WILEY

HYDRODYNAMICS AND WATER QUALITY

Modeling Rivers, Lakes, and Estuaries

ZHEN-GANG JI

HYDRODYNAMICS AND WATER QUALITY

MODELING RIVERS, LAKES, AND ESTUARIES

Zhen-Gang Ji

WILEY-INTERSCIENCE

A JOHN WILEY & SONS, INC., PUBLICATION

HYDRODYNAMICS AND WATER QUALITY

The Wiley Bicentennial–Knowledge for Generations

Each generation has its unique needs and aspirations. When Charles Wiley first opened his small printing shop in lower Manhattan in 1807, it was a generation of boundless potential searching for an identity. And we were there, helping to define a new American literary tradition. Over half a century later, in the midst of the Second Industrial Revolution, it was a generation focused on building the future. Once again, we were there, supplying the critical scientific, technical, and engineering knowledge that helped frame the world. Throughout the 20th Century, and into the new millennium, nations began to reach out beyond their own borders and a new international community was born. Wiley was there, expanding its operations around the world to enable a global exchange of ideas, opinions, and know-how.

For 200 years, Wiley has been an integral part of each generation's journey, enabling the flow of information and understanding necessary to meet their needs and fulfill their aspirations. Today, bold new technologies are changing the way we live and learn. Wiley will be there, providing you the must-have knowledge you need to imagine new worlds, new possibilities, and new opportunities.

Generations come and go, but you can always count on Wiley to provide you the knowledge you need, when and where you need it!

William J. Pesce
President and Chief Executive Officer

Peter Booth Wiley
Chairman of the Board

HYDRODYNAMICS AND WATER QUALITY

MODELING RIVERS, LAKES, AND ESTUARIES

Zhen-Gang Ji

WILEY-INTERSCIENCE

A JOHN WILEY & SONS, INC., PUBLICATION

Published by John Wiley & Sons, Inc., Hoboken, New Jersey
Published simultaneously in Canada

Library of Congress Cataloging-in-Publication Data:

Ji, Zhen-Gang.
Hydrodynamics and water quality : modeling rives, lakes, and estuaries / Zhen-Gang Ji,
p. cm.
Includes index.
ISBN 978-0-470-13543-3 (cloth)
1. Streamflow—Mathematical models. 2. Sediment transport—Mathematical models.
4. Hydrodynamics. 4. Water quality—Measurement—Mathematics. I. Title.
TC175.J52 2008
627—dc22 2007044567

Printed in the United States of America

10 9 8 7 6 5 4 3 2 1

To Yan, Emily, and Tiffany

CONTENTS

FOREWORD

The management of surface water resources is essential for human and ecosystem health and social and economic growth and development. Water resources professionals use a wide range of technical management tools firmly based on the physical, biological, mathematical, and social sciences. This work addresses the fundamental physical and biological processes in surface water systems that provide the basis for both deeper understanding and management decision making. The complexity of the natural surface water environment combined with the ever increasing capabilities of computers to simulate the temporal evolution of systems represented by differential equations has made hydrodynamic and water quality models essential tools for both science and management. Although the present work discusses modeling and presents case studies involving model applications, the author has appropriately chosen to emphasize processes and their commonality and differences between different surface water body types.

This book is organized as follow: An introductory chapter precedes four chapters on fundamental hydrodynamic and water quality processes, followed by a pair of chapters that discuss modeling in the context of regulatory programs and model credibility and performance. The book concludes with three chapters on rivers, lakes, and coastal water bodies. The overarching emphasis of the presentation is the interaction of hydrodynamic and water quality or physical and biogeochemical processes. Chapter 2 presents the fundamentals of surface water hydrodynamics in the context of the three-dimensional, Reynolds averaged, hydrostatic or primitive equations of motions, as well as related dimensionally reduced formulations including the shallow water and St. Venant equations. The understanding of and ability to predict surface water hydrodynamics is important in its on right, addressing topics including riverine floods, water supply reservoir operations, coastal surges, and estuarine salinity intrusion. It readily follows that the physical transport and fate of dissolved and suspended materials is governed by hydrodynamic advection and turbulent diffusion. The term water quality is used in two general contexts in this book as well as in current professional practice. The most general context includes the presence and behavior of dissolved and suspended materials in amounts undesirable for human and ecosystem health, as well as agricultural and industrial use. The more limited historical context, often referred to as conventional water quality, addresses pathogenic organisms and dissolved oxygen dynamics including eutrophication and aquatic carbon, nitrogen, and phosphorous cycles.

The remaining three process oriented chapters address three broad water quality categories: sediment transport, toxic contaminants, and eutrophication. Sediment transport, which is also important in water supply and navigation, has important water quality implications related to water clarity, habitat suitability, and its ability to transport adsorbed materials. The chapter on toxics contaminants provides an overview of the transport and fate of heavy metals and hydrophobic organic compounds, both of which adsorb to inorganic and organic sediments. The final process chapter presents the traditional water quality or water column eutrophication process formulations, as well as the associated remineralization or diagensis of settled organic material. The presentation of process formulations in these four chapters is complimented by the inclusion of illustrative results from actual studies.

Many scientific and engineering studies of surface water systems are in response to regulatory requirements directed at protection of human and aquatic ecosystem health. In the United States, major regulatory programs include the National Point Discharge Elimination System (NPDES), Total Maximum Daily Load (TMDL), and Superfund Remedial Investigation-Feasibility Study (RI/FS). Chapter 6 provides an overview of the role of hydrodynamic and water quality modeling in TMDL development that leads to the following chapter on model performance evaluation.

The use of models for decision making requires the establishment of the model's scientific credibility using accepted quantitative methods that are outlined in Chapter 7. The book concludes by focusing on specific aspects of three major groups of surface water systems, streams and rivers, lakes and reservoirs, and estuaries and coastal regions. Many of the example case studies are based on the author's professional experience. These case studies, as well as those integrated into earlier chapters, provide excellent guidance in the organization and execution of hydrodynamic and water quality studies.

In Hydrodynamics and Water Quality, Dr. Ji has produced a work that should be an essential reference for practicing engineers, scientist, and water resource managers, as well as a text for advance undergraduates and graduate students in engineering and the environmental sciences. The author has brought extensive professional experience and insight to the field and it has been my pleasure to have worked and collaborated with him over the past decade.

Tetra Tech, Inc. JOHN M. HAMRICK
Fairfax, VA

PREFACE

The objective of this book is to present an integrated coverage of hydrodynamics, sediment processes, toxic fate and transport, and water quality and eutrophication in surface waters, including rivers, lakes, estuaries, and coastal waters. The book is intended to serve as a reference book for graduate students and practicing professionals with interest in surface water processes and modeling. Mathematical modeling of surface waters has made great progress in past decades and has become a powerful tool for environmental and water resources management. There are growing needs for integrated, scientifically sound approaches that identify surface water problems and simulate these waterbodies numerically.

This book illustrates principles, basic processes, mathematical descriptions, and practical applications associated with surface waters. Instead of trying to give detailed coverage of every aspect of hydrodynamics, sediment transport, toxics, and eutrophication processes, this book focuses on solving practical problems in rivers, lakes, estuaries, and coastal waters. After Chapter 1 (Introduction), each of the next 5 chapters (2–6) is devoted to one basic and important topic: hydrodynamics, sediment transport, pathogens and toxics, water quality and eutrophication, and external sources and total daily maximum load (TMDL), respectively. Chapter 7 provides general discussions on mathematical modeling and statistical analysis. Based on the theories and processes presented in Chapters 2–7, rivers, lakes, and estuaries and coastal waters are discussed in Chapters 8, 9, and 10, respectively. Each chapter (after Chapter 1) is organized as follows: it begins with an introduction of basic concepts, proceeds to discussions of physical, chemical, and/or biological processes and their mathematical representations, and concludes with case studies. Organizing the book in this application-oriented approach allows readers to easily locate information that is needed for their studies and to focus on the relevant chapters–sections.

Most of the theories and technical approaches presented in the book have been implemented in mathematical models and applied to solve practical problems. Throughout the book, case studies are presented to demonstrate: (1) how the basic theories and technical approaches are implemented into models; and (2) how these models are applied to solve practical environmental–water resources problems. These examples and cases studies are based on either simplified analytical solutions or my professional practice.

A memorable quote from the James Bond movie, From Russia with Love, is that "training is useful, but there is no substitute for experience", which is

directly applicable to the modeling of rivers, lakes, and estuaries. Experience is a key element of modeling and is also one of the primary reasons why modeling is often called an "art". The case studies described in detail throughout the book exemplify this premise. A slightly modified version of this quote also perfectly describes the relationship between modeling and field sampling: modeling is useful, but there is no substitute for field sampling. Law ordains that a person is innocent until proved guilty. A numerical model (and its results), in my opinion, is guilty until proved innocent by data. This highlights the importance of calibrating models against measured data.

This book is about processes and modeling these processes. It is not about models. Detailed discussions on models are refereed to their manuals and reports and are minimized in this book. The theories, processes, and the modeling of these processes presented in this book are generally applicable to numerical models, not just a particular model. It is my intention to make the book unique in three ways:

1. This book will cover state-of-the-art hydrodynamics, sediment transport, toxics fate and transport, and water quality in surface waters in one comprehensive text. In the past 10 years, environmental engineering, water resources engineering, and computer engineering have changed dramatically, especially with respect to progress in mathematical models and computer technology. Comprehensive mathematical models are now routinely used in solving practical engineering problems. This book provides essential and updated information.
2. Instead of trying to cover every detail of hydrodynamics, sediment transport, toxics, and water quality, this book will focus on how to solve practical problems in surface waters. Basic theories and technical approaches are presented, so that mathematical models can be understood and applied to simulate processes in surface waters. From the book, readers will not only understand basic principles, but also learn how to use the models/tools to solve their problems in professional practice. Information is only presented on a need-to-know basis. For example, tides, salinity, and open boundary conditions are not discussed until Chapter 10, where estuaries and coastal waters are covered, since these topics are more likely to be relevant in the modeling of estuaries rather than in the modeling of rivers or lakes.
3. A modeling package on a CD, including electronic files of numerical models, case studies, and model results, is attached to the book. Relevant user manuals and technical reports are also available. This becomes helpful when a reader plans to use the models and tools described in the book to solve practical problems in surface waters. The input files of the case studies described in the book can also serve as templates for new studies.

ACKNOWLEDGMENTS

Many people have contributed to this book over the years that it has taken to write. My former and present colleagues provided great support and encouragement in my professional career and while I was drafting the manuscript, including Robert LaBelle, James Kendall, and Walter Johnson of Minerals Management Service; James Pagenkopf and Leslie Shoemaker of Tetra Tech; Alan Blumberg of HydroQual; and George Mellor of Princeton University. Prof. Cesar Mendoza, my former advisor at Columbia University, helped me in revising the manuscript. Prof. Ji-Ping Chao of National Marine Environmental Forecast Center, China, guided me through my early years of scientific research.

I would like to thank the colleagues and friends who took time from their work to review the chapters of this book. Their comments and advice added to the usefulness of the book. I would like to acknowledge their thoughtful reviews of the manuscript and discussions over the years with them. I am most grateful to Yi Chao (Jet Propulsion Laboratory), Sayedul Choudhury (George Mason University), Tal Ezer (Old Dominion University), Weixing Guo (Schlumberger Water Services), Earl Hayter (U.S. Environmental Protection Agency), Michio Kumagai (Lake Biwa Environmental Research Institute, Japan), Chunyan Li (Louisiana State University), Cesar Mendoza (University of Missouri-Rolla), Leo Oey (Princeton University), Kyeong Park (University of South Alabama), Jian Shen (Virginia Institute of Marine Science), Andy Stoddard (Dynamic Solutions), Dong-Ping Wang (State University of New York at Stony Brook), Tim Wool (U.S. Environmental Protection Agency), Yan Xue (National Oceanic and Atmospheric Administration), Zhaoqing Yang (Battelle Marine Sciences Laboratory), Kirk Ziegler (Quantitative Environmental Analysis), and Rui Zou (Tetra Tech).

My colleague and friend, John Hamrick of Tetra Tech, deserves a special acknowledgment. My close working relationship with John contributed greatly to my professional development and the writing of this book. I feel fortunate and privileged to have worked with him over the past years. I benefited enormously from his guidance, support, and encouragement. I also benefited greatly from working and collaborating with Kang-Ren Jin of South Florida Water Management District. My gratitude extends to Jian Shen of the Virginia Institute of Marine Science and Yongshan Wan, Tom James, and Gordon Hu of South Florida Water Management District. All of whom have stimulated me with their own experience and practical insights.

My gratitude also goes to Mac Sisson (Virginia Institute of Marine Science) and Sharon Zuber (College of William and Mary) who carefully edited the

entire manuscript. Wei Xue provided assistance in drawing some of the graphics. I also like to thank Bob Esposito (John Wiley & Sons, Inc.) for his help in publishing this book and Kenneth McCombs (Elsevier) for initiating and encouraging me to start this long journey of book writing.

Last, but not least, I would like to express my deepest gratitude to my wife (Yan) and our two daughters (Emily and Tiffany). Their encouragement and support, as well as their tolerance of my long hours, made this book a reality. Also I would like to thank the grandparents who helped us raising our daughters and encouraged me to do my best in my career.

ABBREVIATIONS

A	
AOCR	Dissolved oxygen/carbon ratio
B	
BC	Boundary condition
BRI	Blackstone River Initiative
C	
CBOD	Carbonaceous biochemical oxygen demand
cfs	Cubic feet per second
Chl *a*	Chlorophyll *a*
cms	Cubic meters per second
C.L.	Confidence limit
COD	Chemical oxygen demand
CSOD	Carbonaceous sediment oxygen demand
CWA	Federal Clean Water Act
D	
1D, 2D, 3D	One-, two-, three- dimensional
DA	Drainage area
DIN	Dissolved organic nitrogen
DDT	Dichloro-Diphenyl-Trichloroethane
DIP	Dissolved inorganic phosphorus
DM	Dissolved matter
DMR	Discharge monitoring reports
DO	dissolved oxygen
DOC	Dissolved organic carbon
DON	Dissolved organic nitrogen
DOP	Dissolved organic phosphorus
E	
E. coli	*Escherichia coli*
ECOM	Estuarine, Coastal, and Ocean model
EFDC	Environmental Fluid Dynamics Code
EOF	Empirical orthogonal function
EPA	U.S. Environmental Protection Agency

F	
Feb	Fecal coliform bacteria
FFT	Fast Fourier Transform
FPIP	Fraction of predated phosphorous produced as inorganic phosphorus
G	
GUI	Graphic User Interface
GPC	Game and Parks Commission
H	
HSPF	Hydrologic Simulation Program-FORTRAN
I	
IRL	Indian River Lagoon
L	
LA	Local allocations
LHS	Left-hand side
LOEM	Lake Okeechobee Environmental Model
LNG	Liquefied natural gas
LPOC	Labile particulate organic carbon
LPON	Labile particulate organic nitrogen
LPOP	Labile particulate organic phosphorus
M	
MAE	Mean absolute error
ME	Mean error
MOS	Margin of safety
MPN	Most probable number
MRRE	Mean relative RMS error
MSL	Mean sea level
NBOD	Nitrogenous biochemical oxygen demand
NDEQ	Nebraska Department of Environmental Quality
NH4	Ammonia nitrogen
Nit	Nitrification rate
NO3	Nitrate nitrogen
NOAA	National Oceanic and Atmospheric Administration
NPDES	National Pollutant Discharge Elimination System
O	
OBC	Open boundary conditions
ON	Organic nitrogen
OP	Organic phosphorus
P	
PAH	Polycyclic aromatic hydrocarbons
PBAPS	Peach Bottom Atomic Power Station

PC	Personal computer and Principal component
PCB	Polychlorinated biphenyls
PCS	Permit Compliance System
pH	Power of hydrogen
PM	Particulate matter
PO4p	Particulate phosphate
PO4d	Dissolved phosphate
PO4t	Total phosphorus
POM	Princeton Ocean Model
PON	Particulate organic nitrogen
ppb	Parts per billion
ppt	Parts per thousand
R	
RAE	Relative absolute error
RHS	Right-hand side
RMS	Root mean square
RMSE	RMS error
RPD	Rooted plant shoot detritus
RPE	Rooted plant epiphyte
RPOC	Refractory particulate organic carbon
RPON	Refractory particulate organic nitrogen
RPOP	Refractory particulate organic phosphorus
RPR	Rooted plant root
RPS	Rooted plant shoot
RRE	Relative RMS error
S	
SA	Available silica and Surface area
SAV	Submerged aquatic vegetation
SG	Specific gravity
SLE	St. Lucie Estuary
SMB	Sverdrup, Munk, and Bretschneider
SRP	Soluble reactive phosphorus
SSC	Suspended sediment concentration
SU	Particulate biogenic silica
SWAN	Simulation Wave Nearshore
T	
TAM	Total active metal
TDS	Total dissolved solids
TKN	Total Kjeldahl nitrogen
TMDL	Total Maximum Daily Load
TOC	Total organic chemicals
TP	Total phosphorus
TSS	Total suspended solids

U

UBWPAD	Upper Blackstone Water Pollution Abatement District
USACE	U.S. Army Corps of Engineers
USGS	U.S. Geological Survey

W

WLA	Waste load allocations

HYDRODYNAMICS AND WATER QUALITY

CHAPTER 1

Introduction

This chapter introduces surface water systems and the modeling of these systems. The contents of this book are also summarized here.

1.1 OVERVIEW

Surface water systems are waters naturally open to the atmosphere, such as rivers, lakes, reservoirs, estuaries, and coastal waters. The most common uses of surface waters include the followings:

1. Aquatic life support.
2. Water supply.
3. Recreation such as swimming, fishing, and boating.
4. Fisheries.
5. Transportation.

People rely on surface waters for recreation, water supply, and fish production. Surface waters are also critical for the survival of many species. Tens of thousands of birds, mammals, fishes, and other wildlife depend on surface waters as habitats to live, feed, and reproduce.

Rivers are naturally flowing waterbodies. They are a watershed's self-formed gutter system and usually empty into an ocean, lake, or another river. An example is the Illinois River watershed, located in Oklahoma and Arkansas (Fig. 1.1.1). The watershed acts as a collector of all kinds of water (and pollution) discharges. Lakes (and reservoirs) often act as receiving basins downstream from the surrounding watershed. Lakes modify these inflows from the watershed, serving both as filters and buffers. They retain water, sediment, toxics, and nutrients in response to in-lake hydrodynamic, chemical, and biological processes and dampen the extremes of discharges. Estuaries may also act as filters for the sediment and nutrients discharged from rivers and surface runoff.

Hydrodynamics and Water Quality: Modeling Rivers, Lakes, and Estuaries, by Zhen-Gang Ji

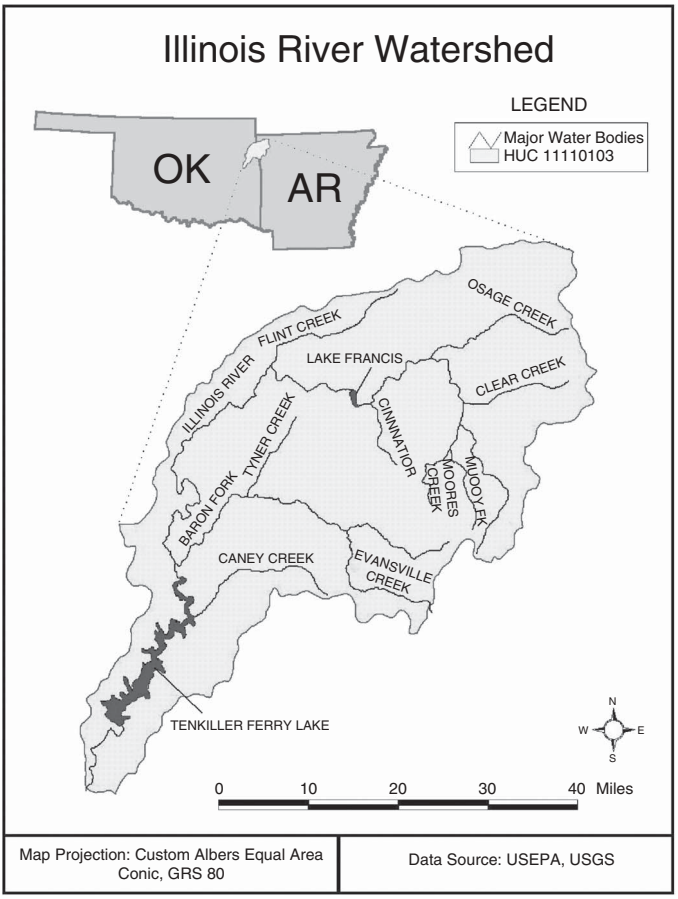

Fig. 1.1.1 Illinois River watershed, Lake Tenkiller drainage basin, the lake, and its main tributaries.

Surface waters are at once resilient and fragile. They are constantly changing as a result of both natural and human forces. The ecosystem of surface waters is an interactive system that includes hydrodynamic characteristics (e.g., water depth and flow velocity), chemical characteristics (e.g., solids, dissolved oxygen, and nutrients), and characteristics associated with the biological community of the water column and benthos. Large amounts of nutrients and contaminants enter into a variety of surface waters. Under siege from all directions, the ecosystems often face assault in the form of increasing populations; inadequately planned land use; and pollutants from farms, homes, and factories. Although every surface water system is unique, many face similar environmental problems: eutrophication, pathogen contamination, toxic chemicals, loss of habitat, and declines in fish and wildlife. These problems, in turn, can cause declines in water quality, living resources, and overall ecosystem health.

TABLE 1.1.1 The Distribution of Water on Earth[a]

Region	Volume (10^3 km^3)	% of total
Oceans	1,350,000	94.12
Groundwater	60,000	4.18
Ice	24,000	1.67
Lakes	230	0.016
Soil moisture	82	0.006
Atmosphere	14	0.001
Rivers	1	—

[a]Based on Lvovich (1971).

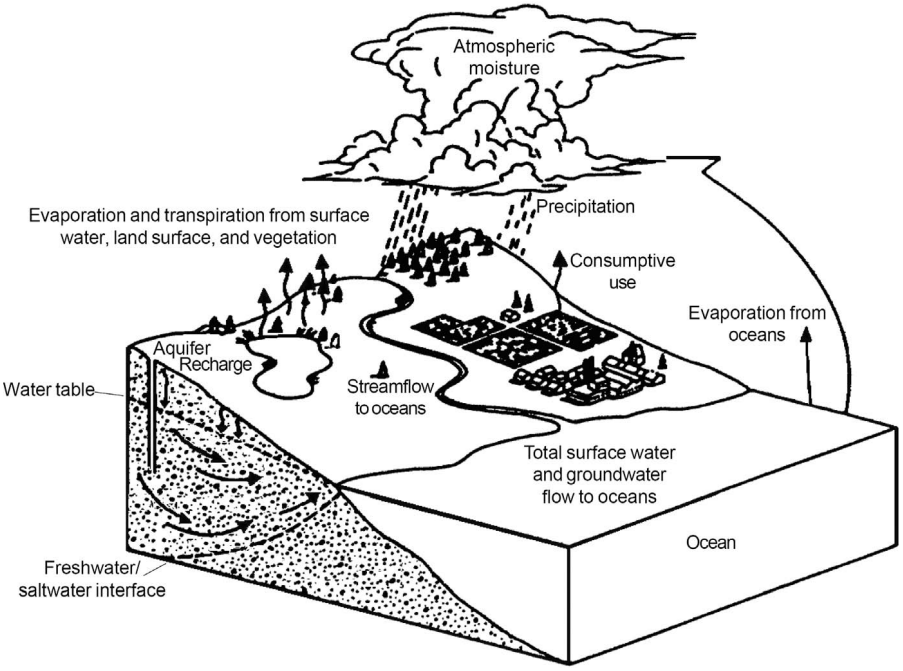

Fig. 1.1.2 Water's natural cycle (EHC, 1998).

Table 1.1.1 is a water budget showing the distribution of water over the earth (Lvovich, 1971). Rivers and lakes, though critical to civilization, contain a very small fraction of the total water budget. The water cycle (also known as the hydrologic cycle) represents the movement and endless recycling of water between the atmosphere, the land surface, and the ground. No matter what water quality problems that an ecosystem is associated with, its water cycle is often a key factor affecting the problems. From raging streams to the slow movement of water through the ground, as illustrated in Fig. 1.1.2, water is in constant motion. The water cycle begins with water evaporation from the

earth's water surface, soil, and plants. The vast majority of evaporation occurs from the oceans. Once in the air, the water vapor is transported by winds and may later condense into clouds. A portion of the water vapor falls to the ground as precipitation in the form of rain or snow.

As the precipitation returns water to the land surface, a portion of it seeps into the ground and becomes groundwater. The remaining portion, which does not infiltrate the soil but flows over the surface of the ground to a stream, is called surface runoff. The water flowing through the ground can also return to the surface to supply water to rivers and lakes. All of the land that eventually drains to a common river or lake is considered to be in the same watershed. By a network of streams that flows into larger and larger streams, the water that is not evaporated back into the atmosphere eventually reaches the oceans. Therefore, land use activities in a watershed can affect the water quality of surface waters, such as rivers, lakes, and estuaries, as contaminants are carried by runoff and groundwater to these surface waters. To accurately estimate pollution loadings to a surface water system, the water cycle of the watershed must be considered accordingly.

1.2 UNDERSTANDING SURFACE WATERS

Three important tools used in supporting water quality management are (1) observation, (2) theoretical analysis, and (3) numerical modeling. Although each tool has advantages, each has certain disadvantages. The appropriate way to apply these tools is to better understand and make use of them according to their properties (Ji, 2004). Also, in the end, the professional judgment of the engineers and the managers inevitably comes into play.

In terms of helping decision makers identifying the scope of the environmental problems, reliable measured data are invaluable. Observation is the only way to know the real characteristics of the ecosystem and to provide the basis for theoretical analysis and numerical modeling. Only after certain observations are made can theoretical analysis and numerical modeling help the understanding of hydrodynamic and water quality processes and produce reliable results for supporting decisionmaking. These processes, in many cases, cannot be described well in mathematical models before they are measured in real waterbodies.

But measured data alone are rarely sufficient to make informed decisions on water quality management plans, especially when it comes to large and complex waterbodies. Due to budget, time, and technical constraints, field measurements are often limited to certain small areas (or fixed locations) and within certain periods of time. Measured data can go only so far in pointing the direction toward sound water quality policies and practices. Further, data errors can result in ambiguous interpretation and misunderstanding of the real physical, chemical, and biological processes. In these cases, theoretical analysis and numerical modeling become important. Through calibration and verifica-

tion, numerical models are capable of realistically representing the hydrodynamic, sediment, toxic, and water quality conditions of the waterbody. The models can then be used as tools to support decisionmaking.

Key parameters used to represent the hydrodynamic and water quality conditions of surface waters include: (1) water temperature, (2) salinity, (3) velocity, (4) sediment, (5) pathogens, (6) toxics, (7) dissolved oxygen (DO), (8) algae, and (9) nutrients.

Water temperature is an important parameter representing the conditions of a waterbody. It also affects when animals and plants feed, reproduce, and migrate. Periodic power plant discharges can cause sudden changes in temperature and be disruptive to a local ecosystem. If water temperature rises too high, the DO level deceases, directly threatening aquatic life and contributing to eutrophication. In estuaries and coastal waters, salinity is a key parameter representing the environmental conditions. Water velocity plays a key role in transporting and mixing water quality variables.

Sediments enter surface waters from many sources and can alter the habitat of benthic organisms once they settle. Sediments can cause siltation in harbors and navigation channels. Sediments cloud the water, making it difficult for plants, such as underwater grasses, to receive sufficient sunlight to survive. Sediments are also important carriers of pollutants. Sediment transport can move the pollutants far away from their sources.

Pathogens, toxic metals, and organic chemicals are often derived from wastewater, farms, and feedlots. They can be transported to beaches and recreational waters, causing direct human exposure and disease. Pathogens may also accumulate in aquatic biota, such as oysters, clams, and mussels, causing disease when consumed by humans.

Dissolved oxygen is one of the most important parameters of water quality and is used to measure the amount of oxygen available for biochemical activity in water. Adequate DO concentrations are a requirement for most aquatic animals. The natural balance of DO can be disrupted by excessive wastewater loads of nutrients. Nutrients can come from wastewater treatment plants, fertilizers, and atmospheric deposition. Nutrients are essential for plants and animals, but excessive nutrient loading can cause algae overproduction, disrupting the natural balance. When algae die and decay, they deplete the dissolved oxygen in water.

Water quality management needs information to identify and evaluate various alternatives for achieving economic and water quality goals. Economic goals are often to achieve cost effectiveness, whereas water quality goals are usually set to meet certain water quality standards. The effectiveness of management alternatives may be measured in terms of how well they accomplish these goals. To determine this effectiveness often requires an assessment of the current state of the waterbody and how it has changed over time. Information is needed about the likely response of the waterbody to the management alternatives, such as decreasing nutrient loads from specific sources or increasing water inflows to the ecosystem, which may require a significant amount of

infrastructure investment. It is paramount to be able to predict the consequences and effectiveness of the alternatives as accurately as possible, thus incorporating this information into decisionmaking.

Assessing the water quality of a surface water system requires expertise from many disciplines. Although the various processes may be described independently, they interact in complex ways. Multiple disciplines (hydrodynamics, sediment transport, pathogens and toxics, eutrophication, etc.) interact with each other to address water quality objectives. The result is not simply the assemblage of multiple disciplines working independently on a problem. Physical, chemical, and biological processes also vary over a broad spectrum, both in time and space. Spatial variations largely depend on the topography of the waterbody and external loadings. Temporal variations may have long-term (yearly), seasonal (monthly), diurnal (hourly), and short-term (minutes) time scales.

Often water quality is defined in terms of concentrations of the various dissolved and suspended substances in the water, for example, temperature, salinity, DO, nutrients, phytoplankton, bacteria, and heavy metals. The distribution of these substances has to be calculated by the water quality model. Based on the principle of conservation of mass, the concentration change can be represented simply in a one-dimensional (1D) form (Ji, 2000a):

$$\frac{\partial C}{\partial t} = -U\frac{\partial C}{\partial x} + \frac{\partial}{\partial x}\left(D\frac{\partial C}{\partial x}\right) + S + R + Q \tag{1.2.1}$$

where C = substance concentration, t = time, x = distance, U = advection velocity in x direction, D = mixing and dispersion coefficient, S = sources and sinks due to settling and resuspension, R = reactivity of chemical and biological processes, Q = external loadings to the aquatic system from point and nonpoint sources.

It would be an oversimplification to say that this book is all about Eq. (1.2.1), but it is safe to say that this equation includes the major elements of hydrodynamics, sediment, toxics, and eutrophication. Many discussions in this book can be related to this equation directly or indirectly.

The changes of concentration C in Eq. (1.2.1) are determined by the following:

1. The hydrodynamic processes control the water depth (D), the advection (represented by the U term), and mixing (represented by the D term), which will be described in Chapter 2.
2. The size and properties of sediment (or particular organic matter) affect the settling and resuspension (represented by the S term), which will be illustrated in Chapter 3.
3. The chemical and biological reactions of pathogens, toxics, and/or nutrients are represented by the R term, which will be presented in Chapters 4 and 5.

4. External loadings from point and nonpoint sources are included by the Q term, which will be elaborated in Chapter 6.

The applications of Eq. (1.2.1) (and its more complicated versions) to rivers, lakes, and estuaries are presented in Chapters 8–10, respectively.

1.3 MODELING OF SURFACE WATERS

"Modeling is a little like art in the words of Pablo Picasso. It is never completely realistic; it is never the truth. But it contains enough of the truth, hopefully, and enough realism to gain understanding about environment systems" (Schooner, 1996). The two primary reasons to conduct modeling are (1) to better understand physical, chemical, and biological processes and (2) to develop models capable of realistically representing surface waters, so that the models can be used to support water quality management and decisionmaking.

The modeling of surface waters is complex and evolving. Presently, the success of a modeling study, especially sophisticated three-dimensional (3D) and time-dependent modeling studies, still depends heavily on the experience of the modeler. There is not a complete agreement among the professionals regarding the "best" approach to modeling rivers, lakes, estuaries, and coastal waters.

Water quality management needs to understand key processes affecting environmental problems in order to evaluate management alternatives. Examples of such environmental problems include:

1. Thermal pollution due to power plant discharges.
2. Sedimentation in harbors causing siltation and high dredging costs.
3. Eutrophication due to excessive nutrient loadings.
4. Low DO conditions caused by waste water discharges.
5. Accumulation of toxic materials in the sediment bed.

Water quality management increasingly depend on accurate modeling. This dependency is further amplified by the adoption of the watershed-based approach to pollution control. Models enable decision-makers to select better, more scientifically defensible choices among alternatives for water quality management. In many cases, the models are used to evaluate which alternative will be most effective in solving a long-term water quality problem. The management decisions require the consideration of existing conditions, as well as the projection of anticipated future changes of the water system. In these applications, the models not only need to represent the existing conditions, but also have to be predictive and give conditions that do not yet exist. Models are also used to provide a basis for economic analysis, so that decision makers

can use the model results to evaluate the environmental significance of a project, as well as the cost–benefit ratio.

Three key factors have contributed to the great progress in the modeling of surface waters:

1. Better understanding and mathematical descriptions of physical, chemical, and biological processes in rivers, lakes, estuaries, and coastal waters.
2. Availability of fast and efficient numerical schemes.
3. Progress in computer technology.

The powerful, yet affordable computers in combination with fast numerical algorithms have enabled the development of sophisticated 3D hydrodynamic and water quality models. These advanced models contain very few simplifying approximations to the governing equations.

Personal computers (PCs) have evolved rapidly to become the standard platform for most engineering applications (with the exception of very large-scale problems). The PCs represent the most widely used computer platform today. Models developed on a PC can be transformed to other PCs without much difficulty. The relatively low prices of PCs also make modeling more cost effective. Due to the rapid advances in computer technology, PCs are now widely used in surface water modeling studies. As a matter of fact, all of the case studies presented in this book are conducted on PCs.

Models play a critical role in advancing the state-of-the-art of hydrodynamics, sediment transport, and water quality, and of water resources management. Because of their requirements for precise and accurate data, models also ultimately contribute to the design of field data collection and serve to identify data gaps in characterizing waterbodies. Models are used to analyze the impact of different management alternatives and to select the ones that result in the least adverse impact to the environment.

Models are often used to improve the scientific basis for theory development, to make and test predictions, and to clarify cause-and-effect relationships between pollutant loadings and the receiving waterbody. Reliable predictions stand out as a salient requirement for models, because decisions can have costly social and economic consequences on businesses, municipalities, and even entire states. Models are often used to evaluate and test potentially expensive water quality management alternatives prior to their implementation. The cost of a hydrodynamic and water quality modeling study is usually a small fraction of the implementation cost. Models can simulate changes in an ecosystem due to changes in internal and/or external conditions, such as water elevation variations or increased external pollutants. These simulations predict positive or negative changes within the ecosystem due to the management actions, such as improved sewage treatment or reduced agricultural runoff. These simulations are obviously far more cost effective than testing expensive management actions on a trial-and-error basis, thus making

models a useful tool for water quality management. Since huge financial investment is at stake, accurate model results are imperative to support the costly implementation.

In the past decades, hydrodynamic and water quality models have evolved from simplified 1D, steady-state models, such as the legendary QUAL2E model (Brown and Barnwell, 1987), to complex 3D, time-dependant models of hydrodynamics, sediment, toxics, and eutrophication. Three-dimensional modeling has matured from a research subject to a practical engineering tool. Over this same period, computational requirements for realistic 3D modeling have changed from supercomputers, to high-end workstations, and then to PCs.

These advanced 3D and time-dependant models, which can also be readily applied for 1D- and two-dimensional (2D) problem settings, provide a powerful computational tool for sediment transport, water quality, eutrophication, and toxic chemical fate and transport modeling studies. Their hydrodynamic submodel provides: (1) flow field, (2) water depth, (3) temperature and salinity, (4) mixing, and (5) bottom stress.

The flow field, water depth, and mixing are used to determine mass transport of solids, toxics and other constituents. Bottom stress is used to estimate the exchange between the water column and sediment bed as a result of sediment deposition and resuspension. Since the mid-1980s, these models (e.g., Blumberg and Mellor, 1987; Hamrick, 1992; Sheng, 1986) have successfully transformed from academic research to practical tools for managing surface water systems.

Numerous models have been developed in the past decades. Many of them are actually based on similar theories and numerical schemes, even though the input and output formats of these models may look very different. For example, the Estuarine, Coastal and Ocean Model (ECOM) (HydroQual, 1991a, 1995a) and the Environmental Fluid Dynamics Code (EFDC) (Hamrick, 1992) both have hydrodynamic theories similar to the Princeton Ocean Model (POM) (Blumberg and Mellor, 1987). The POM, ECOM, EFDC, and CH3D (Sheng, 1986) models all use the sigma coordinate in the vertical and a curvilinear grid in the horizontal. The CE-QUAL-ICM model (Cerco and Cole, 1994), the WASP model (Wool et al., 2002), and the EFDC model have the eutrophication theories similar to the RCA model (HydroQual, 2004). The Chesapeake Bay sediment flux model (Di Toro and Fitzpatrick, 1993) and its modified versions have almost become the "standard" sediment diagenesis model in eutrophication modeling.

These advanced models often include several coupled submodels for different physical, chemical, biological processes in surface waters, such as (1) the hydrodynamic, (2) the wind wave, (3) the sediment, (4) the toxic, (5) the eutrophication, (6) the sediment diagenesis, and (7) the submerged aquatic vegetation (SAV) model.

As an example, Fig. 1.3.1 illustrates the major components of the EFDC model. In addition to computational modules, these advanced models tend to

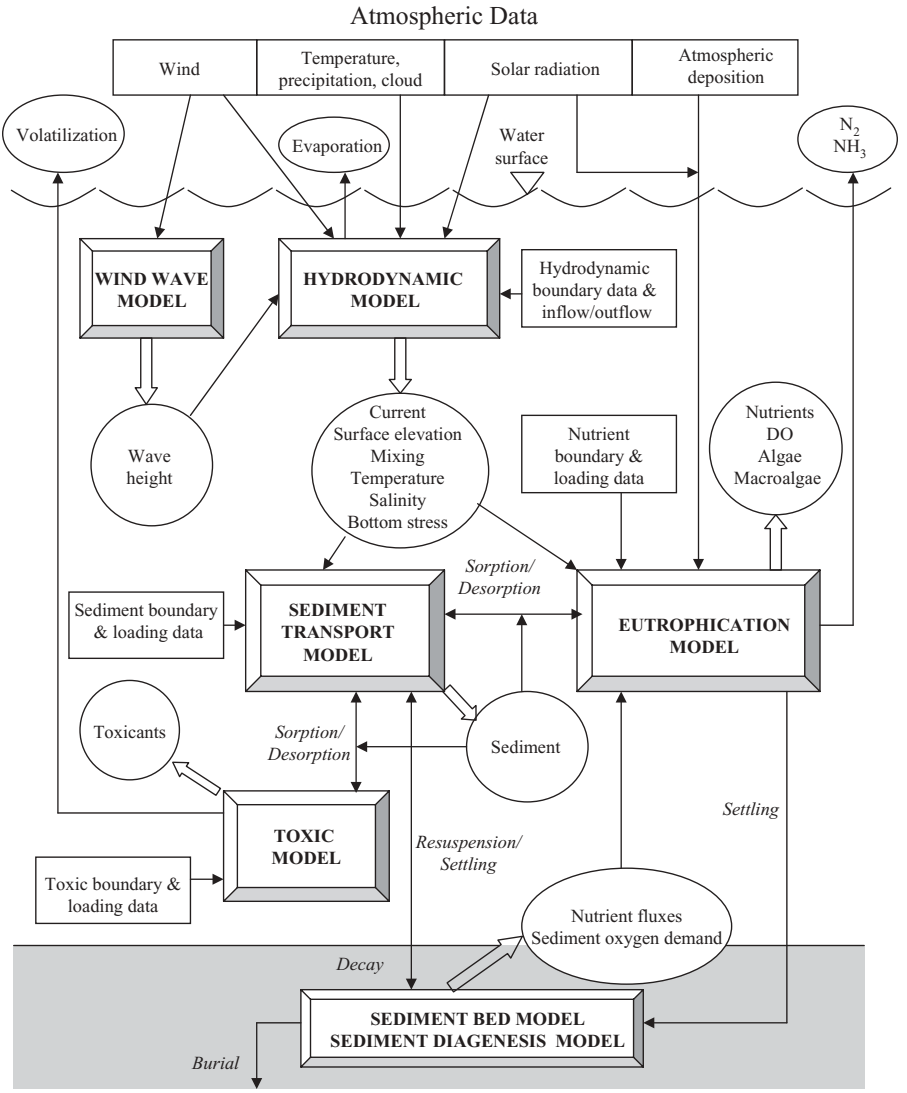

Fig. 1.3.1 Major components (submodels) of the EFDC model.

evolve into complex software systems, comprising many tools and sources of information. They may contain components for grid generation, data analysis, preprocessing, postprocessing, statistical analysis, graphics, and other utilities. Examples of these modeling packages include EFDC, ECOM, MIKE 3 (DHI, 2001) and TRIM (Casulli and Cheng, 1992).

Whereas the basic theories of the aforementioned models (and other models) might have been universally agreed upon, choosing the "best" model for a particular application is the subject of considerable controversy. It is

beyond the scope of this book to get into the subtleties of this controversy. This book does not review models and does not recommend the so-called "best" model for surface water modeling. There are dedicated reports covering particular aspects of model review and model selection (e.g., Tetra Tech, 2001; Imhoff et al., 2004; HydroGeoLogic, 1999).

Note that models are rarely either right or wrong: they either lead the modelers to proper conclusions or to improper conclusions. Thus how to use and interpret model results are as important as the model results themselves. In this light, models are similar to other tools in engineering: they can either be productively used or abused. The experience of the modeler plays a vital role in a successful modeling application. This primary reason is why modeling is also called an "art".

1.4 ABOUT THIS BOOK

This book is about processes, their modeling, and how to use models to support decisionmaking. Instead of addressing models, this book is focused on theories, mathematical representations, and numerical modeling of processes in surface waters. Through case studies, the modeling of rivers, lakes, estuaries, and coastal waters is illustrated.

Chapters 2–5 are dedicated to four important subjects, respectively, (1) hydrodynamics (Chapter 2), (2) sediment transport (Chapter 3), (3) pathogens and toxics (Chapter 4), and (4) water quality and eutrophication (Chapter 5).

After external sources and total daily maximum load (TMDL) are discussed in Chapter 6, and mathematical modeling and statistical analyses are described in Chapter 7, the rest of book is focused on different types of surface waterbodies: (1) rivers (Chapter 8), (2) lakes and reservoirs (Chapter 9), and (3) estuaries and coastal waters (Chapter 10).

Each chapter (after Chapter 1) introduces concepts, processes, and mathematical representations at a level sufficient to meet the modeling needs, but elementary enough to allow the readers to have a good understanding of the topic. The organization of each chapter is similar: it begins by introducing basic concepts, proceeds to the discussions of physical, chemical, and/or biological processes and their mathematical representations, and concludes the chapter with case studies.

The best way to understand theories is via examples and case studies. This book (Chapters 2–10) presents a range of applications designed to be representative of surface water systems, including rivers, lakes, and estuaries. Each chapter typically includes two case studies on two different waterbodies. The case studies are useful for understanding the theories and processes presented in the previous sections of that chapter. They detail key features of surface water systems and exhibit varying levels of complexity. They provide real-world examples of how models can be set up on a practical level, used to

TABLE 1.4.1 Waterbodies Discussed in This Book as Case Studies and Examples

Waterbody Name	Waterbody Type	Physical Feature	Major Problems	Chapters
Blackstone River, MA	Small river	Shallow (<1 m) Narrow (<20 m)	Sedimentation, Toxic metals	3, 8
Susquehanna River, PA	Deep river	Deep (>10 m)	Thermal pollution	8
Lake Okeechobee, FL	Lake	Large (1730 km^2) Shallow (3.2 m)	Phosphorus, Eutrophication	2, 3, 5, 7, 9
Lake Tenkiller, OK	Reservoir	Long (48 km) Deep (>45 m)	Eutrophication	9
Rockford Lake, NE	Reservoir	Small (0.6 km^2) Shallow (3.7 m)	Pathogens	4
St. Lucie Estuary and Indian River Lagoon, FL	Estuary-lagoon	Small (29 km^2) Shallow (2.4 m)	Salinity intrusion, Eutrophication	2, 4, 5, 10
Morro Bay, CA	Estuary	Small (8.5 km^2) Shallow (<2.5 m)	Sedimentation Pathogen	10

simulate surface waters, and applied to support decisionmaking. A primary objective of presenting these case studies is that the modeling approaches, the analysis methods, and the discussions on processes in these case studies are useful for readers to conduct their own modeling studies on similar waterbodies.

The case studies are carefully selected, so that they represent different types of waterbodies. All of the case studies originated from real engineering projects. None of them is just an "idealized" exercise. The contents of these case studies are based on either published journal papers or technical reports. Physical features of these waterbodies and major problems addressed in the cases studies are summarized in Table 1.4.1. Electronic files of two case studies are included in the modeling package:

1. Lake Okeechobee: Shows the modeling and applications of hydrodynamics, wind wave, sediment transport, water quality, and SAV.
2. St. Lucie Estuary and Indian River Lagoon: Presents the applications of hydrodynamics, sediment transport, toxic metal, and water quality.

Sample input files and output files of these studies are included in the modeling package. Readers can use these input files as templates for their own applications and avoid developing the entire input files from scratch.

CHAPTER 2

Hydrodynamics

Hydrodynamics studies the motion of water and the forces acting on water. This chapter discusses the fundamentals of hydrodynamics in surface waters, such as rivers, lakes, estuaries, and coastal waters. The materials presented in this chapter will be used throughout this book.

Hydrodynamics is the driving mechanism for the transport of sediments, toxics, and nutrients and is critical to the movement of pollutants through the environment. A hydrodynamic model can provide crucial information to sediment, toxic, and eutrophication models, including water velocities and circulation patterns, mixing and dispersion, water temperature, and density stratification. Therefore, it is necessary to have a good understanding of hydrodynamic processes in a water system, before proceeding to the studies of sediment, toxic, and/or water quality.

In this book, Chapters 2–5, 8–10 are organized in a similar manner. They typically have the following contents:

1. What this chapter is about and how the contents in this chapter relate to other chapters.
2. How the contents of this chapter are applicable to practical problems.
3. Basic concepts, theories, and processes.
4. Analytical solutions and/or simplified cases that are helpful for understanding the theories and processes.
5. Model parameters and data that are commonly used/adjusted in modeling.
6. Case studies.

In this chapter, the basic hydrodynamic processes are discussed in Section 2.1, governing hydrodynamic equations, in 1D, 2D, and 3D forms, are presented in Section 2.2. Water temperature and thermal processes are discussed in Section 2.3. Hydrodynamic modeling is discussed in the Section 2.4, in which major hydrodynamic model parameters, data required in hydrodynamic

Hydrodynamics and Water Quality: Modeling Rivers, Lakes, and Estuaries, by Zhen-Gang Ji

modeling, and case studies are presented. The two case studies described in this chapter are the modeling of Lake Okeechobee and the modeling of St. Lucie Estuary and Indian River Lagoon. These two waterbodies are also used as cases studies in other chapters of this book.

2.1 HYDRODYNAMIC PROCESSES

Hydrodynamic processes are integral components of complex surface water systems. Water movements at different scales and of different types significantly affect not only the distribution of temperature, nutrients, and dissolved oxygen, but also the aggregation and/or distribution of sediments, contaminants, and algae. Circulation, wave phenomena, and turbulent mixing are major influences on the distribution of biota and the productivity of natural waterbodies. This section illustrates fundamental laws and basic processes in hydrodynamics.

2.1.1 Water Density

Water density has unique physical properties. Water is less dense as a solid than as a liquid. Consequently, ice floats on water. Water density does not monotonically decrease with increasing temperatures. Instead, water has its maximum density at 4 °C. Water becomes less dense as the temperature either increases or decreases from 4 °C. As a result, a lake in the summer tends to have a layer of warm water floating on the top of the denser, colder water below. Conversely, in the winter, if the lake's surface drops <4 °C, it creates a layer of cold water that floats on the top of the denser, warmer (~4 °C) water below. Further, the temperature–density relation is nonlinear. The density difference between 20 and 21 °C is approximately equal to the density difference between 5 and 10 °C. Beside, water density is also significantly influenced by salinity and sediment concentrations. These density differences between the surface water and the bottom water create stratifications and inhibit vertical mixing. Because of this density–temperature relationship, many lakes and estuaries tend to stratify, that is, they separate into distinct vertical layers.

Water density is a basic parameter in hydrodynamic and water quality studies. Accurate hydrodynamic calculations require accurate water densities. The density (ρ) is largely determined by three parameters: (1) temperature (T), (2) salinity (S), (3) concentration of total suspended sediment (C).

The relationship between the four variables, ρ, T, S, and C, can be written as:

$$\rho = f(T, S, C) \tag{2.1.1}$$

and is referred to as the equation of state. The actual form of function f is established empirically.

It is convenient to express the equation of state in differential form as follows:

$$d\rho = \left(\frac{\partial \rho}{\partial T}\right)_{S,C} dT + \left(\frac{\partial \rho}{\partial S}\right)_{T,C} dS + \left(\frac{\partial \rho}{\partial C}\right)_{T,S} dC \tag{2.1.2}$$

Consequently, it has

$$\rho = \rho_T + \Delta\rho_S + \Delta\rho_C \tag{2.1.3}$$

where ρ_T = density of pure water as a function of temperature (kg/m^3), $\Delta\rho_S$ = density increment due to salinity (kg/m^3), $\Delta\rho_C$ = density increment due to total suspended sediment (kg/m^3).

A variety of empirical equations have been proposed to describe the density of pure water as a function of temperature. The one presented by Gill (1982, p. 599) is commonly used in hydrodynamic modeling (e.g., Hamrick, 1992; Cole and Buchak, 1995):

$$\begin{aligned}\rho_T = {} & 999.842594 + 6.793952\times10^{-2}\,T - 9.095290\times10^{-3}\,T^2 + \\ & 1.001685\times10^{-4}\,T^3 - 1.120083\times10^{-6}\,T^4 + 6.536332\times10^{-9}\,T^5\end{aligned} \tag{2.1.4}$$

where T = water temperature (°C).

The water density increment due to salinity, $\Delta\rho_S$, is given by (Gill, 1982).

$$\begin{aligned}\Delta\rho_S = {} & S(0.824493 - 4.0899\times10^{-3}\,T + 7.6438\times10^{-5}\,T^2 - 8.2467\times \\ & 10^{-7}\,T^3 + 5.3875\times10^{-9}\,T^4) + S^{3/2}\,(-5.72466\times10^{-3} + \\ & 1.0227\times10^{-4}\,T - 1.6546\times10^{-6}\,T^2) + S^2\,4.8314\times10^{-4}\end{aligned} \tag{2.1.5}$$

where S = salinity, kg/m^3. Based on Eqs. (2.1.4) and (2.1.5), Fig. 2.1.1 gives the variations of water density with water temperature under salinity values of 0, 10, 20, 30, and 40 ppt. It shows that the water density varies from 992.2 kg/m^3 at 40 °C and 0 ppt to 1032.1 kg/m^3 at 0 °C and 40 ppt.

The total suspended sediment, C, includes two parts: The total suspended solid (TSS) and the total dissolved solid (TDS). Ford and Johnson (1986) presented the following equation to calculate water density increment due to TSS and TDS:

$$\Delta\rho_C = \mathrm{TSS}\,(1\text{-}1/\mathrm{SG})\times10^{-3} + \mathrm{TDS}\,(8.221\times10^{-4} - 3.87\times10^{-6}\,T + 4.99\times10^{-8}\,T^2) \tag{2.1.6}$$

where TSS = total suspended solids concentration (g/m^3), TDS = total dissolved solid concentration (g/m^3), SG = specific gravity of the total suspended solid (=2.56).

The SG is a dimensionless ratio of the density of a fluid (or solid) to the density of pure water. As a rule of thumb, an increment of water density by

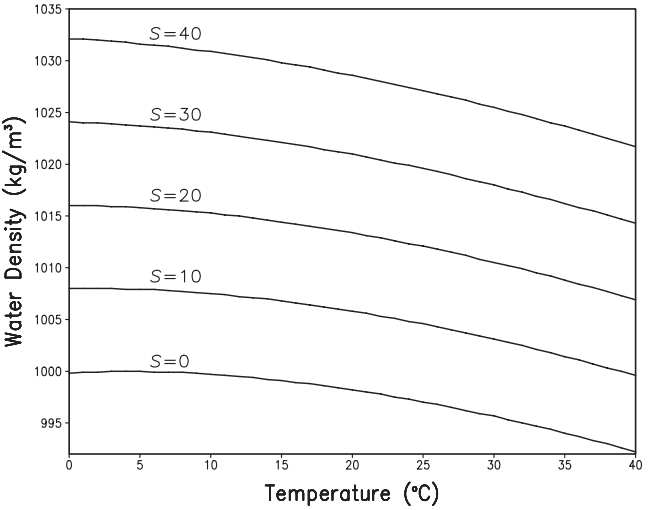

Fig. 2.1.1 Variations of water density with water temperature under salinity values of 0, 10, 20, 30, and 40 ppt.

one-tenth of one percent (0.1%) needs a decrease of ~5 °C or an increase of ~1.2 ppt salinity, that is, the changes of 1 ppt salinity has similar affect on water density variation as the change of 4 °C temperature.

Because of the small variations in water density, it may be necessary to know the density to at least five decimal places in some modeling studies. A variable, called sigma-*t* (σ_t), is defined as:

$$\sigma_t = \rho - 1000 \tag{2.1.7}$$

Both ρ and σ_t have the unit of kilograms per cubic meters (kg/m^3). When studying density variation and vertical stratification, it is sometimes more convenient to present σ-*t* than to directly present density. For example, Ahsan and Blumberg (1999) used sigma-t to illustrate the seasonal variation of vertical density distributions in a lake.

2.1.2 Conservation Laws

The conservation laws that govern hydrodynamic processes include (1) the conservation of mass, (2) the conservation of energy, and (3) the conservation of momentum. These three conservation laws form the theoretical basis of hydrodynamics and are used routinely in the studies of hydrodynamics and water quality. While basic equations in hydrodynamic models are frequently manipulated, simplified, and renamed, they all come from the same conservation laws. The conservation of mass and the conservation of momentum are

discussed here. The conservation of energy will be described in Section 2.3 when heatfluxes are presented.

2.1.2.1 Conservation of Mass. The law of conservation of mass states that mass can neither be produced nor destroyed. It is often expressed in a mass balance equation (also called continuity equation), which accounts for the flux of mass going into a defined area and the flux of mass leaving the defined area. For an incompressible fluid (which is a very accurate description of surface waters) in a defined area, the water flux in must equal the flux out. It has

$$\text{Mass accumulation} = \text{Mass in} - \text{Mass out} + \text{Source} - \text{Sink} \tag{2.1.8}$$

In hydrodynamics, the equation for conservation of mass is frequently illustrated in and applied to water columns. A water column is a portion of a waterbody, or a hypothetical "cylinder" of a waterbody, extending from the surface of a waterbody to the bottom. It is an imaginary vertical column of water used as a control volume for computational purposes. A control volume is a spatial domain for analysis separated from the rest of the spatial domain by a defined boundary. Variables may enter and leave this volume and be stored within it, but its shape and position in space remain unchanged. For a given water column, the inflow minus outflow must equal the volume change over time. Equation (2.1.8) can be resated as:

$$dm = (m_{\text{in}} - m_{\text{out}} + m_r) \cdot dt \tag{2.1.9}$$

where dm = mass accumulation, m_{in} = the rate of mass in flux, m_{out} = the rate of mass out flux, m_r = the net rate of production from all source and sink terms, and dt = time increment.

To develop an equation in terms of mass flux (the rate at which mass enters or leaves a water column), Eq. (2.1.9) is divided by the time increment, dt. It yields the following mass balance equation for water (or a particular pollutant):

$$\frac{dm}{dt} = \frac{\partial m}{\partial t} + \nabla \cdot (m\vec{v}) = m_{\text{in}} - m_{\text{out}} + m_r \tag{2.1.10}$$

If other compounds react to form this pollutant, the net rate of production, m_r, will be positive. If this pollutant reacts to form some other compounds, resulting in a loss of this pollutant, m_r will be negative. Equation (2.1.10) is the basic equation for mass conservation and is used extensively in hydrodynamic and water quality studies.

If a pollutant increases in a waterbody (say, in a lake), it must be due to one (or both) of the following reasons:

1. There are external sources that have discharged into the lake.
2. There are in-lake chemical/biological reactions from other compounds that formed this pollutant.

If chemical/biological reactions caused the pollutant to increase, they must also have caused a corresponding decrease in some other compounds. Thus, the conservation of mass, as expressed in Eq. (2.1.10), provides a means of compiling a pollutant budget in the lake. This budget tracks the amount of the pollutant entering the lake, leaving the lake, and the amount formed or destroyed by chemical and biological reactions.

When the reactions and the inflow/outflow are neglected, the differential equation for the conservation of mass can be further derived from Eq. (2.1.10) as

$$\frac{\partial \rho}{\partial t} + \nabla \cdot (\rho \vec{v}) = 0 \tag{2.1.11}$$

where ρ = density of water, $\vec{v}$ = velocity vector , and ∇ = gradient operator.

Equation (2.1.11) is also called the continuity equation. For incompressible flow ($d\rho/dt = 0$), the continuity equation simplifies to

$$\nabla \cdot \vec{v} = 0 \tag{2.1.12}$$

It means that the net rate of mass flow across any closed surface is zero. Under the Cartesian coordinates, Eq. (2.1.12) has

$$\frac{\partial u}{\partial x} + \frac{\partial v}{\partial y} + \frac{\partial w}{\partial z} = 0 \tag{2.1.13}$$

where u, v, and w are velocity components in x, y, and z directions, respectively.

2.1.2.2 Conservation of Momentum. The conservation of momentum can be derived from Newton's second law:

$$\vec{F} = m \cdot \vec{a} \tag{2.1.14}$$

where $\vec{F}$ = external force , m = mass of the object, and $\vec{a}$ = acceleration of the object.

In addition to external forces (e.g., wind), there are three forces important to hydrodynamics:

1. Gravitational force.
2. Force from water pressure gradient.
3. Viscous force.

Gravitational force is due to the gravitational attraction of the earth. Water pressure gradient is caused by pressure gradient in a waterbody. Viscous force

is due to water viscosity and turbulent mixing. Hence, the momentum equation stated in Eq. (2.1.14) can be expressed as:

$$\rho\frac{d\vec{v}}{dt}=\frac{\partial\rho\vec{v}}{\partial t}+\nabla\cdot(\rho\vec{v}\vec{v})=\rho\vec{g}-\nabla p+\overrightarrow{f_{\text{vis}}} \tag{2.1.15}$$

where $\overrightarrow{f_{\text{vis}}}$ = viscous force, p = water pressure, $\vec{g}$ = gravitational force, ρ = water density, and ∇ = gradient operator.

Equation (2.1.15) does not include wind forcing, which can be incorporated as boundary conditions in Eq. (2.2.30). The negative sign for the pressure gradient is to indicate that the pressure gradient force is directed opposite to the gradient. For an incompressible Newtonian fluid, the viscous force can be expressed as:

$$\overrightarrow{f_{\text{vis}}}=\nabla\cdot\vec{\tau}=\mu\nabla^2\vec{v} \tag{2.1.16}$$

where $\vec{\tau}$ = shear stress, μ = absolute (or dynamic) viscosity, assumed to be constant, and ∇^2 = the Laplacian operator.

A Newtonian fluid is the one where the stress is linearly proportional to the rate of deformation. Most common fluids are Newtonian, such as water, air, and gasoline. However, some fluids have a nonlinear relationship between stress and the rate of deformation. These fluids are called non-Newtonian. Examples of non-Newtonian fluids are toothpaste and butter.

Under Cartesian coordinates, the water shear stress has

$$\tau_{xy}=\mu\frac{dv}{dx} \tag{2.1.17}$$

$$\tau_{yx}=\mu\frac{du}{dy} \tag{2.1.18}$$

where u = velocity component in x direction and v = velocity component in y direction.

Here a double subscript notation is used to label the shear stress components (τ_{xy} and τ_{yx}). For example, the first subscript of τ_{xy} indicates the plane on which the stress acts (in this case, a surface perpendicular to the x axis). The second subscript indicates the direction in which the stress acts.

When considering the rotation of earth and external forces, Eq. (2.1.15) is changed to

$$\frac{d\vec{v}}{dt}=\frac{\partial\vec{v}}{\partial t}+\nabla\cdot(\vec{v}\vec{v})=\vec{g}-\frac{1}{\rho}\nabla p+\nu\nabla^2\vec{v}-2\vec{\Omega}\times\vec{v}+\overrightarrow{F_{\text{fr}}} \tag{2.1.19}$$

where $\vec{\Omega}$ = angular velocity of the earth, $\overrightarrow{F_{\text{fr}}}$ = external forces, and $\nu=\frac{\mu}{\rho}=$ kinematic viscosity.

The angular velocity of the earth, $\vec{\Omega}$, is related to the Coriolis parameter, f, by the following:

$$f = 2\Omega \sin\varphi \tag{2.1.20}$$

where Ω = the magnitude of the earth angular velocity $\vec{\Omega}\,(= 7.292\times10^{-5}\ \mathrm{s}^{-1})$ and φ = the latitude.

Equation (2.1.19) is the Navier–Stokes equation, valid for incompressible Newtonian flows. The meanings of each term in Eq. (2.1.19) are

1. The acceleration term, $d\vec{v}/dt$, is composed of the local rate of change due to time variation $(\partial\vec{v}/\partial t)$, plus the rate of change due to advection of the flow $[\nabla\cdot(\vec{v}\vec{v})]$. This term is the acceleration, $\vec{a} = \vec{F}/m$, given in Eq. (2.1.14). The terms on the right-hand side of Eq. (2.1.19) are all the forces that cause this acceleration. One of the most important objectives in hydrodynamic studies is to find out how the currents change with time, which is specified by this term.
2. The gravitational force, $\vec{g}$, acts toward the center of the earth.
3. The pressure gradient term, $-1/\rho\nabla p$, represents the effects of spatial variation of water pressure. The pressure gradients cause water movement to occur. The two contributing factors to pressure gradients are water surface level slopes (the barotropic component) and changes in density (the baroclinic component).
4. The viscous term, $\nu\nabla^2\vec{v}$, includes the effects of water viscosity. This term can also be modified to represent turbulent mixing.
5. The Coriolis force term, $-2\vec{\Omega}\times\vec{v}$, represents the effect of earth rotation on water movement. It is significant only when large waterbodies are studied.
6. The external force term, $\overrightarrow{F_{\mathrm{fr}}}$, is often used to include wind forces.

There are no analytical solutions to the Navier–Stokes equation, Eq. (2.1.19). It is also too complex to be solved numerically for large domains over long periods of time. Further simplifications to the Navier–Stokes equation, Eq. (2.1.19), are needed in hydrodynamic models and will be described later in Section 2.2.1.

2.1.3 Advection and Dispersion

When a pollutant load is discharged into a waterbody, it is subject to fate and transport processes that modify the pollutant concentration. The principal factors determining the pollutant concentration are hydrodynamic transport and chemical/biological reactions.

Chemical/biological reactions play an important in a pollutant's fate in the environment. An equally important aspect is the hydrodynamic transport of

the pollutant. Hydrodynamic transport acts to move pollutants from the location at which they are generated, resulting in impacts that can be distant from the pollution source. On the other hand, some pollutants, such as wastewater discharges, can be degraded in the receiving waterbody, if they are sufficiently diluted. For these pollutants, slow ambient water velocity and weak mixing can result in excessively high pollutant concentrations and lead to increased adverse impacts on the environment.

Hydrodynamic transport includes the following processes: (1) advection, (2) dispersion, and (3) vertical mixing and convection. Material in water systems can be transported by one or all of these processes. Collectively, these three processes are referred to as hydrodynamic transport. Both horizontal and vertical transport should be considered since, for flow fields with a complex spatial topography, material transport is usually three dimensional.

Advection refers to horizontal transport by flows that move patches of material around, but do not significantly distort or dilute them. In rivers and estuaries, advection often represents the primary transport process of pollutant in the longitudinal direction. Lateral advection across a river is usually small. In a straight channel (Fig. 2.1.2), the velocity profile indicates that the maximum advection occurs in the middle of the channel and that the minimum advection occurs near the banks. The lateral velocity differences cause the flow at the center of the river moving faster than the flow near the banks. This lateral variation promotes dispersion across the river. In contrast to advection, convection refers to vertical transport of water and pollutants. Convection in rivers, lakes, and estuaries is usually very small. Vertical turbulent mixing and its mathematical description will be described in Section 2.2.3.

Dispersion is the horizontal spreading and mixing of water mass caused by turbulent mixing and molecular diffusion. Dispersion reduces the gradient of material concentration. This process involves not only an exchange of water mass, but also of any substance dissolved in it, such as salinity and dissolved pollutants. Hence, in addition to hydrodynamic variables, such as temperature and salinity, dispersion processes are also of importance to the distributions of sediment, toxics, and nutrients in waterbodies. Dispersion in the direction of water flow is called longitudinal dispersion. Dispersion perpendicular to the direction of flow is called lateral dispersion. Longitudinal dispersion is generally much stronger than lateral dispersion in rivers.

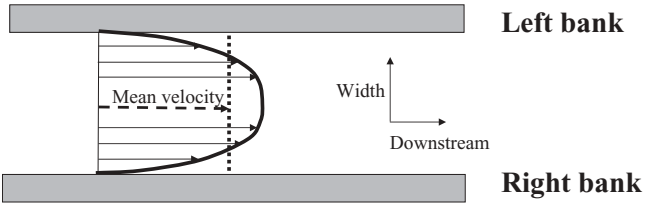

Fig. 2.1.2 Velocity profile in a channel.

Turbulent mixing is often the dominant component of dispersion in rivers, lakes, and estuaries and is much more rapid than molecular diffusion. Turbulent mixing is the result of the momentum exchange between water parcels in a turbulent flow. It spreads chemical or biological constituents in various directions depending on the flow characteristics. Diffusion is a transport process at the microscopic level, owing to the scattering of particles by random molecular motions. Diffusion is the movement of material from an area of high to an area of low concentration due to the concentration gradients. If a drop of colored dye is put into a bottle containing still water, the dye will spread in the water. Eventually, the bottle will contain uniformly colored water. The reason is that the dye tends to move from higher concentration to lower concentration, just as heat transfers from higher temperature to lower temperature. Molecular diffusion occurs much more slowly and so is important only on a very small scale, such as right at the bottom of a lake. Diffusion can be described by Fick's law and the classical diffusion equation.

Advection and dispersion are the major processes by which dissolved materials are transported along and distributed throughout a river or an estuary (Fig. 2.1.2). As water flows along the river, it transports dissolved materials with it via advection. It leads to a net transport of dissolved materials from areas of high concentration to areas of low concentration via dispersion. Hence, horizontal transport of a material consists of two components: (1) advective flux and (2) dispersive flux.

Both fluxes are defined as the mass of concentration crossing a unit area per unit time, with units of mass/(time length^2) (M/T/L^{-2}). The unit conventions are M for mass units, L for length units, and T for time units. The movement of pollutant mass due to advective flux is in the same direction as the fluid flow, while the dispersive flux moves mass from areas of high concentration to areas of low concentration. The advective flux density ($\overrightarrow{J_a}$) depends on concentration (C) and flow velocity ($\vec{v}$):

$$\overrightarrow{J_a} = C \cdot \vec{v} \tag{2.1.21}$$

About the dispersive flux, Fick's law states that the rate of mass movement resulting from molecular diffusion is inversely proportional to the gradient of mass concentration:

$$J = -D\frac{dC}{dx} \tag{2.1.22}$$

where J = the dispersive mass flux density (M/L^2/T), C = the concentration of mass in the water (M/L^3), D = diffusion coefficient (L^2/T), and x = the distance (L).

The negative sign indicates that the diffusing mass flows in the direction of decreasing concentration. Equation (2.1.22) states, in simple terms, that mass will naturally move from areas of high concentration to areas of low

concentration, and that the rate of that movement is greatest when the greatest change in concentration occurs over the shortest distance, that is, the greater the concentration gradient is, the greater the mass flux density will be.

Turbulent mixing results from the random scattering of particles by turbulent flow and can be considered roughly analogous to molecular diffusion. It is assumed that the dispersive flux also follows Fick's law, Eq. (2.1.22), only that the magnitude of the diffusion coefficient (D) is different. Dispersion by turbulent mixing typically results in much larger rates of diffusion and transport and often plays a dominant role in dispersive transport.

The total mass flux across a boundary can be calculated as:

$$\frac{dm}{dt} = (J_a + J)A \tag{2.1.23}$$

where m = mass, J_a = the magnitude of advective flux $\overline{J_a}$ $(\mathrm{M/L^2/T})$, and A = area of the boundary that perpendicular to the direction of the flow.

In most natural waterbodies, the advective flux (J_a) is larger than the dispersive flux (J). When the flow velocity is very small, the advection flux becomes small and can be neglected. The conservation of mass described by Eq. (2.1.10) can then be simplified as:

$$\frac{\partial C}{\partial t} = -\frac{\partial J}{\partial x} \tag{2.1.24}$$

Combining Eqs. (2.1.22) and (2.1.24) yields

$$\frac{\partial C}{\partial t} = D\frac{\partial^2 C}{\partial x^2} \tag{2.1.25}$$

This is the classical diffusion equation from Fick's law. Its solution needs one initial condition and two boundary conditions. Two simple solutions to Fick's law are described below.

Constant release. This case has the following:

$$\text{Initial condition: } C(x, 0) = 0 \tag{2.1.26a}$$

$$\text{Boundary Condition: } C(0, t) = C_0 \tag{2.1.26b}$$

$$C(\infty, t) = 0 \tag{2.1.26c}$$

This is the case that a source with constant concentration C_0 at $x = 0$ is added in a river, starting from $t = 0$. The solution to Fick's law under these conditions is

$$C(x, t) = C_0 \mathrm{erfc}\left[\frac{x}{2\sqrt{Dt}}\right] \tag{2.1.27}$$

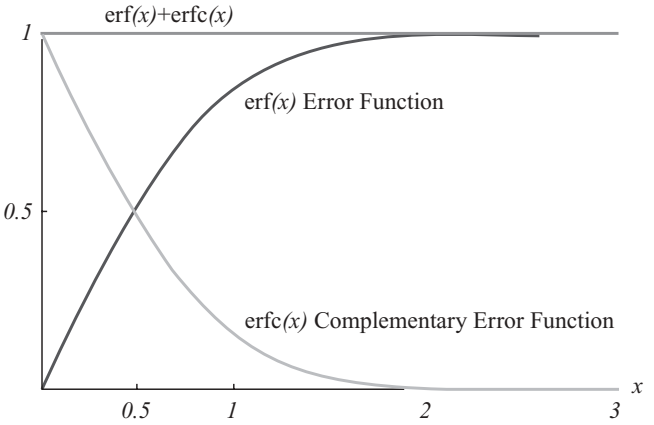

Fig. 2.1.3 Error function and complementary error function.

where the complementary error function, erfc(x), equals 1 minus the error function, erf(x). It has

$$\text{erfc}(x) = 1 - \text{erf}(x) = \frac{2}{\sqrt{\pi}} \int_x^\infty e^{-u^2} du \tag{2.1.28}$$

The complementary error function, erfc(x), has the following properties:

1. erfc(0) = 1
2. erfc(∞) = 0
3. erfc(r) is monotonically decreasing with x

Figure 2.1.3 gives the values of erf(x) and erfc(x).

Instantaneous release. If a slug is released into a river at $t = 0$ and $x = 0$, the initial condition and boundary conditions are

$$\text{Initial condition: } C(x, 0) = 0 \tag{2.1.29}$$

$$\text{Boundary condition : } \int C(x, t) dx = M \tag{2.1.30}$$

$$C(x, \infty) = 0 \tag{2.1.31}$$

where M is the mass initially deposited at $x = 0$. Equation (2.1.30) does not actually specify a boundary value, but requires that the total dye mass at any time t should be equal to the dye mass initially released at $t = 0$. In this case, the solution to (2.1.25) is

$$C(x, t) = \frac{M}{\sqrt{\pi D t}} e^{\left(-\frac{x^2}{4Dt}\right)} \tag{2.1.32}$$

Figure 2.1.4 expresses the solution (2.1.32) graphically.

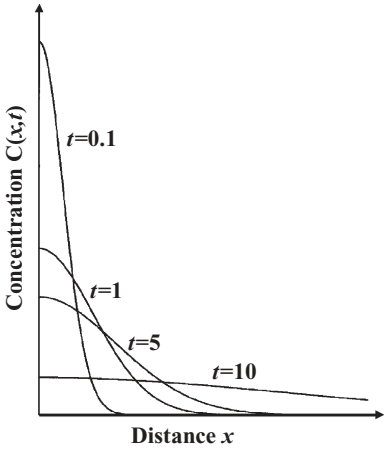

Fig. 2.1.4 Longitudinal distribution for contaminant deposited instantaneously at $x = 0$, according to Eq. (2.1.32).

2.1.4 Mass Balance Equation

Based on the principle of conservation of mass, the concentration change of a reactant can be calculated using mass balance equation (2.1.10), which is simply an accounting of mass inputs, outputs, reactions, and net change. Its 1D form can be simplified as (Ji, 2000a):

$$\frac{\partial C}{\partial t} = -U\frac{\partial C}{\partial x} + \frac{\partial}{\partial x}\left(D\frac{\partial C}{\partial x}\right) + S + R + Q \tag{2.1.33}$$

Net change of concentration | Advectiion | Dispersion | Settling | Reactivity | Load

where C = reactant concentration, t = time, x = distance, U = advection velocity in x direction, D = mixing and dispersion coefficient, S = sources and sinks due to settling and resuspension, R = reactivity of chemical and biological processes, and Q = external loadings to the aquatic system from point and nonpoint sources.

Equation (2.1.33) indicates that net changes of pollutants in water involve five main processes:

1. The advection term accounts for the mass inputs and outputs by water current and specifies the movement of the pollutant with waters as it flow downstream.

2. The dispersion term describes the spreading of the pollutant that occurs due to turbulent mixing and molecular diffusion.
3. The settling term represents the particle settling to and resuspension from the bed, which will be discussed in Chapter 3.
4. The reactivity term refers to chemical and/or biological processes that take place within the water column, which will be described in Chapters 4 and 5.
5. The load term indicates external sources, which will be presented in Chapter 6.

It is evident that the diffusion equation from the Fick's law, Eq. (2.1.25), is just a special case of the mass balance equation, when the terms of advection, settling, reactivity, and external load are neglected in Eq. (2.1.33). In addition to the two analytical solutions, Eqs. (2.1.27) and (2.1.32), another two solutions to the mass balance equations are given below.

Instantaneous release with mean flow. The case of instantaneous release without mean flow is already discussed with the diffusion equation and the solution is given by Eq. (2.1.32). For an instantaneous release with mean flow, Eq. (2.1.33) is

$$\frac{\partial C}{\partial t} = -U\frac{\partial C}{\partial x} + D\frac{\partial^2 C}{\partial x^2} \tag{2.1.34}$$

In the case of the instantaneous point source (slug injection) described by Eqs. (2.1.29)–(2.1.31), the solution to Eq. (2.1.34) is

$$C(x,t) = \frac{M}{B\sqrt{4\pi Dt}} e^{\left(-\frac{(x-Ut)^2}{4Dt}\right)} \tag{2.1.35}$$

where $C(x,t)$ = cross-sectional averaged tracer concentration, M = mass of tracer injected at $x = 0$ and $t = 0$, and B = cross-sectional area of the channel.

If the initial concentration is a Gaussian distribution:

$$C(x,0) = \frac{M}{\sqrt{2\pi}\sigma}\exp\left(-\frac{x^2}{2\sigma^2}\right) \tag{2.1.36}$$

where σ is the standard deviation of the Gaussian distribution, the solution to Eq. (2.1.34) is

$$C(x,t) = \frac{M}{\sqrt{2\pi(\sigma^2 + 2Dt)}}\exp\left(-\frac{(x-Ut)^2}{2(\sigma^2 + 2Dt)}\right) \tag{2.1.37}$$

Figure 2.1.5 shows the downstream travel of the dye concentrations at different times. In field studies, Eq. (2.1.37) can be helpful in estimating the values

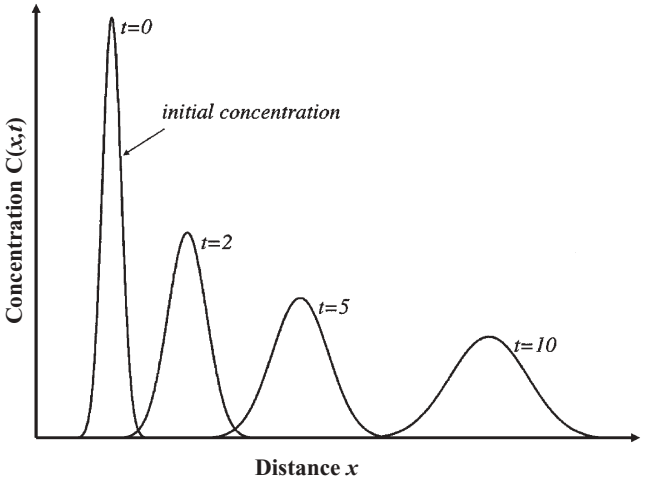

Fig. 2.1.5 Spreading of contaminant in time and space in a steady uniform flow.

of the dispersion coefficient (D) in a river. Equation (2.1.37) can also be valuable in evaluating the accuracy of a numerical model in a simple channel test.

2.1.5 Atmospheric Forcings

The description of a surface water system is usually premised on the identification and understanding of external forcings to the system. Surface waters are subjected to forcings over a broad range of periods, ranging from hourly to seasonal variations. Major external forcings to surface waters include (1) atmospheric forcings, (2) point and nonpoint sources, and (3) forcings from open boundaries.

Atmospheric forcings will be discussed in this section. Point and nonpoint sources will be described in Section 6.1. Forcings from the open boundary will be presented in Section 10.5, where estuarine and coastal modeling is discussed.

Major atmospheric forcings include (1) wind, (2) air temperature, (3) solar radiation, and (4) precipitation. Besides, the atmospheric humidity, cloud cover, and atmospheric pressure can also affect a surface water system via evaporation and heatflux transfer on the air–water interface. As an example, Fig. 2.1.6 gives the photo of Station LZ40 in Lake Okeechobee, Florida. The data measured at LZ40 are frequently used in the Lake Okeechobee modeling and the modeling results are discussed extensively in this book.

Wind is usually a major source of energy in large lakes, coastal waters, and some estuaries. The wind exerts a drag on the water surface and pulls floating objects in the wind direction. The Coriolis force can deflect the movement of the floating objects. Wind driven currents are a major mechanism in the

Fig. 2.1.6 Sampling station LZ40 in Lake Okeechobee, FL. Its location in the lake is shown in Fig. 2.4.2. The data measured at LZ40 are used extensively in this book. (Photo taken by Zhen-Gang Ji.)

transport and distribution of floating pollutants, such as spilled oil. If the distance over which the wind blows and the wind duration are sufficient, wind driven surface currents can approach a velocity equal to 2–4% of the wind speed. But, given the lengths of open water found in most rivers, lakes, and estuaries, it is likely that the resulting current velocity will be less than this magnitude. For example, currents in a narrow estuary may be predominantly tidal and the wind has minimum impact on the flow in a long run. On the other hand, if the estuary is wide, wind stresses can generate currents of considerable importance. The wind may modify the circulation and become a major force on occasions, but the wind cannot be responsible for the mean circulation over extended periods of time.

Winds vary on a variety of time scales, including diurnal variations (sea–land breeze), the time scale of weather systems (a few days), and the seasonal

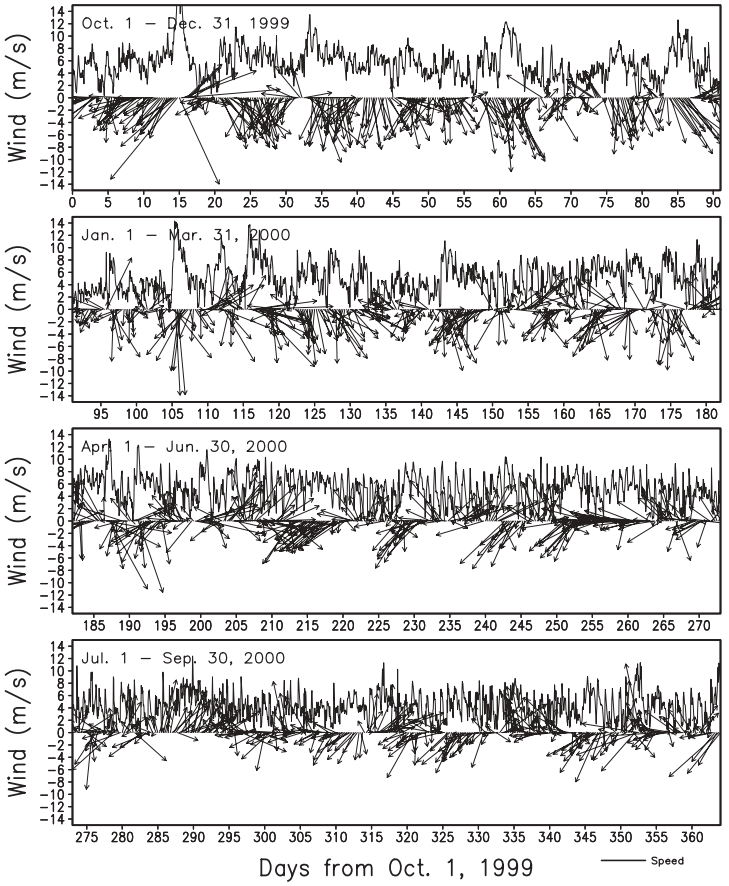

Fig. 2.1.7 Measured wind at Station LZ40 in Lake Okeechobee, FL.

change in prevailing winds. The sea–land breeze is a phenomenon caused by the different heat capacities between land and large waterbodies (e.g., oceans and large lakes). Surface water can respond to an applied wind stress within a few hours and to the cessation of the wind in about the same time frame. Wind forcings can generate waves and storm surges. Seasonal weather patterns in a particular area can generate persistent circulation patterns in a particular water system.

For example, wind is the dominant force in driving the circulation and in generating turbulent mixing in Lake Okeechobee, FL. Because of the wind forcing, the lake circulations are typically dominated by a two-gyre pattern, especially in the winter (Ji and Jin, 2006). The wind driven circulation has a time scale of a few days, the same as the period of local weather systems. Figure 2.1.7 gives the measured wind in the lake between 10/1/1999 and 9/30/2000. It shows that wind patterns in the summer and in the winter are quite different,

causing different effects on Lake Okeechobee. Early summer winds generally are caused by differential heating of land and water, exhibiting a diurnal pattern. Winter winds are associated with cold fronts passing through the area and are much stronger and more persistent than summer winds. These winds constantly mix the water columns.

Strong winds may also cause storm surge in surface waters. Storm surge is simply the phenomenon that water is pushed toward the shore by the winds. Strom surges can cause large water level fluctuation, which can have devastating effects on low-lying coastal regions. Both local and remote winds can play a large role in storm surges in coastal regions. For large lakes, such Lake Okeechobee, storm surges are also a significant threat to the local areas (SFWMD, 2002). Strong storms cause large flows and increased transports and mixing in surface water systems. For example, Jin and Ji (2004) reported that although the typical mean flow in Lake Okeechobee is <5 cm/s, episodic storm currents can >30 cm/s and last for several days.

Air temperature affects surface waters via heatflux and evaporation exchange between the air and the water. The temperature differences between the air and the water strongly influence the exchange of heatflux and moisture between the two. Figure 2.1.8 is the measured air temperature in Lake Okeechobee between 10/1/1999 and 9/30/2000, the same period as the one shown in Fig. 2.1.7. The wind velocity in Fig. 2.1.7 and the air temperature in Fig. 2.1.8 are frequently mentioned in the case studies on the modeling of Lake Okeechobee. In addition to diurnal changes, the air temperature has strong seasonal variations. Figure 2.1.8 indicates that the air temperatures in the lake area can be >30 °C in the summer and a few degrees centigrade in the winter, but never <0.

Solar radiation is often the most important heatflux component that acts as a heat source to a waterbody. Detailed discussions on solar radiation, heatfluxes, and evaporation will be presented in Section 2.3, where thermal processes are described. Precipitation is usually treated as an input of freshwater to a waterbody. For large subtropical lakes like Lake Okeechobee, the direct rainfall to the lake surface is one of the major water sources. For water systems with relatively small surface water areas, such as rivers, the direct precipitation can be insignificant, comparing to inflows from tributaries and runoffs.

For coastal waters, atmospheric pressure affects sea level through the "inverse barometer effect" that low atmospheric pressure causes the sea level to be higher than normal (~1 cm/millibar). This effect, coinciding with storm surge, wind waves, and tides, can cause severe flooding in coastal areas. For most rivers, lakes, and estuaries, however, the hydrodynamic impacts of atmospheric pressure changes are usually small.

Wind stress is the tangential force per unit area due to the horizontal movement of the wind over the water surface. It is determined by the wind speed and direction, and factors transforming the wind speed into wind stress. The latter is usually described by a drag coefficient and is estimated using several

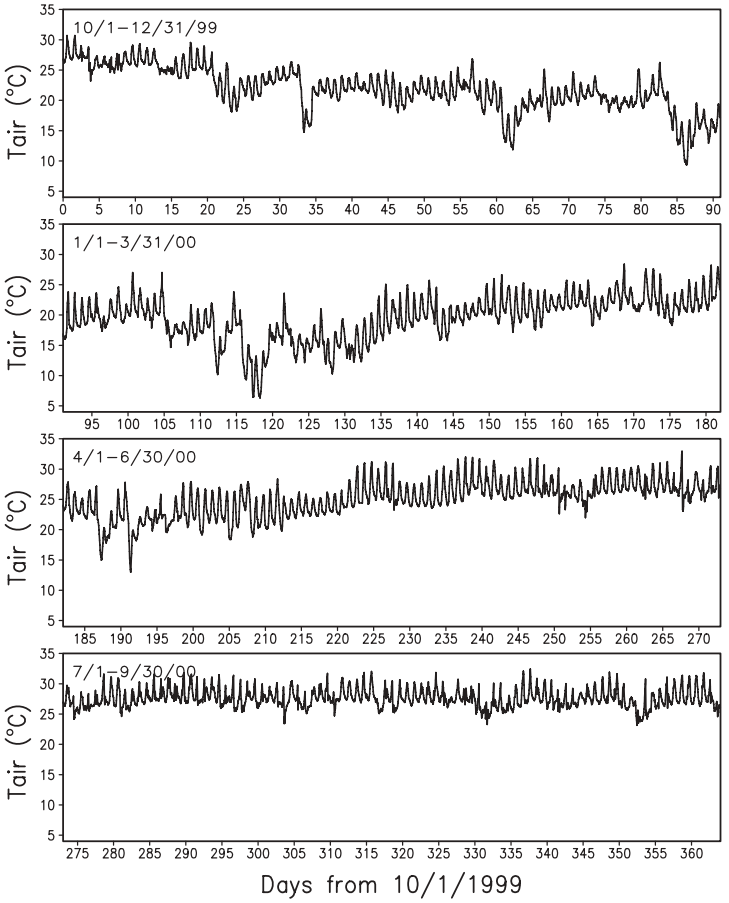

Fig. 2.1.8 Measured air temperature at LZ40 in Lake Okeechobee, FL.

water and air parameters. The wind speed is the dominant parameter determining wind stress:

$$\tau = C_D \rho_A U^2 \tag{2.1.38}$$

where U = the wind speed at 10 m above the water surface (m/s), ρ_A = the density of the air (kg/m^3), C_D = the wind stress coefficient, dimensionless, and τ = wind stress (N/m^2).

The density of air varies with temperature, pressure, and humidity, with typical values being 1.2–1.3 kg/m^3. The wind stress coefficient, C_D, generally increases with wind speed. Hick (1972) found that C_D is equal to 1.0×10^{-3} for wind speed up to 5 m/s and increases linearly to 1.5×10^{-3} for wind speed of 15 m/s. For wind speed between 6 and 22 m/s, Smith (1980) suggested

$$C_D = (0.61 + 0.063 \cdot U) \times 10^{-3} \tag{2.1.39}$$

Hamrick (1992) used the following formulas for calculating wind stress in hydrodynamic models:

$$\tau_x = 1.2 \times 10^{-6}(0.8 + 0.065U) \cdot U \cdot u \tag{2.1.40}$$

$$\tau_y = 1.2 \times 10^{-6}(0.8 + 0.065U) \cdot U \cdot v \tag{2.1.41}$$

where τ_x = wind stress in x direction (N/m^2), τ_y = wind stress in y direction (N/m^2), u = wind speed in x direction (m/s), and v = wind speed in y direction (m/s).

For shallow waterbodies (less than a few meters), the longer water waves will not be able to develop fully and the water surface will remain smoother. Hicks et al. (1974) showed that under such conditions, C_D remains close to 1.0 $\times 10^{-3}$ for all wind speeds. Fischer et al. (1979) reported that the stability of the air column also has a strong influence on the value of C_D. Warm winds blowing over a cold waterbody are stabilized by the temperature difference, which in turn results in less friction. The value of C_D can be reduced by as much as 40% for stable conditions and increased equally by up to 40% for very unstable air flows. Lake Okeechobee is a large lake with mean depth ~3 m. The long waves in this shallow lake can not fully develop and the lake should have relatively smoother surface. AEE (2005) used the following wind stress formulas for the lake modeling:

$$\tau_x = 1.2 \times 10^{-6}(0.8 + 0.065U) \cdot \alpha \cdot U \cdot u \tag{2.1.42}$$

$$\tau_y = 1.2 \times 10^{-6}(0.8 + 0.065U) \cdot \alpha \cdot U \cdot v \tag{2.1.43}$$

where α is an empirical coefficient for including the shallow water effects reported by Fisher et al. (1979) and Hicks et al. (1974). AEE (2005) reported that by setting α to 0.8, the modeled currents are consistent with the measured data well. It should be mentioned that Eqs. (2.1.39)–(2.1.43) are all empirical formulas, there are other formulas (e.g., Mellor, 1998; Sheng, 1986) that are similar to but slightly different from the ones presented here.

2.1.6 Coriolis Force and Geostrophic Flow

The Coriolis force term in Eq. (2.1.19), $-2\vec{\Omega} \times \vec{v}$, represents the effects of earth rotation. It was first described by the nineteenth century French engineer–mathematician Gustave–Gaspard Coriolis in 1835. Coriolis force is significant only when the spatial scale of the study area is very large, such as the Great Lakes and the Chesapeake Bay. Jin et al. (2002) reported that Coriolis force can be significant to circulations in Lake Okeechobee, a subtropical lake with spatial scale of 50 km. In hydrodynamic studies, the Coriolis parameter, $f = 2\Omega \sin\varphi$, can be treated as a constant and its variation with latitude (φ) is often insignificant.

The Coriolis force: (1) becomes evident in large waterbodies due to Earth rotation; (2) deflects motion to the right (left) in the Northern (Southern) Hemisphere; (3) allows geostrophic flow; and (4) leads to inertial oscillations. Owing to the Coriolis force, moving objects are deflected a few degrees to the right in the Northern Hemisphere and to the left in the Southern Hemisphere. In estuaries wide enough to be affected by this force, the effect is to deflect the seaward flow (freshwater flow) to the right side (looking toward the sea) of the estuary and to deflect landward flow (seawater flow) to the left. If the effect is strong, the net flow averaged over time can produce a secondary circulation, with a persistent seaward flow of freshwater along the right bank and a landward flow of seawater along the left bank.

When frictional forces are neglected, the steady-state flow is determined by the balance between the pressure gradient force and the Coriolis force. Equation (2.1.19) can be simplified to

$$2\vec{\Omega}\times\vec{v} = -\frac{1}{\rho}\nabla p \tag{2.1.44}$$

Under Cartesian coordinates, it has

$$-fv = -\frac{1}{\rho}\frac{\partial p}{\partial x} \tag{2.1.45}$$

$$fu = -\frac{1}{\rho}\frac{\partial p}{\partial y} \tag{2.1.46}$$

This balance is known as geostrophic flow. As shown in Fig. 2.1.9, particles in the geostrophic flow move along the lines of constant pressure, with high pressure on their right (left) in the Northern (Southern) Hemisphere (looking in the direction of the flow). The geostrophic flow can be computed from these

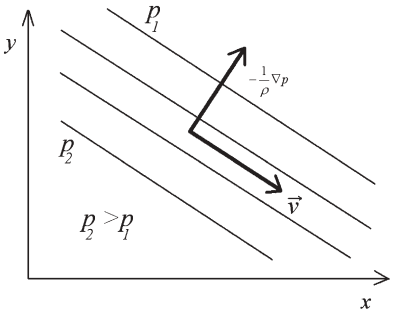

Fig. 2.1.9 Pressure gradient and geostrophic flow.

equations using the pressure gradient obtained by integrating the hydrostatic equation,

$$\rho g = -\frac{\partial p}{\partial z} \tag{2.1.47}$$

which in turn uses density calculated from temperature and salinity.

Equation (2.1.19) can also be simplified to describe inertial oscillations:

$$\frac{\partial u}{\partial t} - fv = 0 \tag{2.1.48}$$

$$\frac{\partial v}{\partial t} + fu = 0 \tag{2.1.49}$$

These momentum equations have the following solution:

$$u = A \sin ft \tag{2.1.50}$$

$$v = A \cos ft \tag{2.1.51}$$

Equations (2.1.50) and (2.1.51) indicate that the inertial oscillations with amplitude A have the current vector rotating clockwise with the inertial period of

$$T_f = \frac{2\pi}{f} \tag{2.1.52}$$

The inertial period T_f is frequently dominating in current observations in the interior of large basins. T_f is equal to 18.61h at 40 °N.

The importance of the Coriolis force can be estimated using a dimensionless Kelvin number, K, which is defined as the ratio of the domain size to the Rossby radius:

$$K = \frac{B}{R_0} \tag{2.1.53}$$

where the Rossby radius is given by

$$R_0 = \frac{C_0}{f} = \frac{\sqrt{gH}}{f} \tag{2.1.54}$$

In Eqs. (2.1.53) and (2.1.54), B is the domain size, f is the Coriolis parameter, R_0 is the external Rossby radius, $C_0 (= \sqrt{gH})$ is the phase speed of external gravity wave, and H is an average depth. For lakes and estuaries with K around (or >) 1.0, the earth's rotation becomes important and the effects of Coriolis

force should be considered. The opposite is also true: the Coriolis force can be neglected when K is much less than 1.0. Lake Okeechobee has $B = 50\,\text{km}$, $H = 3.2\,\text{m}$, $\varphi = 27\,^{\circ}\text{N}$, which yields $K = 0.6$. Therefore, the Coriolis force can be significant to the lake circulations. The geostrophic flow in Lake Okeechobee will be discussed in Section 2.4.2, where the hydrodynamic modeling of the lake is presented as a case study.

The internal structure of a deep lake or estuary can be more responsive to the Coriolis force, because it is controlled by motions with smaller phase speeds. In this case, the Rossby radius is calculated using a reduced gravity:

$$R_0 = \frac{C_i}{f} \tag{2.1.55}$$

where C_i is the phase speed of the first baroclinic wave produced as a result of the density difference. A rough estimate for C_i is 1–2 m/s corresponding to a water depth of 20 m and a density difference of 5–20 kg/m^3. For a mid-latitude estuary with f of $10^{-4}\,\text{s}^{-1}$, the Rossby radius is equal to 10–20 km.

2.2 GOVERNING EQUATIONS

This section describes the governing equations in hydrodynamic models. After introducing the commonly used assumptions in hydrodynamic modeling, the governing equations in 1D, 2D, and 3D are presented. Initial and boundary conditions for the governing equations are also discussed in this section.

2.2.1 Basic Approximations

As discussed previously in this chapter, conservation of momentum, mass, and energy provides the fundamental principles needed to develop hydrodynamic models. Even with advanced computers, these conservation equations are too complex to be solved numerically for large domains over long periods of time. Therefore, further simplifications are needed. This section discusses the approximations that are widely used in the studies of surface water systems: (1) Boussinesq approximation, (2) hydrostatic approximation, and (3) Quasi-3D approximation. These approximations are commonly used in the development and application of hydrodynamic models. It is essential to keep these approximations in mind when applying models to solve practical problems.

A widely used approximation in the studies of river, lakes, estuaries, and coastal waters is the so-called shallow water approximation. The shallow water (or long wave) approximation assumes that horizontal scales of interest are much larger than the depth of the water. When the water depth is much smaller than the wave length, it has.

$$H \ll \frac{1}{k} = \frac{L}{2\pi} \tag{2.2.1}$$

where H = water depth, k = wave number, and L = wave length. Under the shallow water approximation, the surface gravity wave speed, c, only depends on water depth and has the form of

$$c = \sqrt{gH} \tag{2.2.2}$$

In this case, the wave is nondispersive and the wave speed does not depend on wave number ($k = 2\pi/L$). Similarly, the sallow water approximation in hydrodynamics states that the horizontal scale of motion, L, is much larger than the vertical scale of motion, H, that is,

$$\frac{H}{L} \ll 1 \tag{2.2.3}$$

This approximation is justified for most hydrodynamic processes in rivers, lakes, estuaries, and coastal waters, except for studies, such as jet plume modeling. The sallow water approximation is often assumed to be valid when $H/L \leq 0.05$. The Boussinesq approximation, the hydrostatic approximation, and the quasi-3D approximation represent different aspects of a shallow water system.

2.2.1.1 Boussinesq Approximation. A good approximation in describing surface water systems is to assume that the flows are incompressible, which means that the water density does not change with water pressure. Boussinesq approximation is used to represent buoyancy in an incompressible fluid, in which the density is not related to water pressure. In the Boussinesq approximation, variations in water density are ignored, except when the gravitational force and buoyancy are considered.

The Boussinesq approximation is justified for most surface waters on the basis of small variations in density within the waterbodies. Typically, the density varies less than a few percent in a water column. The Boussinesq approximation does not depend on the shallow water approximation. Density changes due to local pressure gradients in the horizontal momentum equations are negligible. The water is treated as incompressible. The Boussinesq approximation excludes sound and shock waves in surface waters.

2.2.1.2 Hydrostatic Approximation. Many surface waters exhibit a common feature: Their ratio of horizontal scale to water depth is very large (shallow water approximation). This leads to a widely used approximation in hydrodynamics, meteorology, and oceanography: the hydrostatic approximation. The hydrostatic approximation assumes that the vertical pressure gradient is almost balanced by the forcing due to buoyancy excess. The vertical acceleration then is a much smaller term and can be omitted.

From Eq. (2.1.19), a vertical momentum equation is typically written as:

$$\frac{dw}{dt} + g + \frac{1}{\rho}\frac{\partial p}{\partial z} = 0 \tag{2.2.4}$$

where w = vertical velocity, g = gravitational acceleration, ρ = density, p = water pressure, t = time, and z = vertical coordinate.

The hydrostatic approximation omits the term $\frac{dw}{dt}$ and leads to the hydrostatic equation:

$$\frac{1}{\rho}\frac{\partial p}{\partial z} = -g \tag{2.2.5}$$

The hydrostatic equation relates the vertical pressure gradient to the vertical distribution of density. Most of the 2D (vertical plane) and 3D hydrodynamic models use this approximation (e.g., Blumberg and Mellor, 1987; Hamrick, 1992). In these models, the vertical momentum equation is reduced to the hydrostatic equation (2.2.5).

The hydrostatic approximation implies that vertical pressure gradients are due only to density. When horizontal scales are much greater than vertical scales, the hydrostatic approximation is justified and in fact, is identical to the shallow water approximation for continuously stratified waters. Given that the horizontal scale of natural waterbodies, such as river, lakes, and estuaries, is so much greater than their depth, this is generally a valid approximation. However, when the vertical scale of motion approaches to the horizontal scale, the hydrostatic approximation becomes no longer valid. At these scales, the pressure at some point in the waterbody is also a function of the water velocity. For example, convective plumes from wastewater discharge diffusers are non-hydrostatic motions (Blumberg et al., 1996).

2.2.1.3 Quasi-3D Approximation. An alternative to deriving a fully 3D model is to treat the system as a set of horizontal layers that interact via source–sink terms representing water exchanges with overlying and underlying layers. This approach allows for eliminating the momentum equation in the vertical direction. For most surface water applications, the quasi-3D approximation ensures computational efficiency and model accuracy.

Most 3D hydrodynamic models used in rivers, lakes, and estuaries are actually quasi-3D models (e.g., Blumberg and Mellor, 1987; Hamrick, 1992). By using the hydrostatic approximation, the models have momentum equations only in the horizontal direction; and the vertical momentum equation is simplified to the hydrostatic equation, Eq. (2.2.5). This often prevents the application of these models to near field problems, where a high degree of turbulence occurs. For example, a model that does not include vertical momentum equation cannot resolve momentum transfer due to a submerged jet. Except when jet plumes are simulated, the quasi-3D approximation is frequently used in hydrodynamic studies with sufficient computational accuracy. In most 2D laterally averaged models (e.g., Cole and Wells, 2000), a similar approach is also used so that the vertical momentum equation is not computed.

2.2.2 Equations in Cartesian Coordinates

Based on the Navier–Stokes equation presented in Section 2.1, the governing equations under the Cartesian coordinates in 1D and 2D are described. After the sigma coordinate is introduced, this subsection also gives the 3D governing equations with the Cartesian coordinates in the horizontal and the sigma coordinate in the vertical.

Natural waterbodies are all three dimensional. The hydrodynamic and water quality variables in these systems have spatial variations over length, width, and depth. There are instances in which a simplification in the governing equations is permissible. The relevant equations can then be reduced from 3D to 2D or even 1D. Justifiable reductions in dimensionality result in savings in model development, simulation, and analysis costs. A numerical model developed for a waterbody should only include the dimension(s) in which spatial variations affect the water quality analysis significantly.

A numerical model can be

1. Zero-dimensional (0D).
2. One-dimensional (1D).
3. Two-dimensional (2D).
4. Three-dimensional (3D).

Zero-dimensional models assume a well-mixed waterbody and do not have spatial variations. A small lake or pond that is completely mixed in all directions is a good example. Zero-dimensional models calculate water quality variables based on the conservation of mass. They may be used in preliminary estimations of water quality conditions in lakes.

One-dimensional models simulate the spatial change over a single dimension, typically oriented longitudinally down the length of a river or a narrow estuary. A 1D model in the vertical may also be applicable to a small, but well-stratified lake. Two-dimensional models consider spatial variations in the lateral and longitudinal directions (in horizontal plane) or in vertical and longitudinal directions (in vertical plane). Three-dimensional models describe changes that occur over all three spatial dimensions and provide the most detailed assessment of pollutant distributions.

A 3D model should be easily applied to 1D or 2D studies by using only 1D or 2D model grid with little changes to the 3D model. For example, with a single layer in the vertical dimension, a 3D model can be reduced to a 2D model and can be applied to shallow, well-mixed waterbodies (e.g., Ji et al., 2001). Again, with a single cell in the lateral direction, the 3D model can be further reduced to a 1D model and can then be applied to shallow and narrow rivers (e.g., Ji et al., 2002a).

Eliminating a dimension in a numerical model implies neglecting spatial variation in that dimension. For example, use of a 1D model in the longitudinal direction implies small deviations in concentrations from the cross-sectional

mean, both laterally and vertically. The transport behavior of the river (or estuary) studied and the objectives of the study are the two major factors determining the dimensionality of the model needed.

2.2.2.1 1D Equations. The 1D model is defined with one space coordinate, that is, model state variables are averaged over the other two directions. Use of 1D model implies that the variation in directions perpendicular to the main channel is either neglected or not computed. It assumes well-mixed properties in the vertical, zero velocity across the main channel, and so on. These models describe flow and water quality concentrations in the direction of flow. One-dimensional models are often well suited to river flow problems, but are less suited to lake–estuarine problems. The most likely application is for run-of-the-river. This kind of free-flowing rivers is shallow and has high velocity, characterized by steep hydraulic profiles. They may have low-head dams or locks along the river. The Blackstone River, MA is a typical one and will be described in Chapters 3 and 4 as case studies (Ji et al., 2002a).

After neglecting the Coriolis force, the 1D continuity equation and momentum equation can be derived as:

$$\frac{\partial H}{\partial t} + \frac{\partial (Hu)}{\partial x} = Q_H \tag{2.2.6}$$

$$\frac{\partial (Hu)}{\partial t} + \frac{\partial (Huu)}{\partial x} = -gH\frac{\partial \eta}{\partial x} - C_B|u|u + \frac{\partial}{\partial x}\left(HA_H\frac{\partial u}{\partial x}\right) + \tau_x \tag{2.2.7}$$

where $H = h + \eta$ = total water depth, h = the equilibrium water depth, η = surface displacement from the equilibrium, u = water velocity in the x direction, $|u|$ = water speed, and Q_H = water inflow/outflow from the external sources, C_B = bottom drag coefficient, A_H = horizontal eddy viscosity, g = gravity acceleration, and τ_x = wind stress in the x direction.

In Eq. (2.2.7), the first term represents the time rate of change of horizontal momentum and the second is the horizontal advection of momentum in x direction. The first term on the right-hand side (RHS) of Eq. (2.2.7) is the force due to the horizontal pressure gradient. The second term on the RHS is the force due to bottom friction, and the third term on the RHS is the horizontal dispersion of momentum in the x direction. The last term on the RHS is the wind forcing, which is already discussed in Section 2.1.5.

In hydrodynamic models, the subgrid scale influence of turbulent mixing is parameterized using horizontal and vertical eddy diffusivity coefficients. The horizontal eddy viscosity represents the internal shear forces created by the transfer of momentum between faster and slower regions of flow by means of turbulent mixing. Its value cannot be directly measured nor observed. It affects velocity distributions and should be calibrated based on measured velocity data. In general, the higher its value, the more uniform the velocity distribution.

The horizontal eddy viscosity is not only related to the turbulence in the flow, but also influenced by the way that Eq. (2.1.19) or (2.2.7) is solved. Greater numerical dispersion results in lower horizontal eddy viscosity needed in a numerical model, when Eq. (2.1.19) or (2.2.7) is solved using a coarser grid or averaged over longer time periods. The horizontal eddy viscosity, A_H, can be calculated using the Smagorinsky subgrid scale scheme (Smagorinsky, 1963), which can be generally written in 2D Cartesian coordinates as:

$$A_H = C\Delta x\Delta y\left[\left(\frac{\partial u}{\partial x}\right)^2 + \left(\frac{\partial v}{\partial y}\right)^2 + \frac{1}{2}\left(\frac{\partial u}{\partial y} + \frac{\partial v}{\partial x}\right)^2\right]^{1/2} \tag{2.2.8}$$

where C = horizontal mixing constant, Δx = model grid size in x direction, and Δy = model grid size in y direction.

The parameter C has typical values between 0.10 and 0.20. The Smagorinsky formula links numerical models' horizontal mixing to current shear and model grid size. The parameter A_H is small if velocity gradients are small. If the horizontal spatial resolution (Δx and Δy) is sufficiently fine so that major features of the bottom topography and the horizontal advection can be resolved in the model, the horizontal eddy viscosity, A_H, will be very small. Accordingly, the horizontal dispersion transport associated with A_H will be very small and can be neglected. For coarse spatial resolution, horizontal diffusion should be retained to represent the unresolved advective mixing and transport processes. Horizontal diffusion in a numerical model is also closely related to the numerical scheme used. Both the flow condition and the numerical scheme affect horizontal dispersion in a numerical model.

Friction accounts for the dissipation of energy by small-scale turbulent motion. Friction forces retard or change the direction of water flow. Friction terms are included in momentum equations to parameterize the turbulent transfer of momentum within the water column or between the water and the boundaries, such as between the atmosphere and the water [the wind stress τ_x term in Eq. (2.2.7)] or between the water and the bottom (the term of $-C_B|u|u$). In Eq. (2.2.7), the bottom drag coefficient, C_B, can be a spatial varying parameter. It represents the effects of bottom roughness on energy losses in flowing water. In addition to C_B, Manning's coefficient is another commonly used parameter to represent bottom friction. The two can be linked together with the following formula (Johnson et al., 1991):

$$C_B = \frac{gn^2}{H^{7/3}} \tag{2.2.9}$$

where n = Manning's coefficient.

The 1D mass transport equation of a material concentration is

$$\frac{\partial(HC)}{\partial t} + \frac{\partial(uHC)}{\partial x} = \frac{\partial}{\partial x}\left(HA_C\frac{\partial C}{\partial x}\right) + S + R + Q_C \tag{2.2.10}$$

where C = concentration of a vertically and laterally averaged constituent, A_C = horizontal eddy diffusivity for mass transport, which is often set to equal to A_H, S = sources or sinks due to settling and resuspension, R = reactivity of chemical and biological processes, and Q_C = external loadings to the system from point and nonpoint sources.

2.2.2.2 2D Vertically Averaged Equations. Two-dimensional models are defined along two spatial coordinates and the model state variables are averaged over the third remaining spatial coordinate. They can be either 2D vertically averaged or 2D laterally averaged. The 2D vertically averaged equations are presented here. The 2D laterally averaged equations are described next.

In shallow waterbodies, such as broad and well-mixed lakes and estuaries, a weak vertical stratification allows a strong coupling of surface wind stresses and bottom friction stresses. The vigorous mixing minimizes vertical gradients in the water column. The physical transport is dominated by essentially depth-uniform horizontal advection. These conditions allow the general 3D equations to be approximated by 2D, vertically integrated equations and eliminate all vertical structure (e.g., Hayter et al., 1998). Shallow and broad lakes, lagoons, and bays may be well represented with 2D vertically averaged models. Morro Bay, CA is a good example of vertically mixed waterbody (Ji et al., 2001). Its simulation will be presented later in Section 10.5.2 as a case study.

The 2D vertically averaged conservation of mass and momentum equations can be expressed as:

$$\frac{\partial H}{\partial t}+\frac{\partial (uH)}{\partial x}+\frac{\partial (vH)}{\partial y}=Q_H \tag{2.2.11}$$

$$\frac{\partial (uH)}{\partial t}+\frac{\partial (u^2H)}{\partial x}+\frac{\partial (uvH)}{\partial y}-fHv=-gH\frac{\partial \eta}{\partial x}-C_B|u|u+\frac{\partial}{\partial x}\left(HA_H\frac{\partial u}{\partial x}\right)+\frac{\partial}{\partial y}\left(HA_H\frac{\partial u}{\partial y}\right)+\tau_x \tag{2.2.12}$$

$$\frac{\partial (vH)}{\partial t}+\frac{\partial (uvH)}{\partial x}+\frac{\partial (v^2H)}{\partial y}+fHu=-gH\frac{\partial \eta}{\partial y}-C_B|u|v+\frac{\partial}{\partial x}\left(HA_H\frac{\partial v}{\partial x}\right)+\frac{\partial}{\partial y}\left(HA_H\frac{\partial v}{\partial y}\right)+\tau_y \tag{2.2.13}$$

where v = velocity in the y direction, $|u|=\sqrt{u^2+v^2}$ = water speed, and τ_y = wind stress in the y direction.

In Eq. (2.2.12), the first term represents the time rate of change of horizontal momentum, and the second and third terms are the horizontal advection of momentum in x and y directions, respectively. The fourth term represents the Coriolis force. The first term on the RHS of Eq. (2.2.12) is the force

imposed by the horizontal pressure gradient. The second term on the RHS is the force due to bottom friction, and the third and fourth terms on the RHS are the horizontal dispersion of momentum in x and y directions, respectively. The last term on the RHS is the wind forcing and its formulas are presented in Section 2.1.5. The terms in Eq. (2.2.13) have meanings similar to the ones in Eq. (2.2.12). The Smagorinsky formula, Eq. (2.2.8), can be used to calculate the horizontal eddy viscosity, A_H.

The mass transport equation is

$$\frac{\partial(HC)}{\partial t}+\frac{\partial(uHC)}{\partial x}+\frac{\partial(vHC)}{\partial y}=\frac{\partial}{\partial x}\left(HA_C\frac{\partial C}{\partial x}\right)+\frac{\partial}{\partial y}\left(HA_C\frac{\partial C}{\partial y}\right)+S+R+Q_C \tag{2.2.14}$$

where C = concentration of a vertically averaged constituent.

The vertical integrated models are relatively straightforward to program and can produce physically interesting results with only modest computational demands. Their major deficiencies are the absence of any vertical structure and the need for a simplistic parameterization of the bottom stress. Besides, in many 2D studies on rivers, the models usually have fixed river width at any particular river section and disallow river width changing with flow rates. Therefore, the flow is confined within the bounds of the 2D numerical grid, and the riverbanks are considered to be solid vertical walls. To realistically simulate this kind of riverbank flooding events, the model should have the so-called wetting and drying capability (e.g., Ji et al., 2001).

2.2.2.3 2D Laterally Averaged Equations. The other type of 2D models is the laterally averaged model. In narrow and deep lakes, reservoirs, and estuaries (especially fjords), the effects of narrow width may result in near uniform distributions of hydrodynamic and water quality variables in the lateral direction. The primary transport in these systems is longitudinal advection and vertical mixing. These systems may be represented well with a 2D laterally averaged model.

As shown in Fig. 2.2.1, the x coordinate represents the horizontal variation and the z coordinate represents the vertical variation. The bathymetry slope shown in the left plot of Fig. 2.2.1 is approximately represented by "stairs" in the Cartesian (x, z) coordinates in the right plot. By neglecting the Coriolis force, the laterally averaged momentum equation can be derived from the Navier–Stokes equation:

$$\frac{\partial\eta}{\partial t}+\frac{\partial(uB)}{\partial x}+\frac{\partial(wB)}{\partial z}=Q_H \tag{2.2.15}$$

$$\frac{\partial(uB)}{\partial t}+\frac{\partial(u^2B)}{\partial x}+\frac{\partial(uwB)}{\partial z}=-\frac{1}{\rho}\frac{\partial Bp}{\partial x}+\frac{\partial}{\partial x}\left(BA_H\frac{\partial u}{\partial x}\right)+\frac{\partial}{\partial z}\left(BA_v\frac{\partial u}{\partial z}\right)+\tau_x \tag{2.2.16}$$

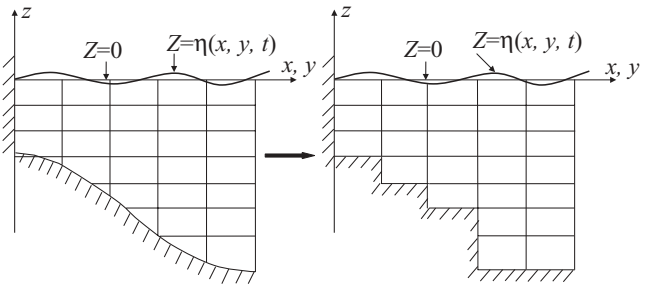

Fig. 2.2.1 The x–z coordinates.

where B = water width, z = vertical Cartesian coordinate, w = vertical velocity, p = water pressure, and A_v = vertical turbulent momentum mixing coefficient.

In Eq. (2.2.16), the first term represents the time rate of change of horizontal momentum, and the second and third terms are the horizontal and vertical advection of momentum. The first term on the RHS of Eq. (2.2.16) is the force imposed by the horizontal pressure gradient. The second term on the RHS is the horizontal dispersion of momentum, and the third term is the vertical dispersion of momentum due to turbulent eddy mixing. The last term on the RHS is the wind forcing. The calculation of A_v will be discussed in Section 2.2.3.

The mass transport equation is

$$\frac{\partial(BC)}{\partial t}+\frac{\partial(uBC)}{\partial x}+\frac{\partial(wBC)}{\partial z}=\frac{\partial}{\partial x}\left(BA_H\frac{\partial C}{\partial x}\right)+\frac{\partial}{\partial z}\left(BA_b\frac{\partial C}{\partial z}\right)+S+R+Q \tag{2.2.17}$$

The free water surface elevation has

$$\frac{\partial(B_s\eta)}{\partial t}=\frac{\partial}{\partial x}\int_{-h}^{\eta}uBdz-\int_{-h}^{\eta}Q_HBdz \tag{2.2.18}$$

where B_s = surface water width, $-h$ = coordinate of the water bottom, η = coordinate of the water surface, Q_H = lateral boundary inflow/outflow, and A_b = vertical turbulent mass mixing coefficient.

2.2.2.4 3D Equations in Sigma Coordinate. In deep surface waters, vertical density stratification can suppress vertical turbulent mixing, resulting in significant vertical variations of hydrodynamic and water quality variables. These systems are most appropriately modeled with 3D models. A 3D model is defined along three spatial coordinates (length, width, and depth), under which the hydrodynamic and water quality variables vary over all

three spatial coordinates. A 3D model is the most physically realistic representation for a waterbody, in which water quality variables have significant gradients in the longitudinal, lateral, and vertical dimensions. Deep and large lakes, reservoirs, estuaries, and coastal waters commonly need a 3D representation.

In hydrodynamic modeling, 3D equations are often written in the Cartesian coordinate in the horizontal directions and in a sigma coordinate in the vertical direction. Therefore, before the 3D equations are presented, it is necessary to introduce the sigma coordinate.

Sigma coordinate. To provide uniform resolution in the vertical, a time variable mapping or stretching transformation is desirable. The mapping or stretching is given by

$$z = \frac{z^* + h}{\eta + h} \tag{2.2.19}$$

where z = the stretched, dimensionless vertical coordinate, or so-called sigma coordinate and z^* = the physical vertical coordinate, or the Cartesian coordinate.

In Eq. (2.2.19) and in Fig. 2.2.2, * denotes the original physical vertical coordinates and $-h$ and η are the physical vertical coordinates of the bottom topography and the free surface respectively. It has

$$z = 0 \qquad \text{at bottom topography} \qquad z^* = -h$$

$$z = 1 \qquad \text{at free surface} \qquad z^* = \eta$$

This so-called "sigma" coordinate was originally outlined by Phillips (1957). As shown in Fig. 2.2.2, the sigma coordinate allows smooth representation

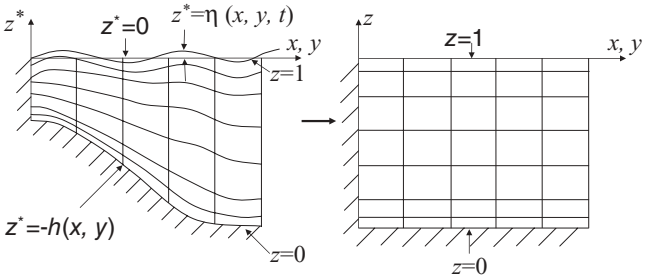

Fig. 2.2.2 A vertical sigma coordinate system. z^* = Cartesian coordinate in the vertical direction, z = the sigma coordinate, and (x, y) = Cartesian coordinates in the horizontal directions.

of the bathymetry and same order of accuracy in shallow and deep waters. Water depths are divided into same number of layers in the sigma coordinate. The bottom is transformed into $z = 0$ plane and the unknown water–surface elevation is exactly transformed into the $z = 1$ plane, which is fixed in the computational plane. With such transformation, the equations are transformed from the x–y–z^* into the x–y–z coordinate systems. Details of the transformation may be found in Vinokur (1974) or Blumberg and Mellor (1987). Free-surface boundary condition allows the air–water interface to evolve freely. One advantage of sigma coordinate is that even under free surface boundary conditions, the water surface is always at $z = 1$, which is very convenient in numerical modeling. Figure 2.2.3 shows a water column with three sigma layers. Variable locations in a numerical model are also indicated in Fig. 2.2.3.

As shown in Fig. 2.2.2, the sigma coordinate has the same number of vertical layers, no matter what the water depths are. The thickness of each vertical layer for each grid cell is variable, since the thickness is computed from the number of vertical layers and the water column depth at each grid cell. This kind of terrain following coordinate has computational efficiency and is able to represent currents with uniform number of vertical layers. However, when the topography is very steep, large bathymetry gradient could lead to extra dissipation between the grid cells in shallow waters and the ones in deep waters. In this case, special attention should be given to avoid large model truncation errors and artificial vertical mixing from the sigma coordinate. In deep water areas, the sigma coordinate might lead to insufficient vertical resolution in representing the surface mixing in the mixing layer. Besides, the vertical velocity in the sigma coordinate should be transferred back to the real vertical velocity in the Cartesian coordinate, before it is used for model–data comparisons.

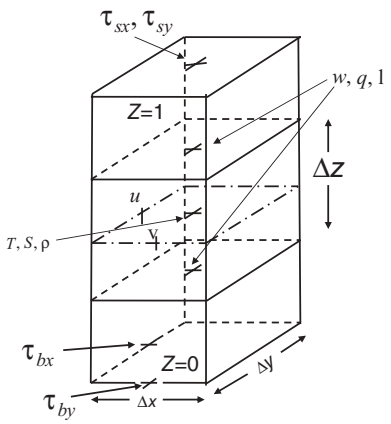

Fig. 2.2.3 Sigma coordinate and variable locations.

3D equations in sigma coordinate. The 3D mass and momentum equations in sigma coordinate are (Hamrick, 1992)

$$\frac{\partial H}{\partial t}+\frac{\partial Hu}{\partial x}+\frac{\partial Hv}{\partial y}+\frac{\partial w}{\partial z}=Q_H \tag{2.2.20}$$

$$\frac{\partial (Hu)}{\partial t}+\frac{\partial (Huu)}{\partial x}+\frac{\partial (Huv)}{\partial y}+\frac{\partial (uw)}{\partial z}-fHv=-H\frac{\partial (p+g\eta)}{\partial x}+\left(-\frac{\partial h}{\partial x}+z\frac{\partial H}{\partial x}\right)\frac{\partial p}{\partial z}+\frac{\partial}{\partial z}\left(\frac{A_v}{H}\frac{\partial u}{\partial z}\right)+Q_u \tag{2.2.21}$$

$$\frac{\partial (Hv)}{\partial t}+\frac{\partial (Huv)}{\partial x}+\frac{\partial (Hvv)}{\partial y}+\frac{\partial (vw)}{\partial z}+fHu=-H\frac{\partial (g\eta+p)}{\partial y}+\left(-\frac{\partial h}{\partial y}+z\frac{\partial H}{\partial y}\right)\frac{\partial p}{\partial z}+\frac{\partial}{\partial z}\left(\frac{A_v}{H}\frac{\partial v}{\partial z}\right)+Q_v \tag{2.2.22}$$

$$\frac{\partial p}{\partial z}=-gH\frac{(\rho-\rho_0)}{\rho_0}=-gHb \tag{2.2.23}$$

$$(\tau_{xz},\tau_{yz})=\frac{A_v}{H}\frac{\partial}{\partial z}(u,v) \tag{2.2.24}$$

where p is excess water column hydrostatic pressure; b is the buoyancy; and τ_{xz} and τ_{yz} are vertical shear stresses in x and y directions.

The total depth, $H = h + \eta$, is the sum of the depth below and the free-surface displacement relative to the undisturbed physical vertical coordinate origin, $z^* = 0$. The pressure p is the physical pressure in excess of the reference density hydrostatic pressure, $\rho_0 gH(1 - z)$, divided by the reference density, ρ_0:

$$p=\frac{\rho_0 gH(1-z)}{\rho_0}=gH(1-z) \tag{2.2.25}$$

The 3D temperature transport equation is

$$\frac{\partial (HT)}{\partial t}+\frac{\partial (HuT)}{\partial x}+\frac{\partial (HvT)}{\partial y}+\frac{\partial (wT)}{\partial z}=\frac{\partial}{\partial z}\left(\frac{A_b}{H}\frac{\partial T}{\partial z}\right)+HR_T+Q_T \tag{2.2.26}$$

where R_T = heating due to solar radiation and Q_T = horizontal turbulent diffusion and external sources–sinks.

As what will be discussed in Section 2.3, solar radiation at the water surface attenuates with depth through the water column. The vertical

velocity in the sigma coordinate (w) is related to the physical vertical velocity w^* by

$$w = w^* - z(\partial_t \eta + u\partial_x \eta + v\partial_y \eta) + (1-z)(u\partial_x h + v\partial_y h) \tag{2.2.27}$$

The mass balance equation for salinity (or a pollutant) is similar to Eq. (2.2.26) for temperature. The only difference is that the former should exclude the solar radiation term in Eq. (2.2.26).

Vertical boundary conditions in sigma coordinate. The vertical boundary conditions for vertical velocity are

$$w(0) = w(1) = 0 \tag{2.2.28}$$

which means that the vertical velocities at the surface and at the bottom are zeroes (Fig. 2.2.3).

Vertical boundary conditions for the momentum equations are kinematic shear stresses at the water bottom ($z = 0$) and water surface ($z = 1$). Expressions for shear stresses are

$$A_v H^{-1} \partial_z (u, v)_{z=0} = (\tau_{bx}, \tau_{by}) = C_B \sqrt{u_{bl}^2 + v_{bl}^2}(u_{bl}, v_{bl}) \tag{2.2.29}$$

$$A_v H^{-1} \partial_z (u, v)_{z=1} = (\tau_{sx}, \tau_{sy}) = C_D \sqrt{U_w^2 + V_w^2}(U_w, V_w) \tag{2.2.30}$$

where τ_{bx} and τ_{by} = shear stresses at the bottom ($z = 0$), τ_{sx} and τ_{sy} = shear stresses at the surface ($z = 1$), U_w and V_w = wind velocity components at 10 m above the water surface, C_B = bottom drag coefficient, C_D = wind stress coefficient, and bl = subscribe referring to water velocity at the mid-point of the bottom layer.

In a sigma coordinate model, the bottom drag coefficient C_B is usually calculated using (Mellor, 1998)

$$C_B = \frac{\kappa^2}{(\ln(\Delta z_b / 2z_o))^2} \tag{2.2.31}$$

where $\kappa = 0.4$ = the von Karman constant, Δz_b = the dimensionless thickness of the bottom layer, $z_o = z_o^*/H$ = the dimensionless roughness height, and z_o^* = the bottom roughness height.

Numerically, Eq. (2.2.31) is applied to the first sigma grid point nearest the bottom. When the bottom of a water system is not well resolved by the vertical model layers, $\Delta z_b/2z_o$ can be very large and leads to very small C_B. In this case, C_B is set to be a constant of 0.0025 in a numerical model (Blumberg and Mellor, 1987).

The wind stress coefficient, C_D, has a format similar to what discussed in Section 2.1.5:

$$C_D = 1.2 \times 10^{-6} \left(0.8 + 0.065\sqrt{U_w^2 + V_w^2}\right) \tag{2.2.32}$$

where U_w and V_w are wind velocity components in meters per second (m/s).

The vertical boundary conditions on temperature and salinity are

$$\frac{A_v}{H}\left(\frac{\partial T}{\partial z}, \frac{\partial S}{\partial z}\right) = -(<wT(1)>, <wS(1)>) \qquad z \to 1 \tag{2.2.33}$$

$$\frac{A_v}{H}\left(\frac{\partial T}{\partial z}, \frac{\partial S}{\partial z}\right) = 0 \qquad z \to 0 \tag{2.2.34}$$

where $<wT\ (0)>$ = temperature flux at the surface (m/s °C), and $<wS(0)>$ = salinity flux at the surface (m/s ppt).

More discussions on temperature modeling and the related boundary conditions will be presented in Section 2.3. It is important to mention that the 3D equations can be simplified to 2D laterally averaged equations by eliminating terms associated with differentiations of x or y. The 2D vertically averaged equations can also be derived from the 3D equations. A 3D model should be easily applied to 1D or 2D studies by simply using 1D or 2D model grid.

2.2.3 Vertical Mixing and Turbulence Models

Turbulence processes play a critical role in vertical mixing. Shallow waters, including rivers, lakes, estuaries, and coastal waters, have turbulence generated at the water bottom or surface. Vertical transport by turbulent diffusion can be sufficient to completely mix the water column. To accurately calculate the vertical turbulent mixing coefficients, A_v and A_b, in the equations of momentum and mass transport, it is necessary to have turbulence models that can represent the vertical mixing realistically. Only the basic concepts and theories that are commonly used in hydrodynamic models are presented here. Detailed discussions on turbulence theories are referred to the numerous books and papers on this topic (e.g., Canuto et al., 2001, 2002).

Turbulent flow is characterized by irregular, random-velocity fluctuations. In turbulent mixing, mass is transferred through the mixing of turbulent eddies within the water system. It is the random motion of the water that does the mixing. This is fundamentally different from the process of molecular diffusion, which is caused by the random motion of molecules. In natural surface waters, the turbulent diffusion is usually much stronger than the molecular diffusion. Turbulence generated by vertical shear in the flow tends to mix dissolved constituents and acts to reduce sharp vertical gradients. Major turbulence-generating mechanisms include the following:

1. Water velocity shear.
2. Wave breaking due to high wind and/or bathymetry change.
3. Tides in estuaries and coastal areas.
4. Inflows/outflows, such as rivers entering lakes or estuaries and water releases from reservoirs.

Some other mechanisms may also affect turbulence in a waterbody but are often negligible. For example, swimming fish may increase local dissipation rates by 10-fold compared to background levels (Farmer et al., 1987) and phytoplankton exudates can increase seawater viscosity and suppress turbulent dissipation rates (Jenkinson, 1986).

Generally, the stronger the flows, the more turbulent the water column. In a lake environment, vertical mixing is generally caused by wind action on the surface, through which eddy turbulence is transmitted to the lower portion of the water columns by shear stresses. The flow-through action in deep reservoirs also causes internal mixing. In estuaries, typically the vertical mixing is induced by the internal turbulence driven by the tidal flows, in addition to surface wind effects. In each environment, however, the amount of vertical mixing is controlled, to a large extent, by the density stratification in the waterbody. Strong vertical stratification inhibits vertical mixing in waterbodies. The vertical stratification can be measured by the gradient Richardson number, which represents the ratio of the buoyancy force to the vertical velocity shear:

$$R_i = -\frac{g}{\rho}\frac{\partial \rho/\partial z}{(\partial v/\partial z)^2} \tag{2.2.35}$$

where

R_i = gradient Richardson number, dimensionless

$\frac{\partial \rho}{\partial z}$ = density vertical gradient (kg/m^4)

$\frac{\partial v}{\partial z}$ = velocity vertical gradient (s^{-1})

The gradient Richardson number provides quantitative information on the relation between the stabilizing effect of buoyancy and the destabilizing effect of velocity shear. It indicates the tendency of the water column to either mix (weak stratification) or resist mixing (strong stratification). Large values of the gradient Richardson number indicate strong stratification, while small values are indicative of weakly stratified, well-mixed conditions.

If $R_i > 0$, the flow is stably stratified with lighter water floating over denser water, especially when $R_i >> 0$. As the gradient Richardson number increases, the resistance to mixing increases. Generally, a value of 10 often indicates the presence of strong vertical stratification and almost complete inhibition of vertical mixing. As a result of strong stratification in a waterbody, for example, significant depletion of dissolved oxygen may occur in the bottom. The mixing of atmospheric oxygen to the bottom is restricted by the strong stratification. If $R_i < 0.25$, mixing occurs between the stratified layers. As R_i nears zero, the flow approaches a neutral condition and the density is the same throughout

the water column. If $R_i < 0$, flows are unstable and heavier water overlies lighter water. Many lakes and reservoirs destratify in the fall of the year, when colder air temperatures and decreased solar radiation cause surface cooling. When the upper cooler layers are denser than the lower layers, lake overturning occurs, which causes rapid mixing of nutrient-laden bottom waters throughout the water column.

In numerical models, turbulent transport and mixing with spatial scales smaller than model grid resolution are represented by vertical and horizontal turbulent dispersion. Horizontal dispersion, for example, can be represented by the Smagorinsky scheme in Eq. (2.2.8). Treatment of vertical mixing in mathematical models is generally achieved through the vertical eddy viscosity. The simplest approach is to represent turbulent mixing using empirical relationships to specify a constant mixing coefficient. Advanced hydrodynamic models, such as Blumberg and Mellor (1987), Hamrick (1992), and Sheng (1986), employ two-equation closure methods to provide internal calculations of vertical eddy diffusivity. The closure models provide the vertical turbulent diffusion coefficients necessary to represent vertical diffusive mass transport. There is a trade-off between the complexity of the turbulence closure and the computational cost. In the 2D laterally averaged equations and the 3D equations, there are two parameters representing the vertical mixing: (1) the vertical turbulent momentum mixing coefficient (A_v) and (2) the vertical turbulent mass mixing coefficient (A_b). These two parameters can be calculated using turbulence models.

The original Navier–Stokes equations, such as Eq. (2.1.19), include all details of turbulence fluctuations and can only be solved by introducing time averaged mean quantities. To account for the transport and history of eddy effects, two variables related to turbulence features in a two-equation turbulence model can be derived from the Navier–Stokes equations. Two-equation turbulence closure models usually have turbulence variables such as turbulence kinetics energy and diffusivity (k-ε model) (e.g., Jones and Launder, 1972) or turbulence kinetics energy and turbulence length scale (k-l) (e.g., Mellor and Yamada, 1982). The turbulence closure scheme calculates vertical turbulent momentum diffusion (A_v) and mass diffusion (A_b) coefficients. The turbulence model described here was developed by Mellor and Yamada (1982) and modified by Galperin et al. (1988) and Blumberg et al. (1992). The model relates A_v and A_b to vertical turbulence intensity (q), turbulence length scale (l), and the Richardson number (R_q) by

$$A_v = \phi_v q l = 0.4 \frac{(1+8R_q)ql}{(1+36R_q)(1+6R_q)} \tag{2.2.36}$$

$$A_b = \phi_b q l = \frac{0.5ql}{(1+36R_q)} \tag{2.2.37}$$

$$R_q = -\frac{gH\dfrac{\partial b}{\partial \sigma}}{q^2}\left(\frac{l^2}{H^2}\right) \tag{2.2.38}$$

where the stability functions ϕ_v and ϕ_b (Galperin et al., 1988) account for reduced and enhanced vertical mixing in stable and unstable vertically density-stratified environments, respectively. Turbulence intensity and the turbulence length scale are determined by solving transport equations for q^2 and q^2l:

$$\frac{\partial(Hq^2)}{\partial t}+\frac{\partial(Huq^2)}{\partial x}+\frac{\partial(Hvq^2)}{\partial y}+\frac{\partial(wq^2)}{\partial z}=$$
$$\frac{\partial}{\partial z}\left(\frac{A_q}{H}\frac{\partial q^2}{\partial z}\right)+2\frac{A_v}{H}\left[\left(\frac{\partial u}{\partial z}\right)^2+\left(\frac{\partial v}{\partial z}\right)^2\right]+2gA_b\frac{\partial b}{\partial z}-2\frac{Hq^3}{B_1 l}+Q_q \quad (2.2.39)$$

$$\frac{\partial(Hq^2l)}{\partial t}+\frac{\partial(Huq^2l)}{\partial x}+\frac{\partial(Hvq^2l)}{\partial y}+\frac{\partial(wq^2l)}{\partial z}=\frac{\partial}{\partial z}\left(\frac{A_q}{H}\frac{\partial(q^2l)}{\partial z}\right)+E_1 l\frac{A_v}{H}\left[\left(\frac{\partial u}{\partial z}\right)^2+\right.$$
$$\left.\left(\frac{\partial v}{\partial z}\right)^2\right]+gE_1 lA_b\frac{\partial b}{\partial z}-\frac{Hq^3}{B_1}\left[1+E_2\left(\frac{l}{\kappa Hz}\right)^2+E_3\left(\frac{l}{\kappa H(1-z)}\right)^2\right]+Q_l \quad (2.2.40)$$

where $\kappa = 0.4$ is the von Karman constant, B_1, E_1, E_2, and E_3 are empirical constants equal to 16.6, 1.8, 1.33, and 0.25 respectively. The parameters Q_q and Q_l are additional source-sink terms, such as subgrid scale horizontal diffusion.

The vertical kinetic energy diffusion coefficient, A_q, has

$$A_q = 0.2ql \quad (2.2.41)$$

For stable stratification, Galperin et al. (1988) suggested limiting the length scale according to

$$1 \le 0.52\frac{q\sqrt{H}}{\sqrt{-g\dfrac{\partial b}{\partial z}}} \quad (2.2.42)$$

or

$$\sqrt{R_q} \le 0.52 \quad (2.2.43)$$

The boundary conditions for turbulence intensity and the turbulence length scale in Eqs. (2.2.39) and (2.2.40) are

$$(q^2(1), q^2\ell(1)) = (B_1^{2/3}u_*^2(1), 0) \quad (2.2.44)$$

$$(q^2(0), q^2\ell(0)) = (B_1^{2/3}u_*^2(0), 0) \quad (2.2.45)$$

where B_1 (= 10.1) is one of the turbulence closure constants and u_* is the friction velocity at the top or bottom as denoted. The friction velocity is defined as:

$$u_* = \sqrt{\tau_s/\rho} \quad (2.2.46)$$

where τ_s = shear stress and can be calculated using Eqs. (2.2.29) and (2.2.30).

2.2.4 Equations in Curvilinear Coordinates

Although circulations in a waterbody are largely controlled by winds, tides, freshwater inflow, and/or density gradients, water motion is also influenced by boundary geometry, such as shoreline and bathymetry. A difficulty in surface water modeling is to accurately resolve the effects of the boundary geometry. A model grid is a network of grid cells (or points) covering the spatial area of a numerical model. The grid discretizes the spatial area of the waterbody into one or more dimensions and forms the basis for application of the numerical model. In order to conduct an accurate hydrodynamic and water quality simulation, the grid representation of boundary geometry should be as realistic as possible.

2.2.4.1 Curvilinear Coordinates and Model Grid. The continuity and the momentum equations are traditionally expressed in the Cartesian coordinates. These equations are applied in numerical modeling using rectangular grids, which are generally effective in waterbodies with relatively regular boundaries. The rectangular grid is the simplest and frequently used grid to represent the shoreline and bottom boundary of a waterbody. Each grid cell is rectangular and the spacing between the grid points in each dimension is fixed. A "staircase" configuration, similar to what shown in Fig. 2.2.1, is fitted to irregular boundaries.

The complexity of surface waters often requires a grid that will result in a scientifically credible, yet computationally feasible model. The grid should provide a compromise between depicting the physical realities of the water system and the computational feasibility. In waterbodies with irregular shorelines, islands, and/or shipping channels, numerical models need very small grid sizes to resolve these boundaries in detail, which may require a very large number of grid cells and make the model computationally uneconomical. For these highly irregular waterbodies, as often seen in some estuaries and reservoirs, curvilinear grids provide better representation. It is often convenient to formulate the governing equations in curvilinear and orthogonal coordinates in the horizontal, so the grid can fit boundary well and achieve sufficient model resolution with reasonable number of grid cells. Since flows close to solid boundaries are usually parallel to those boundaries, curvilinear coordinates are more efficient in representing the effects of irregular boundaries.

Figure 2.2.4 shows a section of a meandering river in a plan view. The curvilinear coordinates are denoted by x (across the river) and y (along the river). The origin of the curvilinear coordinate system is located at Point 1. The coordinates of Point 1, 2, 3, and 4 are (0, 0), (0, y), (x, y), and (x, 0), respectively. The x lines (of y = constants) and y lines (of x = constants) are curved and at right angels to each other (orthogonal). The orthogonal requirement eliminates several terms from the transformed equations and therefore leads to a simpler model. The x lines are generally parallel to the riverbank. For a narrow river, the along river velocity (y component) should be dominant, and the

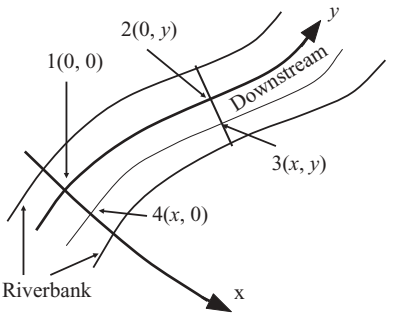

Fig. 2.2.4 An orthogonal curvilinear coordinate system for a meandering river.

across river velocity (x component) should be minimal. Because of meandering and/or width change, for a given increment in y, the down stream distances vary with the value of x. For example, the distance L_{12} (the distance between Points 1 and 2) is usually not equal to the distance L_{43}. Similarly, across river distances for a given increment in x vary with the value of y. The distance L_{14} is usually not equal to the distance L_{23}. Metric coefficients are defined so that a distance increment satisfies the following relation:

$$dL^2 = m_x^2 dx^2 + m_y^2 dy^2 \tag{2.2.47}$$

where dL = a differential distance, dx = a differential distance in x direction, dy = a differential distance in y direction, and m_x and m_y = metric coefficients.

For distances along the x axis, it has

$$dL^2 = m_x^2 dx^2 \tag{2.2.48}$$

and

$$L_{23} = \int_0^x m_x(x', y)dx' \tag{2.2.49}$$

For distances along the y axis, it has

$$dL^2 = m_y^2 dy^2 \tag{2.2.50}$$

and

$$L_{43} = \int_0^y m_y(x, y')dy' \tag{2.2.51}$$

In this curvilinear coordinate system, the velocity components are

$$u = m_x \frac{dx}{dt} \tag{2.2.52}$$

$$v = m_y \frac{dy}{dt} \tag{2.2.53}$$

where u = velocity component in x direction and v = velocity component in y direction.

The metric coefficients are functions of x and y. The average value of the metric coefficient m_x along the line 2-3 is

$$\overline{m_x} = \frac{L_{23}}{L_{14}} \tag{2.2.54}$$

Similarly, the average value of m_y along the line 4-3 is

$$\overline{m_y} = \frac{L_{43}}{L_{12}} \tag{2.2.55}$$

The Cartesian coordinate system is a special case of $m_x = m_y = 1$.

To derive the equations in the curvilinear coordinate systems, mathematical transformation techniques are used to convert the equations from the Cartesian coordinates into the curvilinear coordinates. Figure 2.2.5 shows that for an irregular study domain on the left, a uniform model domain is obtained in the curvilinear coordinate system after the coordinate transformation. Curvilinear coordinates allow great flexibility in the placement of horizontal grid points. They map the irregular geometry into a rectangular computational

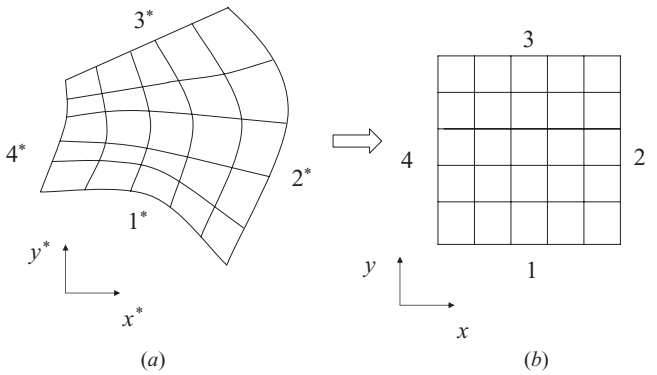

Fig. 2.2.5 (*a*) Curvilinear grid in a study domain. (*b*) Curvilinear grid after curvilinear grid transformation.

grid. In critical areas like shipping channels in an estuary, the curvilinear system allows higher grid resolution to describe processes in these areas in detail.

One of the most commonly used numerical methods is the finite-difference method, in which time and space are divided into discrete (finite) intervals (e.g., Blumberg and Mellor, 1987; Hamrick, 1992). As illustrated in Fig. 2.2.6, the grid has u located at $\pm\Delta x/2$ away from where the water depth (H) and the free surface elevation (η) are defined, and v located at $\pm\Delta y/2$ away from where the H and η are. Choosing variable locations in this way is to achieve computational efficiency and accuracy. Since concentration variables, such as temperature, salinity, and water quality variables, are defined at the center of the grid and velocities are defined at the boundaries of the grid, spatial averaging of velocities is not required to compute changes in concentration variables over time. Also, the horizontal gradients of the free surface elevation and density (ρ) can be used in the horizontal velocity calculation, without requiring spatial averaging of η and ρ.

The model grid is essential for developing a hydrodynamic and water quality model. Three key factors should be considered in grid generation:

1. Theories and basic assumptions used in the model.
2. Objectives of the study and data availability.
3. Computational feasibility.

All of the major models that are currently used for the modeling of rivers, lakes, and estuaries, such as Blumberg and Mellor (1987), Hamrick (1992), and

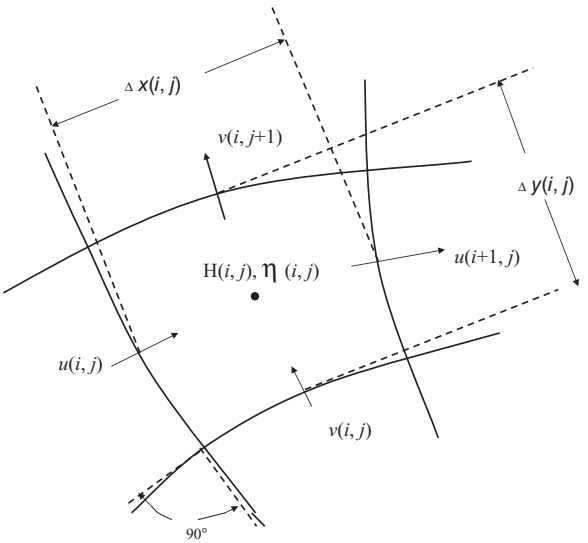

Fig. 2.2.6 Model variable locations on a curvilinear grid.

Sheng (1986), have a common approximation: the so-called shallow water approximation described in Section 2.2.1. The shallow water approximation states that the horizontal scale of motion should be much larger than the vertical scale of motion. Generally, the shallow water approximation requires the ratio of the horizontal scale to the water depth is much larger than one (say ≥20). Having a much finer grid does not necessarily increase the model accuracy. This is an important consideration for determining the model grid size.

Generation of model grid is the first step to setup the model. It is critical to represent domain bathymetry in the study area properly and to limit open boundary uncertainty. A good model grid will minimize computational errors and improve model efficiency. When using a curvilinear grid, the following should be taken into consideration:

1. The grid should properly fit the shorelines.
2. The grid should have the resolution to resolve navigation channel, if there is any.
3. The model open boundary should extend to the area where boundary conditions can be specified.
4. The grid should have sufficient resolution to describe key processes while maintain computational efficiency for long-term simulation.
5. The grid should be kept as uniform as possible to minimize possible numerical problems related to wave propagation and accuracy. The grid orthogonality is often required in finite difference models.
6. Special attention is needed when converting the velocities from curvilinear grid back to Cartesian grid for graphics and model-data comparison. Equations (2.2.27) and (2.2.65) gives relationship between the sigma vertical velocity and the physical vertical velocity. The modeled horizontal velocities need to be rotated back into the directions of true north and true south, before they can be compared with measured data.
7. The great flexibility of curvilinear coordinates in fitting boundaries is offset by the additional terms in the governing equations like Eqs. (2.2.56) and (2.2.57), which cost additional computational time in a numerical simulation.
8. Unlike the Cartesian ones, curvilinear grids need special tools–programs for grid generation, which can be time consuming.

2.2.4.2 3D Equations in Sigma and Curvilinear Coordinates. Under the curvilinear coordinates in the horizontal and the sigma coordinate in the vertical, the momentum, continuity, temperature, and salinity equations are (Hamrick, 1992):

$$\begin{aligned}&\partial_t(m_x m_y Hu)+\partial_x(m_y Huu)+\partial_y(m_x Hvu)+\partial_z(m_x m_y wu)-m_x m_y f_e Hv\\&\quad=-m_y H\partial_x(p+g\eta)-m_y(\partial_x h-z\partial_x H)\partial_z p+\partial_z(m_x m_y H^{-1}A_v\partial_z u)+Q_u\end{aligned} \tag{2.2.56}$$

$$\partial_t(m_x m_y Hv) + \partial_x(m_y Huv) + \partial_y(m_x Hvv) + \partial_z(m_x m_y wv) + m_x m_y f_e Hu$$
$$= -m_x H\partial_y(p + g\eta) - m_x(\partial_y h - z\partial_y H)\partial_z p + \partial_z(m_x m_y H^{-1} A_v \partial_z u) + Q_v \tag{2.2.57}$$

$$\partial_z p = -gHb = -gH(\rho - \rho_o)\rho_o^{-1} \tag{2.2.58}$$

$$\partial_t(m_x m_y H) + \partial_x(m_y Hu) + \partial_y(m_x Hv) + \partial_z(m_x m_y w) = Q_H \tag{2.2.59}$$

$$\partial_t(m_x m_y H) + \partial_x\left(m_y H\int_0^1 u dz\right) + \partial_y\left(m_x H\int_0^1 v dz\right) = \int_0^1 Q_H dz \tag{2.2.60}$$

$$m_x m_y f_e \equiv m_x m_y f - u\partial_y m_x + v\partial_x m_y \tag{2.2.61}$$

$$\rho = \rho(S, T) \tag{2.2.62}$$

$$\partial_t(m_x m_y HS) + \partial_x(m_y HuS) + \partial_y(m_x HvS) + \partial_z(m_x m_y wS)$$
$$= m_x m_y \partial_z(H^{-1} A_b \partial_z S) + Q_S \tag{2.2.63}$$

$$\partial_t(m_x m_y HT) + \partial_x(m_y HuT) + \partial_y(m_x HvT) + \partial_z(m_x m_y wT)$$
$$= m_x m_y \partial_z(H^{-1} A_b \partial_z T) + Q_T \tag{2.2.64}$$

where x and y = the curvilinear-orthogonal coordinates z = vertical sigma coordinate, u and v = the horizontal velocity components in x and y directions, m_x and m_y = the metric coefficients, and w = the vertical velocity in the stretched and dimensionless vertical coordinate z.

The metric coefficients, m_x and m_y, are equal to one under Cartesian coordinates. By setting m_x and m_y equal to one, Eqs. (2.2.56)–(2.2.64) are returned back to the 3D equations under the Cartesian coordinates in the horizontal and sigma in the vertical, that is, the set of equations (2.2.20)–(2.2.26).

The sigma vertical velocity w is related to the physical vertical velocity w^* by

$$w = w^* - z(\partial_t \eta + um_x^{-1}\partial_x \eta + vm_y^{-1}\partial_y \eta) + (1 - z)(um_x^{-1}\partial_x h + vm_y^{-1}\partial_y h) \tag{2.2.65}$$

The source term Q_H in the continuity equation (2.2.59) represents direct rainfall, evaporation, groundwater interaction, water withdrawals, and other point and nonpoint sources. As shown in Fig. 2.2.2, the total depth, $H = h + \eta$, is the sum of the depth below $z^* = 0$ and the free surface displacement relative to $z^* = 0$, The pressure p is given by Eq. (2.2.25).

In the momentum equations (2.2.56) and (2.2.57), f_e is the effective Coriolis parameter defined by Eq. (2.2.61), which incorporates the actual Coriolis parameter, f, and the grid curvature accelerations. Hence, large grid curvature in a curvilinear grid may cause a large value of f_e, which might become an obstacle to computational stability and accuracy and should be avoided.

In Eqs. (2.2.63) and (2.2.64), the source and sink terms, Q_S and Q_T, include subgrid scale horizontal diffusion and thermal sources and sinks, while A_b is the vertical turbulent diffusivity. The density, ρ, is a function of temperature (T) and salinity (S). Salinity equation (2.2.63) can also be used to describe conservative tracers in dye studies. More details on the temperature transport equation (2.2.64) are presented later in Section 2.3.

The buoyancy, b, is defined in Eq. (2.2.58) as the normalized deviation of density from the reference value:

$$b = \frac{\rho - \rho_0}{\rho_0} \tag{2.2.66}$$

Equations (2.2.56)–(2.2.66) provide a closed system for the variables u, v, w, p, η, ρ, S, and T, when the vertical turbulent viscosity and diffusivity (A_v and A_b) and the source and sink terms (Q_u, Q_v, Q_H, Q_S, and Q_T) are specified.

To provide the vertical turbulent viscosity and diffusivity, the turbulence closure model developed by Mellor and Yamada (1982) and modified by Galperin et al. (1988) are used. Similar to what has described in Section 2.2.3, the turbulence intensity and the turbulence length scale are determined by a pair of transport equations (Hamrick, 1992):

$$\begin{aligned}&\partial_t(m_x m_y H q^2) + \partial_x(m_y H u q^2) + \partial_y(m_x H v q^2) + \partial_z(m_x m_y w q^2)\\ &\quad = \partial_z(m_x m_y H^{-1} A_q \partial_z q^2) + 2m_x m_y H^{-1} A_v((\partial_z u)^2 + (\partial_z v)^2) +\\ &\quad 2m_x m_y g A_b \partial_z b - 2m_x m_y H B_1^{-1} l^{-1} q^3 + Q_q\end{aligned} \tag{2.2.67}$$

$$\begin{aligned}&\partial_t(m_x m_y H q^2 l) + \partial_x(m_y H u q^2 l) + \partial_y(m_x H v q^2 l) + \partial_z(m_x m_y w q^2 l)\\ &\quad = \partial_z(m_x m_y H^{-1} A_q \partial_z q^2 l) + m_x m_y H^{-1} E_1 l A_v((\partial_z u)^2 + (\partial_z v)^2) + m_x m_y g E_1 l A_b \partial_z b -\\ &\quad m_x m_y B_1^{-1} H q^3 \left[1 + E_2\left(\frac{l}{\kappa H z}\right)^2 + E_3\left(\frac{l}{\kappa H(1-z)}\right)^2\right] + Q_l\end{aligned} \tag{2.2.68}$$

By setting $m_x = m_y = 1.0$, Eqs. (2.2.67) and (2.2.68) are simplified to the ones under the Cartesian coordinates given in Section 2.2.3.

2.2.5 Initial Conditions and Boundary Conditions

Initial conditions and boundary conditions are needed to solve hydrodynamic and water quality equations. In a modeling study, it is impossible and unnecessary to simulate the whole universe. Generally, an area of interest is selected for the modeling, along with a certain surrounding boundary. The equations of the mathematical model describe the physical, chemical, and biological processes within the waterbody. In order to solve these equations numerically, initial and boundary conditions need to be set and are often critical for the modeling.

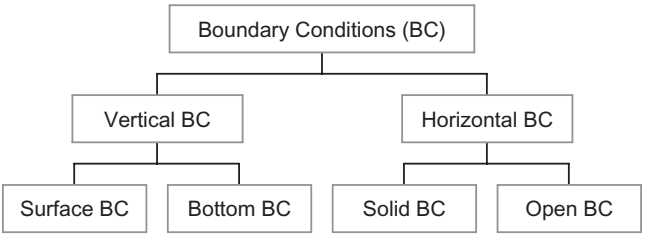

Fig. 2.2.7 Boundary conditions.

Initial conditions specify the state of the waterbody at the beginning of the simulation. The value of the boundary conditions cannot be obtained from the equations used to describe the physical phenomena, but must be inserted on the basis of other information. Boundary conditions and external forcings to the study area are driving forces for model simulations. A model does not calculate boundary conditions for itself, but are affected by them. For example, air temperature and wind speeds are not modeled but are specified to the model as vertical boundary conditions. They affect hydrodynamic processes, such as currents, mixing, and heat transfer.

Different boundary conditions may lead to quite different model results. Improper sets of boundary conditions may cause significant errors in model results, while a proper set of boundary conditions can avoid that. The number and type of initial and boundary conditions depend strongly on the nature of the particular waterbody, on the specific problem of interest, and on the type of the model used.

Boundary conditions include vertical boundary conditions and horizontal boundary conditions (Fig. 2.2.7). The vertical boundary conditions, including surface boundary conditions and bottom boundary conditions, are already discussed previously in this section, where the governing equations are presented. The horizontal boundary conditions include solid boundary conditions and open boundary conditions. Only the solid boundary conditions are discussed here. The open boundary conditions will be presented later in Chapter 10, where estuaries and costal waters are discussed.

2.2.5.1 Initial Conditions. Initial conditions are required only when a time-dependent simulation is conducted. For a steady-state model, by definition, initial conditions are not needed. For any time-dependent numerical simulation, initial conditions are used to set the initial environment values at the beginning of simulation. The system evolution will start from this initial condition. The initial condition should reflect the real waterbody, or at least, it should be an acceptable simplification of the real waterbody.

Spin-up time is the time taken for a numerical model to reach a state of statistical equilibrium under the applied forcings. A cold start occurs when a model is first initialized and needs to be spun up. A cold start can be from

the climatology, an analysis of data, results from a different model, or a combination of the above. The model is then run until a statistical equilibrium is achieved. A hot start is a restart of a model from the saved results of a previous simulation, which is used to eliminate or reduce the model spin up time.

Generally, initial conditions are important when the simulation period is shorter than the time required for these initial conditions to be "flushed out". For example, when modeling water temperature in a deep lake, the initial water temperature in the lake bottom may persist for more than a few months or even more than a year, before the wind and heatfluxes from the surface change it. If the spin-up time and the simulation period are too short, the initial water temperature could affect modeling results significantly. For example, Lake Tenkiller has retention time of 1–2 years (Ji et al., 2004a), errors in the initial conditions may affect the modeling results.

In numerical models, current velocities are usually set up within relatively short period of time and are often set to zero at the beginning of the simulation for convenience. The initial surface water elevation can be critical to the modeling of water systems with long retention times, such as some lakes and reservoirs, since it determines the initial water mass in the system and may have lasting effects on the hydrodynamic and water quality processes. To minimize the impact of initial water temperature and salinity, large and deep waterbodies, say a reservoir or a fjord, usually need a long spin-up time.

Similar to real waterbodies, a numerical model has a limited memory on transport, mixing, and boundary forcings. It is reasonable to believe that the evolution of model variables sometime in the future does not depend on present conditions, if the simulation time is sufficiently long. In the event that the model is not allowed sufficient time to erase impacts caused by initialization, the model results might not be reliable. An effective way to reduce the impact of initial conditions on model results is to have adequate model spin-up time before conducting model-data comparison, so that the effects of the initial conditions can be minimized. Appropriate open boundary conditions can also help overcome any inconsistencies in initial conditions by letting disturbances propagate out of the study area rapidly.

In the modeling of systems with short retention times, such as a rapid flowing river, its initial conditions may have limited impact on the model results. In this case, the initial values are rapidly flushed out of the system and the model "forgets" the initial conditions in a short period of time. For example, the surface elevation of a steep river dynamically links to the flow conditions and the slope of the riverbed. It is difficult (if not impossible) to set a realistic initial water surface elevation. In the modeling of Blackstone River, MA, the river was artificially set to have very deep water depths at the beginning of the simulation (Ji et al., 2002a). The water elevation was then dynamically adjusted by the hydrodynamic processes in the model and established a more realistic profile along the river shortly afterward.

2.2.5.2 Solid Boundary Conditions. Mathematical models should be properly designed to represent the boundary influences of shorelines and open waters on the interior domain of the model. The solid boundary conditions include no-slip conditions and free slip conditions. They are described here. The open boundary conditions are presented in Chapter 10, in which estuaries and coastal waters are discussed.

At a solid boundary without mass fluxes crossing, the water flow must be tangential to it. This means that the component of water velocity normal to the boundary must be zero, that is,

$$\vec{v} \cdot \vec{n} = 0 \tag{2.2.69}$$

where $\vec{v}$ = the current velocity at the boundary and $\vec{n}$ = the unit vector normal to the boundary.

Equation (2.2.69) can also be written as:

$$v_n = 0 \tag{2.2.70}$$

where v_n = velocity component normal to the boundary.

At solid boundaries, water must adhere to the solid, if the water viscosity is significant. It means that the velocity component tangential to the boundary, v_t, is equal to zero:

$$v_t = 0 \tag{2.2.71}$$

This is the no-slip boundary condition. It means that there is no flow along the boundary, as well as through it. The no-slip boundary condition is commonly used in hydrodynamics models (e.g., Sheng, 1986; Blumberg and Mellor, 1987; Hamrick, 1992). If the viscosity is negligible, however, it may be assumed that the water slips along the surface without appreciable drag. It yields:

$$\frac{\partial v_t}{\partial n} = 0 \tag{2.2.72}$$

where n represents the coordinate in the direction normal to the boundary. This is the free slip boundary condition, which means that there can be flow along the boundary, but not perpendicular to it.

For temperature, salinity, and other pollutant concentrations (c), the solid boundary condition states that

$$\frac{\partial c}{\partial n} = 0 \tag{2.2.73}$$

Equation (2.2.73) means that no flux of c across the solid boundary, which is usually a quite accurate approximation in most modeling studies.

2.3 TEMPERATURE

Temperature is a measure of the heat content of a physical body. It indicates the average kinetic energy of the molecules of the substance. The greater the kinetic energy, the higher the temperature. In other words, temperature is a measure of the degree of hotness or coldness of the body. Water temperature represents one of the most important physical characteristics of surface waters. It is a crucial factor in hydrodynamic and water quality studies due to a number of reasons:

1. Vertical temperature profile in a water system affects the stratification, a critical element for vertical mixing.
2. Dissolved oxygen solubility is largely determined by water temperature. Generally, the warmer the water, the less DO.
3. Many biochemical and physiological processes are governed by temperature. Increased temperatures can increase metabolic and reproductive rates throughout the food chain.
4. Some processes, such as reaeration, volatilization, and sorption of organic chemicals to particulate matter, are affected by temperature. Temperature increases can lead to increased dissolved toxic compounds, which is usually the most bioactive.
5. Many aquatic species can tolerate only a limited range of temperatures, and large temperature change can have profound effects on species composition.
6. Water temperature is also of particular economic importance, such as for industrial cooling and for the formation of ice in navigable waterways.

Because of solar radiation, water temperature exhibits strong diurnal variation. Figure 2.3.1 is the measured water temperature in Lake Okeechobee, FL for 72 hours, starting from August 24, 1999 at the middle night. It shows that the lake has the highest water temperature of the day in the afternoon and the lowest temperature in the morning.

Stratification of a waterbody is the arrangement of water masses into separate, distinct, horizontal layers as a result of differences in density. It may be caused by differences in temperature and dissolved or suspended solids. Figure 2.3.2 is the vertical temperature profiles in Lake Wister, OK from November 1992 to June 1993. It shows a seasonal cycle of heating and cooling as well as vertical stratification and destratification. Throughout the winter, temperatures remain fairly constant from top to bottom. In January and February, temperatures are the lowest at 8 °C or lower. In spring and summer, the uppermost layer of the lake grows warmer and the mixing between this surface water and the cooler bottom water slows. In July and August, water tempera-

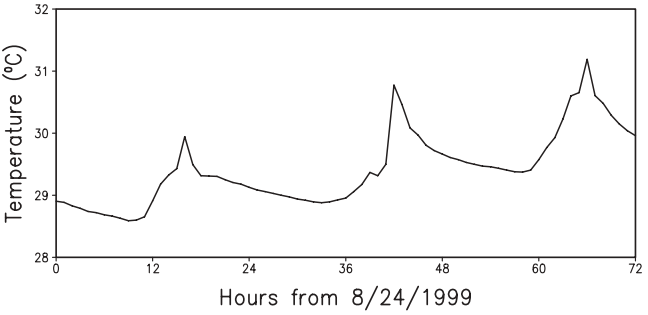

Fig. 2.3.1 Hourly water temperature in Lake Okeechobee, Florida for 72 h, starting from August 24, 1999 at the middle night.

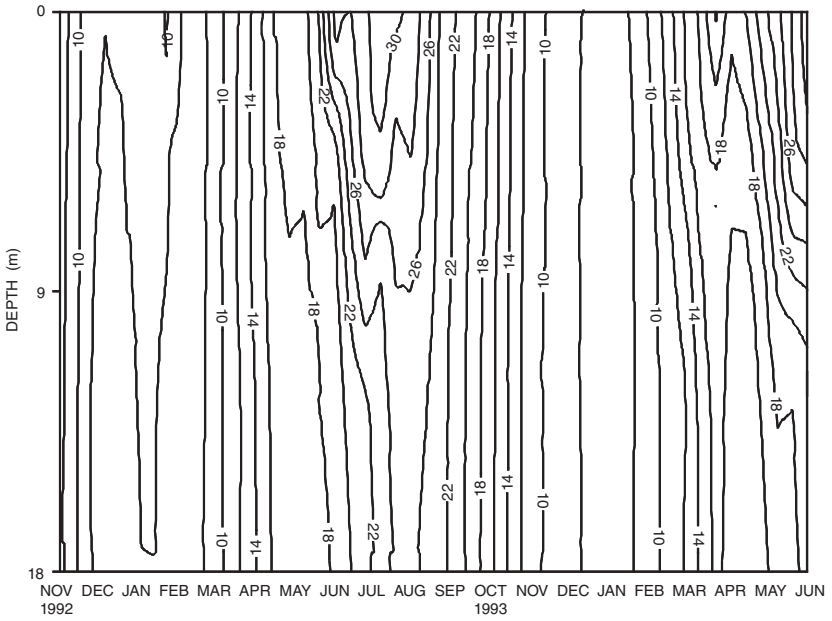

Fig. 2.3.2 Seasonal stratifications of water temperature profiles in Lake Wister, OK (OWRB, 1996).

tures are stratified, and the surface temperatures peak at 30 °C or higher. As air temperatures cool through the fall, the surface water becomes increasingly cold and increases in density. The surface water mass ultimately sinks, when its density becomes greater than that of the underlying water mass. As the surface water moves down, mixing occurs and nutrients from the bottom are

redistributed toward the surface. This introduction of nutrients to surface waters fuels phytoplankton growth. The temperature stratification of a lake can have profound impacts on the hydrodynamic and water quality processes, and will be discussed in detail in Chapter 9.

The term "thermal pollution" is used to describe water quality deterioration caused by inputs of heated water, mostly from industrial cooling processes. Electric power plants draw large quantities of water for cooling from lakes, rivers, or oceans and pump it through condensers at the plants, before returning the water to its source. When the water is discharged, it is sometimes >10 °C warmer than the ambient water. Heated water from electric generating plants is not the sole source of thermal pollution. Urban runoff can also be heated as it passes over highways, pavements, and buildings. The releasing of the heated water can increase surrounding water temperature and dramatically affect life in the vicinity of the thermal plume in a waterbody. A large steam-electric power plant requires an enormous amount of cooling water. For example, a power plant located near Morro Bay, CA discharges about 32-m^3/s cooling water (Tetra Tech, 1999a). Another type of thermal pollution can be caused by discharging very cold water. For example, the proposed Port Pelican project (USCG, 2003) would import liquefied natural gas (LNG) into the U.S. Gulf Coast to meet the gas supply need. To regasify the LNG, large amount of seawater would be used to heat up the LNG. The discharged seawater could be up to 20 °C lower than the surrounding water. This may have significant impact on the local ecosystem.

Sudden change in temperature caused by periodic power plant discharges can make it difficult for the local ecology to ever acclimate. The heated water discharged from power plants can lower DO levels, cause eutrophication, affect the life processes of aquatic organisms, and/or damage the quality of water for drinking or recreational use. If water temperatures rise too high, DO levels drop, directly threatening aquatic life and contributing to eutrophication. Although some members of aquatic ecosystems can adapt to the heated water, many are incapable of doing so and either die or forced to relocate. For some species, such as trout and salmon, any increase in temperature is undesirable. Most plants and animals associated with water systems are incapable of regulating their internal body temperature. Therefore, the temperature of such organisms fluctuates in accordance with ambient temperature of the environment. The organisms incapable of functioning optimally at the new temperature eventually disappear. Most algae have a limited temperature range in which they can grow and survive. In addition, there is an optimum range at which algae exhibit the highest primary production. Many species regulate the timing of important events, such as reproduction and migration, according to specific water temperatures.

However, there are some circumstances when warmed water might be considered beneficial. Within certain limits, thermal addition can promote fish growth and fishing may actually be improved in the vicinity of a power plant.

Water temperature also influences the rate of plant photosynthesis, the metabolic rates of aquatic organisms, and the sensitivity of organisms to toxic wastes, parasites, and diseases. Temperature affects the solubility and, in turn, the toxicity of many other parameters. Generally, the solubility of solids increases with increasing temperature, while gases tend to be more soluble in cold water. As water temperature increases, two factors combine to make it more difficult for aquatic life to get sufficient oxygen to meet its needs. The first is that metabolic rates increase with temperature and therefore increase oxygen demand. The second is that at the same time, the available DO is reduced, because that the amount of DO that the water can hold decreases with temperature. Thus, as temperature increases, the demand for oxygen goes up while the amount of DO available goes down.

2.3.1 Heatflux Components

Water temperature is a function of both surface heatflux and the transport of water into and out of the system. The total heat budget for a waterbody includes the effects of heat exchanges with the atmosphere and with the water bottom, inflows/outflows, and heat generated by chemical/biological reactions. The dominant process controlling the heat budget is the atmospheric heat exchange. In addition, it is also important to include the proper boundary conditions for advective exchange (e.g., rivers, thermal discharges, or tidal flows).

The heat exchanges between the atmosphere and water columns are largely transferred by

1. Radiative processes, including shortwave radiation from the sun and the longwave radiation emitted by the atmosphere and the water surface.
2. Turbulent heat transfers, including latent heat transfer due to water evaporation and sensible heat transfer due to the temperature difference between the water and the overlying air.

Figure 2.3.3 summarizes the major four heatflux components. The plus (+) sign indicates heat input (a gain) to the waterbody. The negative (–) sign indicates heat output (a loss) from the waterbody. The direction of sensible heat transfer depends on the air–water temperature difference. In Fig. 2.3.3:

1. The solar radiation is the short wave radiation from the sun that reaches the water surface.
2. The longwave radiation is the net longwave radiation from the atmosphere and the waterbody.
3. The latent heat is the heat transfer due to water evaporation.

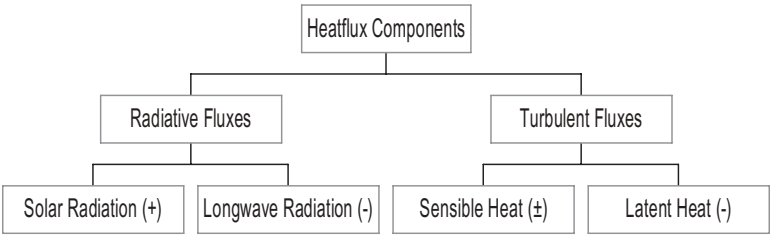

Fig. 2.3.3 Heatflux components.

4. The sensible heat is the conductive heat transfer between the atmosphere and the waterbody.

The net heatflux can be described by

$$H_{\text{net}} = H_S + H_L + H_E + H_C \tag{2.3.1}$$

where H_{net} = net heatflux across the air/water interface, H_S = shortwave solar radiation flux, H_L = net longwave radiation flux from the atmosphere and the waterbody, H_E = latent heatflux due to evaporation and, H_C = sensible heatflux due to conduction. In addition to the major four heatflux components shown in Fig. 2.3.3, other minor heat sources includes the following:

1. Heat generated from chemical/biological reactions.
2. Heat exchange between the water and the water bottom.
3. Heat generated from current friction.

These minor sources are negligible in most applications.

Figure 2.3.4 presents measured hourly averaged heatflux components in the Japan/East Sea (40° N and 134° E) between January 16, 2000 and February 5, 2000 (Lee et al., 2000). During daytime, the solar radiation has the largest values and can be >500 W/m^2. Since there were large air–water temperature differences during the winter, the latent and sensible heatfluxes governed variability in the net surface heatflux, and produced strong heat losses during the winter. Figure 2.2.5 gives the daily averaged heatflux components (in W/m^2) measured in the central Arabian Sea (15° 30′ N, 61° 30′ E) between October 15, 1994 and 20, 1995 (Dickey, 2002). Compared with the ones in Fig. 2.3.4, the heatfluxes in Fig. 2.3.5 were measured at much lower latitude, were daily averaged, and covered the entire four seasons. The daily averaged heatfluxes indicate clearly that generally, the solar radiation is the primary heat source while the latent heat transfer is the primary heat sink. The contributions from longwave radiation and sensible heat transfer are smaller than the two. Figures 2.2.4 and 2.2.5 illustrate the typical values and variation ranges of the four

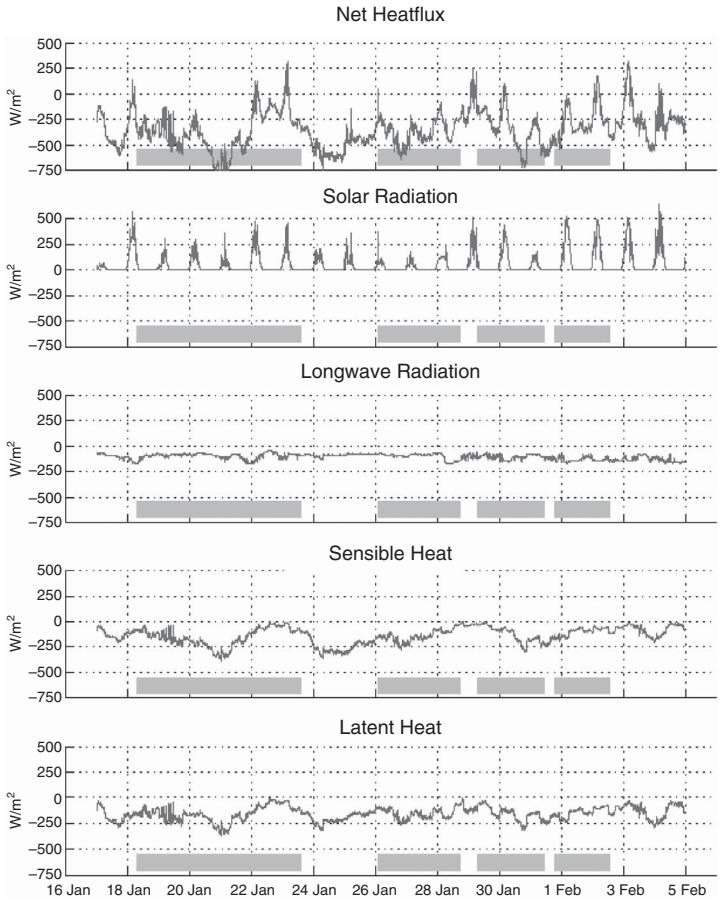

Fig. 2.3.4 Hourly averaged heatflux components measured on the Japan/East Sea (~40 °N and 134 °E) between January 16 and February 5, 2000 (based on Lee et al., 2000).

heatfluxes components. A big difference between the two figures is that Fig. 2.3.4 is hourly averaged, while Fig. 2.3.5 is daily averaged. This explains that why the former has much larger solar radiation amplitude than the latter.

2.3.1.1 Solar Radiation. Among the four heatflux components in Eq. (2.3.1), the solar radiation (also called short wave radiation) is often the most important one in terms of magnitude. Figures 2.3.4 and 2.3.5 give typical values of solar radiation. Unlike the other three heatflux components (longwave radiation, sensible heat, and latent heat), which all occur only at the water surface, solar radiation is penetrative, distributing its heat through a significant range of the water column.

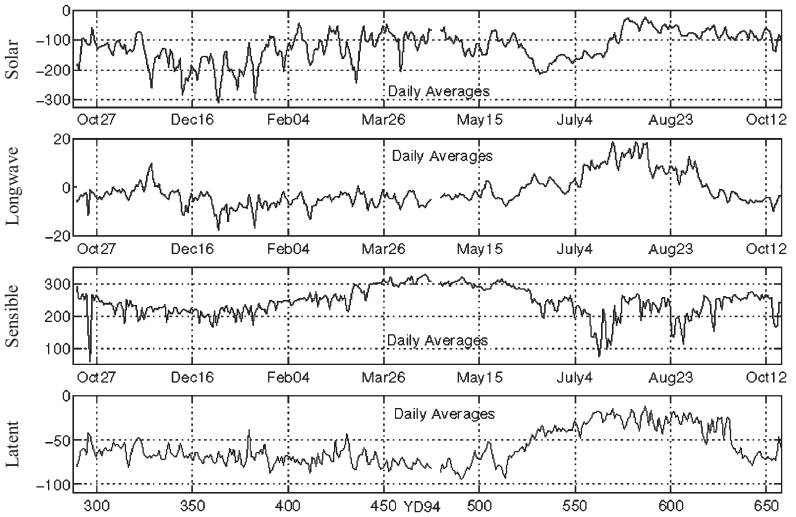

Fig. 2.3.5 Daily averaged heatflux components (in W/m^2) measured in the central Arabian Sea (15° 30′N, 61° 30′E) between October 15, 1994 and October 20, 1995. First panel: solar radiation; second panel: longwave radiation; third panel: sensible heat; fourth panel: latent heat (based on Dickey, 2002).

When solar radiation enters the earth's atmosphere, a portion of the energy is removed by scattering and adsorption. The amount of solar radiation that enters the waterbody depends on

1. The altitude of the sun, which varies daily as well as seasonally for a fixed location on the earth.
2. The dampening effect of scattering and absorption in the atmosphere due to cloud cover.
3. The reflection from the water surface.

A variety of empirical formulas are proposed to estimate the solar radiation. In order to account for the reflection, scattering, and absorption incurred in the atmosphere, a great deal of empiricism should be involved. However, since the solar radiation is often the most important heatflux component and errors from those empirical formulas can be significant, it is desirable to use measured solar radiation in modeling studies. Another effect is that shading from trees and steep riverbanks can significantly reduce the incoming solar radiation to the water surface, resulting in water temperatures much lower than those in unobstructed areas. When modeling narrow rivers and reservoirs, the shading effect can be significant for accurately simulating the local water temperature. To illustrate solar radiation changes, Fig. 2.3.6 shows the measured net solar radiation in Lake Okeechobee, FL between October 1, 1999 and

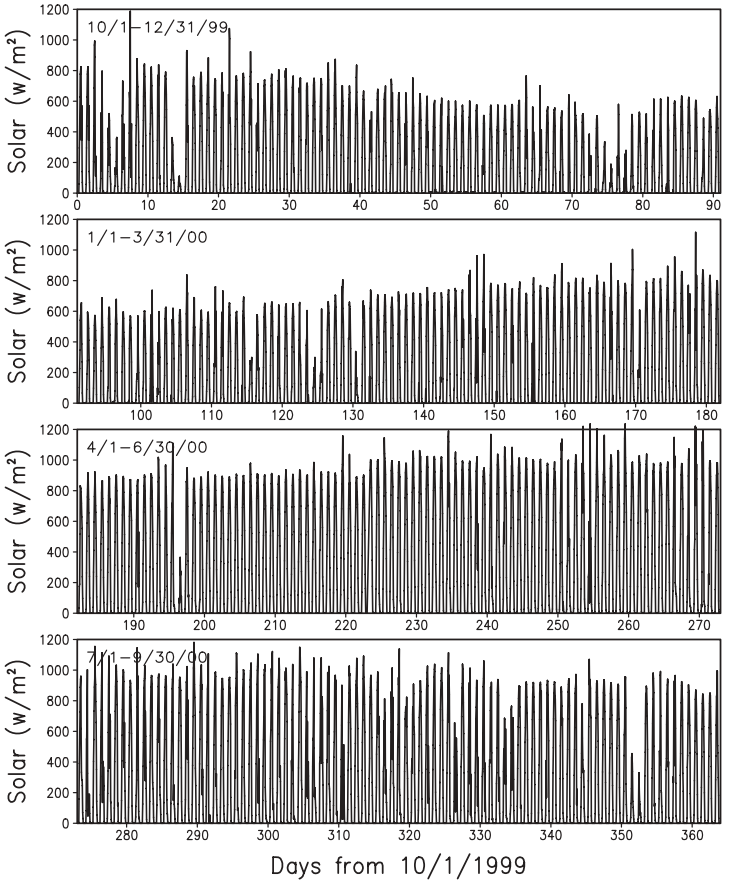

Fig. 2.3.6 Hourly measured solar radiation in Lake Okeechobee, FL.

September 30, 2000. It is seen that in addition to the large diurnal variation, the solar radiation also has large seasonal variations with typical winter values of 600 W/m^2 and summer values of >1000 W/m^2.

2.3.1.2 Longwave Radiation. The magnitude of longwave radiation is proportional to the fourth power of the absolute temperature and is determined by the Stephan–Boltzmann law:

$$H_R = \varepsilon\sigma T^4 \tag{2.3.2}$$

where H_R = the heatflux of longwave radiation (w/m^2), ε = the emissivity (= 0.97 for water), σ = the Stefan–Boltzmann constant (= 5.67×10^{-8} W/m^2/K^4), and T = the absolute temperature in kelvin (= 273.15 + °C).

The net longwave radiation on the water-air surface is the results of two processes: (1) the downward radiation from the atmosphere and (2) the upward radiation emitted by the water surface.

The atmospheric radiation is characterized by much longer wavelengths than solar radiation, and is related to atmospheric temperature, cloudiness, and other atmospheric conditions. During the night and during cloudy condition, the atmospheric radiation can be a significant component for heat balance and water temperature calculation.

The typical values of longwave radiation are shown in Figs. 2.3.4 and 2.3.5. The formula by Swinbank (1963) is commonly used in modeling studies:

$$H_L = \varepsilon\sigma\{[9.37\times10^{-6}(T_a+273.15)^6][1+0.17C^2]-(T+273.15)^4]\} \quad (2.3.3)$$

where H_L = net longwave radiation (W/m^2), ε = emissivity of the waterbody (= 0.97), σ = Stefan–Boltzmann constant (= 5.67×10^{-8} W/m^2/K^4), T = water temperature (°C), T_a = atmospheric temperature (°C), and C = cloud fraction (= 0 = cloudless, = 1 = full cloud coverage).

The first term on the RHS of Eq. (2.3.3) represents the net longwave radiation from the atmosphere, in which an empirical formula is used to determine the overall atmospheric emissivity by considering the cloudiness. The second term represents the longwave radiation from the water, as described by the Stephan–Boltzmann law, Eq. (2.3.2).

2.3.1.3 Evaporation and Latent Heat. Evaporation is a cooling process by which water at the water surface is converted from the liquid to the vapor state. The latent heat due to evaporation is the major heat loss for a waterbody. It mostly balances the heat input from the solar radiation. In order to determine evaporation, radiation, air temperature, vapor–pressure gradient, and temperature of the water need to be estimated accurately. Typical values of latent heat are shown in Figs. 2.3.4 and 2.3.5. Latent heatflux can be calculated using

$$H_E = \rho L_E E \quad (2.3.4)$$

where H_E = latent heatflux due to evaporation (W/m^2), ρ = water density (kg/m^3), L_E = latent heat of water (J/kg) and, E = evaporation rate (m/s).

The latent heat of water required to evaporate 1 g of water varies slightly with both temperature and salinity. An average value is 2400 J, that is, the typical value of L_E is 2.4×10^6 J/kg. This large latent heatflux is supplied directly from heat stored in the water. Hence, the cooling power of evaporation is very large.

After the latent heatflux (H_E) is estimated from empirical formulas, such as the ones given below, Eq. (2.3.4) can also be used to calculate evaporation rate E, which can be a significant component in water balance, especially for subtropical lakes where evaporation rate is very high due to high water

temperatures. The water depth change due to evaporation can be calculated from

$$\Delta z = E\Delta t = \frac{H_E}{\rho L_E}\Delta t \tag{2.3.5}$$

where Δt = time interval (s) and Δz = water depth change over the period of Δt (m).

When precipitation is considered, the increase in water depth is given by

$$\Delta z = R\Delta t \tag{2.3.6}$$

where R = rate of precipitation (m/s).

Partial pressure is the pressure exhibited by a single gas in a gas mixture. An important parameter in latent heat calculation is the actual vapor pressure of air, which is defined as the partial pressure exerted by water vapor. The relative humidity (R_h) is the ratio of the actual vapor pressure (e_a) to the saturation vapor pressure (e_s):

$$R_h = \frac{e_a}{e_s} \tag{2.3.7}$$

The parameter R_h is usually expressed as a percentage rather than as a fraction. The actual vapor pressure, e_a, can then be expressed as:

$$e_a = e_s \frac{R_h(\%)}{100} \tag{2.3.8}$$

The saturation vapor pressure is the maximum vapor pressure that is thermodynamically stable and is a function of the air temperature. Bolton (1980) proposed an empirical formula for the calculation of saturation vapor pressure:

$$e_s = 6.112\exp\left(\frac{17.67T}{T+243.5}\right) \tag{2.3.9}$$

where T = air temperature in °C and e_s = saturation vapor pressure in mb. Errors of Eq. (2.3.9) are <0.3% within the temperature range between –35 and 35 °C, which should be accurate enough for most hydrodynamic and water quality studies.

The latent heat of evaporation is the quantity of heat energy that must be absorbed to break the hydrogen bonds between water molecules in the liquid state to convert them to vapor. Evaporation increases as the difference between air and water temperature increases. Various theoretical and empirical formulas have been proposed to estimate the latent heatflux. A common approach is to link the latent heatflux with (1) wind speed, and (2) the difference

between the saturated vapor pressure at the water surface temperature and the actual vapor pressure in the overlying air (Edinger et al., 1974). It is usually written as:

$$H_E = f(w)(e_s - e_a) \tag{2.3.10}$$

where H_E = evaporation heatflux (W/m^2), $f(w)$ = wind speed function (W/m^2/mb), w = wind speed (m/s), e_s = saturated vapor pressure at water surface temperature (mb), and e_a = actual vapor pressure in the overlying air (typically 10 m above the water) (mb).

Equation (2.3.10) states that the latent heatflux is proportional to the difference between the saturation vapor pressure of the surface layer and the actual vapor pressure of the overlying air. The greater the difference, the higher the rate of evaporation and latent heatflux. The turbulence factor is parameterized by using the wind speed, w, at a specified height above the surface, usually 10 m. The wind speed function has the general format of

$$f(w) = a_0 + a_1 w + a_2 w^2 \tag{2.3.11}$$

The coefficients a_0, a_1, and a_2 can vary in large ranges (Cole and Buchak, 1995). Ahsan and Blumberg (1999) applied

$$f(w) = 6.9 + 0.345 w^2 \tag{2.3.12}$$

to a lake study.

Therefore, after $f(w)$ and e_a are known, the latent heatflux due to evaporation can be calculated from Eq. (2.3.10) and the evaporation rate, E, can be calculated from Eq. (2.3.4).

2.3.1.4 Sensible Heat. In addition to latent heat, as illustrated in Fig. 2.3.3, the sensible heat is also transferred by turbulence activities on the air–water interface. Typical values of sensible heat are shown in Figs. 2.3.4 and 2.3.5. Sensible heat exchange (or conduction) is the heatflux transferred between water and the atmosphere due to a temperature difference between the two. The heat exchange takes place by conduction and convection and is not related to water evaporation. This heat exchange

1. May be upward or downward.
2. Occurs only in a very thin layer of the air–water boundary.
3. Depends on the temperature difference between the air and the water.

The process of sensible heat transfer occurs somewhat analogously to evaporation. Both are affected by turbulence activities and the density stratification. Empirical formulas of sensible heat transfer are also similar to those for latent heat transfer. For example, it is assumed that the heat transfer increases as the temperature difference between water and air increases, and that heat transfer

increases with increasing wind speed, where wind speed is used as a parameter for turbulent transfer across the air–water interface.

The direct measurement of sensible heatflux and latent heatflux requires continuous and detailed monitoring of wind, air and water temperature, and air humidity. It can be difficult and expensive to maintain such a monitoring program for long periods. Because the transfer by conduction is a function of the same variables as evaporation, the commonly used approach is to use the Bowen ratio (Bowen, 1926) to link the latent heatflux and the sensible heatflux. The Bowen ratio is defined as the ratio of sensible heatflux to latent heatflux and has the following:

$$B = \frac{H_C}{H_E} = C_B \frac{p_a}{p_0} \frac{T - T_a}{e_s - e_a} \tag{2.3.13}$$

where B = Bowen ratio, H_C = sensible heatflux due to conduction (W/m^2), H_E = latent heatflux due to evaporation (W/m^2), C_B = Bowen coefficient (= 0.62 mb/°C), p_a = atmospheric pressure (mb), and p_0 = reference atmospheric pressure at sea level (= 1013 mb), T = water temperature (°C), T_a = air temperature (°C), e_s = saturation vapor pressure at water temperature (mb), and e_a = actual vapor pressure of air (mb).

Some studies suggest that the two processes do not scale simply as Bowen suggested, but given the large uncertainty in knowing what is indeed the correct empirical formulas for sensible heatflux and latent heatflux, the Bowen ratio is still a quite accurate approximation in hydrodynamic studies.

By using Bowen ratio, the sensible heatflux, H_C, can be calculated as:

$$H_C = C_B \frac{p_a}{p_0} f(w)(T - T_a) \tag{2.3.14}$$

For practical purposes, the ratio of p/p_0 can be taken to be unity, unless that the study area is located at high altitude and p_a is significantly $<p_0$.

2.3.2 Temperature Formulations

Water temperature is largely determined by external heatfluxes, inflows/outflows, and hydrodynamic processes within the waterbody. Factors influence water temperature include water depth, season, horizontal dispersion, vertical mixing due to wind and tides, stratification, temperature of inflows, and human influences (e.g., heated water discharged from power plants and release from wastewater treatment plants).

2.3.2.1 Basic Equations. The temperature transport equation in sigma coordinate, Eq. (2.2.26), can is rewritten as:

$$\frac{\partial(HT)}{\partial t} + \frac{\partial(HuT)}{\partial x} + \frac{\partial(HvT)}{\partial y} + \frac{\partial(wT)}{\partial z} = \frac{\partial}{\partial z}\left(\frac{A_b}{H}\frac{\partial T}{\partial z}\right) + \frac{\partial I}{\partial z} + Q_T \tag{2.3.15}$$

where x and y = Cartesian coordinates in the horizontal, z = sigma coordinate in the vertical, H = water depth, A_b = vertical turbulent mass mixing coefficient, I = solar radiation, and Q_T = horizontal turbulent diffusion and external sources/sinks.

The hydrodynamic transport, (u, v, w), and the turbulent mixing, A_b, are provided by a hydrodynamic model. The depth distribution of the solar radiation heating is exponential in form and can be expressed as:

$$I = rI_s \exp(-\beta_f H(1-z)) + (1-r)I_s \exp(-\beta_s H(1-z)) \tag{2.3.16}$$

where I = the solar radiation at water depth z (W/m^2), I_s = the incident solar radiation at water surface (z = 1) (W/m^2), β_f = fast scale attenuation coefficients (1/m), β_s = slow scale attenuation coefficients (1/m), and r = a distribution fraction between 0 and 1. For shallow water environments, r is set to one, which eliminates the second term on the RHS of Eq. (2.3.16), and β_f is usually within the range of 0.2–4 m^{-1}.

A simpler form of Eq. (2.3.16) is the Beer's law:

$$I(D) = I_s e^{-K_e D} \tag{2.3.17}$$

where $I(D)$ = solar radiation at depth D below the surface (W/m^2), I_s = solar radiation at the surface (D = 0) (W/m^2), D = water depth (m), and K_e = light extinction coefficient (1/m). By letting r = 1, $\beta_f = K_e$, and $D = H(1 - z)$, Eq. (2.3.16) and Eq. (2.3.17) are identical. Hence, the Beer's law is a special case of Eq. (2.3.16).

Solar radiation that penetrates the surface of the water is absorbed by the water. This absorption, as represented in Eq. (2.3.15), heats the water column and takes place over a considerable depth. In most surface waters, much of the solar radiation penetrating the surface is absorbed in the first a few meters. In the modeling of shallow waters, the solar radiation is often distributed within the top model layer, since the turbidity in these waters is usually high and solar radiation decays rapidly with water depth. However, in very clear lakes, solar heating of the water may occur at depths of tens of meters.

The solar radiation at the surface, I_s, is a function of location, time of the year, time of the day, meteorological conditions, and other factors. The light extinction coefficient (also called light attenuation coefficient) is the measure for the reduction (absorption) of light intensity within a water column, and will be discussed again in Section 3.2.5, where turbidity and Secchi depth are discussed. Equation (2.3.17) will also be used in photosynthesis calculation in Section 5.2.3, where sunlight for algal growth is described.

2.3.2.2 Surface Boundary Condition. At the water surface (z = 1), the boundary condition for the temperature transport equation (2.3.15) is

$$-\frac{\rho c_p A_b}{H}\frac{\partial T}{\partial z} = H_L + H_E + H_C \tag{2.3.18}$$

where ρ = water density, c_p = water specific heat, A_b = vertical turbulent mass mixing coefficient, and H = water depth. In Eq. (2.3.18), the heatfluxes of longwave radiation (H_L), latent heat (H_E), and sensible heat (H_C) can be estimated using Eqs. (2.3.3), (2.3.10), and (2.3.14), respectively.

Based on the approach proposed by Rosati and Miyakoda (1988), Hamrick (1992) applied the following to the temperature boundary condition at water surface:

$$H_L = \varepsilon\sigma T_s^4(0.39 - 0.05e_a^{1/2})(1 - B_c C) + 4\varepsilon\sigma T_s^3(T_s - T_a) \tag{2.3.19}$$

$$H_E = c_e \rho_a L_E w(e_s - e_a)\left(\frac{0.622}{p_a}\right) \tag{2.3.20}$$

$$H_C = c_h \rho_a c_{pa} w(T_s - T_a) \tag{2.3.21}$$

where ε = emissivity of the waterbody (= 0.97), σ = Stefan–Boltzmann constant (= 5.67×10^{-8} W/m^2/K^4), e_a = actual vapor pressure (mb), C = cloud fraction (=0 = cloudless, =1 = full cloud coverage), B_c = an empirical constant (= 0.8), T_s = water surface temperature (°C), T_a = air temperature (°C), c_e = c_h = turbulent exchange coefficients (= 1.1×10^{-3}), ρ_a = atmospheric density (= 1.2 kg/m^3), c_{pa} = specific heat of air (= 1.005×10^3 J/kg/K), L_E = latent heat of evaporation (= 2.501×10^6 J/kg), w = wind speed (m/s), e_s = saturation vapor pressure at surface water temperature (mb), e_a = actual vapor pressure (mb), and p_a = atmospheric pressure (mb).

Comparing Eq. (2.3.19) with Eq. (2.3.3), Eq. (2.3.20) with Eq. (2.3.10), and Eq. (2.3.21) with Eq. (2.3.14), it is evident that there are differences between these equations, even though they have similarities.

When the temperature of a discharge is significantly different from the temperature of the receiving water, the discharge can have thermal and ecological impacts on the receiving water. A typical example is the cooling water discharge from a power plant. The heat energy added to a receiving waterbody can be estimated using:

$$H_T = Q_c \rho c_p \Delta T \tag{2.3.22}$$

where H_T = rate of heat energy exchange (J/s), Q_c = discharge rate (m^3/s), ρ = water density (kg/m^3), c_p = specific heat of water (= 2400 J/kg/°C), and ΔT = temperature difference between the discharged water and the receiving water (°C) Equation (2.3.22) can be used in the external heat source term, Q_T, in Eq. (2.3.15).

2.3.2.3 Bed Heat Exchange. In addition to the surface heatfluxes, the heat exchange on the interface of water column–sediment bed can also affect temperature in the water column. The heat exchange with the sediment bed is generally much smaller than the surface exchange and is frequently neglected

in modeling studies. However, this heat exchange can be significant for accurately simulating vertical temperature profiles. Tsay et al. (1992) demonstrated that in modeling lake stratification, it is important to include the exchange with the sediments in the heat budget. HydroQual (1995b) also simulated temperature stratifications in a lake by including the sediment bed heatflux.

The heatflux through the interface of the water–sediment bed varies with the seasonal changes of water temperature. Heat energy flows from the water to the bed during the summer and early fall and then back into the water during the winter. The magnitude of this seasonal heatflux depends primarily on the seasonal temperature range of the overlying water column and secondarily, on the thermal properties of the sediment bed. In the summer, sediment bed heatflux is a very small percentage of the total heatflux to water columns and is generally insignificant in the overall heat budget. During the winter, especially when the lake is covered with ice and the water temperature is very low, the heatflux from sediment bed can be significant.

A typical formula for sediment bed heatflux is similar to the one for sensible heatflux, Eq. (2.3.14), and is proportional to the temperature difference between the water and the sediment:

$$H_B = -K_B(T - T_b) \tag{2.3.23}$$

where H_B = heatflux between water–sediment bed (W/m^2), K_B = heat exchange coefficient (W/m^2/°C), T = water temperature (°C), and T_b = sediment bed temperature (°C). Cole and Buchak (1995) reported that K_B has value of 7×10^{-8} W/m^2/°C, approximately two orders of magnitude smaller than the surface heat exchange coefficients. The sediment temperature has a typical value of annual mean air temperature.

In shallow surface waters, the solar radiation may penetrate the entire water column. The remaining irradiance at the sediment bed–water interface is adsorbed into the sediment bed. Jin et al. (2000) utilized a simple heat balance equation for the sediment bed:

$$\frac{\partial(H_b T_b)}{\partial t} = \frac{I_b}{\rho_b c_{pb}} - c_{hb}\frac{\rho c_p}{\rho_b c_{pb}}\sqrt{u_1^2 + v_1^2}\,(T_b - T_1) \tag{2.3.24}$$

where I_b = irradiance at the bed determined from Eq. (2.3.16), T_b = bed temperature, H_b = active thermal thickness of the bed, ρ = water density, ρ_b = sediment density, c_p = specific heat of the water, c_{pb} = specific heat of the water–sediment bed mixture, and c_{hb} = a dimensionless convective heat exchange coefficient.

The subscript 1 denotes velocity components and water temperature in the bottom hydrodynamic model layer. Therefore, the vertical boundary condition at the bottom ($z = 0$) can be written as:

$$\frac{A_b}{H}\frac{\partial T}{\partial z} = -c_{hb}\frac{\rho c_p}{\rho_b c_{pb}}\sqrt{u_1^2 + v_1^2}\,(T_b - T_1) \tag{2.3.25}$$

where A_b = vertical turbulent mass mixing coefficient, H = water depth, and z = sigma coordinate. Equations (2.3.24) and (2.3.25) couple the sediment bed with the water column.

2.4 HYDRODYNAMIC MODELING

Using a numerical model to simulate a water system only works when the modeler fully understands the model's limitations and the physical processes involved, and conducts adequate calibration and verification. General discussions on mathematical models, statistical analysis, and model calibration and verification will be presented in Chapter 7. This section is focused on issues directly related to hydrodynamic modeling. After major parameters and data needed in hydrodynamic modeling are discussed, two case studies are presented to demonstrate how hydrodynamic modeling is applied to practical problems in surface waters.

Hydrodynamic transport and mixing are fundamental to the simulation of pollutant transport in waterbodies. Hydrodynamic models that can be generally applied to rivers, lakes, estuaries, and coastal waters typically have the following features:

1. Three dimensional and time dependent.
2. Complete thermodynamic processes.
3. Vertical turbulence mixing.
4. Free surface.

Besides, models using finite difference schemes often use (1) curvilinear horizontal coordinates and (2) sigma vertical coordinate.

Detailed discussions on these features have been presented in the previous sections of this chapter. Fig. 2.4.1 gives the structure of the EFDC hydrodynamic model (Hamrick, 1992). The model include modules for dynamics (water depth, 3D currents, and mixing), dye dispersion simulation, water temperature, salinity, near-field plume simulation, and particle drifting simulation.

When conducting surface water modeling with sophisticated 3D models, small, simple mistakes in setting up the model could lead to huge errors in model results. It is essential to pay close attention to the details, such as:

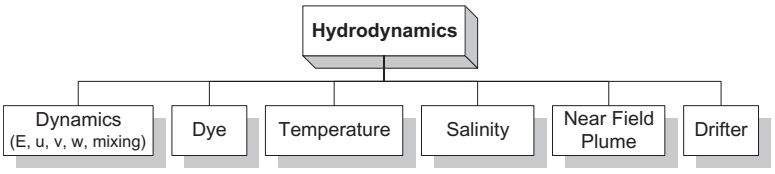

Fig. 2.4.1 The structure of the EFDC hydrodynamic model.

1. All external forcings, including open boundary conditions, point and nonpoint sources, and meteorological forcings, should cover the entire modeling period.
2. Meteorological forcings, such as wind velocity, air temperature, solar radiation, and precipitation, should be specified in correct units.
3. Point sources, nonpoint sources, and open boundary conditions should be specified in proper grid cells.
4. For hydrodynamic models, the parameter determining the bottom friction, such as the bottom roughness height in Eq. (2.2.31), is often the most adjusted in model calibration.
5. The time step for integration should be small enough to ensure computational stability.
6. Unless a model uses a wetting and drying scheme (e.g., Ji et al., 2001 and Section 10.5.2), the water depths of the model cannot be too small. Otherwise, strong wind, evaporation, and/or large tides may cause grid cells dry. The negative (or zero) water depths may lead to computational instability.
7. When the sigma coordinate is used in a model, high horizontal grid resolution is needed in areas with rapidly varying bathymetry. Otherwise, the sigma coordinate may introduce extra errors into the model result.
8. In a sigma coordinate model, the depth of each vertical layer changes with time, as the water surface fluctuates. This is especially important when conducting modal–data comparison in shallow areas with strong tides, where the thickness of each sigma layer can change largely with time.

2.4.1 Hydrodynamic Parameters and Data Requirements

This section discusses the commonly used hydrodynamic parameters and the data required for setting up a hydrodynamic model.

2.4.1.1 Hydrodynamic Parameters. Even though there can be tens of parameters in a hydrodynamic model, many of them, such as the turbulent parameters of Mellor–Yamada model (Mellor and Yamada, 1982), are usually not adjusted in the model calibration process, unless there are well-justified reasons to do so. Values of model parameters are generally obtained through: (1) direct measurement, (2) estimation from other measured data, (3) literature values, and (4) model calibration.

Model calibration is often required to determine certain key parameter values, regardless of how the initial values are selected. It is essential to set the parameter values, especially those site-specific ones, based on measured data. The parameters that are frequently adjusted in hydrodynamic calibrations include the following:

1. Parameter determining the bottom friction, such as the bottom roughness height in Eq. (2.2.31).
2. Horizontal momentum diffusion coefficient.

The bottom roughness height, z_o^* in Eq. (2.2.31), is probably the one adjusted first and most in hydrodynamic calibration. It represents the bottom roughness of the bed and is frequently set to 0.02 m, with a typical range between 0.01 and 0.1 m. The horizontal momentum diffusion coefficient (also called horizontal eddy viscosity), A_H in Eq. (2.2.7), can be either prespecified or calculated using the Smagorinsky formula (2.2.8). When Eq. (2.2.8) is used, the empirical parameter, C, needs to be specified. As discussed in Section 2.2, the parameter C has typical values between 0.10 and 0.20. The horizontal mass diffusion coefficient (also called horizontal eddy viscosity for mass transport), A_C in Eq. (2.2.9), is usually set to be equal to A_H.

Values of many model parameters may also depend on how they are used in the model. For example, while the horizontal momentum diffusion coefficient, A_H, represents the horizontal turbulence mixing in a waterbody, an appropriate value of A_H for a model is also linked to (1) the dimensionality of the model, (2) model grid resolution, and (3) the numerical scheme of the model. These factors all influence the dispersion process in a numerical model. For a same waterbody, models of 1D, 2D, or 3D may have different values of A_H; higher model grid resolution leads to smaller A_H; and a highly diffusive numerical scheme also contributes to the diffusivity of the model and leads to smaller A_H needed in the model.

During model calibration, model parameters are adjusted to optimize the comparison of model results to measured data. The tuning of model parameters, including the hydrodynamic parameters, is a recursive process. Based on literature review and/or previous modeling studies, the value of a parameter can be selected from a feasible range, evaluated in the model, and adjusted to minimize the differences between the model results and the measured data, which is usually carried out by comparing the model and the data graphically and statistically. Ideally, the range of feasible values is determined by laboratory observation and/or field measurement. In the event that measured values are not available, the feasible range is determined from previous studies or by the professional judgment of the modeler. More discussions on model calibration and verification will be presented in Section 7.3.

2.4.1.2 Data Requirements. Hydrodynamic modeling, especially 3D and time-dependent modeling, requires comprehensive data sets for model set up, calibration, and verification. The measured data are used to

1. Determine the type of model application required (e.g., dimensionality, time dependency, and state variables).

2. Set up inputs to drive the model (e.g., bathymetry, winds, external loadings, inflows, and open boundary conditions).
3. Provide a basis for adjusting model parameters (model calibration).
4. Evaluate if the model adequately describes the waterbody (model verification).

Data used in models need to be as accurate as possible. The famous adage is "garbage in, garbage out". While models can be run with minimal data, their results are subject to large uncertainty. Limited data limits the applicability of a model. This cannot be stressed enough: there is no substitute for measured data from the field. Data sampling plans should be designed with model requirements in mind. Each surface water system is unique. The data requirement for a particular study is determined by the characteristics of the system, the hydrodynamic processes, and the time and spatial scales of interest. To a large degree, the quantity and quality of the data determine the confidence that can be placed on the model application. Uncertainties in external driving forces, such as winds and inflow rates, propagate in model results. If the data used for model setup and calibration is not reliable, the model results would not be reliable either, no matter how well the model had been applied to other studies before. Therefore, whenever possible, the modeler should be familiar with how the field data are measured, the type of instruments used, the conditions under which the data were obtained, and how the raw data are processed. The field data should not be considered as perfectly accurate. Internal consistency of field data should always be checked.

To set up inputs to a hydrodynamic model, the following data are often needed (1) bathymetry and shoreline, (2) inflows and outflows, (3) meteorological data, and (4) data for specifying open boundary conditions. Accurate information on the bathymetry and shoreline is a primary requirement. They are needed to set up the model grid and to define the model domain. The model grid affects the model's ability to define sharp thermal gradients and needs sufficient longitudinal/vertical resolution. Bathymetry is the term commonly used for the measurement of water depth. Bathymetry means "depth measures" in Greek and is essentially identical to the word topography used to describe elevation, such as hills and valleys on land. The bathymetry of a waterbody changes over time, largely by processes of sediment deposition and resuspension. Such changes can take place rapidly through large discharges from tributaries or by severe storms. Water depths may greatly affect water temperature simulation. Water depth in a model should be at least as deep as the observed data, so that the model–data comparison of water temperature can be conducted.

Accurate inflow and outflow information is desirable for all modeling studies. They are especially critical for waterbodies with short residence times or during high inflow periods. Inflows and outflows include the flows at upstream boundaries of all tributaries, lateral inflows from groundwater or runoff, and flow diversions. If wastewater discharges represent a significant portion of the total

inflow, they should be included in the model. Significant outflows, such as water taken as coolant by a power plant, should also be specified. A substantial amount of inflow can be unaccounted for when only using gauged inflows (e.g., Ji et al., 2007a). To estimate the missing inflows, a hydrologic model might be needed to determine inflows during storm events. Evaporation can be the most important component of water loses in a waterbody, especially in large, subtropical lakes. For example, evaporation accounts for >50% of the total water loss of Lake Okeechobee, FL (AEE 2005). Seepage gains or losses should also be considered when they are significant. For inflows from shallow streams, the air temperature is sometime used as the inflow temperature, in the event that measured water temperature data are unavailable.

Meteorological data include (1) wind speed and direction, (2) air temperature, (3) solar radiation, (4) precipitation, (5) cloud cover, (6) humidity, and (7) atmospheric pressure. To simulate the diurnal and seasonal variations of a waterbody, ideally, the meteorological data should have hourly (or shorter) time intervals. For example, mixing in a reservoir is often driven by wind forcing and heat exchange between the water and the atmosphere. Equations (2.1.40) and (2.1.41) show that the wind energy input is a function of the wind speed cubed. A daily averaged wind speed can be much less than the hourly wind speeds and result in much less wind energy input. Daily average also eliminates diurnal variation of the air temperature, resulting in damped diurnal variations in the reservoir. A common source of meteorological data is weather stations. However, when the weather stations are located in different terrain and at large distances from the study site, it can be a challenge to extrapolate meteorological data at these weather stations to the study site. Methods for addressing these problems include use of an alternative weather station, averaging data from several weather stations, and separating a waterbody into regions applying data from different meteorological stations (Cole and Wells, 2000).

The performance of a model is a graphical and qualitative measure of the degree to which the model faithfully reproduces the measured data. Calibration data are used to provide initial and boundary conditions and to assess model performance during calibration. Verification data are another independent set of measured data not used in calibration and are utilized to provide an independent check on model performance. The model state variables that are often used in hydrodynamic model calibration and verification include (1) surface water elevation, (2) velocity, (3) temperature, and (4) salinity. Measured data of these variables are needed inside the model domain for model calibration and verification. They are also needed on open boundaries.

Data needed for the hydrodynamic and water modeling can be acquired from a host of databases. In the United States, large databases are often supported and maintained by government agencies, including

1. The Unites States Environmental Protection Agency (EPA).
2. National Oceanic and Atmospheric Administration (NOAA).

3. United States Geological Survey (USGS).
4. United States Army Corps of Engineers (USACE).
5. State and local government agencies.

A convenient way to have updated information on these databases is by searching their websites. This book will not discuss these databases.

Based on the data availability inside the study domain and on the open boundaries, it is necessary to determine a time period for model calibration and a time period for model verification. It is ideal that the periods have

1. Continuous observation data at boundaries.
2. Good observation data inside the model domain that can be compared with model results.
3. Different environmental conditions, for example, a dry period for calibration and a wet period for verification.
4. Complete meteorological data.

The hydrodynamic data mentioned here are the ones that a hydrodynamic model can use in a modeling study, so it is like a "wish list". Practically, available data in a particular study are often less comprehensive. Theoretical and/or empirical methods are often needed to fill up the gaps of missing data.

2.4.2 Case Study I: Lake Okeechobee

Lake Okeechobee is a large, shallow subtropical lake, located in south Florida (Fig. 2.4.2). The lake has an area of 1730 km^2, with a mean depth of only ~3.2 m and a maximum depth of <6.5 m. There are many large lakes (with a surface area >500 km^2) in the world. Thirty-seven percent (37%) of them have mean depths <5 m and 52% of them have mean depths <10 m (Herdendorf, 1984). These large and shallow lakes are strongly influenced by physical forcing functions, such as wind–wave effect. Thus, results from the studies on Lake Okeechobee can be useful for understanding processes in other large, shallow lakes.

The modeling of Lake Okeechobee is the most comprehensive EFDC model application conducted so far. It took years of effort to reach this stage that the model can be used to simulate the lake with confidence. There are few published studies that have taken such solid steps/approaches to model large, shallow lakes. A series of related papers have been published (Jin and Ji, 2001, 2004, 2005; Ji and Jin, 2006; Jin et al., 2000, 2002, 2007). What accompanying the modeling studies are a series of field data sampling studies (SFWMD, 2002). These field sampling studies are designed for and tailored to the model calibration, verification, and validation. Consequently, the modeling efforts were supported by a comprehensive data set for model setup, external loadings, and model calibrations, verification, and validation. These parallel

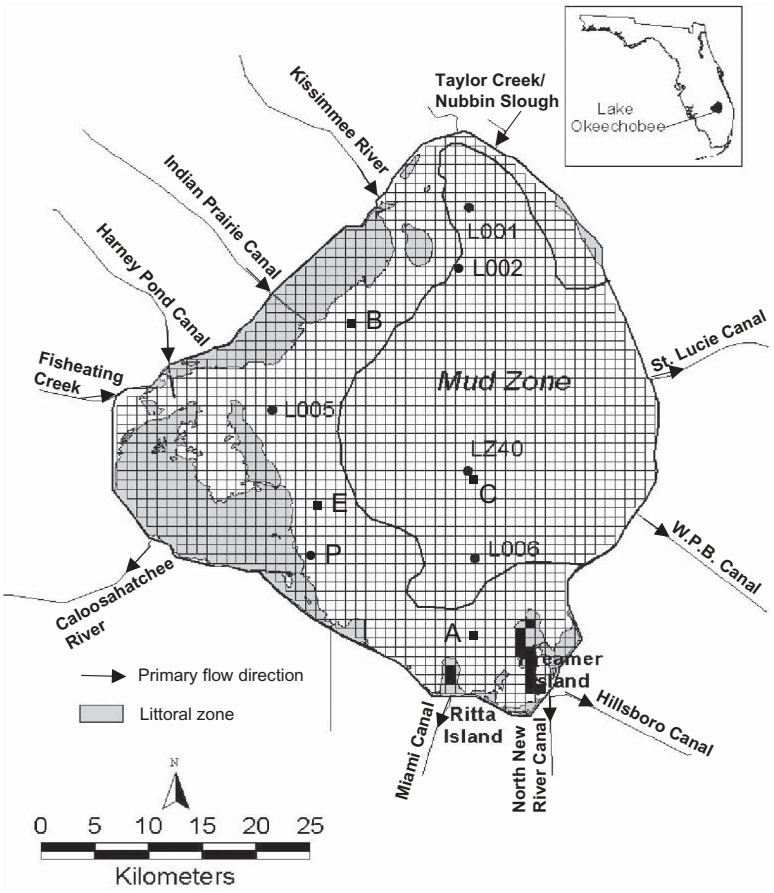

Fig. 2.4.2 Lake Okeechobee, the Lake Okeechobee Environmental Model (LOEM) grid, data sampling stations, and major inflows–outflows.

efforts of modeling and field sampling are well coordinated and well prepared for the development of tools for the understanding and managing the water resources and ecosystem in the lake. These efforts provide unique and excellent examples for demonstrating the modeling of hydrodynamics, wind wave, sediment process, water quality, and SAV in surface waters.

Based on these studies, Lake Okeechobee and its modeling are used as case studies in this book. The modeling of Lake Okeechobee is covered in the following subsections:

1. Hydrodynamic processes and their modeling (this section).
2. Wind wave modeling (Section 3.6.5).
3. Sediment modeling (Section 3.7.2).

4. Water quality and SAV modeling (Section 5.9.2).
5. Application of power spectral analysis (Section 7.2.3).
6. Application of empirical orthogonal function analysis (Section 7.2.4).
7. Applications of the model for lake management (Section 9.4.2).

The modeling approaches, the analysis methods, and the discussions on processes in these case studies are useful for a reader to conduct his own modeling study on similar waterbodies. This is a primary objective of presenting these case studies. A set of input and output files of the LOEM, which is developed based on the EFDC model, is included in the modeling package, so that the files can be used as a template for other modeling studies. Also enclosed in the modeling package are the source code and the executable code of LOEM.

2.4.2.1 Background. The physical, chemical, and biological characteristics of Lake Okeechobee have been extensively documented (e.g., Aumen, 1995; James et al., 1995a, 1995b; Havens et al., 1996, 2007; Steinman et al., 2002). Therefore, only a brief overview is provided here.

Lake Okeechobee was originated ~6,000 years ago during oceanic recession. In the Seminole Indian language, "Okeechobee" means "Big Water". This is an appropriate name for this third largest lake wholly within the United States, after Lake Michigan and Alaska's Iliamna Lake. Lake Okeechobee links the Atlantic and Gulf sides of Florida via the St. Lucie Canal on the east side of the lake and the Caloosahatchee River on the lake's west side (Fig. 2.4.2). South Florida's climate is subtropical and humid, with average annual rainfall between 1 and 1.7 m. More than one-half of the rainfall occurs in the wet season, which is June–September.

Lake Okeechobee is a major component of the Kissimmee–Okeechobee-Everglades hydrologic system. Numerous canals and streams are connected to the lake (Fig. 2.4.2), with water normally entering from tributaries to the north and leaving through canals to the east, west, and south. In 1926 and 1928, hurricane waters destroyed the dikes on the lake's southern edge, which resulted in thousands of deaths. The lake is now encircled by a flood control dike built from 1930s to 1960s and currently has a storage capacity of ~4 billion m^3 of water. Today, the U.S. Army Corp of Engineers (USACE) and the South Florida Water Management District (SFWMD) direct the waters via dikes, canals and floodgates in order to protect against flooding, to prevent saltwater intrusion, and to provide water for agricultural irrigation and drinking water supplies to large urban areas in south Florida. Except for Fisheating Creek, all canal and stream discharges are regulated by flow control structures (e.g. gates, pumps, culverts, and locks) according to a USACE flood control schedule.

Over the last several decades, Lake Okeechobee has experienced accelerated eutrophication due to excessive phosphorus loads from agricultural

runoff (Havens et al., 1996). Much of these excessive loads have accumulated in the lake sediments. Recycling of phosphorus from bottom sediments through resuspension is critical to the lake eutrophication (James et al., 1997). Because sediment resuspension in Lake Okeechobee is impacted by lake-wide circulation patterns and wind–wave action (Sheng, 1991; Mei et al., 1997), a clear understanding of the lake hydrodynamics is required. The accuracy of predicted circulation patterns directly affects the accuracy of predicted phosphorus concentrations. The circulation patterns are influenced by wind, temperature, inflows, outflows, and the Coriolis force. Inflows and outflows have only localized effects, due to the lake's large surface area. As with other large, shallow lakes, wind is the major driving force, with temperature also being important. The lake is well mixed most of the time. However, thermal stratification can be observed, when the wind diminishes.

The objective of this case study is to demonstrate the calibration and verification of the 3D hydrodynamic submodel of the LOEM model and how to use the model to better understand the lake hydrodynamics. The LOEM model included the following periods for calibration, verification, and validation:

1. Calibration: October 1, 1999–September 30, 2000.
2. Verification: October 1, 2000–September 30, 2001.
3. Validation: October 1, 2001–October 30, 2002.

For simplicity, only the model calibration results are presented here. The discussions on model verification and validation are referred to the published papers (Jin and Ji, 2004, 2005; Ji and Jin 2006; Jin et al., 2000, 2002).

2.4.2.2 Data Sources. The data needed in a numerical model are generally in two categories: the input data for setting up the model and the data in the study domain for model–data comparison. A 1-year calibration of the lake hydrodynamic model covered the period from October 1999 to September 2000. The simulated parameters include water depth, current, and water temperature. The bottom of the lake is relatively flat (Fig. 2.4.3). The lake is deepest in its east-central region, and shallowest to the south, west, and northwest. An extensive littoral zone exists in the shallowest areas (Fig. 2.4.2). External forcings included (1) wind velocity, (2) solar radiation, (3) rainfall, (4) lake inflows/outflows, (5) inflow/outflow temperatures, (6) air temperature, and (7) relative humidity.

Rainfall, air temperature, relative humidity, and solar radiation data were collected every 15 min at four in-lake stations shown in Fig. 2.4.2, that is, LZ40, L001, L005, and L006. Station LZ40, shown in Fig. 2.1.6, is located near the center of the lake. Hourly averaged meteorological data at LZ40 are used in the LOEM model. The meteorological data from the other three stations have values similar to the ones of LZ40. Model sensitivity tests indicated that

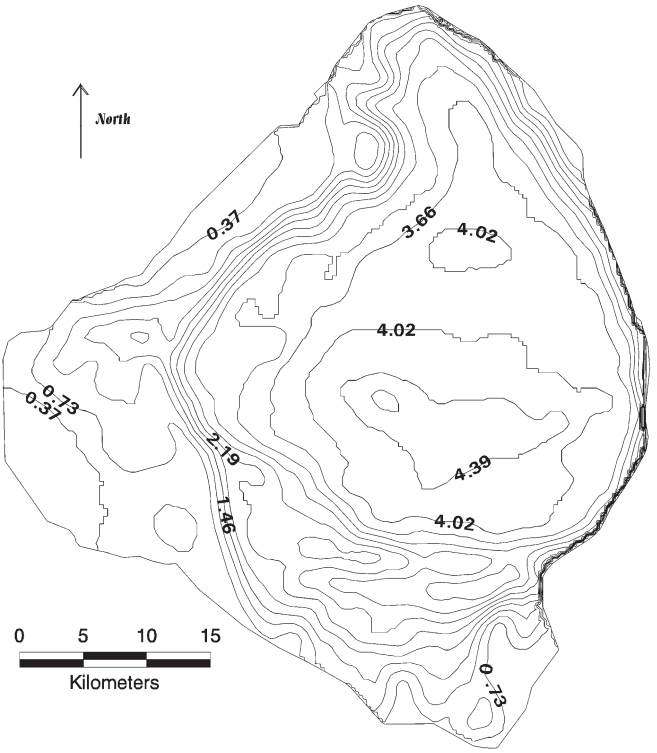

Fig. 2.4.3 Lake Okeechobee bathymetry (unit in meters) (SFWMD, 2002).

using the data from the other three meteorological stations did not change model results significantly. Tributaries include 25 inflows and outflows of the lake. Their daily flow rates are measured by the USACE and SFWMD. The major ones are shown in Fig. 2.4.2.

The wind velocity at LZ40 between October 1, 1999 and September 30, 2000 is already given in Fig. 2.1.7. The corresponding air temperature and solar radiation are also shown in Figs. 2.1.8 and 2.3.6, respectively. Figure 2.4.4 is the total inflow (solid line) and the total outflow (dashed line) of the lake between October 1, 1999 and September 30, 2000. Fig. 2.4.4 indicates that during the period of lake recession in May 2000, large amount of water was discharged out of the lake to lower the lake's water level for lake management purposes.

The data used for model calibration are water surface elevation, water temperature, and water velocity. Available 15-min surface water elevations were collected at stations LZ40, L006, L001, and L005. Velocity profile data were collected every 15 min by Acoustic Doppler Current Profilers (ADCP) at these four stations for 48 days, from 1/18/2000 to 3/5/2000.

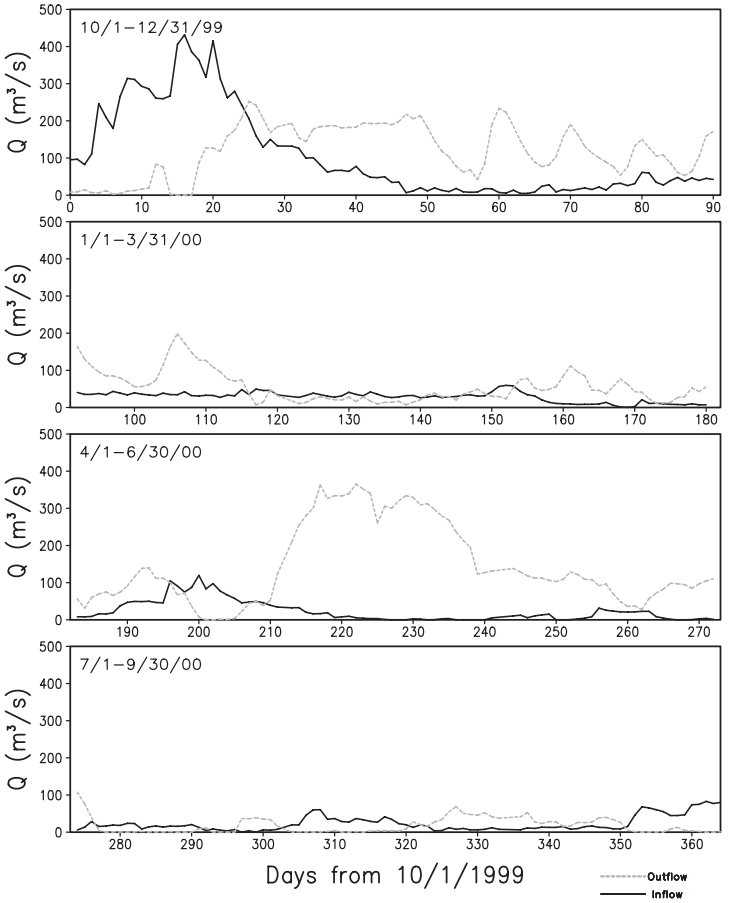

Fig. 2.4.4 Measured total inflow (solid line) and total outflow (dashed line).

2.4.2.3 Model Setup. The LOEM is developed based on the EFDC (Hamrick, 1992). The general theories of the EFDC hydrodynamic model are already covered in previous sections of this chapter. Additional information on the EFDC model is given in Appendix A.

Although the EFDC model is coded under a general orthogonal-curvilinear coordinate system, Cartesian coordinates were considered sufficient for the lake, given its relatively simple shape. The computational grid had 58×66 horizontal cells and 2123 active water cells (Fig. 2.4.2). The grid cells have sizes of 912×923 m. For this large and shallow lake with very flat topography, the horizontal grid is generally sufficient to resolve the hydrodynamic processes in the lake. The initial water depth in each grid ranges from 0.2 m in the shallow region to 4 m in the deep central region. A time step of 200 s was used

throughout the simulation. Approximately 1 CPU hour was required for a one-year hydrodynamic simulation on a 3.6 Ghz Pentium IV PC.

Applying a sigma coordinate to water systems with very steep bathymetry might cause undesirable spurious circulation (Mellor et al., 1998); however, Lake Okeechobee should be an ideal case study for using a sigma coordinate, because the lake's bathymetry is quite uniform with slopes <0.001 (Jin et el., 2000). With mean value of 3.2 m, the lake depths vary from 0.5 to 5.5 m during the simulation period. Numerical tests indicated that for this shallow lake, five equally spaced vertical layers in the model were generally sufficient to resolve the vertical structure of the lake. Model sensitivity tests using 10 vertical layers yielded results similar to the ones of the five-layer model. Except for special statement, all modeling results of Lake Okeechobee presented in this book are from the five-layer model.

Initial conditions were set for water depths, flow velocities, and water column and lake bed temperatures. Depths were based on Richardson and Hamouda (1995) bathymetry data (Fig. 2.4.3), and velocities were set to zeros at the beginning of the simulation. Water column and lake bed temperatures were initialized to 26.7 °C. Because these values only approximated actual initial conditions, a model warm-up period of a few days was required. Sensitivity tests indicate that this large, shallow lake reaches equilibrium with external forgings within a few days.

The LOEM model considered vegetation resistance in the littoral zone of the lake (Fig. 2.4.2). Bottom roughness varies depending on sediment type and vegetation. In the western littoral zone of the lake, bottom roughness and vegetation resistances range from 0.02 to 0.1 m to simulate the effects of emergent and submergent plants and irregularities in bottom depth. In the mud zone of the lake, the bottom is assumed to be hydraulically smooth, while the remaining portion of the lake has a roughness height of 0.02 m (Jin and Ji, 2004).

In the littoral zone, the roughness height is calculated based on the study of Moustafa and Hamrick (2000). Sensitive analysis and tests were conducted to analyze the effects of bottom roughness height on the hydrodynamic results of this study. It was concluded that the model results are insensitive to the bottom roughness change in the littoral zone because flow velocities are very small in the littoral zone due to the resistance of vegetation (Jin et al., 2000).

2.4.2.4 Model Calibration. With its mean depth of 3.2 m, Lake Okeechobee is primarily driven by wind and has a spin-up period of a few days. The model outputs included time series of water surface elevation, horizontal current components, and water temperature at 1-h intervals at locations corresponding to the field observations. The period of model calibration is 365 days, between October 1, 1999 and September 30, 2000.

To quantify the model's prediction of each variable, statistical analyses were used to compare simulated versus observed values for water surface elevation, water temperature, and velocity. Statistical analyses included the mean error, mean absolute error, root-mean-square (RMS) error, maximum absolute

error, and the relative RMS error (RRE). Section 7.2.1 gives the details of the statistical analysis methods. The average of the RRE of water depth, current, and water temperature are 3.07% (Table 2.4.1), 15.80% (Table 2.4.2), and 9.18% (Table 2.4.3), respectively.

Lake Okeechobee displays seasonal variations in water level, caused primarily by changes in precipitation input to the watershed, water evaporation, and the regulation schedule of the USACE. In the middle of October 1999, a Category I hurricane (Irene) passed by south Florida, generating wind speeds up to 23 m/s around Lake Okeechobee. A time series of simulated and observed

TABLE 2.4.1 Error Analysis of Observed and Modeled Water Depth at Four Stations from 10/1/1999 to 9/30/2000

Station	Obs. Mean (m)	Modeled Mean (m)	Mean Abs. Error (m)	RMS Error (m)	Obs. Change (m)	RRE (RMSE ÷ Data Range) (%)
L006	3.814	3.839	0.039	0.049	1.853	2.624
L001	3.881	3.909	0.040	0.050	1.498	3.306
LZ40	4.500	4.505	0.028	0.034	2.184	1.573
L005	3.379	3.407	0.039	0.045	0.935	4.775

TABLE 2.4.2 Error Analysis of Observed and Modeled Horizontal Currents in the East–West Direction (U) and in the North–South (V) Direction from 1/18/2000 to 3/5/2000[a]

Station	Obs. Mean (cm/s)	Modeled Mean (cm/s)	Mean Abs. Error (cm/s)	RMS Error (cm/s)	Obs. Change (cm/s)	RRE (RMSE ÷ Data Range) (%)
L006_UB	–0.06	0.57	2.66	3.39	17.9	18.95
L006_VB	1.06	0.67	1.93	2.47	21.1	11.71
L006_US	0.34	1.11	3.68	4.57	25.1	18.21
L006_VS	0.33	0.54	2.72	3.50	34.0	10.29
L001_UB	0.24	–0.96	2.00	2.68	15.0	17.88
L001_VB	0.96	0.37	2.14	2.76	19.3	14.29
L001_US	–0.82	–1.79	2.84	3.83	27.9	13.73
L001_VS	–1.04	0.36	3.24	4.54	24.8	18.32
LZ40_UB	–0.12	–1.25	2.34	2.91	22.5	12.95
LZ40_VB	0.44	1.69	2.66	3.33	24.6	13.52
LZ40_US	–1.05	–2.45	2.58	3.30	23.0	14.36
LZ40_VS	–0.33	2.86	4.31	5.17	21.5	24.04
L005_UB	–0.12	–0.26	1.93	2.50	18.4	13.58
L005_VB	0.00	0.57	2.12	2.70	18.2	14.82
L005_US	–0.26	–0.57	2.27	3.02	19.7	15.35
L005_VS	0.09	0.95	3.42	4.22	20.3	20.79

[a]The bottom layer (B) is located at ~10% of total depth above the lake bed and the surface layer (S) is located at ~90% of total depth above the lake bed.

TABLE 2.4.3 Error Analysis of Observed and Modeled Water Temperature from 10/1/1999 to 9/30/2000[a]

Station	Obs. Mean (°C)	Modeled Mean (°C)	Mean Abs. Error (°C)	RMS Error (°C)	Obs. Change (°C)	RRE (RMSE ÷ Data Range) (%)
L006_S	23.68	22.93	1.63	2.09	26.65	7.83
L006_M	23.45	22.88	1.21	1.53	20.79	7.38
L001_S	17.84	18.27	1.05	1.51	14.17	10.67
L001_M	17.49	17.88	1.01	1.31	12.24	10.67
LZ40_S	22.64	22.94	1.74	2.14	24.32	8.79
LZ40_M	23.42	22.87	1.13	1.36	20.86	6.52
L005_S	21.98	22.98	2.47	3.07	29.26	10.49
L005_M	21.47	22.90	1.81	2.23	20.13	11.07

[a]Measured water temperature located at ~17% (*S*, surface layer) and 40% (*M*, middle layer) of total depth above lake bed.

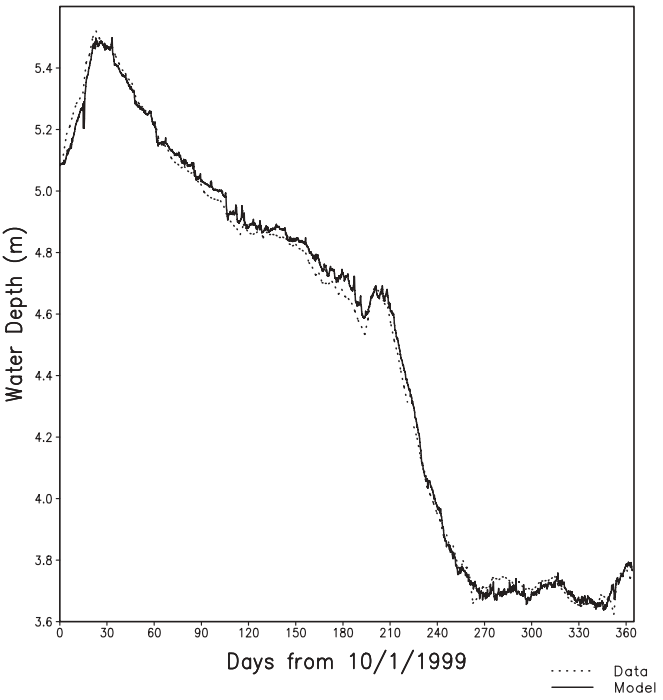

Fig. 2.4.5 Observed (dotted line) and modeled (solid line) water depths at LZ40.

water level at sample station LZ40 (Fig. 2.4.5) shows that the model results match the trend and dynamics of the observed data. In the spring of 2000, the lake levels were lowered in a managed recession to enhance the submerged aquatic vegetation in the lake and to improve the water quality. Figure 2.4.4

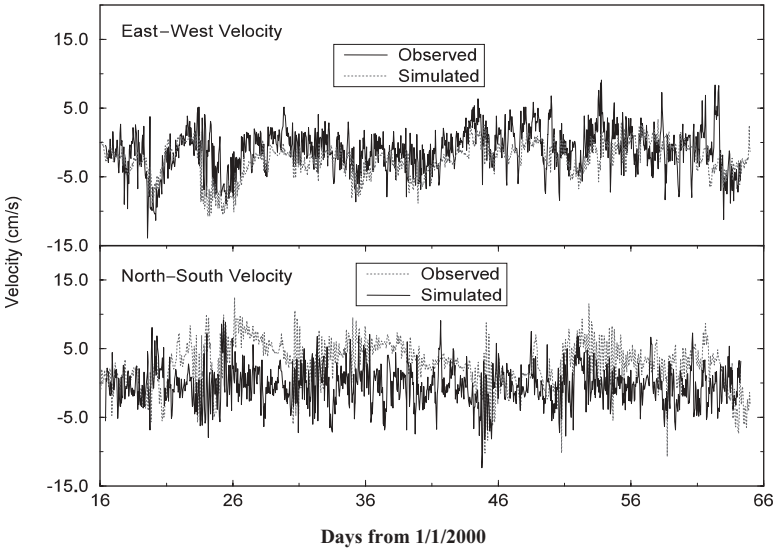

Fig. 2.4.6 Observed (dotted line) and simulated (solid line) surface currents at LZ40 for 48 days, from 1/18/2000 to 3/5/2000.

shows that large amount of water were discharged out of the lake in May and June of 2000. This managed recession was followed by a severe drought. Table 2.4.1 shows that the mean absolute errors of the modeled water depths are ~0.028–0.040 m, and the root-mean-square errors range from 0.034 m to 0.050 m, and the average RRE is 3.07%. Both Table 2.4.1 and Fig. 2.4.5 indicate that although the lake level changed dramatically during this period, the model accurately reproduced lake levels through the recession and drought period.

Figure 2.4.6 presents the observed and simulated surface current at LZ40 for 48 days, from 1/18/2000 to 3/5/2000. This is the period that the measured currents data are available. The corresponding results of the bottom currents are shown in Fig. 2.4.7. The statistical results are already given in Table 2.4.2. Graphical comparisons indicate that the model reproduced general trends at station LZ40. Many short-term fluctuations also are reproduced, although errors exist. In general, agreement between observed and simulated data is good.

Figure 2.4.8 gives the observed and simulated water temperature at LZ40 for 48 days, from 1/18/2000 to 3/5/2000, the same period as the ones in Figs. 2.4.6 and 2.4.7. Table 2.4.3 gives the statistical results. The model reasonably represented water temperature at eight sampling depths at the four lake stations. The LOEM captured the major variance of water temperature both in the middle and the surface layers in the lake, as shown in Fig. 2.4.8. Due to sensor failure, the period used for model-data comparison at station L001 was from November 19, 1999 to May 10, 2000 and was shorter than the data periods

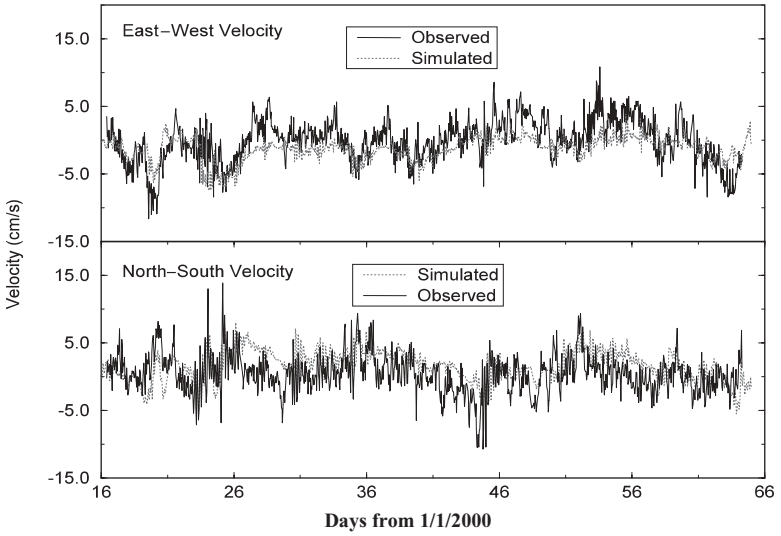

Fig. 2.4.7 Observed (dotted line) and simulated (solid line) bottom currents at LZ40 for 48 days, from 1/18/2000 to 3/5/2000.

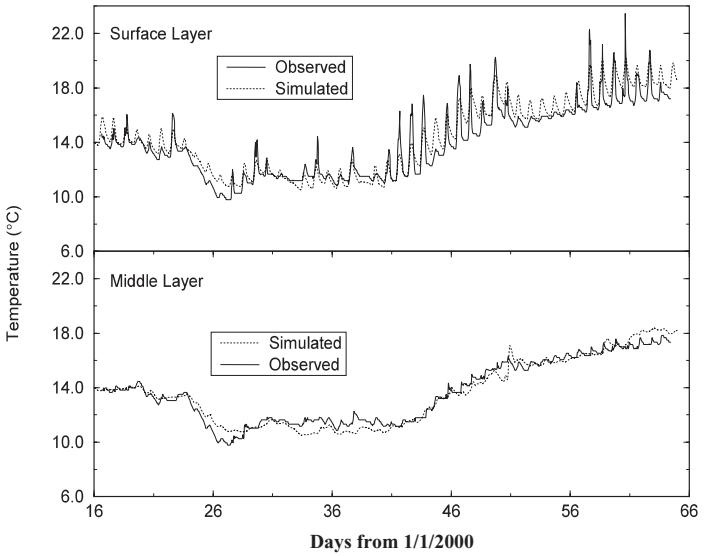

Fig. 2.4.8 Observed and simulated water surface temperatures at LZ40 for 48 days, from 1/18/2000 to 3/5/2000.

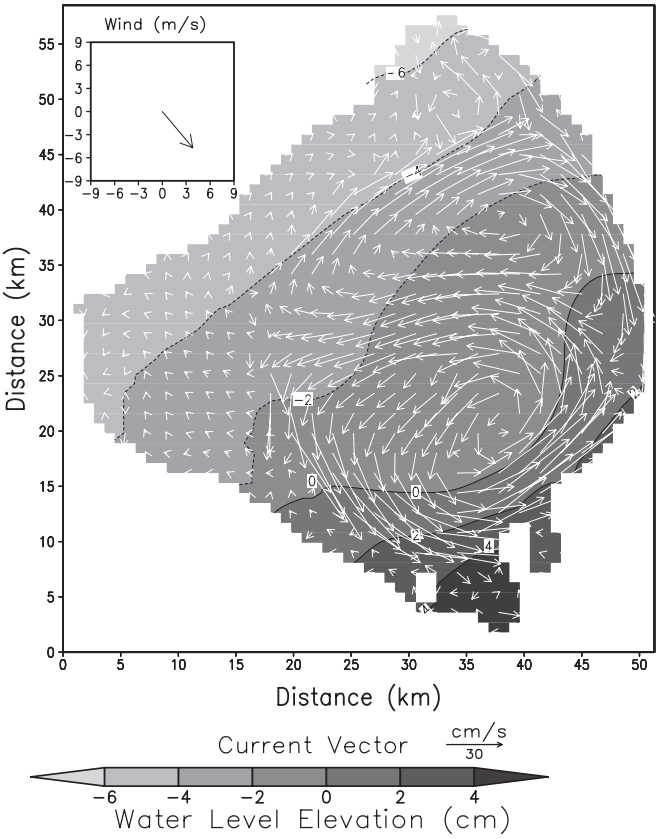

Fig. 2.4.9 Simulated surface current velocity and the water level elevation on January 21, 2000. The water level elevation is the difference between the present surface water elevation and the initial surface water elevation.

of the other stations. Thus the mean temperatures at L001 are much lower than the ones at the other three stations (Table 2.4.3). In general, the simulated water temperatures also agree with observed data very well.

Figure 2.4.9 shows the simulated surface current velocity and the water level elevation on 1/21/2000. The water level elevation is the difference between the present surface water elevation and the initial surface water elevation and is a good indicator of water surface elevation changes. The initial surface water elevation at the beginning of the simulation is set to be uniform. Figure 2.4.9 shows a surface water elevation difference (up to 12 cm) caused by the consistent northwest wind in the lake. The simulated bottom circulation patterns are similar to the surface ones shown in Fig. 2.4.8, but have smaller velocities. Figure 2.4.9 reveals that there are two gyres in the lake: one in the north and one in the south. The current speed of the two gyres varies from <2 to >30 cm/s. The two gyres form a dominant circulation pattern in the lake and play a

significant role in the hydrodynamic, sediment transport, and water quality processes in the lake. Statistical analysis on the two gyres will be presented in Section 7.2.4. Formation mechanisms of the two gyres will be discussed in Section 9.2.4.

2.4.2.5 Hydrodynamic Processes in the Lake. After the successful calibration, verification, and validation of the LOEM, the model was applied to investigate hydrodynamic processes in Lake Okeechobee (Jin and Ji, 2004, 2005; Ji and Jin 2006; Jin et al., 2000, 2002).

Wind-driven current. Wind is the dominant factor driving the lake currents. With mean volume of 4 billion m^3 and annual inflow of $50\,m^3/s$, the lake has a hydraulic retention time of 2.5 years. These features make the influences of lake inflows and outflows secondary. Modeling tests also confirm this phenomenon.

In Lake Okeechobee, the most important driving force for lake currents and surface water elevation gradient is wind stress. Under most meteorological conditions, wind stresses determine the variations of the currents and water surface elevation gradient in the lake. A flat water surface elevation is assumed at the beginning of the run. During the 365 days of simulation, the variation of water surface elevation gradient is dominated by the wind stresses. For example, a strong northwest wind established surface water elevation gradients with the highest elevation at the southeast corner and the lowest at the northwest corner on 1/21/2000 (Fig. 2.4.9). The elevation difference was >12 cm. This is a typical example showing how wind influences the lake surface water elevation and current patterns.

Geostrophic current. In shallow lakes, the motion and mixing of waters are often dominated by wind. However, secondary driving forces, such as Coriolis force and inflow/outflow, may also affect shallow water dynamics during calm wind periods. An interesting current pattern in Lake Okeechobee is the geostrophic current. Because the lake is located at 27 °N and is with a spatial scale of >50 km and a surface area of ~1730 km^2, the Coriolis force may become an important factor in determining the flow patterns and the water surface elevation, when the wind is calm.

As stated in Section 2.1.6, the geostrophic current is formed when the Coriolis force and pressure gradient reach a balance, which can be derived from Eqs. (2.1.45) and (2.1.46) as

$$fv = g\partial\eta/\partial x \tag{2.4.1}$$

$$fu = -g\partial\eta/\partial y \tag{2.4.2}$$

where η is the surface water elevation. The Coriolis parameter, f, is equal to 6.62×10^{-5}/s in Lake Okeechobee area.

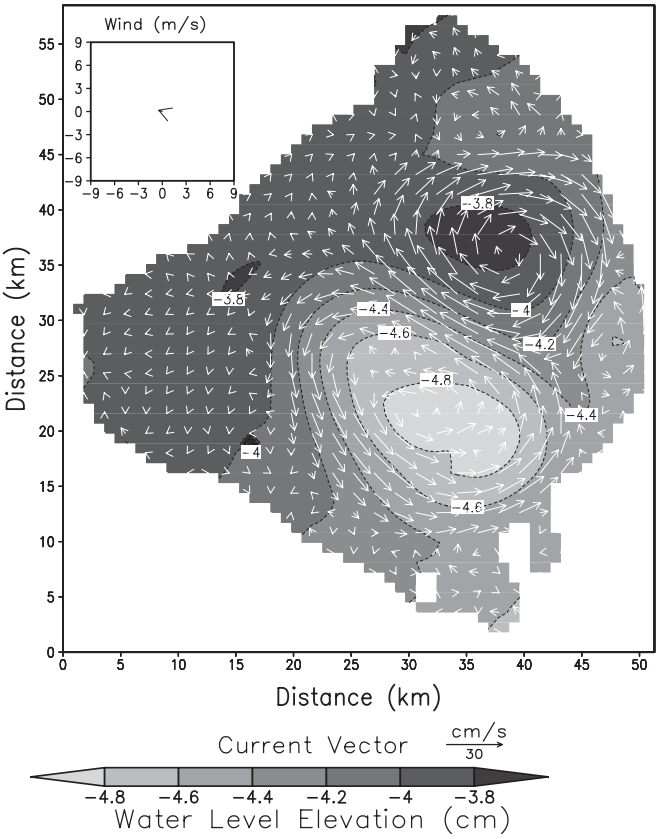

Fig. 2.4.10 Simulated surface current velocity and water level elevation on 1/30/2000.

The geostrophic balance was achieved on 1/30/2000 with wind speed less than 0.2 m/s (Fig. 2.4.10). Two gyres formed in the lake, one in the south and one in the north. The south gyre had a low water elevation center of –6.0 cm, created by a cyclonic current pattern. The north gyre had a relatively high water elevation of –3.7 cm and formed a typical anticyclone. The corresponding circulation patterns in the bottom layer are similar to the surface ones. The two gyres lasted ~2 days. Numerical calculations show that the values of the Coriolis force (fu and fv) were the same order of magnitude as the pressure gradient terms ($g\,\partial h/\partial x$ and $-g\,\partial h/\partial y$). For example, by taking typical values of $v = 0.15$ m/s, $g = 9.8$ m/s^2, $\Delta h = 0.024$ m, and $\Delta x = 24$ km, it yields $fv = 9.83 \times 10^{-6}$ m/s^2 and $g\partial\eta/\partial x = 9.80 \times 10^{-6}$ m/s^2. It means that under the conditions shown in Fig. 2.4.10, the Coriolis force term (fv) and the water elevation gradient term ($g\partial\eta/\partial x$) are approximately in equilibrium. These gyres are clear indications that at times of calm wind, geostrophic currents can be formed in

the lake and the Coriolis force can be a significant factor in determining the circulation pattern.

It should be pointed out that the strong currents shown in Fig. 2.4.10 are the residual circulations from the previous wind-forcing events. Strong or moderate winds induce circulations in the lake. When the wind speed is suddenly reduced, the remaining currents can readjust and reach a geostrophic equilibrium with the surface water elevation gradient, as shown in Fig. 2.4.10. Since the lake is shallow, the geostrophic flow can last no more than a few days, before the lake bottom friction slows down the currents significantly.

Thermal stratification. Jin et al. (2000, 2002) observed large diurnal thermal gradients in the early summer of 1989. The strong diurnal thermal stratification also occurred in the winter of 2000. Diurnal thermal gradients at station L001 were most pronounced during the afternoons, with little or no wind, as shown in Fig. 2.4.11. The temperature difference between surface and bottom layers reached 8.6 °C at 3:00 pm on 2/12/2000. Strong diurnal thermal gradients could create a density barrier that reduces vertical mixing and turbulence under calm wind situations. Low wind stresses impacted only the surface layer of the water column on this day. When wind speeds intensified after 5:00 pm, the vertical transport of momentum and energy increased dramatically between surface and bottom layers, reducing the temperature gradient and allowing mixing of the water column.

Although temperature data suggested that mixing in Lake Okeechobee also can be limited in shallower near-littoral areas, current velocity data showed

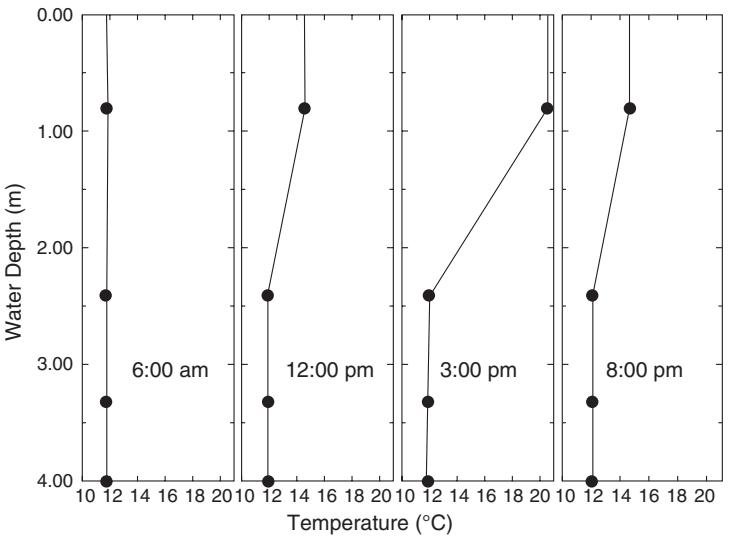

Fig. 2.4.11 Temperature profiles in Lake Okeechobee at L001 on 02/12/2000. From Jin et al. (2002). (Reprinted by permission of American Society of Civil Engineers.)

that mixing generally increases as water depths decrease. In general, vertical mixing is low when wind stresses are low, and strong wind events are required to mix the entire water column in the lake's deeper areas. When the stratification separated a well-mixed warm region from the cold undisturbed region, and generated a vertical density gradient, it prevented the vertical transport of momentum and energy.

Simulated temperature profiles also demonstrated a diurnal cycle of stratification and mixing (Fig. 2.4.8). As shown in Fig. 2.4.8, the temperature difference between surface and bottom layers can reach 8 °C or 2.5 °C/m at LZ40. Strong diurnal thermal gradients can create a density barrier that reduces vertical mixing under calm wind conditions. Typically, early in the day, the water column was well mixed. As the day progressed, surface heating caused the top layer to warm, and a thermocline developed. Initially, afternoon wind stresses lacked sufficient energy and duration to mix the entire water column, but eventually mixing occurred in the later afternoon and in the evening. In addition to water temperature, as what will be discussed in Chapter 3, a high concentration of suspended solids can also enhance the vertical stratification by changing the sunlight absorption and water density profile in the water column.

2.4.2.6 Discussions and Conclusions. This case study presents a 3D hydrodynamic model for Lake Okeechobee (the LOEM model), FL. Conclusions from this modeling study include the following:

1. The LOEM model simulates water surface elevations, velocities, and temperatures with reasonable accuracy.
2. The lake has relatively uniform water depths in the open water areas and the localized bathymetry irregularities are small, which enables the LOEM with grid resolution of 912 × 923 m to represent the hydrodynamic processes reasonably well.
3. Like many other large, shallow lakes in the world, Lake Okeechobee is primarily driven by wind. Wind is the major driving force of horizontal and vertical water movement. Air temperature and solar radiation affect the lake thermal balance. The meteorological data used to drive the LOEM is directly measured on the lake and is able to present the forcing conditions realistically. Tributary inflows and outflows have only local impacts on lake hydrodynamics.
4. The circulation patterns for the top and bottom layers of the lake in high wind events are similar. High wind results in a de-stratification of the lake in most instances. Under low wind conditions, it appears that the Coriolis force can play a significant role on the hydrodynamic processes in the lake, producing a north cyclonic and south anti-cyclonic circulation.

The LOEM can be used as a tool for quantifying the hydrodynamic characteristics and for examining the transport processes in the lake. It is also

useful for aiding further sediment and water quality studies and for guiding field data collections. Other hydrodynamic features, such as lake seiches and lake gyres, will be analyzed in Section 7.2 using statistical tools, and their mechanisms will be discussed in Section 9.2, where lake hydrodynamic processes are described. As case studies, the sediment modeling of Lake Okeechobee will be presented in Chapter 3, the water quality modeling will be described in Chapter 5, and applications of the LOEM model will be illustrated in Chapter 9.

2.4.3 Case Study II: St. Lucie Estuary and Indian River Lagoon

The St. Lucie Estuary (SLE) is a riverine estuary located on the East coast of south Florida (Fig. 2.4.12). The SLE and Indian River Lagoon (IRL), Florida is one of the most biologically diverse ecosystems in the world (SFWMD, 1999). The SLE/IRL and its modeling are used as case studies to illustrate the hydrodynamic and water quality processes in estuaries and how modeling tools are used for water resources management (Ji et al., 2007a, 2007b; Wan et al., 2007). The case studies and examples include the following:

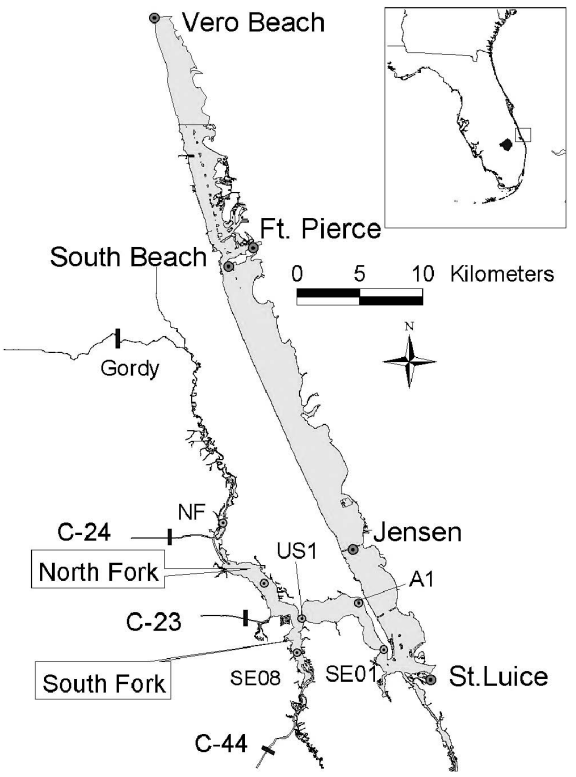

Fig. 2.4.12 The St. Lucie Estuary and Indian River Lagoon, FL.

1. Hydrodynamic processes and their modeling (Section 2.4.3).
2. Heavy metal modeling (Section 4.5.1).
3. Water quality modeling (Section 5.9.3).
4. Stratifications in the SLE (Section 10.3.2).
5. Flushing time in the SLE (Section 10.3.4).
6. Applications of the 3D hydrodynamic and water quality model in the SLE/IRL (Section 10.5.2).

A set of input and output files of the SLE/IRL model is included in the modeling package, which can be used as templates for the modeling of other estuaries.

In this section, the hydrodynamic modeling of SLE is discussed. To illustrate hydrodynamic processes in the estuary, detailed discussions on the model results and the new findings are also presented in this case study.

2.4.3.1 Background. The SLE discharges into the southern end of the IRL, which is connected with the Atlantic Ocean via the St. Lucie Inlet (Fig. 2.4.12). Except for the manmade navigational channel, the IRL is very shallow, with an average depth ~1 m. Because of the restricted connections with the ocean, tidal ranges in the lagoon are often small. The freshwater comes from rivers, canals, surface runoff, and groundwater seepage. The intense solar radiation leads to large evaporation, so that the lagoon may have greater salinity levels than that of the adjacent Atlantic Ocean.

The St. Lucie River is 56-km long and has two major forks: the North Fork and the South Fork (Fig. 2.4.12). The SLE has been highly altered at both its upstream and seaward ends. The system was essentially a freshwater river until 1892, when the St. Lucie Inlet was dredged to provide direct access to the ocean, thus changing the St. Lucie from a river to an estuary. This event resulted in significant saltwater intrusion. Lake Okeechobee (Fig. 2.4.2) is located to the southwest of the SLE. The St. Lucie Canal (C 44) was constructed to provide a connection from Lake Okeechobee to the South Fork of the SLE and then to the Atlantic Ocean. Since the 1950s, the SLE has been a drainage basin for >1800 km^2.The SLE has a total area of ~29 km^2 with ~6.9 $\times 10^7$ m^3 water. The mean water depth is 2.4 m. Five major canals and tributaries deliver freshwater into the SLE. The gauged tributaries supply ~75% of the total freshwater inflow (Morris, 1987). The SLE is a partially mixed estuary with stratification occurring at higher freshwater discharges (Morris, 1987; Doering, 1996).

The SLE is a very complex estuary. The complexity of the bathymetry with navigation channel, multiple inlets, and shallow disposal area results in a unique estuary–lagoon system, where both surface runoff and sub-estuary exchange affect the estuary circulation. The delicate balance of the salinity and nutrients in the St. Lucie Estuary is a key to maintaining the health of all estuarine species in the waterbody. The estuary can suffer from too much

freshwater from basin runoff. The lack of storage in the areas surrounding the estuary causes large amount of water to be released through local drainage canals during periods of heavy rain. It is necessary to keep desired salinity levels and to maintain the health and integrity of the estuary.

The objective of this SLE/IRL study is to develop a water resource management tool for determining nutrient loading ranges to support healthy biological communities in the SLE. To fulfill this goal, development of an advanced 3D hydrodynamic and eutrophication model for the SLE/IRL is required. The calibrated and verified model should be able to

1. Link estuary water quality to nutrient loads from both point and nonpoint sources.
2. Determine nutrient loading ranges to support healthy biological communities.
3. Simulate long-term trend of estuary eutrophication process and hypoxia development.
4. Facilitate establishment of Pollutant Loads Reduction Goals of SLE and the total daily maximum loads (TMDLs).

The development of an advanced model is highly dependent on a good understanding of estuary hydrodynamics, transport processes, and physical, chemical, and biological fate of water quality variables. Over the past years, the South Florida Water Management District (SFWMD) has conducted a substantial research effort. Large amounts of hydrodynamic and water quality data were collected (Germain, 1998). A numerical model was applied to study the freshwater impact of the estuary (Hu, 1999; Hu and Unsell, 1998). These data and studies have provided a basis for understanding the estuary characteristics and modeling requirements.

A 3D hydrodynamic, sediment, toxic, and water quality model is developed in the SLE/IRL area and is calibrated and verified using the following two periods (Ji et al., 2007a, 2007b; Wan et al., 2007): (1) calibration: using the data in 1999 and (2) verification, using the data in 2000.

The development and calibration of the SLE/IRL hydrodynamic model is summarized here. The results of sediment and copper modeling will be presented in Chapter 4. The water quality study on the estuary will be presented in Chapter 5. The applications of the SLE/IRL model for environmental management will be presented in Chapter 10.

2.4.3.2 Model Setup. The model used in this study is developed under the framework of the EFDC model (Hamrick, 1992). Generation of model grid is the first step to setup the model. A primary goal of this study is to simulate multiyear (up to 10 years) processes in the study area. It is essential to design a model grid that has sufficient spatial resolution to represent key hydro-

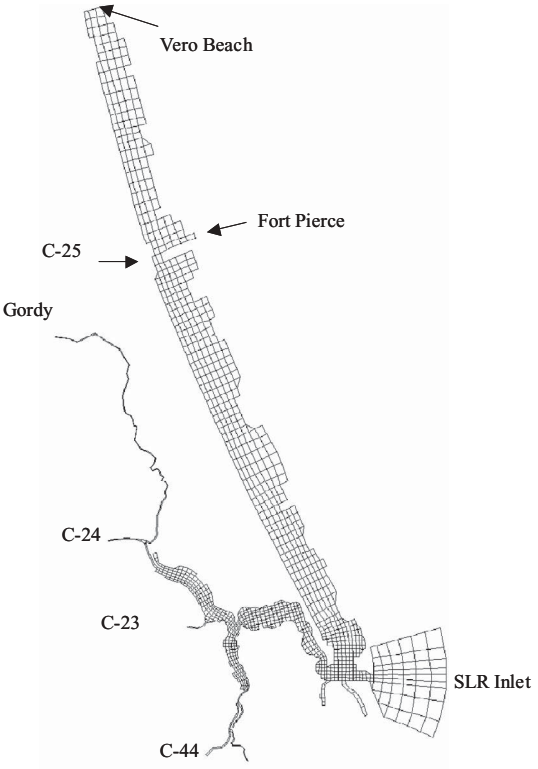

Fig. 2.4.13 Model grid of the SLE/IRL model.

dynamic and water quality processes. And at the same time, the model grid should be computationally efficient, so that long-term (e.g., 10 year) simulations can be accomplished within a reasonable CPU time.

The SLE/IRL is bounded by a complex shoreline. It is further complicated by its navigation channels and shallow areas. Based on the features of the study area, a curvilinear-orthogonal grid is needed to represent the complex geometry of the SLE/IRL (Fig. 2.4.13). The model grid consists of 1161 grid cells, with grid size ranging from 40 to 400 m in the SLE and up to 900 m in the IRL. The grid orientation closely follows the navigation channel. In order to accommodate potential applications of the model in the future, the model domain has extended to the Vero Beach in the IRL. The model includes both the North Fork and the South Fork of the SLE. Portion of three major canals (Canal 47, Canal 49, and Canal 80) are included in the model grid. The upper boundaries of these tributaries and canals are extended to the locations of gages or dam structures, where model boundaries can be described. In the estuary, the measured bathymetry profiles have resolutions varying from tens of meters to >100 m. The model grid resolution is similar to the resolution of the bathy-

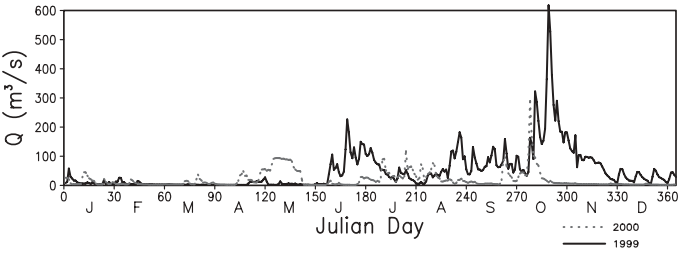

Fig. 2.4.14 Total freshwater inflow in 1999 (solid line) and 2000 (dotted line).

metry measurements. This is a key reason for choosing the current model grid resolution.

The model has three vertical layers. Sensitivity tests with a six-layer model indicate that the three-layer model is adequate to represent the vertical structure of the study area most of the time. The tidal forcing makes this shallow waterbody (with mean depth of 2.4 m) well-mixed vertically, except when large amount of freshwater is discharged into this area. The fully developed version of the SLE/IRL model, including hydrodynamics, sediment processes, toxics, and water quality, takes ~9 CPU hours to finish a 1-year simulation on a Pentium IV 2.4 GHz PC, or ~3.5 days for a 10-year scenario run. This is a feasible time for water resources management applications.

Figure 2.4.14 gives the total freshwater inflow rates in 1999 (solid line) and in 2000 (dotted line). Year 1999 is a wet year with high freshwater discharge from June to November. The highest freshwater discharge occurs in October. The annual mean freshwater inflow in 1999 is 36.7 m^3/s. In contract to 1999, Year 2000 is a dry year with annual mean inflow of 16.5 m^3/s, only 44% of the 1999 value. These two very different years, one wet and one dry, provide ideal periods for model calibration and verification.

The hourly meteorological data used as external forcings to the model include: wind velocity, solar radiation, air temperature, rain, humidity, and cloud cover. Hydrodynamic variables, including tidal elevation, salinity, temperature, and current were observed during 1999–2000. The observed data at St Lucie Inlet, Fort Pierce, and Vero Beach are incorporated into the model as open boundary conditions (Fig. 2.4.12).

2.4.3.3 Tidal Elevation and Current in SLE/IRL. Understanding tidal processes is essential for the success of this modeling effort. The tidal propagation characteristics in an estuary can be quantified by the astronomical tidal constituents. Section 10.2 gives more detailed discussions on tidal processes. Ten major tidal constituents, M_2, S_2, O_1, K_1, Q_1, P_1, K_2, N_2, MF, and MM, are included in the model. The tidal elevations force the model at the three open boundaries shown in Fig. 2.4.12: (1) St. Lucie Inlet, (2) Fort Pierce, and (3) Vero Beach. Via harmonic analysis discussed in Section 10.2.3, the tidal constituents at the

open boundaries were computed from the observation data at these stations in 1999 and 2000.

In calibrating the hydrodynamic model, the value of the bottom roughness height, z_o^* in Eq. (2.2.31), was adjusted to minimize the difference of amplitudes and phases between the simulated and the observed. A constant value of 0.01 m was used in the model. The model results of amplitudes and phases are compared with available data in Tables 2.4.4 and 2.4.5, respectively. Both the model and the data show that M_2 tide is the dominant tidal constitute in the SLE/IRL, followed by K_1, N_2, and O_1. The modeled amplitude of M_2 tide ranges from 0.13 to 0.17 m and is much larger than other constitutes. Overall, the model results are consistent with the data very well. The amplitude errors between the simulated and the observed are <2 cm in the SLE and <4 cm in the IRL. Due to the short horizontal distance of the estuary, the tide is almost in phase inside the SLE.

The sensitivity of the modeled surface elevations to the bottom roughness height was tested twice with bottom roughness values of 0.005 and 0.02 m, respectively. It is found that changes of dominant tidal constituent (M_2 tide) is <1.5 cm as the results of bottom roughness changes. Changes of tidal phases are small as well. In summary, the modeled tidal amplitudes and phases are not very sensitive to this parameter.

An example of time series comparisons between the modeled and the observed surface elevation at A1 is given in Fig. 2.4.15. Station A1 is located in the middle of the estuary and has relatively more measured data for model–data comparison. Time series of temperature and salinity at A1 during the same time period will also be given later. Due to the lack of reliable data at the open boundaries and missing data inside the SLE, only the results in the last 100 days of 1999 (9/24–12/31/99) are shown here. In Fig. 2.4.15, the dotted line is the observed data and the solid line is the modeled results. It shows that the model not only correctly modeled surface fluctuation due to astronomical tides, but also simulated subtidal fluctuations due to variations in the open ocean and freshwater discharges.

Table 2.4.6 lists the statistics at three locations: A1, US1, and NF. It shows that the model calculated the tidal elevations very well. The relative RMS errors (RRE) (= RMS error divided by the data range) vary from 5.0% at A1 to 10.8% at NF. As shown in Fig. 2.4.12, the NF station is located in the narrow channel of the upper stream SLE, influenced by both freshwater and tides. A pulse of large freshwater discharge can cause a sudden change of elevation, which then propagates downstream like a wave. As the estuary becomes wider downstream, the freshwater discharge diffuses into a larger surface area, and the impact of freshwater discharge is gradually reduced. Therefore, errors in freshwater discharges have the largest impact on water elevation in the North Fork section. This contributes to the relatively large model errors at NF. Another possible cause of errors is that in the NF section, the model has only one grid cell across the estuary, which might be insufficient to represent the flooding events.

TABLE 2.4.4 Tidal Amplitude of Harmonic Constituents (m)

Constituent	A1ASLR		US1		NF		Jensen		South Beach	
	Observed	Modeled	Observed	Modeled	Observed	Modeled	Observed	Modeled	Observed	Modeled
M_2	0.13	0.15	0.15	0.15	0.15	0.16	0.16	0.12	0.21	0.17
S_2	0.02	0.02	0.02	0.01	0.02	0.01	0.02	0.01	0.03	0.02
N_2	0.02	0.03	0.03	0.02	0.02	0.03	0.03	0.02	0.05	0.03
K_1	0.04	0.03	0.03	0.03	0.03	0.03	0.04	0.03	0.04	0.04
O_1	0.03	0.03	0.03	0.03	0.03	0.03	0.03	0.02	0.04	0.03
K_2	0.00	0.01	0.00	0.01	0.00	0.02	0.01	0.01	0.01	0.01
P_1	0.01	0.01	0.02	0.01	0.01	0.01	0.01	0.01	0.02	0.02
Q_1	0.00	0.01	0.01	0.01	0.01	0.01	0.01	0.00	0.01	0.01
MF	0.02	0.02	0.03	0.02	0.04	0.02	0.03	0.02	0.03	0.02
MM	0.01	0.02	0.01	0.02	0.02	0.02	0.01	0.02	0.05	0.01

TABLE 2.4.5 Tidal Phase of Harmonic Constituents (h)

Constituent	A1ASLR		US1		NF		Jensen		South Beach	
	Observed	Modeled	Observed	Modeled	Observed	Modeled	Observed	Modeled	Observed	Modeled
M2	1.5	1.3	2.0	1.5	2.5	1.7	1.4	1.7	–0.6	–0.6
S2	4.4	2.3	4.8	2.4	5.8	2.5	4.3	2.4	2.2	1.4
N2	1.8	1.5	2.4	1.9	2.9	2.0	1.8	2.0	–0.8	–0.5
K1	–5.2	–5.6	–4.6	–5.3	–4.3	–5.1	–5.8	–5.0	–7.8	–8.0
O1	–9.8	–10.0	–9.4	–9.7	–9.1	–9.6	–10.1	–9.3	–12.3	–12.7
K2	8.2	–4.6	8.9	–4.5	6.3	–4.3	–4.0	–4.2	5.8	6.0
P1	–6.9	–5.9	16.3	–5.6	–6.3	–5.5	–6.7	–5.6	–8.9	–8.8
Q1	–9.9	–9.1	–7.3	–8.6	–9.0	–8.4	–9.8	–7.9	–12.3	–11.9
MF	–86.1	–87.9	–81.5	–87.5	–68.4	–87.8	–77.9	–78.5	–94.7	–67.4
MM	96.0	–522.5	133.6	–521.3	89.3	–523.0	215.6	–545.5	212.7	–601.2

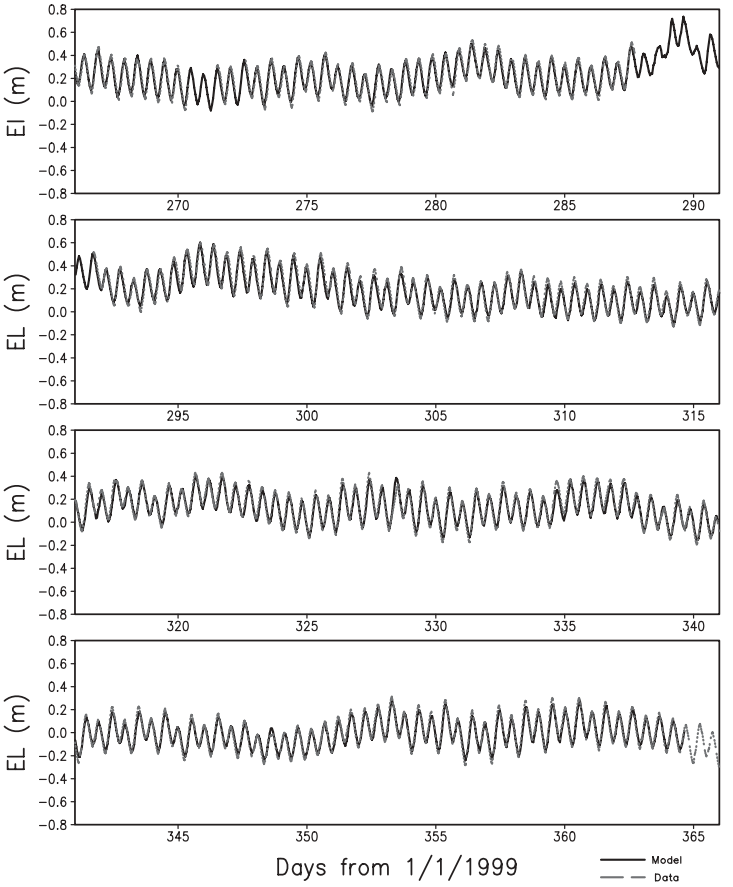

Fig. 2.4.15 Time series of the modeled tidal elevation (solid line) and the measured data (dotted line) at A1 in 1999.

TABLE 2.4.6 A Summary of Relative Errors of Tidal Elevation

Station	Year	RRE (%)	RMS (m)	Data Range (m)	No. of Observations
A1	1999	5.0	0.07	1.40	7225
A1	2000	8.4	0.07	0.83	6257
US1	1999	5.1	0.08	1.57	5670
US1	2000	7.2	0.08	1.11	8261
NF	1999	6.4	0.11	1.72	8019
NF	2000	10.8	0.12	1.11	6195

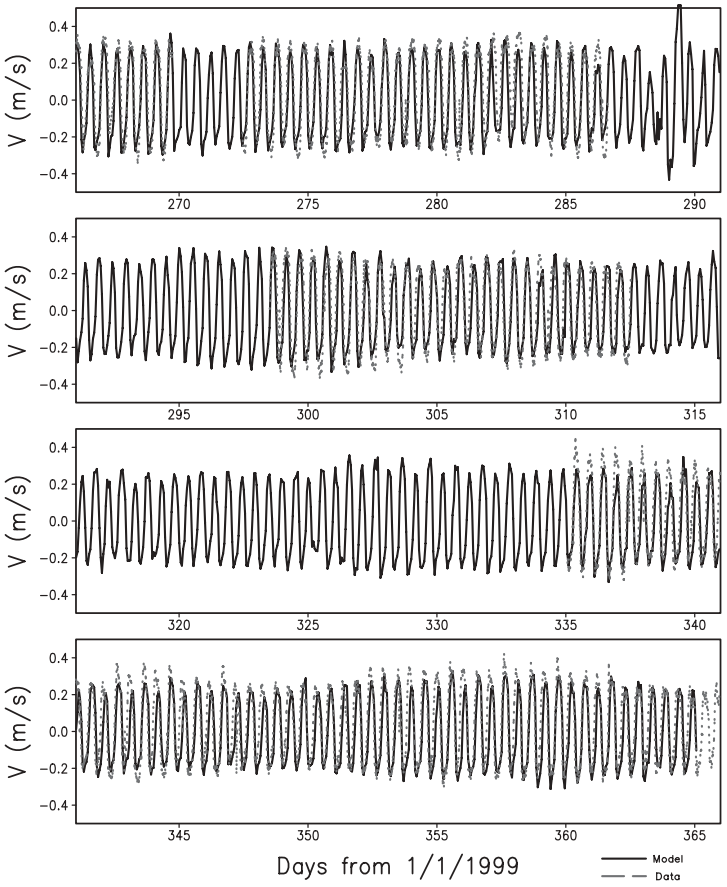

Fig. 2.4.16 Time series of the modeled velocity (solid line) and the measured data (dotted line) at NF in 1999.

North Fork is the only station with available current observation data in 1999 and 2000. The vertically averaged currents from the model are compared with the observed data in Fig. 2.4.16. The current direction is in the orientation of the main channel. The dotted lines are observation results and solid lines are model results. The values of RRE for 1999 and 2000 are both 14 %. The RMS errors are 0.114 and 0.112 m/s for 1999 and 2000, respectively. Overall, the model simulated the currents reasonably well.

2.4.3.4 Temperature and Salinity. The model calibration and verification for temperature use observed data at five stations: SE01, A1, US1, NF, and SE08 (Fig. 2.4.12). The statistics of model results against observations are listed in Table 2.4.7. The averaged RRE in 1999 and 2000 is 11.3%. Table 2.4.7 shows that the model simulated water temperatures satisfactorily. The time series of

TABLE 2.4.7 A Summary of Statistics of Temperature Simulations in 1999 and 2000

Station	Year	Observed Mean (°C)	Modeled Mean (°C)	RMS (°C)	RRE (%)	Number of Obs. Data	Data Range (°C)
SE01	1999	24.7	24.7	1.3	12.2	12	11.0
A1	1999	24.8	24.8	1.5	12.8	14	11.3
US1	1999	25.0	25.0	1.5	13.6	14	11.0
NF	1999	24.9	24.8	1.5	12.2	12	12.4
SE08	1999	25.5	25.9	1.4	13.1	12	10.8
SE01	2000	25.2	25.5	1.1	10.2	16	10.5
A1	2000	25.5	25.5	0.6	5.4	15	11.4
US1	2000	25.5	25.3	0.6	5.3	15	11.4
NF	2000	24.8	24.0	1.4	12.7	13	10.8
SE08	2000	25.8	25.1	1.5	11.6	13	12.5

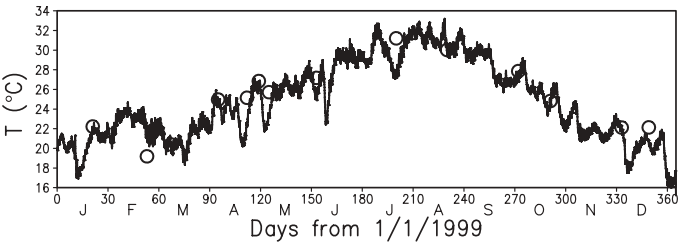

Fig. 2.4.17 Time series of the modeled water temperature (solid line) and the measured data (open circles) at A1 in 1999.

water temperature at A1 in 1999 is presented in Fig. 2.4.17. The solid line is the modeled temperature near the surface and the circles are observation data. Unlike the measured data of tidal elevation, current and salinity, which are available at hourly time intervals, the available temperature data are only at monthly interval. Figure 2.4.17 indicates that the model simulated the seasonal variations well.

Table 2.4.8 is a summary of the statistics of salinity simulation at three stations in 1999 and 2000. Figure 2.4.18 shows a comparison between the modeled and the observed surface salinity at A1 in 1999. The model simulated salinities at A1 and US1 very well. Table 2.4.8 indicates that the errors at NF are relatively large. The NF station is located in the narrow channel and its salinity is strongly influenced by both tides and freshwater discharges. Errors in freshwater input can affect the salinity simulation significantly. Despite the data limitations, the model simulated the salinity transport processes satisfactorily and described the overall seasonal variations well, both in the wet season and in the dry season.

To illustrate the tidal transport process in the estuary, Fig. 2.4.19 gives the hourly averaged salinity and current from the model on January 9, 1999 at 11

TABLE 2.4.8 A Summary of Statistics of Salinity Simulations in 1999 and 2000

Station	Layer	Year	Observed mean (ppt)	Modeled mean (ppt)	RMS (ppt)	RRE (%)	Range (ppt)	Number of Obs. Data	RRE (%) Without Lateral Inflow
A1	Surface	1999	12.7	12.9	3.2	9.9	32.3	2952	9.9
	Bottom	1999	17.2	17.1	4.3	13.0	33.1	2952	12.7
US1	Surface	1999	6.2	6.0	1.6	7.7	20.8	2906	9.6
	Bottom	1999	7.7	7.5	2.5	11.5	21.7	2906	12.4
NF	Surface	1999	1.4	1.3	1.5	13.3	11.3	3766	14.2
	Bottom	1999	1.6	1.7	2.0	17.6	11.4	3766	20.2
A1	Surface	2000	21.6	21.5	2.2	8.1	27.2	2709	9.2
	Bottom	2000	24.7	25.4	2.9	10.5	27.6	2709	10.9
US1	Surface	2000	15.2	14.9	1.7	7.4	23.0	3607	10.9
	Bottom	2000	16.2	17.2	2.5	10.3	24.3	3607	14.0
NF	Surface	2000	5.7	8.3	3.8	26.2	14.5	5368	37.2
	Bottom	2000	6.6	11.6	5.2	32.2	16.1	5368	43.3

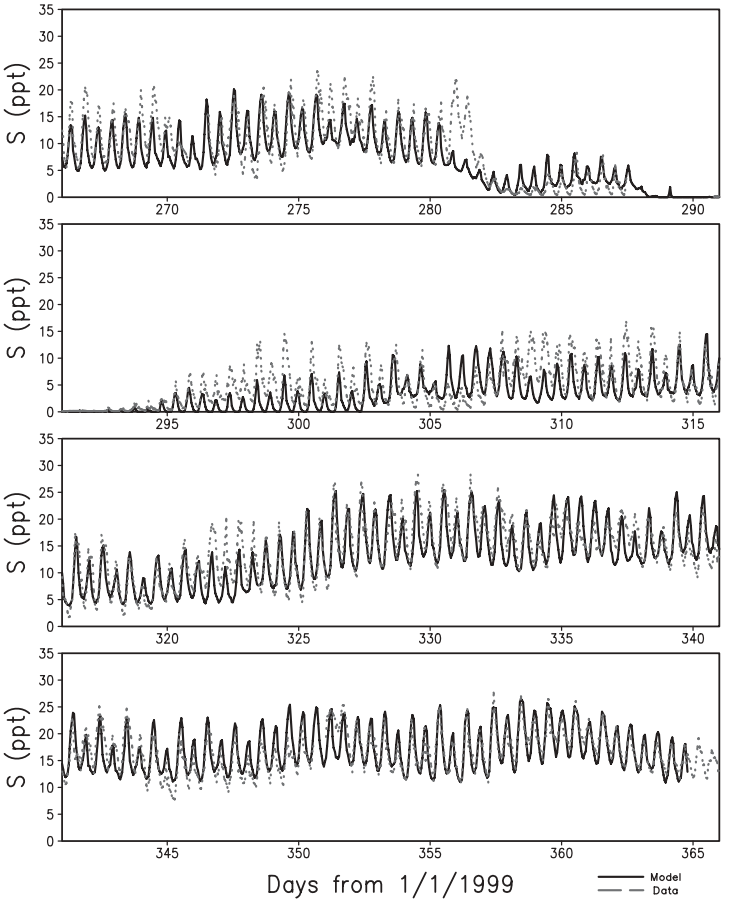

Fig. 2.4.18 Time series of the modeled salinity (solid line) and the measured data (dotted line) at A1 in 1999.

PM. The small plot in Fig. 2.4.19 indicates the tidal amplitude at St. Lucie Inlet. Figure 2.4.19 shows that during the low tide, water is flushed out of the estuary with typical flow velocities around tens of centimeters per second. Salinity is <8 ppt in the North Fork area and is >30 ppt at the estuarine mouth.

2.4.3.5 Discussions on Hydrodynamic Processes. After the SLE/IRL model is calibrated and verified, the model can be used to study hydrodynamic processes in the estuary. Four estuarine processes are the focus of this modeling study: (1) estuarine stratification, (2) salinity intrusion, (3) flushing time, and (4) lateral inflows. They are all key processes affecting the hydrodynamic transport and contaminant dilution in the estuary. The impact of lateral inflows will be described here. The estuarine stratification and salinity intrusion in the SLE will be discussed in Section 10.3.3. The flushing time will be presented in Section 10.3.4.

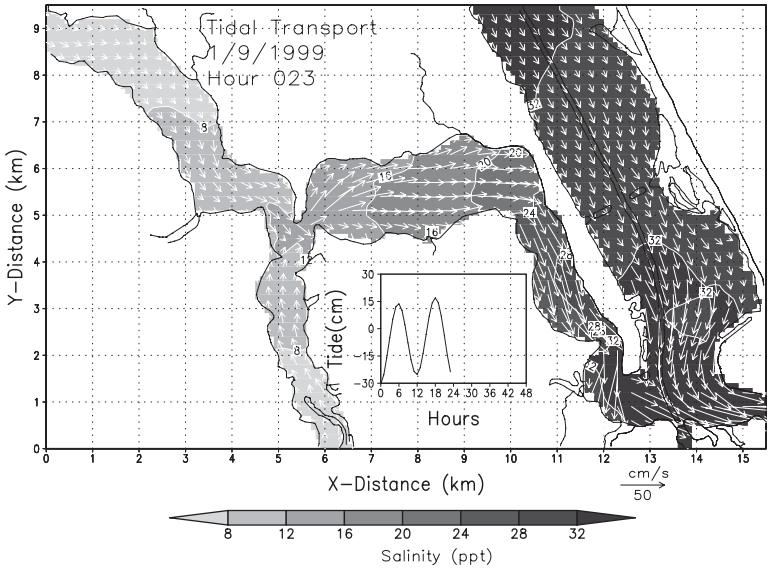

Fig. 2.4.19 Hourly averaged salinity and current from the model on January 9, 1999 at 11 p.m. The small plot indicates the tidal amplitude at St. Lucie Inlet.

Freshwater inflows to a waterbody are often measured by gauges located in the tributaries or upstream of the waterbody. These gauged flow rates are incorporated into a numerical model as inflows to the study area. However, many waterbodies have small, ungauged stream inflows and surface runoffs, which are difficult to measure and are sometimes neglected in modeling studies. Even though this kind of "lateral" inflows may be small individually, their total inflow can be significant to the waterbody. The SLE is a good example.

Freshwaters are discharged into the SLE through four major canals: C-44, C-23, C-24, and North Fork. Data analysis and watershed modeling (Wan et al., 2003) indicated that these inflows contribute ~65–70% of the total freshwater discharges. The rest of the freshwater is from lateral inflows and other small tributaries. The lateral inflows of the SLE contribute ~23% of total discharge in 1999 and 37% in 2000. Therefore, the impact of lateral inflow is significant to the hydrodynamic processes in the estuary.

The impact of lateral inflow on salinity is investigated by model experiments, in which all of the boundary conditions and external forcings are the same as the ones used in model calibrations and verification in 1999 and 2000, except that no lateral inflows discharge to the SLE. Fig. 2.4.20 gives the total lateral flow rate in 2000 and the salinity differences with and without lateral inflows. The salinity is vertically averaged and is at A1. It shows that the lateral inflow affects salinity significantly. The modeled salinity can increase more than 6 ppt, when the lateral inflows are neglected. The last column in Table 2.4.8 gives the values of RRE from the model results without lateral inflow. Comparing with the model results with lateral inflow shown in the seventh column of Table 2.4.8,

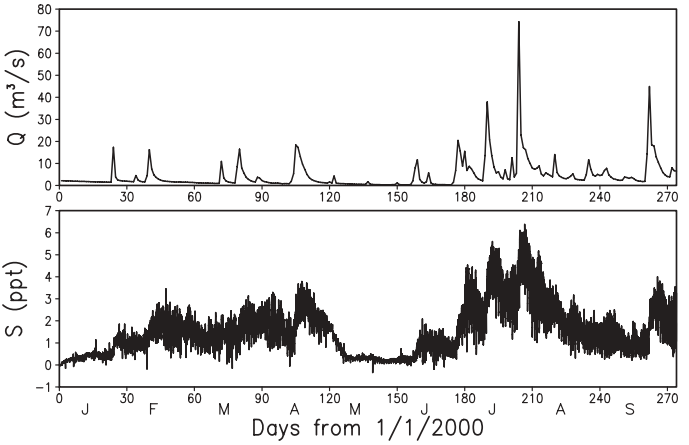

Fig. 2.4.20 Salinity difference without and with lateral inflows at A1 (S) and the rate of total lateral inflow (Q) in 2000.

the RRE without lateral inflows increased significantly, up to 43.3% at NF. Without lateral inflows, the model systematically overestimated salinity.

In addition to salinity, lateral inflows can also affect water elevation in the study area. Results from the SLE/IRL model indicate that the lateral inflows during a flooding period can change surface elevations up to 10 cm, a value that is comparable to the tidal amplitudes in the SLE. At normal lateral inflow rates, however, the influence of lateral inflow on elevation is <0.5 cm.

2.4.3.6 Conclusions. A hydrodynamic model for the SLE/IRL was developed. The model has three open boundaries at St. Lucie Inlet, Vero Beach, and Fort Pierce. Other external forcings to the model include meteorological data and freshwater inflows from the tributaries. The model included 10 major tidal constituents: M_2, S_2, O_1, K_1, Q_1, P_1, K_2, N_2, MF, and MM. The dominant tidal constituent in the estuary is the M_2 tide. The tidal elevation simulation was calibrated with observed data in 1999 and verified with observed data in 2000. The model simulated the tidal variations very well and captured elevation variation in both the dry year and the wet year. The simulated currents were also consistent with the data well. The temperature and salinity were simulated reasonably well in both 1999 and 2000.

Freshwater discharge is an important factor in the simulations of water elevation and salinity. The lateral inflows can change surface elevation up to 10 cm in narrow channels, a value that is comparable to the tidal amplitudes in the SLE. The influence of lateral inflow on salinity is also significant. Without lateral inflows, the salinity can be overestimated by >6 ppt. Other hydrodynamic features of the SLE/IRL, such as estuarine circulation, salinity intrusion, and flushing time, will be presented in Chapter 10, where estuarine processes are discussed.

CHAPTER 3

Sediment Transport

Sediment consists of particles of all sizes that are derived from rocks or biological materials. Sediment can either be suspended in a water column or settle and accumulate on the bottom of a waterbody. Sediment transport is simply the process of eroding sediment from one place, carrying it in the flow, and depositing it in another place. Erosion occurs when the shear stress applied to the sediment bed exceeds a critical value of the shear stress. Deposition takes place when the transport capacity of the flow is exceeded.

To understand the sediment transport processes, it is critical to have a good knowledge of the hydrodynamic processes (discussed in Chapter 2). The sediment transport processes presented in this chapter also play an important role in contaminant fate and transport (Chapter 4) and eutrophication processes (Chapter 5).

Section 3.1 gives an overview of the general features of sediment transport; Section 3.2 discusses the basic processes of sediment transport; Section 3.3 is focused on cohesive sediment; Section 3.4 is on noncohesive sediment; Section 3.5 discusses the geomechanics of the sediment bed; Section 3.6 presents wind waves that are essential to sediment resuspension and deposition in shallow waters; and Section 3.7 is devoted to sediment modeling and applications.

3.1 OVERVIEW

Sediment processes are interesting to a broad spectrum of scientists and engineers. These processes are not merely of academic interests, but are important to the understanding of many pressing environmental problems including eutrophication, contaminant transport, sediment bed erosion, siltation, and waste disposal.

Total suspended sediment is important to the water quality and eutrophication processes because of their influence on density, light penetration, and nutrient availability. Increased TSS reduces light penetration in the water column, thus influencing water temperature, which in turn affects biological

Hydrodynamics and Water Quality: Modeling Rivers, Lakes, and Estuaries, by Zhen-Gang Ji

and chemical reaction rates. The strength of solar radiation in the water column directly affects algae and vegetation growth. The availabilities of sunlight and nutrients, which are closely linked to TSS concentrations, largely control algal production. Total suspended sediment, besides being a very important water quality parameter in its own right, also can have a very strong relationship with chemical species dissolved in the water through adsorption–desorption. Nutrients and toxic chemicals may attach to sediment particles on land and then empty into surface waters, where the pollutants may settle with the sediment or detach and become soluble in the water column. Nutrient (and toxic) concentrations may also be affected by TSS through sorption and settling, as will be discussed in Chapter 4 on toxics and Chapter 5 on nutrients.

3.1.1 Properties of Sediment

Sediments either settle at the bottom of waterbodies or are suspended in water columns. Suspended sediments are commonly transported by either flow or ice. Sediments come from the erosion of soil or from the decomposition of plants and animals. In this sense, sediments are at the end of the path for natural and anthropogenic materials and are at the root of contaminated sediment problems.

Sediments are generally a matrix of materials and consist of four main components:

1. *Interstitial Water:* The largest volume is occupied by interstitial water, which fills the space between sediment particles.
2. *Inorganic Sediment:* Inorganic fraction (silts, clays, etc.) includes the rock and shell fragments and mineral grains that result from the natural erosion of terrestrial materials.
3. *Organic Sediment:* Organic fraction (algae, zooplankton, bacteria, detritus, etc.) usually occupies a low volume, but is an important component of sediment because it can regulate the sorption and bioavalibility of many contaminants.
4. *Contaminants:* Contaminants attached to sediments, such as nutrients, polychlorinated biphenyls (PCBs), and heavy metals, are a very small portion by volume but are often critical to studies of contaminant transport and water quality.

Typically, the average specific gravity of a sediment is close to that of quartz (= 2.65). Total suspended sediments or TSS refer to the matter that is suspended or dissolved in water. Sediment concentration is the weight of dry sediment in a water–sediment mixture per volume of mixture and is often expressed in milligrams/liter (mg/L). When a water sample is evaporated, the residue left in the vessel is the TSS. The suspended particulates in water can be retained on a filter; however, the dissolved sediments are small enough to

pass through a filter. Therefore, the distinction between "particulate" and "dissolved" is primarily a function of the filter used. Traditionally, a 0.45-μm pore size membrane fiber filter is used. According to the Code of Federal Regulation (APHA, 2000), the TDS are defined as those elements that will pass through a 0.45-μm membrane filter. The TSS are those elements that are retained by a 0.45-μm membrane filter. The total solids are the sum of all dissolved and suspended (filterable and nonfilterable) solids.

One of the most basic properties of sediment is the particle size, defined in terms of its diameter. The diameter is usually determined by the mesh size of a sieve that just allows the particles to pass through it. This is also called the sieve diameter of the particle. Based on their sizes, sediment particles are classified into six general categories: (1) clay, (2) silt, (3) sand, (4) gravel, (5) cobbles, and (6) boulders.

Because such classifications are essentially artificial, many schemes have been proposed in the literature to distinguish them. Only clay, silt, and sand are commonly considered in the modeling of sediment transport for water quality studies. Table 3.1.1 gives representative size ranges of clay, silt, sand, and gravel (USACE, 2002). Even though different grading schemes might give slightly different ranges, Table 3.1.1 is relatively consistent with both engineering and geological interpretations. As shown in Table 3.1.1, the range of sediment sizes is enormous, covering several orders of magnitude. Gravel is generally referred to as particles with a size between 2.0 and 20.0 mm in diameter. Sand is referred to as particles with a size between 0.06 and 2.0 mm. This category can also be further divided into very coarse, coarse, medium, fine, very fine, and so on. In practical terms, very fine sand is about the smallest grain size that can still be seen with the naked eye. Silt is referred to as particles with a size between 0.0039 and 0.06 mm. Clay is referred to as particles with a size <0.0039 mm.

Another way to express sediment grain size is by the Wentworth Scale (Wentworth, 1922), which is based on a phi-unit (ϕ) scale and is defined as:

$$\phi = -\log_2 d = -3.3219 \log_{10} d \tag{3.1.1}$$

where d = grain diameter in millimeters.

TABLE 3.3.1 The Types and Sizes of Sediment Particles

Type	Size Range (mm)
Gravel	2.0–20.0
Sand	0.06–2.0
Silt	0.0039–0.06
Clay	<0.0039

The following formula converts ϕ unit into millimeters:

$$d(mm) = 2^{-\phi} \tag{3.1.2}$$

For example, a 2ϕ sand grain has a diameter of 0.25 mm and a 9ϕ clay grain has a diameter of 0.00195 mm.

In natural waterbodies, sediment samples do not have a uniform size. They usually have a grain-size distribution. However, it is frequently necessary to characterize the sample using a single typical grain diameter as a measure of the size distribution. In engineering practice, it is common to classify the sediment by its median grain size, written as d_{50}. The median grain size is the size that divides the sediment sample so that one-half of the sample, by weight, has particles coarser than that size. For example, the median diameters of the sediment in Lake Okeechobee, d_{50}, range from 0.4 to 15 μm in different lake areas (Hwang and Mehta, 1989), which are the sizes of clay and silt (Table 3.1.1). Other similarly sized fractions are also used in characterizing an aggregation of particles. For example, d_{90} is the diameter for which 90% of the sediment, by weight, has a smaller diameter.

Sediments can also be classified as cohesive or noncohesive. A conceptual model of the sediment transport processes is illustrated in Fig. 3.1.1, where a distinction is made between cohesive and noncohesive sediments. "Cohesive" refers to sediment in which interparticle bonding is primarily a result of physicochemical attractions between particles. Unlike noncohesive particles, cohesive particles are subject to the interparticle bonding forces that are significant when compared to the gravitational force. These forces allow the cohesive sediment to be subject to flocculation. In general, the smaller the particle size,

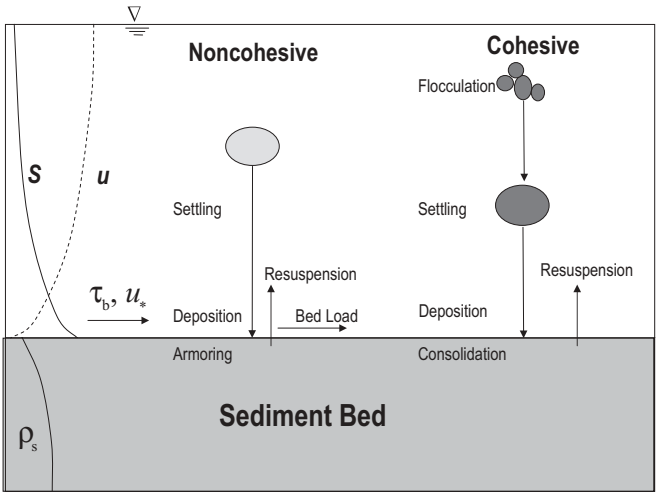

Fig. 3.1.1 Sediment transport processes.

the greater the surface area/volume ratio and the greater the physicochemical attractions between particles. In terms of contaminated sediments, the stronger the interparticle attractions, the greater the sorptive capacity for transporting adsorbed contaminants. Cohesive sediment particles are small and adhere to each other as aggregates of hundreds or thousands of particles, whereas noncohesive sediment particles are generally larger in diameter, and the particles are easily separable. Figure 3.1.1 also illustrates that, due to sediment consolidation and compaction, the bed density (especially for cohesive sediment) increases gradually with depth. In Table 3.1.1, clays are cohesive and have a high sorptive capacity, whereas sands are noncohesive and have essentially no sorptive capacity.

Clay particles are <0.0039 mm in size. Because its particles are so small, clay has a large surface area compared to its volume and is highly sorptive to contaminants. On the other hand, the size of sand is in the range from 0.06 to 2.0 mm. At this size, the force of gravity acting on individual sand grains dwarfs the surface attraction forces between those sand grains. Sand grains (except for very fine sand grains) are noncohesive and generally do not stick together. Silt particles are intermediate between sand and clay. Silt particles remain in suspension far longer than sand grains and can exhibit both cohesive and noncohesive properties, depending on their particle size and composition. A watery mixture of clay and silt is often called mud, which is typically composed of minor amounts of sand and organic material. Mud exhibits strong cohesive properties due to the large surface attraction forces between particles.

3.1.2 Problems Associated With Sediment

The increased loading of sediments and contaminants into surface waters has resulted in the siltation and degradation of water quality. Many of the nutrients and contaminants are now found in the bottom sediments of rivers, lakes, and estuaries and can be returned to the water column via sediment resuspension or diffusion.

Sediment in the water column affects turbidity, heat absorption, and the depth of the eutrophic zone. The problems associated with clean and contaminated sediment are not the same. Clean sediment can cause siltation and reduce light availability in a waterbody. The major concerns regarding contaminated sediment are the pollutants released into the water column, bioaccumulation, and biomagnification. Sediment may carry contaminants into surface waters. In this way, nutrients and toxic chemicals attach to sediment particles on land and ride the particles into surface waters where the pollutants may settle with the sediment or become soluble in the water column. Elevated sediment concentrations cause a number of environmental problems, including the following:

1. Sedimentation in reservoirs, lakes, and harbors causes siltation, diminished navigability, and high costs for maintenance dredging.

2. Sediment serves as a carrier of heavy metals, pesticides, and other contaminants that could be buried in the sediment bed for a long time before being released into the water column again and/or transported over a long distance with the sediment.
3. Sediment obstructs the penetration of sunlight needed for plant growth and affects water temperature.
4. Sediment reduces the recreational quality and overall appearance of a waterbody.
5. Sediment alters aquatic life populations by blanketing fish nesting and spawning areas.

The siltation of rivers, lakes, harbors, and estuaries by sediments is a continuous process. Under low flow conditions, suspended sediments may cause siltation problems, because the materials settle out and impact the substrate on rivers or fill in reservoirs or the upper ends of estuaries.

Under high flow conditions, such as during a storm event, large amounts of sediment from the watershed can be discharged into the receiving waterbody and then be deposited in relatively low-flowing areas. Many harbor basins and navigation channels suffer from rapid siltation, forcing managing authorities to carry out expensive maintenance programs to safeguard navigation. A further influential factor of sediment is the presence of considerable amounts of small clay and silt-sized particles, either in suspension or in the bed sediments. These fine sediments may affect the flow of water through water temperature, density, and sedimentation effects. Occasionally, sediments are delivered back to the land by floods and overflows. The deposition of this previously eroded material can have varying effects depending on what type of soil it is. Alluvial soil, some of the most fertile and productive soils in the world, can certainly increase the productivity of agricultural land. Unfortunately, sand and gravel are the most frequently deposited soils during floods and thus limit production.

Sediment contamination is a widespread environmental problem that can pose a threat to a variety of aquatic ecosystems. Suspended sediments can serve as carriers of contaminants, which readily cling to suspended particles and thus undergo settling, scour, and sedimentation. Sediments are capable of transporting loads of adsorbed contaminants, such as nutrients, pesticides, herbicides, PCBs, polycyclic aromatic hydrocarbons (PAHs), heavy metals, and other toxins. Thus, sediment functions as a reservoir for these chemicals. Sediment deposited on the bottom of a waterbody is often polluted because of the contaminants absorbed from water. Contaminated sediments may be directly toxic to aquatic life or can be a source of contaminants for bioaccumulation in the food chain. Therefore, sediment transport processes must be considered in most toxic chemical studies, which will be the focus of Chapter 4.

The most obvious effect of high-sediment concentrations on water quality is turbidity. The suspended sediment concentrations can limit light penetration and algae productivity. Since settling velocities of fine sediment particles are

very small, they can be easily transported by waves and currents. The presence of these particles in the water column affects heat absorption and depth of the eutrophic zone. These particles increase the attenuation of light in the water column, which leads to an inhibition of photosynthetic activity and reduces the ability of algae to produce food and oxygen. This, in turn, affects the higher organisms that depend on the primary production. As presented in Section 5.8, the light limitation due to high sediment concentration is a primary factor inhibiting SAV growth.

Sediment interferes with recreational activities and the aesthetic enjoyment at waterbodies by reducing water clarity and filling in waterbodies. Although sediment and its transport occur naturally, changes in sediment concentration and particle size can have negative impacts on a waterbody. Fine sediment can severely alter aquatic communities. These particles settle to the bottom where they smother fish eggs and bottom-dwelling animals and impair the benthic habitat. Sediment may clog and abrade fish gills, suffocate eggs and aquatic insect larvae on the bottom, and fill in the pore space between bottom cobbles where fish lay eggs (USEPA, 2000e).

3.2 SEDIMENT PROCESSES

Sediment transport is simply the process of eroding sediment from one place, transporting it in the flow, and depositing it in another place. Erosion occurs when the shear stress applied on the sediment bed exceeds the critical shear stress. Deposition takes place when the transport capacity of the flow is exceeded. The sediment deposited on the bed can be consolidated over time. The four basic sediment processes are

1. Resuspension of the sediment bed.
2. Transport of sediment in the forms of suspended load and bed load.
3. Settling of suspended sediment and deposition on the bed.
4. Consolidation and compaction of the sediment bed.

These processes strongly depend on the flow hydrodynamic conditions and on the sediment properties, such as particle properties: their size, shape, density, and composition.

The sediment exchange between the sediment bed–water column interface, that is, deposition and resuspension, is very complex, depending not only on the water column processes, but also on the detailed sediment properties within the bed. Suspended sediment is transported through turbulent flows. For large and shallow waters where wind waves can develop and their energy can reach the water bottom, wind waves also affect sediment resuspension and deposition. Interactions between sediment particles and the flow may also be significant. In addition to modifying water density, as included in Eq. (2.1.6), high sediment concentrations may dampen turbulent kinetic energy.

Many sediment processes, especially for cohesive sediments, are not yet completely understood. The problem is not only the lack of measured data, but also a lack of understanding the physical processes involved. Mathematical models, including the 3D models described in this chapter, are needed in sediment studies. The physical understanding and mathematical description of the processes, however, are still lagging behind modeling developments, especially with respect to the sediment exchanges near the bed.

3.2.1 Particle Settling

Settling velocity is the most fundamental property governing the motion of the sediment particles in water. It is defined as the terminal velocity at which a single particle falls through quiescent water. While simple in concept, the precise calculation/measurement of settling velocity is usually not. Settling velocity depends principally on the size, shape, and density of the particle and the viscosity and density of the water. Larger particles fall faster. Smaller sized sand particles can be more easily brought into suspension and maintained there by turbulent fluctuations.

For sediment transport modeling, the settling velocity of particles and their resistance to resuspension under shear stress, once they are deposited, are most significant. Settling velocities are also used to calculate the downward movement of sorbed contaminants through the water column. The settling characteristics of particles may vary, as they respond to hydrodynamic conditions in the waterbody. Sediment particles in the water column are brought to the bottom by settling. Once they are near the bottom, deposition governs their removal from the water column. Thus, settling and deposition are fundamentally different.

The settling of a particle in a water column can be determined by the balance between the viscous drag force and the gravitational force. As shown in Fig. 3.2.1, the particle is settling in a water column in response to the gravitational force, F_g, an upward buoyancy force, F_b, and the drag force F_d. It can be derived that

$$F_g = \rho_p \left(\frac{\pi}{6 d_p^3} \right) g \tag{3.2.1}$$

$$F_b = \rho_w \left(\frac{\pi}{6 d_p^3} \right) g \tag{3.2.2}$$

where g = gravitational acceleration (cm/s^{-2}), ρ_p = particle density (g/cm^3), d_p = particle diameter (cm), and ρ_w = water density (g/cm^3). The drag force is the result of frictional resistance to the water flow past the surface of the particle. This resistance depends on the speed at which the particle is falling through the water column, the size of the particle, and the water viscosity.

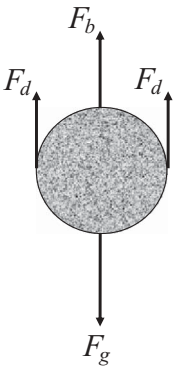

Fig. 3.2.1 The forces acting on a particle settling through a water column.

The Reynolds number (*Re*) is defined as:

$$Re = \rho_w V d_p / \mu \tag{3.2.3}$$

where μ = water's absolute viscosity in g/cm/s and V_s = settling velocity of the particle in cm/s.

Under the assumptions that the flow is laminar and the *Re* is <1, Stoke's law states that:

$$F_d = 3\pi\mu d_p V_s \tag{3.2.4}$$

For particles with constant settling velocity, the gravitational force is equal to the summation of drag force and buoyancy force:

$$F_g = F_b + F_d \tag{3.2.5}$$

Using this relationship, the settling velocity for a uniform spherical particle can be estimated as:

$$V_s = \frac{g(\rho_p - \rho_w)d_p^2}{18\mu} \tag{3.2.6}$$

This is a fundamental equation that helps to estimate terminal settling velocities of particles in a water column. Because it is based on Stoke's law for the drag force, this equation is also often referred to as Stoke's law, and the settling velocity is often called the Stoke's velocity. Equation (3.2.6) reveals that the settling velocity is linearly proportional to the density difference between the particle and the water. Another fundamental result of Eq. (3.2.6) is that the settling velocity increases as the square of the particle diameter, so that larger particles settle much faster than smaller particles. This information is useful for understanding settling processes in water.

Although Eq. (3.2.6) is classic and presents the key processes associated particle settling, it is more useful for understanding those processes than for actually calculating settling velocity. Because the assumptions made to derive Eq. (3.2.6) are often invalid in real waterbodies (e.g., the assumption of laminar flow with $Re < 1$), Eq. (3.2.6) is rarely used to actually calculate the settling velocity. Instead, many empirical formulas are proposed for estimating the settling velocities, especially the settling velocity of cohesive sediments. The choices are too numerous to give a complete list, yet no single formula has been proved superior to the others for general applications. Generally, the settling of cohesive sediment is more complex than that of noncohesive sediment. Section 3.3.3 will present a few empirical formulas for the cohesive sediments. Section 3.4.2 will give more detailed discussions on the settling of noncohesive sediments.

Settling velocities are usually estimated using direct measurement. However, the settling velocity measured in a settling tube may not be accurate and cannot be directly used in a numerical model because of the reduction (or lack) of turbulence in the tube. The turbulence (and flow) condition in the tube can be very different from the one in the waterbody studied. Sediment settling velocities in a model are often used as adjusting parameters to fit measured sediment data. Besides, most models lump sediments of many sizes into one or a few groups (or classes), so that representative values of sediment parameters (e.g., particle diameter, shape, and density) are difficult to define, which makes it unnecessary (and impossible) to specify the accurate values of these parameters. It is more direct to simply use the settling velocity as a calibration parameter in sediment models.

Settling velocity is also partially dependent on the type of model used. For example, a lake model with one vertical layer could have smaller settling velocities than the one with multiple vertical layers, since the latter is capable of representing the vertical transport process better, such as upwelling and vertical turbulent mixing, which may effectively reduce the net settling velocity.

3.2.2 Horizontal Transport of Sediment

The major mechanisms for sediment transport are currents and wind waves. Suspended sediments enter waterbodies from point discharges, land surface runoff, bank erosion, and/or bed scour. Currents, winds, inflows, and tides (in estuaries and coastal waters) are the predominant factors responsible for sediment transport in a waterbody. The effects of all of these mechanisms are complicated by variations in temperature, topography, and salinity throughout the system, which increase the difficulties of describing sediment transport. Using a K-ε turbulence model, Ji (1993) and Ji and Mendoza (1993, 1997, 1998) studied the connection between the instability of flows near the sediment bed and the sediment transport and concluded that the sediment transport is also significantly influenced by the instability of the near bed flows.

Sediments transported by flows can vary significantly in size, from dissolved material (<0.45 μ in diameter) to suspended particles, such as clay, silt, and sand (Table 3.1.1). These particles are the main concern in sediment modeling studies. The total sediment load is the sum of suspended load and bed load:

$$\text{Total sediment load} = \text{suspended load} + \text{bed load} \tag{3.2.7}$$

Sediment is moved as suspended load and/or bed load. Suspended load is the portion of the sediment load that is transported in suspension in the water column. The suspended load includes sediments resuspended from the bed and the wash load brought from upstream. The wash load has relatively fine material in near-permanent suspension that is transported through the system without deposition. It is typically comprised of particle sizes finer than those found in the bed. Cohesive sediments are only transported as suspended load. They are transported by advection (carried with the ambient water at the flow velocity) and dispersion (moved from areas of high sediment concentration to low concentration).

Noncohesive sediments can be transported as suspended load and bed load. Bed load is comprised of particles that move on or near the bed by saltation, rolling, or sliding in the bed layer. Bed load movement occurs intermittently in a thin layer of several grain diameters in thickness, on or in close contact with the bed. Saltation is the process by which individual sediment grains make isolated or serial jumps along the bed. Saltation provides a transition from bed-load transport that takes place immediately above the bed to suspended load transport that takes place in the overlying water column. Although, conceptually, there are clear differences between the suspended load and bed load, it is often difficult to distinguish completely between the two modes of sediment transport in a natural waterbody. It is also difficult to separately measure these two modes in a waterbody. In sediment models, however, separate equations are usually applied for each mode of transport for convenience. Also, for contaminant transport, suspended load is usually of greater interest, since contaminants are often attached to and transported by sediments in suspension.

Shear stress is the frictional force per unit of bed area exerted on the bed by the flowing water. It is an important factor in the movement of bed material. Not only is shear stress a real physical stress on the bed sediment, but also it is a useful parameter in describing sediment transport as well as erosion and deposition. Equation (2.2.29) gives the formulas for shear stress calculation. When water flows over the sediment bed, as either steady flow or oscillatory flow under tides and waves, it exerts a shear stress on the bed. The energy that sets sediment particles into motion is derived from the effect of faster water flowing past slower water. This velocity gradient happens because the water in the main body of flow moves faster than water flowing at the boundaries. The momentum of the faster water is transmitted to the slower boundary water. In doing so, the faster water tends to roll up the slower water: The shear stress moves bed particles in a rolling motion downstream (Fig. 3.2.2). Whether

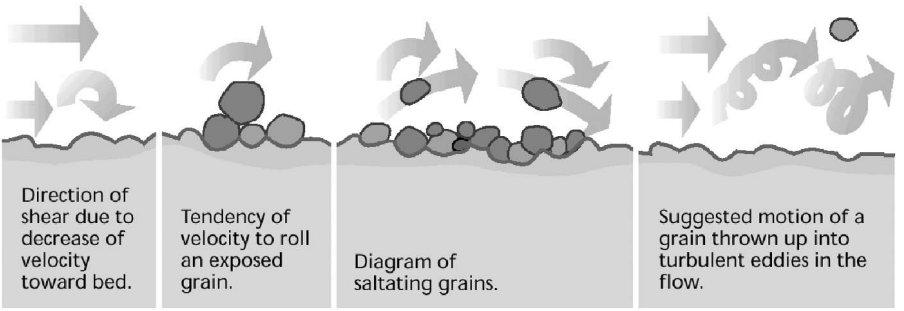

Fig. 3.2.2 Forcing of water shear stress on particles near the sediment bed (FISRWG, 1998).

sediment materials remain on the bed or stay suspended depends on the shear stress. If the shear stress is greater than a critical shear stress, only a fraction of the suspended material will be deposited. If the bed shear stress is less than the critical shear stress, suspended sediment will be deposited on bed gradually.

Generally, two types of hydrodynamic processes generate bottom shear stress: current velocity and waves. In rivers, current velocity is the dominant component of bottom shear stress. In lakes, wind waves can be a primary contributor to bottom shear stress, especially during storms. In large and shallow lakes, such as Lake Okeechobee, the wind waves are a major factor in the calculation of bottom shear stress (Jin and Ji, 2004). In estuaries, wind waves, tidal waves, and mean currents can all significantly affect the bottom shear stress. The relative importance of each component to the total shear stress depends on the specific features of the estuary.

Mathematically, the combined shear stress of current and wind waves, $\vec{\tau}_{cw}$, can be written as the vector sum of the time-averaged component associated with current, $\vec{\tau}_c$, plus the maximum component associated with the wind waves, $\vec{\tau}_{ww}$, expressed as:

$$\vec{\tau}_{cw} = \vec{\tau}_c + \vec{\tau}_{ww} \tag{3.2.8}$$

The magnitude of the current stress, τ_c, has the form:

$$\tau_c = C_c \rho_w u^2 \tag{3.2.9}$$

where u = the current speed near the bed (m/s), ρ_w = the density of the water (kg/m^3), C_c = the bottom friction coefficient (dimensionless), and τ_c = current stress (N/m^2). The current stress equation (3.2.9) is very similar to the wind stress equation (2.1.38).

The magnitude of the wind wave stress, τ_{ww}, has

$$\tau_{ww} = C_{ww} \rho_w u_{ww}^2 \tag{3.2.10}$$

where u_{ww} = the orbital velocity of the wind wave near the bed (m/s), C_{ww} = the bottom friction coefficient due to wind wave (dimensionless), and τ_{ww} = the wind wave stress (N/m^2). (Details about the bottom shear stress calculations are presented in Section 3.6, where wind waves are discussed.)

Sediment particles are picked up by water flow, once the magnitude of water shear stress exceeds the resisting forces of the particle to remain at rest. For a stationary particle on the bed, shear forces are balanced by the forces of gravity, interparticle friction, and cohesion. Mathematically, the following equation can be used to describe erosion:

$$F_s = F_w + F_f + F_c \tag{3.2.11}$$

where F_s = the resuspension force due to the water shear stress imposed on the particle, F_w = the gravity force due to the weight of the particle, F_f = the force resisting resuspension due to the friction between the particle and the bed, and F_c = the force resisting resuspension due to the cohesion between the particle and the bed.

As the flow increases, the left-hand side of this equation increases approximately as the square of the velocity. The initiation of individual particle movement is dependent on a variety of factors, both deterministic and random. When the applied shear stress is low, particles are not brought into motion. As applied shear stress is increased, a critical shear stress is reached at which particles will begin to move. Sediment particles are picked up and carried away from their place of origin whenever the resuspension force, F_s, is large enough to resuspend the particles, that is, $F_s > (F_w + F_f + F_c)$. The formerly stationary particles leave the bed and begin to move. The shear stress at which this occurs is known as the critical shear stress for erosion. The value of the critical stress will depend primarily on the size and density of the particles and secondarily on their shape and packing and the cohesive forces acting between particles. Once this shear stress drops to where $F_s < (F_w + F_f + F_c)$, the particle will settle out to the bottom.

As shown in the first and the second panels of Fig. 3.2.2 (FISRWG, 1998), the shear stress from water flow tends to roll a grain downstream. In slow-moving water, the predominant mode of transport is sediment grains moving along the bottom in the form of bed load. Particle movement on the bed begins as a sliding or rolling motion that transports particles along the bed in the direction of flow. Some particles also may move above the bed surface by saltation, as shown in the third panel of Fig. 3.2.2. These rolling, sliding, and saltation movements result in frequent contact of the moving particles with the bed, and the sediment is transported as bed load.

As the flow velocity (and shear stress) is further increased, particles begin to be suspended and are subject to turbulent forces. At higher shear stresses, the suspension phase develops and the upward diffusion of turbulence maintains the particles in suspension against gravity. The sediment grains are thrown up into suspension and the sediment is transported as suspended load (the fourth panel of Fig. 3.2.2).

3.2.3 Resuspension and Deposition

It is often difficult to separately identify the phase of resuspension and the phase of deposition in natural waterbodies. For the purpose of physical description and mathematical simulation, however, sediment resuspension and deposition need to be described separately. McNeil et al. (1996) designed and used a flume, called SEDflume, to measure the erosion of sediments at high shear stresses and with sediment depth. They determined the critical shear stress for erosion as a function of depth and the erosion rate as a function of both shear stress and depth. Advances in sediment erosion measurement devices (e.g., Roberts et al., 2003 and Jepsen et al., 2002) have facilitated advances in sediment transport modeling.

The terms "erosion" and "resuspension" are often used synonymously. Sediment resuspension is controlled primarily by bottom shear stress. Site-specific bed properties are also a primary factor in determining erosion rates and scour depths. Sediment on the bed will be eroded and transported when the bottom shear stress exceeds a critical value. As described in Eq. (3.2.11), a particle is raised into suspension when the bottom shear stress is sufficient to overcome the stabilizing forces of the sediment. For noncohesive sediment, the main stabilizing force is the immersed particle weight. For cohesive sediment with bulk density [defined in Eq. (3.5.2)] close to the water density, the main forces are interparticle adhesion and organic binding. Typically, cohesive sediment beds are layered with density and shear strength increasing downward. Sediment moves whenever the shear stress transmitted to the bed by water flow and wind waves reaches a critical shear stress for resuspension that is equal to the shear strength "holding" the sediment to the bed.

Once in suspension, sediments will tend to settle out at a rate determined by the sediment concentration, the settling velocity, and the turbulence intensity. Sediment deposition is a process by which suspended sediments leave the water column, either temporarily or permanently, and become part of the bottom sediments. The critical shear stress for deposition of noncohesive sediment is only slightly less than that for erosion. A noncohesive particle settles to the bed almost as soon as the shear stress is too small to erode it, whereas a cohesive sediment floc settles quite differently. The critical shear stress for deposition of cohesive sediment can be much smaller than that for erosion. An accurate analysis requires on-site experimentation to determine values for critical shear stress and other parameters controlling sediment transport.

The probability of deposition depends on the bottom shear stress, the suspended sediment size, and the cohesiveness of the sediment. In order to be deposited, the particles must overcome resistances due to turbulence in the water column, resistances due to the thin viscous sublayer at the interface, and resistances due to chemical or biological activity after they reach the bottom.

The deposition rate can be estimated as the product of the settling velocity and the probability of deposition on contact with the bed, which can vary from

0 for very turbulent systems to 1 for stagnant ponds. The rate of deposition per unit bed area, D, or flux of material to the bed per unit time, is calculated as the sum over a number of classes of settling flux:

$$D = \sum_i p_i w_{si} S_{bi} \tag{3.2.12}$$

where w_{si} = the settling velocity of settling class i, p_i = the probability of deposition of class i, and S_{bi} = the concentration of class i near the bed.

Evaluation of D requires information on w_{si}, p_i, and S_{bi}. The probability of deposition is the probability that a particle reaching the bed will remain there. The settling behaviors of cohesive sediment and noncohesive sediment are different in many ways, and lead to different approaches for estimating settling velocities. The probability of deposition is determined by the sediment properties and the hydrodynamic processes in the waterbody and usually exhibits different features for noncohesive and cohesive sediments. The settling of cohesive sediments will be discussed in Section 3.3.3 and the settling of noncohesive sediments will be discussed in Section 3.4.2.

For streams and rivers, Graf (1971) illustrated the relationships among sediment size, current velocity, and sediment deposition and resuspension (Fig. 3.2.3) that can serve as a preliminary guidance for the understanding of

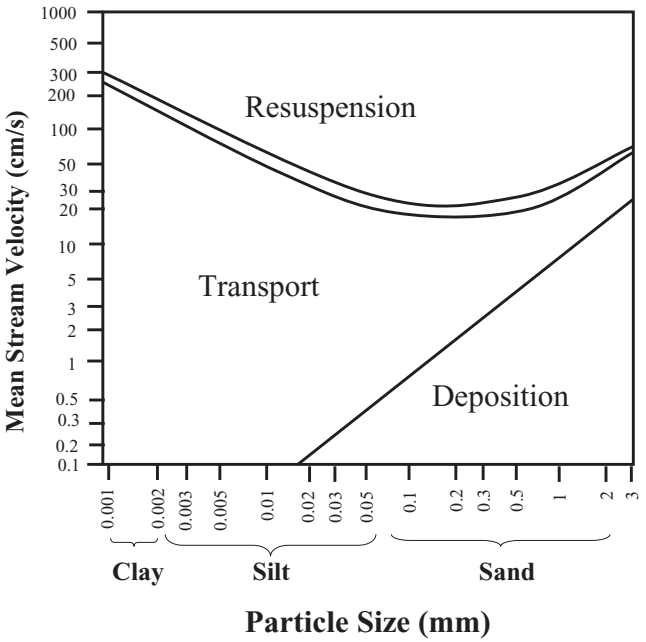

Fig. 3.2.3 Relationship between stream velocity, particle size, and the regimes of sediment erosion, transport, and deposition (based on Graf, 1971).

sediment transport, deposition, and resuspension. For example, fine sand with a diameter of 0.2 mm is expected to settle when current velocity is less than 1.5 cm/s and to resuspend when current velocity is more than 30 cm/s, whereas for very fine silt of 0.004 mm in diameter, settling is not expected. It should be mentioned that the relationships shown in Fig. 3.2.3 are for initial estimations only. Site-specific data are needed to have reliable estimates of the sediment deposition and resuspension.

3.2.4 Equations for Sediment Transport

The temporal and spatial variations of suspended sediment concentration in water columns are governed by the mass conversation equation, also called the transport equation. Within the water column, cohesive particles are advected by flow in the same way that noncohesive particles are. Therefore, the same transport equation is used to describe the motion of all sediment size classes. The transport equation for suspended sediment concentration can be derived from Eq. (2.1.10). Under the Cartesian (in the horizontal directions) and sigma (in the vertical direction) coordinates, it has the form:

$$\partial_t(HS)+\partial_x(HuS)+\partial_y(HvS)+\partial_z(wS)-\partial_z(w_sS)=\partial_x(HA_H\partial_xS)+$$
$$\partial_y(HA_H\partial_yS)+\partial_z\left(\frac{A_v}{H}\partial_zS\right)+Q_s \tag{3.2.13}$$

where H = the water depth, u and v = the horizontal velocity components in the Cartesian horizontal coordinates x and y, w = the vertical velocity in the vertical sigma coordinate z, w_s = the sediment settling velocity, S = the sediment concentration, A_v and A_H = the vertical and horizontal turbulent diffusion coefficients, and Q_s = external sources and sinks.

No decay term is included in Eq. (3.2.13), since suspended sediment can be assumed to be conservative. For noncohesive sediment, the settling velocity, w_s, is a function of the particle's size, density, and shape, and is usually not associated with sediment concentration. For cohesive sediment, the vertical velocity can be related to sediment concentration and other factors such as flow shear.

Vertical boundary conditions for the sediment transport equation at the water surface ($z = 1$) and at the bed ($z = 0$) are

$$-\frac{A_V}{H}\partial_zS-w_sS=0 \qquad \text{at} \quad z=1 \tag{3.2.14}$$

$$-\frac{A_V}{H}\partial_zS-w_sS=J_o \qquad \text{at} \quad z=0 \tag{3.2.15}$$

where J_o ($=J_d + J_r$) is the net sediment flux from the bed to the water column, which is equal to the total of sediment deposition flux (J_d) and sediment resuspension flux (J_r).

Equation (3.2.14) indicates that, at the water surface ($z = 1$), there is no net transport across the free surface, and the diffusion flux, $-A_v/H\partial_z S$, always balances the settling flux, $w_s S$. At the sediment bed ($z = 0$), the net sediment flux, J_0, is equal to the total of the sediment erosion flux and the sediment deposition flux. The sediment flux term, J_0, serves as the means of exchanging sediment between the bed and the water column. Calculating J_0 represents a significant part of the difficulty in sediment modeling.

The gravitational settling flux ($w_s S$) and the sediment net fluxes on the water–sediment bed interface (J_0) represent two important mechanisms in sediment transport. The characteristics of the sediment concentration profile are quite sensitive to the time histories of erosion and deposition, since they represent the source or sink to the total sediment in suspension. The net sediment flux (resuspension minus deposition), J_0, is usually determined by empirical formulas based on measured data.

The sediment transport equation (3.2.13) is similar to the salinity transport equation (2.2.63), just like all transport equations should be. One major difference between Eqs. (3.2.13) and (2.2.63), however, is that Eq. (3.2.13) includes a sediment settling term, $-\partial_z(w_s S)$, which represents the suspended sediment falling out of the water column due to gravitational settling. Another major difference is that the vertical boundary condition for the sediment has vertical flux (J_0) at the bottom of the water column, while the salinity equation (2.2.63) usually has no such kind of vertical boundary conditions, since salinity does not originate from the bottom of a water system under normal circumstances.

An accurate description of sediment transport behavior, which is typically performed through numerical solutions of the sediment mass transport equation, is strongly contingent on an understanding of the structure of the vertical profile of sediment concentrations and the interaction with the flow field. The vertical distribution of suspended sediment concentrations depends on turbulence intensity and on the particle settling velocity. The faster the settling velocity, the stronger turbulence will be required to maintain sediment in transport. For steady and horizontally uniform flows without external source–sinks (Q_s), Eq. (3.2.13) can be reduced to a simple 1D formation:

$$-\frac{A_v}{H}\frac{dS}{dz} - w_s S = 0 \tag{3.2.16}$$

which is similar to the vertical boundary conditions stated in Eq. (3.2.14) and is valid throughout the water column in this case. The solution to Eq. (3.2.16) is

$$S = S_0 \, \mathrm{e}^{-\frac{w_s H}{A_v}(z - z_0)} \tag{3.2.17}$$

where S_0 is the reference sediment concentration at z_0.

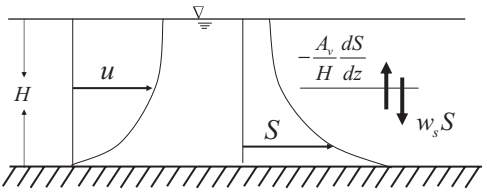

Fig. 3.2.4 Vertical profiles of suspended sediment concentration and the corresponding current in a channel.

This simple analytical solution, Eq. (3.2.17), presents the basic and important relationship that the suspended sediment concentration has with sediment settling velocity, vertical turbulence mixing, and water depth. The schematic illustration of (3.2.17) and the corresponding current in a channel are shown in Fig. 3.2.4. Equation (3.2.16) states that in a water column, the upward turbulent diffusion of sediment $[-(A_v/H)(dS/dz)]$ is balanced by the sediment's tendency to fall out of suspension (w_sS), resulting in a concentration profile that decreases with distance from the bed, as described by Eq. (3.2.17) and Fig. 3.2.4. The vertical density gradient caused by the decreasing sediment concentration can stably stratify the near-bed flow, if the sediment has a large settling velocity and the concentrations are high enough. As indicated in Eq. (3.2.17), if the settling velocity is too large, little sediment will be suspended into the water column, and the resulting suspended sediment will be insignificant. If the settling velocity is very small, large amounts of sediment will be mixed uniformly throughout the water column.

3.2.5 Turbidity and Secchi Depth

Turbidity is a measure of water clarity (or transparency): to what extent the material in water decreases the passage of light through the water column. Water turbidity indicates how cloudy or muddy the water is. The greater the amount of TSS in the water, the murkier it appears and the higher the measured turbidity. Turbidity (and TSS) often increases sharply during and immediately following a rainfall. The flow of stormwater runoff increases flow velocity and the erosion rates of riverbanks and the river bed. Highly turbid water has many effects on the water quality. If the waterbody is excessively turbid over long periods, its health and productivity can be greatly impaired.

Three factors determine turbidity:

1. Suspended sediment (including clay, silt, and sand).
2. Tiny floating organisms (e.g., algae and zooplankton).
3. Colored materials.

Dredging operations, increased flow rates, or even too many bottom-feeding fish may stir up bottom sediments and increase the turbidity. If the zooplank-

ton populations have dropped off reducing the grazing of algae, the increase of algae will result in increased turbidity. Sources of turbidity include the following:

1. Soil erosion from construction, logging, or agricultural activities.
2. Excessive algal growth and reduced zooplankton populations.
3. Waste discharge.
4. Urban runoff.
5. Shoreline erosion.
6. Recirculation of bottom sediment from flooding, dredging, boat traffic and jet skis, or bottom-feeding animals.
7. Discoloration of the water from wetland runoff and/or plant decomposition.

Secchi depth is a measure of water turbidity (or clarity). It is determined by lowering a weighted Secchi disk into a waterbody to the point where it is no longer visible. Secchi disk measurement is perhaps one of the oldest, simplest, and most durable of all water quality measurements. It originated with Italian astrophysicist Pietro Angelo Secchi, who in April l865 first used some white disks to measure the clarity of water in the Mediterranean. The most frequently used Secchi disk is the one with a 20-cm radius that is divided into four equal quadrants of alternating black and white colors (Fig. 3.2.5). The disk is lowered into water until it disappears from view. It is then raised until just visible. The mean of these two measurements is the Secchi depth.

The Secchi disk is a useful tool to estimate water clarity. It can provide a great deal of information on water quality at a low cost, as compared with measuring other nutrients (e.g., phosphorus and nitrogen) and chlorophyll *a*, which are typically monitored at a much reduced frequency and at a higher cost. Secchi depth is well correlated with turbidity and the depth of the biological photic zone. Together with total phosphorus and chlorophyll *a*, Secchi depth is often used as a measure of lake trophic status (e.g., Carlson, 1977). Secchi disk measurements often have a long historical record and provide the basis for identifying trends in trophic status over time because of the large

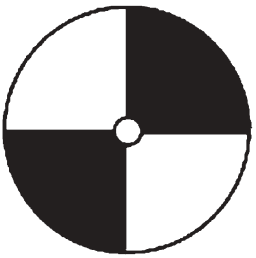

Fig. 3.2.5 A Secchi disk.

number of observations that can be gathered in a given season and the ability to gather numerous years of data at little cost.

Several factors can influence the readings of Secchi depth, such as the eyesight of the viewer, the time of day that the readings are taken, the reflectance of the disk, and so on. Secchi depth is also often used in estimating algal concentrations in waterbodies. However, care must be used in interpreting Secchi data, since Secchi depth measurements are inadequate for nutrient level estimations in waterbodies with colored water. In such instances, total nitrogen and total phosphorus measurements are more accurate indicators of eutrophication.

The light extinction coefficient in Eq. (2.3.17) is another parameter that is frequently used to measure water turbidity (or transparency). Based on data collected at 42 stations in Lake Okeechobee, Jin and Ji (2005) examined the features of Secchi depth, the light extinction coefficient, and total suspended solids (Figs. 3.2.6 and 3.2.7). Figure 3.2.6 is the total suspended solid versus light extinction coefficient based on the measured data in Lake Okeechobee, in which the solid line is an empirical formula derived from the measured data and has the following form:

$$K_e(1/m) = 0.12189 * \mathrm{TSS(mg/L)} + 1.23589 \tag{3.2.18}$$

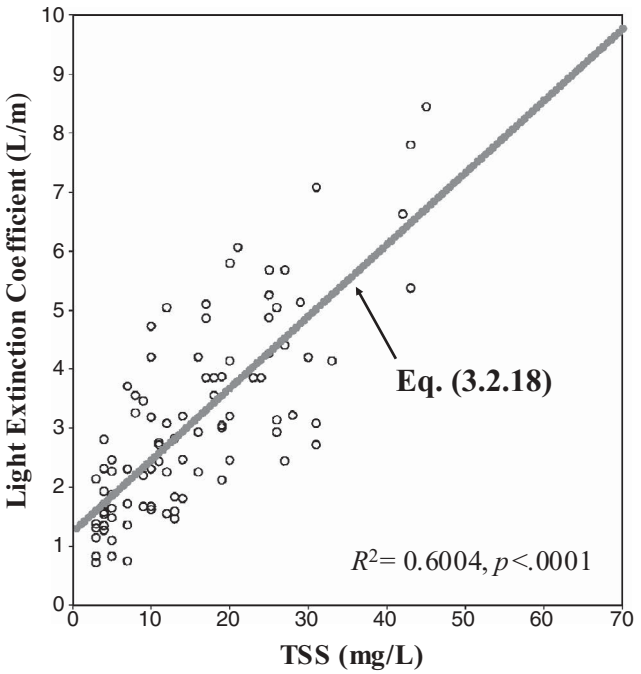

Fig. 3.2.6 Total suspended solid versus light extinction coefficient based on data measured in Lake Okeechobee (Jin and Ji, 2005).

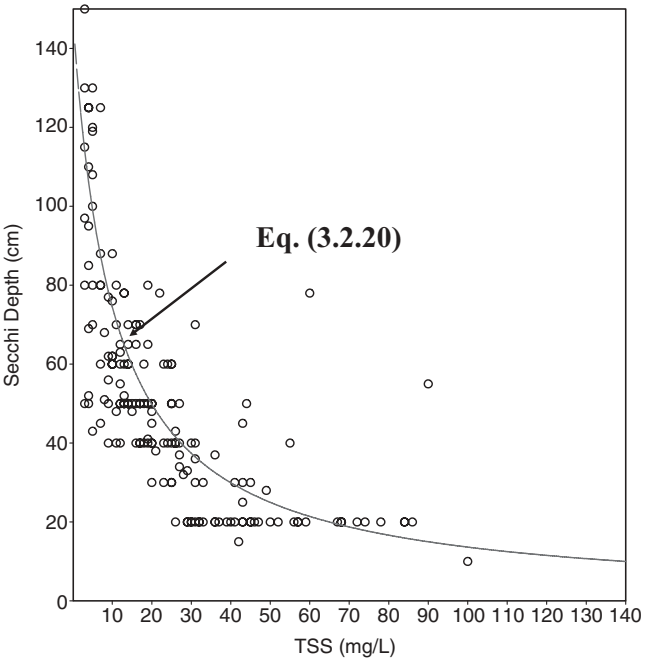

Fig. 3.2.7 Total suspended solid versus Secchi depth based on measured data in Lake Okeechobee (Jin and Ji, 2005).

where K_e = light extinction coefficient in m^{-1} and TSS = total suspended solids in mg/L.

In the past, numerous measurements of Secchi depth have been made in waterbodies. Beeton (1958) and others have developed empirical relationships between the Secchi depth, Z_s, and the light extinction coefficient as given by

$$K_e = C/Z_s \tag{3.2.19}$$

where C is a constant with typical values between 1.7 and 1.9. In Lake Okeechobee, based on the measured data in 1999 and 2000, the parameter C was found to be 1.83, a value that is consistent with the previous studies. From Eqs. (3.2.18) and (3.2.19), the Secchi depth in Lake Okeechobee can be estimated as:

$$Z_s(m) = \frac{1.83}{0.12189 * \text{TSS(mg/L)} + 1.23589} \tag{3.2.20}$$

Figure 3.2.7 is the total suspended solid versus the Secchi depth based on the measured data in Lake Okeechobee. The solid curve is the empirical formula from Eq. (3.2.20).

3.3 COHESIVE SEDIMENT

The management of surface waters often requires accurate and detailed knowledge of cohesive sediment processes to deal with various environmental and engineering problems. Major concerns about cohesive sediment include (1) sediment siltation and (2) environmental pollution.

Cohesive sediments play a significant role on sediment siltation related problems, such as reservoir siltation, maintenance of navigation channels and docks, dredging, and dredged material relocation. The high adsorptive affinity of cohesive sediment for chemical constituents in water causes it to act as a carrier for pollutants with consequent implications for related water quality problems. Many contaminants, such as phosphorus, heavy metals, and PCBs, are attached to cohesive sediments and can be transported, deposited, and/or resuspended with the cohesive sediments. Cohesive sediments deposited on the bottom may function as a source of contaminants to the water column, if they are disturbed by resuspension forces, such as wind waves and strong currents. Lake Okeechobee is a typical example. This lake exhibits signs of eutrophication mainly due to increased internal phosphorus cycling between the water column and the sediment bed (Jin and Ji, 2004). Therefore, it is also essential to understand the cohesive sediment processes for the studies of contaminant transport (Chapter 4) and eutrophication processes (Chapter 5).

Cohesive sediment consists of fine particles, which may be single or, more likely, an aggregation of flocs. Cohesive sediment has a small size and a large particle surface area relative to its mass. The essential properties of cohesive sediment include (1) grain size, (2) mineralogical composition, (3) percentage of organics, and (4) cation exchange capacity.

For cohesive sediments, the bulk properties, physiochemical particle behaviors, and interpartical bonding are of fundamental importance. The characterization for cohesive sediment is more complex than that for coarse-grained material because aggregate properties depend upon the type of sediment, the type and concentration of ions in water, and the flow condition.

Cohesive sediments are those in which the attractive forces, predominantly electrochemical, between sediment grains are stronger than the force of gravity drawing each to the sediment bed. The properties most important for cohesive sediments are interparticle bonding and chemical behavior because they make cohesive sediment respond quite differently to hydrodynamic forces than do noncohesive sediments. The interparticle bonding forces play a significant role in cohesive sediment behaviors, which cause small particles to stick together and form larger aggregates. The strength of the cohesive bond is a function of the grain mineralogy and water chemistry, particularly salinity. Thus, coarse silt may be noncohesive in a freshwater river, but can become cohesive when flowing into an estuary. Therefore, it is easier to define cohesive sediment by behavior than by grain size.

Cohesive sediments often exist in the form of mud in waterbodies. Muds are typically composed of a wide range of materials, thus it is difficult to

provide a unique definition of mud composition. In general, muds include clay and nonclay minerals in the clay- and silt-size ranges, organic matter, and, sometimes, small quantities of fine sand. When large amounts of coarse detritus including sand, gravel, and shell occur with mud, the interactive behavior between different-sized sediments becomes quite complex and it is necessary to treat the coarse material separately from mud. As an example, Table 3.3.1 lists the size distributions of muds at five locations in Lake Okeechobee. The median diameter, d_{50}, varies from 0.003 to 0.015 mm and includes the sizes of clay and silt.

The boundary between cohesive sediment and noncohesive sediment is not clearly defined and generally varies with the type of material. It is, however, appropriate to state that the dominance of interparticle cohesion over gravitational force increases with decreasing particle size. Thus, clays (particle size <0.0039 mm in Table 3.1.1) exhibit more pronounced cohesive behaviors than silts (0.0039–0.06 mm). Silt-sized material, particularly the coarse silts listed in Table 3.1.1, is often weakly cohesive. The mobility of noncohesive sediment can be estimated approximately by knowing the grain size and shape, specific gravities of the sediment and water, and the viscosity or temperature of the water (i.e., physical properties). The mobility of cohesive sediment, however, is more complex, as will be discussed later in this section.

Key processes of cohesive sediments include (1) suspension and transport, (2) flocculation and settling, (3) deposition, (4) consolidation of deposited sediment, and (5) resuspension/erosion of sediment bed.

Because of their small settling velocities, cohesive sediments can be easily transported by flows. The transport processes of cohesive sediments are particularly important in wave-dominated water systems, such as in shallow lakes and estuaries, since they may repeatedly settle to the bed and be resuspended throughout the water column by periodic forces such as wind-induced waves and/or astronomical tides. The concentration of suspended cohesive sediment is the result of horizontal and vertical sediment fluxes and processes within the bed. Cohesive sediments are often transported as aggregates (flocs) rather than as individual particles. Suspended clay particles bond with one another by cohesive forces to form larger masses, which eventually can settle

TABLE 3.3.1 Size Distributions of fine particles at five locations in Lake Okeechobee[a]

Site No.	d_{75} (mm)	d_{50} (mm)	d_{25} (mm)
1	0.015	0.010	0.002
2	0.024	0.015	0.001
3	0.013	0.007	0.0006
4	0.008	0.004	0.0007
5	0.010	0.003	0.0006

[a]Based on Hwang and Mehta, 1989.

as groups (flocs) to the bed. As a result of flocculation into larger particles, the observed settling velocity may be orders of magnitude larger than the Stoke's velocity of the individual particles. The dynamics of these flocs, including flocculation, settling, breakup, and consolidation, affects the suspended sediment concentration. Cohesion of particles in the deposited bed increases the resistance to resuspension and is often a function of the consolidation history. Cohesive sediment processes are very complex, and extensive field and theoretical studies are needed to decipher these processes further (Lick, 2006).

3.3.1 Vertical Profiles of Cohesive Sediment Concentrations

The capacity by currents and waves to transport sediment in suspension is controlled by the amount of energy available in the flow. Suspended sediment is often not well mixed over the water column and stratification occurs due to settling, resulting in a very high sediment concentration near the bed. Figure 3.3.1 is a sketch of the vertical profiles of cohesive sediment concentration $S(z)$ and the corresponding flow velocity $u(z)$, which shows that cohesive sediment can have three distinct regions:

1. The uppermost region is the mixed layer and has a relatively low sediment concentration.
2. The thin fluid mud layer is differentiated from the mixed layer by a steep concentration gradient termed "lutocline" (Parker and Kirby, 1982).
3. The bottom region is a fluid mud layer.

In the mixed layer, the vertical diffusion by turbulence is strong, and the sediment concentration is relatively well mixed. The lutocline is a key feature of vertical profiles of cohesive sediments and is characterized by a steep concentration gradient. The sediment concentrations can be orders of magnitude

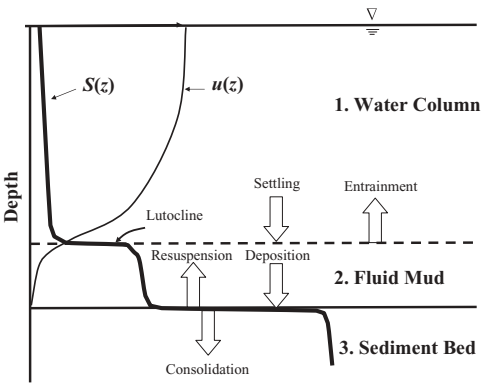

Fig. 3.3.1 Vertical profiles of cohesive sediment concentration and velocity.

higher near the bed than at the water surface. Below the lutocline, there is a fluid mud layer of high sediment concentration. The fluid mud layer is maintained by the turbulent energy of the flow, when there is an equilibrium between the depositional flux and the vertical turbulent transport flux. The fluid mud layer is thin and therefore frequently undetected. Deposition takes place at both interfaces: between the water column and the fluid mud and between the fluid mud and the sediment bed. At the fluid mud–bed interface, the fluid mud deposits, and consolidates to the point where it is too dense to remain fluid.

The fluid mud layer is a static or moving intermediate state between suspension and deposition, analogous to the bed load transport of noncohesive sediments. This mud layer flows downhill by gravity or in the direction of the flow, dragged along by the shear stress of the water flowing above it. The fluid mud layer represents the region where the sediment–water mixture behaves as a fluid and is associated with high sediment concentrations with a sharp mud–water interface. The fluid mud is like a uniform dense viscous fluid and is a well-defined interface between the sediment bed and the water column: sediment on the bed remains at rest while that in the water column moves with the water. The fluid mud is denser than water, less dense than the bed, still capable of motion, but slower than the ambient flow (USACE, 2002).

The lighter water flowing above the denser fluid mud may induce waves on the interface. Wind–wave activity in the upper layer increases the interfacial waves, transforming energy from the mixed layer to the fluid mud. Fluid mud remains stable until a critical shear stress is exceeded. As the difference in flow rates increases, the interfacial wave energy increases until breaking occurs, putting some fluid mud back in suspension and entraining clearer water in the fluid mud. The instability of the fluid mud–water interface and associated entrainment of sediment particles contribute to the cohesive deposition and resuspension (USACE, 2002). Entrainment occurs when the water turbulence incorporates fluid mud into the mixed layer and is controlled by density differences between the two layers, particle settling, and flow conditions.

Depending on the turbulence intensity level, the thickness of the fluid mud layer can change significantly (Hwang and Mehta, 1989). The concentrations in the fluid mud layer can be on the order of 10 g/L, but can also be much higher. Therefore, the total amount of sediment that is transported in the fluid mud layer can be significant. At concentrations above a critical value of tens of grams per liter, the particle interactions start to modify the turbulence. When the turbulence intensity is low, the sediment in the fluid mud layer deposits on the sediment bed. The formation of fluid mud layers, their structures, and subsequent evolution are governed by the settling flux of suspended sediment toward the bed. This flux is the product of the sediment concentration and the settling velocity. The interactions between the water flow and the fluid mud layer are still not well understood. The fluid mud layer is not always observed in every surface waterbody. The conditions for the formation of the fluid mud layer need further study.

3.3.2 Flocculation

Flocculation is the process by which suspended fine particles are assembled into larger groupings (flocs). Flocs are the collections of smaller particles aggregated into larger, more easily settleable particles through chemical, physical, and/or biological processes. Cohesive sediments rarely settle as individual grains in Nature. They tend to stick together when they come close enough for the cohesive forces to overcome the flow shear and the gravity that keep them apart. Flocculation involves two aspects of particles: (1) cohesion and (2) collision.

The process of particle collision and cohesion is also termed aggregation or coagulation. Flocs are larger than individual grains and usually settle faster than the constituent particles. Because of the entrapped water, the density of flocs is less than that of the constituent particles. The settling velocity of a floc is a function of its size, shape, and relative density. Floc formation is dependent on the type and concentration of the suspended particles, the ionic characteristics of the environment, and the fluid shear and turbulence intensity of the flow environment.

Cohesion (particle attraction) is governed by the electrochemistry of the sediment mineral and water. Particle cohesion depends primarily on the mineralogical composition, particle size, and cation exchange capacity of the sediment. Other parameters affecting cohesion include salinity, pH, and temperature of the water. The boundary between cohesive and noncohesive sediments is not clearly defined. It can be stated, however, that cohesion increases with decreasing particle size for the same type of material. For example, clays are much more cohesive than silts. Turbulence can increase the collisions, whereas salinity can increase the cohesion between particles. The effective density of the flocs may vary considerably from that of the individual particles, thus making prediction of the settling velocities difficult and requiring site-specific data for model calibration. Sediment may also be biologically cohesive due to the presence of organisms like diatoms, which can bind the sediment particles together with mucus. Biological cohesion is even more difficult to predict than electrochemical cohesion, providing another reason for using settling velocities as a tuning parameter in cohesive sediment model calibration.

Collisions between small cohesive particles lead to flocculation and the formation of flocs. The frequency of collisions often increases with the sediment concentration and the velocity gradient. However, as the increasing velocity gradient becomes too large, flocs may be broken apart, dispersed, and form new flocs later. Particle collision strongly affects the sizes, settling velocities, strength, and densities of the flocs. Continued flocculation results in larger sized aggregates (flocs) that can be characterized by higher porosity, increased irregularity and fragility, and higher settling rates. The following three factors largely determine the particle collision: (1) velocity gradient, (2) settling velocity difference between particles, and (3) Brownian motion.

These processes occur simultaneously. Under different flow conditions, one process may dominate over the others. Brownian motion is only significant for particles <1 μ in diameter, while velocity gradient and settling velocity differences are important for particles >1 μ diameter (Lick et al., 1993). The effects of the velocity gradient are dominant in high-turbulence regions. Suspended particles follow the motion of the water, travel at different velocities, and produce interparticle contacts. Turbulence intensity affects the collision among suspended particles. Flocs produced by velocity gradients are stronger and denser. At low concentrations, a small amount of shear helps to bring small flocs together to form larger ones. A higher velocity gradient tends to pull the flocs apart (USACE, 2002). The flocs most prone to disruption are the largest ones that have the greatest settling velocity and contain the greatest mass. Under high flow velocities, the flocs may experience a continuous flocculation and breakup, resulting in a quasi-equilibrium condition, in which the properties of the resulting flocs are especially influenced by the history of the aggregated particles. It is very difficult to simulate this process in the laboratory, especially because of the difficulty in correctly simulating the turbulent structure of natural flows, as well as the biological effects.

Settling velocity difference causes more rapidly settling particles to intercept slower settling particles beneath them. It becomes a significant factor when the water current shearing is relatively small, especially in open waters away from shore where differential settling may become the dominant mechanism for flocculation (Lick et al., 1993). This mechanism is a function of the size of the particles or flocs: the greater the difference in size, the faster the rate of flocculation. This mechanism is especially significant after large flocs have been generated in the water column.

Brownian motion is sometimes the least influential mechanism of the three, in which thermal effects lead to the random motion of small particles. Transport by Brownian diffusion depends only on the thermal effects and is independent of factors, such as water flow, gravity force, and salinity. Brownian motion produces ragged, weak flocs that are easily dispersed by velocity gradients (CSCRMDE, 1987). Because sediments in a natural waterbody are often subjected to a certain degree of measurable velocity gradients and turbulence, the Brownian motion effect can be neglected in general. In areas where turbulence is weak, however, Brownian motion can be significant. It may also become important when the concentration of suspended particles is high.

3.3.3 Settling of Cohesive Sediment

Settling is the downward motion of a particle due to the gravitational force, buoyancy, and viscous drag on the particle (Fig. 3.2.1). The settling of cohesive sediment is more complex than that of noncohesive sediment and is closely linked to flocculation, by which individual cohesive sediment particles aggregate to form flocs. This aggregation leads to the settling characteristics of the

flocs being significantly different from those of the individual particles. The flocculation process may result in settling velocities that are several orders of magnitude larger than that of the constituent particles.

Settling velocity is often a more important parameter of cohesive sediment than grain size. Settling velocity is a direct measure of the sediment's behavior in the water column, while grain size only gives the parameter for estimating the settling velocity. As indicated in Eq. (3.2.16), sediments remain suspended in a moving waterbody when the vertical mixing due to turbulence is equal to or greater than the rate of settling of individual particles. As velocities slow down, the vertical mixing decreases and deposition will gradually begin to occur.

There are a variety of empirical formulas for estimating the settling velocities of cohesive sediments. An approach to describe the flocculation and settling, which has met with reasonable success, is the parameterization of the settling velocity of flocs in terms of

1. Cohesive and organic material fundamental particle size (d).
2. Sediment concentration (S).
3. Vertical shear of the horizontal velocity (du/dz).
4. Turbulence intensity in the water column (q).

Therefore, one can have

$$w_s = w_s\left(d, S, \frac{du}{dz}, q\right) \tag{3.3.1}$$

For example, studies using mud from the Severn Estuary in the United Kingdom (Thorn and Parsons, 1980) showed that the following settling velocity can be obtained

$$w_s = 0.513S^{1.29} \qquad \text{for } S < 2\,\text{g/L} \tag{3.3.2}$$

where w_s is in millimeters per second. Equation (3.3.2) is a special case of Eq. (3.3.1). It represents that the settling velocity increases due to the added particle collision and flocculation in increasing sediment concentrations.

A widely used empirical expression proposed by Ariathurai and Krone (1976) also relates the effective settling velocity to the sediment concentration:

$$w_s = w_{so}\left(\frac{S}{S_o}\right)^{\alpha} \tag{3.3.3}$$

with the "o" subscript denoting reference values. Depending on the reference concentration and the value of α, this equation predicts either increasing or decreasing settling velocity as the sediment concentration increases.

Based on observations of settling at six sites in Lake Okeechobee, Hwang and Mehta (1989) proposed

$$w_s = \frac{aS^n}{(S^2 + b^2)^m} \tag{3.3.4}$$

Equation (3.3.4) does not have a dependence on flow characteristics, but is based on data from an energetic field condition having both currents and wind waves (Fig. 3.3.2). This equation has a general parabolic shape with the settling velocity decreasing with decreasing concentration at low concentrations and decreasing with increasing concentration at high concentrations. A least-squares fit method can be used to determine the four parameters, a, b, m, and n, in Eq. (3.3.4). Hwang and Mehta (1989) estimated that the mean values of the four parameters in Lake Okeechobee are $a = 33.38$, $b = 3.7$, $m = 1.78$, and $n = 1.6$, when w_s is in millimeters per second and S is in grams per liter.

Ziegler et al. (1989) proposed a formulation to express the effective settling as:

$$w_s = 2.5(SG_1)^{0.12} \tag{3.3.5}$$

The water column vertical shear stress (G_1) at which the flocs are formed is calculated as:

$$G_1 = \sqrt{\tau_{xz}^2 + \tau_{yz}^2} \tag{3.3.6}$$

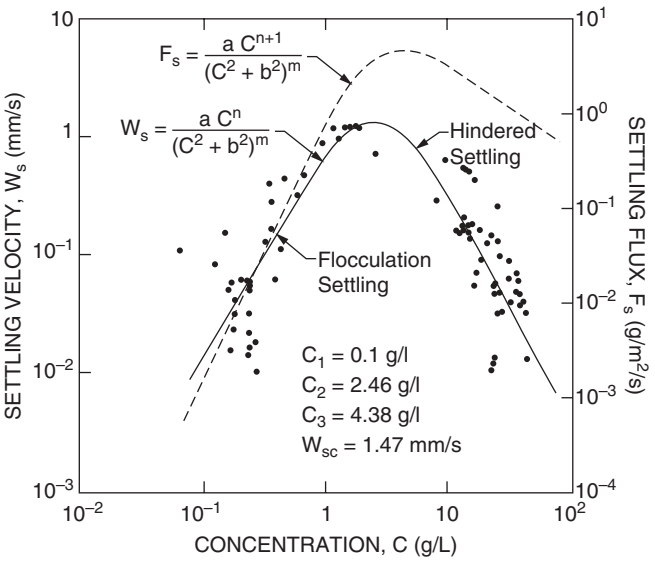

Fig. 3.3.2 Settling velocity and settling flux variations with sediment concentration in Lake Okeechobee (Hwang and Mehta, 1989).

From Eq. (2.2.24), it has the form:

$$G_1 = \frac{A_v}{H}\sqrt{\partial_z u^2 + \partial_z v^2} \tag{3.3.7}$$

where z is the sigma coordinate defined by Eq. (2.2.19). Shrestha and Orlob (1996) proposed another settling velocity equation, which has the form:

$$w_s = S^{\alpha} \exp(-4.21 + 0.147 G_2) \tag{3.3.8}$$

where

$$\alpha = 0.11 + 0.039 G_2 \qquad \text{and} \qquad G_2 = \sqrt{(\partial_z u)^2 + (\partial_z v)^2} \tag{3.3.9}$$

where G_2 is the magnitude of the vertical shear of the horizontal velocity.

Dyer et al. (2000) used the field experiment data set collected in the Tamar Estuary in the United Kingdom and found a dependence of settling velocity on turbulence intensity and sediment concentration:

$$w_s = -0.243 + 0.000567 S + 0.981 G_3 - 0.0934 G_3^2 \tag{3.3.10}$$

and the turbulence parameter G_3 is

$$G_3 = u_* \sqrt{\frac{u}{\nu H}} \tag{3.3.11}$$

where S = sediment concentration (g/L), u^* = the shear velocity (m/s), u = water velocity (m/s), H = water depth (m), and ν = kinematic viscosity (m^2/s).

Even though many empirical formulas for cohesive sediment settling have been reported, the limited knowledge on the flocculation and settling still makes the accurate calculation of settling velocities difficult. The use of a constant settling velocity is the simplest and requires the least number of parameters among the available settling velocity equations and is especially useful if it is measured carefully by laboratory experiments for site-specific applications. By comparing a variety of flocculation formulas with measured settling velocity, Violeau et al. (2000) reported that while some formulas incorporate more of the physical processes than others, they are not necessarily more accurate. The most accurate one, when compared to the *in situ* measurements, still used a constant settling velocity. No one particular flocculation model has been proven to be universally better than the others. There is even significant uncertainty regarding the measurement of settling velocities. Therefore, the simplest flocculation model is recommended, unless measured settling velocity data is available to justify selecting a more complex model. In fact, successful simulations of sediment transport using constant settling

velocities have been reported, such as the studies of Ji et al. (2002a) and Jin and Ji (2004).

Settling velocity is commonly measured by field settling tubes. However, measuring settling velocity in this way may lead to deviations between values measured and their real values in Nature, since:

1. The turbulence condition in the tube is quite different from the real waterbody. As discussed previously, turbulence plays an essential role in cohesive sediment flocculation.
2. The breakup of large flocs near the bottom may be underestimated due to the weaker turbulence intensity in the tube.
3. The limited dimensions of the settling tube (diameter and length) may also affect the flocculation and settling process.

3.3.4 Deposition of Cohesive Sediment

The deposition (and resuspension) of cohesive sediments is extremely complicated. In spite of numerous studies in the past decades, many uncertainties associated with cohesive sediment deposition and resuspension still exist. The difficulties in accurate and realistic data sampling are one major obstacle:

1. Laboratory sediment experiments do not necessarily represent real world conditions.
2. It is difficult to measure all of the important parameters required for developing deposition and resuspension models.

Erosion takes place when the bottom shear stress exceeds the resistance forces of the bed (i.e., the critical shear stress), which in turn, depends on many other bed parameters, such as sediment composition, water content, salinity, and time history of bed consolidation. Consequently, models for the sediment bed are generally very empirical and site specific. Deposition, on the other hand, is more directly affected by hydrodynamic processes in the water column, and hence is more amenable to rigorous models.

High shear stress near the bed breaks up large flocs before they can settle. Then, the resulting smaller flocs and individual particles are resuspended. When a settling floc touches the sediment bed, the weight of sediment grain forces out the pore water, and the floc structure collapses slowly at the bottom. The overlying, weakly held flocs can be easily resuspended and erosion continues until the shear strength of the bed balances the imposed bed shear stress. The rearrangement of the particles gives the bed increased shear strength and resistance to resuspension, primarily due to consolidation and armoring.

Consolidation occurs over time and increases the cohesion between individual particles and flocs and their resistance to erosion. Armoring of the

surface layer also increases with time. It breaks weak interparticle bonds, promotes stronger rebonding arrangements, and renders the deposit more erosion resistant. More discussions on bed consolidation and armoring will be given in Section 3.5.

As stated by Eq. (3.2.12), the deposition flux, J_d, is proportional to the settling velocity and can be expressed as the product of a sediment concentration near the bed, the settling velocity, and the probability of deposition. The water column–sediment bed exchange of cohesive sediments is controlled by the near-bed flow environment and the geomechanics of the deposited bed. After considering the probability of deposition, the effective deposition velocity can be approximately expressed in terms of the effective settling velocity by

$$w_{\mathrm{de}} = w_s\left(\frac{\tau_{\mathrm{cd}} - \tau_b}{\tau_{\mathrm{cd}}}\right) \qquad \tau_b \le \tau_{\mathrm{cd}} \tag{3.3.12}$$

where τ_b = the bed stress or stress exerted by the flow on the bed, τ_{cd} = a critical stress for deposition, w_s = settling velocity, and w_{de} = effective deposition velocity.

The critical deposition stress is generally determined from laboratory or *in situ* field observations. As the bed shear stress increases above the critical deposition value, deposition ceases.

Based on Eq. (3.3.12), the depositional flux can be expressed as:

$$J_d = \begin{cases} -w_s S_d\left(\dfrac{\tau_{\mathrm{cd}} - \tau_b}{\tau_{\mathrm{cd}}}\right) & \tau_b \le \tau_{\mathrm{cd}} \\ 0 & \tau_b \ge \tau_{\mathrm{cd}} \end{cases} \tag{3.3.13}$$

where $J_{\mathrm{d}} = dm/dt$ = sediment depositional flux (g/cm^{-2}/s), m = the sediment mass deposited on bed per unit area (g/cm^{-2}), τ_b = the stress exerted by the flow on the bed, τ_{cd} = the critical stress for deposition, and S_d = the near bed depositing sediment concentration. Equation (3.3.13) states that when the strength of a cohesive sediment bed is strong enough to withstand the near-bed shear stress, the cohesive sediments stick to the bed. It provides the depositional sediment flux stated in the boundary condition by Eq. (3.2.15).

The near-bed flow and the bed properties control the water column–sediment bed exchange of cohesive sediments. The critical deposition stress, τ_{cd}, is generally determined from laboratory or *in situ* field observations; its values ranging from 0.06 to 1.1 N/m^2 have been documented in the literature (e.g., Hwang and Mehta, 1989; Ziegler and Nesbitt, 1994, 1995). Given this wide range of reported values and in the absence of site-specific data, the critical depositional stress is generally treated as a calibration parameter. In addition to the difficulty in determining the critical stress for erosion, the calculation of the bottom shear stress is also crucial and will be discussed in detail later in this chapter.

3.3.5 Resuspension of Cohesive Sediment

Resuspension (erosion) of deposited sediment results from bottom shear stresses imposed by currents and waves. Erosion begins when the bottom shear stress is equal to the shear strength of the surface layer of the sediment bed. The cohesive sediment bed consists of individual particles, but is more likely made up of grain groups held together by cohesion. Erosion occurs where cohesion is weakest. The erosion rate and the depth in the bed to which erosion occurs are strongly dependent on the profile of bed strength. This profile typically shows increasing strength with depth due to increasing consolidation with depth. When the bed strength is insufficient to resist the erosive forces, resuspension begins.

The behavior of cohesive sediments is complex and depends not only on the flow condition, but also on the electrochemical properties of the sediments. Factors, such as hydrodynamic conditions, particle size distribution, vegetation type and distribution, the biochemical property of the bed, and the time history of bed sediments, may all affect the erosion of a cohesive sediment bed. Due to the cohesion, consolidated sediments require higher forces to mobilize, making them more resistant to erosion. The critical shear stress for the erosion of a cohesive bed is often significantly greater than the critical shear stress for deposition. In other words, once a particle has been deposited on the bed, the cohesive bond with other particles makes it more difficult to remove than the particle alone would need. However, once cohesive sediments are resuspended, they can be transported at much lower velocity than is required for the initiation of erosion.

Resuspension (or erosion) of cohesive sediment beds can be classified in two modes: (1) surface erosion and (2) mass erosion. Surface erosion occurs by separation of individual sediment particles from the bed surface, when the bottom shear stress exceeds the critical shear stress of the bed. Mass erosion (or bulk erosion) occurs when the sediment bed structure fails at some level beneath the bed surface, where the bed shear strength is unable to withstand the shear stress imposed by the flow. In this case, the resuspension process happens by dislodging large pieces of the sediment.

Surface erosion typically occurs under mild-to-moderate flow conditions. Surface erosion is described as the wearing away of surface particles, particle by particle. It occurs gradually when the bottom shear stress is less than the bed shear strength near the surface (so mass erosion does not occur), but greater than a critical resuspension shear stress. The surface erosion rate increases with shear stress until the shear stress becomes sufficient to dislodge large pieces of the bed. After that, mass erosion begins. A typical scenario under conditions of accelerating flow and increasing bed stress first would involve the occurrence of gradual surface erosion, followed by a rapid interval of mass erosion, followed by another interval of surface erosion. Alternately, if the bed is well consolidated with a sufficiently high shear strength profile, only gradual surface erosion would occur (Tetra Tech, 2002). Lick et al. (1987)

reported that, as a result of cohesion and consolidation, only a finite amount of cohesive sediment may be resuspended at a given shear stress. The amount of cohesive sediment entrained is a function of the time after deposition, the shear stress, and a site-specific critical shear stress. Erosion continues until the imposed shear stress by the overlying flow is less than the bed shear strength. Lick et al. (2004) developed a theoretical description of the initiation of movement of sediments consisting of uniformly sized quartz particles. These sediments behave in a noncohesive manner of coarse-gained particles, but show cohesive behavior for fine-grained particles. They reported that the erosion of cohesive sediments occurs not only as particle erosion, but as erosion of chunks or aggregates of particles. As particles erode, the aggregates become more exposed and eventually will erode as the lift and drag on the aggregates become sufficiently large to overcome the gravitational force.

When the bed shear stress is greater than the critical shear stress, surface erosion occurs and may be represented by

$$J_r = \frac{dm_e}{dt}\left(\frac{\tau_b - \tau_{ce}}{\tau_{ce}}\right)^{\alpha} \quad \tau_b \geq \tau_{ce} \tag{3.3.14}$$

or

$$J_r = \frac{dm_e}{dt}\exp\left(-\beta\left(\frac{\tau_b - \tau_{ce}}{\tau_{ce}}\right)^{\gamma}\right) \tau_b \geq \tau_{ce} \tag{3.3.15}$$

where J_r = sediment erosion rate, $\frac{dm_e}{dt}$ = the surface erosion rate per unit surface area of the bed, τ_b = the bottom shear stress due to waves and currents, τ_{ce} = the critical shear stress for surface erosion or resuspension, and α, β, and γ = site-specific parameters. Equation (3.3.14) is more appropriate for consolidated beds, while Eq. (3.3.15) is appropriate for partially consolidated beds (Tetra Tech, 2002). The parameters in Eqs. (3.3.14) and (3.3.15) are generally determined from laboratory or *in situ* field experimental observations.

Based on laboratory and field data, Gailani et al. (1991) proposed the following formula to estimate cohesive sediment erosion:

$$E = \frac{a_0}{T_d{}^m}\left(\frac{\tau_b - \tau_{cr}}{\tau_{ce}}\right)^n \qquad \tau_b > \tau_{ce} \tag{3.3.16}$$

Here E = the resuspension potential (mg/cm^2), a_0 = a site-specific constant, T_d = the time after deposition (day), τ_b = the bottom shear stress due to waves and currents, and τ_{cr} = the effective critical shear stress (dyn/cm^2), m = a consolidation parameter, and n = a shear stress parameter.

The resuspension potential, E, is the net mass of resuspended sediment per unit surface area. Laboratory studies (Tsai and Lick, 1987; MacIntyre et al.,

1990) indicate that consolidation effects on cohesive sediment resuspension are typically minimal after ~7 days of consolidation, which leads to $T_{\mathrm{d,\,max}} = 7$ days. The consolidation parameter (m) varies from 0.5 to 2, depending on whether the sediment bed is in a higher energy environment (0.5) or a relatively quiescent body of water (2). The shear stress parameter (n) depends on local bed properties and ranges from 2 to 3. For different sites, the constant a_0 can vary by an order of magnitude. Ziegler and Nesbitt (1994) used the following parameter values in the study of the Pawtuxet River: $m = 0.5$, $n = 2$, $T_{d,\max} = 7$ days, $\tau_{\mathrm{cr}} = 1\,\mathrm{dyn/cm^2}$, and $a_0 = 0.638$.

Equation (3.3.16) determines the net resuspension; however, it is the sediment resuspension flux, J_r, that is needed in the boundary condition (3.2.15) for sediment transport modeling. Experimental results show that the total amount of sediment is not resuspended instantaneously, but it is eroded approximately over a 1-h period (Tsai and Lick, 1987; MacIntyre et al., 1990). Thus, the sediment resuspension flux, J_r, is taken as:

$$J_r = \begin{cases} \dfrac{E}{T_r} = \dfrac{a_0}{T_r T_d^{\,m}} \left(\dfrac{\tau_b - \tau_{\mathrm{cr}}}{\tau_{\mathrm{ce}}} \right)^n & 0 < t \le T_r \\ 0 & t > T_r \end{cases} \tag{3.3.17}$$

where T_r is a parameter representing the resuspension period and is set to 3600 s (HydroQual, 1995a).

The nonlinear relationship between J_r and the bottom shear stress, τ_b, in Eq. (3.3.17) is important. The quadratic stress law shown by Eqs. (3.2.9) and (3.2.10) indicates that bottom shear stress increases as the square of the current velocity (u) and bottom orbital velocity (u_{wm}). Thus, for a current-dominated environment (e.g., a river), the sediment resuspension flux, J_r, is a highly nonlinear function of the current velocity, with J_r being proportional to u raised to the fourth to sixth power. This nonlinear dependence on current velocity amplifies the importance of storm events to sediment transport. Similar phenomenon can also be found in wave-dominated waterbodies. For example, wind waves in Lake Okeechobee play a dominant role in sediment resuspension (Jin and Ji, 2004). Comparison between Eqs. (3.3.14) and (3.3.17) indicates that the two equations have a similar format, even though the two have different parameters to be determined by field data.

The critical erosion stress depends on the sediment type and the state of consolidation of the bed. The cohesion between sediment particles can be considered as inversely proportional to the distance between particles. The closer the particles are to each other, the stronger the cohesive bond and the greater the shear stress needed to separate them. It is convenient (and logical) to link the critical shear stress to the density of the bed. Based on measured data, Miznot (1968) proposed the following relation:

$$\tau_{\mathrm{ce}} = c\rho_s^d \tag{3.3.18}$$

where τ_{ce} = the critical stress for surface erosion, ρ_s = the dry density of the bed, and *c, d* = site-specific parameters. Hayter (1983) found that Eq. (3.3.18) is approximate, but can still be useful in the absence of a better correlation between bed properties and τ_{ce}.

Hwang and Mehta (1989) proposed the following relationship:

$$\tau_{ce} = a(\rho_b - \rho_l)^b + c \tag{3.3.19}$$

where τ_{ce} = the critical stress for surface erosion (N/m^2), ρ_b = the bulk density of the bed (g/cm^3), ρ_l = the bulk density of the uppermost bed level (g/cm^3), and *a, b, c* = site-specific parameters. Hwang and Mehta (1989) set *a, b, c,* and ρ_l equal to 0.883, 0.2, 0.05, and 1.065, respectively.

Surface erosion rates (dm_e/dt) ranging from 0.005 to 0.1 g/s-m^2 have been reported in the literature. They generally decrease with increasing bulk density. Based on experimental observations, Hwang and Mehta (1989) proposed

$$\log_{10}\left(\frac{dm_e}{dt}\right) = 0.23\exp\left(\frac{0.198}{\rho_b - 1.0023}\right) \tag{3.3.20}$$

for the erosion rate in milligrams per hour-squared centimeters (mg/h-cm^2) and the bulk density in grams per cubic centimeters (g/cm^3).

The process of mass erosion is "explosive" in nature. Mass erosion occurs rapidly when the bed stress exerted by the flow exceeds the bed shear strength. Transport into the water column by mass erosion can be expressed in the form of (Tetra Tech, 2002):

$$J_r = \begin{cases} 0 & \tau_b < \tau_s \\ \dfrac{m_{\text{me}}}{T_{\text{me}}} & \tau_b \geq \tau_s \end{cases} \tag{3.3.21}$$

where J_r = the mass erosion flux, m_{me} = the dry sediment mass per unit area of the bed, τ_s = the bed shear strength, and T_{me} = a transfer time scale for the mass erosion.

Hwang and Mehta (1989) indicated that the maximum rate of mass erosion is on the order of 0.6 g/s-m^2. The shear strength of the cohesive sediment bed is generally a linear function of the bed bulk density, such as:

$$\tau_s = a_s\rho_b + b_s \tag{3.3.22}$$

where τ_s = the shear strength of the cohesive sediment bed (N/m^2), ρ_b = the bulk density of the bed (g/cm^3), and a_s, b_s = parameters. Hwang and Mehta (1989) gave a_s and b_s values of 9.808 and –9.934 for bulk density greater than 1.065 g/cm^3.

It should be pointed out that most erosion studies have been performed in laboratory flumes. These laboratory experiments do not always simulate the turbulence spectrum, particle size distribution, and sediment composition in natural waterbodies. Further research is needed to determine the quantitative dependence of erosion rates on parameters representative of real-world conditions. Due to the lack of reliable techniques and experiments for accurately examining the processes of cohesive sediment, empirical formulas, such as the ones listed here, are necessary.

3.4 NONCOHESIVE SEDIMENT

Noncohesive sediments, usually sand and other granular material, are the materials of interest for many beds and banks of rivers and lakes. In addition, these materials may also constitute the bulk of the mass in the bed, which is usually the main component of the total solid mass transport. Important properties of noncohesive sediments include (1) particle size, (2) shape, and (3) specific gravity.

Particle size is the most significant sediment property of noncohesive sediments. Frequently, the particle size alone is used to characterize a sediment particle. Noncohesive sediments typically include gravel, sand, and some silt, as listed in Table 3.1.1. They generally are found on open coasts, in tidal inlets, and in upper reaches of fluvial channel, where there is high-velocity flow. Hydrodynamic processes often control the behaviors of the noncohesive sediment in water.

Much of the classic literature on sediment transport has been concerned with noncohesive sediments. Numerous empirical formulas have also been proposed for quantitatively describing the sediment behaviors, especially for the estimations of equilibrium concentration and the bed load transport. This section will not give detailed discussions on these topics but will only introduce some basic concepts in noncohesive sediment transport.

3.4.1 Shields Diagram

When flow velocity (or wave orbital velocity) increases, so does the bottom shear stress on a noncohesive sediment bed. As depicted in Fig. 3.2.2, the bottom shear stress can increase to a critical point to induce particle motion. Once started, the particle motion can be sustained by water velocities that are less than the critical value required to initiate the particle motion.

Because of variations in material shape and size, grain-size distribution, and water-flow characteristics, there are numerous empirical and theoretical relationships between water flow and sediment transport capacity. Shields relationship between dimensionless shear stress (or Shields parameter) and the boundary *Re* is a reliable predictor. The ratio of the erosion force (bottom shear stress) to the stabilizing forces (submerged weight) is essential in non-

cohesive sediment transport. This ratio, called the Shields parameter or dimensionless shear stress (Shields, 1936), is defined as:

$$\tau_* = \frac{\tau_s}{(\rho_s - \rho_w) g d_s} = \frac{u_*^2}{g' d_s} \tag{3.4.1}$$

where τ_* = Shields parameter (dimensionless bottom shear stress), τ_s = the bottom shear stress (N/m^2), ρ_s = the density of bed sediment (kg/m^3), ρ_w = the density of bed water (kg/m^3), g = the gravitational acceleration (m/s^2), d_s = the diameter of sediment grain (m), $u_* = \sqrt{\tau_s/\rho_w}$ = shear velocity (m/s), and $g' = \left(\frac{\rho_s - \rho_w}{\rho_w}\right) g$ = reduced gravitational acceleration (m/s^2).

The boundary *Re* is defined as:

$$R_* = \frac{u_* d_s}{\nu} \tag{3.4.2}$$

where R_* = boundary Reynolds number, $u_* = \sqrt{\tau_s/\rho_w}$ = shear velocity (m/s), ρ = water density (kg/m^3), d_s = diameter of sediment gain (m), and ν = kinematic viscosity of water (m^2/s).

Shields parameter and the boundary Re number are both dimensionless so that any consistent units of measurement may be used in their calculation. A critical value of the Shields parameter is defined as:

$$\tau_{*\mathrm{cr}} = \frac{\tau_{\mathrm{scr}}}{(\rho_s - \rho_w) g d_s} = \frac{u_{*\mathrm{cr}}^2}{g' d_s} = f(R_*) \tag{3.4.3}$$

where $\tau_{*\mathrm{cr}}$ = critical Shields parameter, τ_{scr} = critical bottom shear stress for erosion (N/m^2), $u_{*\mathrm{cr}} = \sqrt{\tau_{\mathrm{scr}}/\rho_w}$ = shear velocity (m/s), and $f(R_*)$ = a function of R_* obtained from experimental data.

Figure 3.4.1, known as the Shields diagram, is a graph of the Shields parameter, τ_*, versus the boundary Reynolds number, R_*. Shields obtained his critical values for τ_* experimentally, using uniform bed material and measuring sediment transport at decreasing levels of bed shear stress. The Shields curve separates the regions of motion and no motion for noncohesive sediments and represents the relationship between $\tau_{*\mathrm{cr}}$ and R_* given in Eq. (3.4.3). The Shields curve should be interpreted as representing a "gray area" of sediment erosion. When the bottom shear stress is less than the critical shear stress for a particular grain size, then no particle motion takes place and there is no transport. For flow conditions in the vicinity of $\tau_* \approx \tau_{*\mathrm{cr}}$, sporadic particle movement may occur. When the bed shear velocity exceeds the critical shear velocity but remains less than the settling velocity, then some of the noncohesive sediment is transported as bed load. Finally, when the bed shear velocity exceeds both the critical shear velocity and the settling velocity, then noncohesive particles may be entrained into the water column and transported as suspended load.

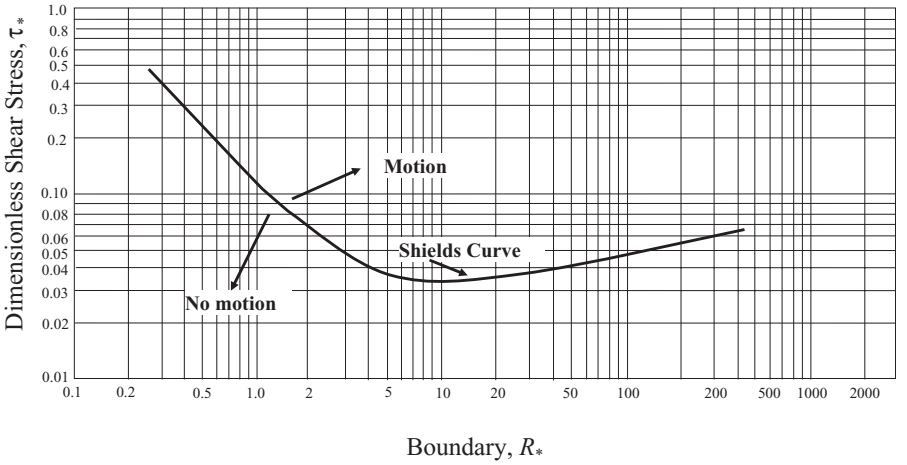

Fig. 3.4.1 Shields diagram: dimensionless bottom shear stress (Shields parameter) versus the boundary Reynolds number. (After Vanoni, 1978.)

The Shields diagram is used to predict whether a given bottom shear stress is sufficient to move a given bed sediment. Figure 3.4.1 shows that the critical Shields parameter, τ_{*cr}:

1. Has approximately a constant value of 0.06 for $R_* > 100$.
2. Increases steadily from a minimum of 0.035, as R_* decreases from the value at 10.

Despite the Shields diagram's usefulness for understanding the resuspension process of noncohesive sediments, it has its limitations. The Shields diagram was developed for uniform sediment and did not account for the effects of the grain-size distribution. However, natural sediments often have a distribution of sediment grain sizes. Deviations from the Shields curve will occur for nonuniform sediments. In this case, smaller particles will be removed at a lower velocity, while the larger particles are not. This process tends to erode the surface layer of smaller particles and leaves a surface with only larger particles exposed. The larger particles are not as easy to erode as the smaller particles and make the sediment surface more resistant to erosion. This phenomenon is known as armoring. Bed forms, such as ripples and dunes that develop with sediment transport, affect the calculation of the Shields parameter. The Shields curve given by Eq. (3.4.3) and Fig. 3.4.1 is somewhat inconvenient to use, because the critical shear velocity (u_{*cr}) is involved in both R_* and τ_*. The Shields diagram is implicitly derived for sandy to gravelly beds. Fine sediment tends to be more nonuniform, in terms of grain size, and cohesive. The Shields diagram also does not consider the effects of cohesive sediment.

3.4.2 Settling and Equilibrium Concentration

Particles are raised into suspension when the turbulence in the flow is sufficient to overcome the gravitational force on the particles. Once in suspension, the particles tend to settle out at a rate determined by the settling velocity and the turbulence intensity. The relative balance between the settling velocity and the flow turbulence determines sediment concentration, as illustrated in the analytical solution, Eq. (3.2.17).

At low concentrations, noncohesive sediments settle as discrete particles. The effective settling velocity (W_{se}) equals the settling velocity of a discrete particle (W_s):

$$W_{se} = W_s \tag{3.4.4}$$

At high concentrations, hindered settling and multiphase interactions can be important. The effective settling velocity of noncohesive sediment is less than the discrete velocity and can be expressed in the form of

$$W_{se} = \left(1 - \frac{S}{\rho_s}\right)^n W_s \tag{3.4.5}$$

where ρ_s = the sediment particle density, S = sediment concentration, n = empirical constant with values of 3 or 4 (van Rijn, 1984a, 1984b).

Lumley (1978) suggested that particle interaction can be neglected for volumetric sediment concentration $<3 \times 10^{-3}$, which is equivalent to a mass concentration of 8 g/L for sediment with specific gravity of 2.65. Since the maximum sediment concentrations in a water column are generally <8 g/L, the interactions between the noncohesive sediment grains are often neglected in sediment modeling studies.

Based on the formula proposed by Cheng (1997), the relationship between the settling velocity and the grain size for noncohesive sediments is presented in Fig. 3.4.2. For grain size between 75 and 500 μm, which is in the size range of sand (Table 3.1.1), the settling velocity varies from 280 to 5000 m/day.

After the settling velocity is determined, all parameters in the equation governing the suspended sediment concentration, Eq. (3.2.13), are known. To solve this equation, it is necessary to specify boundary conditions. One boundary condition, Eq. (3.2.14), is simply that no sediment is transported through the water surface. At the sediment bed ($z = 0$), the boundary condition for cohesive sediment is often expressed as the net sediment flux across the water column–sediment bed interface, represented in Eq. (3.2.15). For noncohesive sediment modeling, however, a commonly used bottom boundary condition is expressed as the near-bed equilibrium concentration at a reference distance above the bed.

At the water column–sediment bed interface, the net flux of noncohesive sediment is controlled primarily by the bottom shear stress, the particle size, and the particle density. Under steady conditions, an equilibrium distribution

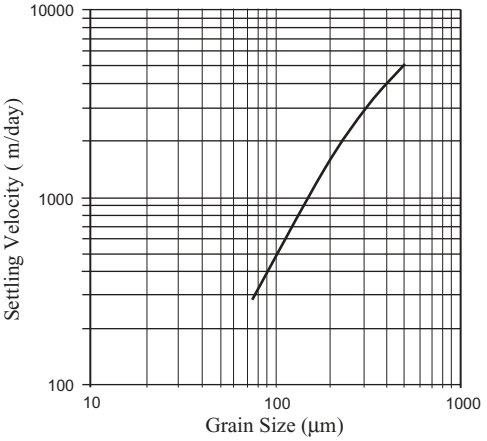

Fig. 3.4.2 Grain size and settling velocity of noncohesive sediment (based on Cheng, 1997).

of suspended sediment can be established with the erosion and deposition fluxes canceling each other. The equilibrium sediment concentration at a reference distance above the bed can then be expressed analytically. Garcia and Parker (1991) evaluated eight empirical formulas for determining the near-bed equilibrium concentrations. All of the formulas essentially specify the equilibrium concentration in terms of hydrodynamic and sediment parameters (Tetra Tech, 2002):

$$S_{\text{eq}} = S_{\text{eq}}(d_s, \rho_s, \rho_w, w_s, u_*, \nu) \tag{3.4.6}$$

where d_s = the sediment particle diameter, ρ_s = the sediment density, ρ_w = the water density, u_* = the bed shear velocity, w_s = the sediment settling velocity, and ν = the kinematic molecular viscosity of water. Garcia and Parker (1991) concluded that the representations of Smith and McLean (1977) and van Rijn (1984a, b), as well as their own proposed representation, perform acceptably when tested against experimental and field observations.

Smith and McLean's formula for the equilibrium concentration is

$$S_{\text{eq}} = \rho_s \frac{0.65\gamma_o T}{1 + \gamma_o T} \tag{3.4.7}$$

where γ_o is a constant equal to 2.4×10^{-3} and T is given by

$$T = \frac{\tau_b - \tau_{\text{cs}}}{\tau_{\text{cs}}} = \frac{u_*^2 - u_{*\text{cs}}^2}{u_{*\text{cs}}^2} \tag{3.4.8}$$

where τ_b is the bed stress and τ_{cs} is the critical Shields stress. The use of Smith and McLean's formulation requires that the critical Shields stress be specified for each sediment size class.

The formula by van Rijn (1984a, b) is

$$S_{\text{eq}} = 0.015\rho_s \frac{d}{z^*_{\text{eq}}} T^{3/2} R_d^{-1/5} \tag{3.4.9}$$

where z^*_{eq} is the dimensional reference height and R_d is a sediment grain Reynolds number, defined as:

$$R_d = \left(g\left(\frac{\rho_s}{\rho} - 1 \right) d_s \right)^{1/2} \frac{d_s}{\nu} \tag{3.4.10}$$

van Rijn suggested setting the dimensional reference height equal to three grain diameters. Garcia and Parker's (1991) general formula for multiple sediment size classes is

$$S_{\text{jeq}} = \rho_s \frac{A(\lambda Z_j)^5}{\left(1 + 3.33A(\lambda Z)^5\right)} \tag{3.4.11}$$

$$Z_j = \frac{u_*}{w_{\text{sj}}} R_{\text{dj}}^{3/5} F_H \tag{3.4.12}$$

$$F_H = \left(\frac{d_j}{d_{50}} \right)^{1/5} \tag{3.4.13}$$

$$\lambda = 1 + \frac{\sigma_\phi}{\sigma_{\phi o}} (\lambda_o - 1) \tag{3.4.14}$$

where A = a constant equal to 1.3×10^{-7}, d_{50} = the median grain diameter based on all sediment classes, λ = a straining factor, F_H = a hiding factor, σ_ϕ = the standard deviation of the sedimentological phi scale of sediment size distribution, and j = subscript for the jth sediment class.

Garcia and Parker's formulation accounts for armoring effects when multiple sediment classes are simulated. For the simulation of a single noncohesive size class, the straining factor and the hiding factor are set to 1.

Madsen (1993) proposed the following formula for estimating equilibrium concentration:

$$S_{\text{eq}} = \gamma C_b \left(\frac{\tau_b}{\tau_{\text{cs}}} - 1 \right) \tag{3.4.15}$$

in which γ is a resuspension parameter and C_b is the volume concentration of the bed sediment, generally taken as 0.65 for a noncohesive sediment bed (Smith and McLean, 1977). The resuspension parameter γ in Eq. (3.4.15) is

closely related to the choice of the reference distance above the bed. There is considerable uncertainty associated with the adoption of these γ values. The γ values reported in the literature can be used only in conjunction with their particular reference distance values. When the reference distance is 7 times the grain size, Wikramanayake and Madsen (1994) set $\gamma = 2 \times 10^{-3}$ for a rippled bed and $\gamma = 2 \times 10^{-4}$ for a flat bed.

3.4.3 Bed Load Transport

As illustrated in Fig. 3.2.2 (FISRWG, 1998), sediment particles can undergo three distinct modes of motion: (1) rolling and/or sliding, (2) saltating or jumping, and (3) in suspension. Flowing water exerts a shear stress on the bed material in the flow direction. The faster the water velocity, the greater the shear stress. When flow and sediment characteristics combine to produce a Shields parameter greater than the critical value (Fig. 3.4.1), sediment is set in motion. For values of the Shields parameter slightly above the critical value, sediment particles begin rolling and/or sliding, while remaining in continuous contact with the bed. As water velocity and shear stress increase, the particles then move along the bed in a series of more-or-less regular jumps, called "saltation". At even higher levels of bed shear stress, upward turbulent forces can lift sediment particles from the bed and carry them into the water column. If these forces are greater than the submerged weight of particles, the particles will remain in suspension (Fig. 3.2.2).

"Sediment load" denotes the material being transported and can be divided into bed load and suspended load. The transport of particles near the bed by rolling, sliding, and saltating is called bed load transport, whereas the transport of particles in suspension is called suspended load transport. Bed load transport and suspended load transport often occur simultaneously. In contrast with suspended load, bed load is the bed material that mostly moves in continuous contact with the bed. Bed load transport takes place in a thin layer close to the bed. Visual observations suggest that the bed load particles move within a region of <10–20 particle-diameter heights (Chanson, 1999). The transition between both modes of transport is not well defined. Bed load transport is highly dependent on water velocity. Slight changes in velocity can have a major effect on the rate of bed load transport.

Even though most of the sediment carried in waterbodies moves as suspended load, bed load can be essential to noncohesive sediment transport. For example, bed formation usually occurs as bed load, which is important to channel migration and can create a major hazard to navigation in large rivers. Bed load movement produces bed forms, such as ripples, bars, and dunes, which in turn affect the flow conditions, the bank stability, and the conditions for navigation (Tetra Tech, 2002).

The bed load transport rate can be defined as:

$$q_B = hS_0V_s \tag{3.4.16}$$

where q_B = bed load transport rate (mass-per-unit time-per unit-width normal to the flow direction), h = average thickness of the bed load layer or mean saltation height, S_0 = mean sediment concentration within the bed load layer, and V_s = average speed of sediment moving within the bed load layer. Bed load transport can be an important process resulting in transporting, sorting, and reordering the particles and size-class fractions within a waterbody. During bed load motion, particles are transported by rolling and/or saltating just above the bed surface. A number of bed load transport formulas have been developed. Bed load sediment transport formulas have the general semiempirical relation of

$$\frac{q_B}{\rho_s d_s \sqrt{g' d_s}} = \Phi(\tau_*, \tau_{*\mathrm{cr}}) \tag{3.4.17}$$

where Φ is a function of the Shields parameter (τ_*) and its critical value ($\tau_{*\mathrm{cr}}$). Many attempts have been made to determine the bed load transport by direct measurements and by the use of empirically or theoretically deduced formulas. None of these methods, however, have been universally accepted as completely adequate for the determination of bed load transport (Tetra Tech, 2002).

Two widely used bed load formulas are the ones of Meyer-Peter and Muller (1948) and Bagnold (1956) and their derivatives. The Meyer-Peter and Muller formulas are typified by

$$\Phi = \phi_1(\tau_* - \tau_{*\mathrm{cr}})^{3/2} \tag{3.4.18}$$

where ϕ_1 is a function of $(\tau_* - \tau_{*\mathrm{cr}})$.

The Bagnold formulas are typified by

$$\Phi = \phi_2(\tau_* - \tau_{*\mathrm{cr}})\left(\sqrt{\tau_*} - \gamma\sqrt{\tau_{*\mathrm{cr}}}\right) \tag{3.4.19}$$

where γ is a parameter and ϕ_2 is a function of $(\tau_* - \tau_{*\mathrm{cr}})$. Based on Bagnold's formula, Ji (1993) and Ji and Mendoza (1997) studied bed load processes using a weakly nonlinear theory, and demonstrated the importance of advection and diffusion of the flow to bed load transport.

The bed load formulation by van Rijn (1984a, b) is represented as:

$$\Phi = \frac{0.053}{R_d^{1/5}}\left(\frac{\tau_* - \tau_{*\mathrm{cr}}}{\tau_{*\mathrm{cr}}}\right)^{2.1} \tag{3.4.20}$$

where the sediment grain Reynolds number (R_d) is defined by Eq. (3.4.10).

3.5 SEDIMENT BED

Sediment bed plays an important role in sediment transport and in the transport and fate of water quality constituents. Sediments (and the sorbed

contaminants) buried in the bed by deposition may be released to the water column by erosion later. The bed properties, mainly the grain size distribution and interparticle cohesion, significantly affect resuspension from a cohesive sediment bed. If sediment is deposited in locations where the critical shear stress is not exceeded, or is exceeded only infrequently, then the sediment will slowly consolidate, increasing in both density and strength. The critical shear stress for erosion is a function of the consolidation or density of the bed. The closer the particles are to each other, the stronger the cohesive bond and the greater shear force needed to separate them. As bed density increases, so the stress threshold for erosion increases, and the sediment deposit becomes more stable and less likely to be eroded by natural forces.

3.5.1 Characteristics of Sediment Bed

Sediment beds are comprised of three phases: solid, water, and gas. The solid phase consists of minerals and/or organic matter that form the skeleton of the sediment. Soil pores exist between solid particles and hold water and gases. Pore water (or interstitial water) is the water found in the interstices between the solid particles. The gas phase in the sediment bed is usually insignificant and is often neglected in the studies of sediment transport. But there are also exceptions. For example, Jepsen et al. (2000) measured the erosion rates and bulk properties of sediments from 11 sites in the Grand River in Michigan. They reported that high concentrations of gas, up to 5% by volume, were present in the sediments. This significantly affected the sediment bulk density and erosion rates.

The solid particle density, ρ_s, is defined as:

$$\rho_s = \frac{M_s}{V_s} \tag{3.5.1}$$

where M_s = the mass of the solid and V_s = the volume of the solid. The solid particle density is a function of the mineral composition of the particle. A value of 2.65 g/cm^3 is usually used for sand particles. Equation (3.5.1) defines a density relating to a particle itself. In order to account for the aggregations of sediments and the void spaces around sediment particles, porosity and bulk density are introduced.

Bulk density refers to a group of particles and is defined as:

$$\rho_b = \frac{M_s}{V} \tag{3.5.2}$$

where V is the volume of sediment bed:

$$V = V_s + V_w \tag{3.5.3}$$

and where V_w = the volume of water.

The solid and water volumes are calculated by

$$V_s = (1-\theta)V = \frac{V}{(1+\varepsilon)} = \frac{M_s}{\rho_s} \tag{3.5.4}$$

$$V_w = \theta V = \frac{\varepsilon V}{(1+\varepsilon)} = \frac{M_w}{\rho_w} \tag{3.5.5}$$

where ρ_w = water density, M_w = water mass, θ = porosity, and ε = void ratio.

Porosity is defined as the ratio of pore space (or voids) to the total volume of the sediment sample. Void ratio is the ratio of water volume over solid volume. Porosity is a function of how tightly the grains are packed together, and thus, is not a constant for a given sediment. In the sediment layer, porosity is the fraction of the total volume in the water phase. The void ratio (ε) and porosity (θ) are related by

$$\varepsilon = \frac{\theta}{(1-\theta)} = \frac{V_w}{V_s} \tag{3.5.6}$$

$$\theta = \frac{\varepsilon}{(1+\varepsilon)} = \frac{V_w}{V} \tag{3.5.7}$$

The sediment or solids concentration in a bed control volume, S, is defined as the ratio of sediment mass over the total volume:

$$S = \frac{M_s}{V} = \rho_s(1-\theta) = \rho_s\left(\frac{1}{1+\varepsilon}\right) \tag{3.5.8}$$

In Lake Okeechobee (Hwang and Mehta, 1989), for example, $\theta = 0.45$ and $\rho_s = 2.0\,\text{g/cm}^3$, and the concentration of solids in the sediment layer is $1.1\,\text{g/cm}^3$.

Hwang and Mehta (1989) collected sediment core data at 31 sites in Lake Okeechobee. They described the vertical structures of the core samples and measured bed bulk density and shear strength profiles at each site. They reported that, despite data scatter, the sediment bulk density and shear strength are closely related. Table 3.5.1 lists the values of bed depths, densities, and shear strengths of a core sample. Figure 3.5.1 shows the corresponding results graphically. These measured data indicate that bulk density generally increases with depth. Hwang and Mehta (1989) reported that sediment bed density is not only related to bed shear strength, but is also dependent upon mud composition. Typically, mud density ranges from $1.01\,\text{g/cm}^3$ up to $1.25\,\text{g/cm}^3$ with a maximum value of $1.3\,\text{g/cm}^3$. The surface mud layers with small shear strength can be easily resuspended under moderate wind conditions due to wind waves and currents, whereas the lower mud layers are difficult to be resuspended, except under severe weather conditions.

Rivers and streams with mostly gravel or coarser bed material usually possess a surface coarser than the underlying material. This characteristic,

TABLE 3.5.1 Bulk Density and Shear Strength of Sediment Bed in Lake Okeechobee[a]

Depth (cm)	Density (g/cm^3)	Shear Strength (N/m^2)
0–5	1.106	386
5–10	1.084	531
10–15	1.099	627
15–20	1.102	1448
20–25	1.131	1448
25–30	1.112	1979

[a]Hwang and Mehta, 1989.

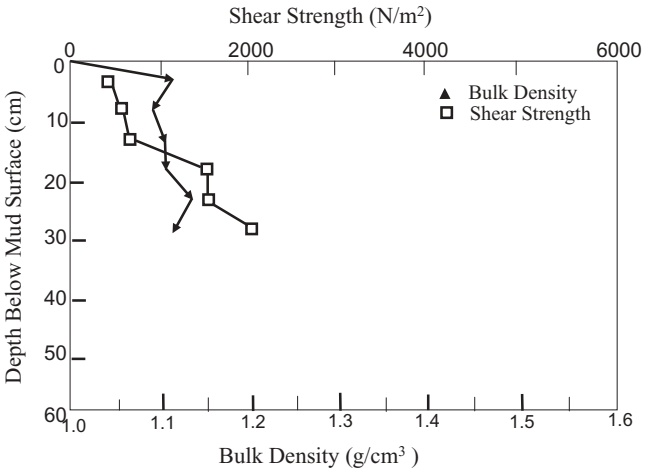

Fig. 3.5.1 Bulk density and shear strength of the sediment bed in Lake Okeechobee. (After Hwang and Mehta, 1989.)

called armoring, occurs in a wide variety of mountain and alluvial streams, which have a large range of different flows, sediment transport rates, and size distribution of bed materials. Armoring is the process of progressive coarsening of a noncohesive sediment bed layer by removal of fine particles until it becomes resistant to scour. In rivers, the coarse layer acts to control the movement of stored sediment and protects the finer materials below from excessive scour during floods. Armoring is also a temporary condition; higher flows may destroy an armored surface layer. Neglecting armoring effects may lead to overestimating erosion in certain river sections.

3.5.2 A Model for Sediment Bed

There is a need for information on the bed material properties. How much sediment is available for resuspension? What is the critical shear stress for

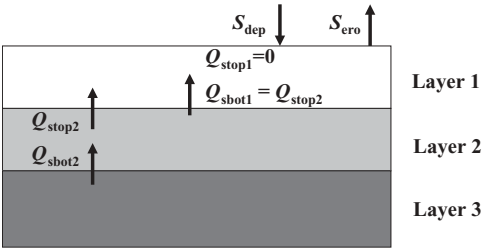

Fig. 3.5.2 Schematic presentation of sediment bed layers.

sediment resuspension? Some of these questions could be answered if a reliable sediment bed model became available. Even though the mathematical representations of a sediment bed vary widely, there are still many similarities and common features among the models. The cohesive sediment bed model used in the study of Lake Okeechobee (Tetra Tech, 2002; Jin and Ji, 2004) is described here.

The sediment bed model couples with the sediment transport model in the water column and updates the bed erosion/deposition based on flow conditions and sediment bed conditions. Since the bed thickness is much less than the bed horizontal scale, the mass conservation laws used in the sediment bed models are essentially 1D in the vertical. The sediment bed is discretized into layers in the model (Fig. 3.5.2). Two types of bed layers are considered: an uppermost layer and one or more lower layers. When deposition occurs, the uppermost layer increases in volume. When net erosion occurs, the volume of the top layer decreases. When the top layer erodes completely, the next bed layer is exposed to scour.

Conservation of sediment mass in a bed control volume is given by

$$\frac{d}{dt} M_s = \rho_s Q_{\text{sbot}} - \rho_s Q_{\text{stop}} + A W_{\text{de}} S_{\text{dep}} - A W_{\text{ee}} S_{\text{ero}} \tag{3.5.9}$$

where M_s = sediment mass, Q = volumetric flux (volume/time), ρ_s = sediment density, A = area of the control volume, W_{de} = sediment-effective deposition velocity, W_{ee} = sediment-effective erosion velocity, S_{dep} = concentration of sediment settling into the control volume from the water column, S_{ero} = concentration of sediment eroding from the control volume into the water column, subscribe stop = sediment volumetric flux out of the top surface of the control volume, and subscribe sbot = sediment volumetric flux into the bottom surface of the control volume.

In Eq. (3.5.9), a positive volumetric flux indicates upward transport. The third and fourth terms on the right-hand side of Eq. (3.5.9) represent the deposition and erosion in the uppermost layer adjacent to the water column, but are omitted in the lower layer. The volumetric flux Q_{stop} is also set to zero in the uppermost layer.

As illustrated in Fig. 3.5.2, the uppermost layer (Layer 1) has sediment deposition and erosion fluxes, and the sediment volumetric flux out of the top surface of Layer 1, Q_{stop1}, is set to zero. Layer 2 (and the remaining lower layers) have volumetric fluxes Q_{stop2} and Q_{sbot2}.

Similarly, conservation of water mass in a bed control volume is given by

$$\frac{d}{dt}M_w = \rho_w Q_{\text{wbot}} - \rho_w Q_{\text{wtop}} + \varepsilon_d A \frac{\rho_w}{\rho_s} W_{\text{de}} S_{\text{dep}} - \varepsilon A \frac{\rho_w}{\rho_s} W_{\text{ee}} S_{\text{ero}} \qquad (3.5.10)$$

where M_w = water mass, Q = volumetric flux (volume/time), ρ_w = water density, ε = void ratio in sediment bed, and ε_d = void ratio in water column near the sediment bed, subscript wtop = water volumetric flux out of the top surface of the control volume, and subscript wbot = water volumetric flux into the bottom surface of the control volume.

Sediment erosion is a time- and material-dependent process. The bed model needs to track sediment layering: the composition and state of each sediment layer at each grid point in the model, which is more a bookkeeping function than numerical modeling. During each time step of simulation, either erosion or deposition occurs, depending on the shear stresses on the bed. If deposition occurs, then sediment is deposited on the top layer of the sediment bed. When the shear stress imposed on the bed surface exceeds the critical shear stress, erosion occurs. This process proceeds downward through layers of the original bed, as long as the shear stress imposed exceeds the critical shear stress at each layer. During each time step, if the computed erosion depth is greater than the thickness of the top layer, then erosion continues on to the next sediment bed layer (Tetra Tech, 2002).

The sediment bed can be represented by discrete layers of thickness B_k. Under the assumption that the bed sediment density and void ratio do not change with time, the sediment mass conservation equation (3.5.9) can be written separately for the top layer ($k = 1$) and the underlying layers ($k > 1$) as:

$$S_1 \frac{\partial B_1}{\partial t} = J_{1-} - J_0 \qquad \text{for Layer 1} \qquad (3.5.11)$$

$$S_k \frac{\partial B_k}{\partial t} = J_{k-} - J_{k+} \qquad \text{for Layer } k \qquad (3.5.12)$$

where S_k = the sediment concentration at Layer k, J_k = the sediment flux at Layer k, J_0 = the net sediment flux at the surface of the sediment bed, and B_k = the sediment bed depth at Layer k, subscript + = parameter value at the top of the layer, and subscript – = parameter value at the bottom of the layer.

From Eq. (3.5.8), the bed sediment concentration, S_k, is expressed as:

$$S_k = \frac{\rho_s}{1 + \varepsilon_k} \qquad (3.5.13)$$

Hence, the sediment density, ρ_s, the void ratio, ε_k, and the sediment concentration, S_k, are constant. The net sediment flux at the surface of the sediment bed, J_0, is also needed in the boundary condition (3.2.15) for the sediment transport equation (3.2.13). the parameter J_0 is the summation of sediment resuspension and resuspension fluxes at the water column–sediment bed interface.

Similarly, the corresponding water mass conservation equations are obtained from Eq. (3.5.10):

$$\left(\frac{\varepsilon_1}{1+\varepsilon_1}\right)\frac{\partial B_1}{\partial t} = q_{1-} - q_{1+} - \frac{1}{\rho_s}(\varepsilon_1 \max(J_0, 0) + \varepsilon_d \min(J_0, 0)) \qquad \text{for Layer 1} \tag{3.5.14}$$

$$\left(\frac{\varepsilon_k}{1+\varepsilon_k}\right)\frac{\partial B_k}{\partial t} = q_{k-} - q_{k+} \qquad \text{for Layer } k \tag{3.5.15}$$

After the sediment mass conservation equations (3.5.11) and (3.5.12) are solved, the water mass conservation equations, (3.5.14) and (3.5.15), can be solved successively downward.

To further simplify the sediment bed model, the internal sediment fluxes, J_k, can be set to zero. In this way, the change in the bed thickness of the top layer, B_1, is determined directly using Eq. (3.5.11). The thicknesses of the underlying layers are not changed with time unless the top layer is completely eroded and the lower layer is exposed to the water flow. In the study of Lake Okeechobee, the sediment bed model is configured to have a prespecified maximum number (=3) of sediment bed layers (Jin and Ji, 2004). At the start of a simulation, the number of layers containing sediment at specific horizontal locations is specified. Under continued deposition, a new sediment layer is created when the thickness of the top layer exceeds a prespecified value. Under continued resuspension, the layer underlying the top layer becomes the new top layer adjacent to the water column after all sediment is resuspended from the existing layer.

3.6 WIND WAVES

The primary reason for considering wind waves in this chapter is that wind waves can significantly affect sediment deposition and resuspension in shallow waters, thus affecting transports of contaminants (e.g., metals) and eutrophication processes (e.g., phosphorus transport). Here shallow waters are areas of a waterbody where wind wave energy can reach the bottom of the water column and contribute significantly to the bottom shear stress calculation.

In deep waterbodies, wind waves usually do not reach the bottom, and hence have little impact on sediment resuspension. In shallow waterbodies,

however, coupling among the various processes is much more pronounced and wind waves can be significant in sediment modeling. Even though the wave-induced mass transport is negligible compared to the wind- or tide-driven currents, wind waves in shallow waters can substantially increase sediment resuspension from the bed. The wind wave-induced oscillatory motion can increase the bottom shear stress, soften the sediment bed, and then lead to sediment resuspension. In the presence of currents, the combined wave-current shear stress can be quite large, and the bed sediment can be resuspended by the combined wave-current shear stress and be transported by the currents (Jin and Ji, 2004).

This section describes the general features of wave processes, wind waves, and the combined flow of wind waves and currents. After two types of wind wave models are introduced, the modeling of wind waves in Lake Okeechobee is presented as a case study.

3.6.1 Wave Processes

As illustrated in Fig. 3.6.1, the terms used to describe waves include the following:

1. *Wave Crest:* The highest part of the wave that is elevated above the mean water level.
2. *Wave Trough:* The lowest part of the wave that is depressed below the mean water level.
3. *Wavelength (L):* The distance between two consecutive wave crests or wave troughs.
4. *Wave Height (H_s):* The vertical distance between a wave crest and the next trough.
5. *Wave Amplitude (A):* The vertical distance between a wave crest (or trough) and the mean water level.
6. *Wave Period (T_s):* The time that it takes for two consecutive wave crests or wave troughs to pass a given point.
7. *Wave Direction:* The direction from which waves approach a location.

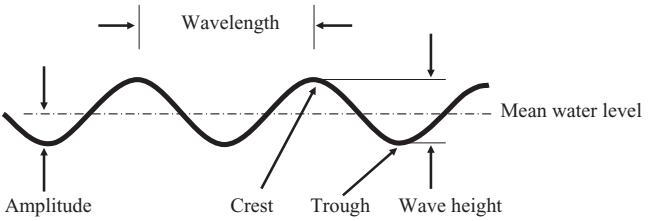

Fig. 3.6.1 Sketch of a sinusoidal wave.

The relationships are

$$L = \frac{2\pi}{k} = \frac{c}{f} = cT_s \tag{3.6.1}$$

where k = wave number, c = wave phase speed, and f = wave frequency.

For a wave process, the vertical motion of particles is significant and the nonhydrostatic equations should be used. After neglecting the nonlinear effects, water viscosity, turbulence activity, and Coriolis forcing, the Navier–Stokes equation, Eq. (2.1.19), can be simplified to

$$\frac{\partial u}{\partial t} = -\frac{1}{\rho}\frac{\partial p}{\partial x} \tag{3.6.2}$$

$$\frac{\partial v}{\partial t} = -\frac{1}{\rho}\frac{\partial p}{\partial y} \tag{3.6.3}$$

$$\frac{\partial w}{\partial t} = -\frac{1}{\rho}\frac{\partial p}{\partial z} - g \tag{3.6.4}$$

where u, v, and w are the velocity components under Cartesian coordinates (x, y, z). The corresponding continuity equation is Eq. (2.2.11). Wave processes are often analyzed using analytical and numerical methods (e.g., Ji and Chao, 1986, 1990). The water pressure, p, can be expressed as:

$$p = p_a - g\rho z + p'(x, y, z, t) \tag{3.6.5}$$

where p_a = atmospheric pressure and $p'(x, y, z, t)$ = disturbed water pressure.

The vertical boundary conditions at the water surface ($z = \eta$) are

$$\frac{\partial \eta}{\partial t} = w \tag{3.6.6}$$

$$p'(x, y, z, t) = g\rho\eta \tag{3.6.7}$$

The vertical boundary condition at the water bottom ($z = -H$) is

$$w = 0 \tag{3.6.8}$$

Under the linear wave theory, the wave solutions to the above equations can lead to the following relationship between wave phase speed and wave number:

$$c = \sqrt{\frac{g}{k}\tanh(kH)} \tag{3.6.9}$$

where c = wave phase speed (or celerity), $k = 2\pi/L$ = wave number, L = wavelength, and H = mean water depth. Equation (3.6.9) is also called the dispersion relationship of surface waves.

According to the values of kH ($=2\pi H/L$), waves can be classified as:

1. Short waves (or deep waves), as $KH >> 1$.
2. Longwaves (or shallow waves), as $KH << 1$.
3. Intermediate waves, as $KH \sim 1$.

The distinction between short waves and long waves has little to do with absolute water depth, but is determined by the ratio of water depth to wavelength. Practically, they are often defined as:

1. Short waves (or deep waves), as $H > L/2$.
2. Longwaves (or shallow waves), as $H < L/20$.
3. Intermediate waves, as $L/20 \le H \le L/2$.

It is important to point out that only longwaves (shallow waves) can significantly affect bottom shear stress and thus influence sediment resuspension. Since the wave energy decreases exponentially with water depth, the short waves (or deep waves) add little to the bottom shear stress.

Water particle velocities under the linear wave theory are maximal at the surface and decrease exponentially with depth. Figure 3.6.2 shows the particle orbital motion in deep water in which the water particles perform orbital motions in cycle and the amplitude decreases by depth. The wave-induced orbit is the greatest at the surface where the radius is equal to the wave amplitudes [i.e., one-half of the wave height (H_s)]. Below the water surface, the orbital radius of particles decreases.

Short waves have $kH >> 1$ and $\tanh kH \approx 1$. Equation (3.6.9) becomes

$$c = \sqrt{\frac{g}{k}} = \sqrt{\frac{gL}{2\pi}} \tag{3.6.10}$$

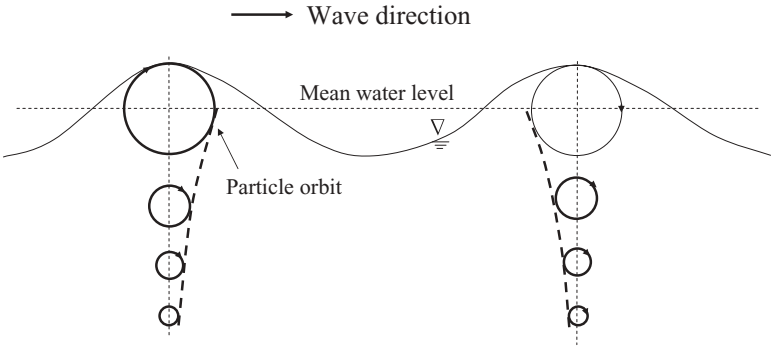

Fig. 3.6.2 Particle orbital motion in deep water.

which indicates that short waves are dispersive and their phase speed, c, depends on wavelength, L.

When waves move into shallow water, the waves begin to interact with the bottom and to affect orbital motion. Their horizontal motion components are maintained while the vertical components decrease. The orbits become flattened circles or ellipses. When the water depth is between $L/2$ and $L/20$, the wave speed is slowed, and the waves in this depth range are called intermediate waves.

When the waves finally enter the area with $H < L/20$, the waves become longwaves (shallow waves). With $kH \ll 1$ and $\tanh kH \approx kH$, Eq. (3.6.9) becomes:

$$c = \sqrt{gH} \tag{3.6.11}$$

Equation (3.6.11) indicates that short wave speed is determined by water depth. In contrast to the circular orbits in deep water (Fig. 3.6.2), wave orbits become increasing flatter or elliptical (Fig. 3.6.3) as waves enter a shallow water area. The elliptical paths followed by the water particles flatten to horizontal lines, particularly at the bottom where no vertical flow is allowed. As the orbits flatten, the motion of the water becomes essentially a horizontal oscillation.

Wavelength can also be calculated based on Eq. (3.6.9):

$$L = L_0 \tanh\left(\frac{2\pi H}{L}\right) = \frac{gT_s^2}{2\pi}\tanh\left(\frac{2\pi H}{L}\right) \tag{3.6.12}$$

where $L_0 = gT_s^2/2\pi$ = wave length in deep water. For a wind wave with a period of 3 s, the wave length in deep water is 14 m. After the wave period (T_s) and water depth (H) are known, an iteration method is often used to calculate wavelength L in Eq. (3.6.12).

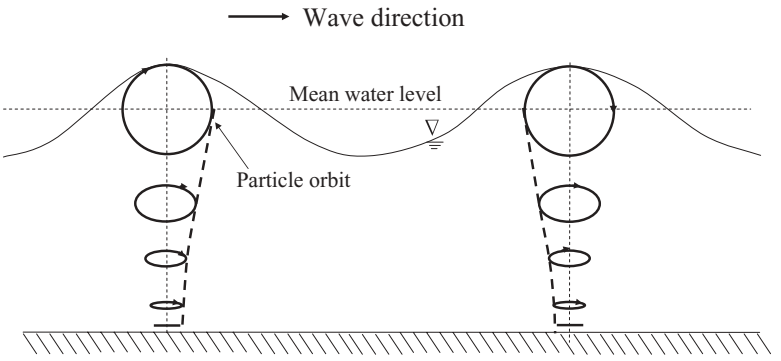

Fig. 3.6.3 Particle orbital motion in shallow water.

The maximum orbital velocity of wave motions near the bottom becomes:

$$u_{\max} = \frac{2\pi H_s}{T_s \sinh\left(\frac{2\pi H}{L}\right)} \tag{3.6.13}$$

where $u_{\max}$ = maximum orbital velocity (m/s), H_s = significant wave height (m), T_s = wave period (s), H = water depth (m), L = wavelength (m), and sinh(x) = hyperbolic sine function. Equation (3.6.13) reveals that orbital velocity is a function of wave height (H_s), wave period (T_s), water depth (H), and wavelength (L).

The maximum shear stress exerted by wind wave, τ_b, is

$$\tau_b = C_f \rho\, u_{\max}^2 \tag{3.6.14}$$

where ρ is the water density, and C_f is the bottom friction coefficient, which depends on both the bed roughness and the flow characteristics in the wave boundary layer. Chapra (1997) reported that for shallow lakes, where currents are generally small, Eq. (3.6.14) can be approximated by

$$\tau_b = 0.3 u_{\max}^2 \tag{3.6.15}$$

where τ_b = maximum bottom shear stress (dyn/cm^2) and $u_{\max}$ = maximum orbital velocity (m/s).

Although wave particles remain approximately at the same position on average, wave energy sets water particles in motion. The surface water particles trace an orbit with a diameter equal to the wave height. This same type of motion is present in the water particles below the surface, but as less energy of motion is present in the water particles, the orbits become smaller and smaller with depth. At a depth equal to one-half the wavelength, the orbital motion decreases to almost zero. Figure 3.6.4 schematizes a "snap-shot" of

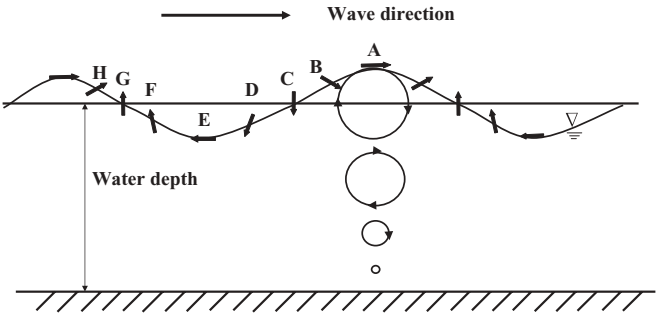

Fig. 3.6.4 Schematic representation of particle motion under a surface wave.

particle motions at different wave phases using local velocity vectors. The diagram uses vertical exaggeration for clarity.

At the wave crest (Point A), the particle motion is horizontal and in the direction of the wave. As the crest passes, the particles begin to fall and their forward motion slows (Point B). They reach a maximum falling speed and a zero forward speed at the midpoint between crest and trough (Point C). As the trough advances, the particles slow in falling speed and start to move backward (Point D). At the bottom of the trough, the particles reach the maximum backward speed and neither rise nor fall (Point E). The velocity at Point E is reversed, but is of the same magnitude as at the crest (Point A). As the remainder of the trough passes, the particles begin to slow in their backward motion and start to rise (Point F). At the midpoint between the trough and crest (Point G), the particles reach a maximum rising speed and a zero backward motion. As the crest approaches (Point H), the particles keep rising and begin to move forward. This cycle of motion creates a circular path (an orbit) for the water particles. These descriptions are based on linear wave theory. When nonlinear wave processes are included, effects such as Stokes shift should be considered.

3.6.2 Wind Wave Characteristics

In ascending order of wavelengths, water waves can also be classified by their generating forcings:

1. *Meteorological Forcings (Wind and Atmospheric Pressure):* Wind waves belong to this category.
2. *Earthquakes:* They generate tsunamis.
3. *Astronomical Forcings:* They generate tides.

These three waves are all gravitational waves, that is, they have gravity as the restoring force. Wind waves are discussed in this section. Tsunamis are long-period ocean waves generated by geological and tectonic disturbances below sea level. Tsunamis travel at speeds of up to 800 km/h in the open ocean where they are of low height. However, tsunamis can rise to a height of 10 m or more as they approach land. Tsunamis will not be discussed in this book. Tidal waves will be discussed in Chapter 10 along with estuaries.

Wind waves are formed by wind blowing over the water surface. They typically have periods of 1 to a few tens of seconds. Wind waves are characterized by a range of wave heights, periods, and wavelengths. At any given instant in time, a waterbody always has more than one single harmonic oscillation. For many studies, such as sediment transport modeling, only the highest waves are of interest. A significant wave height is the average wave height of the highest one-third of all waves in a given sample period. A significant wave period is the averaged period corresponding to the highest one-third waves.

The effect of the wind on water waves depends on the distance over which the wind can blow. This distance is known as the fetch, which is defined as the horizontal distance over water that the wind has blown uninterrupted by land. When computed along the direction of the prevailing wind, the fetch length can provide an indication of wave heights.

When the wind blows over a large surface water area, wind energy is transferred to the waterbody. Wave energy is imported by wind stress and lost to bottom friction. The duration of the wind and the time and direction from which it blows are important factors in the ultimate height of a wave. Wind energy is first absorbed by surface waves and then quickly dissipated into the underlying water columns by wave-breaking processes and turbulence. These waves grow in size and length as a result of the continuing push of the wind on the back of the waves and of the shearing or tangential force between the wind and the water. As waves form, the surface becomes rougher, and it is easier for the wind to grip the roughened water surface and add energy. This process results in increased frictional drag between the air and the water. Wind energy is then increased, and the oscillations of the water surface become larger.

Figure 3.6.5 gives the measured wind speed, significant wave height, and suspended sediment concentration in Lake Okeechobee for 4 days, from May

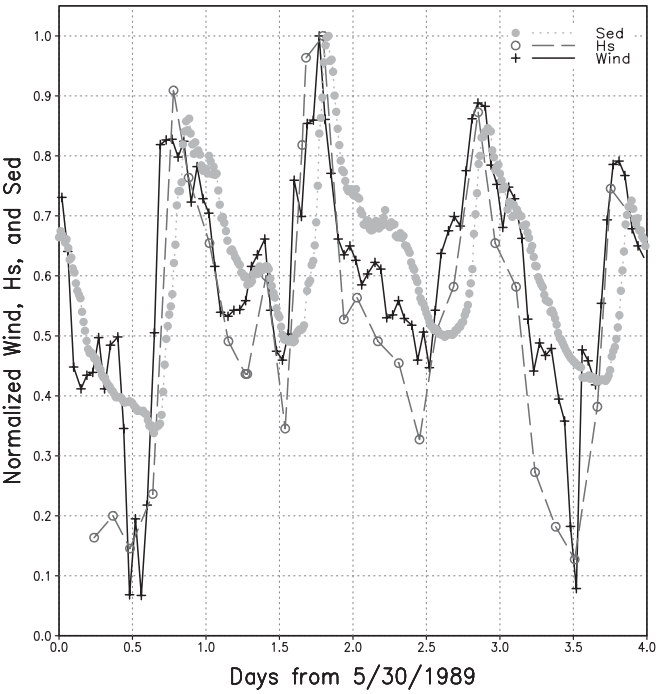

Fig. 3.6.5 Measured wind speed (Wind), significant wave height (Hs), and suspended sediment concentration (Sed) in Lake Okeechobee from May 30 to June 2, 1989.

30, 1989 to June 2, 1989. The horizontal axis is days from May 30, 1989. The vertical axis represents the normalized wind speed, significant wave height, and sediment concentration. The normalized wind speed, which is equal to the wind speed divided by its maximum value (=8.77 m/s), is represented by a solid line and crosses (+). The dashed line and the empty circles (○) represent the normalized values of significant wave height, which has a maximum value of 0.402 m. The dotted line and the filled circles (•) represent the normalized values of suspended sediment concentration (with a maximum value of 88.5 mg/L). At ~Day 1.7, the wind speed, the significant height, and the sediment concentration all reach their maximum values.

Figure 3.6.5 indicates clearly that wind speed, significant wave height, and sediment concentration are closely related. Wind generates wind waves (and currents) that affect sediment concentrations. When wind speed increases, the significant wave height increases accordingly. Along with the currents, the wind waves increase the bottom shear stress and the sediment resuspension from the bed and then lead to higher sediment concentration in the water column. Figure 3.6.5 also shows that, generally, the variation of sediment concentration lags behind the variation of wind speed by 1 to 2 h. This lagged correlation provides another indication that wind is the driving mechanism in sediment resuspension. The wind speed and the significant wave height correlate very well, both during high wind speed periods and during low wind speed periods. On the other hand, the sediment concentration correlates with the wind speed better during the periods of high wind speed than during the periods of low wind speed. This indicates that when wind speed is high, sediment resuspension is largely controlled by wind, whereas when wind speed is low, the sediment deposition and transport can also be affected by other mechanisms such as currents and stratification. The importance of wind waves to sediment processes is clearly demonstrated in Fig. 3.6.5. To study sediment transport in shallow waters, the effects of wind waves must be considered.

3.6.3 Wind Wave Models

Wind waves are often simulated using empirical equations or numerical models. Two representative wind wave models, one empirical and one numerical, are introduced here.

Since Sverdrup and Munk (1947) introduced the first empirical formulation to estimate the significant wave heights in a sea, the development in wind wave simulation and prediction has made great progress. Based on empirical data from Lake Okeechobee and the Gulf of Mexico, Bretschneider (1958) presented graphic relations for significant wave height, wave period, water depth, and wind fetch and developed a semiempirical wave forecasting relationship. Ijima and Tang (1966) converted these graphic relations into empirical formulas. This type of empirical formulation is sometimes called the SMB (Sverdrup, Munk, and Bretschneider) model. Kang et al. (1982) studied wave action and

bottom shear stress in Lake Erie and summarized a series of mathematical formulas for describing wind wave processes.

The shallow wave model SMB is an empirical model based on dimensional analysis:

$$\frac{gH_s}{U^2} = 0.283 \tanh\left[0.53\left(\frac{gH}{U^2}\right)^{0.75}\right] \tanh\left[\frac{0.0125\left(\frac{gF}{U^2}\right)^{0.42}}{\tanh\left(0.53\left(\frac{gH}{U^2}\right)^{0.75}\right)}\right] \quad (3.6.16)$$

$$\frac{gT_s}{2\pi U} = 1.2 \tanh\left[0.833\left(\frac{gH}{U^2}\right)^{0.375}\right] \tanh\left[\frac{0.077\left(\frac{gF}{U^2}\right)^{0.25}}{\tanh\left(0.833\left(\frac{gH}{U^2}\right)^{0.375}\right)}\right] \quad (3.6.17)$$

where H_s = significant wave height (m), T_s = significant wave period (s), U = wind speed (m/s), F = fetch length (m), H = mean water depth along the fetch length (m), and g = gravitational acceleration (m/s^2). The coefficients in Eqs. (3.6.16) and (3.6.17) may vary slightly for different formulations.

To derive Eqs. (3.6.16) and (3.6.17), the basic assumptions of the SMB model are

1. The wind has been blowing long enough in one direction so that the wave field has had enough time to come into equilibrium with the wind.
2. The wind speed and water depth are spatially uniform over the fetch.

The wind input to the model is typically averaged over 1-h intervals. Sheng and Chen (1993) applied solutions similar to Eqs. (3.6.16) and (3.6.17) to Lake Okeechobee. They reported that the results are usually satisfactory if the variation in wind direction is <45° and the variation in wind speed is <2.5 m/s. In Eqs. (3.6.16) and (3.6.17), the consequences of assuming a uniform depth are that, in shallow waters, the effects of depth-dependent processes, such as refraction, shoaling, and wave dissipation, are poorly described. Another limitation of this method is that the wave direction is not given, which is necessary information when the combined flows of waves and currents are calculated for sediment modeling (to be discussed in Section 3.6.4). Despite these limitations, the SMB model and its variations are commonly used for giving quick, order-of-magnitude estimates for wind waves.

Considerable effort has been spent to construct numerical models to simulate wind forcing, nonlinear interaction, and dissipation. A variety of wind wave models are available for use in practical engineering and research problems. One of the widely used wind wave models is the SWAN model (acronym for Simulation WAve Nearshore) (SWAN, 1998). The SWAN model

covers refraction, shoaling, and blocking in wave propagation and shifting frequency due to space variation. The model does not include wave diffraction or reflection, and is therefore most useful in applications where accuracy of the computed wave field is not required in the immediate vicinity of obstacles.

The SWAN model is a finite difference model and can directly use a Cartesian or curvilinear grid that is used in a hydrodynamic and sediment model. It has the ability to compute a time-varying solution rather than just a series of steady-state solutions. In the event that wind–driven waves do not have sufficient time to reach equilibrium with wind forcing, for example during hurricanes and other fast moving storms, the SWAN model has this important advantage over other steady state wind wave models, since storm and hurricane events are often the most important periods for sediment transport. Accurately predicting wind waves during storm and hurricane periods is critical for sediment modeling.

In the SWAN model, a single governing equation characterizes the process of wave transformation through a model domain. This action balance equation is composed of six terms that define energy inputs or losses in the system:

$$\frac{\partial}{\partial t}N+\frac{\partial}{\partial x}c_x N+\frac{\partial}{\partial y}c_y N+\frac{\partial}{\partial \sigma}c_\sigma N+\frac{\partial}{\partial \theta}c_\theta N=\frac{S}{\sigma} \tag{3.6.18}$$

where σ = the relative frequency (as observed in a frame of reference moving with the action propagation velocity), θ = the wave direction (the direction normal to the wave crest of each spectral component), $N(\sigma,\theta)$ = action density spectrum, $S(\sigma,\theta)$ = wave energy sources and sinks (e.g., wind-induced growth, depth-induced breaking), and c = propagation velocities of wave action (energy and currents).

In Eq. (3.6.18), the first term is the change in action density with time. The second and third terms represent wave propagation in geographical space. The fourth term represents the shifting of the relative frequency due to variations of depth and currents, and the fifth term represents changes in the action spectrum due to depth and current-induced refraction. Details of the SWAN model are given by SWAN (1998).

3.6.4 Combined Flows of Wind Waves and Currents

Waves tend to loosen and resuspend bed sediment. On the other hand, waves are an inefficient transporting mechanism, and to the first order and on average, wave motion does not cause net sediment transport in the horizontal direction. Currents, even with very small speeds, can cause a net transport. A simplified picture is that, in shallow waters, wind waves act to stir the sediment bed and the weak currents carry away the suspended sediment. In the immediate vicinity of the sediment bed, however, the wave and current motions cannot be treated separately and then superposed. Rather, there are nonlinear interactions between the two flows.

How waves and currents interact with the bottom to determine bottom shear stress and move sediment has been investigated intensively in the past decades. Wave–current interaction plays a significant role in the study of shallow-water sediment transport and in affecting both the erosion and deposition of sediments. Grant and Madsen (1979) parameterized the wave–current interaction by using two different eddy viscosity formulations for the current boundary layer and the wave boundary layer. Styles and Glenn (2000) further improved the boundary layer interaction model.

The wave–current interaction is associated with the nonlinear coupling of the wave and current boundary layers (Styles and Glenn, 2000). It combines the flows of wind waves and currents that control sediment resuspension. Typically, an oscillatory wave boundary layer nests within a relatively steady current boundary layer. This superposition of flows of different time scales, and hence different boundary layer scales, is determined by the nonlinear interaction of waves and slowly varying currents. In shallow waters, the bottom shear stress due to wind waves can be much larger than that due to currents. The combined bottom shear stress is a nonlinear function of the instantaneous wave plus current velocity.

A predominant mechanism of wind wave attenuation is in the thick, viscous boundary layer of fluid mud (Fig. 3.3.1). The wave energy is converted to work done in moving the fluid mud against viscous shear. According to Eq. (3.6.13), a wind wave with 0.3 m in significant wave height and 3 s in period can produce a near-bottom orbital velocity exceeding 0.11 m/s in depths <4 m. Due to the oscillatory nature of the orbital velocity, the wave bottom boundary layer has only a limited time (approximately one-half of a wave period) to grow, and is very thin immediately above the bottom. The high-velocity shear within the wave bottom boundary layer produces strong turbulence and large bottom shear stress. In contrast to the wave motion, a wind-driven (or tidal) current varies over a much longer time scale, up to hours or longer. The velocity shear, turbulence intensities, and bottom shear stress are much lower for the current than for the wind wave motion.

Sediment concentration might also affect the boundary layer dynamics. The sediment concentration can result in a stable or unstable density stratification, thus suppressing or enhancing turbulent mixing in the vertical direction in much the same fashion as temperature stratification. The relative motion between sediment particles can directly dampen turbulence intensity. The suspended sediment concentration near the bed may become exceedingly high and thus form a fluid mud system within which hindered settling is important and the flow behaves like a non-Newtonian one.

The wave and the current interact to generate a shear stress that varies in magnitude and direction. The high turbulence within the thin wave bottom boundary layer causes the current to experience a higher bottom resistance in the presence of waves than it would if waves were absent. The combined shear stress can be calculated using

$$\vec{\tau}_{cw} = \vec{\tau}_c + \vec{\tau}_{ww} \tag{3.6.19}$$

where $\vec{\tau}_{cw}$ = maximum combined shear stress, and $\vec{\tau}_c$ = current shear stress, and $\vec{\tau}_{ww}$ = maximum shear stress due to wind wave.

Expressing the stresses in terms of their respective shear velocities and taking the magnitude gives (Styles and Glenn, 2000):

$$u_{*cw}^2 = \sqrt{u_{*c}^4 + 2u_{*c}^2 u_{*ww}^2 \cos\phi_{cw} + u_{*ww}^4} \tag{3.6.20}$$

where ϕ_{cw} = the angle between the wave and current ($0 \le \phi_{cw} \le \pi/2$), $u_{*cw} = \sqrt{\tau_{cw}/\rho}$ = combined shear velocity, $u_{*c} = \sqrt{\tau_c/\rho}$ = current shear velocity, $u_{*ww} = \sqrt{\tau_{ww}/\rho}$ = maximum wind wave shear velocity, and ρ = the water density.

The maximum wind wave shear stress, $\vec{\tau}_{ww}$, can be estimated using Eq. (3.6.14), after the maximum orbital velocity, u_{max}, is calculated using wind wave models, such as the SMB model or the SWAN model discussed in this section. Styles and Glenn (2000) adopted the following gradient transport relation for the current shear velocity:

$$u_{*c}^2 = \lim_{z \to z_0} \left(K \frac{\partial U}{\partial z} \right) \tag{3.6.21}$$

where K = the eddy viscosity, U = the magnitude of the horizontal current, z = the vertical coordinate measured positive upward from the bed, and z_0 = the bottom roughness.

3.6.5 Case Study: Wind Wave Modeling in Lake Okeechobee

The characteristics of Lake Okeechobee and its hydrodynamic modeling are already presented in Section 2.4.2. In this section, the discussions are focused on wind wave modeling (Jin and Ji, 2001). The modeling of sediment transport in the lake will be given in Section 3.7.2 as another case study.

3.6.5.1 Background. Sediment resuspension in Lake Okeechobee is caused by currents and wind waves. In both cases, the bottom shear stress must exceed the sediment's critical shear stress for resuspension to occur. With typical values <10 cm/s, currents in the lake are usually too small to cause sediment resuspension. Thus, wind wave forcing is the primary resuspension mechanism in this shallow lake. Energy associated with these waves quickly propagates through the water column to the lake's bottom. When the wind subsides, wind-induced movements in the water column dissipate over time. Similar phenomena have also been observed in other lakes, including Lake Kasum-

igaura, Japan (Otsubo and Muraoka, 1987), Lake Balaton, Hungary (Luettich et al., 1990), and Lake Biwa, Japan (Kumagai, 1988).

3.6.5.2 Measured Data and Model Setup. The wind and wave data used for model calibration were collected by Sheng (1991) at 2 stations near Station LZ40 (Fig. 2.4.2). The data period is from April 27 to May 3, 1989. Wind data were collected at 15-min intervals, and wave height was measured every 0.5 s. The wind data presented a typical spring season wind pattern in Lake Okeechobee (Fig. 3.6.6). The representative wind speed usually was ~6 m/s. The peak wind speed usually occurred between 6 and 10 pm and was between 9 and 10 m/s.

The data used for model verification was collected by the South Florida Water Management District (SFWMD) from March 27 to April 2, 1996. During this period, wave height and wind velocity were measured at another three stations for six consecutive days. Wind speed and direction data were collected every 15 min, and wave height was measured simultaneously at a recording frequency of every 2 s.

Significant wave height, defined by Sverdrup and Munk (1947), is the average of the highest one-third heights of the data recorded during a specified period (e.g., 1 h). It can also be determined from the RMS value of collected

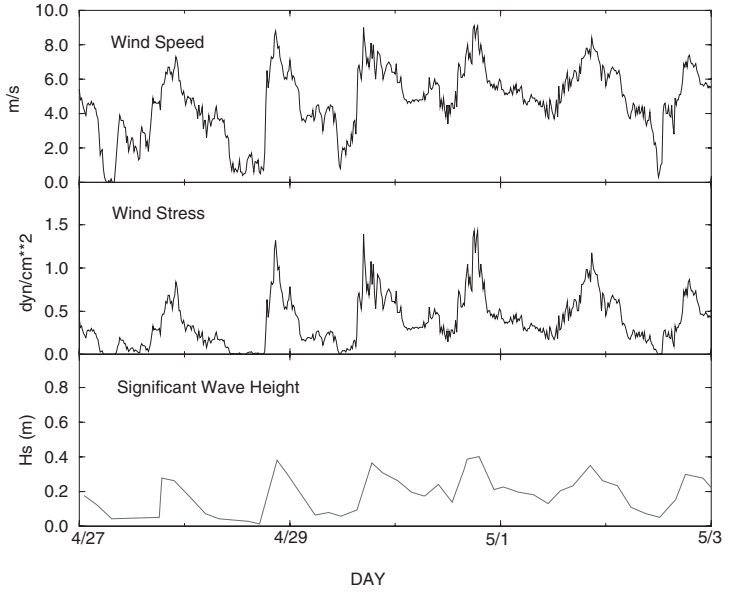

Fig. 3.6.6 Measured wind speed, wind stress, and significant wave height in Lake Okeechobee at a location near LZ40 from 4/27/89 to 5/3/89 (Jin and Ji, 2001).

data during the specified period. The significant wave height, H_s, computed from the RMS value of measured wave heights, is given as:

$$H_s = 1.416\sqrt{\frac{\sum_{i=0}^{N} H_i^2}{N}} \tag{3.6.22}$$

H_i represents each individual wave height converted from measured data and N denotes the total number of wave heights used within a selected time interval.

The SWAN model (SWAN, 1998) was used for this study. The Cartesian grid was the same as that of the hydrodynamic model described in Section 2.4.2, with 59 × 67 cells and a resolution of 910 × 923 m (Fig. 2.4.2). The nonstationary mode of the SWAN model was employed to simulate time-dependent features of wind waves. Sensitivity tests indicated that time steps ≤10 min were able to produce consistent results, and a time step of 10 min was used for this study.

3.6.5.3 Model Calibration and Verification. Figure 3.6.7 presents the comparisons between the simulated and measured significant wave heights at a location near LZ40 (Fig. 2.4.2) for the model calibration period, from April 27 to May 3, 1989. Model results were satisfactory in both the moving trend and the significant wave height fluctuation when compared to the measured data. Jin and Ji (2001) presented the details of the model-data comparison.

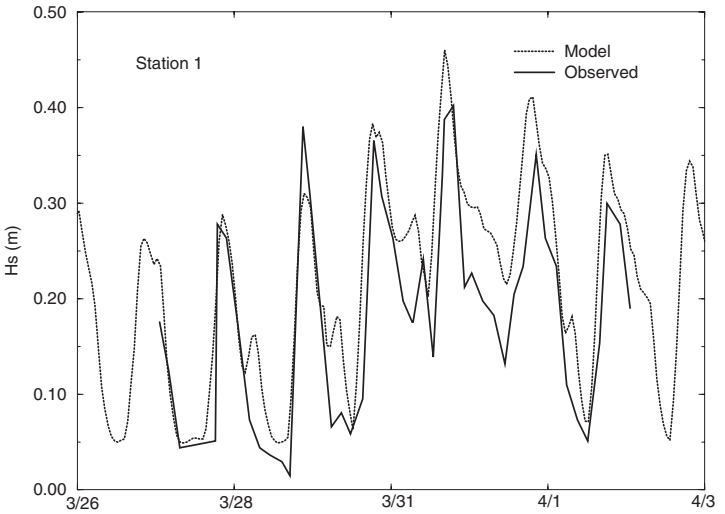

Fig. 3.6.7 Time series comparison between simulated and observed significant wave heights in Lake Okeechobee from 4/27/89 to 5/3/89 (Jin and Ji, 2001).

TABLE 3.6.1 Error and Correlation Analysis for Observed and Simulated Significant Wave Height

Station	Observed Mean (m)	Modeled Mean (m)	Mean Absolute Error (m)	Observed Change (m)	RMSE (m)	Relative RMSE (%)	Correlation Coefficient
1	0.23	0.19	0.06	0.40	0.07	17	0.89
2	0.18	0.14	0.04	0.29	0.06	20	0.87
3	0.17	0.17	0.04	0.27	0.058	22	0.76
4	0.21	0.21	0.06	0.55	0.084	15	0.78
5	0.24	0.21	0.08	0.66	0.10	15	0.79

Statistical analyses also indicated that model results agreed well with observed significant wave heights. Table 3.6.1 gives station names (Column 1), observed means (Column 2), modeled means (Column 3), mean absolute errors (Column 4), observed changes (Column 5), RMS errors (Column 6), relative RMS errors (Column 7), and correlation coefficients between the measured and the observed for the periods of calibration (Stations 1 and 2) and verification (Stations 3–5). Table 3.6.1 indicated that the model results have errors varying from 15% at Stations 4 and 5 to 22% at Station 3. Since Stations 2 and 3 were located near the lake bank or the littoral zone, the reflection and deflection affected the significant wave height data. The correlation coefficients between the model results and the observed data were 0.79–0.89. Overall, the model calibration and verification results were reasonable and satisfactory.

The calibrated and verified wind wave model was applied to simulate wind waves in the lake. Figure 3.6.8 is the simulated significant wave height at LZ40 from 10/1/1999 to 9/30/2000. This 12-month period is the period used for the LOEM model calibration. When Hurricane Irene passed by south Florida in the middle of October 1999, wind speeds were recorded at 23 m/s around Lake Okeechobee. The significant wave height during the hurricane period was up to 1.4 m at LZ40 (Fig. 3.6.8). Wind waves had a significant impact on sediment resuspension and transport in Lake Okeechobee. For a typical winter wind (6 m/s), the hourly averaged significant wave height reached 75 cm on January 21, 2000, at 11 p.m. (Fig. 3.6.9). These wave results will be used for the sediment simulation described in Section 3.7.2.

3.6.5.4 Discussions. Fine sediment on the bottom of Lake Okeechobee is suspended into the water column by waves and currents. Bottom stresses resulting from wind waves are the major cause of sediment resuspension in many large and shallow lakes. Due to shallow depths in Lake Okeechobee and small current velocities (1–10 cm/s), the resuspension processes of fine sediments are particularly dominated by waves (Mei et al., 1997; Sheng, 1991). A

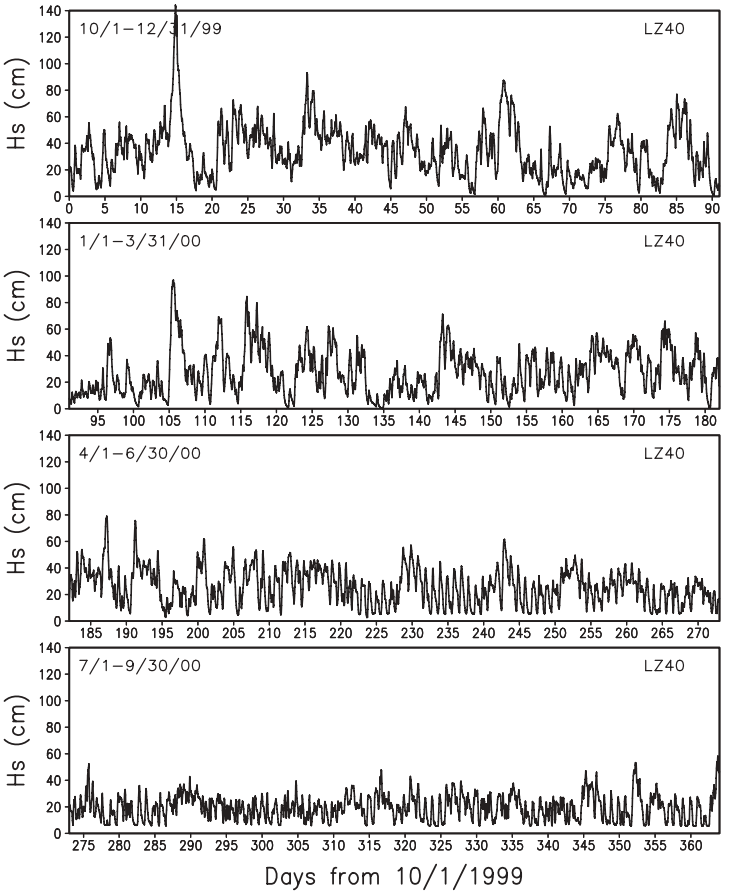

Fig. 3.6.8 Modeled significant wave height at LZ40.

wind wave model can provide temporal and spatial variations of wave heights for the estimation of bottom shear stresses.

The sediment resuspension in Lake Okeechobee is determined by the transmitted energy from the surface, and the amount of transmitted energy is dependent on the wind velocity and fetch. In general, as fetch and wind velocity increase, so does wave height. For example, the significant wave height on January 21, 2000, increases from the northwest to the southeast shore with a northwesterly wind (Fig. 3.6.9). The significant wave heights and their distribution patterns are clearly related to the fetch. Wind speed and direction significantly impact the wave motion and the propagation of the surface waves in the lake.

Due to the shallow depths in Lake Okeechobee, bottom stresses resulting from wind-generated surface waves are the major cause of sediment resuspen-

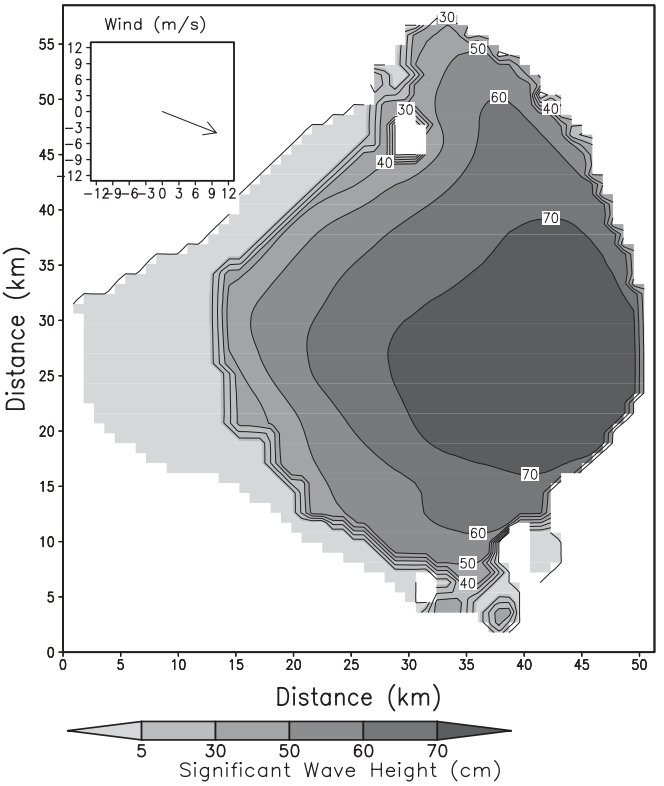

Fig. 3.6.9 Simulated significant wave heights on January 21, 2000 at 11 p.m.

sion (James et al., 1997; Jin and Ji, 2004). The output of this wind wave model is useful for driving the sediment model of Lake Okeechobee. This integrated model, with its ability to simulate wind wave processes and their effects on sediment transport, can significantly improve the modeling of hydrodynamics and sediment transport in the lake. As a case study, the sediment modeling of Lake Okeechobee will be presented in Section 3.7.2.

3.7 SEDIMENT TRANSPORT MODELING

Management of surface waters often requires accurate and detailed knowledge about sediment transport. Sediment transport models and their applications are an important part of analyzing the physical processes of sediment transport. A comprehensive sediment model often includes the following submodels: (1) a hydrodynamic model, (2) a wind wave model, (3) a wave-current model, and (4) a sediment transport model.

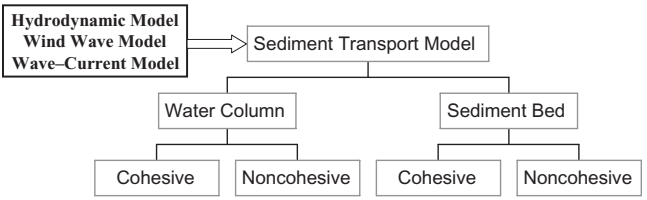

Fig. 3.7.1 Structure of a sediment model.

An indispensable condition for the application of sediment transport modeling is the correct simulation of the hydrodynamics. The hydrodynamic model provides hydrodynamic conditions such as water depth, velocity, turbulence mixing, temperature, and salinity. The hydrodynamic calibration should be adequate, and the flow field must be correctly understood before attempting to evaluate sediment transport.

Wind wave models (e.g., the SWAN model discussed in Section 3.6.3) provide significant wave height, wave period, and wave direction. The wave–current model (e.g., the one discussed in Section 3.6.4) combines the currents and wind waves to accurately estimate bottom shear stress. Both the wind wave model and the wave–current model are only needed in the simulation of large, shallow waterbodies, where wind waves are significant.

Based on these model outputs, sediment transport models simulate flocculation, settling, deposition, consolidation, and resuspension and then calculate sediment concentrations in the water column and sediment mass on the bed. Figure 3.7.1 gives the structure of the sediment model used in the modeling of Lake Okeechobee (Jin and Ji, 2004). The model simulates sediment processes in the water column and the sediment bed. Depending on the type of the problem being investigated, the sediments considered can be cohesive, noncohesive, and/or both.

3.7.1 Sediment Parameters and Data Requirements

Sediment transport is a very site-specific phenomenon that depends on sediment composition, bed characteristics, and hydrodynamic conditions. Sediment models are sensitive to various model parameters, such as settling velocity and critical shear stress. For a sediment model to be reliable, the model needs to be calibrated and verified to the site-specific conditions. In order to use a sediment model in a new study area, a number of site-specific parameters and data should be collected from either laboratory or field measurements, such as:

1. Suspended sediment concentration (SSC).
2. Settling velocity.

3. Critical shear stresses for deposition and for resuspension.
4. Sediment composition and grain size.
5. Sediment bed parameters.

The SSC is the primary variable of sediment models. Even though the SSC is most commonly used in model–data comparison, using the SSC alone for model calibration has its limitations. For example, considering the case of a steady-state equilibrium between erosion and deposition, one has

$$E = \rho w_s S \tag{3.7.1}$$

where E is the erosion rate and $\rho w_s S$ is the deposition rate from Eq. (3.2.12). Rearranging Eq. (3.7.1) yields

$$S = \frac{E}{\rho w_s} \tag{3.7.2}$$

Equation (3.7.2) indicates that a sediment model may reproduce the observed S with different values of E, as long as ρw_s is changed accordingly. This difference can have a direct impact on the choice of remedial action for contaminated waterbodies. For example, small erosion at high bottom shear stresses indicates that the contaminated sediment are being buried over a long time and are unlikely to be resuspended again during high flow events. Hence, natural recovery is probably the best choice of action. Large erosion at high bottom shear stresses indicates that the buried contaminants can be resuspended during high flow events and will contaminate surface waters. Dredging or capping may be necessary for the remediation.

The settling velocity is an important parameter in sediment transport. For cohesive sediment, the settling velocity in a model is actually not the velocity of a particle, but the one corresponding to the vertical settling flux of particles–flocs of many different sizes, as indicated in Eq. (3.2.12). It is the result of the interaction between the flow and the individual particles and the flocs. The sediment settling velocity can be measured either directly or indirectly, such as using the settling column, an image processing technique, and/or a sediment vertical profile. Generally, each of these methods, when deployed simultaneously, may yield considerable differences in settling velocity. This is one of the primary reasons that the settling velocity is often used as a calibration parameter that is tuned within a certain range to make the model results better match the data.

The actual critical shear stresses for deposition and resuspension depend on many factors and vary with time and sediment bed depth. The large variation in measured critical shear stresses is partially due to the difficulty in accurately measuring the critical shear stress, especially after the surface layer is eroded and the bed becomes uneven. In sediment modeling, the critical shear stresses for deposition and resuspension are often used as

adjusting parameters as well. The sediment composition is dependent on the source material, which can be inorganic and/or organic. The parameters used in the sediment bed models vary greatly. The basic parameters include sediment porosity, sediment density, and total sediment mass in the bed.

Data collection for sediment studies can be expensive, particularly the data needed for the development and calibration of rigorous sediment process models. The input data needed for a sediment model is often sediment loads entering the waterbody. Different types of sediment can be supplied to a waterbody by a variety of sources. River bank erosion and general catchment runoff produce large quantities of sand, silt, and clay. Catchment runoff also delivers organic matter. Coastal processes can supply large quantities of sand to an estuary. Wind action on dunes and sandy banks also carries fine sand into estuaries and coastal waters.

On a long-term basis, the suspended load delivered by rivers constitutes the majority of sediment entering estuaries and the marine environment. River sediment discharge is highly episodic. The vast majority of annual sediment load in many tributaries is delivered in a relatively short time period, ~30 days out of a year. It is therefore essential to carry out long term and continuous gauging of river discharge and sediment load. For example, Lick et al. (1994) calculated the resuspension and transport of fine-grained sediment in Lake Erie and reported that major storms, despite their infrequent occurrence, are responsible for most of the resuspension and transport of fine-grained sediments. In order to estimate sediment loading in a sediment model, it is common to establish a regression relation between the measured inflow rate and the sediment load. Figure 3.7.2, for example, expresses the relationship between TSS and flow at Station S49 in the St. Lucie Estuary (AEE, 2004a). The location of S49 is given in Fig. 5.9.11. It has the following empirical formulation:

$$\text{TSS Load (kg/day)} = 6.0019 \times \text{Flow rate (ft}^3\text{/s)}^{1.0971} \tag{3.7.3}$$

Equation (3.7.3) and Fig. 3.7.2 show that the load increases as flow increases. Although limited data are used to establish the loading relationship, the overall results are satisfactory.

3.7.2 Case Study I: Lake Okeechobee

In the modeling of sediment transport, one of the difficult problems is to simulate cohesive sediments because these fine-grained solids settle slowly, are easily transported by horizontal currents, and are repeatedly resuspended and settled. Lake Okeechobee is an ideal case study, since fine-grained sediments cover 44% of the total lake bed area (Reddy et al., 1995). The hydrodynamic calibration and verification of the LOEM have been discussed in Section 2.4.2. The wind wave model of Lake Okeechobee is presented in Section 3.6.5. Both

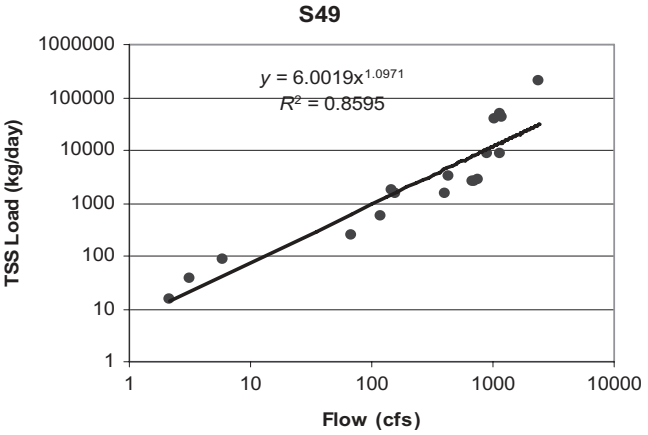

Fig. 3.7.2 Regression results between flow and total suspended solids at Station S49 in the St. Lucie Estuary (AEE, 2004a).

models are indispensable for the success of the sediment modeling in the lake.

The primary goal of this case study is to develop the sediment submodel of the LOEM and to use the model to simulate sediment transport processes in the lake (Jin and Ji, 2004, 2005). Output from the LOEM sediment model will also be used in a water quality submodel to analyze the impact of hydrodynamics and suspended sediment concentrations on lake eutrophication (Section 5.9.2). The LOEM will eventually be used to provide detailed long-term information regarding circulation patterns, sediment distributions, and water quality variations under different hydrological and management scenarios (Section 9.4.2).

3.7.2.1 Background. Sediments in shallow waters can impact the physical and chemical environment of a water column through resuspension and transport. Increased suspended sediments can reduce light availability, which impacts algal and aquatic vegetation growth (Blom et al., 1992). Sediment resuspension also affects the cycling of nutrients through adsorption and desorption of dissolved nutrients to and from the water column (Cerco and Cole, 1994). Finally, sediment resuspension can also impact the water quality by resuspension of organic pollutants and heavy metals (Blom, et al., 1992; Ji et al., 2002a).

Sediment resuspension and deposition in large, shallow waters are primarily driven by wind-induced waves, and sediment transport is dominated by circulation patterns (Mei et al., 1997). Dynamic behaviors of suspended sediments and wind wave effects in shallow lakes have been widely studied in past decades. Recent studies (Jin and Ji, 2004, 2005) show that wind-induced waves are a major driving force in sediment deposition/resuspension in Lake

Okeechobee. Variation in wind velocity results in dramatic changes in water column transparency and suspended solids. In the summer, when an evening sea breeze is a dominant forcing function, there are strong diurnal changes in SSC. In the winter, when frontal systems generate strong winds for multiple days, the water column SSC remains quite high compared to summer conditions.

Lake Okeechobee (Fig. 2.4.2) has a surface area of ~1730 km^2 and is very shallow, with mean and maximum depths of 2.7 and 5.5 m, respectively. The large lake surface area leads to long fetches and strong wind waves in the lake. The shallow water depths allow the energy of surface wind waves to propagate to the lake bottom quickly, and then to affect the bottom shear stress significantly. In the central region of Lake Okeechobee, sediments are a heterogeneous mix of fine-grained bed materials with high organic content (Fig. 3.7.3). In the shallower regions of the lake, sediments are comprised of sand, peat, or exposed bedrock. Approximately one-fifth of the lake supports a littoral community of emergent plants. In the littoral zone, water depths are generally <1.5 m, and the sediments have a high organic content. Figure 3.7.4 shows that

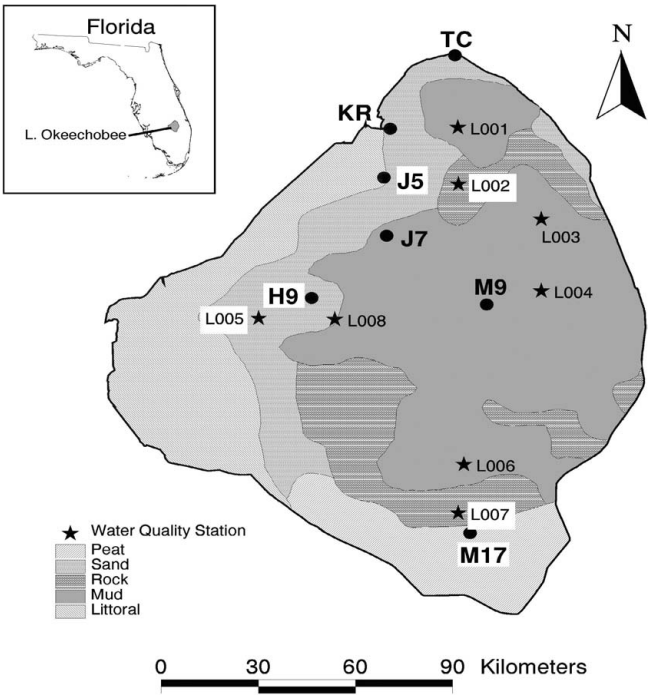

Fig. 3.7.3 The five sediment zones in Lake Okeechobee. The bed sediments can be divided into five principal sediment zones based on physical characteristics. Shown are the stations used in the sediment characterization and the nutrient exchange experiments (SFWMD, 2002).

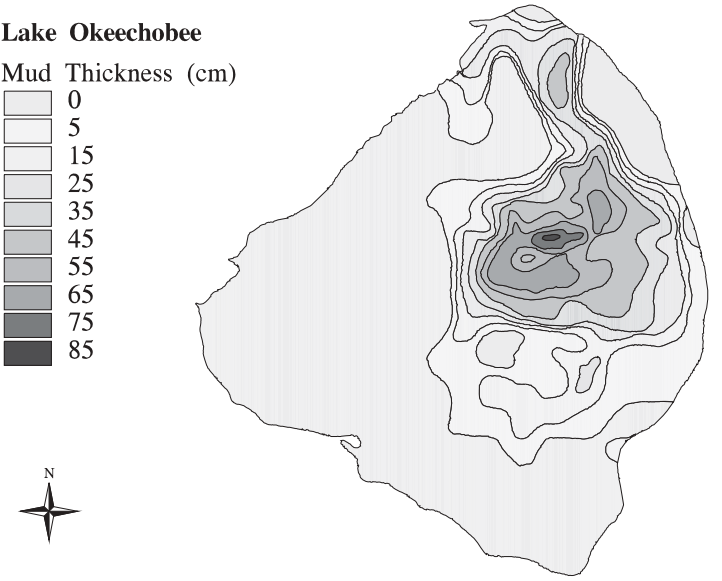

Fig. 3.7.4 Lake Okeechobee mud sediment thickness (based on Kirby et al., 1989).

mud sediments cover the largest area of the lake and have a maximum thickness of ~80 cm (Kirby et al., 1989). The water column in the mud sediment region of the lake has an average depth of 4 m.

Water quality in the lake has changed dramatically in the last century, largely as a result of nutrient inputs from agriculture and other human activities in the watershed (Havens et al., 1996). There has been a rapid and massive buildup of phosphorus-rich mud sediment in the lake. Since the early 1980s, Lake Okeechobee has experienced accelerated eutrophication due to excessive phosphorus loads from agricultural runoff. In-lake total phosphorus concentrations, closely linked to the declining ecosystem health, have nearly doubled since the late 1970s. Recent studies show that the fine-grained sediments in the central region of the lake have accumulated large amounts of phosphorus (P) from these excessive nutrient inputs. Phosphorus cycling is greatly influenced by lake sediments. Resuspended sediments act as a sink by adsorbing dissolved phosphorus and settling out of the water column. Lake sediments are a major source of P to the water column (Reddy et al., 1995). Under proper conditions, such as low dissolved oxygen concentrations, the sediment bed also releases phosphorus. On an annual basis, sediments in Lake Okeechobee produce an internal inorganic P load that is approximately equal to external P loads. This internal P load significantly impacts algal growth and water quality in the lake (Olila and Reddy, 1993; Moore et al., 1998). The accuracy of predicted circulation patterns and sediment concentration directly affects the accuracy of predicted phosphorus concentrations.

3.7.2.2 Model Configuration. Based on the EFDC model (Hamrick, 1992; Tetra Tech, 2002), a sediment transport submodel was added to the LOEM to simulate the transport and fate of multiple-size classes of cohesive and noncohesive solids. The numerical results presented in this case study are based on a single sediment class (cohesive sediment). Similar to the hydrodynamic model described in Section 2.4.2, the sediment model of Lake Okeechobee also has the computational grid of 58×66 horizontal cells, with 2126 active water cells and 5 vertical layers (Fig. 2.4.2).

For a large shallow lake, such as Lake Okeechobee, the major physical processes that determine the structure of the near-bottom flow are the interaction of high-frequency surface waves with relatively low-frequency currents and the interaction of this combined flow with a movable sediment bed. This nonlinear wave–current interaction, a dominant mechanism in shallow water sediment transport, can significantly enhance the roughness of the bed and the stress generated by the current. In general, the near-bottom wave orbital velocity and associated bottom shear stress are greater than (or of the same order of magnitude as) the near-bed current velocity and associated bottom shear stress in a shallow water system (Sheng, 1991; Mei et al., 1997; Jin and Ji, 2004). The combined bottom shear stress, which varies in magnitude and direction over a wave period, is a nonlinear function generated by the instantaneous wave and current velocity. In this study, a wave–current model (Grant and Madsen, 1979; Glenn and Grant, 1987; Styles and Glenn, 2000) is used to calculate bottom shear stresses generated by waves and currents. Section 3.6.4 gives more details on the wave–current interactions.

In general, the TSS in water columns includes cohesive and noncohesive materials. Since the cohesive sediment is the major component in the lake, and the data collected in Lake Okeechobee did not specify TSS components, the TSS in the lake is represented as cohesive sediment in this study. The critical bottom shear stresses for sediment deposition and resuspension are two important parameters for sediment transport modeling. Hwang and Mehta (1989) report that the critical shear stress for cohesive sediment in Lake Okeechobee varied from 0.125 to 0.525 N/m^2, the sediment settling velocity varied from 1.0×10^{-5} to 1.0×10^{-3} m/s, and the resuspension rate varied from 0.005 to 0.1 $g/m^2/s$. A critical shear stress value of 0.18 N/m^2 is used in this study. The critical resuspension shear stress (=0.216 N/m^2) is usually taken as 1.2 times the critical deposition shear stress (Ji et al., 2002a). For simplicity and due to the lack of measured data, the settling velocity of the cohesive sediment is set to be constant. A settling velocity of 1×10^{-5} m/s and resuspension rates of 0.06 $g/m^2/s$ are used for cohesive fine-grain sediment.

3.7.2.3 Model Calibration and Verification. Based on the availability of measured data, the period of model calibration was 28 days, from May 16 to June 13, 1989. A time step of 200 s was used throughout the simulation. The model calibration results are summarized in Table 3.7.1. Statistical parameters used were mean value, mean absolute error, RMSE, and RRE. Section 7.2.1

TABLE 3.7.1 Error Analysis of Observed and Modeled Suspended Sediment Concentrations in 1989

Station	Water Column Location	Obs. Mean (mg/L)	Modeled Mean (mg/L)	Mean Abs. Error (mg/L)	RMSE (mg/L)	Obs. Change (mg/L)	RRE (%)
A	Middle	7.36	4.17	3.77	5.13	19.73	25.99
B	Bottom	21.60	21.87	4.28	8.46	113.80	7.44
C	Bottom	57.20	56.99	5.72	7.79	56.69	13.75
C	Middle	56.35	56.48	5.65	7.79	59.75	13.03
C	Surface	47.35	55.75	8.87	11.60	57.73	20.09
E	Bottom	32.71	32.78	6.23	8.81	52.94	16.64

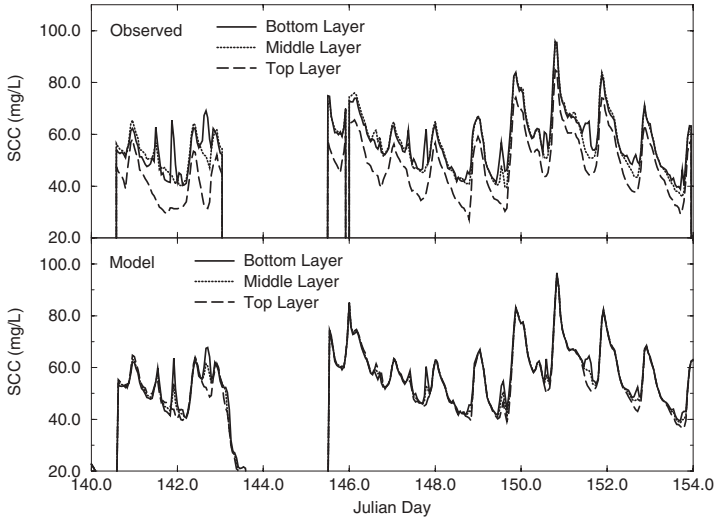

Fig. 3.7.5 Observed and simulated suspended sediment concentrations at Station C from May 16 to June 13, 1989. The Julian day is in reference to January 1, 1989. From Jin and Ji (2004). (Reprinted by permission of American Society of Civil Engineers.)

gives the definitions of these statistical parameters. The station locations are shown in Fig. 2.4.2. In Table 3.7.1, the mean absolute errors are ~3.8–8.9 mg/L, and the RMSE ranges from 5.1 to 11.6 mg/L. The average RRE is 16.16%. Figure 3.7.5 is the time series comparison between the modeled and the observed suspended sediment concentrations at Station C.

A mean relative RMS error (MRRE) can be calculated using the values in the last column of Table 3.7.1. In this study, MRRE is used to evaluate the overall model performance and to reveal model sensitivity to parameters. The MRRE in Table 3.7.1 is 16.16%. When the sediment settling velocity is changed

TABLE 3.7.2 Error Analysis of Observed and Modeled Suspended Sediment Concentrations at Eight Water Depths from 1/18/2000 to 3/5/2000[a]

Station	Obs. Mean (mg/L)	Modeled Mean (mg/L)	Mean Abs. Error (mg/L)	RMS Error (mg/L)	Obs. Change (mg/L)	RRE (%)
L006_M	88.64	86.75	18.54	26.07	158.69	16.43
L006_S	88.66	86.43	18.45	25.83	142.21	18.16
L001_B	73.30	85.90	25.55	31.35	106.81	29.35
L001_M	69.75	84.40	24.12	30.47	105.47	28.89
LZ40_B	116.98	89.34	33.73	49.42	192.38	25.69
LZ40_M	113.34	88.91	30.34	44.00	182.94	24.05
L005_M	62.55	81.86	28.80	34.71	74.71	46.46
L005_S	65.25	81.22	27.43	33.26	72.51	45.87

[a]Measured suspended sediment concentration located ~17% (B, bottom layer), 40% (M, middle layer), and 80% (S, surface layer) of total depth above the lake bed.

±50%, the MRRE changes <6%. When the critical deposition shear stress is changed ±50%, the MRRE changes <9%. In summary, the model results are not very sensitive to the model parameters, and the values of critical deposition (and resuspension) shear stress affect the sediment concentrations more than the other parameters.

The model verification results from January 17 to March 3, 2000 are summarized in Table 3.7.2, which shows that the simulated SSC during the verification period agreed well with the observed data. The mean absolute errors were ~18.5–33.7 mg/L, and the RMS errors ranged from 25.8 to 49.4 mg/L. The average RRE was 29.36%. The maximum variance of monthly observed SSCs, 192.38 mg/L, occurred at station LZ40 bottom layer, with a 25.69% RRE. The simulated results also showed that the model could predict SSC satisfactorily and reproduce the trend at each station during the verification period. For this verification period, the worst model results (RRE = 46.46%) occurred at L005. Three factors may have contributed to the errors:

1. Even though the modeled results at L005 have RMS errors comparable to those at the other three stations, the observed changes of SSC at L005 are significantly smaller compared to the ones at the other stations (Table 3.7.2), which leads to a larger RRE.
2. The SWAN model simulates the wind wave in the full lake domain and is not capable of separating the lake into littoral zones and open water areas. This lack of domain separation leads to an overestimation of the wind fetch (and consequently the bottom shear stress) in the L005 area when wind is blowing from the west or northwest. It also explains why the modeled mean SSC at L005 is higher than the observed mean.
3. The particle size of the sediment at L005 is generally larger than those in other areas of the lake. In this model, one sediment class is used to

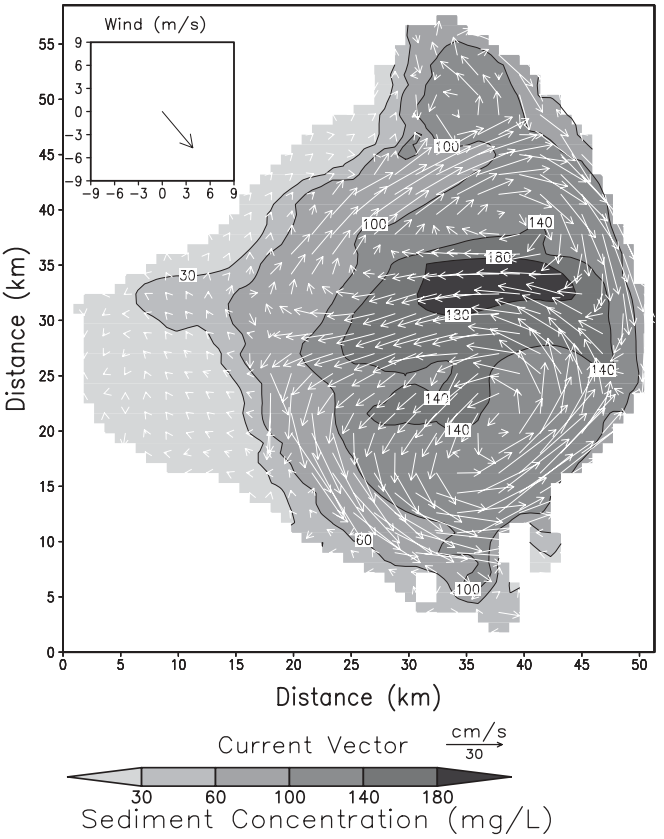

Fig. 3.7.6 Simulated surface velocity and suspended sediment concentrations on January 21, 2000.

represent the sediment bed of the lake. Multiple sediment classes might be needed to represent the sediment grain size distribution in future studies.

Figure 3.7.6 gives the daily averaged surface velocity and suspended sediment concentration on January 21, 2000, the same day that the wind waves (Fig. 3.6.9) and the water level elevations (Fig. 2.4.9) were presented. The patterns of the simulated currents and SSC were very similar at the top and bottom layers of the lake, even though the currents were generally larger at the surface than near the bed, whereas the SSCs were greater near the bed than at the surface. Northwest winds moved surface currents toward the southeast, parallel to the littoral zone and along the lake's east shore. Bottom currents paralleled surface currents along the littoral zone and the northeast shore, suggesting that the lake was well mixed in these shallow areas. Currents

in the littoral zone were very weak (<1 cm/s). Two gyres formed in the lake, one in the south and the other in the north. The south gyre was created by a cyclonic-type current pattern, whereas the north gyre formed a typical anticyclone. The mechanisms of gyre formation will be discussed in Section 9.2.4.

3.7.2.4 Discussions and Conclusions. This case study describes the calibration and verification of the sediment submodel of the LOEM. The hydrodynamic model is very important to the sediment model. Lack of reliable hydrodynamic information may lead to a major uncertainty in the overall estimation of sediment and contaminant transport. Sediment resuspension in Lake Okeechobee is caused by currents and wind wave action (Sheng, 1991; Mei et al., 1997; Jin and Ji, 2004). The SWAN wind wave model is used to compute the significant wave height and the wave period. The wave–current model, developed by Styles and Glenn (2000), is used to calculate the combined bottom shear stress due to current velocity and wind waves.

The process of sediment resuspension in Lake Okeechobee begins with wind energy that is delivered to the water surface and creates waves. When the wind energy is transmitted from the lake surface to the bottom of the lake, the energy dissipates and decreases with increasing depth. This transmission process can be described by fluid particle trajectories induced by wave motion in the vertical direction (Fig. 3.6.3). Combined with current velocities, orbital velocities at the sediment–water interface exert shear stresses that resuspend sediment into the water column.

A comparison has been conducted with and without the wave–current interaction algorithms activated. The impacts of the wind waves on sediment simulation are shown in Table 3.7.3. The second column of the table represents the modeled mean SSC at eight water depths when the SWAN model and the Styles–Glenn model are used in the LOEM. The third column in Table 3.7.3

TABLE 3.7.3 Comparison of the Modeled Mean SSC at Eight Water Depths from 1/18/2000 to 3/5/2000[a]

Station	SSC with Wind Wave (mg/L)	SSC without Wind Wave (mg/L)	SSC Difference (mg/L)
L006_M	86.75	75.44	11.31
L006_S	86.43	73.92	12.51
L001_B	85.90	51.14	34.76
L001_M	84.40	49.83	34.57
LZ40_B	89.34	73.75	15.59
LZ40_M	88.91	72.41	16.5
L005_M	81.86	55.34	26.52
L005_S	81.22	53.49	27.72

[a]Column 2: SSC with wind wave forcing; Column 3: SSC without wind wave forcing; and Column 4: Column 3–Column 4.

is the case without wind wave forcing. The fourth column represents the SSC differences between the two cases. It is obvious that the SSC is significantly underestimated without considering wind wave forcing. The SSC differences between the two cases can be >34 mg/L.

The bottom shear stresses resulting from current velocities are the secondary causes of sediment resuspension in Lake Okeechobee because current velocities typically range from 1 to 10 cm/s, whereas the orbital velocities range from a few centimeters per second to >40 cm/s in this study. Although much higher SSC occurred in the winter season, the orders of magnitude of current velocities in the summer (calibration period) and in the winter (verification period) are about the same (Jin and Ji, 2004). Therefore, the primary role of currents is transporting and carrying suspended sediment solids to other areas in the lake.

Major conclusions of this case study include the following:

1. The LOEM sediment model was developed based on the well-calibrated and verified hydrodynamic model (Section 2.4.2), which was essential for calculating the sediment transport in the lake.
2. The wind wave model (SWAN) was also well calibrated based on the measured data in the lake (Section 3.6.5), which was critical for simulating significant wind wave heights in the lake.
3. The wave–current model (Glenn and Grant, 1987; Styles and Glenn, 2000) used in this study provided the coupling mechanism for the interactions between the wind wave boundary and the current boundary, which was important for accurately calculating the bottom shear stress, a parameter that is essential for sediment modeling.
4. Based on the submodels mentioned above, the sediment model of LOEM was developed, calibrated, and verified using lake data measured in 1989 and 2000, and the model was used to study the unique features of this large and shallow lake. The importance of wind wave, currents, and their interactions with sediment transport was then investigated.
5. By using the comprehensive data set for model calibration and verification, the LOEM model was proven to be a reliable tool for water source management in the lake and is currently being used for analyzing management scenarios, the primary goal of this modeling study. The successful development of the sediment model was also essential for the development of the water quality model of the lake, which will be presented in Section 5.9.2.

3.7.3 Case Study II: Blackstone River

In many ways, sediment transport processes in rivers are different from those in lakes. In large and shallow lakes (e.g., Lake Okeechobee), wind waves play a dominant role in sediment resuspension. Lake currents are relatively weak,

are less important to sediment resuspension, and often play a primary role in transporting the suspended sediments. For rivers, especially for small rivers like the Blackstone River, however, the wind wave effects on sediment are often minimal. The short fetches of rivers limit the growth of wind waves. The primary driving force for sediment resuspension is the river flow.

Based on the study of Ji et al. (2002a), the sediment modeling of the Blackstone River is described in this section. The modeling of metal transport in the river will be provided later in Section 8.4.1. This case study also serves as an example of river modeling.

3.7.3.1 Background. The United States Environmental Protection Agency (USEPA, 1997) documented widespread contamination of the sediment beds of many urban-industrial rivers, lakes, harbors, and estuaries with heavy metals and toxic chemicals. The EPA emphasized the need for credible modeling tools that can be used to quantitatively evaluate the impacts of point sources, nonpoint sources, and internal transport processes for issuing permits under the National Pollutant Discharge Elimination System (NPDES), for TMDL assessment, and for evaluation of remediation alternatives for management decision making.

It is a challenge to apply coupled hydrodynamic, sediment process, and contaminant fate and transport models to the studies of surface water systems. Complex 1D/2D/3D hydrodynamic models have been available in a routine operational sense for only about the past decade. It is critical that appropriate tools are available to perform various types of sediment assessments in 1D/2D/3D environments. Contaminant models are dependent on hydrodynamic models and sediment transport models since heavy metals and toxic chemicals can preferentially adsorb and desorb with solids in the water column and sediment bed. High flow events, such as storms, increase solid loadings from the watershed, increase river flow velocity, reintroduce previously deposited chemicals back into the water column via resuspension, and transport the resuspended contaminants further downstream until they settle out in deposition zones.

The Blackstone River basin (Fig. 3.7.7) consists of ~1657 km^2 including 30 cities and towns. The Blackstone River flows from Worcester, MA, to Pawtucket, Rhode Island. The river is 77 km in length and has 133 m of total fall, resulting in an average drop of 1.73 m/km. The distances shown in Fig. 3.7.7 are river kilometers from the Slaters Mill Dam. There are presently 14 dams and impoundments on the mainstem of the Blackstone that are significant to the hydrodynamic and water quality processes in the river. One of them, the Tupperware Dam, is shown in Fig. 3.7.8. The main tributaries of the Blackstone are the Kettle Brook and the Quinsigamond, Mumford, West, Branch, and Mill Rivers. The Kettle Brook is confluent at the Blackstone's head.

The Blackstone has been the largest source of pollutants discharging into the Narragansett Bay, principally from the industrial discharge of metals and the resuspension of contaminated sediments behind the low head dams in the

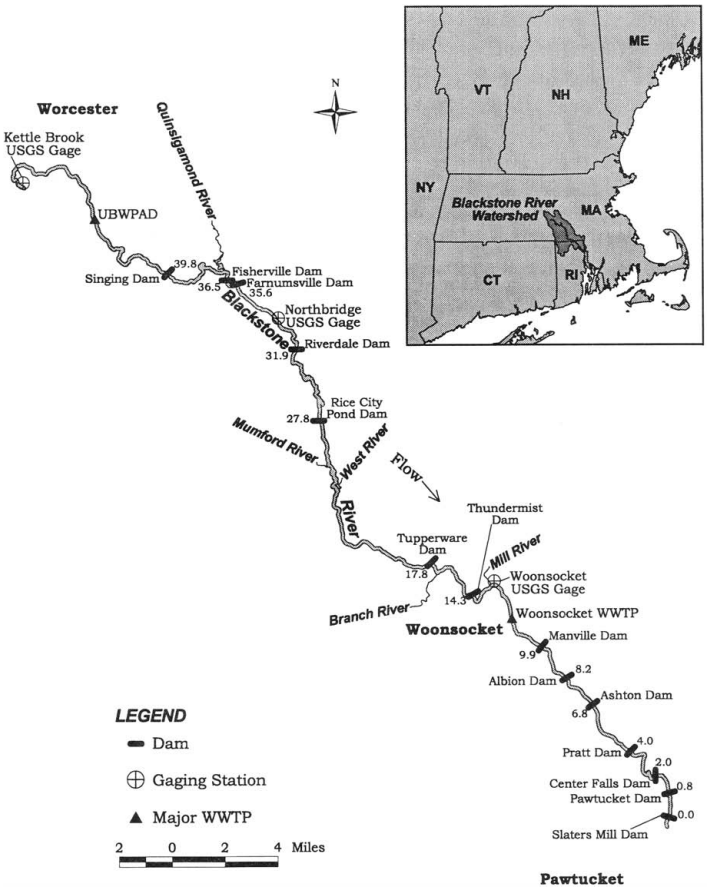

Fig. 3.7.7 Blackstone River study area. The distances are river kilometers from Slaters Mill Dam.

river. Sediment and metals on certain sections of the river bed, such as in the Rice City Pond (at km = 44.0 in Fig. 3.7.7), can be traced back 200 years to the American industrial revolution (USEPA, 1996a). The Upper Blackstone Water Pollution Abatement District (UBWPAD) wastewater treatment facility in Worcester is the largest source of pollution entering the Blackstone in Massachusetts. The Blackstone is a small river when it flows through Worcester, thus it provides minimal dilution for domestic and industrial discharges from the city. In the summer, the UBWPADs discharge of $2.0\,m^3/s$ (cms) can actually account for up to 80% of the total river flow. The plant accounts for 77–96% of the cadmium, copper, chromium, nickel, and zinc discharged into the Blackstone River in Massachusetts. The river also receives wastes in Rhode Island.

Fig. 3.7.8 Tupperware Dam on the Blackstone River (photo taken by Zhen–Gang Ji on February 3, 1998).

There were two major Blackstone River studies conducted in the 1990s: (1) the Blackstone River water reconnaissance investigation by the U.S. Army Corps of Engineers (USACE) (1997), and (2) the Blackstone River Initiative (BRI) by the USEPA (1996a). The USACE study assessed the watershed's problems and presented a comprehensive review of previous studies on the Blackstone. The BRI was a multiyear and multimillion dollar study sponsored by USEPA. Extensive samplings, up to 16 stations at 4-h time intervals, were conducted along the Blackstone River and its tributaries during three storm events. The measured data captured sediment and metal transport along the entire river in detail. The BRI data is the primary data set in the present study. So far, few published studies on sediment and metal modeling in rivers are able to have such comprehensive data sets to drive and to calibrate numerical models.

This Blackstone River modeling study was intended to provide the EPA with a relatively simplified example of how complex models can be used to evaluate the significance of point and nonpoint sources and internal transport processes on the distribution of heavy metals in a shallow, narrow urban–industrial river. The objectives of this study are

1. To apply a 3D numerical model to a 1D sediment and metal study in the Blackstone River. The model used in this study is the Environmental Fluid Dynamics Code (EFDC) (Hamrick, 1992). USEPA (1999) has listed the EFDC model as a tool for water quality management. Among the >100 documented EFDC studies, most of them are 3D applications. It is critical to test the model's versatility in 1D/2D/3D applications and

to demonstrate the model's validity as a contaminant management tool in different surface water systems. This verification is the primary goal of this USEPA-funded study.

2. To calibrate the Blackstone River Model. The BRI provided comprehensive data to capture the transport and resuspension processes of sediments and metals during storm events in detail. The Blackstone River Model can realistically represent external loadings and have sufficient sediment and metal concentration data in water columns for model calibration. Statistical analysis will be conducted to quantify the comparisons between the model results and the data.
3. To investigate the transport processes of sediment and metals and the impacts of various contaminant sources in the river. Because of the relatively simple geometric setting of the river, the model has the advantage of simulating these processes with minimum influences from some other factors, which often complicate sediment and metal transport processes in water systems, such as winds, model boundaries, and tides. The calibrated Blackstone River Model will be used to analyze and clarify the contributions of point source, nonpoint source, and the resuspension process to the calculation of sediment and metal concentrations.

3.7.3.2 Data Sources and Model Setup. During the BRI surveys (USEPA, 1996a), water quality data were collected along the Blackstone River and its tributaries under both wet and dry weather conditions. Compared to the wet weather surveys, the dry weather surveys have much less data and are insufficient to describe the time-varying features of sediment and metals transport in the river. In this study, the wet weather data are used as the primary data source and include flow rate, total suspended solids, and concentrations of five metals (Ca, Cr, Cu, Ni, and Pb). The periods of three wet weather surveys were September 22–24, 1992, November 2–6, 1992, and October 12–14, 1993, respectively. During each of the three storm events, data were collected at up to 16 locations and at 4-h time intervals. This comprehensive data set provides an important source for model input and model calibration.

In addition to BRI data, the following data sources are also used

1. *The HEC-2 Data*. The HEC-2 (1991) program computes water surface profiles for 1D flow in rivers. The data of the HEC-2 model has probably the most detailed information on river morphology in the United States. Numerous HEC-2 studies were conducted in the past decades. The bathymetry and dam elevation data of this study are configured based on the HEC-2 data and the USACE report (1997).
2. *Permit Compliance System (PCS) Data*. The PCS (US Code, 1977), a national computerized management information system, contains the water and contaminant discharges from point sources. The PCS data are incorporated with the BRI data to provide input to the Blackstone River

Model. At USWPAD discharge, daily flow varies from 1.0 to 2.6 cms, and monthly metal concentrations have typical values of 4, 15, 64, 40, and 5 μg/L for Cd, Cr, Cu, Ni, and Pb, respectively.

3. United States Geological Survey (USGS) gauging data. Figure 3.7.7 shows that there are six significant tributaries that discharge into the Blackstone. The USGS daily flow rate data are combined with the BRI tributary data as model input.

Originally constructed as a 3D model, the EFDC model can also be readily applied to 1D or 2D studies by using a 1D or 2D model grid and without any modification to the code. The Blackstone River Model in this study is a 1D application of the EFDC model. Most of the previous EFDC studies are 2D or 3D applications. To test EFDC's versatility and validity as a water quality management tool, the present study is the first 1D EFDC application that has been documented in detail, and the justifications for using the 1D model will be presented later.

According to the BRI report (USEPA, 1996a), 14 significant dams are present on the river's mainstem (Fig. 3.7.7). These 14 dams segregate the river into 14 reaches. The typical width of the Blackstone River is ~25 m, varying from <10-m upstream to >35-m downstream. An exception is in the Rice City Pond section (<300 m long), where the river can be >100 m wide. Since it has an average drop of 1.73 m/km, the Blackstone is a gravity-driven river. The grid of the Blackstone River Model has one cell across the river and one layer in the vertical. Along the river, there are 256 grid cells with varying cell widths and a uniform cell length of 300 m.

Using a 1D and steady-state model, Limno-Tech (1993) computed metals in the Blackstone River and concluded that the 1D model results were generally consistent with observed data. The reasons for using a 1D grid in this study include:

1. The Blackstone River is small and narrow. One grid cell across the river is able to represent most of the river sections well. Also, there is no measured data available to indicate that more grid cells across the river are needed.
2. This gravity-driven river is shallow, has a typical flow speed of 0.3–1.0 m/s, and is well mixed in the vertical. This makes a one-layer model suitable for application.
3. There are needs for credible and versatile models that can be used for 1D/2D/3D contaminant studies, such as evaluating USEPA NPDES permits. One objective of this study is to test the versatility and validity of the 3D EFDC model in 1D applications. The 1D Blackstone River Model serves this purpose ideally.

3.7.3.3 Hydrodynamic and Sediment Simulation. The Blackstone River Model includes a hydrodynamic model, a sediment model, and a toxicant

model. These three models are coupled together and are executed simultaneously. The hydrodynamic model simulates velocity, water elevation, and turbulence mixing for sediment modeling. The outputs of the hydrodynamic and sediment models are linked to the toxicant model to simulate the five metals in the river. In order to minimize the influence of the initial hydrodynamic conditions, the model is spun up for 60 days before model-data comparisons are conducted. A time step of 30 s is used throughout the simulation. On a 400-Mhz Pentium II PC, ~3 CPU hours are required for a 168-day simulation to cover the three storm events. In this section, the hydrodynamic and sediment simulations are presented. The results of metal modeling in the river will be described in Section 8.4.1.

The following parameters are used in this study: (1) a constant sediment settling velocity of 0.002 m/s, (2) a critical deposition shear stress of 0.25 N/m^2, and (3) a critical resuspension shear stress of 0.3 N/m^2. The sediment settling velocity of 0.002 m/s falls into the range of cohesive sediment settling velocity discussed by Hwang and Mehta (1989). Considering that larger size sediments are resuspended during storm events and that the Blackstone River Model uses one class of sediment to simulate the combination of both cohesive and noncohesive sediment, a setting velocity of 0.002 m/s is considered to be representative. There is no measured critical shear stress data available for this study. Hwang and Mehta (1989) reported that the critical shear stress for cohesive sediment varied from 0.125 to 0.525 N/m^2. The value of 0.25 N/m^2 used in this study is within this range. In the EFDC model, critical resuspension shear stress (=0.3 N/m^2 in this study) is usually taken as 1.2 times the critical deposition shear stress. The bottom roughness height is set to 0.02 m, a typical value that has been commonly used in many other studies (e.g., Ji et al., 2001). Parameter sensitivity tests will be discussed later.

The bed sediment plays an important role in the transport of sediment and metals. Sediment-sorbed metals can be buried in the bed by deposition and can be released back to the water column by resuspension. The bed sediment model has one vertical layer in this study. Due to the lack of sediment core data along the river, the initial sediment bed conditions are assumed to be uniform in the river and have the identical values that Limno-Tech (1993) used in the 1D and steady-state metal modeling. The bed sediments had a density of 2 kg/L and a porosity of 0.725, which are determined from professional judgment supplemented by Blackstone River sediment characteristics reported in McGinn (1981). An active sediment layer depth of 5 cm is assigned to all reaches. The bed has initial concentrations of 10 mg/kg for the five metals. Chapra (1997) reported 10 mg/kg of bed zinc in Lake Michigan. Thomann et al. (1993) reported typical bed cadmium concentrations of 2.5–5.0 mg/kg in the Hudson River. To minimize the influence of the bed initial conditions, the Blackstone River Model for this study has 60 days of spin-up time. The river's high flow velocity (typically 0.3–1.0 m/s) and the external loadings from the point and nonpoint sources also reduce the impacts of the initial conditions. The high river velocities resuspend the bed sediment along the river and

redeposit the sediment in low-velocity areas behind the dams. Model sensitivity tests indicate that simulations with 90 days of spin-up time have results similar to those with 60 days of spin-up time. The diffusion coefficient for sediment bed mixing is set to 10^{-9} m^2/s, which is consistent with the range reported by USEPA (1984).

During each BRI storm event, samplings were conducted at up to 16 stations along the Blackstone River and its tributaries at 4-h time intervals for up to 3 days. Data at 12 stations along the Blackstone River are used for model–data comparison. The 12 stations have a total of 120, 192, and 144 records for each measured variable for Storm 1, Storm 2, and Storm 3, respectively.

Figures 3.7.9 and 3.7.10 present the time series of the modeled and measured flow rates (Q) and TSS concentrations along the Blackstone River

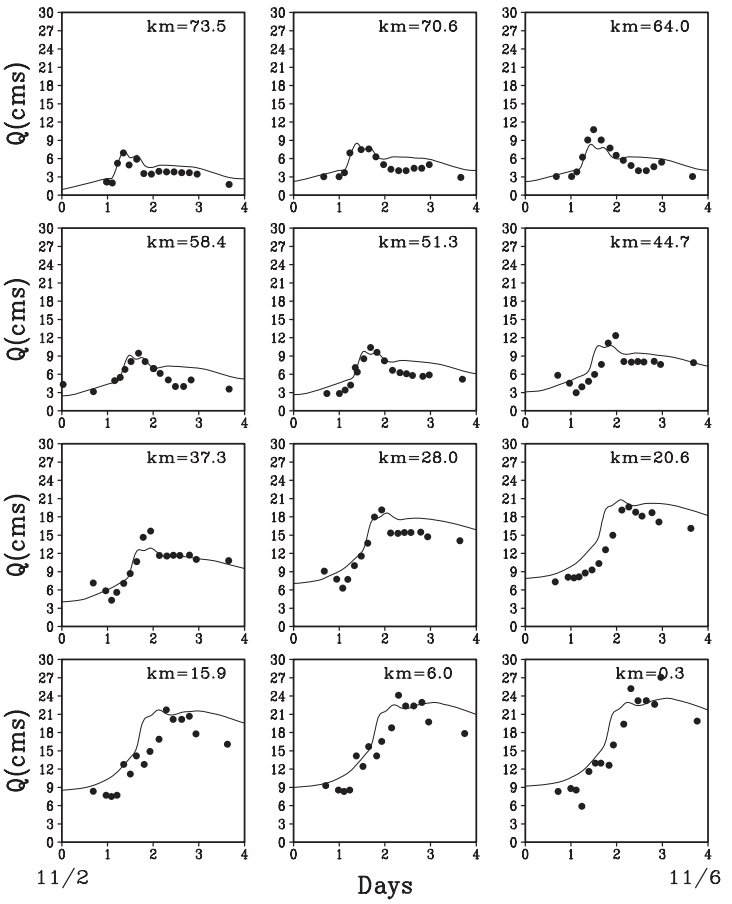

Fig. 3.7.9 Measured and modeled flow rate along the Blackstone River during Storm 2.

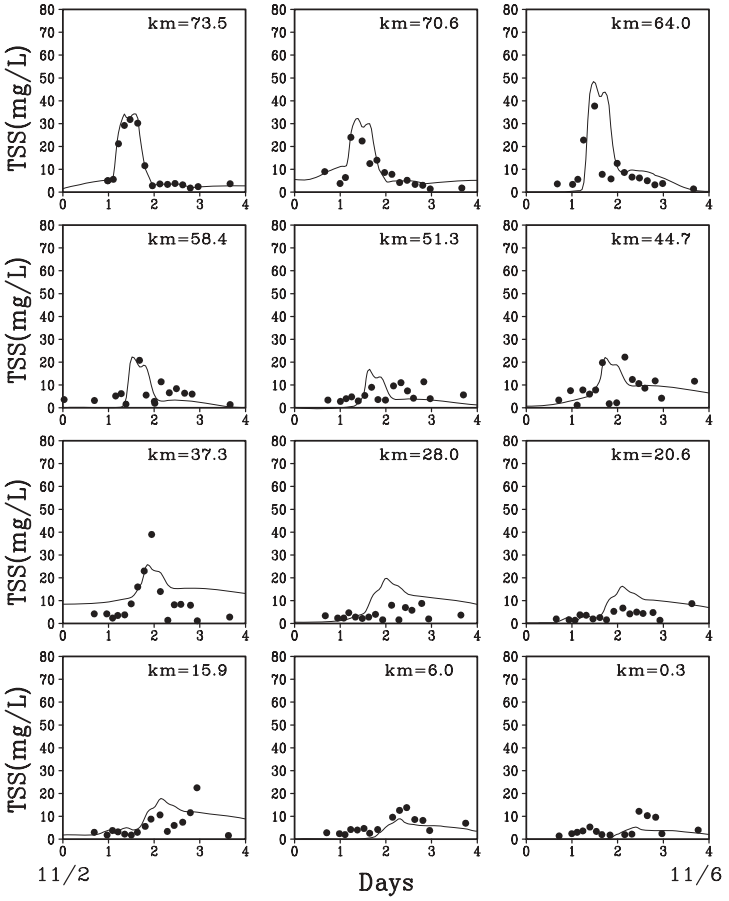

Fig. 3.7.10 Measured and modeled sediment concentration along the Blackstone River during Storm 2.

during Storm 2 (11/2/92–11/6/92). Statistical analysis of the model results of the three storms will be given in Tables 8.4.1–8.4.3. The 12 small plots in Fig. 3.7.9 are the flow rates along the Blackstone River during the survey period of Storm 2. The horizontal axis is in days from November 2, 1992, and the vertical axis is in cubic meters per second. The river kilometers are also shown in the plots. The black dots represent the measured flow rate, and the solid line represents the model results. It is seen in Fig. 3.7.9 that each station has about 16 flow rate records and the 12 stations have a total of 192 records. The upper-left plot of Fig. 3.7.9 shows that the peak flow rate near the river head at Kilometer 73.5 is ~7 cms at Day 1.3. The lower-right plot shows that the peak flow rate near the end of the river (km = 0.3) is around 25 cms at Day 2.3, ~1.0 day later than at the river head. The model simulates both the magnitude and moving speed of the peak flow reasonably well.

TSS in this study is represented by the cohesive sediment in the EFDC model. Figure 3.7.10 is the same as Fig. 3.7.9, except for TSS. As shown in Figs. 3.7.9 and 3.7.10, both the model and the data reveal that high sediment concentrations coincide with high flow rates. The model successfully simulates the sediment resuspension processes at the dams, including Singing Dam (km = 64.0), Fisherville Dam (km = 58.4), Riverdale Dam (km = 51.3), and Rice City Pond Dam (km = 44.7). The high sediment concentration at Kilometer 37.3 is caused by inflows from the upstream and the tributaries.

After the hydrodynamic and sediment processes were simulated successfully, the Blackstone River Model was also applied to simulate metals in the river. This information will be presented in Section 8.4.1. More discussions on this modeling effort are also given in Section 8.4.1.

CHAPTER 4

Pathogens and Toxics

Pathogens are disease-causing microorganisms that include bacteria, viruses, and protozoa. The term "toxics" is used to describe a variety of toxic pollutants in waterbodies, including toxic organic chemicals and toxic metals.

Contaminated water is responsible for the spread of many contagious diseases. Most contaminants, especially the toxics, are associated with sediments in waters. Sorption of metal and organic toxicants to sediments is one of the most important processes affecting their fate and transport. Therefore, an accurate description of hydrodynamic processes (Chapter 2) and sediment processes (Chapter 3) is essential to the fate and transport of pathogens and toxics.

This chapter discusses processes associated with pathogens and toxics and their mathematical modeling. Section 4.1 gives an overview of contaminant problems and sources; Section 4.2 is focused on pathogens; Section 4.3 explains toxics substances, including toxic organic chemicals and metals; Section 4.4 describes processes associated with the fate and decay of the contaminants; and Section 4.5 illustrates the modeling of pathogens and toxics.

4.1 OVERVIEW

A contaminant is a chemical or biological substance in a concentration that can potentially cause adverse affects on the physical, chemical, or biological properties of a waterbody. It includes pathogens, toxic metals, toxic organic chemicals, and other harmful substances. Contamination of surface waterbodies poses serious risks to both aquatic ecosystems and human health. Contaminants in a waterbody can be taken up by aquatic organisms in a process called bioaccumulation. When larger animals feed on these contaminated organisms, the toxicants are taken into their bodies, moving up the food chain in increasing concentrations in a process known as biomagnification. When contaminants bioaccumulate in fish, shellfish, and other food sources, they pose a threat to human health.

Hydrodynamics and Water Quality: Modeling Rivers, Lakes, and Estuaries, by Zhen-Gang Ji

Most contaminants are associated, to a greater or lesser degree, with suspended and deposited particles in natural systems. Although contaminants and nutrients can be transported into the waterbodies in dissolved forms, much of the contaminants and nutrients adsorb onto fine sediment particles. Sediments are both a carrier and a possible source of contaminants in aquatic systems. Sorption of metal and organic toxicants to suspended sediment is one of the most important processes affecting their fate, transport, and bioavailability. Contaminants can be transported through a waterbody by suspended sediment, deposited to the bottom and/or resuspended from the sediment bed, and transformed by chemical, biological, and hydrodynamic factors. Thus, an accurate treatment of sediment processes is essential to the fate and transport of sediment-associated toxics, such as heavy metals and toxic organic chemicals. The slow-settling velocity of dispersed fine sediment, with which many toxicants are associated, suggests the importance of accurate hydrodynamic simulations as part of any toxicant transport and fate study.

Contaminated sediments may kill/affect benthic organisms and reduce the food available to larger animals, such as fish. Some of the contaminants may have been released years ago, while other contaminants are still discharged every day. Some contaminants flow directly from industrial and municipal waste dischargers, while others come from polluted runoffs in urban and agricultural areas. Contaminants may also be carried through the air and deposited in lakes and streams far from the facilities that produced them. Even after the elimination of the primary contaminant sources, contaminants deposited in a sediment bed can still be a major source of pollution for many years to come.

A typical contamination scenario could start with the discharge of a contaminant into a river. The discharged contaminant is sorbed to the sediment, is carried downstream, and then settles into the sediment bed where the river flow slows down. Under a storm event, the deposited sediment, along with the contaminant, could be resuspended into the water column and pose risk to the environment. Elimination of the contaminant discharge would still not remove the contaminant source on the sediment bed.

Examples of contaminant sources are sewage treatment plants, urban runoffs, storm sewers, failing septic systems, industrial discharges, and contaminated sediments (Fig. 4.1.1). The origins of contaminants can be divided into point and nonpoint sources. Point source pollution comes from a specific, identifiable source, such as a pipe. Nonpoint source pollution cannot be traced to a specific spot. Point sources include wastewater treatment plants, overflows from combined sanitary and storm sewers, and industry discharges. Nonpoint sources include runoffs from urban, agriculture, and mining areas. Sometimes contaminants are localized around the discharging location. In other cases, rivers and streams can carry the sediments and the contaminants downstream for a long distance. Atmospheric deposition is another source of nonpoint pollution. Temporal variability of nonpoint sources is directly related to watershed hydrologic variability. High runoff is usually accompanied by high loads

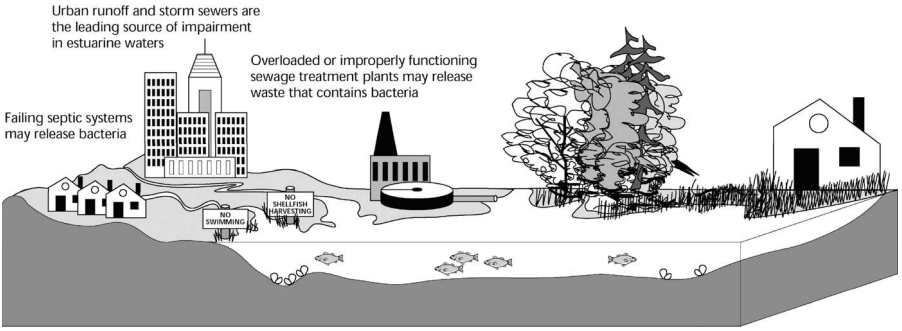

Fig. 4.1.1 Sources of contaminants (USEPA, 2000a).

of sediments that may contain organic contaminants and heavy metals. For example, mining is a significant source of sediment contamination in some regions. Agricultural runoff can contribute arsenic, mercury, and a wide variety of pesticides. Urban runoff is a frequently mentioned source of heavy metals and PAHs. Atmospheric deposition can be one of the major sources of arsenic, lead, mercury, and some pesticides.

4.2 PATHOGENS

Microorganisms are rampant in waterbodies. Many of them are beneficial, functioning as agents for chemical decomposition, and are essential components of the biogeochemical cycles. The survival of ecosystems is impossible without the decomposers. These microorganisms are responsible for converting organic matter to inorganic nutrients that can be used by other plants and animals. They function as decomposers by breaking down plant and animal remains. This activity releases nutrients previously locked up in the organic matter into the food web. For example, bacteria convert ammonia to nitrite and then convert nitrite to nitrate. These nutrients are used by plants. In humans and animals high on the food chain, microorganisms resident in the digestive tract aid in the digestion process and are excreted in large numbers.

Human activities may introduce pathogenic (disease-causing) bacteria into a waterbody. Of the vast number of species of microorganisms present in the environment, pathogens are a small group of microorganisms that are capable of causing varying degrees of diseases in humans. While some pathogens are naturally occurring in the environment, the source of pathogens is usually feces or other wastes of humans and various other warm-blooded animals. These microorganisms may enter waters through a number of routes, including agriculture and urban runoffs, malfunctioning septic tanks or sewage plants, or combined storm/sanitary sewer overflows that bypass treatment during storms.

Pathogens are small in size. Once released into the environment, they are easily transported by water and are often found densely packed on suspended particulate matters. Pathogens are commonly grouped into three general categories: (1) bacteria, (2) viruses, and (3) protozoa.

Pathogens can infect humans through skin contact or ingestion of contaminated water or food. Examples of pathogens include (1) bacteria responsible for cholera and typhoid fever; (2) viruses responsible for hepatitis and respiratory disease; and (3) protozoa responsible for giardiasis. Human exposure can occur not only from eating contaminated shellfish, but also from swimming or engaging in water contact sports in contaminated waters. Fish and shellfish concentrate pathogens in their tissues and may cause illness in persons consuming them. Pathogen contamination can also occur in conjunction with other inorganic pollutants. Runoff from a livestock area, for example, may contain not only pathogens, but high levels of nutrients as well.

Since pathogens tend to be in very low concentrations and there are many different pathogens, direct testing for pathogens is very expensive and impractical. The use of indicators provides evidence that a waterbody may contain pathogens harmful to humans. Pathogens are often associated with fecal waste. The four indicators most commonly used today are total coliform, fecal coliform, *Escherichia coli* (*E. coli*), and enterococci. The indicators are bacteria that are normally prevalent in the intestines and feces of warm-blooded animals, including wildlife, farm animals, pets, and humans. The indicator bacteria themselves are usually not pathogenic.

4.2.1 Bacteria, Viruses, and Protozoa

Bacteria are single-celled microorganisms and usually vary in size from 0.5 to 10 μm. Bacteria are capable of synthesizing cellular material from either inorganic or organic materials. Certain bacteria can function in the absence of oxygen (anaerobic growth), whereas others require high levels of oxygen for growth. Pathogenic bacteria found in surface waters are often attributed to excretions from human and warm-blooded animals. Bacteria of the coliform group are the primary indicators of fecal contamination and are often used to assess water quality. It is important to note, however, that most types of bacteria are not pathogenic. The most important group of bacteria with respect to water quality is those associated with the transmission of disease. Table 4.2.1 shows some of the waterborne diseases and effects associated with bacteria, viruses, and protozoa.

Viruses are the simplest form of microorganisms. They require a host to live and cannot grow outside another living organism. Once inside the host, the virus reproduces and manifests the associated illness. The host cell produces more viral particles and liberates them to the environment for further attacks. Viruses attack many types of cells, including bacteria, algae, and animal cells. The most significant virus group affecting water quality and human health originates in the gastrointestinal tract of infected animals. Viruses, such as

TABLE 4.2.1 Waterborne Pathogens (USEPA, 1999)

	Pathogen	Disease	Effects
Bacteria	*E. coli* (enteropathogenic)	Gastroenteritis	Vomiting, diarrhea, death in susceptible populations
	Legionella pneumophila	Legionellosis	Acute respiratory illness
	Leptospira	Leptospirosis	Jaundice, fever (Weil's disease)
	Salmonella typhi	Typhoid fever	High fever, diarrhea, ulceration of the small intestine
	Salmonella	Salmonellosis	Diarrhea, dehydration
	Shigella	Shigellosis	Bacillary dysentery
	Vibrio cholerae	Cholera	Extremely heavy diarrhea, dehydration
	Yersinia enterolitica	Yersinosis	Diarrhea
Protozoans	*Balantidium coli*	Balantidiasis	Diarrhea, dysentery
	Cryptosporidium	Cryptosporidiosis	Diarrhea
	Entamoeba histolytica	Amedbiasis (amoebic dysentery)	Prolonged diarrhea with bleeding, abscesses of the liver and small intestine
	Giardia lamblia	Giardiasis	Mild-to-severe diarrhea, nausea, indigestion
	Naegleria fowleri	Amoebic meningoencephalitis	Fatal disease; inflammation of the brain
Viruses	Adenovirus (31 types)	Respiratory disease	
	Enterovirus (67 types, e.g., polio, echo, and Coxsackie viruses)	Gastroenteritis	Heart anomalies, meningitis
	Hepatitis A	Infectious hepatitis	Jaundice, fever
	Norwalk agent	Gastroenteritis	Vomiting, diarrhea
	Reovirus	Gastroenteritis	Vomiting, diarrhea
	Rotavirus	Gastroenteritis	Vomiting, diarrhea

hepatitis A, are excreted in the feces of infected individuals. These enteric viruses present a major threat to human health.

Protozoa are also single-celled microorganisms that reproduce by binary fission and occur primarily in aquatic environments. Pathogenic protozoa exist in water as cysts. Once ingested, the cysts hatch, grow, and multiply, causing the associated illness. Many diseases can be transmitted by pathogens in water systems. It is important, therefore, to observe whether the disease-causing pathogens are present in a water system and at what level. It is then possible to evaluate the risk of the disease being transmitted to the general public.

4.2.2 Pathogen Indicators

Waterborne pathogens pose a threat to human health when people contact or ingest the contaminated water or food. Analytical techniques for identification and enumeration of pathogenic bacteria in a waterbody are time consuming, require well-trained technicians, and usually are expensive. Indicator organisms are frequently used to represent the potential presence of pathogenic organisms. These indicators need to have certain properties, such as:

1. They should be easily detected by simple laboratory methods.
2. They should be associated with human sources, so that their occurrence in water would indicate contamination by humans.
3. They should not grow in natural surface water.
4. Their concentrations should be directly linked to the extent of contamination.

Laboratory methods have been developed to study the presence and concentration of indicator organisms. The presence of the indicator organisms shows that a waterbody might be contaminated. The concentration of the indicator organisms correlates to the concentration of the pathogen. Although the indicator organisms may not cause disease, they can be accompanied by a rogue's gallery of pathogenic organisms that cause hepatitis, cholera, or gastrointestinal illnesses. Therefore, swimming areas, wells, and/or shellfish beds may be closed to the public when the indicator concentrations rise above certain water quality criteria.

The four commonly used indicators are (1) total coliform, (2) fecal coliform, (3) *E. coli*, and (4) enterococci. These indicators are easy to grow in a lab and will be present in large numbers if recent fecal contamination has occurred. Total coliform bacteria include a collection of relatively harmless microorganisms that live in large numbers in the intestines of humans and warm- and cold-blooded animals. They aid in the digestion of food. Total coliform consist of both fecal and nonfecal components. Fecal coliform is the most important

subgroup of the total coliform bacteria. They can be separated from the total coliform group by their ability to grow at elevated temperatures and are associated only with the fecal material of warm-blooded animals. Although coliform bacteria are usually not pathogenic themselves, their presence indicates fecal contamination and, probably, disease-causing pathogens.

Total coliforms are not very useful for testing recreational or shellfishing waters. Some species in this group are naturally found in plant material or soil, so their presence does not necessarily indicate fecal contamination. Total coliforms are useful, however, for testing treated drinking water where contamination by soil or plant material would not be a concern (Ohrel and Register, 2006). Fecal coliform is a more fecal-specific indicator. It is widely used to test recreational waters. However, even this group can have a nonfecal origin. Studies also found that all members of the coliform group can regrow in natural surface water (Gleeson and Gray, 1997).

Escherichia coli is a subgroup of the fecal coliform bacteria and is also used as an indicator of fecal contamination in water. In 1885, German bacteriologist Theodor von Escherich discovered *E. coli* bacteria in the human colon and showed that certain strains of the bacteria were responsible for infant diarrhea and gastroenteritis. Although *E. coli* has often been in the news as a waterborne or food-borne pathogen, the vast majority of *E. coli* strains are harmless, including those commonly used by scientists in genetics laboratories. Enterococci bacteria are also a valuable indicator for determining the extent of fecal contamination of surface waters. One factor favoring enterococci as a pathogen indicator is its resistance to environmental factors, particularly saline environments, enhancing its ability as a suitable indicator for marine waters.

EPA (USEPA, 1986, 2002) concluded that for freshwater, *E. coli* and enterococci are best suited for predicting the presence of gastrointestinal illness-causing pathogens, and that for marine waters, enterococci is best suited. Fecal coliform, the indicator originally recommended in 1967 by the Federal Water Pollution Control Administration of the U.S. Department of the Interior (USEPA, 1999), had less correlation to swimming-associated gastroenteritis than *E. coli* (in fresh waters) and enterococci (in both fresh and marine waters). As an indicator, *E. coli* has a major advantage over fecal coliform: it is more fecal specific. Even though EPA recommends enterococci or *E. coli* for testing recreational waters, many states still use fecal coliform. This is partly for the sake of continuity, so that new data can be directly compared with historical data. Another reason is due to economics: the EPA-approved method for enterococci testing requires the use of an expensive growth medium (Ohrel and Register, 2006).

Water quality criteria for pathogens are concentrations of indicator organisms that should not be exceeded in order to protect human health from pathogen-caused illness. As shown below, the EPA criteria for bathing in recreational waters are 33 enterococci/100 mL and 126 *E. coli*/100 mL for freshwaters, and 35 enterococci/100 mL for marine waters (USEPA, 1998).

EPA Criteria for Bathing (Full-Body Contact) Recreational Waters

Freshwater	
Based on a statistically sufficient number of samples (generally not less than five samples equally spaced over a 30-day period), the geometric mean of the indicated bacterial densities should not exceed either of the following[a]:	
E. coli	126/100 mL, or
Enterococci	33/100 mL.
No sample should exceed a one-sided confidence limit (C. L.) calculated using the following guidelines, based on a site-specific log standard deviation:	
Designated bathing beach	75% C.L.
Moderate use for bathing	82% C.L.
Light use for bathing	90% C.L.
Infrequent use for bathing	95% C.L.
If site data are insufficient to establish a log standard deviation, then one should use 0.4 as the log standard deviation for both indicators.	
Marine Water	
Based on a statistically sufficient number of samples (generally not less than five samples equally spaced over a 30-day period), the geometric mean of the enterococci densities should not exceed 35/100 mL.	
No sample should exceed a one-sided confidence limit using the following as guidelines, based on a site specific log standard deviation.:	
Designated bathing beach	75% C.L.
Moderate use for bathing	82% C.L.
Light use for bathing	90% C.L.
Infrequent use for bathing	95% C.L.
If site data are insufficient to establish a log standard deviation, then one should use 0.7 as the log standard deviation.	

[a]Only one indicator should be used. The regulatory agency should select the appropriate indicator for its conditions.

4.2.3 Processes Affecting Pathogens

Pathogen concentrations are controlled primarily by two mechanisms: hydrodynamic processes and degradation. Factors that may influence pathogen concentrations in water include (1) hydrodynamic transport, dilution, and settling; (2) sunlight; (3) temperature; (4) salinity; (5) predation; (6) nutrient levels; (7) toxic substances; and (8) other environmental factors.

Hydrodynamic processes transport and dilute pathogens discharged to a waterbody. Pathogens slowly settle and often attach to other faster settling aggregates. This results in an apparent decrease in bacterial numbers in the water column. Sorption and flocculation can affect this settling process. On the other hand, the pathogens that have settled to the bottom of the waterbody may adversely affect shellfish. Therefore, the settling process is actually the removal of pathogens from the water column to the bed, and a reduction in pathogen levels in the water column may simply signify an increase of pathogen levels in the bed.

In clear water, sunlight is an important factor for pathogen removal. Visible and ultraviolet (UV) light can kill *E. coli*. There is a direct link between sunlight intensity and coliform decay rates. A high level of sunlight may cause a much higher *E. coli* decay rate than that which could occur in the dark. In turbid water, however, the sunlight's ability to remove pathogens is limited, due to the poor penetration of UV light.

Temperature is the single most important modifier of decay rates, especially in freshwater and in the dark. Favorable temperature stimulates bacterial growth in the presence of adequate food and favorable environmental conditions. Decay rates of pathogens, such as *E. coli*, are proportional to salinity in marine water. Nutrient concentrations may be important in determining the decay rates under certain conditions. Some protozoa can ingest bacteria. Several species of organisms have been shown to attack and destroy *E. coli*. Other environmental factors, such as pH, heavy metals, and toxic substances, can have significant effects on the decay rates of pathogens. It is found that when fecal coliform undergoes the transition from the generally low oxygen environment of sewage to higher oxygen levels in surface waters, the oxygen shock promotes rapid coliform reduction (Kott, 1982).

The studies of pathogens in surface waters usually focus on indicator organisms, such as fecal coliform, *E. coli*, or enterococci. Modeling indicator organisms usually involves the use of a simple first-order decay expression. The fate and decay of fecal coliform (or other indicators) can be expressed as:

$$\frac{dC}{dt} = -k \cdot C \tag{4.2.1}$$

or

$$C = C_0 e^{-k \cdot t} \tag{4.2.2}$$

where C = fecal coliform concentration, MPN/100 mL or count/100 mL, C_0 = initial fecal coliform concentration, MPN or count/100 mL, k = decay rate, and t = time. Fecal coliform is often expressed in most probable number (MPN) per 100 mL (MPN/100 mL). The decay rate (also called the die-off rate), k, depends on the particular type of waterbody (i.e., river, lake, or estuary) and is a function of environmental factors, such as the ones listed previously.

The 3D equation for pathogen modeling in the Cartesian coordinates can be expressed as:

$$\frac{\partial C}{\partial t} + \frac{\partial (uC)}{\partial x} + \frac{\partial (vC)}{\partial y} + \frac{\partial (wC)}{\partial z} = \frac{\partial}{\partial x}\left(K_x \frac{\partial C}{\partial x}\right) + \frac{\partial}{\partial y}\left(K_y \frac{\partial C}{\partial y}\right) + \frac{\partial}{\partial z}\left(K_z \frac{\partial C}{\partial z}\right) + S_C \tag{4.2.3}$$

where C = concentration of a indicator organism (MPN/100 mL); u, v, and w = velocity components in the x, y, and z directions, respectively; K_x, K_y, and K_z = turbulent diffusivities in the x, y, and z directions, respectively; and S_C = internal and external sources and sinks.

In Eq. (4.2.3), the last three terms on the left-hand side (LHS) account for the advective transport, and the first three terms on the RHS account for the diffusive transport. These six terms of hydrodynamic transport are the same as those in the sediment transport equation, Eq. (3.2.13). The last term in Eq. (4.2.3) represents kinetic processes and external loads.

The kinetic equation of the indicator organism is

$$\frac{\partial C}{\partial t} = S_C \tag{4.2.4}$$

which may be expressed as:

$$\frac{\partial C}{\partial t} = -k \cdot \theta^{T-20} C + Q \tag{4.2.5}$$

where k = first-order die-off rate at 20 °C (day^{-1}), θ = effect of temperature on decay of coliform bacteria, and Q = external loads of coliform bacteria (MPN/100 mL/day). Equations similar to Eqs. (4.2.3) and (4.2.4) are also commonly used in water quality and eutrophication modeling (Chapter 5).

4.3 TOXIC SUBSTANCES

Toxic substances are those substances that can cause short- or long-term damage to human health and the environment. Ingestion, inhalation, or direct skin contact are the routes of exposure to the toxic substances. Toxic organic chemicals (TOCs) and heavy metals are two major toxic substances in the natural environment. Toxic substances, such as metals, PAHs, PCBs, and pesticides, are a concern in surface waters. These substances enter waterways through municipal and industrial discharges; runoffs from lawns, streets, and farmlands; and deposition from the atmosphere. Many toxic contaminants are also found in sediments and can be resuspended into the water columns by currents, wind waves, and/or tides. Drifting atmospheric pollutants that are eventually deposited in waterbodies also contribute to water contamination. For example, EPA estimates that 76–89% of PCB loadings to Lake Superior have come from air pollution (USEPA, 1994a).

Toxic substances in a waterbody can exist in two basic forms: the dissolved and the particulate phase. The former is transported with water flows, and the latter is often attached to and transported with sediments (or particulate organic carbons). It is primarily the ones in the dissolved phase that cause harm to the environment. Compared with the conventional pollutants, such

as nitrogen and phosphorus, the toxic substances can be considered harmful at very low concentrations, such as in a few micrograms per milliliters (μg/L).

Historical releases of metals and TOCs have left a legacy of sediment beds enriched with these contaminants. The characteristics of local contamination are usually related to the land use activities within the watershed. Rivers, lakes, and estuaries in industrialized/urbanized areas tend to have elevated levels of metals and organic compounds. While the use of certain chemicals (e.g., PCBs) might have since been banned or tightly restricted, these contaminants have accumulated to levels that may still pose an unacceptable human health and ecological risk. For example, the Blackstone River, MA, has high level of toxic metals, which can be traced back 200 years, to the American industrial revolution (USEPA, 1996a).

Distinct processes that many toxic substances undergo are bioaccumulation and biomagnification, which do not pertain to many conventional pollutants, such as nitrogen and phosphorus. Bioaccumulation is the process by which some persistent contaminants concentrate and accumulate as they travel via digestive processes to higher levels of the food chain. Biomagnification is the magnification of contaminant concentrations in biota at each successive trophic level in a food chain. The concentration of chemical contaminants progressively increases from the bottom of the food chain (e.g., phytoplankton and zooplankton) to the top of the food chain (e.g., fish-eating birds). Bioaccumulation is the build-up of a toxic substance by aquatic organisms to concentration levels much higher than the surrounding environment. This is primarily due to the uptake and retention of a chemical by living organisms, as a result of direct contact with or inhalation of the chemical, or eating contaminated food or drinking contaminated water. For example, if a predator eats a large number of preys, with each having a small amount of a pollutant in its body, the predator's tissues could become contaminated with whatever pollutant existed in the prey's tissues. Through this biomagnification process, toxic substances can move through the food web and become more concentrated in animals at higher levels in the food chain. In this way, certain chemicals, such as mercury, PCBs, and some pesticides, can be concentrated from very low levels in the water to toxic levels in animals. Indeed, concentrations of PCBs in the tissue of some animals can reach literally hundreds of thousands of times greater than the surrounding water.

Many chemicals in aquatic systems are toxic at certain concentrations. There is a growing need for development of mathematical and numerical models that can be used for calculating safety levels and establishing water quality criteria. In order for a substance to be considered toxic, several factors should be considered, including the following:

1. The potential that the environment is exposed to the substance.
2. The potential that living organisms are exposed to the substance.
3. The effects that are derived from the exposure.

Toxic contaminants can threaten human and ecological health either directly or through bioaccumulation in and up the food chain. Certain chemicals (e.g., mercury) can be particularly harmful: many pose risks even at very low concentrations and can remain potentially dangerous for long periods of time while they bioaccumulate in animal or human tissue. These chemicals can be acutely poisonous to humans at low levels of exposure. The pollutants can settle to the bottom of waterbodies, creating "hot spots" of contamination. Concentrations of contaminants gather in bottom-dwelling animals that work their way through the food chain, ultimately leading to human exposure.

The most frequently mentioned effects resulting from the exposure to toxic substances are acute and chronic toxicity. Acute toxicity is the toxic effect that is severe enough to rapidly induce an effect within a short period of time, usually 96 h or less. Acute toxicity is not always measured in terms of mortality. Any harmful biological effect may be the result. Chronic toxicity is the toxic effect that lingers or continues for a relatively long period of time and produces an adverse effect on human health and the environment. These effects could include mortality, reduced growth, and/or reduced reproduction.

To assess the effects of a toxic substance, the fate and transport processes of the substance in the environment should be determined, including the following:

1. Hydrodynamic processes, such as advection and dispersion of the toxics in the water column.
2. Sediment processes, such as sediment transport in the water column; deposition and resuspension of sorbed toxics due to sediment movement; and sorption and desorption of the particulate toxics with the sediment.
3. External sources, such as point sources from wastewater treatment plants, nonpoint sources from runoffs, and atmospheric depositions.
4. Decay and transformation processes, such as photolysis, hydrolysis, and biodegradation, which will be discussed in Section 4.4.

Because of the preference for toxic substances to sorb to sediment, an accurate description of sediment concentration is important to the study of toxic substances. A change in the sediment mass balance will ultimately affect the overall toxic mass balance. In addition to sediment, toxic substances may also attach to particulate organic carbon. In this case, sediment and organic carbon should both be considered in the modeling of toxic substances.

Toxic substances in a water system are not necessarily conservative. Processes that can take the toxic substances out of the water system include the following:

1. Sedimentation and burial to the deep sediment layers, so that the toxics are out of the water system.

2. Chemical reactions, so that the toxics are transformed to become nontoxic or less dissolved, since the dissolved form is most likely the one directly causing adverse effects.
3. Sorption by things, such as aquatic plants, so that the toxics are no longer available to the system.

4.3.1 Toxic Organic Chemicals

Toxic organic chemicals are synthetic compounds that contain carbon. Historical releases of TOCs into waterbodies have left a legacy of aquatic sediment enriched with these contaminants. In some sediments, these contaminants have accumulated to levels that may pose an unacceptable human health and ecological risk. These TOCs persist in the environment and bioaccumulate and magnify in the food web. The TOCs can be categorized based on their usage and chemical classes (CEQ, 1978). Toxic organic chemicals that are frequently cited as causing environmental damage include (1) PCBs, (2) PAHs, (3) pesticides, and (4) dioxins and furans.

In modern societies, TOCs have been manufactured, used, and disposed of in large quantities. Many of the TOCs are considered to be refractory, which refers to the chemicals that resist degradation and remain in the environment for a very long time. These TOCs tend to persist and accumulate in the environment and do not readily break down in natural ecosystems. Some of the toxic TOCs, such as DDT and PCBs, have been banned from use in the United States for decades yet continue to cause environmental problems. It is well documented, for example, that DDT built up through the levels of the food chain and caused severe damage to the ecosystem.

The PCBs are a group of banned synthetic organic chemicals that were manufactured as coolants and lubricants for electrical equipment, until they were banned in the 1970s. They are resistant to biological and chemical degradation and can persist in the environment for decades. They are accumulated by aquatic organisms and become amplified in the food chain when animals eat PCB-contaminated organisms. These highly persistent chemicals can still be found in older electrical equipment and industrial waste sites. Problems associated with PCBs include cancer, fertility problems, and nervous system impairment.

The PAHs are a complex mix of organic compounds, including fossil fuels and their combustion. They are commonly the byproducts of oil burning. Exposure generally occurs by breathing smoke or exhaust from automobiles or other combustion processes. They can cause breathing difficulties and are carcinogenic. Many PAHs can be broken down over a period of weeks or months by microorganisms.

Pesticides are another major category of toxics. They are chemicals used to control or eliminate undesirable organisms, such as insects, fungi, or others that may reduce crop yields or impact the health of livestock. Many of them break down into nontoxic chemicals within a few days of application. Some

pesticides are refractory and can build up in sediments or bioaccumulate in food chains, posing potential health risks to humans or wildlife. For example, DDT is a highly toxic poison that is capable of killing many different species. It was used extensively in the 1940s–1960s as a pesticide and was banned in the United States in 1972, but it continues to be measured in sediment and in the tissues of aquatic animals.

Dioxins and furans are families of chemicals that are present in combustion emissions and are known to be highly toxic to humans and wildlife. They are the byproducts created in two major ways: (1) when materials are burned at low temperatures, and (2) by the processes used to manufacture some products. Once they have entered the environment, dioxins and furans can persist for a long time.

4.3.2 Metals

The definition of a metal can be based on its physical properties, such as electrical conductivity, reflectivity, and strength. By a broader definition, however, an element can be called metal if the element loses one or more electrons to form a cation in water. Heavy metals usually refer to those metals between atomic numbers 21 and 84. From the point of view of those studying water quality, however, a heavy metal is often referred to as a metal that is toxic. Heavy metals are a serious pollution problem when their concentration exceeds water quality standards.

Compared with TOCs, heavy metal pollutants are pervasive and more persistent. They frequently have natural background sources from the dissolution of rocks and minerals. Heavy metals can be in a dissolved and in a particulate phase. The metals in a dissolved phase move freely in a waterbody. The metals in a particulate phase are often sorbed to and transported with sediment. Interchange between the particulate and the dissolved metal occurs via sorption–desorption mechanisms. In the sediment bed, metal ions in pore water of the sediment can diffuse to the overlying water column and vice versa, depending on the concentration gradient. In addition, volatile metals (e.g., mercury) are emitted from industrial stack gases and can be directly deposited to surface water.

Characteristics of heavy metals include (1) bioaccumulation and biomagnification, (2) long decay time, (3) natural occurrences, (4) toxicity closely linked to the metal's dissolvability, and (5) many chemical forms. Frequently cited heavy metals include lead, cadmium, mercury, and others. Heavy metals in the environment are a source of concern because of their toxicity, reactivity, and mobility in water systems. Certain metals can persist in the environment, allowing time for biological processes to incorporate metals into food chains and for biomagnification to occur. Although metal concentration in a waste discharge may be small, the concentration can be magnified many times by aquatic organisms in the waterbody. Some heavy metals are essential for plant and animal health. However, at concentrations above those necessary to

sustain life, toxicity may also occur. High concentrations of metals are often reported appearing in fish tissues rather than in the water column, because the metals accumulate in greater concentrations in predators near the top of the food chain.

Lead and mercury rank highest with respect to real or anticipated environmental hazard. They can be converted into methyl mercury and methyl lead, which are strong human nerve poisons. Lead is particularly harmful to children and developing fetuses. Since the ban on lead as a gasoline additive, its concentration in the environment has been dropping steadily. Mercury has long been known as toxic, persistent, and bioaccumulative, and can travel great distances in the atmosphere. The primary health impacts from mercury are on the development of the brain and nervous system. When mercury becomes deposited within a waterbody, it can accumulate in the tissues of fish to concentrations much higher than in the surrounding water. Mercury is the most common contaminant in fish in the United States and Canada.

The decay times of metals are very different from the ones of TOCs. The character of a TOC is dependent on its structure; once that structure is destroyed, the toxic effect disappears. Metals, however, persist indefinitely in one form or another. In this sense, metals pose a much longer threat to the environment than do TOCs. Since decay mechanisms are often omitted, metal modeling can be relatively simpler than TOC modeling.

Unlike TOCs, which are manmade, toxic metals can be naturally occurring from dissolution of rocks and minerals. Human activities, such as industrial processes and mining, have altered the distribution of metals in the environment. Metals can be present in municipal treatment plants, industrial effluents, landfill leachates, and nonpoint source runoffs. In addition, many old industrial areas have soils with high concentrations of heavy metals due to past industrial practices (e.g., mining). Abandoned mines are a continuing source of toxic metals in many streams.

Dissolved metals, rather than total metals, are responsible for the toxicity to organisms. Dissolved metal is defined as the fraction that passes through a 0.45-μm filter, and particulate metal is defined as total metal minus dissolved metal. The dissolved fraction of a metal is a better representation of the biologically active portion of the metal than is the total fraction. This is not to say that particulate metal is nontoxic, only that particulate metal appears to exhibit substantially less toxicity than does dissolved metal. The EPA (USEPA, 1996b) recommends that concentrations of dissolved metal, not total metal, should be used in the water quality standards, because dissolved metal more closely approximates the bioavailable fraction of metal in the water column than does total metal. Sediments play an important role in regulating dissolved concentrations in natural waters. Heavy metals are often largely present in nonbioavailable forms and are sorbed to sediment particles. Environmental conditions, such as pH, temperature, and salinity, affect the metal solubility significantly. In general, metal solubilities are lower at near-neutral pH than in acidic or highly alkaline waters.

A single metal can have many different chemical forms. Owing to the tremendous number of interactions related to the metal in water, the metal concentration should include all of these forms. Therefore, metal total concentration, rather than one or a few particular chemical forms of the metal, should be considered in the sampling and modeling of heavy metals.

4.3.3 Sorption and Desorption

Contaminated sediments are a major source of pollution. They can accumulate on the bottom of a waterbody and contain toxic materials at concentrations that may adversely affect human health or the environment. Many toxic substances sorb strongly onto particulates. The sorption–desorption processes influence the concentration of contaminants. Sorption with solids is a major pathway for the transport of toxic chemicals in natural waters. Due to the interactions with particulate matter, the behavior of contaminants is affected by the transport, deposition, and resuspension of sediments. The dissolved toxic substances are directly linked to environmental damage. The corresponding particulate toxic substances are often considered unavailable to biological activity, and hence do not directly pose severe water quality problems. In addition to metals and toxic organic chemicals, nutrients (e.g., phosphorus) can also sorb to and be transported with sediments, which will be discussed in Chapter 5 when eutrophication processes are presented.

Sorption is the transfer of a substance from the aqueous to the solid phase. Desorption is the process by which substances are released from the particles back into water. Sorption represents the interaction of a contaminant with a solid and can be further divided into adsorption and absorption. Adsorption is the process by which substances adhere to the surface of particles, while absorption is the process by which substances actually penetrate into the structure of the particles. These two processes often have different time scales. Under most circumstances, however, this distinction serves little purpose, since often there is no specific and sufficient information to separate the two. Therefore, the term sorption is used in a generic way to include both phenomena. Sorption may be either absorption or adsorption, or a combination of the two. Sorption may cause a contaminant to accumulate in a bed sediment or bioconcentrate in fish.

Finer fractions of materials (e.g., clays, silts, and organic detritus) are often most important for toxic transport. These fine particles are characterized by size, shape, density, surface area, and surface physical and chemical properties. In general, the smaller the particle size, the greater the surface area/volume ratio and the greater the sorptive capacity for transporting sorbed contaminants. Clays have a high sorptive capacity, while sand has essentially no sorptive capacity. Particle surface areas also affect the capacity for contaminants to interact with particles. As small particles have greater surface/volume ratios than large particles, it is the smaller (silt- and clay-sized) particles that tend to

be more important in determining contaminant behavior. Smaller particles are also more readily carried by flows and waves than large particles.

Figure 4.3.1 illustrates key factors that determine the fate and transport of toxic substances, including (1) inflow and outflow; (2) settling of particulates in the water column; (3) sorption and desorption in both the water column and the bed; (4) exchange between the water column and the bed via deposition/resuspension, diffusion, and bioturbation; (5) losses by burial and volatilization; and (6) bioaccumulation and transformation.

A toxic substance, such as a heavy metal, can be in a particulate or dissolved phase in the sediment bed or the overlying water column. The metal in suspension is advected and dispersed in the water column, and transported by inflow and outflow. In the water column and the sediment bed, interchange between the dissolved metal and particulate metal occurs via sorption/desorption processes. Bed sediments can be scoured and enter the water column, while suspended sediments can undergo settling and be deposited on the bed. The heavy metal can be deposited into the water column from the atmosphere. Dissolved metal in pore water of the sediment bed can diffuse to the overlying water column and vice versa, depending on the concentration difference between the two. The processes of bioaccumulation and chemical transformation can remove the heavy metal out of the water system. The heavy metal can also be buried into the deep sediment layer and then be permanently removed from the surface water system. Depending on the properties of the substance, the importance of these processes varies. Not all of these physical, chemical, and biological interactions shown in Fig. 4.3.1 are essential for every toxic substance.

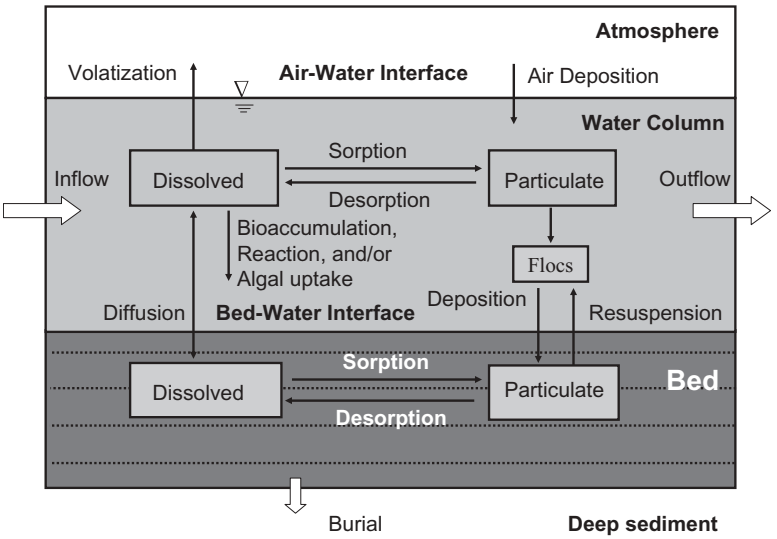

Fig. 4.3.1 Fate and transport processes for a toxicant.

Sorption–desorption processes are usually fast relative to other environmental processes, such as the time step of model integration or the time scales for decay. For this reason, the sorptive interaction between the dissolved and particulate components can be treated as in instantaneous equilibrium, that is, the equilibrium is assumed to be instantaneously established between the particulate phase of a toxic substance and its dissolved phase. In this case, the solubility of the substance can be measured by its solubility product, which is the product of the concentrations of the ionic species involved in the dissolution. This product is considered as a constant under given environmental conditions. For a heavy metal with the following reaction:

$$M_m A_a \rightarrow mM + aA \tag{4.3.1}$$

the solubility product has

$$k_s = [M]^m [A]^a \tag{4.3.2}$$

where k_s = solubility product, $[M]$ = molar concentration of the metal ion, and $[A]$ = molar concentration of the corresponding chemical component.

As discussed before, the concentration of a toxic substance is composed of a dissolved component, C_d, and a particulate component, C_p:

$$C = C_d + C_p \tag{4.3.3}$$

The particulate component can be expressed as a product of the toxic solid-phase concentration, r, and the sediment concentration, S:

$$C_p = r \cdot S \tag{4.3.4}$$

The toxic solid-phase concentration, r, is expressed in solid dry weight. For a given volume of sampled water, the toxic solid-phase concentration is defined as:

$$r = \frac{\text{Mass of toxics sorbed to sediment in } \mu\text{g or mg}}{\text{Mass of sediment in mg or g}} \tag{4.3.5}$$

Assuming that equilibrium exists between the dissolved and particulate phases, which is usually valid in toxic modeling studies, the partition coefficient, P, is defined as:

$$P = \frac{\textit{Toxics} \text{ sorbed to sediment (mass of toxics/mass of sediment)}}{\text{Dissolved toxics (mass of toxics/water volume)}} = \frac{r}{C_d} \tag{4.3.6}$$

Equation (4.3.6) indicates that the partition coefficient is the ratio of the toxics in the particulate phase (sorbed to the sediment) to the toxics in the

dissolved phase. The partition coefficient is usually expressed as liters per gram (L/g) or liters per milligram (L/mg). The value of the partition coefficient for a given substance is affected by a number of factors. Some empirical evidence has suggested that the partition coefficient is inversely related to the sediment concentration, while in other cases, the partition coefficients are independent of sediment concentrations (O'Connor, 1988; Ji et al., 2002a). In order to accurately calculate the dissolved and particulate phases, it is recommended to use measured data to estimate the values of P.

From measured data, the partition coefficient can be estimated as:

$$P = \frac{C_p}{C_d}\frac{1}{S} \tag{4.3.7}$$

The meaning of P becomes apparent in Eq. (4.3.7): the partition coefficient is the ratio of the particulate concentration to the dissolved concentration per unit concentration of suspended solid. For example, measured data indicate that metals in the Blackstone River, MA, have partition coefficients varying from 0.1 to 1.0 L/mg (Ji et al., 2002a). Figure 4.3.2 gives the cadmium partition coefficient as a function of sediment concentration in the Blackstone River (Tetra Tech, 1999b).

The particulate fraction of a toxic (f_p) and the dissolved fraction of a toxic (f_d) are defined as:

$$f_p = \frac{C_p}{C} = \frac{PS}{\theta + PS} \tag{4.3.8}$$

$$f_d = \frac{C_d}{C} = \frac{\theta}{\theta + PS} = 1 - f_p \tag{4.3.9}$$

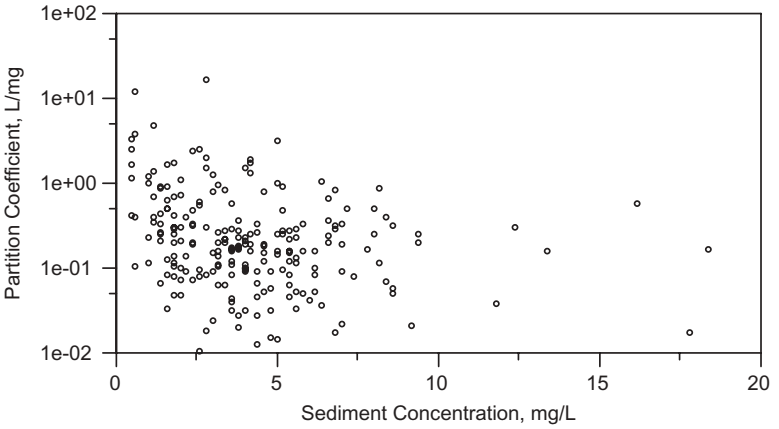

Fig. 4.3.2 Cadmium partition coefficient as a function of sediment concentration in the Blackstone River, MA.

where θ is the porosity (~1 for the water column). The product $P \cdot S$ is a dimensionless parameter. The distribution of a toxicant between dissolved and particulate phases therefore depends on the partition coefficient and the sediment concentration. For a single metal element, there can be a variety of chemical complexes. In most measurements and simulation models, however, all dissolved metal complexes are lumped with the free ion to give the total dissolved metal concentration, and all particulate metal complexes are lumped with all sorbed species to give the total particulate metal concentration.

Toxic chemical models can represent a toxicant by either two- or three-phase partitioning. A two-phase partition defines the total concentration of a toxicant as the sum of the dissolved and particulate fractions, as what is represented in Eq. (4.3.3). The assumption of equilibrium partition between the dissolved and the particulate, as expressed in Eqs. (4.3.8) and (4.3.9), is one of the simplest methods of representing sorption–desorption process, but by no means a general method. For example, a three–phase model partitions the toxicant into three forms: a truly dissolved (bioavailable) phase, a dissolved organic carbon (DOC) phase (not bioavailable), and a particulate organic carbon phase. The three-phase model couples DOC with the toxicant. The three-phase model is most useful for waterbodies with a significant proportion of organic matter produced internally by biological processes, rather than externally supplied.

4.4 FATE AND TRANSPORT PROCESSES

Contaminants in aquatic systems include nutrients, organic toxicants, heavy metals, and pathogens. If no degradation reactions occurred in Nature, every single contaminant discharged in the past would still be polluting the environment. Fortunately, natural purification processes dilute, transport, remove, and degrade contaminants. It is essential to understand the kinetics of reactants and to describe them mathematically. This section summarizes the decay and transport of contaminants and their mathematical formulations.

The fate and transport processes of contaminants are controlled by two factors: their reactivity and their hydrodynamic transport. Reactivity includes (1) chemical processes, (2) biological processes, and (3) biouptakes. Hydrodynamic transport includes three mass transport processes: (1) advection of water current, (2) diffusion and turbulent mixing within the water column, and (3) deposition and resuspension on the water-sediment bed interface.

4.4.1 Mathematical Formulations

How long contaminants remain in a waterbody depends on the nature of the compound. Most chemicals undergo chemical or biological decay. Some chemicals are conservative and do not undergo these types of reactions, even though it is very difficult to find a truly conservative chemical in Nature. A substance is assumed to be conservative when the rate of reaction is very low. Many of

the TOCs, such as PCBs and DDT, do not degrade for many years and can concentrate in the sediment and in the tissues of local aquatic animals. Humans, in turn, can be harmed by consuming these aquatic animals that are exposed to contaminated sediment. Nonconservative substances react chemically or biologically. These fate and decay processes include volatilization, hydrolysis, photolysis, and biodegradation.

The fate and decay of a contaminant represent the gradual decrease in the amount of a substance in an environmental system, as the result of various sink processes, including chemical and biological transformation, or dissipation/deposition to other environmental systems. The fate and decay processes are contaminant specific. However, they have comparable kinetics so that similar formulations can be used. Based on the principle of conservation of mass, the concentration change of a contaminant can be calculated using mass balance equations.

Although reaction kinetics in aquatic systems can be described in numerous ways, the form for a single reactant is generally expressed as:

$$\frac{dC}{dt} = R = -kC^m \tag{4.4.1}$$

where m = the order of reaction and k = rate constant of the m-order reaction. In natural waters, the commonly used forms of Eq. (4.4.1) are with m = 0, 1, and 2.

Zero-Order Reactions. A zero-order reaction ($m = 0$) represents irreversible degradation of a reactant that is independent of the reactant concentration. The solution to Eq. (4.4.1) is

$$C = C_0 - kt \tag{4.4.2}$$

where C_0 = the initial concentration at $t = 0$. In this case, a plot of concentration versus time should yield a straight line with a slope of k, as shown in the left panel of Fig. 4.4.1. Zero-order reactions have their reaction rates determined by some factor other than the concentration of the reacting materials. Methane production and release of hydrolysis products from anaerobic sediment are examples of zero-order reactions (Schnoor, 1996).

First-Order Reactions. First-order reactions ($m = 1$) have their reaction rates proportional to the concentration of the reactant and are most commonly used in describing chemical and biological reactions. For first-order reactions, the solution to Eq. (4.4.1) is

$$C = C_0 e^{-kt} \tag{4.4.3}$$

Equation (4.4.3) indicates that for first-order reactions, reactant concentration decreases exponentially with time. In this case, a plot of logarithm concentration versus time should yield a straight line with a slope of k, as shown in the middle panel of Fig. 4.4.1. Most of the reactions found in the environment can

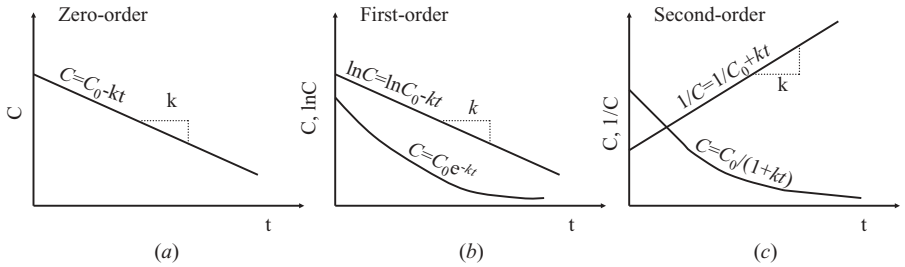

Fig. 4.4.1 (*a*) Concentration versus time for zero-order reaction. (*b*) Concentration and logarithm concentration versus time for first-order reaction. (*c*) Concentration and inverse concentration versus time for second-order reaction.

be conveniently expressed by a first-order approximation without much error. Examples of first-order reactions include biochemical oxygen demand in surface waters, death and respiration rates for bacteria, and production reaction of algae (Thomann and Mueller, 1987). Noted that, although most kinetic formulations are parameterized by first-order reactions, derivation of the reaction rate constant k might require a significant amount of data.

Second-Order Reactions. For second-order reactions ($m = 2$), the solution to Eq. (4.4.1) is

$$\frac{1}{C} = \frac{1}{C_0} + kt \tag{4.4.4}$$

Therefore, if a reaction is indeed second order, a plot of inverse concentration of C ($1/C$) with time should yield a straight line with a slope of k (the right panel of Fig. 4.4.1). Equation (4.4.4) can also be expressed as:

$$C = \frac{C_0}{1 + kC_0 t} \tag{4.4.5}$$

which reveals that, similar to the first-order reaction, the resulting concentration of a second-order reaction also decreases and approaches zero as time increases. Processes that might be described by second-order reactions include atmospheric gas reactions and zooplankton death rates.

The mathematical equations for describing toxic substances, including heavy metal and TOCs, are similar. The 3D transport equation for total toxic concentration C (dissolved plus particulate phases) is

$$\begin{aligned} &\partial_t(HC) + \partial_x(HuC) + \partial_y(HvC) + \partial_z(wC) - \partial_z(w_s f_p C) \\ &= \partial_x(HK_H \partial_x C) + \partial_y(HK_H \partial_y C) + \partial_z\left(\frac{K_v}{H}\partial_z C\right) + R + Q_c \end{aligned} \tag{4.4.6}$$

where w_s = sediment settling velocity, R = reactivity of chemical and biological processes, Q_c = external toxic sources and sinks, x and y = Cartesian coordinates in the horizontal directions, and z = sigma coordinate in the vertical direction, defined in Eq. (2.2.19).

Comparing Eq. (4.4.6) with the pathogen equation (4.2.3) reveals that the major difference between the two is that Eq. (4.4.6) includes the sediment settling term, $-\partial_z(w_s f_p C)$. In Eq. (4.4.6), the total toxic concentration, C, is modeled, instead of calculating the dissolved and the particulate phases separately. Equations (4.3.8) and (4.3.9) specify C_d and C_p, after C and the particulate fraction, f_p, are known. It is the particulate fraction (f_p) and the sediment settling velocity (w_s) that link the toxics with the suspended sediment concentration. The sediment concentration, as shown in Eq. (4.3.8), affects the particulate fraction and thus affects the settling and transport of the toxics described in Eq. (4.4.6). In the modeling of heavy metals, the fate and decay mechanisms, represented by the reactivity term in Eq. (2.1.33), are usually neglected. In this sense, the modeling of metals is simpler than the modeling of some TOCs.

Vertical boundary conditions for the transport equation (4.4.6) are

$$\begin{aligned} -\frac{K_V}{H}\partial_z C - w_s f_p C &= F_o \qquad \text{at water–sediment bed interface } (z \approx 0) \\ -\frac{K_V}{H}\partial_z C - w_s f_p C &= 0 \qquad \text{at the water surface } (z = 1) \end{aligned} \tag{4.4.7}$$

The net flux of toxics from the sediment bed to the water column, F_o, is given by

$$F_o = \max(J_o, 0)\left(\frac{f_p^b}{S^b} + \varepsilon_r \frac{\rho_w}{\rho_s} f_d^b\right) C^b + \min(J_o, 0)\left(\frac{f_p^w}{S^w} + \varepsilon_d \frac{\rho_w}{\rho_s} f_d^w\right) C^w \tag{4.4.8}$$

where the w and b superscripts define water column and sediment bed conditions at the water column–sediment bed interface, respectively, ρ_s is sediment density, ρ_w is water density, and ε_r and ε_d are the sediment bed void ratios under conditions of resuspension and deposition, respectively. The parameter J_o is the net sediment flux from the bed to the water column. This form of net flux consistently accounts for entrainment and expulsion of water and dissolved toxics from and to the bed due to sediment resuspension and deposition (Tetra Tech, 2002; Ji et al., 2002a).

4.4.2 Processes Affecting Fate and Decay

The fate and decay of toxic substances can result from physical, chemical, and/or biological reactions. In addition to sorption and desorption, processes that can significantly affect the fate and decay processes include (1) mineral-

ization and decomposition, (2) hydrolysis, (3) photolysis, (4) biodegradation, (5) bioconcentration, and (6) volatilization.

Transformation processes are those in which toxic substances are essentially irreversibly destroyed, changed, or removed from the water system. These transformation processes are often described by kinetic equations similar to Eq. (4.4.1). Most decay processes are expressed as first-order reactions. The first-order decay coefficients for individual processes are additive and can be linearly superimposed to form a net decay coefficient:

$$k_d = k_m + k_h + k_p + k_{bd} + k_{bc} + k_v \tag{4.4.9}$$

where k_d = net decay coefficient, k_m = mineralization coefficient, k_h = hydrolysis coefficient, k_p = photolysis coefficient, k_{bd} = biodegradation coefficient, k_{bc} = bioconcentration coefficient, and k_v = volatilization coefficient.

In modeling studies, either the net degradation coefficient or the individual coefficients can be specified. In Chapter 5, where the water quality and eutrophication processes are discussed, these processes will be discussed again and their mathematical representations will be described in detail. This section introduces the basic concepts of these processes.

4.4.2.1 Mineralization and Decomposition. Mineralization is the process by which a dissolved organic substance is converted to dissolved inorganic form. Mineralization makes nutrients, such as nitrogen and phosphorus, available for a fresh cycle of plant growth. Decomposition is the breakdown of organic materials into simpler organic or inorganic components through microbial action.

Bacteria decompose organic material to obtain energy for growth. Plant residue is broken down into glucose that is then converted to energy:

$$C_6H_{12}O_6 + O_2 \xrightarrow{\text{energy released}} CO_2 + H_2O \tag{4.4.10}$$

In water quality models, the term "mineralization" often represents the process by which dissolved organic matter is converted to dissolved inorganic form, and thus includes both heterotrophic respiration of dissolved organic carbon and mineralization of dissolved organic phosphorus and nitrogen (Cerco and Cole, 1994). Mineralization is a key process in the water quality models discussed in Chapter 5.

4.4.2.2 Hydrolysis. Hydrolysis is the reaction of a chemical with water, in which splitting of a molecular bond occurs in the chemical and there is a formation of a new bond with either the hydrogen (H^+) component or the hydroxyl (OH^-) component of a water molecule. This involves ionization of the water as well as splitting of the compound hydrolyzed:

$$RX + H_2O \rightarrow ROH + HX \tag{4.4.11}$$

Essentially, water enters a polar location on a molecule and inserts itself, with an H^+ component going to one part of the parent molecule and an OH^- component going to the other. The two components then separate. The concentration of hydrogen and hydroxide ions, and therefore pH, is often an important factor in assessing the rate of a hydrolysis reaction. Hydrolysis is a major pathway for the degradation of many toxic organics. Products of hydrolysis may be either more or less toxic than the original compound.

Hydrolysis is one of the most important fate and decay processes in waterbodies. In water quality models, hydrolysis is used to represent the process by which particulate organic substances are converted to dissolved organic form (Cerco and Cole, 1994; Park et al., 1995). The mathematical representation and simulation of hydrolysis processes will be described in Chapter 5, when water quality and eutrophication processes are discussed.

4.4.2.3 Photolysis. Photolysis (photodegradation) is the transformation of a compound that results directly from the adsorption of light energy. Compounds that absorb sunlight may gain sufficient energy to initiate a chemical reaction. Some of these photochemical reactions result in the decomposition or transformation of a substance.

The energy of light varies inversely with its wavelength. Longwave light lacks sufficient energy to break chemical bonds. Short wave light (X- and γ-rays) is very destructive. Fortunately for life on earth, this type of radiation largely is removed by the upper atmosphere. Light near the visible spectrum reaches the earth's surface and can break the bonds of many organic compounds, which can be important in the decay of organic chemicals in a water system.

The basic characteristics of photolysis are

1. Photolysis has two types of energy absorption: direct photolysis and indirect photolysis. The direct photolysis is the result of direct absorption of sunlight by the toxic chemical molecule. Indirect photolysis is the result of energy transfer to the toxic chemical from some other molecule that has absorbed the sunlight.
2. Photolysis is the destruction of a compound activated by the light energy and is an irreversible decay process.
3. Products of photolysis may remain toxic and the photolysis process does not necessarily lead to detoxification of the system.
4. The photolysis coefficient in Eq. (4.4.9) is usually a function of the quantity and wavelength distribution of incident light, the light adsorption characteristics of the compound, and the efficiency at which absorbed light produces a chemical reaction.

4.4.2.4 Biodegradation. Biodegradation (biolysis) is the breakdown of a compound by enzyme-mediated transformation, primarily due to bacteria, and

to a lesser extent, fungi. Although these types of microbial transformations can detoxify and mineralize toxics, they can also activate potential toxics. The rate of biodegradation can be very rapid, which means that biodegradation is often one of the most important transformation processes in water.

Even though the biodegradation process is largely mediated by bacteria, the growth kinetics of the bacteria is complicated and is not well understood. As a result, toxic models often assume constant decay rates rather than modeling the bacteria activity directly. The first-order decay rate is commonly used. Biodegradation rate is influenced by water temperature and can be represented by an Arrhenius function:

$$k_b = k_{b20}\theta^{(T-20)} \tag{4.4.12}$$

where k_b = biodegradation rate, k_{b20} = biodegradation rate at 20 °C, T = water temperature in °C, and θ = temperature correction factor. The effect of the Arrhenius function is that a higher temperature will cause a faster chemical reaction rate. It gives a quantitative relationship between the reaction rate and its temperature.

Biodegradation rate is also related to the contaminant concentration and can be expressed by a typical Michaelis–Menton formulation:

$$k_b = k_{b\max}\frac{c}{c + c_{1/2}} \tag{4.4.13}$$

where $k_{b\max}$ = the maximum biodegradation rate, c = the contaminant concentration, and $c_{1/2}$ = half saturation (Michaelis) constant.

The combination of the above two formulations yields

$$k_b = k_{\max}\theta^{(T-20)}\frac{c}{c + c_{1/2}} \tag{4.4.14}$$

where $k_{\max}$ = maximum decay rate due to biodegradation. Equation (4.4.14) combines the effects of contaminant concentration and water temperature on the biodegradation process. As will be discussed in Section 5.1.5, the Arrhenius function and the Michaelis–Menton formulation are commonly used in water quality models.

4.4.2.5 Volatilization. Volatilization represents a chemical substance entering the atmosphere by evaporation from water. Volatilization is often treated as an irreversible decay process, because of its mathematical similarities to these decay processes. However, volatilization is actually a reversible transfer, in which the dissolved concentration in water attempts to equilibrate with the gas phase concentration in the overlying atmosphere. Equilibrium occurs when the partial pressure exerted by the chemical in water equals to the partial pressure of the chemical in the atmosphere.

Henry's law states that, at a given temperature, the solubility of a gas is proportional to the pressure of the gas directly above the water. Volatilization is often treated similarly to surface oxygen exchange, where the volatilization flux is proportional to the difference between the chemical concentration in water and the saturation concentration, as:

$$F_v = k_v(c_w - c_{ws}) \tag{4.4.15}$$

where F_v = volatilization flux, k_v = transfer rate, c_w = dissolved concentration of the chemical in water, and c_{ws} = saturation dissolved concentration of the chemical in water.

Equation (4.4.15) indicates that the chemical enters the water when the chemical in the water is unsaturated ($c_w < c_{ws}$), and the chemical leaves (volatizes from) the water when the chemical in the water is oversaturated ($c_w > c_{ws}$). The saturation dissolved concentration is dependent on the atmospheric partial pressure and Henry's law constant for the chemical. The transfer rate, k_v, depends on the properties of the chemical, as well as the characteristics of the waterbody and the atmosphere, including the molecular diffusion coefficient of the chemical in the water and in the atmosphere, the temperature, the wind speed, the current velocity, and the water depth. The conditions favoring volatilization include high vapor pressure, high diffusivity, and low gas solubility. Empirical correlations are often developed to link transfer rates directly to physical parameters, such as wind velocity, water density, and water viscosity.

For many chemicals (with oxygen as a noticeable exception), the partial pressure in the atmosphere is negligible, and the saturation dissolved concentration (c_{ws}) is much smaller than the dissolved concentration (c_w). In this case, Eq. (4.4.15) reduces to

$$F_v = f_v k_v c_w \tag{4.4.16}$$

where f_v = a correction factor.

4.4.2.6 pH. Water quality models (e.g., Cerco and Cole, 1994; Park et al., 1995) often do not simulate inorganic carbon and the associated variables of pH and alkalinity. Carbon dioxide (and total inorganic carbon) is produced by respiration, consumed by algal growth, and replenished by atmospheric exchange. This inorganic carbonate system can be important for many chemical reactions. The rate of chemical reactions can be significantly altered by changing the pH. The solubility and bioavailability of many chemicals are also dependent on pH. Biological processes, such as reproduction, cannot function in acidic or alkaline waters. Heavy metals become more water soluble under acid conditions. This phenomenon aggravates toxic contamination problems by releasing toxic chemicals stored in sediments. Common sources of acidity include mine drainage, runoff from mine tailings, and atmospheric deposition.

The letters pH stand for "power of hydrogen", and pH is a measure of the concentration of hydrogen ions. It indicates how acidic or basic (alkaline) a waterbody is. The pH value is defined as the exponent to the base 10 of the hydrogen ion concentration:

$$\mathrm{pH} = -\log_{10}[\mathrm{H}^+] \tag{4.4.17}$$

where $[H^+]$ = molar concentration of hydrogen ions.

The pH scale is used to determine the acidic or alkaline nature of water. It ranges from 0 to 14 pH units, with pH 0 being the most acidic, pH 7 being neutral, and pH 14 being the most alkaline (basic). Pure water is neutral with a pH of 7. For each 1.0 change of pH, acidity or alkalinity changes by a factor of 10. For example, a pH of 5 is 10 times more acidic than a pH of 6 and 100 times more acidic than a pH of 7. The lower the pH is, the greater is the acidity of the water. Alkaline waters have a pH factor of >7, with a relatively low concentration of hydrogen ions.

The pH of a waterbody results from the ratio of H^+ to OH^-. In natural waters, this usually is dependent on the carbonic acid equilibrium. When carbon dioxide (CO_2) from the atmosphere enters a waterbody, small amounts of carbonic acid are formed. The hydrogen ion can be produced by carbon dioxide reacting with water:

$$\mathrm{H_2O} + \mathrm{CO_2} \rightarrow \mathrm{H^+} + \mathrm{HCO_3^-} \tag{4.4.18}$$

This reaction increases the hydrogen ion concentration, and therefore lowers the pH. Because CO_2 is in the atmosphere and can also be produced by algal growth in water, CO_2 reacting with water is a common process that affects pH values in an aquatic system. There is an inverse relation between pH and CO_2. When aquatic plants remove CO_2 from the water to form organic matter through photosynthesis, the pH increases.

Dissolved calcium carbonate (limestone) exists commonly in water. When an acid interacts with limestone, the following reaction occurs

$$\mathrm{H^+} + \mathrm{CaCO_3} \rightarrow \mathrm{Ca^{2+}} + \mathrm{HCO_3^-} \tag{4.4.19}$$

Unlike the reaction in Eq. (4.4.18), which decreases pH value, this reaction consumes hydrogen ions, thus increasing the pH value.

Daily variation of pH can be caused by aquatic vegetation growth. In daytime, algal photosynthesis uses carbon dioxide and releases dissolved oxygen. Uptake of CO_2 leads to the decease of hydrogen ions and the increase of pH. At night, photosynthesis stops and algae release CO_2, which leads to the decrease of pH. Light availability decreases with water depth, so does the rate of algal photosynthesis. In a deep lake, large algal photosynthesis in surface water reduces CO_2 concentration, leading to an increase in pH. In deeper water, however, algal respiration is the principal biological process,

resulting in an increase in CO_2 and a decrease in pH. Therefore, pH (CO_2) in the afternoon tends to be higher (lower) in surface water than in deeper water. Highly eutrophic lakes may exhibit a large difference in pH (CO_2) between the surface and the bottom layers.

4.5 CONTAMINANT MODELING

The fate and transport of contaminants are complicated processes that include physical transport and chemical and biological kinetics. Contaminants in a waterbody may be the result of either past or present disposal practices. Shutting off the sources does not always solve the problem (e.g., DDT persists many years). Consequently, it is essential that mathematical models for assessing contaminants are accurate and reliable. In the past decades, significant progress has been made in numerical model development, data collection, and computer software and hardware. These developments have helped mathematical models to become reliable tools for environmental management and engineering applications.

A toxicant is usually composed of two forms: dissolved and particulate. A typical toxic model should include the following:

1. A hydrodynamic and sediment model that provides the transport and settling information.
2. Sorption–desorption interaction between dissolved and particulate toxics.
3. Interactions and exchanges between the sediment bed and the overlying water column.
4. Transport, fate, and decay of the toxics in the water column and the sediment bed.
5. External loadings to the system.

Figure 4.5.1 gives the structure of a typical toxic model (Tetra Tech, 2002; Ji et al., 2002a). The preconditions for a successful simulation of toxics transport are the appropriate description of the hydrodynamics and the sediment transport. The coupling of a well-developed hydrodynamic and sediment transport model with a toxic model is a key component for toxic modeling. First, the hydrodynamic calibration should be reasonable and the flow field must be correctly understood, since the hydrodynamic model provides current, turbulence mixing, and water depth. Second, the cohesive sediment transport should be simulated realistically, since it is often the carrier of the particulate toxicant. Finally, based on these model outputs, the toxic transport model calculates toxic concentrations, including the dissolved and the particulate ones, in the water column and in the sediment bed.

In the event that the sorption–desorption processes are secondary to the contaminant modeling (e.g., coliform die-off), a simple first-order decay model

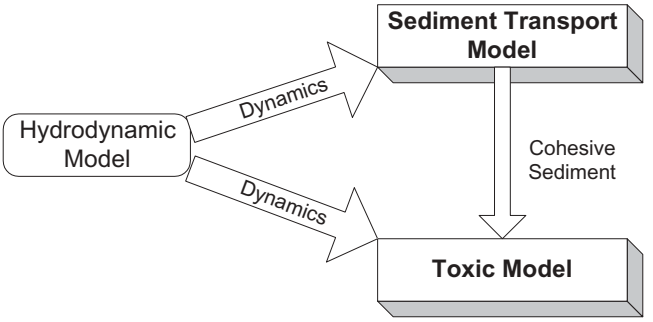

Fig. 4.5.1 Structure of a typical toxic model.

can be used and the sediment transport processes may then be neglected in the modeling.

In addition to the hydrodynamic and sediment parameters, toxic modeling often requires adjustment of the following parameters:

1. Partition coefficient (mostly adjusted in toxic metal and TOC modeling).
2. Decay rate (mostly adjusted in pathogen and TOC modeling).

For different contaminants, such as pathogens, TOCs, or metals, the values of these parameters vary significantly and are often temperature dependent. These parameters should be estimated, whenever possible, based on measured data taken from the site studied, since they are generally site specific and vary dramatically from contaminant to contaminant. In the event that measured data are not available for parameter estimation, values from literature reviews should be used as references. There are many publications on this topic, such as Bowie et al. (1985), Thomann and Mueller (1987), Chapra (1997), and Schooner (1996).

Data used in a toxic model include the following:

1. Concentrations of the contaminants (pathogens, metals, or TOCs) in the water column. For metals and TOCs, the concentrations should be separated into dissolved and particulate phases.
2. Concentrations of the contaminants in the sediment bed.
3. External toxic loadings to the waterbody.

4.5.1 Case Study I: St. Lucie Estuary and Indian River Lagoon

A hydrodynamic, sediment, toxic, and water quality model has been developed in the St. Lucie Estuary and Indian River Lagoon (SLE/IRL), Florida (Ji et al., 2007a, 2007b; Wan et al., 2007). The hydrodynamic modeling of the

SLE/IRL is already introduced in Section 2.4.3 as a case study. The water quality modeling will be discussed in Section 5.9.3 as another case study. This section is focused on the analysis and modeling of copper (Cu) in this area (Ji et al., 2007b).

Heavy metals in the environment are a source of concern because of their toxicity, reactivity, and mobility in water systems. Tetra Tech (1998a, 1999c, 2000a) conducted a series of studies on copper and nickel in the Lower South San Francisco Bay, including source characterization, impairment assessment, and calculation of Total Maximum Daily Loads (TMDLs). Together, these studies were used to assess the impairment of beneficial uses in the South Bay and the need to complete the TMDLs. The conceptual model proposed by Tetra Tech provides a summary of the existing knowledge on the behavior of copper and nickel and factors that control the cycling and toxicity of these metals in the ecosystem.

Previous studies indicate that biotas of the SLE/IRL are stressed by excessive heavy metals and toxic chemicals (Haunert, 1988). Pesticide residues and heavy metals originating in the watershed tend to accumulate in sediments and may become part of the food chain. Haunert (1988) reported that pesticide and heavy metal concentrations, especially the Cu concentration, are highest in muddy sediments found in relatively deep, low-energy benthic environments. Copper is commonly used in agriculture as a trace metal for citrus crops. Copper sulfates are employed to control aquatic weeds in canals and ditches as a fungicide. These agriculture uses of copper may account for the relatively high concentrations of this metal in C-24 (Fig. 2.4.12). Besides, antifouling paints on boat hulls constantly leach copper into the water and are considered the primary source of copper in marine sediment. To understand the fate of heavy metals, a numerical model with the capability of simulating the transport of toxic substances will provide a cost-effective management tool.

4.5.1.1 Analysis of Measured Copper Data. A survey of Cu concentration in SLE was conducted in 1982 (Haunert, 1988). The observations are shown in Fig. 4.5.2. The Cu concentration has units of microgram per gram (μg/g), that is, (μg Cu)/(g sediment). Figure 4.5.2 shows that in 1982, Cu deposition occurred in the North Fork, in the South Fork, and in the middle of the estuary. In the area near the entrance of the estuary, the Cu concentration in the sediment bed is relatively small, presumably due to high flushing in this area (Ji et al., 2007a).

Another set of Cu data was provided by Hameedi and Johnson (2005). This NOAA data set (Fig. 4.5.3) includes Cu concentrations in the sediment bed in 2002, 20 years after the Haunert data. By comparing Fig. 4.5.2 with Fig. 4.5.3, it is readily seen that the Cu concentration has increased by 100–200% in the North Fork during these 20 years. In the South Fork, the Cu concentration has increased by ~100%. In the middle of the estuary, the Cu concentration is slightly increased from 1982 to 2002. In the area near the entrance to the estuary, the Cu concentration is more or less the same.

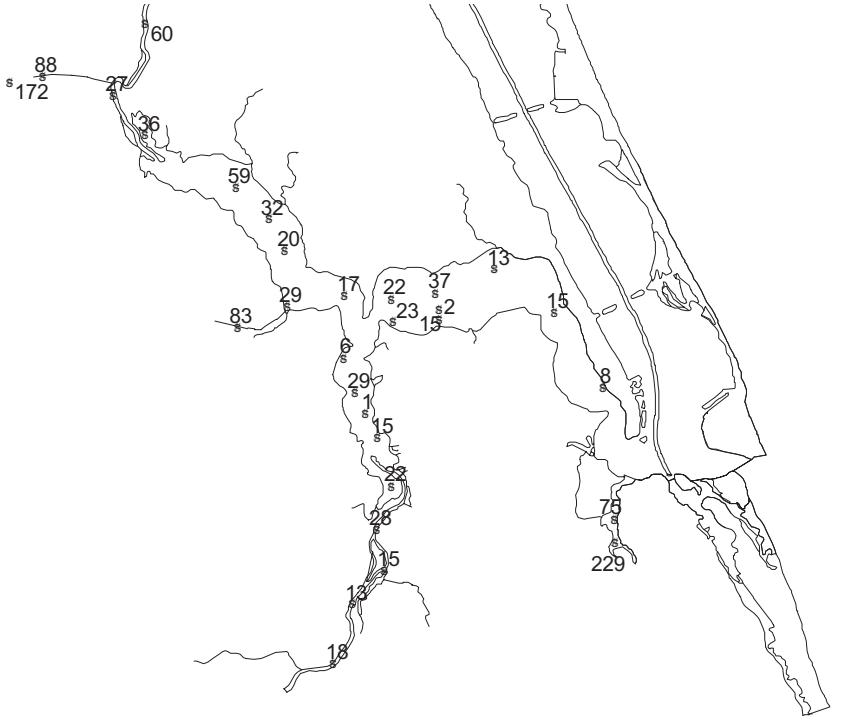

Fig. 4.5.2 Observed Cu concentration (in μg/g) in the sediment bed in 1982.

In addition to external loading conditions, this pattern of Cu deposition should be closely linked to the flushing characteristics in the estuary (Ji et al., 2007a and Section 10.3.4). The North Fork has relatively weak flushing, and therefore has the highest deposition rate. The South Fork frequently receives a large amount of freshwater from Lake Okeechobee, which reduces the Cu deposition in the South Fork and in the middle of the estuary. This might explain why Cu deposition is less in these two areas compared with the North Fork area. High flushing at the entrance of the estuary limits the Cu deposition and leads to Cu concentration almost unchanged in the area in the 20 years.

Figure 4.5.4 gives the measured Cu concentration data in the water column in 2002 (Kelly, 2005). Figure 4.5.4 indicates that Cu concentrations are generally higher in the North Fork and the South Fork than in the middle of the estuary and the entrance area. The large fluctuations in Cu concentration indicate that the external loadings and the internal cycling processes should have large time variations. The large values in Cu concentration are most likely associated with Cu resuspension from the sediment bed, which occurs when a large amount of freshwater is discharged into the SLE. The high Cu values of 99 and 69.3 μg/L were measured in the North Fork area, consistent with the

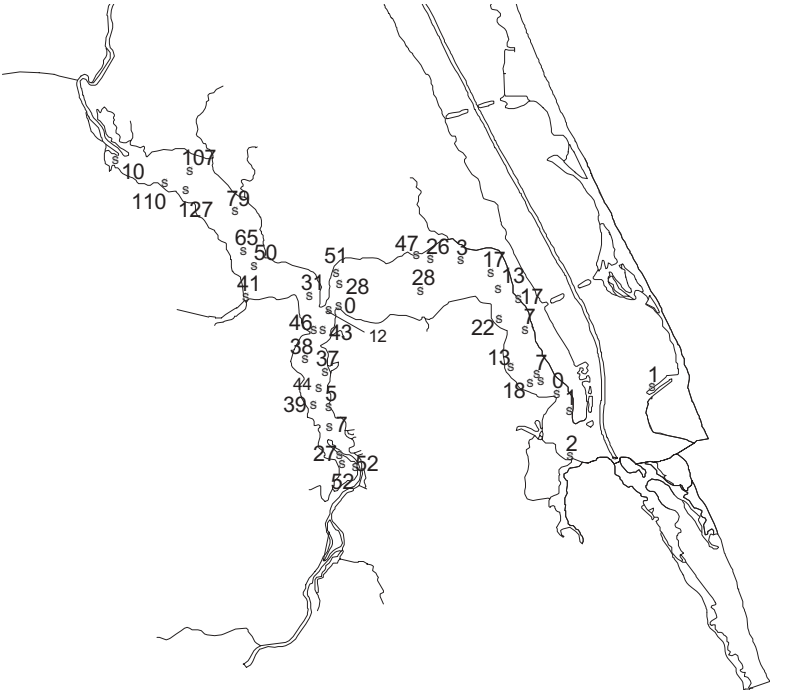

Fig. 4.5.3 Observed Cu concentration (in μg/g) in the sediment bed in 2002.

Cu distribution patterns shown in Fig. 4.5.3, in which the Cu concentration in the sediment bed also has large values in the North Fork.

4.5.1.2 Sediment and Copper Modeling Results. In this study, the EFDC (Hamrick, 1992) is selected as the framework for the development of the SLE/IRL heavy metal model. A 3D hydrodynamic model of the SLE/IRL is calibrated and verified using data in the following two periods (Ji et al., 2007a and Section 2.4.3):

1. *Calibration*: using the data in 1999.
2. *Verification*: using the data in 2000.

The grid of the sediment and metal model contains 1161 horizontal grid cells and three vertical layers, which is the same as the hydrodynamic model grid (Fig. 2.4.12). Sensitivity tests with a six-layer model indicate that the three-layer model is adequate to represent the vertical structure of the study area most of the time (Ji et al., 2007a). The SLE/IRL copper model consists of four interrelated model components: (1) copper sources to the SLE/IRL; (2) hydrodynamic transport; (3) sediment transport, deposition, and resuspension; and (4) copper cycling in the water column and sediment bed.

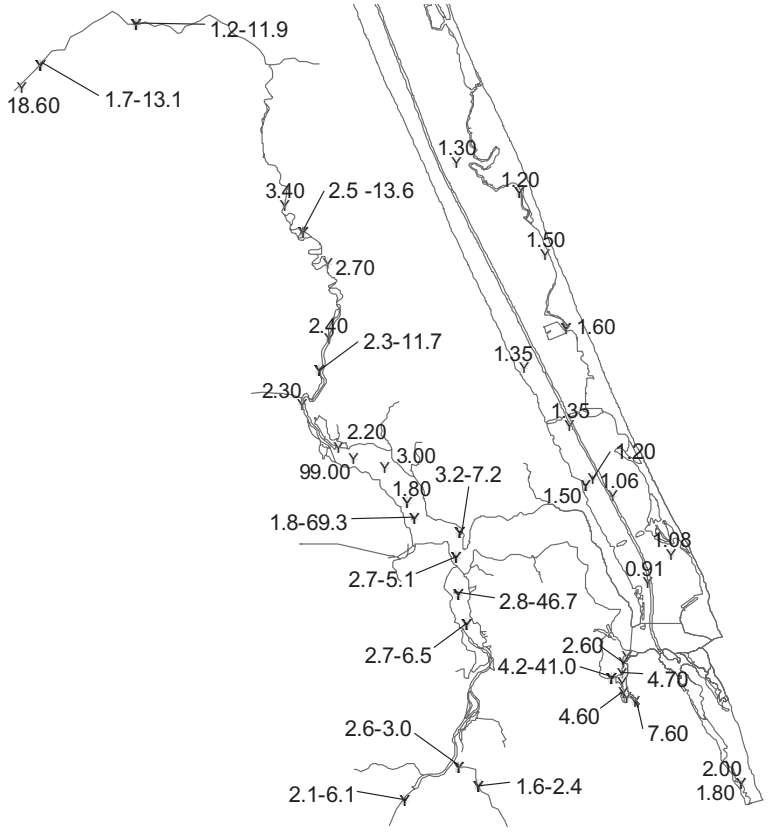

Fig. 4.5.4 Measured Cu concentrations (in μg/L) in the water column in 2002.

To set up the sediment model, a sediment layer with thickness of 6 cm was set at the bottom as the initial condition. The porosity was assumed to be 0.5. Since the initial condition is not well defined due to the lack of measured data, the model was spun up for a year to reach dynamic equilibrium. The sediment model was calibrated based on the 1999 flow condition. The loading was estimated based on the sediment data collected in the past. The comparisons of model results and observations at SE01 in 1999 are shown in Fig. 4.5.5. The location of SE01 is shown in Fig. 2.4.12. In general, the model captured the major features and variability of the TSS reasonably well. Table 4.5.1 presents the statistical error analysis for TSS in the SLE. In Table 4.5.1, the absolute error varies from 5.98 mg/L at SE05 to 8.12 mg/L at SE04. The RMS error varies from 7.11 mg/L at SE06 to 14.67 mg/L at SE03. The RRE varies from 16.92% at SE04 to 66.62% at SE02. The MRRE is defined as the mean value of the last column in Table 4.5.1 and is used as an indicator of the overall model performance. From Table 4.5.1, the MRRE is 44.48% in 1999. The sediment

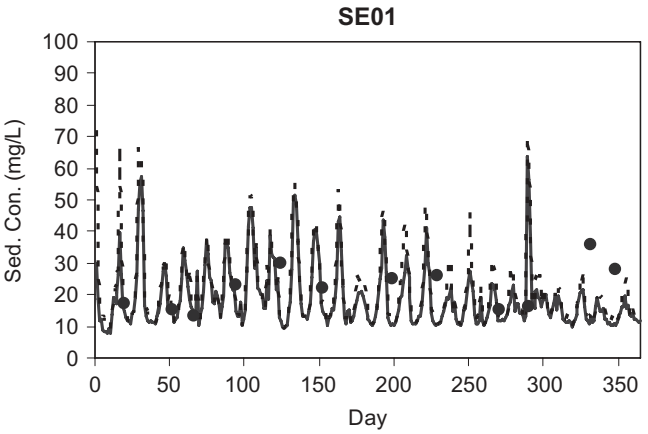

Fig. 4.5.5 Comparison of suspended sediment concentrations in 1999. The dashed line is for the middle layer and the solid line is for the surface layer. The dots are the measured data.

TABLE 4.5.1 Statistical Analysis of Observed and Modeled Suspended Sediment Concentrations in 1999

Station	Number of Data	Obs. Mean (mg/L)	Modeled Mean (mg/L)	Mean Abs. Error (mg/L)	RMS Error (mg/L)	Obs. Change (mg/L)	Relative RMS Error (%)
SE01	12	22.17	21.16	7.96	12.76	23.00	55.47
SE02	13	15.31	19.72	6.54	11.99	18.00	66.62
SE03	14	16.07	18.00	7.98	14.67	40.00	36.66
SE04	12	20.08	19.16	8.12	13.03	77.00	16.92
SE05	14	11.36	15.40	5.98	8.68	18.00	48.20
SE06	12	8.12	12.62	6.17	7.11	17.50	40.65
SE07	10	9.10	13.66	7.20	7.67	33.50	22.89
SE08	14	12.07	17.35	6.03	9.51	15.00	63.40
SE09	12	9.46	15.90	7.02	11.42	21.50	53.10
SE10	13	9.85	16.07	7.96	10.44	25.50	40.92

model is verified using the sediment data in 2000. Table 4.5.2 presents the statistical analysis for TSS. The MRRE is 32.88% in 2000.

One of the key model parameters is the partition coefficient. Based on the Indian River Lagoon data reported by Trefry et al. (1983), the partition coefficient is estimated using the ratio of particulate and dissolved Cu concentrations. The estimated partition coefficient is 0.036 L/mg. The measured Cu concentrations in 1982 (Fig. 4.5.2) were interpolated to the model grid cells as the initial condition in the sediment bed. Figure 4.5.6 gives the differences of Cu concentrations (μg/g) in the sediment bed between the end of 1999 and

TABLE 4.5.2 Statistical Analysis of Observed and Modeled Suspended Sediment Concentrations in 2000

Station	Number of Data	Obs. Mean (mg/L)	Modeled Mean (mg/L)	Mean Abs. Error (mg/L)	RMS Error (mg/L)	Obs. Change (mg/L)	Relative RMS Error (%)
SE01	13	14.98	17.12	6.97	8.34	35.2	23.69
SE02	13	17.56	17.64	11.09	12.76	38.4	33.23
SE03	12	16.31	17.13	8.12	10.82	37.4	28.92
SE04	13	11.45	16.81	10.25	11.58	34.0	34.06
SE05	13	10.76	16.73	8.04	9.45	20.0	47.26
SE06	10	10.80	12.11	4.01	5.16	13.5	38.25
SE07	13	8.80	13.41	6.30	7.35	16.0	45.92
SE08	10	24.25	17.95	8.94	10.95	41.2	26.58
SE09	10	15.93	15.12	4.74	7.96	36.5	21.82
SE10	13	31.34	16.72	21.49	43.85	150.8	29.08

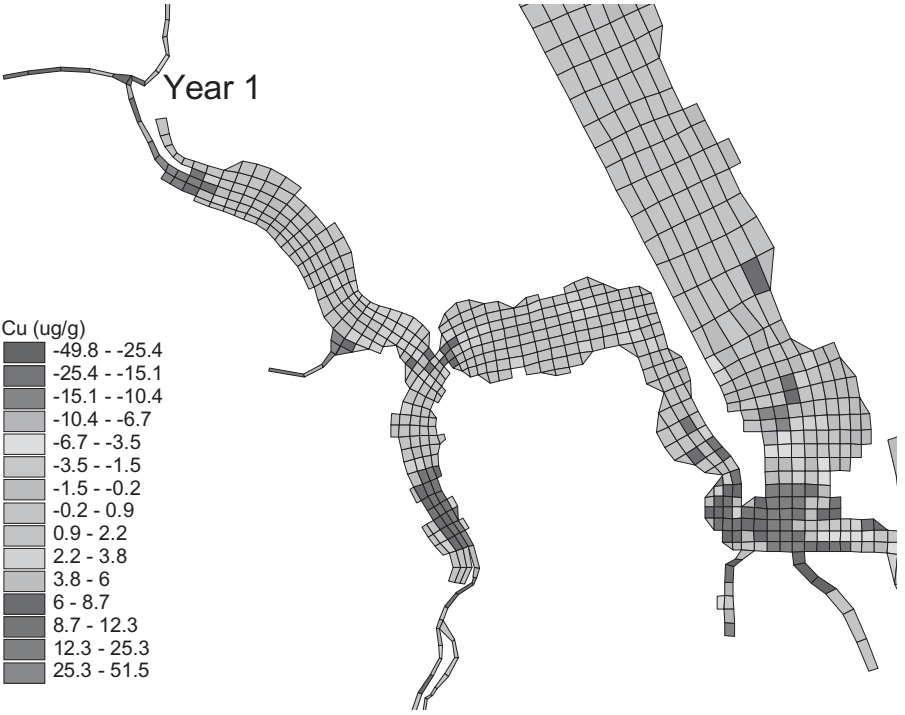

Fig. 4.5.6 Differences of Cu concentration (μg/g) in the sediment bed between Year 1 (1999) and the initial condition.

the initial condition. Because of large inflows from Lake Okeechobee, a large amount of sediment (and the associated Cu) was discharged into the SLE. This caused Cu deposition and Cu concentration to increase in the South Fork. The Cu concentration in the South Fork increased up to 20 μg/g. Cooper concentrations also increased in the North Fork, in the middle of the estuary, and in the entrance area (Fig. 4.5.6). Similar Cu deposition patterns were also observed in 2000. Remember, however, that Fig. 4.5.6 presents the general annual trend, which should have larger variations than the long-term trend with a time scale of decades. Figures 4.5.2 and 4.5.3 give the long-term variation of Cu in 20 years, whereas Fig. 4.5.6 depicts the annual Cu variation in 1999.

Figures 4.5.7 and 4.5.8 give the temporal variations of the modeled Cu concentration in the water column in 1999 at SE01 and SE02, respectively. The dashed (solid) line is for the middle (surface) layer Cu concentration. The results are daily averaged and the M_2 tidal signal is removed. The modeled results in Figs. 4.5.7 and 4.5.8 are in the same range of the measured data shown in Fig. 4.5.4. Also, Fig. 4.5.7 indicates a large spring-neap variation of 15 days or so. In the SE01 area (Fig. 2.4.12), tides are a major driving force in Cu transport, deposition, and resuspension. Since SE01 is near the estuary entrance, variations in tidal amplitude and phase greatly affect Cu concentration in the water column. Figure 4.5.8, however, exhibits much weaker spring-neap tidal signals. The inflows play a more dominant role. For example, ~Day 289, the large increase in Cu concentration is primarily caused by the large inflow during that period.

Figures 4.5.7 and 4.5.8 show that the Cu concentrations can have vertical stratification. For example, in Fig. 4.5.7 ~Day 260, the model results clearly indicate that the Cu concentrations are vertically stratified. From time to time, the middle layer Cu concentration can also be higher than the surface layer

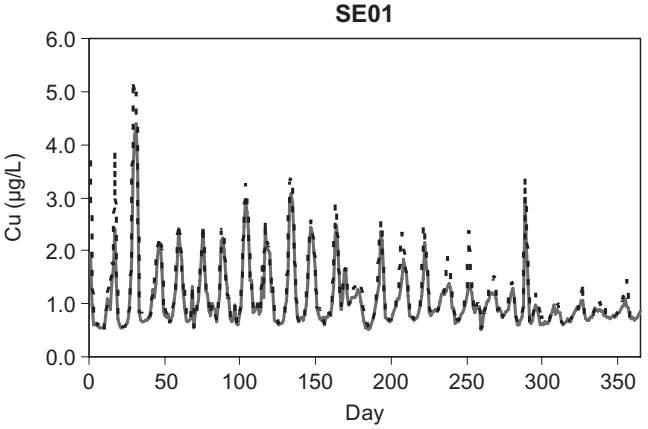

Fig. 4.5.7 Modeled Cu concentration (μg/g) at SE01 in 1999. Dashed line = middle layer, solid line = surface layer.

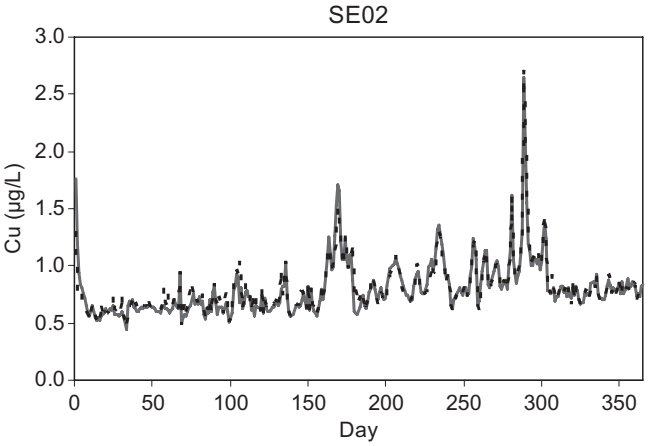

Fig. 4.5.8 Modeled Cu concentration (µg/g) in 1999. Dashed line = middle layer, solid line = surface layer.

Cu concentration, say ~Day 170 in Fig. 4.5.8. This phenomenon is primarily caused by two factors: large external Cu loading and strong vertical stratification. When a large amount of freshwater is discharged into the SLE, it causes salinity stratification and brings a large amount of Cu into the SLE. As the result of the estuarine circulation (Ji et al., 2007a), the fresher water with higher Cu concentration stays on the surface, while the more saline water with lower Cu concentration stays at the bottom. This is the reason that, in Fig. 4.5.8, the middle layer Cu concentration can be lower than the surface Cu concentration from time to time. This also demonstrates the importance of using a 3D model to simulate this shallow estuarine system.

4.5.1.3 Summary and Discussions. Data analysis and 3D numerical modeling were conducted to investigate the sediment and copper processes in the St. Lucie Estuary. Data collected from the estuarine sediment bed in 1982 and 2002 are used to characterize the Cu deposition patterns in the SLE during these 20 years.

Despite the progress in metal studies in the past decades, there are few published papers on the modeling of metal processes in estuaries using 3D coupled hydrodynamic, sediment, and metal models. Based on the 3D hydrodynamic and water quality model of the SLE/IRL (Ji et al., 2007a; Wan et al., 2007), this study presents the 3D modeling of sediment and copper processes in the estuary. The developed model is applied to simulate Cu in the estuary. The modeling results are qualitatively consistent with the measured Cu data.

The uncertainty in the model results can be attributed to several factors, including parameter errors, loading errors, and missing external sources. A series of test runs were also conducted to investigate the model's sensitivity. It was found that external loadings and partition coefficients are two key

factors controlling Cu concentration in the system. For sediment model calibration, it is crucial to have measured data with adequate temporal resolution, so that the dynamic behaviors of sediment resuspension, deposition, and transport can be reasonably represented. The SLE/IRL area is influenced by semidiurnal tidal processes. The sediment data available to this study have time intervals of 2 weeks or longer, which is less than satisfactory for sediment model calibration purposes. Sediment data at hourly time intervals are necessary for fully calibrating the sediment model.

The following processes are important to the study of Cu related processes in the SLE/IRL and should be the focus of future studies: (1) sediment deposition and resuspension; (2) copper sorption, desorption, and internal cycling; (3) measured sediment and Cu data in water column and sediment bed; (4) point and nonpoint sources, and (5) Cu speciation and pH. It is expected that after the copper model is calibrated and verified with measured data, the model will be useful for examining copper processes in the area.

4.5.2 Case Study II: Rockford Lake

This case study originated from a project for the State of Nebraska (Tetra Tech, 1999d). The focus of this study is pathogens in Rockford Lake, Nebraska. Most case studies in this book are on modeling complex water systems and with comprehensive data sets for model setup and calibration. This case study, however, is on a small and simple waterbody and with very limited data for model setup and calibration.

4.5.2.1 Background. The Rockford Lake watershed is located in the State of Nebraska (Fig. 4.5.9). Land use within the watershed consists primarily of agriculture and rangeland. Rockford Lake is located in the west of the watershed and was formed to control floods and to create a multipurpose recreational area when an earthen dam was built in 1968. Table 4.5.3 summarizes the characteristics of Rockford Lake. The lake surface extends >0.6 km^2. The lake's overall storage volume at normal pool is 2.2×10^6 m^3. It drains a watershed of ~34.8 km^2. Its maximum depth is 10.4 m and its mean depth is 3.7 m. Like many reservoirs, the mean depth of Rockford Lake is approximately one-third the maximum depth, which indicates that the reservoir has relatively conical or V-sloped sides.

Rockford Lake's drainage area to surface area (DA/SA) ratio is ~58:1, warranting the assumption that watershed pollutant loads could significantly affect reservoir water quality. A DA/SA ratio of <10:1 implies that shoreline and nearshore activities are likely to dominate reservoir water quality. A DA/SA ratio >50:1 implies that activities in the watershed are likely to dominate reservoir water quality. Aspect ratio (the ratio of lake length to lake width) indicates how important longitudinal versus lateral gradients might be in a waterbody. An aspect ratio >4.0 implies that longitudinal gradients are more important than lateral gradients in water quality. Rockford Lake's aspect

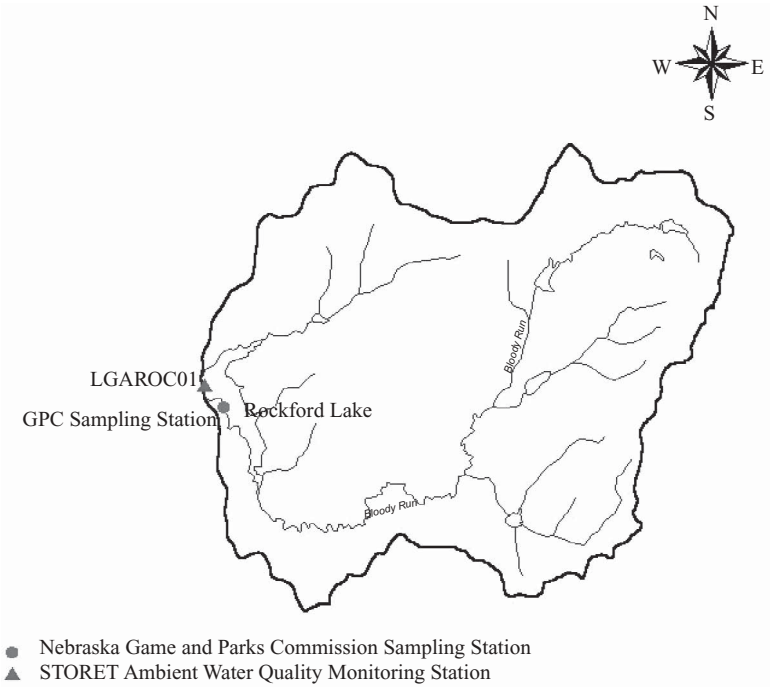

Fig. 4.5.9 Rockford Lake and its watershed.

TABLE 4.5.3 Characteristics of Rockford Lake

Physical Characteristic	Value
Surface area	0.6 km^2
Watershed area (drainage area)	34.8 km^2
Length	1.90 km
Mean width	0.31 km
Maximum depth	10.4 m
Mean depth	3.7 m
Volume	2.2×10^6 m^3
Mean depth/maximum depth	0.36 m
Drainage area/surface area	58 km^2
Aspect ratio (length/width)	6.13

ratio is 6.13. Thus, the longitudinal gradients should be considered in the analysis of the system.

The Nebraska Department of Environmental Quality (NDEQ) has listed Rockford Lake as not meeting applicable Nebraska standards for pathogens in waters used for primary contact recreation. Pathogens are of utmost concern in waters designated for primary contact recreation. Direct contacts with con-

taminated waters, via activities, such as swimming and water skiing, put human health at risk. Fecal coliform concentrations are the commonly used indicator of potential pathogen contamination, because fecal coliform bacteria are common and relatively easy to detect.

Water quality standards are the cornerstone of water quality management programs. Water quality standards define a use for a waterbody and describe the specific water quality criteria to achieve that use. Because of the difficulties in analyzing for and detecting the many possible pathogens organisms, concentrations of fecal bacteria, including fecal coliforms, enterococci, and *E. coli*, are used as primary indicators of pathogenic contamination. Nebraska's water quality standards state the following criteria for measurements of fecal coliform in surface water (NDEQ, 1996):

Bacterial Criteria to Protect Primary Contact Use of Surface Water

Bacteria of the fecal coliform group shall not exceed a geometric mean of 200/100 mL, nor equal or exceed 400/100 mL, in >10% of the samples. These criteria are based on a minimum of five samples taken within a 30-day period. This does not preclude fecal coliform limitations based on effluent guidelines.

The NDEQ classifies a waterbody as impaired if its fecal coliform criteria are exceeded during the high recreation period, from May 1 through September 30, and the waterbody is designated to be used for primary contact recreation. Rockford Lake is a recreational reservoir. Water quality measurements show its waters have exceeded these criteria.

4.5.2.2 Data Sources and Model Setup. Fecal coliform bacteria have not been monitored frequently in the Rockford Lake watershed. The primary sources of available water quality information for the Rockford Lake are

1. Fecal coliform bacteria samples collected by the Nebraska Game and Parks Commission (GPC).
2. Ambient water quality monitoring data retrieved from STORET (USEPA, 2004).

Fecal Coliform Bacteria Samples Collected by GPC. From 1986 through 1988 and 1991 through 1997, the GPC conducted sampling in Rockford Lake to assess whether the lake was supporting its primary contact recreation beneficial use. From one to five samples were collected during the designated recreation months (May–September). A total of 102 samples were collected from 1986 through 1988 and 1991 through 1997. Location of the GPC sampling station is shown in Fig. 4.5.9.

Ambient Water Quality Monitoring Data Retrieved from STORET. The STORET database was queried to obtain water quality data for fecal coliform in the Rockford Lake watershed. This database contains data collected by NDEQ, the United States Geological Survey (USGS), the USACE, and the EPA. Only one station (USEPA LGAROC01) was found inside the watershed with limited data for fecal coliform from 1990 to 1992. Location of the LGAROC01 station is also shown in Fig. 4.5.9.

To simulate the critical conditions associated with fecal coliform in Rockford Lake, a linked model regime was developed. The model consisted of a comprehensive watershed model linked to a 3D lake hydrodynamic and water quality model. The model of the Rockford Lake watershed was developed based on the HSPF model (USEPA, 1996c). The watershed model provides all flow and pollutant loads entering the lake. Four inflows to the lake represented the watershed contributions and were in the form of daily average flows and daily total fecal coliform loads.

The EFDC model (Hamrick, 1992) was used to simulate fecal coliform transport in Rockford Lake. Appendix A of this book gives a brief description of the EFDC model. Since the focus of this study is the fate and transport of fecal coliform, the interactions between fecal coliform and sediment are considered secondary in the lake, and the sediment processes in the lake are not modeled. Instead, the first-order decay process is applied to describe the die-off of fecal coliform. The setup of the EFDC required evaluation of the lake's physical and chemical characteristics, including bathymetry, inflow, outflow, and water quality variables. The EFDC model configuration involved the construction of a horizontal grid for Rockford Lake and development of EFDC input files.

As part of the lake model development, the study area was divided into a grid of discrete cells (Fig. 4.5.10). The grid cells in Fig. 4.5.10 represent the computational (I, J) grid and are not drawn to the physical scale. The cells in the narrow incoming streams were represented with one cell across the stream. Multiple cells were used to obtain adequate resolution in the lake. Cell widths were adjusted according to the incoming river and lake widths. The numerical grid consists of 65 cells in the horizontal plane and one vertical layer. A single vertical layer was used because the lake is shallow, with a mean depth of 3.7 m. A typical grid cell has a uniform length of 80 m in the x direction and 120 m in the y direction. The grid was designed to resolve velocity shears and at the same time allow a time step suitable for efficient computation. Solutions to the hydrodynamics were obtained using a 96-s time step. In modeling studies, such as the ones illustrated in this book, grid maps similar to Fig. 4.5.10 are helpful for modelers to setup the model, to debug, and to analyze model outputs.

Figure 4.5.11 summarizes the pathogen modeling procedure. The first component in the procedure is characterizing the point and nonpoint sources of pathogens from the watershed and establishing the loading rates to the lake,

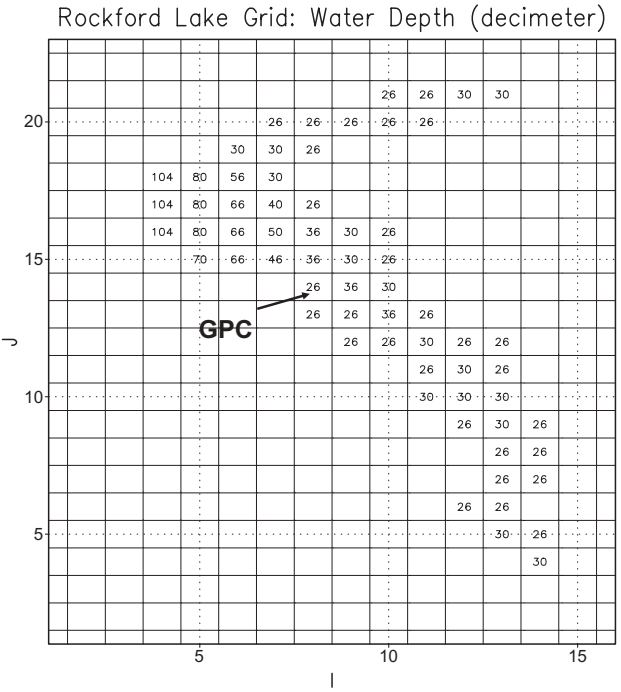

Fig. 4.5.10 Computational grid (I, J) and typical water depths (in decimeter) in Rockford Lake.

which is accomplished using the HSPF model. The second component is calculating the fate and transport processes and estimating the pathogen distribution in the lake, which is achieved using the EFDC model. The third component is interpreting the model output to find whether the pathogen concentrations are in violation of the water quality standards and to develop the pathogen TMDL accordingly. The TMDL development is described by Tetra Tech (1999d) and will not be presented here.

4.5.2.3 Model Results. For bacteria analysis and modeling, model results of the same order of magnitude as data are often considered accurate enough (USEPA, 1990). The EPA compiled bacteria decay rates from studies involving salty and freshwaters (USEPA, 1990). They can be used as a guideline to select initial rates for a particular study. Generally, the decay rates for coliforms are on the order of 1/day, but can be as high as 48/day for marine outfalls. After selecting an initial value for the decay rate, adjustment should be made to fit the prediction results to actual measurement by trial and error.

As shown in Fig. 4.5.9, there are four inflows to the lake from creeks in the watershed. Output from the HSPF model was used to represent the flow rates

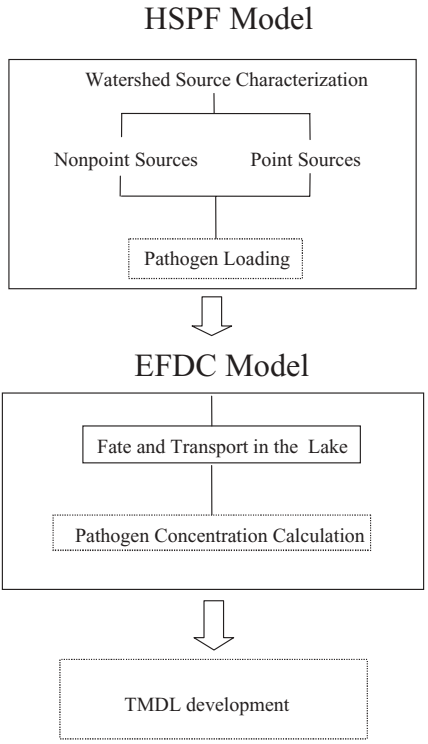

Fig. 4.5.11 Components of pathogen modeling in Rockford Lake.

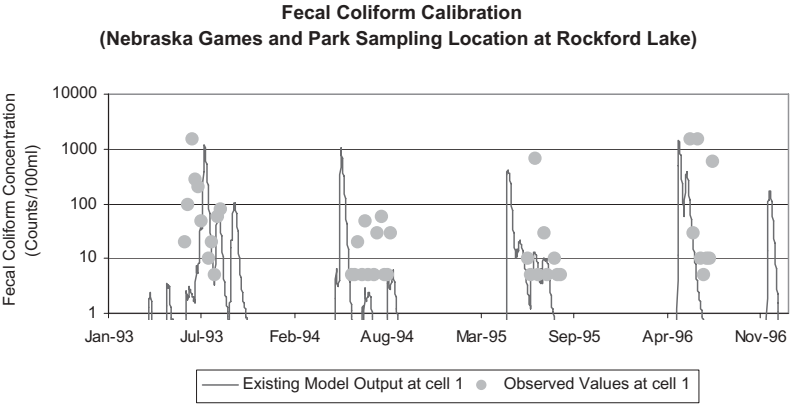

Fig. 4.5.12 Modeled and observed fecal coliform concentration at GPC sampling location in Rockford Lake.

from these creeks. Because hydrodynamic data were not available for model calibration, default parameters were used in the EFDC model. These default parameters had been previously tested and widely used in other EFDC studies. The mass balance (inflows to and outflows from the lake) was verified over the 4-year simulation period (1993–1996) to assure appropriate simulation. The 4-year mean inflow to the lake was ~0.2 m^3/s with a residence time of 128 days.

Based on the availability of fecal coliform data in the lake, the period from 1993 to 1996 was selected as the calibration period. The model calibration was performed by comparing the fecal coliform results of the EFDC model with the measured fecal coliform data at the GPC sampling station. The main model parameter adjusted was the fecal coliform decay rate. It was tuned to 0.4 day^{-1}, which is within the acceptable range (Bowie et al., 1985). Figure 4.5.12 presents both the model and observed data on a logarithmic scale. The solid line represents the modeled daily fecal coliform concentration. The dots represent the observations. As shown in Fig. 4.5.12, the model is able to simulate the fecal coliform conditions in the lake reasonably well. Both the observed data and the model show that high fecal coliform concentrations typically occur during the summer months.

Note, however, that the results presented are just preliminary ones. The lack of measured data, including both hydrodynamic data and pathogen data, hindered further verification of the Rockford Lake model.

CHAPTER 5

Water Quality and Eutrophication

Water quality represents the physical, chemical, and biological characteristics of water and measures the ability of a waterbody to support beneficial use to society. Eutrophication is a process of nutrient overenrichment of a waterbody, resulting in accelerated biological productivity (growth of algae and weeds). Symptoms of eutrophication include algal blooms, reduced water clarity, and oxygen depletion. In modeling studies, water quality and eutrophication are sometimes used interchangeably to represent the processes of waterbody enrichment with nutrients.

Hydrodynamic processes control the transport of algae, nutrients, and DO in a waterbody. Nutrients, such as phosphorus, can attach to sediments in water systems. The sorption and desorption of phosphorus to sediments affect the phosphorus transport and uptake processes. Accurate descriptions of hydrodynamic processes (Chapter 2) and sediment processes (Chapter 3) are essential to the modeling of water quality processes. The sorption/desorption and the fate processes described in Chapter 4 are also important to the understanding of nutrient cycles and eutrophication in aquatic systems.

This chapter covers the water quality and eutrophication processes and their mathematical modeling by focusing on algae, nutrients, DO, sediment diagenesis processes, and submerged aquatic vegetation. Since these processes are closely linked to each other, it is impossible to discuss one without mentioning the others (Ji, 2005a, 2005b). Section 5.1 gives a general overview of water quality processes and the basic concepts. It serves as a prelude to detailed discussions about eutrophication processes in the following sections. Section 5.2 describes algae and related topics; Section 5.3 is focused on organic carbon; Section 5.4 presents nitrogen processes; Section 5.5 illustrates phosphorus processes; Section 5.6 discusses DO; Section 5.7 is devoted to the sediment diagenesis processes in the sediment bed; Section 5.8 describes submerged aquatic vegetation; and Section 5.9, the last section of this chapter, demonstrates the modeling of water quality processes in surface waters.

Hydrodynamics and Water Quality: Modeling Rivers, Lakes, and Estuaries, by Zhen-Gang Ji

5.1 OVERVIEW

Algae, nutrients, and DO are closely linked to each other. Water quality in a waterbody responds to the watershed, the regional climate, as well as the geometry and internal characteristics and processes of the system. Meteorological forces, internal processes, inflows, and outflows are highly dynamic and can be dominant factors in determining the water quality. One fundamental challenge to prevent (or to reduce) eutrophication is to understand this complex chain of events and impacts. Before they are presented in detail in the later sections of this chapter, basic concepts of algae, nutrients, and DO are introduced in this section. The governing equations for water quality modeling are also presented here, along with empirical formulas that are often used to parameterize water quality processes.

5.1.1 Eutrophication

Eutrophication (from the Greek—meaning "well nourished") is a natural process, but human activities can accelerate the process by increasing nutrient loadings into a waterbody. Natural eutrophication is a process that is measured in terms of thousands of years, whereas the culture eutrophication due to human activities is the result that takes only a few decades (or even years) to develop. This book focuses on the culture eutrophication (or simply called eutrophication). Eutrophication is one of the leading environmental problems, which leads to excessive plant growth: algae in the open water, periphyton (attached benthic algae) on the bottom of the waterbody, and macrophytes (large vascular rooted plants that are often called weeds) in shallow water areas.

Based on its biological productivity and nutrient conditions, a waterbody can generally be categorized as oligotrophic, mesotrophic, and eutrophic:

1. "Oligotrophic" describes a waterbody with low biological activity and excellent water quality, since the water is low in nutrients and algae and both primary production and biomass are severely limited.
2. "Mesotrophic" describes a waterbody with medium biological activity and good water quality.
3. "Eutrophic" describes a waterbody with excessive biological activity and poor water quality. The water has abundant nutrients and high rates of primary production, frequently resulting in oxygen depletion in the bottom layer.

As shown in Fig. 5.1.1, a system low in nutrients is described as oligotrophic. An oligotrophic lake is poorly supplied with nutrients and supports little plant growth. As a result, biological activity is generally low, the water is clear, and the water column is often well supplied with oxygen throughout the year. As

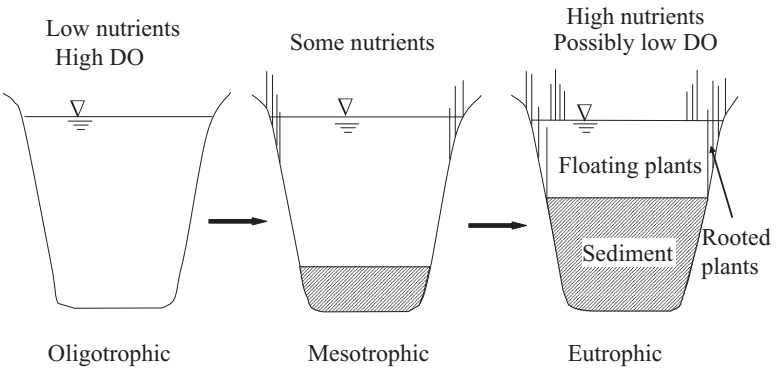

Fig. 5.1.1 The eutrophication process: the progression from oligotrophic through mesotrophic to eutrophic.

the nutrient supply increases, the system is successively described as mesotrophic and eutrophic. Small increases in nutrient supply can result in an increase in production without serious damaging to the ecosystem, but further increases in nutrient loads result in more serious impacts on water and sediment quality. A mesotrophic lake is moderately supplied with plant nutrients and has moderate plant growth. As it becomes eutrophic, the lake is richly supplied with plant nutrients and has heavy plant growth. As a result, the biological productivity is generally high, and the water is turbid because of the dense growth of phytoplankton. The deepest waters often exhibit reduced DO concentrations. The bottom of the eutrophic lake often has a thick sediment layer laden with organic matters.

The trophic state of a waterbody is largely controlled by nutrient loadings from point and nonpoint sources, climatologic conditions (e.g., sunlight, air temperature, precipitation, and water inflow rates), and the shape of the waterbody (e.g., depth, volume, and surface area). Because of variations in geographical and climatological conditions, there are no numeric criteria that are universally applicable to quantifying the trophic states of rivers, lakes, and estuaries.

Different areas may have different nutrient background and atmospheric precipitation. The variables used mostly for representing trophic states are total phosphorus (TP), total nitrogen (TN), chlorophyll, and Secchi depth (or another turbidity parameter). Since eutrophication is largely caused by either too much N or P or some combination of the two, TN and TP are often described as causal variables. Chlorophyll and Secchi depth are initial response variables. Other variables, such as DO, are also useful in representing the eutrophication status of a waterbody.

Nutrient sources include point and nonpoint sources, such as sewage discharges, industrial wastewaters, agricultural runoff, and urban runoff. When eutrophication occurs, the waterbody becomes overwhelmed by excessive

nutrients, such as nitrogen and/or phosphorus. The excessive nutrients produce more phytoplankton/vegetation than can be consumed by the waterbody. This overproduction can lead to a variety of problems, including (1) low DO, especially near the bottom of the waterbody; (2) high suspended solids, often enriched with organic material; (3) high nutrient concentrations; (4) high algal concentrations; (5) low light penetration and low water clarity; (6) odors from algae or anaerobic muds; and (7) changes in species composition.

Dissolved oxygen is consumed in the decomposition of algae. Nutrient enrichment can lead to blooms of algae that eventually die and decompose. Their decomposition removes oxygen from the water. The DO concentration is usually lowest in summer, when the water temperature is high and the vertical stratification is large. If decomposition rates are high, then DO concentration can decrease to the point of affecting other oxygen-dependent organisms to survive, such as causing fish kills. Photosynthesis and respiration of excessive plant growth, as well as the microbial breakdown of dead plant matter, contribute to wide fluctuations in DO levels. The dense phytoplankton concentrations and their consequences are often perceived as serious water quality degradation, because the impacts can be tangible, such as fish kills and strong odors. Algal blooms prevent light from reaching submerged vegetation that depend on light for photosynthesis. Dramatic changes in the ecosystem can occur when species that die as a result of eutrophication are replaced by species that can tolerate eutrophic conditions.

Eutrophication studies require knowledge of physical, chemical, geological, and biological processes. Factors important to eutrophication processes in a waterbody include

1. Geometry of the waterbody: depth, width, surface area, and volume.
2. Flow velocity and turbulent mixing.
3. Water temperature and solar radiation.
4. Total suspended solids.
5. Algae.
6. Nutrients: phosphorus, nitrogen, and silica.
7. Dissolved oxygen.

The first four factors are discussed in previous chapters. The last three water quality variables, algae, nutrients, and DO (and associated processes), will be discussed in this chapter.

5.1.2 Algae

Algae are a group of aquatic plants that contain chlorophyll and grow by photosynthesis. Most algae have chlorophyll as the primary pigment for carbon fixation. Algae uptake nutrients, including phosphate, ammonium, nitrate, silica, and carbon dioxide, from the water or benthic sediments and release

oxygen to the water. Algae may be free-floating or rooted on the bottom of a waterbody. The majority of free-floating algae are not visible to the naked eye. An overabundance of algae is known as eutrophication.

Plankton, a name derived from the Greek word *planktos* for "wandering", is a group of tiny plants and animals that live in water and are floating passively or swimming weakly. Plankton usually drift in the water and are subject to the action of waves and currents. Plankton include phytoplankton (plants) and zooplankton (animals). Some phytoplankton are able to migrate short distances up and down in water column with changes in sunlight levels from day to night. In water quality modeling studies, phytoplankton are referred to as (free-floating) algae. Phytoplankton are primary producers and form the base of an aquatic ecosystem's food web. Via photosynthesis, they transfer the sun's energy into plant matter and provide nourishment for the next trophic level of organisms. Small aquatic animals eat algae and in turn are eaten by larger animals, which are eaten by larger fish. Thus, energy and nutrients originating from the phytoplankton cascade through the food web. In most cases, phytoplankton are more important than rooted aquatic vegetations in the basic food production of an ecosystem. They are the most biologically active plants in aquatic ecosystems and generally have a greater influence on water quality than other plants.

Phytoplankton exist in numerous forms and live in nearly all kinds of environments. A simulation of an algal bloom at the level of individual species is unlikely to be successful. It is more appropriate to focus on algal groups. From the modeling point of view, algae are often grouped based on algal adaptability to environmental conditions, such as temperature, light, and nutrient conditions. Groups of algae include (1) cyanobacteria (blue-green algae), (2) green algae, and (3) diatoms.

Except for their chlorophyll-based photosynthesis, blue-green algae are actually bacteria. They are very important primary producers in both freshwater and marine systems. When present in large groups or blooms, these algae appear as a blue-green discoloration in the water. Many species of blue-green algae are undesirable. They can grow prolifically in waters, produce chemicals that are harmful to both animals and humans, form scum on the water surface, and may cause a bad odor and taste in drinking water. Blue-green algae are known to cause water problems owing to the release of dissolved organic residuals and are generally considered to be objectionable when they occur in large concentrations. Thus, they generally receive the greatest amount of research and management attention.

Blue-green algae have several characteristics that enable them to dominate and create nuisance or noxious conditions. They are extremely tolerant in environmentally stressed situations. Some blue-green species can float or sink depending on light conditions and nutrient supply, allowing them to control their position in the water column and giving them an advantage over other algae. Positive buoyancy of the blue-green algae can result in mass accumulations at the surface, depending on the conditions of sunlight, wind speed, and

vertical mixing (e.g., Ganf, 1974). Such scum then dramatically reduces light availability to aquatic plants (e.g., SAV) below the surface. Some blue-green algae are capable of fixing nitrogen (N_2) gas, which is derived from the atmosphere and dissolved in the water, as a nitrogen source. This fixing allows them to grow when other algal forms are starved for nitrogen.

Green algae exist in diverse sizes, shapes, and growth forms. They are dependent on vertical mixing in the water column to cycle them through the euphotic zone. Diatoms are a group of phytoplankton species utilizing silica as a structural component of the cell wall. They depend on water turbulence to remain suspended. Diatoms are generally a preferred phytoplankton group to support higher trophic levels.

In natural waters, some species of algae bloom for a period of time and then give way to other species that are more compatible with changed conditions, such as temperature, sunlight, and/or nutrient concentrations. Typically, the first algae to increase in early spring are frequently the diatoms (Fig. 5.1.2), followed by green algae, and then blue-green algae. There may be another algal bloom as the temperature stratification vanishes in fall, before algal concentrations reduce to low levels during winter. Although this general pattern is often observed, it can also have significant variations, depending on the characteristics of a particular waterbody (USEPA, 2000b).

According to Liebig's "Law of Minimum", the shortage of any essential nutrient can limit algal growth. In most waterbodies, however, phosphorus and nitrogen are the most likely limiting nutrients. In order for algae to grow, both nitrogen and phosphorus must be present. In rivers, lakes, and other freshwater systems, phosphorus concentrations are often low and limit algal growth. So, increased nitrogen loadings usually do not lead to large increases in algae. For example, if a lake has an abundant supply of all nutrients except phosphorus, then the algal growth will be controlled by the phosphorus concentration. If phosphorus is added to the water, algal growth will increase. In estuaries and coastal waters, however, phosphorus is usually more abundant and nitrogen may limit algal growth. As nitrogen inputs increase, algal concentration in these systems increases and blooms may occur.

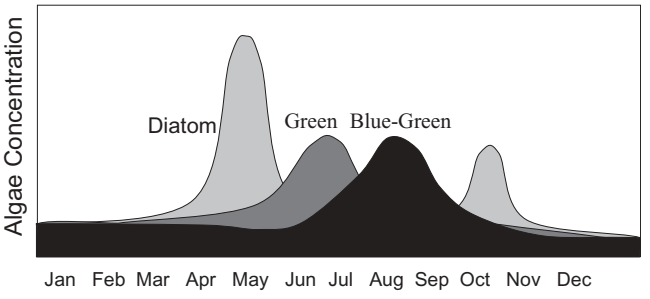

Fig. 5.1.2 Typical seasonal variations of algal concentration.

5.1.3 Nutrients

Nutrients are chemical elements or compounds necessary for the growth of living organisms. Nitrogen, phosphorus, carbon dioxide, and silica are essential nutrients required for algal growth and survival. Silicon is important only for diatoms; it forms the basis for their skeletal structure. In addition to these nutrients, algal growth requires a host of other micronutrients, such as iron, manganese, potassium, sodium, copper, zinc, and molybdenum. However, these minor nutrients are generally not considered in water quality models because they are needed only in trace amounts and they are usually present in quantities sufficient for algal growth.

Although nutrients are essential to algae, excessive nutrient levels can be harmful to ecosystems. Nutrients are considered as pollutants when their excessive concentrations cause eutrophication and overstimulate the growth of aquatic weeds and algae. Nutrients are one of the leading causes of water impairment, along with sediment siltation and pathogens. In addition to causing eutrophication, nutrients can also result in human health problems. For example, nitrate levels of >10 mg/L in drinking water may cause potentially fatal low oxygen levels in the blood when ingested by infants. Nutrient-enriched waters commonly lead to high costs in water treatment to attain acceptable drinking water quality.

Nutrients can exist in different forms:

1. In the water column as dissolved and particulate nutrients.
2. In the sediment bed sorbed to the sediments in particulate form and in the pore water as in dissolved form.
3. In forms contained in algae, fish, and other living organisms.

In most studies, the forms of phosphorus and nitrogen are operationally defined based on available analytical methods. As discussed in Section 3.1.1, the distinction between particulate and dissolved forms depends on the pore size of the filter used to separate the two fractions. Filters with pore size of 0.45 μm are commonly used to separate the particulate and the dissolved.

Understanding the relationship between the forms of nutrients and their bioavailability is important. Nutrients can also be grouped into organic and inorganic. Bioavailable nutrients are in a dissolved form, free of adsorption or other complexity, such that they are readily assimilated (absorbed) by plants. The directly available forms are mainly inorganic, although some algae are able to use organic forms (Darley, 1982). The two nutrients of greatest concern are nitrogen and phosphorus, which have dissolved inorganic forms of ammonium (NH_4), nitrite (NO_2), nitrate (NO_3), and orthophosphate (PO_4).

In addition to the internal recycling, nutrients are introduced into a waterbody through point and nonpoint sources, such as sewage treatment plant discharges, runoff from urban areas and agricultural lands, groundwater inflow from leaking septic systems, and atmospheric deposition. Nitrogen can also

enter and leave a waterbody in the form of free N_2 gas through atmospheric exchange and some species of blue-green algae can also obtain nitrogen from the atmosphere through nitrogen-fixation processes.

The trophic status of a waterbody should be based on total nutrient concentrations, such as TP and TN, instead of just dissolved inorganic phosphorus (DIP) or dissolved inorganic nitrogen (DIN). Inorganic nutrients can be depleted and recycled rapidly in a waterbody. For this reason, most monitoring programs focus on total nutrient concentrations, rather than just the dissolved fractions. Compared with DIN and DIP concentrations, TP and TN concentrations better reflect the trophic status of a waterbody, since algal growth significantly affects the dissolved inorganic nutrients. Algae directly utilize DIN and DIP and deplete them during the algal growth season. Thus, moderately low levels of DIN or DIP do not necessarily result in low algal concentrations. There can still be sufficient supplies of DIN or DIP in the water column that can be transformed from N and P. For example, Fig. 5.1.3 shows the N/P ratios in Lake Okeechobee, FL, calculated from measured data. It shows that algal growth in the spring and summer of 1999 reduced DIN (and DIN/DIP ratio) significantly, while the ratio of TN/TP kept relatively constant throughout the year. The ratio of TN/TP, instead of DIN/DIP, is a better representation of the overall trophic condition of the lake.

Nutrients are difficult to control because they cycle throughout an ecosystem. Rather than leaving the waterbody, nutrients can cycle among the water column, algae, and the bottom sediment. Therefore, gradual inputs of nutrients may cause nutrient accumulation in the waterbody over time. For example, nutrients are taken up by algae. Algal settling and algal mortality result in the transfer of nutrients to the sediment bed. In the summer, with increased temperature, the nutrients return to the water column when the algae decompose and mineralize in the water bottom. The nutrients released from the sediment bed can support the summer algal bloom. This key cycle should be represented well in water quality models.

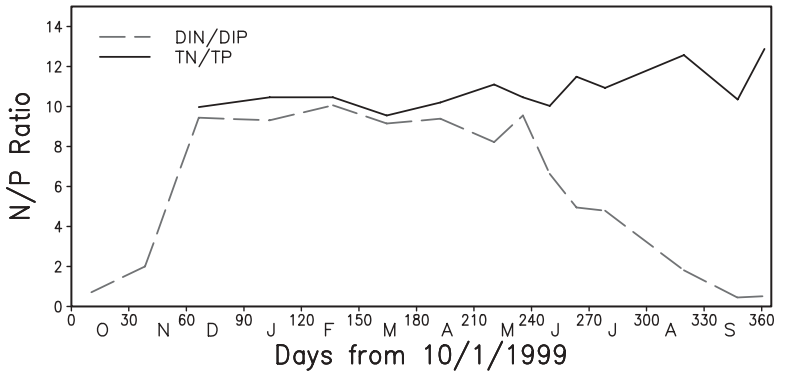

Fig. 5.1.3 The N/P ratios at LZ40 in Lake Okeechobee, calculated from measured data. DIN = NH_4 + NO_2 + NO_3 and DIP = dissolved inorganic phosphorus.

Major processes affecting nutrient concentration and cycling include (1) algal uptake, (2) hydrolysis converting particulate organic nutrients into dissolved organic form, (3) mineralization and decomposition of dissolved organic nutrients, (4) chemical transformations of nutrients, (5) sediment sorption and desorption, (6) settling of particulate matters, (7) nutrient fluxes from the sediment bed, and (8) external nutrient loadings. These processes and their mathematical representations will be discussed in detail in this chapter.

5.1.3.1 Nitrogen Cycle. Nitrogen is one of the most abundant elements on Earth, making up 78% of Earth's atmosphere by volume (~75% by mass). Nitrogen is used primarily by plants and animals to synthesize protein. It is a major component of proteins, is found in the cells of all living organisms, and is continually recycled by plants and animals. Nitrogen enters the ecosystem in several chemical forms.

Organic nitrogen is a form of nitrogen bound to an organic compound. Inorganic nitrogen may exist in a free state as a gas (N_2), or as nitrate (NO_3), nitrite (NO_2), or ammonia (NH_3). Ammonia is often the primary form of nitrogen dissolved in an aquatic system and is the major form of nitrogen used for algal growth. Since NO_2 concentrations are relatively small, nitrate is often referred to the sum of nitrite plus nitrate ($NO_2 + NO_3$) in water quality models.

Ammonia is a dissolved inorganic form of nitrogen. Total ammonia includes ammonium ion (NH_4^+) and un-ionized NH_3. NH_4 concentration is normally much higher than NH_3 concentration (Section 5.5.2.3). This is why that NH_4 is sometimes used to represent (total) ammonia in discussions. Both NH_4 and $NO_2 + NO_3$ are used for algal uptake. While NH_4 is the preferred form of nitrogen for algal growth, algae will utilize $NO_2 + NO_3$ for growth as the NH_4 concentration becomes depleted. Under specific conditions of temperature and pH, the un-ionized component of NH_3 can be toxic to aquatic life; toxicity increases as pH (or temperature) increases. A majority of the ammonia produced in the world is used in fertilizers. Since the decomposition of urea and protein can also produce ammonia, it is often found in domestic wastewater.

All nutrients required for algal growth, such as nitrogen, phosphorus, carbon, and silica, undergo constant recycling between inorganic and organic forms. A nutrient cycle represents the natural cyclic conversions of the nutrient from one form to another within an ecosystem. To study the eutrophication process, it is essential to understand the nutrient cycles. The nitrogen cycle comprises several forms in the water column, in the air, and in the sediment bed. Because it does not sorb strongly to sediment, nitrogen moves easily between the sediment bed and the water column and cycles continuously. The diagram in Fig. 5.1.4 shows an overview of the nitrogen cycle in aquatic environments. It includes the following major phases:

1. Organic nitrogen (ON).
2. Ammonia (NH_3) and ammonium (NH_4).

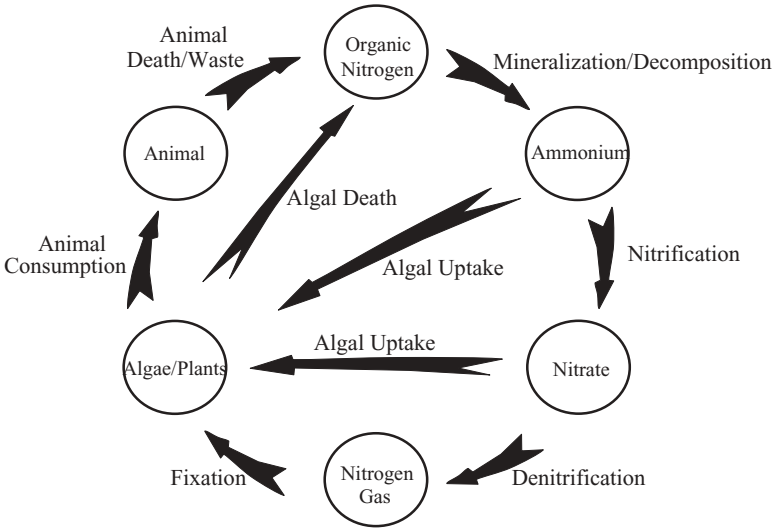

Fig. 5.1.4 Nitrogen cycling processes in an aquatic system.

3. Nitrite and nitrate ($NO_2 + NO_3$).
4. Nitrogen gas (N_2).
5. Algae and plants.
6. Zooplankton and aquatic animal.

The major components of the nitrogen cycle are organic nitrogen, ammonia, and nitrate. Organic nitrogen is one of the primary forms of the external nitrogen loadings. Organic nitrogen undergoes bacterial decomposition and is mineralized to ammonia (Fig. 5.1.4).

Nitrification is the oxidation of ammonium salts via bacteria to nitrites and the further oxidation of nitrites to nitrates. In the presence of nitrifying bacteria and oxygen, ammonia is quickly converted to nitrite and subsequently nitrate via the nitrification process. Nitrate can be converted to nitrogen gas through denitrification under low DO conditions. The nitrogen gas produced leaves the aquatic system and is released into the atmosphere. Denitrification near the bottom of a waterbody, such as a lake, can be a major nitrogen-loss mechanism. Nitrogen fixation is the biological process in which N_2 from the atmosphere is consumed by algae and is converted to organic nitrogen. As mentioned previously in this chapter, some species of blue-green algae are able to fix N_2 directly from the air, when nitrate and ammonia are not readily available. This makes it difficult to use nitrogen as a limiting nutrient to control algal growth.

Both NH_4 and $NO_2 + NO_3$ are removed from the water column by algae and aquatic plants during photosynthesis and then are incorporated into the

food chain. Aquatic animals get their nitrogen by eating algae and plants. The waste from and the death of animals provide new sources of organic nitrogen. Dissolved inorganic nutrients are returned to the water through the hydrolysis of particulate organic nitrogen and the mineralization of dissolved organic nutrients. This completes the nitrogen cycle sketched in Fig. 5.1.4.

5.1.3.2 Phosphorus Cycle. Phosphorus (P) is one of the vital nutrients for algal growth and is a key component in converting sunlight into usable energy forms. However, too much phosphorus in a waterbody can cause excessive algal growth and lead to eutrophication problems. Phosphorus is the limiting nutrient in many freshwater systems, that is, the nutrient in the lowest concentration relative to the stoichiometric ratio required for algal growth. Therefore, phosphorus concentration can be very influential in algal growth. Phosphorus is a very reactive element. It reacts with many cations, such as iron and calcium, and readily sorbs to suspended solids in the water column, reducing its availability for algal uptake. Total phosphorus consists of phosphorus in particulate and dissolved forms. Dissolved phosphates and particulate organic phosphorus are the main components of total phosphorus. Phosphorus does not have a gaseous phase. The technology for removing phosphorus is generally more advanced and less expensive than that for nitrogen removal.

Phosphate is the primary form of phosphorus for algal uptake. Compared with NO_3, the major form of nitrogen for algal uptake, phosphates dissolve less readily and tend to attach to sediment particles. Phosphates exist in three forms:

1. **Orthophosphate**, frequently used to represent soluble reactive phosphorus (SRP), is a salt that contains phosphorus as PO_4^{-3}. It is the only phosphorus compound readily available for algal uptake without further breakdown and provides a measure of the phosphorus immediately available for plant growth. Orthophosphate constitutes the majority of phosphates. Major man-influenced sources include sewage and runoff from farmland and lawns. Orthophosphate, of course, is usually in very low concentrations in unpolluted waters.
2. **Polyphosphate (or metaphosphate)** is used for treating boiler waters and in detergents. In water, they can be transformed into orthophosphate and become available for algal uptake.
3. **Organic phosphate** is often found in plant tissue, waste solids, or other organic material. They may exist in solution, as particles and loose fragments, or in the bodies of aquatic organisms. After decomposition, they can be converted to orthophosphate.

Phosphorus undergoes continuous transformations and cycles repeatedly within an aquatic system, contributing to increased biological activity, before it is finally removed from the system by sedimentation or by outflows. The phosphorus cycle involves physical, chemical, and biological interactions, and

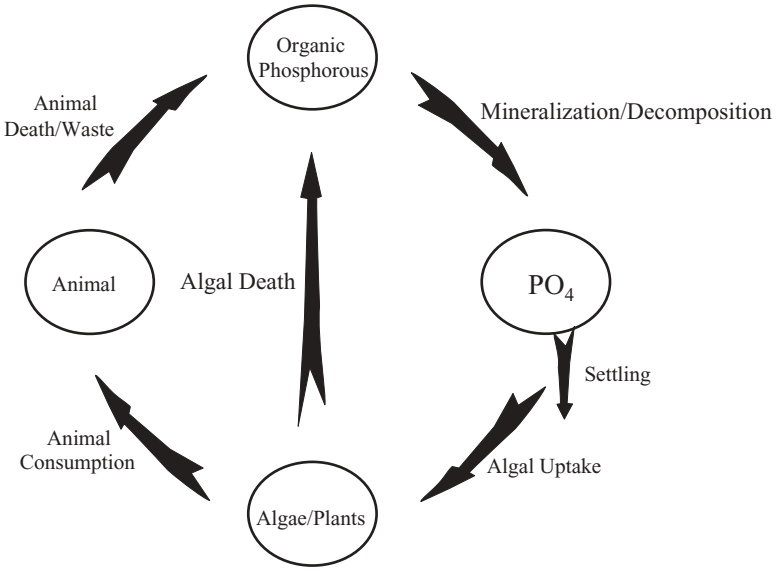

Fig. 5.1.5 Phosphorus cycling processes in an aquatic system.

has the following major forms (Fig. 5.1.5): (1) organic phosphorus, (2) phosphates (largely orthophosphates), (3) algae and plants, and (4) zooplankton and aquatic animal.

The phosphorus cycle operates similarly to the nitrogen cycle in many aspects. Organic forms of phosphorus are generated by the death of algae and then are mineralized to phosphates. Particulate phosphates sorb to sediments and settle to the sediment bed. Dissolved phosphate (largely PO_4) is taken up by algae and plants, incorporated into the food chain, and eventually returned to the water as organic phosphorus. This completes the cycling processes shown in Fig. 5.1.5.

Nitrogen and phosphorus have different chemical properties, and therefore have different cycling processes. The major differences between the nitrogen cycle and the phosphorus cycle are

1. Unlike the nitrogen cycle, the phosphorus cycle does not have a gas phase that can be a major nutrient loss mechanism in an aquatic system.
2. Forms of inorganic nitrogen are easily dissolved in water, while phosphates are often strongly sorbed to sediment. Therefore, phosphates can settle with sediment solids to the bottom of a waterbody and later become a phosphorus source to the waterbody. In many waterbodies, bottom sediments contain enough phosphorus to accelerate eutrophication even after external sources have been terminated.

5.1.3.3 Limiting Nutrients. In addition to nitrogen and phosphorus, algal growth is affected by light, water temperature, and various trace nutrients, which are difficult to control in natural waterbodies. Because some control can be exerted over the concentration of nitrogen and phosphorus, significant studies are conducted on how to make nitrogen or phosphorus a limiting nutrient, so that eutrophication can be controlled in a waterbody.

Algae consume nutrients in a fixed stoichiometric ratio and this ratio is relatively constant. Disparity in the ratio of nutrients supplied often leads to depletion of one nutrient (or nutrient deficit), while the others remain available. This nutrient, which is least available for algal growth, is called the limiting nutrient. When the limiting nutrient is depleted, according to the Liebig's Law of the Minimum, the algal concentrations stop increasing and the eutrophication process is retarded or even reversed.

The concept of a limiting nutrient is the basis for many eutrophication control approaches. The idea is that by identifying and reducing the supply of the limiting nutrient, the algal growth and eutrophication can be controlled. Carbon is seldom in short supply and is often not the limiting nutrient. Silica receives little emphasis in water quality management, because its abundant supply from natural sources is difficult to control. In most aquatic systems, the limiting nutrient is phosphorus or, to a lesser degree, nitrogen. The supply of these nutrients can be altered by controlling loadings from point and nonpoint sources. To control eutrophication in a waterbody, the essential questions are (FISRWG, 1998):

1. Is there a limiting nutrient?
2. Which nutrient is limiting?
3. Is one nutrient limiting during all periods of concern?
4. Could control of a nutrient make it limiting?

In general, seawater is most often limited by nitrogen, whereas freshwater lakes are most often limited by phosphorus. Compared with phosphorus, nitrogen is often more difficult to control, because it is almost impossible to control the nitrogen exchange between the atmosphere and water. Also, some blue-green algae can fix nitrogen directly from the atmosphere and are therefore not limited by nitrogen. In freshwaters, phosphorus is often the limiting element. Reducing phosphorus loading (and concentration) can control the eutrophication in a water system. For example, to control algal growth in a small pond, chemical precipitation, such as alum, can be added to the pond to remove phosphorus in the water column. This treatment leads to a dramatic reduction of phosphorus concentration, and then, the decline of algal concentration, even though there are still excessive amounts of other nutrients in the system.

The ratio of nitrogen to phosphorus (N/P) in an aquatic system is used as an indicator of the nutrient limiting conditions for algal growth. To help illustrate the relative amounts of nitrogen and phosphorus required for algal

growth, the following chemical equation is often used to represent algal photosynthesis (Stumm and Morgan, 1981):

$$106\,CO_2 + 16\,NO_3^- + HPO_4^{2-} + 122\,H_2O + 18H^+ \rightarrow C_{106}H_{263}O_{110}N_{16}P + 138\,O_2 \quad (5.1.1)$$

Therefore, the N/P weight ratio in the algae is

$$\frac{N}{P} = \frac{16 \times 14}{1 \times 31} = 7.2 \quad (5.1.2)$$

Equations (5.1.1) and (5.1.2) reveal that nitrogen and phosphorus are taken up by algae in an approximately constant ratio of 16 atoms of nitrogen/1 atom of phosphorus, or 7.2 : 1 by weight. For a first approximation then, it takes about seven times more nitrogen than phosphorus to produce a given amount of algae. The practical range around this number is 10–20. Waters with N/P ration of <10 might lack nitrogen for algal uptake and nitrogen limits plant growth. When N/P is >20, the converse is often true: phosphorus becomes the limiting nutrient for algal production. Figure 5.1.6 is the average annual TN/TP ratio in Lake Okeechobee between 1973 and 2000. The lake algae were limited by phosphorus in the early 1970s. But the years of excessive phosphorus loads and the successful reduction of nitrogen loads have resulted in the lake becoming nitrogen (and light) limited. The TN/TP ratio in the lake changed from 29 in 1973 to 13 in 2000.

Similarly, the carbon to phosphorus ratio (C/P) is

$$\frac{C}{P} = \frac{106 \times 12}{1 \times 31} = 41 \quad (5.1.3)$$

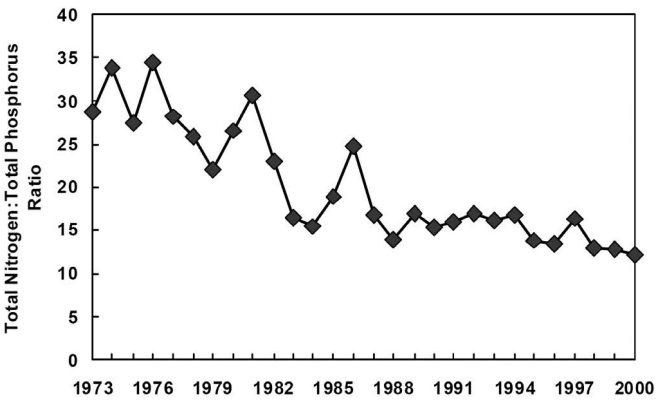

Fig. 5.1.6 Average annual ratio of total nitrogen to total phosphorus in Lake Okeechobee, FL (SFWMD, 2002).

Equations (5.1.2) and (5.1.3) show that the ratios by weight for an average community of algae are ~1P:7N:41C.

Liebig's Law states that the effective way to control eutrophication is to reduce the concentration of the limiting nutrient. Reducing other nutrient(s) will not provide efficient control, unless its concentration decreases to the point where it becomes the limiting nutrient. Although phosphorus is the limiting factor for most lakes and reservoirs, some regions are actually nitrogen-limited due to abundant phosphorus sources. However, reducing phosphorus loading will have much less of an effect on a lake that is nitrogen limited. An exception exists when some species of blue-green algae are able to fix nitrogen directly from the atmosphere, and therefore are not limited by nitrogen. In this case, phosphorus limitation seems to be the only means to control the growth of nitrogen-fixing blue-green algae, whether or not phosphorus is initially the limiting nutrient.

In addition to nutrients, algae also need sunlight for growth. In certain waterbodies, both nitrogen and phosphorus are in sufficient supply and the factor limiting algal growth is light. There can also be multiple factors that limit algal growth. A good example is Lake Okeechobee. The limiting factor in the lake can change seasonally and regionally (SFWMD, 2002). Both nitrogen and light can be the limiting factors. Because of high suspended solid concentration and algal growth, the Secchi depth of the lake can be very small. In this case, only the top thin layer of the water column, sometimes <20 cm, has adequate sunlight for algal growth. More detailed discussions on this topic will be presented in Section 5.9.2, where Lake Okeechobee water quality modeling is presented as a case study.

5.1.4 Dissolved Oxygen

Dissolved oxygen is the amount of oxygen that is dissolved in water, which occurs when microscopic bubbles of gaseous oxygen are mixed in water. Dissolved oxygen is one of the most important parameters of water quality and is used to measure the amount of oxygen available for biochemical activity in water.

Dissolved oxygen is a basic requirement for a healthy aquatic ecosystem. Most fish and aquatic insects need DO to survive. Fish, especially larvae, will die when the DO levels get too low. Low DO is a sign of possible pollution in a waterbody. As DO levels in water drop <5.0 mg/L, aquatic life is put under stress. The lower the concentration, the greater is the stress. Oxygen concentrations <2 mg/L are considered hypoxic. In some cases, the water may lose all of its oxygen and become anoxic. Oxygen levels that remain hypoxic for a prolonged period can result in large fish kills.

Dissolved oxygen is depleted by oxidation of organic carbon, nitrification, and respiration, and is replenished by surface exchange and photosynthesis. Oxygen enters the water by reaeration from the atmosphere and by plant photosynthesis; oxygen concentrations in the water column fluctuate (under

natural conditions), but severe oxygen depletion usually results from human pollution. Bacteria use oxygen to decompose organic materials. In polluted waters, bacterial consumption of oxygen can rapidly outpace oxygen replenishment from the atmosphere and plant photosynthesis. This consumption results in a DO deficit and a reduction of DO concentrations. For example, a large area (6000–7000 miles^2) of hypoxia (DO <2 mg/L) located off the Gulf of Mexico (Texas–Louisiana) Shelf is primarily caused by the excessive nutrients emptied into the Gulf of Mexico from the Mississippi River drainage and the interaction of riverine freshwater with currents in the Gulf. The hypoxia can cause stress or death in bottom-dwelling organisms that cannot move out of the hypoxic zone. Depletion of DO for the water column has resulted in virtually no biological activity in the hypoxic zone (USEPA, 2000c).

Since light availability decreases with depth, the rate of algae photosynthesis tends to decrease with depth. Therefore, in the daylight, there is a net increase in DO above certain water depth. Below this depth, there is a net decrease in DO. Dissolved oxygen is typically higher in surface water than in deeper water, due to reduced photosynthesis and reduced DO downward mixing from the surface. Weather also influences DO concentrations. On clear days, there is sufficient light for increased rates of photosynthesis and DO concentrations normally are high in the afternoon. On cloudy days, photosynthesis is limited by insufficient light and DO concentrations can be relatively low.

Algal growth produces oxygen, while algae respiration consumes oxygen. Prolonged hot weather can deplete oxygen concentrations and may cause fish kills, since warm water cannot contain as much oxygen as cold water. Warm conditions further accelerate oxygen depletion by stimulating bacterial activity and by increased benthic sediment oxygen demand. Under such conditions, minor additions of pollution-containing organic materials can severely depress oxygen levels in a waterbody.

Figure 5.1.7 shows the measured DO for 20 months, from November 1992 to June 1994, in Lake Wister, OK (OWRB, 1996). The corresponding water temperature of the lake is already shown in Fig. 2.3.2. The lake exhibits strong seasonal DO variation. During the winter months (November–January), DO in the lake is high with values ~10 mg/L and is well mixed in the vertical. During the summer, DO is very stratified with values <1.0 mg/L in the lower portion of the lake (water depth from 9 to 18 m), while the surface DO can still be 8 mg/L or higher. This strong DO variation in the vertical is caused primarily by temperature stratification of the lake, biochemical processes in the water column, and benthic oxygen demand in the bed. Discussions on these processes will be presented throughout this chapter, especially in Section 5.6.

5.1.5 Governing Equations for Water Quality Processes

As was discussed in Chapter 2, a hydrodynamic model typically includes the following governing equations: (1) momentum equations (3), (2) a continuity

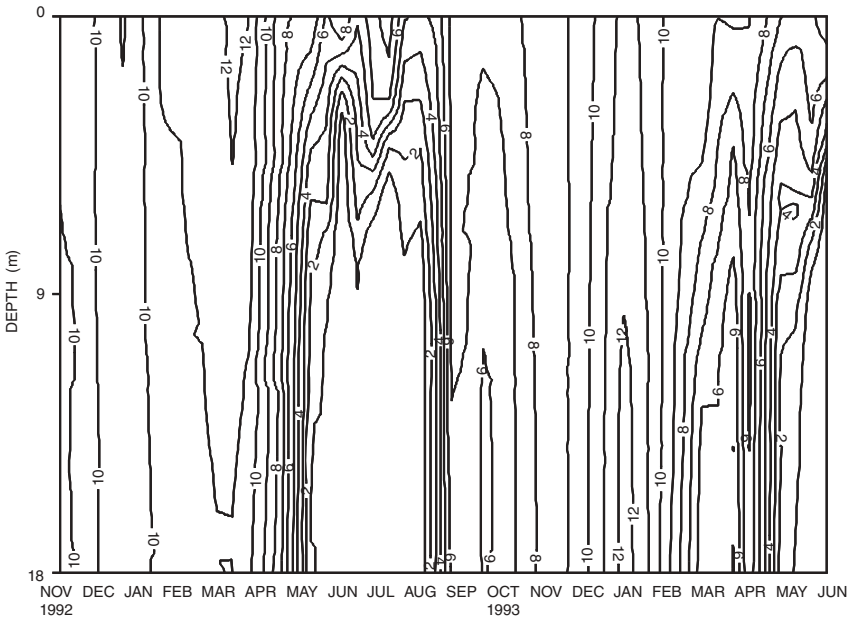

Fig. 5.1.7 Dissolved oxygen (in mg/L) in Lake Wister, OK (OWRB, 1996).

equation (1), (3) a temperature equation (1), (4) a salinity equation (1), and (5) turbulence equations (2). These equations (a total of 8) constitute the fundamental elements of a hydrodynamic model. A water quality model, on the other hand, is based on the mass balance equation (also called conservation of mass equation).

A hydrodynamic model and sediment model provide information needed in a water quality model, including water depth, currents, turbulence mixing, temperature, salinity, and sediment concentration. The water quality model itself is built based on the following:

1. Conservation of mass.
2. Laws governing chemical, biochemical, and biological processes.
3. Boundary conditions and initial conditions.

These will be the focus of this chapter.

Figure 4.3.1 is used to explain toxic transport, but can also be applied to illustrate processes affecting the water quality in an aquatic system:

1. *Physical (or Hydrodynamic) Transport.* Nutrients are advected and dispersed within the water column and are transported into the system by inflow and out of the system by outflow.

2. *Exchange With the Atmosphere.* The atmospheric deposition adds nutrients to the waterbody, while volatilization removes gaseous nutrients out of the waterbody. Reaeration adds DO to the waterbody.
3. *Sorption and Desorption.* For some nutrients (e.g., P), the exchange between the particulate and the dissolved can be approximately represented by the equilibrium partitioning process and is affected by the total suspended solids concentration and the partition coefficient.
4. *Reaction and Algal Uptake.* Biochemical reactions transform nutrients, and algal uptake reduces the concentration of dissolved nutrients.
5. *Exchange on the Bed–Water Interface.* Dissolved nutrients are exchanged between the sediment bed and the water column via the diffusion process. Particulate nutrients can settle on (or be resuspended from) the bed, depending on the flow conditions.
6. *Sediment Diagenesis.* In the sediment bed, the sediment diagenesis (or decay) can be a significant factor for determining the nutrient cycling and oxygen balance in the water column.

Not all of the processes shown in Fig. 4.3.1 are important to every nutrient. For example, volatilization is insignificant to the phosphorus cycling, and sorption and desorption are not essential to nitrogen transformation.

To represent these processes mathematically, water quality variables, such as algae, nutrients, and DO, are described using a set of coupled mass conservation equations. The conservation of mass, as stated in Eq. (2.1.10), accounts for the material entering/leaving a waterbody, transport of the material within the water body, and physical, chemical, and biological transformations of the material. Hence, all of the governing equations for water quality processes have a similar form (Cerco and Cole, 1994; Park et al., 1995, 2005):

$$\frac{\partial C}{\partial t}+\frac{\partial (uC)}{\partial x}+\frac{\partial (vC)}{\partial y}+\frac{\partial (wC)}{\partial z}=\frac{\partial}{\partial x}\left(K_x\frac{\partial C}{\partial x}\right)+\frac{\partial}{\partial y}\left(K_y\frac{\partial C}{\partial y}\right)+\frac{\partial}{\partial z}\left(K_z\frac{\partial C}{\partial z}\right)+S_C \tag{5.1.4}$$

where C = concentration of a water quality state variable; u, v, w = velocity components in the x, y, and z directions, respectively; K_x, K_y, K_z = turbulent diffusivities in the x, y, and z directions, respectively; and S_C = internal and external sources and sinks per unit volume.

Equation (5.1.4) incorporates transport due to flow advection and dispersion, external pollutant inputs, and the kinetic interaction between the water quality variables. The last three terms on the LHS of Eq. (5.1.4) account for the advection transport, and the first three terms on the RHS of Eq. (5.1.4) account for the diffusion transport. These six terms for physical transport are the same as those in the mass balance equation for temperature and salinity

in a hydrodynamic model [e.g., Eq. (2.4.15) for temperature]. The last term in Eq. (5.1.4) represents the kinetic processes and external loads for each of the state variables.

Some water quality models decouple the kinetic processes (represented by S_C) from the physical transport processes (Cerco and Cole, 1994; Park et al., 1995, 2005). Therefore, the equation for physical transport has the same form as the salinity equation:

$$\frac{\partial C}{\partial t}+\frac{\partial (uC)}{\partial x}+\frac{\partial (vC)}{\partial y}+\frac{\partial (wC)}{\partial z}=\frac{\partial}{\partial x}\left(K_x\frac{\partial C}{\partial x}\right)+\frac{\partial}{\partial y}\left(K_y\frac{\partial C}{\partial y}\right)+\frac{\partial}{\partial z}\left(K_z\frac{\partial C}{\partial z}\right) \tag{5.1.5}$$

It represents the physical transport of flows and turbulence activities. The equation for kinetic processes and external loadings, called kinetic equation, has

$$\frac{\partial C}{\partial t}=S_C \tag{5.1.6}$$

Equation (5.1.6) is used to describe the kinetic processes in a waterbody. The term kinetics refers to the mathematical description of the time dependency of any dynamic process, which can be physical (e.g., sorption and atmospheric deposition), chemical (e.g., nitrification), or biochemical (e.g., algal growth and uptake). First-order kinetics, derived by linearizing S_C with respect to C, is used in most water quality models:

$$\frac{\partial C}{\partial t}=k\cdot C+R \tag{5.1.7}$$

where k = kinetic rate (time^{-1}) and R = source/sink term due to external loadings and/or internal reactions (mass/volume/time).

The governing equations, Eqs. (5.1.5) and (5.1.7), are widely used in water quality modeling studies. A major task for a water quality model is to formulate k and R in Eq. (5.1.7), so that water quality processes can be represented realistically. Water quality and eutrophication processes are very complicated. Even though all kinetic equations are based on the same mass balance equation, empirical formulations are often used as an approximation for specifying the model parameters (e.g., k and R). Therefore, the same water quality process might be described mathematically by a variety of approaches. Major differences between water quality models are primarily in

1. How the kinetic equation, Eq. (5.1.7), is specified.
2. How many nutrients are simulated.
3. How many state variables are included to describe each nutrient cycle.

The focus of this chapter is to specify Eq. (5.1.7) for algae, carbon, nitrogen, phosphorus, silica, and DO, so that these water quality variables can be described mathematically and then be calculated numerically in water quality models. In this chapter, descriptions of water quality models are primarily based on the reports of Cerco and Cole (1994) and Park et al. (1995). The notation convention for the water quality variables by Park et al. (1995) is also used here. This is for the convenience of understanding the attached source code of the EFDC model, since the model is directly coded from these formulations and uses a similar notation convention.

It should be emphasized that the equations, the theories, and the models described in this chapter are by no means the "best" ones. Differences do exist among water quality models (e.g., Brown and Barnwell, 1987; Wool et al., 2002; HydroQual, 1995c). This book does not review models and does not recommend the so-called "best" model for surface water modeling. There are dedicated reports covering particular aspects of model review and model comparison (e.g., Tetra Tech, 2001; Imhoff et al., 2004; HydroGeoLogic, 1999).

5.1.5.1 Hydrodynamic Effects. Water quality processes are significantly controlled by complex hydrodynamic processes. Inflows, water temperature, wind, and sunlight all modulate algal growth by influencing horizontal transport, vertical mixing, sedimentation, and primary production. The time scales of these forcings vary from hourly (or shorter) wind variation, 12.42-h tidal period, 24-h sunlight cycle, several days of weather events, to seasonal cycles of sunlight and temperature. Hydrodynamic transport describes how chemical or biological material is moved from one location to another. Other factors (e.g., salinity, temperature, and sunlight) influence the kinetic processes. For example, temperature regulates the decay rates of organic matters and light availability is a key factor controlling algal photosynthesis.

The role of temperature in eutrophication is both physical and biological. Water temperature strongly affects algal growth rates, nutrient recycle kinetics, and biological decomposition. Temperature, and to a lesser degree salinity, influence the solubility of DO. Differences in water temperature and salinity can create spatial and temporal gradients in DO in a waterbody. Temperature and salinity also affect water column density, an important factor in hydrodynamic circulation. Density stratification within the water column can lead to low DO in the bottom water, because the stratification reduces the vertical mixing between the surface oxygen-rich water with the bottom oxygen-deficient water. Highly stratified systems are more prone to hypoxia than are vertically mixed systems, since stratification limits downward transport of oxygen from atmospheric reaeration. Conversely, density stratification can

limit algal growth by trapping nutrient-rich water below the thermocline of a lake.

Water residence time can affect the amount of algae in the water. A waterbody that flushes rapidly (i.e., has a short residence time) exports nutrients rapidly downstream, resulting in low nutrient concentrations in the waterbody. In addition, a waterbody with flushing shorter than the doubling time of algal cells inhibits formation of algal blooms, since the algae may not reach the concentration in which nutrients are limiting the algal growth.

5.1.5.2 Temperature Effects. Most water quality processes are temperature dependent. Temperature significantly influences the kinetic rates of nutrient transformations; the rate of chemical reactions increases with temperature. The kinetic rate, k, in Eq. (5.1.7), is usually linked to the water temperature. Kinetic equations often represent reactions with a temperature-corrected kinetic rate, called the Arrhenius relationship:

$$k = k_{20}\theta^{(T-20)} \tag{5.1.8}$$

where k = kinetic rate at temperature T, (L/time); T = temperature, (°C), k_{20} = kinetic rate at 20 °C, (L/time), and θ = temperature effect constant, unitless, which usually has a value of slightly >1.

Algal growth rate is controlled by temperature, water movement, nutrients, and light. It increases with temperature until an optimum is reached, after which further temperature increase will inhibit growth. The value of this optimum temperature varies with the species concerned and with light and nutrients. This temperature effect can be expressed as:

$$f_3(T) = \begin{cases} e^{-\mathrm{KTG1}_x(T-\mathrm{TM1}_x)^2} & if\ T < \mathrm{TM1}_x \\ 1.0 & if\ \mathrm{TM1}_x \le T \le \mathrm{TM2}_x \\ e^{-\mathrm{KTG2}_x(T-\mathrm{TM2}_x)^2} & if\ T > \mathrm{TM2}_x \end{cases} \tag{5.1.9}$$

where $f_3(T)$ = algal growth function; $\mathrm{TM1}_x$ = lower end of optimal temperature range for algal growth for algal group x; $\mathrm{TM2}_x$ = upper end of optimal temperature range for algal growth for algal group x; $\mathrm{KTG1}_x$ = effect of temperature below $\mathrm{TM1}_x$ on growth for algal group x; and $\mathrm{KTG2}_x$ = effect of temperature above $\mathrm{TM2}_x$ on growth for algal group x, and subscript $x = c$ for cyanobacteria, d for diatom, and g for green algae.

Equation (5.1.9) gives a temperature–optimum curve by combining two exponential functions, one describing the rising limb of the curve below the optimum temperature and the other describing the falling limb of the curve above the optimum temperature. By using different values of $\mathrm{KTG1}_x$ and $\mathrm{KTG2}_x$, an asymmetric growth curve can be generated. The two optimum temperatures, $\mathrm{TM1}_x$ and $\mathrm{TM2}_X$, are used to express an optimum temperature range, rather than a single optimum temperature value. For $\mathrm{TM1}_x$ = 20 °C,

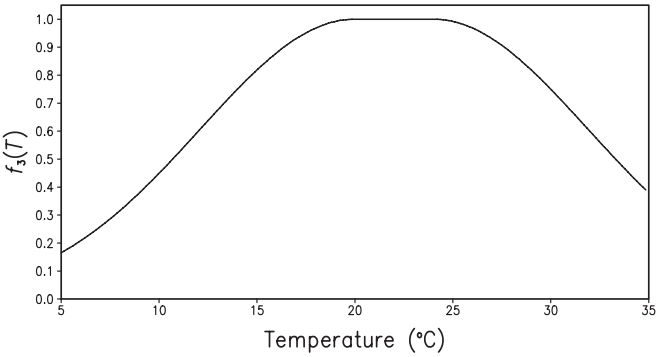

Fig. 5.1.8 Algal growth limiting function for temperature.

$TM2_x$ = 24°C, $KTG1_x$ = $KTG2_x$ = 0.008 $(°C)^{-2}$, the curve of $f_3(T)$ is shown in Fig. 5.1.8. The algal growth for temperature reaches maximum (= 1) within the optimal temperature range ($TM1_x \le T \le TM\ 2_x$). Out of this range, the growth rate decreases gradually.

Temperature change is one of the major factors causing seasonal variations (and dominance) of different algal groups (blue-greens, diatoms, greens, etc.). Algal growth usually thrives within a certain temperature range. Outside of this range, algal growth is depressed significantly. Different algal species have different optimum temperatures for growth. In general, blue-green algae have higher optima than green algae, which in turn have higher optima than diatoms (Fig. 5.1.2). As a result of different optimum temperatures, there may be seasonal variation of algal species, with diatoms dominating during spring with low temperatures and green algae and blue-green algae dominating in summer with higher temperatures. The temperature–optimum curve shown in Fig. 5.1.8 is generally more appropriate than a linear formulation or simple exponential formulation. This approach allows different algae to be dominant in different seasons, a feature that is essential for algae models.

5.1.5.3 Michaelis–Menton Formulation. The effects of nutrient concentrations on algal growth are quite complex. The Michaelis–Menton formulation, also referred as the Monod formulation (Monod, 1949), is widely used to represent the rates of algal growth and other reactions. It has

$$k_C = k_{\max} \frac{C}{C_H + C} \tag{5.1.10}$$

where k_c = algal growth rate (L/time), $k_{\max}$ = maximum algal growth rate (L/time), C = nutrient concentration (mg/L), and C_H = half-saturation concentration (mg/L).

Half-saturation concentration is the nutrient concentration at which the growth rate is one-half of the maximum rate. It defines the nutrient uptake

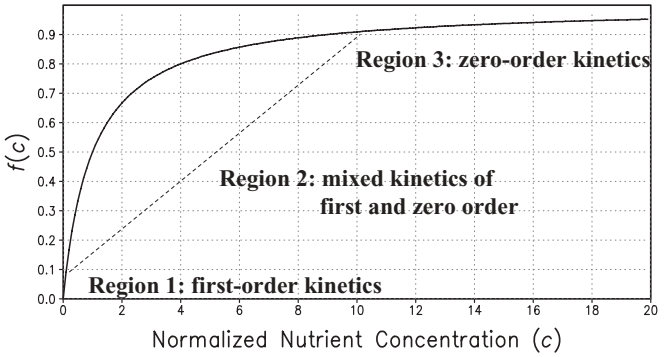

Fig. 5.1.9 Schematic representation of the Michaelis–Menton formulation.

characteristics of different algal species. A low half-saturation concentration indicates the ability of the algal group to thrive under low nutrient conditions.

Equation (5.1.10) can be modified to

$$k_C = k_{\max} \frac{C/C_H}{1 + C/C_H} = k_{\max} f(C) \tag{5.1.11}$$

where the Michaelis–Menton function, $f(c)$, is defined as:

$$f(c) = \frac{C/C_H}{1 + C/C_H} = \frac{c}{1 + c} \tag{5.1.12}$$

in which the nutrient concentration is normalized by the one-half saturation concentration. The values of $f(c)$ are plotted versus the normalized nutrient concentration $c = C/C_H$ in Fig. 5.1.9. The relationship between the normalized nutrient concentration, c, and the Michaelis–Menton function, $f(c)$, are

1. When $c = 1$, $f(c) = 0.5$.
2. When $c = 10$, $f(c) = 0.9$.
3. When $c >> 1$, $f(c) \rightarrow 1.0$.

According to Eq. (5.1.10), there is no growth at zero-nutrient concentration. The growth rate becomes linearly proportional to nutrient concentration at low nutrient concentration. As the nutrient level continues to increase and is at high concentration ($C >> C_H$), the effect on the algal growth rate is saturated. At this point, the nutrient is no longer limiting, so further increases in the external nutrient supply do not affect growth.

As discussed in Section 4.4.1, kinetic reactions can be represented as zero-, first-, second-order, and so on. The Michaelis–Menton formulation is actually

a combination of the zero-order ($m = 0$) and the first-order ($m = 1$). Equations (5.1.12) and (4.4.1) yield

$$\frac{dc}{dt} = -k_0 \frac{c}{1+c} c^m \tag{5.1.13}$$

where k_0 = a constant.

When $m = 0$ and $c \le 0.1$, Eq. (5.1.13) yields

$$\frac{dc}{dt} = -k_0 c(1-c) \approx -k_0 c \tag{5.1.14}$$

which approximates the first-order kinetics well, since c^2 is very small and negligible.

When $m = 0$ and $c \ge 10$, Eq. (5.1.13) yields

$$\frac{dc}{dt} = -k_0 \left(1 - \frac{1}{c}\right) \approx -k_0 \tag{5.1.15}$$

which represents the zero-order kinetics well.

Figure 5.1.9 expresses the specific growth rate as a function of normalized concentration given by Eq. (5.1.12). Figure 5.1.9 shows that the algal growth rate is a function of nutrient concentrations up to a saturating condition, above which it remains almost constant (= k_{max}). The growth rates can be approximately categorized into three regions:

1. In Region 1 ($0 < c \le 0.1$), the Michaelis–Menton formulation approximates first-order kinetics, in which as c increases, $f(c)$ increases proportionally, as what is described in Eq. (5.1.14).
2. In Region 2 ($0.1 < c < 10$), the formulation has mixed kinetics of first and zero order.
3. In Region 3 ($c \ge 10$), the formulation represents the zero-order kinetics, in which $f(c)$ remains almost unchanged when c varies, as described in Eq. (5.1.15).

Nitrogen and phosphorus are required by all algal species, while silica is required only by diatoms. Liebig's Law of the Minimum indicates that algal growth is controlled by the nutrient in least supply. With more than one nutrient accounted for, the algal growth rate can be calculated by

$$k_C = k_{max} \text{minimum} \left(\frac{C_N}{C_{HN} + C_N}; \frac{C_P}{C_{HP} + C_P}; \frac{C_{Si}}{C_{HSi} + C_{Si}} \right) \tag{5.1.16}$$

where $C_{N,P,Si}$ = concentrations of available inorganic nitrogen (including ammonia, nitrate, and nitrite), orthophosphate, and available silica; and $C_{HN,P,Si}$ = half saturation concentrations of N, P, and Si.

5.1.5.4 State Variables in Water Quality Models. In order to simulate eutrophication processes in aquatic systems, a water quality model requires a large suite of state variables. Candidate state variables are measurable water quality variables that can be used to evaluate the condition of eutrophication in a waterbody. A water quality model typically has the following water quality variable groups: (1) algae, (2) organic carbon, (3) phosphorus, (4) nitrogen, (5) silica, and (6) other water quality variables.

Each group consists of several state variables representing different components of the group. For example, a nutrient can be dissolve, particulate, refractory, or labile. Inorganic matters include all compounds that do not contain carbon chemically bound to hydrogen. Organic matters are compounds that contain carbon chemically bound to hydrogen. The specific variables of each group may vary from one water quality model to another, but they are similar in many ways (e.g., Brown and Barnwell, 1987; Park et al., 1995; Cerco and Cole, 1994; HydroQual, 1995c). For example, the EFDC water quality model has 22 state variables (Table 5.1.1). The schematic

TABLE 5.1.1 The EFDC Water Quality Model State Variables[a]

Water Quality Variable Group	Variable Number and Name
Algae	(1) Cyanobacteria (blue-green algae) (B_c)
	(2) Diatom algae (B_d)
	(3) Green algae (B_g)
	(22) Macroalgae (B_m)[b]
Organic carbon	(4) Refractory particulate organic carbon (RPOC)
	(5) labile particulate organic carbon (LPOC)
	(6) dissolved organic carbon (DOC)
Phosphorus	(7) refractory particulate organic phosphorus (RPOP)
	(8) labile particulate organic phosphorus (LPOP)
	(9) dissolved organic phosphorus (DOP)
	(10) total phosphate (PO4t)
Nitrogen	(11) refractory particulate organic nitrogen (RPON)
	(12) labile particulate organic nitrogen (LPON)
	(13) dissolved organic nitrogen (DON)
	(14) ammonia nitrogen (NH4)
	(15) nitrate nitrogen (NO3)
Silica	(16) particulate biogenic silica (SU)
	(17) available silica (SA)
Other	(18) chemical oxygen demand (COD)
	(19) dissolved oxygen (DO)
	(20) total active metal (TAM)[c]
	(21) fecal coliform bacteria (Feb)[d]

[a]Parkert et al., 1995.
[b]The macroalgae variable was added later to the EFDC water quality model.
[c]Total active metal was introduced for sorption and desorption of phosphate and silica in the water quality model (Cerco and Cole, 1994). Since it is easier to obtain measured sediment data and more realistic to use sediment for sorption and desorption, TAM will not be discussed in this chapter.
[d]Fecal coliform bacteria is already discussed in Chapter 4.

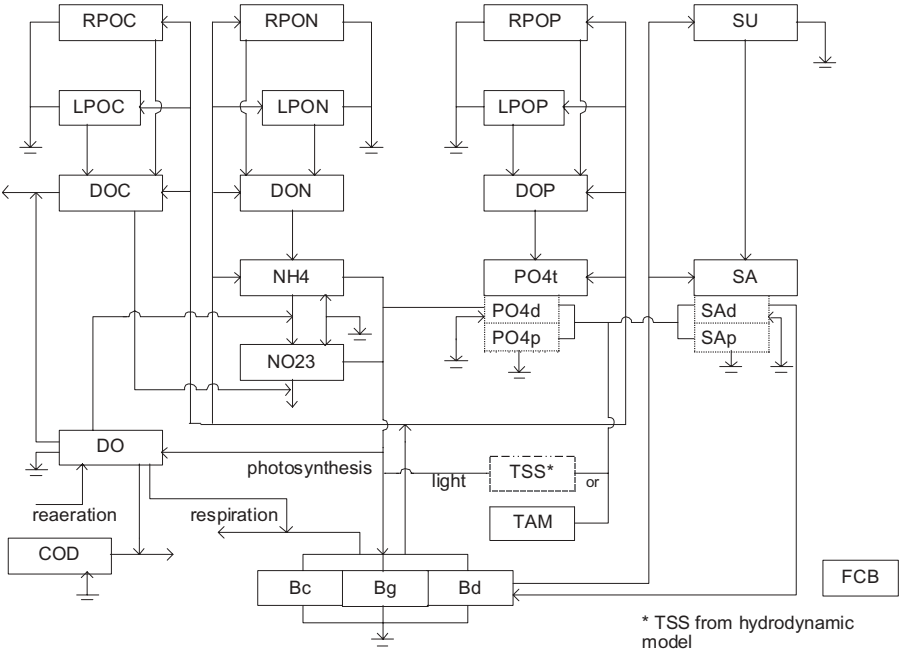

Fig. 5.1.10 Schematic diagram for the EFDC water quality model (Park et al., 1995).

representation of the relationship between the 22 state variables is shown in Fig. 5.1.10. The kinetic processes included in the EFDC water quality model are mostly from the Chesapeake Bay 3D water quality model, CE-QUAL-ICM (Cerco and Cole, 1994).

Features of these water quality state variables are (Cerco and Cole, 1994; Park et al., 1995):

Algae. Algae are represented by four state variables in the EFDC model: cyanobacteria, diatoms, greens, and macroalgae. The grouping is based upon the distinctive characteristics of each alga and upon the significant role that the characteristics play in the ecosystem. Cyanobacteria, commonly called blue-green algae, are unique in that some species fix atmospheric nitrogen. Diatoms are distinguished by their requirement of silica as a nutrient to form cell walls. Phytoplankton that do not fall into the preceding two groups are lumped into the heading of green algae. Macroalgae is incorporated into the water quality model to represent aquatic plants that attach to the bed.

Organic Carbon. Three organic carbon state variables are considered: dissolved, labile particulate, and refractory particulate. Labile and refractory

distinctions are based upon the time scale of decomposition. Labile organic carbon decomposes on a time scale of days to weeks while refractory organic carbon requires more time. Labile organic carbon decomposes rapidly in the water column or the sediments. Refractory organic carbon decomposes slowly, primarily in the sediments, and may contribute to sediment oxygen demand years after deposition.

Nitrogen. Nitrogen is first divided into organic and inorganic fractions. Organic nitrogen state variables are DON, labile particulate organic nitrogen, and refractory particulate organic nitrogen. Two inorganic nitrogen forms are considered, ammonium and nitrate, and both are utilized for algal growth. Ammonium is oxidized by nitrifying bacteria into nitrate and this oxidation can be a significant sink of oxygen in the water column and the sediment bed. Nitrite concentrations are usually much less than nitrate and are combined with nitrate for modeling purposes. Hence, the nitrate state variable actually represents the sum of nitrite plus nitrate ($NO_2 + NO_3$).

Phosphorus. As with carbon and nitrogen, organic phosphorus is considered in three states: dissolved, labile particulate, and refractory particulate. Only a single inorganic form, total phosphate, is considered. Partition coefficients are used to distribute the total phosphate between the dissolved phosphate and the particulate phosphate.

Silica. Silica is divided into two state variables: available silica and particulate biogenic silica. Available silica is primarily dissolved and can be utilized by diatoms. Particulate biogenic silica cannot be utilized. In the model, particulate biogenic silica is produced through diatoms mortality. Particulate biogenic silica undergoes dissolution to available silica or settles to the bottom sediments.

Chemical Oxygen Demand. In the EFDC water quality model, COD is the concentration of reduced substances that are oxidizable by inorganic means. In saline water, the primary component of COD is sulfide released from sediments. Oxidation of sulfide to sulfate may remove substantial quantities of DO from the water column. In freshwater, the major COD is methane (CH_4).

Dissolved Oxygen. Dissolved oxygen is a central component of the water quality model.

Total Active Metal. Both phosphate and dissolved silica sorb to inorganic solids, primarily iron and manganese. Sorption and subsequent settling is one pathway for removal of phosphate and silica from the water column. Consequently, the concentration and transport of iron and manganese can be represented in the model as TAM. It is partitioned between particulate and dissolved phases by an oxygen-dependent partition coefficient.

Fecal Coliform. Fecal coliform is used as indictor for pathogens in a waterbody.

In data monitoring programs, total nutrient usually covers all forms of the nutrient in the water, including the organic nutrient in living organisms (mostly algal biomass). In water quality models, however, the state variables of the organic nutrient generally do not include the nutrient in algae. For example, Table 5.1.1 has ON = RPON + LPON + DON. When compared with measured data, the modeled TN should include the ON in the modeled algal biomass. The same argument is also applicable to the modeled TP, TOC, and total silica.

In addition to the 22 state variables listed in Table 5.1.1, the following three variables are also important to the water quality modeling:

Temperature. Temperature is a primary determinant of the rate of biochemical reactions. Reaction rates increase as a function of temperature although extreme temperatures result in the mortality of organisms. Temperature is calculated in the hydrodynamic model.

Salinity. Salinity is a conservative tracer that provides verification of the transport component of the model and facilitates examination of conservation of mass. Salinity influences the DO saturation concentration and is used in the determination of kinetic constants that differ in saline and fresh water. Salinity can also affect the mortality of certain algal species. Salinity is simulated in the hydrodynamic model.

Total Suspended Solids. When sediment processes are simulated, particulate phosphate and particulate silica can be considered attaching to the TSS (or suspended cohesive sediment) and are carried around with the TSS by flows. In this case, the state variable of total active metal is not used in the water quality modeling. Compared with using TAM, it is more appropriate to use TSS for the modeling of particulate nutrients, since it is easier to obtain measured TSS data, and sediment processes can be modeled more reliably using the sediment model.

5.2 ALGAE

Phytoplankton (free-floating algae) and aquatic plants (macrophytes) are the two major primary producers in surface water. Primary producers are able to utilize light, carbon dioxide, and nutrients to synthesize new organic material. Algae play a key role in the eutrophication process and are essential for water quality modeling. Algae affect the nitrogen cycle, the phosphorus cycle, the DO balance, and the food chain, primarily through nutrient uptake and algae death. As algae grow and die, they form part of the nutrient cycles.

As shown in Fig. 5.2.1, algae uptake dissolved inorganic nutrients (PO_4, NO_3, NH_4, and SA) during the photosynthesis process and recycle the nutrients in the forms of organic phosphorus (OP), ON, and unavailable silica (particulate biogenic silica) (SU). The settling process removes these particulate materials to the bed. Via the sediment diagenesis in the bed and the mineralization and

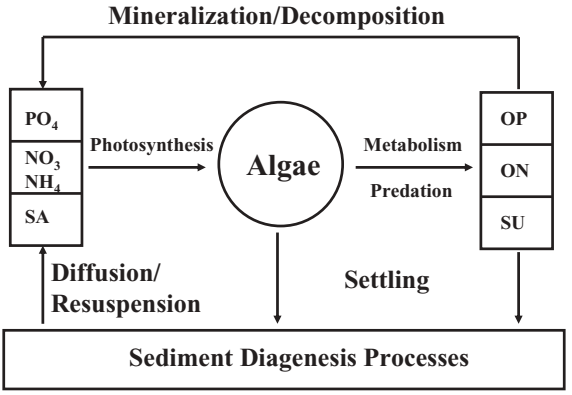

Fig. 5.2.1 Algal kinetics.

decomposition in the water column, the particulate nutrients are transformed back into inorganic forms available for the next round of algal uptake. This completes the algae cycle.

In a water quality model, the primary linkages between algae and the other water quality variables are

1. Nutrient kinetics is closely linked to algal kinetics. A principal component in the nutrient cycles is the nutrient uptake associated with algal growth, which is the main process of removing dissolved nutrients from a waterbody. Algal respiration and decay provide organic nutrients to the nutrient cycles. Algal growth requires inorganic nutrients and sunlight. The metabolism of algae often regulates the concentrations of nitrogen and phosphorus in natural waters.
2. Diurnal and seasonal DO variations can be significantly affected by algal processes. During the day, algae increase DO concentrations via photosynthesis. At night, algae reduce the DO concentrations via respiration. In stratified waterbodies, such as reservoirs, algal production may also affect seasonal DO variations, since the organic materials derived from algae settle to the bottom and later (especially in the summer) become a major source of oxygen depletion.

In addition to nutrient cycles and DO variations, algal growth can significantly change pH value. When algae consume dissolved CO_2 for growth during the day, the value of pH increases. The value of pH decreases when algae release CO_2 during respiration at night.

5.2.1 Algal Biomass and Chlorophyll

Biomass constitutes the amount of a living organism or assemblage of organisms within a specific volume or area of an ecosystem, usually measured in

units, such as wet weight, dry weight, biovolume, or nitrogen content. This biological measurement designates groups of living organisms, as opposed to numbers of individuals. Algal concentration is typically expressed in biomass as carbon per unit volume (e.g., mg C/L) in water quality models. For a given volume of a water sample, the relationship between the algae biovolume and the algal biomass as carbon can be estimated from formulas given by Strathmann (1967). For diatoms, it has

$$\log C = -0.422 + 0.758 \log V \tag{5.2.1}$$

For other algae, it has

$$\log C = -0.460 + 0.866 \log V \tag{5.2.2}$$

where C = algal biomass in 10^{-12} g as carbon and V = algae biovolume in $10^{-6}\,m^3$.

There can be a variety of algal species in an aquatic system. For most monitoring programs, microscopic enumeration of all algae is prohibitively costly and technically impossible. In practice, total algal biomass is often represented by chlorophyll *a*, which is much easier to measure and provides a reasonable estimate of algal biomass. Chlorophyll *a* (Chl) is most commonly available as an estimate of algal biomass, and is considered to be directly proportional to the concentration of algal biomass. It is applied to represent lake trophic status (Carlson, 1977) and to set up water quality criteria. For example, Oregon has set an endpoint of 10 μg/L for natural lakes that thermally stratify and 15 μg/L for natural lakes that do not thermally stratify (NALMS, 1992). Similarly, North Carolina uses a standard of 40 μg/L for warm waters and 15 μg/L for cold waters (NALMS, 1992).

Chlorophyll is a group of green pigment, including chlorophyll *a, b, c*, and *d*, which occurs primarily in many plants and some bacterial cells. Pigments are chemical compounds that reflect only certain wavelengths of visible light making them appear "colorful". Chlorophyll transforms light energy into chemical energy in photosynthesis. There are seven types of chlorophyll. Chlorophyll *a*, because of its primary role in photosynthesis, is frequently used as a measure of algal biomass in natural waters. To measure chlorophyll *a*, the sampled water is filtered through a fine glass-fiber filter to collect all of the particulate material greater than ~1 μ in size. The chlorophyll *a* in this material is then extracted with a solvent and quantified using a spectrophotometer or a fluorometer. Therefore, chlorophyll *a* is an indirect measure of the overall algae population and does not distinguish different algal groups (e.g., diatoms, blue-greens).

To simulate eutrophication processes, water quality models often express algal biomass as carbon. Using either a fixed or variable carbon/chlorophyll ratio, modeled algal concentrations (as carbon) can be converted to algal concentrations as chlorophyll *a*, and then the modeled and the measured algal

concentrations (now both as chlorophyll *a*) can be compared. Chlorophyll *a* can be converted to algal biomass using

$$B = \alpha \text{Chl} \tag{5.2.3}$$

where B = algal biomass concentration as carbon (C) (mg C/L), Chl = chlorophyll *a* concentration (mg Chl/L), and α = carbon to chlorophyll ratio, mg C/mg Chl.

The value of α varies widely depending on the makeup of the algae population, typically ranging from 15 to 100 (Bowie et al., 1985, Table 6-4). When both the measured data of Chl and B are available, the value of α can be calculated. In many applications, however, α is initially given based on literature values, and then used as a tuning parameter for model calibration. One weakness of using chlorophyll *a* to represent algal biomass is that the amount of chlorophyll *a* per algal cell can vary widely, either seasonally or annually due to the species composition, light conditions, and nutrient availability. Laws and Chalup (1990) reported that the chlorophyll/carbon ratio in algae could vary up to a factor of 5. It should use caution when applying Chl as an indicator of algae in a waterbody. In addition, it may also be important to examine the algal community microscopically, since the mix of species may influence water quality management decisions. Steinman and Lamberti (1996) and Stevenson (1996) presented general methods for algal biomass determination.

Nutrient uptake kinetics is a principal component in modeling algal growth. Stoichiometric ratios give quantitative relationships between nutrients and algae. Most water quality models assume that the nutrient compositions of algal cells and the stoichiometric ratios are constant. Under this assumption, nutrient uptake rates can be estimated as:

$$V_s = \alpha_s \mu B \tag{5.2.4}$$

where V_s = uptake rate for a particular nutrient (nutrient mass/volume–time), α_s = nutrient fraction of algal cells (stoichiometric ratio) (mass nutrient/mass algae), μ = growth rate of algae (L/time), and B = algal concentration (algal mass/volume).

5.2.2 Equations for Algal Processes

Factors controlling algal concentration include physical transport [described by Eq. (5.1.5)] and algal kinetics [described in Eq. (5.1.7)]. The physical transport of algae is similar to other hydrodynamic and water quality variables and is not the focus of this chapter. The kinetics will be discussed in detail in this chapter.

Water quality models usually do not simulate a specific algal species. Instead, algae are aggregated into either a single group (e.g., total algae or Chl) or a few groups (e.g., blue-green algae, diatoms, and green algae). For water quality models intended for short-term simulations (days to weeks), the single group

approach can represent the algal variation reasonably well, since a single type of algae is likely the dominant one during the simulation period. However, for long-term simulations (seasons to years), water quality processes are often associated with different types of algae in different seasons, which means that more than one group of algae are needed in water quality modeling. It is essential to include these algal groups in order to realistically describe nutrient and algal kinetics. Since most water quality studies need to consider seasonal (and annual) variations, a water quality model with multialgal groups is often necessary (e.g., Table 5.1.1).

Algal kinetics is governed by the following: (1) algal growth; (2) metabolism, including respiration and excretion; (3) predation; (4) settling; and (5) external sources. A general equation that includes all of these processes can be expressed as:

$$\text{Net algal production} = \text{algal growth} - \text{metabolism} - \text{predation} - \text{settling} + \text{external sources} \tag{5.2.5}$$

Equation (5.2.5) forms the basis for almost all algae models, in which the net algal production (growth) is expressed as the difference between the growth, the death (metabolism and predation), the settling, and the external source. Major differences between different algae models are primarily in the number of algal groups considered, and the specific empirical formulations used for each term (process) in Eq. (5.2.5). Because of these differences, it is critical to understand the assumptions of a particular model when selecting model parameters, extracting parameter values from one model and applying them to another, and/or comparing model results with measured data.

The kinetic equation, Eq. (5.2.5), can now be written for algae as (Park et al., 1995):

$$\frac{\partial B_x}{\partial t} = (P_x - \mathrm{BM}_x - \mathrm{PR}_x)B_x + \frac{\partial}{\partial z}(\mathrm{WS}_x \cdot B_x) + \frac{\mathrm{WB}_x}{V} \tag{5.2.6}$$

where B_x = algal biomass of algal group x (g C/m^3), t = time (day), P_x = production rate of algal group x (day^{-1}), BM_x = basal metabolism rate of algal group x (day^{-1}), PR_x = predation rate of algal group x (day^{-1}), WS_x = settling velocity of algal group x (m/day), WB_x = external loads of algal group x (g C/day), V = volume (m^3), and subscript x = c, d, g.

As listed in Table 5.1.1, algae are grouped into three model state variables: cyanobacteria (blue-green algae), diatoms, and green algae. The algal biomass concentration, B_x, is expressed as carbon (C). The subscript, x, is used to denote three algal groups: c for cyanobacteria, d for diatoms, and g for green algae. Hence, the algal kinetic equation (5.2.6) is the same for the three algal groups, but contains different parameter values to characterize the differences between the groups. The volume, V, is represented by the model grid volume.

In Eq. (5.2.6), the algal production rate, P_x, is a complicated function of nutrient concentrations, water temperature, and sunlight. Algal biomass decreases through basal metabolism and predation. The basal metabolism in Eq. (5.2.6) is the sum of all internal processes that decrease algal biomass, and largely consists of two parts: respiration and excretion. The settling removes algae from the water column and deposits it onto the bottom of the waterbody. External loads include point and nonpoint sources from tributaries, surface runoffs, groundwater, and atmospheric deposition. The right-hand terms of Eq. (5.2.6) will be discussed in detail in the forthcoming sections.

5.2.3 Algal Growth

Algal growth is the most important process for algae modeling. The algal growth rate is a complicated function of temperature, light, and nutrients and is often the determining factor for the net algal production in Eqs. (5.2.5) and (5.2.6).

Primary production determines the rate of algal growth. Primary producers are able to utilize light, CO_2, and nutrients to synthesize new organic materials. They represent the process whereby new organic matter is formed and accumulated through photosynthesis activity of primary producers. The rate of primary production is estimated by measuring the amount of oxygen released and the amount of carbon assimilated by the plant. Primary producers, such as algae, convert solar energy and nutrients into organic matters that are incorporated into the tissues of plants. Primary producers are at the base of the food chain and serve as a food source for higher organisms in ecosystems. Algae are one of two main primary producers in surface waters. The other primary producers are the rooted or floating aquatic plants (macrophytes), which are generally restricted to shallow waters. In most cases, algae are more important in the food production than are rooted aquatic plants.

When the conditions of nutrients, sunlight, and water temperature are favorable, algal blooms may occur. The algae will continue to bloom until one or more of the key factors promoting algal growth is no longer available, a condition(s) commonly referred to as "limiting". That is, the lack of sunlight or nutrients or other factors limits the algal growth. The effects of these processes are considered to be multiplicative and can be mathematically expressed in a general form as:

$$P_x = PM_x \cdot f_1(N) \cdot f_2(I) \cdot f_3(T) \tag{5.2.7}$$

where PM_x = maximum growth rate for algal group x (day^{-1}), $f_1(N)$ = growth limiting function for nutrients ($0 \le f_1 \le 1$), $f_2(I)$ = growth limiting function for light intensity ($0 \le f_2 \le 1$), $f_3(T)$ = growth limiting function for temperature ($0 \le f_3 \le 1$).

In estuaries, freshwater algae coming from upstream rivers can die rapidly in saline water. The increased mortality of freshwater organisms may be represented by retaining the salinity toxicity term in the growth equation:

$$P_x = PM_x \cdot f_1(N) \cdot f_2(I) \cdot f_3(T) \cdot f_4(S) \tag{5.2.8}$$

where $f_4(S)$ = growth limiting function for salinity ($0 \le f_4 \le 1$).

In a modeling study, the value of maximum growth rate, PM_x, is initially estimated based upon previous studies and upon literature values (e.g., Bowie et al., 1985), and subsequently adjusted as a tuning parameter during the model calibration and verification process. In Eqs. (5.2.7) and (5.2.8), each growth limiting function can vary from 0 to 1. A value of 1 indicates that the factor does not limit growth, and a value of 0 means that the limiting is so severe that growth is stopped entirely.

Temperature is one of the most important factors controlling algal growth. Each algal group has its own optimum temperature range for growth. The temperature dependency of algal growth, $f_3(T)$, is already given in Eq. (5.1.9). The formulations of f_1 and f_2 will be discussed later in this section.

Biologically, estuaries are a distinct part of the river system. The freshwater algae from upstream rivers can die rapidly due to salinity toxicity. Hence, the growth of freshwater blue-green algae in saline water can be limited by (Cerco and Cole, 1994):

$$f_4(S) = \frac{STOX^2}{STOX^2 + S^2} \tag{5.2.9}$$

where $STOX$ = salinity at which algal growth is halved (ppt) and S = salinity in water column (ppt).

5.2.3.1 Nutrients for Algal Growth. The major limiting nutrients for algal growth are phosphorus and nitrogen, with the addition of silicon for diatoms. Most water quality models only include these nutrients in the algal growth calculation. Carbon is also a major nutrient needed for algal growth. However, since carbon is often available in excess relative to phosphorus and nitrogen, carbon limitation is commonly excluded from algal growth formulations.

Nitrogen can be the limiting nutrient for algal growth when the waterbody has high phosphorus concentration or is an estuary or a coastal area. Algae use NH_4 and $NO_2 + NO_3$ to form proteins during photosynthesis. Some species of blue-green algae can fix atmospheric nitrogen for photosynthesis, which makes it difficult for nitrogen to be a limiting nutrient in some natural systems. Phosphorus is one of the primary nutrients for algal growth. In many freshwaters, phosphorus is the limiting nutrient. Orthophosphate is the inorganic form of phosphorus that can be directly consumed by algae. Dissolved silica (Si) is consumed by diatoms for providing the structural skeleton and can limit diatoms growth. Similar to phosphorus, silica can sorb to suspended solids. Its

concentration is closely associated with the partition coefficient and the concentration of total suspended solids.

Most algae models directly link algal growth and nutrient uptake with fixed stoichiometry. These models use the Michaelis–Menton formulation to describe growth limiting functions for nutrients and assume that the nutrient composition of the algal cells remains constant. In this approach, the algal growth rates are determined by the external nutrient concentrations in the water. In natural waters, however, nutrient uptake and algal growth are actually two separate processes. Nutrient uptake depends on the internal nutrient levels in the algal cells and the external nutrient concentrations in the water. Algal growth is actually determined by the internal nutrient levels in the cells, rather than external concentrations in the water. The internal stoichiometry of the algae may vary with changes in the external nutrient concentrations. To describe these two processes separately in two steps, more complex formulations (and therefore more model parameters) are needed than fixed stoichiometry models. In this book, therefore, only the fixed-stoichiometry approach is used to describe nutrient uptake for algal growth.

A fixed-stoichiometry approach computes a growth limiting function for each nutrient, and then combines these functions together to form the growth limiting function, $f_1(N)$, in Eq. (5.2.7). Based on the Michaelis–Menten kinetics discussed in Section 5.1.5, the growth limiting functions for nutrients can be expressed as:

$$f_1(\mathrm{NH_4} + \mathrm{NO_3}) = \frac{\mathrm{NH_4} + \mathrm{NO_3}}{\mathrm{KHN} + \mathrm{NH_4} + \mathrm{NO_3}} \tag{5.2.10}$$

$$f_1(\mathrm{PO_4}) = \frac{\mathrm{PO_4}}{\mathrm{KHP} + \mathrm{PO_4}} \tag{5.2.11}$$

$$f_1(\mathrm{SAd}) = \frac{\mathrm{SAd}}{\mathrm{KHS} + \mathrm{SAd}} \tag{5.2.12}$$

where $NH_4 + NO_3$ = ammonia and nitrate concentrations (mass/volume), PO_4 = orthophosphate concentration (mass/volume), SAd = available dissolved silica concentration (mass/volume), KHN = half saturation constant for nitrogen (mass/volume), KHP = half saturation constant for phosphorus (mass/volume), KHS = half saturation constant for silicon (mass/volume).

Values of the half saturation constants are listed in many previous studies, such as Table 6–10 of Bowie et al. (1986), in which the values vary widely, up to three orders of magnitude. Different limiting formulations (multiplicative, minimum, or harmonic mean) also lead to different values of half saturation constants. Equations (5.2.7) and (5.2.8) are multiplicative formulations.

The decision to include specific nutrients for algal growth in a water quality model depends on the algae considered and the aquatic system. Nitrogen and phosphorus are the two most commonly used. Using Liebig's Law of the

Minimum, which states that growth is determined by the nutrient in least supply, the nutrient limitation for growth of blue-green algae and green algae is expressed as:

$$f_1(N) = \text{minimum}\left(\frac{NH_4 + NO_3}{KHN_x + NH_4 + NO_3}, \frac{PO_4 d}{KHP_x + PO_4 d}\right) \quad (5.2.13)$$

where KHN_x = nitrogen half saturation constant for algal group x (mass/volume), KHP_x = phosphorus half saturation constant for algal group x (mass/volume), and subscript x = c for cyanobacteria and g for green algae, respectively (mass/volume).

For nitrogen-fixing cyanobacteria (blue-green algae), the nitrogen limitation in Eq. (5.2.13) may be omitted, although the algae's nitrogen kinetics should still be included in the model for describing the nitrogen cycle. For example, James et al. (2005) modeled the algal growth in Lake Okeechobee, and assumed that, when DIN concentration is <100 μg/L, the cyanobacteria growth is no longer limited by nitrogen and DIN is no longer removed from the water column.

When diatoms are considered, silicon limitation should be included, and Eq. (5.2.13) is modified to

$$f_1(N) = \text{minimum}\left(\frac{NH_4 + NO_3}{KHN_d + NH_4 + NO_3}, \frac{PO_4 d}{KHP_d + PO_4 d}, \frac{SAd}{KHS + SAd}\right) \quad (5.2.14)$$

where KHN_d = nitrogen half saturation constant for diatoms (mass/volume) and KHP_d = phosphorus half saturation constant for diatoms, mass/volume.

5.2.3.2 Sunlight for Algal Growth and Photosynthesis. Ecosystems are fueled, ultimately, by solar energy. Sunlight is the major source of heat to the water column and has a fundamental role in aquatic primary production. Photosynthesis is the metabolic process by which plants convert CO_2 and H_2O into carbon compounds and O_2 using light as an energy source. Photosynthesis is essential to the primary production of phytoplankton and submerged aquatic vegetation. In photosynthesis, plants capture solar energy and store it as chemical energy in organic compounds. Photosynthesis is essential in producing the food base of an aquatic system and is an important source of oxygen. The chemical process opposite of photosynthesis is respiration, the "burning" of carbon compounds to power metabolism.

Photosynthesis is a complex series of reactions. A simplified version of this chemical reaction is to utilize water, carbon dioxide, and light energy to produce a simple sugar (glucose) and oxygen. The equation governing photosynthesis is

$$6\,CO_2 + 6\,H_2O + \text{light energy} \xrightarrow[\text{Inorgnic nutrients}]{\text{Pigments}} C_6H_{12}O_6 + 6\,O_2 \quad (5.2.15)$$

in which the glucose ($C_6H_{12}O_6$) represents any organic matter in plants. Plants (phytoplankton) that utilize light energy to create chemical energy to store within the cell tissue are known as primary producers, since they create organic materials from inorganic forms. Equation (5.2.15) indicates that sunlight is the major driving force for photosynthesis. As a result, the geographic location, the seasonality, and the hour of the day, which affect incident sunlight, are all important factors to the eutrophication process in natural waters.

The maximum depth at which algae can grow is determined by light levels. The euphotic zone is the upper portion of the water column where sunlight is sufficient (more than ~1% incident light) for photosynthesis to occur. A general rule of thumb is that this depth is about two to three times the Secchi depth. The euphotic zone is reduced by the increased light attenuation coefficient. Actively growing algae only exist in the euphotic zone. At or near the water surface, photosynthesis occurs at or near maximum rates due to high light intensities, while at depths below the euphotic zone, photosynthesis stops due to insufficient light.

Water transparency affects the extent of sunlight penetration into the water column, and reduced water transparency reduces the euphotic zone. The absorption and attenuation of light by the water column are a major factor controlling photosynthesis. Incident light is absorbed by the water itself and any colored material dissolved in it. Particulate matters reflect the light and create a scattering effect. The net result of these factors is an attenuation of light intensity with depth. The deeper into the water column that light can penetrate, the deeper photosynthesis can occur. The light intensity (or solar radiation) in a water column can be calculated using Beer's law, Eq. (2.3.17), which states that light decreases exponentially with depth and can be represented by the negative exponential equation:

$$I(D) = I_s e^{-K_e D} \tag{5.2.16}$$

where $I(D)$ = light intensity (or solar radiation) at depth D below the surface (W/m^2), I_s = solar radiation at the surface ($D = 0$) (W/m^2), D = water depth (m), and K_e = light extinction coefficient (1/m).

The key parameter in Eq. (5.2.16) is the light extinction coefficient, K_e, which is determined by the water transparency (or turbidity). The light extinction coefficient is a measure of the vertical light attenuation through the water column, and total suspended solids (e.g., algae, organic detritus, or inorganic sediment) attenuate light and reduce transparency. There also may be high concentrations of light-absorbing dissolved materials. There are different approaches to calculate K_e. When the simulation period is short and the water turbidity has small changes, the light extinction function can be taken as constant. For seasonal and annual simulations, however, water turbidity varies significantly by the changes of TSS concentration and algal concentration. The light extinction coefficient increases with concentrations of the total suspended solids and algae, and can be estimated using the following:

$$K_e = K_0 + K_1 \cdot \mathrm{TSS} + K_2 \cdot B \tag{5.2.17}$$

where K_0 = light extinction coefficient for all absorption components (except TSS and algae) (1/length), TSS = total suspended solid concentration (mass/volume), K_1 = factor for light extinction coefficient for TSS [volume/(mass length)], B = total algal concentration (mass/volume), and K_2 = factor for light extinction coefficient for algae [volume/(mass length)].

The effect of water color is included in K_0. When TSS is unknown, the turbidity effect of TSS should also be included in K_0. The total algal concentration, B, is the sum of all algae in the water column, and can be represented by (B_c + B_d + B_g) as defined in Table 5.1.1. Shading can prevent light from reaching photosynthesizing organisms. The factor for the light extinction coefficient for algae, K_2, is also called the self-shading factor, representing that the algal growth itself can also increase water turbidity and reduce available sunlight for further algal growth.

After the light intensity (I) is calculated using Eqs. (5.2.16) and (5.2.17), the growth limiting function for light intensity, $f_2(I)$, is given as (Steele, 1962):

$$f_2(I) = \frac{I}{I_k}\exp\left(1 - \frac{I}{I_k}\right) \tag{5.2.18}$$

where I_k = optimum light intensity. As shown in Fig. 5.2.2, $f_2(I)$ reaches maximum (= 1) when $I = I_k$.

Since light varies continuously with time, some models integrate the light limitation function >24 h to get a daily average value. Cerco and Cole (1994) and Park et al. (1995) used the daily and layer integrated form of $f_2(I)$ in their water quality models:

$$f_2(I) = \frac{2.718 \cdot \mathrm{FD}}{\mathrm{Kess} \cdot \Delta z}\left(e^{-\alpha_B} - e^{-\alpha_T}\right) \tag{5.2.19}$$

where

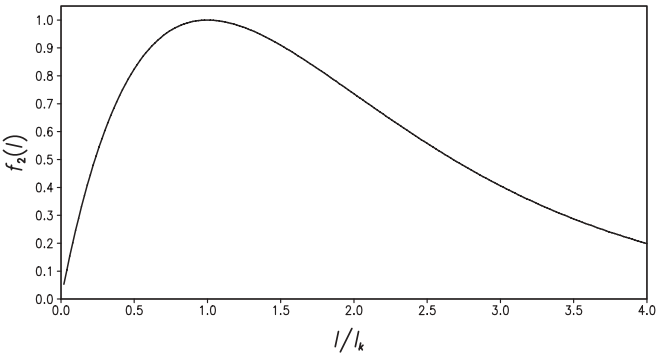

Fig. 5.2.2 Algal growth limiting function for light intensity, $f_2(I)$.

$$\alpha_B = \frac{I_o}{\mathrm{FD}\cdot(I_s)_x}\cdot\exp(-\mathrm{Kess}[H_T+\Delta z]) \tag{5.2.20}$$

$$\alpha_T = \frac{I_o}{\mathrm{FD}\cdot(I_s)_x}\cdot\exp(-\mathrm{Kess}\cdot H_T) \tag{5.2.21}$$

where FD = fractional daylength ($0 \le \mathrm{FD} \le 1$), Kess = K_e = total light extinction coefficient (m^{-1}), Δz = layer thickness (m), I_o = daily total light intensity at water surface (langleys/day), $(I_s)_x$ = optimal light intensity for algal group x (langleys/day), and H_T = depth from the free surface to the top of the layer (m).

The total light extinction coefficient, Kess, is given by

$$\mathrm{Kess} = Ke_b + Ke_{\mathrm{TSS}}\cdot\mathrm{TSS} + Ke_{\mathrm{Chl}}\cdot\sum_{x=c,d,g}\left(\frac{B_x}{\mathrm{CChl}_x}\right) \tag{5.2.22}$$

where Ke_b = background light extinction (m^{-1}), Ke_{TSS} = light extinction coefficient for total suspended solids (m^{-1} per g/m^3), TSS = total suspended solid concentration provided from the hydrodynamic model (g/m^3), Ke_{Chl} = light extinction coefficient for chlorophyll a ($m^{-1}/mg\,Chl/m^3$), CChl_x = carbon/chlorophyll ratio in algal group x (g C/mg Chl). Equation (5.2.22) is similar to Eq. (5.2.17). The optimal light intensity (I_s) for photosynthesis is expressed as:

$$(I_s)_x = \mathrm{minimum}[(I_o)_{\mathrm{avg}}\cdot e^{-\mathrm{Kess}\cdot(D_{\mathrm{opt}})_x}, (I_s)_{\mathrm{min}}] \tag{5.2.23}$$

where $(D_{\mathrm{opt}})_x$ = depth of maximum algal growth for algal group x (m) and $(I_0)_{\mathrm{avg}}$ = adjusted surface light intensity (langleys/day).

A minimum, $(I_s)_{\mathrm{min}}$, in Eq. (5.2.23) is specified so that algae do not thrive at extremely low-light levels. The adjusted surface light intensity, $(I_0)_{\mathrm{avg}}$, is estimated as:

$$(I_0)_{\mathrm{avg}} = CI_a\cdot I_0 + CI_b\cdot I_1 + CI_c\cdot I_2 \tag{5.2.24}$$

where I_1 = daily light intensity 1 day preceding model day (langleys/day), I_2 = daily light intensity 2 days preceding model day (langleys/day), and CI_a, CI_b, and CI_c = weighting factors for I_0, I_1, and I_2, respectively: $CI_a + CI_b + CI_c = 1$.

5.2.4 Algal Reduction

Algal concentration is determined by a balance between growth and reduction rates. After the algal growth is described in the previous section, this section describes algal reduction caused by basal metabolism, predation, and settling, which are represented by the terms in Eq. (5.2.6).

5.2.4.1 Basal Metabolism. Basal metabolism is a general term for biochemical processes that occur in living organisms by which energy is provided

for vital processes and activities. The basal metabolism term in Eq. (5.2.6), ($-BM_xB_x$), includes algal reduction due to respiration and excretion.

Respiration is the metabolic process by which organic carbon is oxidized to CO_2 and H_2O with a net release of energy. Algal respiration occurs continuously day and night, and the aerobic respiration of algae requires oxygen. During respiration, oxygen is consumed and carbon dioxide is released. Plant residue is broken down into glucose, which is then converted to energy. This chemical reaction can be described by the following simplified equation:

$$C_6H_{12}O_6 + 6\,O_2 \rightarrow 6\,CO_2 + 6\,H_2O + \text{released energy} \tag{5.2.25}$$

Comparing Eq. (5.2.25) with Eq. (5.2.15), it is easy to see that respiration is the reverse process of photosynthesis and contributes to the reduction of algal biomass.

Excretion is the removal of waste products or substances present in excess. Nutrient excretion by algae and zooplankton is one of the major components of nutrient recycling. Respiration and excretion are generally combined and modeled as a single term, such as in Eq. (5.2.6), which includes all metabolic losses and excretory processes.

Most models express basal metabolism as either a constant loss term or as a function of temperature. The general expression is

$$BM_x = BMR_x \cdot f_{BM}(T - TR_x) \tag{5.2.26}$$

where BMR_x = basal metabolism rate at TR_x for algal group x (1/time), $f_{BM}(T)$ = temperature function for basal metabolism (dimensionless), and TR_x = reference temperature for basal metabolism for algal group x (°C).

One commonly used form of Eq. (5.2.26) is the Arrhenius relationship with a reference temperature of 20°C. Similar to Eq. (5.1.8), it has the form:

$$BM_x = BMR_x \cdot \theta^{(T-20)} \tag{5.2.27}$$

where θ temperature effect constant (dimensionless).

Cerco and Cole (1994) described the basal metabolism in an exponentially increasing function of temperature:

$$BM_x = BMR_x \cdot e^{KTB_x \cdot (T-20)} \tag{5.2.28}$$

where KTB_x = effect of temperature on metabolism for algal group x, ($°C^{-1}$).

Note that, with parameter values commonly used in the literature, Eqs. (5.2.27) and (5.2.28) actually lead to similar values for BM_x. For example, with θ = 1.045 (Di Toro and Matystik, 1980) for Eq. (5.2.27) and $KTB_x = 0.04\,°C^{-1}$ for Eq. (5.2.28), the two temperature functions for basal metabolism, $\theta^{(T-20)}$ and $e^{KTB_x \cdot (T-20)}$, yield very close values (Fig. 5.2.3).

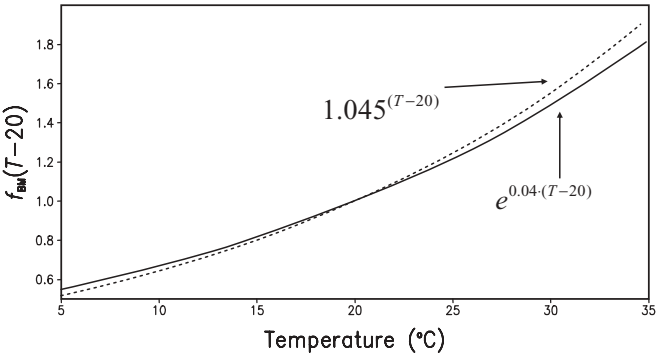

Fig. 5.2.3 Temperature functions for basal metabolism.

5.2.4.2 Algal Predation. Zooplankton is the plankton consisting of animal life that is moved aimlessly by flows. It includes the larval forms of large adult organisms (e.g., crabs, fish) and small animals that never get larger than several millimeters. Zooplankton consumes algae, bacteria, detritus, and sometimes other zooplankton, and is in turn eaten by small fish. Algal predation is the consumption of algae by zooplankton or other aquatic organisms.

Zooplanktons form an important link in the food web. Zooplankton grazing can be a key loss mechanism for algae, depending on the time of the year, zooplankton population, and zooplankton grazing rate. These organisms consume algae by filtering the surrounding water and then clearing off the algae. This filtering rate is closely linked to the water temperature and the algal concentration. Some phytoplankton species are consumed more readily and are preferentially selected by zooplankton. For example, single-celled diatoms and green algae are readily consumed, while some blue-green algae are avoided. Dense populations of zooplankton (and other algae consumers) may lead to negligible algal biomass in a waterbody, in spite of high levels of nutrients. In this case, the waterbody is often characterized by an increase in dissolved nutrients, reduced turbidity, and proliferation of macrophytes.

Some models include equations for zooplankton in order to calculate algal predation. However, limited data on zooplankton usually exclude detailed formulation of zooplankton population. Instead, the rate of zooplankton grazing is often treated as a constant in Eq. (5.2.6):

$$\mathrm{PR}_x = \text{constant} \tag{5.2.29}$$

where PR_x = predation rate of algal group x (day^{-1}).

Another approach to describe algal predation rate without directly modeling zooplankton is to link PR_x with temperature and algal biomass. Similar to

the formulation for basal metabolism, Eq. (5.2.28), the following equation can be used for algal predation (Tetra Tech, 2006):

$$\mathrm{PR}_x = \mathrm{PRR}_x \cdot \left(\frac{B_x}{B_{xP}}\right)^{\alpha_P} \cdot e^{\mathrm{KTB}_x(T-\mathrm{TR}_x)} \tag{5.2.30}$$

where PRR_x = predation rate at reference temperature TR_x for group x, (day^{-1}), B_{xP} = reference algal concentration for predation ($\mathrm{g\,C/m^3}$), and α_P = exponential dependence factor.

The advantage of Eq. (5.2.30) is that when algal concentration (B_x) is much smaller (larger) than the reference algal concentration, B_{xP}, the predation rate will be very small (large). This effectively reduces the fluctuation of algal concentration in the model.

Even though the basal metabolism and the algal predation have similar formulations, as described in Eqs. (5.2.28) and (5.2.30), the two processes have different distributions of end products for organic carbon, nitrogen, phosphorus, and silica. The end products of algal predation should be largely particulate organic matter, whereas the end products of basal metabolism should be largely dissolved organic matter and dissolved inorganic matter.

5.2.4.3 Algal Settling. In addition to basal metabolism and algal predation, algal settling is another important mechanism that physically removes algae from the water column. Settling is represented in the algal kinetic equation, Eq. (5.2.6), as $(\partial/\partial z)(\mathrm{WS}_x \cdot B_x)$. Algae is usually slightly heavier than water, thus, settling occurs even though the density difference between algae and water is very small. This process results in the removal of algae from the euphotic zone. In waters with strong vertical mixing, algae settling is usually weak but can still contribute to the overall algal reduction.

Algal settling in natural waters is a complex phenomenon and depends on many factors, such as:

1. The density, size, and shape of the algae.
2. The density, velocity, turbulence strength, and viscosity of the water.

The algal settling velocity may also depend on the model used. In one-layer (or vertically averaged) models, algal settling represents the removal of algal biomass to the benthic sediments and thus is a sink term for the water column. In models with multiple vertical layers, algal settling represents the vertical displacement of algal particles to the lower layer and thus is a sink term for the upper layer while a source term for the lower layer. Therefore, the definition of settling rate is different, depending on the vertical resolution of the model. In addition, a water quality model with one vertical layer might not be able to adequately resolve the vertical transport process, such as upwelling and vertical circulations. Consequently, to compensate for such inadequacy, the one-layer model might also need to specify settling velocities different

from those of a multiple-layer model. It is impractical to calculate the algal setting velocity in a water quality model. Most models specify algal settling velocities as model parameters, such as the ones for three algal groups, WS_c, WS_d and WS_g in Eq. (5.2.6). Published values of algal settling velocities can differ by up to a few orders of magnitude, typically ranging from 0.05–15 m/day (Bowie et al., 1985, Table 6-19).

The settling algae can be a significant source of nutrients to the sediment bed and can play an important role in the sediment diagenesis process. The settled algal biomass undergoes bacterial and biochemical reactions in the bed, and then releases nutrients back to the water column. The sediment diagenesis process discussed in Section 5.7 will establish the linkage of algae and nutrients in the sediment bed to the ones in the water column.

5.2.5 Silica and Diatom

Silica is included in water quality modeling only when diatoms are considered.

Silicon (Si) is a nonmetallic element and is one of the most abundant elements in the earth's crust. Silicon reacts rapidly with oxygen and water, and is usually not in its pure form in Nature. Instead, silicon exists mostly in silicate formations (in rocks). Most silicon is not available to algal uptake due to its insoluble nature. When combined with water, silicates can convert to orthosilicic acid, $Si(OH)_4$, the form that can directly be consumed by diatoms. In eutrophication studies, silica (SiO_2) is often used to represent the silicon needed for diatom growth.

Silica in waterbodies largely originates from the weathering and erosion of rocks on land. Surface runoff carries it into streams and rivers and, then, into lakes and estuaries. Silica from upstream rivers is the dominant external source of silicon to estuaries. Silica sources from human activities are usually minor, including wastewater treatment plants (from household detergents) and paper production industry. Because it is largely from natural sources, silica is usually not selected as a nutrient for algal growth control and eutrophication management.

Silica may become a limiting nutrient for diatom growth. All algae, such as blue-green algae and green algae, require phosphorus and nitrogen as nutrients, but only diatoms also require silica for growth. Diatoms accumulate silica as a structural element in their cell walls. The nutrient ratios, N/Si/P, affect which algae is dominant in a waterbody. Malone et al. (1996) reported that the Chesapeake Bay can exhibit strong Si limitation, with the ratio of available nutrients (Si/P) in the range of 100–300.

Diatoms tend to grow rapidly, if there are adequate nutrients (Si, P, and N) available. In natural waters, diatoms are often dominant in the spring, when large amounts of silica are brought into the system from surface runoff. The diatom bloom ends, after the available silica in water is used up and stored in the diatoms. This nutrient depletion can lead to the sharp decline of diatom

concentrations and the growth of other (nondiatom) algae. As diatoms settle to the bottom of the waterbody, they slowly dissolve and then release silica back into the water column. The silica and diatom cycling in the water column and on the bed is also affected by the concentrations of others nutrients (P and N). The increased P and N loadings from human activities lead to increased diatom production and rapid silica uptake in the water column. The settling of diatoms removes silica from the water column onto the sediment bed resulting in a reduced Si supply to the waterbody and altered N/Si and P/Si ratios. The consequence is that Si is more limited to diatom growth.

As listed in Table 5.1.1, silica can be represented by two state variables: SU and SA. Biogenic silica represents the silica unavailable to diatom growth. Available silica has two phases: dissolved and particulate. The dissolved available silica, *SAd*, represents the silica that is directly available for diatom uptake. The equation for diatoms given in Eq. (5.2.6), is the same as the ones for blue-green algae and green algae. The nutrient limiting function, $f_1(N)$, needs to use Eq. (5.2.14) to include silica into the consideration. Biogenic silica has the following sources and sinks (Cerco and Cole, 1994): (1) diatom basal metabolism (BM_d) and predation (PR_d), (2) dissolution to available silica, (3) settling, and (4) external loads.

The corresponding kinetic equation is

$$\frac{\partial \mathrm{SU}}{\partial t} = (\mathrm{FSP}_d \cdot \mathrm{BM}_d + \mathrm{FSPP} \cdot \mathrm{PR}_d)\mathrm{ASC}_d \cdot B_d - K_{\mathrm{SUA}} \cdot \mathrm{SU} + \frac{\partial}{\partial z}(w_s \cdot \mathrm{SU}) + \frac{\mathrm{WSU}}{V} \tag{5.2.31}$$

where SU = concentration of particulate biogenic silica ($\mathrm{gSi/m^3}$), FSP_d = fraction of metabolized silica by diatoms produced as particulate biogenic silica, FSPP = fraction of predated diatom silica produced as particulate biogenic silica, ASC_d = silica/carbon ratio of diatoms (gSi/gC), K_{SUA} = dissolution rate of particulate biogenic silica ($\mathrm{day^{-1}}$), w_s = settling velocity of cohesive sediment (m/s), and WSU = external loads of particulate biogenic silica (gSi/day).

Available silica includes the following sources and sinks:

1. Diatom basal metabolism (BM_d), predation (PR_d), and uptake (P_d).
2. Settling of sorbed (particulate) available silica.
3. Dissolution from particulate biogenic silica.
4. Sediment–water exchange of dissolved silica in the bottom layer.
5. External loads.

The kinetic equation describing these processes is

$$\frac{\partial \mathrm{SA}}{\partial t} = (\mathrm{FSI}_d \cdot \mathrm{BM}_d + \mathrm{FSIP} \cdot \mathrm{PR}_d - P_d)\mathrm{ASC}_d \cdot B_d + K_{\mathrm{SUA}} \cdot \mathrm{SU} + \frac{\partial}{\partial z}(w_s \cdot \mathrm{SAp}) + \frac{\mathrm{BFSAd}}{\Delta z} + \frac{\mathrm{WSA}}{V} \tag{5.2.32}$$

where SA = concentration of available silica (g Si/m^3), SAd = dissolved available silica (g Si/m^3), SAp = particulate (sorbed) available silica (g Si/m^3), FSI_d = fraction of metabolized silica by diatoms produced as available silica, FSIP = fraction of predated diatom silica produced as available silica, BFSAd = sediment–water exchange flux of available silica (g Si/m^2/day) applied to bottom layer only., Δz = the thickness of the bottom layer in the numerical model, and WSA = external loads of available silica (g Si/day).

The available silica includes both the dissolved (SAd) and the particulate (SAp):

$$\mathrm{SA} = \mathrm{SAd} + \mathrm{SAp} \tag{5.2.33}$$

In Eqs. (5.2.31) and (5.2.32), the terms expressed as a function of diatom biomass (B_d) represent the effects of diatoms on silica, including basal metabolism and predation. Fractions, FSP_d, FSI_d, FSPP and FSIP, account for the silica released by both basal metabolism and predation, and they must satisfy $FSP_d + FSI_d = 1$ for basal metabolism, and FSPP + FSIP = 1 for predation.

Other features of these two equations include

1. Available silica is consumed for diatom growth (P_d), but SU is not.
2. Dissolution (K_{SUA}) converts SU to SA.
3. Only the particulate available silica (SAp) is settleable, instead of the total SA.
4. Only the dissolved available silica (SAd) produced by sediment diagenesis processes in the bed is exchanged on the sediment-water interface, instead of the total SA.

The available silica is sorbed to cohesive sediment and is affected by the sorption–desorption process. Similar to Eqs. (4.3.8) and (4.3.9) for toxics, available silica has the following relationships with sediment:

$$\mathrm{SAp} = \frac{K_{\mathrm{SAp}} \cdot S}{1 + K_{\mathrm{SAp}} \cdot S} \mathrm{SA} \tag{5.2.34}$$

$$\mathrm{SAd} = \frac{1}{1 + K_{\mathrm{SAp}} \cdot S} \mathrm{SA} = \mathrm{SA} - \mathrm{SAp} \tag{5.2.35}$$

where K_{SAp} = partition coefficient for available silica (per g/m^3) and S = sediment concentration (g/m^3).

The dissolution rate, K_{SUA}, is expressed as an exponential function of temperature:

$$K_{\mathrm{SUA}} = K_{\mathrm{SU}} \cdot e^{\mathrm{KT_{SUA}}(T - \mathrm{TR_{SUA}})} \tag{5.2.36}$$

where K_{SU} = dissolution rate of particulate biogenic silica at TR_{SUA} (day^{-1}), KT_{SUA} = effect of temperature on dissolution of particulate biogenic silica

($^oC^{-1}$), and TR_{SUA} = reference temperature for dissolution of particulate biogenic silica (^oC). Equation (5.2.36) has a format similar to Eq. (5.2.28) for basal metabolism and Eq (5.2.30) for predation.

5.2.6 Periphyton

Periphyton is a group of organisms attached to a substrate (e.g., rocks, larger plants, or the bottom of a waterbody). The organisms include algae, fungi, bacteria, and protozoa. Attached algae are the most important group of periphyton and are usually the focus of periphyton studies. When abundant, periphyton removes nutrients from the water column, thereby reducing the risk of algal blooms. Periphyton also is an important food source for invertebrates and fish.

The major characteristic differences between periphyton (attached algae) and other free-floating algae (e.g., blue-green algae, diatoms, and green algae) are

1. Periphyton remains in a fixed location by attaching to the bottom of the waterbody, while other algae float freely in the water column.
2. Periphyton often prevails in lotic systems, such as rivers, while other algae can thrive in waterbodies that may or may not be lotic, such as lakes and estuaries.

Periphyton usually exists in shallow hard-bottom environments and can influence nutrient uptake and diurnal oxygen variability. Periphyton can be sensitive indicators of water quality in lotic systems. Quinn (1991) reported that excessive periphyton growth causes:

1. Reduced clarity, altered color, and floating mats due to sloughed material.
2. Large diurnal fluctuations in pH and DO that can stress or eliminate sensitive species.
3. Blockage of water intake screens and filters.
4. Dense mats on the bed reducing intergravel flow and habitat quality for benthic invertebrates and fish spawning.
5. Restriction or degradation of swimming and other water-based recreation due to aesthetic degradation.

Periphyton has similar growth requirements as other algae (blue-green algae, diatom, and green algae) and is subject to the same basic processes of growth, basal metabolism, and predation. From Eq. (5.2.6), it has the form:

$$\frac{\partial B_m}{\partial t} = (P_m - \mathrm{BM}_m - \mathrm{PR}_m)B_m \tag{5.2.37}$$

where B_m = algal biomass of periphyton (gC/m^2), t = time (day), P_m = production rate of periphyton (day^{-1}), BM_m = basal metabolism rate of periphyton (day^{-1}), and PR_m = predation rate of periphyton (day^{-1}).

The terms of settling loss and external loading in Eq. (5.2.6) are omitted here. The periphyton population is treated as one group and is represented in algal biomass as carbon. Because of the characteristic differences, the modeling techniques for periphyton (attached algae) should be different from those for free-floating algae, including

1. *Horizontal Transport:* Periphyton is attached to the bed and is not subject to hydrodynamic transport.
2. *Flow Velocity:* The availability of nutrients to periphyton can be influenced by flow velocity.
3. *Vertical Settling:* Periphyton does not have settling losses, but instead it may have additional losses due to sloughing or scouring from the bed.
4. *Units:* Periphyton is expressed in terms of areal densities rather than volumetric concentrations.
5. *Availability of Bottom Substrate:* Since periphyton usually present in shallow hard-bottom environments, the features of bottom substrate can also limit periphyton growth.

The production rate of periphyton, P_m, can b expressed as (Warwick et al., 1997; USEPA, 2000d):

$$P_m = \mathrm{PM}_m \cdot f_1(N) \cdot f_2(I) \cdot f_3(T) \cdot f_4(V) \cdot f_5(B_m) \tag{5.2.38}$$

where PM_m = maximum growth rate for periphyton (day^{-1}), $f_1(N)$ = growth limiting function for nutrients ($0 \le f_1 \le 1$), $f_2(I)$ = growth limiting function for light intensity ($0 \le f_2 \le 1$), $f_3(T)$ = growth limiting function for temperature ($0 \le f_3 \le 1$), $f_4(V)$ = growth limiting function for velocity ($0 \le f_4 \le 1$), and $f_5(B_m)$ = growth limiting function for periphyton biomass ($0 \le f_5 \le 1$).

In Eq. (5.2.38), the first three limiting functions, f_1, f_2, and f_3, represent processes similar to those given in Eq. (5.2.7). Growth limiting functions, f_4 and f_5, are added for periphyton growth. Flow velocity has a dual effect on periphyton growth. Water currents enhance periphyton growth by mixing the overlying waters with nutrient-poor waters that develop around cells and by reducing the thickness of the nutrient-depleted laminar boundary layer on the water–periphyton interface (Whitford and Schumacher, 1964). Increased exchange of nutrients between the periphyton and the overlying water increase periphyton growth. Water currents also constantly scour periphyton from its substrate. Horner et al. (1990) reported that periphyton growth is positively correlated to flow velocity to a certain level. Above this level, scouring and sloughing decrease biomass growth.

For simplicity, the growth limiting function for velocity, $f_4(V)$, can be represented by a Michaelis–Menton equation:

$$f_4(V) = \begin{cases} \dfrac{V}{\mathrm{KMV} + V} & V \ge V_{\min} \\ \dfrac{V_{\min}}{\mathrm{KMV} + V_{\min}} & V < V_{\min} \end{cases} \tag{5.2.39}$$

where V = flow velocity (m/s), $V_{\min}$ = reference minimum flow velocity (m/s), and KMV = half saturation velocity (m/s).

The Michaelis–Menton equation limits periphyton growth at low velocities. The half saturation velocity, KMV, is the velocity at which half the maximum growth rate occurs. This approach is analogous to the nutrient limitations discussed in Section 5.2.3. However, the Michaelis–Menton equation is too limiting at low velocities and could lead to no periphyton growth in still waters. To avoid this problem, Eq. (5.2.39) sets $f_4(V)$ to a constant ($=\frac{V_{\min}}{\mathrm{KMV}+V_{\min}}$), when V is very small ($<V_{\min}$).

Equation (5.2.39) does not include the scouring effect that occurs when the flow velocity is very large. A formulation similar to the one for temperature effect, Eq. (5.1.9), can be applied here:

$$f_4(V)=\begin{cases} e^{-\mathrm{KVM1}\cdot(V-V_1)^2} & \text{if } V<V_1 \\ 1.0 & \text{if } V_1\le V\le V_2 \\ e^{-\mathrm{KVM2}\cdot(V-V_2)^2} & \text{if } V>V_2 \end{cases} \tag{5.2.40}$$

where V_1 = lower end of optimal velocity range for periphyton growth, V_2 = upper end of optimal velocity range for periphyton growth, KVM1 = effect of velocity below $V1$ on periphyton growth, and KVM2 = effect of velocity above $V2$ on periphyton growth. Equation (5.2.40) reflects the phenomenon that high velocities may cause scouring and reduction of periphyton. A curve of Eq. (5.2.40) should be similar to the one for temperature in Fig. 5.1.8.

Periphyton growth is also affected by the availability of suitable substrate, and high periphyton density can limit periphyton productivity. A Michaelis–Menton equation can be used to represent this relationship:

$$f_5(B_m)=\frac{\mathrm{KMB}}{\mathrm{KMB}+B_m} \tag{5.2.41}$$

where KMB = half saturation constant for periphyton biomass, ($\mathrm{g\,C/m^2}$) and B_m = algal biomass of periphyton ($\mathrm{g\,C/m^2}$).

Equation (5.2.41) indicates that when there is no periphyton on the bed ($B_m=0$), the limiting function for periphyton density is equal to 1.0 and is not limiting periphyton growth. When B_m is equal to the half saturation constant, KMB, half the maximum growth rate occurs. Caupp et al. (1991) used a KMB value of $5.0\,\mathrm{g\,C/m^2}$ for a river in California.

5.3 ORGANIC CARBON

Carbon is one of the most abundant elements in living matter and is an essential component of organic material. Total carbon consists of organic and inor-

ganic forms that can be both dissolved and particulate. Photosynthesis converts inorganic carbon to organic carbon. Because algae need sunlight to grow, the photosynthesis process only happens in the upper layer of a waterbody where there is sufficient sunlight. As discussed in Chapter 4, inorganic carbon directly affects pH values in the water column. Since it is usually available in excess, inorganic carbon is often excluded in eutrophication models (e.g., Cerco and Cole, 1994), unless pH modeling is involved.

The production of organic carbon is a key process in eutrophication study. The organic carbon cycle consists of photosynthesis, respiration, and decomposition. Because some organic carbons decay at faster rates than others, organic carbon can be divided into those that decay at a fast rate (labile) and those that decay at a slower rate (refractory). In water quality models, organic carbon can be categorized as (Table 5.1.1, Fig. 5.3.1): (1) RPOC, (2) LPOC, and (3) DOC. Total organic carbon is the sum of all organic carbon compounds and can be expressed as:

$$\mathrm{TOC} = \mathrm{RPOC} + \mathrm{LPOC} + \mathrm{DOC} \tag{5.3.1}$$

Labile particulate organic carbon has a decomposition time scale of days to weeks and decays rapidly either in the water column or sediment bed. Refractory particulate organic carbon has a decomposition time scale of months to seasons, after being settled to the sediment bed. Through the sediment diagenesis processes, the settled RPOC in the bed may affect the water quality in the water column for a long time (seasons and even years). Sources of organic carbon include excretion and death of living organisms (e.g., algae) and external loadings (Fig. 5.3.1). The discharges of organic matter from point sources (e. g., wastewater treatment plants) can be a major source of organic carbon, leading to large DO deficits and violation of water quality standards. Organic materials derived from vegetation in the contributing watershed are typically

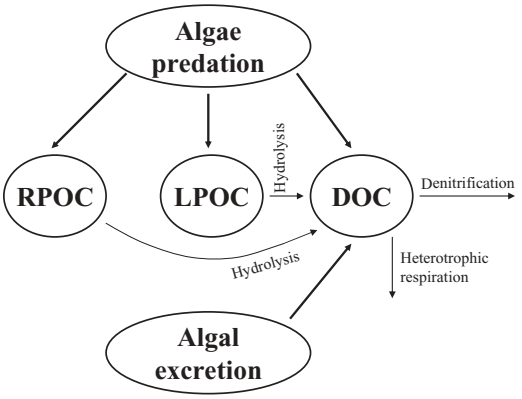

Fig. 5.3.1 Organic carbon state variables and their transformations.

low in LPOC and high in RPOC. Organic materials from fertilizers and municipal wastewater often have a high LPOC content.

Organic carbon transformations are represented in a cascade approach (Fig. 5.3.1):

1. Algal predation and algal excretion contribute to RPOC, LPOC, and DOC.
2. Hydrolysis converts RPOC and LPOC to DOC.
3. Denitrification and heterotrophic respiration remove DOC.

5.3.1 Decomposition of Organic Carbon

Bacteria decompose organic material to obtain energy for growth, break it down into simpler organic substances, and eventually convert it into inorganic substances. This decomposition exerts an oxygen demand and removes DO from the water column. A simplified representation of this decomposition is the same as the equation for respiration, Eq. (5.2.25), and is given by the following:

$$C_6H_{12}O_6 + O_2 \xrightarrow{\text{energy released}} CO_2 + H_2O \tag{5.3.2}$$

where glucose ($C_6H_{12}O_6$) represents organic compounds. The chemical energy released by the conversion of glucose to carbon dioxide and water is used for various cell processes. Equation (5.3.2) represents the reaction opposite to the one shown in Eq. (5.2.15) for photosynthesis. Equation (5.3.2) indicates that oxygen is required to oxidize organic material, which can be an important source for oxygen depletion in an aquatic system. The dynamics of carbon and oxygen are closely related. Oxygen is produced when organic carbon is produced, while oxygen is consumed when organic carbon is decomposed.

Under anaerobic conditions, certain bacteria can use nitrate instead of oxygen, but they present only in the sediment bed or in the bottom of a stratified waterbody, after prolonged oxygen depletion has occurred. When insufficient oxygen is available, the resulting anaerobic decomposition is performed by completely different microorganisms. They produce end products that can be highly objectionable, including hydrogen sulfide (H_2S), ammonia (NH_3), and methane (CH_4). Anaerobic decomposition can be represented by the following:

$$\text{Organic matter} \xrightarrow{\text{micoorganisms}} CO_2 + CH_4 + \text{New cells} + \text{Unstable products} \tag{5.3.3}$$

5.3.2 Equations for Organic Carbon

For brevity, all forms of carbon discussed in this book represent concentrations as carbon. For example, a concentration of 10-mg/L dissolved organic carbon

refers to 10 mg of carbon in the form of dissolved organic carbon in 1 L of water.

Except for the time scale of decomposition, LPOC and RPOC have similar properties and are primarily controlled by the following processes (Fig. 5.3.1): (1) algal predation, (2) hydrolysis to DOC, (3) settling, and (4) external loads. Consequently, the governing equation for particulate organic carbon (POC) should have the following format:

$$\text{Net change of POC} = \text{algal predation} - \text{hydrolysis} - \text{settling} + \text{external loads} \tag{5.3.4}$$

In Eq. (5.3.4), the algal predation includes all kinds of algae, including cyanobacteria (blue-green algae), diatoms, and green algae. Mathematically, Eq. (5.3.4) can be written for RPOC and LPOC as (Cerco and Cole, 1994):

$$\frac{\partial \text{RPOC}}{\partial t} = \sum_{x=c,d,g} \text{FCRP} \cdot \text{PR}_x \cdot B_x - K_{\text{RPOC}} \cdot \text{RPOC} + \frac{\partial}{\partial z}(\text{WS}_{\text{RP}} \cdot \text{RPOC}) + \frac{\text{WRPOC}}{V} \tag{5.3.5}$$

and

$$\frac{\partial \text{LPOC}}{\partial t} = \sum_{x=c,d,g} \text{FCLP} \cdot \text{PR}_x \cdot B_x - K_{\text{LPOC}} \cdot \text{LPOC} + \frac{\partial}{\partial z}(\text{WS}_{\text{LP}} \cdot \text{LPOC}) + \frac{\text{WLPOC}}{V} \tag{5.3.6}$$

where RPOC = concentration of refractory particulate organic carbon (g C/m^3), LPOC = concentration of labile particulate organic carbon (g C/m^3), FCRP = fraction of predated carbon produced as refractory particulate organic carbon, FCLP = fraction of predated carbon produced as labile particulate organic carbon, K_{RPOC} = hydrolysis rate of refractory particulate organic carbon (day^{-1}), K_{LPOC} = hydrolysis rate of labile particulate organic carbon (day^{-1}), WS_{RP} = settling velocity of refractory particulate organic matter (m/day), WS_{LP} = settling velocity of labile particulate organic matter (m/day), WRPOC = external loads of refractory particulate organic carbon (g C/day), and WLPOC = external loads of labile particulate organic carbon (g C/day).

The processes for DOC are more complicated than the ones for RPOC and LPOC (Fig. 5.3.1). They include: (1) algal excretion, (2) algal predation, (3) hydrolysis from RPOC, (4) hydrolysis from LPOC, (5) heterotrophic respiration of DOC, (6) denitrification, and (7) external loads. This yields

$$\text{Net change of DOC} = \text{algal excretion} + \text{algal predation} + \text{RPOC hydrolysis} + \text{LPOC hydrolysis} - \text{DOC heterotrophic respiration} - \text{denitrification} + \text{external loads} \tag{5.3.7}$$

These seven processes control the variation of DOC concentration and lead to the following governing equation for DOC:

$$\frac{\partial \mathrm{DOC}}{\partial t} = \sum_{x=c,d,g}\left[\mathrm{FCD}_x + (1-\mathrm{FCD}_x)\frac{\mathrm{KHR}_x}{\mathrm{KHR}_x + \mathrm{DO}}\right]\mathrm{BM}_x \cdot B_x + \sum_{x=c,d,g}\mathrm{FCDP}\cdot\mathrm{PR}_x \cdot B_x + K_{\mathrm{RPOC}}\cdot\mathrm{RPOC} + K_{\mathrm{LPOC}}\cdot\mathrm{LPOC} - K_{\mathrm{HR}}\cdot\mathrm{DOC} - \mathrm{Denit}\cdot\mathrm{DOC} + \frac{\mathrm{WDOC}}{V} \tag{5.3.8}$$

where DOC = concentration of dissolved organic carbon ($\mathrm{gC/m^3}$) FCD_x = a constant for algal group x ($0 < \mathrm{FCD}_x < 1$), KHR_x = half saturation constant of DO for algal DOC excretion for group x ($\mathrm{gO_2/m^3}$) DO = dissolved oxygen concentration ($\mathrm{gO_2/m^3}$), FCDP = fraction of predated carbon produced as dissolved organic carbon, K_{HR} = heterotrophic respiration rate of dissolved organic carbon ($\mathrm{day^{-1}}$), Denit = denitrification rate ($\mathrm{day^{-1}}$) given in Eq. (5.5.31), and WDOC = external loads of dissolved organic carbon (gC/day).

Two algal processes affect organic carbon concentrations: algal excretion and algal predation by zooplankton. They are represented by the terms with summation ($\Sigma_{x=c,d,g}$) in Eqs. (5.3.5), (5.3.6), and (5.3.8). In the governing equation for algae, Eq. (5.2.6), the basal metabolism term ($-\mathrm{BM}_x \cdot \mathrm{B}_x$)actually includes two separated processes: the algal excretion and respiration. While both processes reduce algal concentration, they have different end products of organic carbon. Respiration produces CO_2, while excretion primarily produces dissolved organic carbon. The CO_2 from respiration is an inorganic form and is often excluded in the eutrophication modeling (e.g., Cerco and Cole, 1994). The DOC from excretion is included in the first term on RHS of Eq. (5.3.8). Zooplankton consumes algae and recycles carbon back to the water as RPOC, LPOC, and DOC. Since zooplankton are not modeled directly, three empirical parameters, FCRP, FCLP, and FCDP, are used to distribute algal carbon among RPOC, LPOC, and DOC, and their summation should be equal to 1.0, as follows:

$$\mathrm{FCRP} + \mathrm{FCLP} + \mathrm{FCDP} = 1.0 \tag{5.3.9}$$

5.3.3 Heterotrophic Respiration and Dissolution

The fifth term on the RHS of Eq. (5.3.8), $-\mathrm{K_{HR}}\cdot\mathrm{DOC}$, represents the heterotrophic respiration that converts DOC into CO_2. Heterotrophic respiration needs oxygen. A Michaelis–Menton function can be used to represent the dependency of heterotrophic respiration rate, K_{HR}, on DO concentration. It has the form:

$$K_{\mathrm{HR}} = \frac{\mathrm{DO}}{\mathrm{KHOR_{DO}} + \mathrm{DO}} K_{\mathrm{DOC}} \tag{5.3.10}$$

where $KHOR_{DO}$ = oxic respiration half saturation constant for DO ($g\,O_2/m^3$) and K_{DOC} = heterotrophic respiration rate of dissolved organic carbon at infinite dissolved oxygen concentration (day^{-1}).

The dissolution (hydrolysis) rates of RPOC and LPOC and the heterotrophic respiration rate of DOC, K_{RPOC}, K_{LPOC}, and K_{DOC}, can be specified by the following:

$$K_{RPOC} = (K_{RC} + K_{RCalg} \sum_{x=c,d,g} B_x) \cdot e^{KT_{HDR}(T-TR_{HDR})} \tag{5.3.11}$$

$$K_{LPOC} = (K_{LC} + K_{LCalg} \sum_{x=c,d,g} B_x) \cdot e^{KT_{HDR}(T-TR_{HDR})} \tag{5.3.12}$$

$$K_{DOC} = (K_{DC} + K_{DCalg} \sum_{x=c,d,g} B_x) \cdot e^{KT_{MNL}(T-TR_{MNL})} \tag{5.3.13}$$

where K_{RC} = minimum dissolution rate of refractory particulate organic carbon (day^{-1}), K_{LC} = minimum dissolution rate of labile particulate organic carbon (day^{-1}), K_{DC} = minimum respiration rate of DOC (day^{-1}), K_{RCalg} and K_{LCalg} = constants that relate dissolution of refractory and labile particulate organic carbon, respectively, to algal biomass ($day^{-1}/g\,C/m^3$), K_{DCalg} = constant that relates respiration to algal biomass ($day^{-1}/g\,C/m^3$) KT_{HDR} = effect of temperature on hydrolysis of particulate organic matter ($^oC^{-1}$), TR_{HDR} = reference temperature for hydrolysis of particulate organic matter (^oC), KT_{MNL} = effect of temperature on mineralization of dissolved organic matter ($^oC^{-1}$), and TR_{MNL} = reference temperature for mineralization of dissolved organic matter (^oC).

Equation (5.3.11)–(5.3.13) indicate that RPOC and LPOC are converted to DOC via an hydrolysis process, while DOC is converted to CO_2 via a mineralization process. Hydrolysis and mineralization are both discussed in Section 4.4, and will also be used to describe the conversions of organic phosphorus and organic nitrogen later in this chapter.

5.4 PHOSPHORUS

Phosphorus (P) is one of the key nutrients for algal growth. Unlike nitrogen, which is very soluble, phosphorus has low solubility and is strongly sorbed to suspended solids that settle out of the water column. This settling can lead to a build-up of phosphorus on the bed. Nitrogen has a gaseous form (N_2), but phosphorus does not. Although algae consume much less phosphorus than nitrogen, phosphorus plays a key role in algal growth. Phosphorus is often the limiting nutrient, especially in freshwaters. Phosphorus concentrations in streams in pristine (unaffected by human activities) areas generally are small. Stream sampling in 63 relatively unaffected basins indicated a median total phosphorus concentration of 0.016 mg/L (Alexander et al., 1996). Phosphorus is not a toxic element, unless it is present in very high levels. The primary concern about high phosphorus concentrations in a waterbody has to do with excessive aquatic plant productivity and eutrophication. The rapid growth of

aquatic vegetation and/or increase in the algal population is detrimental to the ecosystem, causing high algal biomass, excessive growth of macrophytes, reduced transparency, and oxygen depletion.

The main natural reservoirs of phosphorus are poorly soluble minerals. Erosion of these minerals from terrestrial sources and their runoff to surface waters are important sources of new phosphorus. Prior to widespread phosphate bans in detergents, surface waters received a considerable portion of phosphorus from detergents. The ban resulted in decreased P concentrations in many waters. Point sources of P include wastewater treatment plants and industrial discharges. Nonpoint sources include natural weathering of rocks and minerals, surface runoff, atmospheric deposition, and direct input by animals. In pristine natural waters, the primary source of P is runoff from the watershed and flux from the sediment bed. The atmospheric deposition of phosphorus is relatively small. Phosphorus used in agriculture, industry, and other human activities lead to increased loadings to receiving waters. Excessive P loadings may cause algal bloom or nuisance growth of aquatic plants. Therefore, limiting the point and nonpoint sources of P is essential to eutrophication control.

Phosphorus exists in organic and inorganic forms. Both forms include particulate and dissolved phases. Total phosphorus is a measure of all forms of phosphorus and is widely used for setting trophic state criteria. As shown in Table 5.1.1 and in Fig. 5.4.1, TP can be split into the following state variables in a water quality model: (1) RPOP, (2) LPOP, (3) DOP, and (4) PO4t.

The relative proportion of each form depends on the nature and origin of these materials. Inorganic P compounds can be associated with different forms of Fe, Al, Ca, and other elements. Organic P forms are generally associated with living organisms, and consist of easily decomposable P compounds (LPOP)

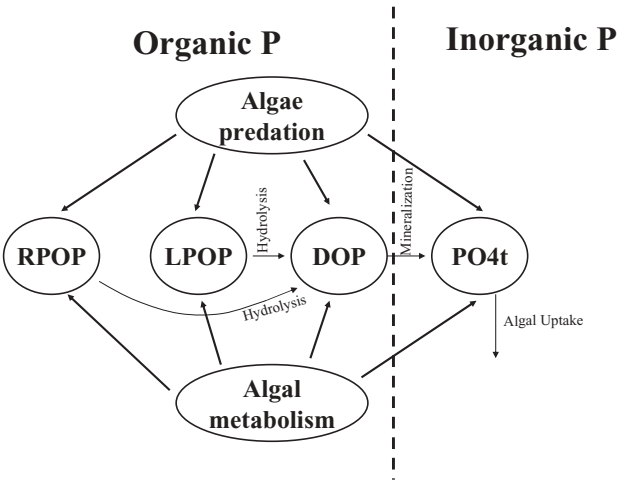

Fig. 5.4.1 Phosphorus state variables and their transformations.

and slowly decomposable organic P compounds (RPOP). The inorganic phosphorus is summarized as total phosphate (PO4t), which includes both the dissolved and the particulate phases of phosphate. The particulate phosphate (PO4p) is assumed to be in equilibrium condition with the dissolved phosphate (PO4d) via a partition process. The PO4d represents the phosphorus that can be directly taken by algae, although some assimilation of organic phosphorus may occur, especially during periods of P deficiencies. Soluble reactive phosphorus (SRP) is a mixture of dissolved inorganic and organic species measured by the method described by APHA (2000).The SRP represents P that is readily available to algae and aquatic plants. In water quality modeling studies, PO4d is often compared with the measured SRP data in model–data comparison. The SRP may overestimate the concentration of PO4d, since SRP is actually a combination of orthophosphorus and low molecular weight organic phosphorus. The low molecular weight organic phosphorus components are rapidly cycled and ultimately taken up by algae; thus, SRP is still an acceptable measure of dissolved bioavailable phosphorus (Sheng and Chen, 1993).

Fig 5.4.1 describes the transformations between P state variables. The major internal sources of P are algal metabolism and algal predation by zooplankton. Algae are consumed by zooplankton, which return the nutrients back into the system via zooplankton death, mostly in organic forms. Particulate organic phosphorus represents living and dead particulate matter, such as algae and detritus. Dissolved organic phosphorus includes organic phosphorus excreted by organisms and soluble P compounds. Dissolved phosphate interacts with particulate phosphate via a sorption–desorption mechanism. Dissolved phosphate is taken up by algae for growth and is incorporated into algal biomass. In water quality models (e.g., Cerco and Cole, 1994), the organic forms undergo hydrolysis and mineralization or bacterial decomposition into inorganic phosphorus before algae can consume them.

Phosphorus transformations can be represented in a cascade approach (Fig. 5.4.1): (1) hydrolysis converts RPOP and LPOP to DOP, (2) mineralization converts DOP to PO4t, and (3) algal uptake PO4d for growth.

The fate and transport processes of phosphate are strongly influenced by the sediment processes. Fig. 4.3.1 illustrates the fate and transport processes for a toxicant and is also helpful for explaining key factors that determine the fate and transport of phosphates, except that phosphates do not experience the bioaccumulation shown in Fig. 4.3.1. The total phosphate includes particulate and dissolved phases in the sediment bed and in the water column. The atmosphere can add phosphorus into the water column via air deposition, and the phosphates can be buried into the deep sediment layer and be permanently removed from the waterbody. Algae also consume dissolved phosphate for growth. The key processes include

1. Inflow and outflow.
2. Settling of the particulate phosphorus in the water column.
3. Sorption and desorption in both the water column and the bed.

4. Exchange between the water column and the bed via deposition/resuspension and diffusion.
5. Losses by burial.
6. Algal uptake and metabolism.

The phosphorus and sediments in suspension are advected and dispersed in the water column, where dissolved phosphorus sorbs to sediment particles under aerobic conditions. Subsequent settling of the suspended sediments and sorbed phosphorus can provide a significant loss mechanism of phosphorus from the water column to the sediment bed. In the water column and the sediment bed, interchange between the dissolved and the particulate phosphorus occurs via the sorption/desorption process. Bed sediments can be scoured and enter the water column, whereas suspended sediments can undergo settling and be deposited on the bed. Under anaerobic conditions, the phosphate sorbed to sediment particles may become dissolved again and becomes bioavailable. This reabsorption is a key component of the growth and decay cycle. Dissolved phosphate in pore water of the sediment bed may diffuse to the overlying water column and vice versa, depending on the concentration difference between the two.

The above processes for phosphates are similar to the ones for toxicants described in Section 4.3 in many ways. However, differences between the two include

1. Toxicants can be removed from the water column via bioaccumulation and transformation, whereas dissolved phosphate is taken up by algae for growth.
2. Some toxicants can be converted into a gaseous phase and released into the atmosphere via volatilization, but phosphate cannot.

Phosphorus processes are closely linked to sediment processes, especially in large, shallow waters. It is critical to have a good representation of sediment processes, before phosphorus processes can be described realistically. For example, phosphorus is of particular concern in Lake Okeechobee, FL (SFWMD, 2002; Jin and Ji, 2005). The annual mean P concentration has increased dramatically from 55 μg/L in 1973 to >110 μg/L in 2000. Wind-induced sediment resuspension is estimated to transport 6–18 times the amount of P to the water column as diffusive flux, and up to six times the amount of P in external loads.

5.4.1 Equations for Phosphorus State Variables

For brevity, all forms of phosphorus discussed in this book represent concentrations as phosphorus. For example, an orthophosphate concentration expressed as 10 mg/L refers to an orthophosphate concentration of 10 mg/L as phosphorus. As listed in Table 5.1.1 and Fig. 5.4.1, the EFDC model uses four

state variables for phosphorus: three organic forms (refractory particulate, labile particulate and dissolved) and one inorganic form (total phosphate).

5.4.1.1 Particulate Organic Phosphorus. As illustrated in Figs. 5.1.5 and 5.4.1, the POP are largely determined by (1) algal metabolism, (2) algal predation, (3) hydrolysis of POP to dissolved organic phosphorus, (4) settling, and (5) external loads.

The kinetic equation for POP (RPOP and LPOP) can be described as:

$$\text{The change of POP} = \text{Algal basal metabolism} + \text{algal predation} - \text{POP hydrolysis} - \text{settling} + \text{external source} \quad (5.4.1)$$

Therefore, the kinetic equations for RPOP and LPOP are (Cerco and Cole, 1994; Park et al., 1995):

$$\frac{\partial \text{RPOP}}{\partial t} = \sum_{x=c,d,g} (\text{FPR}_x \cdot \text{BM}_x + \text{FPRP} \cdot \text{PR}_x)\text{APC} \cdot B_x - K_{\text{RPOP}} \cdot \text{RPOP} + \frac{\partial}{\partial z}(\text{WS}_{\text{RP}} \cdot \text{RPOP}) + \frac{\text{WRPOP}}{V} \quad (5.4.2)$$

and

$$\frac{\partial \text{LPOP}}{\partial t} = \sum_{x=c,d,g} (\text{FPL}_x \cdot \text{BM}_x + \text{FPLP} \cdot \text{PR}_x)\text{APC} \cdot B_x - K_{\text{LPOP}} \cdot \text{LPOP} + \frac{\partial}{\partial z}(\text{WS}_{\text{LP}} \cdot \text{LPOP}) + \frac{\text{WLPOP}}{V} \quad (5.4.3)$$

where RPOP = concentration of refractory particulate organic phosphorus (g P/m^3), LPOP = concentration of labile particulate organic phosphorus (g P/m^3), FPR_x = fraction of metabolized phosphorus by algal group x produced as RPOP, FPL_x = fraction of metabolized phosphorus by algal group x produced as LPOP, FPRP = fraction of predated phosphorus produced as RPOP, FPLP = fraction of predated phosphorus produced as LPOP, APC = mean phosphorus/carbon ratio in all algal groups (g P/g C), K_{RPOP} = hydrolysis rate of RPOP (day^{-1}), K_{LPOP} = hydrolysis rate of LPOP (day^{-1}), WRPOP = external loads of RPOP (g P/day), and WLPOP = external loads of LPOP (g P/day).

5.4.1.2 Dissolved Organic Phosphorus. Major processes affecting dissolved organic phosphorus are (Figs. 5.1.5 and 5.4.1): (1) algal metabolism, (2)algal predation, (3) hydrolysis from RPOP and LPOP, (4) mineralization to phosphate phosphorus, and (5) external loads.

These processes can be expressed as:

$$\text{The change of DOP} = \text{Algal basal metabolism} + \text{algal predation} + \text{POP hydrolysis} - \text{mineralization} + \text{external source} \tag{5.4.4}$$

The corresponding kinetic equation is

$$\frac{\partial \text{DOP}}{\partial t} = \sum_{x=c,d,g} (\text{FPD}_x \cdot \text{BM}_x + \text{FPDP} \cdot \text{PR}_x)\text{APC} \cdot B_x + K_{\text{RPOP}} \cdot \text{RPOP} + K_{\text{LPOP}} \cdot \text{LPOP} - K_{\text{DOP}} \cdot \text{DOP} + \frac{\text{WDOP}}{V} \tag{5.4.5}$$

where DOP = concentration of dissolved organic phosphorus (gP/m^3), FPD_x = fraction of metabolized phosphorus by algal group x produced as DOP, FPDP = fraction of predated phosphorus produced as DOP, K_{DOP} = mineralization rate of DOP (day^{-1}), and WDOP = external loads of DOP (gP/day).

Comparing Eqs. (5.4.2), (5.4.3), and (5.4.5) for organic phosphorus with Eqs. (5.3.5), (5.3.6), and (5.3.8) for organic carbon reveals that the two sets of kinetic equations are mathematically very similar.

5.4.1.3 Total Phosphate. Total phosphate (PO4t) includes dissolved phosphate (PO4d) and sorbed phosphate (PO4p):

$$\text{PO4t} = \text{PO4d} + \text{PO4p} \tag{5.4.6}$$

The amount of total phosphate in a waterbody depends on

1. Algal metabolism, predation, and uptake.
2. Mineralization from dissolved organic phosphorus.
3. Settling of PO4p.
4. Exchange of PO4d at the sediment bed–water column interface.
5. External loads.

The corresponding kinetic equation is

$$\frac{\partial \text{PO4}t}{\partial t} = \sum_{x=c,d,g} (\text{FPI}_x \cdot \text{BM}_x + \text{FPIP} \cdot \text{PR}_x - P_x)\text{APC} \cdot B_x + K_{\text{DOP}} \cdot \text{DOP} + \frac{\partial}{\partial z}(\text{WS}_{\text{TSS}} \cdot \text{PO4p}) + \frac{\text{BFPO4d}}{\Delta z} + \frac{\text{WPO4t}}{V} \tag{5.4.7}$$

where PO4t = total phosphate (gP/m^3), PO4p = particulate (sorbed) phosphate (gP/m^3), FPI_x = fraction of metabolized phosphorus by algal group x produced as inorganic phosphorus, FPIP = fraction of predated phosphorus

produced as inorganic phosphorus, WS_{TSS} = settling velocity of suspended sediment (m/day), provided by the sediment model, BFPO4d = sediment–water exchange flux of phosphate (g P/m^2/day), applied to the bottom layer only, and WPO4t = external loads of total phosphate (g P/day).

5.4.2 Phosphorus Processes

This section discusses the following processes that affect phosphorus concentrations:

1. Sorption and desorption of phosphate to sediment particles.
2. Algal metabolism and algal predation.
3. Mineralization and hydrolysis.

5.4.2.1 Sorption and Desorption of Phosphate. The mathematical description of sorption and desorption of phosphate is similar to that of the sorption and desorption of toxicants described in Section 4.3.3.

In the presence of oxygen, dissolved phosphates combine with suspended particles. These particles eventually settle to the sediment bed and are temporarily removed from the cycling process. The settling of suspended solids and sorbed phosphorus can provide a significant loss mechanism of phosphorus from the water column to the bed. The sorption–desorption processes of phosphate are much faster than those for biological kinetics. The former are on the order of minutes; the latter are on the order of days. This difference permits an instantaneous equilibrium assumption for the calculation of phosphate. The dissolved phosphate and the particulate (sorbed) phosphate can then be treated as a single state variable in a water quality model. Similar to the discussions on toxicants in Section 4.3.3, the dissolved and particulate phosphates may be expressed as:

$$\mathrm{PO4p} = \frac{K_{\mathrm{PO4p}} \cdot S}{1 + K_{\mathrm{PO4p}} \cdot S} \mathrm{PO4t} \tag{5.4.8}$$

$$\mathrm{PO4d} = \frac{1}{1 + K_{\mathrm{PO4p}} \cdot S} \mathrm{PO4t} \tag{5.4.9}$$

where K_{PO4p} = partition coefficient of phosphate (m^3/g) and S = sediment concentration (g/m^3).

Equation (5.4.8) and (5.4.9) for phosphates are similar to Eqs. (4.3.8) and (4.3.9) for the toxicants. Phosphates are most likely to sorb to cohesive sediment. When concentrations of both cohesive sediment and noncohesive sediment are available, it is the cohesive sediment concentration (not the total sediment concentration) that should be used in Eqs. (5.4.8) and (5.4.9). In order to simulate the water quality and eutrophication processes realistically, it is necessary to describe the sediment process in detail.

Dividing Eq. (5.4.8) by Eq. (5.4.9) gives

$$K_{\mathrm{PO4p}} = \frac{\mathrm{PO4p}}{\mathrm{PO4d}} \frac{1}{S} \tag{5.4.10}$$

The meaning of K_{PO4p} becomes apparent in Eq. (5.4.10): the partition coefficient is the ratio of the particulate concentration to the dissolved concentration per unit concentration of suspended solid. When measurements of PO4p, PO4d, and S are available, K_{PO4p} can be estimated using Eq. (5.4.10). A wide range of partition coefficients for phosphorus is found in the literature, with typical values ranging from 0.01 to 0.1 m^3/g (Cerco and Cole, 1994; Park et al., 1995).

5.4.2.2 Effects of Algae on Phosphorus. As algae grow, dissolved inorganic phosphorus (PO4d) is taken up, stored, and incorporated into algal biomass. Living algal cells are a major component of the total phosphorus pool in the water. Settling of algae to the bottom sediments is a major loss pathway of phosphorus from the water column. As algae respire and die, algal biomass (and the phosphorus) is recycled to nonliving organic and inorganic matters. The effects of algae are represented by the summation terms ($\sum_{x=c,d,g}$) in Eqs. (5.4.2), (5.4.3), (5.4.5), and (5.4.7) and are illustrated in Fig. 5.4.1. The total algal loss by basal metabolism, that is, the term of $\mathrm{BM}_x \cdot \mathrm{B}_x$ in Eq. (5.2.6), is split using distribution coefficients FPR_x, FPL_x, FPD_x, and FPI_x, and they should satisfy:

$$\mathrm{FPR}_x + \mathrm{FPL}_x + \mathrm{FPD}_x + \mathrm{FPI}_x = 1 \tag{5.4.11}$$

where x = c, d, and g, representing cyanobacteria (blue-green algae), diatoms, and green algae, respectively.

The algal predation is accounted for by the terms associated with PR_x, the predation rate of algal group x. The total loss by predation, the term of $\mathrm{PR}_x \cdot \mathrm{B}_x$ in Eq. (5.2.6), is split using distribution coefficients, FPRP, FPLP, FPDP, and FPIP:

$$\mathrm{FPRP} + \mathrm{FPLP} + \mathrm{FPDP} + \mathrm{FPIP} = 1 \tag{5.4.12}$$

Algae consume PO4d for growth, and algal uptake of phosphate is represented by $(-\mathrm{P}_x \cdot \mathrm{APC} \cdot \mathrm{B}_x)$ in Eq. (5.4.7). In water quality models, algal biomass is often expressed in units of carbon per volume of water. In order to estimate the nutrients contained in algal biomass, the ratio of phosphorus-to-carbon, APC, should be known.

Algal composition varies as a function of nutrient availability and adapts to ambient phosphorus concentration. When the concentrations of available phosphorus and nitrogen are low, algae adjust their composition so that smaller

quantities of these nutrients are needed to produce carbonaceous biomass (Di Toro, 1980). Algal phosphorus content is high when ambient phosphorus is high, and is low when ambient phosphorus is low. Based on measured data, Cerco and Cole (1994) reported large variations of the algal phosphorus/carbon ratio and used the following empirical formulation to estimate the algal phosphorus/carbon ratio:

$$\mathrm{APC} = \frac{1}{\mathrm{CP_{prm1}} + \mathrm{CP_{prm2}} \cdot e^{-\mathrm{CP_{prm3}} \cdot \mathrm{PO4d}}} \tag{5.4.13}$$

where $\mathrm{CP_{prm1}}$ = minimum carbon/phosphorus ratio (g C/g P), $\mathrm{CP_{prm2}}$ = difference between minimum and maximum carbon/phosphorus ratio (g C/g P), and $\mathrm{CP_{prm3}}$ = effect of dissolved phosphate concentration on carbon/phosphorus ratio (per g P/m^3).

5.4.2.3 Mineralization and Hydrolysis. Organic nutrients undergo hydrolysis and mineralization to become inorganic nutrients before being consumed by algae. The hydrolysis of particulate organic phosphorus is represented by the term of K_{RPOP} in Eq. (5.4.2) and the term of K_{LPOP} in Eq. (5.4.3). The mineralization of dissolved organic phosphorus is represented by the term of K_{DOP} in Eq. (5.4.5). The formulations for hydrolysis and mineralization rates are (Park et al., 1995):

$$K_{\mathrm{RPOP}} = \left(K_{\mathrm{RP}} + \frac{\mathrm{KHP}}{\mathrm{KHP} + \mathrm{PO4d}} K_{\mathrm{RPalg}} \sum_{x=c,d,g} B_x \right) \cdot e^{\mathrm{KT_{HDR}}(T - \mathrm{TR_{HDR}})} \tag{5.4.14}$$

$$K_{\mathrm{LPOP}} = \left(K_{\mathrm{LP}} + \frac{\mathrm{KHP}}{\mathrm{KHP} + \mathrm{PO4d}} K_{\mathrm{LPalg}} \sum_{x=c,d,g} B_x \right) \cdot e^{\mathrm{KT_{HDR}}(T - \mathrm{TR_{HDR}})} \tag{5.4.15}$$

$$K_{\mathrm{DOP}} = \left(K_{\mathrm{DP}} + \frac{\mathrm{KHP}}{\mathrm{KHP} + \mathrm{PO4d}} K_{\mathrm{DPalg}} \sum_{x=c,d,g} B_x \right) \cdot e^{\mathrm{KT_{MNL}}(T - \mathrm{TR_{MNL}})} \tag{5.4.16}$$

where K_{RP} = minimum hydrolysis rate of refractory particulate organic phosphorus (day^{-1}), K_{LP} = minimum hydrolysis rate of labile particulate organic phosphorus (day^{-1}), K_{DP} = minimum mineralization rate of dissolved organic phosphorus (day^{-1}), K_{RPalg} and K_{LPalg} = constants that relate the hydrolysis of refractory and labile particulate organic phosphorus to algal biomass (day^{-1}/g C/m^3), K_{DPalg} = constant that relates mineralization to algal biomass (day^{-1}/g C/m^3), and KHP = mean half saturation constant for algal phosphorus uptake (g P/m^3).

The mean half saturation constant for algal phosphorus uptake, KHP, is calculated using

$$\mathrm{KHP} = \frac{1}{3} \sum_{x=c,d,g} \mathrm{KHP}_x \tag{5.4.17}$$

Equations (5.4.14)–(5.4.16) reveal that these rates are functions of water temperature and dissolved phosphate, and their values increase exponentially with water temperature.

5.5 NITROGEN

Nitrogen is essential to the production of plant and animal tissue. It is a key constituent of organic matter and is used primarily by plants and animals to synthesize protein. Protein averages ~16% nitrogen. While nitrogen is an indispensable nutrient for aquatic plant growth, too much nitrogen is harmful to the ecosystem. Nitrogen exists in several chemical forms and the nitrogen cycle is complex (Fig. 5.1.4). Some bacteria and blue-green algae, via nitrogen fixation, can extract nitrogen gas from the atmosphere and transform it into organic nitrogen. Some other bacteria release nitrogen gas back into the atmosphere via a denitrification process.

It may seem unusual that nitrogen could limit algal growth, given that the atmosphere is ~78% nitrogen gas; however, only a few life-forms (e.g., blue-green algae) have the ability to fix nitrogen gas directly from the atmosphere. Most algal species can use nitrogen only if it is in inorganic and dissolved forms, such as NH_4 or NO_3. A nitrogen limited system is often a greater problem than a phosphorus limited system. In many eutrophic waters, algal blooms are primarily due to blue-green algae that can directly fix atmospheric nitrogen. Thus, eliminating manmade nitrogen sources may have a very limited effect on improving the eutrophic condition in these waters.

In addition to being an essential nutrient to algal growth, nitrogen also plays important roles in other water quality processes and may constitute a problem in its own right. For example:

1. The oxidation of NH_4 to NO_3 during the nitrification process consumes oxygen and may contribute significantly to the oxygen depletion of a waterbody.
2. High concentrations of un-ionized NH_3 can be toxic to aquatic life.
3. The common form of nitrogen in water is NO_3, which itself is not toxic. However, bacteria in the intestinal tract of infants can convert nitrates to highly reactive NO_2, which may cause the so-called "blue baby" syndrome and death from suffocation. There are strict regulations governing the amount of nitrate that can be present in drinking water.

Nitrogen and phosphorus are major nutrients in an aquatic system. There are important differences between the two:

1. *Fixation:* Nitrogen can be fixed from the atmosphere in the form of nitrogen gas (N_2) by some bacteria and blue-green algae, whereas phosphorus cannot. Thus, controlling N sources is more difficult than controlling P sources.

2. *Oxygen Consumption:* Nitrogen processes can consume DO via oxidation of ammonia to nitrate (nitrification process), whereas phosphorus process cannot uptake DO via the transformation of one form of phosphorus to another.
3. *Toxicity:* One form of nitrogen, NH_3, can be toxic to fish and other aquatic organisms, hereas phosphorus is generally nontoxic in an aquatic system.
4. *Denitrification:* Nitrite and nitrate nitrogen can be converted to N_2 and then removed from the waterbody to the atmosphere, whereas no forms of phosphorus can. Denitrification can be a major mechanism of nitrogen reduction.
5. *Settling:* Forms of nitrogen are not strongly attached to suspended sediments and therefore do not settle with the suspended sediments to the sediment bed, whereas phosphorus can sorb to the suspended solids and total phosphorus concentration can be significantly influenced by the sorption–desorption process and sediment settling.

These differences illustrate that the two nutrients behave differently in the eutrophication processes and that different approaches should be used for eutrophication control and water quality management. When the available phosphate is depleted and becomes the limiting nutrient, no additional phosphorus supplies are available from the atmosphere. Nitrogen, on the other hand, can be fixed directly from the atmosphere by blue-green algae and some bacteria, which makes the control of nitrogen sources more difficult. In addition, nitrogen is not as often limiting to plant growth as phosphorus in many natural waters, especially in freshwaters. Thus, most of the eutrophication management efforts are focused on phosphorus control.

5.5.1 Forms of Nitrogen

Nitrogen exists in many chemical forms (compounds or species), both organic and inorganic. It occurs in the gas, dissolved, and particulate phases. Organic nitrogen is associated with carbon, while inorganic nitrogen is associated with elements other than carbon. The inorganic forms are highly mobile and bioavailable. Organic forms require mineralization before becoming available to algae.

In an oxidation reaction, an element loses one or more electrons and its oxidation state increases. In a reduction reaction, an element gains one or more electrons and its oxidation state decreases. The oxidation–reduction reactions of nitrogen are mediated by biological, chemical, and physical factors. For example, the first stage of nitrification is

$$2NH_4^+ + 3O_2 \rightarrow 2NO_2^- + 2H_2O + 4H^+ \qquad (5.5.1)$$

TABLE 5.5.1 Nitrogen Forms and Their Oxidation States

Nitrogen Forms	Names	Oxidation States	Notes
HNO_3, NO_3^-	Nitric acid, nitrate ion	+5	Most oxidized, available to algal uptake
NO_2	Nitrogen dioxide	+4	
HNO_2, NO_2^-	Nitrous acid, nitrite ion	+3	Unstable
NO	Nitrogen monoxide (nitric oxide)	+2	
N_2O	Nitrous oxide (laughing gas)	+1	
N_2	Nitrogen gas or elemental nitrogen	0	Available to algae via fixation
NH_2OH	Hydroxylamine	–1	
N_2H_4	Hydrazine	–2	
NH_3, NH_4^+	Unionized ammonia, ammonium ion	–3	Most reduced, preferred to algal uptake

Oxidation is always accompanied by reduction and the two reactions occur simultaneously. Reactions in which oxidation and reduction are occurring are usually called redox reactions.

Nitrogen is an extremely reactive element. The many forms of nitrogen are the result of nitrogen's ability to gain and lose electrons to other elements. The oxidation state is positive as the atom loses electrons and is negative as the atom gains electrons. The ability of nitrogen to vary its oxidation state makes it highly reactive. Understanding the transformation of nitrogen between the different states is critical to studies of nitrogen processes. Table 5.5.1 presents several nitrogen forms and their oxidation states. Nitrogen in its most reduced state is found in ammonium and various organic nitrogen forms. Ammonium is immediately available for phytoplankton uptake, as is nitrate, but an organism needs more energy to uptake nitrate than ammonium. This is why most algae prefer to use ammonium over nitrate.

In natural waters, primary forms of nitrogen include

1. Nitrate ion (NO_3^-).
2. Nitrite ion (NO_2^-).
3. Dissolved nitrogen gas (N_2).
4. Dissolved ammonia gas (NH_3) and ammonium ion (NH_4^+).
5. Organic nitrogen (ON).

It is relatively easy to measure organic nitrogen, ammonia, and nitrate and nitrite, which is one of the reasons that nitrogen forms are categorized in detail in a water quality model (with five state variables in Table 5.1.1). The dissolved

NH_3 and NH_4^+ are often treated together as one group in water quality models.

Total nitrogen is the sum of all nitrogen forms and can be represented as:

$$TN = NO_2 + NO_3 + NH_3/NH_4 + ON \tag{5.5.2}$$

Organic nitrogen can exist in considerable proportions and contribute substantially to total nitrogen. Nitrate is the common form of inorganic nitrogen in water. Nitrite is generally unstable in water and contributes little to the total nitrogen. Ammonium ions, nitrites, and nitrates are readily available to algal uptake and have direct impact on algal growth and the eutrophication process. In data colleting and monitoring, TN usually covers all forms of nitrogen in the water including the ON in living organisms (mostly algal biomass). In water quality models, however, ON generally does not include the nitrogen in algae. For example, Table 5.1.1 has ON = RPON + LPON + DON. It is essential that, when comparing with measured data, the modeled TN should include the ON in the modeled algal biomass. The same argument is also applicable to the modeled TP, TOC, and total silica.

The total Kjeldahl nitrogen (TKN) test involves digestion and distillation to determine both organic nitrogen and ammonia in a water sample. It has the form:

$$TKN = NH_3/NH_4 + ON = TN - NO_2 - NO_3 \tag{5.5.3}$$

In water quality models, the forms of nitrogen can be grouped as (Cerco and Cole, 1994): (1) RPON, (2) LPON, (3) DON, (4) NH_4, and (5) NO_3.

These five variables are summarized in Table 5.1.1 and illustrated in Fig. 5.5.1. Two of the nitrogen state variables are in inorganic forms: NH_4 and NO_3. The other three are in organic forms: refractory, labile, and dissolved. The three major nutrients, C, P, and N, all have their organic forms grouped into similar categories. As illustrated in Fig. 5.5.1, nitrogen transformations are represented in a cascade approach: (1) hydrolysis converts RPON and LPON to DON, (2) mineralization converts DON to NH_4, (3) nitrification converts NH_4 to NO_3, (4) algal uptake NH_4 and NO_3 for growth, and (5) denitrification removes NO_3 out of the aquatic system.

5.5.2 Equations for Nitrogen State Variables

For brevity, all forms of nitrogen discussed in this book represent concentrations as nitrogen. For example, an ammonia concentration expressed as 10 mg/L refers to an ammonia concentration of 10 mg/L as nitrogen.

5.5.2.1 Particulate Organic Nitrogen. Organic nitrogen includes all substances in which nitrogen is bonded to carbon. It occurs in both dissolved and particulate forms. Particulate organic nitrogen (PON) includes small

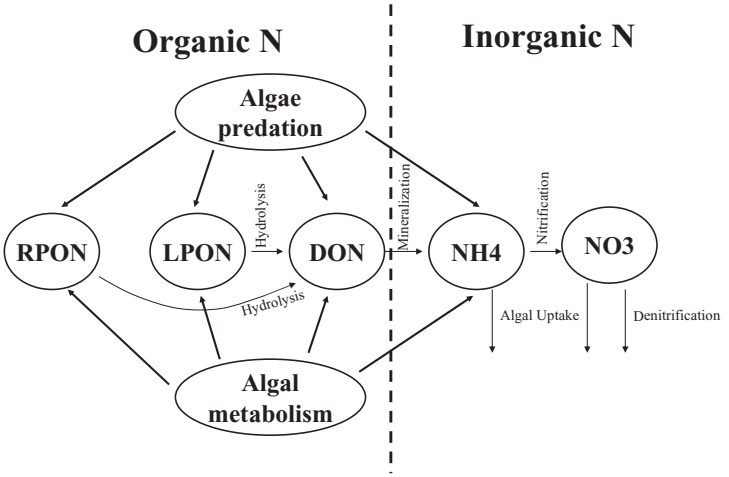

Fig. 5.5.1 Nitrogen state variables and their transformations.

organisms (algae, bacteria, etc.), both living and dead, and fragments of organisms. Dissolved organic nitrogen is mostly from wastes excreted by organisms or from the hydrolysis of PON. Particulate organic nitrogen, including RPON and LPON, has the following sources and sinks (Figs. 5.1.4 and 5.5.1): (1) algal basal metabolism, (2) algal predation, (3) hydrolysis to DON, (4) settling, and (5) external loads.

The corresponding mass balance equation can be described as:

$$\text{The change of PON} = \text{Algal basal metabolism} + \text{algal predation} - \text{PON hydrolysis} - \text{settling} + \text{external source} \quad (5.5.4)$$

Therefore, the kinetic equations for RPON and LPON are (Park et al., 1995):

$$\frac{\partial \text{RPON}}{\partial t} = \sum_{x=c,d,g} (\text{FNR}_x \cdot \text{BM}_x + \text{FNRP} \cdot \text{PR}_x)\text{ANC}_x \cdot B_x - K_{\text{RPON}} \cdot \text{RPON} + \frac{\partial}{\partial z}(\text{WS}_{\text{RP}} \cdot \text{RPON}) + \frac{\text{WRPON}}{V} \quad (5.5.5)$$

and

$$\frac{\partial \text{LPON}}{\partial t} = \sum_{x=c,d,g} (\text{FNL}_x \cdot \text{BM}_x + \text{FNLP} \cdot \text{PR}_x)\text{ANC}_x \cdot B_x - K_{\text{LPON}} \cdot \text{LPON} + \frac{\partial}{\partial z}(\text{WS}_{\text{LP}} \cdot \text{LPON}) + \frac{\text{WLPON}}{V} \quad (5.5.6)$$

where RPON = concentration of refractory particulate organic nitrogen (gN/m^3), LPON = concentration of labile particulate organic nitrogen (gN/m^3), FNR_x = fraction of metabolized nitrogen by algal group x as refractory particulate organic nitrogen, FNL_x = fraction of metabolized nitrogen by algal group x produced as labile particulate organic nitrogen, FNRP = fraction of predated nitrogen produced as refractory particulate organic nitrogen, FNLP = fraction of predated nitrogen produced as labile particulate organic nitrogen, ANC_x = nitrogen/carbon ratio in algal group x (gN/gC), K_{RPON} = hydrolysis rate of refractory particulate organic nitrogen (day^{-1}), K_{LPON} = hydrolysis rate of labile particulate organic nitrogen (day^{-1}), WRPON = external loads of refractory particulate organic nitrogen (gN/day), and WLPON = external loads of labile particulate organic nitrogen (gN/day).

By examining the field data in the Chesapeake Bay, Cerco and Cole (1994) showed that the variation of nitrogen-to-carbon stoichiometry was small and thus used a constant algal nitrogen/carbon ratio, ANC_x. In this chapter, all refractory organic nutrients, including C, P, and N, have the same settling velocity of WS_{RP}, and all liable organic nutrients have the same settling velocity of WS_{LP}.

5.5.2.2 Dissolved Organic Nitrogen. Sources and sinks for DON include (Figs. 5.1.4 and 5.5.1): (1) algal basal metabolism, (2) algal predation, (3) hydrolysis from RPON and LPON, (4) mineralization to ammonium, and (5) external loads.

These sources and sinks are similar to the ones for DOP. The kinetic equation describing these processes is

$$\frac{\partial \mathrm{DON}}{\partial t} = \sum_{x=c,d,g} (\mathrm{FND}_x \cdot \mathrm{BM}_x + \mathrm{FNDP} \cdot \mathrm{PR}_x)\mathrm{ANC}_x \cdot B_x + K_{\mathrm{RPON}} \cdot \mathrm{RPON} + K_{\mathrm{LPON}} \cdot \mathrm{LPON} - K_{\mathrm{DON}} \cdot \mathrm{DON} + \frac{\mathrm{WDON}}{V} \quad (5.5.7)$$

where DON = concentration of dissolved organic nitrogen (gN/m^3), FND_x = fraction of metabolized nitrogen by algal group x produced as dissolved organic nitrogen, FNDP = fraction of predated nitrogen produced as dissolved organic nitrogen, K_{DON} = mineralization rate of dissolved organic nitrogen (day^{-1}), and WDON = external loads of dissolved organic nitrogen (gN/day).

5.5.2.3 Ammonium Nitrogen. In natural waters, ammonia exists in two forms: un-ionized (NH_3) and ionized (NH_4^+). The equilibrium relationship between the two is defined by the following reversible reaction:

$$\mathrm{H_2O} + \mathrm{NH_3} \rightleftarrows \mathrm{NH_4^+} + \mathrm{OH^-} \quad (5.5.8)$$

Ammonia is a colorless gas with a strong pungent odor. It is very soluble in water and is relatively toxic to aquatic life. Ammonia is produced from the breakdown of protein for energy, originating from feces, decaying food, dead

aquatic animals, and decomposing plants. Mineralization (and decomposition) of organic matter results in release and accumulation of ammonia. Ammonia, in the presence of nitrifying bacteria and oxygen, is oxidized to nitrite and to nitrate (nitrification). Under anaerobic conditions, nitrification of ammonia to nitrate stops and ammonia accumulates, often at the bottom of stratified waterbodies (e.g., deep lakes).

Ammonium is made by reaction between ammonia and water and is less toxic. How much of the NH_3 turns into NH_4^+ depends on the temperature and the pH level of the water. The higher the temperature (or pH), the less NH_3 becomes NH_4^+. Therefore, the toxic level of ammonia is both pH and temperature dependent. Toxicity increases as temperature (or pH) increases.

The concentrations of NH_3 and NH_4^+ at equilibrium are determined by pH and temperature and are related by the following equation:

$$K_e = \frac{[NH_3][H^+]}{[NH_4^+]} \tag{5.5.9}$$

where K_e = ammonia equilibrium constant (mol/L), $[NH_3]$ = NH_3 concentration (mol/L), $[NH_4^+] = NH_4^+$ concentration (mol/L), and $[H^+]$ = H^+ concentration (mol/L).

The ammonia equilibrium constant, K_e, is a function of temperature (Wright et al., 1961):

$$\text{Log}_{10} K_e = 0.2976 - 0.001225 \cdot T - \frac{2835.76}{T + 273.15} \tag{5.5.10}$$

where T is water temperature in °C and K_e has a value of 5.7×10^{-10} at 25 °C.

Total ammonia concentration in mol/L, [TA], has the form:

$$[TA] = [NH_3] + [NH_4^+] \tag{5.5.11}$$

Equations (5.5.9), (5.5.11), and (4.4.17) yield

$$\frac{[NH_4^+]}{[TA]} = \frac{[H^+]}{K_e + [H^+]} = \frac{10^{-pH}}{K_e + 10^{-pH}} \tag{5.5.12}$$

$$\frac{[NH_3]}{[TA]} = \frac{K_e}{K_e + [H^+]} = \frac{K_e}{K_e + 10^{-pH}} \tag{5.5.13}$$

Equation (5.5.12) gives the proportion of ammonia in ionized form. Equation (5.5.13) gives the proportion of ammonia in un-ionized form and shows that the proportion of un-ionized ammonia is determined by the pH and temperature of the water. High pH and high water temperature can promote NH_3 toxicity. As pH or temperature increases, the proportion of un-ionized ammonia and the toxicity also increase. Based on Eqs. (5.5.12) and

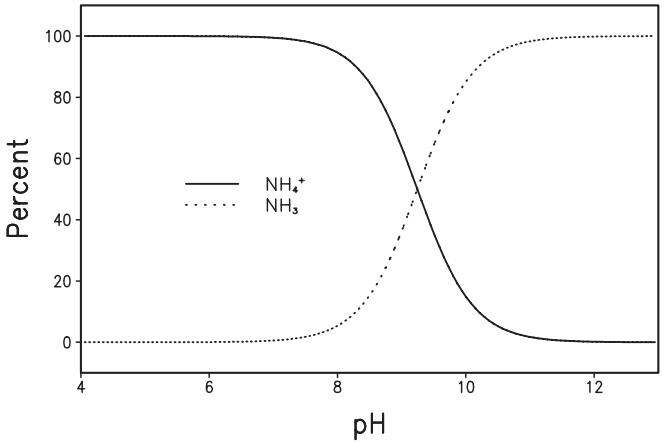

Fig. 5.5.2 Percentage of NH_4^+ and NH_3 as functions of pH at a water temperature of 25°C.

(5.5.13), Fig. 5.5.2 shows how NH_4^+ and NH_3 concentrations vary with pH at 25 °C. Figure 5.5.2 indicates that, at a pH of 7, the un-ionized form (NH_3) is almost 0%. At a pH of 9, the un-ionized form is ~40% of the total ammonia, indicating much greater potential toxicity to aquatic life. Detailed simulation of ammonia concentrations, including NH_3 and NH_4^+, requires the simulation of pH. However, if pH does not vary significantly, it is adequate to simulate ammonium concentrations without simulating pH. This is the approach described in this chapter. Figure 5.5.2 also indicates that in the pH range of most natural waters (i.e., pH between 7 and 8), NH_4^+ is the dominant form and usually has much higher concentrations than NH_3. For this reason, only NH_4^+ concentrations are commonly simulated in water quality models.

Major sources and sinks for ammonia nitrogen include (Figs. 5.1.4 and 5.5.1): (1) algal basal metabolism, predation, and uptake; (2) mineralization from dissolved organic nitrogen; (3) nitrification to nitrate; (4) exchange at the sediment bed–water column interface, and (5) external loads.

The kinetic equation for NH4 can be described as:

$$\begin{aligned}\text{The change of NH4} = {} & \text{Algal contributions} + \text{DON mineralization} - \\ & \text{Nitrification} + \text{bottom flux of NH4} + \text{external source}\end{aligned} \tag{5.5.14}$$

Hence, the mathematical equation for ammonium is

$$\begin{aligned}\frac{\partial \text{NH4}}{\partial t} = {} & \sum_{x=c,d,g} (\text{FNI}_x \cdot \text{BM}_x + \text{FNIP} \cdot \text{PR}_x - \text{PN}_x \cdot P_x)\text{ANC}_x \cdot B_x + \\ & K_{\text{DON}} \cdot \text{DON} - \text{Nit} \cdot \text{NH4} + \frac{\text{BFNH4}}{\Delta z} + \frac{\text{WNH4}}{V}\end{aligned} \tag{5.5.15}$$

where FNI_x = fraction of metabolized nitrogen by algal group x produced as inorganic nitrogen, FNIP = fraction of predated nitrogen produced as inorganic nitrogen, PN_x = preference for ammonium uptake by algal group x ($0 < PN_x < 1$), given by Eq. (5.5.20), Nit = nitrification rate (day^{-1}) given in Eq. (5.5.28), BFNH4 = sediment–water exchange flux of ammonium ($gN/m^2\,day$), applied to the bottom layer only, and WNH4 = external loads of ammonium (gN/day).

Algae can uptake both ammonia and nitrate; however, ammonia is the preferred form of nitrogen for algal growth and is characterized by the parameter PN_x, which will be given later in Eq. (5.5.20). The NH_4 flux from the sediment bed, BFNH4, can be either specified based on measured data or calculated by simulating the sediment diagenesis process (Section 5.7).

5.5.2.4 Nitrate Nitrogen. Nitrogen oxides (NO_x) represent inorganic compounds containing both nitrogen and oxygen, including NO_2, NO_3, and others. Nitrate nitrogen (NO_3^-) is highly soluble and can be reduced to form nitrite (NO_2^-). Microorganisms transform ammonia to nitrite and then nitrate through the process of nitrification. This oxidation process can only happen under aerobic conditions. Although this process has two steps, nitrite is unstable and can be oxidized to form nitrates. The amount of nitrite present in natural waters is usually very small. Most of the oxidized nitrogen is in the form of nitrate nitrogen, and nitrate is often used to represent both nitrate and nitrite in water quality models, as listed in Table 5.1.1.

Major sources and sinks for nitrate nitrogen include (Figs. 5.1.4 and 5.5.1): (1) algal uptake, (2) nitrification from ammonium, (3) denitrification to nitrogen gas, (4) NO_3 flux at the sediment bed–water column interface, and (5) external source.

The NO_3 kinetic equation describing these processes can be expressed as:

$$\begin{aligned}\text{The change of } NO_3 = &-\text{Algal uptake} + \text{nitrification} - \text{denitrification}\\ &+ \text{bottom flux of NO3} + \text{external source}\end{aligned} \tag{5.5.16}$$

Mathematically, it has the form:

$$\frac{\partial \text{NO3}}{\partial t} = -\sum_{x=c,d,g}(1-\text{PN}_x)P_x\cdot\text{ANC}_x\cdot B_x + \text{Nit}\cdot\text{NH4} - \text{ANDC}\cdot\text{Denit}\cdot\text{DOC} + \frac{\text{BFNO3}}{\Delta z} + \frac{\text{WNO3}}{V} \tag{5.5.17}$$

where ANDC = mass of nitrate nitrogen reduced per mass of dissolved organic carbon oxidized (0.933 gN/gC), BFNO3 = sediment–water exchange flux of nitrate ($gN/m^2/day$), applied to the bottom layer only, and WNO3 = external loads of nitrate (gN/day). The NO3 flux from the sediment bed, BFNO3, can be either specified based on measured data or calculated by simulating the sediment diagenesis process, which will be described in Section 5.7.

5.5.3 Nitrogen Processes

Processes affecting nitrogen concentrations include

1. *Algal Uptake:* Algae consume NH_4 and NO_3 for growth via the photosynthetic process.
2. *Mineralization and Hydrolysis:* Particulate organic nitrogen is decayed into DON via hydrolysis, and then DON is converted to NH4 via mineralization.
3. *Nitrification:* Ammonia is oxidized to nitrite (NO_2^-) and then to nitrate (NO_3^-) via nitrification.
4. *Denitrification:* Under anaerobic conditions, nitrate is reduced to nitrogen gas (N_2) and then released from the modeling system.
5. *Nitrogen Fixation:* Some blue-green algae can directly fix N_2 from the atmosphere. This process is an important external source to a waterbody and can affect the nitrogen dynamics significantly. However, NH4 and NO3 are preferred forms of nitrogen for algae consumption.

These processes and their mathematical representations are discussed in this section.

5.5.3.1 Effects of Algae. The terms within summation ($\sum_{x=c,d,g}$) in Eqs. (5.5.5)–(5.5.7), (5.5.15), and (5.5.17) represent the effects of algae on nitrogen. As described in the nitrogen kinetic equations and in Fig. 5.5.1, algae can influence nitrogen processes through: (1) algae death, (2) algal growth, (3) algal preference for ammonia over nitrate, and (4) nitrogen fixation.

Figure 5.5.1 illustrates that through algal metabolism and algal predation, the nitrogen of algal biomass can be recycled to organic nitrogen and inorganic nitrogen, and is represented by the distribution coefficients. For algal basal metabolism:

$$\mathrm{FNR}_x + \mathrm{FNL}_x + \mathrm{FND}_x + \mathrm{FNI}_x = 1 \tag{5.5.18}$$

and for algal predation:

$$\mathrm{FNRP} + \mathrm{FNLP} + \mathrm{FNDP} + \mathrm{FNIP} = 1 \tag{5.5.19}$$

Two forms of nitrogen, NH_4 and nitrate NO_3, are used during algal uptake and growth, and NH_4 is the preferred form of nitrogen over NO_3 for algal growth. The value of the ammonia preference factor, PN_x in Eqs. (5.5.15) and (5.5.17), is a function of the ammonia and nitrate concentrations, and is expressed as:

$$\mathrm{PN}_x = \mathrm{NH4}\frac{\mathrm{NO3}}{(\mathrm{KHN}_x + \mathrm{NH4})(\mathrm{KHN}_x + \mathrm{NO3})} + \mathrm{NH4}\frac{\mathrm{KHN}_x}{(\mathrm{NH4} + \mathrm{NO3})(\mathrm{KHN}_x + \mathrm{NO3})} \tag{5.5.20}$$

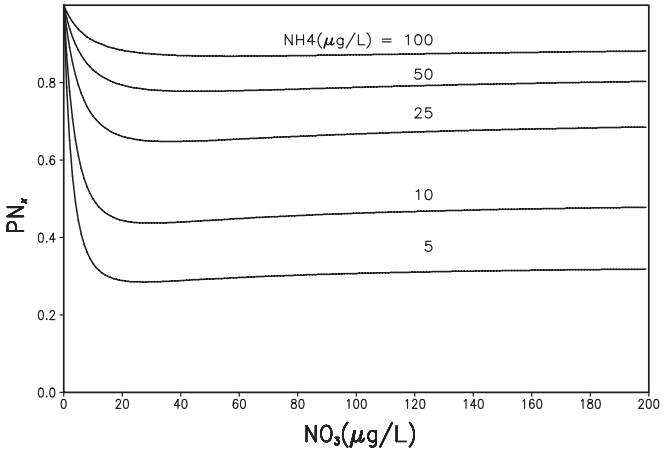

Fig. 5.5.3 Preference for ammonia uptake, PN_x, as functions of NO3 at KHN_x = 10 μg/L.

Equation (5.5.20) is somewhat similar to the Michaelis–Menton formulation that has been used to describe limiting functions in this chapter. The half saturation constant, KHN_x, is firstly introduced in Eq. (5.2.13) for growth limiting function for nutrients, $f_1(N)$. The PN_x partitions the nitrogen uptake between ammonia and nitrate, with values ranging from 0 to 1. The preference for ammonium is 1 when nitrate is absent and is 0 when ammonium is absent. At PN_x = 1, NO3 is zero and algae uptake nitrogen only in the form of NH_4. At PN_x = 0, NH4 is zero and algae uptake nitrogen only in the form of NO_3. This approach is commonly used in water quality models (e.g., Cerco and Cole, 1994; Park et al., 1995). At KHN_x = 10 μg/L, the values of PN_x (Fig. 5.5.3) show that PN_x is most sensitive at low values of NH4 and NO3. For a given concentration of NH4, PN_x is almost a constant when NO3 is >20 μg/L.

5.5.3.2 Mineralization and Hydrolysis. Decomposition of organic detritus and dead algae releases both dissolved organic and dissolved inorganic nutrients to the water. Organic nitrogen undergoes bacterial decomposition into ammonia nitrogen before consumption by algae. As illustrated in Fig. 5.5.1, hydrolysis breaks down particulate organic nitrogen into dissolved organic nitrogen, and NH_3/NH_4^+ is released when organic matter is mineralized.

The hydrolysis of particulate organic nitrogen is represented by the term of K_{RPON} in Eq. (5.5.5) and the term of K_{LPON} in Eq. (5.5.6). The mineralization of dissolved organic nitrogen is represented by the term of K_{DON} in Eq. (5.5.7). Similar to the equations for the phosphorus processes, Eqs. (5.4.14)–

(5.4.16), the three parameters, K_{RPON}, K_{LPON}, and K_{DON}, have the following formulations:

$$K_{RPON} = \left(K_{RN} + \frac{KHN}{KHN + NH4 + NO3} K_{RNalg} \sum_{x=c,d,g} B_x \right) \cdot e^{KT_{HDR}(T - TR_{HDR})} \tag{5.5.21}$$

$$K_{LPON} = \left(K_{LN} + \frac{KHN}{KHN + NH4 + NO3} K_{LNalg} \sum_{x=c,d,g} B_x \right) \cdot e^{KT_{HDR}(T - TR_{HDR})} \tag{5.5.22}$$

$$K_{DON} = \left(K_{DN} + \frac{KHN}{KHN + NH4 + NO3} K_{DNalg} \sum_{x=c,d,g} B_x \right) \cdot e^{KT_{MNL}(T - TR_{MNL})} \tag{5.5.23}$$

where K_{RN} = minimum hydrolysis rate of refractory particulate organic nitrogen (day^{-1}), K_{LN} = minimum hydrolysis rate of labile particulate organic nitrogen (day^{-1}), K_{DN} = minimum mineralization rate of dissolved organic nitrogen (day^{-1}), K_{RNalg} and K_{LNalg} = constants that relate hydrolysis of refractory and labile particulate organic nitrogen to algal biomass ($day^{-1}/gC/m^3$), K_{DNalg} = constant that relates mineralization to algal biomass ($day^{-1}/gC/m^3$), and KHN = mean half-saturation constant for algal nitrogen uptake (gN/m^3), which has the form:

$$KHN = \frac{1}{3} \sum_{x=c,d,g} KHN_x \tag{5.5.24}$$

5.5.3.3 Nitrification. Nitrification is the process in which an NH_4^+ is oxidized to NO_2^- and then to NO_3^-. The process of nitrification in natural water is complex, mainly depending upon: (1) dissolved oxygen concentration, (2) nitrogen concentrations, (3) water temperature, (4) nitrifying bacteria, and (5) pH level.

Nitrification is a two-stage process. The first stage is the oxidation of ammonia to NO_2^- mediated by the nitrifying bacteria Nitrosomonas. The second stage is the oxidation of nitrite to NO_3^- mediated by the nitrifying bacteria Nitrobacter. They can be expressed as:

$$\text{Stage 1} \qquad 2\,NH_4^+ + 3\,O_2 \rightarrow 2\,NO_2^- + 2\,H_2O + 4\,H^+ \qquad \text{(Nitrosomonas)} \tag{5.5.25}$$

$$\text{Stage 2} \qquad 2\,NO_2^- + O_2 \rightarrow 2\,NO_3^- \qquad \text{(Nitrobacter)} \tag{5.5.26}$$

Combining Stages 1 and 2 yields

$$NH_4^+ + 2\,O_2 \rightarrow NO_3^- + H_2O + 2\,H^+ \tag{5.5.27}$$

Nitrite is unstable and is often an intermediate product in the nitrogen transformations. In order to reduce the number of state variables required in water quality models, nitrite and nitrate are often incorporated together as a single-state variable ($NO_2 + NO_3$), as listed in Table 5.1.1.

The nitrifying bacteria are commonly found in natural waters and require DO to survive. Nitrification is only allowed to occur if oxygen is present. Therefore, aerobic conditions are essential to the reactions described by Eqs. (5.5.25) and (5.5.26). The nitrification of ammonia has the potential for removing large amounts of oxygen from a waterbody. The stoichiometry of reactions indicates that 2 mol of oxygen are required to nitrify 1 mol of ammonium into nitrate: 3.43 (=1.5 × 32/14) g O_2/g N for transforming ammonia to nitrite in Eq. (5.5.25) and 1.14 (=0.5 × 32/14) g O_2/g N for transforming nitrite to nitrate in Eq. (5.5.26). Thus, for every gram of ammonium nitrogen oxidized, 4.57 (=2 × 32/14) g of oxygen are consumed. However, Wezernak and Gannon (1968) reported that due to the effect of nitrifying bacteria, <2 mol of oxygen are actually consumed per mole of ammonium nitrified, and a total of 4.33 g of oxygen is required to oxidize 1.0 g of ammonia nitrogen. This explains why AONT has the value of 4.33 (instead of 4.57) g O_2/g N in the DO equation, Eq. (5.6.9).

The nitrification process is often represented in first-order kinetics, as in the term of (–Nit·NH4) in Eq. (5.5.15). The nitrification rate, Nit, can be formulated as a function of NH_4, DO, and temperature:

$$\text{Nit} = \frac{\text{DO}}{\text{KHNit}_{\text{DO}} + \text{DO}} \frac{\text{NH4}}{\text{KHNit}_{\text{N}} + \text{NH4}} \text{Nit}_m \cdot f_{\text{Nit}}(T) \tag{5.5.28}$$

and

$$f_{\text{Nit}}(T) = \begin{cases} e^{-\text{KNit1}\cdot(T-\text{TNit})^2} & \text{if } T \le \text{TNit} \\ e^{-\text{KNit2}\cdot(\text{TNit}-T)^2} & \text{if } T > \text{TNit} \end{cases} \tag{5.5.29}$$

where KHNit_{DO} = nitrification half saturation constant for dissolved oxygen (g O_2/m^3), KHNit_{N} = nitrification half saturation constant for ammonium (g N/m^3), Nit_m = maximum nitrification rate at TNit (day^{-1}), TNit = optimum temperature for nitrification (°C), KNit1 = effect of temperature below TNit on nitrification rate ($°C^{-2}$), and KNit2 = effect of temperature above TNit on nitrification rate ($°C^{-2}$). Equation (5.5.28) shows that the nitrification process can be limited by low concentrations of DO and NH4.

5.5.3.4 Denitrification. Denitrification is the process in which nitrate is reduced to nitrite and then to nitrogen gas by bacteria. The necessary conditions for denitrification include oxygen depletion and freely available nitrate or nitrite. Because of the lack of oxygen for normal aerobic respiration, bacteria use oxygen bound in nitrate and remove the oxygen from the nitrate,

which reduces nitrate to nitrite. Nitrite is further reduced to nitrogen gas, and then released into the atmosphere. Denitrification can cause significant losses of nitrogen from a waterbody.

Therefore, by denitrification, nitrogen is lost from the nitrogen cycle in an aquatic system (Figs. 5.1.4 and 5.5.1). Some scientists postulate that the continued activity of denitrifying microorganisms throughout geological history is the reason why nitrogen is the principal component of the earth's atmosphere (Stevenson, 1972). Denitrification is an anaerobic process in which nitrate, instead of oxygen, is used during the oxidation of organic carbon compounds to yield energy (respiration). The net denitrification reaction is described by the following equation:

$$5CH_2O + 4NO_3^- + 4H^+ \rightarrow 5CO_2 + 2N_2 + 7H_2O \qquad (5.5.30)$$

In water columns, denitrification usually contributes little to nitrogen loss. However, under the anaerobic conditions found in the sediment bed or during extremely low oxygen conditions in the water column, denitrification can be important and may remove a substantial fraction of the nitrogen from a waterbody by converting nitrate and nitrite into nitrogen gas. Denitrification oxidizes DOC and converts NO_3 to NO_2, and then to nitrogen gas (N_2). Denitrification removes both DOC and NO_3 from the system, and is represented by the term of (–Denit·DOC) in Eq. (5.3.8) and the term of (–ANDC·Denit·DOC) in Eq. (5.5.17), respectively. The Michaelis–Menton function is used to express the denitrification rate, Denit:

$$\text{Denit} = \frac{\text{KHOR}_{\text{DO}}}{\text{KHOR}_{\text{DO}} + \text{DO}} \frac{\text{NO}_3}{\text{KHDN}_{\text{N}} + \text{NO}_3} \text{AANOX} \cdot K_{\text{DOC}} \qquad (5.5.31)$$

where $KHDN_N$ = denitrification half saturation constant for nitrate (gN/m^3) and AANOX = ratio of denitrification rate to oxic dissolved organic carbon respiration rate.

In Eq. (5.5.31), AANOX is a constant (=0.5 in Park et al., 1995) that makes the anoxic respiration slower than oxic respiration. The parameter K_{DOC} is given in Eq. (5.3.13). $KHOR_{DO}$ is also used to calculate the heterotrophic respiration rate, K_{HR}, in Eq. (5.3.10). The modified Michaelis–Menton term is to suppress the reaction in the presence of a small amount of oxygen. Equation (5.5.31) includes three factors that largely control the denitrification process:

1. *Dissolved Oxygen.* Denitrification rate declines as DO levels rise above zero.
2. *Nitrate Concentration.* A standard Michaelis–Menton formulation is used to represent the effect of NO3 on denitrification.
3. *Temperature.* K_{DOC} is associated with temperature in Eq. (5.3.13).

5.5.3.5 Nitrogen Fixation. The nitrogen gas (N_2) is relatively inert and unreactive. It combines with other elements only at high temperature and pressure or when mediated by certain microorganisms. Nitrogen fixation is the process by which nitrogen gas is converted into biologically usable NH_4^+ and NO_3^-. It is both a natural process that is accomplished by bacteria or by lightning and an industrial process that requires large amounts of energy, such as the production of fertilizer. The reaction can be represented as

$$N_2 + 3\,H_2 \rightarrow 2\,NH_3 \quad \text{(ammonia); or } NH_4^+ \text{ (ammonium ion)} \qquad (5.5.32)$$

Nitrogen fixation is carried out by a variety of organisms; however, those responsible for most of the fixation in natural waters are certain species of blue-green algae. Although all aquatic plants require N compounds, very few are able to utilize N_2. The ability of blue-green algae to fix nitrogen is frequently cited as one of the reasons that phosphorus, not nitrogen, is considered to be the limiting nutrient in most lakes.

Nitrogen increase in lakes due to nitrogen fixation can be significant in nutrient-enriched waters. The potential importance of nitrogen fixation in nutrient budgets for primary production has been established in a number of marine and freshwater ecosystems. Rates of nitrogen fixation may be influenced by the nitrogen supply to the lake, by N/P ratios; and by other chemical and physical factors. Lake research has revealed numerous cases of nitrogen limitation of phytoplankton production. For example, nitrogen fixation in Lake Okeechobee may be a major contributor to the nitrogen budget of the lake and help to resolve the missing source of nitrogen in modeling efforts (Phlips and Ihnat, 1995). Nitrogen fixation can be viewed as a source of external nitrogen loading. Without knowledge of nitrogen fixation rates and the environmental factors that influence these rates, detailed representation of nitrogen fixation cannot be incorporated into a model.

5.6 DISSOLVED OXYGEN

As discussed in Section 5.1.4, DO is one of the most important water quality variables in aquatic systems. Dissolved oxygen is a basic requirement for a healthy aquatic ecosystem and indicates the capability of the waterbody to support a balanced ecosystem. Fish and aquatic insects need DO to survive. When DO levels are low, aquatic life may be impaired and large mortalities may occur. Dissolved oxygen concentration is probably the single state variable that provides maximum information about water quality conditions in natural waters. For this reason, water quality standards are set for DO to meet the designated uses for most waterbodies.

The DO conditions in aquatic systems are often categorized as aerobic, hypoxic, or anaerobic:

1. An "aerobic" (or oxic) condition is characterized by the presence of DO. "Aerobic" is also used to describe biological or chemical processes that occur in the presence of oxygen.
2. "Hypoxia" is an environmental condition in which the concentration of DO is low enough to have biological effects. The EPA defines hypoxic water as water with oxygen concentrations of 2 mg/L or less (USEPA, 2000b).
3. "Anaerobic" (or anoxic) condition is characterized by zero oxygen levels. Literally, anaerobic means "without oxygen". Practically, it is often used synonymously with anoxia in water quality studies, representing environmental conditions that contain very little or no oxygen. Anaerobic is also used to describe biological or chemical processes that occur in the absence of oxygen.

Dissolved oxygen concentrations fluctuate under natural conditions, but can be lowered severely as a result of human activities, such as introducing large quantities of oxygen-demanding wastes or from eutrophication. The wastes are oxidized in the receiving waterbody and reduce the amount of DO available. When large amount of nutrients (e.g., phosphorus or nitrogen) are discharged into a waterbody, the plants and algae begin to grow more rapidly than normal. As this happens, there is also an excess die-off of the plants and algae. These organic matters are later decomposed in water and add to the DO depletion. As a result, eutrophication often causes excessive oxygen production in surface waters (even super saturated DO in some cases) and hypoxia or even anoxia in deep waters.

When bottom waters go anoxic, denitrification may serve as the main mechanism for removing nitrate from the bottom of stratified waters. An anaerobic condition also changes metal solubility. For example, the presence of nitrate will inhibit manganese reduction. Following the denitrification of nitrate, manganese species in the sediment bed are reduced from insoluble forms to soluble forms, which diffuse into the overlying water column. Under anaerobic conditions, phosphates sorbed to sediment particles can be liberated from the particles very rapidly and released back into the water column. Hence, the sediments may serve as a major phosphorus source during anaerobic periods.

Low DO concentrations favor anaerobic bacteria that produce noxious gases or foul odors. As DO levels fall, undesirable odors, tastes, and colors impair the uses of a waterbody. Fermentation is a process by which, under an anaerobic condition, organic matter is decomposed and converted into another organic matter and carbon dioxide to generate energy by microorganisms. Low or zero DO leads to anaerobic conditions and makes fermentation the major energy production mechanism. The fermentation process, most prevalent in the sediment bed, releases gases, such as CH_4 and hydrogen sulfide (H_2S), to the water column. Carbon is converted to methane instead of carbon dioxide, and sulfur is converted to hydrogen sulfide. Not only do these gases impair

the taste of the water, but they may also be toxic and have severe consequences for the ecosystem.

Fish and other aquatic organisms can survive short periods of low DO, but prolonged periods of depressed oxygen can dramatically alter the ecosystem. As DO levels drop, aquatic life is threatened and, in the extreme case, perishes. Prolonged exposure to low DO conditions can suffocate fish or starve fish by suffocating its prey. Most sport fish species (e.g., trout and salmon) suffer if DO concentrations fall below a concentration of 3–4 mg/L. Larvae and juvenile fish are more sensitive and require even higher DO concentrations, ranging from 5 to 8 mg/L.

Dissolved oxygen may exhibit strong diurnal variation, primarily caused by the diurnal variation of sunlight, and more directly, caused by the following two competing mechanisms:

1. Photosynthesis and respiration of algae and aquatic plants.
2. Diurnal variation of water temperature.

Photosynthesis is usually the dominant process in determining DO diurnal variations, especially in eutrophic waters. The water temperature effect is often secondary. The two mechanisms have opposite phases of variation. As an example, Fig. 5.6.1 shows the measured DO in Lake Okeechobee for 72 h, starting from August 24, 1999. The corresponding water temperature is already given in Fig. 2.3.1. In daylight, photosynthesis uses carbon dioxide and releases DO, resulting in an increase in DO concentration. This explains why DO concentrations usually reach their daily maxima in the afternoon and before dusk. At night, photosynthesis stops, but respiration continues causing DO to decline. Aquatic animals are affected most by minimum DO, rather than by its daily means. Hence, monitoring for water quality should include the diurnal minimum DO.

Coinciding with the diurnal DO cycle caused by algal photosynthesis is the diurnal cycle of water temperature. Comparing DO concentrations in Fig. 5.6.1 with water temperatures in Fig. 2.3.1, it is evident that the two are related: both are controlled by the diurnal variation of solar radiation. Dissolved oxygen solubility in water is directly linked to water temperature. Higher water temperature leads to lower DO concentration. In addition, oxygen-consuming reactions, such as the decomposition of organic matters, are also affected by water temperature. A higher water temperature generally leads to a higher oxygen consumption rate and a lower DO concentration. Therefore, the diurnal variation of water temperature should lead to a lower DO in the afternoon and a higher DO in the early morning, exactly in the opposite phase of photosynthesis. Nevertheless, photosynthesis causes a much larger DO variation than does water temperature, and the diurnal variation shown in Fig. 5.6.1 is largely the result of algal photosynthesis.

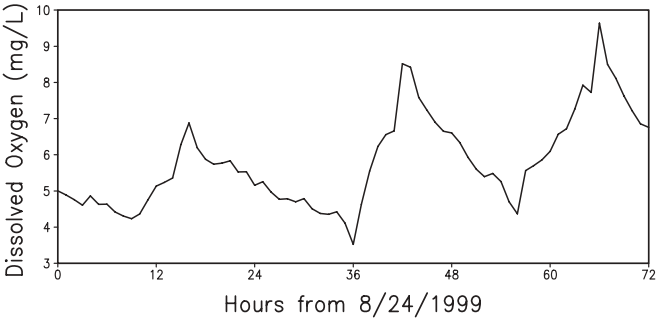

Fig. 5.6.1 Measured DO in Lake Okeechobee for 72 h, starting from August 24, 1999 at midnight.

5.6.1 Biochemical Oxygen Demand

Biochemical oxygen demand (BOD) is a measure of the total amount of oxygen removed from water biologically or chemically in a specified time and at a specific temperature. It indicates the total concentration of DO that is required during the degradation of organic matter and the oxidation of some inorganic matter. Microorganisms require oxygen to decompose organic matter. Oxygen depletion can also result from oxygen-demanding chemical reactions, such as the nitrification process discussed in Section 5.5.3. In short, BOD is an indicator rather than a true physical or chemical substance.

Since wastewaters are usually high in BOD, and DO concentration is a primary indicator of aquatic systems, BOD is widely used to measure water quality pollution and has traditionally been the most important parameter for organic pollutions. For a variety of reasons, the validity of BOD as a measure of water quality has often been questioned. However, BOD remains a key measurement of wastewater treatment plant discharges.

Biochemical oxygen demand is determined from a standardized test that has not changed substantially through the years. To conduct a BOD test, a test sample is placed in a bottle and then the bottle is filled with dilution water. The initial DO concentration is measured. The bottle must be shielded from light sources to keep algae from adding oxygen by photosynthesis, and the bottle should be sealed to keep air from replenishing DO that has been removed by biodegradation. The sample is incubated at 20 °C for a specific period, usually 5 days. At the end of the period, the DO concentration is measured again. The BOD is then calculated from Eq. (5.6.1):

$$\mathrm{BOD} = (\mathrm{DO}_i - \mathrm{DO}_f)\frac{V_b}{V_s} \tag{5.6.1}$$

where DO_i = initial DO concentration, DO_f = final DO concentration, V_b = the volume of the bottle, and V_s = the volume of sample added to the bottle.

In BOD tests, BOD values are calculated using Eq. (5.6.1). The term BOD generally refers to the standard 5-day BOD test. The 5-day BOD, or BOD_5, is the total amount of oxygen consumed during the first 5 days of the test. Regulatory agencies often write wastewater discharge permits in terms of 5-day BOD (e.g., USEPA, 1993).

The oxidation process is usually carried out in two stages: carbonaceous and nitrogenous (nitrification). Carbonaceous biochemical oxygen demand (CBOD) involves the breakdown of organic carbon compounds, which are discussed in Section 5.3. Nitrogenous biochemical oxygen demand (NBOD) involves the oxidation of ammonia to nitrate (nitrification) and is presented in Section 5.5.3. There is a time lag between the carbonaceous oxidation and the nitrification, and the two processes tend to occur at different decaying rates. In domestic wastewaters, CBOD typically occurs before NBOD, giving rise to the well-known two-stage BOD curve (Fig. 5.6.2). In the beginning of BOD utilization, bacteria are responsible for decomposition of organic matter (CBOD). The oxidation of ammonia (NBOD) only becomes significant after >7 or 8 days. This is one reason for limiting a BOD test to 5 days. In natural waters, however, the two processes can occur simultaneously. The BOD tests can also be conducted with a nitrification inhibitor, so that the test measures only the oxidation of carbonaceous material and the results are considered to be CBOD.

The amount of oxygen removed from waters varies with the concentration of organic matter and many other factors, such as the concentration of bacteria, water temperature, the nature of organic matter, and the type of bacteria. For simplicity and in practice, it is often assumed that the rate of decomposition of organic matter is proportional to the amount of organic matter and can be described as a first-order reaction:

$$\frac{dL}{dt} = -k \cdot L \tag{5.6.2}$$

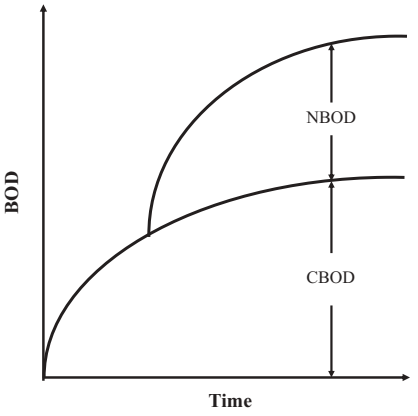

Fig. 5.6.2 Sketch of the typical two-stage DO uptake by CBOD and NBOD.

where L = the concentration of organic matter expressed as O_2 (mg O_2/L), k = BOD reaction rate (time^{-1}), and t = time (day).

Equation (5.6.2) indicates that the rate at which the oxygen is consumed, dL/dt, is proportional to the concentration of biologically degradable organic material and chemically oxidizable substances. Integration of this expression yields

$$L = \mathrm{BOD}_u \cdot e^{-k \cdot t} \tag{5.6.3}$$

where BOD_u is the ultimate biochemical oxygen demand, a measure of the total (ultimate) amount of oxygen removed from water by aerobic microorganisms. In Eq. (5.6.3), L also represents the amount of BOD left in water after time t and BOD_u represents the amount of BOD in water at $t = 0$.

The amount of BOD exerted at time t, BOD_t, is equal to the difference between the ultimate biochemical oxygen demand (BOD_u) and the BOD remaining at time t (L). That is,

$$\mathrm{BOD}_t = \mathrm{BOD}_u - L = \mathrm{BOD}_u \cdot (1 - e^{-kt}) \tag{5.6.4}$$

The values of k vary significantly, typically ranging from 0.05 to 0.4 day^{-1}. Given a set of BOD values, the BOD reaction rate (k) and the ultimate BOD (BOD_u) may be calculated using Eq. (5.6.4). Equations (5.6.3) and (5.6.4) are represented by the curves shown in Fig. 5.6.3, in which the solid line is the percent of BOD removed from the water (=$\mathrm{BOD}_t/\mathrm{BOD}_u$) and the dashed line is the percent of BOD remaining in the water (=L/BOD_u). Figure 5.6.3 shows that, with $k = 0.23$ day^{-1}, half of the total BOD is removed from the water after ~3 days.

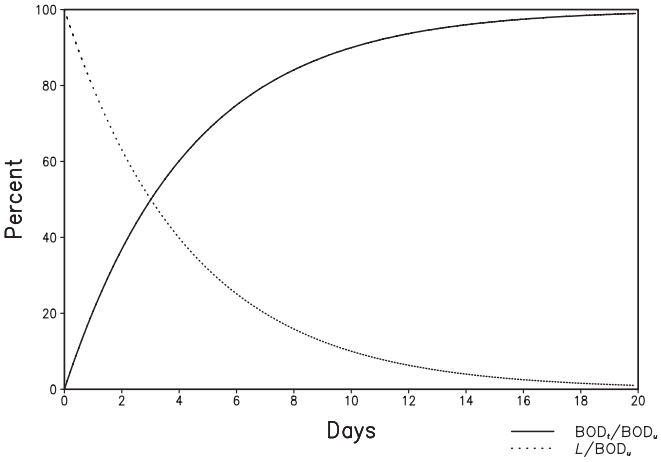

Fig. 5.6.3 Percent of BOD removed from the water (solid line) and percent of BOD remaining in the water (dashed line) at $k = 0.23$ day^{-1}.

The BOD reaction is highly affected by temperature. As temperature increases, so does the rate of biodegradation. The temperature adjustment equation is similar to the other bacterial temperature equations, such as Eq. (5.1.8):

$$k = k_{20} \cdot \theta^{(T-20)} \tag{5.6.5}$$

where k_{20} = BOD reaction rate at 20 °C and θ = a constant typically assumed to be 1.047.

Biochemical oxygen demand combines the effects of several oxygen-consuming processes into one variable (e.g., Fig. 5.6.2) and is often oversimplified for water quality modeling studies. A more realistic approach is to separate oxygen demands into various components, such as oxygen demands from decomposition of organic matter, from nitrification, and from oxidation of other substances. This approach is commonly used in water quality models (e.g., Ambrose et al., 1993; Cerco and Cole, 1994; and Park et al., 1995). The BOD is a key parameter for wastewater discharges and is routinely measured and reported. To apply measured BOD data to water quality modeling, empirical formulations are often needed to relate BOD to organic matters. In studying New York City municipal wastewater discharges, HydroQual (1991b) employed the following relationship to link BOD_5 to total organic carbon:

$$\text{TOC} = 18 + 0.7 \times \text{BOD}_5 \tag{5.6.6}$$

where TOC = total organic carbon (mg/L) and BOD_5 = 5-day biochemical oxygen demand (mg/L).

Some water quality models do not directly simulate BOD as a state variable. In order to use measured BOD data for model–data comparison, state variables of a water quality model, such as the ones listed in Table 5.1.1, need to be converted to BOD, so that model results can be directly compared with the measured BOD. Using the approach taken in the Long Island Sound Study (HydroQual, 1991b), the following equation approximately calculates BOD_5 based on the state variables listed in Table 5.1.1 (Tetra Tech, 1999e):

$$\begin{aligned}\text{BOD}_5 = 2.67 \cdot [&\text{LPOC} \cdot (1 - e^{-5 \cdot K_{\text{LPOC}}}) + \text{DOC} \cdot (1 - e^{-5 \cdot K_{\text{HR}}}) + \\ &\text{COD} \cdot (1 - e^{-5 \cdot KCOD}) + \sum_{x=c,d,g} B_x \cdot (1 - e^{-5 \cdot \text{BM}_x})] + 4.33 \cdot \text{NH4} \cdot (1 - e^{-5 \cdot \text{Nit}})\end{aligned} \tag{5.6.7}$$

where *KCOD* is the oxidation rate of chemical oxygen demand (day^{-1}) and is given by Eq. (5.6.21). The parameters K_{LPOC}, K_{HR}, BM_x, and Nit are already given by Eqs. (5.3.12), (5.3.10), (5.2.28), and (5.5.28), respectively.

5.6.2 Processes and Equations of Dissolved Oxygen

Dissolved oxygen concentrations are a function of physical and chemical processes that control the solubility, transport, production, and consumption of

DO. Oxygen and nutrients are linked in a cycle of uptake and release in which DO concentrations are usually greatest in surface waters due to both surface reaeration and photosynthetic production. The vertical transport of oxygen and nutrients depends upon the turbulent diffusion in the water column. Oxygen concentration generally decreases with depth.

Total suspended solids (and water turbidity) may influence DO concentration via: (1) light availability, (2) water temperature, and (3) DO consumption. High TSS increases the light attenuation coefficient and reduces the amount of light available for photosynthesis. This leads to less DO production. Suspended particles absorb heat and cause water temperature to increase. The ability of water to hold oxygen is influenced by temperature and salinity. Since warm water holds less DO than cold water, a temperature increase causes a reduction in DO concentrations. Total suspended solids often consists of a large content of suspended organic matters. Their decomposition also consumes oxygen.

Major sources and sinks of DO are summarized in Fig. 5.6.4. If the contribution of DO sources is less than the summation of DO sinks, there is an oxygen deficit in the waterbody. The major DO sources include (1) reaeration, (2) photosynthesis, and (3) external loads.

Water obtains oxygen directly from the atmosphere via reaeration and from plants via photosynthesis. Vertical mixing between surface and deep waters transfers DO to lower levels. Reaeration from the atmosphere occurs in direct proportion to the DO deficit in the waterbody. The DO deficit is the difference between the saturated DO concentration and the existing DO concentration in the waterbody. With adequate sunlight, algae and aquatic plants consume nutrients and produce oxygen as a result of photosynthesis. In water layers where photosynthetic rates are very high, such as during an algal bloom, the water may become supersaturated, that is, the oxygen content may exceed the DO saturation concentration. During periods of strong stratification, photosynthesis is the only potential source of DO in the deeper waters, and this occurs only if light penetrates to the deeper layers. External loads can be either a DO source increasing the DO concentration in the receiving water or a DO sink decreasing the DO concentration, depending on the inflow DO concentration.

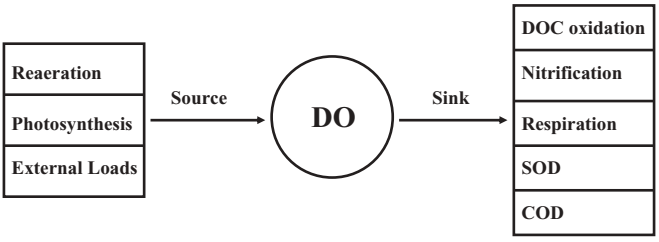

Fig. 5.6.4 Major sources and sinks of DO.

Major DO sinks consist of (1) oxidation of organic matter, (2) nitrification, (3) algal respiration, (4) sediment oxygen demand due to sediment diagenesis in the bed, and (5) chemical oxygen demand due to reduced substances released from the sediment bed.

As discussed in Section 5.3.1, the oxidation and decomposition of organic matter consume oxygen. The nitrification process uptakes oxygen to oxidize NH_4^+ to NO_2^- and then to NO_3^- (Section 5.5.3). Algal respiration needs oxygen to convert organic carbon to carbon dioxide and water (Section 5.2.4). Chemical and biological processes in the sediment bed often uptake oxygen from the water column. Oxygen is consumed by the sediment organism respiration and the benthic decomposition of organic material, which can be a significant fraction of the total oxygen demand in a waterbody. Sediment oxygen demand is used to represent the oxygen depletion due to benthic reactions. It is the rate of oxygen consumption exerted by the bottom sediment on the overlying water. Sulfide and methane provide additional oxygen demands. Microbial activities tend to increase with increased temperature. The stratification may prevent DO in the surface layer from reaching the bottom. Therefore, the benthic effects can be particularly acute in summer under low-flow conditions (in a river) or highly stratified conditions (in a deep lake). Details on SOD will be discussed in the next section of this chapter, where sediment diagenesis processes are presented.

Since the pioneering work of Streeter and Phelps (1925), DO has been modeled for many decades. A variety of well-tested models are available for DO calculation. As shown in Fig. 5.6.4, the change in DO concentration should be determined by the summation of the DO source and DO sinks, that is,

$$\begin{aligned}\text{Net change of DO} = {} & \text{photosynthesis} - \text{respiration} - \text{nitrification} - \\ & \text{DOC decomposition} - \text{COD} + \text{Reaeration} - \\ & \text{SOD} + \text{external loads}\end{aligned} \tag{5.6.8}$$

The corresponding DO kinetic equation is

$$\begin{aligned}\frac{\partial \text{DO}}{\partial t} = {} & \sum_{x=c,d,g}\left((1.3-0.3\cdot \text{PN}_x)P_x - (1-\text{FCD}_x)\frac{\text{DO}}{\text{KHR}_x+\text{DO}}\text{BM}_x\right) \\ & \text{AOCR}\cdot B_x - \text{AONT}\cdot \text{Nit}\cdot \text{NH4} - \text{AOCR}\cdot K_{\text{HR}}\cdot \text{DOC} - \frac{\text{DO}}{\text{KH}_{\text{COD}}+\text{DO}} \\ & \text{KCOD}\cdot \text{COD} + K_r(\text{DO}_s - \text{DO}) + \frac{\text{SOD}}{\Delta z} + \frac{\text{WDO}}{V}\end{aligned} \tag{5.6.9}$$

where PN_x = preference for ammonium uptake by algal group x ($0 \le \text{PN}_x \le 1$), given by Eq. (5.5.20) and Fig. 5.5.3; AONT = mass of DO consumed per unit mass of ammonium nitrogen nitrified (4.33 g O_2/g N; see discussions on nitrification in Section 5.5.3); AOCR = dissolved oxygen/carbon ratio in respiration (2.67 g O_2/g C); K_r = reaeration coefficient (day^{-1}), applied to the surface layer

only; DO_s = saturation concentration of dissolved oxygen ($g\,O_2/m^3$), SOD = sediment oxygen demand ($g\,O_2/m^2/day$), applied to the bottom layer only; a direction of positive is towards the water column; WDO = external loads of dissolved oxygen ($g\,O_2/day$).

5.6.3 Effects of Photosynthesis and Respiration

Detailed discussions on photosynthesis and respiration are presented in Sections 5.2.3 and 5.2.4, respectively. This section focuses on the effects of photosynthesis and respiration on DO in a waterbody, which are represented by the first two terms on the right-hand side of Eq. (5.6.9). Oxygen is a byproduct of aquatic plant photosynthesis. Through photosynthesis and respiration, phytoplankton, periphyton, and rooted aquatic plants (macrophytes) can significantly affect the DO levels in a waterbody and can have a profound effect on the variability of the DO throughout a day or from day to day. Aquatic plants provide a net addition of DO to a waterbody on a daily average basis through photosynthesis, yet respiration can cause low DO levels at night that can affect the survival of aquatic organisms.

In water quality modeling, respiration and photosynthesis are considered as the same reaction but occur in opposite directions. However, photosynthesis only occurs during daylight hours, whereas respiration and decomposition proceed at all times and are not dependent on solar energy. These reactions can be represented by the following simplified equation:

$$6\,CO_2 + 6\,H_2O \underset{\text{Respiration}}{\overset{\text{Photosynthesis}}{\rightleftharpoons}} C_6H_{12}O_6 + 6\,O_2 \tag{5.6.10}$$

where glucose, $C_6H_{12}O_6$, represents organic compounds in plants. In this reaction, photosynthesis converts carbon dioxide and water into glucose and oxygen and leads to a net gain of DO in the waterbody. Conversely, respiration converts glucose and oxygen into carbon dioxide and water resulting in a net loss of DO in the waterbody. Plants generally produce more organic matter and oxygen than they use.

The daily DO maximum commonly occurs in mid-afternoon during which time photosynthesis is the dominant mechanism (Fig. 5.6.1). The daily DO minimum typically occurs in the early morning during which time respiration and decomposition have the greatest effect on DO, and photosynthesis is not occurring. Therefore, excessive algal growth can cause large diurnal DO variation, which might be harmful to an aquatic ecosystem and lead to violations of DO standards. Photosynthesis can also lead to DO supersaturation, a phenomenon whereby the DO concentration in water is above the saturation concentration. Supersaturation occurs when the oxygen sources (Fig. 5.6.4) provide more oxygen to the water column than the oxygen sinks take up.

Because algal growth requires sunlight and nutrients, quantifying photosynthetic oxygen production needs to address algae-nutrient kinetics. The RHS terms associated with B_x in Eq. (5.6.9) account for the effects of algae on DO.

Algae produce oxygen through photosynthesis (the term of P_x) and consume oxygen through respiration (the term of BM_x). The quantity of DO produced also depends on the form of nitrogen utilized for algal growth. Morel (1983) gave the following equations for DO production:

$$106\,CO_2 + 16\,NH_4^+ + H_2PO_4^- + 106\,H_2O \rightarrow \text{protoplasm} + 106\,O_2 + 15\,H^+ \tag{5.6.11}$$

$$106\,CO_2 + 16\,NO_3^- + H_2PO_4^- + 122\,H_2O + 17\,H^+ \rightarrow \text{protoplasm} + 138\,O_2 \tag{5.6.12}$$

where protoplasm is the living substance of algae cells. It is a chemically active mixture of protein, fats, and many other complex substances suspended in water.

Equation (5.6.11) indicates that, when ammonium is the nitrogen source, 1 mol of oxygen is produced per mole of carbon dioxide fixed. Equation (5.6.12) shows that, when nitrate is the nitrogen source, 1.3 (= 138/106) mol of oxygen are produced per mole of carbon dioxide fixed. These two equations are reflected in the first term on the RHS of Eq. (5.6.9) by the quantity of $(1.3–0.3{\cdot}PN_x)$, which is the photosynthesis ratio and represents the molar quantity of oxygen produced per mole of carbon dioxide fixed. When the entire nitrogen source is from ammonium (ammonium preference factor, $PN_x = 1.0$), the quantity is 1.0. When the entire nitrogen source is from nitrate ($PN_x = 0.0$), the quantity is 1.3.

The rate of oxygen production (and nutrient uptake) is proportional to the algal growth rate. Equation (5.6.10) reveals that, for each gram of algae carbon produced by photosynthesis, 32/12 (or ~2.67) g of O_2 are produced. Conversely, for every gram of algae carbon consumed by respiration, 32/12 g of oxygen are also consumed. Hence, the dissolved oxygen/carbon ratio, AOCR, in Eq. (5.6.9) should have AOCR = 2.67 g O_2/g C.

5.6.4 Reaeration

Reaeration is a process by which oxygen is transferred across the interface between the atmosphere and a waterbody, usually resulting in the net transfer of oxygen to the water. Oxygen gas (O_2) constitutes ~21% of the atmosphere and readily dissolves in water. Reaeration is the most important route for introducing oxygen into surface waters. Compared with algal photosynthesis, which can only add DO to water in daylight, reaeration brings DO to water day and night. Natural or artificial reaeration brings the level of DO to saturation. Natural processes, such as winds and water waves, can enhance the rate of oxygen transfer. Artificial agitation can also increase DO in a waterbody. For example, when agitation introduces air into the lower layers of a reservoir, air bubbles form and rise through the water column. The oxygen in the air dissolves into the water and replenishes the DO. The rising air bubbles also

cause the bottom waters to rise to the surface where they take on more oxygen from the atmosphere.

The rate of reaeration is proportional to the DO deficit, which is the difference between the DO concentration and the oxygen saturation value. The term of K_r on the RHS of Eq. (5.6.9), $K_r(DO_s - DO)$, represents the reaeration process mathematically. It indicates that the larger the DO deficit, the higher the rate of reaeration. The conditions of the atmosphere and the waterbody determine the rate of reaeration rate, K_r. The DO deficit is a useful water quality parameter and is influenced by temperature, salinity, and atmospheric pressure.

Typically, oxygen is transferred from the atmosphere into the water, since DO levels in natural waters are generally below saturation. However, when photosynthesis produces supersaturated DO levels (e.g., in the afternoon of a eutrophic reservoir) the net transfer of oxygen can be from the water into the atmosphere.

Reaeration occurs by diffusion of oxygen from the atmosphere into the water (when DO is not saturated) and by the turbulent mixing of water and air. In general, the reaeration rate in natural waters depends on (1) water flow speed and wind speed, (2) water temperature and salinity, and (3) water depth.

Large water flow speed and wind speed lead to strong turbulence activities in the atmosphere and the water. Turbulence and mixing increase reaeration, while quiescent, stagnant conditions reduce reaeration. For example, due to less turbulence and weaker atmospheric exchange of DO, a slow-moving lake may show a greater diurnal DO variation compared to a fast-flowing river. At higher temperatures, water can hold less oxygen when saturated. This condition results in less oxygen being directly available. In addition, the metabolic rate of organisms increases with increasing temperature, which leads to more oxygen consumption. A deeper waterbody tends to be more stratified and more difficult for the surface DO replenished from the atmosphere to be transferred to the lower levels. Water system restoration techniques often take advantage of these relationships, for example, by the installation of artificial cascades to increase reaeration.

Many empirical formulations have been developed for estimating the reaeration rate. When wind effects are excluded, the empirical formulas for the reaeration rate coefficient are based solely on velocity and depth:

$$K_r(20\,^\circ\mathrm{C}) = A \cdot \frac{V^B}{D^C} \tag{5.6.13}$$

where: K_r (20 °C)= reaeration rate at 20 °C (day^{-1}), V = water velocity (m/s), D = water depth (m), and A, B, C = empirical parameters.

When Eq. (5.6.13) is used in a multilayer model, the water depth, D, should be replaced with the thickness of the top layer, Δz. Equation (5.6.13) indicates

TABLE 5.6.1 Values of Empirical Parameters for Reaeration Coefficients

Formulas	A	B	C	Applicable Waters
O'Connor and Dobbins (1958)	3.93	0.50	1.50	Slower, deeper rivers
Churchill et al. (1962)	5.026	0.969	1.673	Moderately deep, faster streams
Owens et al. (1964)	5.34	0.67	1.85	Shallow streams

that a large water velocity and a small water depth lead to a high reaeration coefficient. The values of A, B, and C are listed in Table 5.6.1 for three commonly used formulas: O'Connor and Dobbins (1958) for slower, deeper rivers, Churchill et al. (1962) for moderately deep, faster streams, and Owens et al. (1964) for shallow streams.

Equation (5.6.13) and Table 5.6.1 pertain to the reaeration rate at 20 °C. The effects of water temperature on the reaeration rate are expressed as:

$$K_r = K_r(20\,^{\circ}\mathrm{C}) \cdot 1.024^{(T-20)} \tag{5.6.14}$$

where K_r = reaeration rate at T °C and T = water temperature in °C.

Numerous relationships also exist to include wind-induced reaeration. For example, Banks and Herrera (1977) used the following:

$$K_r = \left(K_{\mathrm{ro}} \sqrt{\frac{u_{\mathrm{eq}}}{h_{\mathrm{eq}}}} + W_{\mathrm{rea}} \right) \frac{1}{\Delta z} \cdot KT_r^{T-20} \tag{5.6.15}$$

where K_{ro} = proportionality constant = 3.933 in MKS units, u_{eq} = weighted velocity over cross-section (m/s), h_{eq} = weighted depth over cross-section (m), W_{rea} = wind-induced reaeration (m/day), KT_r = constant for temperature adjustment of DO reaeration rate, and Δz = the thickness of the surface layer in numerical model.

The wind-induced reaeration is expressed as:

$$W_{\mathrm{rea}} = 0.728U_w^{1/2} - 0.317U_w + 0.0372U_w^2 \tag{5.6.16}$$

where U_w = wind speed (m/s) at the height of 10 m above surface.

For models with sufficient layers to resolve the vertical stratification, the modeled DO concentration should not be that sensitive to the empirical formulas of reaeration rate. The empirical formulas are only applied in the top layer, where DO is often near the saturation concentration no matter which empirical formula is used. Ji et al. (2004a) reported that even when the bottom DO is almost zero in a very stratified reservoir, the surface DO can still be around the saturation concentration. This makes the modeled DO concentrations less sensitive to the reaeration rate.

Water temperature affects the saturated DO concentration. Lower water temperature leads to higher saturated DO concentration. The saturated DO concentration is empirically expressed as a function of temperature and salinity (APHA, 2000):

$$\begin{aligned} DO_s = \exp\Bigg[& -139.3441 + \frac{1.575701 \times 10^5}{T_k} - \frac{6.6423 \times 10^7}{T_k^2} \\ & + \frac{1.2438 \times 10^{10}}{T_k^3} - \frac{8.621949 \times 10^{11}}{T_k^4} \\ & - S\left(1.7674 \times 10^{-2} - \frac{1.0754 \times 10^1}{T_k} + \frac{2.1407 \times 10^3}{T_k^2} \right) \Bigg] \end{aligned} \tag{5.6.17}$$

where T_k = temperature in K (= 273.15 + °C) and S = salinity in ppt.

By fitting a second-order polynomial curve to measured data, Chapra and Canale (1998) derived a regression equation for DO_s:

$$DO_s = 0.0035 \cdot T^2 - 0.3369 \cdot T + 14.407 \tag{5.6.18}$$

where T = water temperature in °C. Equation (5.6.18) yields DO saturation concentrations very similar to the ones from Eq. (5.6.17) at $S = 0.0$. The RMS error (difference) between the two is only 0.08 mg/L for water temperatures between 0 and 40 °C, even though Eq. (5.6.18) is much simpler than Eq. (5.6.17). Figure 5.6.5 gives the values of DO_s from Eq. (5.6.17) at $S = 0$, 15, and 35 ppt. Fig. 5.6.5 reveals that as temperature (or salinity) increases, the amount of oxygen that water can hold decreases substantially. For example, at 10 °C, saturation DO is 11.29 mg/L for freshwater and is only 9.02 mg/L for water with 35 ppt salinity. At 30 °C, saturation DO is 7.56 mg/L at $S = 0.0$ and is only 6.24 mg/L at $S = 35$ ppt.

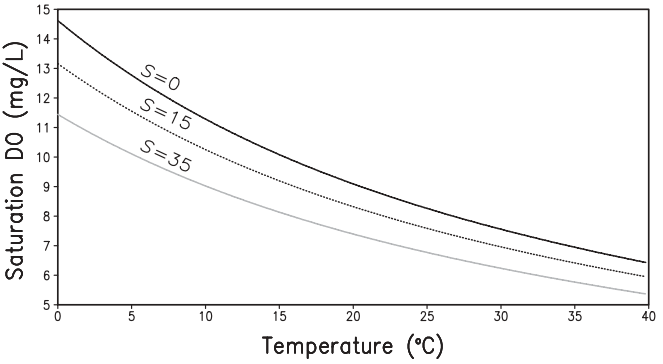

Fig. 5.6.5 Saturation DO concentration (mg/L) as a function of temperature (°C) at salinity equal to 0, 15, and 35 ppt.

Hyer et al. (1971) derived another empirical formula for saturation DO by including the effect of salinity:

$$DO_s = 14.6244 - 0.367134 \cdot T + 0.0044972 \cdot T^2 + S \cdot (-0.0966 + 0.00205 \cdot T + 0.0002739 \cdot S) \quad (5.6.19)$$

5.6.5 Chemical Oxygen Demand

There are a variety of definitions for COD. Generally, COD represents the reduction of DO caused by chemical reactions. Chemical oxygen demand is widely used to represent the overall level of organic contamination in wastewater. The larger the COD value, the more oxygen the wastewater discharge demands from the receiving waterbody. However, in some water quality models (e.g., Cerco and Cole, 1994; Park et al., 1995), COD is used to represent the oxygen demand from reduced substances, such as sulfide in saline water or methane in freshwater. Both sulfide and methane are quantified in units of oxygen demand and are treated with the same kinetic formulation. The COD source is from the sediment diagenesis process in the sediment bed. The kinetic equation is

$$\frac{\partial \mathrm{COD}}{\partial t} = -\frac{\mathrm{DO}}{\mathrm{KH_{COD}} + \mathrm{DO}} \mathrm{KCOD} \cdot \mathrm{COD} + \frac{\mathrm{BFCOD}}{\Delta z} + \frac{\mathrm{WCOD}}{V} \quad (5.6.20)$$

where COD = COD concentration (g O_2-equivalents/m^3); KH_{COD} = half saturation constant of DO required for oxidation of COD (g O_2/m^3); KCOD = oxidation rate of COD (day^{-1}); BFCOD = COD sediment flux (g O_2-equivalents/m^2/day), applied to the bottom layer only and estimated in Section 5.7; and WCOD = external loads of COD (g O_2-equivalents/day).

The external loads, WCOD, are usually 0. An exponential function is used to describe the temperature effect on the oxidation rate of COD:

$$\mathrm{KCOD} = K_{\mathrm{CD}} \cdot e^{\mathrm{KT_{COD}}(T - \mathrm{TR_{COD}})} \quad (5.6.21)$$

where K_{CD} = oxidation rate of COD at TR_{COD} (day^{-1}), KT_{COD} = effect of temperature on oxidation of COD ($°C^{-1}$), TR_{COD} = reference temperature for oxidation of COD (°C).

5.7 SEDIMENT FLUXES

As discussed in Chapters 3 and 4, sediment not only affects water turbidity, but also carries chemicals, such as nutrients and toxic materials, that can affect water quality. Particulate organic matters deposited into the sediment bed undergo a decomposition or mineralization process, referred to as diagenesis. The dissolved inorganic nutrients in the sediment bed can then be recycled

back to the water column in the form of sediment fluxes. Nutrients released from the sediment bed and SOD can contribute significantly to eutrophication problems, even after external sources have been substantially reduced. Therefore, a critical aspect of water quality modeling, particularly for long-term simulations, is to describe sediment diagenesis processes in the sediment bed and to estimate sediment fluxes released from the bed.

Sediment diagenesis processes presented in this chapter are different from the sediment processes described in Chapter 3, in which cohesive and noncohesive sediments are discussed. Physically, the same sediment bed of a waterbody is addressed in both chapters. However, Chapter 3 is focused on the transport, deposition, and resuspension of sediments, while this chapter deals with the diagenesis processes and the sediment fluxes that affect the eutrophication processes. Historically, the sediment transport modeling (in Chapter 3) and the water quality modeling (in this chapter) were mostly carried out by two different groups of modelers with different application objectives, and these two types of models are generally not closely coupled. For example, the changes of bed thickness due to sediment deposition–resuspension are generally not reflected in sediment diagenesis models (e.g., Cerco and Cole, 1994). The linkage between the sediment processes and the water quality processes is often via the sorption and desorption of phosphorus and silica to the suspended sediment (Park et al., 1995). It is necessary to directly link the benthic processes in the sediment model with the ones in the water quality model. Section 5.7.6 will discuss how sediment resuspension affects nutrient entrainment from the sediment bed.

Particulate organic matters, such as algae, settle to the bottom of the water column and decompose via aerobic or anaerobic processes. High levels of organic matter in sediments may create a significant SOD when the organic matters break down. Decomposing organic matter reduces oxygen concentrations and can lead to or maintain anoxic conditions. Nutrient concentrations in the pore waters and bottom waters, particularly ammonia and phosphate, may build up to high concentrations. Nitrate in the anoxic water column and sediment bed may become denitrified. Under oxic conditions, the ammonia released from sediments is directly transformed into nitrate (nitrification). The sediment bed often represents a major storage of phosphorus in a waterbody. Phosphorus released from the sediments to the overlying water is increased under anoxic conditions. Sediment fluxes also depend on the characteristics of the bed. A sandy bed contains relatively little organic matter for the sediment diagenesis process because the sand is often unstable and nutrient deficient. A muddy bottom often contains abundant nutrient sources.

Internal recycling of nitrogen and phosphorus from the sediment bed can sustain eutrophic conditions for long periods even if external loading is reduced. Shallow lakes with a long history of receiving nutrient-rich inflows are especially likely to maintain high rates of internal recycling. These internal loads occur through diffusion and sediment resuspension from the bed to the water column. As a result, lake restoration through reduction of external loads

may take decades to succeed (Rossi and Premazzi, 1991). For example, Lake Okeechobee is shallow with an average depth of 3.2 m. The internal phosphorus load is approximately equivalent to the external loads. This internal load resulted from decades of excessive P loads to the lake (Havens et al., 1996). Despite the continuous reduction in external loads of TP and TN in two decades (1979–1998), the improvement of the lake water quality is not statistically significant. The lack of a response of water column TP to reductions in external P loads is in part attributed to this internal sediment P load (James et al., 1995a, b).

The sediment diagenesis model described in this section is primarily based on the Chesapeake Bay Sediment Flux Model developed by Di Toro and Fitzpatrick (1993), which is now commonly accepted and used in water quality modeling (e.g., Cerco and Cole, 1994; Park et al., 1995; HydroQual, 1995c). Complete model documentation can be found in Di Toro and Fitzpatrick (1993) and Di Toro (2001). Many discussions and equations in this chapter originate from the report by Park et al. (1995).

5.7.1 Sediment Diagenesis Model

Benthic environment refers to the environment at the bottom of an aquatic system. Diagenesis includes the net effect of all physical and biogeochemical processes active in the sediment bed. In the sediment diagenesis model, diagenesis is used to represent the decay process of organic matters (Di Toro and Fitzpatrick, 1993). An example of diagenesis is the transformation of particulate organic nitrogen to ammonia under an aerobic condition.

Sediment fluxes from the bed due to diagenetic reactions can be substantial nutrient sources or oxygen sinks. During organic matter decomposition in benthic sediments, there is considerable oxygen demand that must be supplied from the overlying water column. This SOD may comprise a substantial fraction of the total oxygen consumption in an aquatic system. The occurrence of anoxia, partially due to SOD, can dramatically increase certain nutrient fluxes. Over long time scales (e.g., decades), benthic sediments act as sinks for nutrients and other substances that are removed from the water column. Certain fractions of deposited nutrients, such as nitrogen, phosphorus, and silica, are buried in deeper sediment layers and are permanently removed from the aquatic system. However, over a time scale of months and seasons, benthic sediments can be significant nutrient sources to the overlying water, especially during summer. Warm water may lead to enhanced chemical and biological processes in the sediments and a large amount of dissolved nutrients released back into the overlying water.

Approaches to incorporate sediment fluxes into water quality models include the following:

1. Specifying the fluxes based on measured data and literature values and adjusting the fluxes as model calibration parameters

2. Calculating the fluxes from a sediment diagenesis model and coupling this model with the water quality model of the overlying water

The first approach is traditionally used in water quality models that do not dynamically simulate benthic processes (e.g., Brown and Barnwell, 1987). Spatially varying fluxes are specified for dissolved nutrients and SOD. Time functions may also be utilized to reflect seasonal changes. The sediment fluxes are site-specific and are determined largely by model calibration to make model results fit measured data. With this approach, the difficulty arises when SOD values need to be predicted for future conditions, such as wasteload reduction scenarios for water resource management. Thus, this approach does not lead to a robust estimate of benthic fluxes and introduces major uncertainty in the use of a water quality model as a predictive and management tool.

Significant efforts have been made to realistically simulate the diagenetic reactions and the sediment fluxes. Sediment diagenesis models describe the sediment processes that control nutrient fate in the sediments. These models are useful for evaluating sediment response to changes in external nutrient loads and for predicting nutrient fluxes across the sediment-water interface. Since the sediment fluxes can affect the water quality process in the overlying water column significantly, it is necessary to couple the sediment diagenesis model with the water quality model, especially for long-term (multi-season or multi-year) simulations.

The sediment diagenesis model (Di Toro and Fitzpatrick, 1993), like water quality models, is based on the principle of mass conservation. The benthic sediment receives fluxes of POC, PON, POP, particulate silica (Si), and algae from the water column (Fig. 5.7.1). The amount of POM in benthic sediments increases as algae and organic detritus settle to the bottom and decrease as the sediments decompose. The sediments undergo decay processes similar to the ones in the water column, but with the decay products going to the interstitial water rather than the overlying water. These decay products can react in the aerobic and anaerobic layers. The nutrients in the interstitial waters

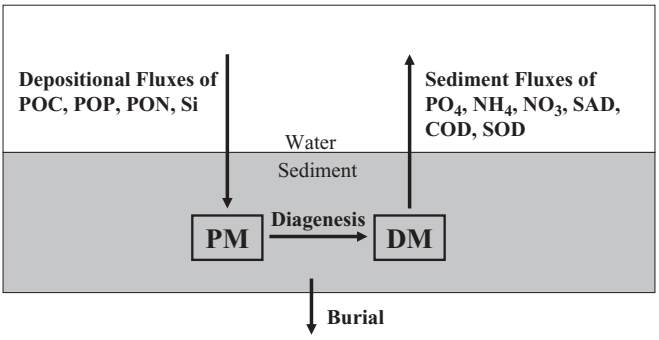

Fig. 5.7.1 Components of a sediment diagenesis model.

diffuse to the overlying water at a rate depending on the concentration difference between the interstitial water and overlying water. The model also includes the burial of nutrients into deeper sediment layers, which permanently removes the nutrients from the aquatic system.

Primary features of the sediment diagenesis model include (Di Toro and Fitzpatrick, 1993):

1. *Three Fluxes:* the model represents the depositional fluxes of particulate matters from the water column to the benthic bed, the diagenesis (decay) fluxes of the particulate matters in the bed, and sediment fluxes of the dissolved nutrients from the bed back into the overlying water.
2. *Two-Layer Structure of the Benthic Bed:* the upper layer is thin and is often aerobic, and the lower layer is permanently anaerobic (Fig. 5.7.2).
3. *Three G Classes of Benthic Sediments:* The particulate organic matters are split into three fractions (G classes) with different decay rates.

These features are presented in this section.

5.7.1.1 Three Fluxes of the Sediment Diagenesis Model. The sediment diagenesis model can be schematically represented in three principal fluxes (components) (Fig. 5.7.1):

1. The deposition of particulate matters (PM) from the water column to the sediment bed.
2. Diagenesis (or decay) process in the bed converting the PM into dissolved matter (DM).
3. The sediment fluxes transporting the DM from the bed to the overlying water and the burial of dissolved and particulate matters into deeper sediment layers.

First, the sediment bed receives depositional fluxes of POC, POP, PON, and particulate Si from the overlying water (Fig. 5.7.1). These four depositional fluxes provide the external sources to the benthic sediments. For a sediment diagenesis model with a two-layer structure (Fig. 5.7.2), the upper layer is often aerobic and thin, but the lower layer is anaerobic. Because of the negligible thickness of the upper layer, the deposition is treated as occurring directly from the water column to the lower layer.

Second, the diagenesis (decay) process converts the deposited particulate matters into dissolved matters within the lower layer and produces diagenesis fluxes. The mineralization of POM leads to dissolved organic matter, and the hydrolysis of particulate silica yields dissolved Si. The diagenesis fluxes are the sources for the sediment fluxes.

Third, dissolved matters react in the aerobic and anaerobic layers of the sediment bed. The DM produced by diagenesis in the lower layer are either

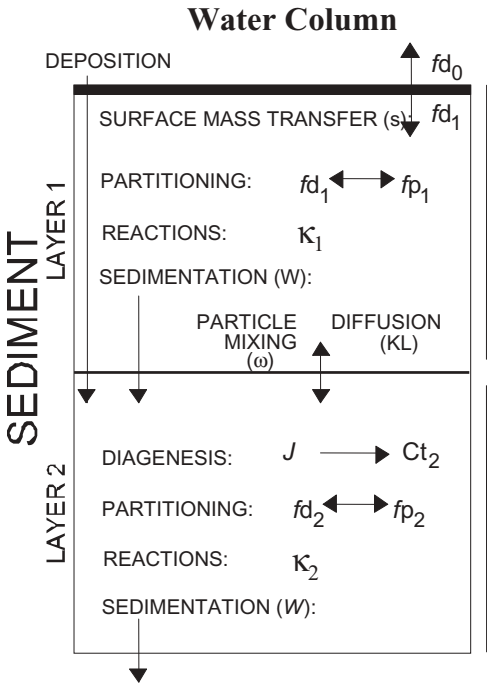

Fig. 5.7.2 Sediment layers and processes included in the sediment diagenesis model (Di Toro and Fitzpatrick, 1993).

transferred to the upper layer and then to the overlying water as sediment fluxes or buried to the deeper layer. The sediment diagenesis model includes sediment fluxes of six variables: PO_4, NH_4, NO_3, SAD, COD, and SOD (Fig. 5.7.1). These sediment fluxes are caused by diffusion between the water column and the sediment bed. The sediment resuspension discussed in Chapter 3 can entrain large amounts of sediment and POM from the bed into the water column when the bottom shear stress is large. This nutrient transfer mechanism will be discussed in Section 5.7.6.

5.7.1.2 Two-Layer Structure of Benthic Sediment. Figure 5.7.2 represents a two-layer structure of a sediment diagenesis model (other processes shown in Fig. 5.7.2 will be discussed later). The upper layer is a thin layer in contact with the water column and may be aerobic or anaerobic, depending on the DO concentration in the overlying water. The thickness of this thin layer is determined by the DO concentration in the water overlying the sediment and by the rate of oxygen consumption in the sediment. The lower layer is permanently anaerobic, with typical depths ranging from 5 to 15 cm. Due to the negligible thickness of the upper layer, PM from the water column is assumed to be deposited directly to the lower, anaerobic layer. The deposited

organic matter is oxidized in the upper aerobic layer, but is reduced in the lower anaerobic layer. A portion of the deposited material is also buried in the deeper layer via sedimentation and is permanently removed out of the aquatic system.

The thickness of the upper, aerobic layer is determined by the penetration of oxygen into the sediment and is only a small fraction of the total depth. It has the form:

$$H = H_1 + H_2 \approx H_2 \tag{5.7.1}$$

where H = the total depth (typically 10 cm), H_1 = the upper layer depth (typically 0.1 cm), H_2 = the lower layer depth.

The total depth of benthic sediment, H, is an important parameter in the sediment diagenesis model. It represents the active depth of the benthic organism mixing and determines the volume of the anaerobic layer. Active depths of 5–15 cm have been reported for estuaries. A value of 10 cm seems appropriate (Di Toro and Fitzpatrick, 1993). Sediments below this depth cannot be recycled into the active layer and are assumed to be permanently removed from the aquatic system. In the study of the sediment–water flux of hydrophotic organic chemicals, however, Lick (2006) argued that a well-mixed layer of benthic sediment bed often may not exist, and, when it does, it is slow to form, that its depth is difficult to define and even harder to quantify.

The memory of the sediment bed is much longer than the memory of the water column. The magnitude of H (or H_2) controls the long-term response time of the bed. The thickness of the active sediment layer should reflect the influence from the overlying water and have a reasonable time memory. If H is too small, the model will remember or be influenced by recent deposition, occurring only within the last one or two years. If H is too large, the model results will be averaged over a period that is too long and does not reflect the recent changes in the external loadings, for example, the reduction of nutrient loadings from a wastewater treatment plant. The sedimentation rate of the deposited material also affects the memory of the sediment diagenesis model. It is ideal to have measured data for estimating the active sediment thickness. However, in the event that there is no measured data available, which is often the case in many modeling studies, it is necessary to have the benthic sediment depth, together with the sedimentation rate, to provide for a multiyear memory of the sediment bed. In the study of Norwalk Harbor, Connecticut, for example, Lung (2001) selected the sediment layer depths and the sedimentation rates so that the memory of the bed was ~10 years.

5.7.1.3 Three G Classes of Sediment Organic Matter. After being deposited on the bottom of a waterbody, POM experience diagenesis pro-

cesses at different decay rates. The readily degradable POM are depleted shortly, while more refractory materials remain. Beginning with the early work of Berner (1964), diagenetic models with a few different decay rates, termed "G class" models (after the symbols used to identify POM in each class), have met with much success in fitting measured data (Westrich and Berner, 1984).

Three G classes (or fractions) are commonly used in water quality models (e.g., Di Toro and Fitzpatrick, 1993). They are derived from different forms of organic matters in the benthic sediments and categorized as rapidly degrading, moderately degradable, or nondegradable (refractory). These classes are termed G_1, G_2, and G_3, respectively. Each class represents a portion of the organic material that decays at a specific rate, and each G class has its own mass conservation equation. The decay rates for each class are approximately an order of magnitude smaller than the previous class:

1. The G1 (labile) fraction has a half-life on the order of 20 days.
2. The G2 (refractory) fraction has a half-life on the order of 200 days.
3. The G3 (inert) fraction has no significant decay before being buried into deep, inactive sediments.

The decay rates of the G classes control the production rates of diagenesis fluxes and the sediment fluxes. If a large portion of the deposited POM is in the G1 class, then the diagenesis fluxes will respond to the depositional fluxes rapidly, and the sediment fluxes will also increase shortly afterward since there will be a short time lag introduced by mineralization.

5.7.1.4 State Variables of the Sediment Diagenesis Model. The sediment diagenesis model developed by Di Toro and Fitzpatrick (1993) has been incorporated into surface water quality models (e.g., Cerco and Cole, 1994; HydroQual, 1995c). In the EFDC model (Park et al., 1995), the sediment diagenesis submodel has 27 state variables/fluxes (Table 5.7.1). The particulate organic matters, including POC, PON, and POP, are all split into three G classes and exist only in Layer 2 (Fig. 5.7.2), since they are deposited from the water column directly into the lower layer. For the same reason, the particulate biogenic silica (state variable 10 in Table 5.7.1) also is present in Layer 2 only.

State variables 11–20 in Table 5.7.1 represent the five inorganic substances (sulfide/methane, NH_4, NO_3, PO_4, and SA) in the 2 layers. These substances are primarily the products of the diagenesis (decay) processes of the deposited particulate matters from the water column. The nitrate state variables (15, 16, and 22) represent the sum of nitrate (NO_3) nitrogen and nitrite (NO_2) nitrogen. State variables 21–26 are the six sediment fluxes that feed back to the overlying water. Four of them (NH_4, NO_3, PO_4, and SA) provide nutrients to

TABLE 5.7.1 EFDC Sediment Diagenesis Model State Variables and Fluxes[a]

(1) Particulate organic carbon G1 class in Layer 2
(2) Particulate organic carbon G2 class in Layer 2
(3) Particulate organic carbon G3 class in Layer 2
(4) Particulate organic nitrogen G1 class in Layer 2
(5) Particulate organic nitrogen G2 class in Layer 2
(6) Particulate organic nitrogen G3 class in Layer 2
(7) Particulate organic phosphorus G1 class in Layer 2
(8) Particulate organic phosphorus G2 class in Layer 2
(9) Particulate organic phosphorus G3 class in Layer 2
(10) Particulate biogenic silica in Layer 2
(11) Sulfide–methane in Layer 1
(12) Sulfide–methane in Layer 2
(13) Ammonia nitrogen in Layer 1
(14) Ammonia nitrogen in Layer 2
(15) Nitrate nitrogen in Layer 1
(16) Nitrate nitrogen in Layer 2
(17) Phosphate phosphorus in Layer 1
(18) Phosphate phosphorus in Layer 2
(19) Available silica in Layer 1
(20) Available silica in Layer 2
(21) Ammonia nitrogen flux
(22) Nitrate nitrogen flux
(23) Phosphate phosphorus flux
(24) Silica flux
(25) Sediment oxygen demand
(26) Release of chemical oxygen demand
(27) Sediment temperature

[a]Park et al., 1995.

the water column. The other two (SOD and COD) uptake oxygen from the water column. In the event that the sediment diagenesis submodel is not utilized in the water quality model, these six sediment fluxes need to be specified as model input parameters. When integrated into the water quality model, the sediment diagenesis model simulates the nutrient exchanges across the sediment–water interface at each model time step, thus providing a true dynamic representation of the system (Park et al., 1995).

Sediment temperature (state variable 27) is calculated based on the diffusion of heat between the water column and the bed:

$$\frac{\partial T}{\partial t} = \frac{D_T}{H^2}(T_W - T) \tag{5.7.2}$$

where T = temperature of the benthic sediment (°C), T_W = temperature in the overlying water column (°C), calculated in the hydrodynamic model, and D_T = heat diffusion coefficient between the water column and sediment ($= 1.8 \times 10^{-7}\,m^2/s$).

5.7.2 Depositional Fluxes

Benthic sediments in a waterbody come from two major sources:

1. External loads provide inorganic particulates and some organic materials, which form coarse sediments around a receiving area and become finer away from the receiving area.
2. Detritus from the dead aquatic organisms within the waterbody settle to the bottom and generate the "rain" of particulate matters, which tend to accumulate in deep areas, whereas in shallower areas, the constant mixing recycles them back into the water column.

Deposition is a key process that couples the water quality model of the water column with the sediment diagenesis model. In the previous sections of this chapter, all of the PM, including algae, POC, POP, PON, and silica, have a settling term in their kinetic equations [e.g., Eq. (5.2.6) for algae]. The general form is

$$\frac{\partial \mathrm{PM}}{\partial t} = \text{kinetics} + \frac{\partial}{\partial z}(\mathrm{WS_{PM}} \cdot \mathrm{PM}) + \text{loadings} \tag{5.7.3}$$

where PM = concentration of the particulate matter and $\mathrm{WS_{PM}}$ = settling velocity of the particulate matter.

The settling velocity, $\mathrm{WS_{PM}}$, represents the net deposition to the sediment bed due to the difference between the downward settling flux and the upward resuspension flux. It represents a long-term average of POM settling and does not reflect short-term fluctuations caused by sediment resuspension and deposition. The settling flux of ($\mathrm{WS_{PM}} \cdot \mathrm{PM}$) leaves the water column, settles on the sediment bed, and becomes the depositional flux in the sediment diagenesis model.

In the water quality model, the following state variables contribute to the depositional fluxes:

1. Three algal groups, cyanobacteria, diatoms and green algae [Eq. (5.2.6)].
2. Refractory and labile particulate organic carbon [Eqs. (5.3.5) and (5.3.6)].
3. Refractory and labile particulate organic phosphorus [Eqs. (5.4.2) and (5.4.3)] and particulate phosphate [Eq. (5.4.7)].
4. Refractory and labile particulate organic nitrogen [Eqs. (5.5.5) and (5.5.6)].
5. Particulate biogenic silica [Eq. (5.2.31)] and sorbed available silica [Eq. (5.2.32)].

The sediment diagenesis model receives the depositional fluxes of POC, PON, POP, and particulate biogenic silica (PSi), and they are treated

analogously. Since the sediment model has three G classes of PM, the depositional fluxes for the ith G class (i = 1, 2, or 3) are expressed as:

$$J_{\mathrm{POC},i} = \mathrm{FCLP}_i \cdot \mathrm{WS}_{\mathrm{LP}} \cdot \mathrm{LPOC} + \mathrm{FCRP}_i \cdot \mathrm{WS}_{\mathrm{RP}} \cdot \mathrm{RPOC} + \sum_{x=c,d,g} \mathrm{FCB}_{x,i} \cdot \mathrm{WS}_x \cdot B_x \tag{5.7.4}$$

$$J_{\mathrm{PON},i} = \mathrm{FNLP}_i \cdot \mathrm{WS}_{\mathrm{LP}} \cdot \mathrm{LPON} + \mathrm{FNRP}_i \cdot \mathrm{WS}_{\mathrm{RP}} \cdot \mathrm{RPON} + \sum_{x=c,d,g} \mathrm{FNB}_{x,i} \cdot \mathrm{ANC}_x \cdot \mathrm{WS}_x \cdot B_x \tag{5.7.5}$$

$$J_{\mathrm{POP},i} = \mathrm{FPLP}_i \cdot \mathrm{WS}_{\mathrm{LP}} \cdot \mathrm{LPOP} + \mathrm{FPRP}_i \cdot \mathrm{WS}_{\mathrm{RP}} \cdot \mathrm{RPOP} + \sum_{x=c,d,g} \mathrm{FPB}_{x,i} \cdot \mathrm{APC} \cdot \mathrm{WS}_x \cdot B_x + \gamma_i \cdot \mathrm{WS}_{\mathrm{TSS}} \cdot \mathrm{PO4p} \tag{5.7.6}$$

$$J_{\mathrm{PSi}} = \mathrm{WS}_d \cdot \mathrm{SU} + \mathrm{ASC}_d \cdot \mathrm{WS}_d \cdot B_d + \mathrm{WS}_{\mathrm{TSS}} \cdot \mathrm{SAp} \tag{5.7.7}$$

where $J_{\mathrm{POM},i}$ = depositional flux of POM (M = C, N, or P) routed into the ith G class (g/m^2/day); J_{PSi} = depositional flux of PSi (g Si/m^2 day); FCLP_i, FNLP_i, and FPLP_i = fraction of water column labile POC, PON, and POP, respectively, routed into the ith G class in sediment; FCRP_i, FNRP_i, and FPRP_i = fraction of water column refractory POC, PON, and POP, respectively, routed into the ith G class in sediment; $\mathrm{FCB}_{x,i}$, $\mathrm{FNB}_{x,I}$, and $\mathrm{FPB}_{x,i}$ = fraction of POC, PON, and POP, respectively, in the algal group x (=c, d, g) routed into the ith G class in sediment; and γ_i = an index.

Equations (5.7.4)–(5.7.7) give a total of 10 (=3 × 3 + 1) depositional fluxes from the water column to the bed, corresponding to the first 10 state variables in Table 5.7.1. The settling velocities, $\mathrm{WS}_{\mathrm{LP}}$, $\mathrm{WS}_{\mathrm{RP}}$, and WS_x, are net settling velocities.

In Eq. (5.7.6), the settling of particulate phosphate is determined by the settling velocity of the total suspended solids, $\mathrm{WS}_{\mathrm{TSS}}$, which comes from the sediment models discussed in Chapter 3. The index, γ_i, has the form:

$$\gamma_i = \begin{cases} 1, & \text{if } i = 1 \\ 0, & \text{if } i = 2 \text{ or } 3 \end{cases} \tag{5.7.8}$$

which means that all of the particulate organic phosphate, PO4p, is mapped into G1 class.

In Eqs. (5.7.4)–(5.7.6), the POM fluxes from the water column are split into three portions (G classes) using the distribution coefficients. For example, FCLP_1 represents the fraction of LPOC from the water column that is mapped into the G_1 class, and $\mathrm{FCB}_{c,3}$ represents the fraction of POC in cyanobacteria (blue-green algae) that is mapped into the G_3 class. Silica is not subject to the diagenesis (decay) process and is not split into G classes. Instead, dissolution converts particulate silica into dissolved silica, which then can be transferred back into the overlying water.

The sum of the distribution coefficients should be unity:

$$\sum_{i=1}^{3} \mathrm{FCLP}_i = \sum_{i=1}^{3} \mathrm{FNLP}_i = \sum_{i=1}^{3} \mathrm{FNLP}_i = 1 \qquad \text{for labile organic matters} \tag{5.7.9}$$

$$\sum_{i=1}^{3} \mathrm{FCRP}_i = \sum_{i=1}^{3} \mathrm{FNRP}_i = \sum_{i=1}^{3} \mathrm{FPRP}_i = 1 \qquad \text{for refractory organic matters} \tag{5.7.10}$$

$$\sum_{i=1}^{3} \mathrm{FCB}_{x,i} = \sum_{i=1}^{3} \mathrm{FNB}_{x,i} = \sum_{i=1}^{3} \mathrm{FPB}_{x,i} = 1 \qquad \text{for algae} \tag{5.7.11}$$

5.7.3 Diagenesis Fluxes

The kinetic equation for POM in a sediment bed is derived based on the mass balance equation:

$$\text{Net POM change} = -\text{decay of POM} - \text{burial} + \text{depositional flux} \tag{5.7.12}$$

Because the upper layer thickness is negligible [Eq. (5.7.1)], the depositional fluxes are considered to proceed directly to the lower layer, and the diagenesis occurs in the lower layer only. The kinetic equations are similar for POC, PON, and POP and for different G classes. In the lower, anaerobic layer and for the ith G class (i = 1, 2, or 3), Eq. (5.7.12) is expressed as:

$$H_2 \frac{\partial G_{\mathrm{POM},i}}{\partial t} = -K_{\mathrm{POM},i} \cdot \theta_{\mathrm{POM},i}^{T-20} \cdot G_{\mathrm{POM},i} \cdot H_2 - W \cdot G_{\mathrm{POM},i} + J_{\mathrm{POM},i} \tag{5.7.13}$$

where $G_{\mathrm{POM},i}$ = concentration of POM (M = C, N or P) in the ith G class in Layer 2 (g/m^3), $K_{\mathrm{POM},i}$ = decay rate of the ith G class POM at 20 °C in Layer 2 (day^{-1}), $\theta_{\mathrm{POM},i}$ = constant for temperature adjustment for $K_{\mathrm{POM},i}$, T = sediment temperature (°C), and W = burial rate (m/day).

In Eq. (5.7.13), the G_3 class is treated as inert and has $K_{\mathrm{POM},3} = 0$. The sedimentation process buries a portion of the POM into the deeper sediment layers and permanently removes the POM from the aquatic system. The depositional fluxes, $J_{\mathrm{POM},i}$, are the source terms that drive the diagenesis process.

The POM settle on the bed and increase the overall thickness of sediment. Since the total depth, H in Eq. (5.7.1), is set to be constant in the model, the active layer moves upward as the total depth increases. The speed at which the layer moves vertically is referred to as "burial rate". This mechanism causes a permanent loss (or burial) of sediment from the active layer (and from the sediment diagenesis model). The magnitude of the burial per unit area per day is $W \cdot G_{\mathrm{POM},i}$.

In Eq. (5.7.13), the inert class (G3) produces no diagenesis fluxes. The decay of the two reactive G classes produces the diagenesis fluxes:

$$J_M = \sum_{i=1}^{2} K_{\mathrm{POM},i} \cdot \theta_{\mathrm{POM},i}^{T-20} \cdot G_{\mathrm{POM},i} \cdot H_2 \tag{5.7.14}$$

where J_M = diagenesis flux (g/m^2/day) of carbon (M = C), nitrogen (M = N), or phosphorus (M = P).

5.7.4 Sediment Fluxes

As shown in the previous two sections, the calculations of depositional fluxes and the diagenesis fluxes are relatively simple and straightforward. The calculation of sediment fluxes, however, is much more complex in the sediment diagenesis model. The diagenesis (decay) of POM produces soluble intermediate products that are quantified as the diagenesis fluxes in Eq. (5.7.14). These intermediate products react in the upper, aerobic layer and in the lower, anaerobic layer. Portions of the end products are returned to the overlying water as sediment fluxes. This section describes the calculation of sediment fluxes for ammonium, nitrate, phosphate, sulfide/methane, and the sediment oxygen demand. The sediment flux of silica will be discussed in Section 5.7.5.

The kinetic equations of the dissolved nutrients and DO in the water column are typically formulated as:

$$\frac{\partial \mathrm{DM}}{\partial t} = \text{kinetics} + \frac{B\mathrm{Flux}}{\Delta z} + \text{loadings} \tag{5.7.15}$$

where DM = concentration of the dissolved matter, BFlux = sediment flux of the dissolved matter, and Δz = the thickness of the bottom layer in the water column model.

The sediment flux, BFlux, can be a significant fraction of the total nutrient (or SOD) source. This contribution is particularly true in stratified water systems during high-temperature periods. For example, SOD can be significantly large due to decomposition of organic matter and nitrification and cause severe DO depletion in the bottom of the water column.

Generally, processes affecting sediment fluxes include (Fig. 5.7.2):

1. Diagenesis in the lower layer.
2. Reactions in both layers.
3. Partitioning between particulate and dissolved fractions in both layers.
4. Sedimentation from the upper to lower layer and from the lower layer to deep inactive sediment.
5. Particle mixing between the layers.
6. Diffusion between the layers.
7. Mass transfer between the upper layer and the water column.

As an example, Table 5.7.2 gives the measured sediment fluxes in Lake Okeechobee (Fisher et al., 2005). Measured dissolved reactive phosphorus (DRP) is often treated as PO4d defined by Eq. (5.4.9) when conducting model-

TABLE 5.7.2 Shows the Averaged Sediment Fluxes of DRP, NH_4, and SOD in Lake Okeechobee[a,b]

Station	DRP ($mg/m^2/day$)	NH_4 ($mg/m^2/day$)	SOD ($mg/m^2/day$)
Taylor Creek	0.39 (±0.23)	40.1 (±5.7)	863 (±202)
Kissimmee River	0.58 (±0.05)	21.1 (±2.4)	652 (±159)
J5	0.37 (±0.36)	12.2 (±4.4)	471 (±159)
J7	0.62 (±0.29)	26.8 (±4.4)	891 (±117)
M9	1.01 (±0.03)	5.2 (±2.8)	718 (±55)
H9	0.51 (±0.39)	10.7 (±9.3)	539 (±118)
M17	2.12 (±1.16)	15.9 (±10.3)	893 (±223)
Average	0.78 (±0.58)	18.8 (±11.7)	718 (±173)

[a]Standard deviations are in parentheses.
[b]Fisher et al., 2005.

data comparison. Table 5.7.2 shows that the averaged sediment fluxes in milligram per square meter per day ($mg/m^2/day$) are 0.78 for DRP, 18.8 for NH_4, and 718 for SOD.

5.7.4.1 Basic Equations. On the bottom of a waterbody, nutrients are constantly exchanged between the sediment bed and the overlying water. This exchange is largely a diffusion process, controlled by the difference in the nutrient concentrations between the sediment and the overlying water. Nutrients diffuse from a region of high concentration to a region of low concentration. Fick's law indicates that the rate of nutrient transfer due to diffusion is inversely proportional to the gradient of nutrient concentration:

$$J = -D\frac{\partial C}{\partial z} \tag{5.7.16}$$

where J = nutrient flux ($ML^{-2}T^{-1}$), C = nutrient concentration (ML^{-3}), D = diffusion coefficient (L^2/T), and z = vertical distance (L).

In an eutrophic system, nutrient concentration in the sediment bed is generally higher than the concentration in the overlying water. This difference leads to the net nutrient flux from the bed to the overlying water (Fig. 5.7.3). Dissolved oxygen concentration is usually lower in the bed than in the water column, which leads to a net DO flux from the water column to the bed (or equivalently, a SOD flux from the bed to water column). Water flow (and the turbulence) also affects the diffusion between the sediment bed and the overlying water. Water flow may physically disturb the sediments and increase the efficiency of diffusion. The flushing mechanism introduced by water flow maintains a low nutrient concentration in the overlying water and prevents a decline in the concentration gradient. In the sediment bed, transport of nutrients and SOD commonly occurs through diffusion and through the mixing of the upper 5–15 cm of the sediment (Di Toro, 2001).

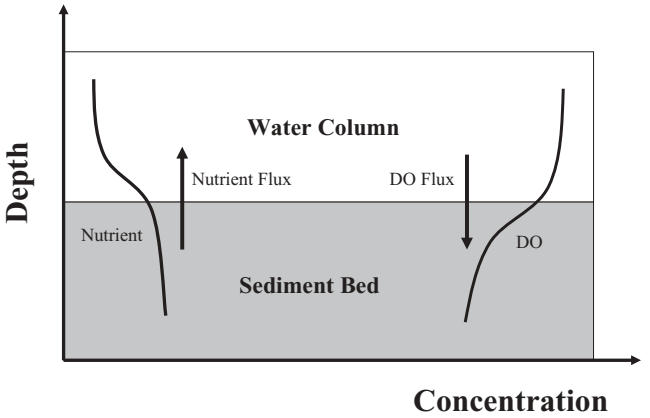

Fig. 5.7.3 Variation of nutrient and DO concentrations with depth in the sediment bed and overlying water.

In the sediment diagenesis model, Fick's law is used to quantify the sediment fluxes between the sediment bed and the overlying water in the following format:

$$J = s \cdot (C_1 - C_0) \tag{5.7.17}$$

where s = surface mass transfer coefficient (LT^{-1}), C_1 = dissolved nutrient concentration in Layer 1 (ML^{-3}), and C_0 = dissolved nutrient concentration in the overlying water (ML^{-3}).

In order to calculate the sediment flux, it is necessary to know the surface mass transfer coefficient, s, and the nutrient concentration, C_1, in Layer 1. The concentration in the overlying water, C_0, is provided by the water quality model in the water column.

Other factors that have direct or indirect influences on sediment fluxes include (1) sediment temperature, (2) benthic organisms, (3) organic and physical characteristics of the sediment, (4) current velocity over the sediments, and (5) chemistry of the interstitial water. These factors may also be interrelated. For example, temperature and available oxygen can be changed by the transport process in the water column or biochemical process in the sediment bed. These processes need to be considered in sediment flux computation.

Nutrients in the sediment bed can be described, similarly, using the mass/balance equation. In the upper, aerobic layer, the following processes should be included (Fig. 5.7.2):

1. Exchange of the dissolved fraction between Layer 1 and the overlying water.
2. Diffusion exchange of the dissolved fraction between Layers 1 and 2.

3. Particle mixing exchange of the particulate fraction between Layers 1 and 2.
4. Deposition to Layer 2.
5. Removal by reaction.
6. Internal sources.

Since the upper layer is quite thin ($H_1 \sim 0.1$ cm) and the surface mass transfer coefficient (s) is on the order of 0.1 m/day, the residence time in the upper layer is on the order of $H_1/s \sim 10^{-2}$ days, which is much shorter than the typical time scales of benthic processes. Hence, a steady-state approximation is appropriate in the upper layer, and the time differentiation term is set to zero. The mass/balance equation for ammonium, nitrate, phosphate, or sulfide/methane in the upper layer is derived by taking into account the six processes above:

$$H_1 \frac{\partial Ct_1}{\partial t} = s(fd_o \cdot Ct_o - fd_1 \cdot Ct_1) + \mathrm{KL}(fd_2 \cdot Ct_2 - fd_1 \cdot Ct_1) + \omega(fp_2 \cdot Ct_2 - fp_1 \cdot Ct_1) - W \cdot Ct_1 - \frac{\kappa_1^2}{s} Ct_1 + J_1 = 0 \qquad (5.7.18)$$

where Ct_1 and Ct_2 = total concentrations in Layers 1 and 2, respectively (g/m^3), Ct_o = total concentration in the overlying water (g/m^3), s = surface mass transfer coefficient (m/day), KL = diffusion velocity for dissolved fraction between Layers 1 and 2 (m/day), ω = particle mixing velocity between Layers 1 and 2 (m/day), fd_o = dissolved fraction of total substance in the overlying water ($0 \le fd_0 \le 1$), fd_1 = dissolved fraction of total substance in Layer 1 ($0 \le fd_1 \le 1$), fp_1 = particulate fraction of total substance in Layer 1 ($=1 - fd_1$), fd_2 = dissolved fraction of total substance in Layer 2 ($0 \le fd_2 \le 1$), fp_2 = particulate fraction of total substance in Layer 2 ($=1 - fd_2$), W = sedimentation (or burial) rate (m/day), κ_1 = reaction velocity in Layer 1 (m/day), and J_1 = sum of all internal sources in Layer 1 (g/m^2/day).

In Eq. (5.7.18), the diagenesis flux, included as an internal source (J_1), provides the sources for the concentration change. The reactions include, for example, the oxidation of sulfide that results in sediment oxygen demand. The first term on the RHS of Eq. (5.7.18) represents the exchange across the sediment–water interface. The sediment flux from Layer 1 to the overlying water (J_{aq}), which couples the sediment model with the water column model, may be expressed as:

$$J_{aq} = s(fd_1 \cdot Ct_1 - fd_o \cdot Ct_o) \qquad (5.7.19)$$

The convention used in Eq. (5.7.19) is that positive flux tranfers from the sediment to the overlying water. Equation (5.7.19) states that nutrient fluxes are the result of a gradient in nutrient concentration between the overlying water and the interstitial water of the sediment.

The dissolved and the particulate fractions have the following relations:

$$fd_0 + fp_0 = 1 \tag{5.7.20}$$

$$fd_1 + fp_1 = 1 \tag{5.7.21}$$

$$fd_2 + fp_2 = 1 \tag{5.7.22}$$

The nutrients in the sediment bed may be present in both the dissolved and particulate phases. The sorption and desorption processes control the fractions, similar to the sorption and desorption of toxic materials discussed in Chapter 4. From Eqs. (4.3.8) and (4.3.9), the dissolved and particulate fractions are computed as:

$$fd_1 = \frac{1}{1 + m_1 \cdot \pi_1} \qquad fp_1 = \frac{m_1 \pi}{1 + m_1 \cdot \pi_1} \tag{5.7.23}$$

$$fd_2 = \frac{1}{1 + m_2 \cdot \pi_2} \qquad fp_2 = \frac{m_2 \pi}{1 + m_2 \cdot \pi_2} \tag{5.7.24}$$

where m_1 and m_2 = solid concentrations in Layers 1 and 2, respectively (kg/L) and π_1 and π_2 = partition coefficients in Layers 1 and 2, respectively (per kg/L).

In the lower, anaerobic layer, the processes included in the mass balance equation are (Fig. 5.7.2):

1. Diffusion exchange of dissolved fraction between Layers 1 and 2.
2. Particle mixing exchange of particulate fraction between Layers 1 and 2.
3. Deposition from Layer 1 and burial to the deep inactive sediments.
4. Removal by reaction.
5. Internal sources.

The corresponding mass balance equation for ammonium, nitrate, phosphate, or sulfide/methane in the lower layer is

$$H_2 \frac{\partial Ct_2}{\partial t} = -\mathrm{KL}(fd_2 \cdot Ct_2 - fd_1 \cdot Ct_1) - \omega(fp_2 \cdot Ct_2 - fp_1 \cdot Ct_1) + W(Ct_1 - Ct_2) - \kappa_2 \cdot Ct_2 + J_2 \tag{5.7.25}$$

where κ_2 = reaction velocity in Layer 2 (m/day), and J_2 = sum of all internal sources including diagenesis in Layer 2 (g/m^2/day).

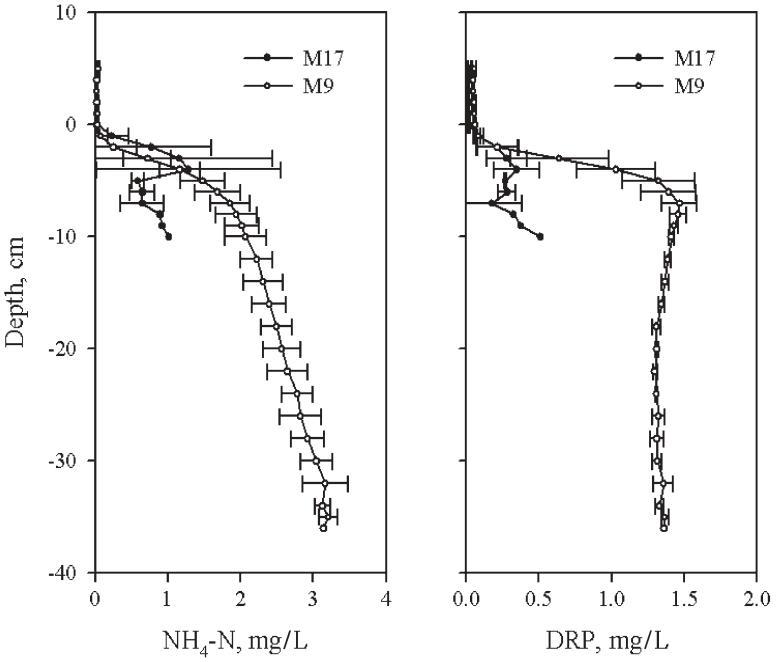

Fig. 5.7.4 Sediment pore water concentrations of DRP and ammonium (NH_4-N) at stations M9 and M17 in July 1999 (Fisher et al., 2005).

All of the parameters in Eqs. (5.7.18) and (5.7.25) for different state variables are the same, except for the reaction velocities (κ_1 in Layer 1 and κ_2 in Layer 2) and the internal sources (J_1 in Layer 1 and J_2 in Layer 2), which have different mathematical formulations for different state variables. Silica is not subject to the diagenesis process and will be discussed in Section 5.7.5.

As an example, Fig. 5.7.4 gives the vertical profiles of NH_4 and DRP at two stations in Lake Okeechobee in July 1999 (Fisher et al., 2005). At station M9 (the central mud region), the concentration of DRP increased from 0.02 in the overlying lake water to 1.5 mg/L in the sediment pore water at a depth of 5 cm below the sediment–water interface. The corresponding P flux averaged 0.83 mg/m^2/day. The NH_4-N concentration in the sediment–water column increased from 0.03 in the water column to 2 mg/L in the sediment pore water at a depth of 5 cm below the sediment–water interface. The diffusive NH_4-N flux was estimated as 3.1 mg/m^2/day. At station M17 (the southern peat region), the lake water concentrations of DRP and NH_4-N averaged 0.02 and 0.03 mg/L, respectively. Porewater concentrations increased to ~0.5 mg/L (DRP) and 1 mg/L (NH_4-N) at a depth of 10 cm below the sediment–water interface.

5.7.4.2 Parameters for Sediment Fluxes. The mass balance equations of (5.7.18) and (5.7.25) need a total of 13 parameters: W, H_2, m_1, m_2, π_1, π_2, s, ω, KL, κ_1, κ_2, J_1 and J_2, which can be categorized into four groups:

1. Common parameters specified as input (4): W, H_2, m_1, and m_2.
2. Variable-specific partition coefficients specified as input (2): π_1 and π_2.
3. Common parameters calculated by model (3): s, ω, and KL.
4. Variable-specific parameters calculated by model (4): κ_1, κ_2, J_1, and J_2.

Parameters of the first group, W, H_2, m_1, and m_2, are specified as input parameters in the sediment diagenesis model and are the same for all state variables. Some discussions on the burial rate (W) and the depth of the lower layer (H_2) have already been presented in the previous section, where the two-layer structure of the benthic bed is discussed. The partition coefficients, π_1 and π_2, are variable-specific and are also given as input parameters. The third group represents the vertical mixing and exchange rates between Layer 1 and the overlying water (s), and between Layer 1 and Layer 2 (ω and KL). They are common to the state variables. Parameters of the fourth group, κ_1, κ_2, J_1, and J_2, vary from state variable to state variable. These parameters in the sediment diagenesis model need to be evaluated from field data and through model calibration. The parameter values used in the Chesapeake Bay (Cerco and Cole, 1994) may serve as a starting point for model application. Park et al. (1995) also evaluated these parameters in detail.

Surface mass transfer coefficient(s). Di Toro et al. (1990) reported that the surface mass transfer coefficient, s, is related to the SOD and can be calculated used the following formulation:

$$s = \frac{D_1}{H_1} = \frac{\text{SOD}}{\text{DO}_0} \tag{5.7.26}$$

where D_1 = diffusion coefficient in Layer 1 (m^2/day).

Particle Mixing Velocity (ω). Benthic organisms provide the major mechanism causing particle mixing. The physical properties of bottom sediments are affected by the burrowing, particle sorting, and tube building activities of benthic fauna (e.g., invertebrates). These activities may alter the density, water content, shear strength, and mixing of bed sediments. Bioturbation is the disturbance of sediments due to displacement by living organisms. For example, bioturbation in the benthic habitat resulting from burrowing of organisms, such as worms, insect larvae, and decapods, increases nutrient exchanges with the overlying water. Fish grazing along the mud–water interface, as well as birds wading in shallow waters, also contribute to bioturbation. As sketched in Fig. 5.7.3, particle mixing transfers nutrients upward into the overlying water and DO downward into the interstitial water. The depth of bioturbation is limited by oxygen availability. Most of burrowing organisms are found within the top few centimeters of the sediment. To calculate particle mixing velocity, it is necessary to consider the factors affecting bioturbation.

In the sediment diagenesis model, particle mixing velocity between Layers 1 and 2 is assumed to be proportional to the benthic biomass and is largely controlled by bioturbation. The particle mixing velocity between Layers 1 and 2, ω, is parameterized as:

$$\omega = \frac{Dp \cdot \theta_{Dp}^{T-20}}{H_2} \frac{G_{\mathrm{POC,1}}}{G_{\mathrm{POC,R}}} \frac{\mathrm{DO}_0}{\mathrm{KM}_{Dp} + \mathrm{DO}_0} f(\mathrm{ST}) + \frac{Dp_{\min}}{H_2} \tag{5.7.27}$$

where Dp = apparent diffusion coefficient for particle mixing (m^2/day), θ_{Dp} = constant for temperature adjustment for Dp, $G_{\mathrm{POC,R}}$ = reference concentration for $G_{\mathrm{POC,1}}$ ($g\,C/m^3$), KM_{Dp} = particle mixing half saturation constant for oxygen ($g\,O_2/m^3$), ST = accumulated benthic stress (day), f(ST) = benthic stress function (dimensionless), $0 \le f(\mathrm{ST}) \le 1$, and $Dp_{\min}$ = minimum diffusion coefficient for particle mixing (m^2/day).

In Eq. (5.7.27),

1. H_2 represents the effect of bed thickness.
2. Dp represents the bioturbation.
3. θ_{Dp}^{T-20} is the temperature effect.
4. $\frac{G_{\mathrm{POC,1}}}{G_{\mathrm{POC,R}}}$ assumes that the particle mixing is proportional to the labile particulate organic carbon ($G_{\mathrm{POC,1}}$), which is assumed to be proportional to the benthic biomass.
5. $\frac{\mathrm{DO}_0}{\mathrm{KM}_{Dp} + \mathrm{DO}_0}$ is the Michaelis–Menton type oxygen dependency, accounting for the oxygen dependency of the benthic biomass.
6. f(ST) is a function representing the effects of anoxia/hypoxia on the benthic biomass.
7. $Dp_{\min}$ represents the minimum (or background) diffusion for particle mixing.

There is a hysteresis (or time lag) between bottom water oxygen and the benthic biomass. For example, the benthic biomass in a stratified lake increases as the summer progresses. However, the occurrence of anoxia/hypoxia reduces the biomass drastically and imposes stress on benthic activities. In the fall, the bottom water oxygen increases, but the biomass (and the particle mixing velocity) does not immediately increase. The recovery of benthic biomass following hypoxic events depends on many factors, including severity and longevity of hypoxia, constituent species, and salinity (Diaz and Rosenberg, 1995). The benthic stress function, f(ST), is used to represent this phenomenon. The concept is that low DO in the overlying water imposes stress on the benthic population and that the increased benthic stress reduces

particle mixing. The equation for the accumulated benthic stress is expressed as:

$$\frac{\partial \mathrm{ST}}{\partial t} = \begin{cases} -K_{\mathrm{ST}} \cdot \mathrm{ST} + \left(1 - \dfrac{\mathrm{DO}_0}{\mathrm{KM}_{Dp}}\right) & \text{if } \mathrm{DO}_0 < \mathrm{KM}_{Dp} \\ -K_{\mathrm{ST}} \cdot \mathrm{ST} & \text{if } \mathrm{DO}_0 > \mathrm{KM}_{Dp} \end{cases} \tag{5.7.28}$$

where ST = accumulated benthic stress (day) and K_{ST} = first-order decay rate for ST (day^{-1}). The benthic stress function, $f(\mathrm{ST})$, can be expressed as (Park et al., 1995):

$$f(\mathrm{ST}) = 1 - K_{\mathrm{ST}} \cdot \mathrm{ST} \tag{5.7.29}$$

For constant DO_0, the analytical solution to Eq. (5.7.28) is

$$\mathrm{ST} = \begin{cases} \dfrac{1}{K_{\mathrm{ST}}}\left(1 - \dfrac{\mathrm{DO}_0}{\mathrm{KM}_{Dp}}\right) + \left[\mathrm{ST}_0 - \dfrac{1}{K_{\mathrm{ST}}}\left(1 - \dfrac{\mathrm{DO}_0}{\mathrm{KM}_{Dp}}\right)\right] e^{-K_{\mathrm{ST}} \cdot t} & \text{if } \mathrm{DO}_0 < \mathrm{KM}_{Dp} \\ \mathrm{ST}_0 \cdot e^{-K_{\mathrm{ST}} \cdot t} & \text{if } \mathrm{DO}_0 > \mathrm{KM}_{Dp} \end{cases} \tag{5.7.30}$$

where ST_0 = initial benthic stress at $t = 0$.

Equation (5.7.30) gives the values of benthic stress under constant DO in the overlying water but without considering the hysteresis effect. In the sediment diagenesis model, the reduction in particle mixing due to the benthic stress, $f(\mathrm{ST})$, is estimated in the following approach (Fig. 5.7.5):

1. The benthic stress, ST, is calculated with Eq. (5.7.28).
2. Once DO_0 drops below a critical concentration, $\mathrm{DO}_{\mathrm{ST},c}$, for $\mathrm{NC}_{\mathrm{hypoxia}}$ consecutive days or more, the benthic stress is not allowed to decrease until t_{MBS} days of $\mathrm{DO}_0 > \mathrm{DO}_{\mathrm{ST},c}$. It means that when the overlying water experiences hypoxic days that are longer than the critical hypoxia days ($\mathrm{NC}_{\mathrm{hypoxia}}$), the maximum benthic stress will remain for a specified period (t_{MBS} days), regardless of DO_0.
3. No hysteresis occurs if DO_0 does not drop below $\mathrm{DO}_{\mathrm{ST},c}$ or if hypoxia lasts $<\mathrm{NC}_{\mathrm{hypoxia}}$ days. When applying maximum stress for t_{MBS} days, the subsequent hypoxic days are not included in t_{MBS}. The values of $\mathrm{DO}_{\mathrm{ST},c}$ are often set to 3 mg/L.

Three parameters relating to hysteresis, $\mathrm{DO}_{\mathrm{ST},c}$, $\mathrm{NC}_{\mathrm{hypoxia}}$ and t_{MBS}, are site specific. Diaz and Rosenberg (1995) reported that the parameters are functions of many factors, such as severity and longevity of hypoxia, constituent species, and salinity. The critical overlying oxygen concentration, $\mathrm{DO}_{\mathrm{ST},c}$, also depends on how DO_0 is calculated in the water column and its vertical distance to the bed. The critical hypoxia days, $\mathrm{NC}_{\mathrm{hypoxia}}$, depends on the tolerance of

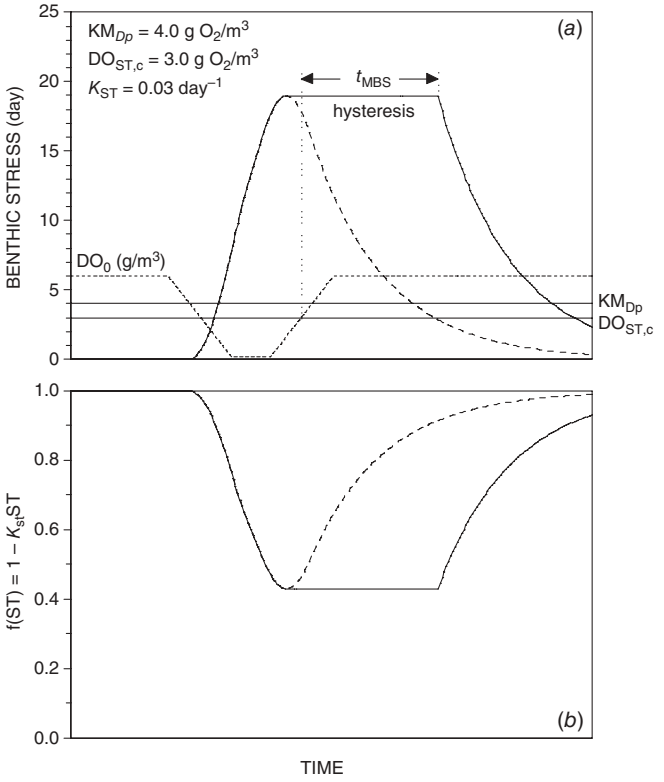

Fig. 5.7.5 Benthic stress (*a*) and its effect on particle mixing (*b*) as a function of overlying water column DO concentration (Park et al., 1995).

benthic organisms to hypoxia. The hysteresis (time lag) for the recovery of the benthic biomass following hypoxic events, t_{MBS}, tends to be longer for higher salinity.

Diffusion Velocity (KL). After the particle mixing velocity (ω) is determined by Eq. (5.7.27), the diffusion velocity for the dissolved fraction between Layers 1 and 2, KL, can be parameterized to include molecular diffusion and bioirrigation by benthic organisms:

$$\mathrm{KL} = \frac{Dd \cdot \theta_{Dd}^{T-20}}{H_2} + R_{\mathrm{BI,BT}} \cdot \omega \tag{5.7.31}$$

where Dd = diffusion coefficient in pore water (m^2/day), θ_{Dd} = constant for temperature adjustment for Dd, and $R_{\mathrm{BI,BT}}$ = ratio of bioirrigation to bioturbation. The last term in Eq. (5.7.31) accounts for the enhanced mixing by organism activities.

5.7.4.3 Ammonium Nitrogen Flux. The reaction velocities and the internal sources of ammonia/ammonium in Eqs. (5.7.18) and (5.7.25), κ_1, κ_2, J_1, and J_2, are specified here. The nitrogen cycle illustrated in Fig. 5.1.4 can be used to explain the transformation of nitrogen in benthic sediments.

As shown in Fig. 5.7.2, the sediment diagenesis model has two layers. It is assumed that diagenesis does not occur in the upper layer because of its thin depth. The only ammonia source in the sediment bed is from the diagenesis in the lower layer. Therefore, the internal sources, J_1 and J_2, in Eq. (5.7.18) and (5.7.25) are expressed as:

$$J_{1,\mathrm{NH4}} = 0 \tag{5.7.32}$$

$$J_{2,\mathrm{NH4}} = J_N \tag{5.7.33}$$

where $J_{1,\mathrm{NH4}}$ = internal source of NH_4 in Layer 1, $J_{2,\mathrm{NH4}}$ = internal source of NH_4 in Layer 2, and J_N = diagenesis flux of nitrogen, given by Eq. (5.7.14).

The reaction (and loss) of ammonia in the benthic sediment is through nitrification. Ammonia is nitrified to nitrate under aerobic conditions and is largely determined by DO concentrations, NH_4 concentrations, and temperature. A Michaelis–Menton expression is used for the ammonia concentration dependency and for the oxygen dependency of the nitrification rate. The temperature dependence takes a format similar to Eq. (5.1.8). Consequently, the reaction velocity for ammonium in the upper, aerobic layer is expressed as:

$$\kappa^2_{1,\mathrm{NH_4}} = \frac{\mathrm{DO_0}}{2\cdot \mathrm{KM_{NH4,O2}} + \mathrm{DO_0}} \frac{\mathrm{KM_{NH4}}}{\mathrm{KM_{NH4}} + \mathrm{NH4_1}} \kappa^2_{\mathrm{NH4}} \cdot \theta^{T-20}_{\mathrm{NH4}} \tag{5.7.34}$$

where $\mathrm{KM_{NH4,O2}}$ = nitrification half saturation constant for dissolved oxygen ($\mathrm{g\,O_2/m^3}$), $\mathrm{NH4_1}$ = total ammonia nitrogen concentration in Layer 1 ($\mathrm{g\,N/m^3}$), $\mathrm{KM_{NH4}}$ = nitrification half saturation constant for ammonia ($\mathrm{g\,N/m^3}$), κ_{NH4} = optimal reaction velocity for nitrification at 20 °C (m/day), and θ_{NH4} = constant for temperature adjustment for κ_{NH4}.

Therefore, the fifth term on the RHS of Eq. (5.7.18) gives the nitrification flux:

$$J_{\mathrm{Nit}} = \frac{\kappa^2_{1,\mathrm{NH4}}}{s} \cdot \mathrm{NH4_1} \tag{5.7.35}$$

where J_{Nit} = nitrification flux ($\mathrm{g\,N/m^2/day}$).

Since ammonium is present only in dissolved form in benthic sediments, it has

$$\pi_{1,\mathrm{NH4}} = \pi_{2,\mathrm{NH4}} = 0 \tag{5.7.36a}$$

$$fd_{1,\mathrm{NH4}} = fd_{2,\mathrm{NH4}} = 1 \tag{5.7.36b}$$

$$\omega = 0 \tag{5.7.36c}$$

There is no nitrification in the lower, anaerobic layer:

$$\kappa_{2,NH4} = 0 \tag{5.7.37}$$

The sediment flux of ammonia to the overlying water, $J_{aq,NH4}$, can be calculated using Eq. (5.7.19), after $NH4_1$ is known by solving Eq. (5.7.18).

5.7.4.4 Nitrate Nitrogen Flux. The reaction velocities and the internal sources of nitrate in Eqs. (5.7.18) and (5.7.25), κ_1, κ_2, J_1, and J_2, are specified here.

There is no diagenetic source for nitrate in either sediment layer. Nitrification flux in the upper, aerobic layer, J_{Nit}, given by Eq. (5.7.35), is the only source of nitrate in the benthic sediment:

$$J_{1,NO3} = J_{Nit} \tag{5.7.38}$$

and

$$J_{2,NO3} = 0 \tag{5.7.39}$$

Since nitrate is present only in dissolved form in benthic sediments, it has

$$\pi_{1,NO3} = \pi_{2,NO3} = 0 \tag{5.7.40a}$$

$$fd_{1,NO3} = fd_{2,NO3} = 1 \tag{5.7.40b}$$

$$\omega = 0 \tag{5.7.41}$$

Denitrification removes nitrate in both layers with the following reaction velocities:

$$\kappa^2_{1,NO3} = \kappa^2_{NO3,1} \cdot \theta^{T-20}_{NO3} \tag{5.7.42}$$

$$\kappa_{2,NO3} = \kappa_{NO3,2} \cdot \theta^{T-20}_{NO3} \tag{5.7.43}$$

where $\kappa_{NO3,1}$ = reaction velocity for denitrification in Layer 1 at 20 °C (m/day), $\kappa_{NO3,2}$ = reaction velocity for denitrification in Layer 2 at 20 °C (m/day), and θ_{NO3} = constant for temperature adjustment for $\kappa_{NO3,1}$ and $\kappa_{NO3,2}$.

From the fifth term on the RHS of Eq. (5.7.18) and the fourth term on the RHS of Eq. (5.7.25), the denitrification flux out of sediments as a nitrogen gas becomes:

$$J_{N2(g)} = \frac{\kappa^2_{1,NO3}}{s} NO3_1 + \kappa_{2,NO3} \cdot NO3_2 \tag{5.7.44}$$

where $J_{N2(g)}$ = denitrification flux ($gN/m^2/day$), $NO3_1$ = total nitrate nitrogen concentration in Layer 1 (gN/m^3), and $NO3_2$ = total nitrate nitrogen concentration in Layer 2 (gN/m^3).

Once Eqs. (5.7.18) and (5.7.25) are solved for $NO3_1$ and $NO3_2$, the sediment flux of nitrate to the overlying water, $J_{aq,NO3}$, can be calculated using Eq. (5.7.19).

Denitrification flux, as stated by Eq. (5.7.44), is an important pathway for the removal of nitrogen from an aquatic system. The primary source of nitrate for denitrification, as expressed in Eq. (5.7.38), is from previously nitrified ammonia. When oxygen is freely available, a large fraction of the ammonia produced in the sediments is nitrified to nitrate and then is denitrified to nitrogen gas in the lower, anaerobic layer. This process removes nitrogen out of the aquatic system and leads to less ammonium released back into the water column. The reduction of ammonium concentration in the water column may reduce algal production, the supply of carbon to the bottom sediments, and oxygen consumption. This mechanism indicates that a slight improvement in DO concentration near the bed can start a positive feedback reaction.

On the other hand, when oxygen is absent in the sediments, denitrification is limited to the rate at which nitrate is supplied by diffusion from the water column. Under hypoxia conditions, nitrification is diminished, and the supply of nitrite for denitrification is reduced. In this scenario, most ammonia produced in the sediment bed is released to the overlying water. The ammonia becomes available for algal uptake after vertical mixing brings it up to the surface layer where photosynthesis occurs. Algal carbon settles to the bottom, consumes oxygen, and further diminishes denitrification. Hence, the anaerobic condition may cause a positive feedback that promotes ammonia release and algal production (and eutrophication) in an aquatic system.

5.7.4.5 Phosphate Phosphorus Flux. Compared with nitrogen, phosphorus in benthic sediments is differentiated by two major characteristics:

1. *Sorption and Desorption.* Unlike ammonia and nitrate, which do not significantly sorb to solids, phosphate phosphorus is easily attached to sediment. Sorption and desorption processes greatly affect the dissolved phosphate concentration.
2. *No Removal Reaction.* Nitrate can be denitrified to nitrogen gas and then released into the atmosphere, whereas phosphorus cannot be removed out of the system by biochemical reactions. Burial to the deeper, inactive sediment layers is the only removal mechanism.

These two characteristics of phosphorus have important implications for water quality modeling and eutrophication management. For phosphorus, sorption and desorption affect the interstitial water concentrations, and through which, change phosphorus flux. Dissolved oxygen concentration in the overlying water affects the partition between the dissolved and the particulate phosphate, which is an important factor in phosphorus flux calculation. Phosphorus fluxes are enhanced under anaerobic conditions. Without chemical reactions that can remove phosphorus, the deposited phosphorus in the benthic

sediments can stay in the bottom for a long time, say many years, and later be released into the water column to cause eutrophication problems. This is a major mechanism that causes eutrophication in many lakes, even long after the external sources have been significantly reduced.

In the sediment bed, detrital algae decompose and yield both organic and inorganic phosphorus. A fraction of the end product, dissolved inorganic phosphorus, remains in the interstitial water and is not sorbed onto the benthic solids. Exchange of the dissolved phosphorus with the overlying water column, similar to that of ammonia, nitrate, and DO, transfers the phosphate to the water column. In the sediment diagenesis model, there is no internal source of phosphorus in the upper layer, and phosphate is produced by the diagenetic breakdown of POP in the lower layer. Hence, the last terms of Eqs. (5.7.18) and (5.7.25) are

$$J_{1,\mathrm{PO4}} = 0 \tag{5.7.45}$$

$$J_{2,\mathrm{PO4}} = J_P \tag{5.7.46}$$

where J_p = diagenesis flux of phosphorus, given by Eq. (5.7.14).

A portion of the produced phosphate remains in the dissolved form, and a portion becomes particulate phosphate, depending on the partition coefficients, $\pi_{1,\mathrm{PO4}}$ and $\pi_{2,\mathrm{PO4}}$, in Eqs. (5.7.23) and (5.7.24). Partitioning and phosphate flux are strongly affected by the DO concentration in the overlying water (DO_0). As DO_0 approaches zero, the partition coefficients decrease and the sediment flux of phosphate increases. It has

$$\pi_{1,\mathrm{PO4}} = \begin{cases} \pi_{2,\mathrm{PO4}} \cdot (\Delta\pi_{\mathrm{PO4},1}) & \mathrm{DO}_0 > (\mathrm{DO}_0)_{\mathrm{crit,PO4}} \\ \pi_{2,\mathrm{PO4}} \cdot (\Delta\pi_{\mathrm{PO4},1})^{\frac{\mathrm{DO}_0}{(\mathrm{DO}_0)_{\mathrm{crit,PO4}}}} & \mathrm{DO}_0 \le (\mathrm{DO}_0)_{\mathrm{crit,PO4}} \end{cases} \tag{5.7.47}$$

where $\pi_{1,\mathrm{PO4}}$ and $\pi_{2,\mathrm{PO4}}$ = partition coefficients of PO4 in Layers 1 and 2, respectively (per kg/L), $\Delta\pi_{\mathrm{PO4},1}$ = factor to enhance sorption of PO4 in Layer 1 (>1.0), and $(\mathrm{DO}_0)_{\mathrm{crit,PO4}}$ = critical dissolved oxygen for PO4 sorption (mg/L).

Smaller partition coefficients lead to a higher dissolved fraction in Eq. (5.7.23) and a higher PO_4 flux in Eq. (5.7.19). Equation (5.7.47) makes $\pi_{1,\mathrm{PO4}}$ in the upper, aerobic layer larger than $\pi_{2,\mathrm{PO4}}$ in the lower, anaerobic layer. When DO_0 exceeds the critical DO for PO4 sorption, $(\mathrm{DO}_0)_{\mathrm{crit,PO4}}$, sorption in the upper layer is enhanced by $\Delta\pi_{\mathrm{PO4},1}$ times. When DO_0 is $<(\mathrm{DO}_0)_{\mathrm{crit,PO4}}$, sorption in the upper layer is gradually reduced to $\pi_{2,\mathrm{PO4}}$ as DO_0 goes to zero.

There is no removal reaction for phosphate in either layer:

$$\kappa_{1,\mathrm{PO4}} = \kappa_{2,\mathrm{PO4}} = 0 \tag{5.7.48}$$

Once Eqs. (5.7.18) and (5.7.25) are solved for $\mathrm{PO4}_1$ and $\mathrm{PO4}_2$, the sediment flux of phosphate to the overlying water, $J_{\mathrm{aq,PO4}}$, can be calculated using Eq. (5.7.19).

5.7.4.6 Chemical Oxygen Demand and Sediment Oxygen Demand. As described in Section 5.6.5, the COD is a parameter for the content of oxygen-consuming substances in water. In the sediment diagenesis model, COD represents the oxygen demand of sulfide gas in saline water (or methane gas in freshwater) that is produced in the sediment bed.

The sediment oxygen demand (SOD) represents the oxygen demand required for the oxidation of organic matter in benthic sediments. The SOD in the sediment diagenesis model consists of two components: (1) carbonaceous sediment oxygen demand (CSOD) due to sulfide oxidation, and (2) NSOD due to nitrification. Sediment oxygen demand can be a significant portion of total oxygen demand in a waterbody. Similar to the BOD, COD and SOD are both oxygen equivalents. They are indicators rather than true physical or chemical substances. Compared with COD flux, SOD flux often plays a much more significant role in affecting DO concentration in the overlying water.

Sulfide (H2S). In saline water, sulfide is used to calculate the COD from the benthic sediments. There is no internal source of sulfide in the upper layer of the model. In the lower, anaerobic layer, sulfide is produced by the diagenetic breakdown of POC and is decremented by the organic carbon consumed due to denitrification. Hence, the last terms of Eqs. (5.7.18) and (5.7.25) are

$$J_{1,\mathrm{H2S}} = 0 \tag{5.7.49}$$

$$J_{2,\mathrm{H2S}} = a_{\mathrm{O2,C}} \cdot J_{\mathrm{C}} - a_{\mathrm{O2,NO3}} \cdot J_{\mathrm{N2(g)}} \tag{5.7.50}$$

where $a_{\mathrm{O2,C}}$ = stoichiometric coefficient for carbon diagenesis consumed by sulfide oxidation (2.6667 g O_2-equiv/g C), $a_{\mathrm{O2,NO3}}$ = stoichiometric coefficient for carbon diagenesis consumed by denitrification (2.8571 g O_2-equiv/g N), J_C = diagenesis flux of carbon (g/m^2/day), given by Eq. (5.7.14), and $J_{\mathrm{N2(g)}}$ = denitrification flux (g N/m^2/day), given by Eq. (5.7.44).

Sulfide in the sediment bed can be removed via sulfide oxidation and sulfide flux between the bed and the overlying water. Sulfide oxidation occurs only in the upper, aerobic layer, in which both dissolved sulfide and particulate sulfide are oxidized, and oxygen is consumed in the process. There is no sulfide oxidation in the lower, anaerobic layer. Hence, the reaction velocities in Eqs. (5.7.18) and (5.7.25) are expressed as:

$$\kappa^2_{1,\mathrm{H2S}} = \left(\kappa^2_{\mathrm{H2S},d1} \cdot fd_{1,\mathrm{H2S}} + \kappa^2_{\mathrm{H2S},p1} \cdot fp_{1,\mathrm{H2S}}\right)\theta^{T-20}_{\mathrm{H2S}} \frac{\mathrm{DO}_0}{2 \cdot KM_{\mathrm{H2S,O2}}} \tag{5.7.51}$$

$$\kappa_{2,\mathrm{H2S}} = 0 \tag{5.7.52}$$

where $\kappa_{\mathrm{H2S},d1}$ = reaction velocity for dissolved sulfide oxidation in Layer 1 at 20 °C (m/day), $\kappa_{\mathrm{H2S},p1}$ = reaction velocity for particulate sulfide oxidation in

Layer 1 at 20 °C (m/day), θ_{H2S} = constant for temperature adjustment for $\kappa_{H2S,d1}$ and $\kappa_{H2S,p1}$, and $KM_{H2S,O2}$ = constant to normalize the sulfide oxidation rate for oxygen ($g\,O_2/m^3$). The constant, $KM_{H2S,O2}$, is used to scale the oxygen concentration in the overlying water. At $DO_0 = KM_{H2S,O2}$, the reaction velocity for sulfide oxidation rate is at its nominal value.

The oxidation reactions in the upper, aerobic layer consume oxygen and cause oxygen flux to the sediment (SOD). In the sediment diagenesis model, the CSOD is computed from the rate of oxygen utilization during sulfide oxidation, that is, the fifth term on the RHS of Eq. (5.7.18). The NSOD is calculated based on the nitrification flux given by Eq. (5.7.35). By convention, SOD is positive and is expressed as:

$$\mathrm{SOD} = \mathrm{CSOD} + \mathrm{NSOD} = \frac{\kappa_{1,\mathrm{H2S}}^2}{s}\,\mathrm{H2S}_1 + a_{\mathrm{O2,NH4}} \cdot J_{\mathrm{Nit}} \tag{5.7.53}$$

where $H2S_1$ = total sulfide concentration in Layer 1 ($g\,O_2$-equiv/m^3) and $a_{O2,NH4}$ = stoichiometric coefficient for oxygen consumed by nitrification ($4.33\,g\,O_2/g\,N$).

Equation (5.7.53) is nonlinear for SOD, because the RHS contains s (=SOD/DO_0) so that SOD appears on both sides of the equation. In addition, the nitrification flux (J_{Nit}) given by Eq. (5.7.35) is also a function of s.

When the DO in the overlying water is low, the sulfide may not be completely oxidized in the upper layer, and the remaining sulfide can diffuse into the overlying water. This sediment flux of sulfide contributes to the COD in the water column and is calculated according to Eq. (5.7.19):

$$J_{\mathrm{aq,H2S}} = s(fd_{1,\mathrm{H2S}} \cdot \mathrm{H2S}_1 - \mathrm{COD}) \tag{5.7.54}$$

The sulfide released from the sediment reacts very quickly in the water column when oxygen is available, but can accumulate in the water column under anoxic conditions. As given in Eq. (5.6.20), the only source of COD in the water column model is from the sediment COD flux. Sulfide is quantified as oxygen equivalents to represent COD in the water column.

Methane (CH_4). Instead of sulfide, methane is used for COD calculation in freshwater. Similar to H_2S in saline water, CH_4 is produced by carbon diagenesis and is decremented by the organic carbon consumed by denitrification in the lower layer (Park et al., 1995). No diagenetic production of CH_4 occurs in the upper layer. Hence, the last terms of Eqs. (5.7.18) and (5.7.25) are the same as the ones given by Eqs. (5.7.49) and (5.7.50) for sulfide:

$$J_{1,\mathrm{CH4}} = 0 \tag{5.7.55}$$

$$J_{2,\mathrm{CH4}} = a_{\mathrm{O2,C}} \cdot J_{\mathrm{C}} - a_{\mathrm{O2,NO3}} \cdot J_{\mathrm{N2(g)}} \tag{5.7.56}$$

The dissolved methane produced takes two pathways: (1) oxidation in the oxic upper layer causing CSOD or (2) escape from the sediment as aqueous flux or as gas flux:

$$J_{2,\mathrm{CH4}} = \mathrm{CSOD} + J_{\mathrm{aq,CH4}} + J_{\mathrm{CH4(g)}} \tag{5.7.57}$$

where $J_{\mathrm{aq,CH4}}$ = aqueous methane flux ($\mathrm{gO_2}$-equiv/$\mathrm{m^2}$/day), $J_{\mathrm{CH4(g)}}$ = gaseous methane flux ($\mathrm{gO_2}$-equiv/$\mathrm{m^2}$/day).

A portion of dissolved methane that is produced in the anoxic layer diffuses into the oxic layer where it is oxidized. This methane oxidation causes CSOD in the freshwater sediment (Di Toro et al., 1990) and is calculated as:

$$\mathrm{CSOD} = \mathrm{CSOD}_{\max} \cdot \left(1 - \mathrm{sech}\left[\frac{\kappa_{\mathrm{CH_4}} \cdot \theta_{\mathrm{CH_4}}^{T-20}}{s}\right]\right) \tag{5.7.58}$$

$$\mathrm{CSOD}_{\max} = \mathrm{minimum}\left\{\sqrt{2 \cdot \mathrm{KL} \cdot \mathrm{CH4}_{\mathrm{sat}} \cdot J_{2,\mathrm{CH4}}}, J_{2,\mathrm{CH4}}\right\} \tag{5.7.59}$$

$$\mathrm{CH4}_{\mathrm{sat}} = 100\left(1 + \frac{h + H_2}{10}\right)1.024^{20-T} \tag{5.7.60}$$

where $\mathrm{CSOD}_{\max}$ = maximum CSOD occurring when all the dissolved methane transported to the oxic layer is oxidized, κ_{CH4} = reaction velocity for dissolved methane oxidation in Layer 1 at 20 °C (m/day), θ_{CH4} = constant for temperature adjustment for κ_{CH4}, and $\mathrm{CH4}_{\mathrm{sat}}$ = saturation concentration of methane in the pore water ($\mathrm{gO_2}$-equiv/$\mathrm{m^3}$).

The hyperbolic secant function, sec h (x), is defined as:

$$\mathrm{sech}(x) = \frac{2}{e^x + e^{-x}} \tag{5.7.61}$$

If the overlying water oxygen is low, the methane that is not completely oxidized can escape the sediment into the overlying water either as aqueous flux or as gas flux. The aqueous methane flux, which contributes to the COD in the water column, is modeled using (Di Toro et al., 1990):

$$J_{\mathrm{aq,CH4}} = \mathrm{CSOD}_{\max} - \mathrm{CSOD} = \mathrm{CSOD}_{\max} \cdot \mathrm{sech}\left[\frac{\kappa_{\mathrm{CH_4}} \cdot \theta_{\mathrm{CH_4}}^{T-20}}{s}\right] \tag{5.7.62}$$

Methane is only slightly soluble in water. If its saturation concentration, $\mathrm{CH4}_{\mathrm{sat}}$ given by Eq. (5.7.60), is exceeded in the pore water, it forms a gas phase that escapes as bubbles. The gaseous methane flux, $J_{\mathrm{CH4(g)}}$, is calculated using Eq. (5.7.57), with $J_{2,\mathrm{CH4}}$ from Eq. (5.7.56), CSOD from Eq. (5.7.58), and $J_{\mathrm{aq,CH4}}$ from Eq. (5.7.62) (Di Toro et al., 1990).

5.7.5 Silica

Silica is included in water quality modeling only when diatoms are considered. The production of silica in benthic sediments is different from the production of carbon, nitrogen, and phosphorus. The former is the result of the dissolution of particulate biogenic silica and is treated as independent of bacterial processes, whereas the latter is the result of the mineralization of POM by bacteria.

Even though silica and POM experience different processes in the benthic sediments, they are described analogously in the sediment diagenesis model. More specifically, silica is treated similarly to phosphate. The kinetic equation for silica (PSi) in the sediment bed can be derived based on the mass balance equation:

$$\text{Net PSi change} = -\text{dissolution of PSi} - \text{burial} + \text{depositional flux} + \text{detrital flux} \tag{5.7.63}$$

The corresponding kinetic equation in the lower layer is

$$\mathrm{H}_2 \frac{\partial \mathrm{PSi}}{\partial t} = -H_2 \cdot S_{\mathrm{Si}} - W \cdot \mathrm{PSi} + J_{\mathrm{Psi}} + J_{\mathrm{DSi}} \tag{5.7.64}$$

where PSi = concentration of particulate biogenic silica in the sediment (g Si/m^3), S_{Si} = dissolution rate of PSi in Layer 2 (g Si/m^3/day), J_{PSi} = depositional flux of PSi (g Si/m^2/day) given by Eq. (5.7.7), J_{DSi} = detrital flux of PSi (g Si/m^2/day) to account for PSi settling to the sediment that is not associated with the algal flux of biogenic silica.

Mathematically, Eq. (5.7.64) is analogous to the diagenesis equation for POM, Eq. (5.7.13). The dissolution rate, S_{Si}, is formulated as:

$$S_{\mathrm{Si}} = K_{\mathrm{Si}} \cdot \theta_{\mathrm{Si}}^{T-20} \frac{\mathrm{PSi}}{\mathrm{PSi} + \mathrm{KM}_{\mathrm{Psi}}} (\mathrm{Si}_{\mathrm{sat}} - fd_{2,\mathrm{Si}} \cdot \mathrm{Si}_2) \tag{5.7.65}$$

where K_{Si} = dissolution rate for PSi at 20 °C in Layer 2 (day^{-1}), θ_{Si} = constant for temperature adjustment for K_{Si}, $\mathrm{KM}_{\mathrm{PSi}}$ = silica dissolution half saturation constant for PSi (g Si/m^3), and $\mathrm{Si}_{\mathrm{sat}}$ = saturation concentration of silica in the pore water (g Si/m^3). In Eq. (5.7.65), the dissolution rate is proportional to the solubility deficit, ($\mathrm{Si}_{\mathrm{sat}} - fd_{2,\mathrm{Si}} \cdot \mathrm{Si}_2$), and is related to the PSi concentration in a Michaelis–Menton function.

The mass balance equations for mineralized silica can be described using Eqs. (5.7.18) and (5.7.25). There is no source/sink term and no reaction in the upper layer:

$$J_{1,\mathrm{Si}} = \kappa_{1,\mathrm{Si}} = 0 \tag{5.7.66}$$

In the lower layer, silica is produced by the dissolution of particulate biogenic silica and is modeled using Eq. (5.7.64). The two terms in Eq. (5.7.64) correspond to the source and reaction terms in Eq. (5.7.25):

$$J_{2,\mathrm{Si}} = K_{\mathrm{Si}} \cdot \theta_{\mathrm{Si}}^{T-20} \frac{\mathrm{PSi}}{\mathrm{PSi} + \mathrm{KM}_{\mathrm{PSi}}} \mathrm{Si}_{\mathrm{sat}} \cdot H_2 \tag{5.7.67}$$

$$\kappa_{2,\mathrm{Si}} = K_{\mathrm{Si}} \cdot \theta_{\mathrm{Si}}^{T-20} \frac{\mathrm{PSi}}{\mathrm{PSi} + \mathrm{KM}_{\mathrm{PSi}}} f_{d2,\mathrm{Si}} \cdot H_2 \tag{5.7.68}$$

The silica dissolved from particulate silica exists in two forms: one attaching to solids and the other remaining in dissolved form. The partition coefficients, $\pi_{1,\mathrm{Si}}$ and $\pi_{2,\mathrm{Si}}$, in Eqs. (5.7.23) and (5.7.24) control the partitioning. Similar to phosphate, silica has the following partition coefficient in the upper layer:

$$\pi_{1,\mathrm{Si}} = \begin{cases} \pi_{2,\mathrm{Si}} \cdot (\Delta\pi_{\mathrm{Si},1}) & \mathrm{DO}_0 > (\mathrm{DO}_0)_{\mathrm{crit,Si}} \\ \pi_{2,\mathrm{Si}} \cdot (\Delta\pi_{\mathrm{Si},1})^{\frac{\mathrm{DO}_0}{(\mathrm{DO}_0)_{\mathrm{crit,Si}}}} & \mathrm{DO}_0 \le (\mathrm{DO}_0)_{\mathrm{crit,Si}} \end{cases} \tag{5.7.69}$$

where $\pi_{1,\mathrm{Si}}$ and $\pi_{2,\mathrm{Si}}$ = partition coefficients of Si in Layers 1 and 2, respectively (per kg/L), $\Delta\pi_{\mathrm{Si},1}$ = factor to enhance sorption of Si in Layer 1 (>1.0), $(\mathrm{DO}_0)_{\mathrm{crit,Si}}$ = critical dissolved oxygen for Si sorption (mg/L). Once Eqs (5.7.18) and (5.7.25) are solved for Si_1 and Si_2, the sediment flux of silica to the overlying water, $J_{\mathrm{aq,Si}}$, can be calculated using Eq. (5.7.19).

5.7.6 Coupling With Sediment Resuspension

In deep waterbodies, such as the Chesapeake Bay (Cerco and Cole, 1994) and Lake Tenkiller (Ji et al., 2004a), nutrients in the sediment bed are largely released in the dissolved form via diffusion. These diffusion fluxes are the sediment fluxes described in the sediment diagenesis model (Di Toro and Fitzpatrick, 1993). In these deep waters, the overall contributions from sediment resuspension to nutrient budget can be secondary.

A distinctive feature of shallow waters, however, is the close coupling between the water column and the sediment bed, and sediment resuspension can contribute significantly to the total nutrient budget. In addition to diffusion fluxes, the coupling between the water column and the sediment bed occurs via settling and resuspension of particulate matter. The bottom nutrients can be brought into the water column during high wind events, when bottom sediments are resuspended into the water column. Before the resuspended sediments are deposited back onto the bottom, nutrients that are absorbed onto the sediment particles can be released into the water column, contributing to the total nutrient budget in the water column.

Lake Okeechobee is a good example of how sediment resuspension significantly affects nutrient cycling in the waterbody. In the LOEM, AEE (2005)

considered the influence of sediment resuspension on the nutrient budget. The sediment transport submodel of LOEM was explicitly coupled with the water quality submodel. In the LOEM model, both diffusion and sediment resuspension brought nutrients from the sediment bed into the water column. For example, the sediment–water exchange flux of RPON is linked directly to the sediment resuspension flux (AEE, 2005):

$$\text{BFRPON} = C_{\text{NS}} \cdot J_r \tag{5.7.70}$$

where BFRPON = sediment–water exchange flux of RPON (g N/m^2/day), C_{NS} = ratio of PON concentration to solid concentration in the sediment bed (g N/kg solid), and J_{r} = sediment resuspension flux (kg solid/m^2/day), calculated in a sediment model.

Among the three G classes of benthic sediments, the G1 fraction is labile and decays rapidly in the bed, whereas G3 fraction is inert and has no significant decay. The G3 fraction resuspended into the water column would behave similarly to the sediment solid and have little impact on the nutrient supply, before the suspended nutrient is settled back into the bed again. Under these circumstances and for simplicity, the G2 fraction is used to calculate the nutrient resuspension flux in the Okeechobee modeling study (AEE, 2005). The PON resuspended with sediment is approximately represented by the PON in the G2 class in Layer 2 ($G_{\text{PON,2}}$) and the ratio, C_{NS}, has the form:

$$C_{\text{NS}} = \frac{G_{\text{PON,2}}}{m_2} \tag{5.7.71}$$

where m_2 is the solid concentration in Layer 2 used in Eq. (5.7.24).

With the added sediment–water exchange flux of RPON, the equation for RPON, Eq. (5.5.5), is modified to

$$\frac{\partial \text{RPON}}{\partial t} = \sum_{x=c,d,g} (\text{FNR}_x \cdot \text{BM}_x + \text{FNRP} \cdot \text{PR}_x)\text{ANC}_x \cdot B_x - K_{\text{RPON}} \cdot \text{RPON} + \frac{\partial}{\partial z}(\text{WS}_{\text{RP}} \cdot \text{RPON}) + \frac{\text{WRPON}}{V} + \frac{\text{BFRPON}}{\Delta z} \tag{5.7.72}$$

in which the BFRPON term is applied to the bottom layer only.

To account for the PON loss in the sediment bed due to sediment resuspension, the equation for $G_{\text{PON,2}}$, Eq. (5.7.13), should also be modified to

$$H_2 \frac{\partial G_{\text{PON,2}}}{\partial t} = -K_{\text{PON,2}} \cdot \theta_{\text{PON,2}}^{T-20} \cdot G_{\text{PON,2}} \cdot H_2 - W \cdot G_{\text{PON,2}} + J_{\text{PON,2}} - \text{BFRPON} \tag{5.7.73}$$

In this way, BFRPON acts to modify the depositional flux $J_{\text{PON,2}}$. Similar approaches are also applied to POP, POC, and PSi to account for the

contributions of sediment resuspension to the nutrient budget (AEE, 2005). See Section 9.3.4 for further discussion about internal cycling of nutrients in shallow lakes.

5.8 SUBMERGED AQUATIC VEGETATION

Aquatic plants include thousands of species. Macrophytes are aquatic plants that are large enough to be observed by the naked eye. They can be classified into four categories: (1) freely floating, (2) floating leaved, (3) emerged, and (4) submerged.

These four groups of macrophytes are defined by their connection to the waterbody substrate (Fig. 5.8.1). Free-floating macrophytes typically float on or just under the water surface with their roots suspended in the water column. They absorb nutrients entirely from the water column. Floating-leaved macrophytes are rooted to the bottom with leaves that float on the water surface. They may also have underwater leaves. Emerged macrophytes grow near the banks of surface waters, typically in depths of water <1 m. They have their basal portions submerged in water and have their upper structural biomass growing in the air.

Submerged macrophytes, also called submerged aquatic vegetation (SAV), are a diverse group that grows completely (for the most part) under the water. A few species of SAV have flowers that stick above the surface. Hundreds of SAV species are known from freshwater and marine habitats. The definition of SAV usually excludes algae, floating plants, and plants that grow above the water surface.

A stand-alone SAV model commonly includes three groups of state variables: (1) SAV variables, including shoots, roots, and epiphytes; (2)nutrients, and (3) algae. Nutrients and algae have been discussed in previous sections of

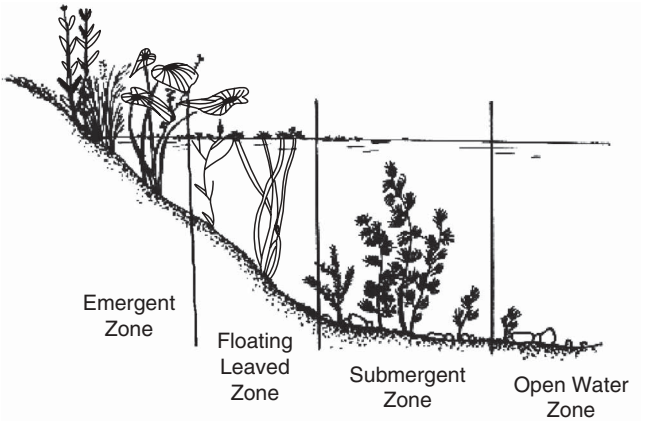

Fig. 5.8.1 Macrophytes in the littoral zone (redrawn from Caduto, 1990).

this chapter; therefore, the focus of this section will be on the SAV variables and their processes. The SAV theories and algorithm presented in this section primarily originated from the SAV modeling study on Lake Okeechobee (Hamrick, 2004; AEE, 2005) and the SAV modeling in Florida Bay (Cerco et al., 2002).

5.8.1 Introduction

The SAV found in most waterbodies is often a desirable component of the ecosystem and is widely recognized as a barometer of a waterbody's health. Management activities are directed to ensure their continual presence. Submerged aquatic vegetation forms the critical link between the physical habitat and the biological community (Fig. 5.8.2). SAV can (1) uptake and release nutrients, (2) reduce shear stress on and shelter the sediment bed, (3) increase total resistance to flow and dampen wave, and (4) provide a healthy ecosystem and support fish and bird populations.

Submerged aquatic vegetation makes significant contributions to the total primary production and nutrient cycling in many waterbodies. These

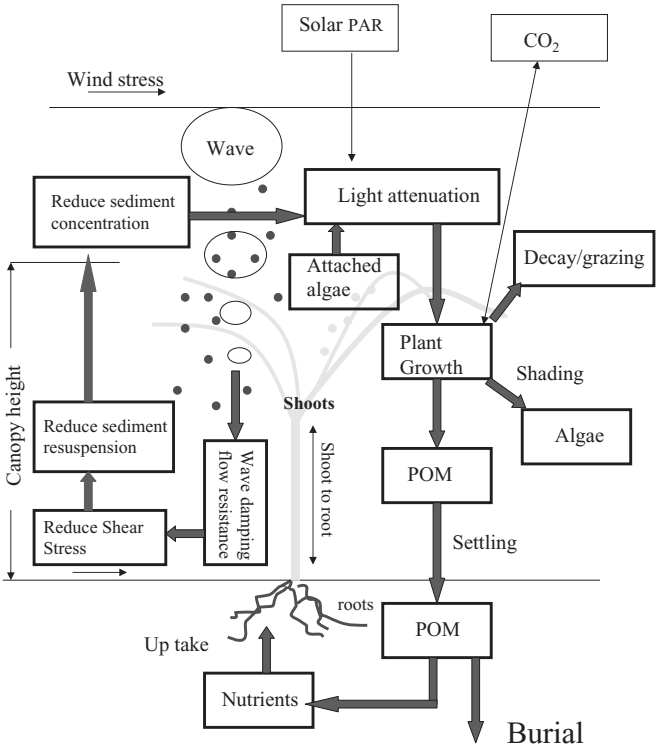

Fig. 5.8.2 Submerged aquatic vegetation processes and the modeling approach.

micropaytes can inhibit phytoplankton growth by competing for nutrients. During the SAV growth seasons (spring and summer), SAV consumes large quantities of nutrients, which are contained in the SAV biomass throughout the warm seasons. As the SAV dies and decays in fall and winter, it slowly releases nutrients back into the water column at a time when algal blooms pose less of a problem. Through primary production and respiration, SAV also affects the DO and CO_2 concentrations, alkalinity, and pH of a waterbody.

Submerged aquatic vegetation binds the sediments to the bottom and stabilizes sediments, which could be easily resuspended if the plants are lost. By retarding water currents, SAV allows suspended sediments to settle and water clarity is improved. Without SAV to stabilize the sediment bed, sediments, along with the nutrients, are easily resuspended from the bottom, blocking the light needed for SAV photosynthesis and increasing nutrients available for algal blooms. It often buffers the shoreline and minimizes erosion by dampening the energy of incoming waves. Submerged aquatic vegetation provides critical habitat for fish, wading birds, and other wildlife. Besides, SAV produces oxygen in the lower portion of the water column through photosynthesis, which is beneficial to aquatic organisms, especially to the benthic organisms.

Not all healthy surface waters have the physical and chemical properties necessary to support SAV. Key factors that control SAV growth include (Fig. 5.8.3) (1) light availability, (2) nutrients, (3) substrate characteristics, and (4) temperature.

Light availability is often the single most crucial factor regulating SAV growth. SAV can grow only in water areas that are shallow enough and clear enough to receive sufficient sunlight for photosynthesis. As illustrated in

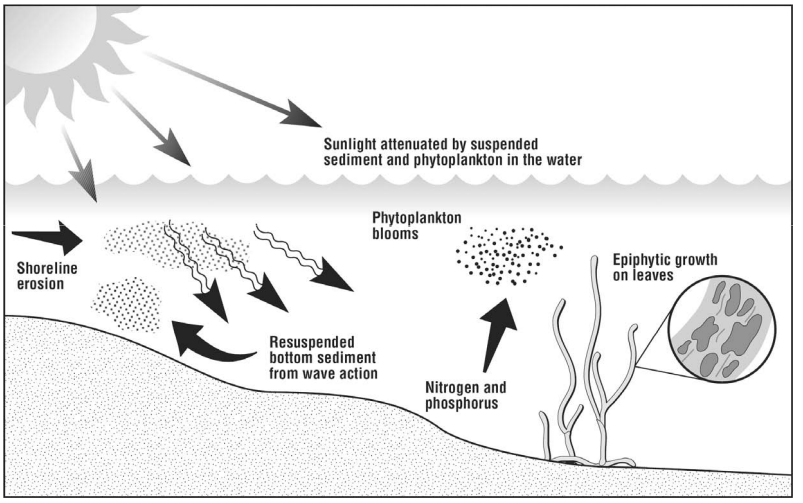

Fig. 5.8.3 Impacts on SAV. Sediments, nutrients, algal blooms, and epiphytic growth can affect the amount of sunlight reaching the plants (USEPA, 2006).

Eq. (5.2.16), the light for photosynthesis decreases when water depth increases or water clarity decreases. Submerged aquatic vegetation species require 20% of daily incident light for their survival in comparison with phytoplankton, which require only 1% of daily incident light (Dennison et al., 1993; Kenworthy and Haunert, 1991). This light requirement often restricts the maximum depth of SAV occurrence to 1–2 m.

The amount of total suspended solids, nutrients, and algae in the water column affects water clarity and plays a major role in controlling SAV growth. As illustrated in Fig. 5.8.3, SAV density may be suppressed when algal densities are high because the algae and/or epiphytes on plant surfaces shade out SAV. Conversely, if SAV is dense, algal growth can be limited (Scheffer, 1989; Scheffer et al., 1993). Excessive nutrients stimulate algal blooms that cloud the water column and reduce water clarity. The nutrients may also trigger a thick growth of epiphytes that prevent the sunlight from reaching the leaf surfaces. As the light availability decreases, the SAV density decreases, leading to fewer nutrients consumed by SAV and the increased possibility of algal blooms. Thus, shaded, turbid, and deep waters have fewer SAV.

Submerged aquatic vegetation draws nutrients from both the sediment bed and the water and competes with algae for nutrients. Nutrients removed by SAV are released into the overlying water, as SAV tissue decays, and contribute to the internal loading of nutrients. The SAV species primarily live in areas where the plants remain submerged. Some species can withstand exposure during low-water periods (e.g., low tide), but a large tidal range (e.g., >2 m) may lead to SAV being exposed for a relatively long time and being desiccated and/or frozen. The physical aspects of the substrate are also important to SAV growth. Some bottom types are too rocky or too sandy for the plants to anchor themselves. In addition, sandy substrate can be nutritionally poor for SAV growth. Areas with severe wave action or deep water may also not be suitable for SAV growth. Like any other algae or plants, SAV growth is also affected by water temperature.

5.8.2 Equations for a SAV Model

Three components are required in order to simulate SAV growth (Figs. 5.8.2 and 5.8.3). The first is a SAV model that describes SAV biomass growth and decay. The second is a water quality model that provides light, temperature, nutrients, and other forcing functions of the SAV model. The third is a coupling algorithm that links the water quality model to the SAV model. The water quality model has been discussed in previous sections of this chapter; therefore, the SAV model and its coupling with the water quality model will be described in this section.

The SAV model (Fig. 5.8.4) incorporates three state variables: (1) shoots (biomass in the water column), (2) roots (biomass in the sediment bed), and (3) epiphytes (plants that grow on the surface of SAV leaves). Shoots consume nutrients from water and from sediments via roots. Epiphytes uptake nutrients

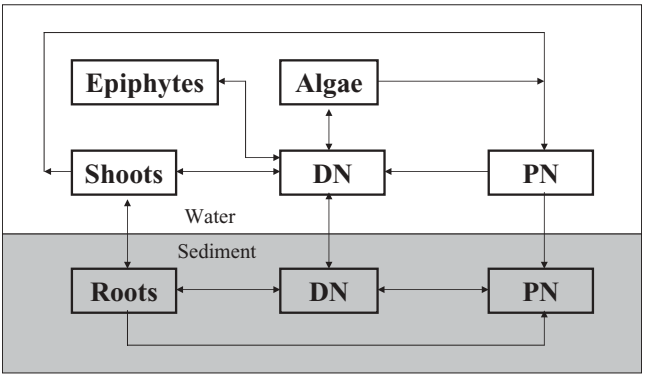

Fig. 5.8.4 SAV model state variables (boxes) and mass flows (arrows). DN = dissolved nutrients; PN = particulate nutrients.

from water, and roots exchange nutrients with sediments. The kinetic mass balance equations for rooted plant shoots, roots, and epiphytes growing on the shoots are (Hamrick, 2004; Cerco et al., 2002):

$$\frac{\partial(\mathrm{RPS})}{\partial t} = ((1 - F_{\mathrm{PRPR}}) \cdot P_{\mathrm{RPS}} - R_{\mathrm{RPS}} - L_{\mathrm{RPS}})\mathrm{RPS} + \mathrm{JRP}_{\mathrm{RS}} \tag{5.8.1}$$

$$\frac{\partial(\mathrm{RPR})}{\partial t} = F_{\mathrm{PRPR}} \cdot P_{\mathrm{RPS}} \cdot \mathrm{RPS} - (R_{\mathrm{RPR}} + L_{\mathrm{RPR}})\mathrm{RPR} - \mathrm{JRP}_{\mathrm{RS}} \tag{5.8.2}$$

$$\frac{\partial(\mathrm{RPE})}{\partial t} = (P_{\mathrm{RPE}} - R_{\mathrm{RPE}} - L_{\mathrm{RPE}})\mathrm{RPE} \tag{5.8.3}$$

where t = time (day), RPS = rooted plant shoot biomass (g C/m^2), F_{PRPR} = fraction of production directly transferred to roots ($0 < F_{\mathrm{PRPR}} < 1$), P_{RPS} = production rate for plant shoots (day^{-1}), R_{PRS} = respiration rate for plant shoots (day^{-1}), L_{RPS} = nonrespiration loss rate for plant shoots (day^{-1}), $\mathrm{JRP}_{\mathrm{RS}}$ = carbon transport positive from roots to shoots (g C/m^2/day^{-1}), RPR = rooted plant root biomass (g C/m^2), R_{RPR} = respiration rate for plant roots (day^{-1}), L_{RPR} = nonrespiration loss rate for plant roots (day^{-1}), RPE = rooted plant epiphyte biomass (g C/m^2), P_{RPE} = production rate for epiphytes (day^{-1}), R_{PRE} = respiration rate for epiphytes (day^{-1}), and L_{RPE} = nonrespiration loss rate for epiphytes (day^{-1}).

The governing equation for shoots, Eq. (5.8.1), establishes a balance between sources and sinks of the SAV biomass in the water column. The governing equation for roots, Eq. (5.8.2), establishes a balance between sources and sinks of the SAV biomass in the sediment bed. The mass flows and interactions among the state variables are shown in Fig. 5.8.4.

An additional state variable is used to account for shoot detritus at the bottom of the water column:

$$\frac{\partial(\mathrm{RPD})}{\partial t} = F_{\mathrm{RPSD}} \cdot L_{\mathrm{RPS}} \cdot \mathrm{RPS} - L_{\mathrm{RPD}} \cdot \mathrm{RPD} \tag{5.8.4}$$

where RPD = rooted plant shoot detritus biomass (g C/m^2), F_{RPSD} = fraction of shoot loss to detritus ($0 < F_{\mathrm{RPSD}} < 1$), and L_{RPD} = decay rate of detritus (day^{-1}), which is assumed to be constant.

The above equations of the SAV model have a general format of

$$\frac{dC}{dt} = a \cdot C + b \tag{5.8.5}$$

where C = concentration, a = constant, and b = constant.

This equation can be solved using an implicit scheme as in the following:

$$\frac{C^{n+1} - C^n}{\Delta t} = a \cdot C^{n+1} + b \tag{5.8.6}$$

where n = the nth time step.

Equation (5.8.6) yields

$$C^{n+1} = \frac{1}{1 - a \cdot \Delta t}(C^n + \Delta t \cdot b) \tag{5.8.7}$$

Equation (5.8.7) gives the general formula used to solve the differential equations of the SAV model.

5.8.2.1 Shoots Production and Respiration. The SAV growth is limited by light, temperature, water column nutrients, sediment nutrients, and salinity (if in saline water). If these resources are in short supply, they can be considered limiting factors for SAV growth. Light availability often plays a key role in SAV development. High concentrations of suspended sediments, algae, or floating aquatic plants are not conducive to SAV growth.

The production or growth rate for plant shoots is given by

$$P_{\mathrm{RPS}} = \mathrm{PM}_{\mathrm{RPS}} \cdot f_1(N) \cdot f_2(I) \cdot f_3(T) \cdot f_4(S) \cdot f_5(\mathrm{RPS}) \tag{5.8.8}$$

where: $\mathrm{PM}_{\mathrm{RPS}}$ = maximum growth rate under optimal conditions for plant shoots (day^{-1}), $f_1(N)$ = effect of suboptimal nutrient concentration ($0 \le f_1 \le 1$), $f_2(I)$ = effect of suboptimal light intensity ($0 \le f_2 \le 1$), $f_3(T)$ = effect of suboptimal temperature ($0 \le f_3 \le 1$), $f_4(S)$ = effect of salinity on freshwater plant shoot growth ($0 \le f_4 \le 1$), and f_5(RPS) = effect of shoot self-shading on shoot growth ($0 \le f_5 \le 1$).

Nutrient limitation is specified in terms of both water column and bed nutrient levels by

$$f_1(N) = \text{minimum}\left(\frac{(NH_4 + NO_3)_w + \frac{KHN_{RPS}}{KHN_{RPR}}(NH_4 + NO_3)_b}{KHN_{RPS} + (NH_4 + NO_3)_w + \frac{KHN_{RPS}}{KHN_{RPR}}(NH_4 + NO_3)_b}, \frac{PO_4 d_w + \frac{KHP_{RPS}}{KHP_{RPR}} PO_4 d_b}{KHP_{RPS} + PO_4 d_w + \frac{KHP_{RPS}}{KHP_{RPR}} PO_4 d_b} \right) \tag{5.8.9}$$

where NH_4 = ammonium nitrogen concentration (g N/m^3), NO_3 = nitrate + nitrite nitrogen concentration (g N/m^3), KHN_{RPS} = half saturation constant for nitrogen uptake from water column (g N/m^3), KHN_{RPR} = half saturation constant for nitrogen uptake from bed (g N/m^3), PO_{4d} = dissolved phosphate phosphorus concentration (g P/m^3), KHP_{RPS} = half saturation constant for phosphorus uptake from water column (g P/m^3), KHP_{RPR} = half saturation constant for phosphorus uptake from bed (g P/m^3), subscript w= water column, and subscript b = bed.

Submerged aquatic vegetation are capable of absorbing nutrients from either the sediment or the water column. Equation (5.8.9) indicates that depending on the eutrophic status, N or P may be the limiting nutrient in SAV biomass accumulation. Both P and N may be taken up by SAV from sediments and the water column. Water column measurements of nutrient concentrations are usually not indicative of SAV growth potential. However, nutrient concentrations in sediment pore water affect SAV growth significantly. Since nutrient concentrations are usually greater in the sediment than in the water column, sediments represent a major source of nutrients for SAV growth.

Light available to the shoots and epiphytes is calculated in the same way as in the water quality model. The light effect on growth is given by Steele's equation, Eq. (5.2.18). By integrating the portion of the water column from the bed to the average top of the plant shoots and over a time period, it has the form:

$$f_2(I) = \frac{2.718 \cdot FD}{Kess \cdot H_{RPS}} (\exp(-\alpha_B) - \exp(-\alpha_T)) \tag{5.8.10}$$

$$\alpha_B = \frac{I_O}{FD \cdot I_{SSO}} \cdot \exp(-Kess \cdot H) \tag{5.8.11}$$

$$\alpha_T = \frac{I_O}{FD \cdot I_{SSO}} \cdot \exp(-Kess \cdot (H - H_{RPS})) \tag{5.8.12}$$

where FD = 1 for instantaneous solar radiation or daylight fraction for daily averaged solar radiation ($0 \le FD \le 1$), Kess = total light extinction coefficient (m^{-1}), I_O = instantaneous solar radiation (FD = 1) or averaged solar radiation during day light (FD < 1) at water surface (Langley/day), I_{SSO} = optimal light intensity on shoot surface for rooted plant growth (Langley/day), H = depth of the water column (m), and H_{RPS} = average height of shoots above bed (m).

The total light extinction coefficient is

$$\text{Kess} = \text{Ke}_b + \text{Ke}_{\text{TSS}} \cdot \text{TSS} + \text{Ke}_{\text{RPE}}\left(\frac{\text{RPE}}{\text{CChl}_{\text{RPE}}}\right) + \text{Ke}_{\text{Chl}} \sum_{m=1}^{M}\left(\frac{B_m}{\text{CChl}_m}\right) \quad (5.8.13)$$

where Ke_b = background light extinction (m^{-1}), Ke_{TSS} = light extinction coefficient for total suspended solids ($m^{-1}/g/m^3$), TSS = total suspended solid concentration (g/m^3) provided from the hydrodynamic model, Ke_{RPE} = light extinction coefficient for epiphyte chlorophyll (m^{-1}/mg Chl/m^2), CChl_{RPE} = carbon/chlorophyll ratio for epiphytes (g C/mg Chl), Ke_{Chl} = light extinction coeffi-cient for algae chlorophyll (m^{-1}/mg Chl/m^3), B_m = concentration of algal group m (g C/m^3), and CChl_m = carbon/chlorophyll ratio in algal group m (g C/mg Chl).

The optimum light intensity for shoot growth is given by

$$I_{\text{SSO}} = \min(I_O \cdot e^{-\text{Kess}\cdot(H_{\text{opt}} - 0.5H_{\text{RPS}})}, I_{\text{SSOM}}) \quad (5.8.14)$$

where H_{opt} = optimum water depth for maximum growth of rooted aquatic vegetation (m), and I_{SSOM} = maximum value for optimum solar radiation for growth (Langley/day).

In some applications where the daylight averaged solar radiation is used, it may be desirable to average the water surface radiation over the current and preceding days using Eq. (5.2.24). It is evident that Eqs. (5.8.10)–(5.8.14) are similar to the ones described in Section 5.2.3 on light for algal growth and photosynthesis.

Similar to Eq. (5.1.9), the effect of temperature on shoot growth is given by

$$f_3(T) = \begin{cases} \exp(-\text{KTP1}_{\text{RPS}}[T - TP1_{\text{RPS}}]^2) & \text{if } T \le TP1_{\text{RPS}} \\ 1 & \text{if } TP1_{\text{RPS}} < T < TP2_{\text{RPS}} \\ \exp(-\text{KTP2}_{\text{RPS}}[T - TP2_{\text{RPS}}]^2) & \text{if } T \ge TP2_{\text{RPS}} \end{cases} \quad (5.8.15)$$

where T = temperature (°C) provided from the hydrodynamic model, $TP1_{\text{RPS}} < T < TP2_{\text{RPS}}$ = optimal temperature range for shoot production (°C), KTP1_{RPS} = effect of temperature below TP1_{RPS} on shoot production ($°C^{-2}$), and KTP2_{RPS} = effect of temperature above TP2_{RPS} on shoot production ($°C^{-2}$).

Similar to Eq. (5.2.9), the effect of salinity on freshwater plant shoot growth is calculated by

$$f_4(S) = \frac{\text{STOXS}^2}{\text{STOXS}^2 + S^2} \tag{5.8.16}$$

where STOXS = salinity at which growth is halved (ppt).

The representation of self-shading by shoots is to incorporate density-limiting functions into the model, since shoot abundance will ultimately be limited by the reduced light available to the SAV growth. The effect of shoot self-shading on shoot growth is given by (AEE, 2005):

$$f_5(\text{RPS}) = e^{-K_{\text{SH}} \cdot \text{RPS}} \tag{5.8.17}$$

where K_{SH} = attenuation due to shoot self-shading (m^2/g).

The respiration rate for plant shoots is assumed to be temperature dependent and uses a formula similar to Eq. (5.2.28) for algae:

$$R_{\text{RPS}} = \text{RM}_{\text{RPS}} \cdot \exp(\text{KTR}_{\text{RPS}}[T - \text{TR}_{\text{RPS}}]) \tag{5.8.18}$$

where TR_{RPS} = reference temperature for shoot respiration (°C), RM_{RPS} = shoot respiration rate at TR_{RPS} (L/time), and KTR_{RPS} = effect of temperature on shoot respiration ($^\circ C^{-1}$). The nonrespiration loss rate for shoots, L_{RPS}, is assumed to be constant.

5.8.2.2 Carbon Transport and Roots Respiration. The carbon transport from roots to shoots is defined as positive to the shoots. Two different formulations can be utilized, the first based on the observed ratio of shoot-to-root biomass ratios:

$$\text{JRP}_{\text{RS}} = \text{KRPO}_{\text{RS}} \cdot (\text{ROSR} \cdot \text{RPR} - \text{RPS}) \tag{5.8.19}$$

where KRPO_{RS} = shoot-to-root transfer rate to follow observed ratio (day^{-1}) and ROSR = observed ratio of shoot carbon to root carbon (dimensionless).

The second formulation transfers root carbon-to-shoot carbon under unfavorable light conditions for the shoots:

$$\text{JRP}_{\text{RS}} = \text{KRP}_{\text{RS}}\left(\frac{I_{\text{SS}}}{I_{\text{SS}} + I_{\text{SSS}}}\right)\text{RPR} \tag{5.8.20}$$

where KRP_{RS} = shoot-to-root transfer rate (day^{-1}), I_{SS} = solar radiation at shoot surface (Langley/day), and I_{SSS} = half saturation solar radiation at shoot surface (Langley/day).

The respiration rate for plant roots is assumed to be temperature dependent:

$$R_{\text{RPR}} = \text{RM}_{\text{RPR}} \cdot \exp(\text{KTR}_{\text{RPR}}[T - \text{TR}_{\text{RPR}}]) \tag{5.8.21}$$

where TR_{RPR} = reference temperature for root respiration (°C), RM_{RPR} = root respiration rate at TR_{RPR} (day^{-1}), and KTR_{RPR} = effect of temperature on root respiration ($°C^{-1}$). The nonrespiration loss rate for roots, L_{RPR}, is assumed to be constant.

5.8.2.3 Epiphytes Production and Respiration. Nutrient enrichment also enhances epiphytic growth on SAV leaf surfaces, which can limit the light available to SAV for photosynthesis. The production or growth rate for epiphytes on plant shoots is given by

$$P_{RPE} = PM_{RPE} \cdot f_1(N) \cdot f_2(I) \cdot f_3(T) \cdot f_4(S) f_5(RPS) \tag{5.8.22}$$

where PM_{RPE} = maximum growth rate under optimal conditions for epiphytes (day^{-1}), $f_1(N)$ = effect of suboptimal nutrient concentration in the water column ($0 \le f_1 \le 1$) $f_2(I)$ = effect of suboptimal light intensity ($0 \le f_2 \le 1$), $f_3(T)$ = effect of suboptimal temperature ($0 \le f_3 \le 1$), $f_4(S)$ = effect of salinity on freshwater epiphyte growth ($0 \le f_4 \le 1$), f_5(RPS) = effect of shoots on epiphyte growth ($0 \le f_5 \le 1$).

Nutrient limitation for epiphytes is given by

$$f_1(N) = \text{minimum}\left(\frac{NH4 + NO3}{KHN_{RPE} + NH4 + NO3}, \frac{PO4d}{KHP_{RPE} + PO4d}\right) \tag{5.8.23}$$

where KHN_{RPe} = half saturation constant for nitrogen uptake for epiphytes (g N/m^3) and KHP_{RPE} = half saturation constant for phosphorus uptake for epiphytes (g P/m^3).

Light limitation is specified by

$$f_2(I) = \frac{2.718 \cdot FD}{Kesse \cdot H_{RPS}} (\exp(-\alpha_B) - \exp(-\alpha_T)) \tag{5.8.24}$$

$$\alpha_B = \frac{I_O}{FD \cdot I_{SSOE}} \cdot \exp(-Kesse \cdot H) \tag{5.8.25}$$

$$\alpha_T = \frac{I_O}{FD \cdot I_{SSOE}} \cdot \exp(-Kesse \cdot (H - H_{RPS})) \tag{5.8.26}$$

where Kesse = total light extinction coefficient for epiphytes (m^{-1}) and I_{SSOE} = optimal light intensity for epiphyte growth (Langley/day).

$$Kesse = Ke_b + Ke_{TSS} \cdot TSS + Ke_{Chl} \sum_{m=1}^{M} \left(\frac{B_m}{CChl_m}\right) \tag{5.8.27}$$

The optimum light intensity for epiphyte growth is given by

$$I_{SSOE} = \min(I_O \cdot e^{-Kesse \cdot (H_{opt} - 0.5 H_{RPS})}, I_{SSOEM}) \tag{5.8.28}$$

where I_{SSOEM} = maximum value for optimum light for epiphyte growth (Langley/day). In some applications where the daylight averaged solar radiation is used, it may be desirable to average the water surface radiation over the current and preceding days using Eq. (5.2.24).

The effect of temperature on epiphyte growth is given by

$$f_3(T) = \begin{cases} \exp(-\mathrm{KTP1_{RPE}}[T - \mathrm{TP1_{RPE}}]^2) & \text{if } T \le \mathrm{TP1_{RPE}} \\ 1 & \text{if } \mathrm{TP1_{RPE}} < T < \mathrm{TP2_{RPE}} \\ \exp(-\mathrm{KTP2_{RPE}}[T - \mathrm{TP2_{RPE}}]^2) & \text{if } T \ge \mathrm{TP2_{RPE}} \end{cases} \tag{5.8.29}$$

where $\mathrm{TP1_{RPE}} < T < \mathrm{TP2_{RPE}}$ = optimal temperature range for epiphyte production (°C), $\mathrm{KTP1_{RPE}}$ = effect of temperature below $\mathrm{TP1_{RPE}}$ on epiphyte production ($°C^{-2}$), and $\mathrm{KTP2_{RPE}}$ = effect of temperature above $\mathrm{TP2_{RPE}}$ on epiphyte production ($°C^{-2}$).

The effect of salinity on freshwater epiphyte growth is given by

$$f_4(S) = \frac{\mathrm{STOXE}^2}{\mathrm{STOXE}^2 + S^2} \tag{5.8.30}$$

where STOXE = salinity at which growth is halved (ppt).

Since epiphytes grow on shoots, the surface area of the shoots affects the epiphyte growth. It has the form:

$$f_5(\mathrm{RPS}) = \frac{\mathrm{RPS}}{\mathrm{RPSH} + \mathrm{RPS}} \tag{5.8.31}$$

where RPSH = RPS concentration at which growth is halved (g C/m^2).

The respiration rate for epiphytes is assumed to be temperature dependent and uses a formula similar to Eq. (5.2.28):

$$R_{\mathrm{RPE}} = \mathrm{RM_{RPE}} \cdot \exp(\mathrm{KTR_{RPE}}[T - \mathrm{TR_{RPE}}]) \tag{5.8.32}$$

where $\mathrm{TR_{RPE}}$ = reference temperature for epiphytes respiration (°C), $\mathrm{RM_{RPE}}$ = epiphytes respiration rate at $\mathrm{TR_{RPE}}$ (L/Time), and $\mathrm{KTR_{RPE}}$ = effect of temperature on epiphytes respiration ($°C^{-1}$). The nonrespiration loss rate for epiphytes, L_{RPE}, is assumed to be constant.

5.8.3 Coupling With the Water Quality Model

It is assumed that SAV has a fixed nutrient composition. Nitrogen and phosphorus in SAV biomass are represented in terms of carbonaceous biomass. The SAV respiration releases nutrients back to the sediment bed and water column. As illustrated in Figs. 5.8.2 and 5.8.3, the SAV model has direct linkages with the water quality model:

1. Growth and decay of the SAV link to the nutrient pool of the water quality model.

2. Photosynthesis and respiration of SAV link to DO dynamics.
3. Settling of POM and nutrient uptake affect nutrients in the water column and in the sediment bed.
4. Shoot detritus, RPD, is located at the bottom of the water column and is coupled with the water quality model at the bottom layer only.

When integrated into the water quality model, the SAV model is completely coupled with the water quality model in the water column and the sediment diagenesis model in the sediment bed. All of the state variables are updated at each model time step, providing a true dynamic representation of the system (AEE, 2005).

5.8.3.1 Organic Carbon Coupling. The interaction of organic carbon between the SAV model and the water quality model is given by

$$\frac{\partial \mathrm{RPOC}_W}{\partial t} = \frac{1}{H}(\mathrm{FCR}_{\mathrm{RPS}} \cdot R_{\mathrm{RPS}} + (1 - F_{\mathrm{RPSD}}) \cdot \mathrm{FCRL}_{\mathrm{RPS}} \cdot L_{\mathrm{RPS}})\mathrm{RPS} + \frac{1}{H}$$
$$(\mathrm{FCR}_{\mathrm{RPE}} \cdot R_{\mathrm{RPE}} + \mathrm{FCRL}_{\mathrm{RPE}} \cdot L_{\mathrm{RPE}})\mathrm{RPE} + \frac{1}{\Delta z}\mathrm{FCRL}_{\mathrm{RPD}} \cdot L_{\mathrm{RPD}} \cdot \mathrm{RPD} \tag{5.8.33}$$

$$\frac{\partial \mathrm{RPOC}_B}{\partial t} = \frac{1}{B}(\mathrm{FCR}_{\mathrm{RPR}} \cdot R_{\mathrm{RPR}} + \mathrm{FCRL}_{\mathrm{RPR}} \cdot L_{\mathrm{RPR}})\mathrm{RPR} \tag{5.8.34}$$

$$\frac{\partial \mathrm{LPOC}_W}{\partial t} = \frac{1}{H}(\mathrm{FCL}_{\mathrm{RPS}} \cdot R_{\mathrm{RPS}} + (1 - F_{\mathrm{RPSD}}) \cdot \mathrm{FCLL}_{\mathrm{RPS}} \cdot L_{\mathrm{RPS}})\mathrm{RPS} + \frac{1}{H}$$
$$(\mathrm{FCL}_{\mathrm{RPE}} \cdot R_{\mathrm{RPE}} + \mathrm{FCLL}_{\mathrm{RPE}} \cdot L_{\mathrm{RPE}})\mathrm{RPE} + \frac{1}{\Delta z}\mathrm{FCLL}_{\mathrm{RPD}} \cdot L_{\mathrm{RPD}} \cdot \mathrm{RPD} \tag{5.8.35}$$

$$\frac{\partial \mathrm{LPOC}_B}{\partial t} = \frac{1}{B}(\mathrm{FCL}_{\mathrm{RPR}} \cdot R_{\mathrm{RPR}} + \mathrm{FCLL}_{\mathrm{RPR}} \cdot L_{\mathrm{RPR}})\mathrm{RPR} \tag{5.8.36}$$

$$\frac{\partial \mathrm{DOC}_W}{\partial t} = \frac{1}{H}(\mathrm{FCD}_{\mathrm{RPS}} \cdot R_{\mathrm{RPS}} + (1 - F_{\mathrm{RPSD}}) \cdot \mathrm{FCDL}_{\mathrm{RPS}} \cdot L_{\mathrm{RPS}})\mathrm{RPS} + \frac{1}{H}$$
$$(\mathrm{FCD}_{\mathrm{RPE}} \cdot R_{\mathrm{RPE}} + \mathrm{FCDL}_{\mathrm{RPE}} \cdot L_{\mathrm{RPE}})\mathrm{RPE} + \frac{1}{\Delta z}\mathrm{FCDL}_{\mathrm{RPD}} \cdot L_{\mathrm{RPD}} \cdot \mathrm{RPD} \tag{5.8.37}$$

$$\frac{\partial \mathrm{DOC}_B}{\partial t} = \frac{1}{B}(\mathrm{FCD}_{\mathrm{RPR}} \cdot R_{\mathrm{RPR}} + \mathrm{FCDL}_{\mathrm{RPR}} \cdot L_{\mathrm{RPR}})\mathrm{RPR} \tag{5.8.38}$$

where RPOC = concentration of refractory particulate organic carbon (g C/m^3), LPOC = concentration of labile particulate organic carbon (g C/m^3), DOC =

concentration of dissolved organic carbon (g C/m^3), FCR = fraction of respired carbon produced as refractory particulate organic carbon, FCL = fraction of respired carbon produced as labile particulate organic carbon, FCD = fraction of respired carbon produced as dissolved organic carbon, FCRL = fraction of nonrespired carbon loss produced as refractory particulate organic carbon, FCLL = fraction of nonrespired carbon loss produced as labile particulate organic carbon, FCDL = fraction of nonrespired carbon loss produced as dissolved organic carbon, H = depth of water column, B = depth of bed, Δz = bottom layer thickness, subscript W = water column, and subscript B = bed.

The terms related to detritus, RPD, are only applied in the bottom layer of the water quality model. Equations (5.8.33)–(5.8.38) represent very similar mechanisms: the organic carbons (RPOC, LPOC, and DOC) in the water column (W) and bed (B) are increased due to the respiration and nonrespiration loss of shoots (RPS), roots (RPR), epiphytes (RPE), and/or shoot detritus (RPD).

5.8.3.2 Dissolved Oxygen Coupling. The interaction of rooted plants and epiphytes with DO is given by

$$\frac{\partial \mathrm{DO}_W}{\partial t} = \frac{1}{H}(P_{\mathrm{RPS}} \cdot \mathrm{RPSOC} \cdot \mathrm{RPS} + P_{\mathrm{RPE}} \cdot \mathrm{RPEOC} \cdot \mathrm{RPE}) \tag{5.8.39}$$

where DO = concentration of dissolved oxygen (g O_2/m^3), RPSOC = oxygen/carbon ratio for plant shoots (g O_2/g C), and RPEOC = oxygen/carbon ratio for epiphytes (g O_2/g C). Equation (5.8.39) indicates that the production of shoots (RPS) and epiphytes (RPE) increases DO in the water column.

5.8.3.3 Phosphorus Coupling. The interaction of rooted plants and epiphytes with phosphorus is given by

$$\begin{aligned}\frac{\partial \mathrm{RPOP}_W}{\partial t} = {} & \frac{1}{H}(\mathrm{FPR}_{\mathrm{RPS}} \cdot R_{\mathrm{RPS}} + (1 - F_{\mathrm{RPSD}}) \cdot \mathrm{FPRL}_{\mathrm{RPS}} \cdot L_{\mathrm{RPS}}) \cdot \mathrm{RPSPC} \cdot \mathrm{RPS} + \\ & \frac{1}{H}(\mathrm{FPR}_{\mathrm{RPE}} \cdot R_{\mathrm{RPE}} + \mathrm{FPRL}_{\mathrm{RPE}} \cdot L_{\mathrm{RPE}}) \cdot \mathrm{RPEPC} \cdot \mathrm{RPE} + \\ & \frac{1}{\Delta z} \mathrm{FPRL}_{\mathrm{RPD}} \cdot L_{\mathrm{RPD}} \cdot \mathrm{RPSPC} \cdot \mathrm{RPD}\end{aligned} \tag{5.8.40}$$

$$\frac{\partial \mathrm{RPOP}_B}{\partial t} = \frac{1}{B}(\mathrm{FPR}_{\mathrm{RPR}} \cdot R_{\mathrm{RPR}} + \mathrm{FPRL}_{\mathrm{RPR}} \cdot L_{\mathrm{RPR}}) \mathrm{RPRPC} \cdot \mathrm{RPR} \tag{5.8.41}$$

$$\begin{aligned}\frac{\partial \mathrm{LPOP}_W}{\partial t} = {} & \frac{1}{H}(\mathrm{FPL}_{\mathrm{RPS}} \cdot R_{\mathrm{RPS}} + (1 - F_{\mathrm{RPSD}}) \cdot \mathrm{FPLL}_{\mathrm{RPS}} \cdot L_{\mathrm{RPS}}) \mathrm{RPSPC} \cdot \mathrm{RPS} + \\ & \frac{1}{H}(\mathrm{FPL}_{\mathrm{RPE}} \cdot R_{\mathrm{RPE}} + \mathrm{FPLL}_{\mathrm{RPE}} \cdot L_{\mathrm{RPE}}) \mathrm{RPEPC} \cdot \mathrm{RPE} + \\ & \frac{1}{\Delta z} \mathrm{FPLL}_{\mathrm{RPD}} \cdot L_{\mathrm{RPD}} \cdot \mathrm{RPSPC} \cdot \mathrm{RPD}\end{aligned} \tag{5.8.42}$$

$$\frac{\partial \mathrm{LPOP}_B}{\partial t} = \frac{1}{B}(\mathrm{FPL}_{\mathrm{RPR}} \cdot R_{\mathrm{RPR}} + \mathrm{FPLL}_{\mathrm{RPR}} \cdot L_{\mathrm{RPR}})\mathrm{RPRPC} \cdot \mathrm{RPR} \quad (5.8.43)$$

$$\begin{aligned}\frac{\partial \mathrm{DOP}_W}{\partial t} = {} & \frac{1}{H}(\mathrm{FPD}_{\mathrm{RPS}} \cdot R_{\mathrm{RPS}} + (1 - F_{\mathrm{RPSD}}) \cdot \mathrm{FPDL}_{\mathrm{RPS}} \cdot L_{\mathrm{RPS}})\mathrm{RPSPC} \cdot \mathrm{RPS} \\ & + \frac{1}{H}(\mathrm{FPD}_{\mathrm{RPE}} \cdot R_{\mathrm{RPE}} + \mathrm{FPDL}_{\mathrm{RPE}} \cdot L_{\mathrm{RPE}})\mathrm{RPEPC} \cdot \mathrm{RPE} \\ & + \frac{1}{\Delta z}\mathrm{FCDL}_{\mathrm{RPD}} \cdot L_{\mathrm{RPD}} \cdot \mathrm{RPSPC} \cdot \mathrm{RPD}\end{aligned} \quad (5.8.44)$$

$$\frac{\partial \mathrm{DOP}_B}{\partial t} = \frac{1}{B}(\mathrm{FPD}_{\mathrm{RPR}} \cdot R_{\mathrm{RPR}} + \mathrm{FPDL}_{\mathrm{RPR}} \cdot L_{\mathrm{RPR}})\mathrm{RPRPC} \cdot \mathrm{RPR} \quad (5.8.45)$$

$$\begin{aligned}\frac{\partial \mathrm{PO4}t_W}{\partial t} = {} & \frac{1}{H}(\mathrm{FPI}_{\mathrm{RPS}} \cdot R_{\mathrm{RPS}} + (1 - F_{\mathrm{RPSD}}) \cdot \mathrm{FPIL}_{\mathrm{RPS}} \cdot L_{\mathrm{RPS}})\mathrm{RPSPC} \cdot \mathrm{RPS} \\ & \frac{1}{H}(\mathrm{FPI}_{\mathrm{RPE}} \cdot R_{\mathrm{RPE}} + \mathrm{FPIL}_{\mathrm{RPE}} \cdot L_{\mathrm{RPE}})\mathrm{RPEPC} \cdot \mathrm{RPE} \\ & + \frac{1}{\Delta z}\mathrm{FPIL}_{\mathrm{RPD}} \cdot L_{\mathrm{RPD}} \cdot \mathrm{RPSPC} \cdot \mathrm{RPD} \\ & - \frac{1}{H}F_{\mathrm{RPSPW}} \cdot P_{\mathrm{RPS}} \cdot \mathrm{RPSPC} \cdot \mathrm{RPS} - \frac{1}{H}P_{\mathrm{RPE}} \cdot \mathrm{RPEPC} \cdot \mathrm{RPE}\end{aligned} \quad (5.8.46)$$

$$\begin{aligned}\frac{\partial \mathrm{PO4}t_B}{\partial t} = {} & \frac{1}{B}(\mathrm{FPI}_{\mathrm{RPR}} \cdot R_{\mathrm{RPR}} + \mathrm{FPIL}_{\mathrm{RPR}} \cdot L_{\mathrm{RPR}})\mathrm{RPRPC} \cdot \mathrm{RPR} \\ & - \frac{1}{H}(1 - F_{\mathrm{RPSPW}})P_{\mathrm{RPS}} \cdot \mathrm{RPRPC} \cdot \mathrm{RPS}\end{aligned} \quad (5.8.47)$$

$$F_{\mathrm{RPSPW}} = \frac{\mathrm{KHP}_{\mathrm{RPR}}\mathrm{PO4}d_w}{\mathrm{KHP}_{\mathrm{RPR}}\mathrm{PO4}d_w + \mathrm{KHP}_{\mathrm{RPS}}\mathrm{PO4}d_b} \quad (5.8.48)$$

where RPOP = concentration of refractory particulate organic phosphorus (g C/m^3), LPOP = concentration of labile particulate organic phosphorus (g C/m^3), DOP = concentration of dissolved organic phosphorus (g C/m^3), PO4t = total phosphate (g P/m^3) = PO4d + PO4p, PO4d = dissolved phosphate (g P/m^3), PO4p = particulate (sorbed) phosphate (g P/m^3), FPR = fraction of respired phosphorus produced as refractory particulate organic phosphorus, FPL = fraction of respired phosphorus produced as labile particulate organic phosphorus, FPD = fraction of respired phosphorus produced as dissolved organic phosphorus, FPI = fraction of respired phosphorus produced as total phosphate, FPRL = fraction of nonrespired phosphorus produced as refractory particulate organic phosphorus, FPLL = fraction of nonrespired phosphorus produced as labile particulate organic phosphorus, FPDL =

fraction of nonrespired phosphorus produced as dissolved organic phosphorus, FPIL = fraction of nonrespired phosphorus produced as total phosphate, RPSPC = plant shoot phosphorus/carbon ratio (g P/g C), RPRPC = plant root phosphorus/carbon ratio (g P/g C), RPEPC = epiphyte phosphorus/carbon ratio (g P/g C), F_{RPSPW} = fraction of PO4*d* uptake from the water column, $\mathrm{KHP_{RPS}}$ = half saturation constant for phosphorus uptake from the water column (g P/m^3), and $\mathrm{KHP_{RPR}}$ = half saturation constant for phosphorus uptake from the bed (g P/m^3).

The terms related to detritus, RPD, are only applied to the bottom layer of the water quality model. Equations (5.8.40)–(5.8.45) represent very similar mechanisms: the fractions of organic phosphorus (RPOP, LPOP, and DOP) in the water column (*W*) and bed (*B*) are increased due to the respiration and nonrespiration loss of shoots (RPS), roots (RPR), epiphytes (RPE), and/or shoot detritus (RPD). Equations (5.8.46) and (5.8.47) describe the impacts of RPS, RPR, RPE, and RPD on total phosphate (PO_4t) in the water column and the bed. They show that RPS can uptake PO_4 from the water column and the bed, whereas RPE can only consume PO_4 in the water column. Equations (5.8.46) and (5.8.47) represent the key mechanism by which SAV competes with phytoplankton for phosphorus during the SAV growth season.

5.8.3.4 Nitrogen Coupling. The nitrogen coupling between the SAV model and the water quality model is given by

$$\begin{aligned}\frac{\partial \mathrm{RPON}_W}{\partial t} = {} & \frac{1}{H}(\mathrm{FNR_{RPS}}\cdot R_{\mathrm{RPS}} + (1-F_{\mathrm{RPSD}})\cdot \mathrm{FNRL_{RPS}}\cdot L_{\mathrm{RPS}})\cdot \mathrm{RPSNC}\cdot \mathrm{RPS} \\ & \frac{1}{H}(\mathrm{FNR_{RPE}}\cdot R_{\mathrm{RPE}} + \mathrm{FNRL_{RPE}}\cdot L_{\mathrm{RPE}})\cdot \mathrm{RPENC}\cdot \mathrm{RPE} \\ & + \frac{1}{\Delta z}\mathrm{FNRL_{RPD}}\cdot L_{\mathrm{RPD}}\cdot \mathrm{RPSNC}\cdot \mathrm{RPD} \end{aligned} \tag{5.8.49}$$

$$\frac{\partial \mathrm{RPON}_B}{\partial t} = \frac{1}{B}(\mathrm{FNR_{RPR}}\cdot R_{\mathrm{RPR}} + \mathrm{FNRL_{RPR}}\cdot L_{\mathrm{RPR}})\mathrm{RPRNC}\cdot \mathrm{RPR} \tag{5.8.50}$$

$$\begin{aligned}\frac{\partial \mathrm{LPON}_W}{\partial t} = {} & \frac{1}{H}(\mathrm{FNL_{RPS}}\cdot R_{\mathrm{RPS}} + (1-F_{\mathrm{RPSD}})\cdot \mathrm{FNLL_{RPS}}\cdot L_{\mathrm{RPS}})\mathrm{RPSNC}\cdot \mathrm{RPS} \\ & + \frac{1}{H}(\mathrm{FNL_{RPE}}\cdot R_{\mathrm{RPE}} + \mathrm{FNLL_{RPE}}\cdot L_{\mathrm{RPE}})\mathrm{RPENC}\cdot \mathrm{RPE} \\ & + \frac{1}{\Delta z}\mathrm{FNLL_{RPD}}\cdot L_{\mathrm{RPD}}\cdot \mathrm{RPSNC}\cdot \mathrm{RPD} \end{aligned} \tag{5.8.51}$$

$$\frac{\partial \mathrm{LPON}_B}{\partial t} = \frac{1}{B}(\mathrm{FNL_{RPR}}\cdot R_{\mathrm{RPR}} + \mathrm{FNLL_{RPR}}\cdot L_{\mathrm{RPR}})\mathrm{RPRNC}\cdot \mathrm{RPR} \tag{5.8.52}$$

$$\frac{\partial \mathrm{DON}_W}{\partial t} = \frac{1}{H}(\mathrm{FND}_{\mathrm{RPS}} \cdot R_{\mathrm{RPS}} + (1 - F_{\mathrm{RPSD}}) \cdot \mathrm{FNDL}_{\mathrm{RPS}} \cdot L_{\mathrm{RPS}})\mathrm{RPSNC} \cdot \mathrm{RPS} + \frac{1}{H}(\mathrm{FND}_{\mathrm{RPE}} \cdot R_{\mathrm{RPE}} + \mathrm{FNDL}_{\mathrm{RPE}} \cdot L_{\mathrm{RPE}})\mathrm{RPENC} \cdot \mathrm{RPE} + \frac{1}{\Delta z}\mathrm{FNDL}_{\mathrm{RPD}} \cdot L_{\mathrm{RPD}} \cdot \mathrm{RPSNC} \cdot \mathrm{RPD} \quad (5.8.53)$$

$$\frac{\partial \mathrm{DON}_B}{\partial t} = \frac{1}{B}(\mathrm{FND}_{\mathrm{RPR}} \cdot R_{\mathrm{RPR}} + \mathrm{FNDL}_{\mathrm{RPR}} \cdot L_{\mathrm{RPR}})\mathrm{RPRNC} \cdot \mathrm{RPR} \quad (5.8.54)$$

$$\frac{\partial \mathrm{NH4}_W}{\partial t} = \frac{1}{H}(\mathrm{FNI}_{\mathrm{RPS}} \cdot R_{\mathrm{RPS}} + (1 - F_{\mathrm{RPSD}}) \cdot \mathrm{FNIL}_{\mathrm{RPS}} \cdot L_{\mathrm{RPS}})\mathrm{RPSNC} \cdot \mathrm{RPS} + \frac{1}{H}(\mathrm{FNI}_{\mathrm{RPE}} \cdot R_{\mathrm{RPE}} + \mathrm{FNIL}_{\mathrm{RPE}} \cdot L_{\mathrm{RPE}})\mathrm{RPENC} \cdot \mathrm{RPE} + \frac{1}{\Delta z}\mathrm{FPRL}_{\mathrm{RPD}} \cdot L_{\mathrm{RPD}} \cdot \mathrm{RPSNC} \cdot \mathrm{RPD} - \frac{1}{H}\mathrm{PN}_{\mathrm{RPSw}} \cdot \mathrm{F}_{\mathrm{RPSNW}} \cdot P_{\mathrm{RPS}} \cdot \mathrm{RPSNC} \cdot \mathrm{RPS} - \frac{1}{H}\mathrm{PN}_{\mathrm{RPE}} \cdot P_{\mathrm{RPE}} \cdot \mathrm{RPENC} \cdot \mathrm{RPE} \quad (5.8.55)$$

$$\frac{\partial \mathrm{NH4}_B}{\partial t} = \frac{1}{B}(\mathrm{FNI}_{\mathrm{RPR}} \cdot R_{\mathrm{RPR}} + \mathrm{FNIL}_{\mathrm{RPR}} \cdot L_{\mathrm{RPR}})\mathrm{RPRNC} \cdot \mathrm{RPR} - \frac{1}{H}\mathrm{PN}_{\mathrm{RPSb}}(1 - F_{\mathrm{RPSNW}})P_{\mathrm{RPS}} \cdot \mathrm{RPSNC} \cdot \mathrm{RPS} \quad (5.8.56)$$

$$\frac{\partial \mathrm{NO3}_W}{\partial t} = -\frac{1}{H}(1 - \mathrm{PN}_{\mathrm{RPSW}})\mathrm{F}_{\mathrm{RPSNW}} \cdot P_{\mathrm{RPS}} \cdot \mathrm{RPSNC} \cdot \mathrm{RPS} - \frac{1}{H}(1 - \mathrm{PN}_{\mathrm{RPE}})P_{\mathrm{RPE}} \cdot \mathrm{RPENC} \cdot \mathrm{RPE} \quad (5.8.57)$$

$$\frac{\partial \mathrm{NO3}_B}{\partial t} = -\frac{1}{H}(1 - \mathrm{PN}_{\mathrm{RPSb}})(1 - F_{\mathrm{RPSNW}})P_{\mathrm{RPS}} \cdot \mathrm{RPSNC} \cdot \mathrm{RPS} \quad (5.8.58)$$

$$\mathrm{PN}_{\mathrm{RPSW}} = \frac{\mathrm{NH4}_W \cdot \mathrm{NO3}_W}{(\mathrm{KHNP}_{\mathrm{RPS}} + \mathrm{NH4}_W)(\mathrm{KHNP}_{\mathrm{RPS}} + \mathrm{NO3}_W)} + \frac{\mathrm{NH4}_W \cdot \mathrm{KHNP}_{\mathrm{RPS}}}{(\mathrm{NH4}_W + \mathrm{NO3}_W)(\mathrm{KHNP}_{\mathrm{RPS}} + \mathrm{NO3}_W)} \quad (5.8.59)$$

$$\mathrm{PN}_{\mathrm{RPSb}} = \frac{\mathrm{NH4}_B \cdot \mathrm{NO3}_B}{(\mathrm{KHNP}_{\mathrm{RPS}} + \mathrm{NH4}_B)(\mathrm{KHNP}_{\mathrm{RPS}} + \mathrm{NO3}_B)} + \frac{\mathrm{NH4}_B \cdot \mathrm{KHNP}_{\mathrm{RPS}}}{(\mathrm{NH4}_B + \mathrm{NO3}_B)(\mathrm{KHNP}_{\mathrm{RPS}} + \mathrm{NO3}_B)} \quad (5.8.60)$$

$$PN_{RPE} = \frac{NH4 \cdot NO3}{(KHNP_{RPE} + NH4)(KHNP_{RPE} + NO3)} + \frac{NH4 \cdot KHNP_{RPE}}{(NH4 + NO3)(KHNP_{RPE} + NO3)} \quad (5.8.61)$$

$$F_{RPSNW} = \frac{KHN_{RPR}(NH4 + NO3)_w}{KHN_{RPR}(NH4 + NO3)_w + KHN_{RPS}(NH4 + NO3)_b} \quad (5.8.62)$$

where RPON = concentration of refractory particulate organic nitrogen (g N/m^3), LPON = concentration of labile particulate organic nitrogen (g N/m^3), DON = concentration of dissolved organic nitrogen (g N/m^3), NH4 = ammonia (g N/m^3), NO3 = nitrate + nitrite nitrogen (g N/m^3), FNR = fraction of respired nitrogen produced as refractory particulate organic nitrogen, FNL = fraction of respired nitrogen produced as labile particulate organic nitrogen, FND = fraction of respired nitrogen produced as dissolved organic nitrogen, FNI = fraction of respired nitrogen produced as ammonia, FNRL = fraction of nonrespired nitrogen produced as refractory particulate organic nitrogen, FNLL = fraction of nonrespired nitrogen produced as labile particulate organic nitrogen, FNDL = fraction of nonrespired nitrogen produced as dissolved organic nitrogen, FNIL = fraction of nonrespired nitrogen produced as ammonia, RPSNC = plant shoot nitrogen/carbon ratio (g N/g C), RPRNC = plant root nitrogen/carbon ratio (g N/g C), F_{RPSNW} = plant shoot fraction of NH4 and NO3 uptake from the water column, PN_{RPS} = ammonia nitrogen preference fraction for plant shoots, $KHNP_{RPS}$ = saturation coefficient for nitrogen preference for plant shoots (g N/g C), PN_{RPE} = ammonia nitrogen preference fraction for epiphytes, $KHNP_{RPE}$ = saturation coefficient for nitrogen preference for epiphytes (g N/g C), KHN_{RPS} = half saturation constant for nitrogen uptake from the water column (g N/m^3), and KHN_{RPR} = half saturation constant for nitrogen uptake from bed (g N/m^3).

The terms related to detritus, RPD, are only applied to the bottom layer of the water quality model. Equations (5.8.49)–(5.8.54) represent very similar mechanisms: the fractions of organic nitrogen (RPON, LPON, and DON) in the water column (*W*) and bed (*B*) are increased due to the respiration and nonrespiration loss of shoots (RPS), roots (RPR), epiphytes (RPE), and/or shoot detritus (RPD). Equations (5.8.55)–(5.8.58) describe the impacts of RPS, RPR, RPE, and RPD on dissolved inorganic nitrogen (NH4 and NO3) in the water column and the bed. They show that RPS can uptake NH4 and NO3 from the water column and the bed, whereas RPE can only consume NH4 and NO3 in the water column. Equations (5.8.55)–(5.8.58) represent the key mechanism by which SAV competes with phytoplankton for nitrogen during the SAV growth season.

5.8.3.5 Total Suspended Solid Coupling. The effects of SAV on stabilizing the sediment bed can be included in sediment modeling. A simplified

approach is to modify the settling velocity of the TSS, so that the increased settling velocity will lead to lower TSS (Cerco et al., 2002). It has the form:

$$\frac{\partial \text{TSS}}{\partial t} = \text{net transport} - \frac{1}{H}(W_s + W_{\text{SAV}} \cdot \text{RPS}) \cdot \text{TSS} \qquad (5.8.63)$$

where W_s = TSS settling velocity, W_{SAV} = a parameter representing the effect of SAV on reducing the TSS concentration in the water column, and RPS = rooted plant shoot biomass (g C/m^2).

5.9 WATER QUALITY MODELING

Scientifically credible numerical models can enhance water resource management by helping evaluate management options. However, the dynamic simulation of eutrophication in a surface water system can be a very complicated and computationally intensive endeavor due to the time variations of a large number of chemical, biological, and biochemical processes; reaction rates; and external inputs. A water quality model is a mathematical representation of water quality processes that occur within a waterbody. It typically includes one or more groups of algae, inorganic and organic nutrients (N, P, C), and DO. The model simulates water quality processes, including external inputs, nutrient recycling, and algal growth in rivers, lakes, and estuaries. It generally incorporates features such as circulation and mixing, point and nonpoint sources, photosynthesis, water temperature, DO dynamics, behaviors of the various nutrient forms, the effects of atmospheric loadings, and SOD. As an example, Fig. 5.9.1 gives the structure of the EFDC water quality model (Park et al., 1995) in which the water quality model is directly coupled with the hydrodynamic, sediment, and SAV models (AEE, 2005).

Mathematical modeling of water quality presents a special challenge and demands integration of multiple disciplines. Compared with the hydrodynamics and sediment transport, water quality modeling is often more difficult to work with because of the complexity of the algal biology, the nonlinear interactions between nutrients and aquatic plants, and the interactions between the sediment bed and the water column. As discussed in the previous sections of this chapter, water quality models typically take into account three factors: hydrodynamic transport, external inputs, and chemical and biological reactions within the system. For water quality models, processes of temperature, oxygen, nutrients, and algae are considered and often interact with each other. The sediment fluxes from the bed are also of concern. Water quality models are dependent on hydrodynamics to describe the movement of water and the mixing. Knowledge of hydrology, meteorology, and atmospheric physics is needed for specifying external loadings and conditions at the air–water interface. The model also draws on chemical kinetics and biochemistry for determination of the fate of dissolved and particulate nutrients.

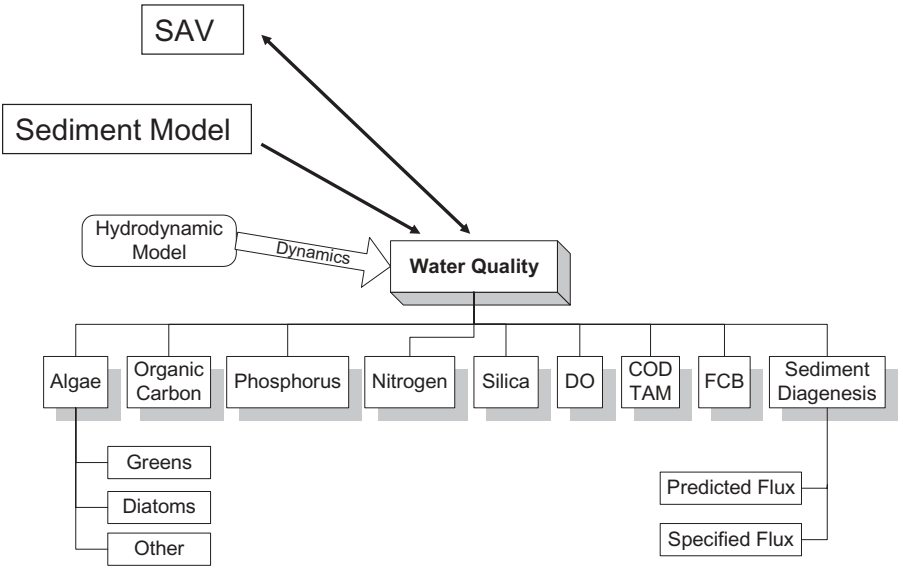

Fig. 5.9.1 Structure of the EFDC water quality model.

Hydrodynamic models provide essential information to water quality models, including advection, dispersion, vertical mixing, temperature, and salinity. Water quality models can be linked with hydrodynamic models directly or indirectly. In a direct approach, the hydrodynamic transport and water quality processes are simulated concurrently. That is, the hydrodynamics and water quality algorithms are contained within the same computer code and run simultaneously (e.g., Park et al., 1995). In an indirect approach, the hydrodynamic simulation is conducted separately and the hydrodynamic results are saved as inputs to a water quality model (e.g., HydroQual, 1995c). The hydrodynamic results may be averaged over space and time to allow the use of coarser time or space scales in water quality modeling. However, this time and space averaging may encounter difficulties, since important advective and diffusive information may be lost in the spatial and temporal averaging. In the modeling of the Chesapeake Bay, Cerco et al. (2002) reported that a great deal of uncertainty still remained when computing hydrodynamics for water quality utilization. In particular, they found that alternate hydrodynamic computations that produce similar computations of salinity can produce dramatically different computations of DO and other water quality parameters. They concluded that hydrodynamic models cannot be calibrated in isolation and, subsequently, used to drive water quality models. Instead, hydrodynamic and water quality models must be calibrated together to produce simultaneous, satisfactory computations of both transport processes and water quality.

5.9.1 Model Parameters and Data Requirements

This section covers information about parameters and data used in the water quality modeling of rivers, lakes, and estuaries.

5.9.1.1 Water Quality Parameters. Water quality models are based on the principle of mass conservation. In order to represent water quality processes mathematically, water quality models utilize numerous empirical formulations and parameters, much more than the ones in hydrodynamic and sediment models. For example, the EFDC water quality model (Park et al., 1995) has >130 model parameters categorized into six groups. One group represents the parameters used in the sediment diagenesis model. The other five groups represent algae, organic carbon, phosphorus, nitrogen, and the oxygen cycle in the water column. Determining the values of these parameters is the key step in water quality model calibration.

A major consequence of so many water quality parameters is that it takes much more effort to tune the parameters and to calibrate the water quality model. For example, the net algal production in Eq. (5.2.6) depends on algal growth, metabolism, predation, settling, and external sources. It is desirable to obtain actual measurements of water quality parameters. In practice, however, many of these parameter values are often determined via model calibration. This is necessary since the parameters vary with environmental conditions, such as temperature, light, and nutrient concentrations, all of which change continually with time. Since water quality processes are interrelated, adjusting one parameter may affect several processes. It requires significant expertise to adjust the water quality parameters of a water quality model, because of the complexity of the interactions between the processes involved. In order to simulate a system well, it is vital to understand the processes being modeled and the controlling factors of the system.

The evaluation of water quality parameters is an iterative process. Literature values are used for establishing reasonable ranges for the parameters (e.g., Bowie et al., 1984). Typically, an initial parameter set is selected from the literature, followed by revisions to improve agreement between model results and measured data. Final parameters are then chosen to optimize the agreement between the modeled results and the measured data. Ideally, the range of feasible values is determined by measured data. For some parameters, however, no observations are available. Then, the feasible range is determined by parameter values employed in similar models or by the judgment of the modeler (Cerco and Cole, 1994).

For example, HydroQual (1995c) reported that in the modeling of Massachusetts Bay, although the set of potentially adjustable model parameters used in the study numbers >100, in reality a much smaller subset of parameters were actually adjusted during the study. A number of the model coefficients have proved to be "universal" across a number of estuarine and coastal ecosystems similar to the Massachusetts Bay. This subset of model

parameters has been successfully applied to eutrophication models for other studies. For example, the parameter values established in the application to the Chesapeake Bay (Cerco and Cole, 1994) may serve as a starting point for model application to estuaries in the eastern United States.

Major differences between water quality models include the number of algae and nutrient groups considered and the specific empirical formulations used for each term (process). Because of these differences, it is critical to understand the assumptions of a particular model when selecting model parameters, extracting values from one model and applying them to another, and/or comparing model results with measured data. Detailed discussions about water quality parameters are beyond the scope of this book and are referred to other literatures.

When conducting a modeling study on a specific waterbody, more information on water quality parameters is generally available from

1. Technical reports and papers on model parameters. These documents present general discussions on parameter values and their ranges (e.g., Bowie et al., 1985).
2. Manuals and reports for the model that is used in the study. These documents usually give parameter values that are relevant and applicable to the specific model.
3. Technical reports and papers on the waterbody studied. These documents often provide parameter values that are specifically applicable to this study site.

5.9.1.2 Data Requirements. Numerical models are simply a tool to quantify the physical, chemical, and biological processes. Due to the empirical nature of mathematical formulations used in water quality models, adequate data are the key to model setup, calibration, and verification. The credibility of model results is judged, to a large degree, by their agreement with measured data. Reliable initial and time-varying boundary conditions are essential to a water quality model. If external nutrient loadings are not adequately characterized, it would be impossible for the model to accurately reproduce the eutrophication processes. These point and nonpoint sources are often determined by measured data, watershed models, and/or regression analysis.

For example, regression analysis can be used to resolve intense storm events, since these events generally have the highest loadings to a waterbody. It is common to establish a regression relation between the measured inflow rate and the nutrient loadings. Figure 5.9.2, for example, shows the relationship between TP in kg/day and flow (Q) in cubic meters per second (m^3/s) at Station TT151 in the Florida Bay. It has the following form:

$$\text{TP Load (kg/day)} = -1.46 + 3.95Q - 0.118Q^2 - 0.00247Q^3 \qquad (5.9.1)$$

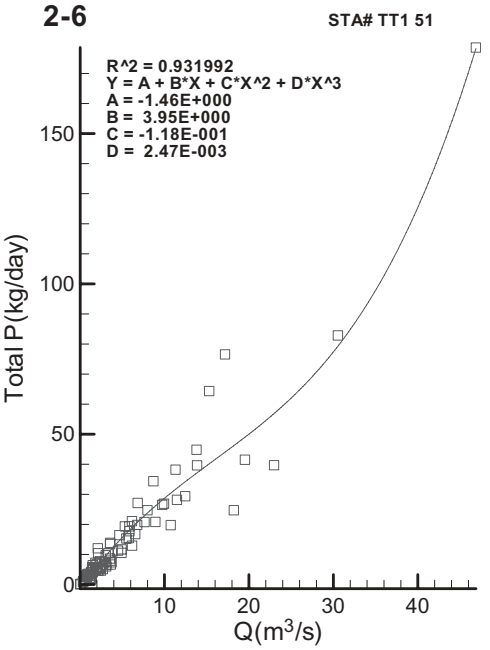

Fig. 5.9.2 Regression results between flow and total phosphorus at Station TT151 in the Florida Bay.

Equation (5.9.1) and Fig. 5.9.2 show that the load increases as the flow increases. Although limited data are used to establish the loading relationship, the overall results are satisfactory, with R^2 values of 0.93. More discussion on regression analysis will be given in Section 7.2.2.

A literature review is a good place to obtain a preliminary understanding of the processes in a water system and to obtain baseline data information. A literature review may also help to highlight the key factors affecting the water quality process and to reduce data requirements. For example, literature data may show that a certain tributary source is unlikely to contribute much to the nutrient budget. Consequently, it might be possible to eliminate the sampling of that tributary and to assign it the values from literature sources.

In addition to data collected from new sampling programs, water quality data may exist in various databases. The EPA reports (USEPA, 2000b, 2000c, 2001) give a long list of relevant databases. Among these databases, EPAs national database for water quality and biological data, STORET, is probably the one used most in water quality studies (USEPA, 1994b). The database STORET is a compendium of data supplied by Federal, State, and local organizations that is used to evaluate environmental conditions in the United States. It includes physical, chemical, and biological data measured in waterbodies throughout the United States and has operated continuously since the

1960s. Interested parties may view the database on the World Wide Web (http://www.epa.gov/storet/).

The type, amount, and quality of water quality data needed depend on a number of factors, such as which state variables are used and what water quality processes are involved. The physical, chemical, and biological characteristics of the waterbody studied should be considered in determining the data requirements. Frequently, a practical consideration is the availability of funding for the study. Another consideration is the nature of the relationship between nutrient loads and the response of the waterbody. For example, minimum requirements for one year of limnological data have been developed by the EPA as part of the Clean Lakes Program (USEPA, 2000b).

5.9.2 Case Study I: Lake Okeechobee

The hydrodynamic modeling of Lake Okeechobee is discussed in Section 2.4.2. The sediment transport modeling of the lake is given in Section 3.7.2. In addition, Jin and Ji (2004, 2005) also discussed the hydrodynamic and sediment modeling of the lake in detail. As a case study, this section discusses the water quality and SAV modeling in the lake (Jin et al., 2007; AEE, 2005). The developed water quality model and the SAV model constitute two submodels of the LOEM.

This case study is focused on the following efforts:

1. Calibration of the LOEM water quality model: October 1999–September 2000.
2. Verification of the LOEM water quality model: October 2000–September 2001.
3. Validation of the LOEM water quality model: October 2001–October 2002.
4. Simulating SAV in the lake: October 1999–October 2002.

The applications of the LOEM model will be presented in Section 9.4.2 as another case study.

5.9.2.1 Background. Despite the progress in 3D hydrodynamic, water quality, and sediment diagenesis models and their successful applications in estuaries and bays, few 3D water quality modeling studies on lakes have been published. In the modeling of Lake Okeechobee, Jin and Ji (2004, 2005) clearly demonstrated 3D features of the lake and the importance of 3D modeling. They reported that the lake can exhibit strong vertical stratifications when the wind is calm. Ji et al. (2004a) used a 3D hydrodynamic, sediment, and water quality model to simulate water quality and eutrophication in a reservoir and illustrated the importance of 3D water quality modeling. They demonstrated that neither a 2D laterally averaged nor a 2D vertically averaged model was

capable of representing the DO and temperature profiles in the reservoir; therefore, a 3D model must be used in the study (Section 9.4.1).

Lake Okeechobee is the largest subtropical lake in North America. This large shallow lake (area 1730 km^2, mean depth 3.2 m) contains a littoral habitat that comprises 20% of its surface area (Fig. 2.4.2). The lake functions as the central part of a large interconnected aquatic ecosystem in south Florida. Lake Okeechobee is known for sport fishing, and it is home to migratory water fowl, wading birds, and the federally endangered Everglade Snail Kite. Agricultural activities around the lake area include cattle ranching, dairy farming, and crop production of sugarcane, winter vegetables, and citrus. The seasonal variations of algae in Lake Okeechobee, like many tropical and subtropical lakes, do not follow the classic pattern of spring bloom and winter minima in temperate lakes. Algal blooms have been observed in all months of the year (Havens et al., 1996). The lack of a winter freeze and reduced interseasonal variation in solar radiation and air temperature play a significant role in the water quality processes in the lake. Wind is a primary driving force for the lake (Ji and Jin, 2006). Contrary to the general tendency toward phosphorus limitation in temperate freshwater systems, nitrogen and light limitation are most common in Lake Okeechobee (Aldridge et al., 1995).

Water quality in this lake has changed dramatically in the last several decades, largely as a result of nutrient inputs from agriculture and other human activities in the watershed. Because of the excessive P loads to Lake Okeechobee, the lake has changed from a P-limited system in the 1970s to a N-limited system in the 1990s (Havens et al., 1996). High rates of external phosphorus loading from the watershed and internal phosphorus loading from the lake sediment bed are responsible for the high concentrations of phosphorus in the lake. Total phosphorus concentrations have increased dramatically from 42 ppb in the early 1970s to >120 ppb in 2000 (Havens and James, 2005). The phosphorus-rich mud sediments in the center of the lake are frequently resuspended by wind and transported to ecologically sensitive shoreline areas, especially during times of high lake levels (James and Havens, 2005).

Submerged and emergent vegetation comprise ~20% of the lake area. The uptake of phosphorus by this vegetation can play a role in the lake's phosphorus dynamics. Submerged aquatic vegetation has the capability to reduce water column phosphorus concentrations by a number of processes including reduced resuspension, uptake of phosphorus, and coprecipitation of phosphorus with calcium. During years when the lake water level is low, the lake can support a large spatial extent of SAV (Havens et al., 2004). When the lake water level is high, the growth of SAV is suppressed due to light limitations caused by the deeper water and the high turbidity.

5.9.2.2 Model Setup and Data Sources. The LOEM model is developed within the framework of the Environmental Fluid Dynamics Code (EFDC) (Hamrick, 1992; Park et al., 1995). Model parameters used in this study are similar to the ones used in the Peconic Bay study (Tetra Tech, 1999e), the

Christina River study (Tetra Tech, 2000b), the Long Island Sound study (HydroQual, 1991b), the Massachusetts Bay study (HydroQual, 1995c), and the Lake Okeechobee study (James et al., 2005). Di Toro (2001) reported that the parameters used in the sediment diagenesis models are also very similar to those used in the studies of Cerco and Cole (1994), HydroQual (1991b), and HydroQual (1995c). The values of major water quality parameters used in this study are listed in Table 5.9.1.

The water quality data available to this study included eight water quality parameters collected monthly at 25 in-lake stations in water years (October–September, WY) 2000, 2001, and 2002. These parameters are DO, Chl, TP, SRP, total Kjeldahl nitrogen (TKN), NH_4, NO_x (NO_2 + NO_3), and silica (SI). The water quality model also simulates chloride (Cl) in the lake to check the model's conservation of mass. The locations of water quality stations are shown in Fig. 5.9.3. Note that all of the 25 water quality stations are located in the open water area and none of them are in the littoral zone area. The lack of measured water quality data in the littoral zone will affect model calibration in this area. The littoral zone is not addressed here also because it typifies a wetland more than a lake ecosystem. These observed measurements are available on the South Florida Water Management District's DBHYDRO database (http://www.sfwmd.gov/org/ema/dbhydro/index.html). External loadings of nutrients and solids are provided at monthly intervals using methods described by James et al. (1995a). The atmospheric deposition data at the Kennedy Space Center (Station FL99) are obtained from the National Atmospheric Program (http://nadp.sws.uiuc.edu/nadpdata/). Limited in-lake sediment flux data are available, but are insufficient for direct model–data comparison.

TABLE 5.9.1 Major Water Quality Parameters

PMc = maximum growth rate for cyanobacteria (L/day)	2.5
KHNc = nitrogen half saturation for cyanobacteria (mg/L)	0.01
KHPc = phosphorus half saturation for cyanobacteria (mg/L)	0.001
BMRc = basal metabolism rate for cyanobacteria (L/day)	0.01
WSc = settling velocity for cyanobacteria (m/day)	0.25
WSrp = settling velocity for refractory POM (m/day)	0.8
WSlp = settling velocity for labile POM (m/day)	0.8
KRP = minimum hydrolysis rate of refractory particulate organic phosphorus (L/day)	0.005
KLP = minimum hydrolysis rate of labile particulate organic phosphorus (L/day)	0.075
KDP = minimum hydrolysis rate of dissolved organic phosphorus (L/day)	0.1
KRN = minimum hydrolysis rate of refractory organic nitrogen (L/day)	0.005
KLN = minimum hydrolysis rate of labile particulate organic nitrogen (L/day)	0.075
KDN = minimum hydrolysis rate of dissolved organic nitrogen (L/day)	0.02
NitM = maximum nitrification rate (L/day)	0.07

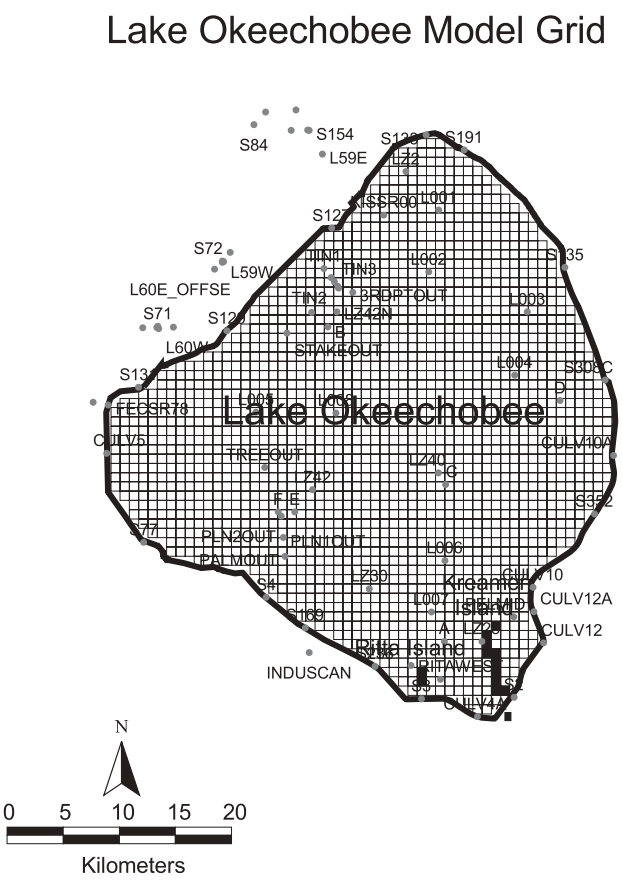

Fig. 5.9.3 Locations of water quality data stations (SFWMD, 2002).

5.9.2.3 Water Quality Modeling Results. The water quality model uses the grid of the hydrodynamic submodel, containing 2121 horizontal grid cells (Fig. 2.4.2) and 5 vertical layers. Integration time step was 200 s. The 3D model results were averaged and saved daily. It takes ~6 h of CPU time for a 1-year simulation on a 3 GHz PC. In this study, three sets of independent data in WY 2000, WY 2001, and WY 2002 were used to calibrate, verify, and validate the LOEM model. General discussions on model calibration, verification, and validation are not presented here, but will be given in Section 7.3.

The water quality model was calibrated against WY 2000 data (from 10/1/1999 to 9/30/2000). Comparisons were made between the model results and observations for the eight observed water quality parameters. Some sampling sites had a few measured data in WY 2000 that were insufficient for statistical analysis. Only measured data that had monthly samples (i.e., the total data number is >12) were used in the statistical analysis. In previous studies, water quality modeling results are often presented as spatially and temporally

averaged manner. For example, the Chesapeake Bay Model (Cerco and Cole, 1994) compared model results with observations that were averaged by month and over aggregated grid subdivisions. In this study, however, the water quality data are presented without any averaging in space or time and are compared directly with the model results. All of the available data at the 25 stations are used for model–data comparison. Direct comparison without any additional manipulation is a more rigorous way to check model performance. Detailed calibration and verified results are presented at one site, L002, which is in the north central region of the lake (Fig. 2.4.2). Data from other sites were compared to the model results in the same fashion.

The relative root-mean-square error (RRE) at L002 varies from 11.95% for DO to 32.88% for TKN (Table 5.9.2). The RRE is defined as the ratio of RMSE to the observed change and is often used in hydrodynamic and water quality modeling (e.g., Blumberg et al., 1999; Jin and Ji, 2004, 2005). In the calculation of DO errors, traditionally, the mean DO, instead of DO variation, is used to calculate relative errors (e.g., Martin and McCutcheon, 1999; USEPA, 1990). This study also followed this approach. There are insufficient measured data of NH_4 and SI for statistical analysis. The mean RRE for six parameters evaluated at L002 is 22.6% for the calibration period. Another way to measure the relative errors of model results is the relative absolute error (RAE), which is the absolute error divided by the mean observation. The absolute error and the RAE are also presented to show that the model generally has comparable RRE and RAE, even though the mean RAE is slightly higher than the mean RRE.

The RRE results for each station and water year are summarized (Table 5.9.3). As an example, the mean RRE of 22.6% at L002 in WY2000 comes from Table 5.9.2. The Mean RRE values for the 25 sample locations in Lake Okeechobee ranged from a low of 22.5% at site L008, in the south central region of the lake, to 36.1% at PELMID, in the south east region of the lake (Fig. 5.9.3, Table 5.9.3). In general, the RRE was smaller for sites located toward center of the lake. The overall mean RRE during the calibration period is 27.8%, which indicates that the model simulates the water quality variations in the lake reasonably well.

Table 5.9.4 gives the mean values of the observed and modeled water quality variables. For example, the observed mean DO value in WY 2000, 8.357 mg/L, is the average of DO data at the 25 stations during the period of 10/1/1999 and 9/30/2000, which includes ~25 (number of stations) × 14 (number of data at each station in WY 2000) of DO measurements. The corresponding modeled mean DO value of 8.328 mg/L is calculated using the modeled DO at the same locations and at the same measurement times. It is evident that the model simulated the mean values of the measured data satisfactorily.

Time series plots of the observed data (circles) and model simulation (solid line) demonstrate the model goodness-of-fit at site L002 (Fig. 5.9.4*a* and *b*) because the model results generally compare favorably to the observed data. Observed data were taken from 1 *m* below the surface of the water column. Because DO profiles in Lake Okeechobee rarely indicate hypoxia or anoxia,

TABLE 5.9.2 Error Analysis of Observed and Modeled Water Quality Variables at L002 from 10/1/1999 to 9/30/2000

Variable	Number of Observations	Obs. Mean (mg/L)	Modeled Mean (mg/L)	RMS Error (mg/L)	Abs. Error (mg/L)	Obs. Change (mg/L)	RRE (%)	RAE (%)
DO	13	8.474	8.159	1.013	0.732	1.630	11.95	8.64
Chl(μg/L)	15	28.193	18.275	18.636	12.836	76.800	24.27	45.52
TP	15	0.130	0.130	0.033	0.025	0.205	16.16	19.50
SRP	14	0.035	0.043	0.016	0.012	0.065	24.57	35.10
TKN	15	1.343	1.371	0.369	0.295	1.122	32.88	21.97
NO2+NO3	14	0.271	0.276	0.160	0.106	0.596	26.83	39.07
Cl	14	52.960	53.250	3.483	2.936	16.240	21.45	8.64
Mean							22.60	25.1

TABLE 5.9.3 Summary of Station-Averaged RRE for WY 2000–WY 2002

Station Name	Relative Root-Mean-Square Error %		
	WY 2000	WY2001	WY2002
3RDPTOUT	29.2		38.6
L001	26.5	32.5	27.6
L002	22.6	33.1	33.6
L003	24.1	28.5	31
L004	23.9	32.2	33
L005	24.5	34	34.8
L006	28.6	33.8	39.8
L007	26.2		48.3
L008	22.5	31.7	26.4
LZ2			31.9
LZ30	32.4	32.9	45.6
LZ40	25	36.3	32.6
LZ42	28.6	35.1	37.3
LZ42N	27.5		28.2
PALMOUT	31.1		32.7
PELMID	36.1		36.6
PLN2OUT	28.3		44.6
POLE3S	35.8		35.5
POLESOUT	28.3		28.8
RITAEAST	28.2		
RITAWEST	28.7		33.2
STAKEOUT	24.4		29.9
TREEOUT	28.9		32
Mean	27.78	33.01	34.55

the water column is considered well mixed in DO. The model reproduces the marked spring bloom, both in time and in magnitude (Panel a2 in Fig. 5.9.4*a*), but appears to underestimate the algal concentration in September 2000.

There are 25 stations in the lake. Similar high algal concentrations exist at L002 and 2 more stations to the northwest of LOO2, that is, in the northwest corner of the lake (the area near the Kissimmee River inflow and its nearby littoral zone). These high algal concentrations occurred only in this small area and only in the fall of 2000. The LOEM model simulated the water temperature very well, as reported in the previous studies (e.g., Fig. 2.4.8 and Table 2.4.3). It is unlikely that small errors in temperature simulation could cause such large errors in algae simulation. The high algal concentrations might be associated with the inflows from the Kissimmee River and nearby littoral zone activities. The littoral zone is largely covered with emergent vegetation.

The LOEM does not have a submodel to realistically describe the emergent vegetation in the littoral zone. Even though the littoral zone consists of relatively isolated areas and is largely separated by the dense emergent vegetation, the littoral zone could have an impact on the water quality in the nearby area.

TABLE 5.9.4 Mean Values of Observed and Modeled Water Quality Variables for WY 2000–WY 2002

Variable	WY 2000		WY2001		WY2002	
	Obs. Mean (mg/L)	Modeled Mean (mg/L)	Obs. Mean (mg/L)	Modeled Mean (mg/L)	Obs. Mean (mg/L)	Modeled Mean (mg/L)
DO	8.357	8.328	8.061	7.960	8.242	8.379
Chl(μg/L)	21.371	20.556	21.243	19.379	30.058	27.486
TP	0.099	0.119	0.117	0.081	0.093	0.123
SRP	0.038	0.043	0.025	0.026	0.029	0.024
TKN	1.338	1.344	1.538	1.487	1.447	1.572
NO2+NO3	0.265	0.268	0.117	0.066	0.083	0.028
Cl	54.412	52.958	78.135	76.486	72.282	72.443

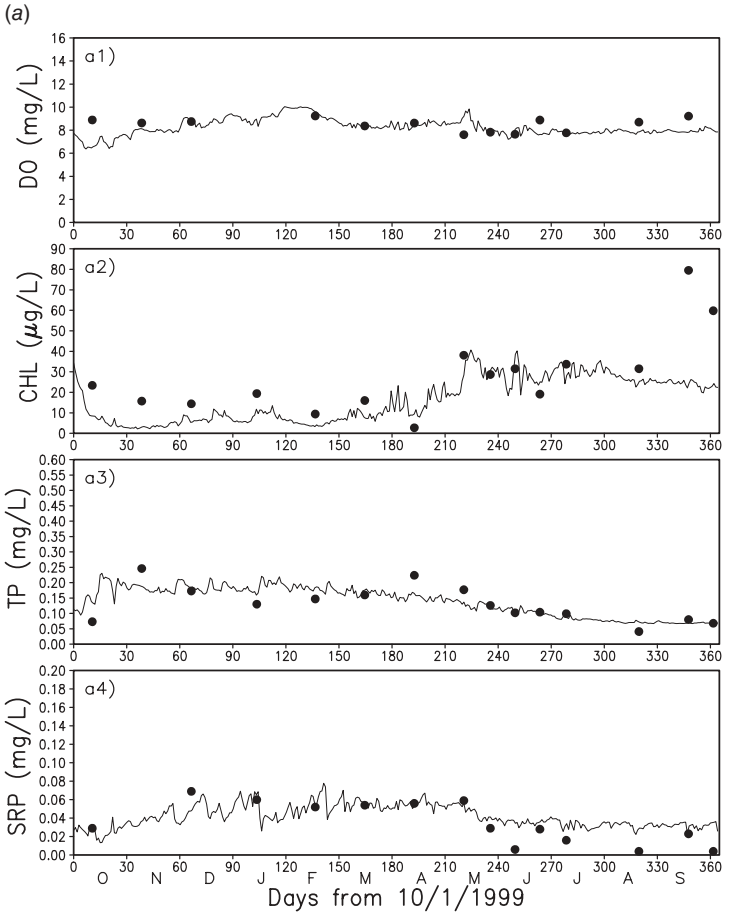

Fig. 5.9.4(*a*) Time series of water quality variables at L002 between 10/1/1999 and 9/30/2000. Closed cycle = measured data; solid line = modeled results.

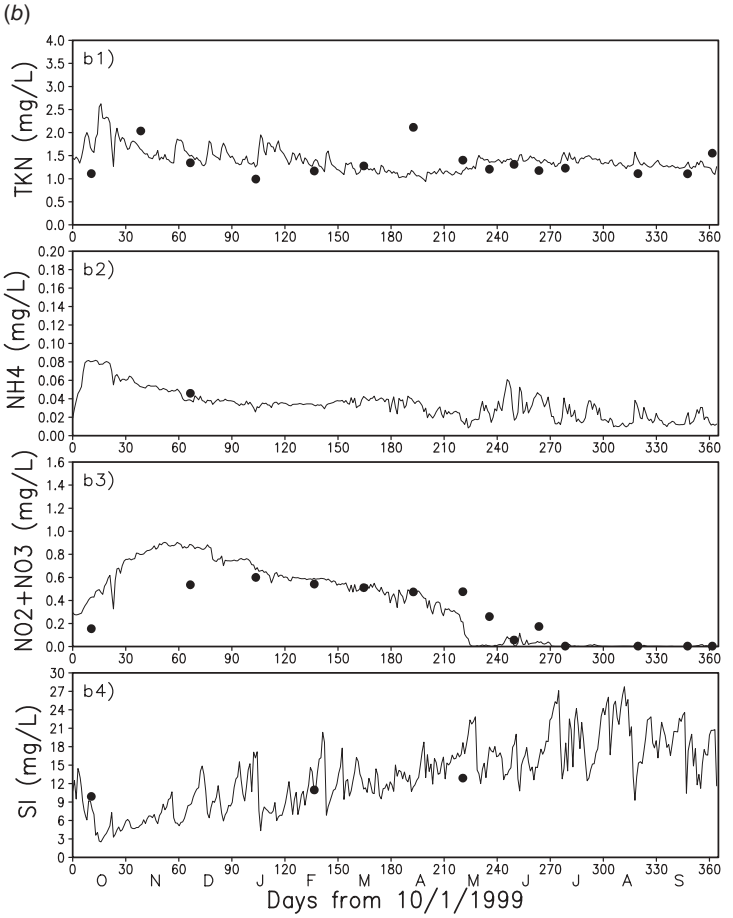

Fig. 5.9.4(*b*) Time series of water quality variables at L002 between 10/1/1999 and 9/30/2000. Closed cycle = measured data; solid line = modeled results.

In addition, all of the 25 water quality stations are located in the open water area; none of them is in the littoral zone. As a result, modeling errors in the littoral zone might affect the model results in the areas near the littoral zone. Toward the center of the lake and far away from the littoral zone, the model is less affected by errors in the littoral zone. This should also partially explain why the RRE was smaller for sites located toward the center of the lake. It is expected that more realistic representation of the emergent vegetation in the littoral zone should improve the LOEM results.

With respect to the nutrients, the computations are in good agreement with the observed data. The model reproduced the marked declines in nutrients as the spring algal bloom takes place. The model also reproduced the timing of the depletion of NO_x (Panel b3 in Fig. 5.9.4*b*). As the result of algal growth,

TP and SRP decline, and concentrations are relatively low during the algal growth season due to the increased uptake from algae. Weaker wind speeds in this period lead to reduced sediment resuspension, which also contributes to TP and SRP decline. During the summer months, NO_x and NH4 are reduced significantly and nitrogen becomes the limiting nutrient for algal growth (Fig. 5.9.4*b*). Panel b4 in Fig. 5.9.4*b* shows that SI concentration fluctuated to a large extent (James et al., 2005).

The modeled chlorophyll *a* concentration and the water currents on 6/2/2000 are given in Fig. 5.9.5. The small arrow in the upper left corner indicates the wind speed and direction on that day. Phytoplankton biomass, represented by chlorophyll *a* levels, exhibited significant spatial variability. In the open water area, the typical chlorophyll *a* concentrations are in the range of 15–35 μg/L, which are consistent with the measured data.

The LOEM water quality model is verified with observed data from WY2001. The purpose of model verification is to test the performance of the calibrated model under different environmental conditions. During this period (10/1/2000–9/30/2001) a record drought occurred. The lake level dropped to a record low in June 2001. Because of the drought, some stations have only a few measured data in 2001 and are inadequate for statistical analysis. The mean RRE is 33.01% (Table 5.9.3). Overall the model results are consistent with the data (Table 5.9.4, Fig. 5.9.6*a* and *b*). The calibrated and verified LOEM model is further validated using WY 2002 data (10/1/2001 and 9/30/2002) (Table 5.9.3). Overall, the model results are consistent with the observed data (Table 5.9.4). The mean RRE is 34.55%.

5.9.2.4 SAV Modeling Results. Submerged aquatic vegetation is a key component of the shallow nearshore region of the lake, between the littoral zone and the deeper open water zone (Fig. 2.4.2). It plays a critical role in stabilizing sediments, supporting attached algae that remove available nutrients from the water, and providing critical habitat for fish, wading birds, and other wildlife (Havens et al., 2005). The SAV community in the lake is monitored on two different spatial and temporal scales. On a quarterly basis, the biomass is evaluated at fixed locations along 16 shoreline transects (Fig. 5.9.7). Plants are sampled at sites along each transect, starting at the shoreline and progressing lake ward until a site is reached where there are no plants (Havens et al., 2005). When the density of the SAV biomass is more than 5 g dry weight/m^2, the sampled area is considered covered with SAV. On a yearly basis, the entire SAV community is also mapped at a resolution of 1000 × 1000 m (Havens et al., 2005). Collecting these SAV data is a huge, expensive effort. It is fortunate that these data are available to this study. The survey from August to September of 2000 indicated that the lake had 43,845 acres (1 acre = 4047 m^2) of SAV (Fig. 5.9.8).

Figure 5.9.9 gives the modeled water surface elevation (EL) at Station P (shown in Fig. 2.4.2), measured SAV coverage in percentage, and the SAV areas in 2000, 2001, and 2002. The SAV (%) panel is the summary results from

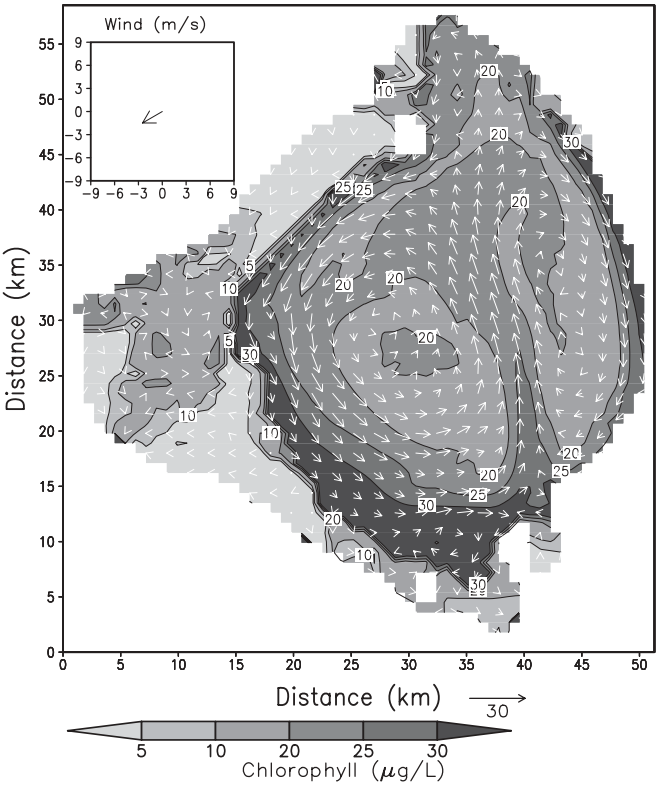

Fig. 5.9.5 Modeled surface Chl concentrations and currents on 6/2/2000.

the SAV transect surveys (Fig. 5.9.7), indicating the percentages of the survey areas that have SAV. For example, the SAV (%) panel indicates that about 20% of the transect area has SAV in October 1999. Even though the SAV (%) panel does not measure the total SAV area, it indicates the trend of SAV growth and coverage in the lake well.

A lower water depth leads to more light available to SAV growth and to a larger SAV area. Higher water depths limit SAV growth. Statistical analysis indicates that the SAV area in the lake is strongly correlated with the water depth. When the SAV time series in the SAV (%) panel lags the water elevation in the EL panel by 79 days, the two have a correlation coefficient of –0.72. With no time lag between the two, the correlation coefficient is reduced to –0.35. In early 2000, the water depth in the lake was very high and the SAV area was very small (Fig 5.9.9). The similar trend of a negative correlation is also shown in 2002. In 2001, however, the extremely low water level resulted in the exposure of a large portion of the lake. This exposure might explain why there is no strong negative correlation between the two in the first one-half of 2001.

The third panel gives the modeled SAV area in 1000 acres (dotted line) and the measured SAV biomass density in grams per square meter (g/m^2) (solid line). The three dots indicate the measured SAV acreage in the summers of 2000, 2001, and 2002. The seasonal and annual variations are well represented by the SAV model. The model is consistent with field observations that indicate increased SAV coverage at low water levels in Lake Okeechobee (Havens et al., 2005; Havens et al., 2004; James and Havens, 2005).

The spatial distribution of SAV predicted by the model for September 2002 is similar to the observed map of SAV from August to September 2002 (Figs 5.9.8 and 5.9.10). Further analysis of the model results also indicates that the distribution of SAV in the lake largely reflects the distribution of light

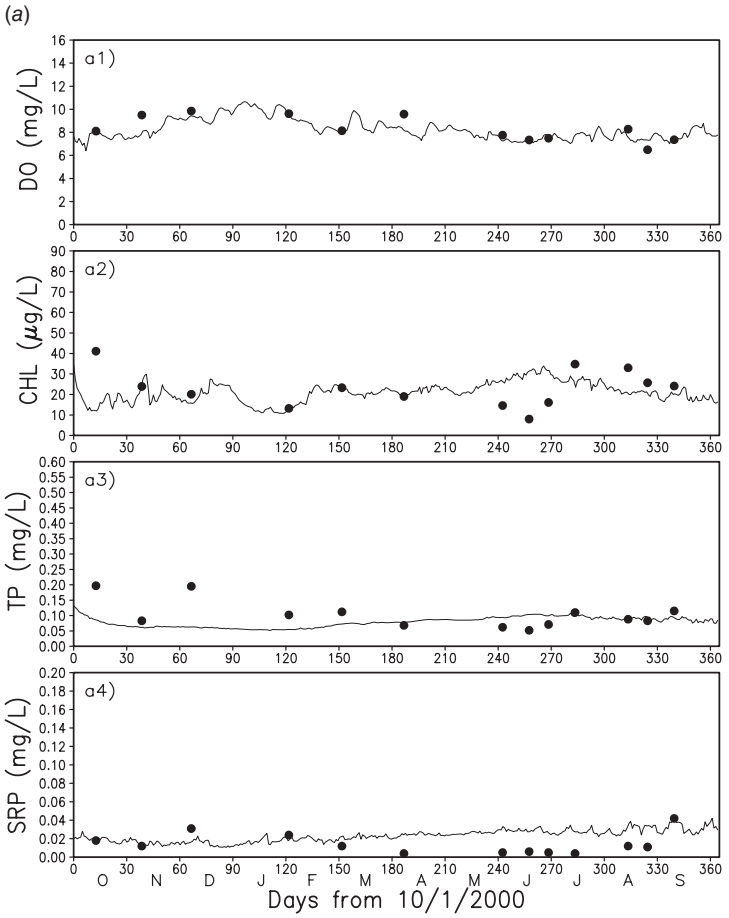

Fig. 5.9.6(*a*) Time series of water quality variables at L002 between 10/1/2000 and 9/30/2001. Closed cycle = measured data; solid line = modeled results.

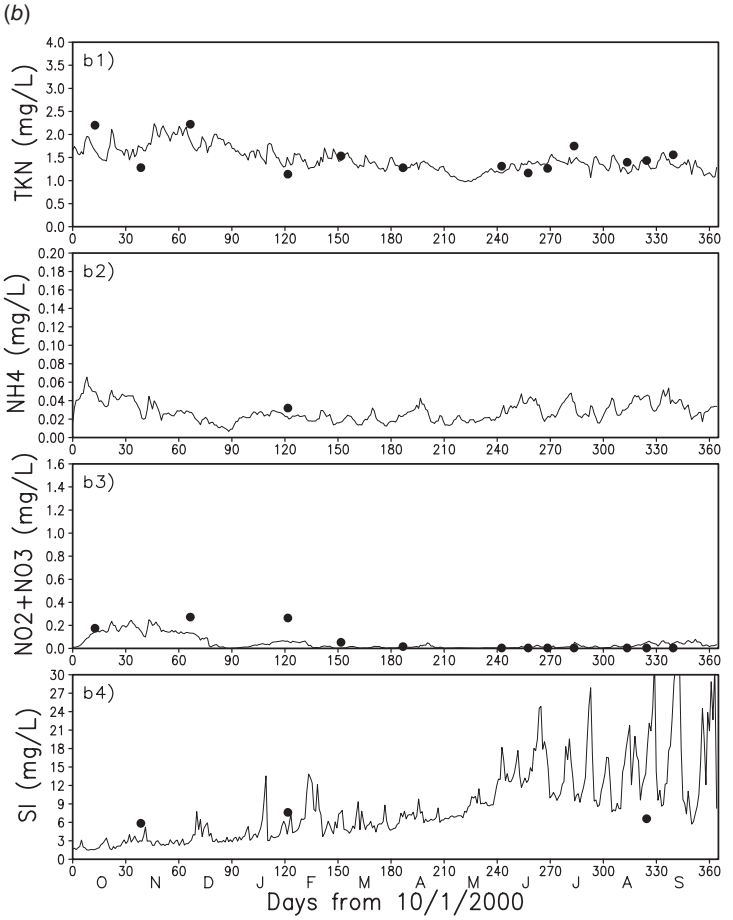

Fig. 5.9.6(*b*) Time series of water quality variables at L002 between 10/1/2000 and 9/30/2001. Closed cycle = measured data; solid line = modeled results.

attenuation. In summary, the SAV model is capable of representing the spatial and temporal variations of SAV in the lake well.

5.9.2.5 Discussions and Summary. This study presents a 3D hydrodynamic, sediment, water quality, and SAV model for Lake Okeechobee, FL. The LOEM model is enhanced based on the well-calibrated and verified hydrodynamic and sediment model (Jin and Ji, 2001, 2004, 2005; Ji and Jin, 2006; Jin et al., 2000, 2002), which is essential for the water quality and SAV modeling. Using three years of measured data, the LOEM water quality and SAV model was calibrated, verified, and validated. The model is capable of reproducing key water quality characteristics of the lake without having to resort to exten-

Fig. 5.9.7 Map of Lake Okeechobee showing the location of 16 transects for quarterly evaluation of submerged aquatic vegetation biomass, taxonomic structure, and water transparency. Plants are sampled at sites along each transect, starting at the shoreline and progressing lakeward until a site is reached where there are no plants (SFWMD, 2002).

sive, site-specific parameter manipulations. It provides a greater degree of confidence that the calibrated, verified, and validated model reproduces the interrelationship between algae, nutrients, and DO in the lake.

Major contributions in this case study include

1. Based on the EFDC model, the LOEM is expanded to include a water quality submodel to simulate eutrophication processes in the lake. The model simulates algae, DO, and nutrient processes in the lake reasonably well.
2. The LOEM model is enhanced to include a SAV submodel to represent SAV processes in the lake. The SAV model is calibrated using measured SAV data in the lake. Collecting these SAV data is a huge, expensive effort. It is fortunate that these data are available to this study.

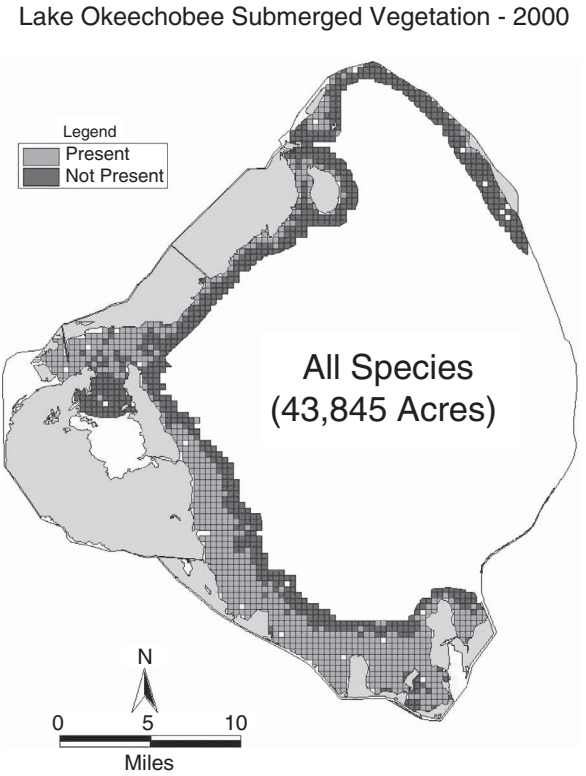

Fig. 5.9.8 Summary results from SAV surveys in August and September of 2000.

The SAV model is capable of representing the spatial and temporal variations of SAV in the lake well. So far, there are few published studies on SAV modeling in lakes that have such detailed model–data comparisons.

Factors that are important to this study include

1. The LOEM is developed under the framework of the EFDC model (Hamrick, 1992; Park et al., 1995). The physical processes and the numerical schemes implanted into the EFDC model have been tested and improved via >100 applications, which is beneficial to the development and application of the LOEM.
2. There are adequate measured water quality and SAV data for model–data comparison.
3. Lake Okeechobee is shallow and is primarily driven by wind. The meteorological data used to drive the LOEM is directly measured on the lake and is able to present the forcing conditions realistically. The lake has

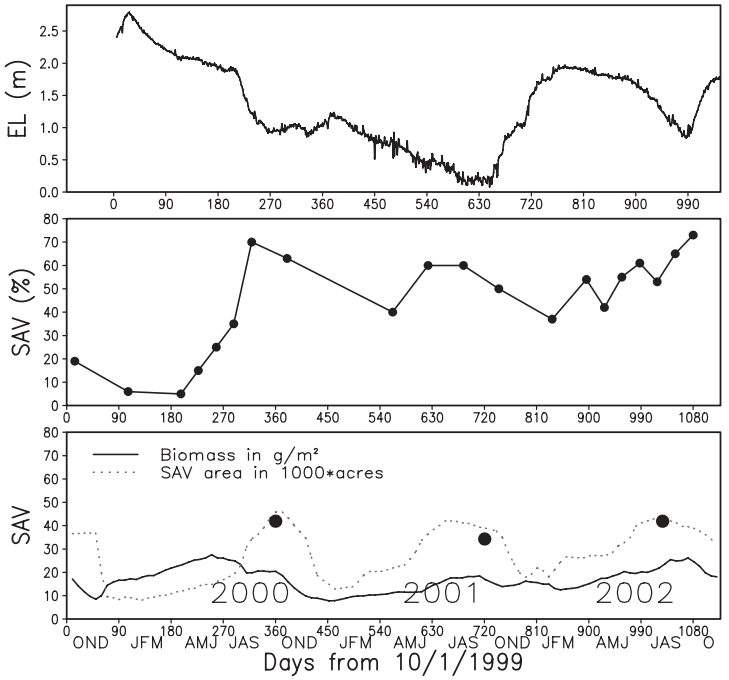

Fig. 5.9.9 Water depth and SAV results from 10/1/1999 to 9/30/2002. First panel from the top: modeled water depth in the near shore zone at Station PALMOUT; second panel: the measured SAV area; third panel: modeled SAV biomass concentration (solid line) and SAV area in 1000 acres (dotted line).

relatively uniform water depths in the open water areas and the localized bathymetry irregularities are small, which enables the LOEM to represent the hydrodynamic processes reasonably well.

4. Intensive studies on the lake have been conducted in recent years (Jin and Ji, 2001, 2004, 2005; Ji and Jin, 2006; Jin et al., 2000, 2002). These studies revealed the general characteristics of the lake in detail and are essential for this modeling effort.

However, there are inadequate sediment diagenesis fluxes data for model–data comparison. An internal net flux between the water column and the sediment bed is the result of (1) the settling of particulate nutrients, (2) the diffusion between the water column and the sediment bed, and (3) the resuspension and deposition of sediment solid. This internal net flux is the residual of these three components and can be much smaller than each of these three components. The lack of measured data is often a challenge in water quality modeling. Further studies are needed to diagnose and to analyze these complex internal exchanges.

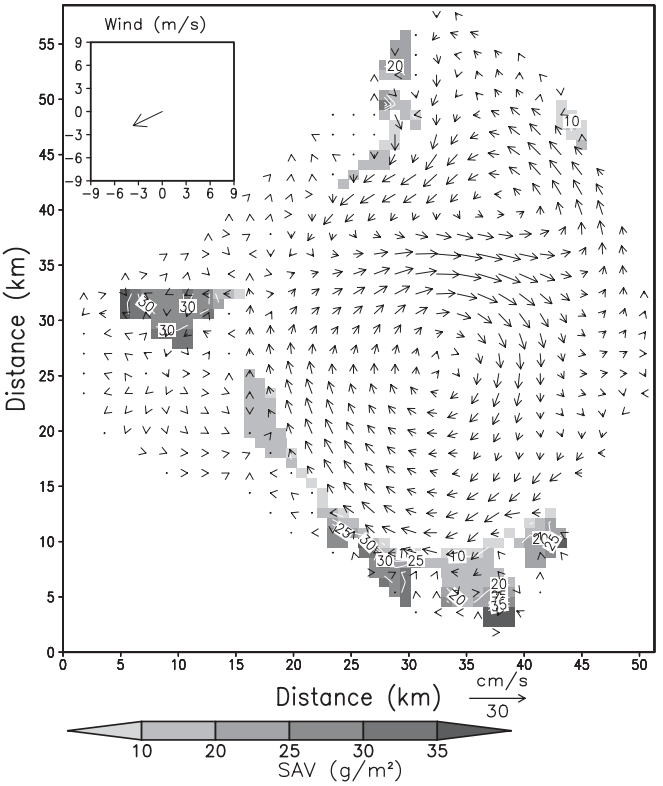

Fig. 5.9.10 Modeled SAV area on 9/19/2000.

5.9.3 Case Study II: St. Lucie Estuary and Indian River Lagoon

The hydrodynamic modeling of the St. Lucie Estuary and Indian River Lagoon (SLE/IRL) has already been discussed in Section 2.4.3 as a case study. This section describes the set up, calibration, and verification of the SLE/IRL water quality model (Wan et al., 2007). Applications of the SLE/IRL model will be presented in Section 10.5.3 as another case study.

The SLE/IRL area has suffered from altered water flow patterns and degraded water quality. The increased drainage and dramatic changes in stormwater runoff have significantly influenced the ecosystem. Floodwater released to the estuary from Lake Okeechobee, combined with excess stormwater runoff from drainage canals, altered the salinity balance and stressed the estuary's unique ecosystem. Surface runoff caused an increase both in freshwater inflows and pollution levels in the SLE/IRL. Seagrasses and oysters, once abundant in the estuary, become virtually absent (Haunert and Startzman, 1980, 1985). The SLE is now a phytoplankton-based system with high chlorophyll *a* concentrations (blooms exceeding 50 μg Chl *a*/l have been

observed, maximum = 73.3 μg Chl *a*/L) with hypoxic and anoxic events in bottom waters (Chamberlain and Hayward, 1996; Doering, 1996). In order to implement a full-scale pollutant load reduction program, nutrient dynamics in the estuary needs to be evaluated. A central tool for aiding in this effort is a fully coupled 3D hydrodynamic and water quality model with capability of simulating estuary circulation, suspended sediment transport, eutrophication processes, and bottom sediment fluxes.

5.9.3.1 Model Setup. The SLE/IRL Model was developed with the Environmental Fluid Dynamics Code (EFDC) (Hamrick, 1992; Park et al., 1995). The water quality model has the same the grid as the SLE/IRL hydrodynamic model, with 1161 horizontal grid cells and 3 vertical layers (Fig. 2.4.13). The time step for the SLE/IRL water quality model is 2 min.

Measured monthly mean concentrations for water quality variables at the St. Lucie Inlet were used as open boundary conditions. Model sensitivity tests showed that the water quality was more sensitive to nutrient loadings from upstream than at the open boundaries. It is acceptable to use the monthly mean concentrations to force the model at the open boundaries. By analyzing the measured data, the total organic nitrogen and phosphorus were split into refractory, labile, and dissolved components, with the weighting coefficients of 0.3, 0.3, and 0.4, respectively. The ratio of carbon/Chl of 0.05 (gC/μg-Chl) was used to convert algal concentrations to carbon.

To develop a water quality model, correctly quantifying nutrient loadings is essential. The sources of nutrients in the SLE are primarily from major canals, lateral inflows, atmospheric deposition, and internal recycles. The loading from upstream through three major canals and the North Fork (at C-24, C-23, and C-44, and Gordy in Fig. 5.9.11) contributes ~65–75% of the total nutrient loads (Wan et al., 2003). Daily freshwater inflows are available at these four stations. During the wet season, large amounts of nutrients are also emptied into the SLE through surface runoff. The nonpoint sources play an important role in the eutrophication processes in the SLE. Daily nonpoint source loads of TN and TP are calculated using the watershed model developed by Wan et al. (2003). It is estimated that the lateral flow contributed ~23 and 37% of the total discharge in 1999 and in 2000, respectively.

The sediment diagenesis model was run iteratively for 5 years with the 1999 nutrient loading. At the end of the fifth year, the model results were used as the initial condition for model simulation. It was found that, after 5 years of iterative simulation, the water quality concentrations in the sediment bed approached dynamic equilibrium.

5.9.3.2 Water Quality Model Calibration and Verification. Phytoplankton and nutrient distributions in the SLE/IRL show strong seasonal variations. Thus, a yearly long calibration period is needed for the water quality model. The period of 1999 was used for model calibration. The period of 2000 was used for model verification. The annual mean freshwater inflow in 1999 is

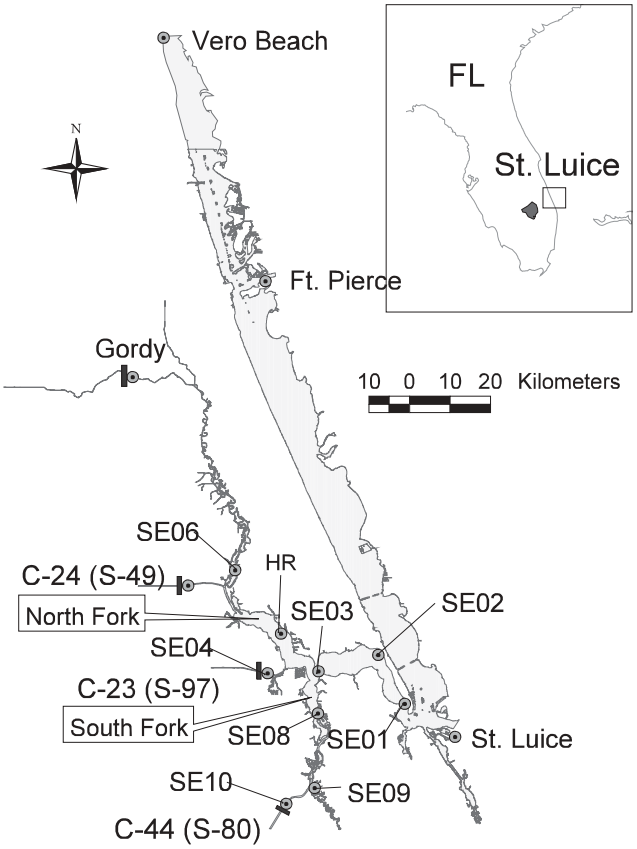

Fig. 5.9.11 St. Lucie Estuary and Indian River Lagoon, FL.

36.7 m^3/s. In contrast to 1999, Year 2000 is a dry year with annual mean inflow of 16.5 m^3/s, only 45% of the 1999 value. These two very different years, one wet and one dry, provide ideal periods for model calibration and verification. The total inflow rates in 1999 and 2000 are already given in Fig. 2.4.14.

Comparisons were made between the model results and observations for six observed water quality variables: algal concentration, TP, orthophosphate (PO4), total Kjeldahl nitrogen TKN, NH_4, and DO at 10 stations (Fig. 5.9.11). However, there were no nitrate and nitrite data available for this study. Observed data were taken approximately from 0.5 m below the surface of the water column. The water quality data are presented without any averaging in space or time and are compared directly with the model results. A statistical comparison between the model results and observations at the 10 stations (Fig. 5.9.11) in 1999 are presented in Tables 5.9.5 and 5.9.6. For the convenience of model-data comparison, the observation data were separated into two groups: inside the SLE (including SE01, SE02, SE03, HR, SE06, and

TABLE 5.9.5 Statistics of Model Results Inside the SLE in 1999

Station	State Variable	RMS	RRE (%)	Range	No. of Obs.	Obs. Mean	Model Mean
SE01	Algae (μg/L)	6.50	31.9	20.40	11	7.26	10.60
SE01	TP (mg/L)	0.04	12.1	0.33	10	0.13	0.11
SE01	PO4 (mg/L)	0.02	18.9	0.11	10	0.04	0.06
SE01	TKN (mg/L)	0.26	24.9	1.04	10	0.55	0.37
SE01	NH4 (mg/L)	0.05	34.6	0.15	8	0.05	0.03
SE01	DO (mg/L)	1.17	17.0	6.87	12	5.76	6.79
SE02	Algae (μg/L)	5.84	29.7	19.70	14	6.79	11.56
SE02	TP (mg/L)	0.06	18.9	0.33	13	0.15	0.13
SE02	PO4 (mg/L)	0.03	31.7	0.09	12	0.05	0.07
SE02	TKN (mg/L)	0.35	33.6	1.04	13	0.60	0.46
SE02	NH4 (mg/L)	0.06	30.2	0.19	11	0.05	0.04
SE02	DO (mg/L)	1.37	18.6	7.35	14	6.00	7.22
SE03	Algae (μg/L)	5.88	31.6	18.60	14	7.51	12.08
SE03-US1	TP (mg/L)	0.10	30.2	0.34	13	0.20	0.14
SE03-US1	PO4 (mg/L)	0.05	30.9	0.17	13	0.07	0.07
SE03-US1	TKN (mg/L)	0.37	32.8	1.13	13	0.73	0.53
SE03-US1	NH4 (mg/L)	0.05	34.3	0.16	11	0.07	0.04
SE03-US1	DO (mg/L)	1.74	25.1	6.92	14	5.70	7.20
SE08	Algae (μg/L)	7.27	34.3	21.20	14	7.83	15.06
SE08	TP (mg/L)	0.10	30.3	0.33	13	0.21	0.14
SE08	PO4 (mg/L)	0.04	32.2	0.12	13	0.07	0.05
SE08	TKN (mg/L)	0.38	27.8	1.36	13	0.82	0.67
SE08	NH4 (mg/L)	0.05	22.1	0.21	11	0.06	0.04
SE08	DO (mg/L)	1.34	14.8	9.01	14	6.67	7.30
HR	Algae (μg/L)	5.81	46.8	12.40	14	6.79	11.77
HR	TP (mg/L)	0.11	25.2	0.44	12	0.21	0.17
HR	PO4 (mg/L)	0.04	31.6	0.13	12	0.06	0.09
HR	TKN (mg/L)	0.35	26.6	1.30	12	0.69	0.55
HR	NH4 (mg/L)	0.13	31.8	0.40	10	0.09	0.04
HR	DO (mg/L)	1.19	12.9	9.28	14	6.35	6.76
SE06-NF	Algae (μg/L)	6.80	31.6	21.50	12	10.55	12.55
SE06-NF	TP (mg/L)	0.12	24.4	0.48	11	0.29	0.21
SE06-NF	PO4 (mg/L)	0.06	44.0	0.13	11	0.08	0.10
SE06-NF	TKN (mg/L)	0.23	21.9	1.05	11	0.77	0.66
SE06-NF	NH4 (mg/L)	0.04	41.0	0.11	9	0.05	0.05
SE06-NF	DO (mg/L)	2.61	40.4	6.45	12	4.78	6.82

SE08) and upstream of the SLE (including SE04, SE07, SE09, and SE10). The RMS error and the RRE for each variable at each station were calculated. The overall RRE of 28.1% indicates that the model results are reasonably good.

Figure 5.9.12 gives the time series comparions between the measurd data (circles) and the model results (solid line) at SE08. Since the daily averaged

TABLE 5.9.6 Statistics of Model Results Upstream of the SLE in 1999

Station	State Variable	RMS	RRE (%)	Range	No. of Obs.	Obs. Mean	Model Mean
SE04	Algae (μg/L)	4.28	21.2	20.20	12	8.36	10.88
SE04	TP (mg/L)	0.14	16.9	0.81	11	0.29	0.33
SE04	PO4 (mg/L)	0.08	18.7	0.41	11	0.11	0.15
SE04	TKN (mg/L)	0.51	27.2	1.86	11	0.84	0.75
SE04	NH4 (mg/L)	0.06	26.9	0.21	10	0.07	0.07
SE04	DO (mg/L)	3.12	38.0	8.21	12	4.68	6.56
SE07	Algae (μg/L)	6.31	23.3	27.10	10	9.39	10.10
SE07	TP (mg/L)	0.12	26.2	0.47	9	0.31	0.30
SE07	PO4 (mg/L)	0.06	34.6	0.16	9	0.10	0.10
SE07	TKN (mg/L)	0.35	20.9	1.65	9	1.01	0.92
SE07	NH4 (mg/L)	0.10	36.4	0.28	8	0.14	0.11
SE07	DO (mg/L)	3.67	29.5	12.44	10	5.96	5.62
SE09	Algae (μg/L)	5.54	38.2	14.50	12	8.10	11.93
SE09	TP (mg/L)	0.09	27.9	0.32	11	0.18	0.23
SE09	PO4 (mg/L)	0.04	40.1	0.10	11	0.07	0.08
SE09	TKN (mg/L)	0.34	28.4	1.18	11	0.82	0.72
SE09	NH4 (mg/L)	0.04	22.2	0.16	9	0.04	0.05
SE09	DO (mg/L)	0.78	9.6	8.11	12	6.39	6.79
SE10	Algae (μg/L)	6.49	41.7	17.00	13	6.82	15.44
SE10	TP (mg/L)	0.10	19.5	0.49	12	0.21	0.22
SE10	PO4 (mg/L)	0.07	26.2	0.25	12	0.08	0.05
SE10	TKN (mg/L)	0.41	30.5	1.33	12	0.88	0.97
SE10	NH4 (mg/L)	0.04	27.3	0.14	10	0.08	0.07
SE10	DO (mg/L)	2.46	31.4	7.83	13	5.92	5.79

model results at SE08 are vertically mixed most of the time, only the surface layer results are given here. The model results exhibit much larger vertical stratificaiton in some areas of the SLE and will be presented in 2D contours later. Both the model and the data in Fig. 5.9.12 indicate that there was no significant algal bloom in 1999. The factors limiting the algal bloom are probably low NH_4 loading and fast movement of water induced by the high freshwater discharge.

The water quality model is verified using the 2000 data. Because no measured data were available for specifying open boundaries after 09/30/2000 (Day 275), the model verification run was conducted for the first 274 days of 2000. The statistics of the model–data comparisons in 2000 have errors comparable to the ones in 1999 (Tables 5.9.5 and 5.9.6). For simplicity, the averaged RRE in 2000 is summarized in Table 5.9.7 for the same six state variables at the same 10 stations that are used in model calibration. For example, the overall DO RRE is 15.0% inside the SLE and 23.2% upstream of the SLE. The overall mean RRE is 30.7% for stations inside SLE and 30.1% for the upstream stations, which are comparable to the ones given

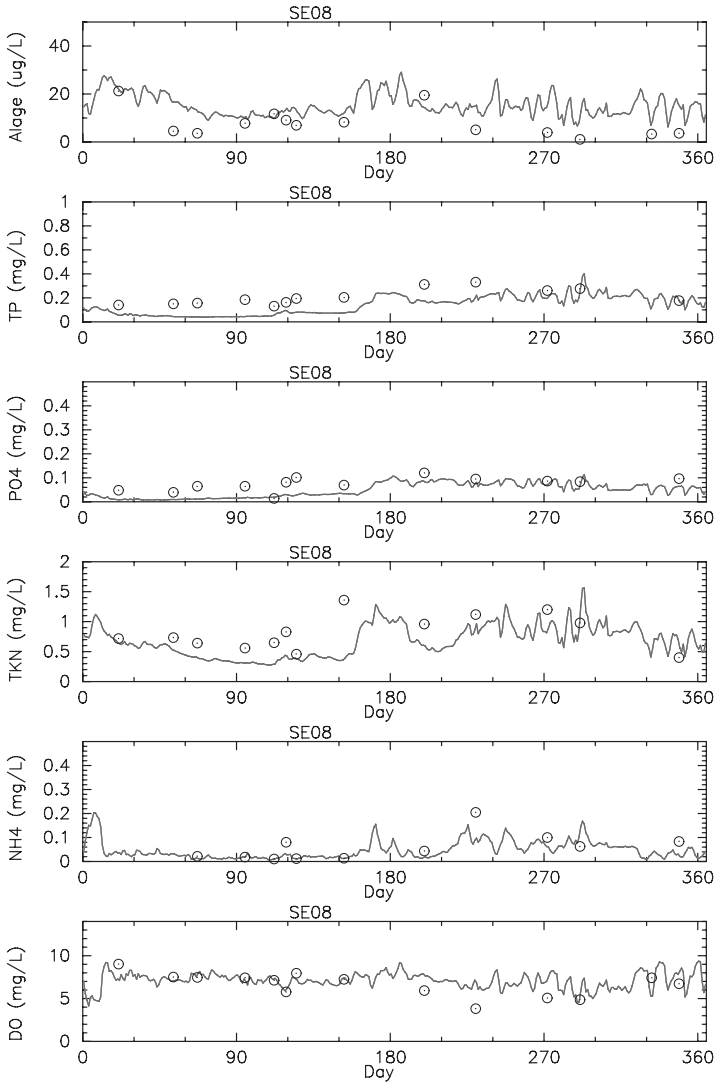

Fig. 5.9.12 Comparison of model results at station SE08 in 1999. The circles represent the measured data; the solid lines give surface layer model results.

in Tables 5.9.5 and 5.9.6. As an example, Fig. 5.9.13 gives the model–data comparisons at SE08 in 2000. The model prediction for nutrients is in the acceptable range. There was an algal bloom in May 2000, and the model realistically captured the timing and amplitude of the bloom. Both the model and the data indicate that the Chl *a* concentration was >40 μg/L around Day 130. A large amount of freshwater was discharged into the SLE from Lake Okeechobee between April and May, which brought high nutrients into the

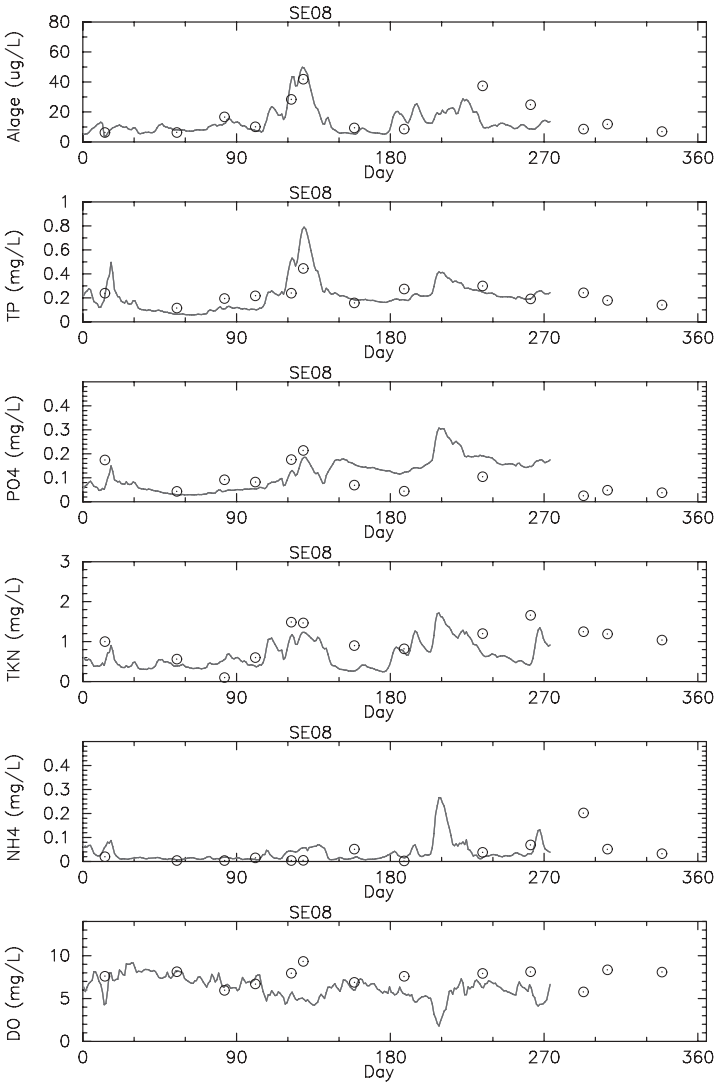

Fig. 5.9.13 Comparison of model results at station SE08 in 2000. The circles represent the measured data; the solid lines give surface layer model results.

SLE and caused the algal bloom. In Fig. 5.9.13, the model underpredicted DO around Day 130, which was possibly caused by over-estimated carbon loading from upstream and lateral sources.

5.9.3.3 Hydrodynamic and Water Quality Processes in the SLE. The calibrated and verified SLE/IRL water quality model was applied to study

TABLE 5.9.7 Summary of Mean Errors in 2000

State Variable	Inside SLE				Upstream of SLE			
	RRE (%)	RMS	Obs. Mean	Model Mean	RRE (%)	RMS	Obs. Mean	Model Mean
Algae (μg/L)	28.7	11.96	13.66	9.59	22.2	8.52	18.57	15.96
TP (mg/L)	30.7	0.08	0.17	0.16	39.4	0.16	0.24	0.32
PO4 (mg/L)	31.4	0.06	0.10	0.11	51.3	0.09	0.11	0.16
TKN (mg/L)	34.6	0.46	0.73	0.46	25.0	0.77	1.14	1.25
NH4 (mg/L)	33.3	0.07	0.06	0.03	19.5	0.13	0.13	0.19
DO (mg/L)	15.0	1.31	6.35	6.53	23.2	2.01	4.92	4.57
Mean RRE	30.7				30.1			

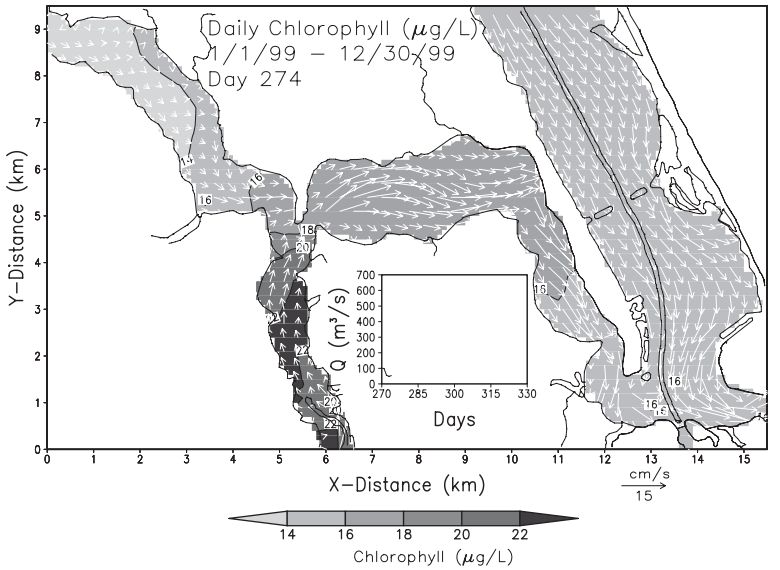

Fig. 5.9.14 Mean surface currents and surface chlorophyll *a* concentrations on 10/1/1999 (Day 274).

hydrodynamic and water quality processes in the area. Figure 5.9.14 shows the daily averaged surface current and surface Chl concentration in the SLE/IRL on Day 274 (10/1/1999). The Chl concentration varies from <14 to >22 μg/L. To indicate inflow conditions, the small inset in the figure gives the total inflow rate to the water system. High algal concentration over 24 μg/L occurred in the South Fork. The mean surface flow in the SLE runs seaward and the mean flow pattern in the IRL runs southward.

Figure 5.9.15 is similar to Fig. 5.9.14 but is for the bottom current and surface TKN. It is evident that the TKN in the estuary is primarily from the

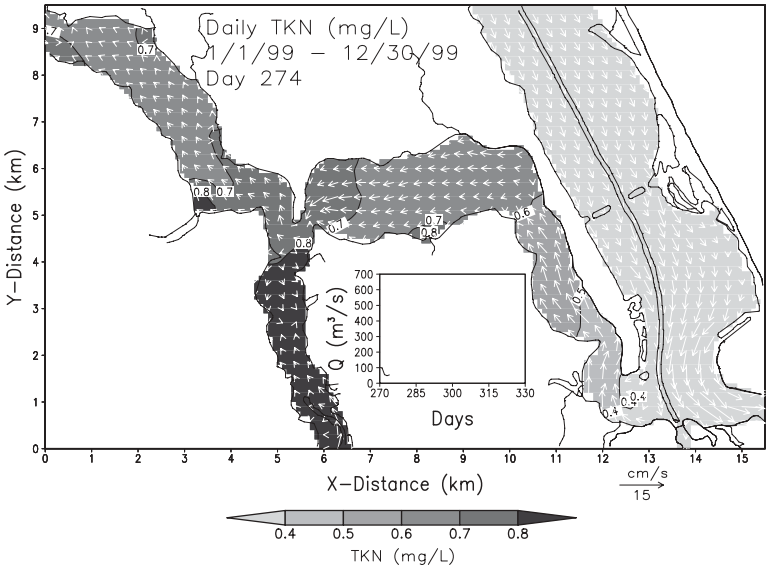

Fig. 5.9.15 Mean bottom currents and surface TKN concentrations on 10/1/1999 (Day 274).

upstream flows and that the TKN concentration in the IRL is small. The mean bottom flow in the SLE is landward, opposite to the direction of the mean surface flow. This describes a typical two-layer velocity profile of an estuary. The two-layer circulation shown in Figs. 5.9.14 and 5.9.15 is a key mechanism for trapping nutrients. Large amounts of nutrients transported to the estuary can be trapped inside the estuary and deposited to the bottom. These deposited nutrients become a potential internal nutrient source and recycle back to the water column through sediment fluxes and the resuspension of sediment. Decay of organic materials generates a large DO demand and creates estuary hypoxia.

By analyzing measured water quality data in SLE, AEE (2005) reported that the DO in the bottom water showed a strong negative correlation with the salinity difference between the surface and bottom. The water column stratification induced by high freshwater discharge, contributes to the development of low DO in SLE. Millie et al. (2004) also reported that in the North Fork of the SLE, bottom water hypoxia occurred during the warmest summer months. A large amount of particulate organic matters were discharged into the estuary and deposited on the bottom. The sediment diagenesis processes in the sediment bed cause high sediment oxygen demand, which significantly reduces the DO concentration at the bottom of the water column. The large freshwater inflows cause stratification in the North Fork, and the stratification reduces vertical exchanges of DO. Hence, the stratification contributes to the bottom hypoxia in the estuary.

Such water column stratification has also been recorded in other shallow estuarine systems. For example, oxygen depletion in Mobile Bay, AL, has been shown to be directly related to the intensity of the water column stratification (Turner et al., 1987). Water column stratification, once formed, inhibits vertical mixing and reduces the oxygen concentration in the bottom waters. Moreover, the bottom water is more likely to become hypoxic in shallow estuaries, because they have a smaller DO reservoir and are more likely to be depleted than in deep estuaries. Many previous studies reported that increased nutrient inputs promote algal blooms and may lead to reduced DO concentration in the bottom of the waterbody. This study indicated that the stratification caused by freshwater inflows may also contribute significantly to the bottom hypoxia in an estuary. In order to restore the estuarine ecosystem, it might not be enough just to decrease the nutrient loadings to the system. Modulating the freshwater discharge pattern (in both the North Fork and the South Fork) should also be considered to mitigate the water column stratification.

5.9.3.4 Summary and Conclusions. This case study documents the development, calibration and verification of the SLE/IRL water quality model. The water quality model is enhanced based on the well-calibrated and verified hydrodynamic model (Ji et al., 2007a), which is essential for water quality modeling. The model is calibrated using the data from 1999 and is verified using the data from 2000. The overall model results are satisfactory. Year 1999 was a normal water year and had no significant algal bloom, whereas Year 2000 was a dry year and had an algal bloom in May 2000. The onset of the algal bloom coincided with the discharge of a large amount of freshwater from Lake Okeechobee. The model realistically simulated the algal bloom in May 2000 and captured the peak algal concentrations. The model sensitivity tests show that the model is sensitive to the loadings from both the upstream and lateral inflows. The high algal concentrations indicate that the estuary was under the stress of eutrophication. High algal concentrations in the upper estuary were likely caused by excessive nutrient supplies and poor flushing, since most nutrients originate from upstream. The model results show that the nitrogen, rather than phosphorus, is limiting the growth of phytoplankton in the SLE.

Low DO generally occurs in summer, especially in the upstream tributaries. The cause of DO variation is primarily due to hydrodynamic conditions, organic loadings, and the release of SOD from the bottom. Both SOD and organic carbon contribute to the low DO in the area. Water column stratification in the wet season is one of the major causes for benthic hypoxia. In the summer of 1999, the large freshwater inflows caused strong stratification and contributed to the hypoxia/anoxia in the area.

Contributions of this study include

1. Based on the EFDC model, the SLE/IRL model is expanded to include a water quality submodel to simulate the eutrophication processes in the

SLE. The model simulates algae, DO, and nutrient processes in the estuary reasonably well.

2. The newly enhanced SLE model is applied to study hydrodynamic and water quality processes in the estuary. The model results reveal that SLE exhibits the typical two-layer circulation pattern of an estuary. This two-layer circulation plays an important role on the nutrient transport and DO stratification.

CHAPTER 6

External Sources and TMDL

Key elements in surface water modeling include the external sources entering a waterbody. As water quality management issues become increasingly complex, the domain of interest in a surface water study is expanded to incorporate pollutant loadings from watershed runoff, atmospheric deposition, and groundwater seepage. This chapter focuses on external sources and processes associated with these external sources. The last section of this chapter discusses the TMDL, a useful tool in water quality management.

6.1 POINT SOURCES AND NONPOINT SOURCES

Pollutant concentrations in a surface water system, such as nutrients and toxics, are controlled by sources external to the system and by internal processes. The internal processes, as discussed in previous chapters, include sediment resuspension, nutrient fluxes from the sediment bed, and nitrogen fixation. External sources include municipal and industrial discharges, stream inputs, atmospheric deposition, surface runoff, groundwater seepage, and other sources surrounding the water system (Fig. 6.1.1). An important task in surface water modeling is to characterize the external sources and estimate the associated pollutant loadings. These external sources can be characterized as either point sources or nonpoint sources, which are governed by different mechanisms and can result in different impacts on the receiving water.

A point source is a source of pollution that can be attributed to a specific physical location and is easily identified because it usually comes out of a "pipe". Examples include sewage treatment plants, industrial plants, livestock facilities, and others. Point sources are regulated by the state water quality agency and EPA. Point sources are issued National Pollutant Discharge Elimination System (NPDES) permits when they meet regulations (USEPA, 1993). Point source loadings from permitted discharges may be determined from discharge monitoring reports (DMRs) available from many state agencies or EPA. Most of these DMRs contain information about conventional pollutants,

Hydrodynamics and Water Quality: Modeling Rivers, Lakes, and Estuaries, by Zhen-Gang Ji

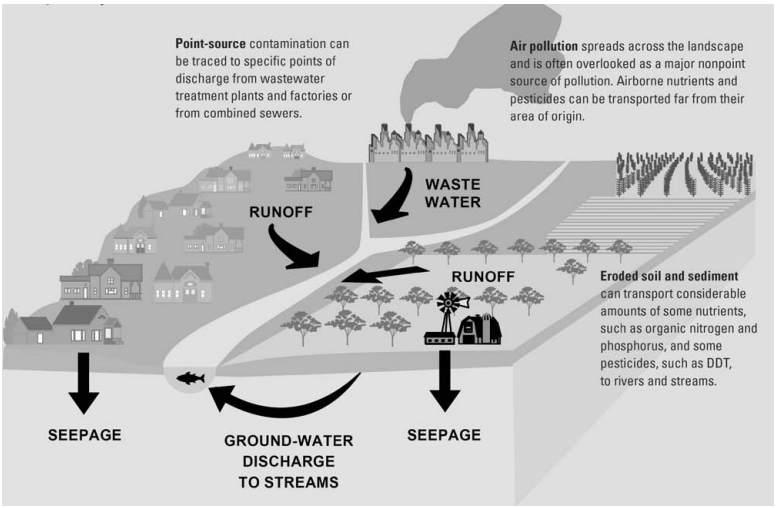

Fig. 6.1.1 Major external sources to a surface water system (USGS, 1999).

such as BOD, NH_4, TKN, suspended solids, and coliform bacteria. Point sources can also include pollutant loadings contributed by tributaries to the main receiving water.

An NPDES permit is issued by EPA or a state regulatory agency that sets specific limits on the type and amount of pollutants that a municipality or industry can discharge into a receiving water. It also includes a compliance schedule for achieving those limits. It is called the NPDES because the permit process was established under the National Pollutant Discharge Elimination System. The NPDES is an EPA program under provisions of the Federal Clean Water Act (CWA) that regulates point source discharges through the issuance of permits to discharges and enforcement of the terms and conditions of those permits. The control of water column pollutants, including toxic materials and nutrients, by imposing limits on point source discharges through NPDES permitting is now well established as a means of water quality management. The program has done much to improve water quality in the United States. More than 200,000 sources are regulated by NPDES permits nationwide (USEPA, 1993).

In contrast to point sources, nonpoint sources come from numerous widespread locations or sources that have no well-defined points of origin and, cumulatively, threaten water quality and natural systems. The regulatory definition of a nonpoint source is “anything not a point source”. Examples of nonpoint sources include agriculture, construction, grazing, forest, lawn care, parking lots, and other urban runoff (Fig. 6.1.1). Nonpoint sources may also originate from the atmosphere. Examples include leaching of excess fertilizer from farmlands and acid rain. Individually, each may not be a serious threat,

but together nonpoint sources may significantly harm the receiving waterbody.

The NPDES program has vastly improved the water quality of many receiving waters. However, many other waters still do not meet water quality standards, even with increasingly stringent discharge standards. Since the later 1960s, people have gradually understood that the dominant source of pollutants in many waters is from nonpoint sources, not from point sources, such as wastewater treatment plants. While point and nonpoint sources contribute to pollution, nonpoint sources often are dominant and present complex management challenges.

Major nonpoint sources include (Fig. 6.1.1): (1) runoff from agricultural lands (sediments, fertilizers, bacteria, and pesticides); (2) runoff from urban areas (oil, grease, toxic chemicals, heavy metals, pathogens, and sediments); (3) atmospheric deposition (toxic chemicals, heavy metals, nutrients, and acid); and (4) seepage from groundwater (nutrient and toxic chemicals).

Agriculture is the leading cause of nonpoint source pollution in the United States (USEPA, 2000a). Urban runoff particularly affects waterbodies that are used by and benefit the largest number of people. Pollutants from atmospheric deposition reach receiving waters via direct deposition to the water or deposition and subsequent washoff from the watershed. Rainfall or snowmelt carries pollutants over and through the ground. The runoff carries away pollutants and deposits them into receiving waters. Toxic chemicals, nutrients, and heavy metals can be deposited at significant rates in urban areas. Groundwater may carry nutrients into a waterbody and contribute to the total nutrient budget.

Nonpoint sources may differ significantly from point sources in their distribution in time and space. Nonpoint sources often involve complex transport through soil, water, and air. Nonpoint sources are more widespread and difficult to identify and quantify than point sources. Thus, developing solutions for nonpoint sources is more difficult. Table 6.1.1 summarizes the major differences between point sources and nonpoint sources. In contrast to the fairly steady flow rates of point sources, the flow rates of nonpoint sources are highly variable, up to several orders of magnitude. The impact of point sources on a receiving water is often more significant during low flow conditions, while the

TABLE 6.1.1 Major Differences between Point Sources and Nonpoint Sources

Characteristics	Point Sources	Nonpoint Sources
Time variation	Relatively steady	Highly variable
Flow magnitude	Variation less than one order of magnitude	Variation up to several orders of magnitude
Impact	Most severe during low flow	Most severe during or following storm events
Predictability	Fairly predictable	Less predictable
Permit	Required under NPDES	Not required

TABLE 6.1.2 Sources and Concentrations of TN and TP from Common Point and Nonpoint Sources[a]

Source	Total Nitrogen (mg/L)	Total Phosphorus (mg/L)
Urban runoff	3–10	0.2–1.7
Livestock operations	6–800	4–5
Atmosphere (wet deposition)	0.9	0.015
90% forest	0.06–0.19	0.006–0.012
50% forest	0.18–0.34	0.013–0.015
90% agriculture	0.77–5.04	0.085–0.104
Untreated wastewater	35	10
Treated wastewater	30	10

[a]FISRWG, 1998.

nonpoint sources assert the most severe impact during or following storm events. The assessment of nonpoint source impacts is often more complicated. Most nonpoint sources are directly or indirectly driven by precipitation; thus, their loadings are inherently dynamic in nature. The carrier of the pollutants is water (and possibly sediment) as the water runs through the watershed. Therefore, detailed watershed processes are needed to describe nonpoint sources. Because of these uncertainties, nonpoint sources are less predictable. Besides, point sources are generally regulated under the NPDES in the United States, while no permit is needed for nonpoint sources. The pollutant concentrations from point and nonpoint sources also differ significantly. Table 6.1.2 lists typical values of TN and TP from different point and nonpoint sources.

From the modeling point of view, discharges to a receiving waterbody, such as tributaries to a river, streams to a lake, and rivers to an estuary, can be treated as point sources to the waterbody, when these tributaries are specified as external sources and are not directly modeled in the study. In this way, both point and nonpoint sources can be incorporated into a numerical model in a similar manner. After a model grid is generated for a study area, all of the point and nonpoint sources are assigned to specific grid cells. For example, in modeling a river, a tributary is just treated as a point source and is assigned to a specific grid cell as an inflow. A nonpoint source from runoff is treated as many small inflows and is assigned to grid cells along the riverbank (e.g., Ji et al., 2002a).

6.2 ATMOSPHERIC DEPOSITION

Atmospheric deposition happens when air pollutants hit the earth's surface (either land or water). Atmospheric pollutants are deposited in either dry or wet form. Air pollutants washed out of the sky by rain or snow are called wet deposition. Air pollutants deposited without precipitation are called dry depo-

sition, which is the settling of particulate matters due to gravity. Wet deposition occurs when particulate matters are removed from the atmosphere by precipitation and is associated with dissolved substances in rainfall (or snow) (Ji, 2000b). Nutrient forms in precipitation are generally soluble and those in dry deposition are generally insoluble. Observations of wet and dry depositions are frequently available (e.g., National Atmospheric Deposition Program http://nadp.sws.uiuc.edu/nadpdata/). As an example, Table 6.2.1 gives atmospheric wet deposition concentrations used in the Peconic Estuary Model (Tetra Tech, 1999e). The corresponding dry deposition rates are given in Table 6.2.2.

TABLE 6.2.1 Atmospheric Wet Deposition Concentrations Used in the Peconic Estuary Model[a]

Parameter	Concentration (mg/L)	Parameter	Concentration (mg/L)
Refractory part. Organic carbon	0.325	Refractory part. Organic nitrogen	0.0
Labile part. Organic carbon	0.325	Labile part. Organic nitrogen	0.0
Dissolved organic Carbon	0.650	Dissolved organic nitrogen	0.648
Dissolved organic Phosphorus	0.045	Ammonia nitrogen	0.18
Orthophosphate	0.016	Nitrate + Nitrite nitrogen	0.33
Available silica	0.0		

[a]Tetra Tech, 1999e.

TABLE 6.2.2 Atmospheric Dry Deposition Rates Used in the Peconic Estuary Model[a]

Parameter	Deposition Rate ($g/m^2/day$)	Parameter	Deposition Rate ($g/m^2/day$)
Refractory part. Organic carbon	0.000387	Refractory part. Organic nitrogen	0.000530
Labile part. Organic carbon	0.000387	Labile part. Organic nitrogen	0.000530
Dissolved organic Carbon	0.000773	Dissolved organic nitrogen	0.000771
Dissolved organic Phosphorus	0.000054	Ammonia nitrogen	0.000214
Orthophosphate	0.000019	Nitrate + Nitrite nitrogen	0.000393
Available silica	0.000247		

[a]Tetra Tech, 1999e.

Atmospheric deposition is increasingly recognized as a significant external source of pollutants to surface waters. A pollutant from the air may be deposited into waterbodies and affect water quality in these systems. Pollutants can be transferred directly or indirectly onto the surface of a waterbody. Direct deposition occurs when pollutants are directly deposited onto the surface of a waterbody. At the air–water interface, exchanges of gases, liquids, and solids happen during both dry- and wet-weather periods and are referred to as dry or wet deposition. Indirect deposition occurs when pollutants are deposited on land first and then are washed into a waterbody. The indirect transfer of pollutants from the air to water is modified by the transport, transformation, and storage of pollutants on land. Storage can introduce a substantial time delay between the time when a pollutant reaches the land and the time when the pollutant shows up in the water. For example, the presence of snow can introduce a time delay in pollution, by which the pollutants attached to snow will be released into surface waters the next spring.

Winds can carry air pollutants substantial distances. For example, in some cases, DDT-tainted materials traveled south-to-north across the entire United States from Mexico and Central and South America. Studies indicated that 80% of the toxic chemicals entering Lake Superior result from atmospheric deposition rather than from water discharges (EHC, 1998). Nitrogen can be deposited from the air directly onto a waterbody. It can also be deposited on the watershed first and then transported to the waterbody.

There are five categories of air pollutants with the greatest potential to harm water quality (USEPA, 2000a): (1) nitrogen, (2) mercury, (3) other metals, (4) combustion emissions, and (5) pesticides.

These categories are based on both method of emission and other characteristics of the pollutants. They all have the ability to settle into waterbodies and damage ecosystems, as well as public health. Nitrogen is in its own category since its effects on ecosystems are so much different than other combustion emissions. Mercury behaves very differently in the environment from other metals and therefore has its own category. Combustion emissions and pesticides are exclusively manmade whereas mercury, other metals, and nitrogen compounds arise from both natural and manmade sources.

Atmospheric deposition is often identified as a major source of mercury, PCBs, and PAHs deposited to aquatic systems. For example, ~63% of the PCB input to Lake Huron is from direct atmospheric deposition, an additional 15% is from atmospheric deposition to the upstream Lakes Superior and Michigan, and the remaining 22% is from other sources (USEPA, 2000a). Bricker (1993) reported that atmospheric deposition contributes 33% of lead and 2% of copper and zinc in the sediment of Narragansett Bay, RI.

While nitrogen, in the forms of NO_x, NH_3, and organic compounds, is a natural part of the earth's atmosphere, human activities are increasing the concentrations and causing harm to some waterbodies. In North America, combustion of fossil fuels (e.g., coal, oil, and gas) by industry, power plants, and vehicles contributes the majority of NO_x to the atmosphere. The largest

TABLE 6.2.3 Selected U.S. Estuaries and the Estimated Percentage of Total Nitrogen Entering the Watershed as Atmospheric Deposition[a]

Albemarle-Pamlico Sounds, NC	38%
Chesapeake Bay	21%
Delaware Bay	15%
Long Island Sound	20%
Narragansett Bay	12%
New York Bight	38%
Waquoit Bay, MA	29%
Delaware Inland Bays	21%
Flanders Bay, NY	7%
Guadalupe Estuary, TX	2–8%
Massachusetts Bays	5–27%
Narragansett Bay	4%
Newport River Coastal Waters, NC	>35%
Potomac River, MD	5%
Sarasota Bay, FL	26%
Tampa Bay, FL	28%

[a]USEPA, 2000a.

sources of NH_3 emissions are fertilizers and domesticated animals (e.g., hogs, chickens, and cows). More studies are needed on the anthropogenic sources of organic nitrogen. As human sources of nitrogen compounds to the atmosphere increase, the importance of atmospheric deposition of nitrogen to surface waters increases as well. Atmospheric deposition of excess nitrogen can be a major contributor to eutrophication: increased primary production, algal blooms, hypoxia/anoxia, fish or shellfish kills, and changes in algal community composition. In some cases, nitrogen pollution can also contribute to acidification of waterbodies.

Nitrogen deposited from the atmosphere can be a large percentage of the total nitrogen load in some areas. Table 6.2.3 shows selected U.S. estuaries and the estimated percentage of total nitrogen entering the watershed as atmospheric deposition (USEPA, 2000a). For example, Albemarle-Pamlico Sound in North Carolina receives 38% of its nitrogen from the atmosphere. Nutrient loading to the Chesapeake Bay is a primary cause of the decline of the Bay's water quality. Recent estimates indicate that ~21% of the nitrogen delivered to the Bay is from the atmosphere, including both direct deposition to the Bay's surface and deposition to the watershed that is later transported to the Bay in runoff.

Airborne nitrogen and sulfur gases (NO_x and SO_x) react with water, oxygen, and other compounds to form nitric acid and sulfuric acid. Acid precipitation is the term used to refer specifically to wet atmospheric deposition—rain or snow containing significant amounts of sulfuric and nitric acid or other

pollutants. The impacts of atmospheric deposition of acids on waterbodies vary greatly, depending on the amount of acid deposited, the amount of acid already present in the waterbody, and the ability of the waterbody to absorb and neutralize acid. Seawater has a noteworthy ability to neutralize acid, so significant acidification does not occur in coastal waters and most estuaries. Some freshwater systems, however, may be very sensitive to atmospheric inputs of acidic compounds (USEPA, 2000a).

In addition to nitrogen, atmospheric deposition may also be a significant source of pollutants such as trace metals and toxic organic compounds. Mercury is a toxic metal released by both natural and manmade processes. Its unique chemical characteristics greatly influence its behavior in the environment and distinguish it from other metals. Although it occurs naturally, human activities have greatly increased its concentration in the environment and presently account for ~75% of worldwide mercury emissions (USEPA, 2000a). Mercury is able to travel great distances in the atmosphere. The primary concern with mercury is that it accumulates within the tissues of wildlife and humans. The concentration of mercury within the tissue of a fish or shellfish may be tens of thousands of times greater than the concentration of mercury in the water. In addition to mercury, manmade processes have led to an increase in concentrations of other metals, such as lead, cadmium, nickel, copper, and zinc.

There are tens of thousands of pesticides used today. Once pesticides are released into the environment, they undergo chemical reactions that break them down into other chemical compounds called byproducts. Many pesticides break down very slowly, and thus, the pesticide and its byproducts can remain in soil, air, or water for decades. Some byproducts can be toxic whereas others can be relatively non-toxic.

6.3 WETLANDS AND GROUNDWATER

Basic characteristics of wetlands and groundwater are discussed in this section.

6.3.1 Wetlands

A wetland is an area that is constantly or seasonally covered by surface water or saturated by groundwater. Saturation with water is the dominant influence on the characteristics of the soil and on the composition of the plant community of a wetland. Wetlands are the vital link between water and land. They form a transition zone between water and land where the soil is occasionally or permanently saturated with water. In this transition zone, the flow of water, the cycling of nutrients, and the energy of the sun combine together to produce a unique ecosystem. Wetlands are often found at the interface between dry terrestrial ecosystems, such as upland forests and grasslands, and permanently

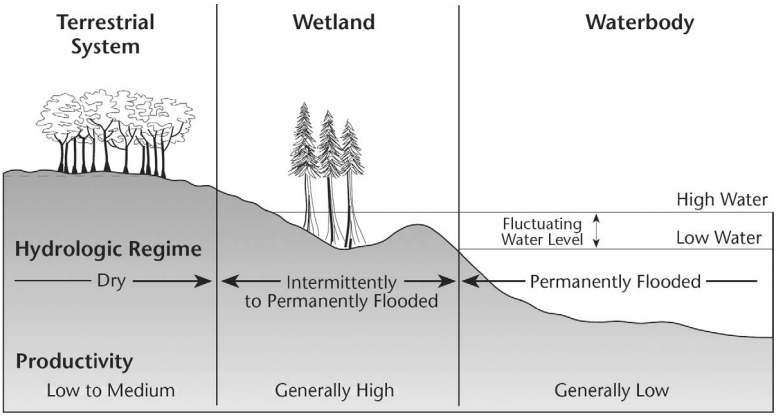

Fig. 6.3.1 A description of a wetland (USEPA, 2000a).

wet aquatic ecosystems, such as rivers, lakes, estuaries, and coastal waters (Fig. 6.3.1).

Unlike rivers, lakes, and estuaries, some wetlands contain little or no surface water and are primarily influenced by high groundwater tables. These wetlands are only seasonally wet and have standing water for just a few months out of the year. In general, wetlands provide critical habitat for a wide variety of fish and wildlife, provide water storage, improve water quality, and stabilize shorelines. In the studies of surface waters, wetlands are often considered as an important component of an integrated system. For example, in the modeling study of Florida Bay, FL, a large portion of the Everglades National Park (wetland) is included in the model (Tetra Tech and AEE, 2005).

Wetlands vary from region to region, but they share three characteristics:

1. *Hydrology*: They are periodically flooded or at least saturated to or near the surface. Water saturation largely determines how the soil develops and what types of plant and animal communities live in and on the soil.
2. *Soils*: They have unique hydric soils characterized by periodic wetness and differing from those of adjacent upland areas. A hydric soil is a soil that formed under conditions of saturation or flooding long enough to develop anaerobic conditions in the upper layer.
3. *Vegetation*: They support plant species that have adapted to or are dependent on periodically wet conditions.

Wetlands include two general categories: coastal (or tidal) wetlands and inland (or freshwater) wetlands. Coastal wetlands are often closely linked to estuaries, where the large salinity variation and the fluctuating tidal elevation combine to create a difficult environment for most plants. Consequently, many shallow

coastal areas are mud flats or sand flats without any vegetation. Some plants, however, have successfully adapted to this environment. Inland wetlands are most common on floodplains along rivers and along the margins of lakes, and in other low-lying areas where the groundwater intercepts the soil surface (USEPA, 2000a).

Wetlands are now recognized for a variety of important ecological functions. Each wetland works in combination with other wetlands, adjacent uplands, and aquatic systems as a part of a complex, integrated system that can deliver a range of benefits to humans, fish, wildlife, and the environment as a whole. Wetlands are popular sites for fishing, hunting, hiking, boating, and wildlife observation. Natural wetlands continue to experience reduction in abundance and distribution. Approximately one-half of the wetlands in the continental United States have been lost since colonial settlement (Frayer et al., 1983).

Depending on their type, location, and geographical factors, wetlands can serve the following functions: (1) fish and wildlife habitat, (2) water storage and groundwater recharge, (3) sediment trapping and water quality improvement, and (4) flood damage reduction.

Wetlands have long been recognized as highly productive habitats for aquatic and terrestrial plants and animals. Many fish and wildlife species depend on wetlands for survival or as seasonal habitats. Wetlands form an important transition zone between terrestrial systems and waterbodies (Fig. 6.3.1). They are often very productive and highly diverse in animal and vegetative composition because they contain elements common to both systems. Wetlands can be thought of as biological "supermarkets" and are among the world's most productive ecosystems (often more productive than artificial agricultural systems). The combination of shallow water, high levels of inorganic nutrients, and high rates of primary productivity is ideal for producing great volumes of organic matter that form the base of the food chain.

Besides serving as important habitat for wildlife, wetlands are a source of groundwater and surface water recharge. Wetlands help store water during floods and release it gradually to downstream areas. Some wetlands maintain stream flow during dry periods; others replenish groundwater.

Water draining from uplands carries sediments, nutrients, and other pollutants. Wetlands absorb these pollutants before they reach rivers, lakes, and other receiving waterbodies; therefore, they greatly influence the flow and quality of water (Fig. 6.3.2). As the water flows through marshes, much of the sediments and pollutants are filtered out. Wetlands can protect receiving waters from pollution by filtering urban and agricultural runoff and trapping sediments that otherwise could harm aquatic life.

Wetland plants and soils also act as a natural buffer between an upland and a waterbody, absorbing flood waters and dissipating storm surges. When rivers overflow, wetlands help to absorb and slow floodwaters. Wetland plants hold the soil in place with their roots, absorb the energy of waves, and slow down currents. Reduced velocity translates into less damage from flood waters. The

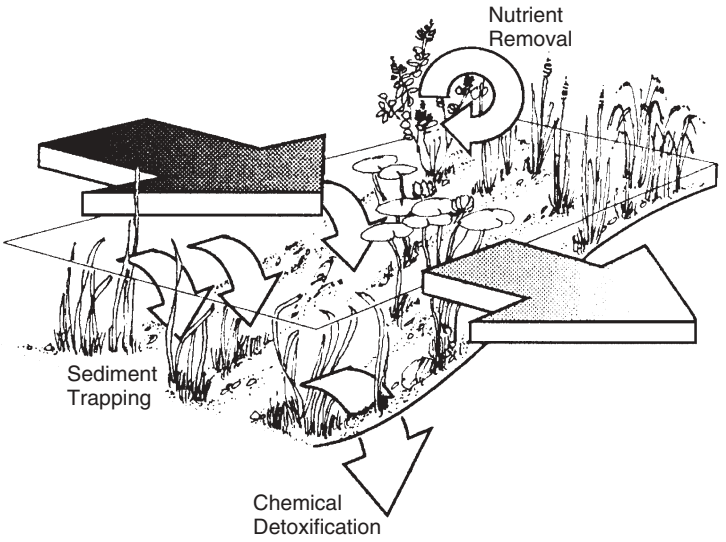

Fig. 6.3.2 Sediment trapping and nutrient removal by wetlands (USEPA, 2000a).

combination of water storage and velocity reduction helps prevent erosion and stabilize the shoreline.

6.3.2 Groundwater

Surface water is the water on the surface of the land, including water in rivers, lakes, and estuaries and runoff moving across the land surface. Groundwater is the water that completely fills the spaces between rocks and soil particles underground, in much the same way as water fills a sponge. Because of its availability and generally good quality, groundwater is widely used for household and other water supplies. Water enters groundwater storage primarily by infiltration/percolation. As water seeps through the soil, it carries with it substances applied to the land, such as fertilizers and toxics. The groundwater moves through aquifers and eventually surfaces in discharge areas, such as rivers, lakes, and estuaries, or it is drawn out of the ground by humans.

Groundwater is a critical component of water resources management. EPA (USEPA, 2000a) reported that in the United States:

1. Approximately 40% of river flow depends on groundwater.
2. About 50% of Americans obtain their drinking water from groundwater.
3. Approximately 95% of rural residents rely on groundwater for their drinking supply.
4. About 50% of agricultural water comes from groundwater.

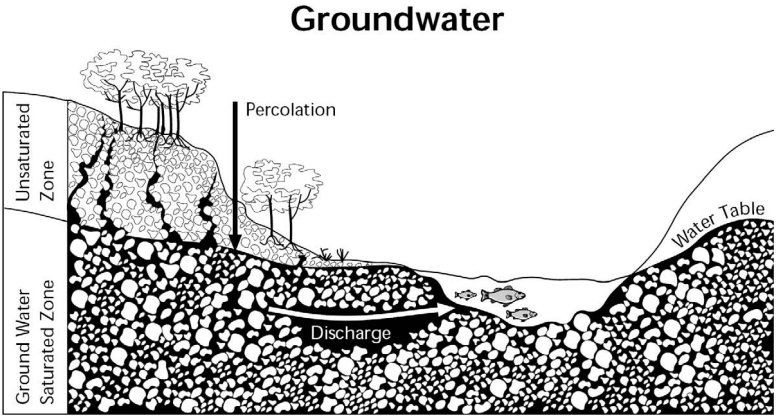

Fig. 6.3.3 Illustration of a saturated and an unsaturated zone (USEPA, 2000a).

Beneath the earth's surface, water resides in two general zones: the saturated zone and the unsaturated zone (Fig. 6.3.3). The area where water fills cracks and spaces in soil, sand, and rocks is called the saturated zone. Groundwater refers to the water in the saturated zone. The top of this zone is called the water table. The unsaturated zone lies between the water table and the land surface. The water table may be deep or shallow and may rise or fall depending on many factors. It may be <1 m below the land's surface or it may be hundreds of meters down. Groundwater supplies are replenished by rain and snow melt. Heavy rains or melting snow may cause the water table to rise. An extended period of dry weather may cause the water table to fall.

Groundwater can be found almost everywhere and is an integral part of the water cycle. As discussed in Section 1.1, the cycle starts with precipitation falling on the surface of the earth. When rain falls to the ground, the water does not stop moving. Some of it flows into rivers, lakes, or estuaries. Some sinks into the ground by percolating through the unsaturated zone. Groundwater is stored in and moves slowly through layers of soil, sand, and rocks called aquifers. Water continues to move within the saturated zone under the influence of gravity from areas where the water table is high toward areas where the water table is lower. Groundwater can move laterally, discharge from the ground, and become surface water. In this way, groundwater can affect surface water quantity and quality (Fig. 6.3.3).

Groundwater is vulnerable to pollution. Contamination occurs when pollutants become dissolved in water at the land surface and are carried down to the aquifer with the water. Groundwater quality can be adversely affected by human activities and natural processes. Except where contaminated water is injected directly into an aquifer, such as deep injection wells (Fig. 6.3.4), essentially all groundwater pollutants enter with water from the land surface. Groundwater can be polluted by (Fig. 6.3.4): (1) landfills, (2) septic systems,

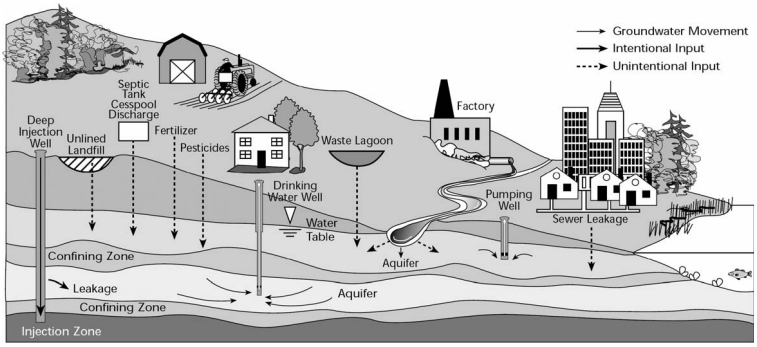

Fig. 6.3.4 Sources of groundwater contamination (USEPA, 2000a).

(3) leaky underground storage tanks, (4) fertilizers and pesticides, (5) industrial facilities, and (6) road salts and chemicals.

Generally, the properties and the amount of the pollutant and the properties of the soil above the aquifer are the major factors determining whether it will cause pollution in an aquifer. The most severe impact often comes from older landfills, which leak many different chemicals at high concentrations. Landfills are supposed to have a protective bottom layer to prevent contaminants from getting into the water. However, if there is no layer or it is cracked, contaminants from the landfill can make their way into the groundwater (USEPA, 2000a). Residential septic systems are designed to slowly drain away human waste underground at a harmless rate. A malfunctioning septic system can leak nutrients, bacteria, and other contaminants into the groundwater. Leakage from storage tanks can be a significant source of groundwater contamination. Agricultural activities add nutrients and pesticides to groundwater. Industrial activities tend to add organic chemicals and metals. Road salts are widely used to melt winter ice. When the ice melts, the salt is washed off the roads and may eventually end up in the groundwater.

It is common to think of surface water and groundwater as separate resources; however, they are interconnected. Surface water can affect the quality and quantity of groundwater. Likewise, groundwater discharge can significantly affect the quality and quantity of surface waters, especially small rivers during low flow seasons. For example, the modeling study of Peconic Bay, NY, illustrates the importance of nutrients from groundwater to the eutrophication in the bay (Tetra Tech, 1999e).

Surface waterbodies, such as rivers, lakes, and estuaries, can be seen visually, but ground waterbodies cannot be seen. Groundwater usually moves much more slowly than surface water. This is because groundwater needs to overcome more friction to move through small spaces between rocks and soil underground. Although the distinction between surface water and groundwater seems simple, they are connected in such a way that surface water can become groundwater and vice versa.

The groundwater component often plays a minor role in the overall water balance and the groundwater seepage is often difficult to measure. For many applications, inflows or losses to groundwater are assumed to be negligible, but this assumption can be questionable. From a nutrient exchange perspective, groundwater transport can be important, especially for closed or semi-closed surface waterbodies (e.g., lakes). When dealing with contaminated groundwater, seepage into surface water can represent a major concern in these types of waterbodies. Groundwater models can be used in simulating the flux of contaminants entering the surface water from the ground (e.g., Tetra Tech, 1999e; Guo and Langevin, 2002).

The exchange between surface water and groundwater can be very important. For example, rivers usually start as small streams and get bigger as they flow downstream. The water they gain is often from groundwater. Aquifers discharge through seepages to feed the rivers and lakes. For groundwater to discharge into a river, the altitude of the water table in the vicinity of the river should be higher than the altitude of the river water surface (e.g., Fig. 8.2.2). It is also possible for rivers (and lakes) to lose water to the ground. In these cases, rivers recharge the aquifer through river bed infiltration (Fig. 8.2.2). Groundwater can be responsible for maintaining the hydrologic balance of rivers, lakes, and wetlands. This is the reason why successful water resource management plans always have a special interest in the groundwater adjacent to the waterbody.

6.4 WATERSHED PROCESSES AND TMDL DEVELOPMENT

There are many published papers and reports on watershed processes and TMDL development (e.g., Shoemaker et al., 1997; Haith and Shoemaker, 1987; Lahlou et al., 1998). This section introduces basic concepts about watershed and TMDL development in surface water systems.

6.4.1 Watershed Processes

Technically, a watershed is the divide separating one drainage area from another (Chow, 1964). The term "watershed" is now commonly used to refer to an area of land that drains water, sediment, and dissolved materials into a common outlet, such as a river, lake, underlying aquifer, estuary, or ocean (e.g., Fig. 1.1.1). Watershed is sometime used synonymously with drainage basin and catchment (Dunne and Leopold, 1978). Watershed forms vary greatly and are tied to many factors including climate, morphology, soils, and vegetation. Watersheds, therefore, occur on multiple scales. There can be subwatersheds within watersheds. They range from the largest river basins, such as the watersheds of the Mississippi, Missouri, and Columbia Rivers, to the watersheds of very small streams of only a few acres in size. Ridges of higher ground generally form the boundaries between watersheds. At these boundaries, rain falling

on one side flows toward the low point of one watershed, while rain falling on the other side of the boundary flows toward the low point of a different watershed.

The watershed is increasingly being accepted as the most appropriate geographic unit for management of water quality. The importance of the relationship between a surface waterbody and its watershed cannot be overemphasized. Over the past decades, point source discharges of nutrients are fairly constant and are controlled by the NPDES permitting (see Section 6.1). While point sources continue to be an environmental threat, it is clear that nonpoint pollutant inputs have increased in recent decades and have degraded water quality in many aquatic systems. For example, besides discharges from industrial or municipal sources, surface waters may be threatened by urban, agricultural, or other forms of polluted runoff. When a waterbody (e.g., a lake) was surrounded primarily by forest, grassland, and/or wetlands, very little nitrogen and phosphorus ran off the land into the water. Most of these nutrients were absorbed or held in place by the natural vegetation. Today, much of the forests and wetlands might have been replaced by farms, cities, and suburbs. As a result, the amount of nutrients entering a lake's water could increase tremendously. Eroded soil and sediment can transport considerable amounts of nutrients to the lake. Consequently, it is essential to protect surface waters from the cumulative impacts of nonpoint sources. Watershed approach has become the most logical basis for managing water resources environmentally, financially, and socially.

Runoff occurs when rainfall (or snowmelt) does not evaporate or infiltrate the ground, but instead flows onto adjacent land or waterbodies. Land cover plays an important role in the runoff process and affects the quality and quantity of the water entering a receiving waterbody. Factors that influence runoff processes include climate, geology, topography, soil characteristics, and vegetation. Heavily vegetated areas can intercept precipitation. When the rate of rainfall (or snowmelt) exceeds infiltration capacity, excess water travels downhill as runoff. As illustrated in Fig. 6.4.1, the flow rate of runoff differs greatly

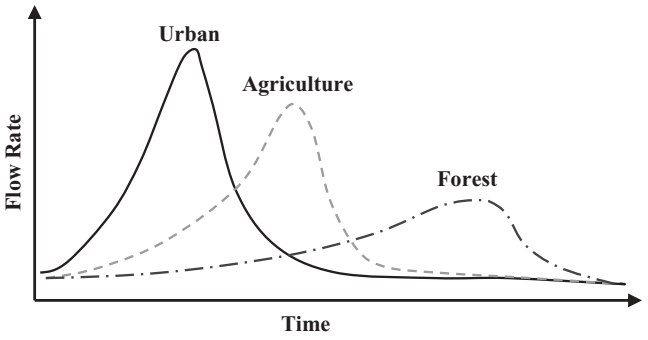

Fig. 6.4.1 Runoff flow rates of different land covers.

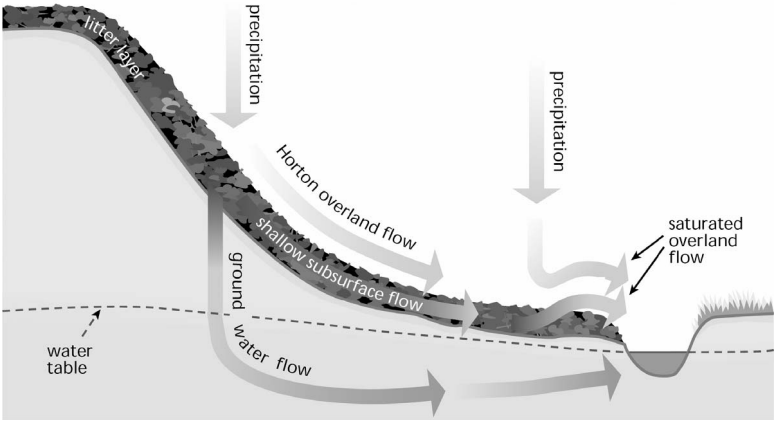

Fig. 6.4.2 Three basic types of runoff: overland flow, subsurface flow, saturated overland flow (FISRWG, 1998).

among different land covers. In urban areas, the high proportion of impervious surfaces prevents rainwater from infiltrating the soil and increases the flow rate. The high peak flow rate can increase erosion on the land and carry large amounts of sediments and nutrients into the receiving water.

There are three basic types of runoff (Fig. 6.4.2): overland flow, subsurface flow, and saturated overland flow (FISRWG, 1998). Each of these runoff types can occur individually or in some combination. When the precipitation rate is higher than the infiltration rate, surface depressions begin to fill and the infiltration rate decreases as the soil becomes wetter. If the precipitation rate continues to be higher than the infiltration rate, runoff begins.

A surface waterbody is often a reflection of its watershed and the activities taking place in the watershed. For example, if a lake suffers from eutrophication, often the cause of the problem can be linked to pollution sources within the watershed. Typically, water quality decreases with an increasing ratio of watershed area to the waterbody area (especially for lakes), because a larger watershed usually involves a larger runoff into the waterbody. The land use within the watershed determines the amount of nutrients that enter the waterbody. A lake and its watershed can be used as an example. Watershed features have a great influence on lake hydrology. Watershed disturbance is a sensitive early warning of lake change. If the lake is small relative to the size of its watershed, the potential is greater for the lake to fill in with sediment or be affected by nutrients. On the other hand, if the watershed has lots of firmly rooted vegetation, it will act as a sponge to trap water and soil and thereby considerably reduce erosion.

Figure 6.4.3 illustrates the linkages of surface water with the watershed and with groundwater. The flow rate, water temperature, sediment concentration, DO, toxics, and nutrients from the watershed are often treated as inputs to a

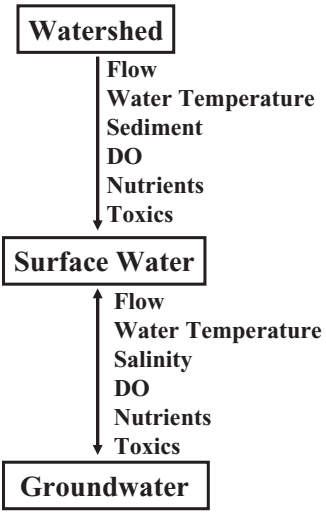

Figure 6.4.3 Coupling of a surface water system with the watershed and groundwater.

surface water model. These inputs can be from either measured data or a watershed model. The interactions between the groundwater and the surface water can also be described (Fig. 6.4.3). In the surface water model, these nonpoint sources from the watershed (and the groundwater) are distributed to each grid cell in proportion to the length of the grid cell.

6.4.2 Total Maximum Daily Load

Proper management of a waterbody needs a comprehensive management plan. The plan should provide strategies for improving and protecting the water quality of the waterbody. Traditional efforts of controlling point sources have been only moderately successful in reducing water pollution, specifically in waterbodies where nonpoint sources are the major contributors. Over recent decades, it has gradually become apparent that many water quality problems are best solved at the watershed level rather than at the individual receiving waterbody level. A watershed protection approach is necessary to manage the waterbodies and to meet the water quality standards. It is essential to have a thorough understanding of how the surrounding watershed influences water quality and how physical, chemical, and biological interactions in the waterbody further modify the water quality.

Water quality standards emanate from state or federal laws or regulations that consist of (1) the designated uses of a waterbody, (2) the numeric and narrative water quality criteria that are necessary to protect the uses of that waterbody, and (3) an antidegradation policy. Water quality standards protect the public health, enhance the quality of water, and serve the purposes of the

Clean Water Act (USEPA, 1994b). Numeric criteria are ambient concentrations developed by EPA or states for various pollutants to protect human health and aquatic life. Narrative criteria are statements that describe the desired water quality goal.

A TMDL is a tool for implementing water quality standards and is based on the relationship between pollution sources and water quality conditions in a waterbody. Assimilative capacity (or loading capacity) is the greatest amount of pollutant load (e.g., TP) that can be discharged to a waterbody without exceeding water quality standards. Assimilative capacity represents the ability of a waterbody to naturally absorb and use a pollutant without violating water quality standards. The TMDLs are obtained by calculating the assimilative capacity of a waterbody and identifying the sources to determine the maximum load that the waterbody is capable of carrying without causing detrimental effects. A TMDL is the sum of the individual waste load allocations (WLA) for point sources and load allocations (LA) for nonpoint sources (including natural background), so that the assimilative capacity of the waterbody is not exceeded. These point and nonpoint sources may be either existing or future sources. A margin of safety (MOS) is required to address uncertainty in the analysis. This uncertainty can be caused by insufficient or poor-quality data, a lack of knowledge about the pollution effects, and/or errors in estimating the loading capacity of the waterbody. The TMDL can be expressed as:

$$\text{TMDL} = \text{WLA} + \text{LA} + \text{MOS} \tag{6.4.1}$$

The MOS may also be incorporated into the conservative estimations on WLA and LA that are used to develop TMDLs. For example, if a receiving waterbody has only one point source, the TMDL is then the sum of that point source's WLA plus the LA for any nonpoint sources. Local association includes natural background sources from groundwater seepage, atmospheric deposition, and weathering of rocks and soils. These sources are often very difficult to control. Atmospheric deposition is caused at the regional or national scale and is impossible to be controlled at the watershed scale. The weathering and dissolution processes of rocks and soil are natural mechanisms and should also be considered as part of the uncontrolled loads.

A key element in TMDL development is to determine the loading capacity of the receiving waterbody. A sound, scientifically credible analysis on the loading capacity is a must for the TMDL development. The purpose is to answer a fundamental question: How much of a specific pollutant can be discharged in a receiving water without violating the water quality standard? This question is often answered by conducting numerical modeling of the waterbody (e.g., Wool et al., 2003a, 2003b).

Watershed models simulate pollutant loadings from point and nonpoint sources discharged into a receiving water. Receiving water models, as discussed extensively in this book, simulate the movement and transformation of pollutants in rivers, lakes, estuaries, and coastal waters. These models establish

a quantitative relationship between pollutant sources and the water quality in the receiving water. For example, in the development of a TMDL for Lake Tenkiller (Tetra Tech, 2000c), a receiving water model was used to determine the phosphorus loading capacity that will protect the lake from accelerated eutrophication (Ji et al., 2004a). A watershed model was used to determine the sources of the phosphorus loads, the magnitude of the loads, and the potential reductions under a variety of management scenarios. Ultimately, the watershed model and the lake model were used to determine the optimum combination of loads for the protection of the water quality in the lake. The modeling of Lake Tenkiller is presented in Section 9.4.1 as a case study.

In addition to external sources, pollutants can be reintroduced into a waterbody from the water bottom by resuspension. Therefore, control of nutrients is further complicated by the internal cycling of nutrients in the waterbody. Understanding the relationships between nutrient loads, the waterbody response, and the processes in the waterbody is the key to making reliable determinations of the total loading capacity. Natural environmental conditions, such as flow velocity, water depth, temperature, nutrient concentrations, sediment oxygen demand, all affect the loading capacity of the waterbody.

The TMDL development involves the identification and evaluation of various management alternatives for achieving economic and water quality goals. Models not only are used to determine relationships between pollutant loads and the water quality response, but also are necessary to project future water quality conditions. Models may assist in the development and evaluation of various components of watershed management plans and, thus, help to achieve the economic and water quality goals. Economic goals are usually expressed in terms of cost effectiveness and cost distribution among the stakeholders, whereas water quality goals are often expressed in terms of water quality standards. The diverse character of nonpoint sources implies that more people may be affected by the management decisions, thus creating a greater burden on the modelers and the decision makers. Noncredible models may lead to unwise decisions with significant financial implications. Because a TMDL program requires the implementation of load reductions that often have enormous financial consequence, the TMDL calculation must be scientifically defensible. The model should be well calibrated and verified before it can be used to link the critical water quality conditions of the receiving waterbody to external loadings.

For rivers receiving organic loads, the low flow with high temperature is often the critical condition. For example, stream analysis often uses a low flow condition of 7Q10 (7-day low flow, once in 10-years) found during the summer high temperature condition. Under wet weather flow conditions, the 7Q10 condition is inappropriate, and nonpoint sources should be considered. For lakes, vertical stratification is often a key parameter in identifying critical conditions for lake TMDL development.

For estuaries and coastal waters, the definition of critical conditions is not so straightforward. Estuaries and coastal waters are complex systems and

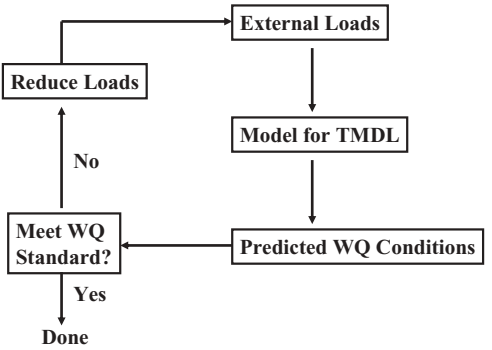

Figure 6.4.4 Use of models for TMDL development.

present a challenge for defining the criteria conditions. Freshwater, tides, wind, sediment transport, and other factors can be important to determining the critical conditions. The goal is to estimate the loading capacity during periods when estuaries and coastal waters are most vulnerable to pollutant sources. For example, a shallow estuary dominated by point sources of nutrients might have low freshwater flow periods as critical conditions due to limited flushing. A deep estuary with strong stratification may set up conditions favorable for algal bloom, eutrophication, and hypoxia.

As shown in Fig. 6.4.4, a model for TMDL development predicts water quality for a specified set of external loads including point sources, nonpoint sources, and natural background sources. The process is iterative. External loads are used as the model input. The model then is applied to predict the corresponding water quality conditions. If the predicted water quality conditions meet the water quality standard set for this waterbody, then the TMDL calculation is done. Typically, the first iteration consists of performing a model simulation using existing loads and then comparing predicted water quality with the water quality standards. Assuming that the existing loads result in violation of the water quality standards, additional model simulations are performed using reduced external loads, until the water quality standards are met. The results of the above approach are also dependent on the year (or years) chosen for the modeling periods. The periods should represent critical or worst-case conditions. The overall intent of the modeling analysis is to define the external loads that will ensure that the waterbody meets established water quality standards.

CHAPTER 7

Mathematical Modeling and Statistical Analyses

This chapter describes mathematical modeling and statistical analyses that are commonly used in the studies of surface water systems.

The three sections of this chapter cover three essential, yet relatively independent, subjects on modeling. Section 7.1 discusses types of mathematical models, numerical models, and the selection of models for modeling surface water systems. Section 7.2 presents the statistical analyses frequently used in hydrodynamic and water quality studies. Section 7.3 focuses on topics related to model calibration, verification, and sensitivity analysis.

7.1 MATHEMATICAL MODELS

In the study of surface waters, models can be divided into two general categories: (1) physical models and (2) mathematical models. A physical model is built to a particular scale and uses water (or some other fluid) to produce a scaled flow that can be measured and related back to the real water system. A mathematical model, on the other hand, represents the water flow and other processes with a set of mathematical equations, which often needs to be solved numerically by a computer. The role of either model compliments that of the other, but strictly speaking, neither model can be completely successful, because surface water systems are so complex and defy exact simulation.

A mathematical model is usually based upon fundamental physical, chemical, and biological principles that describe the spatial and temporal variations of a water system. A mathematical model does not purport to represent all aspects of the actual environment but attempts to incorporate only those features of the problem that are most relevant. The parameters of the model can be adjusted so that the model can realistically represent certain characteristics of the surface water system. In hydrodynamic and water quality modeling, as

Hydrodynamics and Water Quality: Modeling Rivers, Lakes, and Estuaries, by Zhen-Gang Ji

illustrated in the previous chapters, a mathematical model is often a set of coupled, nonlinear, partial differential equations. As no two water systems are alike, parameters of mathematical models need to be adjusted to suit the local circumstances, or even new parameterizations or mechanisms may be required to represent the water system appropriately.

Mathematical models have many forms. They may be empirically derived statistical relationships plotted on a graph, relationships developed based on the law of conservation of mass, or the combination of the two. Each model group has benefits and limitations. Mathematical models can be categorized into a variety of groups based on their characteristics, such as whether they are (1) statistical (empirical) or mechanistic, (2) deterministic or stochastic, and (3) analytical or numerical.

These characteristics represent different aspects of mathematical models. For example, most (if not all) of the 3D hydrodynamic models (e.g., Blumberg and Mellor, 1987; Hamrick, 1992) are mechanistic, deterministic, and numerical models.

Statistical (Empirical) Models and Mechanistic Models Statistical or empirical models are usually expressed in simple mathematical relationships derived by statistically fitting equations to observed data. For example, a linear regression of chlorophyll and P data from a lake is a simple empirical model in which the relationship between chlorophyll and P is expressed in an algebraic equation. Empirical models are usually easy to use and require minimal effort and data. One weakness of empirical models is that they tend to have large standard errors of prediction, especially when there is no adequate site-specific data for model calibration. They are most reliable when applied within the range of observations used to construct the model. Extrapolation from empirical data is known to be uncertain.

In contrast, mechanistic models are based on physical, chemical, and biological mechanisms that govern water systems. When properly calibrated and verified, mechanistic models are capable of addressing many more details of hydrodynamic and water quality processes. Mechanistic models are explanatory and are formulated upon equations that contain directly definable, observable parameters. Extrapolation from mechanistic models usually carries higher confidence than extrapolation using empirical models because mechanistic models usually have a better representation of the physics, chemistry, and biology of the waterbody being studied.

In hydrodynamic and water quality modeling, however, mechanistic models often need empirical formulations to represent processes in the model. For example, the turbulence model described in Section 2.2.3 is largely based on empirical formulations, even though the hydrodynamic model that employs the turbulence model is mechanistic. In Chapter 5, many of the formulations used in the water quality models are empirical, originating from statistically fitting equations to observed data. Therefore, the statistical (empirical) and

mechanistic models often work together in the modeling of surface water systems.

Deterministic Models and Stochastic Models A deterministic model contains no random (stochastic) components. Each component of and input to the model is determined exactly by mathematical equations. The behavior of every variable is completely determined by the governing equations and the initial states of the variables. A given input will always produce the same output, not allowing for random variation. In contrast, a stochastic model contains random (stochastic) components or inputs. The model allows for random, probabilistic elements in the relationship between two or more variables. A given input will produce an output according to some statistical distribution expressed in random variables.

A stochastic model focuses on reproducing certain statistical features of a waterbody. For example, a stochastic model of a river may characterize flow rates in terms of probability distribution, mean, and variance. However, the model is not able to give a specific flow rate at a specific time. A deterministic model, on the other hand, should be able to reproduce certain physical processes of the river. By including all of the external inflow sources to the river, the deterministic model should be able to calculate a specific flow rate at a specific time. Generally, deterministic models are designed to represent internal physical processes, enabling a wide range of model applications that stochastic models are unable to address.

Stochastic components are also often an important part in the calibration and verification of a deterministic model. For example, to calibrate a deterministic model, one has

$$f_{\text{obs}} = f_{\text{model}} + \text{error} \tag{7.1.1}$$

where f_{obs} = observed data, f_{model} = model result, and error = model error.

There is often a set of measured data at different sampling stations and times. Equation (7.1.1) then can be expressed as

$$\sum f_{\text{obs}} = \sum f_{\text{model}} + \sum \text{error} \tag{7.1.2}$$

where Σ represents averaging over all of the data sampling stations and times.

The objective of model calibration and verification is to minimize the term of Σ error, so that the model results can match the measured data as closely as possible. Since Σ error represents the overall cumulative difference between the model and the data, there are a number of factors that can affect the value of Σ error, such as model accuracy and data sampling errors. In this sense, the term of Σ error can be viewed as a stochastic (or random) component, and the purpose of the calibration of a deterministic model is to minimize its stochastic

term, Σ error. Hence, the stochastic component will always play a central role, even for deterministic models (e.g., Ji et al., 2002b, 2004b).

Analytical Models and Numerical Models Mathematical models can be either analytical or numerical. An analytical model has an exact mathematical solution to the differential equations describing processes in a waterbody. Analytical models are available only for relatively restrictive conditions, usually predicting 1D, constant parameters under steady-state conditions (e.g., Ji and Chao, 1989, 1991). In spite of the severe assumptions that must be invoked, analytical models are often used to

1. Check the accuracy of complicated numerical models (e.g., Ji et al., 2003)
2. Provide first-order estimates of relatively simple systems
3. Give insights into hydrodynamic and water quality processes in waterbodies

The famous Streeter-Phelps (1925) equation, Eq. (8.3.4), is an example of an analytical solution that estimates DO concentrations along a river. The vertical profile of sediment concentration, Eq. (3.2.17), is derived from a simplified case, but is still capable of giving insights into the profiles of sediment concentration in waters. Equation (3.2.17) elucidates the importance of sediment settling velocity, vertical diffusion, and water depth to sediment distribution in the vertical direction. It is also a common practice to check the accuracy of a numerical model by comparing analytical solutions to the ones from the numerical model. For instance, Ji et al. (2003) derived analytical solutions to a linearized Navier–Stokes equation and used the solution to describe trajectories of particles in the Gulf of Mexico.

Analytical models are often limited by the assumptions used to derive their solutions. Most models for surface water systems are often too complicated to obtain analytical solutions, and numerical techniques are indispensable to finding solutions to these models.

A numerical model is a discretized version of a set of mathematical equations, such as the continuity equation and momentum equations, that describe processes in a waterbody. The discretized set of equations is then converted into computer code (a computer model). By entering the input data and model parameters into a computer, numerical solutions to the model can be derived. (A computer simulation is a representation of a water system using a computer model.) Given appropriate data, the execution of the computer model yields an approximate solution to the mathematical model.

7.1.1 Numerical Models

Modeling is the use of numerical models to simulate the behavior of a waterbody in response to a specific set of forcing conditions. Models that are cali-

brated and verified are then used to predict the response of a water system to changes in forcing conditions. Numerical models can be classified according to

1. Numerical method: finite difference, finite element, finite volume, spectral, and so on.
2. Grid type: Cartesian grid, curvilinear grid, unstructured grid, and so on.
3. Time-differencing scheme: explicit, implicit, semi-implicit, and so on.
4. Spatial-differencing scheme: upwind, central difference, flux-corrected transport, and so on.

For example, the EFDC model uses a finite difference method, a curvilinear grid, a semi-implicit scheme, and flux-corrected transport (Hamrick, 1992).

In terms of their representations of space and time, numerical models can also be categorized as: (1) steady state or time dependent (dynamic) and (2) Zero, one, two, or three dimensional. The temporal characteristics includes whether the model is steady state (inputs and outputs are constant over time) or time dependent (dynamic) depending on the treatment of the time derivative in the governing equations. Steady-state means that variable values within the system do not change with respect to time. A steady-state model sets time derivatives equal to zero and uses constant values of input variables to produce time-independent results. This condition happens when the inputs and outputs are held constant for a long time. Steady-state models are much easier to apply and require considerably fewer resources than dynamic models. A limited group of waterbodies might be appropriate for the application of steady-state models, such as rivers with low variability of flow and sediment and contaminant loads on the annual scale. Steady-state models can have a certain level of utility for screening purposes.

In contrast, a time-dependent model includes the time derivatives in the governing equations and describes the temporal variability of a waterbody. The model simulates temporal and spatial variations due to varied external loadings, boundary conditions, meteorological conditions, and internal processes within the waterbody.

The spatial characteristics of numerical models include the number of dimensions simulated and the spatial resolution. In modeling shallow and small rivers, 1D models are often used since their vertical and lateral gradients are typically small. For example, Ji et al. (2002a) used a 1D model to simulate the Blackstone River in Massachusetts, which is also described as case studies in Sections 3.7.3 and 8.4.1. For large lakes and estuaries, 2 D or 3D models are more appropriate, because both vertical and horizontal concentration gradients commonly occur, such as the other case studies described in this book.

The 3D models provide the closest approximation to reality by simulating gradients along all three of the spatial dimensions. A number of 3D, time-dependent, free-surface hydrodynamic models are now available for surface water modeling (e.g., Blumberg and Mellor, 1987; Hamrick, 1992; Casulli and Cheng, 1992). Although these models all solve the same 3D Navier–Stokes

equation, Eq. (2.1.19), they can be significantly different in terms of turbulence schemes, numerical methods, grid types, and/or solution algorithms.

The development of a numerical model for a water system can be divided in two phases: (1) the development of a generic model and (2) the development of a site-specific model.

A generic model is a numerical model that incorporates the general theories of hydrodynamics and water quality, but does not include any site-specific information. As shown in Fig. 7.1.1, a generic model is often developed in the following steps:

1. Basic theories are developed and expressed in differential equations.
2. The differential equations are discretized in finite difference (or finite element) equations and are then solved using certain numerical algorithms.
3. Computer programs are developed based on the finite difference equations and the numerical algorithms, so that solutions to the model can be obtained by running the model on a computer.

A set of input file templates are often developed along with the computer programs, so that the computer code can be tested and checked for consistency. At this stage, the generic model is not associated with any specific study area and is configured for general waterbodies, provided that the same types of processes are relevant to the modeling purpose. For example, the EFDC model (Hamrick, 1992) is a generic model that is generally applicable to rivers, lakes, estuaries, and coastal waters.

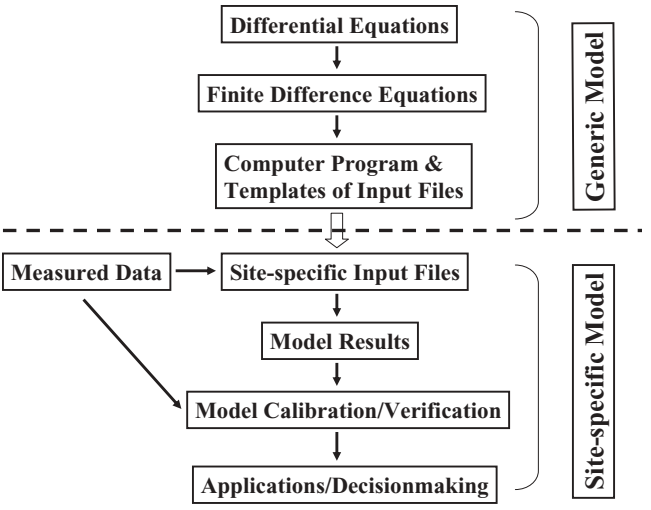

Fig. 7.1.1 Development of a numerical model.

In contrast, a site-specific model is designed for the study of a specific water system and has unique settings. A site-specific model is often derived from a generic model combined with site-specific information, such as topography, model parameters, and boundary conditions. As shown in Fig. 7.1.1, to apply a generic model to a specific site, measured data should be incorporated into the model for (1) setting up input files and (2) model calibration and verification.

As discussed in the previous chapters, input files of a site-specific model, such as the Lake Okeechobee Environmental Model (LOEM) (Jin and Ji, 2005), should originate from the study area. After input files are set up, the site-specific model is ready to run on a computer and to produce results. The model results are compared with the measured data for model calibration and verification. Finally, the calibrated and verified model can be used for applications and for supporting decisionmaking. It is evident that the computer code of a generic model (e.g., the EFDC model) is easily transportable from one study site to another, whereas a model of a specific waterbody (e.g., the LOEM model) is designed for the specific site only.

Unlike analytical models, which cannot deal with complex problems, numerical models are capable of realistically simulating complex water systems. Since the 1990s, 3D hydrodynamic and water quality modeling has been maturing from being a research subject to a practical analysis technology. The rapid progress of computer technologies provides powerful computers for numerical simulation. Computational requirements for realistic 3D modeling have changed from super computers and high-end workstations to desktop personal computers in the past two decades.

Measured data through laboratory and field studies are used to provide insight into hydrodynamic and water quality processes. However, measured data can be difficult and expensive to obtain. Spatial and temporal resolutions of measured data are often inadequate to fully characterize a waterbody. Numerical models can play a key role in understanding and extrapolating measured data. If a numerical model can accurately simulate the measured data from the waterbody, then the model may be used for further applications with confidence. A numerical model can be used to interpolate between observed data and to guide future data sampling efforts. By incorporating measured data in a numerical simulation, such as via data assimilation, even more reliable results can be produced from the numerical model. Data assimilation is becoming a powerful method in hydrodynamic and water quality modeling. Therefore, numerical models are essential tools not only for understanding the hydrodynamic and water quality processes, but also for developing plans for water resources and environmental management.

Numerical models are always a more or less schematized version of real systems, based on some hypotheses and descriptions of processes. The ability to describe water systems in mathematical equations and then in numerical models does not necessarily mean that the water processes are fully understood. Though they can deal with much more complex problems than

analytical models, numerical models still cannot include all the processes and mechanisms that may exist in a water system. In fact, there are many approximations made in numerical models that can lead to errors in the model. Empirical coefficients introduced into these approximations often increase the uncertainty of model results. Also, results of numerical models depend much on external forcings, which are from either measured data collected in the study area or another model. Errors in external forcings can significantly compromise model accuracy. For example, Ji et al. (2007a) reported that in the modeling of St. Lucie Estuary, errors in the freshwater inflow can cause significant errors in salinity simulation from time to time.

7.1.2 Model Selection

Albert Einstein once said, "Make everything as simple as possible, but not simpler." Model selection is the first step in a modeling application. Although a variety of models are available to the study of hydrodynamics and water quality, selecting a model that best matches the study needs is still a complex task. The goal of model selection is to choose a model (or models) capable of meeting all (or most) of the study objectives.

All models are, by definition, representations of actual processes. Assumptions are used to simplify the real system and can impose limitations on the model application. Therefore, it is essential to be familiar with model assumptions before selecting a model. Selection of an appropriate model requires consideration of (1) objectives of the study and (2) time and resources needed, including availability of data, technical expertise, and project cost.

An appropriate model (or models) should be selected based upon the study objectives, waterbody characteristics, available data, model characteristics, literature guidance, and regional experience. Model selection should also be balanced between competing demands. Since time and resources are always limited to one degree or another, the goals should be to identify the model(s) capable of addressing all of the important processes affecting the waterbody and to select the most useful one. Selection of a too simple model can result in the lack of accuracy and certainty that are needed in decisionmaking, while selection of an overly complex model may result in misdirected resources, study delays, and increased cost.

In the process of model selection, it is important to consider model availability and familiarity, documentation quality, technical support, and professional recognition and acceptance of a model. The technical expertise of the modelers is invaluable for specifying model parameters and critically evaluating model results. If a number of future projects will require the use of a particular model, it may be advantageous to use this particular model for the current project, even if the model is not necessarily the simplest one for this application. It is desirable to select a model that meets the most application requirements and has demonstrated applications and continuous support from the developer and user communities. It may be more beneficial to invest heavily in one model than to switch models from project to project. No "warm-

up period" is often a big advantage over learning a new model. It is advantageous to select a model that is well documented and is applicable to a variety of situations. As far the model configuration is concerned, the model should be written in modular form for consistency and easy update. If a model is widely used and accepted in the modeling community, it is easier to establish credibility of the modeling study and to interpret its results.

There is no single model for addressing all hydrodynamic and water quality problems. Each model has inherent assumptions and limitations that must be considered during model selection, application, and interpretation of results. Screening-level models are designed as highly simplified models with only a few state variables and limited key processes. These models are used to provide preliminary estimates of the water quality conditions. Since every waterbody is unique, models may require modification prior to use. Knowledge of the waterbody characteristics and the study objectives are crucial for model modification. It is important to use the model that is best for the study, not necessarily the model most familiar to the modeler. Familiarity with the model is important in model selection, but not to the exclusion of better models. It is helpful to ask the following questions in model selection:

1. What are the key hydrodynamic processes?
2. What are the water quality concerns?
3. What spatial and temporal scales are adequate for resolving these processes?
4. How will the model be used in supporting management decisionmaking?

It might be desirable to choose a simple model for a study. However, in real practice, comprehensive models are often preferred over simple models for a variety of reasons, especially for modeling large, complex water systems. Typical features of comprehensive models include (1) 3D and time dependent; (2) turbulence scheme for the vertical mixing; and (3) hydrodynamic, thermal, sediment, toxic, and eutrophication processes.

Generally speaking, comprehensive models should (but not always) have better mathematical, physical, chemical, and biological representations of water systems than simple models do. Comprehensive models can be applied at various levels of detail. In many cases, it is advantageous to adopt a more detailed model to address various scientific and engineering applications than to switch models from one phase of a project to another or from one project to another (Nix, 1990).

In modeling large, complex water systems, comprehensive models often have advantages over simple models because of the following factors: (1) the evolving understanding of the waterbody, (2) the management needs, (3) the falling costs of computing, and (4) the modelers.

The understanding of a waterbody gets better as the study progresses. A comprehensive understanding of the system is often achieved after the study is finished. Therefore, it is sometimes difficult to know exactly which simple model should be able to describe the system adequately at the beginning of

the study. Consequently, it is convenient to have a model that has the most capability (and potential) to describe the important features (known and to be known) of the system. In the event that the comprehensive model does not include a mechanism that is later found important in the waterbody, the model should already have a good framework for adding this new mechanism, since a comprehensive model generally represents the hydrodynamic and water quality situations better than simple models. The idea is to find a model that best fits the problem at hand and also provides the flexibility for further enhancement and development. An important rule is that comprehensive models can, in general, be applied to simpler systems, but simple models cannot be readily extended to systems more complex than those for which the models were designed.

The needs for supporting management decisionmaking might change frequently and cannot always be foreseeable, say for political reasons. It is necessary to choose a model that has the capability to meet these "expanded" needs. It is often more cost effective to choose a comprehensive model that has the potential to address the current and future needs than to use a simple model that is later revealed as inadequate and has to be replaced by a more advanced one.

The progress in computer technology has dramatically reduced the costs of computing, which makes comprehensive models more affordable. Many comprehensive models are now running on desktop computers. For example, all of the case studies in this book were conducted on PCs. Computer costs often become insignificant compared with the costs of other modeling efforts, such as field data sampling and manpower for modeling. The dramatic increasing in computer power also makes the comprehensive models more feasible in practical applications.

After all, modeling studies are conducted by modelers. A modeler often needs to study the hydrodynamic, sediment, toxic, and/or water quality processes in a variety of waterbodies, and needs models and tools that are versatile enough for these different applications. It is common that a modeler studies several waterbodies at a same time and finishes tens of modeling projects over years. Hence, it is understandable that the modelers would like to use (and understand well) a few models (one if possible), and apply them to most of the modeling studies. Instead of learning to use a variety of models for different applications, modelers often prefer to understand a few (or even one) comprehensive models well, stick with them, and apply them to address most of the modeling needs. It is cost effective to use one (or a limited set of) model, to provide sufficient human and financial resources for the model application, and to contribute to the scientific growth of the model.

Using a comprehensive model requires a modeler to have much training, skill, and experience. The modeler must have a full understanding of the limitations and assumptions of the model. Otherwise, using this model would simply be like running a black-box model. The major obstacles to the applications of comprehensive models include the following:

1. *Expertise.* Comprehensive models need well-trained and experienced modeling professionals, so that the models can be used appropriately and the results can be interpreted correctly.
2. *Measured Data.* Comprehensive models usually need more measured data for model calibration and verification than the simple models do. Data sampling can be expensive and historic data might not be adequate.
3. *Costs.* It usually takes more manpower to use comprehensive models than to use simple models. The relatively long computational time of comprehensive models adds extra costs to a study. For example, it typically takes hours of clock time to finish a one-year simulation in most of the case studies cited in this book.

There is still an important role for simple models that can be implemented quickly, need minimal data, and provide useful management support. However, comprehensive models are often more useful (and cost effective) in the modeling of large, complex water systems. The progress in computer technology, the enrichment of measured data, the enhancement of comprehensive models, and the growing need for supporting decisionmaking all point to this direction.

The studies on Lake Okeechobee are examples of models that began at relatively simple levels of complexity and have subsequently progressed to include more complex kinetics and spatial and temporal detail. The need to support management decisionmaking dictates the ever-increasing level of complexity in the questions being asked about the lake. The statistical models developed by Walker and Havens (1995) provided statistical analysis about the lake. The model later developed by James et al. (1997) was able to describe the spatial variations in the lake. The 3D and time-dependant LOEM (Jin and Ji, 2001, 2004, 2005; Ji and Jin, 2006; Jin et al., 2000, 2002, 2007), which is also used as case studies in this book, is able to address the spatial and temporal variations of the lake in detail and to meet the management needs.

A model must continually be updated and should never be "frozen" in time. It requires enormous amount of resources to maintain, update, and enhance a comprehensive model. Therefore, comprehensive models that are for general purposes, in the public domain, and available from or supported by public agencies (or organizations) are more likely to have competitive advantages in the long run. In support management decisionmaking, a single model might not be able to represent all the water quality components of interest and to explain the complex water quality processes of concern. In this case, a combination of models and tools might be needed.

7.1.3 Spatial Resolution and Temporal Resolution

Spatial and temporal resolutions are important characteristics of a numerical model. They affect the design and construction of the model grid and are related to each other. As the spatial resolution changes, the temporal

resolution (model time step) should be adjusted accordingly to achieve computational stability, accuracy, and efficiency.

The choice of spatial resolution requires considerable judgment and experience. Two critical factors are (1) the extent to which spatial gradients occur and (2) the extent to which these variations need to be considered from a management perspective. Competing factors often must be balanced, such as precision and cost. The spatial and temporal resolutions required for hydrodynamic and water quality modeling vary widely, depending on the water system studied and the processes involved. The rules of thumb are

1. Fine resolution reduces numerical errors in a model, but if the resolution is too fine, it can unnecessarily increase study costs with diminishing improvement to the model results.
2. Coarse resolution may reduce study costs, but if the resolution is too coarse, it can compromise model accuracy and results.

Even though a real water system is always 3D, it may be described by a model of 1D, 2D, or 3D, depending on the characteristics of the system. If the system's variation in a dimension can be considered insignificant or can be represented by averaged values, this spatial dimension can be eliminated from the modeling study. Averaging always leads to a loss in information. This cannot be completely avoided because averaging is essentially a filtering technique. The key is to have adequate resolution, so that the spatial gradients of water variables can be simulated realistically in the model. For example, a 1D river model only describes the spatial variations along the river, but neglects the cross-sectional and vertical variations. This kind of 1D model should be able to represent small and narrow rivers well, as is illustrated in the Blackstone River study in Sections 3.7.3 and 8.4.1. In estuaries, in addition to variations in the longitudinal dimension, those in the vertical are often significant to the simulation, since the saline water and freshwater often lead to vertical stratification. For wide estuaries with significant cross-sectional variations, 3D models are then needed.

Following the determination of an appropriate spatial resolution, the temporal resolution of the model should also be determined. There are no formal guidelines for selecting temporal resolution. The duration of a time-dependent simulation varies widely, typically ranging from weeks to years, and is usually determined by the following factors: (1) size of the study area, (2) flow conditions and water transport features, (3) water quality processes interested, (4) availability of measured data, and (5) needs for supporting decisionmaking.

A basic requirement is that the simulations should be long enough to eliminate the effect of the model's initial conditions. This ensures that errors in the initial conditions do not significantly affect model results. As discussed in Section 2.2.5, the errors from inappropriate initial conditions can be "forgotten" if the simulation is long enough. The flushing time of a waterbody is another reference for determining the minimum duration of simulations. The

period of water quality simulations may range from seasons to years, if seasonal and annual variations of sunlight, temperature, and external loadings are to be included.

Hydrodynamic processes normally control the selection of the model time step. The time step of a model should be small enough to ensure computational stability and convergency, which often reduces the time step length to be on the order of minutes or even seconds. With such small time steps required for hydrodynamic modeling, the model is most likely to have sufficient temporal resolution to represent other processes, such as sediment transport and water quality kinetics, in the waterbody.

7.2 STATISTICAL ANALYSES

Statistical analyses can be used in setting up model inputs, evaluating model performance, and understanding processes in waterbodies.

In a modeling study, it is critical to demonstrate that the model used is capable of representing the water system realistically. Model calibration is often accomplished through a subjective trial-and-error adjustment of model parameters until the model results fit the data well. The experience and judgment of the modeler are a major factor in calibrating a model accurately and efficiently. There are two general approaches for comparing model results with measured data: (1) qualitative comparisons and (2) quantitative comparisons.

Qualitative comparisons are usually based on visual comparisons of the model results with the data via time-series plots and spatial graphics for state variables, and then by determining whether the model reproduces observed patterns in time and in space. A seasoned modeler can examine the plots and form an experience-based judgment on the status of model calibration and verification.

Quantitative (or statistical) comparisons, on the other hand, utilize statistical analyses to give quantitative measures of how good the model results fit the data. Statistical analyses provide a different perspective on model–data comparison that numerically quantifies the state of the model calibration/verification (sometimes referred to as model skill assessment). Statistical analyses are simple to apply and yield well-defined quantitative measures of model performance.

Both approaches have their advantages and disadvantages. The qualitative comparisons are useful in presenting the patterns of model results in time and in space, but are highly subject to the experience and judgment of the modeler. The quantitative comparisons provide more objective measures of model performance, but are less effective in describing the patterns of model performance. The quantitative comparisons can also be significantly affected by the number, location, duration, and processing of the data (Spaulding et al., 2000). A combination of qualitative (visual) comparison and quantitative (statistical) comparison is a good approach for evaluating model performance.

7.2.1 Statistics for Model Performance Evaluation

Although numerous methods exist for analyzing and summarizing model performance, there is not a consensus in the modeling community about a standard set of measures for model performance evaluation. The following statistical variables are useful in model–data comparison for model calibration and verification: (1) mean error (ME), (2) mean absolute error (MAE), (3) root-mean-square (RMS) error, (4) relative error (RE), and (5) relative RMS error (RRE).

The ME is the mean difference between observed and predicted values:

$$\mathrm{ME} = \frac{1}{N}\sum_{n=1}^{N}(O^n - P^n) \tag{7.2.1}$$

where N = number of observation–prediction pairs, O^n = the value of the nth observed data, and P^n = the value of the nth predicted data.

A zero value of mean error is ideal. A nonzero value is an indication that the model may be biased toward either over or under prediction. A positive value indicates that, on average, the model predictions are less than the observations and the model tends to underpredict the observations. A negative value indicates that on average the model predictions are greater than the observed data, and the model tends to overpredict observations.

Only using the ME as the measure of model performance may give a false ideal value of zero (or near zero) and be misleading, if the average of the positive deviations is about equal to the average of the negative deviations. The two may cancel out each other and calculate an average close to zero. Because of this possibility, it is never a good idea to rely solely on this statistic as a measure of model performance. Other statistics are needed.

The MAE is defined as the mean absolute value of the differences between observed and predicted values:

$$\mathrm{MAE} = \frac{1}{N}\sum_{n=1}^{N}|O^n - P^n| \tag{7.2.2}$$

Although it provides no indication of overprediction or underprediction, MAE eliminates the canceling effects of positive and negative errors, and can be viewed as a more definitive measure of observation–prediction agreement. Unlike ME, MAE cannot give a false zero. The magnitude of the MAE indicates the average deviation between model predictions and observed data. An MAE of zero means that the predictions match the observations perfectly.

The RMS error or the standard deviation is the average of the squared differences between observed and predicted values:

$$\text{RMS Error} = \sqrt{\frac{1}{N}\sum_{n=1}^{N}(O^n - P^n)^2} \tag{7.2.3}$$

The RMS error is widely used to evaluate model performance. An RMS error of zero is ideal. The RMS error is an alternative to (and is usually larger than) MAE, and is a more rigorous measure of model performance. It looks like a weighted equivalent to MAE with larger observation–prediction differences given larger weightings.

The above three statistics, ME, MAE, and RMS error, all give absolute values of observation-prediction discrepancies. In the hydrodynamic and water quality modeling, however, it is often useful to express the discrepancies in percentage to measure the model performance. The RE is the ratio of the MAE to the observed mean and is expressed as:

$$\text{RE} = \frac{\text{MAE}}{\text{Observed Mean}} \times 100 = \frac{\frac{1}{N}\sum_{n=1}^{N}|O^n - P^n|}{\bar{O}} \times 100 \tag{7.2.4}$$

where $\bar{O} = \frac{1}{N}\sum_{n=1}^{N} O^n = \text{observed mean}$.

The RE provides the sense of how well the predictions compare to the mean values of the observations. In the modeling of surface waters, however, some state variables may have very large mean values and lead to very small relative errors, which can give a false impression that the model predictions are very accurate, even though the prediction errors might actually be unacceptable. For example, if a mean water temperature is 31 °C and the MAE is 3 °C, then the relative error is only 9.7% and looks acceptable. In reality, however, a MAE of 3 °C is unacceptable in most hydrodynamic and water quality modeling applications. In the modeling of Lake Tenkiller (Ji et al., 2004a), which is also described in Section 9.4.1, the lake has a mean water depth of 41 m at the dam. Even if the predicted water elevation is off by 3 m, the RE could still be only 7.3%, even though an MAE of 3 m would be absolutely unacceptable in the modeling study.

To overcome this shortcoming, the RRE is often used in hydrodynamic and water quality modeling and is defined as the ratio of RMS error to the observed change:

$$\text{RRE} = \frac{\text{RMS Error}}{\text{Observed Change}} \times 100 = \frac{\sqrt{\frac{1}{N}\sum_{n=1}^{N}(O^n - P^n)^2}}{O_{\max} - O_{\min}} \times 100 \tag{7.2.5}$$

where $O_{\max}$ = maximum value of observations and $O_{\min}$ = minimum value of observations.

The RRE is a useful measure of model performance in the modeling of rivers (Ji et al., 2002a), lakes (Jin and Ji, 2004, 2005; Ji et al., 2004a), and estuaries (Blumberg et al., 1999; Ji et al., 2001). The RRE is used extensively in the case studies presented in this book.

7.2.2 Correlation and Regression

There is often a need to know the relationship between two variables, such as the relationship between flow rate and sediment loading from a tributary to a lake. Correlation and regression analyses present the relationship in statistical terms (e.g., Ji and Chao, 1987).

The variance of a variable, s^2, is the average of the square of variable deviations from the variable mean, expressed as:

$$s^2 = \frac{1}{N}\sum_{n=1}^{N}(O^n - \bar{O})^2 \tag{7.2.6}$$

It measures the variability of the variable, that is, how values of the variable are spread about its mean value. The standard deviation, s, is defined as:

$$s = \sqrt{\frac{1}{N}\sum_{n=1}^{N}(O^n - \bar{O})^2} \tag{7.2.7}$$

that measures the typical difference of a variable value from the variable mean.

A correlation coefficient is calculated to quantitatively express the relationship between two variables and is defined as:

$$r = \frac{\sum_{n=1}^{N}(O^n - \bar{O})(P^n - \bar{P})}{\sqrt{\sum_{n=1}^{N}(O^n - \bar{O})^2}\sqrt{\sum_{n=1}^{N}(P^n - \bar{P})^2}} \tag{7.2.8}$$

where r = correlation coefficient, dimensionless and

$$\bar{P} = \frac{1}{N}\sum_{n=1}^{N}P^n = \text{predicted mean}$$

In model–data comparison, correlation coefficients can be a measure of how well the predicted values fit with the observed data. Correlation coefficients vary from 0 (random relationship) to 1 (perfect linear relationship) or –1 (perfect negative linear relationship). If there is no relationship between the predicted and the observed, the correlation coefficient is 0 or very small. As the strength of the relationship between the predicted and the observed increases, the value of the correlation coefficient approaches 1. Eq. (7.2.8) is for linear correlation. Nonlinear correlation, along with significance tests, is refereed to other sources (e.g., Press et al., 1992).

For example, Wang et al. (2003) calculated correlation coefficients between wind speed and SSC at four stations in Lake Okeechobee (Table 7.2.1). The locations of the four stations are shown in Fig. 2.4.2. The results clearly indicate that wind blowing on the lake has a strong effect on the variation of SSC. The

TABLE 7.2.1 Correlation Coefficients for Wind Speed/SSC and Wind Stress/SSC at Stations LZ40, L006, L001 and L005[a]

Stations	Wind Speed vs. SSC Bottom	Wind Stress vs. SSC Bottom	Wind Speed vs. SSC Middle	Wind Stress vs. SSC Middle	Wind Speed vs. SSC Surface[b]	Wind Stress vs. SSC Surface[b]
LZ40	0.715	0.691	0.756	0.744	N/A	N/A
L006	0.733	0.710	0.726	0.698	0.733	0.704
L001	0.700	0.705	0.683	0.680	N/A	N/A
L005	0.527	0.423	0.493	0.401	N/A	N/A

[a]Wang et al., 2003.
[b]N/A = SSC data are not available for calculating the correlation coefficient.

correlation coefficient between wind speed and SSC can be up to 0.756 at Station LZ40.

Regression analysis uses the best-fit approach to establish a mathematical relationship between two variables. In surface water studies, regression analysis is often utilized to establish a simple expression between two sets of measured data. Based on the expression, the values of one variable can be calculated from the other. An example is the relationship between flow rate and nutrient loading from tributaries. Correlation between these two variables is positive. After a regression expression is developed, the flow rate is often used to predict the nutrient loading.

A relationship between two variables is frequently assumed to be linear, and the regression equation can be expressed as:

$$y = a \cdot x + b \tag{7.2.9}$$

where x = the known variable; y = the variable to be calculated; a = slope of the regression line or regression coefficient, and b = intercept value.

Observed data are used to determine the values of a and b, so that Eq. (7.2.9) can fit the measured data (of y) with minimal errors. To measure how well the regression equation represents the relationship between the two variables, the correlation coefficient between the y values calculated from Eq. (7.2.9) and the y values observed is computed. The square of the correlation coefficient, r^2, is often used as an indicator of the goodness-of-fit of the linear regression relationship.

The method of least-squares regression is used to determine the values of the two unknown parameters, the slope (a) and the intercept (b) in Eq. (7.2.9). For a set of data, (x_i, y_i) with $i = 1, \ldots, N$, the least-squares regression ensures that Eq. (7.2.9) has the values of a and b, so that the line best fits the data points. This means that the error between the observed data and the line,

$$\text{error} = \sum_{n=1}^{N} (y_i - (ax_i + b))^2 \tag{7.2.10}$$

reaches a minimum. Mathematically, this can be achieved by differentiating the error with respect to the variables a and b and then setting them equal to zero. After some mathematical manipulations, one has

$$a\sum_{n=1}^{N} x_i^2 + b\sum_{n=1}^{N} x_i = \sum_{n=1}^{N} x_i y_i \tag{7.2.11}$$

$$a\sum_{n=1}^{N} x_i + bN = \sum_{n=1}^{N} y_i \tag{7.2.12}$$

Solving these two equations gives expressions for the coefficients a and b. This is the basis of the least-squares regression.

In modeling studies, regression formulations are often used to relate two variables and to provide loadings to the water quality model. For example, in the St Lucie study (AEE, 2004a), the nutrient concentrations in the tributaries that empty into the estuary are typically measured once or twice every month. From the concentrations and the flow rates, nutrient loadings to the estuary can be calculated. The problem is that the nutrient data sampling frequency of once or twice a month is insufficient for the water quality modeling. Therefore, instead of directly using the nutrient loadings calculated from the measured data, regression relationships between the flow rate and the nutrient loadings are established. Since the flow rates have daily values, the daily nutrient loadings to the estuary can be calculated using the regression equations and then be used as inputs to the model. Figure 7.2.1 gives the regression analysis results at Gordy, a station in the St. Lucie Estuary (AEE, 2004a). Similar regression expressions are also frequently used to estimate loadings of sediment and toxics to surface waters.

7.2.3 Spectral Analysis

Periodic phenomena are common in surface waters, such as diurnal and annual variations of water temperature and DO concentration. Tidal motions in estuaries and seiche motions in lakes are also periodic in time.

Spectral analysis is a useful tool for studying periodic variations in time and in space. Variations of a time series, such as temperature and water surface elevation, can be seen as a composition of periodic components with different frequencies. By analyzing the contributions of these components to the time series, the major frequencies (or periods) can be identified, which can be very helpful in understanding the characteristics of the waterbody. A time series can be decomposed into periodic components, a long-term trend, and random fluctuations. A crucial step for spectral analysis is to separate the periodic oscillations from the long-term trend and the random fluctuations, and to find the variance (energy) associated with the periodic components.

Fourier analysis is a commonly used method for spectral analysis. It extracts periodic signals from what may appear to be a very noisy time series or spatial

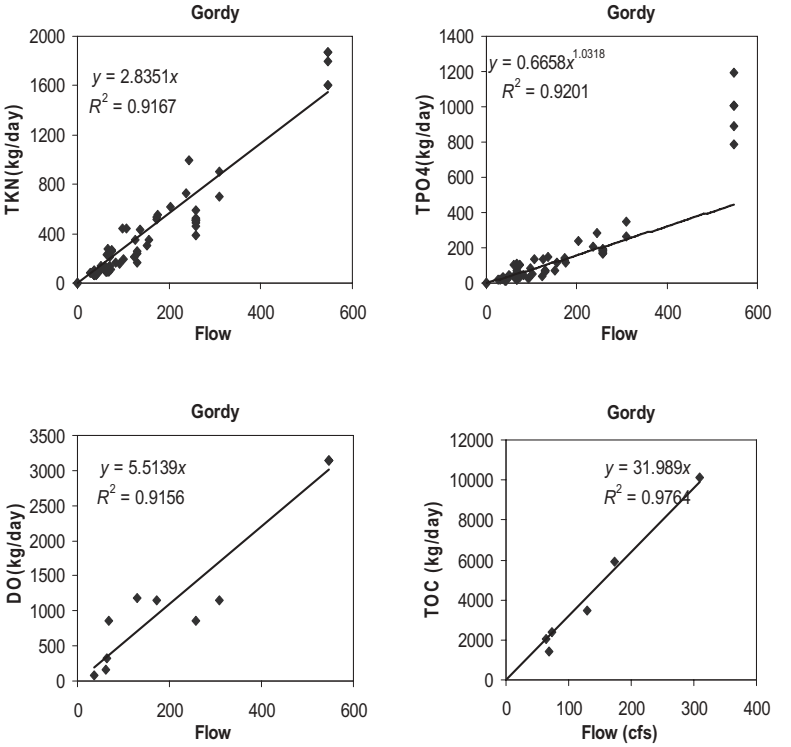

Fig. 7.2.1 Regression results for loadings at Gordy. Flow rates are in cubic feet per second (cfs).

series. For a time series, $\eta(t)$, having $2N$ values at times $t_n = t_1, t_2, \ldots t_{2N}$, the time series can be approximately represented as a combination of sine and cosine functions:

$$\eta(t_n) = a_0 + \sum_{k=1}^{N} [a_k \cos(\omega_k t_n) + b_k \sin(\omega_k t_n)] + \eta_0(t) \tag{7.2.13}$$

where t = time, a_0 = mean value of $\eta(t)$, a_k and b_k = constants (Fourier coefficients), ω_k = angular frequency of the kth periodic component, N = number of frequencies included in Eq. (7.2.13), and $\eta_0(t)$ = residual signal other than the periodic components.

The angular frequency, ω_k, is specified as:

$$\omega_k = \frac{2\pi k}{T} \tag{7.2.14}$$

where $T = 2N \times dt$ = duration of the time series and dt = time interval of the time series.

Equation (7.2.14) indicates that the specified frequencies are integer multiples of the fundamental frequency, $2\pi/T$. The Fourier coefficients, a_k and b_k, define the relative contribution that each oscillatory component of frequency ω_k makes to the time series. The corresponding period of ω_k, T_k, is

$$T_k = \frac{T}{k} = \frac{2N \cdot dt}{k} \tag{7.2.15}$$

Equation (7.2.13) can also be expressed as:

$$\eta(t_n) = a_0 + \sum_{k=1}^{N} A_k \cos\left[\frac{2\pi k}{T} t_n - \phi_k\right] + \eta_0(t) \tag{7.2.16}$$

where A_k = amplitude of the kth periodic component and φ_k = phase of the kth periodic component.

It has

$$A_k^2 = a_k^2 + b_k^2 \tag{7.2.17}$$

and

$$\phi_k = \arctan\left(\frac{b_k}{a_k}\right) \tag{7.2.18}$$

The Fourier transform in Eq. (7.2.13) describes the time series in the frequency domain. The amplitude, A_k, reveals which periodic components have the largest amplitudes (or energy), and therefore are the major contributors to the time series. A commonly used approach to carry out a Fourier transfer is by the Fast Fourier Transform (FFT) method, which is a fast numerical algorithm to determine the values of the coefficients a_k and b_k (Press et al., 1992).

For a time series with time interval of dt and duration of T ($= 2N \times dt$), Eq. (7.2.14) yields a critical frequency, f_c:

$$f_c = \frac{\omega_c}{2\pi} = \frac{1}{2dt} \tag{7.2.19}$$

where $\omega_c = \pi/dt = \omega_N$ = the highest frequency in Eq. (7.2.13). Equation (7.2.19) indicates that the highest frequency that can be represented by the spectral analysis corresponds to two sample points per cycle. Frequencies higher than f_c introduce distortion effects and should be treated as noise.

A good example is the spectral analysis of water surface elevations in Lake Okeechobee, FL (Ji and Jin, 2006). Lake Okeechobee (Fig. 2.4.2) is large (>50 km long) and shallow (a few meters deep). It is expected that seiche motions with periods of a few hours should be significant in the lake. The measured water surface elevations are saved in 15-min time intervals, so that

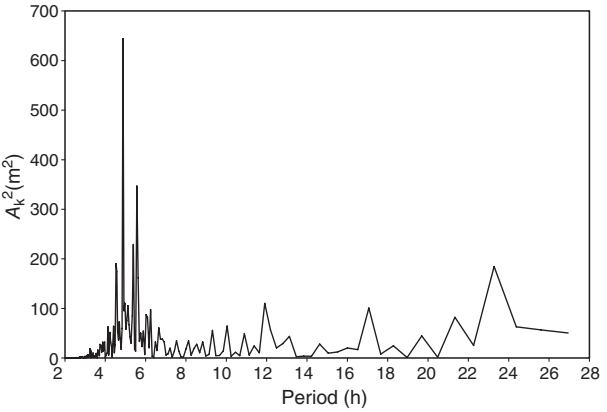

Fig. 7.2.2 Spectral analysis of measured water surface elevation in Lake Okeechobee.

motions with periods of a few hours can be resolved well. A total of 2048 samples ($T = 512$ h) are used to conduct the FFT. In Fig. 7.2.2, the horizontal axis is the harmonic period in hours, and the vertical axis is the squares of the harmonic amplitude in m^2, as defined in Eq. (7.2.17). The dominant feature of Fig. 7.2.2 is that the harmonic components with periods ~5 h are the strongest ones, which are caused by the seiche motions in the lake. More details on seiche motions are presented in Section 9.2.5.

The Fourier transform can also be used to remove unwanted frequencies, so that the harmonic components of interest can be revealed clearly. In this approach, the time series is first Fourier transformed, then the Fourier coefficients corresponding to the unwanted frequencies are set to zero. Finally, a time series is recomposed with the modified Fourier coefficients. For example, to study monthly and seasonal variations of water temperature, diurnal variations can be removed by setting the corresponding Fourier coefficients to zero.

7.2.4 Empirical Orthogonal Function

A key issue in data analysis is how to represent spatially and temporally varying data so that hydrodynamic and water quality processes can best be visualized. The empirical orthogonal function (EOF) method, also known as principal component analysis, is a useful tool for this purpose. The EOF method analyzes and reduces spatially and temporally varying data to a level that potential physical modes may be easily visualized. The EOF method: (1) provides a compact description of the data set in terms of orthogonal functions, (2) finds spatial patterns (or modes) of variability and their time variation, and (3) gives a measure of the importance of each mode. These modes are orthogonal in space and time and the first mode is the one with the largest variance (or energy). Usually, most of the variance of a data set is in the first few

orthogonal functions whose patterns may then be linked to possible hydrodynamic and/or water quality processes.

The EOF analysis is a transform of data and is similar to the Fourier analysis described in Section 7.2.3 in several ways. In both analyses, the original data are projected onto a set of orthogonal functions, even though the choice of the specific orthogonal functions is different. In the Fourier analysis, the orthogonal functions are a set of sines and cosines of various frequencies. This analysis is motivated by the desire to identify the principal modes of oscillation of the system. For a data set expressed in terms of space (x) and time (t), $\psi(x, t)$, the Fourier analysis yields

$$\psi(x,t) = \sum_{n=0}^{N}\left[a_n(t)\cos\left(\frac{2\pi n}{L}\right) + b_n(t)\sin\left(\frac{2\pi n}{L}\right)\right] \tag{7.2.20}$$

where $0 < x < L$. Equation (7.2.20) is similar to the Eq. (7.2.13), except that the former is projected onto Fourier series in space, whereas the latter is projected in time. Now, instead of being expressed as a function of space and time, the data set, $\psi(x, t)$, is expressed in terms of sines and cosines with different spatial wavelengths. The time dependence is expressed in the coefficients $a_n(t)$ and $b_n(t)$ that represent the amplitudes of $\cos(2\pi n/L)$ and $\sin(2\pi n/L)$.

The EOF analysis is conducted in a similar manner, except that the spatial functions, which are sines and cosines in a Fourier analysis, are now not specified beforehand but rather are determined by the data itself. In the EOF analysis, the data set, $\psi(x, t)$, at any given location x, is expressed as the sum of N orthogonal spatial functions $\varphi_i(x)$:

$$\psi(x,t) \approx \sum_{i=1}^{N} \mathrm{PC}_i(t)\phi_i(x) = \mathrm{PC}_1(t)\phi_1(x) + \mathrm{PC}_2(t)\phi_2(x) + \ldots + \mathrm{PC}_N(t)\phi_N(x) \tag{7.2.21}$$

where $\phi_i(x)$ = the ith EOF, nondimensional, $\mathrm{PC}_i(t)$ = the ith principal component (PC), with the dimension of $\psi(x, t)$, and N = number of EOF modes.

The EOF analysis decomposes the spatial and temporal variations of a data set into separate spatial patterns and time series. The spatial patterns of $\phi_i(x)$ are referred as the EOF. The time series of $\mathrm{PC}_i(t)$ are referred as principal components (or amplitudes). The parameter $\mathrm{PC}_i(t)$ represents the temporal variation of the spatial pattern descrbied by $\phi_i(x)$ and shows how the spatial pattern oscillates in time. The parameters $\mathrm{PC}_i(t)$ and $\phi_i(x)$ are calculated by requesting that the values of $\sum_{i=1}^{N} PC_i(t)\phi_i(x)$ best fit the values of $\psi(x, t)$, so that the overall difference between the two reaches the minimum. A number of literature citations (e.g., Preisendorfer, 1988) provide the details on how to calculate $\mathrm{PC}_i(t)$ and $\phi_i(x)$. The number of spatial points used in an EOF analysis is often much larger than the number of EOF modes needed. This is why Eq. (7.2.21) only gives approximate values of $\psi(x, t)$. Also, one should keep in

mind that EOF analysis is a mathematical analysis, and x and t can actually represent any variable. It is for the convenience of discussion to have x representing space and t representing time.

A major difference between the Fourier analysis and the EOF analysis is in the selection of the orthogonal functions. The term "empirical" indicates that the orthogonal functions vary from data set to data set and are not prespecified. In the EOF analysis, the orthogonal spatial functions, $\phi_i(x)$, are derived from the data set and are for the maximization of the projection of the data set on them, while in the Fourier analysis, the orthogonal functions are prespecified sines and cosines.

The EOFs are always orthogonal to each other and have

$$\sum_{k=1}^{N} [\phi_i(x_k)\phi_j(x_k)] = \delta_{ij} \tag{7.2.22}$$

where the Kronecker delta, δ_{ij}, is defined as:

$$\delta_{ij} = \begin{cases} 1, & i = j \\ 0, & i \neq j \end{cases} \tag{7.2.23}$$

The principal components, $PC_i(t)$, also are orthogonal to each other:

$$\sum_{m=1}^{M} [PC_i(t_m) PC_j(t_m)] = \lambda_i \delta_{ij} \tag{7.2.24}$$

where M = number of data values of a time series at a specified location and λ_i = variance of the ith EOF mode.

The total variance (or energy) of the data set can be expressed as:

$$\text{Total variance} = \sum_{i=1}^{TN} \lambda_i \tag{7.2.25}$$

where TN = total number of EOF modes.

The variance of the ith EOF mode in percent is calculated as:

$$\text{variance (\%)} = \frac{\lambda_i}{\sum_{i=1}^{TN} \lambda_i} \times 100 \tag{7.2.26}$$

Thus, the summed variance of the first N EOF modes is expressed as:

$$\text{Summed variance (\%)} = \frac{\sum_{i=1}^{N} \lambda_i}{\sum_{i=1}^{TN} \lambda_i} \times 100 \tag{7.2.27}$$

which represents the percentage of total variance (energy) that is captured by the first N EOFs. A useful EOF analysis should result in a decomposition of

the data set, in which a large percentage of the total variance is represented by the first few EOFs.

The EOF analysis separates a data set into orthogonal functions (or modes). Each mode has an associated variance (λ_i), nondimensional spatial pattern [or EOF, $\phi(x)$], and dimensional time series [or principal components, $PC_i(t)$]. The energy (variance) associated with each mode is ordered according to its corresponding EOF. The first mode contains the highest percentage of the total variance and represents the spatial pattern most frequently realized; the second mode explains the maximum amount of the variance remaining and is the one most commonly realized under the constraint of orthogonality to the first one; and so on.

The EOF analysis is an efficient way to represent a data set and provides the possibility of identifying modes that might be associated with relevant hydrodynamic and/or water quality processes. Since EOFs are ordered by decreasing variance values, the first of a few empirical modes can often account for most of the variance of the data set and can describe the major features of its variability. The EOF analysis is also often employed as a filter to remove unwanted scales of variability, if the summed variance of the first few modes in Eq. (7.2.21) is large enough to capture most of the total variance of the data set. A new and simpler version of the data set can be reconstructed with only the first few terms in Eq. (7.2.21), and the remaining terms are treated as random noise and are eliminated. In this sense, the EOF analysis is similar to the Fourier analysis used to filter out scales of unwanted variability.

It should be pointed out that, while the EOF analysis is an efficient way to decompose a data set, EOF modes do not necessarily correspond to any true hydrodynamic or water quality processes. The hydrodynamic and water processes are governed by the conservation laws and other principles, as discussed in the previous chapters of this book, while the EOF modes are simply results of a statistical analysis. Whether these modes are physically meaningful is subject to interpretation. Besides, one physical process may be reflected by several EOF modes, or more than one process may constitute the spatial pattern of one EOF mode.

7.2.5 EOF Case Study

An EOF analysis was applied to the study of Lake Okeechobee (Ji and Jin, 2006). The lake and its modeling using the LOEM are already discussed in the previous chapters. In this section, the EOF analysis is applied to the daily averaged velocities during the period from October 1, 1999, to September 30, 2000. The data set has 2121 locations (grid cells) and 365 time records (days) at each location, that is, $M = 365$ in Eq. (7.2.24). The EOF results of the modeled surface currents are presented here. Since the lake is well mixed most of the time (Jin and Ji, 2005), the EOF analysis on currents at lower levels yielded similar results.

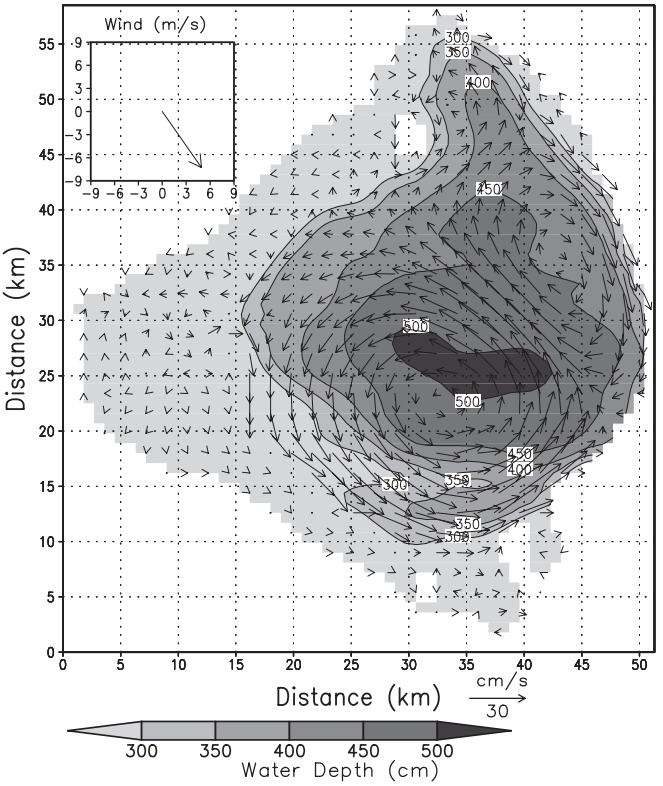

Fig. 7.2.3 Modeled water currents and water depth in Lake Okeechobee on December 25, 1999.

A distinct feature of Lake Okeechobee is the two-gyre pattern in the lake. Figure 7.2.3 shows the daily averaged surface currents and water depths on December 25, 1999, from the LOEM model. The small plot on the upper-left corner gives the daily averaged wind velocity. Under the northwest wind of 8 m/s, a typical wind in the area during winter, the lake has two distinct gyres: a cyclone (a counterclockwise rotation gyre) in the southwest of the lake and an anticyclone (a clockwise rotation gyre) in the northeast.

Figure 7.2.4 gives the mean lake circulations, obtained by averaging the modeled surface currents over 365 days, from October 1, 1999, to September 30, 2000. Figure 7.2.4 shows that the mean lake circulations also exhibit a two-gyre pattern, similar to the winter circulation pattern shown in Fig. 7.2.3. But the velocities of the mean circulations in Fig. 7.2.4 are much smaller than those in Fig. 7.2.3. The former has a typical speed of a few centimeters per second, while the latter can be >25 cm/s.

In order to delineate the major modes of variability in the lake, the modeled velocities were decomposed into EOF modes. The mean velocity field (Fig.

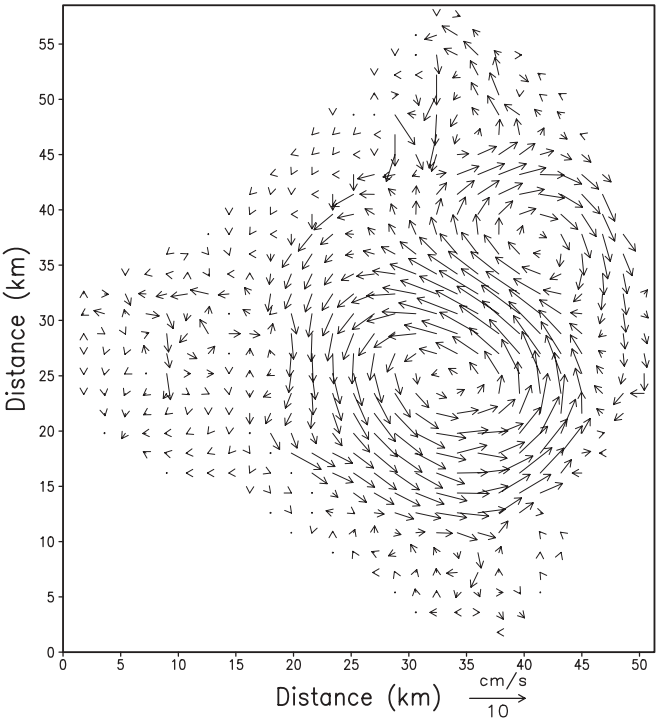

Fig. 7.2.4 Modeled surface currents averaged over 365 days, from October 1, 1999, to September 30, 2000.

TABLE 7.2.2 Variances of the First Seven EOF Modes of Currents in Lake Okeechobee

EOF Mode	Variance (%)	Summed Variance (%)
1	54.4	54.4
2	27.6	82.0
3	5.1	87.2
4	3.4	90.5
5	2.2	92.8
6	1.6	94.3
7	1.1	95.5

7.2.4) was removed before the EOF analysis was conducted. In Table 7.2.2, the variance is calculated using Eq. (7.2.26) and the summed variance is calculated using Eq. (7.2.27). The first seven EOF modes (Table 7.2.2) account for 95.5% of the total variance (or energy). When combined, the first two EOF modes (EOF1 and EOF2) explain >82% of the total variance. Individually, they explain 54.4% and 27.6% of the total variance, respectively. Since the

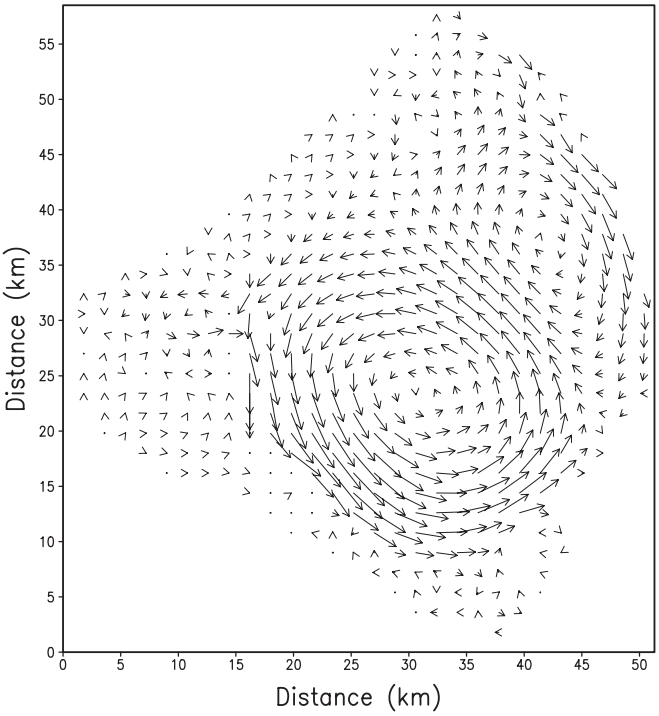

Fig. 7.2.5 Spatial patterns of the first EOF mode (EOF1) of surface currents.

mean velocity field (Fig. 7.2.4) is much smaller than the typical lake velocities, especially in the winter (e.g., Fig. 7.2.3), the first two EOF modes play a key role in explaining the major spatial patterns of the currents in the lake.

The first EOF mode (EOF1), shown in Fig. 7.2.5, exhibits a two-gyre pattern oriented along the northwest–southeast direction, and accounts for 54.4% of the total spatial variance (energy). This pattern can either strengthen the mean circulation pattern (Fig. 7.2.3) when the two are in the same phase, or weaken (or even reverse) the mean circulation pattern when the two are in the opposite phase. It is important to point out that even though the circulation pattern in Fig. 7.2.3 is similar to the one in Fig. 7.2.5, the two actually represent very different variables. Figure 7.2.3 gives the daily averaged flow field in the lake on December 25, 1999, while Fig. 7.2.5 represents the first EOF mode of the currents during the period from October 1, 1999, to September 30, 2000. The fact that the circulation patterns in these two figures are similar means that: (1) the flow pattern on December 25, 1999, shown in Fig. 7.2.3, is a typical winter circulation pattern in the lake, and (2) the two-gyre pattern in Fig. 7.2.5, derived from the EOF analysis, captures this circulation pattern very well.

The two-gyre pattern is one of the key hydrodynamic processes in the lake. The two gyres shown in Figs. 7.2.3 and 7.2.4 are primarily caused by the

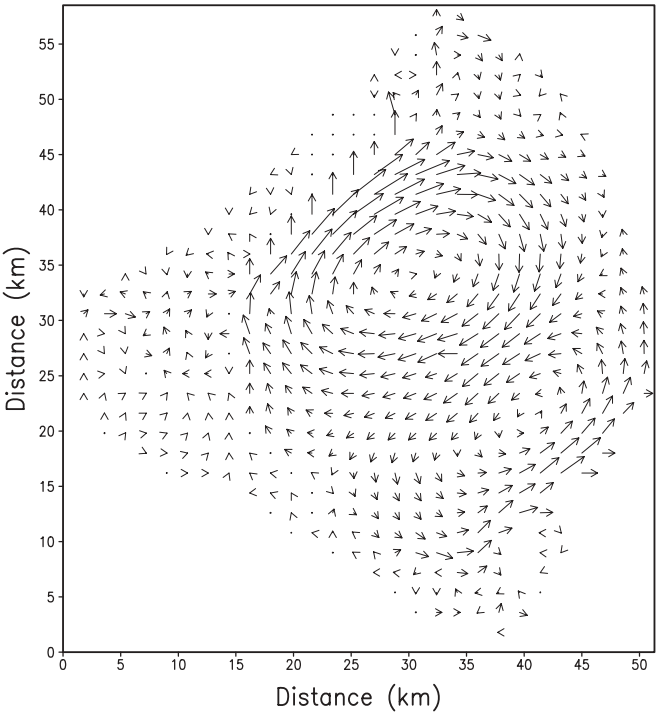

Fig. 7.2.6 Spatial patterns of the second EOF mode (EOF2) of surface currents.

northwest wind and the southeast wind in the area. Because the mean circulation pattern is weak (Fig. 7.2.3), EOF1 plays a significant role in the formation of the two-gyre pattern in the lake. More than one-half (54.4%) of the total energy of the currents is captured by the first EOF mode. The second EOF mode (EOF2) (Fig. 7.2.6) accounts for 27.6% of the total variance and also exhibits a two-gyre pattern. In this mode, the gyres are oriented along the southwest–northeast direction, which is approximately orthogonal (90° difference in angle) to the two-gyre pattern of EOF1. The EOF2 pattern is largely due to the southwest wind and northeast wind in the area. The mechanism for gyre formation in the lake will be discussed later in Section 9.2.4.

Figures 7.2.5 and 7.2.6 display the spatial patterns of the velocity modes. To describe flow velocity patterns at a specific time in the lake, the time series of the amplitudes, also called the PC, should be considered. Figure 7.2.7 gives the time series of principal components of the first mode (solid line) and the second mode (dotted line) of surface currents. Their amplitudes are normalized by the square root of the total variance. Figure 7.2.7 shows that the circulations in the lake have variations of several days. Compared with the measured wind velocity (Fig. 2.1.7), the two-gyre pattern is closely linked to the wind forcing. In Fig. 7.2.7, for example, large PC values ~ Day 15 corre-

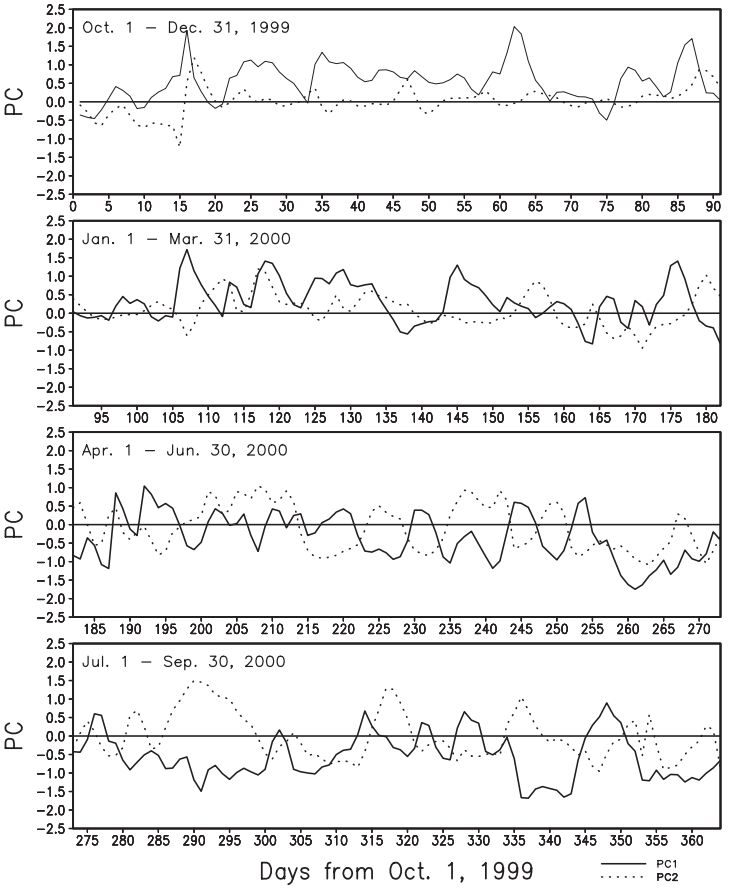

Fig. 7.2.7 Time series of principal components of the first mode (solid line) and the second mode (dotted line) of surface currents. Their amplitudes are normalized by the square root of the total variance.

spond to a hurricane event during that period (Fig. 2.1.7). Since the PC values are positive, the two-gyre pattern in Fig. 7.2.5 represents the true patterns in the lake, that is, a cyclone in the southwest area of the lake, and an anticyclone in the northeast area. Large negative values of PC1 ~ Day 260 indicate that the two-gyre pattern is opposite to the one shown in Fig. 7.2.5, that is, an anticyclone in the southwest and a cyclone in the northeast.

The second principal component represents a correction to the first EOF mode, that is, this mode provides for a slight change in the circulation patterns described by the first mode. For example, ~ Day 107, which corresponds to another strong wind event, the PC1 values are positive, while the PC2 values are negative. Both PC1 and PC2 are often out of phase in the summer and in the fall (Fig. 7.2.7). The combination of the first two modes constitutes a complicated circulation pattern in the lake.

Figure 7.2.7 indicates strong seasonal variation in lake circulations. Between Day 0 and Day 132 (October 1, 1999–February 10, 2000), the PC1 has positive values throughout the winter, except for a few short periods, whereas PC2 has values around zero. This difference strongly indicates that, in the winter, EOF1 is the dominant mode and EOF2 is much less significant, and the circulation pattern shown in Fig. 7.2.5 is the dominant circulation pattern. Large variations of PC1 and PC2 in the summer indicate that EOF1 and EOF2 both can be important in contributing to the circulation patterns in the summer.

7.3 MODEL CALIBRATION AND VERIFICATION

The comparison of model results to measured data is indispensable in model evaluation (or skill assessment). The measured data are either from the laboratory or the field. The objective is to calibrate the model to the observed data, utilizing parameter values that are consistent with the observed data and/or are within the general ranges of literature values. Successful evaluation is essential for developing a credible model for applications. By comparing a model's output against measured data, as illustrated in Fig. 7.3.1, the model can be calibrated, verified, and validated.

A key component in the modeling procedure is how the model parameters are derived and how the model results are interpreted to explain the physical, chemical, and/or biological processes in the waterbody. Treating a model as a black box is a recipe for failure. There is no model that can simply operate in a "plug and play" mode and that requires no calibration. There might be large differences between the modeled and the measured in the first simulations. It

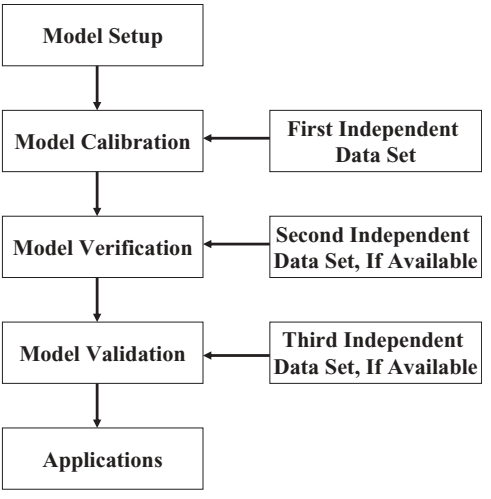

Fig. 7.3.1 Procedure of model calibration, verification, and validation.

is inappropriate to simply use questionable data as input to a model, and then to adopt the output as it is, without a basic understanding of the physical processes and without the knowledge of the model capabilities and limitations. The rule of "garbage in, garbage out" most certainly pertains to surface water modeling. In addition to adequately measured data, the success of model calibration also depends on the experience and skill of the modeler. This required combination is a primary reason why numerical modeling is also called an art.

As illustrated in Fig. 7.3.1, several steps are generally needed in a modeling study: model setup, model calibration, model verification, model validation, and model applications. These steps are associated with the development of a site-specific model. They are generic and can be modified according to available data and the complexity of the waterbody. The data required depend on the objectives of the study and the model selected. In setting up a model, a significant effort must be directed toward gathering and processing data used as input and for model–data comparison.

Model calibration is the adjustment of model parameter values within reasonable and acceptable ranges so that the deviations between the model results and the measured data are minimized and are within some acceptable ranges of accuracy. The deviations are often expressed in statistical variables, such as RMS errors defined by Eq. (7.2.3) and relative RMS errors defined by Eq. (7.2.5). The measured data for model calibration should be an independent data set that is not used in the model setup. The calibrated model is technically valid only for a particular scenario and data set.

Model verification is the subsequent testing of a calibrated model to a second independent data set, usually under different external conditions, to further examine the model's ability to realistically represent the waterbody. The verification process involves running the model with the calibrated parameters and comparing the results to the second independent data set. In some literatures, model verification is also called model validation.

Model calibration and verification provide information necessary to evaluate the accuracy and reliability of the results generated by a model. When a third independent data set is available, model validation can be performed to enhance the model's reliability of representing the waterbody (e.g., Jin and Ji, 2005; AEE 2005). The model developed can then be applied to investigate various operational and management alternatives. Care should still be given in applying the model outside the ranges used in the calibration, verification, and validation.

7.3.1 Model Calibration

Model calibration is generally discussed in this section. Specific procedures of how to calibrate a model are described in the case studies of this book. Mathematical models are generally developed for applications to a wide range of waterbodies for a variety of problems. It is difficult to recommend a general procedure for model calibration. Experience is an essential element in model

calibration. Each modeling study is unique and requires knowledge about the system under investigation.

Model calibration is necessary because of the semiempirical nature of hydrodynamic and water quality models. These models can be generally applied to a variety of waterbodies, since they are usually based on fundamental laws and principles, such as the conservation of mass and the conservation of momentum described in Section 2.1.2. However, some of the key processes, such as the bottom friction in hydrodynamic models and the kinetics in water quality models, are expressed in empirical formulas. A number of parameters in these empirical formulas either cannot be directly measured or have no measured data available in a specific waterbody. One step in the model calibration process is to adjust these model parameters (within reasonable ranges) to enable the model to reproduce measured data (with acceptable accuracy). Whereas the mathematical formulation of a model is more related to science, model calibration has aspects more related to art. The ability of the model to represent a waterbody often depends on how well the model is calibrated. The overall objective is to calibrate the model to the observed data using a set of model parameters that are consistent with the observed data and are within the general ranges of values reported in the literature.

Model calibration is the first stage of tuning a model with a set of field data not used in the model setup. Model calibration is also the process of determining model parameters. When measured data are available, model parameters can be estimated using curve-fitting procedures. The model parameters may also be obtained through a series of test runs. Comparisons are made between model results and measured data graphically and statistically to assess model performance. The value of a model parameter is chosen in a trial-and-error procedure within an acceptable range for the parameter. This process continues until a reasonable reproduction of the observed data is attained or no further improvement is possible. Model parameters should be spatially and temporally uniform, unless there are specific data or information indicating otherwise. Setting model parameters to vary from one model grid to the next to match model results with data is poor practice. Physical, chemical, and biological processes should be consistent over space and time.

Calibration of water quality models is usually more time consuming. As indicated in Chapter 5, many parameters related to algal growth and nutrient recycling are difficult, if not impossible, to determine by measured data. The practical approach of assigning them is to rely on literature values, model calibration, and sensitivity analysis. That is, the parameters are selected from literature values, preferably from previous studies with similar settings. Subsequent model runs are carried out to fine tune these parameters by matching model results with the measured data. Sensitivity analysis, which will be presented in Section 7.3.3, is often performed to clarify the model's reliability.

In model calibration and verification, one of the most perplexing questions is "How good is the model?". This question is generally tackled by comparing model results with measured data via two approaches: graphic comparison and

statistical comparison. No generally accepted criteria exist to measure the accuracy of model results. Whether the model's performance is acceptable depends on study objectives, sensitivity of study outcomes to model results, and reliability of measured data. As stated in Section 7.2.1, the following statistical variables are useful for model calibration and verification: (1) mean error, (2) mean absolute error, (3) RMS error, (4) relative error, and (5) RRE.

In the event that the model cannot be calibrated with acceptable accuracy, possible causes include (1) the model is misused or the model is not setup properly, (2) the model is inadequate for this type of application, (3) there are insufficient data to describe the waterbody, and (4) the measured data are not reliable.

A model is a numerical representation of a waterbody. The formulations used in the model should be continuously tested against measured data. If a formulation fails to describe the processes, then either the formulation should be modified or a new one should be developed. For example, a model with the hydrostatic approximation cannot be used to simulate convective plumes from wastewater discharge diffusers, as discussed in Section 2.2.1. There should be sufficient layers to resolve vertical stratifications and adequate lateral grid cells to resolve horizontal circulations (Ji et al., 2004a). Two (not one) algae groups are usually needed to represent algal blooms that occur twice in a year. When SAV plays a significant role in the eutrophication process, the water quality model then should include a SAV mechanism. If pH is an important factor for the fate of toxic metals, then this mechanism should be included in the model. It requires an experienced modeler to determine whether model formulations are inadequate.

Another possible cause of large model errors can be the lack of data to describe the waterbody adequately. For example, the bathymetry data is inaccurate, or the nutrient loadings to the system are incomplete. Wind forcing may play a critical role in stratification, but there may be no accurate wind data available in the study area. An important assumption in model calibration, though rarely stated explicitly, is that the measured data are without error or uncertainty. This is not always true. Errors in measured data, caused by instrument failures or human error, may contribute to large model–data differences. These types of errors may be identified by judgment according to basic physical principles, the experience of the modeler, and/or comparison of the data against data at nearby stations, and so on. For example, surface water temperature in the summer should generally be higher than the bottom temperature most of the time, and surface sediment concentration should generally be lower than that at the bottom. When this type of data error is identified, the data should be removed from model–data comparison.

Hydrodynamic and water quality models are often used as water resource management tools, which are usually interested in spatial scale of much larger than model grid size and temporal scale of seasons or longer. A model may not give accurate simulations of short-term variations but may still capture the

long-term trend of the water system. In this case, the model can still be useful in determining the system's long-term changes and providing meaningful answers to support decisionmaking.

7.3.2 Model Verification and Validation

A calibrated model does not mean that the model has predictive capability. Calibration alone is insufficient to determine the capability of a model to simulate a waterbody. The model may contain incorrect mechanisms, and the consistency between model results and measured data could be the result of unrealistic parameter values. A set of parameters used in model calibration may not represent the waterbody under a different set of external loadings and/or boundary conditions. Furthermore, certain mechanisms that could be the keys to the future conditions of the system may not even be included in the model.

If a model is used to simulate a waterbody with insufficient measured data, the simulation can be speculative and less credible. If the model is calibrated to an independent data set with acceptable accuracy, the model results would be more reliable. Model verification is to confirm that the calibrated model is useful over an extensive range of conditions in the waterbody. Therefore, it is essential that the data sets for calibration and verification cover the range of waterbody conditions over which model predictions are intended.

Model verification uses an independent data set (the second data set that is not used in model setup, as shown in Fig. 7.3.1). Model verification helps establish greater confidence in the model's capability of predicting future conditions of the system. Values of model parameters obtained from model calibration are not adjusted in the verification phase, and the model results are evaluated graphically and statistically in the same manner used for model calibration, but with a different data set. An acceptable verification demonstrates that the model is capable of simulating the waterbody under different external conditions.

The verified model is still limited to the range of conditions defined by the data sets used in the calibration and verification procedures. Any model prediction outside this range remains uncertain. To enhance the model's credibility, a third data set, if available, should be used to validate the model (Fig. 7.3.1). For example, the LOEM was calibrated with 2000 data, verified with 2001 data, and validated with 2002 data (AEE, 2005). The LOEM results are presented in the chapters throughout this book.

Strictly speaking, model verification means that, with the same parameters obtained through the model calibration, the model is rerun and its output is compared with the second independent data set. In some cases, however, parameter values may have to be adjusted slightly to match the model results with the verification data. For example, some water quality parameters obtained through calibration against conditions in winter (or in a dry year) may not be calibrated well until the verification data in summer (or in a wet year) is used.

In this case, the changes of parameters should be consistent, reasonable, and scientifically defensible. If the model parameters are changed during the verification, the changed parameters should be tested again with the calibration data set.

One type of model evaluation that is often ignored is the model post audit. Generally, a model is calibrated, verified, and even validated, and then applied to certain scenarios to support management decisionmaking, such as calculations of TMDLs. This process is often the end of most modeling studies. There are very few cases in which modeling studies are performed after the implementation of the decisions to check whether the model calculations were accurate and management decisions were appropriate. However, without model postaudit, the overall success (or failure) of a modeling study often cannot be accurately assessed (USEPA, 1990).

7.3.3 Sensitivity Analysis

Model sensitivity to variations in model parameters is an important characteristic of a model. Sensitivity analysis is used to find out how model results vary as model parameters are changed and to identify the most influential parameters in determining the accuracy of model results (e.g., Price et al., 2004). Natural waters inherently have complex, random, and nonlinear processes that cannot be accurately represented mathematically. Model formulations are a compromise between the reality of the waterbody and the approximation of the numerical representation. The accuracy of model output is influenced by a number of uncertainties from measured data, model formulations, and model parameters. Sensitivity analysis is a useful tool to clarify the relationship between uncertainty in parameter values and model results. Sensitivity analysis should be an indispensable component of surface water modeling.

Sensitivity analysis quantitatively examines the changes in model results with respect to changes in model parameters. Typically, sensitivity analysis is performed by changing one model parameter at a time and evaluating the effects on model results. Parameters and input data are varied individually by constant percentages to determine which parameter, initial condition, or boundary condition causes the greatest change in the model results. For simple models with a few parameters, sensitivity analyses are generally straightforward. However, for complex models, sensitivity analyses can be complicated, since there may be nonlinear interactions involved. If the change in a parameter causes a large change in the model results, the model is then considered to be sensitive to that parameter.

Sensitivity analysis can indicate the relative contributions of processes to variations in model results. It may provide insight into the need for additional data collection to refine the estimate of certain loadings, initial conditions, or reaction rates. For example, the cause of low DO can be identified from the contributions of SOD, external loadings, decay of organic carbon, photosyn-

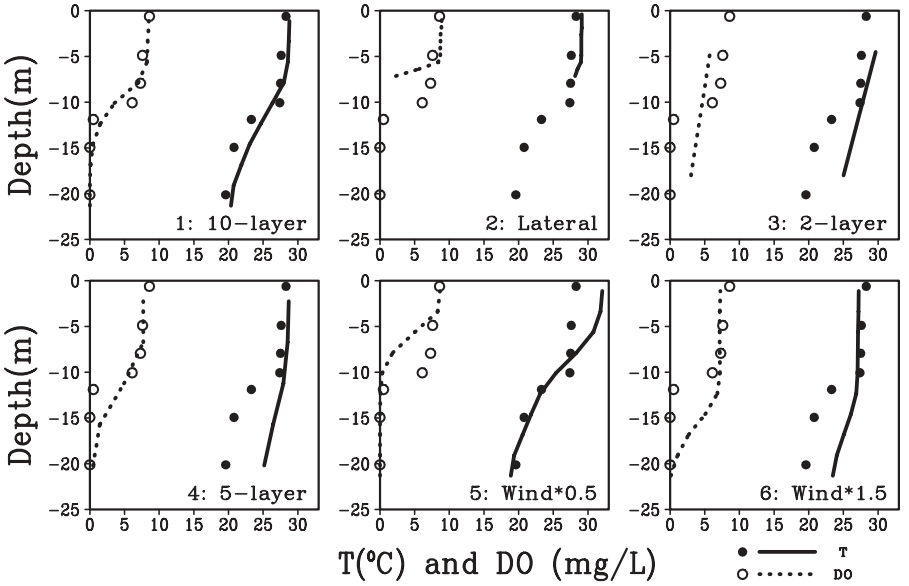

Fig. 7.3.2 Vertical profiles of water temperature (T) and dissolved oxygen (DO) at OKN0165 on August 12, 1986, in 6 different cases. Case 1: 10-layer model, Case 2: lateral cell, Case 3: 2-layer model, Case 4: 5-layer model, Case 5: wind speed reduced by 50%, and Case 6: wind speed increased by 50%.

thesis, nitrification, and/or reaeration. In this case, the ranking can be used to determine which parameters should have higher priority for accuracy. For example, if the DO concentration is sensitive to SOD, then SOD used in the model should either be specified by measured data or be carefully calibrated and verified against measured data, so that the SOD error in the model can be minimized.

Figure 7.3.2 is an illustration of the sensitivity of the Lake Tenkiller model to spatial resolution and wind forcing (Ji et al., 2004a). It gives vertical profiles of water temperature (T) and DO for six different cases:

1. Bench mark results from a 10-layer model.
2. T and DO at a lateral grid cell.
3. T and DO from a 2-layer model.
4. T and DO from a 5-layer model.
5. T and DO with wind speed reduced by 50%.
6. T and DO with wind speed increased by 50%.

Major findings from these sensitivity tests are that (1) 3D modeling is critical to the Lake Tenkiller modeling, and (2) the lake stratification is very sensitive to wind forcing. Section 9.4.1 gives more results on Lake Tenkiller modeling.

CHAPTER 8

Rivers

A river is a naturally flowing waterbody that usually empties into an ocean, lake, or another river. Small rivers are also called streams or brooks.

The general theories and processes of hydrodynamics, sediment transport, pathogens and toxics, and water quality are already presented in Chapters 2–5, respectively. This chapter describes the characteristics of rivers and the hydrodynamic, sediment, and water quality processes in rivers. The modeling of rivers is then presented through two case studies.

8.1 CHARACTERISTICS OF RIVERS

Compared with lakes and estuaries, the most distinct characteristic of a river is its natural downstream flow. Lakes typically have much smaller flow velocities than rivers. Flow velocities in estuaries, though their magnitudes can be comparable to the ones in rivers, are tidally driven and can be in either direction (downstream or upstream). Rivers are complex and dynamic. The health of a river is directly linked to the health of the surrounding watershed. The water quality in a river will deteriorate, if the watershed condition deteriorates. The common designated uses of a river include aquatic life support, water supply, and recreation activities (e.g., swimming, fishing, and boating).

A river often acts as a sink for contaminants discharged along the river, such as effluents from wastewater treatment plants that discharge nutrients, heavy metals, and/or pathogens into the river. Rivers may also act as sinks and sources in the watershed, depending on the time of the year or the section of the river. For example, sediments and heavy metals deposited behind the dams on the Blackstone River, MA, up to 200 years ago can still be released back into the water column during a flood event and become a significant source of contaminants (Ji et al., 2002a).

A tributary is a river or stream that flows into a larger waterbody (another river, lake, or estuary). A river basin is the drainage area of a river and its tributaries. The rivers and their tributaries, normally occupying less than a few

Hydrodynamics and Water Quality: Modeling Rivers, Lakes, and Estuaries, by Zhen-Gang Ji

percent of the total drainage basin, are the conduits of the river basin. They are like a gutter system and transport water, nutrients, sediment, and toxicants downstream (often to an estuary or a large lake). Via rivers, pollutants from point or nonpoint sources can travel hundreds or even thousands of kilometers and cause environmental problems in a waterbody that is located far away from the sources.

River characteristics can change significantly over time in response to human activities and changing climatic and hydrologic conditions. Rivers vary widely by morphological, hydraulic, and ecological characteristics, including (1) river slope, width, and depth; (2) flow rate and flow velocity; (3) water temperature; (4) sediment transport and contaminants deposition; and (5) nutrient inflows and eutrophication processes.

Rivers are very diversified, ranging from the deep, slow-flowing lower Mississippi to the shallow, rapid mountain streams of the Rockies. As shown in Fig. 8.1.1, the longitudinal profile of a river can generally be split into three zones (Schumm, 1977; Miller, 1990; FISRWG, 1998): (1) headwater zone, (2) transfer zone, and (3) depositional zone.

Rivers often start at a natural spring or a snowmelt (e.g., a glacier), thus the headwater zone is the early course of a river and is often in steep, mountain areas with rapidly flowing cold water. River slope is measured as the difference in elevation between two points in the river divided by the river length between the two points. The headwater tributaries collect water and sediment from the watershed as they flow into the river. As a river continues along its course, the surrounding terrain flattens out and the river widens. The transfer zone receives

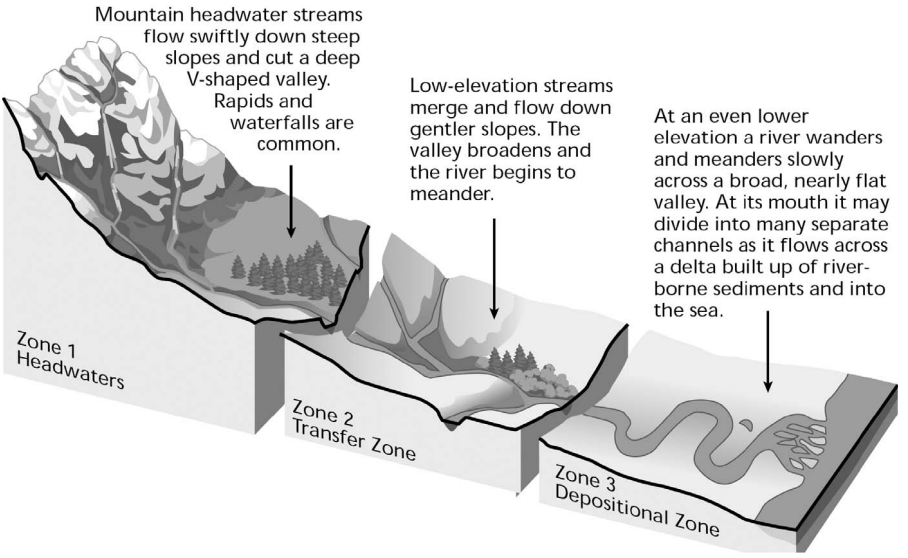

Fig. 8.1.1 A longitudinal profile of a river (from FISRWG, 1998).

some of the eroded material and nutrients from the headwater zone, and is characterized by wider floodplains and gentler downstream flows. The river begins to meander in the transfer zone.

Most rivers end when they flow into an ocean, a lake, or another river. The end of the river is called the river mouth. The depositional zone is characterized by lower slope, increased sediment deposition, broader floodplains, and greater flow rate. The river meanders slowly across a broad, nearly flat valley. The slower flow and larger floodplain allow vegetation and biological communities to thrive. The river-borne sediment is deposited at the river mouth and a large, alluvial area is created. The new land, which is often triangularly shaped, is called a delta, originated from the Greek letter "delta" that is shaped like a triangle. At its mouth, the river may divide into different slow-flowing channels, as it flows across a delta and into the ocean (FISRWG, 1998).

The cross-section (or lateral profile) of a river depicts the shape of the channel in which a river flows. The cross-sectional area is the wet area of the river normal to the direction of flow. Even among different types of rivers, common characteristics of cross-sections are observable from headwaters to the river mouth. As shown in Fig. 8.1.2, cross-sections of most rivers have two major components: a main channel and a floodplain. The main channel is a trench in which a river flows for most of the year. The channel width and depth increase downstream due to the increasing drainage area and discharge. Water and sediment in the river may influence the formation and alteration of the channel. A floodplain is a highly variable area on one or both sides of a main channel. It is dry for most of the year and is inundated by floodwaters at the high water stage. A floodplain is often seasonally inundated and has plants, such as emergent marshes and a floodplain forest. In river models, flows are usually transported in the main channel. The seasonal inundation of a floodplain can be realistically simulated in models that are capable of representing the wetting and drying variations (e.g., Ji et al., 2001).

Point and nonpoint sources have caused a wide range of water quality problems and the deterioration of the ecological state in rivers. Leading pollutants and stressors in the United States include (USEPA, 2000a):

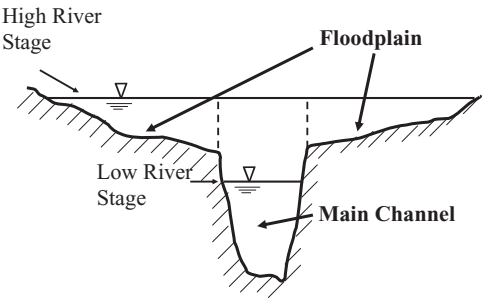

Fig. 8.1.2 A typical cross-section (lateral profile) of a river.

(1) pathogens (bacteria), (2) siltation, (3) habitat alterations, (4) oxygen-depleting substances, (5) nutrients, (6) thermal modifications, (7) toxic metals, and (8) flow alterations.

Pathogens are the most common pollutant affecting rivers and streams in the United States. Bacteria are used as indicators to provide evidence of possible fecal contamination and to determine if rivers are safe for swimming and drinking. Pathogen pollution is a major public health problem especially in the use of river water for water supply and the consumption of fish and shellfish harvested in rivers and estuaries. Bacteria commonly enter surface waters in inadequately treated sewage, fecal material from wildlife, and runoff from pastures, feedlots, and urban areas.

Siltation is the deposition and accumulation of sediment in a waterbody. In the United States, siltation is one of the most widespread pollution problems in rivers (USEPA, 2000a). Suspended matter discharged from sewers and storm sewers and from nonpoint sources change sediment conditions in rivers and affect the living conditions for benthic plants and animals. As shown in Fig. 8.1.3, siltation alters aquatic habitat and suffocates fish eggs and bottom-dwelling organisms. Suspended sediment blocks sunlight and depresses growth of beneficial aquatic vegetations. Excessive siltation can also impair drinking

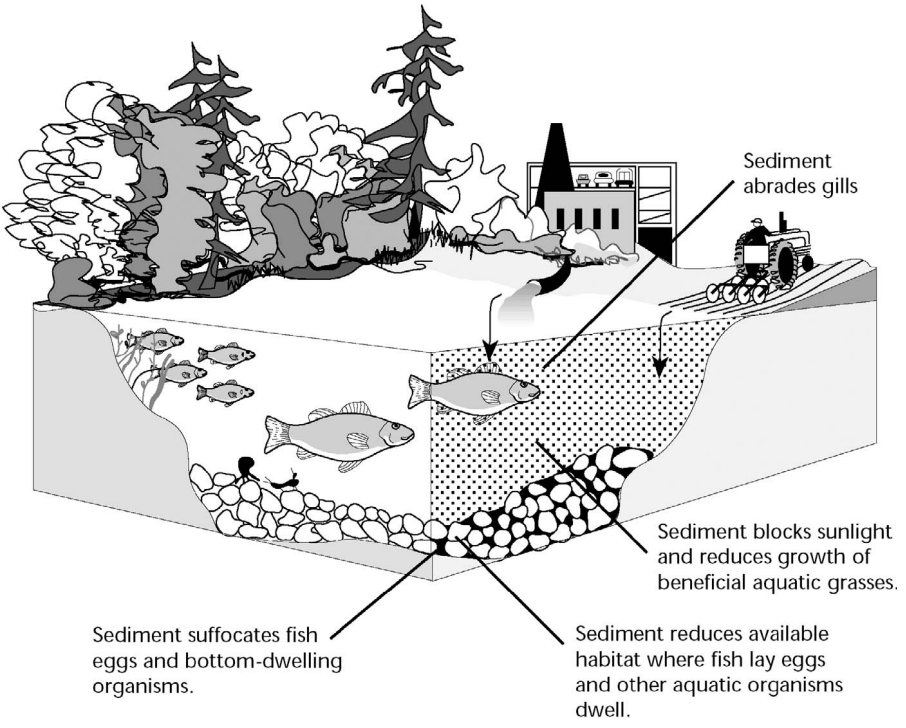

Fig. 8.1.3 Effects of siltation in rivers (USEPA, 2000a).

water treatment processes and recreational use of a river. Over the long-term, unchecked siltation can alter habitat with profound adverse effects on aquatic life. Major sources of siltation include runoff from agricultural lands, forestry operations, and urban areas.

Often, several pollutants and stressors impact a single river reach. For example, habitat modifications can make a river less suitable for inhabitation. Development in urban areas can increase erosion that results in higher sediment runoff to rivers. Discharges from power plant cooling water can elevate river temperature and have a significant impact on a river ecosystem. Effluents from wastewater treatment plants can increase concentrations of toxic chemicals and metals. Excessive levels of nitrogen and phosphorus can cause eutrophication in rivers, depleting the DO concentration needed for fish and beneficial vegetations. Pollutants in rivers can flow to lakes and estuaries and impair water qualities in these waterbodies.

8.2 HYDRODYNAMIC PROCESSES IN RIVERS

Rivers have distinct hydrodynamic characteristics that are different from those of lakes or estuaries. This section focuses on the following: (1) river flow and the Manning equation, (2) advection and dispersion processes in rivers, and (3) flow over dams.

8.2.1 River Flow and the Manning Equation

The flow rate of a river is the volume of water that passes a cross-section of the river in a unit of time, which is usually expressed in cms or cubic feet per second (cfs) and is calculated as:

$$Q = AV \tag{8.2.1}$$

where Q = flow rate in cms or cfs, A = area through which the water is flowing in m^2 or ft^2, and V = average velocity in the downstream direction in m/s or ft/s.

The river flow can generally be separated into two components: (1) base flow and (2) storm flow. Base flow is composed largely of groundwater effluent and sustains river flow during dry weather periods. Storm flow is from the runoff during or shortly after a precipitation event. As described in Section 1.1 on the water cycle, the ultimate source of all flows is precipitation. The water from base flow is the precipitation that percolates into the ground and flows slowly through a long path before reaching the river, whereas the water from storm flow is the precipitation that reaches the river shortly after precipitation through runoff. In addition to base flow from the groundwater and the storm flow from the runoff, point sources, such as wastewater treatment plant discharges and tributaries to the river, also contribute to a river flow.

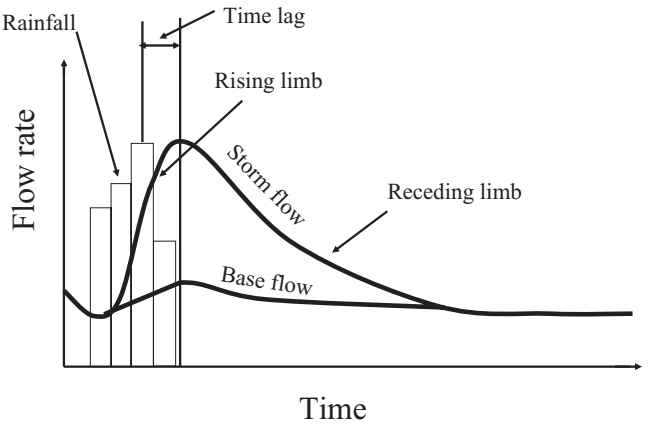

Fig. 8.2.1 A storm hydrograph of a river.

A hydrograph is a graph showing time variation in flow rate or stage (depth) of water in a river. As sketched in Fig. 8.2.1, the river flow is composed of the storm flow and the base flow. After the beginning of a rainfall, the storm flow from runoff starts to increase and reaches its peak some time after the peak rainfall. There is a time lag between the two peaks. The rising limb is the portion of the hydrograph to the left of the peak of the storm flow, which shows how long the river takes to reach its peak flow rate after a rainfall event. The receding limb is the portion of the hydrograph to the right of the peak, which shows how long the river takes to return to the base flow.

Interactions between groundwater and the river vary throughout the watershed. The water table is the top of the water surface in the saturated part of an aquifer. In Fig. 8.2.2*a*, a river receives water from the groundwater flow when the water table is higher than the water level of the river. In this case, the groundwater provides the base flow of the river. When the water table is lower than the water level, the river loses water to the aquifer (Fig. 8.2.2*b*).

High and low flow extremes of a river are usually described statistically. Flow frequency represents the average time interval between occurrences of annual maximum flow rate of a given or greater magnitude. It indicates the probability of exceeding a given flow rate in any given year. For example, if the 100-year recurrence interval flood in a river is given as 1000 cms, a flood of this magnitude or greater will occur, on average, once in 100 years. It means that in any single year, the annual flood flow has a 1% chance, or 0.01 probability, of exceeding the 100-year flood.

In addition to flood events, low flow conditions are also important characteristics of a river. When there is no precipitation contributing to the storm flow, and the base flow from groundwater is low, the river experiences low flow conditions. Low flow results in less water available for dilution of pollutants from point sources, causing high pollutant concentrations in the river. There-

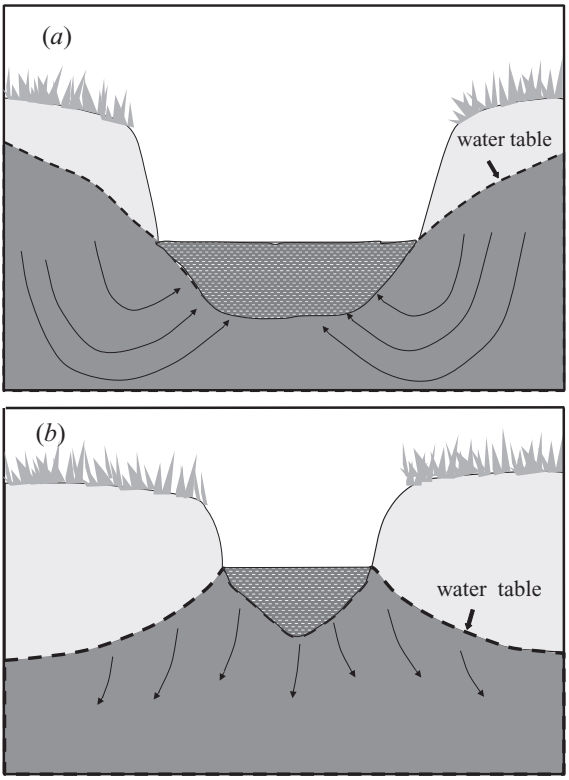

Fig. 8.2.2 Interactions between a river and the groundwater: (*a*) the river gains water from the aquifer, and (*b*) the river loses water to the aquifer.

fore, point source discharges during low flow conditions have the most significant impact on the river's water quality, since the discharge may constitute a larger percentage of river flow. For example, wastewater discharges to the Blackstone River can account for up to 80% of the total river flow in summer (Ji et al., 2002a).

A common parameter for representing low flow condition is the 7Q10 flow, which is the lowest 7-day average flow rate occurring once in 10 years. This probability-based statistic is frequently used in evaluating the impact of point sources on river water quality. For example, the NPDES permits (USEPA, 1993) are often based on the 7Q10 flow. In addition to 7Q10, other types of flows can be estimated from a hydrologic record. For example, the minimum average 7-day flow in a year (7Q1) can be estimated, or the minimum average flow in a given month or season can be computed.

As described in Chapter 2, a hydrodynamic model based on momentum and continuity equations is often used to calculate flow velocity, flow rate, and water depth in a waterbody. A simpler approach to calculate these parameters

is to use the Manning equation, which is an empirical formulation relating velocity (or flow rate), depth, slope, and a channel roughness coefficient in a river. The Manning equation was derived by curve-fitting data measured in rivers and channels. The equation is

$$V = \frac{Q}{A} = \frac{R^{2/3} S^{1/2}}{n} \tag{8.2.2}$$

where V = mean flow velocity (m/s), Q = flow rate (m^3/s), A = cross-sectional area (m^2), R = hydraulic radius (m), S = slope of the channel bed (m/m), and n = Manning roughness coefficient.

The hydraulic radius is defined as:

$$R = \frac{A}{P} \tag{8.2.3}$$

where P is the wetted perimeter in m, which is the length of contact of the water with the channel in m, measured in a direction normal to the flow. The Manning roughness coefficient, n, represents the channel roughness that contributes to the dissipation of flow energy. Table 8.2.1 shows a range of n values for various channels and rivers.

Originally, the Manning equation was developed in the 1880s for uniform flows with constant channel slope, water depth, and hydraulic radius. The Manning equation involves only one coefficient (n) and provides good physical insight into channel flows by integrating the effects of slope and channel geometry. Today, the Manning equation is still widely used in hydraulic calculations with reasonable accuracy. The Manning equation is often used to determine the water surface elevation for a given flow or to estimate water velocity for a given water surface elevation. In hydrodynamic modeling, the Manning equation may serve the purpose of giving a quick estimation of flow conditions

TABLE 8.2.1 Values of the Manning Roughness Coefficient, *n*, for Various Channels and Rivers[a]

Type of Channel	Manning Roughness Coefficient (n)
Smooth concrete	0.012
Ordinary concrete lining	0.013
Earth channels in best condition	0.017
Straight unlined earth canals in good condition	0.020
Natural rivers and canals	0.020–0.035
Mountain streams with rocky beds and rivers with variable sections and some vegetation along banks	0.040–0.050
Alluvial channels without vegetation	0.011–0.035

[a]Chow, 1964.

in a river. However, the Manning equation is an empirical formulation that may not reflect actual conditions of a river. The results from the Manning equation are sensitive to the value of the Manning roughness coefficient, n. It is difficult, if not impossible, to accurately estimate n values in complex natural rivers.

8.2.2 Advection and Dispersion in Rivers

As discussed in Section 2.1.3, advection is the horizontal transport of water properties (e.g., temperature and nutrient concentrations). Dispersion is the mixing of water properties. Natural rivers differ from uniform rectangular channels in several ways: the depth varies irregularly, the channel is likely to curve, and the river banks may also vary irregularly. Bank irregularities have a major effect on lateral dispersion in a river. Generally, the larger the irregularity, the faster lateral mixing occurs.

In rivers, a prominent feature is the longitudinal dispersion: the transport and spreading of pollutants downstream from a point source. When a tracer is released into a river, two distinct processes control the tracer transport: (1) flow advection carries the tracer away from the releasing point and (2) turbulence dispersion spreads out and dilutes the tracer concentration.

Mathematically, the above two processes are represented by the first and second terms on the RHS of Eq. (2.1.33), respectively. Advection results in the pollutant's moving downstream, while longitudinal mixing leads to spreading or smearing in the longitudinal dimension. Lateral and vertical mixing processes determine how long it takes for a pollutant to be completely mixed across a river. The dominant transport process in rivers is the advection due to river flow. Flow velocity controls a river's travel time, the time required by a particle to cross a river reach. Flow velocity, along with temperature and other river characteristics, determines the variations in water quality. The dispersion process in rivers is often less important in the transport of pollutants. The effect of dispersion may be ignored in analyzing a continuous pollutant load to a river. On the other hand, when analyzing transport of storm-driven loadings during wet weather periods, longitudinal dispersion also must be considered, since the pollutant loading is represented as a single "pulse" input rather than a continuous load. Figure 8.2.3 is a velocity vertical profile in a channel. In small rivers, however, the turbulence generated by bed friction is strong, and the depth is generally small, resulting in rivers that are often well mixed vertically.

To illustrate the longitudinal dispersion in a river, an idealized dye release experiment is shown in Fig. 8.2.4, in which *a* gives the plain view of the dye transport in the river and *b* presents the lateral-averaged dye concentration along the river. In the river, a line source of constant concentration is instantaneously released at time $t = 0$, and the longitudinal velocity has parabolic variation across the river. As shown in *a*, the advection process transports the dye downstream, and the dispersion process spreads the dye and reduces the

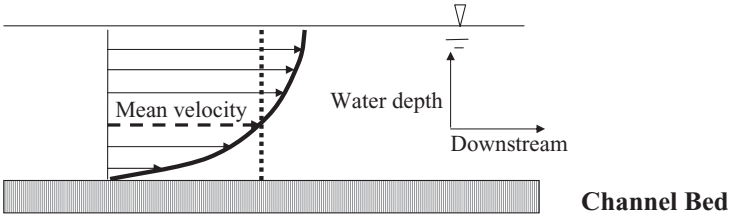

Fig. 8.2.3 Velocity vertical profile in a channel.

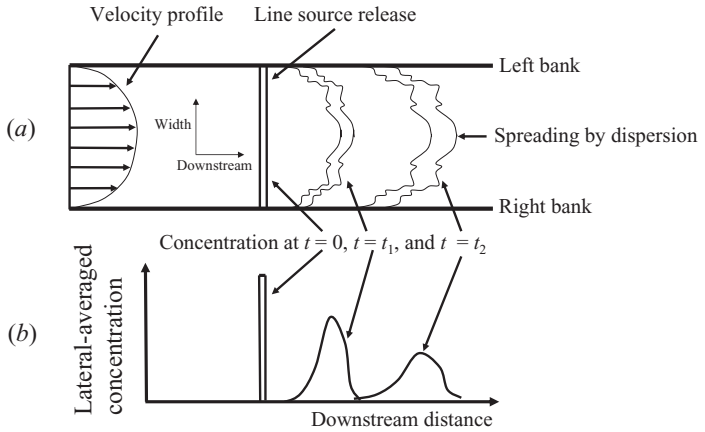

Fig. 8.2.4 Advection and dispersion processes in a river. (*a*) Part *a* gives the plain view of dye transport in the river. (*b*) Part *b* presents the lateral-averaged dye concentration along the river.

maximum concentration. Dye travels downstream faster in the middle of the river than near the banks. As a result, the line source released at $t = 0$ becomes approximately a parabolic shape at $t = t_1$ and $t = t_2$. The concentration profiles at t_1 and t_2 in *a* also reflect the random fluctuations of turbulence activities in the river. Because of variations in flow velocity across the river, dye spreads both along and across the river by dispersion. The laterally averaged dye concentration in *b* also indicates that the velocity shear and turbulent dispersion contribute to the concentration spreading along the river.

8.2.3 Flow Over Dams

A dam is a structure that blocks the flow of a river or other waterway to form a basin and holds water back to make a pond, lake, or reservoir. It usually has facilities to control the release of impounded waters. Dams are present in many rivers for various purposes, such as water supply, flood control, navigation, and generating electric power. In addition to its impact on the hydrody-

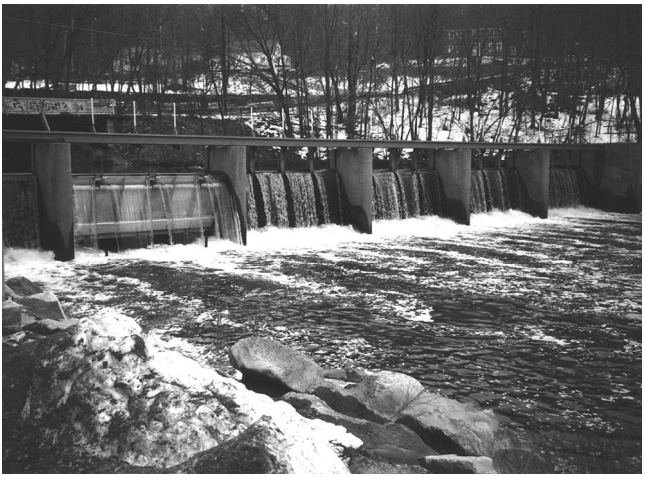

Fig. 8.2.5 Riverdale Dam on the Blackstone River. (Photo taken by Zhen-Gang Ji on February 3, 1998.)

namic processes in a river, a dam can greatly affect sediment and water quality processes. For example, dams slow down the natural flow of the river and allow suspended sediments to settle behind the dams. Over-dam flow can enhance reaeration and reduce dissolved oxygen deficit significantly. As an example, the Riverdale Dam (Fig. 8.2.5) is a low-head dam on the Blackstone River, MA.

When dams are present in a river, the river is actually separated into different reaches by the dams. To simulate river processes, the flow conditions in the dam area should be represented appropriately. For a flow over a dam crest (Fig. 8.2.6), the river energy equation can be written as:

$$\frac{V^2}{2g} + H + B = \frac{V_c^2}{2g} + H_c + E_c \tag{8.2.4}$$

where V = upstream velocity, H = upstream water depth, B = upstream bed elevation, V_c = dam crest velocity, H_c = dam crest water depth, and E_c = dam crest elevation.

The elevations are in reference to mean sea level (MSL) or some other reference level. Equation (8.2.4) states that the total river energy upstream of the dam is equal to the total energy at the dam crest. In a hydrodynamic model, the LHS of Eq. (8.2.4) can be calculated in the upstream grid cell adjacent to the dam. The velocity at the crest reaches the critical flow and is expressed as:

$$V_c = \sqrt{gH_c} \tag{8.2.5}$$

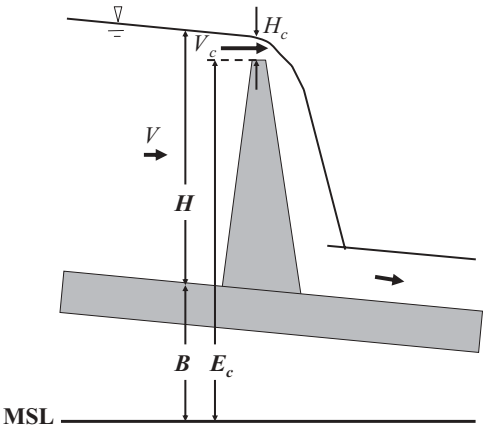

Fig. 8.2.6 Flow over a dam.

Since the river flow slows down significantly when the water approaches the dam, it is assumed that

$$\frac{V^2}{2g} \ll H + B \tag{8.2.6}$$

Hence, Eqs. (8.2.4)–(8.2.6) yield

$$H_c = \frac{2}{3}(H + B - E_c) \tag{8.2.7}$$

The flow rate over the crest is

$$Q = WH_cV_c = W\sqrt{g}H_c^{3/2} = \left(\frac{2}{3}\right)^{3/2}\sqrt{g}W(H + B - E_c)^{3/2} \tag{8.2.8}$$

where W = river width.

A more general form of Eq. (8.2.8) can be expressed as flow rate per unit of river width:

$$\frac{Q}{W} = \left(\frac{2}{3}\right)^{3/2}\sqrt{g}(H + B - E_c)^{3/2} \tag{8.2.9}$$

Since B and E_c are normally known, Eq. (8.2.9) establishes a relationship between the river flow rate, Q, and the water depth at the upstream grid cell, H, which is useful in determining hydrodynamic conditions in a river. Ji et al. (2002a) used Eq. (8.2.9) to calculate over-dam flows in the Blackstone River.

8.3 SEDIMENT AND WATER QUALITY PROCESSES IN RIVERS

Rivers maintain a very delicate balance among the following variables: (1) water inflows from the watershed, (2) water depth and velocity, (3) width and slope of the river, (4) sediment size and concentration, and (5) nutrients and algae. More importantly, this balance is dynamic rather than static. Rivers can act as sinks for water, sediment, and nutrients. When nutrients stimulate algal growth, the designated use of a river, such as recreational use, drinking water supply, and living habitat, can be adversely affected. In addition to nutrients, other factors (e.g., sunlight, sediment load, and grazing) can also affect the water quality in a river.

8.3.1 Sediment and Contaminants in Rivers

Sediment siltation is one of the leading environmental problems in rivers. The filling of river channels, harbors, and estuaries by sediments brings a high cost to society. The condition of a river's watershed greatly affects the amount of sediment delivered into the river. The sediment sources vary among rivers, and even within a particular river, from year to year. Extreme events, such as hurricanes, can produce dramatic changes in the amounts and types of sediments that are delivered into a river. The vulnerability of a river to sediments and contamination reflects a complex combination of upstream flows, land use, and land-management practices.

As discussed in Chapter 3, sediment in rivers (and in other waterbodies) undergoes three primary processes:

1. Erosion (resuspension): The detachment of sediments from a river bed.
2. Transport: The movement of eroded sediments in flowing water.
3. Deposition: The settling of eroded sediments to river bed.

The erosion, transport, and deposition of river sediments are controlled by river flows and sediment loads. River sediment discharge is highly episodic. In river basins, a disproportionate amount of the total annual sediment load is associated with high flows and extreme events. The vast majority of river sediments is discharged during only 10% of the year (36 days), and 90% of the year represents a very small amount of the sediment load (CSCRMDE, 1987). Low flow rates usually result in net deposition conditions. High flow rates may cause net erosion in upstream reaches and net deposition in downstream reaches or in the estuary into which the river flows. In addition, in certain reaches of a river, erosion may occur during the rising limb period of the hydrograph (Fig. 8.2.1), with deposition occurring during the corresponding receding limb period.

Many rivers have dams that form a pond, lake, or reservoir. The impoundments clarify rivers downstream by settling sediment, toxic substances, and nutrients behind the dam. There are both beneficial and adverse effects of

dams in terms of sediment and water quality. Impoundments can benefit a river by removing pesticides and heavy metals through settling. However, these toxic substances do not become entirely harmless when they settle behind the dam. They can be resuspended during episodic high flow events, thereby reintroducing these chemicals into the water column. An example of this process will be presented in Section 8.4.1 on sediment and heavy metals in the Blackstone River (Ji et al., 2002a).

In river studies, 1D and steady-state models are commonly used (e.g., Brown and Barnwell, 1987). When nonpoint sources are identified as the major sources of external loadings, time-dependent modeling is required. The 3D sediment transport equation, Eq. (3.2.13), can be simplified into a 1D form (Ji, 2000a):

$$\partial_t(HS) + \partial_x(HuS) = \partial_x(HK_H\partial_x S) + Q_s + J_0 \tag{8.3.1}$$

where H = water depth, u = velocity component in the Cartesian horizontal coordinate x, S = sediment concentration, K_H = horizontal turbulent diffusion coefficients, Q_s = external point and nonpoint sources, and J_o = net sediment flux (=deposition flux + resuspension flux) from the bed to the water column.

The 1D transport equation for the total concentration (dissolved plus particulate phases) of a toxicant, C, is similar to the sediment transport equation (8.3.1) and can be derived from Eq. (4.4.6):

$$\partial_t(HC) + \partial_x(HuC) = \partial_x(HK_H\partial_x C) + Q_c + F_0 \tag{8.3.2}$$

where Q_c = external point and nonpoint metal sources and F_o = net flux of toxicant from the sediment bed to the water column given by Eq. (4.4.8).

If a river is wide enough to have significant lateral variations or deep enough to develop vertical stratifications, 2D (and even 3D) models may be needed to simulate sediment and toxicant transport in the river. For example, sediment transport within a meandering river is very complex. The velocities are faster at the outer bank and slower at the inner bank. The lateral velocity difference directly influences the sediment transport. There might be erosion occurring along the outer bank and deposition occurring on the inner bank. Using a 1D model to represent the river is equivalent to treating sediment transport as being uniform across the river, eliminating the effect of river meandering on sediment transport and vertical stratifications. A 1D model represents the entire cross-section of the river as being either net depositional or net erosional.

8.3.2 Impacts of River Flow on Water Quality

Water quality processes can be highly dependent on river flow conditions. The time that a pollutant remains within a section of a river is called residence time (or travel time), a concept similar to the retention time often used in lake

studies. The flow velocity and the length of the river section determine the residence time. River flow affects water quality in a river in several ways:

1. *Dilution.* A large volume of flow dilutes concentrations of pollutants that are discharged into the river.
2. *Residence Time.* High flow velocity reduces the residence time and affects the amount of material that can be produced or degraded in the river section.
3. *Mixing.* High flow velocity increases mixing in the river, enhances the assimilative capability of the river, and reduces pollutant concentration gradients.
4. *Erosion.* High flow can erode bed material and destabilize the benthic environment.

The impact of pollutant loadings to a river is largely determined by the magnitudes of the loadings and the flow rate. Rapid transport of pollutants by high flow results in a short residence time and often causes minimal water quality problems. Conversely, slow transport of pollutants by low flow results in a long residence time and can lead to water quality problems, such as oxygen depletion and eutrophication. Channel alteration and watershed disturbance can lead to abnormally high flow rates for a given amount of rain and amplify the impact of floods. Watershed disturbance can also increase sedimentation and harm aquatic biota in a river.

In temperate regions, seasonally high flow typically occurs during the periods of snowmelt in early spring and spring rains, whereas seasonally low flow normally occurs in summer and early fall. The river flow affects the concentration and distribution of water quality variables. Generally, point sources have a larger impact on a river during low flow (dry weather) conditions due to less water diluting the pollutants. Low DO concentrations and high algal growth in a river often occur during low flow periods and hot weather conditions. The combination of low flow, minimum dilution, and high temperature often makes summer and early fall the critical periods for evaluating the impact of point sources (e.g., wastewater treatment plants).

In contrast, nonpoint sources can bring large amounts of pollutants from the watershed into a river during high flow (wet weather) conditions. It is important to examine both point and nonpoint sources in both high and low flow conditions. Point sources of nutrients often cause algal blooms in rivers during low flow conditions, while nonpoint sources may increase nutrient concentrations and turbidity following periods of wet weather events. Municipal discharges, agriculture runoff, and urban runoff are among the most common sources of impairment to rivers. Water quality management plans may require strategies that are based on the seasonal hydrologic and climatological patterns in the area.

In the study of the Blackstone River, for example, Ji et al. (2002a) reported that discharge from a wastewater treatment plant was the dominant point

source of contaminants and had significant impact on the sediment contamination in the river. However, this point source alone is still insufficient to account for the total metal concentrations in the river. Nonpoint sources and the processes of sediment deposition and resuspension are also important factors that control the concentrations of sediment and toxic metals. Sections 3.7.3 and 8.4.1 provide more discussions on the modeling of Blackstone River.

8.3.3 Eutrophication and Periphyton in Rivers

Algae need adequate sunlight and nutrients to grow. Vegetations in riparian wetlands, such as trees and grasses, filter pollutants from runoff and reduce surface erosion. Streamside trees can reduce the amount of light available for photosynthesis and moderate water temperature. River temperature, in turn, affects the availability of DO in the water column for fish and other aquatic organisms.

As discussed in Chapter 5, algae are necessary to support the food chain and nutrients, in turn, are necessary for algal growth and thus for supporting a healthy aquatic ecosystem. In excess, however, nutrients can contribute to algal blooms and low DO, and water quality conditions deteriorate through a process known as eutrophication. Thus, nutrients are a leading cause of river impairment. Nitrogen and phosphorus (especially P) are the primary nutrients that cause nuisance conditions associated with eutrophication in rivers. Phosphorus is frequently the key nutrient controlling algal growth in many freshwaters worldwide. Nitrogen can also become important in waters with a low N/P ratio. When either P or N is limited, algal growth may be limited. Nutrient limitation is an important consideration in river management.

Eutrophication frequently ranks as one of the top causes that result in the impairment of river beneficial uses (e.g., fishing, swimming, and drinking water supply). Excessive algal growths can clog water intake pipes, lead to low DO concentrations, and impair the designated use of a river. Decomposition of excess organic matter and the respiration of algae and plants can severely lower DO concentration.

One distinct feature of river eutrophication is the role of periphyton (attached algae). As discussed in Section 5.2.6, periphyton often prevails in lotic systems, such as fast-moving streams with a gravel/cobble bed, while other algae can thrive in waterbodies that may or may not be lotic, such as lakes and estuaries. Phytoplankton (free-floating algae) is often the major algae component in lakes, while periphyton might play a significant role in eutrophication process in rivers. A modeling study on eutrophication processes in the Christina River, DE, illustrated the importance of periphyton for simulating DO diurnal variations (USEPA, 2000d). In fast-moving streams, most available nutrients are in the water column, and most Chl *a* is on the streambed. Therefore, as listed in Table 8.3.1, it is often more appropriate to classify the tropic state of a stream based on concentrations of benthic Chl *a* (USEPA, 2000c):

TABLE 8.3.1 Boundaries for Trophic Classification of Streams[a]

Variable	Oligotrophic-Mesotrophic Boundary	Mesotrophic-Eutrophic Boundary
Average benthic chlorophyll (mg/m^2)	20	70
Maximum benthic chlorophyll (mg/m^2)	60	200
Total nitrogen (μg/L)	700	1500
Total phosphorus (μg/L)	25	75

[a]Based on USEPA, 2000c.

1. Oligotrophic: Average Chl *a* concentration <20 mg/m^2.
2. Mesotrophic: Average Chl *a* concentration <70 mg/m^2.
3. Eutrophic: Average Chl *a* concentration ≥70 mg/m^2.

The process governing the growth of periphyton in fast-flowing rivers is different from the growth of phytoplankton in lakes and slow-moving rivers. Phytoplankton is usually not the dominant algae in small streams. Fast-moving flow and shallow water depth often favor periphyton growth on the streambed. River eutrophication can result in excessive algal mats and oxygen depletion at times of slow-moving flows and high water temperatures. Periphyton requires a gravel/cobble riverbed to develop high levels of biomass. River currents enhance the exchange of nutrients at the plant cell surface. Instead of being expressed in terms of chlorophyll *a* per unit volume, periphyton biomass in rivers may be represented as chlorophyll *a* per unit area. Table 8.3.2 summarizes factors that affect periphyton and phytoplankton biomass levels in rivers.

8.3.4 Dissolved Oxygen in Rivers

Dissolved oxygen is essential to ecosystems. Section 5.6 details DO processes in waterbodies. Shallow rivers typically have adequate DO concentrations, due to a large water surface/water depth ratio for reaeration and a sufficient water flow to mix DO throughout the water column. A DO concentration of 5 or 6 mg/L is often necessary to maintain healthy water quality conditions. Aquatic lives may experience severe population reduction at DO levels of 3.0 mg/L or less. The condition of DO concentration <2 mg/L is referred to as hypoxia, a DO level below which many species are likely to die.

Processes controlling DO spatial distribution in a river include the following:

1. Oxidation of the BOD: As discussed in Section 5.6.1, BOD is used to represent all sinks of dissolved oxygen, such as the oxidation of

TABLE 8.3.2 Geological, Physical, and Biological Habitat Factors that Affect Periphyton and Phytoplankton Biomass Levels in Rivers and Streams Given Adequate-to-High Nutrient Supply and NonToxic Conditions[a]

Phytoplankton-Dominated Rivers	Periphyton-Dominated Rivers
High Phytoplankton Biomass	*High Periphyton Biomass*
Low current velocity (<10 cm/s)/long detention time (>10 day)	High current velocity (>10 cm/s)
Low turbidity/color	Low turbidity/color
Open canopy	Open canopy
Greater stream depth	Shallow stream depth
Greater depth/width ratio	Minimal scouring
	Limited macroinvertebrate grazing
	Gravel or larger substrata
	Smaller depth/width ratio
Low Phytoplankton Biomass	Low Periphyton Biomass
High current velocity (>10 cm/s)/short detention time (<10 day)	Low current velocity (<10 cm/s)
High turbidity/color	High turbidity/color
Closed canopy	Closed canopy
Shallow stream depth	Greater stream depth
	High scouring
	High macroinvertebrate grazing
	Sand or smaller substrata

[a]Note that only one factor is sufficient to limit either phytoplankton or periphyton biomass (USEPA, 2000c, citing several other sources).

carbonaceous and nitrogenous organic matter, the benthic oxygen demand, and the oxygen utilized by algal respiration.

2. Reaeration of DO from the atmosphere: In addition to atmospheric reaeration, DO produced by photosynthesis and DO contained in incoming flows are also major oxygen sources.
3. Transport due to the river flow: Advection and diffusion processes enhance DO mixing and reaeration within a river.

The pioneering work by Streeter and Phelps (1925), who developed the first water quality model to describe the oxygen depletion in the Ohio River, is useful for understanding DO processes in a river. It can be described in a first-order reaction equation:

$$U\frac{dC}{dx} = -k_d B + k_a(C_s - C) \tag{8.3.3}$$

where x = distance, U = advection velocity in x direction, C = DO concentration, B = BOD concentration, C_s = saturated DO concentration, k_d = deoxygenation rate constant of BOD, and k_a = first-order reaeration rate constant of DO.

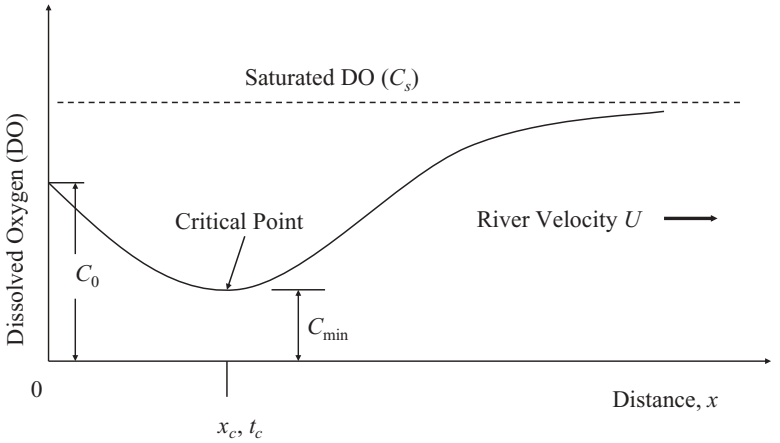

Fig. 8.3.1 Dissolved oxygen sag curve in a river.

By assuming that BOD has a first-order degradation reaction with a decay rate constant of k_r, the solution to Eq. (8.3.3) is the famous Streeter–Phelps equation:

$$C = C_s - \frac{k_d L_0}{k_a - k_r}(e^{-k_r x/U} - e^{-k_a x/U}) - (C_s - C_0)e^{-k_a x/U} \tag{8.3.4}$$

A schematic representation of the Streeter–Phelps equation is shown in Fig. 8.3.1, describing a DO sag curve in a river. The DO sag curve gives DO longitudinal variation as the result of oxygen depletion and recovery, after a BOD load is discharged into a receiving river. Between the discharge point ($x = 0$) and the critical distance ($x = x_c$), oxidation exceeds reaeration (i.e., $k_d B > k_a(C_s - C)$ in Eq. (8.3.3), because of high BOD concentrations and a small DO deficit ($=C_s - C$). Oxygen in the river is consumed faster than it is resupplied. The DO concentration decreases to a minimum C_{min} at a critical distance x_c (or critical time $t_c = x_c/U$). This position is the critical location where the lowest DO concentration occurs, and the oxidation rate and reaeration rate are equal. After passing the critical location, reaeration exceeds oxidation [i.e., $k_d B < k_a(C_s - C)$ in Eq. (8.3.3)] because of a low BOD concentration and a high DO deficit. Thus, oxygen in a river increases gradually. Further downstream, the rate of supply exceeds the utilization rate, resulting in a full recovery of the DO concentration.

The above discussion is a simple illustration of the BOD/DO modeling analysis under the following assumptions:

1. Organic decomposition and reaeration are the dominant processes affecting the DO concentrations.
2. Other processes, such as nitrification and sediment oxygen demand that may significantly affect DO in rivers, are not included.

3. Nonpoint sources, which may depress DO concentration significantly, are not considered.
4. The river is considered as a 1D straight channel, and the effects of complicated river geometry are excluded.

8.4 RIVER MODELING

The data and parameters needed for the modeling of surface waterbodies are generally discussed in Section 2.4.1 for hydrodynamics, Section 3.7.1 for sediment transport, Section 4.5 for toxics, and Section 5.9.1 for water quality and eutrophication, respectively. The selection of numerical models for the modeling of surface water systems is discussed in Section 7.1.2. This section is focused on issues directly related to river modeling. The modeling of the Blackstone River, MA (Ji et al., 2002a) and the modeling of Susquehanna River, MD (Hamrick and Mills, 2001) are presented as case studies in this section.

Transport in rivers is often dominated by the processes of advection and dispersion. One-, two-, and three-dimensional models have been developed to describe these processes. Study objectives, river characteristics, and data availability are key factors determining model applicability. Section 2.2.2 provides model equations in 1D, 2D, and 3D. A 1D model is often used in the modeling of small and shallow rivers. More detailed analysis of flow velocities and directions requires the representation of the river in two and, sometimes, three dimensions. When lateral variation (or vertical stratification) is an important feature of the river, models with 2D variations are needed. For large rivers, especially for rivers that directly flow into estuaries, 3D models might be needed in order to describe the river processes accurately.

One-dimensional models, such as the widely used QUAL2E model (Brown and Barnwell, 1987), are traditionally applied to river modeling. For most small and shallow rivers, these 1D models are often adequate to simulate hydrodynamic and water quality processes. In 1D models, water surface elevation, velocity, and discharge vary only in the longitudinal (along-the-river) direction and are constants in the lateral (across-the-river) direction. This approach provides a simplified mathematical description of river flows.

Rivers with a steep bottom slope often have a relatively high-velocity and a shallow water depth, and are characterized by gravel, cobbles, and rocks in the riverbed. Coarse sands and finer particles are washed out by the high velocity. The dominant gradient of water quality constituents is along the river in the direction of flow. A 1D laterally and vertically averaged model is thus appropriate for describing water flow and the transport of sediment and toxic chemicals. Rivers with a moderate bottom slope result in a low-velocity waterway, often characterized by a sediment bed consisting of a mixture of fine-grained cohesive particles and fine sands. The dominant gradient of water quality constituents in this kind of river is in the direction of the flow and a 1D model may still be adequate. One-dimensional models are limited in their ability to capture the complexity of natural rivers. The assumption that the

characteristics of the river are uniform both vertically and laterally may not be valid for wide, deep rivers. In this case, the 1D approach may fall short of describing the river processes. Transport in these rivers can have significant gradients either laterally or vertically. In this case, a 2D or 3D model is needed to provide a better representation of the river.

Boundary conditions of a river model are often specified by either flow/rate time series or stage time series with the following boundaries:

1. *Upstream Boundary.* An upstream boundary provides inflows to the river and is often specified as flow rate or water surface elevation.
2. *Downstream Boundary.* Water surface elevations or a rating curve are often specified at the downstream boundary.
3. *Lateral Boundary.* Lateral inflows may come from gaged and ungaged areas along the river.

Upstream and downstream boundaries are often specified at locations where flow or water quality data are available or where there are dams, which makes it easier to specify the inflows and the boundary conditions. When a section of the river is ungaged, the characteristics of the contributing watershed may be used to estimate in flows, often via a watershed model. Tidal rivers may have more complicated boundary conditions due to reversing flows.

8.4.1 Case Study I: Blackstone River

The hydrodynamic and sediment modeling of Blackstone River, MA (Fig. 3.7.7) is already discussed in Section 3.7.3. As a continuation, the modeling of heavy metals in the river is presented here (Ji et al., 2002a).

8.4.1.1 Modeling Metals in the Blackstone River. As discussed in Section 3.7.3, the total and dissolved concentrations of the five metals (Ca, Cr, Cu, Ni, and Pb) and TSS were measured during the three BRI surveys (USEPA, 1996a). From these measured data, the partition coefficients P can be estimated using Eq. (4.3.7). Based on the BRI data, Tetra Tech (1999b) reported that while they show a large variability, the partition coefficients of the five metals in the Blackstone River can be represented reasonably by setting P equal to 0.2, 1.0, 0.2, 0.1, and 1.0 L/mg for Cd, Cr, Cu, Ni, and Pb, respectively. Thomann et al. (1993) set Cd's partition coefficient to 0.1 L/mg. The USEPA (1984) reported that in Flint River, MI, the partition coefficients varied from 0.05 to 0.45 L/mg for Cd and 0.02 to 0.1 L/mg for Cu, which are both comparable to the values used in this study. Parameter sensitivity tests will be presented later.

During each BRI storm event, samplings were conducted at up to 16 stations along the Blackstone River and its tributaries at 4-h time intervals for up to 3 days. Data at 12 stations along the Blackstone River are used for model–data comparison. The 12 stations have a total of 120, 192, and 144 records for each measured variable for Storm 1, Storm 2, and Storm 3,

respectively. To conduct statistical analysis, model results were saved at the 12 locations and at the exact sampling times, so the model results could be compared with the data at the same locations and at the same times. Tables 8.4.1–8.4.3 summarize the error analyses of seven observed and modeled variables, including river flow rate (Q), TSS, Cd, Cr, Cu, Ni, and Pb, during Storm 1, Storm 2, and Storm 3, respectively. These tables present the values of observed mean, modeled mean, absolute mean error, RMS error, observed change, and relative RMS error in percentage. In general, these analyses show that the simulated Q, TSS, Cd, Cr, Cu, Ni, and Pb agree well with observed data. For example, Table 8.4.2 shows that compared with the 192 measured data from the 12 locations, the relative RMS errors of Storm 2 modeling range from 6.17% for Q to 17.27% for TSS, and the relative RMS errors for the five metals are no more than 15.03%. Tables 8.4.1–8.4.3 indicate that, statistically, the Blackstone River Model simulates very well the transport processes of hydrodynamics, sediment, and metals during the three storm events.

Figures 8.4.1–8.4.5 present the time series of the modeled and measured Cd, Cr, Cu, Ni, and Pb along the Blackstone River during Storm 2 (11/2/92–

TABLE 8.4.1 Error Analysis of Observed and Modeled River Flow Rate (Q), Total Suspended Sediment (TSS), Cadmium (Cd), Chromium (Cr), Copper (Cu), Nickel (Ni), and Lead (Pb) During Storm 1

Variable	Obs. Mean	Modeled Mean	Mean Abs. Error	RMS Error	Obs. Change	Relative RMS Error (%)
Q (cms)	4.56	4.93	1.03	1.43	8.45	16.88
TSS (mg/L)	6.23	2.60	4.83	7.22	34.60	20.86
Cd (μg/L)	0.66	0.89	0.37	0.54	2.52	21.56
Cr (μg/L)	4.83	0.97	3.86	4.89	17.50	27.95
Cu (μg/L)	18.05	10.27	10.39	13.02	67.80	19.21
Ni (μg/L)	10.88	8.26	4.11	5.48	29.50	18.57
Pb (μg/L)	7.61	2.13	5.63	7.33	30.90	23.71

TABLE 8.4.2 Error Analysis of Observed and Modeled River Flow Rate (Q), TSS, Cadmium (Cd), Chromium (Cr), Copper (Cu), Nickel (Ni), and Lead (Pb) During Storm 2

Variable	Obs. Mean	Modeled Mean	Mean Abs. Error	RMS Error	Obs. Change	Relative RMS Error (%)
Q (cms)	9.53	10.95	1.86	3.42	55.39	6.17
TSS (mg/L)	6.80	8.20	4.54	6.53	37.80	17.27
Cd (μg/L)	0.88	1.22	0.52	0.71	5.12	13.95
Cr (μg/L)	4.08	1.99	2.27	3.17	27.08	11.71
Cu (μg/L)	12.27	12.09	5.77	8.69	57.80	15.03
Ni (μg/L)	7.92	7.73	2.31	3.52	25.70	13.68
Pb (μg/L)	7.52	4.57	4.00	5.43	37.80	14.38

TABLE 8.4.3 Error Analysis of Observed and Modeled River Flow Rate (Q), Total Suspended Sediment (TSS), Cadmium (Cd), Chromium (Cr), Copper (Cu), Nickel (Ni), and Lead (Pb) During Storm 3

Variable	Obs. Mean	Modeled Mean	Mean Abs. Error	RMS Error	Obs. Change	Relative RMS Error (%)
Q (cms)	5.20	9.68	6.18	11.87	50.88	23.33
TSS (mg/L)	11.52	8.40	7.30	11.25	128.70	8.74
Cd (μg/L)	0.40	1.28	0.92	1.84	5.12	35.90
Cr (μg/L)	3.38	2.05	2.20	4.86	47.30	10.28
Cu (μg/L)	14.01	15.53	9.12	14.51	95.80	15.14
Ni (μg/L)	7.99	6.78	3.63	5.75	20.80	27.62
Pb (μg/L)	11.12	6.38	7.80	12.44	66.80	18.63

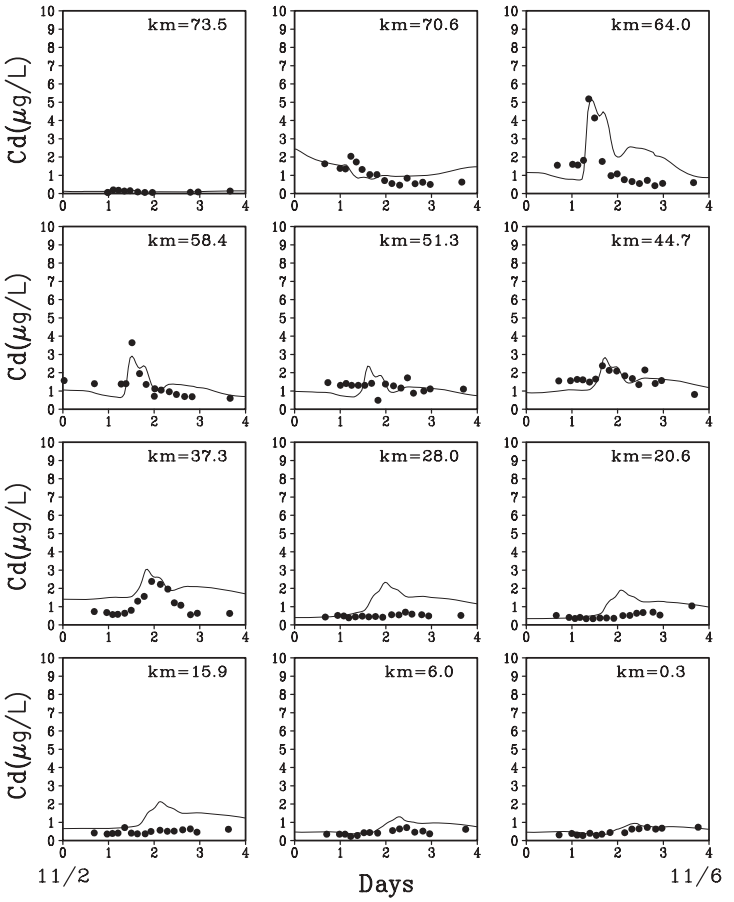

Fig. 8.4.1 Measured and modeled Cd concentration along the Blackstone River during Storm 2.

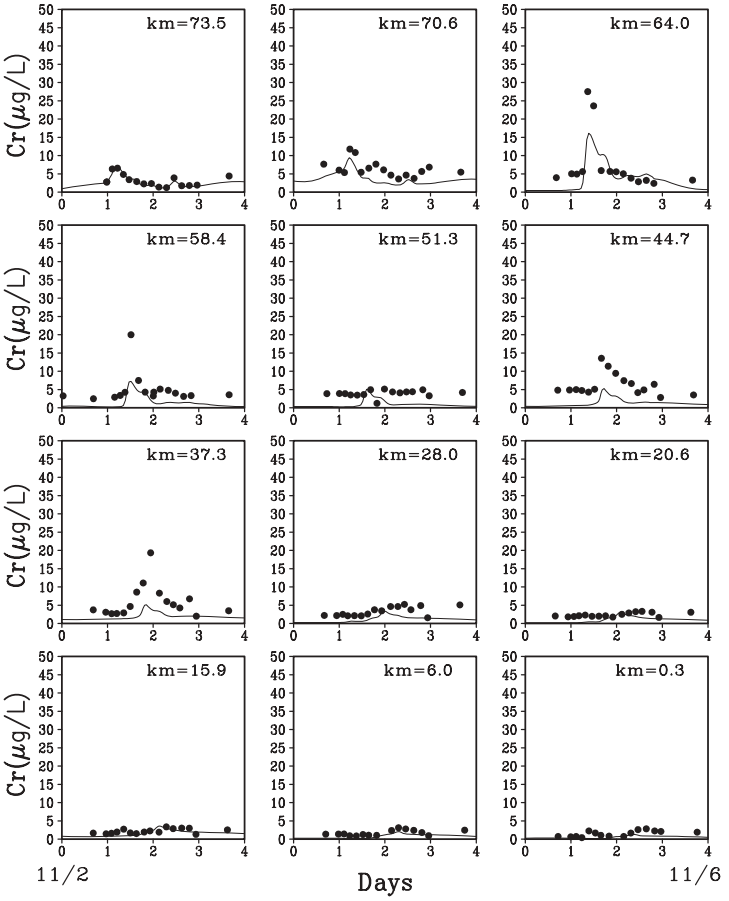

Fig. 8.4.2 Measured and modeled Cr concentration along the Blackstone River during Storm 2.

11/6/92). The 12 small plots in Fig. 8.4.1 are the concentrations of Cd along the Blackstone River during the survey period of Storm 2. The horizontal axis is in days from November 2, 1992. The vertical axis is in micrograms per liter (μg/L). The river kilometers are also shown in the plots. The black dots represent the measured Cd concentration. The solid line represents the model results.

Figure 8.4.1 indicates that at km = 70.6, the Cd concentration increased significantly due to the UBWPAD discharges at km = 71.4. At the peak of Storm 2 (~Day 1.3), the Cd concentration at km = 70.6 dropped slightly, as the result of dilution caused by the high river flow. This phenomenon clearly indicates that, compared with the nonpoint sources from the Blackstone watershed, the UBWPAD is a more significant source of Cd. At km = 64.0 (Singing Dam), the Cd concentration increased abruptly as the result of sediment

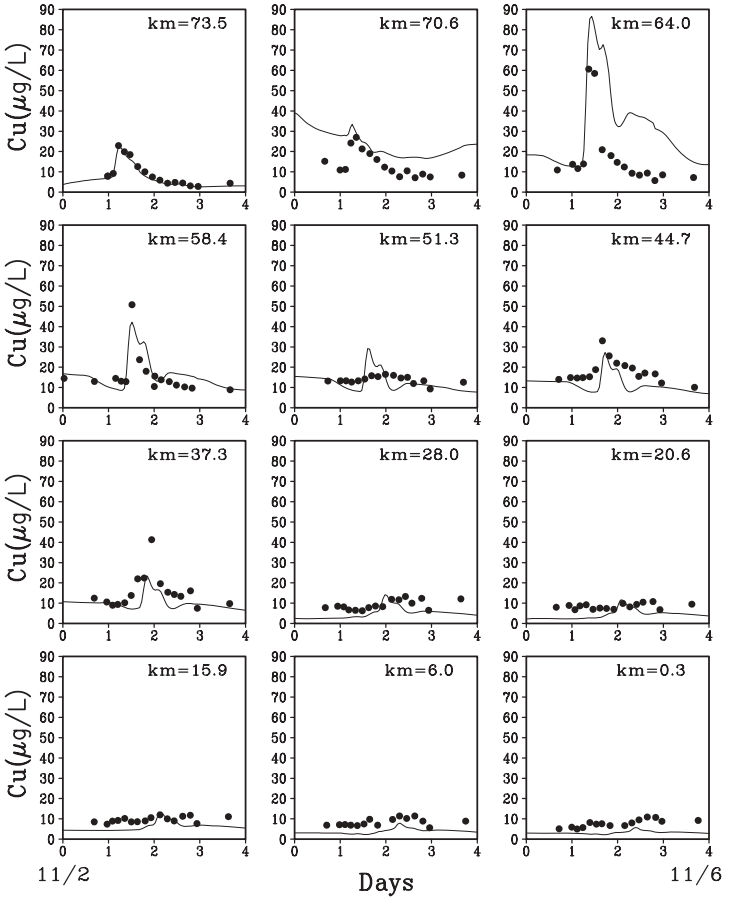

Fig. 8.4.3 Measured and modeled Cu concentration along the Blackstone River during Storm 2.

resuspension near the dam. Both the data and the model indicated a peak Cd value of 5.2 μg/L. At other dams (km = 58.4, 51.3, and 44.7), the Cd concentrations increased with TSS concentrations (shown in Fig. 3.7.10) accordingly. The results in Figs. 3.7.10 and 8.4.1 indicate that the model is able to describe the dilution process and sediment and metals resuspension processes realistically.

Figures 8.4.2–8.4.5 are similar in format to Fig. 8.4.1, but show concentrations for the other four metals (Cr, Cu, Ni, and Pb), which have features similar to the ones presented in Fig. 8.4.1. For example, metal concentrations at km = 64.0 (Singing Dam) in Figs. 8.4.2–8.4.5 all increased significantly as the results of high flow rates and sediment resuspension. It is also interesting to see that during the high flow period at km = 70.6 (immediately downstream from the UBWPAD), whereas concentrations of the other four metals (Cd, Cr, Cu, and Ni in Figs. 8.4.1–8.4.4) did not increase significantly, the Pb concentration in

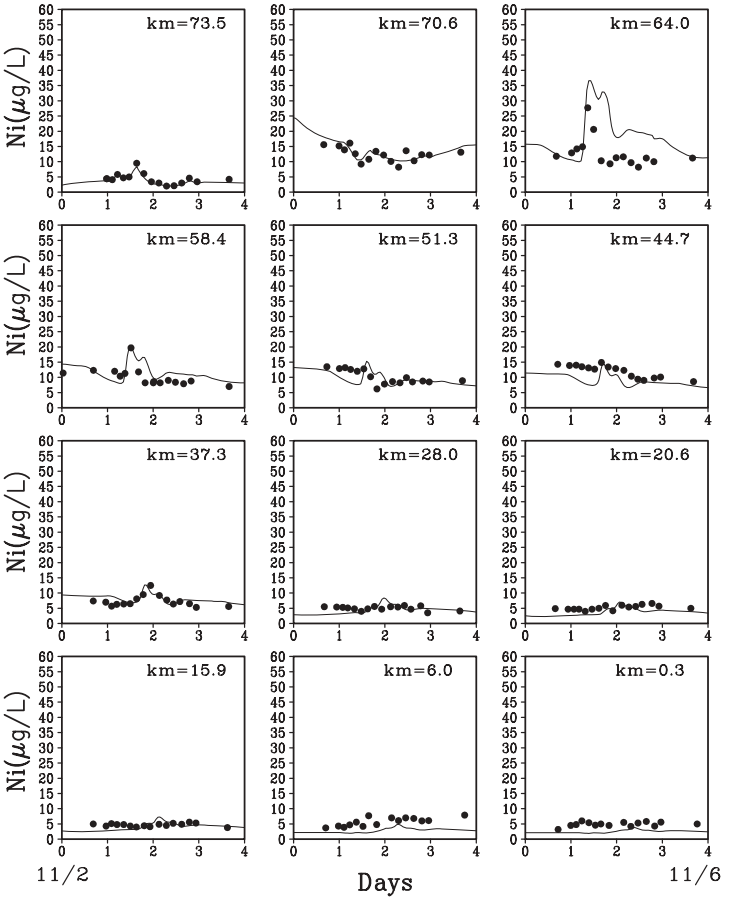

Fig. 8.4.4 Measured and modeled Ni concentration along the Blackstone River during Storm 2.

Fig. 8.4.5 had a large increase. This finding suggests that unlike the other four metals, which are largely from the UBWPAD, Pb from nonpoint sources (watershed) contributes significantly to the Blackstone. Later discussion on the contaminant sources will also support this finding.

Model parameters that are important to this study include the sediment settling velocity, critical deposition shear stress, critical resuspension shear stress, and the partition coefficients for the five metals. A MRRE of each storm simulation can be calculated using the values in the last columns of Tables 8.4.1–8.4.3. In this study, MRRE is used to evaluate the overall model performance and to reveal model sensitivity to parameters. For example, the MRRE of the Storm 2 simulation in Table 8.4.2 is 13.17%. When the partition coefficients (P) are changed ±50%, the MRRE is changed <1.5%. When the sediment settling velocity is changed ±50%, the MRRE is changed <4%. When

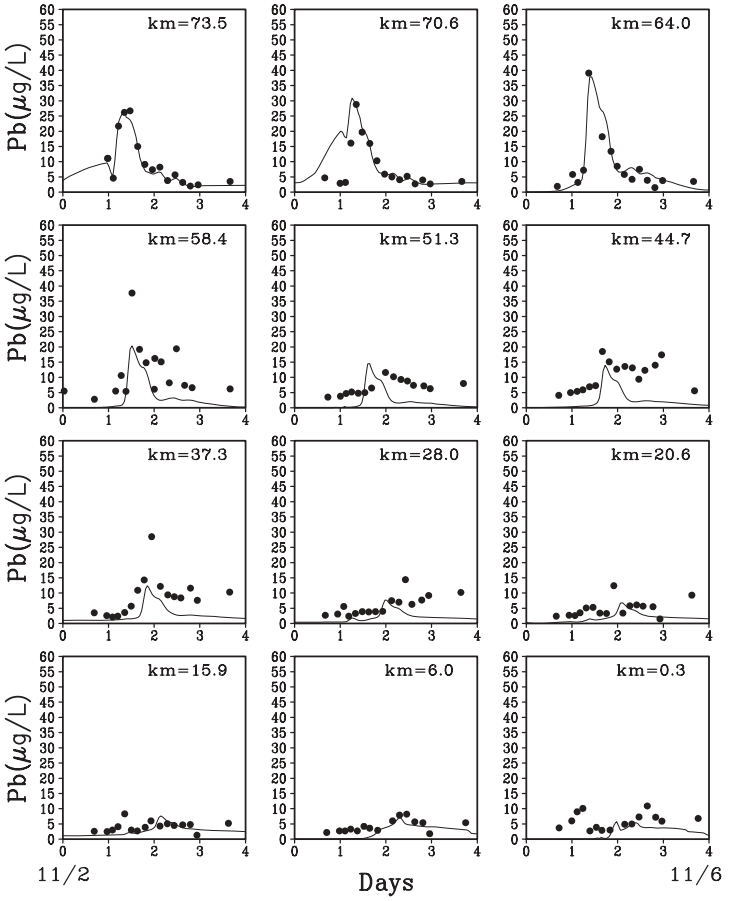

Fig. 8.4.5 Measured and modeled Pb concentration along the Blackstone River during Storm 2.

the critical deposition shear stress is changed ±50%, the MRR is changed <10%.

In summary, the model results are not very sensitive to model parameters, and the values of critical deposition (and resuspension) shear stress affect the sediment and metals concentrations more than other parameters. Under high flow conditions, the sediment resuspension process during a storm event plays a more critical role in sediment and metal calculation than the sediment settling velocity does. This is one major reason that model results are less sensitive to settling velocity changes in the simulation of storm events.

8.4.1.2 Impacts of Sediment and Metals Sources. After it is calibrated against the BRI data, the Blackstone River Model can be used to analyze the impacts of point discharge, nonpoint discharge, and the resuspension process

on the river. The Singing Dam (Fig. 3.7.7, km = 64.0) is used as the site for the analysis. Under identical water inflow rates and hydrodynamic conditions, four scenarios with different sediment and metal loadings and/or resuspension processes were investigated:

1. *Single Point Discharge.* In this case, sediment and metal loadings from all sources are turned off except the ones from UBWPAD at km = 71.4. To eliminate the impact of resuspension from the river bed, the sediment resuspension processes is turned off by setting the critical resuspension shear stress to a very large value.
2. *Nonpoint Source Discharge.* Sediment and metal data collected near the head of the river at km = 73.5 are used to represent the inflows of nonpoint sources from the upstream watershed. In this case, all sediment and metal sources are turned off, except the ones at km = 73.5. The sediment resuspension process is also turned off.
3. *Bed Resuspension.* The resuspension process that brings sediment and metals back to the water column from the river bed is analyzed by turning off all sediment and metal loadings to the river. In this case, the only sources of sediment and metals are from the river bed.
4. *Full Process.* In this case, all above process are included in the model, and the results were shown in Figs. 3.7.9, 3.7.10, and 8.4.1–8.4.5.

Figure 8.4.6 shows the concentrations of TSS, Cd, and Pb at the Singing Dam (km = 64.0) during Storm 2. In Fig. 8.4.6, Panel (1) is the single point discharge case, Panel (2) is the nonpoint source discharge case, Panel (3) is the bed resuspension case, and Panel (4) is the full process case. The small plots in the first column of Fig. 8.4.6 indicate that TSS at the Singing Dam is primarily from upstream nonpoint sources (Panel 2) and bed resuspension (Panel 3). The single point source from UBWPAD (Panel 1) contributes little to the sediment concentration at the Singing Dam. Note that, since sediment transport, deposition, and resuspension are nonlinear processes, the linear superposition of sediment concentrations in Panels (1), (2), and (3) may not be equal to the one in Panel (4).

The small plots in the second column of Fig. 8.4.6 reveal that Cd concentrations at the Singing Dam largely come from UBWPAD and bed resuspension. The nonpoint sources from upstream bring little Cd to the Singing Dam. Figure 8.4.6 also indicates that the dominant Pb source at the Singing Dam is from upstream nonpoint sources. Neither the UBWPAD nor the bed sediment resuspension contribute much to the Pb concentration here. This finding is consistent with the previous discussion regarding Fig. 8.4.5.

Similar analyses were also conducted on Storm 1 and Storm 3, and similar results were obtained. It was found that the sediment and metal transport in shallow rivers is complicated. No single process/source can always be dominant. In order to describe the sediment process and fate and transport of metals, all major sources, including point sources, nonpoint sources, and river

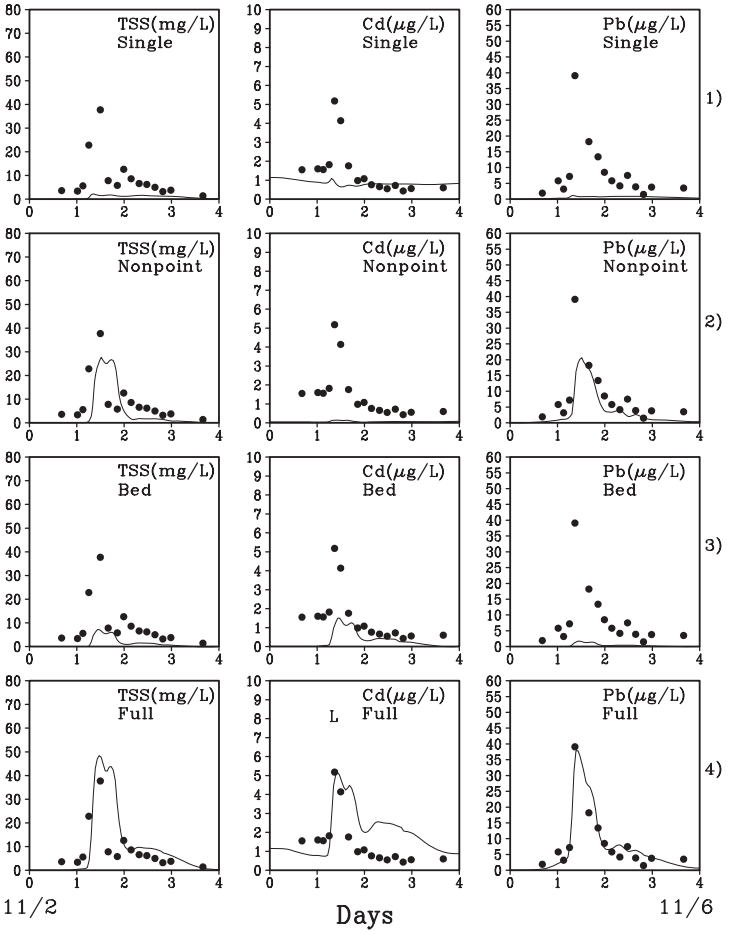

Fig. 8.4.6 Sediment, Cd, and Pb concentrations at Singing Dam (km = 64.0) during Storm 2: (1) single point discharge, (2) nonpoint discharge, (3) bed resuspension, and (4) full process.

bed resuspension, should be considered. Currently, the evaluation of NPDES permits is primarily based on point source discharges. Water quality management tools that can include nonpoint sources and sediment resuspension are needed.

8.4.1.3 Discussion and Conclusions. The Blackstone River Initiative (USEPA, 1996a) carried out surveys on the Blackstone River from 1991–1993. This multiyear and multimillion-dollar project provided the most comprehensive survey on water quality, sediment, and heavy metals in the river, and served as the primary data set for the present modeling study. The Blackstone River Model is applied to simulate the three BRI storm events. The model

simulates the river flow rates well both in amplitude and in phase. The sediment transport and resuspension processes are depicted satisfactorily in the model. The concentrations of TSS and the five metals during the three storm events are also simulated very well.

Conclusions of this study are as follows (Ji et al., 2002a):

1. So far, there are few published modeling studies on sediment and metal transport in rivers that simulate storm events on an hourly basis and use comprehensive data sets for model input and model calibration. With the BRI data and the other data sources, this study is able to simulate the sediment and metal transport processes in detail. Statistical analysis and graphic presentation indicate that the model results are in very good agreement with the data.
2. For shallow and narrow rivers like the Blackstone, the EFDC model with a 1D grid can represent the hydrodynamic, sediment, and metal processes reasonably well in most reaches. In certain reaches, such as the Rice City Pond (<300 m long), more than one cell across the river may be needed.
3. The UBWPAD is the dominant point source of contaminants. It has significant impact on the sediment contamination in the river. The model results also reveal that the discharges from UBWPAD alone are insufficient to account for the total metal concentrations in the river.
4. Nonpoint sources and the processes of sediment deposition and resuspension are also important factors that affect the concentrations of sediment and metals. Because the geometric setting of the river is relatively simple, the transport and resuspension processes of sediment and the associated metals can be directly investigated with minimum interference from other hydrodynamic processes. Contaminants from point and nonpoint sources were discharged into the river, transported downstream, settled on the river bed (especially behind the dams), and resuspended again when a storm event occurs.

Two factors hinder detailed simulation of the sediment and metals on the bed: (1) no sediment core data are available to quantify the sediment depth and distribution along the river, and (2) the accumulation of sediment and contaminants on the river bed is a long-term process with time scales of months, years, and even decades. The BRI data used in this study include three surveys, each lasting only a few days. Therefore, the BRI data cannot (and should not) be used to answer questions on the long-term processes of sediment deposition and contaminant accumulation on the river bed. As indicated in this study, nonpoint sources play an important role in the sediment contamination process. Both field sampling and modeling studies are needed to quantify the nonpoint source influence. One cohesive sediment class is used to represent TSS in the model. Since the TSS in the river includes components

of cohesive, noncohesive, organic, and inorganic materials, it will be helpful for sediment and metal modeling to separate TSS into cohesive and noncohesive sediments.

8.4.2 Case Study II: Susquehanna River

This case study is based on the work of Hamrick and Mills (2001) and Tetra Tech (1998b).

Hydrodynamic and transport models are now commonly applied to predict power plant thermal impacts under design conditions. Predicting the behavior of discharges from a circulating cooling water system has been integral to power plant licensing and permitting. To understand how heated discharges behave in the aquatic environment, it is necessary to understand the hydrodynamic transport processes governing the movement and mixing of the heated and ambient waters. Meteorological events and changes in the circulation greatly affect the thermal processes. To minimize thermal pollution, plants are often regulated to control the temperatures of discharged effluent. Numerical models are also used to provide information on the design and the operation of the power plants. This case study describes the modeling study on the thermal transport in the Conowingo Pond associated with the Peach Bottom Atomic Power Station's discharge.

8.4.2.1 Background. The Susquehanna River flows through Pennsylvania and Maryland, emptying into the Chesapeake Bay. Conowingo Pond is located on the Susquehanna River in Maryland and Pennsylvania and serves as a cooling reservoir for the Peach Bottom Atomic Power Station (PBAPS). As shown in Fig. 8.4.7, the pond is bounded to the north by the Holtwood Dam and to the south by the Conowingo Dam.

The geometry features of the pond are (1) volume: $3 \times 10^8\,m^3$, (2) length: 23 km, (3) width: 800–2400 m, and (4) average depth: 7 m.

Tetra Tech (1998b) summarized and analyzed the historical flow and thermal data in the pond collected during the summers of 1996 and 1997. A 145-day period, spanning from May through the middle of September 1997, was selected for model simulation. A curvilinear grid containing 954 cells was developed to represent the pond (Fig. 8.4.7). The intake and discharge locations of PBAPS are also shown in the figure. Horizontal grid resolution ranges from ~100 m in the vicinity of the PBAPS to 2 km near the upstream and downstream dams. Bathymetric data for the grid was digitized from a recreational chart of the pond. Model simulations were conducted using eight sigma layers in the vertical. Hydrologic and flow forcing for the model include inflow to the pond at the Holtwood Dam and outflow at the Conowingo Dam (Fig. 8.4.8), direct rainfall, and model-calculated evaporation. The PBAPS cooling flow of $94.6\,m^3/s$ (cms) prior to September 1 and 78.2 cms thereafter is withdrawn from the model domain at the cooling water intake and returned at the discharge (Fig. 8.4.7).

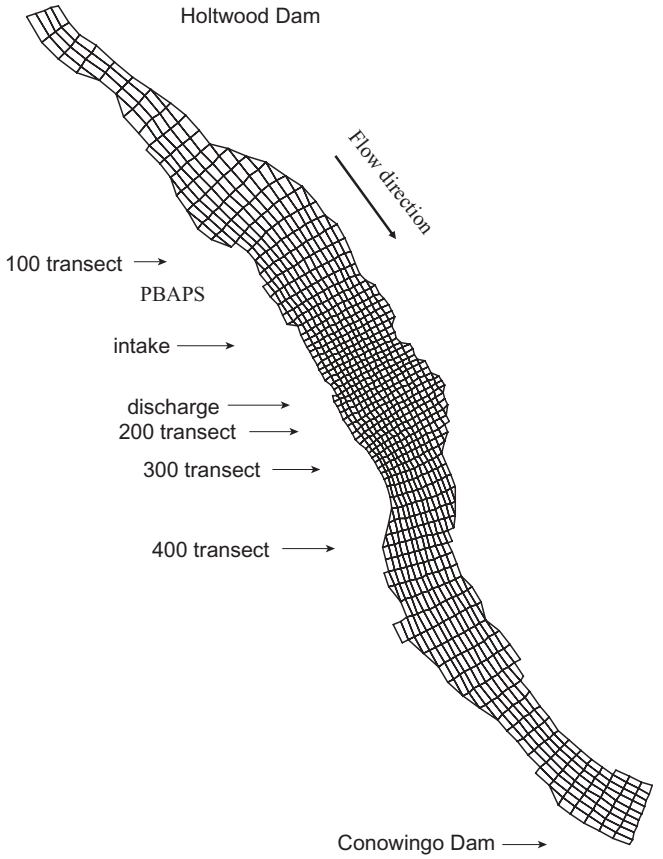

Fig. 8.4.7 Horizontal curvilinear–orthogonal grid of Conowingo Pond (Tetra Tech, 1998b).

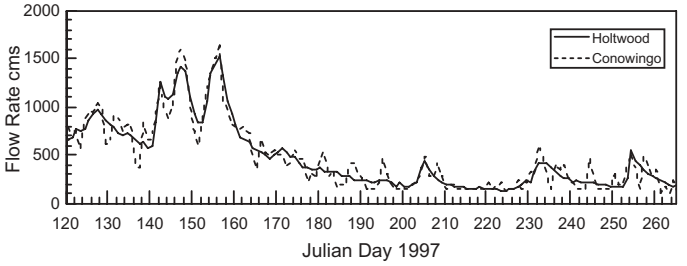

Fig. 8.4.8 Flow rates at Holtwood and Conowingo Dams (Tetra Tech, 1998b).

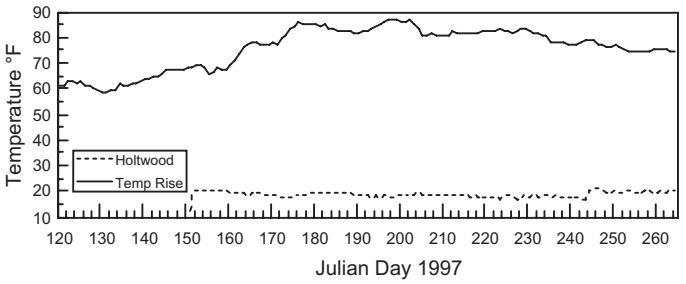

Fig. 8.4.9 Holtwood Dam inflow temperature and PBAPS condenser temperature rise (Tetra Tech, 1998b).

Thermal forcing for the model included inflow temperature at the Holtwood Dam and temperature rise through the PBAPS condenser (Fig. 8.4.9) and atmospheric thermal exchange. Atmospheric data necessary for thermal simulation, including air temperature, pressure, relative humidity, direct rainfall, and wind speed and direction, were obtained from the National Climate Data Center for measurements taken at the Wilmington, Delaware Airport, the closest comprehensive observation station.

8.4.2.2 Model Application. The EFDC model (Hamrick, 1992) was used to simulate thermal transport and the temperature distribution in the Conowingo Pond during the summer of 1997. The model simulation began on May 1, with a uniform initial temperature distribution of 57 °F. The rapid temperature response to the high river flows during May resulted in conditions independent of the 57 °F initial temperature. Thermal calibration of the model primarily involved adjustment of the sensible and latent heat transfer coefficients.

Preliminary model performance was graphically judged by comparison of observed and predicted PBAPS cooling water intake temperatures and observed and predicted temperatures at 16 observation locations in the pond. Figure 8.4.10 shows the cooling water intake temperature. The model predictions tend to be slightly higher than the observations but exhibit the same trends. Figure 8.4.11 shows model predicted and observed temperatures at Station 102, in the 100 transect, which is ~3-km northwest of the cooling water intake and located midway across the pond. The temperature at this station responds primarily to inflow from the Holtwood Dam and local atmospheric thermal forcing. Figure 8.4.12 shows model predicted and observed temperatures at Station 201, in the 200 transect, ~500-m southeast of the cooling water discharge on the west shore of the pond. This station shows the most pronounced influence of the heated discharge. Model predictions at this station are fair, with the model showing overall lower temperature and strong vertical stratification. Figure 8.4.13 shows model predicted and observed temperature at Station 301 in the 300 transect, ~1-km southeast of the discharge. Although

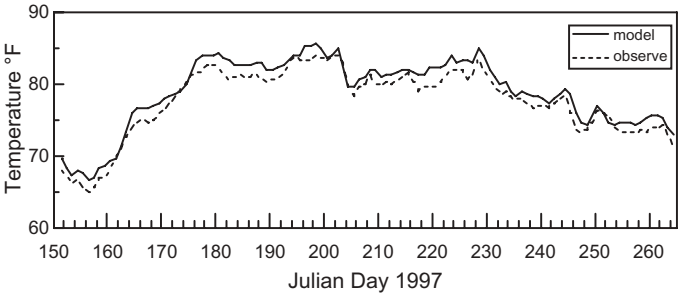

Fig. 8.4.10 Model predicted and observed temperatures at the PBAS cooling intake (Tetra Tech, 1998b).

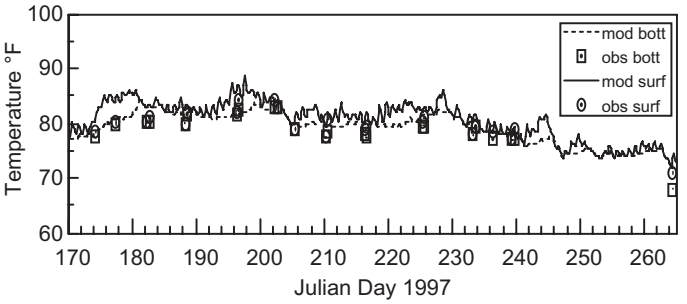

Fig. 8.4.11 Model predicted and observed temperature at Station 102 (Tetra Tech, 1998b).

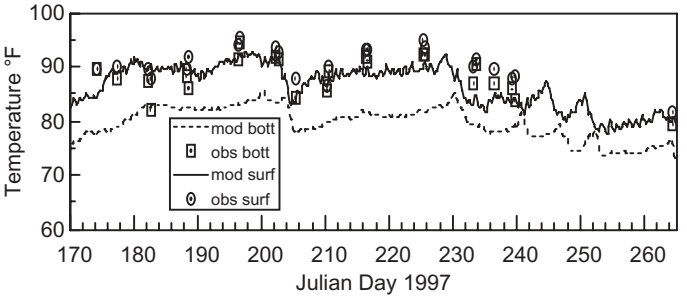

Fig. 8.4.12 Model predicted and observed temperature at Station 201 (Tetra Tech, 1998b).

predicted temperatures are slightly lower than observed, the model does an excellent job in predicting thermal stratification at this station. The highest observed temperatures during the summer 1997 sampling period occurred on July 16. Figure 8.4.14 shows surface temperature contours on this day at 4 p.m. in the afternoon. It is seen in Fig. 8.4.14 that the impact of PBAPS dis-

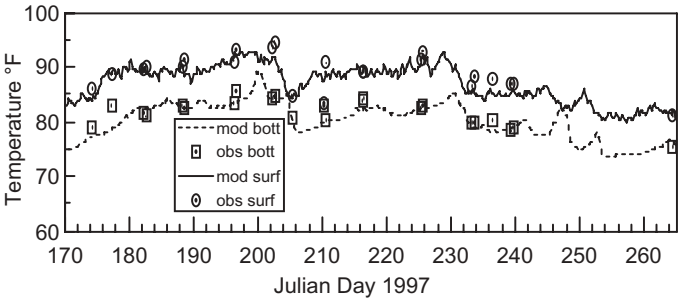

Fig. 8.4.13 Model predicted and observed temperature at Station 301 (Tetra Tech, 1998b).

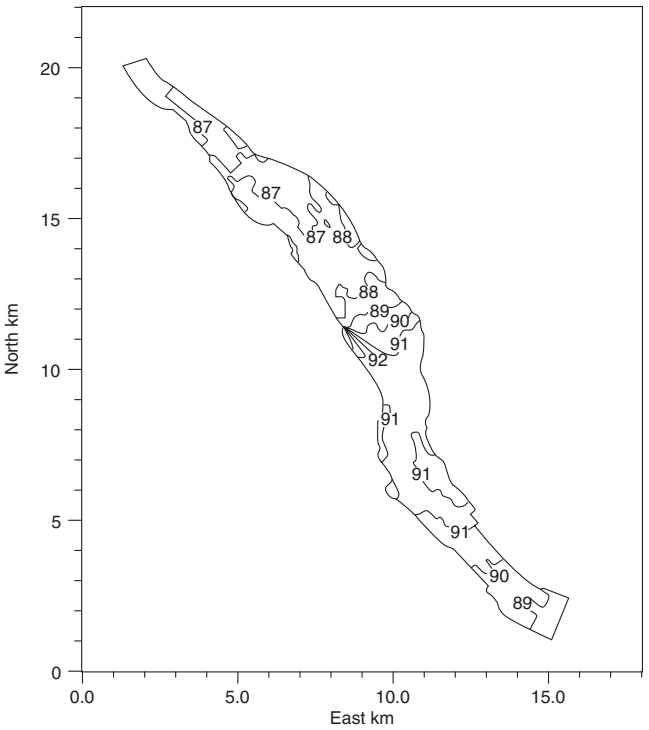

Fig. 8.4.14 Model predicted surface temperature on July 16, 1997, at 4 p.m. (Tetra Tech, 1998b).

charge on the pond is evident. The water temperature upstream near the Holtwood Dam is 87 °F. In the discharging area, the surface water temperature is up to 94 °F, ~7 °F higher than the upstream water temperature. Even 10-km downstream from PBAPS near the Conowingo Dam, the surface water temperature is still at 89 °F.

8.4.2.3 Discussions. This case study has presented an application of simulating the impact of the Peach Bottom Atomic Power Station's cooling discharge on Conowingo Pond. The comparison of model results with field observations from Summer 1997 indicates that the model is capable of predictive thermal simulation on seasonal and annual time scales. Operation of the model is economical with a 145-day simulation taking approximately 12 h on a 400-MHz personal computer. Once configured for thermal simulation of water systems impacted by power plant discharges, the model can be extended to address biological and eutrophication issues and the transport and fate of sorptive metal and toxic organic contaminants.

CHAPTER 9

Lakes and Reservoirs

Even though the terms "lakes" and "reservoirs" are sometimes used interchangeably, a lake is commonly referred to as a natural waterbody formed by geological processes, such as receding glaciers, volcanoes, and earthquakes. A reservoir is often referred to as a manmade water system formed by a dam or other engineering structures that impound water for flood control, navigation, recreation, power generation, and/or water supply.

The general theories and processes of hydrodynamics, sediment transport, pathogens and toxics, and water quality are presented in Chapters 2–5, respectively. This chapter describes characteristics of lakes and reservoirs; their hydrodynamic, sediment, and water quality processes; and case studies on the modeling of lakes and reservoirs.

9.1 CHARACTERISTICS OF LAKES AND RESERVOIRS

Lakes are distributed throughout the world and are abundant in high latitudes, particularly in areas subjected to glacial action. Lakes and their watersheds are valuable ecosystems for both people and nature. More than 90% of all available liquid surface freshwater in the world is contained in lakes. Lake ecosystems commonly include significant wetlands along the shore as well as open waters. Communities surrounding lakes often depend heavily on the lakes for water, food, and way of life. Lakes also provide important habitat for many plants, fish, and waterfowl that depend on lakes for survival.

The designated uses of a lake include (1) water supply for drinking, irrigation, and industrial use; (2) recreation, such as swimming, fishing, and boating; (3) flood control; (4) power generation; and (5) navigation. Compared with rivers and estuaries, the distinctive characteristics of lakes include (1) relatively low flow velocity; (2) relatively low inflows and outflows, (3) development of vertical stratification, and (4) acting as sinks of nutrients, sediments, toxins, and other substances originating from point and nonpoint sources.

Hydrodynamics and Water Quality: Modeling Rivers, Lakes, and Estuaries, by Zhen-Gang Ji

A major difference between rivers and lakes is in the speed of water flow. Water speeds are generally much smaller in lakes than in rivers. Thus, on the right side of Eq. (2.1.33), the first term (the advection term) is generally much larger than the second term (the mixing term) in rivers, while the first term may be comparable to or even smaller than the second term in lakes. The fast-flowing nature of rivers often results in well-mixed profiles in the vertical and lateral directions and rapid downstream transport, whereas the deeper, slower-moving water in lakes tends to have stratified vertical profiles and lateral variations. Lakes are also distinguished from estuaries that have interchanges with the ocean and are subject to tides.

Due to its relatively large velocity, a river, especially a shallow, narrow river, can often be well represented one-dimensionally. By contrast, a lake generally has much more complicated circulation patterns and mixing processes, which are largely affected by lake geometry, vertical stratification, hydrological conditions, and meteorological conditions. Lakes and reservoirs tend to store water over seasons and years. Such a long retention time often makes internal chemical and biological processes significant in the lake water column and the sediment bed, whereas these processes might be negligible in rapid-flowing rivers.

9.1.1 Key Factors Controlling a Lake

This section introduces key factors that influence the water quality in a lake. Knowledge of the formation and history is important to understanding a lake. Hutchinson (1957, 1967, 1975) listed 76 different types of lakes based solely on their origins. The characteristics of a lake depend on many factors, including (1) formation and history, (2) human activities in the past, (3) climate, (4) size and shape of the drainage basin, and (5) physical features.

A lake is closely linked to its drainage basin (watershed). Therefore, the watershed features, such as land use, climate, size, and shape, directly or indirectly influence the hydrodynamic and water quality conditions in the lake. A large ratio of lake drainage area (DA) to surface area (SA), DA/SA, usually indicates the potential for high sediment and nutrient loads.

A variety of lake factors control the in-lake hydrodynamic conditions, including (1) depth, length, width, volume, and surface area; (2) inflows and outflows; (3) hydraulic residence time; and (4) lake stratification. A lake's geometry, formally called morphometry, can largely be described by the length, width, depth, volume, and surface area of the lake. Water depth and hydraulic residence time are the two key indices representing the physical features of a lake. The mean depth of a lake (Z) is equal to the volume (V) divided by the surface area (A):

$$Z = \frac{V}{A} \tag{9.1.1}$$

Lakes can be generally classified as shallow (<7 m) and deep (>7 m), and can be divided into short residence time (<1 year) and long residence time (≥1 year) (Chapra, 1997; Hutchinson, 1957; Wetzel, 1975). In general, mean depth is inversely related to a lake's biological productivity (growth of algae and weeds). Lakes with large mean depths generally are less productive than lakes with small mean depths.

The average time required to completely empty the lake water through outflow is called the hydraulic residence time (flushing time or retention time), which is defined as the ratio of lake volume to the lake outflow rate (Q):

$$\tau = \frac{V}{Q} \tag{9.1.2}$$

where τ is hydraulic residence time.

Hydraulic residence time represents the average length of time that water resides in a lake, ranging from several days in small impoundments to years in large lakes. Inflows supply nutrients to the lake. Hydraulic residence time can have a significant influence on the responses of a lake to nutrient enrichment. A short hydraulic residence time can reduce the time available for plant growth and result in less accumulation of biomass. Long residence times result in recycling and greater nutrient retention. For example, if the lake volume is small and the outflow is high, the hydraulic residence time will be short. This condition causes nutrients to be quickly flushed out of the lake. On the other hand, if the lake has a long hydraulic residence time, nutrients can reside in the lake for a long time, and algae can have more of a chance to grow. Kimmel et al. (1990) reported that algae do not accumulate at hydraulic residence times <7 days.

9.1.2 Vertical Stratification

One of the most significant factors responsible for the vertical gradients in water quality is the density stratification due to temperature. Lakes are typically not well mixed, due to surface heating by solar radiation and insufficient vertical mixing. In summer, buoyancy confines the warmed waters to the near-surface layer. This vertical structure generally varies from year to year due to differences in solar energy, wind, and inflow. Stratification can form in lakes of only a few meters deep (e.g., Jin and Ji, 2004). A typical temperature profile of a lake in summer is shown in Fig. 9.1.1, which indicates that lakes may become physically stratified into three identifiable layers: (1) epilimnion, (2) thermocline (metalimnion), and (3) hypolimnion.

The epilimnion is the upper layer where the temperature is relatively uniform over depth. This layer is usually well mixed by wind action at least some portion of the day and represents the less dense, warmer water in the lake.

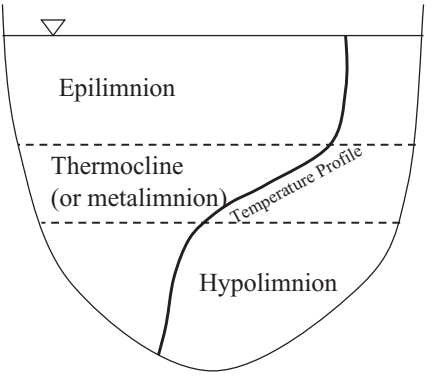

Fig. 9.1.1 Vertical layers and a temperature profile in a lake.

Beneath the epilimnion is the thermocline (or metalimnion), which is the middle zone that represents the transition from warm surface water to cooler bottom water. It exhibits the minimum vertical mixing and the maximum rate of temperature decrease with respect to the depth. Although the term "thermocline" is often used synonymously with metalimnion, the thermocline actually represents the plane of maximum rate of temperature decreases within the metalimnion. An important feature of the thermocline is its effectiveness in putting a limit on the vertical exchange of turbulent kinetic energy generated either by surface wind or by friction at the bed. Since the downward momentum transfer is severely inhibited, the upper layer of the water column is easily moved by wind stress on the water surface.

The hypolimnion is the layer that extends to the bottom of the lake where the temperature steadily decreases. Compared with the epilimnion, water in the hypolimnion is much colder. The hypolimnion is typically the coldest layer in the summer, is relatively undisturbed from wind mixing, and is often too dark for much plant photosynthesis to occur. The density gradient in the thermocline can act as a physical barrier that prevents vertical mixing between the epilimnion and the hypolimnion during the summer.

Vertical temperature profiles of lakes vary with season. At the end of winter, a lake is often well mixed from top to bottom as the result of winter meteorological conditions (e.g., cold air temperature, strong wind, and weak solar radiation). Lake stratification begins in spring and reaches its peak in late summer. Surface water temperature decreases gradually from the end of the summer and through the winter, and eventually the lake temperature becomes vertically homogenous in winter. A good example of lake stratification and its seasonal variations are shown in Fig. 9.1.2, which illustrates the seasonal variations of water temperature and DO of Lake Tenkiller, OK (Ji et al., 2004a). A detailed discussion of the modeling of Lake Tenkiller is presented in Section 9.4.1 as a case study.

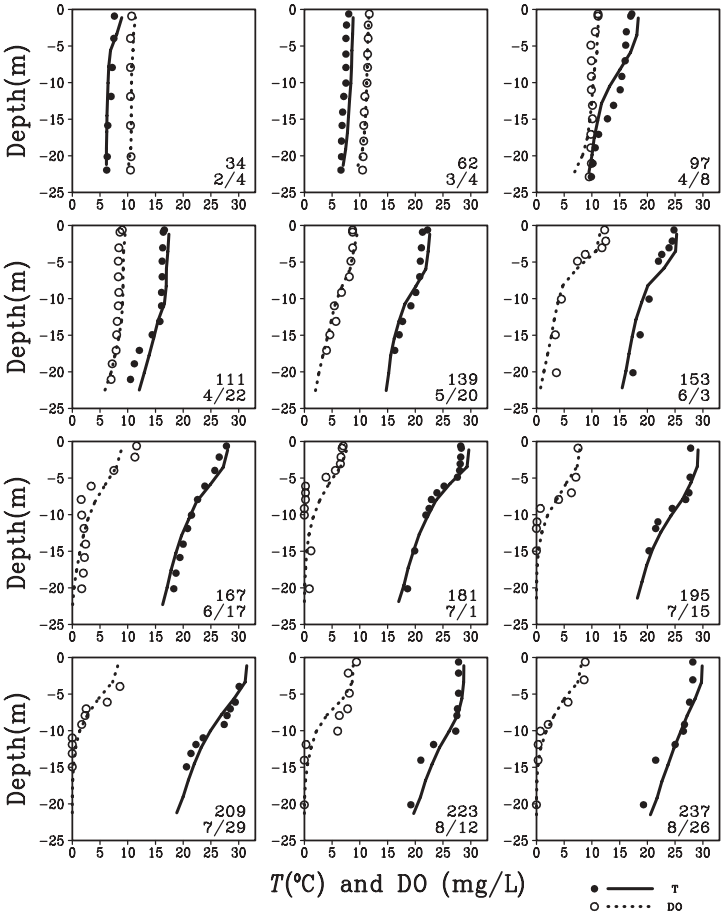

Fig. 9.1.2 Vertical profiles of water temperature (T) and dissolved oxygen (DO) at OKN0166 in Lake Tenkiller, OK. The corresponding date and Julian Day are shown in the lower right corner of each plot. Solid line = modeled T, closed circle = measured T, dashed line = modeled DO, and open circle = measured DO (Ji et al., 2004a).

Thermal behaviors in lakes and reservoirs have significant impact on water quality processes and engineering applications, such as lake management, power plant setting considerations, and thermal effects of power plant discharges on ecosystems. Temperature stratification is the most common type of density stratification, but other factors may also produce density stratification. For example, high suspended sediment concentrations increase water densities and reduce mixing. Higher sediment concentration near the bottom of the water column can cause density stratification and hinder the mixing of the bottom water with the overlying water.

9.1.3 Biological Zones in Lakes

Based on its temperature profiles, as discussed in the previous section, a lake can stratify into three distinct vertical layers: epilimnion, thermocline, and hypolimnion. Based on its biological communities, a lake can be separated into three distinct biological zones (Fig. 9.1.3): (1) littoral zone, (2) pelagic zone, and (3) benthic zone.

The littoral zone is a unique habitat found at the edge of the shoreline, where sunlight penetrates all the way to the lake bottom and allows the growth of rooted and floating aquatic plants (macrophytes). In the littoral zone, ~1% (or more) of surface sunlight can reach the sediment bed for the macrophytes to grow. Emergent, submerged, and floating aquatic plants often are abundant in the littoral zone. In addition to being a food source, these aquatic plants provide habitat for fish, invertebrates, and other organisms. In the summer, waters in the littoral zone become very hot with little moderation in temperature. In winter, ice may cover the water, making these zones much colder than deeper areas. Littoral zones are strongly affected by surface wind and inflows surrounding the lake. For example, Fig. 2.4.2 shows the littoral zone in Lake Okeechobee.

The pelagic zone (or open water zone) is the region of a lake where sunlight generally does not penetrate all the way to the lake bottom. The euphotic zone (Fig. 9.1.3) is the layer from the water surface down to the depth where the sunlight is at the level of 1% of the surface sunlight. It is the uppermost layer of the lake that receives sufficient sunlight for photosynthesis and aquatic plant growth. Below the euphotic zone, the sunlight level is too low for photosynthesis. In most lakes, the euphotic zone exists within the epilimnion. In very clean and transparent lakes, however, sunlight can penetrate well below the thermocline, and the euphotic zone (and photosynthesis) can even occur in the hypolimnion.

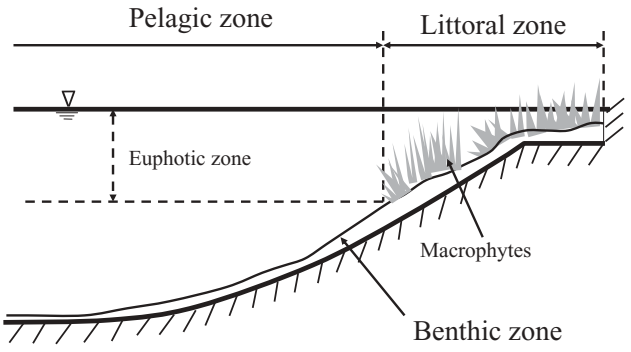

Fig. 9.1.3 Macrophytes and the littoral, pelagic, and benthic zones of a lake.

The depth of the euphotic zone can be estimated from the Secchi depth, Z_s. Eqs. (2.3.17) and (3.2.19) yield:

$$D = -\ln\left(\frac{I(D)}{I_s}\right)\frac{Z_s}{C} \tag{9.1.3}$$

By letting $I(D)/I_s = 0.01$ and $C = 1.83$, which is the value in Lake Okeechobee given by Eq. (3.2.20), the depth of the euphotic zone, D_E, can be estimated using the following:

$$D_E = 2.52Z_s \tag{9.1.4}$$

Equation (9.1.4) indicates that a general rule of thumb is that the depth of the euphotic zone is about two to three times that of the Secchi depth.

The benthic zone is the thin sediment layer on the lake bottom (Fig. 9.1.3). It is typically a few centimeters thick and contains a wide variety of benthic organisms, which are mostly invertebrates. The abundance and species composition of benthic organisms are influenced strongly by the oxygen level in the benthic zone. The bioturbation of benthic organisms can be quantified by the particle mixing velocity in Eq. (5.7.27).

Even though the littoral, pelagic, and benthic zones have different biological activities, the hydrodynamic transport and movement of organisms link the three zones. For deep lakes, the impact of macrophytes on the biological community is relatively small, since aquatic plant growth is restricted to a relatively narrow and limited region. For shallow lakes, intense sediment bed-water column interaction and the abundant aquatic plants in the large littoral zone make the water quality processes in shallow lakes different from those in deeper lakes in many aspects.

9.1.4 Characteristics of Reservoirs

A main function of a reservoir is to stabilize the flow of water by regulating the downstream outflows. Reservoirs are built for widely different purposes, including the following:

1. *Flood Control:* Reservoirs control flooding by storing water during flood periods for later release. They reduce the magnitude of the flood peak, but extend elevated discharges over a longer period.
2. *Navigation:* Reservoirs provide sufficient water to maintain adequate water depth for navigation.
3. *Water Supply:* Reservoirs store water during wet periods for later use during dry periods.
4. *Power Generation:* Hydroelectric power is generated by passing water through turbines.

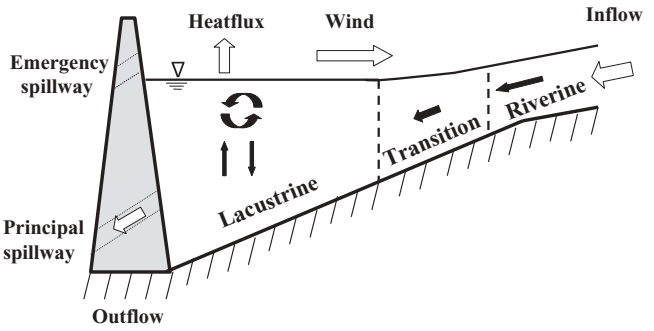

Fig. 9.1.4 The riverine, transition, and lacustrine zones of a reservoir.

Reservoirs vary widely in morphometry, hydrology, and management objectives. They can be small and shallow ponds, large and deep reservoirs, or flow through navigational pools. No generally accepted method of classifying reservoirs exists. Since a primary function of reservoirs is to store water, the hydraulic residence time, which is defined as the reservoir volume divided by the outflow rate, is one of the most important reservoir parameters. If the residence time is long, the internal processes, such as stratification and nutrient fluxes from the bed, are expected to significantly affect the water quality in the reservoir. If the hydraulic residence time is short, water quality in the reservoir is likely to be controlled by the inflow.

The principal spillway of a reservoir (Fig. 9.1.4) is designed to regulate the water level and is used first during normal inflow and flood flows. The emergency spillway is a secondary spillway used to convey floodwaters in excess of the capacity of the principal spillway. It allows inflows from large storms to be released from the reservoir before the water level rises too high to overtop the dam.

As discussed previously in this section, natural lakes often have three distinct biological zones: littoral, pelagic, and benthic. The littoral zone plays a significant role in natural lakes. However, reservoirs, created by a dam located on the main channel of a watershed, often have steep slopes and a very narrow littoral zone, if any. Reservoirs have characteristics of both rivers and lakes and have unique physical characteristics. They are generally long and narrow, compared with natural lakes that can be any shape. They are river-like at the head where major tributaries enter and are more lake-like near the dam. In addition to the vertical stratifications discussed previously, reservoirs can also exhibit significant longitudinal variations in hydrodynamic and water quality properties. With one or more upstream inflows and a downstream outflow, water quality gradients in reservoirs are almost always significant in the longitudinal direction. Reservoirs, such as Lake Tenkiller (Fig. 9.4.1), typically have main inflows and tributaries located far away from the outflow at the dam and can often be divided into three distinct zones (Fig. 9.1.4): (1) riverine, (2) transition, and (3) lacustrine.

The riverine zone is usually narrow and well mixed. In a river, gravitational force due to the slope of water surface drives the flow and transport. As the river flows into the riverine zone (Fig. 9.1.4), the slope decreases and eventually becomes almost flat in the lacustrine zone. In the riverine zone, although the flow is decreasing, the river-like flowing condition is still dominant. In the transport equation (2.1.33), the first term (advection) is much larger than the second term (mixing). The flow still transports significant amounts of suspended particles. As a result, the turbidity is relatively high, and the light penetration is low.

The transition zone features the transition from riverine-like to lake-like conditions. The water surface gradually becomes flat. Because of the decreased water surface slope in this zone, velocities decrease and suspended particles settle, with a subsequent increase in light penetration. Within the transition zone, buoyancy forces due to density differences between inflows and lake waters become significant.

The lacustrine zone is characteristic of a lake-like condition, especially in the forebay area, which is the part of the reservoir immediately behind the dam. In this zone, buoyancy forces dominate the flow patterns. Due to low flow velocity and deep water depth, concentrations of suspended particles are generally low, and light penetration is sufficient to promote algal growth.

Unlike natural lakes that usually discharge surface water, reservoirs can have outlets at different levels so that the quantity and quality of the water released can be controlled. A stratified or unstratified condition can dramatically affect water quality conditions of the reservoir and its releases. Reservoirs with stratification can be used to control the temperature of the water released by allowing discharge from the epilimnion, thermocline, and/or hypolimnion, depending on the needs. Via variable depth outlets, for example, colder bottom water can be released when needed for fish, and warmer surface water can be released when needed for irrigation.

Reservoirs have a great deal of spatial variation in hydrodynamic and water quality variables. For example, sediment in a reservoir typically experiences a longitudinal sorting by grain size. Coarser particles settle first in the upper portion of the reservoir, and finer particles remain in suspension longer and are deposited further down the reservoir. Coarse (inflow derived) organic matter is concentrated at the upstream end of the reservoir. Finer particulate organic matter settles further downstream. River algae may also settle in the upper portion of the reservoir, but are more concentrated in the deepest parts. As these suspended materials settle longitudinally, light penetration increases gradually in the reservoir. The decreasing curve in Fig. 9.1.5 depicts the general pattern of longitudinal reduction in the reservoir, while the increasing curve shows the general pattern of longitudinal increment.

The following variables should decrease gradually downstream and should follow the pattern described by the decreasing curve in Fig. 9.1.5: (1) velocity, (2) suspended matters, and (3) nutrients available to algal growth. The

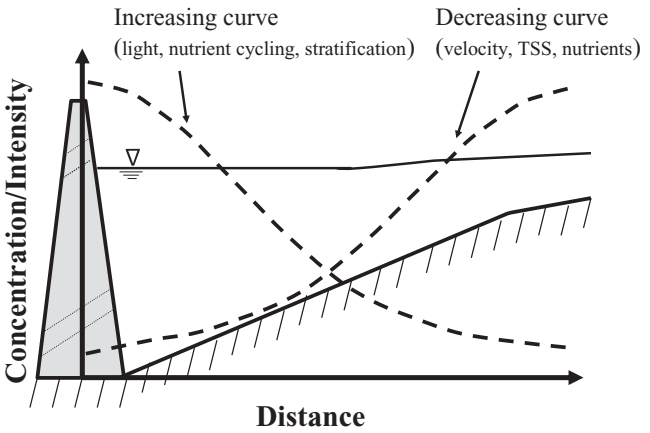

Fig. 9.1.5 Schematic representation of longitudinal distributions of hydrodynamic and water quality variables in a reservoir.

following variables should increase gradually downstream and should follow the pattern described by the increasing curve in Fig. 9.1.5: (1) light penetration, (2) internal nutrient cycling, and (3) vertical stratification.

When the light penetration is increased, algae will have sufficient light for photosynthesis and consume more nutrients. This leads to the reduction of nutrients available to algal growth in the surface layer. The deposited particulate matters in the deep portion of the reservoir go through sediment diagenesis processes in the sediment bed. As a result, nutrients are eventually released back to the water column from the bed. This process of internal nutrient cycling also affects the DO levels in the bottom layer significantly, which may cause the bottom waters to be anoxic due to the SOD from the bed.

The major differences in characteristics between natural lakes and manmade reservoirs include (1) morphometry, (2) biological zones, (3) external loadings, and (4) management objectives. One of the most important distinctions between natural lakes and reservoirs is the shape of the waterbody, which influences the hydrodynamic, sediment, and water quality processes significantly. The deepest portion of a natural lake, such as Lake Okeechobee (Fig. 2.4.3), is often located near the center of the waterbody, with the lake bottom sloping toward the center. Large reservoirs, such as Lake Tenkiller (Fig. 9.4.1), are drowned river valleys and tend to be long and deep. The deepest area of a reservoir is almost always near the dam, with the reservoir bottom sloping toward the dam.

Reservoirs typically have much larger watersheds than natural lakes. The ratio of drainage area to the surface water area of a reservoir is usually much larger than that for a lake. Therefore, reservoirs often have larger sediment loadings, nutrient loadings, and seasonal variation in water inflow rates. With greater sediment and nutrient loadings, many reservoirs have greater sedimentation rates and are more turbid than natural lakes. Also, a lake generally has

the inflow and outflow near the surface, whereas a reservoir can release water at any water depth, ranging from the surface to the bottom.

Reservoirs are most likely located in areas with few or no natural lakes. Reservoirs are often built and managed for specific purposes, such as flood control, navigation, water supply, and/or power generation. The outflow and storage of a reservoir are regulated to achieve a beneficial use. Reservoir management might include extreme water level fluctuations and discharge depth controls, which can significantly influence the transport and mixing patterns and, consequently, the water quality within the reservoir. Most natural lakes have limited control over water depth and discharge depth.

9.1.5 Lake Pollution and Eutrophication

Lakes and reservoirs are waterbodies that can hold water for a long time. Pollutants from point and nonpoint sources can be easily trapped in lakes because of the long hydraulic residence time and relatively small discharge rate. Therefore, lake conditions are especially sensitive to additional pollutants from human activities, which can overload the ecosystem and accelerate eutrophication. Excessive algal growth and low DO levels are common symptoms of accelerated eutrophication in lakes.

The most common pollutants affecting lakes include (1) nutrients, (2) metals and toxic chemicals, and (3) sediments. Lake eutrophication originates from excessive nutrient loadings. Healthy lake ecosystems contain nutrients, such as nitrogen and phosphorus, in small quantities from natural sources. Extra nutrient inputs disrupt the balance of lake ecosystems and may lead to algal blooms, excessive aquatic plant growth, and eventually oxygen depletion (Fig. 9.1.6). Excessive nutrients stimulate blooms of undesirable algae and aquatic plants. This excess can lead to many environmental problems. For example, noxious aquatic plants clog the shoreline and reduce access to the lake. A large biomass eventually results in a large quantity of dead plants sinking to the lake bottom. Bacteria consume dissolved oxygen in the water while decomposing the dead plants. This process, in turn, deprives fish and other oxygen-consuming organisms and impairs the quality of lake water. Fish kills and foul odors may also result if dissolved oxygen is depleted. Nutrients, such as P, can also be carried into lakes via sediment particles, deposited on the lake bottom, and resuspended again at a later time to make lasting impact on the lake water quality. Metals and other organic chemicals, such as mercury and PCBs (discussed in Chapter 4), contaminate sediment, fish, and shellfish. They are a major cause of impairment to lakes. An overabundance of sediments from the surrounding watershed can fill lakes, reduce the life span of reservoirs, and destroy habitat for plants and animals.

The eutrophication of lakes and reservoirs is largely caused by agricultural runoff and untreated industrial and urban discharges. For example, the destruction of shoreline vegetation may lead to the increased erosion of sediment and nutrients into a lake. In the United States, most of the problems associated

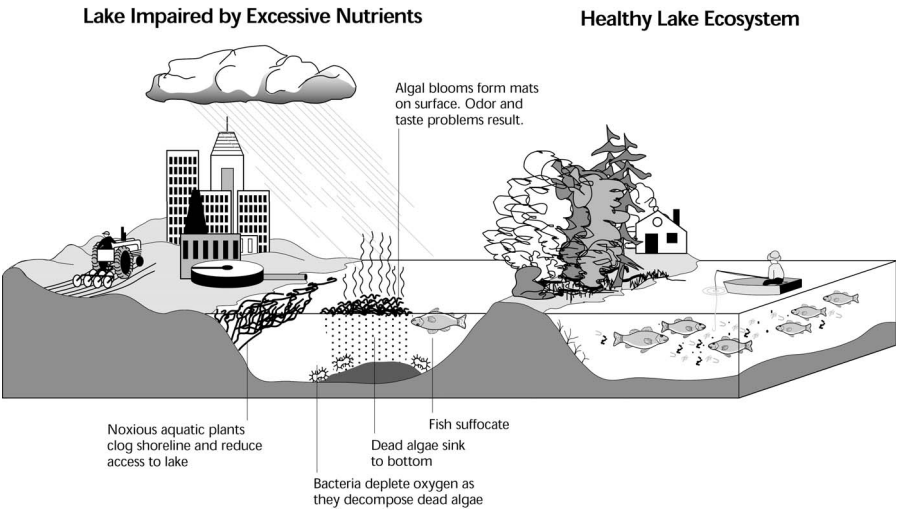

Fig. 9.1.6 Comparison between a lake impaired by excessive nutrients and a healthy lake ecosystem (USEPA, 2000a).

with the direct discharge of domestic wastewater have been successfully mitigated. Now the regulatory focus is on the more difficult problem of controlling nonpoint sources of nutrient pollution, such as agricultural runoff. The prevention of lake eutrophication requires planning and management of the associated watershed (USEPA, 2000a). It needs an understanding of the relationship between nutrient sources and the eutrophication processes in the lake.

A lake's trophic status is a description of the biological condition of the lake. Lakes and reservoirs are commonly grouped into three different trophic statuses (Fig. 5.1.1):

1. Oligotrophic status (low nutrients/low productivity).
2. Mesotrophic status (intermediate nutrients/intermediate productivity).
3. Eutrophic status (high nutrients/high productivity).

The trophic statuses are a useful means of classifying lakes and describing lake processes in terms of the productivity of the system. A lake usually undergoes these three statuses through time. The oligotrophic status is usually associated with deep lakes, in which bottom waters are cold and have high levels of DO throughout the year. The lake has low nutrient concentrations and low plant growth. The sediment bed contains small amounts of organic materials. Biological productivity in terms of phytoplankton, SAV, and fish is low. Water quality in the lake is usually good.

The mesotrophic status is characterized by intermediate levels of nutrient and biological productivity, and the bottom DO in the lake is reduced. The water quality is often deteriorating toward the eutrophic status, but is still adequate for most beneficial uses.

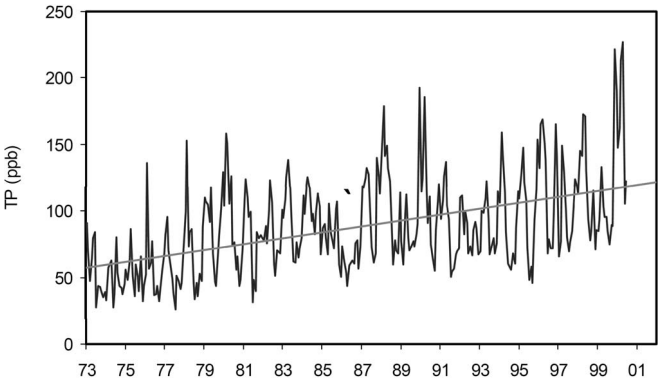

Fig. 9.1.7 Total phosphorus concentration in Lake Okeechobee for the period between 1973 and 2000. The straight line indicates the general trend of P-level increment (SFWMD, 2002).

The eutrophic status is featured with (1) high concentrations of nutrients, (2) high biological productivity, (3) high concentrations of algae, (4) low DO concentrations (especially near the bottom), and (5) thick sediment bed with high organic materials.

In extreme cases of eutrophication, the DO in the lake bottom may reach zero during summer periods. Lake water quality is usually low and may be inadequate for the designated uses. Processes that control eutrophication in lakes and reservoirs include (1) hydrodynamic processes, especially inflow, outflow, and vertical mixing; (2) sediment processes, such as sediment resuspension and phosphorus transport in shallow lakes; and (3) chemical and biological processes.

Modeling eutrophication in lakes, therefore, involves representation of all these processes (see general discussions in Chapters 2, 3, and 5). The unique features of algal growth, nutrient recycling, and DO stratification in lakes will be presented in this chapter.

As an example of lake eutrophication, Fig. 9.1.7 gives the total phosphorus concentration in Lake Okeechobee for the period between 1973 and 2000 (SFWMD, 2002). The straight line indicates the general trend of the P-level increment. The corresponding annual TN/TP ratio in the lake is already given in Fig. 5.1.6. In addition, Fig. 9.1.7 shows that:

1. The lake has strong seasonal variations.
2. The annual mean P concentration has increased dramatically in <3 decades, from 55 μg/L in 1973 to >110 μg/L in 2000.

9.2 HYDRODYNAMIC PROCESSES

This section focuses on the following hydrodynamic processes: (1) inflows and outflows, (2) wind forcing and vertical circulations, (3) seasonal variations of

thermal stratification, (4) gyres, and (5) seiches. These processes are commonly seen and often play significant roles in lakes and reservoirs, but they are not limited to lakes and reservoirs. These processes may also be observed in other waterbodies, such as rivers and estuaries.

9.2.1 Inflow, Outflow, and Water Budget

Inflows to lakes and reservoirs include river flows, watershed runoff, groundwater inflow, and discharges from wastewater treatment plants. An inflow displaces the standing lake water after entering a lake. If there is no density difference between the inflow water and the lake water, the inflow will mix with the lake water rapidly. If there are density differences, turbulent mixing in the lake will be affected, and the inflow will move as a density current in the form of overflow, interflow, or underflow (Fig. 9.2.1*a–c*). Density current is a flow through a larger waterbody, retaining its unmixed identity because of a difference in density. As discussed in Section 2.1.1, temperature, salinity, and suspended sediment are the three primary parameters determining water density.

When river waters are warmer than lake waters, the inflow waters will tend to spread out over the lake surface in the form of overflow (Fig. 9.2.1*a*). Mixing between the lake waters and the inflow waters will increase as temperature difference is reduced. When surface waters are cooling down, river waters are often colder than lake waters, and the inflow will drop below the lake surface and submerge to a depth where the densities of the lake and that of the incoming waters are equal. As a result, the inflow forms a density flow below the warmer surface water, but above the colder bottom water (the interflow shown in Fig. 9.2.1*b*), or the inflow sinks all the way to the bottom of the lake and forms an underflow (Fig. 9.2.1*c*). As an example, Yang et al. (2000) studied temperature and density-driven circulation in Lake Billy Chinook, Oregon, and successfully simulated the three flows (overflow, interflow, and underflow) in the lake.

Plunge point is the location at which the denser inflow plunges beneath the water surface and becomes a density current. As illustrated in Figs. 9.2.1*b* and *c*, the inflow leaves the surface at the plunge point and continues as an underflow (or interflow) in the lake. Due to the velocity shear between the underflow and the overlying lake water, some of the lake water is dragged downwards, and a corresponding counterflow is induced in the upper layer of the lake. Because of this surface velocity pattern, the plunge point is sometimes marked by floating debris on the lake surface.

As discussed in Section 2.1.1, water density varies with temperature and concentrations of dissolved and suspended materials. A same temperature difference causes a greater density difference at high temperature than at low temperature. For example, the density difference due to a temperature difference of 1 °C is about three times greater at 20 than at 5 °C. Therefore, even a small temperature difference at high water temperature (say in the summer)

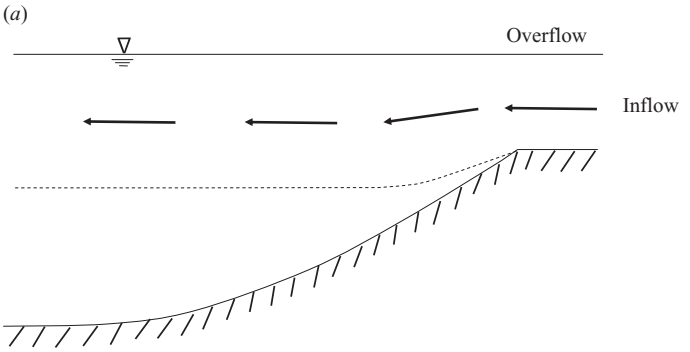

Fig. 9.2.1(a) Density inflow and mixing processes in lakes and reservoirs: overflow.

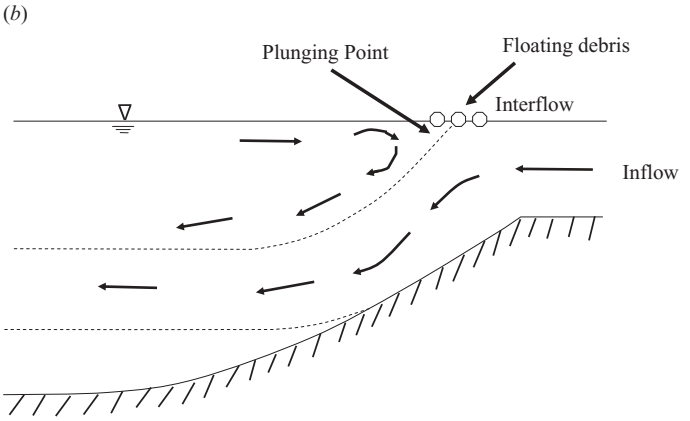

Fig. 9.2.1(b) Density inflow and mixing processes in lakes and reservoirs: interflow.

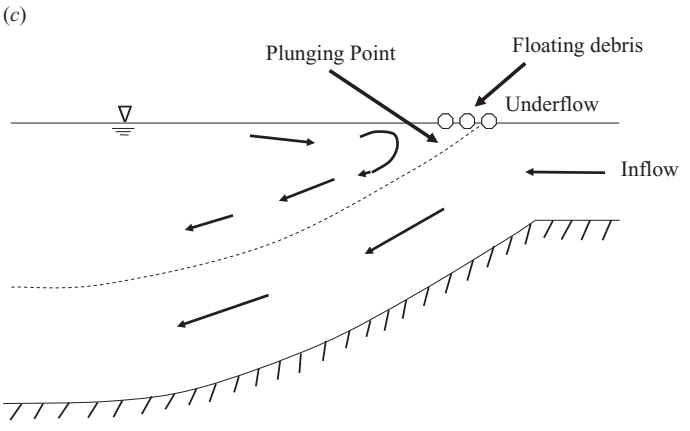

Fig. 9.2.1(c) Density inflow and mixing processes in lakes and reservoirs: underflow.

may cause significant dampening of the turbulent mixing and lead to the formation of density current. This phenomenon is an important reason to the frequent occurrence of turbid density currents in tropical and subtropical waters.

Inflows contribute to lake mixing and serve as a primary source of sediments and nutrients. As shown in Figs. 9.2.1*a–c*, the inflow rate and the density differences between the inflow water and the lake water dictate the distributions of the incoming sediments and nutrients. The timing of nutrient loadings relative to lake seasonal stratification can influence distributions of the nutrients. For example, when an inflow enters a stratified lake in the summer in the form of underflow (Fig. 9.2.1*c*), the nutrient loadings are emptied directly into the bottom of the lake, which is most likely already nutrient-rich. These additional nutrients are not directly available to the eutrophication processes in the euphotic zone (Fig. 9.1.3) and therefore may not have immediate impact on the algal growth in the lake. On the other hand, when an inflow enters a stratified lake in the form of overflow (Fig. 9.2.1*a*), the nutrient loadings are spread out in the euphotic zone, in which algal growth is limited due to the lack of certain nutrients (e.g., P). The incoming nutrients (P) may cause an immediate algal bloom in the lake. In summary, it is necessary to take into account the effects of inflow timing and lake stratification. This possible sequence of events also illustrates why a comprehensive model may be needed to simulate the spatial and seasonal variations in detail (e.g., Ji et al., 2004a).

Outflows include natural releases from lakes and discharges at reservoir dams. Natural lakes often have discharges from the lake surface. For reservoirs, however, discharges are normally regulated by passing through control structures of the dam. When water is released from a reservoir, potential energy is converted into kinetic energy. Mixing is a result of this conversion of energy, and the degree of mixing varies with the location of the discharge outlets. Bottom discharge increases vertical mixing and dissipation of bottom materials, whereas surface discharge has a minimal impact on the bottom materials.

Water balance in lakes and reservoirs is the result of the income of and losses from the waterbody. Inflows and outflows affect the water surface elevation, surface area, and lake volume. Rapid raising and lowering of water levels for power generation, irrigation, and other uses can disrupt the lake's natural ecology, especially along the shore. As a result, it may have a significant impact on lake water quality on an annual, seasonal, daily, and even hourly basis. Mathematically, the water budget of a lake is deceptively simple: income equals to losses plus (or minus) change in storage. In practice, however, measuring the income and losses can be very complicated. The water budget for a lake is

$$\Delta V = V_{\text{new}} - V_{\text{old}} = V_{\text{inflow}} + V_{\text{prec}} \pm V_{\text{ground}} - V_{\text{outflow}} - V_{\text{evap}} \tag{9.2.1}$$

where ΔV = lake volume change, V_{new} = new lake volume, V_{old} = old lake volume, V_{inflow} = inflow volume, V_{prec} = precipitation volume, V_{ground} = ground-

water seepage volume, $V_{outflow}$ = outflow volume, and V_{evap} = evapotranspiration volume.

Lakes interact with all components of the hydrological system: atmospheric water, surface water, and groundwater. As illustrated in Eq. (9.2.1), the change in water storage is a function of the difference between income and loss. The income may consist of tributary inflow, watershed runoff, point source discharges, precipitation on the water surface, and groundwater. Water losses occur through lake discharge, groundwater recharge or seepage, and evapotranspiration. Evapotranspiration is the combination of water that is evaporated and transpired by plants as a part of their metabolic processes. It represents the loss of water in a lake by evaporation from the water surface and by transpiration from aquatic plants. For example, Lake Okeechobee is a large, shallow subtropical lake. Precipitation is the major water source, representing ~54% of the total water input to the lake. The evapotranspiration makes up to 70% of the total water losses (SFWMD, 2002).

9.2.2 Wind Forcing and Vertical Circulations

As shown in Fig. 9.1.4, three external forcings are essential to the hydrodynamic processes in lakes and reservoirs, (1) heatflux exchanges and thermal forcings, (2) inflow and outflow, and (3) wind forcing. Heatflux exchanges and thermal forcings are discussed in Section 2.3. Inflow and outflow are described in Section 9.2.1. This section is focused on wind forcing and vertical circulations in lakes.

Wind forcing is a key factor determining a lake circulation and a major energy source for vertical mixing. This impact is especially true in large lakes, as is illustrated in the case studies of Lake Okeechobee and Lake Tenkiller in this book. When the wind blows across a lake (Fig. 9.2.2), it:

1. Exerts a shear stress on the water surface.
2. Results in momentum transfer from the air into the water.
3. Causes the surface water to move in the direction of the wind.

Wind energy is converted into turbulence in the surface layer and is then transferred to the lower parts of the epilimnion by turbulent diffusion, until the thermal gradient dissipates the energy. The turbulent mixing in the lake has a layered vertical structure, because the water motion is largely confined to the epilimnion and currents in the hypolimnion are weak. Consequently, the depth of turbulence penetration can be restricted. In shallow lakes (e.g., Lake Okeechobee), wind-induced turbulence may occur at all depths, and therefore can significantly enhance nutrient entrainment from the sediment bed. In deeper lakes (e.g., Lake Tenkiller discussed later in Section 9.4.1), however, this wind-induced turbulence cannot reach the bottom except around the lake edges. In such deep lakes, sediment resuspension is weak and nutrients tend to accumulate on the bed.

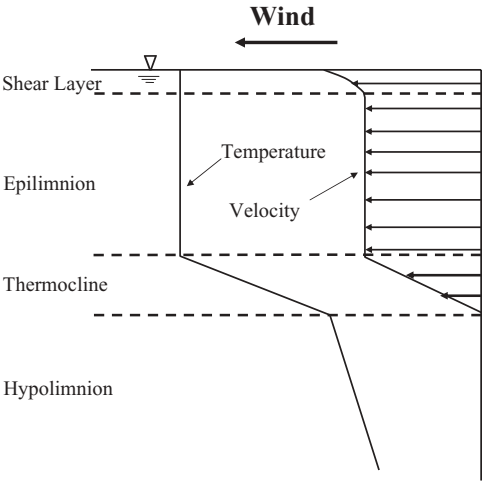

Fig. 9.2.2 Wind forcing processes in a lake.

Another effect of wind forcing is the setup (or set-down) of the water surface elevation. This response can be assessed quantitatively with the following equation:

$$\frac{\partial \eta}{\partial x} = \frac{\tau_x - \tau_b}{\rho g H} \tag{9.2.2}$$

where $H = h + \eta$ = total water depth, h = the equilibrium water depth, η = surface displacement from the equilibrium, τ_x = wind stress in the x direction, and τ_b = bottom shear stress in the x direction.

This equation is obtained by simplifying Eq. (2.2.7). Note from Eq. (9.2.2) that the surface elevation slope has the same sign as the wind direction. A wind blowing in the negative direction produces a negative water elevation slope, since the wind piles up water in the downwind direction. In shallow waters, the effects of bottom friction, τ_b in Eq. (9.2.2), may become significant in the calculation of the surface elevation slope.

When wind blows over a lake, the wind stress results in water movement in the epilimnion and sets up an inclination in the water surface (Fig. 9.2.3). Water moves faster along the surface in the direction of the wind than the returning underflow due to resistance from the bed sediment, aquatic vegetation, and other bottom friction. Hence, the downwind rise in water level. The tilted water surface eventually establishes a hydrostatic pressure gradient to balance the wind stress. In response to the water movement in the epilimnion, a countercurrent in the hypolimnion may also be established (Fig. 9.2.3). Such motions can cause significant horizontal as well as vertical transport in both the epilimnion and the hypolimnion. The setup time of this vertical circulation

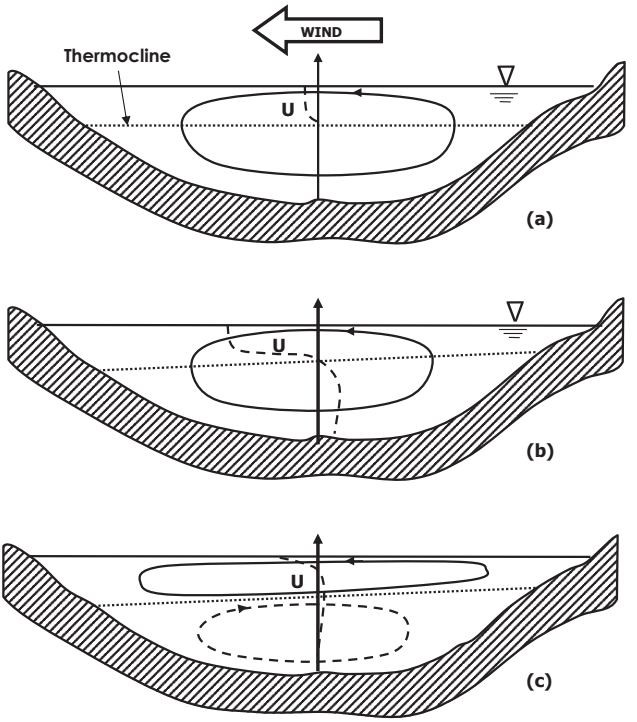

Fig. 9.2.3 Formation of vertical circulation in a lake: (*a*) initiation of motion, (*b*) position of maximum shear stress across the thermocline, and (*c*) steady-state vertical circulation (based on USEPA, 1983).

is proportional to the seiche period of the lake. Discussions on seiches will be presented in Section 9.2.4.

In addition to current circulations, wind forcing also generates wind waves that are important to turbulent mixing and sediment resuspension. The wave motion, especially when waves are breaking, contributes to turbulent kinetic energy in the epilimnion. The orbital velocities of wind waves are critical to sediment resuspension in shallow lakes, as described in Section 3.6.

9.2.3 Seasonal Variations of Stratification

In addition to spatial variations in the horizontal directions, lakes have prominent changes in the vertical, especially during summer. As discussed in Section 9.1.2, stratification is the formation of water layers with different physical, chemical, and/or biological characteristics, such as density or temperature.

In addition to the inflow and outflow discussed in Section 9.2.1, factors controlling lake stratification include (1) solar radiation, (2) wind forcing, (3) water depth, and (4) lake surface area. Stratification typically occurs through

the interaction of wind and solar radiation in the lake surface layer. Heatflux and water depth are two important factors determining the thermal structure of lakes. As discussed in Section 2.3.1, the difference between the heat input and the heat loss determines whether the lake surface is heating or cooling. Heating during the spring and summer may lead to stratification in lakes. Small lakes have short fetch, weak wind waves, and shallow epilimnion; therefore, they are more likely to be stratified. Large lakes generally have a long fetch, strong wind waves, and a deep epilimnion, and therefore, are more likely to stratify in deep water areas only. It is unlikely to have stratification in extremely shallow lakes, because the wind-induced turbulence is strong enough to mix lake waters from the surface to the bottom.

Lake turnover is a vertical mixing process due to density instabilities caused by the cooling of surface water. As the surface water cools, it becomes denser and sinks, mixing with the bottom water. Seasonal temperature changes during spring and fall may cause the water to turnover and mix from top to bottom. Nutrients that are commonly stored in the lake bottom can be stirred up, transferred to the surface layer, and become available for algal growth. A dimictic lake is one that mixes twice a year, in the spring and fall. During the summer and winter (when the lake is covered with ice), there is a thermal stratification, and the vertical mixing is dampened. This pattern (spring turnover—summer stratification—fall turnover—winter stratification) is typical for temperate lakes.

The annual cycle of thermal stratification is well understood and represents one of the most important hydrodynamic processes occurring within a lake. For a lake with negligible inflows and outflows (their impact is discussed in Section 9.2.1), a brief description of seasonal variations of lake stratification is presented here. Even though the discussions are focused on Lake Wister, OK, the processes described are typical and should be generally applicable to many other lakes.

In temperate climates, ice may form on lakes in winters. The surface water temperature is near 0 °C, and the bottom water temperature is usually ~4 °C. Since water has its maximum density at 4 °C, the water column forms a stable stratification with lighter water (near 0 °C) on the top and denser water (~4 °C) at the bottom. As the weather warms, the ice melts. The surface water begins to warm and approaches the temperature of the bottom water. Consequently, there is little thermal stratification to limit vertical mixing in the lake. This period of uniform temperature is referred to as spring turnover.

Lake Wister, OK, shown in Fig. 9.2.4, displays a simple annual cycle. Although it does not experience ice cover and stratification in winters, the lake has clearly distinguishable seasonal variations and serves as a good illustration. The thermal stratification in February of 1993 (~10 °C on the surface and ~8 °C on the bottom) was due to the exceptionally warm weather condition in the area. In the early spring (March, 1993), the temperature (density) of the surface water was equal to that of the bottom water. Very little wind energy was needed to mix the lake completely, and the temperature of the lake became

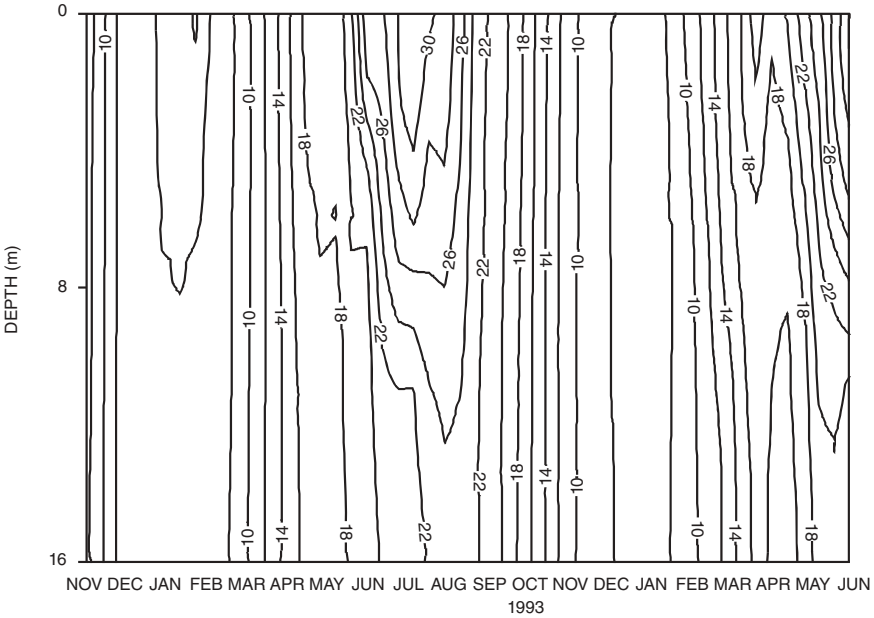

Fig. 9.2.4 Measured temperature profiles in Lake Wister (OWRB, 1996).

uniform near 8 °C. The surface water continued to heat up, and wind forcing continued to stir the water column and distributed this thermal energy into the lower portion of the water column, resulting in an increase in the temperature of the entire water column to 17 °C in early May 1993. As the solar radiation intensified, the density gradient between the surface and bottom increased. The surface water became lighter than the bottom water, and eventually the wind forcing was simply insufficient to completely mix the water column. As a result, a temperature gradient (thermal stratification) was established in the water column in May and June of 1993. The warmer, near-surface water became sufficiently buoyant to resist complete vertical mixing.

In the summer, solar radiation has its highest intensity and the lake becomes stratified into three distinct zones: epilimnion, thermocline, and hypolimnion (Fig. 9.1.1). The thermocline in Fig. 9.2.4 effectively separates the warmer surface layer (epilimnion) from the deeper, cooler layer (hypolimnion). The hypolimnion consists of the coldest water with smaller temperature changes over the year. For example, the surface water temperature has an annual variation up to 23 °C, from 8 to 31 °C, while the bottom temperature varies only 14 °C, from 8 to 22 °C (Fig. 9.2.4). The strong vertical mixing in the epilimnion is important in keeping algae in suspension and remaining within the eutrophic zone. In the thermocline, which is an area of extreme stability, the vertical

transport between the epilimnion and the hypolimnion is limited. During the remaining summer heating season, the lake continues to gain heat by solar radiation. Some of this heat is lost by evaporation and sensible heat transferred to the atmosphere, but some of it is stored in the epilimnion.

In late summer, the rate of heat loss by evaporation and sensible heat exceeds the radiation input, and the lake begins to cool. In the fall, the reductions of solar radiation and air temperature lead to strong cooling of the upper layers. This cooling makes the surface water denser and causes mixing with deeper water and a reduction of the density difference between the epilimnion and the hypolimnion. As fall cooling progresses, winds mix the lake to greater depths, and the surface and bottom waters eventually approach the same temperature and density, a phenomenon called "fall turnover". The lake continues to lose heat to the atmosphere by evaporation and sensible heat, and the water temperature continues to decrease.

In the winter, the water column continues to be vertically mixed (unless the surface water freezes, ice cover prevents wind mixing, and stratification forms under the ice—a situation that does not happen in Lake Wister). As shown in Fig. 9.2.4, water temperature in Lake Wister was never lower than 7 °C in the winter of 1993, and there was no ice formation on the lake. In the months of November–January, the surface water continually cooled, became heavier, and sank. There is little resistance to the stirring action of the wind forcing. The lake remains vertically mixed until the next spring, thus completing the annual stratification cycle.

Lakes exist in a great variety of locations and climates. The above discussion of thermal stratifications in lakes is generally applicable, but, as in most phenomena, there are exceptions. Many shallow lakes, for example, do not stratify (or only stratify for short periods) in the summer. Lake Okeechobee is a good example. The lake may stratify in the afternoon and become vertically mixed at night, as shown in Fig. 2.4.11. In addition to thermal stratifications, a waterbody can also be stratified due to concentrations of dissolved or suspended materials, such as salinity and suspended sediments.

9.2.4 Gyres

A gyre is a circular, rotational circulation pattern, established by winds or other physical forces. In addition to existing in large lakes, gyres are also found in estuaries and open oceans (Fischer et al., 1979).

Gyres have been observed, analyzed, and simulated in many studies. Schwab et al. (2000) reported that the wind-driven circulation pattern in Lake Michigan consisted of two counterrotating gyres: a counterclockwise-rotating gyre to the right of the wind and a clockwise-rotating gyre to the left. The gyres are separated by a convergence zone along the downwind shore with resulting

offshore flow and a divergence zone along the upwind shore with onshore flow. Based on measured data, Lemmin and D'Adamo (1996) analyzed the relationship between atmospheric forcings and a large-scale gyre in Lake Geneva, Switzerland. They concluded that the seasonally persistent gyre is caused by winds and affected by the topography of the surrounding land. The three gyres in Lake Biwa, Japan, induced by both wind and thermal convection, have been studied in detail for many years (e.g., Kumagai et al., 1998). Ishikawa et al. (2002) studied toxic cyanobacterial blooms in Lake Biwa and highlighted the importance of lake gyres in transporting nutrients and algae. They demonstrated that gyres played a key role in cyanobacteria distribution in the lake. Yamashiki et al. (2003) also observed the formation process of three gyres in Lake Biwa using an acoustic Doppler current profiler. They reported that the surface heat transfer process was one of the main driving forces for gyre formation in Lake Biwa. Pan et al. (2002) applied a 3D model to Lake Kinneret, Israel. They indicated that the daily mean wind curl field was responsible for the generation of three lake gyres.

This section uses Lake Okeechobee as an example to discuss the formation mechanism of gyres (Ji and Jin, 2006). As described in Sections 2.4.2 and 7.2.5, a distinct feature of Lake Okeechobee is the two gyres in the lake. Figure 7.2.3 shows the daily-averaged water flows and water depths in the lake on December 25, 1999. Under the forcing of northwest wind of 8 m/s, which is the typical wind pattern in the area during winter, the lake has two distinct gyres: a cyclone in the southwest and an anticyclone in the northeast.

In order to explain the gyres in the lake, the relationship between the wind forcing and the lake circulation is sketched in Fig. 9.2.5. Wind is a primary driving force for lake circulation. When a uniform wind blows over a large and shallow lake that is shallower on the right and deeper on the left, the line of action of the wind forcing is through the centroid of the water surface. Since it is deeper and contains more water on the left, the mass center of the lake water should be toward the deeper side, to the left of the line of centroid. Therefore, the mass center and the line of centroid do not coincide, and a torque is produced. The torque makes the lake water rotate, flowing into the paper on the right and flowing out of the paper on the left. The sign of arrowhead, $\odot$, indicates that the velocity is in the direction out of the paper. The sign of the arrow end, $\otimes$, indicates that the velocity is in the direction into the paper.

Figure 9.2.5 illustrates that, when a constant wind blows over a lake of variable depth, a laterally varying surface current is induced, flowing with the wind in the shallow area and as a return flow against the wind in the deeper area. A counterclockwise rotation (or cyclone) is created by the uniform wind in the direction into the paper. The current on the shallow side (along the shore) is in the wind direction, while the current on the deep side is opposite to the wind direction. Lake Okeechobee has its deepest area in the center

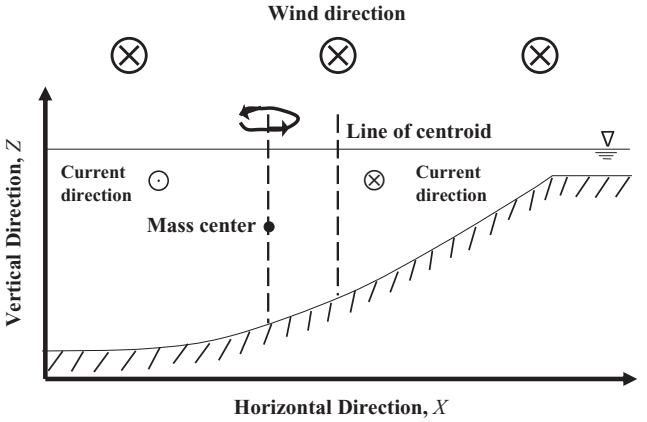

Fig. 9.2.5 A sketch on gyre formation caused by wind forcing. ⊙ = in the direction out of the paper; ⊗ = in the direction into the paper.

of the lake (Fig. 7.2.3). Hence, under the forcing of a uniform wind, the lake should have flows in the wind direction along the shore and opposite to the wind direction in the deep area, just like the two-gyre circulation pattern shown in Fig. 7.2.3. After the wind subsides, the two gyres may last for a few more days and form geostrophic flows, similar to what is shown in Fig. 2.4.10 (Jin et al., 2002).

9.2.5 Seiches

Seiches are standing waves (or periodic oscillations) of the water level in closed or semiclosed waterbodies, such as lakes, estuaries, and harbors. Prolonged wind forcing on a lake produces a surface gradient in which the water level rises in the downwind sector. Oscillations take place when the wind forcing suddenly reduces or changes direction. Because the solid barrier of the lake boundary reflects waves, the superposition of the original and reflected waves gives rise to standing waves called seiches, a prominent feature of closed waterbodies.

Gyres transport sediments, nutrients, and algae largely in the horizontal direction. Seiches, on the other hand, can contribute to the vertical mixing in lakes. Meteorological events can generate both gyres and seiches. The dynamic response of a lake depends on the intensity and the fetch length of the wind, the ambient stratification, and the geometry of the lake. Seiches can be excited by a variety of external perturbations. Strong meteorological events, such as hurricanes, cause large seiches in lakes. In addition to wind, changes in atmospheric pressure and reservoir withdrawals may also excite seiches. For example, a large withdrawal from a reservoir leads to a net flow of

water toward the dam. When the withdrawal suddenly stops, the water elevation gradient and the water momentum keep the water flowing and piling up at the dam. This may induce seiches in the reservoir. Seiches produce horizontal flows in the hypolimnion that may lead to turbulent mixing (Ostrovsky et al., 1996). Seiches can cause spatial and temporal variations in the location of the thermocline, but may not be strong enough to increase vertical transport across the thermocline in deep lakes. Ji et al. (2004a) modeled hydrodynamic and water quality processes in Lake Tenkiller, which will be discussed in detail as a case study in Section 9.4.1. A seiche signal of 2.36 h is found in this lake.

Under the assumptions of constant depth, negligible bottom stress, and steady-state conditions, the 1D equation of motion given by Eq. (2.2.7) can be simplified as:

$$0 = -\rho g H \frac{\partial \eta}{\partial x} + \tau_x \tag{9.2.3}$$

where ρ = water density (kg/m^3), g = 9.8 m/s^2, H = mean water depth (m), η = water elevation deviation (m), x = horizontal distance (m), and τ_x = surface wind stress (N/m^2).

The surface wind stress, τ_x, can be estimated from Eq. (2.1.38). Hence, for a lake of scale L, the surface water elevation difference ($\Delta\eta$) under a steady and uniform wind stress can be estimated as:

$$\Delta\eta = \frac{\tau_x L}{\rho g H} = \frac{C_D \rho_A U^2 L}{\rho g H} \tag{9.2.4}$$

where C_D can be calculated using Eq. (2.1.39).

For Lake Okeechobee, by letting ρ_A = 1.3 km/m^3, U = 6.5 m/s, L = 50 km, ρ = 1000 kg/m^3, H = 3.2 m, the value $\Delta\eta$ = 10 cm is obtained. Therefore, under a typical wind of 6.5 m/s, Lake Okeechobee can have water piling up on one side of the lake that leads to an elevation difference of up to 10 cm. A sudden change in wind may cause oscillations in water elevation and trigger seiches in the lake. As will be shown in Fig. 9.2.8, the measured seiche amplitude also has values ~10 cm, very close to this theoretical estimation.

The mechanism of seiche generation is actually similar to many other free oscillations. An oscillation is initiated if a system is disturbed by an external force, causing it to deviate from its equilibrium condition. The restoring force of the system tries to reestablish the equilibrium, while the inertial motion keeps the system deviated from the equilibrium condition. If the external force causing the initial disturbance disappears, the oscillation will gradually decay due to friction. The free oscillation of a pendulum is a good example. In the case of seiches in a lake, the system is the lake, the equilibrium condition is the leveled surface water elevation, the restoring force is the gravitational force, and the external force is the wind.

Free oscillations in a narrow channel can be described by shallow water equations derived from Eqs. (2.2.6) and (2.2.7):

$$\frac{\partial \eta}{\partial t} = -H\frac{\partial u}{\partial x} \tag{9.2.5}$$

$$\frac{\partial u}{\partial t} = -g\frac{\partial \eta}{\partial x} \tag{9.2.6}$$

which are for a 1D, closed rectangular channel with vertical walls and uniform depth. A wave equation is then obtained from Eqs. (9.2.5) and (9.2.6):

$$\frac{\partial^2 u}{\partial t^2} - gH\frac{\partial^2 u}{\partial x^2} = 0 \tag{9.2.7}$$

A general wave solution to Eq. (9.2.7) is

$$u = u_0 e^{i(kx-\omega t)} \tag{9.2.8}$$

where u_0 = wave amplitude, $\omega = 2\pi/T$ = wave frequency, T = wave period, $k = 2\pi/\lambda$ = wave number, and λ = wavelength.

Substituting Eq. (9.2.8) into Eq. (9.2.7) yields the following dispersion relation:

$$\omega = \sqrt{gH}k \tag{9.2.9}$$

and phase speed:

$$c = \sqrt{gH} \tag{9.2.10}$$

For a channel of length L, the velocity should have the following boundary conditions at the two ends:

$$u(0, t) = u(L, t) = 0 \tag{9.2.11}$$

A specific wave solution that satisfies the boundary conditions (9.2.11) is

$$u = u_0 \cos\omega t \sin k_n x \tag{9.2.12}$$

in which the wave number must have the following discrete values:

$$k_n = \frac{n\pi}{L} \quad n = 1, 2 \ldots \tag{9.2.13}$$

Consequently, there should be discrete modes of standing waves (seiches) in the channel with the following seiche periods:

$$T_n = \frac{2\pi}{\omega} = \frac{2\pi}{\sqrt{gH}k} = \frac{2L}{n\sqrt{gH}} \tag{9.2.14}$$

Equation (9.2.14) is based on the assumption of a rectangular basin with a flat bottom and provides a useful first approximation of the seiche period. The fundamental mode (n = 1) has the longest seiche period:

$$T_1 = \frac{2L}{\sqrt{gH}} \tag{9.2.15}$$

The corresponding wave length is $\lambda = 2L$.

From Eqs. (9.2.12) and (9.2.6), the water elevation is derived as:

$$\eta = \eta_0 \sin\omega t \cos k_n x \tag{9.2.16}$$

where η_0 = wave amplitude of the water elevation.

Based on Eqs. (9.2.12) and (9.2.16), the spatial distributions of the seiche modes are sketched in Fig. 9.2.6 for seiche velocity and in Fig. 9.2.7 for seiche elevation, respectively. Figures 9.2.6 and 9.2.7 show that the fundamental mode (n = 1) has the largest velocity oscillation and the smallest water elevation change in the middle of the channel.

As discussed previously, Lake Okeechobee has a typical length of 50 km and an average water depth of 3.2 m (Ji and Jin, 2006). Therefore, the fundamental mode of the seiches in the lake, according to Eq. (9.2.15), should be

$$T_1 = \frac{2L}{\sqrt{gH}} = \frac{2\times 50\times 10^3}{\sqrt{9.8\times 3.2}} = 5\text{h} \tag{9.2.17}$$

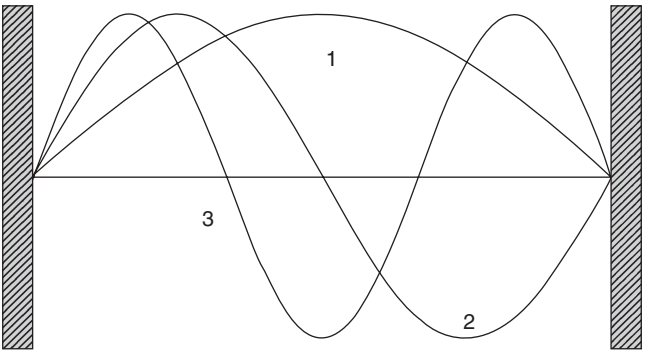

Fig. 9.2.6 The first three velocity modes of seiches in a channel.

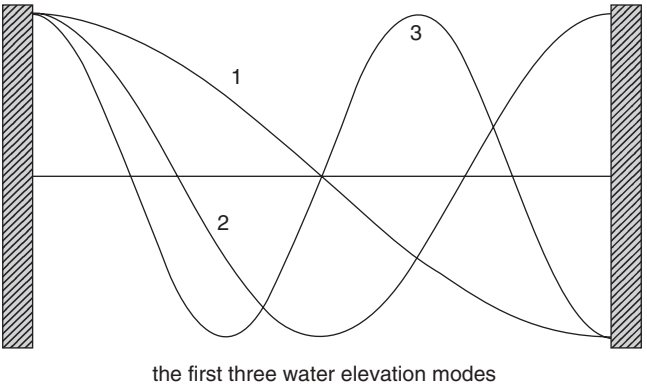

Fig. 9.2.7 The first three water elevation modes of seiches in a channel.

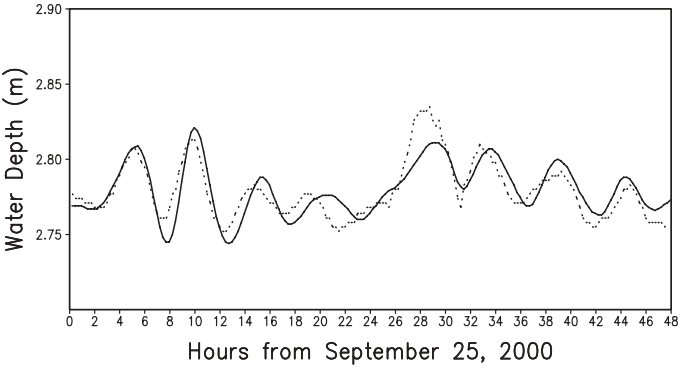

Fig. 9.2.8 Time series of water depth at L001 in Lake Okeechobee. Solid line = model results, dashed line = measured data.

It is expected that the lake should have seiches with a period of ~5 h. Sheng and Lee (1991) also suggested that seiches with a period of ~5 h may occur in Lake Okeechobee.

Measured water elevations at four stations, L006, L001, LZ40, and L005 (Fig. 2.4.2), are studied using the spectra analysis method discussed in Section 7.2.3. The elevation data are at 15-min time intervals, which should be adequate to resolve the 5-h seiche period. Figure 9.2.8 shows the time series of the modeled and the measured water depths at L001 for 48 h, starting from 9/25/2000 at midnight. The solid line is the modeled water depth, and the dashed line is the measured data. It is evident that during the 48 h, the modeled and the measured experience ~9 cycles, consistent with the 5-h period given in Eq. (9.2.17). Both the modeled and the measured have seiche ranges ~10 cm, surprisingly close to the theoretical value given by Eq. (9.2.4). Figure 9.2.9 gives the time series of the modeled v-component at L001 during the same

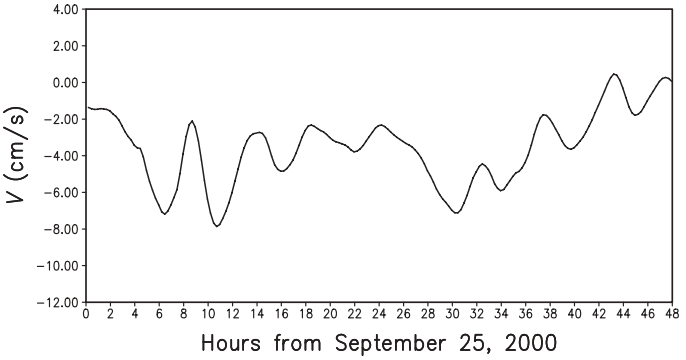

Fig. 9.2.9 Time series of modeled water *v*-velocity at L001 in Lake Okeechobee.

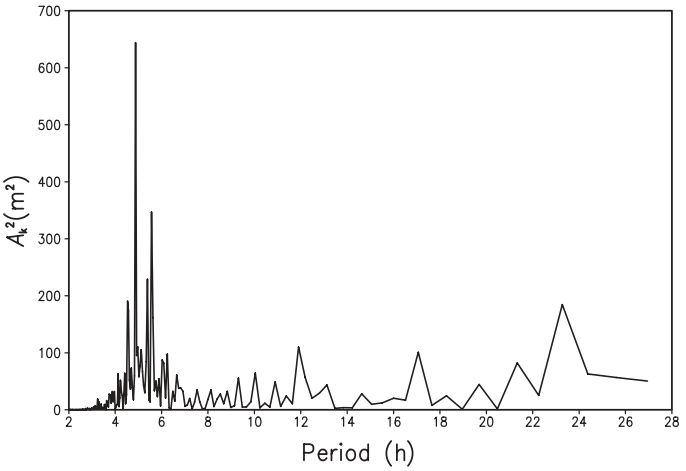

Fig. 9.2.10 Power spectra of modeled water elevation time series at Station L001 in Lake Okeechobee.

period shown in Fig. 9.2.8. There is no measured current data available during this period. Figure 9.2.9 shows that the modeled current has a strong seiche signal as well, with a period of 5 h or so.

Figure 9.2.10 gives the power spectra of modeled water elevations at L001 in 2000, which is from the LOEM. The corresponding power spectra analysis on the measured data is already presented in Fig. 7.2.2. Both the measured data in Fig. 7.2.2 and the model result in Fig. 9.2.10 indicate that within the period range of <28 h, the strongest signal is at 4.9 h, a seiche period that is very close to the theoretical estimation of 5 h. By analyzing the measured elevation data and the modeled results at the four stations (L006, L001, LZ40, and L005), it is found that water elevations at the four stations all have seiche

signals with periods ~5 h, and the seiche signals at L001 are the strongest among the four stations.

As shown in Fig. 2.4.2, a large section of the shoreline in the west of Lake Okeechobee is surrounded by the littoral zone, in which the seiche signals can be dampened. This explains why the seiche signals at L006 and L005 are relatively weak, compared to the ones at L001, since at L001, there is no littoral zone (and vegetation) to dampen seiches that oscillate along the north–south direction. The relatively narrow area around L001 also helps to amplify the seiche signals. Station LZ40 is located near the center of the lake. Figure 9.2.7 indicates that the fundamental mode ($n = 1$) should have a minimum elevation oscillation near the center. This explains why the seiche signals at LZ40 are the weakest among the four stations.

In summary, it is found that Lake Okeechobee exhibits strong seiche signals with a period ~5 h and seiche range ~10 cm. The theoretical results from Eqs. (9.2.4) and (9.2.17), the measured data, and the modeled results all consistently support this finding. The seiche ranges are typical ~10 cm in the lake, as shown in Fig. 9.2.8, and can be >20 cm from time to time. In a lake with mean depth of only 3.2 m, it is expected that seiches can be a significant factor affecting the hydrodynamic and water quality processes in the lake. In shallower areas, such as near L001 that has mean depth of 2.7 m, the seiche effects should be more significant. Further studies are needed to clarify the effects of seiches on the hydrodynamic and water quality processes in the lake.

The LOEM is originally developed for multiple-year simulations of hydrodynamic and water quality processes in the lake. A primary application of the model is to support decisionmaking on water quality management with a time scale of years and even decades. It is surprising (and gratifying) to see that the model also simulates the processes with a time scale of hours so well.

9.3 SEDIMENT AND WATER QUALITY PROCESSES IN LAKES

Lakes and reservoirs often act as sinks for water, sediment, and nutrients. They also have distinct internal cycling mechanisms of sediments and nutrients. This section focuses on sediment and water quality processes in lakes and reservoirs.

9.3.1 Sediment Deposition in Reservoirs and Lakes

Trap efficiency of a lake (or reservoir) represents the proportion of sediment inflow (in tons/year) that is retained within the lake and is defined as:

$$\text{Trap efficiency} = \frac{\text{Sediment inflow} - \text{Sediment outflow}}{\text{Sediment inflow}} \tag{9.3.1}$$

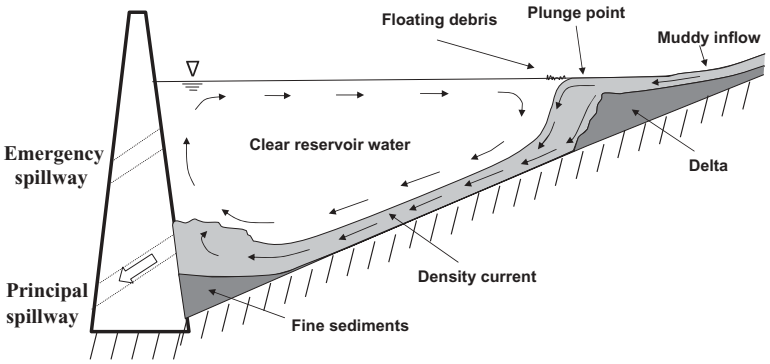

Fig. 9.3.1 Typical sediment deposition pattern in a reservoir.

Trap efficiency is a useful parameter to measure the capability of a lake to retain sediments that flow into the waterbody. Deep lakes and reservoirs often have high sediment trapping efficiencies with little sediment inflow (and sorbed contaminants) leaving the waterbody.

A river carries sediments in the water column as a suspended load and along the river bed as a bed load. The sizes of suspended sediment typically span the range from sand to silt to clay (Table 3.1.1). In rivers, suspended sediments tend to settle to the bed, whereas the turbulent mixing counteracts the gravitational settling and keeps a certain amount of sediments in suspension. When a river reaches a reservoir (or a lake), however, flow velocity and turbulent mixing are greatly reduced, and sediments start to settle in the reservoir. A typical sediment deposition pattern in a reservoir is depicted in Fig. 9.3.1.

Larger suspended particles (gravels, sands, and other coarse sediments) and most of the bed load are deposited in the reservoir headwater and form a reservoir delta. A delta is a deposition zone where a river flows into a standing waterbody, such as a reservoir, a lake, or a sea. Coarser sediment tends to be deposited in the reservoir headwater; finer sediment is carried downstream and deposited in deeper water. Deposition rate is highest in the headwater and decreases significantly down the reservoir. The deposits in the delta may later be resuspended and transported to deeper areas during high flow events.

This deposition pattern results in a longitudinal sorting of suspended sediments by grain size. Coarser particles settle first in the upper portion of the reservoir; finer particles remain in suspension longer and are deposited further down the reservoir; the very smallest particles may remain in suspension for a long time and may even be discharged with the outflow. This mechanism of sediment deposition and transport leads to the formation of a reservoir delta in the headwater and a large accumulation of fine sediments near the dam (Fig. 9.3.1). Since there is a longitudinal sorting by grain size, there may also

TABLE 9.3.1 A Typical Distribution of Deposited Sediments in a Reservoir (USACE, 1987)

Particle Size	Inlet (%)	Mid-Reservoir (%)	Outlet (%)
Sand	5	<1	0
Silt	76	61	51
Clay	19	38	49

be longitudinal gradients of water quality constituents associated with the sediment (Fig. 9.1.5).

A typical distribution of deposited sediments in a reservoir is shown in Table 9.3.1, which gives the percent of deposited sediments in different sections of a reservoir. The size ranges of sand, silt, and clay are given in Table 3.1.1. It is shown in Table 9.3.1 that sand is most likely being deposited in the reservoir delta area (the inlet), whereas clay is most likely being deposited in the dam area (the outlet). Silt has a higher possibility of being deposited in the inlet area than in the outlet area. Sediment deposition patterns are extremely complex and are the results of hydrodynamic, sediment transport, and water quality processes. Human activities may also affect the pattern significantly, such as dredging, dumping of dredged material, and discharging of sediment-laden material.

Sediments tend to settle in low energy areas where both currents and wind waves are weak. The finer the sediments are, the lower the energy should be. Currents and orbital velocities in the lake bottom are usually stronger in shallow areas than in deeper areas. This leads to the accumulation of coarser sediments in shallow water and finer sediments at depth. Consequently, the sediments that are fine-grained and richer in organic materials tend to form a deposition zone at the center (and deeper part) of a lake. This phenomenon is referred to as "focusing" and can play a significant role in the water quality processes in a lake. A good example is Lake Okeechobee. Figures 3.7.3 and 3.7.4 depict that the lake has the mud zone located in the deep-water areas and the sand zone located in the shallower and more dynamic areas.

9.3.2 Algae and Nutrient Stratifications

Vertical stratifications, as discussed in Sections 9.1.2 and 9.2.3, are one of the most distinct features of lakes and reservoirs. The annual cycle of vertical thermal stratification plays a significant role in water quality processes. The onset, duration, strength, and turnover of thermal stratification dictate water quality conditions. The strong mixing in the epilimnion is important in keeping algae in suspension. At the thermocline, the vertical exchange between the epilimnion and the hypolimnion is limited. In a stratified lake, water released at different water depths may have quite different nutrient and DO concentra-

tions. For example, releases from an anoxic hypolimnion may have phosphorus and nitrogen concentrations that are much greater than the ones in the epilimnion. These releases bring a large amount of nutrients that may be needed for farming.

Primary nutrient sources to lakes and reservoirs are (1) external nutrient loadings from point and nonpoint sources and (2) internal nutrient cycling from the bottom of the water. Major point sources include tributaries and wastewater treatment plants. Major nonpoint sources include surface runoff and atmospheric deposition. Rainfall or snowfall events (wet deposition) and dust deposition (dry deposition) can be important sources of nutrients. It is often difficult to accurately quantify these sources. The most difficult source to quantify, as discussed in Section 5.7, is the bottom sediment fluxes caused by diffusion, resuspension, and groundwater seepage. In deep lakes, nutrient-rich bottom waters are a major source of nutrients to the surface layer. During periods of stratification, nutrients may be released from the sediment bed to the bottom waters as a result of the decomposition of bed organic material. The nutrient-rich bottom waters can be entrained into the surface layer and become available for algal growth. During the lake turnover, full mixing of waters occurs and the nutrient-rich bottom waters are mixed throughout the water column. It is these nutrients that support algal growth in the next growing season.

Excessive algae biomass resulting from nutrient enrichment can adversely affect the overall health of a waterbody. Lakes are especially vulnerable to excessive nutrients because of their long residence time. Nutrients are consistently identified as the cause of lake impairments more than any other pollutants. The relationship between nutrient loading and eutrophication is complicated by a variety of physical, chemical, and biological factors. Phenomena of lake eutrophication include algal bloom, surface scum, excessive macrophyte growths, and decreased DO concentrations. Excessive algal growth, coupled with the strong vertical stratification in the summer, can result in significant loss of dissolved oxygen, leading to hypoxia or even anoxia in the lake bottom. Phosphorus and nitrogen are essential nutrients for algal growth. Of these two nutrients, P is often considered to be the nutrient that regulates the production of algae in lakes and is routinely used to estimate the trophic status of lakes. Vollenweider (1968) categorized lakes as:

1. Oligotrophic, if $P < 10\,\mu g/L$.
2. Mesotrophic, if $10\,\mu g/L \le P < 20\,\mu g/L$.
3. Eutrophic, if $P \ge 20\,\mu g/L$.

Vertical mixing affects the distribution and recycling of nutrients within the water column and with the sediment bed. Internal waves or wind mixing during the passage of weather fronts may mix a portion of the nutrient-enriched waters of the hypolimnion into the epilimnion. Reservoir operations,

such as withdrawing water from the hypolimnion, may also promote vertical mixing and entrain nutrients from the bottom to the surface.

In winter, a lake is vertically mixed when ice is not forming on the surface (or after the early spring turnover). This leads to vertically mixed water quality variables (nutrients, algae, DO, etc.). Biological productivity is low in the cold water and consumes fewer nutrients, and nutrient levels are usually high. These elevated nutrient levels later contribute to the algal blooms in the spring.

Vertical mixing due to spring turnover and runoffs from snowmelt often make large amounts of nutrients available to algal growth. Algae influence (and are influenced by) nutrient levels in a lake. Nutrient uptake by algae occurs in the eutrophic zone where photosynthesis takes place (Fig. 9.1.3). During the algal growth season, dissolved nutrients are incorporated into the biomass of algae, which subsequently settles from the epilimnion or is incorporated into higher trophic levels of the food web. With the exception of buoyant algae that can actively maintain their position in the surface layer, there is a net downward movement of nutrients from the epilimnion to the hypolimnion and lake bed. In this way, nutrients are redistributed from the upper layer to the bed as the dead algae gradually sink to the bed and decompose.

In summer, the lake develops thermal stratification (Fig. 9.1.1). Water temperature and water quality variables are mixed in the upper layer (the epilimnion) and have significant gradients in the intermediate layer (the thermocline). The thermocline acts as a barrier to the vertical mixing and practically separates the bottom layer (the hypolimnion) from the epilimnion. Vertical exchanges of water quality variables, such as DO, are greatly dampened. Particulate matters from the biological activity in the epilimnion settle to the lake bottom. Once particles have settled in a deep stratified lake, they commonly do not get resuspended into the surface water again. The nutrients that settle to the bottom are typically released back into the water column in the dissolved form through diffusion. Hence, the hypolimnion usually experiences poor water quality due to high nutrient levels and low DO concentrations, especially in the late summer and the early fall. In shallow lakes, however, nutrients settled to the bottom can be resuspended into the water column and play a key role in the eutrophication process, which will be discussed in Section 9.3.4.

As an example, Fig. 9.3.2 gives measured and modeled water quality variables in Lake Tenkiller, OK (Ji et al., 2004a). The curves are model results. The open circles and the crosses represent measured data in the surface and lower layers, respectively. Figure 9.3.2 shows that, after the algal bloom in June, nutrient concentrations decrease in the surface layer as nutrients are taken up by algae and eventually sink to the bottom when the algae die and settle out. The bottom waters, on the other hand, maintain high levels of nutrients. Therefore, during the period of summer stratification, any additional input of nutrients into the surface layer (epilimnion) may trigger a new algal bloom. More details on the modeling of Lake Tenkiller will be presented in Section 9.4.1.

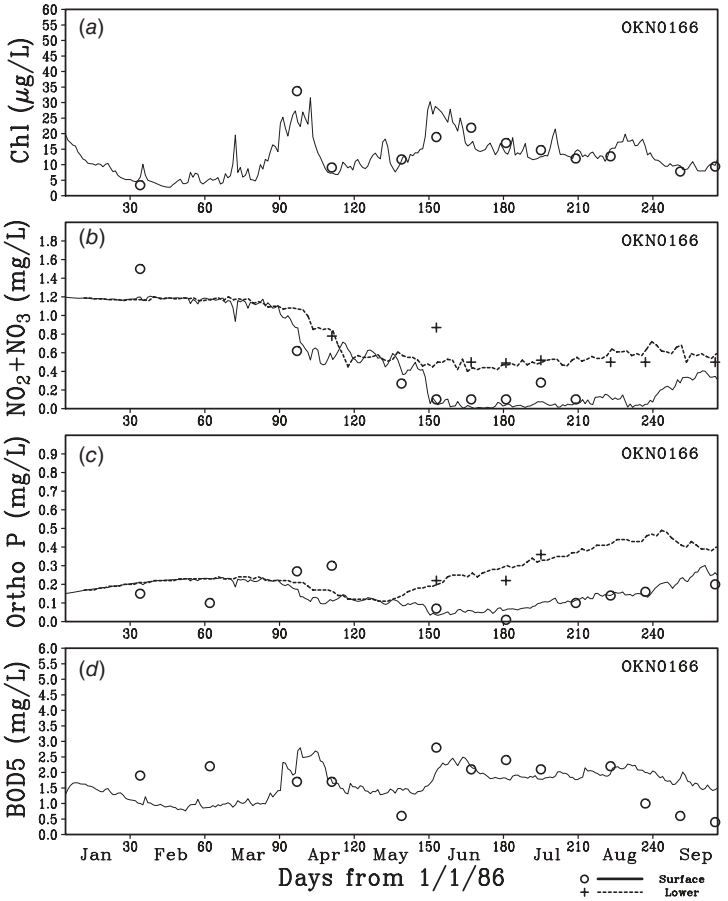

Fig. 9.3.2 Model–data comparison of water quality variables for 262 days at OKN0166. (*a*) Chlorophyll *a*; (*b*) nitrite + nitrate; (*c*) orthophosphorus; and (*d*) 5-day biochemical oxygen demand. Solid line = model results on the surface layer, open circle = measured data on the surface layer (1 m below the water surface), dashed line = model results in the lower layer, and cross = measured data in the lower layer (10 m below the water surface).

9.3.3 Dissolved Oxygen Stratifications

Dissolved oxygen is an integrative measure of a waterbody's ecosystem health. Atmospheric reaeration is the primary DO source to a lake. It brings oxygen to the lake's surface layer and then DO is transferred to lower layers via vertical mixing. Oxygen demand in a waterbody includes two separate but highly interactive fractions: SOD and water column oxygen demand. In contrast to nutrients that may be consumed by algae in the surface layer (e.g., Fig. 9.3.2), the focus for DO in lakes is primarily on the bottom concentrations. Dissolved

oxygen levels typically remain high in the surface water because of reaeration. As the water column becomes stratified, however, DO entrapped in the hypolimnion can be decreased and even depleted.

Profiles of DO and temperature are essential for characterizing whether a lake has a suitable habitat for sensitive fish species and other aquatic organisms. Deep lakes can have warm water fish in the epilimnion and cold water fish in the hypolimnion. For example, trout require cold, oxygen-rich water and primarily live in the hypolimnion of oligotrophic lakes. In a eutrophic lake that is stratified in the summer, warm water fish can live in the epilimnion and be quite productive, while cold water fish can be driven out of the colder bottom waters into warmer, oxygen-rich waters. DO depletion in the hypolimnion can result in the death of aquatic organisms.

Compensation depth is the water depth at which the net oxygen production is zero. It is the water depth at which oxygen production by reaeration and photosynthesis equals oxygen consumption by respiration. Below this depth, there is a net loss in the DO and, above it, a net gain. The compensation depth is a useful indicator of the anoxic condition in lakes, especially during summer stratifications. The euphotic zone (Fig. 9.1.3) is the layer from the water surface down to the depth where the sunlight is at the level of 1% of the surface sunlight. In a eutrophic lake, the compensation depth is about the same as the depth of the euphotic zone and can be roughly estimated using Eq. (9.1.3). In the hypolimnion of a stratified lake, the only source of oxygen is from photosynthesis that occurs only if the water is clear enough to allow the euphotic zone to extend below the thermocline. Therefore, a clear, oligotrophic lake at least has the possibility of having a source of oxygen in the hypolimnion, whereas a eutrophic lake does not.

When the compensation depth ascends above the thermocline, abrupt shifts in the algal community occur in the lake. The strong vertical thermal stratification dampens the entrainment of surface DO to the bottom, and the photosynthesis processes (if any) in the bottom is too weak to replenish the DO consumed. In this case, photosynthetic oxygen production occurs only in very shallow waters, nitrification and subsequent denitrification in deeper waters decline, ammonia accumulation increases, and the phosphorus release from the sediment bed intensifies. The resulting anoxia has a profound effect on the water quality and the ecosystem in the lake. It should also be mentioned, however, that hypoxia (even anoxia) in the hypolimnion is a common feature of many deep lakes due to summer stratification, which does not necessarily mean that the lake is eutrophic.

Eutrophic lakes show wide seasonal changes in their water quality characteristics. They are rich in nutrients and organic matters. Algae in these lakes bloom, die off, and eventually settle to the lake bottom. This “rain of organic matters” causes increased oxygen demand and oxygen depletion in bottom waters. The lake stratification prevents atmospheric oxygen from being entrained into the bottom waters, and the bottom waters are usually too dark for photosynthesis. As a result, there is no oxygen source in the hypolimnion

to replenish the oxygen lost through oxidation. Consequently, the combination of less oxygen produced in the hypolimnion and more oxygen demand due to decomposition may lead to a complete loss of DO below the thermocline during summers (e.g., Fig. 5.1.7 for Lake Wister and Fig. 9.1.2 for Lake Tenkiller).

Figure 9.1.2 represents typical seasonal patterns of temperature and DO in a stratified lake. In the winter, as illustrated in the plot of 2/4 (Day 34) of Fig. 9.1.2, the lake is well mixed with effectively uniform water temperature and DO, due to high turbulence levels. Since the water temperature is low, the ability of water to hold oxygen is high, and the oxygen consumption due to oxidation of organic matters is low. These factors, along with the stronger wind forcing, lead to DO concentrations of >10 mg/L in the winter.

If ice forms in winter (which is not the case in Lake Tenkiller), a eutrophic lake may develop a DO stratification. Since the ice cover blocks sunlight and prevents reaeration, the lake may become too dark for photosynthesis and cannot get oxygen from the atmosphere. In this way, both reaeration and photosynthesis stop providing oxygen to the lake. The oxidation of organic matters in the bottom and the SOD from the sediment bed continue to consume oxygen and may cause DO depletion. This mechanism may lead to fish kill in the winter, known as winter kill—sudden and massive death of fish caused by oxygen depletion or harmful chemicals (e.g., ammonia or hydrogen sulfide). Low DO in the bottom may also cause a release of nutrients from the sediment bed. The nutrients released can be stored in the bottom, be brought back to the surface during the spring turnover, and fuel the algal bloom in the spring.

During the summer months (June, July, and August of 1986 in Fig. 9.1.2), a definite thermocline formed. Exchanges between the epilimnion and the hypolimnion are almost eliminated due to the strong stratification. The DO concentration in the epilimnion remains high throughout the summer because of photosynthesis and diffusion from the atmosphere. The settling and oxidation of particulate organic matter generated in the surface waters cause low DO levels in the bottom. The hypolimnion is effectively cut-off from all sources of oxygen, while organisms continue to respire and consume oxygen. DO is depleted beyond the middle depths of the lake. The vertical DO profile becomes analogous to that for temperature, where the depth of the steepest gradient of DO concentration is coincident with the thermocline.

It is interesting to see that, in Fig. 9.1.2, the measured DO in the plot of 6/17 (Day 167) has two minimum DO concentrations: one in the thermocline at a depth of ~8 m and one near the bottom. A possible explanation is that organic matters from the epilimnion settle at slower rates in the thermocline because of higher viscosity due to lower temperatures. Since the organic matters remain in the thermocline for a longer period, the decomposition occurs over a longer period, consumes more oxygen, and leads to the minimum DO. Besides, higher production of organisms due to rich nutrients in the thermocline may also contribute to the low DO in this layer.

Anoxic conditions are generally associated with the hypolimnion, but anoxic conditions may occur in the thermocline as well. As eutrophication advances, transparency declines, and the compensation depth ascends. The thermocline may become anoxic due to respiration and decomposition of organic matters settling into the thermocline. The plot on 7/1 (Day 181) shows that anoxia existed only 6 m below the water surface and was right in the middle of the thermocline.

During the fall turnover, the lake becomes completely mixed again. The oxygen from the epilimnion is transferred to the oxygen-poor hypolimnion. Nutrients from the bottom are distributed throughout the water column. This completes the seasonal cycles of water temperature, DO, and nutrients in the lake.

9.3.4 Internal Cycling and Limiting Functions in Shallow Lakes

More than 35% of the world's large lakes (>500 km^2) have a mean depth of <5 m (Havens et al., 2004). These large and shallow lakes are strongly influenced by wind forcing (Ji and Jin, 2006) and have distinct characteristics in internal nutrient cycling.

As discussed previously in this section, deep lakes often have a typical pattern of seasonal and annual variations: nutrients in the euphotic zone are consumed by algae and then settle to the lake bottom after the algae die. Phosphorus can also sorb to suspended sediments and be removed from the water column to the sediment bed. Generally, there is a net downward movement of nutrients from the epilimnion to the hypolimnion. In a deep, stratified lake, suspended solids no longer are expected to return to the water column, once they have settled. The mechanism for nutrients in the sediment bed to return to the water column is via diffusion in the form of a dissolved phase. During the period of thermal stratification, the thermocline acts as a barrier to nutrient upward transport into the epilimnion. Only a lake turnover in early spring or later fall may mix the bottom nutrients throughout the water column and make the nutrients available to algal growth in the euphotic zone.

In contrast to deep lakes, large and shallow lakes:

1. Often experience significant interactions between physical, chemical, and biological processes in the water column and the bed sediments.
2. Have irregular seasonal and interannual variation patterns.
3. Are often more productive.
4. Are easily subject to dramatic events, such as storms, and may experience dramatically different states (clear vs. turbid).
5. Are influenced by wind waves.
6. Lack a stable period of summer stratification, but may still develop a temperature gradient vertically through the water column.
7. Do not always readily respond to reductions in external nutrient loading.

In large, shallow lakes, interactions between the sediment bed and the water column can play a major role in determining nutrient concentrations, turbidity, and algal growth. The major interactions include the following:

1. Resuspension of sediments by current and wind wave (Section 3.3.5).
2. Sorption and desorption of nutrients from resuspended sediment (Section 5.4.2).
3. Diffusion exchange of nutrients (sediment fluxes) (Section 5.7.4).
4. Uptake and release of nutrients by SAV and periphyton on the lake bottom (Section 5.8.3).

Nutrient levels in the water column are controlled by the rates of production and reduction. For example, the P production in a large, shallow lake is largely controlled by resuspension from the bed and desorption from the suspended sediments (Havens et al., 2004). The P reduction is primarily determined by algal uptake, sorption to the suspended sediments, and settling to the bed. The upward flux due to wind waves can be much larger than fluxes due to other processes, such as diffusion, bioturbation, and external loading. These processes may become more important in shallow lakes than the ones that are less heavily influenced by wind (e.g., shorter fetch, greater depth, or more consolidated sediment material). The deposition and resuspension of sediments are often the dominant mechanisms controlling P concentrations in lakes heavily influenced by wind (e.g., James et al., 1997).

A lake's sediment bed gradually contains high levels of nutrients (phosphorus) in the process of lake eutrophication. As illustrated in Fig. 9.3.3, the deeper sediment layer with low P reflects the oligotrophic status of the lake in the past; the intermediate layer with moderate P records the mesotrophic status of the lake; and the top layer with high P is the results of the current eutrophic status of the lake. Under the wind forcing, the internal cycling of P may play a dominant role in lake eutrophication.

Large and shallow lakes often display highly irregular seasonal and interannual variations in nutrient concentrations, largely driven by meteorological events. Shallow lakes tend to be more productive than deep lakes, in part because they are generally well mixed, thereby allowing nutrients to remain in suspension and accessible to algae. The epilimnion may completely replace the hypolimnion, so that the lake remains relatively mixed throughout the year. Internal loading of phosphorus is often a more serious threat in shallow lakes than in deep lakes. Consequently, shallow lakes often exhibit the symptoms of eutrophication to a greater extent than do deep ones.

As discussed in Section 3.6, large, shallow lakes are more easily affected by wind forcings. Under the same wind velocity, the larger the lake area, the longer the wind fetch and the stronger the wind wave. This relationship means that the sediments deposited on the bed of a large, shallow lake are easily eroded by wind waves. Havens et al. (2004) reported that variation in wind velocity results in dramatic changes in water column transparency, suspended

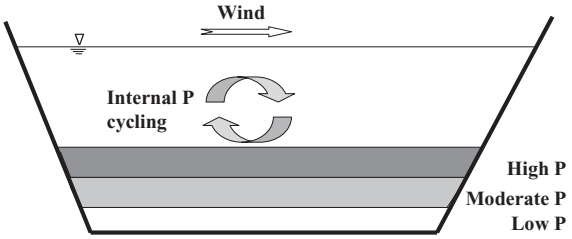

Fig. 9.3.3 Schematic diagram of internal phosphorus cycling in a lake.

sediments, and total P (TP). Wind can be the main driving force behind P dynamics at hourly, daily, and seasonal time scales. In summer, when the evening sea breeze is a dominant forcing function, there are strong diurnal changes in TP. In winter, when frontal systems generate strong winds for multiple days, water column TP remains quite high compared to summer conditions. Hurricanes can result in elevated sediment and TP concentrations in the water column for several months (e.g., Jin and Ji, 2005). Local water depths in the lake can modify wind effects by influencing bottom shearing stress, horizontal distribution of sediment particles, and development of submerged aquatic vegetation.

Due to its long fetch, strong wind waves can develop in a large lake, even under modest wind forcing conditions. If the lake is shallow, the wind wave energy can propagate to the lake bottom and cause sediment resuspension (Section 3.6). Sediments (and the sorbed phosphorus) can be easily resuspended into the water column under the forcing of wind waves and currents. Wind waves, along with currents and seiches, affect the heat exchange between the epilimnion and the hypolimnion. They may also influence nutrient return from the hypolimnion to the epilimnion, when large amounts of nutrients are released from the bed.

Depending on the external and/or internal forcings, shallow eutrophic lakes can exhibit two dramatically different states: clear or turbid. Clear lakes generally have high densities of submerged aquatic plants and low concentrations of sediments, whereas the opposite tendencies occur in turbid lakes. Shallow lakes can "switch" their state from clear to turbid if impacted by strong external and/or internal forcings, such as a dramatic change in water level, a major discharge event, and/or a dramatic increase in external loadings. In regions that are influenced by hurricanes, strong wind events can also transform a lake from a clear to a turbid state (Havens et al., 2004).

A large, shallow lake may also be stratified during the day under sunlight, but often returns to a homogenous condition during the night. During daytime and under low wind, a shallow lake may develop a steep temperature gradient vertically through the water column (e.g., Fig. 2.4.11). Under these conditions, there can be a substantial reduction of oxygen transfer through the water column. With elevated organic material decomposing in the sediment bed, this

may lead to the development of anoxic sediments at the bottom of shallow lakes.

As a consequence of the internal nutrient cycling, shallow lakes do not always respond readily to reductions in external nutrient loading. Since large amounts of in-lake nutrients (especially P) are stored in the sediment bed, the reduction of external nutrient loadings may achieve little immediate improvement in the lake water quality. Phosphorus dynamics in these lakes can be strongly influenced by sediment resuspension at time scales from hours to decades (e.g., Jin and Ji, 2005). The highly eutrophic sediments can remain eutrophic long after the external loadings are reduced and thus delay the recovery of the lake. From a management standpoint, this means that lake responses to external load reductions are likely to occur with a long time lag. After a large and shallow lake becomes eutrophic, it is often a daunting task to restore the lake conditions. Internal P loading makes the lake ecosystem very resilient to changes in its phosphorus concentration when external loadings vary. Even when external loads are dramatically reduced, the lake's sediments act as a phosphorus reservoir and continue to release phosphorus into the water column. During wind events, these sediments are resuspended in the lake, and the phosphorus contained in the sediments is released into the water column impacting the water quality (James et al., 1997).

As discussed in Section 5.2.3, algal growth is a function of temperature, light, and nutrients. The effects of these processes are considered to be multiplicative and can be expressed in the general form of Eq. (5.2.7), which calculates algal limitation functions that range between 0.0 and 1.0. When its value is 1.0, the algal growth is not limited by this parameter. When its value is near zero, the algal growth is severely limited by this parameter. In P-laden lakes, P rarely becomes a limiting nutrient. Therefore, according to Eq. (5.2.13), the potential for nutrient limiting is practically determined by nitrogen levels in the lake. In such lakes, certain species of blue-green algae that can fix atmospheric nitrogen have a clear competitive advantage and frequently become dominant. Light limiting occurs when available irradiance is insufficient for algal growth. High levels of suspended sediments can reduce water transparency and cause light limiting, a prominent characteristic of many large, shallow lakes. Light limiting is particularly common during winter because of low incident light and high sediment concentration induced by strong wind, but it is less common in summer when incoming irradiance is maximal.

As an example, Fig. 9.3.4 gives the growth limiting functions for N, irradiance (I), and temperature (T) in Lake Okeechobee from October 1, 1999, to September 30, 2000, which are calculated using the surface layer results from the Lake Okeechobee Environmental Model (Jin et al., 2007). The solid line is for the limiting function for nitrogen, fN, defined by Eq. (5.2.10). The dashed line is for the limiting function for irradiance, fI, defined by Eq. (5.2.18). The dotted line is for the limiting function for temperature, fT, defined by Eq. (5.1.9). The growth limiting function for phosphorus (P) is always near 1 (not shown). Since the lake has very small Secchi depths most of the time (Jin and

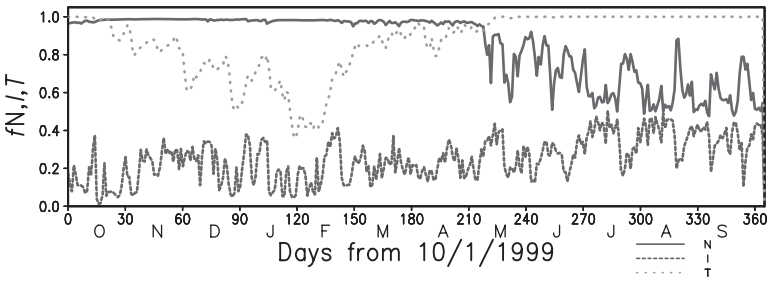

Fig. 9.3.4 The growth limiting functions for N, irradiance (I), and temperature (T) in Lake Okeechobee.

Ji, 2005), the growth limiting function for irradiance, fI, decreases rapidly with water depth, which leads to little algal growth below the surface layer. The daily averaged function for irradiance is generally <0.5. Sunlight is a primary limiting factor for algal growth in Lake Okeechobee. Temperature can limit algal growth in winter. Nitrogen becomes a co-limiting factor in summer, when there is sufficient sunlight for algal growth, and the in-lake nitrogen (NH_4 and NO_x) is used up. This phenomenon explains the negative correlation between fN and fI in the summer. When fI is high, there is sufficient sunlight for algal growth, which consumes nitrogen (and phosphorus) and lowers the in-lake nitrogen to limiting levels. When fI is low, algal growth is limited, and nitrogen consumption is reduced, which leads to a higher nitrogen level and a larger value of fN.

9.4 LAKE MODELING

Modeling of lakes and reservoirs is different from the modeling of rivers and estuaries in many aspects. Due to their long retention times, lakes and reservoirs are typically more sensitive to eutrophication than rivers and estuaries. Studies on lakes and reservoirs are often focused on algal growth and nutrients. Lake models commonly need multiple vertical layers to resolve the stratifications of temperature, algae, DO, and nutrients.

The data and parameters needed for the modeling of surface waterbodies are generally discussed in Sections 2.4.1 for hydrodynamics, Section 3.7.1 for sediment transport, Section 4.5 for toxics, and Section 5.9.1 for water quality and eutrophication, respectively. The selection of numerical models for the modeling of surface water systems is generally discussed in Section 7.1.2. In this section, two modeling case studies are presented (1) a deep reservoir (Lake Tenkiller) and (2) a large, shallow lake (Lake Okeechobee). These two very different water systems serve as good examples of how lakes and reservoirs are modeled using 3D models.

9.4.1 Case Study I: Lake Tenkiller

This case study is primarily based on the work of Ji et al. (2004a).

9.4.1.1 Introduction. Despite the progress in 3D hydrodynamic, water quality, and sediment diagenesis models and their successful applications in estuaries and bays (Cerco, 1999), few similar 3D modeling studies on eutrophication in lakes and reservoirs have been published. It is fairly common to use 2D models to study water quality processes. For example, the W2 model (Cole and Wells, 2000) has been widely used in many 2D laterally averaged water quality studies on lakes and reservoirs. In modeling studies (e.g., Chung and Gu, 1997; Tufford and McKllar, 1999), the importance of 3D modeling of lakes and reservoirs is increasingly realized. In modeling hydrodynamics and sediment transport in rivers and reservoirs, Ziegler and Nisbet (1994, 1995) also illustrated the limitations of laterally averaged models and emphasized the needs for 3D modeling.

Lake Tenkiller is located in the Illinois River watershed, which straddles the Oklahoma-Arkansas boundary and covers 4170 km^2 (Fig. 1.1.1). The Illinois River flows from Arkansas into Oklahoma, where it drains into Lake Tenkiller before flowing into the Arkansas River. Lake Tenkiller is located in the southwestern portion of the basin. The main tributaries to the lake include the Illinois River, Baron Fork, Tahlequah Creek, Flint Creek, and Caney Creek. Figure 1.1.1 shows the location of the Illinois river watershed, the Lake Tenkiller drainage basin, Lake Tenkiller, and its main tributaries. Table 9.4.1 summarizes the physical characteristics of Lake Tenkiller. The lake is 48 km long, up to 3 km wide, and 70 km^2 in area. Its depth varies from >45 m near the dam to <10 m in the upstream section. The lake has a retention time of 1.76 years. With a width of up to 3 km and a large lateral bathymetry gradient, it is expected that this reservoir should have large 3D variability. It is critical to simulate the hydrodynamic and water quality processes using a 3D model so

TABLE 9.4.1 Physical Characteristics of Lake Tenkiller

Physical Characteristic	Value
Surface area	70 km^2
Drainage area above lake	4,170 km^2
Length	48 km
Length of shoreline	209 km
Width	0.8–3 km
Maximum depth	46.3 m
Mean depth	14 m
Volume	810,000–1,520,000 m^3
Retention time	1.76 y
Mean depth/maximum depth	0.33
Drainage area/surface area	59.6

that water quality parameters in the lake can be described in detail and cost-effective water management approaches can be proposed and evaluated.

The US Army Corps of Engineers constructed Lake Tenkiller in 1947 to provide flood control, water supply, flow augmentation, and water conservation. Lake Tenkiller's designated uses also include a cold water fishery and recreational activities. Lake Tenkiller's drainage area/surface area ratio is ~59.6, warranting the assumption that watershed pollutant loads significantly affect reservoir water quality. Lake Tenkiller is identified as a high-priority target for TMDL development by the Oklahoma Department of Environmental Quality (ODEQ, 2000). Major water quality issues include nutrient enrichment, eutrophication, and hypolimnetic DO depletion.

The objectives of this study were

1. To develop a 3D hydrodynamic and water quality model of Lake Tenkiller.
2. To calibrate the Lake Tenkiller Model using the measured data graphically and statistically.
3. To apply the model to study the hydrodynamic and water quality processes in the lake (Ji et al., 2004a; Tetra Tech, 2000c)

9.4.1.2 Data Sources and Model Setup. Approximately twice a month, USACE (1988) monitored 14 stations in the lake area from February to September 1986. The collected data included water temperature (T), DO, Chl a , BOD_5, orthophosphorus (PO_4), and nitrate–nitrogen ($NO_2 + NO_3$). These 14 water quality stations are shown in Fig. 9.4.1, except for OKN0169, which is not located on the lake. The data at OKN0177 and OKN0175 are used to represent tributary loadings from the Illinois River and Caney Creek, respectively. The remaining 11 stations in Fig. 9.4.1 are used for model–data comparison and model calibration.

The hydrodynamic inputs include meteorological forcings and lake inflows/outflows. The hourly meteorological data at Fayetteville, Arkansas include wind speed and direction, air temperature, solar radiation, precipitation, relative humidity, and cloud cover. Hourly inflow and outflow data of the lake were provided by USACE (Miller, 1999). The atmospheric deposition rates of nutrients are based on data from the National Atmospheric Deposition Program (http://nadp.sws.uiuc.edu/nadpdata/).

The Lake Tenkiller model is developed within the framework of the EFDC mode (Hamrick, 1992; Park et al., 1995). Development of a site-specific model generally includes the following steps: (1) collecting and analyzing measured data for input and model–data comparison; (2) generating the model grid; (3) specifying model parameters, boundary conditions, and external forcings; (4) setting up graphic and statistical packages; (5) calibrating the model against measured data; and (6) analyzing hydrodynamic and water quality processes in the water system. The development of the Lake Tenkiller model followed these steps.

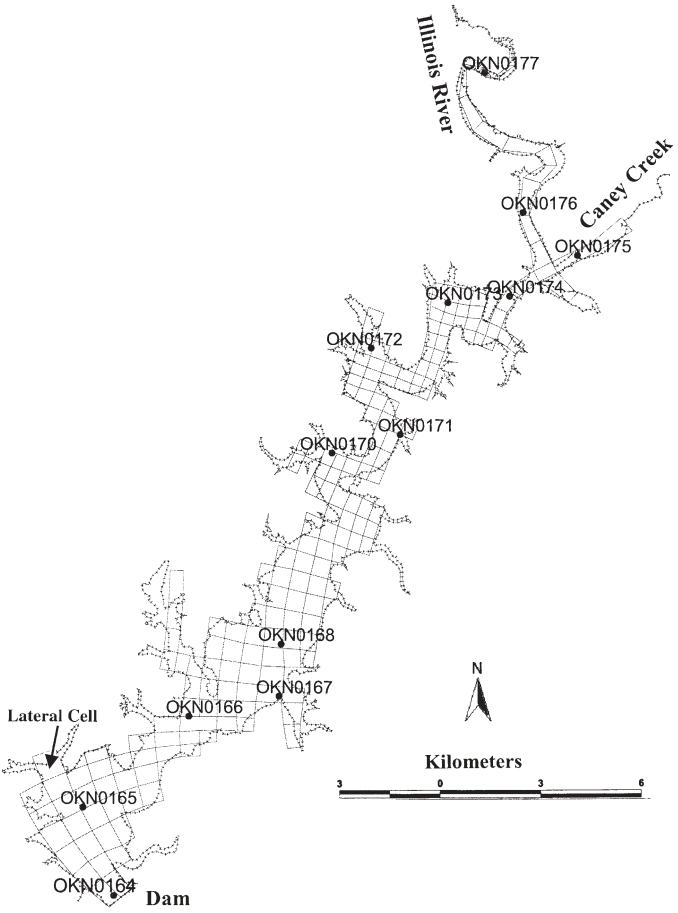

Fig. 9.4.1 Lake Tenkiller study area and model grid.

The study area was divided into a grid of discrete cells. Figure 9.4.1 shows the model grid overlaying an outline of Lake Tenkiller. U.S. Geological Survey bathymetric data of Lake Tenkiller was interpolated to provide water depths. As shown in Fig. 9.4.1, the inflows (Caney Creek and Illinois River) were each represented by one cell across the stream. To obtain adequate resolution in the lake, multiple cells were used in the lateral direction. The numerical grid consisted of 198 cells in the horizontal plane and 10 sigma layers in the vertical. Sensitivity tests indicated that the 10 vertical layers are necessary and important to resolve the vertical temperature and DO profiles in the lake (Ji et al., 2004a).

Solutions to the hydrodynamic and water quality model were obtained using a 90-s time step. The calibration time period of the Lake Tenkiller Model was 262 days (January 5 to September 24, 1986), which is the USACE (1988)

in-lake monitoring period. On a 2.4-GHz Pentium IV PC, ~5 CPU hours are required for a 262-day simulation. To minimize the impact of initial conditions on model results, the model was spun up for 2 years using the 1986 inflow conditions. The end of the 2-year spin-up run was used as the initial condition for the 262-day simulation.

9.4.1.3 Hydrodynamic Simulation. The hydrodynamic variables of the Lake Tenkiller Model include water surface elevation, water temperature, water velocity, and turbulent mixing. Hydrodynamic calibration is needed so that the model can properly characterize the nature, behavior, and pattern of water flow within the lake. The strong vertical temperature stratification and its effect on vertical mixing are also essential to eutrophication processes and water quality modeling.

Modeled versus observed daily averaged water depths at OKN0164 are shown in the Fig. 9.4.2, in which the horizontal axis represents days from January 1, 1986, and the vertical axis represents water depth in meters. The dashed line represents the modeled water depths, and the solid line represents the measured water depth. It is evident that the modeled water depth closely matches the measured data. The statistical methods discussed in Section 7.2.1 are used to compare model simulations and sampling observations. At OKN0164, the mean water depth is 40.9 m, the RMS error is 0.09 m, and the relative RMS error is 3.5%.

Temperature is also an important indicator of hydrodynamic behaviors. The 12 plots in Fig. 9.1.2 show the vertical profiles of temperature and DO at OKN0166. In each plot of Fig. 9.1.2, the horizontal axis represents water temperature in degree Celsius (or DO concentration in mg/L), and the vertical axis represents water depth in meters. The solid line represents the modeled water temperature, and the closed circle represents the measured temperature. The dashed line represents the modeled DO, and the open circle represents the measured DO. The corresponding Julian day and date are shown in the lower right corner of each plot.

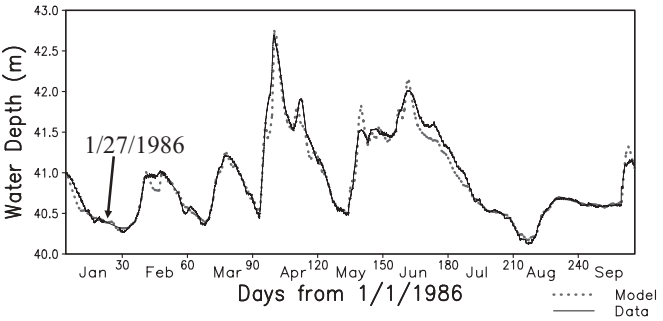

Fig. 9.4.2 Model–data comparison of water surface elevation for 262 days at OKN0164. The solid line is the measured data, and the dashed line is the model results.

In Fig. 9.1.2, both the model and the data reveal that the lake temperature experienced four distinct stages. The lake was

1. Well mixed in the winter (2/4 and 3/4).
2. Starting to be stratified in the spring (4/8 and 4/22).
3. Highly stratified in the summer (7/1, 7/15, and 7/29).
4. Less stratified again in August (8/26).

The strongest vertical stratification occurred in the summer, with a surface-bottom temperature difference of >10 °C. Overall, the model simulated the temperature stratification and seasonal variation very well.

To conduct statistical analysis, modeled temperatures at the 11 stations were saved at the same times and water depths that the measured data were collected. Table 9.4.2 summarizes the statistical analysis of the observed and modeled temperatures at the 11 stations. The number of observed temperatures varies from 42 at OKN0173 to 122 at OKN0164 and OKN0168. The modeled temperature has the smallest relative RMS error of 4.58% at OKN0172 and the largest relative RMS error of 7.97% at OKN0164. The RMS error varies from 1.11 °C at OKN0174 to 1.81 °C at OKN0164. Overall, the water temperature profiles are simulated very well, with a mean relative RMS error of 5.85% among the 11 stations. Since DO modeling and eutrophication processes are closely linked to water temperature, accurate simulation of water temperature is also a vital step toward the successful modeling of water quality processes.

No measured velocity data are available for model–data comparison. Due to its long retention time of 1.76 years, the inflows and outflows of the lake

TABLE 9.4.2 Statistical Analysis of Observed and Modeled Temperature at the 11 Stations Shown in Fig. 9.4.1

Station Name	Obs. Data Number	Obs. Mean (°C)	Modeled Mean (°C)	Mean Abs. Error (°C)	RMS Error (°C)	Obs. Change (°C)	Relative RMS Error (%)
OKN0164	122	19.09	20.47	1.47	1.81	22.7	7.97
OKN0165	113	18.32	19.09	1.18	1.41	22.5	6.25
OKN0166	120	19.13	19.99	1.17	1.40	23.9	5.86
OKN0167	97	20.63	21.68	1.33	1.58	23.7	6.69
OKN0168	122	19.73	20.62	1.14	1.38	23.8	5.79
OKN0170	112	20.47	21.07	0.91	1.20	24.7	4.85
OKN0171	94	21.26	22.15	1.23	1.65	24.0	6.88
OKN0172	94	21.97	22.74	0.94	1.13	24.7	4.58
OKN0173	42	22.14	23.28	1.14	1.26	23.4	5.37
OKN0174	77	22.28	22.71	0.92	1.11	23.0	4.83
OKN0176	63	24.23	25.16	1.00	1.15	21.7	5.30

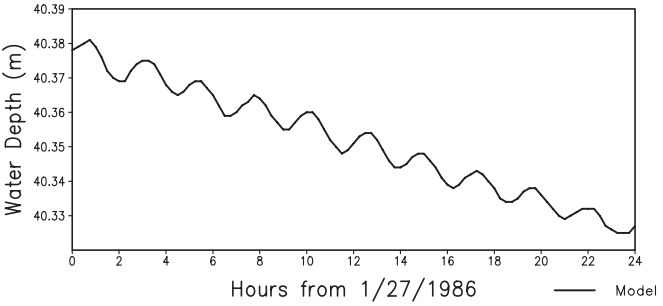

Fig. 9.4.3 Modeled water surface elevation for 24 h on January 27, 1986, at OKN0164.

have a relatively small influence on circulation patterns in the lake. Water currents in the lake are primarily driven by wind. Typically, the modeled surface velocities are ~2–4% of the wind speed.

Lake Tenkiller has a typical length of 48 km and an average water depth of 14 m. The fundamental mode of seiches in the lake can be estimated using Eq. (9.2.15):

$$T_1 = \frac{2L}{\sqrt{gH}} = \frac{2 \times 48 \times 10^3}{\sqrt{9.8 \times 14}} = 2.36\,\text{h} \tag{9.4.1}$$

Therefore, it is expected that the lake should have a seiche period ~2.36 h. The measured water depths shown in Fig. 9.4.2 are at daily time intervals and are inadequate to resolve events with periods of a few hours. The modeled water depths, on the other hand, should be able to resolve seiche signals. By saving modeled results at 15-min intervals, the modeled water depths on January 27, 1986, are shown in Fig. 9.4.3, which is the same time series on January 27, 1986, in Fig. 9.4.2. The water depths in Fig. 9.4.3 exhibit clear periodic behaviors. There are ~10 cycles during the 24 h, consistent with the estimation in Eq. (9.4.1). Similar periodic signals are also found in other sections of the time series in Fig. 9.4.2. The spectral analysis technique discussed in Section 7.2.3 is used to identify periodic signals in water elevations. It is found that the strongest signal is at 2.36 h, the same as the theoretical estimation given in Eq. (9.4.1).

9.4.1.4 Water Quality Simulation. Dissolved oxygen is an important indicator of model performance in water quality modeling. The 12 plots in Fig. 9.1.2 show the vertical profiles of the modeled and the measured DO at OKN0166. The DO is vertically mixed in the winter and is very stratified in the summer. For example, on July 29, 1986 (Day 209), both the model and the data indicate that DO reduced to almost zero at only 11 m below the water surface. As shown in Fig. 9.1.2, DO dynamics in Lake Tenkiller are typical of a lake system: Shortly after the onset of thermal stratification, the hypolimnetic

oxygen content decreases. This condition began at the water–sediment interface because of high oxygen demand from sediment diagenesis. This process transferred nutrients between the sediment bed and the stratified lower water column and progressed upward through the hypolimnion. Hypolimnetic anoxia occurred after stratification formed in the water columns and continued through September.

While the model simulated the DO profiles reasonably most of the time, the model did not resolve the DO stratification well on July 1, 1986 (Day 181). It appears that more vertical layers might be needed in this extremely stratified situation in which DO was reduced to zero only 6 m below the surface. Errors in wind forcing might also cause too much mixing on this day. It is demonstrated that lake stratifications are sensitive to wind forcing (Ji et al., 2004a). More accurate meteorological data might be able to improve the wind forcing and the model's vertical mixing.

Table 9.4.3 presents the statistical analysis of observed and modeled DO at the 11 stations. The relative RMS errors have a mean value of 16.34%, varying from 10.86% at OKN0170 to 28.26% at OKN0176. The modeled DO profiles at OKN0166 (shown in Fig. 9.1.2) have a RMS error of 1.41 mg/L and a relative RMS error of 11.25%. Overall, as shown in Fig. 9.1.2 and Table 9.4.3, the model simulated DO satisfactorily. In the river inflow area, the reservoir is relatively shallow with a water depth of <10 m. The nutrients from the rivers cause algal blooms in the area and DO supersaturation in afternoons. The EFDC water quality model lacks the mechanism to describe the super saturation process and is not able to simulate such large DO variations in these water columns. This partially explains the large relative RMS errors in the shallow sections of the reservoir, such as those at OKN0173, OKN0174, and OKN 0176.

TABLE 9.4.3 Statistical Analysis of Observed and Modeled Dissolved Oxygen at the 11 Stations Shown in Fig. 9.4.1

Station Name	Obs. Data Number	Obs. Mean (mg/L)	Modeled Mean (mg/L)	Mean Abs. Error (mg/L)	RMS Error (mg/L)	Obs. Change (mg/L)	Relative RMS Error (%)
OKN0164	122	6.73	8.28	1.79	2.65	12.6	21.07
OKN0165	113	6.92	7.52	0.96	1.41	12.3	11.50
OKN0166	120	6.46	6.89	1.00	1.41	12.5	11.25
OKN0167	97	6.50	7.26	1.31	1.85	12.4	14.93
OKN0168	122	6.26	6.34	1.08	1.46	13.0	11.26
OKN0170	112	6.48	6.20	1.20	1.56	14.4	10.86
OKN0171	94	6.69	6.08	1.28	1.89	15.7	12.05
OKN0172	94	6.92	6.26	1.47	2.02	16.3	12.37
OKN0173	42	10.05	8.09	2.18	2.63	10.2	25.79
OKN0174	77	8.19	5.74	2.74	3.14	15.4	20.36
OKN0176	63	8.60	6.20	2.83	3.39	12.0	28.26

The USACE (1988) data also include Chl *a*, $NO_2 + NO_3$, PO_4, and BOD_5. But these data lack the quantity and quality to make model–data comparisons in vertical profiles. The four panels of Fig. 9.3.2 show the modeled and the measured Chl *a*, $NO_2 + NO_3$, PO_4, and BOD_5 at OKN0166, the same station whose temperature and DO are shown in Fig. 9.1.2. In Fig. 9.3.2, the open circle represents the measured data on the surface, and the cross represents the measured data in the lower layer, which is 10 m below the water surface. The corresponding model results are represented by the solid and dashed lines, respectively. In the first panel, the model captured the two algal blooms realistically, one in the spring and one in the summer, with algal concentrations varying from <5 μg/L in the winter to >30 μg/L in the spring. In the second panel, both the model and the data indicate that the $NO_2 + NO_3$ concentration is very stratified in the summer as the result of thermal stratification (shown in Fig. 9.1.2) and algal uptake. In the third panel, the PO_4 concentrations are also very stratified in the summer. In the fourth panel, the model and the data show that BOD_5 varies in the range of 0.5–2.5 mg/L. Overall, the model results in Fig. 9.3.2 are consistent with the measured data and represent the seasonal changes reasonably.

The four panels in Fig. 9.4.4 present the modeled fluxes of NH_4, NO_3, PO_4, and SOD, respectively. There are no measured sediment flux data available for the calibration of the sediment diagenesis model in this study. As shown in Fig. 9.4.4, the sediment diagenesis model of Lake Tenkiller simulated seasonal variations of sediment fluxes between the sediment bed and the overlaying water. The positive values represent fluxes from the sediment bed to the overlying water column. Compared with studies on estuaries and bays, there are very limited reports on the measured sediment fluxes in freshwater systems, especially in deep lakes and reservoirs. Di Toro (2001) detailed sediment flux data and modeling in Lake Champlain, a large freshwater system in North America. The average depth of Lake Champlain is 22.8 m, which is comparable with the depths of Lake Tenkiller. The measured data and modeled results of NH_4, NO_3, PO_4, and SOD in the deep waters of Lake Champlain (Di Toro, 2001, Fig. 15.21) are surprisingly similar to the ones shown in Fig. 9.4.4, both in magnitude and in seasonal variation. One exception is that the Lake Tenkiller Model produced much larger PO_4 flux during the summer as the result of the anoxic condition in the lake bottom, while Lake Champlain did not have hypolimnetic anoxia. Since the sediment fluxes play important roles in the water quality and eutrophication processes, the errors in the water quality model results could also be partially due to the lack of data to calibrate the sediment diagenesis model.

9.4.1.5 Discussion and Conclusions. The primary purpose for developing the Lake Tenkiller Model was to use the model as a tool for proposing and testing load-management strategies aimed at limiting eutrophication processes in the lake (Tetra Tech, 2000c). The model was calibrated against measured data in 1986 and represented existing hydrodynamic and water quality pro-

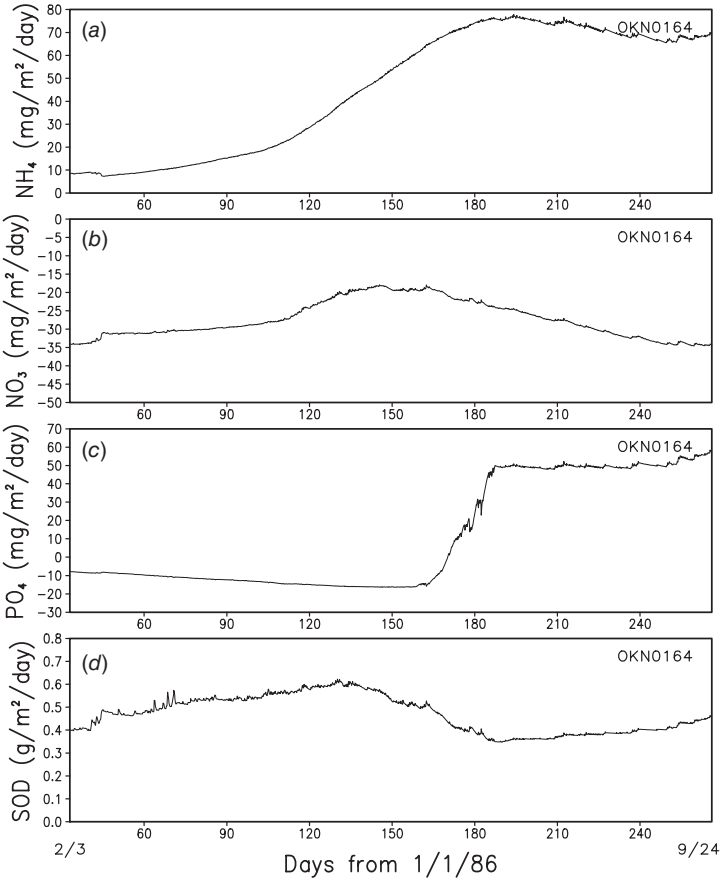

Fig. 9.4.4 Modeled sediment fluxes at OKN0164. (*a*) NH_4; (*b*) NO_3; (*c*) PO_4; and (*d*) SOD.

cesses in the lake satisfactorily. In addition to being compared with the measured data graphically, the model results were also analyzed statistically. This analysis provided a different perspective on model–data comparison that numerically quantified the state of model calibration.

Conclusions from this modeling study include the following:

1. Despite the progress in 3D hydrodynamic, water quality, and sediment diagenesis models and their successful applications in estuaries and bays, few similar 3D modeling studies on eutrophication in lakes and reservoirs have been published. In this study, a 3D hydrodynamic and water quality model has been developed and applied to Lake Tenkiller, OK. The importance of 3D modeling of lake hydrodynamic and eutrophication processes is discussed in detail and demonstrated through a variety of test cases (Section 7.3.3).

2. The model was calibrated against measured data. Particular attention was given to reproducing the seasonal cycles of temperature, algae, and nutrients in the lake. Comparisons of the modeled results with the measured data for all parameters were satisfactory. The seasonal variations of T, DO, Chl, $NO_2 + NO_3$, PO_4, and BOD_5 were replicated reasonably well.
3. Even though the modeled sediment fluxes are similar to those reported by Di Toro (2001), both in magnitude and in seasonal variation, there are no measured data available for calibrating the sediment diagenesis model in this study. This should be one of the error sources in the water quality modeling.

The Lake Tenkiller Model is used as a tool for proposing and evaluating cost-effective approaches for water resources management (Tetra Tech, 2000c).

9.4.2 Case Study II: Lake Okeechobee

The hydrodynamic, sediment, and water quality modeling of Lake Okeechobee is already discussed in previous chapters. It took years of effort to reach the stage that the LOEM can be used to simulate the lake with confidence (Jin and Ji, 2001, 2004, 2005, 2006; Ji and Jin, 2006; Jin et al., 2000, 2002, 2007). So far, there are few published studies that have taken such solid steps/approaches to model a large, shallow lake. This section focuses on the applications of the LOEM.

The LOEM is used to predict the impact of hydrodynamic, sediment, and water quality processes in the lake under different management scenarios and environmental conditions. The LOEM is capable of predicting how phosphorus-rich mud sediments move in the lake and under what conditions the sediments are most likely to be resuspended and transported. This information is useful to evaluating the water quality improvement plan (SFWMD, 2002). This section summarizes three applications (scenarios) of the LOEM model:

1. Sediment and nutrient fluxes from the open water into the Fisheating Bay.
2. Impact of hurricanes on the lake.
3. Impact of SAV growth on water quality conditions in the lake.

9.4.2.1 Sediment and Nutrient Fluxes into the Fisheating Bay. The LOEM model is used to estimate the amounts of sediment and nutrients that are transferred into the Fisheating Bay from the open water (Fig. 2.4.2). The bottom of Lake Okeechobee contains a crescent-shaped ridge of rock along the south and western regions. When water levels are <4.57 m (15 ft) MSL, this ridge restricts water movement between the regions. As a result, less sediment

is transported to the nearshore region, and water quality is improved there. When water levels are high (well >4.57 m MSL), water movements are less restricted, and the resuspended sediment from the mud zone is able to reach the nearshore area. Fisheating Bay, located in the west side of Lake Okeechobee (Fig. 2.4.2), is a shallow area containing SAV and providing critical habitat for fish, wading birds, and other wildlife. Submerged aquatic vegetation in this area plays a role in preventing sediments from resuspension and supporting attached algae. Shoreline areas of Lake Okeechobee supported a large acreage of SAV before 1995, but the acreage was reduced after multiple years of very high water levels.

Lake-wide circulation patterns, associated with a large gyre that is parallel to the shoreline (e.g., Figs. 7.2.3 and 7.2.4), generate a movement of suspended sediment into the Fisheating Bay. Strong, seasonal northern winds produce a well-mixed water column and create a mean current velocity near the shoreline area. Most of the sediment carried by currents into the bay are settled and deposited in this area after losing momentum. The current velocity is drastically reduced by resistance from SAV and the lake bed. The geophysical boundary of Fisheating Bay also decreases current velocities in the area. The deposited sediment can be resuspended back into the water column again due to either increased flow from Fisheating Creek or wind-induced waves. These conditions cause increased turbidity and hinder the growth of SAV during spring, summer, and fall. Therefore, the fluxes of sediment and nutrients from the open water into the Fisheating Bay greatly affect the ecosystem of the bay.

The sediment and nutrient fluxes from the open water into the Fisheating Bay are calculated using the LOEM model. Figure 9.4.5 shows the time series of the modeled total sediment (Sed) and TP flowing into the Fisheating Bay in Water Year (WY) 2000 (10/1/1999–9/30/2000), WY 2001 (10/1/2000–9/30/2001), and WY 2002 (10/1/2001–9/30/2002). Figure 9.4.5 shows that, in WY 2000, ~25×10^3 tons of sediment and 23.5 tons of TP entered the Fisheating Bay. In WY 2001, ~6×10^3 tons of sediment entered the Fisheating Bay, while 2 tons of TP left the Fisheating Bay and entered the open water. In WY 2002, ~18×10^3 tons of sediment and 13 tons of TP entered the Fisheating Bay.

The sediment and TP fluxes exhibited very different patterns in 2000 and 2001. This was primarily due to the fact that the lake had extremely low water elevation in 2001, and a large portion of the lake area became dry during the summer of 2001. Figure 9.4.5 reveals that sediment and TP were transported out of the Fisheating Bay and into the open water in the last 2 months of WY 2001. By carefully examining water inflows from the tributaries and the circulation patterns in the lake, it is found that the large water inflows from the tributaries in the west of the lake caused a net sediment and TP fluxes into the open water in August and September of 2001.

Sheng and Lee (1991) modeled the phosphorus transported into the vegetation area in Lake Okeechobee. They estimated that ~1 ton of phosphorus flux entered the area over a 1-month period, which is equivalent to ~12 tons or so

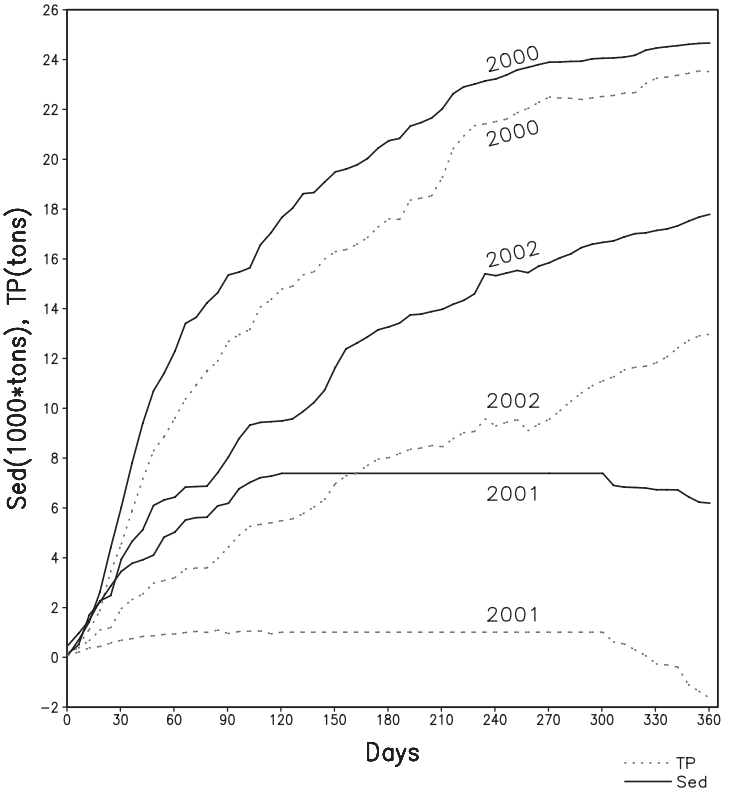

Fig. 9.4.5 Time series of the estimated total sediment (solid line) and total phosphorus (dotted line) into the Fisheating Bay in WY 2000, 2001, and 2002.

per year. Considering the very different input data and very different periods used in the two studies, TP flux from the LOEM is consistent with the one from Sheng and Lee (1991), since the two are on the same order of magnitude.

9.4.2.2 Impact of Hurricane Irene. During the last century, the Florida Peninsula experienced landfall by named tropical storms, on average, once per year, and landfall by a hurricane (wind velocity >120 km/h) every 2–3 years. A "major" hurricane (wind velocity >180 km/h) impacted the Peninsula every 5–6 years (Jin and Ji, 2005). Lake Okeechobee is located in the area that has a high probability for hurricane impacts.

Strong tropical storm events (hurricanes or cyclones) may have strong impacts on the hydrodynamics, sediment transport, and water quality in a lake. Those impacts are often not well documented since it is difficult to predict the timing and paths of hurricanes. There is also a lack of substantive data prior to and after the event. Risk of damage to field equipment and observers makes

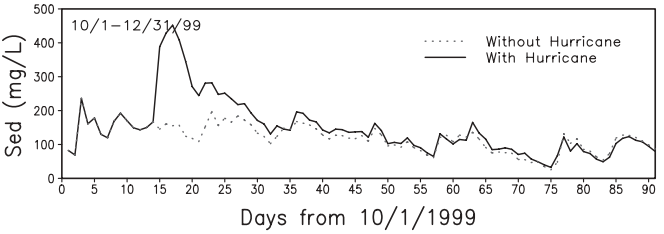

Fig. 9.4.6 Modeled sediment concentrations with (solid line) and without (dotted line) effects of Hurricane Irene.

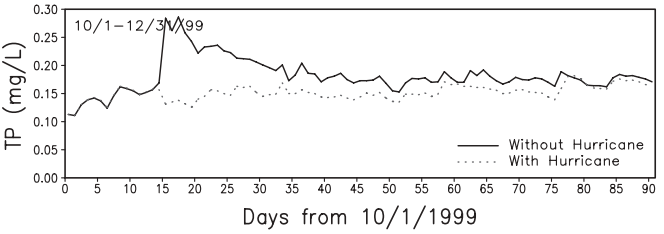

Fig. 9.4.7 Modeled total phosphorus concentrations with (solid line) and without (dotted line) effects of Hurricane Irene.

it very difficult to prepare a data collection plan to study their effects. The LOEM model can be a good alternative tool to investigate the hurricane impacts.

Hurricane Irene, a Category I hurricane, passed by Lake Okeechobee in mid-October, 1999. To study the impact of Hurricane Irene on the lake water quality, the LOEM model is used to calculate the case as if there was no hurricane in October 1999. The no-hurricane case is simulated by replacing the wind velocities between October 15 and 17, 1999, with wind velocities between October 15 and 17, 1989, which leads to modest wind speeds of a few m/s during this period.

Figure 9.4.6 gives the modeled sediment concentrations at LZ40 (shown in Fig. 2.4.2) under the conditions with (solid line) and without (dotted line) Hurricane Irene. It shows that around Day 16, Hurricane Irene caused a large amount of sediment to be resuspended from the lake bottom. The sediment concentration is up to 450 mg/L. The higher sediment concentration lasted for >60 days. Figure 9.4.7 gives the modeled TP concentrations at LZ40 under the conditions with (solid line) and without (dotted line) Hurricane Irene. It shows that around Day 16, the resuspended sediment brought a large amount of particulate phosphorus from the bed into the water column and increased the TP concentration up to 0.28 mg/L. The higher TP concentration lasted for >60 days.

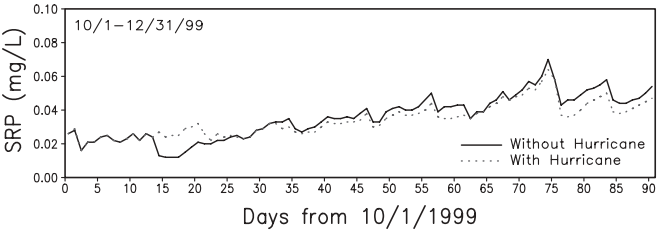

Fig. 9.4.8 Modeled SRP concentrations with (solid line) and without (dotted line) effects of Hurricane Irene.

TABLE 9.4.4 Differences between Model Results for Chl a With and Without SAV in 2000

Station Name	Observed Mean (μg/L)	With SAV Model		Without SAV Model	
		Model Mean (μg/L)	RRE (%)	Model Mean (μg/L)	RRE (%)
PELMID	14.70	24.83	62.82	25.91	67.83
POLE3S	12.85	25.70	60.88	26.59	64.96
RITAWEST	23.77	24.47	25.15	25.17	26.46
RITAEAST	19.74	27.10	33.61	29.38	41.02
TREEOUT	21.89	23.34	38.33	24.69	41.03
PALMOUT	19.79	23.14	43.77	24.31	45.33
Mean	18.79	24.76	44.09	26.01	47.77

Figure 9.4.8 gives the modeled SRP concentrations at LZ40 under the conditions with (solid line) and without (dotted line) Hurricane Irene. SRP is represented by PO4d in the LOEM model using Eq. (5.4.9). It shows that the SRP concentration is significantly decreased during and right after the hurricane event. The primary reason for SRP reduction is due to the high suspended sediment concentration in the water column. As shown in Eq. (5.4.9), the high TSS concentration reduced the SRP concentration.

It should also be mentioned that the results presented in Figs. 9.4.6–9.4.8 are from a sediment model that does not include the mechanism of sediment bed consolidation. The consolidation process should affect how the sediment bed responds to hurricane forcings.

9.4.2.3 Impacts of SAV on Nutrient Concentrations. To analyze the impact of SAV on the water quality in Lake Okeechobee, a test run without SAV was conducted by turning off the SAV submodel of the LOEM model, which is called the run without SAV. This test run is then compared with the model calibration run in 2000, called the run with SAV (Section 5.9.2).

SAV can significantly affect nutrient concentrations, especially in areas where the SAV biomass is large and the water has a limited exchange with the

open water. During the SAV growth season, nutrients are consumed by the SAV and are less available for algal growth in the water column. Table 9.4.4 tabulates the modeled Chl *a* (CHL) concentration at six stations (shown in Fig. 5.9.3) in or near the SAV zone (Fig. 5.9.8). Table 9.4.4 indicates that including SAV in the model consistently reduces the CHL concentration at these six stations. The SAV growth consumes SRP and lowers SRP concentration. At TREEOUT station, for example, the CHL concentration had an observed mean of 21.89 μg/L, a modeled mean of 23.34 μg/L, and an RRE of 38.33%. Without the SAV model, the modeled mean increased to 24.69 μg/L and the RRE increased to 41.03%. Table 9.4.4 shows that on average, the Chl *a* concentrations are reduced by 1.25 μg/L and the model's RRE is reduced by 3.68%, when the SAV is included in the LOEM model.

In the study of SAV impact on the lake water quality, a few things should be kept in mind:

1. Currents bring nutrients from other areas to the SAV zone and reduce the impact of SAV growth on nutrient concentrations in the lake.
2. Compared with other lakes, SAV concentrations in Lake Okeechobee are relatively low (Havens, 2003), only ~20 g/m^2 on average, which also reduces the influence of SAV on nutrient concentrations.
3. SAV makes up only a few percent of the total lake area reducing its influence on lake water quality.
4. SAV growth consumes nutrients. Some of these nutrients are buried in the lake bed and are assumed to be permanently removed from the lake system. But most of the nutrients taken by the SAV are eventually released back into the water column, via respiration and nonrespiration loses. In this way, SAV just recycles most of the nutrients that are consumed for SAV growth.

CHAPTER 10

Estuaries and Coastal Waters

An estuary is defined as a semiclosed coastal waterbody that is freely connected to the open sea and within which seawater is measurably diluted with freshwater derived from land drainage (Pritchard, 1967). This classic definition has been extended to include certain areas of inland lakes that receive riverine water. For example, the backwater reaches draining into the Great Lakes are considered to be estuaries, where the lake water intrudes upstream into these reaches. Coastal water is usually referred to as the part of the ocean affected by its proximity to the land that exerts a measurable influence on the water. For simplicity, estuaries are where rivers meet the oceans, and coastal waters are where the lands meet the oceans.

The general theories and processes of hydrodynamics, sediment transport, pathogens and toxics, and water quality are already presented in Chapters 2–5, respectively. This chapter describes characteristics of estuaries and the hydrodynamic, sediment, and water quality processes in estuaries and coastal waters. At the end of this chapter, case studies are also presented as modeling examples.

10.1 INTRODUCTION

Coastal waters are complex environments characterized by rich biological diversity and natural resources. As the population of coastal communities increases, the deterioration of the coastal environment has become a critical issue. Estuaries are coastal waters where the mouth of the river meets the ocean and where the freshwater of the river mixes with the saline water from the ocean. They are the crossroads of river, ocean, atmosphere, and sediment bed. Salinity variations in estuaries are so large that they affect the mean circulations significantly. Estuaries are often known as bays, harbors, sounds, inlets, lagoons, and so on, even though not all waterbodies by these names are necessarily estuaries. The important characteristic is the mixing of fresh and saline water and not the name. Some familiar estuaries in the Unites States

Hydrodynamics and Water Quality: Modeling Rivers, Lakes, and Estuaries, by Zhen-Gang Ji

include the Chesapeake Bay, New York Harbor, Long Island Sound, Cook Inlet, and Indian River Lagoon.

Enacted in 1972, the Clean Water Act (CWA) is the cornerstone of surface water quality protection in the United States. The statute employs a variety of regulatory and nonregulatory tools to sharply reduce direct pollutant discharges into waterways, finance municipal wastewater treatment facilities, and manage polluted runoff. Under the CWA, the estuary has its own legal definition: All or part of the mouth of a river or stream or other body of water having unimpaired natural connection with the open sea and within which seawater is measurably diluted with freshwater derived from land drainage. The CWA definition of estuary also considers "associated aquatic ecosystems and those portions of tributaries draining into the estuary up to the historic height of migration of anadromous fish or the historic head of tidal influence, whichever is higher". Anadromous fish are fish that live most of their lives in saltwater and return to freshwater to spawn, such as herring and salmon. The definition of estuaries used in the scientific communities is not the same as the legal definition under the CWA.

Estuaries are different from rivers and lakes hydrodynamically, chemically, and biologically. Compared with rivers and lakes, the unique characteristics of estuaries include that (1) tides are a major driving force; (2) salinity and its variations usually play a significant role in hydrodynamic and water quality processes; (3) two directional net flows—seaward in the surface layer and landward in the bottom layer—often control the long-term transport of pollutants; and (4) open boundary conditions are required in numerical modeling.

The primary factors controlling transport processes in estuaries are tides and freshwater inflows. Wind forcing can also be significant for large estuaries. Most estuaries are long and narrow, resembling a channel (Fig. 10.1.1). Rivers are the primary source of freshwater to an estuary, which mixes with saline water as tidal elevation rises and falls. A typical estuary has most of the freshwater being discharged at its head and has a transitional section (near the estuary mouth) between the estuary and the coastal ocean. The freshwater inflow is blocked from streaming into the open ocean by either the surrounding mainland, peninsulas, or barrier islands. As illustrated in Fig. 10.1.1, the river has a downstream flow of freshwater. The tidal river is the reach where although some current reversal occurs, seawater has not penetrated to the region, and the tidal water is still fresh (or brackish). The estuary has reversal currents and saline water.

Key characteristics of coastal waters include sharp horizontal and vertical gradients of salinity and other hydrodynamic and water quality variables. In mathematical models, open boundary conditions, which will be discussed in Section 10.5.1 later, are often needed to describe three sides of a coastal water area: (1) an open offshore boundary adjacent to the open ocean, (2) an upstream open boundary, and (3) a downstream open boundary.

The sharp salinity gradients result from the freshwater inflows and the mixing of the saline water from the open ocean. Horizontal salinity and density

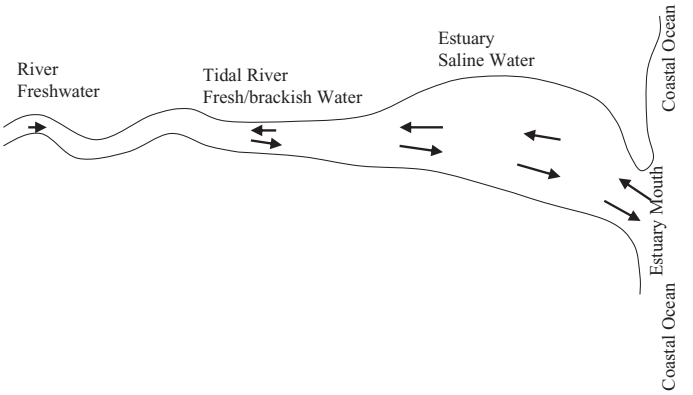

Fig. 10.1.1 Schematic representation of an estuary system.

gradients tend to parallel the contours of the bathymetry. Wind forcing and coastal upwelling and downwelling also affect the gradients of salinity, temperature, and other water quality variables.

Coastal waters and estuaries present the world with a bounty of tangible and intangible benefits. People rely on the coastal waters and estuaries for recreation, livelihoods, and social and economic well being. Coastal oceans account for only 10% of the oceans by area but up to 95% of the world's fishery yield (Walsh, 1988). The United States has >152,000 km of coastline. More than one-half of the United States' population live in coastal areas, and this trend is expected to grow (NRC, 2000). There are ~850 estuaries in the United States (NRC, 1983). Estuaries represent only a tiny proportion of the world's surface waters, but they are among the most productive ecosystems in Nature. Rivers drain into estuaries, bringing in nutrients from uplands. Plants use these nutrients, along with the sun's energy, carbon dioxide, and water, to manufacture food. These waters provide critical habitat for various life stages of commercial fish and shellfish and support popular recreational activities. This mixing of fresh and saline water creates a unique environment that brims with life of all kinds, such as birds, mammals, fish, and other wildlife.

Most riverine pollutants eventually empty into estuaries. Dredged material, municipal discharge, and industrial wastes are the primary point sources to estuaries. Urban runoff and agricultural activities are often the major nonpoint sources. Many estuaries face similar pollution problems: overenrichment of nutrients, pathogen contamination, toxic chemicals, and alteration of freshwater inflow. These problems result in harmful algal blooms, beach and shellfish bed closings, fish kills, disappearance of SAV, and a variety of other environmental problems. Excess nutrient loadings contribute to lower DO levels and SAV losses. Beach closings due to elevated pathogen concentrations are one of the most visible symptoms of marine pollutions.

The characteristics of estuaries vary significantly. Estuaries can be categorized by their distinct characteristics and circulation patterns. Geomorphic classification schemes provide some insight into the circulation patterns. Based on their geomorphic features, estuaries can be divided into four main groups (Pritchard, 1967; Dyer, 1973; Tomczak and Godfrey, 1994): (1) coastal plain estuaries (drowned river valleys), (2) lagoons (bar-built estuaries), (3) fjords, and (4) tectonic estuaries and others.

Coastal plain estuaries (or drowned river valleys) were formed by drowning the ancient river mouth due to the rising sea level at the end of the last ice age. A good example of a coastal plain estuary is the Chesapeake Bay, where the rising sea level invaded a low-lying historic river mouth. These estuaries have little sedimentation and still keep the topography of the ancient river valley. They are commonly broad, shallow (often <30 m deep), and mostly located in the temperate climate zones. With gentle sloping bottoms, these valleys have depths that increase uniformly toward the mouth. Coastal plain estuaries are characterized by well-developed longitudinal salinity gradients. Such estuaries are usually moderately stratified and can be highly influenced by the wind. The majority of estuaries in the United States are of the coastal plain type.

Lagoons (bar-built estuaries) were formed by breaching of the ancient sandbars (barrier islands) and flooding of the region behind it due to the rising sea level over geological time. This feature was formed during the last ice age. Lagoons, such as the Indian River Lagoon shown in Fig. 2.4.12, have large open areas and are very shallow (usually <2 m deep). They are separated from the ocean by barrier islands, which are generally parallel to the shoreline. The barrier islands protect lagoons from the pounding of the ocean waves and may change position and shape in response to coastal processes and human actions. Lagoons may also be separated from the open ocean by barrier coral reefs, such as the Mesoamerican Lagoon along the coast of Belize created by the Mesoamerican Barrier Reef System (Ezer et al., 2005). Lagoons have a limited exchange with the ocean through inlets, which are short, narrow waterways connecting the lagoon with the ocean. Most lagoons are primarily wind dominated and are generally vertically mixed. Some lagoons may experience vertical stratifications, especially in the navigation channels. The water is moved more by the wind than by the tide and does not flow from headwaters to a mouth like a river. The shallow water depths enhance the nutrient exchanges between the water column and the sediment bed. Due to high evaporation, limited exchange with the ocean, and low freshwater inflow, lagoons usually have higher salinities than other estuaries. Lagoons are present on all continents, especially in the subtropics and tropics. In the United States, lagoons are primarily found along the Gulf of Mexico and the lower Atlantic regions.

Fjords are drowned glacial valleys that are formed by moving glaciers during the last ice age (Fig. 10.1.2). The scouring of the river valleys results in very deep estuaries. In contrast to coastal plain estuaries and lagoons, fjords

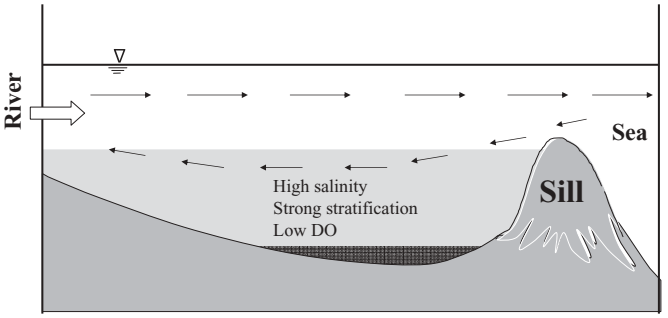

Fig. 10.1.2 Schematic representation of a fjord.

TABLE 10.1.1 Common Characteristics of Coastal Plain Estuaries, Lagoons, and Fjords

Estuary Type	Width	Depth	Location	Stratification	Tides	Examples
Coastal plain estuaries	Wide	Shallow (<30 m)	Temperate zone	Moderate	Strong	Chesapeake Bay
Lagoons	Wide	Very shallow (<2 m)	Subtropics and tropics	Weak	Weak	Indian River Lagoon, FL
Fjords	Narrow	Deep (>200 m)	High latitudes	Strong	Weak in deep waters	Puget Sound, WA

feature a long, narrow, deep arm of the sea with steep sides. Water depths typically are several hundred meters deep. The small ratio of width/depth means that fjords are relatively narrow, even though the width of a fjord is not necessarily less than the width of a lagoon or coastal plain estuary. A shallow sill is situated at the mouth of a fjord, formed by accumulated rocks at the glacier front when the glacier receded (Fig. 10.1.2). Sill depths can be as shallow as 4 m, but typically range between 40 and 150 m (Tomczak and Godfrey, 1994). The higher the sill, the more isolated the bottom water is in the fjord behind it. The sill limits circulation and mixing in deep water, greatly impedes flushing, and makes only the surface waters affected by tidal forcing. Fjords usually are strongly stratified, with hypoxia (or even anoxia) in deep waters. Fjords generally occur at higher latitudes. A good example of a fjord is the Puget Sound, Washington.

Table 10.1.1 summarizes the common characteristics of coastal plain estuaries, lagoons, and fjords. It should be mentioned that not all estuaries exactly fit the characteristics listed in Table 10.1.1, which is more a concept than a description of real estuaries. Comparisons between the different estuary groups clearly show the characteristics of each estuary group, which is helpful

for understanding the estuarine processes and for conducting modeling studies.

In addition to the above three groups, estuaries may also be formed by tectonic activities, volcanic eruptions, or landslides. Tectonic estuaries are created when the sea fills in the large cracks or faults that were formed by the motion of earth's crust. Their geomorphic features vary greatly and may resemble coastal plain estuaries, lagoons, or fjords. A good example of a tectonic estuary is the San Francisco Bay.

10.2 TIDAL PROCESSES

"The tides are the heartbeat of the ocean, a pulse that can be felt all over the world" (Defant, 1958). This section gives brief descriptions on tides, tidal currents, and tidal analysis. The focuses are on those aspects that are important to hydrodynamic, sediment, and water quality processes in estuaries. Many details on tides and tidal dynamics are not covered here and are left to dedicated books and reports on tides (e.g., Pugh, 1987).

10.2.1 Tides

Tides are the alternate rising and falling of water levels resulting from the gravitational attraction between the earth, sun, and moon. Tidal currents are the associated horizontal movement of the water. Tidal currents change speed and direction regularly and are among the strongest in the world's ocean. At high tide at the estuary mouth, the slope of the water surface forces water to rush into an estuary. At low tide, the reversal slope flushes water out of the estuary. Tides and tidal circulation play a significant role in the hydrodynamic, sediment transport, and water quality processes in estuaries and coastal waters.

Tides and wind waves discussed in Section 3.6 are both gravitational waves, that is, both have gravity as the restoring force, and both can be important in the study of estuaries and coastal waters. Major differences between the two waves include (1) wavelength, (2) wave period, and (3) origin.

Tides are long waves with wavelengths spanning thousands of kilometers in the open ocean and with the shortest wavelength of more than a few hundred kilometers in estuaries; whereas wind waves have typical wavelengths of a few (or tens) meters. Therefore, tidal waves are always shallow water waves; whereas wind waves can be either shallow water waves (Fig. 3.6.5) or deep water waves (Fig. 3.6.4), depending on the water depth. Tidal periods are characterized as diurnal (one high and one low per day), semidiurnal (two highs and two lows per day), and mixed (two highs and two lows with unequal heights); in contrast, wind waves have periods of a few seconds or less. The dominant tidal period is usually 12 h 25 min. Tides originate in the deep ocean basins due to the gravitational attraction between the earth, sun, and moon

and then propagate into coastal waters and estuaries; wind waves are formed by wind blowing over water surface.

Tides are important in estuaries, coastal waters, and tidal rivers; however, wind waves can be critical to sediment resuspension and toxicant transport in large and shallow waters. This is also the primary reason that tides are presented in this chapter, whereas wind waves are described in the sediment transport chapter (Chapter 3). Since the tide-generating force is on a global scale, only the major oceans can experience tidal forcing and generate tides. Estuaries are forced by the tides originating from the deep ocean via the connections to the ocean. Wind waves can play a significant role in sediment processes, as long as: (1) the surface area of the waterbody is large enough so that the fetch is sufficiently long and (2) the water depth is shallow enough so that the wind wave energy can propagate to the water bottom.

Because these two types of waves are very different in many aspects, they are usually simulated using very different models. Tidal elevations and currents in estuaries can be described well using the hydrodynamic equations presented in Section 2.2. Wind waves can be simulated using the wind waves models described in Section 3.6.3.

Tides are produced as the result of the gravitational attraction of the moon and the sun. Tidal currents are produced in response to the differences in tidal elevation. Except for the moon and the sun, all other celestial bodies are insignificant to tides. Newton's Law of Gravitation states that gravitational attraction (force) between two bodies is proportional to the product of the masses of the two bodies, divided by the square of the distance between them:

$$F = G\frac{m_1 m_2}{r^2} \tag{10.2.1}$$

where F = the gravitational force on either body, r = distance between the mass centers of the two bodies, m_1 = mass of body 1, m_2 = mass of body 2, and G = the universal constant (or gravitational constant) (= $6.67 \times 10^{-11}\,\mathrm{N\,m^2\,kg^{-2}}$).

Compared to other celestial bodies, the moon is the closest to the earth and has the strongest effect on the tides (Fig. 10.2.1). The longer distance between the sun and the earth creates a tide-generating force of ~46% of that of the moon. Other celestial bodies are too far away from the earth to exert a significant influence on tides.

In addition to the gravitational force, the centrifugal force from the rotation of the earth also affects tides. The balance between the two forces controls the tides in the deep oceans. On the side of the earth facing the moon, as illustrated in the first plot of Fig. 10.2.1, there is a stronger gravitational force due to the shorter distance. On the side away from the moon, there is a weaker gravitational force due to the larger distance. This force difference results in high tides on the side facing the moon (due to the stronger attraction from the

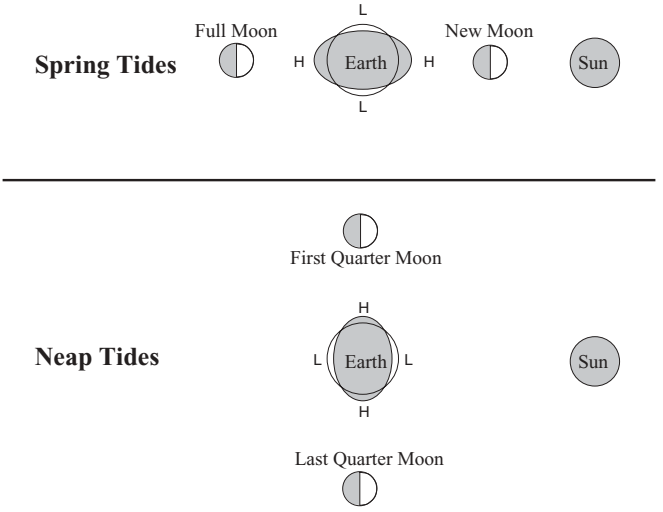

Fig. 10.2.1 Schematic representations of spring and neap tides.

moon) and on the side away from the moon (due to the relatively stronger centrifugal force). This leads to a bulge in the oceans on the two opposing sides of the earth. The corresponding low tides (depressions) are presented in areas with no net excess of gravitational or centrifugal forces.

As the moon rotates around the earth, these bulges and depressions travel across the oceans. The vertical fluctuation of water elevation produces horizontal flows in the form of tidal currents. Because the moon passes over any fixed location on the earth's surface every 24.84 h (called a tidal or lunar day), there are approximately two high and two low tides every day, and there is a maximum tide every 12.42 h, which is called the semidiurnal tide (or M_2 tide). Since the gravitational force is proportional to the masses of the bodies, as given in Eq. (10.2.1), only the earth's large waterbodies, such as the Pacific, Atlantic, and Indian Oceans, experience tidal motions. For example, the moon can causes a bulge of one-half of a meter in the Atlantic Ocean. This bulge and the corresponding depression lead to the propagation of a tidal wave. The topography of ocean basins and estuaries can significantly modify the amplitude and phase of tides and in some regions create extremely large tides, such as those found in the Bay of Fundy in the Gulf of Maine and in Cook Inlet in the Gulf of Alaska (e.g., Oey et al., 2007).

The amplitudes of the semidiurnal tides change as the relative position of the moon and sun changes. As shown in Fig. 10.2.1, spring tides are exceptionally high tides that occur approximately every 2 weeks during new and full moons when the earth, sun, and moon are in alignment, and the lunar tide is in phase with the solar tide. Neap tides are exceptionally low tides that occur approximately every 2 weeks during the moon's first and third quarters, when the earth, sun, and moon are at right angles to each other, and the lunar tide

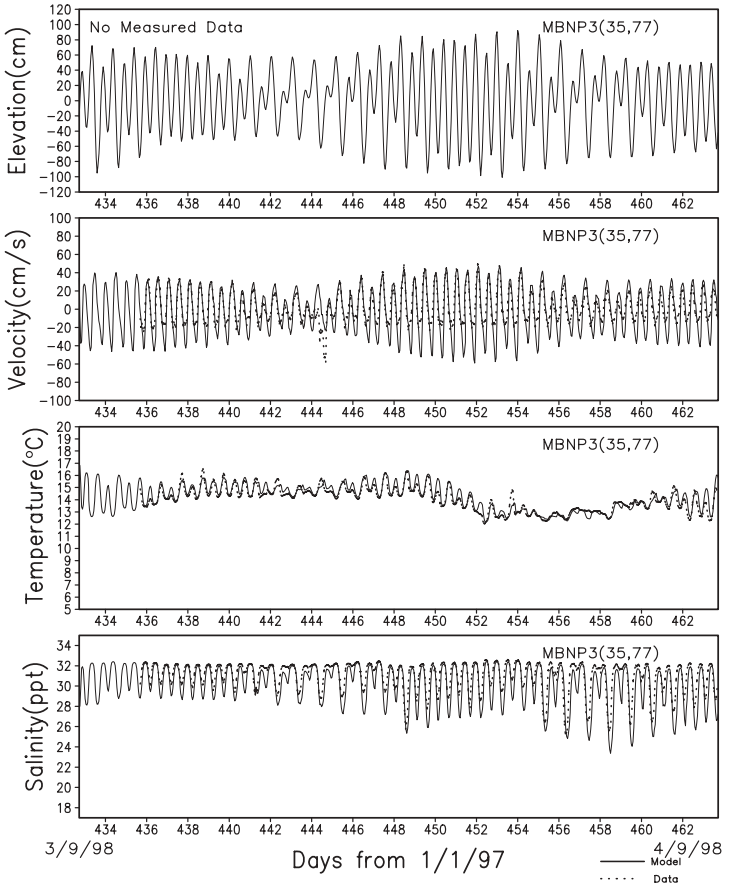

Fig. 10.2.2 Model (solid line) and measured (dashed line) tidal elevation, velocity, temperature, and salinity at MBNP3 in Morro Bay, CA (Ji et al., 2001).

is out of phase with the solar tide. This envelope of the spring-to-neap cycle occurs with a period of ~14.77 days. An example tidal elevation in Morro Bay, CA, is shown in the first panel of Fig. 10.2.2 (Ji et al., 2001), in which the tidal elevation exhibits two amplitude envelopes during the 31 days, from March 12 to April 11, 1998. It is clear that the tidal elevation (top panel of Fig. 10.2.2) shows strong diurnal variability and has a spring-neap variability of 15 days or so. Tidal elevations control the tidal velocity (shown in the velocity panel of Fig. 10.2.2), and therefore control the transport of substances in the estuary, as shown by the salinity time series in the bottom panel of Fig. 10.2.2.

Tides can be represented as the sum of tidal constituents. Each constituent is a harmonic oscillation and has its amplitude, period, and phase, which can be extracted from measured tidal data using the harmonic analysis described in Section 10.2.3. There are hundreds of tidal constituents, but most of them

TABLE 10.2.1 Major Tidal Constituents and Periods

Tidal Symbol	Generating Force	Period (h)
M_2	Moon	12.421
S_2	Sun	12.000
O_1	Moon	25.819
K_1	Moon, Sun	23.935
N_2	Moon	12.659
P_1	Sun	24.067
K_2	Moon, Sun	11.967

have very small amplitudes, and therefore are neglected in tidal analysis. Table 10.2.1 lists the major tidal constituents and their periods. These tidal constituents are the building blocks of the tide. The subscripts of the tidal symbols in Table 10.2.1 indicate the approximate number of cycles per 24 h. Diurnal constituents occur approximately once a day and have a subscript of 1. Constituents with subscripts of 2 are semidiurnal constituents and occur approximately twice per day.

The first five constituents, M_2, S_2, O_1, K_1, and N_2 are often the most important tidal constituents. It is often adequate to include these five constituents in a tidal analysis, even though more than a hundred tidal constituents might be used in official tidal predictions. If the amplitudes for M_2, S_2 and N_2 are large compared to the amplitudes for O_1 and K_1, then the tides in the region are of the semidiurnal type. If O_1 and K_1 amplitudes are large compared to M_2, S_2 and N_2, then the tides are of the diurnal type.

The spring and neap tides shown in Fig. 10.2.1 can also be explained as being caused by the period difference between M_2 and S_2 tides. The S_2 tide has a period of 12.000 h, a little shorter than the M_2 tide's period of 12.421 h. The period difference makes the two constituents in and out of phase. Spring tides are formed when M_2 and S_2 tides are in phase, so that both constituents peak at the same time, causing large tidal amplitude. Neap tides occur when M_2 and S_2 tides are out of phase and tend to cancel each other, reducing tidal amplitude.

10.2.2 Tidal Currents

The back-and-forth flow of tidal currents is the most visible feature of estuaries. Tides and tidal currents are important to estuaries for a variety of reasons, including (1) tides are ubiquitous and are often a major driving force of the system, (2) tides are a major factor controlling the flushing time of many estuaries, (3) tidal currents are largely responsible for mixing in estuaries, and (4) tidal currents can generate residual flow that affect the long-term transport of pollutants.

As illustrated in Fig. 10.2.3, low tide (low water) is the lowest water level reached by a falling tide. High tide (high water) is the highest water level

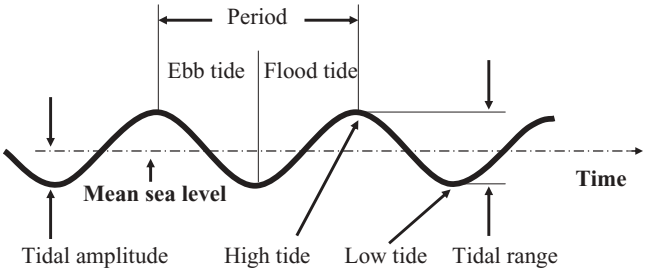

Fig. 10.2.3 Sketch of a tide.

reached by a rising tide. Tidal range is the difference in water level between high and low waters and is two times of tidal amplitude. Ebb tide (falling tide) is the transitional period from the high tide to the succeeding low tide. During the ebb tide, an estuary drains the water to the sea and the water level drops. The associated current (called ebb current) moves seaward. Flood tide (rising tide) is the transitional period between low water and the succeeding high water, during which an estuary receives water from the sea and the water level rises. The associated current (called flood current) moves landward. The period of slack water represents the time of minimum tidal velocity, during which the tidal current changes direction and its velocity is around zero.

Major factors that influence the propagation and amplitude of tides include: (1) bottom friction, (2) water depth and shoreline, and (3) Coriolis force. Interactions of tidal flows with these factors may result in a residual current that could play a significant role in the transport of pollutants. The residual current is generally obtained by averaging tidal velocities over tidal periods. An averaging time of 25 h is often used to remove the semidiurnal tide (M_2 tide).

Tidal currents experience vertical shears from their interaction with the bottom. These shears reduce the vertical stratification. Because of bottom friction, tidal currents are weaker near the bottom than in the interior of the water column. This frictional effect allows the currents near the bottom to respond to tidal elevation change more quickly than the currents in the interior. Hence, tidal phases near the bottom change before those in the interior or near the surface, causing vertical phase differences in the tidal currents. These phase differences are best observed around the times of slack waters.

Due to the rotation of the earth, the Coriolis force deflects currents to the right in the northern hemisphere and to the left in the southern hemisphere. This deflective force can make the ebb and flood currents follow different paths in an estuary and result in spatially asymmetric residual patterns: a counterclockwise residual circulation in the Northern hemisphere. This circulation pattern may affect long-term transport (e.g., salinity and sediment) significantly. For example, this circulation is applied to explain why the mean salinity in the Chesapeake Bay is generally higher on the eastern shore than on the western shore, since the counterclockwise circulation brings more salt into the estuary on the eastern shore.

In estuaries with narrow channels, tidal currents are often bi-directional and flow only back-and-forth along the channel. In open areas, the Coriolis force may make the tidal current change directions (0–360°) continuously during a tidal period. Tidal currents then can be projected onto a principal axis on which the flow components have their largest amplitudes and onto a secondary axis that is at a right angle (or normal) to the principal axis. The components of the tidal currents on the secondary axis often have their smallest amplitudes. This approach is often used in tidal current analysis and for model–data comparison. For example, the velocity panel in Fig. 10.2.2 shows the comparison between the measured and modeled currents after both of them are projected onto the principal axis.

Tidal excursion is the distance that a particle travels from low water to high water or vice versa. This parameter is useful for describing the movement of pollutants in estuaries within tidal cycles. Due to net seaward flow of freshwaters, the ebb tidal excursion is generally larger than the flood tidal excursion.

A component of tidal current (e.g., M_2 tide) can be expressed as:

$$u = u_0 \sin(kx - \omega t) = u_0 \sin\left(\frac{2\pi}{L}x - \frac{2\pi}{T}t\right) \tag{10.2.2}$$

where u = tidal velocity, u_0 = maximum tidal velocity, k = tidal wave number, ω = tidal frequency, L = tidal wave length, and T = tidal period (=12.42 h for the M_2 tide).

Equation (10.2.2) can be used to estimate the tidal excursion. Tidal excursion is much shorter than tidal wave length. The former is often in the order of 10 (or less) kilometers, while the latter is more than hundreds (even thousands) of kilometers. It is reasonable to use the values of u at a fixed location (say $x = 0$) for the calculation of tidal excursion, since the values of u are largely determined by time and are relatively constant within the estimated tidal excursion at a specific time. Hence, the tidal velocity around $x = 0$ can be rewritten as:

$$u = u_0 \sin\left(\frac{2\pi}{T}t\right) \tag{10.2.3}$$

For simplicity, the negative sign from Eq. (10.2.2) is omitted in Eq. (10.2.3). The tidal excursion, L_{TE}, is calculated by integrating over one-half of the tidal period:

$$L_{TE} = \int_0^{T/2} u\,dt = \frac{T}{\pi}u_0 \tag{10.2.4}$$

Freshwater inflows impose a net seaward movement on water particles over a tidal cycle. Hence, the ebb tidal excursion should be slightly larger than the flood tidal excursion. For a typical maximum tidal velocity of 1 m/s and with

a M_2 period of 12.42 h, the tidal excursion, L_{TE}, is 14.2 km, which is indeed much smaller than the tidal wave length. Equation (10.2.4) is useful for estimating the horizontal transport distance associated with either ebb or flood tide.

The rise or fall of tidal elevation propagates along an estuary in the form of a longwave. The phase relation between the tidal elevation and the tidal current varies with water depth. The travel speed of a tidal wave in shallow waters is given by $c = \sqrt{gH}$, which means that the deeper the water, the faster the wave speed. The estuary width (and the water depth) usually decreases as the tide propagates up stream, which may amplify the tidal fluctuation.

When a tidal wave propagates upstream in an estuary, it reaches the water head (e.g., a dam) and is reflected. The reflecting wave interferes with the incoming wave in the estuary. This reflection may lead to a standing wave in the estuary when the reflecting wave and the incoming wave are in phase. Standing waves do not travel horizontally. They are stationary and oscillate back and forth around a fixed point. Figure 10.2.4 illustrates the phase relationship between the tidal elevation and the tidal current: the first panel from the top is the tidal elevation, and the second panel is the tidal velocity of a standing wave. At the end of the estuary, the tidal elevation has the maximum amplitude, and the tidal current is at a minimum. At a distance along the estuary equal to one-quarter of the wavelength, the tidal elevation is unchanged with time, and the tidal velocity has the maximum amplitude.

A reflecting wave will not be produced if the estuary is very long and the friction dissipates the energy of the incoming wave. In this case, the estuary

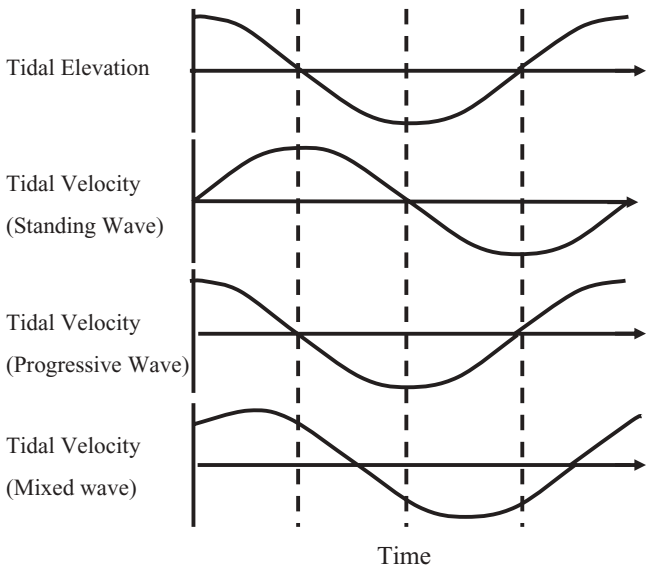

Fig. 10.2.4 The phase relation between tidal elevations and tidal currents.

has a progressive tidal wave. As illustrated in Fig. 10.2.4, the progressive wave has the tidal elevation and the tidal velocity in phase. The maximum tidal currents occur at high or low tide. Tides in estuaries are often a mixture of progressive waves and standing waves, as illustrated in the bottom panel of Fig. 10.2.4.

In certain estuaries, the tidal range is amplified in the upstream section because of resonance effects. Tides in estuaries are generated by tidal forcing from the open ocean. Tidal resonance occurs when the natural period of oscillation of the estuary matches the period of a major tide (e.g., M_2 tide). The amplitudes of tidal resonance depend on the closeness of a resonance period to one of the tidal periods and on the tidal amplitudes in the open ocean. The natural oscillation period of an estuary primarily depends on the depth and the length of the estuary. It is the time that the tidal wave takes to travel from the mouth of the estuary to the opposite end and then reflect and travel back to the mouth of the bay. Since the wave speed is $\sqrt{gH}$ and the distance is $2L$, the oscillation period can be estimated as:

$$T = \frac{2L}{\sqrt{gH}} \tag{10.2.5}$$

where T = natural oscillation period of the estuary, L = estuary length, and H = mean water depth.

The natural oscillation period of Eq. (10.2.5) is similar to the period of the fundamental seiche mode given by Eq. (9.2.15). Both equations are for standing waves in closed or semi-closed waterbodies. Like a father pushing his daughter on a swing, a tide of modest amplitude from the open ocean may be amplified to an enormous oscillation when the tidal forcing is in resonance with a natural oscillation period. A narrowing of the estuarine width in the upstream also favors tidal amplification. The largest tidal range often occurs at the end of the estuary. This phenomenon is described in Fig. 10.2.4 and is similar to the seiche dynamics discussed in Section 9.2.5 (Fig. 9.2.7).

The largest tides in the world occur in the Bay of Fundy on the Atlantic coast of Canada, where the average tidal range is 12 m and can be >16 m. The primary cause of the enormous tides is a resonance of the bay with the tides from the Atlantic Ocean. The bay has a natural oscillation period of ~13 h, very close to the M_2 tide period of 12.42 h. Strong tides in shallow waters produce strong turbulence to keep water columns well mixed and nutrients and sediments in suspension. This mixing is critical to support the ecosystem and the food chain, and these waters are often productive fishing areas.

10.2.3 Harmonic Analysis

Harmonic analysis is a statistical method for determining the amplitude and phase of tidal constituents in a time series. A time series can be decomposed into (1) a series of periodic components, (2) a value of long-term mean, and (3) random fluctuations.

The most obvious characteristic of an estuary is the sinusoidal oscillations containing either semidiurnal tides, diurnal tides, or a combination of the two. To identity these harmonic oscillations (or tidal constituents), it is necessary to separate the harmonic (periodic) oscillations from the mean value and the random fluctuations and to find the amplitudes and phases associated with these oscillations.

The Fourier analysis, as described in Section 7.2.3, is a useful tool in studying periodic variations. Fourier analysis computes Fourier amplitudes at equally spaced frequency intervals determined as integer multiples of the fundamental frequency, ω_1, as given in Eq. (7.2.14). The Fourier transform shown in Eq. (7.2.13) is for a time series with equal time intervals (= dt) and equal frequency intervals given by Eq. (7.2.14). However, the Fourier analysis is not much use when it comes to the analysis of a time series with particular frequencies that are not included in the discrete set of frequencies given by Eq. (7.2.14). In the case of tidal motions, the tidal frequencies (or periods), such as the ones listed in Table 10.2.1, are predetermined based on the astronomical forces and do not have equal frequency intervals. It is inconvenient and inefficient to use the standard Fourier transform in Eq. (7.2.13) to analyze tidal motions.

The underlying principle of harmonic analysis is that tides can be decomposed into a collection of simple sinusoids, such as the tidal constituents listed in Table 10.2.1. A tidal time series can be expressed as the sum over a small set of frequency components. The frequencies (periods) of interest are known, but the associated amplitudes and phases are unknown and are to be determined using the harmonic analysis. Similar to the Fourier analysis, a time series, $\eta(t)$, can be approximately represented as a combination of sine and cosine functions in harmonic analysis:

$$\eta(t) = a_0 + \sum_{k=1}^{N} [a_k \cos(\omega_k t) + b_k \sin(\omega_k t)] + \eta_0(t) \tag{10.2.6}$$

where t = time, a_0 = mean value of $\eta(t)$, a_k and b_k = constants, ω_k = angular frequency of the kth tidal constituent, N = number of tidal constituents included in Eq. (10.2.6), and $\eta_0(t)$ = residual signal other than the periodic components.

The time series, $\eta(t)$, can be either tidal elevation or velocity components. The angular frequency, ω_k, is specified as:

$$\omega_k = \frac{2\pi}{T_k} \tag{10.2.7}$$

where T_k is the tidal period of the kth tidal constituent. Table 10.2.1 lists the major tidal periods.

The major difference between the harmonic analysis and the Fourier analysis is in the angular frequency, ω_k. The angular frequency, ω_k, in Eq. (10.2.6) is predetermined by Table 10.2.1 and has irregular frequency intervals, while the

angular frequency, ω_k, in Eq. (7.2.13) is calculated from Eq. (7.2.14) and has equal frequency intervals.

Equation (10.2.6) can also be expressed as:

$$\eta(t) = a_0 + \sum_{k=1}^{N} A_k \cos\left[\frac{2\pi}{T_k} t - \phi_k\right] + \eta_0(t) \tag{10.2.8}$$

where A_k = amplitude of the kth tidal constituent and φ_k = phase of the kth tidal constituent.

It has

$$A_k^2 = a_k^2 + b_k^2 \tag{10.2.9}$$

and

$$\phi_k = \arctan\left(\frac{b_k}{a_k}\right) \tag{10.2.10}$$

In Eq. (10.2.8), a finite number of constituents (=N) are used in the reconstruction of a tidal signal. Values of the site-specific variables, a_0, A_k, φ_k, and η_0 (t), are computed from measured time series data, usually using a least-squares method.

Harmonic analysis yields the amplitude and phase of the individual cosine waves, each of which represents a tidal constituent identified by its period or the tidal speed (= 360°/period). Once these variables are determined, they can be used to reconstruct the original time series and to predict tides at that place. Subtraction of the reconstructed tidal signal from the original record also yields a time series of residual components of the time series, represented by the sum of a_0 and $\eta_0(t)$ from Eq. (10.2.8). This residual component is often called the subtidal signal, representing effects like wind-driven or mean circulation.

Harmonic analysis estimates the amplitudes of periodic motions with predetermined periods, such as the tidal periods, and finds the best-fit coefficients between the time series and the sinusoids with given frequencies. Since, typically, there are many more data values than the specified frequencies, a least-squares technique has to be used to find the amplitude and phase of each periodic (harmonic) component. The total error between a given time series and the time series composed from the harmonic components is defined as:

$$E = \sum_{m=1}^{M}\left[\eta(t_n) - a_0 - \sum_{k=1}^{N}[a_k \cos(\omega_k t_n) - b_k \sin(\omega_k t_n)]\right]^2 \tag{10.2.11}$$

where t_n = time of the measured data, $n = 1, 2, \ldots, M$, N = number of predetermined harmonic components, M = number of measured data, and E = total error. For simplicity, the sum of a_0 and $\eta_0(t)$ from Eq. (10.2.8) is represented as a_0.

For N predetermined frequencies, there are a total of $2N + 1$ harmonic coefficients. Typically, the number of measured data (M) is much larger than the number of the predetermined harmonic components, that is $M >> 2N + 1$. The least-squares harmonic analysis is used to find values of a_k and b_k, so that the total error, E, can be minimized. Unlike the Fourier transform in Eq. (7.2.13), gaps in the time series of $\eta(t_n)$ in Eq. (10.2.11) are permitted, since times, t_n, used in Eq. (10.2.11) are not required to be evenly spaced. This feature of the least–squares method in tidal analysis is very convenient. An hourly time series of 29 days is usually sufficient to resolve the most energetic tidal constituents.

Taking the partial derivations of Eq. (10.2.11), with respect to the unknown coefficients a_k and b_k, and setting the results to zero, yields $(2N + 1)$ linear equations for the $(2N + 1)$ coefficients of a_k ($k = 0, 1, \ldots N$) and b_k ($k = 1, 2, \ldots N$). The idea is to fit the data according to the least-squares criterion—simply picking the combination of a_k and b_k that causes the sum of the squared differences between the measured and the estimated from Eq. (10.2.6) to be as small as possible. Details of the least-squares harmonic analysis are provided by Emery and Thomson (2001), which contains a wealth of information about this method.

An example of least-squares harmonic analysis is the study of Morro Bay, CA (Ji et al., 2001). The amplitudes and phases of five major constituents (M_2, S_2, N_2, K_1, and O_1) from the model and the field data at two stations are tabulated in Table 10.2.2. The locations of these two stations are shown in

TABLE 10.2.2 Harmonic Analysis of Measured Data and Modeled Results in Morro Bay, CA[a]

Constituent ID	Station MBNT		Station MBST	
	Amplitude (cm)	Phase (deg)	Amplitude (cm)	Phase (deg)
M2-field data	51.1	352.289	52.4	351.193
M2-model	50.4	352.736	47.2	356.305
Difference	0.7	–0.447	5.2	–5.112
S2-field data	17.9	304.599	18.4	305.756
S2-model	17.7	307.445	16.1	314.344
Difference	0.2	–2.846	2.3	–8.588
N2-field data	13.4	272.976	14.1	271.901
N2-model	13.9	271.495	12.6	277.110
Difference	–0.5	1.481	1.5	–5.209
K1-field data	21.4	95.710	21.1	94.000
K1-model	20.8	95.421	19.3	98.885
Difference	0.6	0.289	1.8	–4.885
O1-field data	18.5	138.117	18.3	139.571
O1-model	18.2	139.373	16.8	142.319
Difference	0.3	–1.256	1.5	–2.748

[a]Ji et al., 2001.

Fig. 10.5.1. Both the model results and the field data indicate that after the semidiurnal tide M_2, the diurnal tide K_1 is the second most important tidal component in Morro Bay. This finding is helpful for explaining the strong diurnal behavior of the wetting and drying process in the bay (Section 10.5.2).

10.3 HYDRODYNAMIC PROCESSES IN ESTUARIES

Estuaries exist in many forms, ranging from coastal plain estuaries to narrow-deep fjords, but they all share the common feature of being the transitional region from land to sea and from fresh to saline water. The action of tides and tidal currents further complicate estuarine processes. The hydrodynamic theories, equations, and processes are generally described in Chapter 2. This section focuses on hydrodynamic processes that are commonly observed in estuaries and coastal waters.

The primary factors controlling estuarine hydrodynamic processes are (1) tides and other forcings from open boundaries, (2) freshwater inflows, (3) wind, evaporation/precipitation, and heatflux exchanges with the atmosphere, and (4) geometry and topography of the estuary. The estuarine environment is characterized by considerable longitudinal mixing as a consequence of back-and-forth tidal flow. Since the tides are a deterministic phenomenon and occur at fixed periods, their effects on the estuarine circulation are readily observed and analyzed from measured data. Other external forcings from open boundaries, such as low-frequency water elevation change, can also affect circulation in an estuary.

Rivers and surface runoff are the primary source of freshwater to an estuary. Freshwater discharges, along with tides, largely control the distribution of salinity in an estuary. Freshwater inflow plays a major role in the stratification and net flushing of estuaries. Increased freshwater inflow can change the characteristics of an estuary from well mixed to partially mixed or stratified. Freshwater inflow varies primarily on seasonal scales, but severe storms can dump a large amount of freshwater into an estuary within a short period of time. Large river flow or weak tidal mixing can lead to vertical stratification where freshwater flows above saline water. In rivers, flushing of pollutants is driven primarily by advection. In estuaries, however, both advection and dispersion should be considered.

In addition to the tides and river freshwater inflows, transport and mixing processes in an estuary can also be affected significantly by wind. Wind-induced circulation is transient and interacts with estuarine geometry to produce various circulation patterns. In shallow estuaries, wind stress can dominate transport and produce energy to vertically mix the water column. As shown in Eqs. (2.1.40) and (2.1.41), this energy is proportional to the cube of the wind speed. In contrast to tidally induced vertical mixing that is produced by bottom friction and propagates upward, wind-induced vertical mixing is produced on the atmosphere–water interface and propagates downward.

Under strong, persistent wind and weak stratification, the wind forcing can mix the water column completely. Sea level variations caused by wind forcing in the open ocean can propagate into the estuary via the estuarine mouth. This remote, subtidal variation can be a major contributor to the low-frequency and nontidal variations inside the estuary. Wind waves, as discussed in Section 3.6, can play a major role in sediment resuspension. Evaporation, precipitation, and heatflux exchanges with the atmosphere can also influence the circulation patterns and water temperature.

Estuaries often have restricted connection to the open sea. The geometry and topography of estuaries affect the hydrodynamic transport. Consequently, the combination of the open sea and the estuarine topography greatly affects the internal circulation. As discussed in Section 10.2, estuarine length influences the phase between the tidal current and the tidal elevation. Estuarine depth determines the propagation speed of tidal waves. Shallow estuaries are often vertical mixed, while deep estuaries are generally stratified and have larger upstream salinity intrusion. Shallow sills near the mouth of a fjord (Fig. 10.1.2) limit circulation and flushing of bottom waters. Many estuaries have deep navigational channels, which offer less friction to tidal flows than the wide, shallow tidal flats. This difference leads to stronger tidal flow over the channels than over the flats. The channels may also be stratified and act as pathways to the transport of salinity and other water quality variables. Therefore, 3D models are often needed in estuarine modeling.

10.3.1 Salinity

Salinity is a measure of salt concentration in water: Higher salinity means more dissolved salts. Salinity originated as an oceanographic term and does not have a precise chemical definition. The major elements that determine salinity are similar worldwide, but the exact proportions of the various ions vary in different waters. Salinity is often expressed in parts per thousand (ppt or ‰), which is approximately grams of salt per liter of water. Salinity ranges from 0 to 33 ppt in estuaries and ~35 ppt in the open oceans. The UNESCO Practical Salinity Scale of 1978 (UNESCO, 1981) redefined salinity in Practical Salinity Unit (psu): the conductivity ratio of a sea water sample. The ratio has no unit, so it is not the case that 35 psu exactly equals 35 g of salt per liter of water.

The concentration of dissolved solids in water can be expressed in mass ratio:

$$\text{Concentration} = \frac{\text{Mass of dissolved solids}}{\text{Mass of water}} \tag{10.3.1}$$

The unit of salinity concentration, ppt, has

$$\text{ppt} = 1000 \times \text{mass ratio} = \frac{\text{g}}{1000\,\text{g}} = 0.001 \times \text{mg/L} \tag{10.3.2}$$

Salt concentrations are expressed in ppt in estuaries and are often represented in the form of chloride concentration in milligram per liter in lakes. For near-freshwaters, Eq. (10.3.2) provides an approximate conversion between ppt and mg/L. A typical chloride concentration of 75 mg/L in Lake Okeechobee (AEE, 2005) is equivalent to 0.075 ppt, a very small value compared with the ones in estuaries.

By weight, seawater of 35 ppt has only 96.5% of water. The remaining 3.5% is dissolved solids. Since the dissolved solids are much heavier than freshwater, the density of saltwater is greater than that of freshwater and varies with both salinity and temperature. At a temperature of 20 °C, seawater has a density ~1026 kg/m^3, whereas freshwater has a density of 1000 kg/m^3. This slight difference in density can significantly affect estuarine circulations.

Water density increases with increasing salinity and decreasing temperature. This relationship explains why water of low salinity tends to float above denser water that is colder and of higher salinity. In terms of density variation, increasing 1 ppt of salinity is approximately equal to decreasing 4 °C of water temperature. Therefore, salinity variation often changes estuarine stratification more effectively than temperature variation.

Tides are the major forcing in an estuary and, along with freshwater inflows, control the vertical and horizontal distributions of salinity. Vertically, high tides lead to strong vertical mixing and little stratification, whereas low tides are insufficient to break up the vertical stratification. Horizontally, salinity in small, tidally mixed estuaries can change from completely fresh to saline within a tidal cycle, whereas salinity in larger estuaries is controlled to a greater degree by seasonal freshwater inflows. Wind forcing can also significantly affect vertical mixing in large estuaries.

For marine life, the large salinity variation in estuaries may create a challenging environment. Changes in the balance between freshwater and saltwater can lead to the loss of species sensitive to this balance. Benthic organisms face a great challenge because they may experience both fresh and saltwater in a single tidal cycle. Freshwater algae from upstream rivers can die rapidly due to salinity toxicity, as represented by Eq. (5.2.9). Therefore, an estuary has its own ecosystem, characterized by high tolerance of the salinity variations.

10.3.2 Estuarine Circulation

A few concepts and parameters for describing the characteristics of estuaries are useful and should be presented. Tidal prism is the volume of water contained in the estuary between the elevations of high tide and low tide (i.e., the tidal range shown in Fig. 10.2.3). When the surface area of the estuary does not differ significantly between high and low tide, the tidal prism can be approximately estimated as:

$$\text{Tidal prism} = \text{tidal range} \times \text{area} = 2 \times \text{tidal amplitude} \times \text{area} \quad (10.3.3)$$

In Eq. (10.3.3), the tidal range and the tidal amplitude are both averaged over the estuarine area. Equation (10.3.3) may be used to estimate the order of magnitude of tidal prisms, but should not be considered as an accurate calculation. Ebb (flood) tidal prism is the total volume of water transported through a fixed cross-section of an estuary during an ebb (flood) tide, excluding freshwater inflows. On average, ebb tidal prism and flood tidal prism are both equal to tidal prism, that is, one tidal prism of water is flushed out of the estuary during ebb tide, and one tidal prism of water is flushed into the estuary during flood tide.

Freshwater and tidal flow are the two major driving forces in an estuary. The balance of these two driving forces can be quantified by flow ratio. Assuming that R is the total volume of freshwater entering an estuary during an ebb (or flood) tide, and that V is the tidal prism, the flow ratio is defined as:

$$\text{Flow ratio} = \frac{R}{V} \tag{10.3.4}$$

Flow ratio affects the advection, vertical mixing, salinity distribution, and stratification. It is calculated over one tidal cycle and represents characteristics of mean flow. When evaporation and rainfall are relatively small, flow ratio is a useful parameter to indicate that an estuary belongs to which pattern of stratification and mixing: highly stratified, moderately stratified, or vertically mixed. It should be pointed out that the flow ratio, R/V, controls the estuary stratification and mixing, not the absolute values of R or V. Estuaries can have very different values of R and V and still have a similar stratification pattern, as long as that they have a similar flow ratio.

Estuarine stratification can also be directly measured by salinity ratio, which is defined as the ratio of bottom-top salinity difference (dS) over vertically averaged salinity (S):

$$\text{Salinity ratio} = \frac{dS}{S} \tag{10.3.5}$$

Since salinities are easier to measure than the values of R and V, the salinity ratio is often easier to be estimated in estuarine applications. The salinity ratio and the flow ratio are two useful parameters for characterizing the circulation pattern and stratification of estuaries.

One principal feature of estuaries is the tidal-averaged circulation of two-layer net flow in the vertical, called estuarine circulation (or gravitational circulation). This circulation represents the mean flow that flushes material out of the estuary and affects the distribution of estuarine water quality. Figure 10.3.1 illustrates the typical estuarine net circulation averaged over a tidal cycle. It has a net seaward transport in the surface layer and a net landward transport in the bottom layer. The surface flow has much lower salinity than the bottom flow, and there is a tendency for the less dense freshwater to flow

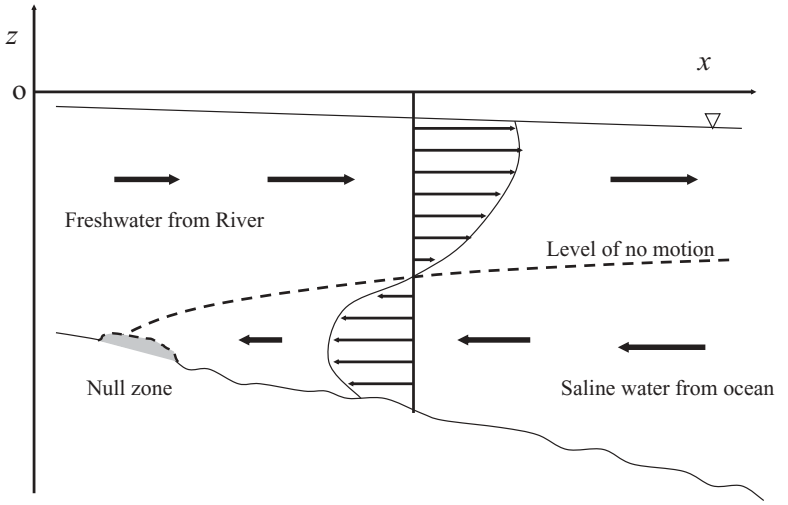

Fig. 10.3.1 A sketch of estuarine circulation.

over the top of the estuarine water. The velocity shear between the two layers causes vertical mixing and entrainment. The entrainment adds water from the bottom to the surface layer. The summation of these two-layer flows should be equal to the net freshwater inflow, even though the magnitudes of two-layer flows can be much larger than the freshwater inflow. Figure 10.3.1 will also be used in discussions on sediment transport in Section 10.4.2.

Frequently, it is convenient to describe an estuary in two vertical layers for the discussion of long-term transport of pollutants in estuaries. The estuarine circulation is a mean (or steady) state and is an idealized concept; it cannot be observed instantaneously. The net (tidal-averaged) velocity in an estuary is often a small fraction of the instantaneous flow. However, due to its steady nature, the net flow can flush material out of the estuary and is important in the long-term transport. For example, Figure 5.9.14 gives the daily averaged surface current in the St. Lucie Estuary, which indicates a downstream flow. Figure 5.9.15 gives the corresponding bottom current, indicating an upstream flow in most of the estuary. The two figures clearly reveal the two-layer estuarine circulation.

10.3.3 Stratifications of Estuaries

Estuaries are classified based on their geomorphology in Section 10.1. Since an important characteristic of estuaries is that their waters are measurably diluted with freshwater from rivers and runoffs, estuaries can also be classified by their patterns of stratification and mixing as: (1) highly stratified, (2) moderately stratified, and (3) vertically mixed.

TABLE 10.3.1 Classification of Estuaries by Patterns of Stratification

Stratification Type	Flow Ratio	Salinity Difference	Vertical Entrainment
Highly stratified estuaries	≥1.0	Large	Strong
Moderately stratified estuaries	<1.0 and ≥0.01	Moderate	Moderate
Vertically mixed estuaries	<0.01	Very small	None

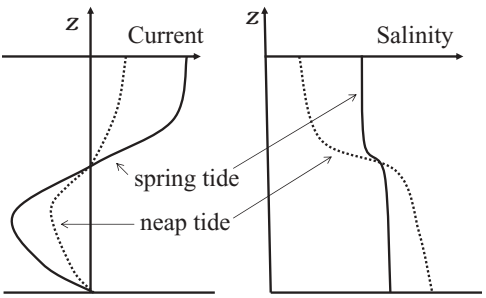

Fig. 10.3.2 Profiles of current and salinity during spring tide (solid lines) and neap tide (dashed lines).

This method of classification groups estuaries with similar circulation and mixing patterns together and is hydrodynamically based (Table 10.3.1). The type of an estuary depends primarily on the relative magnitudes of river and tidal flow and on the geometry of the estuarine basin. Changes in any of these factors may alter the mixing and the estuarine circulation. At one end of this range is the river-dominated, poorly mixed (highly stratified) salt wedge estuary. At the other end is the vertically mixed, laterally homogeneous estuary. Between the two, there is the moderately stratified estuary.

Estuarine stratifications are also affected by spring and neap tides. Estuarine stratification is weaker during spring tides than during neap tides because spring tidal currents are stronger and contribute more energy to mix the water column (Fig. 10.3.2). As a result, the salinity gradient in the vertical is stronger during a neap tide than during a spring tide.

10.3.3.1 Highly Stratified Estuaries. Estuarine stratification can be characterized by a few key elements, including flow ratio, vertical salinity difference, and vertical entrainment of seawater from the bottom to the surface. Generally, highly stratified estuaries have the following characteristics: (1) flow ratio: >1.0, (2) salinity difference: large, and (3) vertical entrainment: strong.

As summarized in Table 10.3.1, highly stratified estuaries typically have a flow ratio larger (or much larger) than 1.0. In these estuaries, river flow

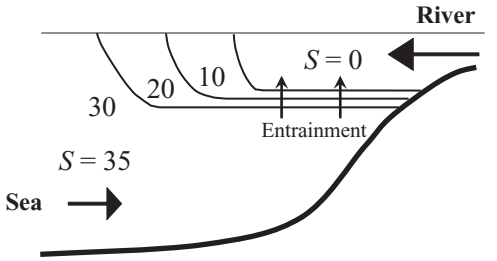

Fig. 10.3.3 Sketch of a highly stratified estuary.

dominates tidal motion and controls the circulation pattern, and freshwater flows over a deeper layer of dense seawater. As shown in Fig. 10.3.3, a feature of a highly stratified system is that the strong density gradient greatly inhibits vertical turbulence, thus reducing mixing across the interface to a very low level. The strong freshwater flow in the upper layer against the tidal current produces a large current shear. This shear may lead to internal wave motion and instability at the transition between the two layers, resulting in the upward transfer of bottom seawater. This upward entrainment of seawater is often strong and carries high salinity water into the low salinity surface layer. Unlike turbulent mixing that exchanges water in both directions, entrainment only carries a fraction of the bottom water into the surface layer in one direction. This entrainment leads to salinity increasing in the surface, whereas the undisturbed portion of the bottom water has salinity unchanged.

Highly stratified estuaries are characterized by the presence of a tongue of higher salinity water (or salt wedge) near the bottom and an overlying layer of freshwater. The salt wedge extends from the estuarine mouth and moves with the tides. River discharges control the circulation and push back the seawater. There is a sharp transition and weak mixing between the two layers. With weak tides and dampened vertical mixing, the salt wedge can penetrate a long distance upstream. The Mississippi and Columbia Rivers in the United States are examples of large salt wedge estuaries.

Another type of highly stratified estuary is a fjord. As discussed in Section 10.1, a fjord is characterized by a deep basin and a shallow sill separating the basin from the sea. Fjords usually have high river input and little tidal mixing. There are two very distinct layers of water (Fig. 10.1.2): the top layer is low in salinity; the bottom layer is cold and high in salinity. The temperature and salinity differences result in two layers of very different density.

10.3.3.2 Moderately Stratified Estuaries. Moderately stratified estuaries (Fig. 10.3.4) generally have the following characteristics: (1) flow ratio: <1.0 and >0.01, (2) salinity difference: moderate, and (3) vertical entrainment: moderate. Moderately stratified estuaries are between highly stratified and vertically mixed estuaries. Their stratification is significant, but is not as large as the

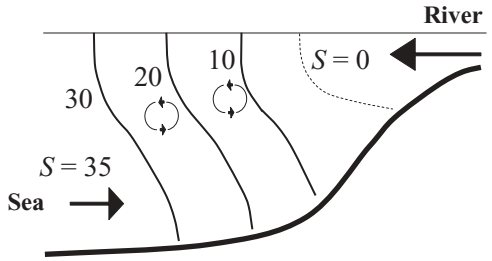

Fig. 10.3.4 Sketch of a moderately stratified estuary.

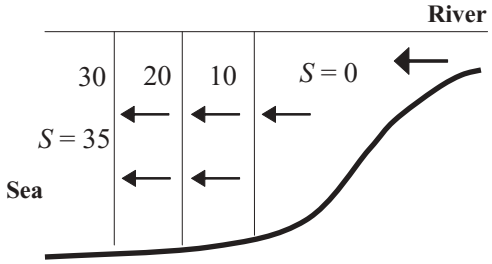

Fig. 10.3.5 Sketch of a vertically mixed estuary.

ones of highly stratified estuaries. Strong tidal flows and large river discharge result in both turbulent mixing and entrainment. This mixing leads to vertical exchanges between the two layers in both directions.

As sketched in Fig. 10.3.4, the salinity varies continuously through the water column, without a distinct interface between the upper and lower layers. The water is stirred into the upper layer, and the freshwater is mixed into the lower layer. Vertically, the salinity can vary as little as 1 ppt and as much as 12 ppt. Horizontally, the salinity increases towards the sea. This type of estuary is widespread around the world. The San Francisco Bay is an example of a moderately stratified estuary.

10.3.3.3 Vertically Mixed Estuaries. Vertically mixed estuaries (Fig. 10.3.5) generally have the following characteristics: (1) flow ratio: <0.01, (2) salinity difference: very small, and (3) vertical entrainment: none. Vertically mixed estuaries have a strong tidal flow and a weak river flow. They are often shallow and large, and there is a net seaward flow at all depths. The mixing is so complete that the vertical salinity distribution is almost uniform with depth. The salinity decreases from the ocean to the river. The Delaware Bay is an example of a vertically mixed estuary.

It is important to stress that real estuaries never fit the above idealized classifications exactly. These three types of estuaries are more concepts than descriptions of real estuaries. The tidal prism of an estuary is relatively

constant throughout the year, but the rate of freshwater inflow can change dramatically, up to a few orders of magnitude, from dry to wet seasons. In addition, large spring and neap tides may also change the tidal prism significantly and affect the flow ratio. Therefore, an estuary's flow ratio can vary a few orders of magnitude and the stratification of the estuary can change dramatically, from highly stratified to moderately stratified or even to vertically mixed. As presented later in this section, there are occasions for which an estuary may have very different stratification patterns even at the same flow ratio (Ji et al., 2007a). The estuarine types represent different patterns of salinity transport and vertical mixing. It is helpful to utilize these types to understand the estuarine processes, even though the estuary may change its type from season to season.

10.3.3.4 An Example of Estuarine Stratifications. The St. Lucie Estuary (SLE) is used as an example to illustrate the stratification of estuaries (Ji et al., 2007a).

Figure 10.3.6 *a* is the measured total freshwater inflow rate (Q); (*b*) is the flow ratio (R/V); (*c*) is the salinity ratio (dS/S); and (*d*) is the distance from 10 ppt isohaline to the mouth of the estuary (the St. Lucie station shown in Fig. 2.4.12). An isohaline is a contour line of equal salinity. Except for (*a*), the other three panels show results from the SLE/IRL model described in Section 2.4.3. The modeled flow ratio and salinity ratio are averaged over a half M_2 tidal cycle during a flood tide and an ebb tide, respectively. Because of the great variation in freshwater inflows over time, the estuary displays different estuarine types at different times. When freshwater flows are extremely small, the estuary can be well mixed. During periods of wet weather, moderately mixed conditions prevail. Under full flood flows, strong stratifications occur.

Figure 10.3.6 *c* shows that the salinity ratio (dS/S) generally increases with the flow ratio (R/V), but when the flow ratio in (*b*) is persistently large for a relatively long time (between Days 120 and 140), the estuary suddenly changes from very stratified to vertically mixed within a few tidal cycles, and dS/S drops to almost zero. In this case, the large freshwater inflow makes it difficult for the seawater to be transported in the bottom layer from the open ocean; the persistent large inflows wash out the salt to the Atlantic Ocean and then the stratification collapses. Figure 10.3.6 reveals that R/V can be a good indicator of estuarine stratifications, but other factors may also affect estuarine circulation significantly.

Freshwater inflow is the key factor limiting saline intrusion in the estuary. Figure 10.3.6 *d* illustrates the rapid downstream flushing that accompanies large inflow events. Tidal flows are very effective in moving salinity upstream. This effect is seen in the relatively quick migration of salinity back up the estuary (between Days 140 and 170) after the major flood has washed the salt downstream. The post-flood recovery of salt in the estuary, which involves an upstream salinity excursion of 30 km or more, takes place in ~30 days. Between days 102 and 125, discharge increased from 2.8 to 93.3 m^3/s. This increase flushed the 10 ppt isohaline downstream some 30 km.

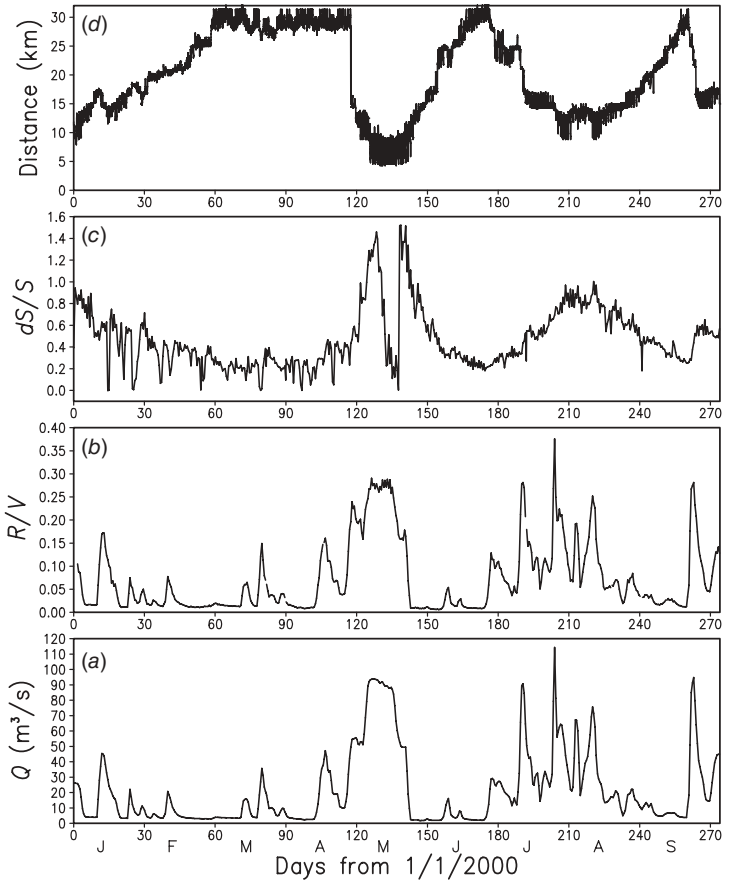

Fig. 10.3.6 Freshwater inflow (Q), flow ratio (R/V), salinity ratio (dS/S), and the distance from 10 ppt isohaline to the mouth of the estuary in 2000.

As discussed in Section 10.2.2, the tidal excursion gives the total distance traveled by a water particle during the flood tide or ebb tide. The "noise" in Fig. 10.3.6 *d* reveals tidal excursions in the estuary indicating that a typical tidal excursion is ~5 km or less. Figure 2.4.16 shows that typical tidal velocities in the St. Lucie Estuary are ~35 cm/s or less. For a maximum tidal velocity of 35 cm/s, Eq. (10.2.4) yields a tidal excursion of 5 km, which is consistent with the results shown in Fig. 10.3.6.

10.3.4 Flushing Time

Flushing time is a useful concept in estuarine management. The harmful effects of a pollutant are usually a function of its concentration. A variety of terms, such as flushing time, residence time, transit time, and turnover time, are used to describe time scales for transport and removal of materials that enter

waterbodies. Flushing time (or residence time) is often used to represent time scales for removing materials (especially pollutants) out of estuaries. The shorter the flushing time, the better flushed the estuary. Typical flushing times range from days in small estuaries to months in large estuaries during low flow conditions. Flushing time can be defined in a number of ways in the literature, and these definitions are sometimes inconsistent and imprecise. Care must be exercised to determine the meaning being used to avoid misinterpretation or incorrect comparisons of data.

Flushing time of estuaries is commonly defined as the time needed to replace the freshwater already in the estuary (freshwater volume) at the rate of freshwater inflow (Dyer, 1973). It represents the average time required to remove a parcel of freshwater (or a conservative tracer) from an upstream location in an estuary to the sea. Since pollutant loadings are often associated with freshwater inflows, the flushing time describes an overall feature of the estuary and is often used in the analysis of pollutant transport in estuaries.

The flushing time of estuaries is different from the hydraulic residence time of lakes, even though that the two are similar in spirit: both express the ratio of freshwater volume over the freshwater flow rate. As stated in Section 9.1.1, the hydraulic residence time of lakes is the average time required to completely empty the lake water with the outflow rate, that is, the ratio of the lake volume to the lake outflow rate. Since estuaries constantly exchange with the sea and can never be "emptied", the flushing time is focused on the freshwater and its transport in estuaries.

The freshwater volume of an estuary, V_f, is calculated using an integration over the estuarine volume:

$$V_f = \int \frac{S_0 - S}{S_0} dV = V\left(1 - \frac{S_m}{S_0}\right) \tag{10.3.6}$$

where S_0 = seawater salinity (or reference salinity outside the estuary), S = salinity in the estuary, S_m = mean salinity in the estuary, and V = estuary volume.

The mean salinity in the estuary is calculated as:

$$S_m = \frac{1}{V} \int S dV \tag{10.3.7}$$

From Eq. (10.3.6), it can be shown that:

1. When $S_m = S_0$, the freshwater volume is zero, and the estuary has no freshwater.
2. When $S_m = S_0/2$, the freshwater volume is one-half of the estuary volume.
3. When $S_m = 0$, the freshwater volume is equal to the estuary volume, and the entire estuary has only freshwater.

Therefore, by its definition, the flushing time of an estuary, T_f, can be calculated as:

$$T_f = \frac{V_f}{R} = \frac{V}{R}\left(1 - \frac{S_m}{S_0}\right) \tag{10.3.8}$$

where R = the rate of total freshwater inflow.

Note that in Eq. (10.3.8), the flushing time is not inversely proportional to the freshwater inflow, since the freshwater inflow also changes the mean salinity, S_m, which is determined by the complex hydrodynamic process in the estuary.

Flushing time affects a wide range of hydrodynamic, sediment, toxic, and water quality processes that respond to external loadings. Flushing time indicates the minimum duration for simulations of dissolved, nonreactive pollutants in an estuary and is often used to determine how much of a potentially harmful substance an estuary can tolerate before its ecosystem is significantly affected. An estuary with very short flushing time is unlikely to have algal blooms, since algae are flushed out of the system before they can grow significantly. Toxics and nutrients, such as heavy metals and phosphorus, interact extensively with benthic sediments. They often require simulation times greatly exceeding flushing times, because their processes are largely controlled by exchanges between the water column and the sediment bed.

As in lakes, flushing time is a major parameter indicating estuarine response to external loads. However, flushing is a more complicated process in estuaries than in lakes, involving not only freshwater flow rate, but also tidal exchange with the sea at the estuarine mouth. As the tide rises, ambient water enters the estuary and mixes with the water in the estuary. On the following ebb tide, a portion of this seawater–freshwater mixture leaves the estuary. The net result is the exchange of some estuarine water with seawater from the ocean. Factors controlling flushing in estuaries include freshwater inflow, tidal range, and wind forcing. All these factors are time variable. Therefore, flushing times vary over a range of time scales. Flushing time averaged over a long term (a season or a year) is often more useful in representing the estuarine characteristics.

Estuarine flushing is largely controlled by two processes: advection by freshwater inflow and longitudinal dispersion by tidal forcing. Large freshwater inflow and strong tides lead to short flushing time. The flow ratio, R/V, quantifies the relative importance of freshwater inflow and tidal forcing. Parameters controlling estuary–ocean exchange include tidal range, tidal frequency (diurnal vs. semidiurnal), and water depth. Flushing time also varies over the spring-neap tide cycle. While the tidal prism of an estuary may be large, it does not necessarily mean that the estuary has a short flushing time and is well flushed. The water transport in the tidal prism is largely oscillatory. Flushing time is quite sensitive to the freshwater inflow rate, with the larger flow rates associated with smaller flushing times, as illustrated in Fig. 10.3.7 in the St. Lucie Estuary. In the first 9 months of 2000, the total freshwater inflow

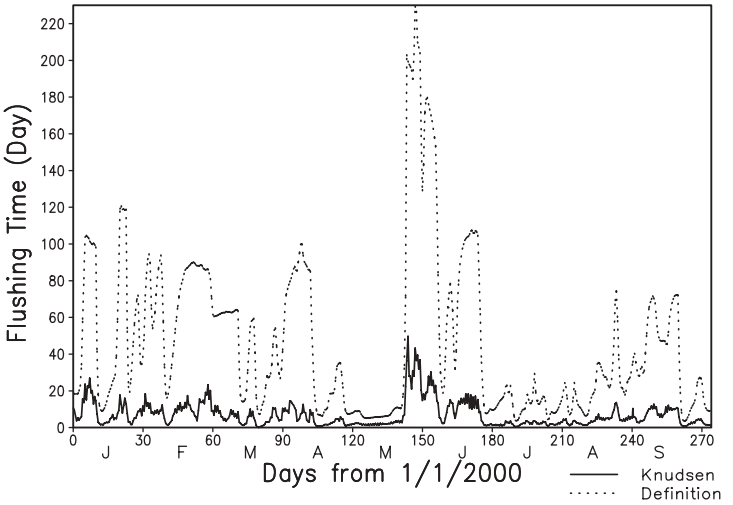

Fig. 10.3.7 Flushing time in the St. Lucie River Estuary in 2000. The solid line is from the Knudsen formula, Eq. (10.3.10). The dashed line is from the definition, Eq. (10.3.8).

varied between 1.8 and 94 m^3/s (Fig. 10.3.6), and the corresponding flushing time varied from 230 to 5.2 days (Fig. 10.3.7).

Wind may also influence estuarine circulation and flushing time. Large and shallow estuaries are more susceptible to wind forcing. The wind-induced surface current may cause a vertical circulation in the estuary and affect flushing. However, wind-induced circulation and flushing are generally secondary, compared with the ones induced by freshwater inflow and tidal forcing.

Flushing time can be calculated by empirical formulas, numerical models, physical models, and/or field studies. Often, some combination of these efforts is the most effective approach. Several empirical formulas have been used to estimate flushing times, including the tidal prism formula and the Knudsen formula (Knudsen, 1900). Flushing time is usually calculated based on an average tidal range and with wind effects neglected. These empirical formulas are screening calculations only and should not be considered accurate. Numerical models calibrated against measured data often give more realistic estimations of flushing times.

The tidal prism formula provides a simple way to estimate the lower limit of flushing time in estuaries. It has the formulation:

$$T_f = \frac{V}{V_{\text{tp}}} T \tag{10.3.9}$$

where V = estuary volume, V_{tp} = the tidal prism, and T = tidal period (=12.42 h for the M_2 tide).

The tidal prism formula is derived by assuming that the seawater brought into the estuary during a flood tide is completely mixed with the freshwater from the river and that the mixture is completely flushed out of the estuary during the following ebb tide. These assumptions are never completely met in real estuaries and lead to the underestimation of flushing time due to incomplete mixing. Freshwater at the head of the estuary may not exit the estuary in one tide cycle, and some water flushed out of the estuary during the ebb tide returns during flood tide. Underestimating flushing times means that pollutants remain in the estuary longer than the estimation from the tidal prism formula. The tidal prism formula in Eq. (10.3.9) gives a lower limit of flushing time, that is, the shortest possible time that pollutants can be flushed out of the estuary. The tidal prism is relatively constant compared with other variables such as freshwater inflow and salinity. Therefore, the tidal prism formula gives constant flushing time, regardless of the rate of freshwater inflow, a major driving forcing in estuaries, which is a major disadvantage of the tidal prism formula.

From the definition of flushing time given by Eq. (10.3.8), it is evident that the key element of calculating flushing time is to estimate the mean salinity in the estuary. Under the assumption of completely mixing in the estuary, the Knudsen formula can be derived by considering the continuity of the water column and the continuity of salt. However, more direct assumptions in deriving the Knudsen formula can be stated as the following:

1. There is a strong two-layer circulation in the estuary (Fig. 10.3.1).
2. Due to this strong circulation, the bottom salinity at the mouth of the estuary (S_b) is equal to the reference salinity outside the estuary (S_0), that is, $S_b = S_0$.
3. The surface salinity at the mouth of the estuary (S_s) is equal to the mean salinity in the estuary (S_m), that is, $S_s = S_m$.

Under these assumptions, the Knudsen formula can be directly derived from the definition, Eq. (10.3.8), as:

$$T_f = \frac{V}{R}\left(1 - \frac{S_s}{S_b}\right) \tag{10.3.10}$$

where the salinities at the mouth, S_s and S_b, can be obtained from measured data.

In real estuaries, however, the bottom salinity at the mouth is generally less than the reference salinity outside the estuary (i.e., $S_b < S_0$) and the surface salinity at the mouth is generally larger than the mean salinity inside the estuary (i.e., $S_s > S_m$). The consequence is that, similar to the tidal prism formula, the Knudsen formula in Eq. (10.3.10) may also consistently underestimate flushing times.

As an example, the flushing time of the St. Lucie Estuary is calculated using the tidal prism formula of Eq. (10.3.9), the Knudsen formula of Eq. (10.3.10), and the flushing time definition of Eq. (10.3.8), respectively. The main body of the estuary (Fig. 2.4.12) has a mean volume of $5.5 \times 10^7 \text{m}^3$ ($=V$) and a tidal prism of $8.9 \times 10^6 \text{m}^3$ ($=V_{tp}$). Therefore, the tidal prism formula of Eq. (10.3.9) gives a flushing time of 3.2 days.

No sufficient measured salinity data were available to be used in Eqs. (10.3.8) and (10.3.10). Instead, the values of modeled salinities from the SLE/IRL model are used here. In Fig. 10.3.7, the solid line is from the Knudsen formula, and the dashed line is from the definition. The corresponding conditions of the estuary are illustrated in Fig. 10.3.6, in which freshwater inflow (Q), flow ratio (R/V), salinity ratio (dS/S), and the distance from 10 ppt isohaline to the St. Lucie Inlet in 2000 are presented.

In Fig. 10.3.7, the Knudsen formula, Eq. (10.3.10), gives a mean flushing time of 7 days, and the definition formula, Eq. (10.3.8), yields a mean flushing time of 47 days. The Knudsen formula consistently underestimates the flushing time by a factor of 6 or 7, even though the two curves in Fig. 10.3.7 have similar fluctuation patterns. During the high flow period between Day 120 and 140 (Fig. 10.3.6), the flushing times from both the Knudsen formula and the definition reduce to only a few days. In the following dry period around Day 150, the total inflow is only a few cubic meters per second. This low flow period leads to the flushing time increasing dramatically, up to 230 days. In this case, the flushing time from Eq. (10.3.8) is ~72 times that from the tidal prism formula, Eq. (10.3.9). Figure 10.3.7 clearly illustrates that the freshwater inflow is a dominant driving force in determining the flushing time in the estuary.

Estuarine flushing is inherently dispersive in nature. In real estuaries, there is no unambiguous point at which the original freshwater/pollutants are completely removed. Therefore, another practical way to estimate estuarine flushing is to define the removal percentage, such as 50%, 75%, or 95% removal. Ji et al. (2001) used a hydrodynamic model to study the flushing process in Morro Bay, CA, Section 10.5.2 will give details of this study as a case study on estuarine modeling.

The Morro Bay Model was used to estimate the flushing half-life, which is defined as the amount of time required for a unit concentration of a substance to decrease to one-half its initial value (i.e., 50% removal). For this analysis, the model input included tide and meteorological conditions during a 31-day period from March 9 to April 9, 1998, the same period used for model calibration. At the beginning of the simulation period, every grid cell in the model was initialized with a unit concentration of dye. The ocean boundary and the freshwater flows were assigned dye concentrations of zero.

The purpose of this flushing exercise was to determine which areas in Morro Bay are susceptible to poor flushing. In Morro Bay, there are two mechanisms available for dilution and flushing of bay waters. The primary mechanism is the exchange with the Pacific Ocean (Estero Bay) through the open boundary at the entrance to Morro Bay (Fig. 10.5.1). Bay water exits the entrance to

Estero Bay during ebb tide, and clean water enters during flood tide. A certain amount of recirculation occurs at the bay entrance at the change from ebb to flood tide flow. This phenomenon is approximated in the Morro Bay Model by setting the inflowing concentration to the last outflowing value for a period of 30 min following the change from ebb to flood flow at the open boundary. After 30 min, the flow entering the open ocean boundary is set to a dye concentration of zero. The second mechanism available for dilution comes from the two streams, Chorro Creek and Los Osos Creek. The stream discharges act to dilute the pollutant in the bay.

The results of the flushing simulation are shown as contours of flushing half-life (in days) in Fig. 10.3.8. As expected, the poorest flushing occurs in the southwest portion of the bay with flushing half-life times on the order of 10–16 days. Another poor area of flushing is inside White Point Marina where

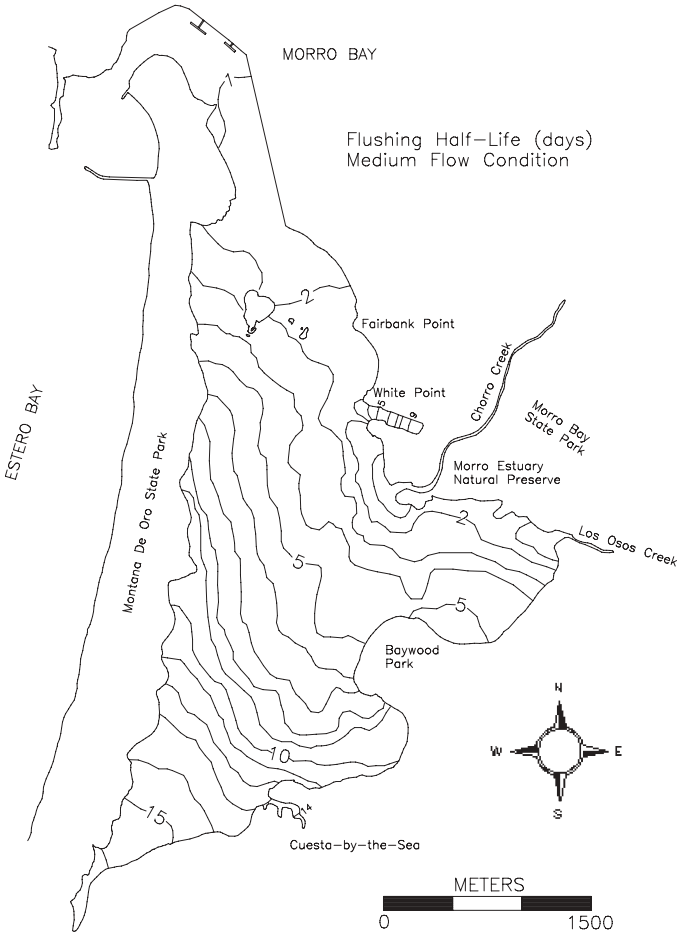

Fig. 10.3.8 Morro Bay flushing analysis.

flushing half-life times range from 5 to 9 days. The flushing analysis has shown that freshwater flows from Chorro Creek and Los Osos Creek have a significant impact on flushing in Morro Bay. The bay is especially susceptible to the build-up of pollutants in certain areas, most notably the southwest portion of the bay and White Point Marina.

Another way of looking at the flushing simulation results is to compute a bay-wide average flushing half-life time. This calculation was accomplished by multiplying the volume of water in each model grid cell at mean tide level times the computed flushing half-life for each grid cell and then dividing by the total bay water volume, resulting in a volume-weighted average flushing rate. The bay-wide average flushing half-life is 3.2 days.

10.4 SEDIMENT AND WATER QUALITY PROCESSES IN ESTUARIES

Diversity of species is often greatest where two ecosystems meet. Estuaries are the meeting place of rivers and oceans and are among the most productive ecosystems on earth. Sediment and water quality processes in estuaries may differ from those in freshwater lakes, because freshwater and seawater have different chemical characteristics. The theories, processes, and equations related to sediment transport and water quality are generally discussed in Chapters 3–5. This section focuses on processes that often occur in estuaries.

10.4.1 Sediment Transport under Tidal Forcing

Compared with rivers and lakes, estuaries have unique mechanisms that affect sediment processes, including (1) tidal forcing, (2) flocculation and settling of fine sediments due to salinity variation, and (3) estuarine circulation and sediment trapping. Sediment processes are complex in estuaries. Erosion, transportation, and deposition are affected by river discharge, tidal currents, meteorological events, biological processes, and chemical reactions. Tidal forcing provides turbulent mixing energy to suspended sediment. The flocculation of fine sediment and the estuarine circulation trap suspended sediment. Wind waves may also affect sediment resuspension in large, shallow estuaries.

Estuarine sediments originate from various sources: rivers, surface runoff, local erosion, atmospheric fallout, and the sea. Concentrations of suspended sediment in the sea are usually low; therefore, watersheds are often more important sources of sediments than the sea. Sediments in estuaries generally consist of fine particles that adsorb more toxics than coarse particles (Hayter and Mehta, 1983). They are responsible for filling the channels, harbors, and waterways in estuaries. These fine particles increase turbidity and absorb phosphate and toxic contaminants. They also carry the majority of toxic metals and organic compounds that are discharged into estuaries. Therefore, sediment transport is an important mechanism of nutrient and toxic transport in estuaries.

Riverborne sediments often constitute the majority of the sediment load entering estuaries. The effect of rivers on an estuary can begin well upstream, far away from the estuary. Upstream changes can cause fluctuations in sediment and water delivery to the estuary (and the ocean). High river discharges during floods are an important mechanism to flush the sediment out of the estuaries. During a flooding period, freshwater flows can be much stronger than tidal flows and transport a large amount of sediment downstream.

The action of wind on exposed sand dunes can transport considerable quantities of sand into an estuary. Morro Bay, CA, is a good example (Tetra Tech, 1999a). Wind waves can influence sediment resuspension and movement. Within the narrow confines of river estuaries, wind waves are small. However, when the dominant wind direction persistently coincides with a long, straight, and wide stretch of an estuary, the long fetch may promote the generation of wind waves. These wind waves can resuspend the deposited sediments.

Under the tidal forcing, the sediment processes are characterized by cycles of deposition and resuspension. Except at slack water, turbulent mixing keeps sediment in suspension throughout the tide. At slack water, individual or groups of particles settle to the bottom. As the current increases at the next stage of the tide, erosion occurs again and removes part or all of the sediments just deposited. This type of erosion-deposition cycle is driven by the back-and-forth tidal currents, often resulting in little net transport of the eroded sediment from its site of erosion.

10.4.2 Flocculation of Cohesive Sediment and Sediment Trapping

As discussed in Section 3.3.2, flocculation is the process by which suspended fine particles are assembled into larger groupings (called flocs or aggregates). Aggregates are formed when cohesive particles collide repeatedly. Fine sediments are eroded from the watershed and are carried by rivers and surface runoffs into estuaries, where these sediments are liable to collide and flocculate into large aggregates in saline water.

Clay sediments become cohesive when the salinity reaches a few parts per thousand (ppt) in an estuary, well before they enter the lower portions of the estuary. Once the river-delivered sediments are in the estuary and exposed to the first traces of seawater, the surface layer of sediment particles is surrounded by ions in the seawater. This process destabilizes the particles and creates a favorable condition for aggregation. These destabilized particles are attracted to each other and start to aggregate. The collision between two particles produces an aggregate, and the process continues until equilibrium is reached to form larger particles (aggregates), which may consist of hundreds of the original particles. As discussed in Section 3.3, the larger aggregates have a much larger settling velocity than the ones of individual particles and are easier to settle. The flocculation of cohesive sediment in saline water, in turn, affects the settling velocity and, subsequently, the transport, resuspension, and deposition of sediments in estuaries.

Estuaries generally act as filters between land and sea, essentially trapping, storing, and recycling significant quantities of sediments, nutrients, and toxic substances. Estuarine processes significantly modify the strength and the form of the signals that the estuary receives from land and sea. Sediments (and pollutants) from watersheds are carried into estuaries by rivers and runoffs and tend to accumulate there; thus, estuaries act as sinks for enormous volumes of sediment. As rivers approach the sea, their mouths broaden and currents slow down, reducing estuarine flushing and trapping sediment and pollutants. During a short period of high sediment discharge, a large amount of sediment may be deposited in an estuary. The effect of seawater is to further enhance sediment settling by the flocculation of cohesive sediments. When allowed to accumulate, the deposited sediments consolidate and undergo various physical and chemical changes. Dams built along upstream rivers for flood control and water storage reduce sediment load to estuaries and coastal areas. Lacking these sediments, however, erosion may occur in the coastal areas.

An important feature of moderately stratified estuaries is the turbidity maximum. The estuarine circulation (Fig. 10.3.1) indicates that in the lower layer, there is a point where the mean flow changes from being downstream to upstream (i.e., the null zone). It is a region of convergence in the lower layer with an upward vertical velocity, giving conditions favoring the accumulation of suspended sediment there, that is, the turbidity maximum. This process creates a zone within which sediment concentrations are higher than those either farther upstream in the river or farther downstream in the estuary and this zone is usually located near the null zone at the head of the salinity intrusion (Fig. 10.3.1). The null zone provides velocity gradients that favor collision and aggregation of suspended particles. The surface layer transports sediment downstream to the middle of the estuary where the sediments settle into the lower layer and then travel upstream again in the residual bottom flow. Consequently, the maximum sediment concentration occurs near the bottom around the null zone. This high concentration also causes rapid deposition in the area. Its position oscillates with the tide along the estuary. An increase in river flow can move its mean position in a seaward direction. As a result, this zone alters its position with changes in river discharge, and the sediments can be deposited over a long distance. Therefore, the estuarine circulation leads to net sediment accumulation within the estuary. The strength and characteristics of the estuarine circulation controls the location and, in part, the strength of the turbidity maximum. This is a major mechanism for maintaining the turbidity maximum in estuaries.

This sediment trapping mechanism has profound impacts on sediment and pollutant transports. The high sediment concentration within this area provides a major site for physical, chemical, and biological reactions between dissolved and particulate materials and for interactions among particulate materials. As a result, the area acts as a filter for removal of dissolved and suspended materials. In general, moderately stratified estuaries have the strongest estuarine circulation patterns and are the most effective filters trapping

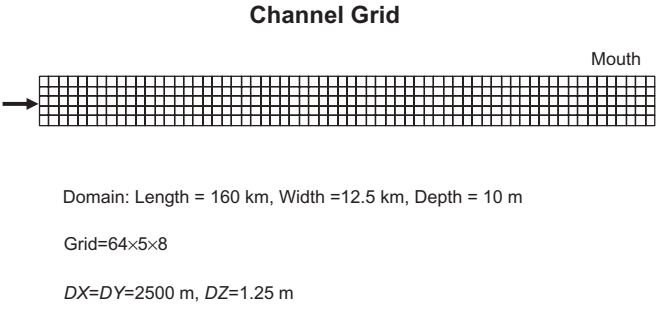

Fig. 10.4.1 Model grids of an idealized channel.

suspended materials. The trapping efficiency drops off quickly as freshwater flows increase. During major floods, for example, the flood flow is sufficient to flush sediments entirely out to sea.

To illustrate the estuarine circulation and the turbidity maximum, an idealized channel is set up for numerical simulation using the EFDC model (Hamrick, 1992). A Cartesian model grid is created to represent a channel of 160 km in length, 12.5 km in width, and 10 m in depth. The grid has 64 cells along the channel and 5 cells across the channel. The cell size is 2500 × 2500 m. Eight vertical layers are used in the model. The grid layout is shown in Fig. 10.4.1. The open boundary is in the east, and the freshwater inflow comes from the channel head in the west.

The hydrodynamic model is forced by an M_2 tide with amplitude of 0.5 m at the mouth. A constant freshwater inflow of 4000 m^3/s is discharged into the channel at the head. To account for the stratification at the mouth, the surface and bottom salinities are set to 32 and 34 ppt, respectively. At the open boundary, outflowing salinity is calculated using the salinity located immediately inside the open boundary. When the flow changes from outflow to inflow, the inflowing salinity is calculated by linearly interpolating the last outflowing salinity and the prespecified salinity at the open boundary. This interpolation is used in the first 1 h after the tidal direction change. Once the flooding time is longer than one hour, the prespecified salinity is used as the boundary condition. The initial condition for salinity is specified to linearly increase from the head to the mouth. To minimize the impact of initial conditions, the model is run for 300 days to reach a dynamic equilibrium.

Figure 10.4.2 shows vertical profiles of salinity (*a*), residual velocity (*b*), sediment concentration (*c*), and toxic concentration (*d*). These profiles are along the middle of the channel. The model results represent a typical partially stratified estuary. Salinity (*a*) increases gradually downstream, and stratification develops, especially in the channel mouth area. The two-layer circulation (*b*) has an upstream residual current at the bottom and a downstream residual current on the surface.

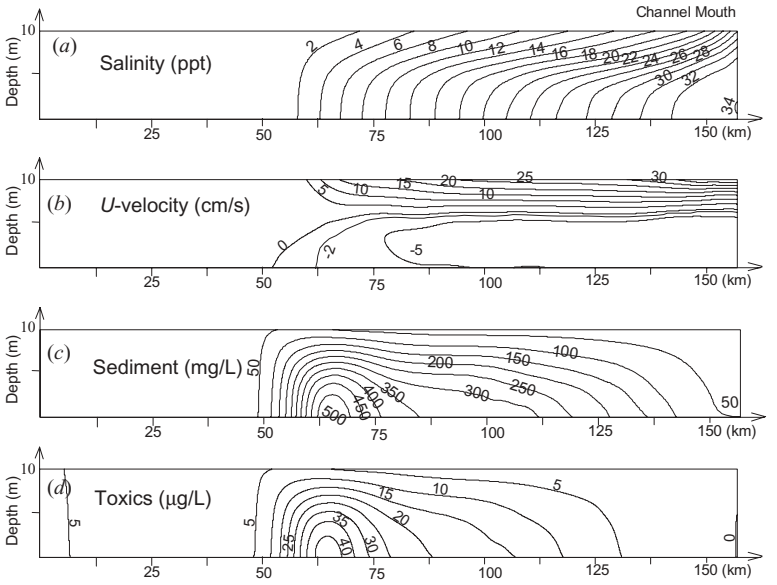

Fig. 10.4.2 Vertical profiles of model results along the channel: (*a*) salinity (ppt), (*b*) *u*-velocity (cm/s), (*c*) sediment concentration (mg/L), and (*d*) toxic concentration (μg/L).

A constant initial sediment concentration of 10 mg/L is specified in the water column. The sediment concentration of freshwater inflow is 60 mg/L. The sediment concentration at the mouth is 25 mg/L on the surface and 50 mg/L at the bottom. The treatment of the open boundary condition for the suspended sediment is the same as the one for salinity. Figure 10.4.2 *c* shows the vertical sediment distribution along the middle of the channel. Higher sediment concentrations occur at the bottom, and lower concentrations occur near the surface. A maximum of sediment concentration forms in the middle of the estuary due to the estuarine circulation.

In this test, the freshwater toxic concentration is 10 μg/L. The initial conditions in both the water column and bottom sediment are 10 μg/L. The toxic concentrations at the mouth are set to 0. Figure 10.4.2 *d* gives the vertical toxic concentration distribution. The high toxic concentration in (*d*) is closely associated with the high sediment concentration shown in (*c*). As the suspended sediment increases and accumulates in the turbidity zone, the toxic concentration increases accordingly.

10.4.3 Eutrophication in Estuaries

As discussed previously, estuaries may act as filters by trapping nutrients and other pollutants from point and nonpoint sources. The underlying sediments can store and transform these pollutants, either releasing them back into the

water column at a later time or burying them permanently. Nutrient overenrichment is one of the leading causes of water quality impairment in estuaries. Eutrophication in estuaries can result in fish kill, brown tide, algal bloom, low dissolved oxygen, and other water quality impairments. Understanding how estuaries respond to nutrient loadings is a critical step toward successful management of these systems.

Freshwater inflow is a primary driving force that defines the ecological character of river-dominated estuaries. Algal growth and biomass accumulation are often directly related to riverborne nutrient inputs. In addition to changing salinity levels, inflows provide nutrients and sediments that are important for overall productivity of the estuary. Loading from freshwater inflows is a function of both flow rate and the concentration of materials. Typically, years with a higher river flow are marked by greater algal biomass. Alteration of inflows can have a significant effect upon the water quality in receiving estuaries. Because it influences the flushing time of material in an estuary, the magnitude of inflows also affects the relative roles of external loadings and internal cycles in establishing nutrient concentrations.

Chlorophyll *a* concentrations vary widely. The values in excess of 12–15 μg/L are likely to cause severe shading of seagrasses. Summer values in the range of 20–40 μg/L are frequently observed in enriched estuaries. In contrast, during the winter, concentrations in overenriched temperate U.S. estuaries may decrease to 1–5 μg/L. Red (and brown) tide is a visible red, brown, green, or yellow coloration of water caused by excessive amounts of certain algae species. These algae decrease water clarity and, upon decay, deplete the oxygen dissolved in the water. Decreased water clarity can also lead to a loss of SAV (USEPA, 2001).

Dissolved oxygen is one of the major parameters for assessment of eutrophication in estuaries. Density stratification in estuaries affects the vertical mixing, limits bottom waters from reaeration, and causes DO stratification. On a seasonal basis, density stratification greatly influences the degree of hypoxia in the bottom of the water system. Even relatively shallow estuaries with moderate tidal forcing may still have pockets of hypoxic water in areas, such as shipping channels. In addition to seasonal variation, DO stratification in estuaries has interannual variations related to river flow and meteorological conditions. Salinity also causes a depression in the amount of oxygen that a waterbody is able to carry (Fig. 5.6.5). For example, at 10 °C, saturation DO is 11.29 mg/L for freshwater but is only 9.02 mg/L for water with 35 ppt salinity. At 30 °C, saturation DO is 7.56 mg/L at S = 0.0 and is 6.24 mg/L at S = 35 ppt.

As mentioned in Section 5.6, hypoxia is an environmental condition in which the concentration of dissolved oxygen is low enough to have biological effects. Hypoxia may occur when decaying organic matter on the bottom depletes oxygen and the stratification blocks the replenishment of the oxygen from the air. As the result, fish and shellfish are deprived of oxygen. The EPA defines hypoxic water as water with oxygen concentrations of 2 mg/L or less

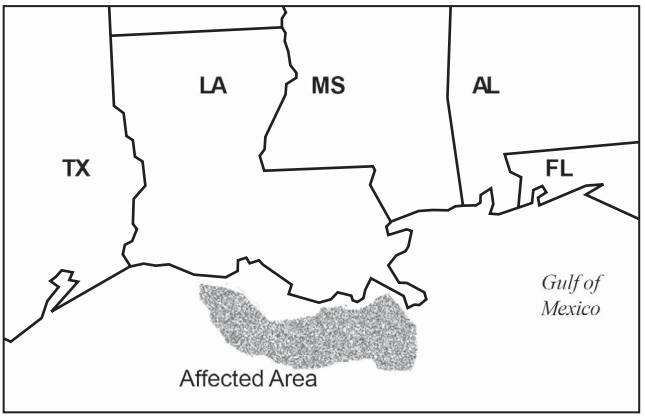

Fig. 10.4.3 Hypoxic waters in the Gulf of Mexico (NSC, 1998).

(USEPA, 2000a). DO concentration of 2 mg/L is generally accepted as the minimum level required to support most animal life and reproduction. Hypoxia occurs in many estuaries around the world. The Mississippi delta area in the northern Gulf of Mexico (Fig. 10.4.3) has one of the largest zones of hypoxic bottom waters in the western Atlantic Ocean. This zone of hypoxic waters, often called the "dead zone", covers an area of up to 7000 miles^2 during part of the year, mainly in the summer. This zone may lack sufficient oxygen to support normal populations of fish and shellfish. The causes of this dead zone are complex; however, excessive nutrients from the Mississippi River are a major contributing factor (NSC, 1998).

Nitrogen and phosphorus are the primary contributors to eutrophication. Silica may limit diatom growth at relatively high levels of N and P. As a general rule, P is often the nutrient limiting freshwater eutrophication. In contrast, eutrophication of most estuaries and coastal waters is primarily limited by nitrogen, with some exceptions. A number of temperate estuaries exhibit seasonal shifts in limiting nutrients with winter–spring P limiting and summer–fall N limiting. There are also cases where both N and P are equally limiting. It is necessary to manage both phosphorus and nitrogen inputs.

As discussed in Section 5.1.3, the N/P ratio is a key parameter for indicating whether a system is N limiting or P limiting. A waterbody is often N limiting when the N/P ratio is low and is P limiting when the N/P ratio is high. The possible reasons that nitrogen limitation tends to be more prevalent in estuaries and coastal waters than in lakes include (1) low N/P ratio in the neighboring ocean, (2) low N/P ratio of freshwater inflow as the result of human activities, (3) less effective nitrogen fixation in saline water than in freshwater, (4) more phosphorus released from the bed in saline water, and (5) denitrification.

Lakes receive nutrients from their watersheds and from the atmosphere, whereas estuaries receive nutrients from these sources, as well as from the

open ocean where nutrients may have a lower N/P ratio. Thus, estuaries are more likely to be nitrogen limiting than lakes. Human activities may lead to large amounts of phosphorus entering the watershed and eventually entering the estuary via rivers and surface runoff, which cause a higher P concentration and a lower N/P ratio in the estuary. This phosphorus input contributes to nitrogen limitation in estuaries. Nitrogen fixation can be less effective in estuaries than in freshwater systems (Howarth et al., 1999), which can lead to a lower N concentration and a lower N/P ratio.

Estuaries often act as filters trapping nutrients within estuaries. Their relatively shallow water depths, often only a few meters to a few tens of meters deep, promote strong sediment bed-water column exchanges. Phosphorus is attached to sediment more tightly in freshwater than in saline water (Caraco et al., 1990). Therefore, phosphorus deposited to the bottom with sediment particles is more easily released back into the water column in estuaries than in lakes.

Denitrification can be a major nitrogen sink in estuaries. The necessary conditions for denitrification include oxygen depletion and freely available nitrate or nitrite. Deep estuaries can develop anoxic conditions and have denitrification as a major channel for releasing nitrogen out of the estuary and into the atmosphere.

For example, Peconic Bay, NY is primarily nitrogen limited (Tetra Tech, 1999e). An analysis of the long-term data shows that inorganic N/P ratios for the winter–spring months of January–April are in the 6–8 range. In the summer–fall months (June–November), the long-term inorganic N/P ratios range from 0.6 to 2.1, clearly indicating a nitrogen-limited system during the period of summer maximum algal productivity. A rule of thumb is that an N/P ratio of <10 indicates N limitation, but >20 indicates P limitation. Figure 10.4.4 gives the summary of N/P ratios in 28 estuaries (USEPA, 2001). Horizontal bars indicate the annual ranges in N/P ratios; solid triangles represent the ratio at the time of maximum productivity. Vertical bands represent the typical range of algal composition ratios.

10.5 ESTUARINE AND COASTAL MODELING

Modeling of estuaries and coastal waters is different from the modeling of rivers and lakes in many ways. Currents in estuaries are driven by tides, freshwater inflows, winds, and density gradients (associated with temperature, salinity, and sediment concentration). Consequently, estuarine currents are complex and generally 3D, turbulent, and time dependent. Except for extremely shallow estuaries, significant vertical variations exist in current, temperature, salinity, and sediment concentrations. Another important feature of estuarine and coastal models is the need for specifying open boundary conditions that link the waterbody to the sea. Section 10.5.1 is devoted to a discussion about open boundary conditions.

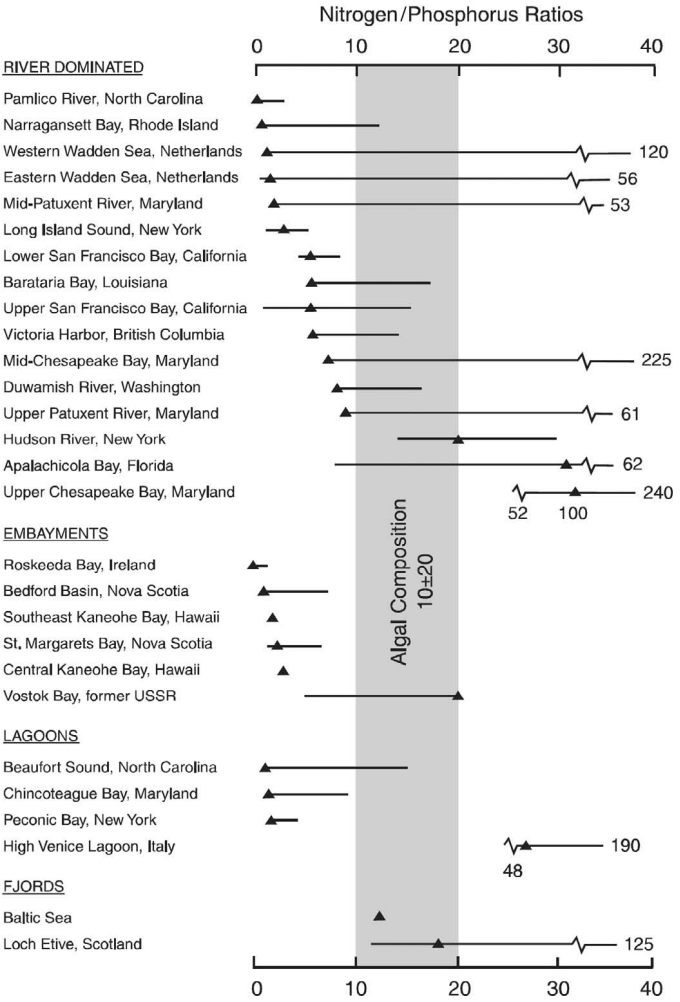

Fig. 10.4.4 Summary of N/P ratios in 28 estuaries. Horizontal bars indicate the annual ranges in N/P ratios; solid triangles represent the ratio at the time of maximum productivity (USEPA, 2001).

The data and parameters needed for the modeling of surface waterbodies are generally discussed in Section 2.4.1 for hydrodynamics, Section 3.7.1 for sediment transport, Section 4.5 for toxics, and Section 5.9.1 for water quality and eutrophication, respectively. The selection of numerical models for the modeling of surface water systems is generally discussed in Section 7.1.2. In this section, two modeling case studies are presented (1) a shallow, vertically mixed estuary with large tidal variations (Morro Bay, CA) and (2) a modestly stratified estuary (St. Lucie Estuary and Indian River Lagoon, FL).

10.5.1 Open Boundary Conditions

As shown in Fig. 2.2.7, BC include vertical BC and horizontal BC. The vertical BC are discussed in Section 2.2.2. The solid BC in the horizontal direction are described in Section 2.2.5. This section focuses on horizontal open boundary conditions (OBC).

The world oceans, coastal waters, and estuaries are all connected and, in theory, behave as parts of one system. However, it is often unpractical (and unnecessary) to simulate the entire system when dealing with a localized estuary or coastal water. A common practice is to enclose the region of interest with an artificial boundary and to conduct modeling studies within this limited domain. When a limited domain is established, conditions for the sides of the domain not bounded by land need to be specified. The interactions between the domain and the outside must be reflected in the model as OBC. In theory, the OBC should accurately represent the responses at the boundary, whether they originate from processes within or outside of the model domain. In practice, however, specifying the OBC is a problem in itself. In the modeling of coastal waters, for example, it can be a challenge to accurately specify the spatial variations of sea surface elevations at the offshore, upstream, and downstream open boundaries.

Estuaries and coastal waters are rich in hydrodynamic and water quality phenomena interacting on multiple scales. Generally, water surface elevations provide the OBC. Salinity, temperature, current, and water quality variables may also be required at the boundaries. Ideal OBC are transparent to disturbances that are generated within the model domain. The OBC allow phenomena generated in the domain of interest to pass through the boundary without undergoing significant distortion and without influencing the interior solution. The idea is to make open boundaries transparent to internally generated motions while prescribing background low frequency forcing (e.g., tides, mean currents). The primary goals for OBC are (1) to allow waves and disturbances originating within the model domain, such as sea level or velocity, to freely leave the domain and (2) to allow waves and disturbances (especially low frequency forcing) originating outside the model domain to freely pass into the domain.

The choice of model domain is often a compromise between cost, suggesting a smaller domain, and reality, suggesting a larger domain. When using and interpreting model results, one should be aware that results near the OBC may be questionable. It is a good practice to use a model where the area of interest is in the interior of the model domain, well away from open boundaries. To minimize the impact of errors originating from the OBC, the general rule is that the farther away the OBC is from the area of interest, the less the OBC errors will affect the model results. In designing the model domain, therefore, the open boundaries should be delineated at a sufficient distance away from the interior, so that the OBC errors do not influence the solution within the interior domain. In general, the OBC should be located beyond the influence

of the discharges being evaluated and should be at places where flow, tides, and/or water quality variables are well monitored. Wherever possible, tidal gauges should be placed at the model boundaries as part of the monitoring program. Upstream boundaries of an estuary model are best located at a dam or at a gage station. Downstream boundaries should be located at the mouth of an estuary, or even extended into the sea. Figures 2.4.13 and 10.5.1 give locations of two open boundaries respectively.

Since there are no general laws to prescribe the OBC, extrapolation, approximation, and/or assumption must be used in order to obtain boundary conditions. A variety of OBC have been proposed in the literature (e.g., Palma and Matano, 1998, 2000). Some of them are based on a linearized version of the momentum equations. Others are relaxation schemes that restore the

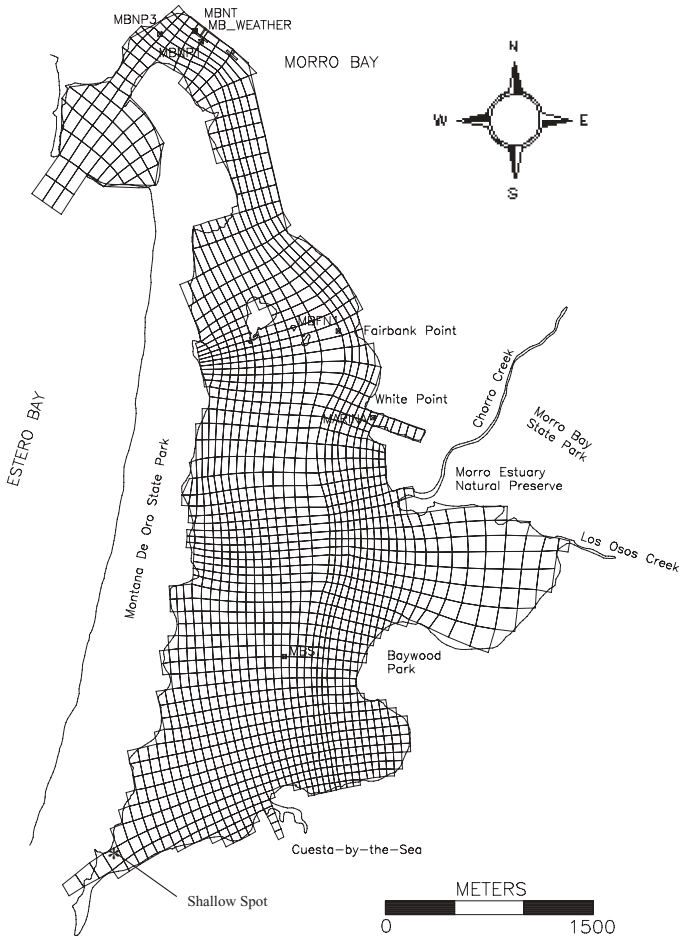

Fig. 10.5.1 Morro Bay model grid and monitoring stations.

model variables to a reference state within specified regions. Examples of the boundary conditions are

1. *Radiation Boundary Conditions*. The most widely used OBC are derived from the radiation equation of Sommerfeld (1949), which provides a simple and stable extrapolation of the interior solution. The Sommerfeld radiation condition suggests that the interior disturbances approaching the boundary should propagate through it in a wave-like way.
2. *Clamped (or Specified) Boundary Conditions*. Boundary conditions on open boundaries can be clamped (or specified) in a number of ways. Time series of observed data can be used. The boundaries can also be set to constants, climatological values, or be interpolated from monthly mean values.
3. *Sponge Boundary Conditions*. The idea is to absorb outward propagating waves and disturbances so that they cannot reflect back into the model domain. In a numerical model, an additional set of grid points is used outside the area of interest to implement the sponge boundary condition.
4. *Nested Grids*. Values at the grid points from a model with a much larger domain are used as OBC in the smaller nested model.
5. *Periodic Boundary Conditions*. These types of conditions are often appropriate for channel flow. Based on the idea that what goes out one side comes back in on the other, it is often used to test models against known analytic solutions. Connolly et al. (1999) also used periodic boundary conditions to simulate currents and pathogens in the coastal waters of Oahu Island, Hawaii.

The simplest and most popular OBC is the radiation condition, originally suggested by Sommerfeld (1949):

$$\partial\phi / \partial t + C \cdot \partial\phi / \partial x = 0 \tag{10.5.1}$$

where ϕ = any variable, C = the phase velocity of the waves, and x = coordinate perpendicular to the open boundary.

This kind of passive OBC has the variables at the open boundary determined by the interior circulation. It is useful when the circulation at the open boundary is unknown or is an integral part of the problem. Here, the primary issue is the proper formulation of the phase velocity of the waves. The radiation method proposed by Orlanski (1976) works reasonably well to establish passive boundary conditions, allowing disturbances to propagate out of the computational domain. The radiation condition is robust. However, the use of radiation conditions alone without clamping to the external data is sometime insufficient to maintain stability. The model solution may drift and eventually becomes numerically unstable in a long-term simulation. The choice of phase

speed value may also be controversial. A common choice is the nondispersive, shallow water wave speed described in Eq. (3.6.11).

The clamped boundary condition is often used to specify the boundary values of either the surface height or current speed with time along the open boundaries. Measured surface height can be used to either directly specify the water elevation at the boundary or applied to calculate current speed. The vertically averaged current perpendicular to the OBC can be specified as:

$$U = \pm \eta_F (g / D)^{1/2} \tag{10.5.2}$$

where η_F is the surface height with time, and D is the water depth. The expression is negative for open boundaries in the positive x and y directions, but positive in the negative x and y directions. Equation (10.5.2) gives U along the open boundary by using the surface height η_F. Since the surface height is specified at any given time, the value of U is also specified (or clamped). A primary disadvantage of the clamped boundary condition is that it does not pass through any longwave energy toward the open boundary from the interior of the model domain. When imposed boundary conditions do not precisely match the natural system response, the clamped boundary conditions cause artificial interactions between the boundary and the interior flow, and waves can be spuriously reflected at the model open boundaries. A good OBC should be transparent and allow wave disturbances within the model domain to escape, without being artificially reflected back into the model domain.

Several modeling techniques have been proposed to alleviate such problems by applying "partially clamped" boundary conditions, which are essentially a combination of the radiation boundary condition and the clamped boundary condition. The purpose is to have a boundary condition that is transparent to outgoing transients yet permits the background tidal and mean elevations to be prescribed and maintained. Blumberg and Kantha (1985) proposed a modified version of the Sommerfeld (1949) radiation condition in the following form:

$$\frac{\partial \eta}{\partial t} + C \frac{\partial \eta}{\partial x} = -\frac{(\eta - \eta_F)}{T} \tag{10.5.3}$$

where t = time, η = modeled tidal elevation, η_F = measured water elevation, including climatological mean and a tidal component, C = the wave phase speed, = $(gD)^{1/2}$, and T = a characteristic time scale.

The OBC described by Eq. (10.5.3) can also be formulated in terms of U or V, instead of η. By applying Eq. (10.5.3) to the Middle Atlantic Bight, Blumberg and Kantha (1985) found that a value of 4 h was chosen as the best value for T. It roughly corresponds to the time that a transient disturbance takes to traverse the entire shelf. The RHS of the Blumberg and Kantha formulation provides for the clamping of the free-wave solution to the measured data. For T large, this formulation approaches the pure radiation condition.

For T small, the left-hand side of the formulation becomes negligible, and the formulation approaches the clamped solution. The partially clamped boundary condition is a good compromise for ensuring that the model solution does not drift in time while allowing energy from the model interior to pass through the open boundary.

Marchesiello et al. (2001) used the radiation condition to determine whether an open boundary is passive (outward propagation) or active (inward propagation). In the case where the boundary is passive, the radiation condition is applied, allowing the information from the interior to pass through the open boundary without excessive reflection. In the active-boundary case, when dynamic equations require external information, the solution can be clamped towards external data without causing an over-specification problem.

The sponge boundary condition uses a region of increased horizontal viscosity near the open boundaries. It has been used with some success in modeling. The method is capable of absorbing disturbances and suppressing computational noise associated with the radiation condition (Palma and Matano, 1998), in particular for outgoing dispersive waves. However, the large variation of viscosity at the boundary produces some reflections, and the method wastes a significant number of grid points close to the boundary.

At present, there is no uniform practice for specifying OBC for the hydrodynamic and water quality applications. It is also beyond the scope of this book to conduct an extensive presentation of OBC problems. In a modeling study, all physical and numerical boundary conditions should be accurately stated to fully reveal the exact treatment of open boundaries.

10.5.2 Case Study I: Morro Bay

This case study is primarily based on the work of Ji et al. (2000, 2001).

10.5.2.1 Introduction. Estuarine and wetland systems can be subject to wetting and drying processes due to surface water elevation changes. Numerical models should be able to account for such processes with a minimum of empiricism and tuning. A variety of approaches have been utilized to represent wetting and drying in finite difference, finite volume, and finite element numerical models for free surface flows. Flather and Hubbert (1990) revie wed a number of approaches used to represent wetting and drying in tidal and storm surge models. They also defined two physical classes of wetting and drying systems applicable to lake, estuarine, coastal, and wetland environments. The first class is associated with smoothly varying topography, whereas the second class is associated with localized rapid variations in topography. Smooth topographic variations generally occur along shorelines of lakes, estuaries, and wetlands. The localized rapid topographic variations are often characterized by well-defined channels passing through areas having otherwise relatively uniform topography. Accurate modeling of wetting and drying in these systems is closely tied to the ability of the model to represent both the

deeper, smaller scale channel systems and the remaining larger scale shallow areas.

Casulli and Cheng (1992) developed and applied a wetting and drying scheme to simulate tidal processes in the San Francisco Bay and in the Lagoon in Venice, Italy. Moustafa and Hamrick (2000) applied a wetting and drying model for the study of wetland processes in the Everglades. Oey (2005, 2006) developed a wetting and drying scheme for the Princeton Ocean Model and applied the model to simulate hydrodynamic processes in Cook Inlet, Alaska. Among these (and other) wetting and drying applications, however, a common problem is the lack of detailed field-measured data to calibrate the model and therefore to verify the wetting and drying schemes. To overcome this lack of field observations, Oey et al. (2007) used satellite observations in validating their wetting and drying model in Cook Inlet, Alaska.

Morro Bay is a natural embayment located on the central coast of California (Fig. 10.5.1). It is a shallow lagoon, ~6.5 km long in the north–south direction and ~2.8 km wide at its maximum width in the east–west direction. Because of sedimentation, the bay has lost more than a quarter of its volume over the last 100 years. At low tide, >60% of the bay area emerges and becomes dry. Water quality concerns include excessive levels of bacteria, nutrients, and heavy metals. The features of Morro Bay bathymetry characterize the two types of topography classified by Flather and Hubbert (1990) well. A shipping channel from the entrance of the bay extends along the east shoreline into the south of the bay, and features localized rapid topographic variations. The depth of the channel varies from 4 to 9 m. The rest of the bay is very flat and shallow with mean water depth ranging from 1 to <0.5 m, featuring smoothly varying topography. Since the tidal elevation differences between high tide and low tide are >2 m at the entrance of the bay, a large portion of the bay area changes between wetting and drying during every M_2 tidal cycle (12.42 h). To simulate the hydrodynamic processes in Morro Bay, the numerical model must be capable of simulating the wetting and drying processes realistically.

The above features of Morro Bay make the bay an ideal site for studying the wetting and drying processes in estuaries and for testing wetting and drying schemes used in numerical models. It is essential to have an adequate field data set available for describing the wetting and drying processes in detail. For this study, comprehensive field measurements were conducted to collect various types of data, including bathymetry, high water lines, low water lines, tidal elevation, temperature, salinity, meteorological data, and hydrological data. The purpose of this study was to develop a hydrodynamic model that is capable of representing the wetting and drying processes in shallow estuaries and to apply the model to realistically simulate the hydrodynamic processes in Morro Bay.

10.5.2.2 Field Data Measurements. In this study, there are six field sampling stations in Morro Bay (Fig. 10.5.1). The sampling period spanned 31 days, from March 9, 1998, to April 9, 1998. The data at the MBNP1 station lasted

only 2.8 days starting from the beginning of the 31-day simulation, which is inadequate for statistical analysis. Therefore the MBNP1 data is only used as a reference for the model's initial condition. The Marina station is located in the small and shallow channel shown in Fig. 10.5.1. Tetra Tech (1999a) reported that there was an undocumented small amount of freshwater entering into the channel that could influence the local hydrodynamic processes, such as the salinity in the channel. Because the focus of this study is on processes with a spatial scale much larger than this channel, and the influence of this small channel on the bay is minimal, the data at the Marina will not be included in the model calibration. In this study, the following field-measured data were available and used for model external forcings or for model–data comparison:

1. Tidal gauge recorders were installed at two locations—MBNT near the entrance to Morro Bay and MBST near the southern end of the bay (Fig. 10.5.1). The tidal elevation data were averaged over 10-min intervals throughout the period.
2. Current data were available at two location—MBNP3 and MBFN1.
3. Water temperature data were available at three different locations—MBNT, MBNP3, and MBST.
4. Salinity values were determined from the conductivity and temperature measurements at one location—MBNP3.
5. Meteorological data at MB_WEATHER included air temperature, relative humidity, solar radiation, wind speed and direction, cloud coverage, and rainfall at 1-h intervals.
6. Hourly stream flow measurements were available from a gauge at Canet Road, which is located ~5.5 km upstream from the mouth of Chorro Creek.
7. The shoreline of Morro Bay was determined from several sources, including 1 : 100,000 scale U.S. Geological Survey Digital Line Graph Data and an AutoCAD drawing of Morro Bay prepared by Philip Williams & Associates (1988). The shoreline was used to develop the spatial extent of the hydrodynamic circulation model.

The data were processed to provide continuous and simultaneous boundary conditions for the hydrodynamic model during the calibration period. The open ocean boundary was defined at the mouth of Morro Bay and extended a short distance into Estero Bay. Two sources of freshwater entered the bay representing Chorro Creek and Los Osos Creek.

To study the wetting and drying processes in estuaries, it is important to have detailed measurement data on bathymetry, low water lines, and high water lines. These data are critical for model grid generation and model verification. The bathymetric survey on Morro Bay was conducted from March 11 to 16 1998. Over 4500 water depths were recorded at a spacing of 9.14 m along

predetermined survey lines. Water depths were measured to an instrumental accuracy of 9 cm and an overall accuracy of 15 cm when the motion of the survey vessel was taken into account. In conjunction with measuring the water depths, the high-water and low-water levels were surveyed for the entire bay using a GPS system and aerial photographs. Details of the survey were reported by Tetra Tech (1999a).

Freshwater inputs to the system consisted of discharges from two streams, Chorro Creek and Los Osos Creek, as well as direct rainfall. The watershed area contributing to Chorro Creek at its mouth is ~111 km^2, and the watershed area at the mouth of Los Osos Creek is ~60 km^2. The hourly flows at the Canet Road gauge on Chorro Creek, Q_{Canet}, provided the basis for determining freshwater flows at the mouth of Chorro Creek, $Q_{\text{ChrroMouth}}$, and at the mouth of Los Osos Creek, $Q_{\text{LosOsosMouth}}$, according to the following equations (Tetra Tech, 1999a):

$$Q_{\text{ChorroMouth}} = 0.8845 Q_{\text{Canet}}^{1.094} \tag{10.5.4}$$

$$Q_{\text{LosOsosMouth}} = 0.007427 Q_{\text{Canet}}^{1.559} \tag{10.5.5}$$

The historical record at the Canet Road gauge indicates that Chorro Creek is an extremely "flashy" stream. It is common for flow rates to change dramatically over a period of a few hours. Therefore, hourly inflow time series were developed for the model in order to preserve the high-frequency resolution during storm events. Compared with the inflows from the two streams, groundwater underflow is very small and is neglected in the hydrodynamic modeling study.

10.5.2.3 Model Setup. The hydrodynamic model of Morro Bay is developed with the Environmental Fluid Dynamics Code (EFDC) (Hamrick, 1992). The model grid (Fig. 10.5.1) contains 1609 horizontal curvilinear grid cells and a single vertical layer. Also shown in Fig. 10.5.1 are the six stations at which tides, velocity, temperature, and/or salinity were measured. The typical cell size varies from 50 to 80 m in the X-direction (east–west) and 50–110 m in the Y-direction (north–south). Since the tidal ranges can be >2 m and the water depths are only a few meters or less, Morro Bay is mixed vertically and can be represented reasonably well with one vertical layer. The model is driven by atmospheric forcings (wind, heatfluxes, precipitation, and evaporation), tributary inflows, and open boundary conditions. Open boundary conditions include the tidal elevation at MBNT, which was used to prescribe the forcing condition at the entrance to Morro Bay. The salinity and temperature data at stations MBNP1 and MBNP3 were applied to the open boundary.

10.5.2.4 Wetting and Drying Approaches. Numerical schemes have been developed for the modeling of wetting and drying processes. The representation of drying in finite difference and finite volume models has traditionally

involved blocking or forcing the flow across cell faces to zero, when the mean depth along the faces falls below a user-specified small value (hereafter termed the cell face drying depth). The general approach to cell face blocking involves checking all cell face depths relative to the cell face drying depth immediately after the water surface elevation or depth distribution has been updated over a time step. After the blocked cell faces have been identified, the identified cell face flows were forced to zero on the next time step (Casulli and Cheng, 1992).

An earlier wetting and drying scheme, designed to avoid negative depths at cell centers, was developed by Leendertse and Gritton (1971). Their scheme is also based on blocking cell face flows when cell face depths fall below a cell face drying depth after a preliminary update of the water surface elevation. Rather than applying the blocking on the next time step, the current updating or time step is repeated with the blocking enforced at the end of the time step, thus achieving a higher level of dynamic consistency. In these schemes, a number of iterations per time step are generally performed with the cell face depths being checked after each iteration. Leendertse and Gritton implemented this scheme using an alternating direction implicit solution for the water surface elevation, which can require a large number of drying iterations since the surface elevation is alternately updated along the two horizontal coordinate directions. In fact, they noted that the final results after the iterative update of the surface elevation field may still be inconsistent and require an additional arbitrary adjustment.

As an alternative to the wetting schemes described above, Hamrick (1994) implemented a wetting and drying scheme that requires no direct logical choices, as to whether a dry cell face is allowed to become wet, which may be considered as a hybrid of the Casulli and Cheng (1992) and Leendertse and Gritton (1971) procedures. The essence of the scheme is to assume that after an update of the water surface elevation and horizontal velocity fields, all cell faces are assumed open to flow at the end of the next update or time step. In this manner, the responsibility of determining whether a cell face is wet or dry is transferred to the drying scheme. In simpler terms, this wetting and drying scheme is based only on determining if a cell face is dry, and doing so in a dynamically consistent manner such that the no-flow condition on a dry face is imposed as part of the surface elevation and velocity field updates. This scheme was demonstrated to be stable and was successfully applied to the 3D simulation of wetlands in the Everglades (Moustafa and Hamrick, 2000). The scheme proposed by Hamrick (1994) and Moustafa and Hamrick (2000) is used in this Morro Bay study. The details of the wetting and drying scheme and the lengthy finite difference equations will not be presented here.

10.5.2.5 Wet Cell Mapping. Three-dimensional numerical models actually have two grids: A grid in physical space (as shown in Fig. 10.5.1) that is curvilinear–orthogonal in the horizontal and stretched in the vertical and a corresponding unit cube grid in computational space (as shown in Fig. 4.5.10). Cells

in both grids are first identified by the usual (*I, J, K*) indexing notation. However, in modeling highly irregular regions, many of the horizontal (*I, J*) locations in physical and computational space may correspond to dry land cells resulting in essentially wasted memory storage, if the 3D array storage convention is used. In the Morro Bay Model, a wet cell mapping technique is used to map only the water cells from the (*I, J*) horizontal indexing to a single (*L*) indexing in the horizontal. In this way, the model grid only includes the cells that might be wet during the simulation period, and the cells that will never be wet are excluded in the model grid. The (*L*) indexing is very efficient in that the locations (*I − 1, J*) and (*I + 1, J*) correspond to (*L − 1*) and (*L + 1*), respectively, whereas lookup tables relate the locations (*I, J − 1*) and (*I, J + 1*) to the single horizontal index locations [*LS*(*L*)] and [*LN*(*L*)], respectively.

For a 3D array of size (IM, JM, KM), the number of loops is changed from IM × JM × KM to LM × KM, where LM is the number of wet cells plus 2. For the Morro Bay Model, IM = 56, JM = 81, KM = 1, and LM = 1611. Compared with the conventional indexing of (*I, J, K*), the wet cell mapping technique used in the Morro Bay Model has the following advantages:

1. Memory storage reduction: The size of a 3D array after wet cell mapping is only 35.5% (= 1611/(56 × 81)) of the original 3D array.
2. Computational efficiency: The number of calculations is therefore reduced to 35.5% of the original (*I, J*) loops accordingly.
3. Vectorization: Wet cell mapping also results in increased model vectorization on vector processors, which might vectorize only the innermost DO loop. The Morro Bay Model would have the vectorized loop length of only 56 using conventional indexing with loops ordered *K, J*, and *I* from the outer to the inner. Single indexing in the horizontal, with an outer *K* and an inner *L* loop, would result in an extremely efficient vectorized inner loop with a length of 1611.
4. Grid generation: The wet cell mapping prescribes that only the number of wet cells is relevant in numerical calculation, and the sizes of IM and JM have little impact on CPU time. It is much more efficient to fit grids to highly irregular regions without the constraint of the sizes of IM and JM.

10.5.2.6 Hydrodynamic Processes in Morro Bay

Model Calibration. Based on the availability of the measured data, the period of model–data comparison was 31 days, between March 9 and April 9, 1998. The model results were compared with measured data in tables, in time series, and in scatter plots. Table 10.5.1 lists the statistics of the model–data comparison for surface tidal elevation (*E*), tidal velocity in the major tidal direction (*V*), water temperature (*T*), and water salinity (*S*). The first column gives station names, the variables, and their units; the second column gives the mean

TABLE 10.5.1 Statistics of Model–Data Comparison for Surface Tidal Elevation (E), Tidal Velocity in the Major Tidal Direction (V), Water Temperature (T), and Water Salinity (S)

Station and Variable	Measured Mean	Modeled Mean	Mean Absolute Error	RMS Error	Measured Change	Relative RMS Error (%)
MBNT: E (cm)	–0.2	0.0	4.7	5.6	194.7	2.85
MBST: E (cm)	0.0	0.0	11.0	13.8	201.5	6.84
MBNP3: V (cm/s)	2.59	–0.82	13.66	17.52	107.41	16.31
MBFN1: V(cm/.s)	5.78	2.66	11.06	13.09	169.45	7.72
MBNT: T (°C)	14.28	14.19	0.30	0.40	4.30	9.39
MBNP3: T (°C)	14.04	14.18	0.34	0.46	4.52	10.24
MBST: T (°C)	15.34	15.06	0.95	1.11	6.41	17.27
MBNP3: S (ppt)	31.03	30.43	0.84	1.19	7.31	16.29

values of the measured data; the third column gives the mean values of the modeled results; the fourth column gives the mean absolute error between the measured and the modeled; the fifth column gives the RMS error; and the sixth column gives the change ranges of the measured data. Variables on Columns 2–6 have units stated in Column 1. The last column in Table 10.5.1 shows the relative RMS error as a percentage, which is the result of RMS error divided by the measured change. Table 10.5.1 indicates that the Morro Bay Model simulates tidal elevation, tidal velocity, water temperature, and water salinity satisfactorily.

The amplitudes and phases of five major constituents (M_2, S_2, N_2, K_1, and O_1) from an harmonic analysis of model results are tabulated and compared with the respective values from field data (Table 10.2.2). Both the model results and the measured data indicate that after the semidiurnal tide M_2, the diurnal tide K_1 is the second most important tidal component in Morro Bay. This finding will be helpful for explaining the strong diurnal behavior of the wetting and drying processes in the bay later. Differences between model results and field data are <5.2 cm for amplitudes of all five constituents and <9° for tidal phases. A phase difference of 1° is equivalent to about a 2-min time difference for semidiurnal tides or about a 4-min difference for diurnal tides.

The time series of model–data comparison at Station MBNT is already shown in Fig. 10.2.2. As shown in Fig. 10.2.2, the modeled tidal elevation (solid line) matches the data (dotted line) almost perfectly. The modeled velocity has an amplitude of 40 cm/s, and there is no measured velocity at MBNT. The modeled temperature is also consistent with the data. The model realistically simulates the semidiurnal temperature variations caused by the tides. There is no measured salinity data at MBNT. The model indicates strong semidiurnal variation of salinity ranging from 24 to 32 ppt.

Since tidal velocity is one of the major factors affecting sediment transport and water quality processes, it is necessary to examine and compare the modeled and measured velocity carefully. Figure 10.5.2 is a scatter plot of the measured velocity versus modeled velocity at MBNF1. The velocities are rotated into the major tidal axis direction so that the maximum v-component and the minimum u-component are obtained. Only the maximum v-components of the measured and the modeled are shown in Fig. 10.5.2. It is clear that generally the model simulated amplitudes of the outward velocity and the inward velocity well, except for a few extreme flow conditions. The exceptions are probably the result of the model having a single vertical layer and not representing the vertical circulation patterns of the bay. Having multiple model layers might allow better representation of tidal velocities in the harbor area of Morro Bay. The discrepancies in tidal currents between the model and the data might be also caused by uncertainty in the very localized bathymetry, which cannot be represented in the model without resorting to extremely fine-scale grid cell sizes. In general, reproducing tidal currents is a more difficult task because, compared with tide elevation, tidal currents are

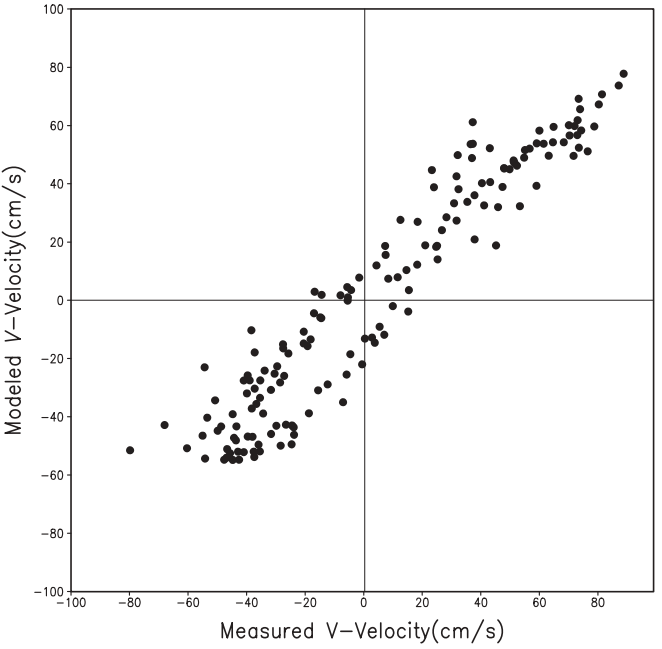

Fig. 10.5.2 Measured velocity versus modeled velocity at MBFN1.

more sensitive to bathymetry, giving rise to a higher degree of uncertainty in field measurements. Scatter plot comparison of velocities at MBNP3 also shows good consistency between the model velocities and the measured velocities. In summary, the model simulated the tidal velocity reasonably well.

Wetting and Drying Processes in the Morro Bay. The wetting and drying processes are a striking feature of Morro Bay. Figure 10.5.3 shows the 30-min averaged water depth at low tide. The black dots represent the low-water line obtained from an aerial photo. The small plot in the upper right corner indicates the surface tidal elevation in cm at the mouth of the bay, which is the tidal driving force of the entire bay. The hours shown by the x-axis label of the small plot are in reference to March 31, 1998, at 00:00. The scale bar at the bottom of the figure shows the water depth, ranging from <20 cm to >700 cm. Considering that the bathymetry measurement error in Morro Bay is 15 cm (Tetra Tech, 1999a), grid cells of the Morro Bay model are switched to "dry" when the water depth is less than a critical water depth of 17 cm, and to "wet" when the water depth is >17 cm. As a result of this wetting and drying scheme, the areas shown in Fig. 10.5.3 are considered dry when the water depth is <20 cm. Sensitivity of model results to this critical water depth will be discussed later. Figure 10.5.3 reveals clearly that the majority of the bay (64.5%) becomes dry at low tide and only the main channel area remains wet, with water depth

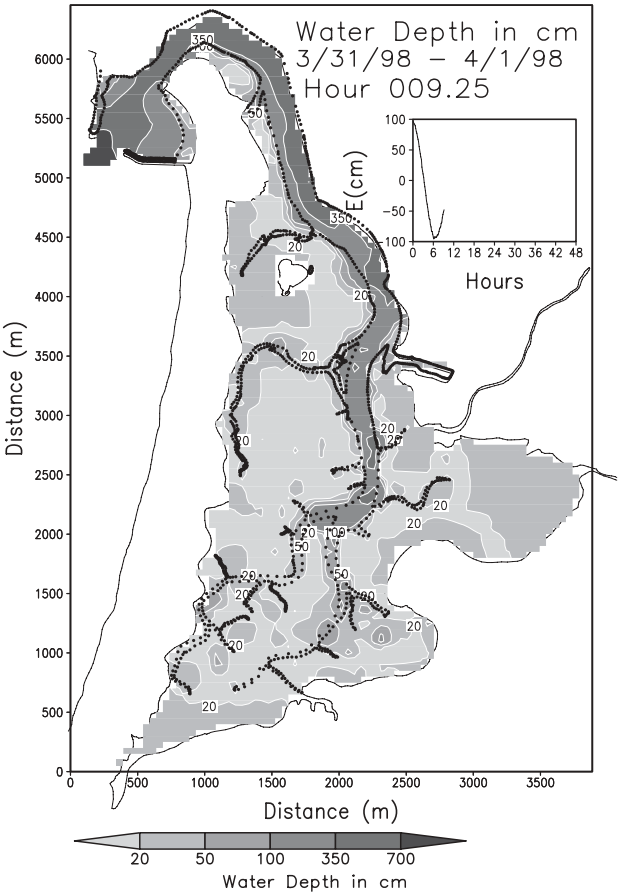

Fig. 10.5.3 Water depth at low tide (30-min average).

ranging from <1 m in the south to >7 m at the entrance of the bay. Comparing the model results with the measured low-water line, it is clear that the model simulated the wet and dry areas very well, except for those small channels shown by the black dots in Fig. 10.5.3 that cannot be resolved by the model grid.

Figure 10.5.4 shows the modeled surface water elevation at high tide, which indicates that the entire bay is full of water with a minimum water depth of >80 cm. Also shown in Fig. 10.5.4 is the measured high-water line represented by the black dots, which is based on an aerial photo. The model results coincide with the high-water line well. In Fig. 10.5.4, the modeled velocities are represented by arrows, and the arrow scale is given at the bottom of the figure. At Hour 27.25, the water is flushing out of the bay in shallow and flat areas and is flushing into the bay along the deep channel.

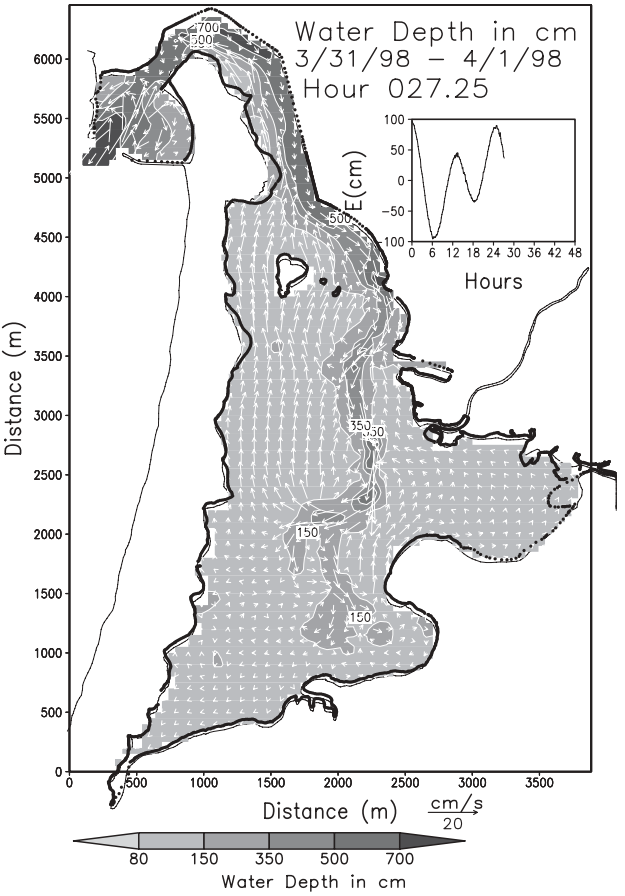

Fig. 10.5.4 Water depth at high tide (30-min average).

To illustrate how the surface water elevation is represented in the wetting and drying calculation, Figure 10.5.5 shows the modeled surface water depth at a shallow spot in the southwest corner of Morro Bay. The shallow spot grid cell has mean water depth of 46 cm, and its location is shown in Fig. 10.5.1. When its water depth is >17 cm, this grid cell is treated just like any other wet cell. When the water depth is not >17 cm, this grid cell becomes "dry" and is taken out of the computation, as indicated in Fig. 10.5.5.

At high tide, the total wet area of the model grid shown in Fig. 10.5.1 is 8.5 km^2. At low tide, the wet area can be reduced by >60%. To illustrate such a large area change caused by the wetting and drying process, Fig. 10.5.6 shows the wet area as a percentage for 48 h from March 31 to April 1, 1998, the same period discussed in Figs. 10.5.3 and 10.5.4. At Hour 9.25, Figs. 10.5.3 and 10.5.6 indicate that only 35.5% of the total bay area is wet, and the rest becomes dry.

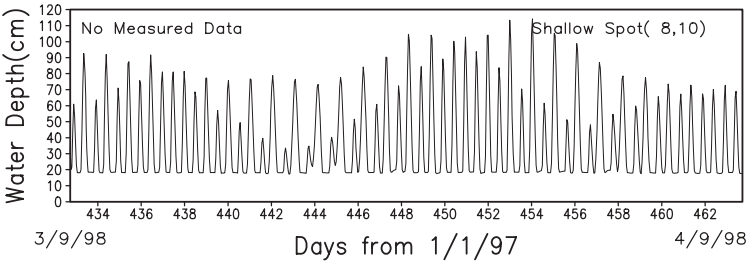

Fig. 10.5.5 Modeled surface water depth at a shallow spot (8, 10).

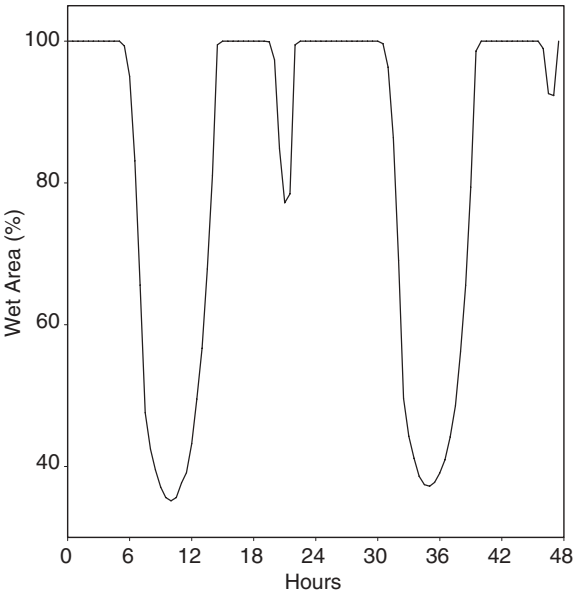

Fig. 10.5.6 Modeled wet area of Morro Bay for 48 h from March 31, to April 1, 1998.

At high tide (e.g., at Hour 27.25 shown in Figs. 10.5.4 and 10.5.6), the entire bay area becomes wet. It is also interesting to notice from Fig. 10.5.6 that a large dry area occurs diurnally, not semidiurnally. This phenomenon is an indication that diurnal tides are also important in Morro Bay. This finding is consistent with the results listed in Table 10.2.2, which states that after the M_2 tide, the diurnal tide K_1 is the second most important component in Morro Bay.

As shown in Fig. 10.5.3, Morro Bay has a shipping channel from the entrance of bay extending to the south of the bay. At low tide, the water depths vary from >7 m at the entrance of bay to <1 m at the south end of the bay. The rest of the bay area is flat and shallow, and it mostly becomes "dry" at low tide.

These two features of Morro Bay represent the two classes of topography discussed by Flather and Hubbert (1990) well. The fact that the Morro Bay Model is able to simulate the wetting and drying processes well, given such a complicated bathymetry, is a strong indication that the wetting and drying scheme employed by the model is robust and reliable.

For numerical modeling, it is important to conduct model sensitivity analysis to clarify the influences of model parameter values on model results. Most of the parameters used in the EFDC model are kept unchanged in most (if not all) of the previous EFDC applications. For example, the parameters related to the Mellor–Yamada turbulence model (Mellor and Yamada, 1982; Galperin et al., 1988) are treated as constants, and their values are the same as the ones used in other hydrodynamic models, such as the Princeton Ocean Model (Mellor, 1998) and the Estuary, Coastal and Ocean Model (HydroQual, 1991a). A parameter that is adjusted frequently in hydrodynamic modeling is the bottom roughness coefficient, which has a typical value of 0.02 meters (HydroQual, 1991a; Hamrick, 1992). In this study, the bottom roughness coefficient has the default value of 0.02 m. It is found that by changing its value from 0.02 to 0.01 and then to 0.03, the Morro Bay Model results have small changes. The relative RMS errors of tidal elevation, temperature, and salinity listed on the last column of Table 10.5.1 are changed <1%. The relative RMS errors of velocity are changed <7%.

Another important parameter in this study is the critical water depth, which is used to determine whether the grid cells are wet or dry during numerical computation. The critical water depth is set to be 17 cm in the Morro Bay Model, under the consideration that the bathymetry measurement error is 15 cm (Tetra Tech, 1999a). Sensitivity tests are conducted to clarify the influences of critical water depth. By changing the critical water depth from 17 to 15 cm and then to 20 cm, the hydrodynamic results are changed insignificantly. For example, the wet areas presented in Fig. 10.5.6 are changed <3% when the critical water depth is set to be 15 or 20 cm.

Successful calibration of the Morro Bay hydrodynamic circulation model indicates that the model can be applied to investigate hydrodynamic processes in the bay. The Morro Bay Model was used to estimate the flushing half-life, and the results have already been presented in Section 10.3.4.

10.5.2.7 Summary and Conclusions. For the wetting and drying simulation of estuarine processes, a hydrodynamic model within the framework of the EFDC has been presented. The hydrodynamic processes in Morro Bay are relatively difficult to model since large areas become "dry" mudflats during low tide. However, the model has been designed to simulate the wetting and drying processes using the numerical schemes developed by Hamrick (1994) and Moustafa and Hamrick (2000).

Morro Bay features a shipping channel, with localized rapid topography variations, but flat and shallow topography in the rest of the area. It represents the two wetting and drying systems classified by Flather and Hubbert (1990)

well. For this modeling study, comprehensive field samplings were conducted to record the wetting and drying processes in detail. The measured data for the model calibration included tidal elevation, current velocity, water temperature, and salinity at six locations in Morro Bay for 31 days, from March 9 to April 9, 1998. The low- and high-water lines were measured to characterize the surface tidal elevation variations. The primary model hydrodynamic forcings included open boundary tidal elevations, solar radiation, surface wind stresses, and freshwater inflows from Chorro Creek and Los Osos Creek.

Comparison between the model results and measured data indicates that the model results match the data reasonably well at the data stations for tidal elevation, current velocity, salinity, and temperature. The model also simulated the wetting and drying variability of Morro Bay realistically. There results are a strong indication that the wetting and drying scheme employed in the model is robust and is applicable to studies on shallow estuaries and wetlands. The calibrated Morro Bay Model was also applied to study the flushing processes in the bay and to identify poor flushing areas.

Understanding the hydrodynamics of a tidal system is vital to environmental studies. Without a detailed description of how water moves through the system, any analysis of water quality issues would be incomplete. The model presented in this case study can be used as a tool for quantifying the hydrodynamic characteristics and examining the transport processes in shallow estuaries as well as to aid further hydrodynamic and water quality studies and to guide field data collection programs.

10.5.3 Case Study II: St. Lucie Estuary and Indian River Lagoon

A 3D water quality model for the SLE and the Indian River Lagoon (IRL), Florida, has been developed using the EFDC model. The SLE/IRL model has been calibrated and verified based on the observation data in 1999 and 2000 (Ji et al., 2007a, 2007b; Wan et al., 2007). As case studies, the modeling of the SLE/IRL is discussed extensively in this book:

1. Hydrodynamic modeling (Section 2.4.3).
2. Heavy metal modeling (Section 4.5.1).
3. Water quality modeling (Section 5.9.3).
4. Estuarine Stratifications (Section 10.3.2).
5. Flushing time (Section 10.3.4).

A primary objective of presenting these case studies is to show how to model an estuary for environmental management. This section is focused on the applications of the SLE/IRL model. Two scenarios are presented (AEE, 2004b): (1) 10-year simulations from 1991 to 2000 and (2) influences of sea level rise on water quality conditions in SLE.

10.5.3.1 Ten-Year Simulations. For long-term simulation of water quality processes, computer resources may become an issue. The SLE/IRL model consists of 1159 horizontal grid cells and 3 vertical layers, with a total of 3477 grid cells. State variables include surface water elevation, temperature, current, salinity, suspended sediment, and 21 water quality variables. The time step used for model simulation is 60 seconds. The computer memory required is ~380 MB. A 1-year simulation requires ~10 h of CPU time on a Pentium IV 1.6 GHz PC. Model results are saved daily on the hard drive and requires 200 MB of hard disk space for each simulation year.

Since the SLE/IRL model was calibrated and verified based on the data in 1999 and 2000, the model's capability for long-term simulation needs to be further tested. The 10-year simulation from 1991 to 2000 is designed to diagnose the model's performance. Real-time meteorological data obtained from nearby stations include temperature, wind speed and direction, and solar radiation. Since real-time tidal forcing data at the open boundaries are unavailable from 1991 to 1998, the tidal constituents obtained from harmonic analysis of real-time data are used to generate hourly tides as boundary conditions. Measured daily discharges from the major tributaries are used as freshwater inflows. The lateral inflows of total phosphorus and total nitrogen are obtained from the watershed model (Wan et al., 2003).

Since real-time nutrient loadings from the upstreams were unavailable, two approaches are tested to generate the nutrient loadings between 1991 and 2000: (1) a regression method and (2) a linear interpolation of measured water quality data. The regression method derives relationships between inflows and loadings obtained from observation data. It was initially used to create loadings for the 21 water quality state variables. After carefully examining the nutrient loadings generated by the regression formulas, it was found that the nutrient loadings were either overestimated or underestimated in some critical periods. The formulas worked for 1999 and 2000, but they did not work for the years from 1991 to 1998. The loadings were often overestimated under high flow conditions. Inconsistent estimation of loadings from Lake Okeechobee often occurs. Since the lake discharge is controlled according to the lake management plan, the relationships between the flow and the loadings obtained through regression are not expected to be accurate. The regression method is often more appropriate if the loading is dominated by natural runoff.

Another approach for estimating the loadings to the system is the linear interpolation of measured water quality data at the boundaries. The water quality data at dams, hydrological structures, and the upstream tributaries are used to estimate the loadings. This approach provided more realistic seasonal and annual nutrient loading variations in the upstreams. In this study, the linear interpolation of the observation data at the boundaries is used to generate daily loadings from 1991 to 1998. The loadings in 1999 and 2000 are kept the same as the ones used in model calibration and verification.

Figure 10.5.7 shows the mean flow discharged into the SLE from 1991 to 2000. It shows that 1994, 1995, and 1998 are wet years, whereas 1997 and 2000

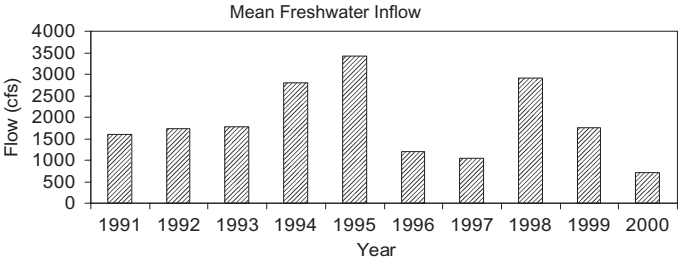

Fig. 10.5.7 Mean freshwater inflow from 1991 to 2000.

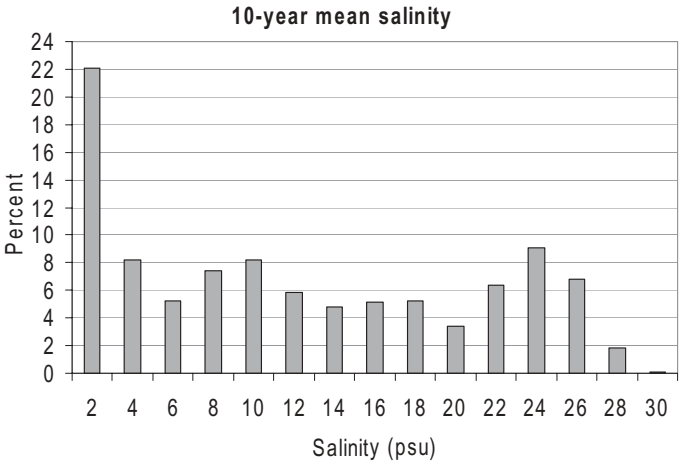

Fig. 10.5.8 Modeled salinity percentiles at US1 between 1991 and 2000.

are dry years. Figure 10.5.8 gives the modeled salinity percentiles at US1 (shown in Fig. 2.4.12) between 1991 and 2000. It describes the mean salinity variation. For example, it shows that salinity at US1 is >27 ppt <2% of the time and is <2 ppt 22% of the time.

Six water quality stations (SE01, A1, US1, SE08, North Fork, and NF in Fig. 2.4.12) have adequate data for model–data comparison. Detailed statistical tables (similar to Table 5.9.5) and figures (similar to Fig. 5.9.12) at the six stations from 1991 to 2000 are not given here, but may be found in the technical report (AEE, 2004b). Table 10.5.2 summarizes the relative RMS error (RRE) of the model results at the six stations. The mean RRE varies from 24% in 1999 to 44% in 1994. Overall, the model results have comparable RRE in these 10 years, even though the values of mean RRE from 1991 to 1998 (except for 1997) are slightly larger than those in 1999 and 2000, since 1999 and 2000 are the periods of model calibration and verification.

For example, Figures 10.5.9 and 10.5.10 give the time series of model results against observations at A1 (Fig. 2.4.12) in 1994 and 1997, respectively. In

TABLE 10.5.2 A Summary of Model's Relative RMS Error (RRE) (%)

State variable	1991	1992	1993	1994	1995	1996	1997	1998	1999	2000	Mean
Algae		52	49	58	32	47	68	28	33	25	44
TP	25	16	27	25	22	35	29	28	23	35	27
PO_4	66	38	32	87	53	32	40	24	31	41	44
TKN	23	20	20	23	22	26	29	28	27	30	25
NH_4	58	28	32	43	30	44	60	23	31	26	38
DO	24	32	31	30	21	32	33	27	2	19	25
Mean	39	31	32	44	30	36	43	26	24	29	34

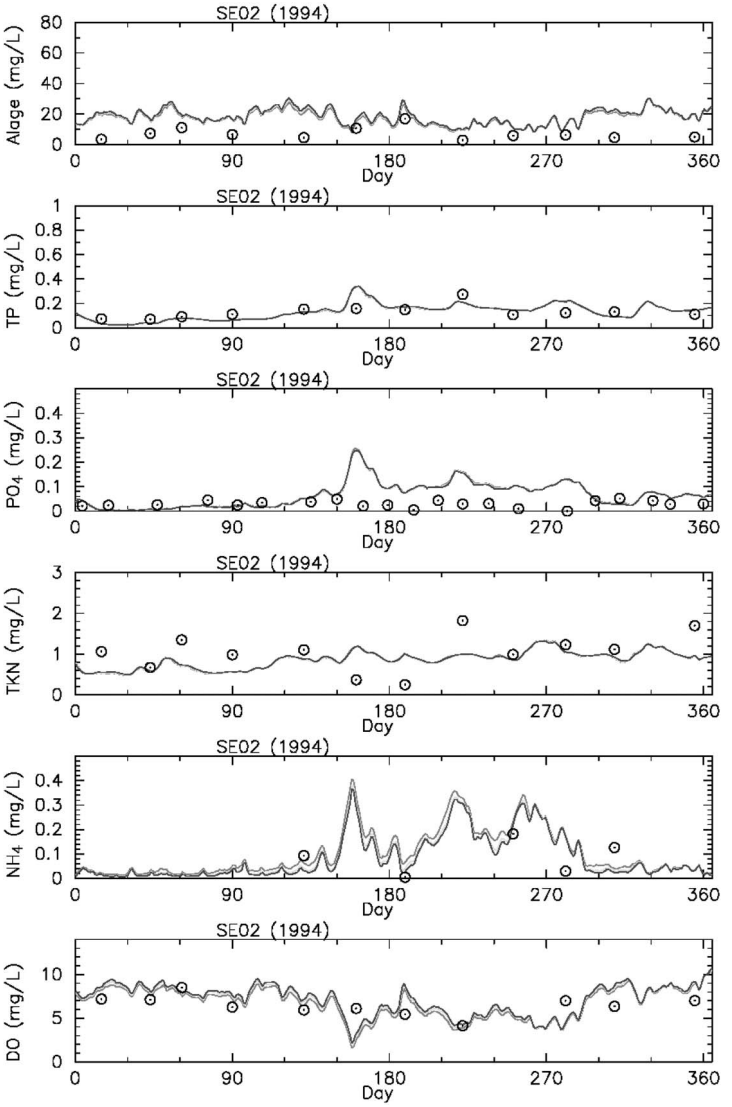

Fig. 10.5.9 Model–data comparisons of algae, TP, PO_4, TKN, NH_4, and DO at SE02 in 1994. In the NH_4 panel, the bottom line is the modeled NH_4 in the surface layer, and the top line is the modeled NH_4 in the bottom layer. In the DO panel, the bottom line is the modeled NH_4 in the bottom layer, and the top line is the modeled NH_4 in the surface layer.

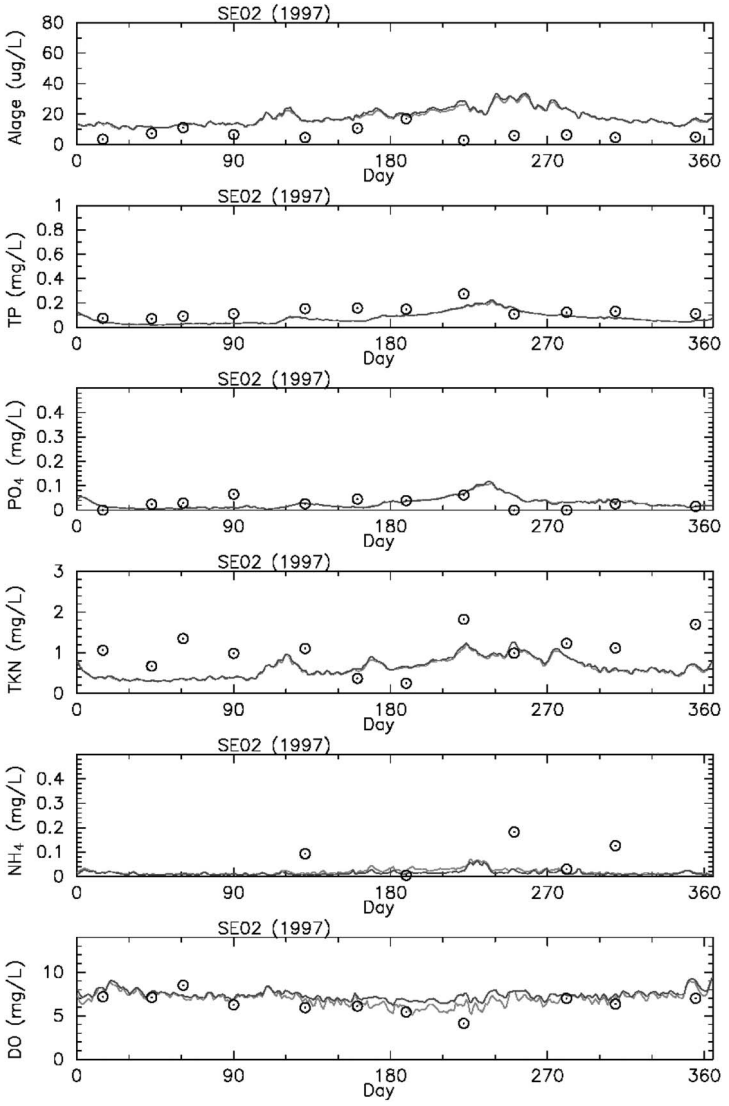

Fig. 10.5.10 Model–data comparisons of algae, TP, PO4, TKN, NH_4, and DO at SE02 in 1997. In the NH_4 panel, the bottom line is the modeled NH_4 in the surface layer, and the top line is the modeled NH_4 in the bottom layer. In the DO panel, the bottom line is the modeled DO in the bottom layer, and the top line is the modeled DO in the surface layer.

general, the model simulated water quality variations in the estuary reasonably well. The model captured the seasonal and annual changes in the water quality conditions in the SLE. However, it appears that the model overestimated PO_4 and underestimated TKN in some years. The consistent overprediction or underprediction is more likely due to the loading inaccuracy in the model.

Correctly predicting a water quality variable, such as DO, depends on a number of factors, including stratification, carbon input, SOD, and algae. The stratification depends on freshwater discharge and water elevation fluctuation at the estuary mouth. The low frequency sea level fluctuation at the St. Lucie Inlet (Fig. 2.4.12) is between –0.4 and 0.3 m (AEE, 2004a). This fluctuation is a reflection of the external wind forcing on the open ocean and influences the stratification, thus the DO concentrations. However, this fluctuation is not included in the SLE/IRL model between 1991 and 1998, since the model uses the harmonic analysis to generate the tides at the open boundary during this period. The carbon loading is also insufficient, especially the input of carbon from the marsh areas. The simulation of DO dynamics can be improved with more accurate boundary conditions and external loadings.

Overall, the SLE/IRL model, which is calibrated using the data in 1999 and verified using the data in 2000, is capable of representing the long-term variations of the system. The 10-year run from 1991 to 2000 indicates that the model simulates the seasonal and annual changes of the water quality conditions reasonably well.

10.5.3.2 Influence of Sea Level Rise on Water Quality. Two long-term runs were conducted to examine the influence of sea level rise on water quality conditions in the SLE (AEE, 2004b). The first run has the sea level rise of 0.8 ft (24.4 cm) and the second run has the sea level rise of 1.2 ft (36.6 cm). Model configurations of these two runs are the same as the benchmark run (the 10-year run), except that the mean sea levels at the three open boundaries (Fig. 2.4.12) are increased by 0.8 and 1.2 ft, respectively. All other controlling factors, such as external loading, benthic fluxes, and freshwater discharges, are unchanged. Therefore, the sea level rise is largely equivalent to the water depth increase in these test runs.

Statistical analyses and graphic comparisons indicate that the differences between the results of the benchmark run and the run of a sea level rise of 0.8 ft are relatively small. Table 10.5.3 lists the differences of the mean model results from a sea level rise of 1.2 ft against the benchmark run. In Table 10.5.3, a negative value means that the sea level rise of 1.2 ft decreases the mean concentration. For most of the years, the mean algal concentration decreases as the sea level rises, except for Years 1995 and 1996. The mean DO concentration also decreases as the sea level rises. Higher sea level leads to greater water depth and stronger stratification, which can lead to lower DO and less light available for algal growth in the bottom water. The algal concentration decrease can also result in less DO production. As algal concentration decreases, nutrient uptake is reduced, resulting in a slight increase of nutrient concentrations

TABLE 10.5.3 A Summary of Statistics of Model Results With a Sea Level Rise of 1.2 ft against the Benchmark Run

Year	Name	Mean Difference	Year	Name	Mean Difference
1991	Chl	–0.65	1996	Chl	0.37
	PO4	0.01		PO4	0.00
	TP	0.01		TP	0.00
	TN	0.00		TN	0.01
	NH4	0.03		NH4	0.00
	DO	–0.33		DO	–0.08
1992	Chl	–0.11	1997	Chl	–0.28
	PO4	0.00		PO4	0.00
	TP	0.00		TP	0.00
	TN	–0.01		TN	–0.02
	NH4	0.00		NH4	0.00
	DO	–0.01		DO	–0.07
1993	Chl	–0.94	1998	Chl	–0.18
	PO4	0.00		PO4	0.01
	TP	0.00		TP	0.01
	TN	–0.04		TN	0.01
	NH4	0.00		NH4	0.01
	DO	–0.18		DO	–0.11
1994	Chl	–0.69	1999	Chl	–0.27
	PO4	0.01		PO4	0.00
	TP	0.01		TP	0.00
	TN	–0.01		TN	0.00
	NH4	0.01		NH4	0.01
	DO	–0.49		DO	–0.17
1995	Chl	1.05	2000	Chl	–0.22
	PO4	0.00		PO4	0.01
	TP	0.00		TP	0.01
	TN	0.02		TN	–0.02
	NH4	0.00		NH4	0.00
	DO	–0.04		DO	–0.23

TABLE 10.5.4 Averaged Salinity Difference Between the Benchmark Condition and the Sea Level Rise Conditions[a]

Station	1995		1996		2000	
	0.8 ft	1.2 ft	0.8 ft	1.2 ft	0.8 ft	1.2 ft
SE01	2.5	3.1	0.8	1.1	0.5	0.8
SE02	1.7	2.2	1.3	1.9	1.0	1.4
SE03	1.0	1.5	1.8	2.6	1.2	1.8

[a]salinity unit in ppt.

in the system. It is important to mention that even though the annually averaged change might not be very large, the changes during a particular period can be significant. For example, Table 10.5.3 lists that the annual mean DO is lowered by 0.49 mg/L in 1994. The DO concentration at SE05 in 1994 can actually be decreased by >4 mg/L in the summer (AEE, 2004b).

Salinities in the SLE are also affected by sea level rise. Table 10.5.4 lists three representative years to illustrate the impact of sea level rise: 1995 (wet year), 1996 (average year), and 2000 (dry year). Table 10.5.4 shows that a sea level rise of 1.2 ft can increase mean salinity by 3.1 ppt at SE01 in 1995.

Via these two 10-year simulations, it is concluded that sea level rise can have adverse impacts on the water quality conditions in the SLE/IRL system, such as reduced DO concentrations and increased salinity concentrations. Statistical analyses indicate that with the sea level rise of 0.8 ft, the adverse impacts are relatively small. The sea level rise of 1.2 ft can lower the mean DO concentration up to 0.49 mg/L and increase salinity concentration by >3 ppt. More measured data are needed to provide better and more accurate boundary conditions and nutrient loadings to the system. Direct coupling with a watershed model will supply more reliable information for setting up the SLE/IRL model and for conducting long-term simulations.

APPENDIX A

Environmental Fluid Dynamics Code

A1 OVERVIEW

The Environmental Fluid Dynamics Code (EFDC) (Hamrick, 1992) is a public-domain modeling package for simulating three-dimensional (3D) flow, transport, and biogeochemical processes in surface water systems, including rivers, lakes, estuaries, reservoirs, wetlands, and coastal regions. The EFDC model was originally developed at the Virginia Institute of Marine Science and is currently supported by the U. S. Environmental Protection Agency (EPA). The EFDC model has been extensively tested and documented in >100 modeling studies. The model is presently being used by universities, research organizations, governmental agencies, and consulting firms.

The EFDC model is an advanced 3D, time-variable model that provides the capability of internally linking hydrodynamic, water quality and eutrophication, sediment transport, and toxic chemical transport and fate submodels in a single source code framework. It includes four major modules (Fig. A1):

1. A hydrodynamic model.
2. A water quality model.
3. A sediment transport model.
4. A toxics model.

The full integration of the four components is unique and eliminates the need for complex interfacing of multiple models to address the different processes. Major processes represented in the EFDC model are already summarized in Fig. 1.3.1. A module to represent the submerged aquatic vegetation (SAV) was recently added to the EFDC model (AEE, 2005).

Representative applications of the EFDC model include modeling of sediment and metals transport in Blackstone River (Ji et al., 2002a), wetting and drying simulation of Morro Bay (Ji et al., 2000, 2001), simulations of Lake Okeechobee hydrodynamic, thermal, sediment, SAV, and water quality processes (Jin and Ji, 2001, 2004, 2005, Ji and Jin, 2006; Jin et al., 2000, 2002, 2007),

Hydrodynamics and Water Quality: Modeling Rivers, Lakes, and Estuaries, by Zhen-Gang Ji

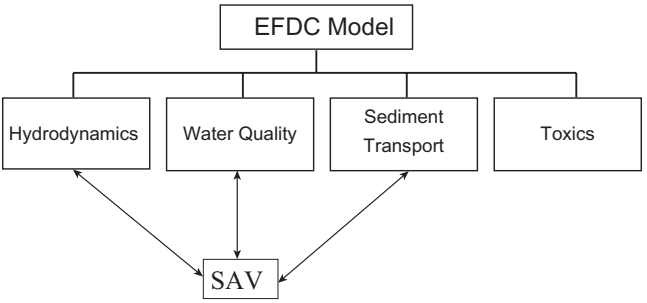

Fig. A1 Primary modules of the EFDC model.

hydrodynamic, sediment, and water quality modeling of St. Lucie Estuary (SLE) and Indian River Lagoon (Ji et al., 2007a, 2007b; Wan et al., 2007), hydrodynamic and water quality modeling of Lake Tenkiller (Ji et al., 2004), hydrodynamic modeling of Lake Billy Chinook Reservoir (Yang et al., 2000), the study of tidal intrusion and its impact on larval dispersion in the James River estuary (Shen et al., 1999), modeling estuarine front and its associated eddy (Shen and Kuo, 1999), modeling for TMDL development in Mobile Bay, Alabama (Wool et al., 2003a), hydrodynamic and water quality modeling of Neuse River Estuary, North Carolina (Wool et al., 2003b), 3D hydrodynamic–eutrophication modeling of Kwang-Yang Bay, Korea (Park et al, 2005), and integrated hydrodynamic and water quality modeling of Wissahickon Creek, Pennsylvania (Zou et al., 2006).

A2 HYDRODYNAMICS

The hydrodynamics of the EFDC model and many aspects of the computational scheme are equivalent to the widely used Blumberg–Mellor model (Blumberg and Mellor, 1987). The hydrodynamic model component is based on the 3D shallow water equations and includes dynamically coupled salinity and temperature transport. Notable extensions to the EFDC hydrodynamic model include representation of hydraulic structures for controlled flow systems, vegetation resistance for wetland systems (Moustafa and Hamrick, 2000), and wetting and drying process (Ji et al., 2001). The EFDC model solves the vertically hydrostatic, free-surface, turbulent-averaged equations of motions for a variable-density fluid. Dynamically coupled transport equations for turbulent kinetic energy, turbulent length scale, salinity, and temperature are also solved. The two turbulence parameter transport equations implement the Mellor–Yamada level 2.5 turbulence closure scheme (Mellor and Yamada, 1982; Galperin et al., 1988). Major processes included in the EFDC hydrodynamic model are already described in Chapter 2.

A3 SEDIMENT TRANSPORT

The EFDC model is capable of simulating the transport of multiple size classes of cohesive and noncohesive suspended sediment, including bed deposition and resuspension. An EPA report detailed a comprehensive evaluation of the EFDC sediment and toxic models and concluded that EFDC is a robust modeling system that can be successfully implemented at contaminated sediment sites (Hayter et al., 2006). The EFDC incorporates advanced formulations based on research findings and understanding of sediment transport processes. The sediment transport capabilities and formulations are consistent with peer models including the USACE's CH3D-SED (Spasojevic and Holly, 1994) and the SEDZL model (Ziegler and Nesbitt, 1995). Water column transport is based on the same high-order advection–diffusion scheme used for salinity and temperature. The EFDC internally computes settling, deposition, and resuspension of cohesive and noncohesive solids as well as sediment bed geomechanics. Water column and bed exchange of particles is represented as functional relationships of bed shear stress for cohesive solids and the Shields parameter for noncohesive solids. The deposited bed may be represented by a single layer or multiple layers. Consolidation of the sediment bed is represented by a surface bed layer and multiple deep bed layers that respond to the accumulation or erosion of solids from the bed. Water column-sediment bed interface elevation changes are also incorporated into the hydrodynamic continuity equation. Technical details of the EFDC sediment model are already given in Chapter 3.

A4 TOXIC CHEMICAL TRANSPORT AND FATE

The EFDC toxic model accounts for multiple toxic chemicals in an integrated model of hydrodynamics, sediment transport, and toxic chemical transport and fate. Total contaminant concentration is simulated in the water column and bed with dissolved and particulate fractions determined by equilibrium partitioning. Water column–bed exchange of dissolved and particulate contaminants includes deposition and associated surface water entrainment, resuspension and associated pore water entrainment, pore water expulsion due to consolidation, and diffusion between the surface water and pore water phases. The contaminant transport capabilities and formulations are consistent with peer models including the TOXI module of the WASP5 model (Ambrose et al., 1993). Chapter 4 covers details of toxic modeling.

A5 WATER QUALITY AND EUTROPHICATION

The EFDC water quality model includes 22 state variables in the water column and is coupled with a 27-state variable sediment diagenesis model. The

nutrient cycling is most similar to the kinetics of the Chesapeake Bay water quality model (Cerco and Cole, 1994). The sediment diagenesis model is based on a recoding of the model developed by DiToro and Fitzpatrick (1993). The water quality model incorporates multiple functional groups of algae, dissolved oxygen, phosphorus, silica, organic carbon, and chemical oxygen demand. Organic carbon and organic nutrients are represented as dissolved and particulate labile and refractory forms. The sediment diagenesis model, upon receiving the particulate organic matter deposited from the overlying water column, simulates the diagenesis and the resulting fluxes of inorganic substances (ammonium, nitrate, phosphate, and silica) and sediment oxygen demand back to the water column. The coupling of the sediment diagenesis model with the water quality model not only enhances the model's predictive capability of water quality parameters, but also enables it to simulate the long-term variations in water quality conditions in response to changes in nutrient loadings. Chapter 5 describes details of the water quality and eutrophication processes.

A6 NUMERICAL SCHEMES

The EFDC model is designed to represent a finite difference computational grid as either a simple Cartesian grid or an orthogonal, curvilinear coordinate system for irregular coastlines. In the vertical domain, EFDC uses a sigma-stretched-grid to represent complex bathymetry. As a fully 3D model, EFDC can be applied to all types of surface waterbodies. Originally constructed as a 3D model, the EFDC model can also be readily applied to 1D or 2D studies by using a 1D or 2D model grid and without any modification to the code.

The numerical scheme employed in EFDC to solve the equations of motion uses second order accurate spatial finite differencing on a staggered or C grid. The model's time integration employs a second-order accurate, three-time level, finite difference scheme with an internal–external mode splitting procedure to separate the internal shear or baroclinic mode from the external or barotropic mode. The external mode solution is semi-implicit and simultaneously computes the 2D surface elevation field by a preconditioned conjugate gradient procedure. The external solution is completed by the calculation of the depth-average barotropic velocities using the new surface elevation field. The mode's semi-implicit external solution allows large time steps that are constrained only by the stability criteria of the explicit central difference or high-order upwind advection scheme used for the nonlinear accelerations (Smolarkiewicz and Clark, 1986; Smolarkiewicz and Grabowski, 1990; Smolarkiewicz and Margolin, 1993). The EFDC model's internal momentum equation solution, at the same time step as the external, is implicit with respect to vertical diffusion. Time splitting inherent in the three-time-level scheme is controlled by periodic insertion of a second-order accurate two-time-level trapezoidal step.

A7 DOCUMENTATION AND APPLICATION AIDS

Extensive documentation of the EFDC model is available. Theoretical and computational aspects of the model are described for hydrodynamics (Hamrick, 1992), sediment transport (Tetra Tech, 2000), toxic contaminants (Tetra Tech, 1999), and water quality (Park et al., 1995). The model user's manual (Hamrick, 1996) also provides details on setup of the EFDC input files.

The original user interface is based on text input file templates. This choice was selected in the interest of maintaining model portability across a range of computing platforms and readily allows the user to modify input files using most text-editing software. The text interface also allows modification of model files on remote computing systems and in heterogeneous network environments.

Several versions of windows-based user interfaces have also been developed in recent years. The preprocessor has a grid generator (GEFDC), an input data checker, and an initial condition generator. The postprocessor converts output data for use by other third-party visualization applications, often without need for intermediate processing. Graphics and visualization software successfully used with EFDC output include APE, AVS, GrADS, IDL, Mathematica, MatLab, NCAR Graphics, PV-Wave, Tecplot, SiteView, Spyglass Transform and Slicer, Voxelview, and EFDC_Explorer (Craig, 2004).

The EFDC modeling system is written in FORTRAN 77. The generic or universal source code has been compiled and executed on most UNIX workstations (DEC Alpha, Hewlett-Packard, IBM RISC6000, Silicon Graphics, Sun and Sparc compatibles), Cray and Convex supercomputers, and PC compatibles and Macintosh personal computers. Intel, Absoft, Lahey, and Microsoft compilers are supported on PC compatibles.

APPENDIX B

Conversion Factors

LENGTH

1 inch (in) = 2.540 cm
1 foot (ft) = 0.3048 m
1 yard (yd) = 0.9144 m
1 mile (mi) = 1.6093 km
1 nautical mile = 1.852 km
1 meter (m) = 3.2808 ft = 39.37 in.

AREA

1 square inch (in^2) = 6.452 cm^2
1 square foot (ft^2) = 0.0929 m^2
1 hectare (ha) = 10,000 m^2 = 2.471 acres
1 square kilometer (km^2) = 0.3861 mi^2
1 acre (ac) = 43,560 ft^2 = 0.404685 ha

VOLUME

1 cubic foot (ft^3) = 7.4805 gal = 28.32 L = 0.02832 m^3
1 cubic meter (m^3) = 35.3147 ft^3 = 264.172 gal = 1000 Liters (L)
1 gallon = 3.785 L = 0.134 ft^3
1 barrel oil (bbl) = 0.15899 m^3 = 42 gal

VELOCITY

1 foot/second (ft/s) = 0.6818 mph = 0.3048 m/s = 16.364 mi/day
1 meter/second (m/s) = 3.2808 ft/s = 86.4 km/day = 2.237 mph

Hydrodynamics and Water Quality: Modeling Rivers, Lakes, and Estuaries, by Zhen-Gang Ji

1 mile/hour (mph) = 1.609 km/h = 1.467 ft/s = 0.4470 m/s
1 knot = 1 nautical mile/h = 1.688 ft/s = 1.151555 mph = 1.853248 km/h

FLOW RATE

1 cubic foot/second (cfs) = 0.028316 m^3/s
1 cubic meter/second (m^3/s) = 35.315 cfs

MASS

1 pound (lb) = 453.592 g
1 kg = 2.2046 lb
1 metric ton (ton) = 1000 kg = 2204.622 lb

DENSITY

1 lb/ft^3 = 16.018 g/m^3
1 g/cm^3 = 1000 kg/m^3 = 62.428 lb/ft^3

CONCENTRATION

1 g/L = 1000 g/m^3 = 1 ppt
1 mg/L = 1 g/m^3 = 1 ppm
1 µg/L = 1 mg/m^3 = 1 ppb

TEMPERATURE

Degrees Celsius (°C) = $\frac{5}{9}[T(°\text{F}) - 32]$

Degrees Fahrenheit (°F) = $\frac{9}{5}T(°\text{C}) + 32$

FORCE

1 Newton (N) = 1 kg m/s^2 = 1×10^5 dyn
1 dyne (dyn) = 1 g cm/s^2

PRESSURE

1 atmosphere = 76.0 cm Hg = 33.8995 ft H_2O (0 °C) = 101.325 kPa
1 Pascal (Pa) = 1 N/m^2

ENERGY

1 calorie (cal) = 4.1868 J
1 Joule (J) = 1 W s = 1 N m
1 kilowatt hour = 3600 kJ = 860 kcal

HEATFLUX

1 Langley/day (ly/day) = 1 cal/(cm^2 day) = 0.4846 W/m^2

POWER

1 Watt (W) = 1 J/s = 1.34×10^{-3} horsepower (hp)

APPENDIX C

Contents of Electronic Files

This modeling package includes the following five folders: (1) Channel, (2) StLucie, (3) LakeOkee, (4) Documents, and (5) UtilityPrograms. The first three folders contain three sample applications, including their source codes, executable codes, input files, output files, and some results in animations. These three studies illustrate modeling applications to a channel, an estuary, and a lake, respectively. These sample applications may serve as templates for possible new applications. The templates allow modelers to modify existing input files to meet their specific modeling needs and to avoid developing the entire input files from scratch. For this purpose, some unnecessary details of the original inputs files are omitted so that the readers can focus on the essentials of the input and output files.

The fourth folder (Documents) contains EFDC manuals, reports, and technical notes. The fifth folder (UtilityPrograms) contains utility programs that are often used in EFDC modeling applications. Dr. John Hamrick of Tetra Tech provided most of the materials in the Documents and UtilityPrograms folders.

A variety of graphic and visualization software is available for presenting and analyzing 3D model results. Which graphic package to use is largely a personal choice. There is no "best" one for graphics and visualization. In this book, most of the graphics from the model results were made using either GrADS (http://www.iges.org/grads/) or Tecplot (http://www.tecplot.com/). The animations files are in avi, gif, or flc format. A free animation player, called Imagen (http://www.gromada.com/download.html), is a simple and useful tool for playing animations.

Several versions of the windows-based Graphic User Interface (GUI) have been developed for the EFDC model in recent years. These GUIs might look easier for setting up a modeling application. However, personally, I feel that directly modifying the major EFDC input files (e.g., efdcwin.inp and wqwin.inp) using a text editor is still a simple and convenient way to set up an EFDC application. After all, understanding the theories and the processes are the key (more difficult) part in a modeling study. It is like a race car, a pretty dashboard looks nice, but the most important things are under the hood!

Hydrodynamics and Water Quality: Modeling Rivers, Lakes, and Estuaries, by Zhen-Gang Ji

It should also be mentioned that the template files provided in this modeling package are intended to be used by readers who already have basic knowledge about the EFDC model and modeling in general. It is recommend that an inexperienced modeler takes a training course before using the EFDC model for practical applications.

C1 CHANNEL MODEL

The Channel folder contains input and output files of a channel model. Some of the model results are given and discussed in Section 10.4.2. The source code and executable code are the same as the SL/IRL model and are given in the St. Lucie folder.

C2 ST. LUCIE ESTUARY AND INDIAN RIVER LAGOON MODEL

The SLE and Indian River Lagoon Model and its applications are discussed extensively in this book. The St. Lucie folder contains three subfolders:

1. 1999: input and output files from the 1999 simulation (the first 30 days).
2. Code: SLE/IRL model source code, which is based on the EFDC model.
3. Animations: Some of the model results in AVI format.

The executable code, StLucie.exe, is compiled using the Intel FORTRAN 8.1 (http://www.intel.com/support/performancetools/fortran/windows/index.htm).

C3 LAKE OKEECHOBEE ENVIRONMENTAL MODEL

The Lake Okeechobee Environmental Model (LOEM) and its applications are discussed extensively in this book. The LakeOkee folder contains three subfolders:

1. 2002: input and output files from the 2002 simulation (the first 30 days).
2. code: LOEM model source code, which is based on the EFDC model.
3. Animations: Some of the model results in GIF or FLC format.

Two utility programs, readHyBin.for and readWqBin.for, are provided to read and process the four major binary output files (hyts.bin, hy3d.bin, wqts.bin, and wq3d.bin). The executable code, LakeOkee.exe, is compiled using the Intel FORTRAN 8.1.

Major differences between the LOEM source code and the SLE/IRL source code are that LOEM includes (1) wind wave model, (2) wave–current interac-

tion model, (3) SAV model, and (4) multiple layers in the sediment bed. Excluding these four features, the LOEM code should be similar to the SLE/IRL code.

C4 DOCUMENTATION AND UTILITY PROGRAMS

The Documents folder contains documents related to the EFDC model, including EFDC user manuals, theoretical reports, application reports, and technical notes.

The UtilityPrograms folder contains six subfolders:

1. gefdc_gridgen: GEFDC is a FORTRAN based grid generation program.
2. harmonicanalysisS: a program that performs a least-squares harmonic analysis on a scalar time series.
3. harmonicanalysisV: a program that performs a least-squares harmonic analysis on a two-component vector time series.
4. STEfdc: a program that generates initial salinity and temperature fields, salt.inp and temp.inp, for the EFDC model.
5. TimeserFilter: a program that filters the high frequencies of a time series.
6. vogg_gridgen: VOGG is a visual orthogonal grid generation tool for hydrodynamic and water quality modeling.

BIBLIOGRAPHY

AEE 2004a. St. Lucie Estuary and Indian River Lagoon Water Quality Model III: Sediment and Water Quality Modeling. Technical Report to South Florida Water Management District. Applied Environmental Engineering, LLC, Florida.

AEE 2004b. St. Lucie Estuary and Indian River Lagoon Water Quality Model IV: Long-Term Water Quality Simulations. Technical Report to South Florida Water Management District. Applied Environmental Engineering, LLC, Florida.

AEE 2005. Three Dimensional Water Quality Model of Lake Okeechobee. Technical Report to South Florida Water Management District. Applied Environmental Engineering, LLC, Florida.

Ahsan, A. K. M. Q. and Blumberg, A. F. 1999. Three-dimensional hydrothermal model of Onondaga Lake, New York. J. Hydraulic Eng., 125(9):912–923.

Aldridge, F. J., Phlips, E. J., and Schelske, C. L. 1995. The use of nutrient enrichment bioassays to test for spatial and temporal distributions of limiting factors affecting phytoplankton dynamics in Lake Okeechobee, FL. N. G. Aumen and R. G. Wetzel (eds.), in Advances in Limnology, Schweizerbart, Stuttgart, Germany.

Alexander, R. B., Slack, J. R., Ludtke, A. S., Fitzgerald, K. K., and Schertz, T. L. 1996. Data from Selected U. S. Geological Survey National Stream Quality Monitoring Networks (WQN): U. S. Geological Survey Digital Data Series DDS-37, 2 disks.

Ambrose, R. B., Wool, T. A., and Martin, J. L. 1993. The Water Quality Analysis and Simulation Program, WASP5: Part A, Model Documentation Version 5.1. U. S. EPA, Athens Environmental Research Laboratory, 210 pp.

APHA 2000. Standard Methods for the Examination of Water and Wastewater. 21st ed. Eaton, A. D., L. C. Clesceri, and A. E. Greenberg (eds.). American Public Health Association, Washington, DC.

Ariathurai, R. and Krone, R. B. 1976. Finite element model for cohesive sediment transport. J. Hydraulic Div. ASCE, 102:323–338.

Aumen, N. G. 1995. The history of human impacts, lake management, and limnological research on Lake Okeechobee, Florida (USA). Arch. Hydrobiol., Adv. Limnol., 45:1–16.

Bagnold, R. A. 1956. The flow of cohesionless grains in fluids. Philos. Trans. R. Soc. London, Ser. A, 249 (964):235–297.

Banks, R. B. and Herrera, F. F. 1977. Effect of wind and rain on surface reaeration. J. Environ. Eng. Div., ASCE, 103:489–504.

Hydrodynamics and Water Quality: Modeling Rivers, Lakes, and Estuaries, by Zhen-Gang Ji

Beeton, A. M. 1958. Relationship between Secchi disk readings and light penetration in Lake Huron, Trans. Am. Fisheries Soc., 87:73–79.

Berner, R. A. 1964. An idealized model of dissolved sulfate distribution in recent sediments. Geochim. Cosmochim. Acta, 28(9):1497–1503.

Blom, G., van Duin, E. H. S., Aalderink, R. H., Lijklema, L., and Toet, C. 1992. Modeling sediment transport in shallow lakes—interactions between sediment transport and sediment composition. Hydrobiologia, 235/236:153–166.

Blumberg, A. F., Galperin, B., and O'Connor, D. J. 1992. Modeling vertical structure of open-channel flow. J. Hydraulic Eng., 118:1119–1134.

Blumberg, A. F., Ji, Z.-G., and Ziegler, C. K. 1996. Modeling outfall plume behaviors using a far field circulation model. J. Hydraulic Eng., 122(11):610–616.

Blumberg, A. F. and Kantha, L. H. 1985. Open boundary conditions for circulation models. J. Hydraulic Eng., 11:237–255.

Blumberg, A. F., Khan, L. A., and St. John, J. P. 1999. Three-dimensional hydrodynamic model of New York Harbor Region, J. Hydraulic Eng., 125(8):799–816.

Blumberg, A. F. and Mellor, G. L. 1987. A description of a three-dimensional coastal ocean circulation model. In Three-Dimensional Coastal Ocean Models, Coastal and Estuarine Science, Vol. 4., Heaps, N. S., (ed.), American Geophysical Union: pp. 1–19.

Bolton, D. 1980. The computation of equivalent potential temperature. Monthly Weather Rev., 108:1046–1053.

Boudreau, B. P. and Ruddick, B. R. 1991. On a reactive continuum representation of organic matter diagenesis. Am. J. Sci., 291:507–538.

Bowen, I. S. 1926. The ratio of heat losses by conduction and by evaporation from any water surface. Phys. Rev., 27:779–787.

Bowie, G. L., Mills, W. B., Porcella, D. B., Campbell, C. L., Pagenkopf, J. R., Rupp, G. L., Johnson, K. M., Chan, P. W. H., and Gherini, S. A. 1985. Rates, Constants, and Kinetics Formulations in Surface Water Quality Modeling, Second Edition, USEPA, Environmental Research Laboratory, Athens, GA, EPA/600/3-85/040.

Bretschneider, C. L. 1958. Revisions in wave forecasting: deep and shallow water. Proceedings of the 6th Conference on Coastal Engineering, pp. 30–67.

Bricker, S. B. 1993. Historical trends in contamination of estuarine and coastal sediments: The history of Cu, Pb, and Zn inputs to Narragansett Bay, Rhode Island, as recorded by salt marsh sediments. Estuaries 16(3B):589–607.

Brown, L. C. and Barnwell, T. O. 1987. The Enhanced Stream Water Quality Models QUAL2E and QUAL2E-UNCAS: Documentation and User Manual. EPA/600/3-87-007. U.S. Environmental Protection Agency, Athens, GA.

Caduto, M. J. 1990. Pond and Brook: A Guide to Freshwater Environments. London: University Press of New England, 1990.

Canuto, V. M., Howard, A., Cheng, Y., and Dubovikov, M. S. 2001. Ocean turbulence. Part I: One-point closure model-momentum and heat vertical diffusivities. J. Phy. Oceanog., 31:1413–1426.

Canuto, V. M., Howard, A., Cheng, Y., and Dubovikov, M. S. 2002. Ocean turbulence. Part II: Vertical diffusivities of momentum, heat, salt, mass, and passive scalars. J. Phys. Oceanog., 32:240–264.

Caraco, N., Cole, J., and Likens, G. E. 1990. A comparison of phosphorus immobilization in sediments of freshwater and coastal marine systems. Biogeochemistry, 9(3):277–290.

Carlson, R. E. 1977. A trophic state index for lakes. Limnol. Oceanog., 22:361–369.

Casulli, V. and Cheng, R. T. 1992. Semi-implicit finite difference methods for three-dimensional shallow water flow. Int. J. Numerical Methods Fluids, 15:629–648.

Caupp, C. L., Brock, J. T., and Runke, H. M. 1991. Application of the Dynamic Stream Simulation and Assessment Model (DSSAM III) to the Truckee River below Reno, Nevada: Model Formulation and Program Description. Report prepared by Rapid Creek Water Works for Nevada Division of Environmental Protection, Carson City, and Washoe County Department of Comprehensive Planning, Reno, NV.

CEQ 1978. Environmental Quality, the Ninth Annual Report of the Council on Environmental Quality. U.S. Government Printing Office, Washington, DC.

Cerco, C. F. 1999. Eutrophication models of the future. J. Environ. Eng., 125(3):209–210.

Cerco, C. F. and Cole, T. 1994. Three-dimensional Eutrophication Model of Chesapeake Bay. Volume 1: Main Report. Technical Report EL-94-4. US Army Corps of Engineers Waterways Experiment Station.

Cerco, C. F., Johnson, B. H., and Wang, H. V. 2002. Tributary Refinements to the Chesapeake Bay Model. Technical Report, U.S. Army Corps of Engineers Waterway Experiment Station, Vicksburg, MS, ERDC TR-02-4.

Chamberlain, R. and Hayward, D. 1996. Evaluation of water quality and monitoring in the St. Lucie estuary, Florida. Water Res. Bull., 32(4):681–696.

Chanson, H. 1999. The Hydraulics of Open Channel Flow: An Introduction. London, UK: Butterworth-Heinemann, 544 pp.

Chapra, S. C. 1997. Surface Water-quality Modeling. New York: McGraw-Hill, 844 pp.

Chapra, S. C. and Canale, R. P. 1998. Numerical Methods for Engineers, with Programming and Scientific Applications. New York: McGraw-Hill, 839 pp.

Cheng, N. S. 1997. Simplified settling velocity formula for sediment particle, J. Hydraulic Eng., 123:149–152.

Chow, V. 1964. Handbook of Applied Hydrology, a Comparison of Water-Resources Technology. New York: McGraw-Hill.

Chung, S.-W. and Gu, R. 1997. Two-dimensional simulations of contaminant currents in stratified reservoir. J. Hydraulic Eng., 124(7):704–711.

Churchill, M. A., Elmore, H. L., and Buckingham, R. A. 1962. The prediction of stream reaeration Rates. J. Sanitary Eng. Div., ASCE, 88(SA4):1–46.

Cole, T. M. and Buchak, E. M. 1995. CE-QUAL-W2: A Two-dimensional, Laterally Averaged, Hydrodynamic and Water Quality Model, Version 2. US Army Corps of Engineers, Waterways Experiment Station, Technical Report El-95-X, Vicksburg, MS.

Cole, T. M. and Wells, S. A. 2000. CE-QUAL-W2: A two-dimensional, Laterally Averaged, Hydrodynamic and Water Quality Model, Version 3.0. Instruction Report EL-2000, US Army Engineering and Research Development Center, Vicksburg, MS.

Connolly, J. P., Blumberg, A. F., and Quadrini, J. D. 1999. Modeling fate of pathogenic organisms in coastal waters of Oahu, Hawaii. J. Environ. Eng., 125(5):398–406.

Craig, P. M. 2004. User's Manual for EFDC_Explorer: A Pre/Post Processor for the Environmental Fluid Dynamics Code. Technical Report, Dynamic Solutions, LLC, P. O. Box 24176, Knoxville, TN.

CSCRMDE 1987. Sedimentation Control to Reduce Maintenance Dredging of Navigational Facilities in Estuaries. Report and symposium proceedings. Committee on Sedimentation Control To Reduce Maintenance Dredging in Estuaries, Washington, DC: National Academy Press.

Darley, W. M. 1982. Algal Biology: A Physiological Approach. Oxford, UK: Blackwell Scientific Publications.

Defant, A. 1958. Ebb and Flow—the Tides of Earth, Air, and Water. Ann Arbor, MI: University of Michigan Press.

Dennison, W. C., Orth, R. J., Moore, K. A., Stevenson, J. C., Carter, V., Kollar, S., Bergstrom, P. W., and Batuik, R. A. 1993. Assessing water quality with submersed aquatic vegetation. Bioscience, 43(2):86–94.

DHI 2001. MIKE 3 Estuarine and Coastal Hydrodynamics and Oceanography, DHI Water & Environment, Danish Hydraulic Institute, Horsholm, Denmark.

Di Toro, D. M. 1980. Applicability of cellular equilibrium and Monod theory to phytoplankton growth kinetics. Ecolog. Modelling, 8:201–218.

Di Toro, D. M. 2001. Sediment Flux Modeling. New York: John Wiley & Sons, Inc.

Di Toro, D. M. and Fitzpatrick, J. 1993. Chesapeake Bay Sediment Flux Model. Contract Report EL-93-2, U. S. Army Engineer Waterways Experiment Station, Vicksburg, MS.

Di Toro, D. M. and Matystik, W. F. 1980. Mathematical Models of Water Quality in Large Lakes, Part 1: Lake Huron and Saginaw Bay. EPA-600/3-80-056. pp. 28–30.

Di Toro, D. M., Paquin, P. R., Subburamu, K., and Gruber, D. A. 1990. Sediment oxygen demand model: methane and ammonia oxidation. J. Environ. Eng., 116(5):945–986.

Diaz, R. J. and Rosenberg, R. 1995. Marine benthic hypoxia: a review of its ecological effects and the behavioural responses of benthic macrofauna. Oceanography and Marine Biology: an Ann. Rev., 33:245–303.

Dickey, T. D. 2002. Personal communication. Ocean Physics Laboratory, University of California Santa Barbra, CA.

Doering, P. 1996. Temporal variability in water quality in the St. Lucie estuary, South Florida. Water Res. Bull., 32 (6):1293–1306.

Dunne, T. and Leopold, L. B. 1978. Water in Environmental Planning. San Francisco, CA: W. H. Freeman Co.

Dyer, K. 1973. Estuaries: A Physical Introduction. New York: Wiley-Interscience. 140 pp.

Dyer, K. R., Bale A. J., Christie, M. J., Feates, N., Jones, S., and Manning, A. J. 2000. The properties of suspended sediment in an estuarine turbidity maximum. Proceedings of 6th International Conference on Nearshore and Estuarine Cohesive Sediment Transport Processes, Delft.

Edinger, J. E., Brady, D. K., and Geyer, J. C. 1974. Heat Exchange and Transport in the Environment. Report No. 14, EPRI Pub. No. EA-74-049-00-3. Electric Power Research Institute, Palo Alto, CA.

EHC 1998. Coastal Challenges: A Guide to Coastal and Marine Issues. Environmental Health Center, 1025 Connecticut Avenue, NW, Suite 1200, Washington, DC.

Emery, W. J. and Thomson, R. E. 2001. Data Analysis Methods in Physical Oceanography. New York: Elsevier, 638 pp.

Ezer, T., Thattai, D. V., Kjerfve, B., and Heyman, W. 2005. On the variability of the flow along the Meso-American Barrier Reef System: A numerical model study of the influence of the Caribbean Curr. Eddies. Ocean Dyn., 55:458–475.

Farmer, D. D., Crawford, G. B., and Osborn, T. R. 1987. Temperature and velocity microstructure caused by swimming fish. Limnol. Oceanog., 32:978–983.

Fischer, H. B., List, E. J., Imberger, J., and Brooks, N. H. 1979. Mixing in Inland and Coastal Waters, New York: Academic Press, 483 pp.

Fisher, M. M., Reddy, K. R., and James, R. T. 2005. Internal nutrient loads from sediments in a shallow, subtropical lake. Lake Reser. Manag., 21(3):338–349.

FISRWG 1998. Stream Corridor Restoration: Principles, Processes, and Practices. By the Federal Interagency Stream Restoration Working Group (FISRWG) (15 Federal agencies of the US government). GPO Item No. 0120-A; SuDocs No. A 57.6/2: EN3/PT.653. ISBN-0-934213-59-3.

Flather, R. A. and Hubbert, K. P. 1990. Tide and surge models for shallow water-Morecambe Bay revisited. In Modeling Marine Systems, Vol. I, Boca Raton, FL: CRC Press, pp. 135–166.

Ford, D. E. and Johnson, M. C. 1986. An Assessment of Reservoir Mixing Processes. Technical Rpt. E-86-7, US Army Engineer Waterways Experiment Station, Vicksburg, MS.

Frayer, W. E., Monahan, T. J., Bowden, D. C., and Grabill, F. A. 1983. Status and Trends of Wetlands and Deepwater Habitats in the Conterminous U.S., 1950s to 1970s. Department of Forests and Wood Sciences, Colorado State University, Fort Collins, CO. 32 pp.

Gailani, J., Ziegler, C. K., and Lick, W. 1991. Transport of suspended solids in the lower Fox River. J. Great Lakes Res., 17:479–494.

Galperin, B., Kantha, L. H., Hassid, S., and Rosati, A. 1988. A quasi-equilibrium turbulent energy model for geophysical flows. J. Atmos. Sci., 45:55–62.

Ganf, G. G. 1974. Diurnal mixing and the vertical distribution of phytoplankton in a shallow equatorial lake (Lake George, Uganda), J. Ecol., 62(2):611–629.

Garcia, M. and Parker, G. 1991. Entrainment of bed sediment into suspension. J. Hydraulic Eng., 117:414–435.

Germain, G. 1998. Surface Water Quality Monitoring Network. Technical memorandum, WRF#356, South Florida Water Management District.

Gill, A. E. 1982. Atmosphere-Ocean Dynamics. New York: Academic Press, 662 pp.

Gleeson, C. and Gray, N. 1997. The Coliform Index and Waterborne Disease. London, UK: E and FN Spon.

Glenn, S. M. and Grant, W. D. 1987. A suspended sediment stratification correction for combined waves and current flows. J. Geophy. Res., 92(C8):8244–8264.

Graf, W. H. 1971. Hydraulics of Sediment Transport. New York: McGraw-Hill.

Grant, W. D. and Madsen, O. S. 1979. Combined wave and current interaction with a rough bottom. J. Geophys. Res., 84(C4):1797–1808.

Guo, W. and Langevin, C. D. 2002. User's Guide to SEAWAT: A Computer Program for Simulation of Three-Dimensional Variable-Density Ground-Water Flow: Techniques of Water-Resources Investigations Book 6, Chapter A7, 77 pp.

Haith, D. A. and Shoemaker, L. L. 1987. Generalized watershed loading functions for stream flow nutrients. Water Res. Bull., 23(3):471–478.

Hameedi, J. and Johnson, E. 2005. Personal communication. NOAA/NOS/NCCOS facility in Silver Spring, MD.

Hamrick, J. M. 1992. A Three-dimensional Environmental Fluid Dynamics Computer Code: Theoretical and Computational Aspects. The College of William and Mary, Virginia Institute of Marine Science, Special Report 317, 63 pp.

Hamrick, J. M. 1994. Application of the EFDC, Environmental Fluid Dynamics Computer Code to SFWMD Water Conservation Area 2A. J. M. Hamrick and Associates, Report JMH-SFWMD-94-01, Williamsburg, VA, 126 pp.

Hamrick, J. M. 1996. Users Manual for the Environmental Fluid Dynamic Computer Code. The College of William and Mary, Virginia Institute of Marine Science, Special Report 328, 224 pp.

Hamrick, J. M. 2004. A Rooted Aquatic Plant and Epiphyte Algae Sub-Model for EFDC. Unpublished technical notes.

Hamrick, J. M. and Mills, W. B. 2001. Analysis of temperatures in Conowingo Pond as influenced by the Peach Bottom atomic power plant thermal discharge. Environ. Sci. Policy, 3:197–209.

Haunert, D. E. 1988. Sediment Characteristics and Toxic Substances in the St. Lucie Estuary, Florida. Technical Publication 88-10, South Florida Water Management District, West Palm Beach, FL.

Haunert, D. E. and Startzman, J. R. 1980. Some Seasonal Fisheries Trends and Effects of a 1000-cfs Fresh Water Discharge on the Fishes and Macroinvertebrates in the St. Lucie Estuary, Florida., Technical Publication 80-3, South Florida Water Management District.

Haunert, D. E. and Startzman, J. R. 1985. Short Term Effects of a Fresh Water Discharge on the Biota of St. Lucie Estuary, Florida. Technical Publication 85-1. South Florida Water Management District.

Havens, K. E. 2003. Submerged aquatic vegetation correlations with depth and light attenuating materials in a shallow subtropical lake. Hydrobiologia, 493:173–186.

Havens, K. E., Aumen, N. G., James, R. T., and Smith, V. H. 1996. Rapid ecological changes in a large subtropical lake undergoing cultural eutrophication. Ambio, 25:150–155.

Havens, K. E., Fox, D., Gornak, S., and Hanlon, C. 2005. Aquatic vegetation and largemouth bass population responses to water-level variations in Lake Okeechobee, Florida (USA). Hydrobiologia, 539:225–237.

Havens, K. E. and James, R. T. 2005. The phosphorus mass balance of Lake Okeechobee, Florida: implications for eutrophication management. Lake Reser. Manag., 21(2):139–148.

Havens, K. E., Jin, K.-R., Iricanin, N., and James, R. T. 2007, Phosphorus dynamics at multiple time scales in the pelagic zone of a large shallow lake in Florida, USA. Hydrobiologia, 581(1):25–42.

Havens, K. E., Sharfstein, B., Brady, M. A., East, T. L., Harwell, M. C., Maki, R. P., and Rodusky, A. J. 2004. Recovery of submerged plants from high water stress in a large subtropical lake in Florida, USA. Aquatic Bot., 78:67–82.

Hayter, E. J. 1983. Prediction of Cohesive Sediment Movement in Estuarial Waters. Ph.D. dissertation, University of Florida, Gainesville.

Hayter, E. J., Bergs, M., Gu, R., McCutcheon, S., Smith, S. J., and Whiteley, H. J. 1998. HSCTM-2D, a Finite Element Model for Depth-averaged Hydrodynamics, Sediment and Contaminant Transport. Technical Report, U.S. EPA Environmental Research Laboratory, Athens, GA.

Hayter, E. J., Mathew, R., Hallden, J., Garland, E., and Salerno, H. 2006. Evaluation of the State-of-the-Art Contaminated Sediment Transport and Fate Modeling System. EPA/600/R-06/108, EPA Ecosystems Research Division, Athens, GA.

Hayter, E. J. and Mehta, A. J. 1983. Modeling Fine Sediment Transport in Estuaries. Report EPA-600/3-83-045, U.S. Environmental Protection Agency, Athens, GA.

HEC-2 1991. Water Surface Profiles, User's Manual. Hydrologic Engineering Center, Davis, CA. 308 pp.

Herdendorf, C. E. 1984. Inventory of the Morphometric and Limnological Characteristics of the Large Lakes of the World. Technical Bulletin, Ohio Sea Grant, Columbus, OH.

Hicks, B. B. 1972. Some evaluations of drag and bulk transfer coefficients over water bodies of different sizes. Boundary-layer Meteorology, 3:201–213.

Hicks, B. B., Drinkrow, R. L., and Grauze, G. 1974. Drag and bulk transfer coefficients associated with a shallow water surface. Boundary-Layer Meteorol., 6:287–297.

Horner, R. R., Welch, E. B., Seeley, M. R., and Jacoby, J. M. 1990. Responses of periphyton to changes in current velocity, suspended sediment, and phosphorus concentration. Freshwater Biol., 24(2):215–232.

Howarth, R. W., Chan, F., and Marino, R. 1999. Do top-down and bottom-up controls interact to exclude nitrogen-fixing cyanobacteria from the plankton of estuaries? An exploration with a simulation model. Biogeochemisty, 46:203–231.

Hu, G. 1999. Two-dimensional hydrodynamic model of St. Lucie estuary. In Environmental Engineering 1999, Proceedings of the ASCE-CSCE National Conference on Environmental Engineering, pp. 434–443.

Hu, G. and Unsell, D. 1998. Tidal circulation in the Southern Indian River Lagoon. Water Resources Engineering 1998, Proceedings of the International Water Resources Engineering Conference, Norfolk, VA, Vol. 1, 844–849.

Hutchinson, G. E. 1957. A Treatise on Limnology, Vol. I. Geography, Physics and Chemistry, New York: John Wiley & Sons, Inc., 1015 pp.

Hutchinson, G. E. 1967. A Treatise on Limnology, Vol. II. Introduction to Lake Biology and the Limnoplankton. New York: John Wiley & Sons, Inc., 1115 pp.

Hutchinson, G. E. 1975. A Treatise on Limnology, Vol. III. Limnological Botany. New York: John Wiley & Sons, Inc., 660 pp.

Hwang, K.-N., and Mehta, A. J. 1989. Fine Sediment Erodibility in Lake Okeechobee, Florida. Technical report to South Florida Water Management District, UFL/COEL-89/019, University of Florida, Gainesville, FL, 140 pp.

HydroGeoLogic, 1999. Selection of Water Quality Components for Eutrophication-related Total Maximum Daily Load Assessments. Task 4: Documentation of Review and Evaluation of Eutriphication models and Components. Technical report to U.S. Environmental Protection Agency, HydroGeoLogic, Inc. and Aqua Terra Consultants, Herndon, VA.

HydroQual 1991a. A Primer for ECOM-3D. Technical report, HydroQual, Inc., Mahwah, NJ.

HydroQual 1991b. Water Quality Modeling Analysis of Hypoxia in Long Island Sound. Technical report, HydroQual, Inc., Mahwah, NJ.

HydroQual 1995a. A Primer for SEDZL-3D. Technical report, HydroQual, Inc., Mahwah, NJ.

HydroQual 1995b. A Hydrodynamic and Water quality Evaluation of the Metro Outfall Relocation in Onondaga Lake. Technical report, HydroQual, Inc., Mahwah, NJ.

HydroQual 1995c. A Water Quality Model for Massachusetts and Cape Cod Bays: Calibration of the Bays Eutrophication Model (BEM). Technical report, HydroQual, Inc., Mahwah, NJ.

HydroQual 2004. User's Guide for RCA. Technical report, HydroQual, Inc., Mahwah, NJ.

Hyer, P. V., Fang, C. S., Ruzecki, E. P., and Hargis, W. J. 1971. Hydrography and Hydrodynamics of Virginia Estuaries, Studies of the Distribution of Salinity and Dissolved oxygen in the Upper York System, Virginia Institute of Marine Science, Williamsburg, VA.

Ijima, T. and Tang, F. L. W. 1966. Numerical calculation of wind waves in shallow water. In Proceedings of the 10th Coastal Engineering Conference, Tokyo, Japan. pp. 38–45.

Imhoff, J. C., Stoddard, A., and Buchak, E. M. 2004. Evaluation of Contaminated Sediment Fate and Transport Models. Final report to National Exposure Research Laboratory, Office of Research and Development, U.S. Environmental Protection Agency, Athens, GA.

Ishikawa, K., Kumagai, M., Vincent, W. F., Tsujimura, S., and Nakahara, H. 2002. Transport and accumulation of bloom-forming cyanobacteria in a large, mid-latitude lake: the gyre-Microcystis hypothesis. Limnology, 3:87–96.

James, R. T., Bierman, Jr., V. J., Erickson, M. J., and Hinz, S. C. 2005. The Lake Okeechobee Water Quality Model (LOWQM) enhancements, calibration, validation and analysis. Lake Reser. Manag., 21:231–260.

James, R. T. and Havens, K. E. 2005. Outcomes of extreme water levels on water quality of offshore and nearshore regions in large shallow subtropical lake. Arc. Hydrobiol., 163:225–239.

James, R. T., Jones, B. L., and Smith, V. H. 1995a. Historical trends in the Lake Okeechobee Ecosystem. II. Nutrient budgets. Arch. Hydrobiol./Suppl. (Monog. Beit.), 107:25–47.

James, R. T., Martin, J., Wool, T., and Wang, P. F. 1997. A sediment resuspension and water quality model of Lake Okeechobee. Am. Water Res. Assoc., 33(3):661–680.

James, R. T., Smith, V. H., and Jones, B. L. 1995b. Historical trends in the Lake Okeechobee Ecosystem. III. Water quality. Arch. Hydrobiol./Suppl. (Monograph. Beitr.), 107:49–69.

Jenkinson, I. R. 1986. Oceanographic implications of non-Newtonian properties found in phytoplankton cultures. Nature (London), 323:435–437.

Jepsen, R., McNeil, J., and Lick, W. 2000. Effects of gas generation on the density and erosion of sediments from the Grand River. J. Great Lakes Res., 26(2):209–219.

Jepsen, R., Roberts, J., Gailani, J., and Smith, S. J. 2002. The SEAWOLF Flume: Sediment Erosion Actuated by Wave Oscillations and Linear Flow. SAND2002-O100. Sandia National Labs, Albuquerque, NM.

Ji, Z.-G. 1993. Stability Analyses for the Formation of Ripples, Dunes and Antidues. D. Eng. Sc. Thesis, Columbia University, New York.

Ji, Z.-G. 2000a. Fate and transport in rivers, lakes, and estuaries. Standard Handbook of Environmental Science, Health, and Technology. New York: McGraw-Hill, pp. 8.47–8.55.

Ji, Z.-G. 2000b. Air pollutants and fugitive dust. Standard Handbook of Environmental Science, Health, and Technology. New York: McGraw-Hill, pp. 5.1–5.5.

Ji, Z.-G. 2004. Use of physical sciences in support of environmental management. Environ. Manag., 34(2):159–169.

Ji, Z.-G. 2005a. Water quality models: chemical principles. In Water encyclopedia, Volume 2: Water Quality and Resources Development. Hoboken, NJ: John Wiley & Sons, Inc., pp. 269–273.

Ji, Z-G. 2005b. Water quality modeling-case studies. In Water encyclopedia, Volume 2: Water quality and resources Development. Hoboken, NJ: John Wiley & Sons, Inc., pp. 255–263.

Ji, Z.-G. and Chao, J. P. 1986. On the influences of large-scale inhomogeneity of sea temperature upon the oceanic waves in the tropical regions—Part II: Numerical analysis. Adv. Atmos. Sci., 3:238–244.

Ji, Z.-G. and Chao, J. P. 1987. Teleconnections of the sea surface temperature in the India Ocean with the sea surface temperature in the eastern equatorial Pacific in the Northern Hemisphere, Adv. Atmos. Sci., 3(4):343–348.

Ji, Z.-G. and Chao, J. P. 1989. Responses of tropical atmospheric circulation to the ocean-land surface heating. Acta Meteorolog. Sinica, 3(2):119–131.

Ji, Z.-G. and Chao, J. P. 1990. Instabilities of oceanic waves in the tropical region. Acta Meteorolog. Sinica, 4(2):136–145.

Ji. Z.-G. and Chao, J. P. 1991. An analytical coupled atmospheric-ocean interaction model. J. Marine Sys., 1:263–270.

Ji, Z.-G., Hamrick, J. H., and Pagenkopf, J. 2002a. Sediment and metals modeling in shallow river. J. Environ. Eng., 128:105–119.

Ji, Z.-G., Hu, G., Shen, J., and Wan, Y. 2007a. Three dimensional modeling of hydrodynamic processes in the St. Lucie Estuary. Estuarine, Coastal Shelf Sci., 73:188–200.

Ji, Z.-G. and Jin, K.-R. 2006. Gyres and seiches in a large and shallow lake. J. Great Lakes Res., 32:764–775.

Ji, Z.-G., Johnson, W. R., and Marshall, C. F. 2004b. Deepwater oil-spill modeling for assessing environmental impacts. Coastal Environment V, Southampton, UK: WIT Press, 349–358.

Ji, Z.-G., Johnson, W. R., Marshall, C. F., Rainey, G. B., and Lear, E. M. 2002b. Oil-spill Risk Analysis: Gulf of Mexico Outer Continental Shelf (OCS) Lease Sales, Eastern

Planning Area, 2003–2007, and Gulfwide OCS Program, 2003–2042. Minerals Management Service, U.S. Department of the Interior, Herndon, Virginia. OCS Report 2002–069.

Ji, Z.-G., Johnson, W. R., Price, J. W., and Marshall, C. F. 2003. Oil-spill risk analysis for assessing environmental impacts. In Proceedings of the 2003 International Oil Spill Conference, Vancouver, Canada.

Ji, Z.-G. and Mendoza, C. 1993. Nonlinear stability analysis of an erodible bed for dune formation. Advances on Hydro-Science and Engineering, ed. S. S. Y. Wang. The University of Mississippi, University, MS, 1B: 1317–1322.

Ji, Z.-G. and Mendoza, C. 1997. Weak nonlinear stability analysis for dune formation. J. Hydraulic Eng., 123(11):979–985.

Ji, Z.-G. and Mendoza, C. 1998. Instability of the viscous sublayer for ripple inception. Mech. Res. Commun., 25(1):3–14.

Ji, Z.-G., Morton, M. R., and Hamrick, J. M. 2000. Modeling hydrodynamic and sediment processes in Morro Bay. In Estuarine and Coastal Modeling: Proceedings of the 6th International Conference, Spaulding, M. L. and Butler, H. L., (eds), New Orleans, LA, 1035–1054.

Ji, Z.-G., Morton, M. R., and Hamrick, J. M. 2001. Wetting and drying simulation of estuarine processes. Estuarine, Coastal Shelf Sci., 53:683–700.

Ji, Z.-G., Morton, M. R., and Hamrick, J. M. 2004a. Three-dimensional hydrodynamic and water quality modeling in a reservoir. In Estuarine and Coastal Modeling: Proceedings of the 8th International Conference, Spaulding, M. L. (ed.), Monterey, CA, pp. 608–627.

Ji, Z.-G., Shen, J., and Browder, J. 2007b. Analysis and modeling of sediment and copper processes in St. Lucie Estuary. Marine Environmental Research (submitted).

Jin, K. R., Hamrick, J. M., and Tisdale, T. 2000. Application of a three-dimensional hydrodynamic model for Lake Okeechobee. J. Hydraulic Eng., 126:758–771.

Jin, K. R. and Ji, Z.-G., 2001. Calibration and verification of a spectral wind-wave model for Lake Okeechobee. Ocean Eng., 28(5):571–584.

Jin, K. R. and Ji, Z.-G. 2004. Case study: modeling of sediment transport and wind-wave impact in Lake Okeechobee. J. Hydraulic Eng., 130(11):1055–1067.

Jin, K. R. and Ji, Z.-G. 2005. Application and validation of three-dimensional model in a shallow lake. J. Waterway, Port, Coastal, Ocean Eng., 131(5):213–225.

Jin, K. R., Ji, Z.-G., and Hamrick, J. M. 2002. Modeling winter circulation in Lake Okeechobee, Florida. J. Waterway, Port, Coastal, Ocean Eng., 128:114–125.

Jin, K. R., Ji, Z.-G., and James, T. 2007. Three dimensional water quality and SAV modeling of a large shallow lake. J. Great Lakes Res., 33:28–45.

Johnson, B. H., Health, R. E., Hsieh, B. B., Kim, K. W., and Butler, H. L. 1991. User's Guide for a Three-dimensional Numerical Hydrodynamic, Salinity, and Temperature Model of Chesapeake Bay. Technical Report HL-91-20, U.S. Army Engineer Waterways Experiment Station, Hydraulic Laboratory, Vicksburg, MS.

Johnson, B., Kim, K., Heath, R., Hsieh, B., and Butler, L. 1993. Validation of a three-dimensional hydrodynamic model of Chesapeake Bay. J. Hydraulic Eng., 119(1):2–20.

Jones, W. P. and Launder, B. E. 1972. The prediction of laminarization with a two-equation model of turbulence. Inter. J. Heat Mass Transfer, 15:301–314.

Kang, S. W., Sheng, Y. P., and Lick, W. 1982. Wave action and bottom shear stress in Lake Erie. J. Great Lakes Res., 8(3):482–494.

Kelly, C. E. 2005. Personal communication. Florida Department of Environmental Protection, Tallahassee, FL.

Kenworthy, W. J. and Haunert, D. E. 1991. The light requirements of seagrasses. Proceedings of a Workshop to Examine the Capability of Water Quality Criteria, Standards and Monitoring Programs to Protect Seagrasses. NOAA Technical Memorandum NMFS-SEFC-287, NOAA.

Kimmel, B. L., Lind, O. T., and Paulson, L. J. 1990. Reservoir primary production. In: Thornton K. W., Kimmel B. L., Payne F. E. (eds.) Reservoir Limnology: Ecological Perspectives. New York: Wiley-Interscience, pp. 133–193.

Kirby, R. R., Hobbs, C. H., and Metha, A. J. 1989. Fine Sediment Regime of Lake Okeechobee, Florida. UFL/COEL-89/009, Coastal and Oceanographic Engineering Department, University of Florida, Gainesville, FL.

Knudsen, M. 1900. Ein Hydrographische Lehrsatz. Annal. Hydrog. Marinen Meteorol., 28:316–320.

Kott, U. 1982. Chemical factors. Symposium on the survival of pathogens in the natural environment. XIII International Congress of Microbiology, Boston, MA.

Kumagai, M. 1988. Predictive model for resuspension and deposition of bottom sediment in a lake. Japan. J. Limnol., 49(3):185–200.

Kumagai, M., Asada, Y., and Nakano, S. 1998. Gyres measured by ADCP in Lake Biwa. Coastal Estuarine Studies, 54:199–208.

Lahlou, M., Shoemaker, L., Choudhury, S., Elmer, R., Hu, A., Manguerra, H., and Parker, A. 1998. Better Assessment Science Integrating Point and Nonpoint Sources. BASINS, Version 2.0 User's Manual. EPA-823-B-98-006. U.S. EPA, Washington, DC, 65 pp.

Laws, E. A. and Chalup, M. S. 1990. A microalgal growth model. Limnol. Oceanog., 35(3):597–608.

Lee, C. M., Jones, B. H., Brink, K. H., Arnone, R., Gould, R., Dorman, C., and Beardsley, R. 2000. Upper Ocean Response to Cold Air Outbreaks in the Japan/East Sea: SeaSoar Surveys at the Subpolar Front. Presented on 18 Dec. 2000 at the American Geophysics Union Meeting, San Francisco, CA.

Leendertse, J. J. and Gritton, E. C. 1971. A Water Quality Simulation Model of Well Mixed Estuaries and Coastal Seas. Vol. 2, Computational Procedures. Rand Corporation, Report R-708-NYC, New York, 53 pp.

Lemmin, U. and D'Adamo, N. 1996. Summertime winds and direct cyclonic circulation: observations from Lake Geneva. Annal. Geophys., 14:1207–1220.

Lick, W. 2006. The sediment-water flux of HOCs due to "diffusion" or is there a well-mixed layer? If there is, does it matter? Environ. Sci. Technol., 40(18):5610–5617.

Lick, W., Huang, H. N., and Jepsen, R. 1993. Flocculation of fine-grained sediments due to differential settling. J. Geophys. Res.-Oceans, 98:10279–10288.

Lick, W., Jin, L. J., and Gailani, J. 2004. Initiation of movement of quartz particles. J. Hydraulic Eng., 130(8):755–761.

Lick, W., Lick, J., and Ziegler, C. K. 1994. The resuspension and transport of fine-grained sediments in Lake Erie. J. Great Lakes Res., 20(4):599–612.

Lick, W., Ziegler, C. K., and Tsai, C. 1987. Resuspension, Deposition and Transport of Fine-gained Sediments in Rivers and Near-shore Areas. Prepared for the USEPA Large Lakes Research Station, Grosse Lie, MI.

Limno-Tech 1993. Field Application of a Steady State Mass Balance Model to Heavy Metals in the Blackstone River. Technical Report, Limno-Tech, Inc., Ann Arbor, MI.

Luettich, Jr., R. A., Harleman, D. R. F., and Somlyódy, L. 1990. Dynamic behavior of suspended sediment concentrations in a shallow lake perturbed by episodic wind events. Limnolog. Oceanog., 35(5):1050–1067.

Lumley, J. L. 1978. Two-phase and non-Newtonian flows. Top. Appl. Phys., 12:289–324.

Lung, W.-S. 2001. Water Quality Modeling for Wasteload Allocations and TMDLs, New York: John Wiley & Sons, Inc.

Lvovich, M. J. 1971. World water balance. In: Symposium on world water balance, UNESCO/IAHS publication 93, Paris, France.

MacIntyre, S., Lick, W., and Tsai, C. H. 1990. Variability of entrainment of cohesive sediments in freshwater. Biogeochemistry, 9:187–209.

Madsen, O. S. 1993. Sediment Transport Outside the Surf Zone. Technical Report, U.S. Army Engineer Waterways Experiment Station, Vicksburg, MS.

Malone, T. C., Conley, D. J., Fisher, T. R., Gilbert, P. M., Harding, L. W., and Sellner, K. G. 1996. Scales of nutrient-limited phytoplankton productivity in Chesapeake Bay. Estuaries, 19(2B):371–385.

Marchesiello, P., McWilliams, J. C., and Shchepetikin, A. 2001. Open boundary conditions for long-term integration of regional oceanic models. Ocean Modeling, 3(1/2):1–20.

Martin, J. L. and McCutcheon, S. C. 1999. Hydrodynamics and transport for water quality modeling. Boca Raton, FL: Lewis Publishers.

McGinn, J. M. 1981. A sediment control plan for the Blackstone River. Department of Environmental Quality Engineering, Office of Planning and Program Management Department of Environmental Quality Engineering, Boston, MA.

McNeil, J., Taylor, C., and Lick, W. 1996. Measurements of erosion of undisturbed bottom sediments with depth. J. Hydraulic Eng., 122(6):316–324.

Mei, C. C., Fan, S., and Jin, K. R. 1997. Resuspension and transport of fine sediments by waves. J. Geophys. Res., 102(C7):15807–15821.

Mellor, G. L. 1998. User's Guide for a Three-Dimensional, Primitive Equation, Numerical Ocean Model. Atmospheric and Ocean Sciences Program, Princeton University, Princeton, NJ.

Mellor, G. L., Oey, L.-Y., and Ezer, T. 1998. Sigma coordinate pressure gradient errors and the seamount problem. J. Atm. Oceanic Technol., 15:1122–1131.

Mellor, G. L. and Yamada, T. 1982. Development of a turbulence closure model for geophysical fluid problems. Rev. Geophys. Space Phys., 20:851–875.

Meyer-Peter, E. and Muller, R. 1948. Formulas for bed-load transport. Proceedings of the International Association of Hydraulic Structures Research, Report of Second Meeting, Stockholm, 39–64.

Miller, A. 1999. Personal communication. U.S. Army Corps of Engineers, Tulsa, OK District.

Miller, G. T. 1990. Living in the Environment: An Introduction to Environmental Science. 6th ed. Wadsworth Publishing Company, Belmont, CA.

Millie D. F., Carrick H. J., Doering, P. H., and Steidinger, K. A. 2004. Intra-annual variability of water quality and phytoplankton in the North Fork of the St. Lucie River Estuary, Florida (USA): a quantitative assessment. Estuarine, Coastal Shelf Sci., 61:137–149.

Miznot, C. 1968. A study of the physical properties of different very fine sediments and their behavior under hydrodynamic action. La Houille Blanche, 7:591–620.

Monod, J. 1949. The growth of bacterial cultures. Ann. Rev. Microbiol., 3:371–394.

Moore, P. A., Reddy, D. R., and Fisher, M. M. 1998. Phosphorus flux between sediment and overlying water in Lake Okeechobee, Florida: spatial and temporal variations. J. Environ. Qual., 27:1428–1439.

Morel, F. 1983. Principles of Aquatic Chemistry. New York: John Wiley & Sons, Inc., 446 pp.

Morris, F. R. 1987. Modeling of Hydrodynamics and Salinity in the St. Lucie Estuary. South Florida Water Management District, Technical Publication 87, West Palm Beach, FL.

Moustafa, M. Z. and Hamrick, J. M. 2000. Calibration of the wetland hydrodynamic model to the Everglades nutrient removal project. Water Quality Ecosystem Modeling, 1:141–167.

NALMS 1992. Developing Eutrophication Standards for Lakes and Reservoirs. North American Lake Management Society, Report prepared by the Lake Standards Subcommittee, Alachua, FL. 51 pp.

NDEQ 1996. Title 117-Nebraska Surface Water Quality Standards. Nebraska Department of Environmental Quality, Lincoln, NE.

Nix, J. S. 1990. Mathematical modeling of the combined sewer system. Chapter 2 in Control and treatment of combined sewer overflows, P. E. Moffa (ed.), pp. 23–78. New York: Van Nostrand Reinhold Company.

NRC 1983. Fundamental Research on Estuaries: the Importance of an Interdisciplinary Approach. National Research Council. Washington, DC: National Academy Press.

NRC 2000. Clean Coastal Waters: Understanding and Reducing the Effects of Nutrient Pollution. National Research Council. Washington, DC: National Academy Press.

NSC 1998. Coastal Challenges: A Guide to Coastal and Marine Issues. National Safety Council, Washington, DC.

O'Connor, D. J. 1988. Models of sorptive toxic substances in freshwater systems. I: Basic equations. J. Environ. Eng., 114(3):507–532.

O'Connor, D. J. and Dobbins, W. E. 1958. Mechanism of reaeration in natural streams. Transactions ASCE, 123:641–684.

ODEQ 2000. Continuing Planning Process. 1999–2000 edition. Oklahoma Department of Environmental Quality, Oklahoma, OK.

Oey, L.-Y. 2005. A wetting and drying scheme for POM. Ocean Modeling, 9:133–150.

Oey, L.-Y. 2006. An OGCM with movable land-sea boundaries. Ocean Modeling, 13:176–195.

Oey, L.-Y., Ezer, T., Hu, C., and Muller-Karger, F. E. 2007. Baroclinic tidal flows and inundation processes in Cook Inlet, Alaska: numerical modeling and satellite observations. Ocean Dynamics, doi: 10.1007/s10236-007-0103-8.

Ohrel, Jr., R. L. and Register, K. M. 2006. Volunteer Estuary Monitoring: A Methods Manual, Second Edition. EPA-842-B-06-003. U.S. Environmental Protection Agency, Office of Water, Washington, DC.

Olila, O. G. and Reddy, K. R. 1993. Phosphorus sorption characteristics of sediments in shallow eutrophic lakes of Florida. Arch. Hydrobiol., 129:45–65.

Orlanski, I. 1976. A simple boundary condition for unbounded hyperbolic flows. J. Comput. Phys., 21:251–269.

Ostrovsky, I., Yacobi, Y. Z., Walline, P., and Kalikhman, I. 1996. Seiche-induced mixing: its impact on lake productivity. Limnol. Oceanog., 41:323–332.

Otsubo, K. and Muraoka, K. 1987. Field studies on physical properties of sediment and sediment resuspension in Lake Kasumigaura. Jpn. J. Limnol., 48:s131–s138.

Owens, M., Edwards, R., and Gibbs, J. 1964. Some reaeration studies in streams. Inter. J. Air Water Pollution, 8:469–486.

OWRB 1996. Oklahoma Water Resources Board, United States Army Corps of Engineers, and Oklahoma State University. Final Report for Cooperative "Clean-Lakes" Project, Phase I: Diagnostic and Feasibility Study on Wister Lake, OK.

Palma, E. D. and Matano, R. P. 1998. On the implementation of passive open boundary conditions for a general circulation model: the barotropic mode. J. Geophys. Res., 103:1319–1341.

Palma, E. D. and Matano, R. P. 2000. On the implementation of passive open boundary conditions for a general circulation model: the three-dimensional case. J. Geophys. Res., 105:8605–8628.

Pan, H., Avissar, R., and Haidvogel, D. B. 2002. Summer circulation and temperature structure of Lake Kinneret. J. Phys. Oceanog., 32:295–313.

Park, K., Jung, H. S., Kim, H. S., and Ahn, S. M. 2005. Three-dimensional hydrodynamic-eutrophication model (HEM-3D): application to Kwang-Yang Bay, Korea. Marine Environ. Res., 60(2):171–193.

Park, K., Kuo, A. Y., Shen, J., and Hamrick, J. M. 1995. A Three-dimensional Hydrodynamic-Eutrophication Model (HEM3D): Description of Water Quality and Sediment Processes Submodels. The College of William and Mary, Virginia Institute of Marine Science. Special Report 327, 113 pp.

Parker, W. R. and Kirby, R. 1982. Time dependent properties of cohesive sediment relevant to sedimentation management—European experience. Estuarine Comparisons, V. S. Kennedy, (ed.), New York: Academic Press, pp. 573–590.

Philip Williams & Associates. 1988. Sedimentation Processes in Morro Bay, California. Prepared for Coastal San Luis Resource Conservation District. Philip Williams and Associates, San Francisco, CA.

Phillips, N. A. 1957. A coordinate system having some special advantage for numerical forecasting. J. Meteorol., 14:184–185.

Phlips, E. J. and Ihnat, J. 1995. Planktonic nitrogen fixation in a shallow subtropical lake (Lake Okeechobee, Florida, USA). Arch. Hydrobiol., Adv. Limnol., 45:191–201.

Preisendorfer, R. W. 1988. Principal Component Analyses in Meteorology and Oceanography. London, UK: Elsevier, 418 pp.

Press, W. H., Teukolsky, S. A., Vetterling, W. T., and Flannery, B. P. 1992. Numerical Recipes in Fortran, the Art of Scientific Computing. 2nd ed., Cambridge University Press, 963 pp.

Price, J. M., Johnson, W. R., Ji, Z.-G., Marshall, C. F., and Rainey, G. B. 2004. Sensitivity testing for improved efficiency of a statistical oil-spill risk analysis model. Environ. Modelling Software, 19:671–679.

Pritchard, D. W. 1967. Observations of circulation in coastal plain estuaries. In Estuaries, Publication No 83, American Association for the Advancement of Science, Washington, DC, pp. 37–44.

Pugh, D. T. 1987. Tides, Surges, and Mean Sea-level. New York: John Wiley & Sons, Inc., 472 pp.

Quinn, J. M. 1991. Guidelines for the Control of Undesirable Biological Growths in Water. National Institute of Water and Atmospheric Research. Consultancy Report No. 6213/2.

Reddy, K. R., Sheng, Y. P., and Jones, B. L. 1995. Lake Okeechobee Phosphorus Dynamics Study: Summary. Vol. I. Contract No. C-91-2554. Report to the South Florida Water Management District, West Palm Beach, FL.

Richardson, J. R. and Hamouda, E. 1995. GIS modeling of hydroperiod, vegetation, and soil nutrient relationships in the Lake Okeechobee marsh ecosystem. Arch. Hydrobiol., Adv. Limnol., 45:95–115.

Roberts, J. D., Jepsen, R. A., and James, S. C. 2003. Measurement of sediment erosion and transport with the adjustable shear stress erosion and transport flume. J. Hydraulic Eng., 29(11):862–871.

Rosati, A. K. and Miyakoda, K. 1988. A general circulation model for upper ocean simulation. J. Phys. Oceanog., 18:1601–1626.

Rossi, G. and Premazzi, G. 1991. Delay in lake recovery caused by internal loading. Water Res., 25:567–575.

Scheffer, M. 1989. Alternative stable states in eutrophic shallow freshwater systems: A minimal model. Hydrobiol. Bull., 23:73–85.

Scheffer, M., Hosper, S. H., Meijer, M. L., Moss, B., and Jeppesen, E. 1993. Alternative equilibria in shallow lakes. Trends Ecol. Evol., 8(8):275–279.

Schnoor, J. L. 1996. Environmental Modeling: Fate and Transport of Pollutants in Water, Air, and Soil. New York: John Wiley & Sons, Inc.

Schumm, S. A. 1977. The Fluvial System. New York: John Wiley & Sons, Inc.

Schwab, D. J., Beletsky, D., and Lou, J. 2000. The 1998 coastal turbidity plume in Lake Michigan. Estuarine, Coastal Shelf Sci., 50:49–58.

SFWMD 1999. Focus on the St. Lucie River. South Florida Water Management District, West Palm Beach, FL, 7 pp.

SFWMD 2002. Lake Okeechobee Surface Water Improvement and Management (SWIM) Plan. South Florida Water Management District, West Palm Beach, FL, 202 pp.

Shen, J., Boon, J., and Kuo, A. Y. 1999. A numerical study of a tidal intrusion front and its impact on larval dispersion in the James River estuary, Virginia. Estuaries, 22(3A):681–692.

Shen, J., and Kuo, A. Y. 1999. Numerical investigation of an estuarine front and its associated eddy. J. Waterway, Port, Coastal Ocean Eng., 125(3):127–135.

Sheng, Y. P. 1986. A Three-dimensional Mathematical Model of Coastal, Estuarine and Lake Currents Using Boundary Fitted Grid. Report No. 585, A.R.A.P. Princeton, New Jersey: Group Titan Systems, New Jersey.

Sheng, Y. P. 1991. Lake Okeechobee Phosphorus Dynamics Study: Hydrodynamics and Sediment Dynamics—A Field and Modeling Study. Vol. VII., South Florida Water Management District, West Palm Beach, FL.

Sheng, Y. P. and Chen, X. J. 1993. Lake Okeechobee Phosphorus Dynamics Study: A Three Dimensional Numerical Model of Hydrodynamics, Sediment Transport, and Phosphorus, Dynamics: theory, model development, and documentation. Final Report to South Florida Water Management District. Coastal and Oceanographic Engineering Department, University of Florida, Gainesville, FL.

Sheng, Y. P. and Lee, H. 1991. The Effect of Aquatic Vegetation on Wind-driven Circulation in Lake Okeechobee. UFL/COEL-91/018. University of Florida, Gainesville, FL.

Shields, A. 1936. Application of Similarity Principles and Turbulent Research to Bed-Load Movement (translation of original in German by W. P. Ott and J. C. van Uchelen, California Institute of Technology), Mitteilungen der Preussischen Versuchsanstalt für Wasserbau und Schiffbau.

Shoemaker, L., Lahlou, M., Bryer, M., Kumar, D., and Kratt, K. 1997. Compendium of Tools for Watershed Assessment and TMDL Development. Report EPA841-B-97-006, Office of Water, U.S. Environmental Protection Agency, Washington, DC.

Shrestha, P. A. and Orlob, G. T. 1996. Multiphase distribution of cohesive sediments and heavy metals in estuarine systems. J. Environ. Eng., 122:730–740.

Smagorinsky, J. 1963. General circulation experiments with the primitive equations, Part I: the basic experiment. Monthly Weather Rev., 91:99–152.

Smith, R. B. 1980. Linear theory of stratified hydrostatic flow past an isolated mountain. Tellus, 32:348–364.

Smith, J. D. and McLean, S. R. 1977. Spatially averaged flow over a wavy bed. J. Geophys. Res., 82:1735–1746.

Smolarkiewicz, P. K. and Clark, T. L. 1986. The multidimensional positive definite advection transport algorithm: further development and applications. J. Comput. Phys., 67:396–438.

Smolarkiewicz, P. K. and Grabowski, W. W. 1990. The multidimensional positive definite advection transport algorithm: nonoscillatory option. J. Comput. Phys., 86:355–375.

Smolarkiewicz, P. K. and Margolin, L. G. 1993. On forward-in-time differencing for fluids: extension to a curvilinear framework. Monthly Weather Rev., 121:1847–1859.

Sommerfeld, A. 1949. Partial Differential Equations. Lecture Notes on Theoretical Physics. Vol. 6. San Diego, CA: Academic Press.

Spasojevic, M. and Holly, F. M. 1994. Three-dimensional Numerical Simulation of Mobile-bed Hydrodynamics. Contract Report HL-94-2, US Army Engineer Waterways Experiment Station, Vicksburg, MS.

Spaulding, M., Swanson, C., and Mendelsohn, D. 2000. Application of qualitative model-data calibration measures to assess model performance. In Estuarine and Coastal Modeling: Proceedings of the 6th International Conference, Spaulding, M. L. and Butler, H. L. (eds.), ASCE, pp. 843–867.

Steele, J. H. 1962. Environmental control of photosynthesis in the sea. Limnol. Oceanog., 7:137–150.

Steinman, A. D., Havens, K. E., Carrick, H. J., and VanZee, R. 2002. The past, present, and future hydrology and ecology of Lake Okeechobee and its watersheds. In J. W. Porter and K. G. Porter (eds.), the Everglades, Florida Bay, and Coastal Reefs of the Florida Keys, an Ecosystem Restoration Sourcebook. Boca Raton, FL: CRC Press.

Steinman, A. D. and Lamberti, G. A. 1996. Biomass and pigments of benthic algae. In Methods in Stream Ecology. Hauer, F. R. and G. A. Lamberti (eds.). San Diego, CA: Academic Press, pp. 295–313.

Stevenson, F. J. 1972. Nitrogen Cycle. In Fairbridge, R. W. (ed.), The Encyclopedia of Geochemistry and Environmental Sciences. New York: Van Nostran Reinhold, pp. 801–806.

Stevenson, R. J. 1996. An introduction to algal ecology in freshwater benthic habitats. In Algal Ecology: Freshwater Benthic Ecosystems. Stevenson, R. J., M. Bothwell, and R. L. Lowe (eds.). San Diego, CA: Academic Press, pp. 3–30.

Strathmann, R. R. 1967. Estimating the organic carbon content of phytoplankton from cell volume or plasma volume. Limnol. Oceanog., 12:411–418.

Streeter, H. W. and Phelps, E. B. 1925. A study of the pollution and natural purification of the Ohio River. III: Factors concerned in the phenomena of oxidation and reaeration. Bulletin Number 146, U.S. Public Health Service.

Stumm, W. and Morgan, J. J. 1981. Aquatic Chemistry, 2d ed., New York: John Wiley & Sons, Inc.

Styles, R. and Glenn, S. M. 2000. Modeling stratified wave-current bottom boundary layers for the continental shelf. J. Geophys. Res. (Ocean), 105(24):119–139.

Sverdrup, H. V. and Munk, W. H. 1947. Wind, Sea and Swell: Theory of Relations for Forecasting, U.S. Navy Hydrographic Office Publication No. 601.

SWAN 1998. SWAN Cycle 2 User Manual, Delft University of Technology, The Netherlands.

Swingbank, W. C. 1963. Longwave radiation from clear skies. Quart. J. R. Meteorol. Soc., 89:339–348.

Tetra Tech 1998a. Copper and Nickel Source Characterization for the Lower South San Francisco Bay TMDL Project. Report prepared for the City of San Jose. Tetra Tech, Inc., Lafayette, CA.

Tetra Tech 1998b. Analysis of Historical Thermal Data in Conowingo Pond Relative to Operations at Peach Bottom Atomic Power Station and Implications for Three-dimensional Modeling. A report to PECO Energy and EPRI. Tetra Tech, Inc., Lafayette, CA.

Tetra Tech 1999a. Morro Bay National Estuary Program: Hydrodynamic Circulation Model. Tetra Tech, Inc., Lafayette, CA.

Tetra Tech 1999b. Pilot Scale Application of Existing Water Quality Models to Derive NPDES Permits Based on Sediment Quality. Technical report to USEPA, Tetra Tech, Inc., Fairfax, VA.

Tetra Tech 1999c. Task 1. Conceptual Model Report for Copper in Lower South San Francisco Bay (Final Report). Report prepared for the City of San Jose. Tetra Tech, Inc., Lafayette, CA.

Tetra Tech 1999d. Fecal Coliform TMDL for the Rockford Lake Watershed, Nebraska. Technical report to USEPA. Tetra Tech, Inc., Fairfax, VA.

Tetra Tech 1999e. Three-dimensional Hydrodynamic and Water Quality Model of Peconic Estuary. For Peconic Estuary Program, Suffolk County, NY. Tetra Tech, Inc., Fairfax, VA.

Tetra Tech 2000a. Task 2. Impairment Assessment Report for Copper and Nickel in Lower South San Francisco Bay (Final Report). Report prepared for the City of San Jose. Tetra Tech, Inc., Lafayette, CA.

Tetra Tech 2000b. Hydrodynamic and Water Quality Model of Christina River basin. Technical Report for U.S. Environmental Protection Agency Region 3. Tetra Tech, Inc., Fairfax, VA.

Tetra Tech 2000c. Water Quality Modeling Analysis in Support of TMDL Development for Tenkiller Ferry Lake and the Illinois River Watershed in Oklahoma. Technical Report for U.S. Environmental Protection Agency Region 6 and Department of Environmental Quality, State of Oklahoma. Tetra Tech, Inc., Fairfax, VA.

Tetra Tech 2001. Technical Evaluation of Existing Water Quality Models and Their Suitability for Use in Developing Sediment Quality-Based NPDES Permits. Technical report to USEPA, Tetra Tech, Inc., Fairfax, VA.

Tetra Tech 2002. Theoretical and Computational Aspects of Sediment and Contaminant Transport in the EFDC Model. Technical Report to USEPA. Tetra Tech, Inc., Fairfax, VA.

Tetra Tech 2006. The Environmental Fluid Dynamics Code Theory and Computation, Volume 3: Water Quality Module. Technical Report to USEPA, Tetra Tech, Inc., Fairfax, VA.

Tetra Tech and AEE 2005. Florida Bay Water Quality Data. Technical report to South Florida Water Management District. Tetra Tech, Inc., Fairfax, Virginia and Applied Environmental Engineering, LLC, Naples, FL.

Thomann, R. V., Merklin, W., and Wright, B. 1993. Modeling cadmium fate at superfund site: impact of bioturbation. J. Environ. Eng., 119:424–442.

Thomann, R. V. and Mueller, J. A. 1987. Principles of Surface Water Quality Modeling and Control. New York: Harper and Row.

Thorn, M. F. C. and Parsons, J. G. 1980. Erosion of cohesive sediments in estuaries: an engineering guide. Proceedings of the Third International Symposium on Dredging Technology, Paper Fl, British Hydraulic Research Association-Fluid Engineering, Bordeaux, France, pp. 349–358.

Tomczak, M. and Godfrey, J. S. 1994. Regional Oceanography: an Introduction. Oxford, England; New York: Pergamon Press, 442 pp.

Trefry, J. H., Sadoughi, M., Sullivan, M. D., Steward, J. S., and Barber, S. 1983. Trace metals in the Indian River Lagoon, Florida: the copper story. Florida Sci., 46(3/4):415–427.

Tsai, C. H. and Lick, W. 1987. Resuspension of sediments from Long Island Sound. Water Sci. Technol., 21(6/7):155–184.

Tsay, T. K., Ruggaber, G. J., Effler, S. W., and Driscoll, C. T. 1992. Thermal stratification modeling of lakes with sediment heat flux. J. Hydraulic Eng., 118(3):407–419.

Tufford, D. L. and McKellar, H. N. 1999. Spatial and temporal hydrodynamic and water quality modeling analysis of a large reservoir on the South Carolina (USA) coastal plain. Ecol. Modeling, 114:137–173.

Turner, R. E., Schroeder, W. W., and Wiseman, Jr., W. J. 1987. The role of stratification in the deoxygenation of Mobile Bay and adjacent shelf bottom waters. Estuaries, 10:13–19.

UNESCO 1981. The Practical Salinity Scale 1978 and the International Equation of State of Seawater 1980. Technical Paper Marine Science, 36: 25 pp.

US Code 1977. Title 33 Navigation and Navigable Water, Chapter 26 Water Pollution Prevention and Control. Clean Water Act of 1977. Washington, DC.

USACE 1987. Engineering and Design: Reservoir Water Quality Analysis. EM 1110-2-1201, U.S. Army Corps of Engineers, Washington, DC.

USACE 1988. Water Quality Report on Tenkiller Ferry Lake, 1985–1986. U.S. Army Corps of Engineers, Tulsa, OK.

USACE 1997. Blackstone River Watershed Reconnaissance Investigation. Volume 1, Main Paper and Appendices; Volume 2, Additional Appendices. U.S. Army Corps of Engineers, New England District, Concord, MA.

USACE 2002. Coastal Engineering Manual. EM 1110-2-1100, U.S. Army Corps of Engineers, Washington, DC.

USCG 2003. Environmental Impact Statement for the Port Pelican LLC Deepwater Port License Application. United States Coast Guard, Vessel and Facilities Operation Standards Division, 2100 Second Street, SW, Washington, DC.

USEPA 1984. Technical Guidance Manual for Performing Waste Load Allocations. Book 2: Streams and Rivers; Chapter 3: Toxic substances. EPA 440/4-84-022, United States Environmental Protection Agency, Washington, DC.

USEPA 1986. Quality Criteria for Water 1986. EPA-440/5-86-001, U.S. Environmental Protection Agency, Office of Water, Washington, DC.

USEPA 1990. Technical Guidance Manual for Performing Waste Load Allocations, Book III: Estuaries. U.S. Environmental Protection Agency, Office of Water, Washington, DC.

USEPA 1993. Training Manual for NPDES Permit Writers. EPA 833-B-93-003, United States Environmental Protection Agency, Washington, DC.

USEPA 1994a. Deposition of Air Pollutants to the Great Waters. U.S. Environmental Protection Agency, Office of Air Quality, Research Triangle Park, NC.

USEPA 1994b. Water Quality Standards Handbook. 2nd ed. EPA-823-B-94-005b, U.S. Environmental Protection Agency, Office of Water, Washington, DC.

USEPA 1996a. Blackstone River Initiative. Phase 1: Dry Weather Assessment Interim Paper of Data 1991. Prepared by U.S. Environmental Protection Agency, Region 1, and the Massachusetts Division of Water Pollution Control, in cooperation with the Rhode Island Department of Management and the University of Rhode Island.

USEPA 1996b. The Metals Translator: Guidance For Calculating a Total Recoverable Permit Limit From a Dissolved Criterion. EPA 823-B-96-007, United States Environmental Protection Agency, Office of Water, Washington, DC.

USEPA 1996c. Hydrologic Simulation Program-FORTRAN, User's Manual for Release 11, EPA 600/3-84/065, United States Environmental Protection Agency, Athens, GA.

USEPA 1997. The Incidence and Severity of Sediment Contamination in Surface Waters of the United States. Volume 1: National sediment quality survey. EPA 823-R-97-006, United States Environmental Protection Agency, Washington, DC.

USEPA 1998. Bacteria Water Quality Standard Status Report. U.S. Environmental Protection Agency, Office of Water, Washington, DC.

USEPA 1999. Review of Potential Modeling Tools and Approaches to Support the BEACH Program. EPA 823-R-99-002. U.S. Environmental Protection Agency, Office of Science and Technology, Washington, DC.

USEPA 2000a. National Water Quality Inventory: 1998 Report to Congress. EPA 841-R-00-001. U.S. Environmental Protection Agency, Office of Water, Washington, DC.

USEPA 2000b. Nutrient Criteria Technical Guidance Manual: Lakes and Reservoirs, First Edition. EPA-822-B00-001. Office of Water, Office of Science and Technology, Washington, DC.

USEPA 2000c. Nutrient Criteria Technical Guidance Manual: Rivers and Streams. EPA-822-B-00-002, Office of Water, Office of Science and Technology, Washington, DC.

USEPA 2000d. Hydrodynamic and Water Quality Model of Christina River Basin. Final Report. United States Environmental Protection Agency, Region III, Philadelphia, PA. 464 pp.

USEPA 2000e. Total Maximum Daily Load (TMDL) for Lake Okeechobee. United States Environmental Protection Agency, Atlanta, GA.

USEPA 2001. Nutrient Criteria Technical Guidance Manual: Estuarine and Coastal Marine Waters. EPA-822-B-01-003. Office of Water, Office of Science and Technology, Washington, DC.

USEPA 2002. Implementation Guidance for Ambient Water Quality Criteria for Bacteria. EPA-823-B-02-003. U.S. Environmental Protection Agency, Office of Water, Washington, DC.

USEPA 2004. STORET Version 2.0.5 Report Module Reference Guide. U.S. Environmental Protection Agency, Office of Water, Washington, DC.

USEPA 2006. Volunteer Estuary Monitoring: A Methods Manual. EPA-842-B-06-003. U.S. Environmental Protection Agency, Office of Wetlands, Washington, DC.

USGS 1999. The Quality of Our Nation's Waters—Nutrients and Pesticides. U.S. Geological Survey, U.S. Geological Survey Circular 1225, 82 pp.

Vanoni, V. A. 1977. Manuals and Reports on Engineering Practice, No. 54. Prepared by the ASCE Task Committee for the Preparation of the Manual on Sedimentation of the Sedimentation Committee of the Hydraulics Division, American Society of Civil Engineers, New York, NY.

van Rijn, L. C. 1984a. Sediment transport, Part I: Bed load transport. J. Hydraulic Eng., 110:1431–1455.

van Rijn, L. C. 1984b. Sediment transport, Part II: Suspended load transport. J. Hydraulic Eng., 110:1613–1641.

Vinokur, M. 1974. Conservation equations of gas dynamics in curvilinear coordinate systems. J. Comput. Phys., 50:71–100.

Violeau, D., Bourban, S., Cheviet, C., Markofsky, M., Petersen, O., Roberts, W., Spearman, J., Toorman, E., Vested, H., and Weilbeer, H. 2000. Numerical simulation

of cohesive sediment transport: intercomparison of several numerical models. 6th Int. Conf. on Nearshore and Estuarine Cohesive Sediment Transport, INTERCOH 2000, Delft, The Netherlands.

Vollenweider, R. A. 1968. The Scientific Basis of Lake and Stream Eutrophication with Particular Reference to Phosphorus and Nitrogen as Eutrophication Factors. Technical Report DAS/DSl/68.27, Organization for Economic Cooperation and Development, Paris, France.

Walker, Jr., W. W. and Havens, K. E. 1995. Relating algal bloom frequencies to phosphorus concentrations in Lake Okeechobee. Lake Reser. Management, 11:77–83.

Walsh, J. J. 1988. On the Nature of Continental Shelves. New York: Academic Press.

Wan, Y., Ji, Z.-G., and Shen, J. 2007. Three-dimensional water quality modeling of the St. Lucie Estuary (unpublished manuscript).

Wan, Y., Reed, C., and Roaza, E. 2003. Modeling watershed with high groundwater and dense drainage canals, Part I: Model development. In International Congress: Watershed Management for Water Supply Systems, Peter E. Black (ed.). American Water Resources Association, Middleburg, VA, TPS-03-2 (CD-ROM).

Wang, K.-H., Jin, K.-R., and Tehrani, M. 2003. Field measurement of flow velocities, suspended solids concentrations, and temperatures in Lake Okeechobee. J. Am. Water Res. Assoc., 39(2):441–456.

Warwick, J. J., Cockrum, D., and Horvath, M. 1997. Estimating non-point source loads and associated water quality impacts. J. Water Res. Planning Management, 123(5):302–310.

Wentworth, C. K. 1922. A scale of grade and class terms for clastic sediments. J. Geol., 30:377–392.

Westrich, J. T. and Berner, R. A. 1984. The role of sedimentary organic matter in bacterial sulfate reduction: the G model tested. Limnol. Oceanog., 29(2):236–249.

Wetzel, R. G. 1975. Limnology. New York: Saunders, 743 pp.

Wezernak, C. T. and Gannon, J. J. 1968. Evaluation of nitrification in streams. J. Sanitary Eng. Div., ASCE, 94(SA5):883–895.

Whitford, L. A. and Schumacher, G. J. 1964. Effect of current on respiration and mineral uptake of Spirogyra and Oedogonium. Ecology, 45:168–170.

Wikramanayake, P. N. and Madsen, O. S. 1994. Calculation of Suspended Sediment Transport by Combined Wave–Current Flows. Contract Report DRP-94-7, U.S. Army Engineer Waterways Experiment Station, Vicksburg, MS.

Wool, T. A., Ambrose, R. B., Martin, J. L., and Cormer, E. A. 2002. Water Quality Analysis Simulation Program (WASP), Version 6.0.

Wool, T. A., Davie, S. R., Plis, Y. M., and Hamrick, J. M. 2003a. The development of a hydrodynamic and water quality model to support TMDL determinations and water quality management of a stratified shallow estuary: Mobile Bay, Alabama. Water Environmental Federation TMDL Specialty Conference, Chicago, IL.

Wool, T. A., Davie, S. R., and Rodriguez, H. N. 2003b. Development of three-dimensional hydrodynamic and water quality models to support total maximum daily load decision process to the Neuse River Estuary, North Carolina. J. Water Res. Planning Management, 129:295–306.

Wright, J. M., Lindsay, Jr., W. T., and Druga, T. R. 1961. The Behavior of Electrolytic Solutions at Elevated Temperatures as Derived from Conductance Measurements. USAEC Comm. R&D report WAPD-TM-204, 32 pp.

Yamashiki, Y., Kumagai, M., Jiao, C., Nezu, I., and Matsui, S. 2003. Numerical simulation of thermally induced gyres in Lake Biwa. Hydrolog. Proc., 17(14):2947–2956.

Yang, Z., Khangaonkar, T., DeGasperi, C., and Marshall, K. 2000. Three-dimensional modeling of temperature stratification and density-driven circulation in Lake Billy Chinook, Oregon. In Estuarine and Coastal Modeling: Proceedings of the 6th International Conference, Spaulding, M. L. and Butler, H. L. (eds.), pp. 411–425.

Ziegler, C. K. and Nesbitt, B. 1994. Fine-grained sediment transport in Pawtuxet River, Rhode Island. J. Hydraulic Eng., 120:561–576.

Ziegler, C. K., and Nesbitt, B. 1995. Long-term simulation of fine-grained sediment transport in large reservoir. J. Hydraulic Eng., 121:773–781.

Ziegler, C. K., Israelsson, P. H., and Connolly, J. P. 2000. Modeling sediment transport dynamics in Thompson Island Pool. Upper Hudson River. Water Quality and Ecosystems Modeling, 1:193–222.

Zou, R., Carter, S., Shoemaker, L., Parker, A., and Henry, T. 2006. Integrated hydrodynamic and water quality modeling system to support nutrient total maximum load development for Wissahickon Creek, Pennsylvania. J. Environ. Eng., 132(4):555–566.

INDEX

Hydrodynamics and Water Quality: Modeling Rivers, Lakes, and Estuaries, by Zhen-Gang Ji